NASA TM X-58168
JSC-09930

PROCEEDINGS OF THE

NASA Earth Resources Survey Symposium

HOUSTON, TEXAS
JUNE 1975

N76-17501 THRU N76-17551 Unclas 14342 G3/43
HC $7.25

FIRST COMPREHENSIVE SYMPOSIUM ON THE PRACTICAL APPLICATION OF EARTH RESOURCES SURVEY DATA

ORIGINAL CONTAINS COLOR ILLUSTRATIONS

Original photography may be purchased from:
EROS Data Center
10th and Dakota Avenue
Sioux Falls, SD 57198

VOLUME I-B

TECHNICAL SESSION PRESENTATIONS

GEOLOGY – INFORMATION SYSTEMS AND SERVICES

"Made available under NASA sponsorship in the interest of early and wide dissemination of Earth Resources Survey Program information and without liability for any use made thereof."

FEB 1976
RECEIVED
NASA STI FACILITY
INPUT BRANCH

National Aeronautics and Space Administration
LYNDON B. JOHNSON SPACE CENTER

(NASA-TM-X-58168-Vol-1-B) NASA EARTH RESOURCES SURVEY SYMPOSIUM. VOLUME 1-B: GEOLOGY, INFORMATION SYSTEMS AND SERVICES First Comprehensive Symposium on the Practical Application of Earth Resources

NASA TM X-58168

NASA ERS Earth Resources Survey Symposium

VOLUME I-B

TECHNICAL SESSION PRESENTATIONS

Geology
Information Systems and Services

PREFACE

The first comprehensive symposium on the practical application of Earth resources survey data was sponsored by the NASA Headquarters Office of Applications from June 9 to 12, 1975, in Houston, Texas. The Lyndon B. Johnson Space Center acted as host.

This symposium combined the utilization and results of data from NASA programs involving LANDSAT, the Skylab Earth resources experiment package, and aircraft, as well as from other data acquisition programs.

The primary emphasis was on the practical applications of Earth resources survey technology of interest to a large number of potential users. Also featured were scientific and technological exploration and research investigations with potential promising applications.

The opening day plenary session was devoted to papers of general interest and an overview. The following 2-1/2 days were devoted to concurrent discipline-oriented technical sessions and to three special sessions covering State and Local Users, Coastal Zone Management, and User Services. These special sessions were structured to provide governmental and private organizations with a comprehensive picture of various applications in the management and implementation of remote-sensing data use in their own programs. The concluding day was a summary with selected state, international, and technical session papers, summaries of significant results from special and technical sessions, and an overview of federal agency and international activities and planning.

Volumes I-A, I-B, I-C, and I-D contain the technical papers presented during the concurrent sessions. Volume II contains the opening day plenary session, special sessions, and the concluding day summary session. Volume III contains a summary of each session by the chairman and session personnel and provides an overview of the significant applications that have been developed from the use of remote-sensing data. Volume III also includes the conclusions and needs identified during the individual sessions and workshops.

Opinions and recommendations expressed in these reports are those of the session members and do not necessarily reflect the official position of NASA.

Olav Smistad
Symposium Coordinator

NASA ERS Earth Resources Survey Symposium

PROGRAM COMMITTEE

Charles W. Mathews, NASA, Chairman
Joseph Carlson, Public Technology, Inc.
Dr. John DeNoyer, U.S. Geological Survey
Dr. M. Frank Hersman, National Science Foundation
Daniel J. Fink, AIAA, Space Applications Board (NRC)
Harold Finger, General Electric Co.
Dr. Stanley Freden, NASA
Willis Hawkins, Lockheed Aircraft Corp.
Russell R. Schweickart, NASA
Pitt Thome, NASA

SYMPOSIUM COORDINATORS

JOHNSON SPACE CENTER
Olav Smistad
Edward O. Zeitler
Earth Resources Program Office
OFFICE OF APPLICATIONS
Dan Richard, User Affairs

ADMINISTRATIVE SUPPORT

Industrial Economics Research Division
Texas A. & M. University

PRECEDING PAGE BLANK NOT FILMED

SESSION LEADERS

AGRICULTURE
(Includes Agriculture, Forestry, Range Resource Inventory and Management)

Richard Baldwin, Chairman
Cargill, Inc., Minneapolis, Minn.
James Murphy
U.S. Department of Agriculture, Agricultural Stabilization and Conservation Service, Houston, Tex.
Ryborn Kirby
NASA Lyndon B. Johnson Space Center, Houston, Tex.
Kenneth Suit
NASA Lyndon B. Johnson Space Center, Houston, Tex.

ENVIRONMENT
(Environmental Surveys and Applications)

Kessler Cannon and Ronald Myles, Chairmen
Department of Environmental Quality, State of Oregon, Portland, Oreg.
Dr. Ralph Shay
Oregon State University, Corvallis, Oreg.
Dr. Lawrence Greenwood
NASA Langley Research Center, Hampton, Va.
Howard Curfman
NASA Langley Research Center, Hampton, Va.

GEOLOGY
(Includes Geological Structure, Landform Surveys, Energy and Extractive Resources)

Dr. Floyd Sabins, Chairman
Chevron Oil Field Research Co., La Habra, Calif.
Dr. Larry Rowan
U.S. Department of the Interior, U.S. Geological Survey, Reston, Va.
Dr. Nicholas Short
NASA Goddard Space Flight Center, Greenbelt, Md.
Robert Stewart
NASA Lyndon B. Johnson Space Center, Houston, Tex.

INFORMATION
(Information Systems and Services)
USER SERVICES

Dr. David Landgrebe, Chairman
Purdue University/Laboratory for Applications of Remote Sensing, West Lafayette, Ind.
Terry Phillips
Purdue University/Laboratory for Applications of Remote Sensing, West Lafayette, Ind.
Timothy White
NASA Lyndon B. Johnson Space Center, Houston, Tex.
Gerald Kenney
NASA Lyndon B. Johnson Space Center, Houston, Tex.

LAND USE
(Includes Regional Planning)
STATE/LOCAL

Charles Parrish, III, Chairman
Department of Natural Resources, State of Georgia, Atlanta, Ga.
Charles Meyers
U.S. Department of Interior, Office of Land Use and Water Planning, Washington, D.C.
Dr. Armond Joyce
NASA Lyndon B. Johnson Space Center, Earth Resources Laboratory, Bay St. Louis, Miss.
Robin Rowley
NASA Lyndon B. Johnson Space Center, Houston, Tex.

MARINE RESOURCES
(Includes Marine Resources, Ocean Surveys)
COASTAL ZONE MANAGEMENT

Senator A. R. (Babe) Schwartz, Chairman
Texas State Senator, Galveston, Tex.
John Sherman, III
National Oceanic and Atmospheric Administration, National Environmental Satellite Service — SPOC Group, Washington, D.C.
E. Lee Tilton, III
NASA Lyndon B. Johnson Space Center, Earth Resources Laboratory, Bay St. Louis, Miss.
William Stephenson
NASA Lyndon B. Johnson Space Center, Houston, Tex.

WATER RESOURCES
(Water Resources Management)

Dr. Daryl Simons, Chairman
Colorado State University, Fort Collins, Colo.
John Teerink
Bookman Edmonston, Inc., Sacramento, Calif.
Dr. Vincent Salomonson
NASA Goddard Space Flight Center, Greenbelt, Md.
Raymond Clemence
NASA Lyndon B. Johnson Space Center, Houston, Tex.

CONTENTS

Paper number		Page
	VOLUME I-A	
	Agriculture	
A-1	ESTIMATING VEGETATIVE BIOMASS FROM LANDSAT-1 IMAGERY FOR RANGE MANAGEMENT Paul M. Seevers, James V. Drew, and Marvin P. Carlson	1
A-2	DISCRIMINATING COASTAL RANGELAND PRODUCTION AND IMPROVEMENTS WITH COMPUTER-AIDED TECHNIQUES C. A. Reeves and D. P. Faulkner	9
A-3	USEFULNESS OF LANDSAT DATA FOR MONITORING PLANT DEVELOPMENT AND RANGE CONDITIONS IN CALIFORNIA'S ANNUAL GRASSLAND David M. Carneggie, Stephen D. DeGloria, and Robert N. Colwell	19
A-4	MONITORING VEGETATION CONDITIONS FROM LANDSAT FOR USE IN RANGE MANAGEMENT R. H. Haas, D. W. Deering, J. W. Rouse, Jr., and J. A. Schell	43
A-5	UTILIZATION OF LANDSAT IMAGERY FOR MAPPING VEGETATION ON THE MILLIONTH SCALE Donald L. Williams and Jerry C. Coiner	53
A-6	LANDSAT-1 DATA, ITS USE IN A SOIL SURVEY PROGRAM F. C. Westin and C. J. Frazee	67
A-7	DELINEATION OF THE BOUNDARIES OF A BURIED PRE-GLACIAL VALLEY WITH LANDSAT-1 DATA J. B. Peterson, F. E. Goodrick, and W. N. Melhorn	97
A-8	ARE CLEAR-CUT AREAS ESTIMATED FROM LANDSAT IMAGERY RELIABLE? Y. Jim Lee	105
A-9	APPLICATIONS OF LANDSAT IMAGERY IN MONITORING THE FOREST OF THAILAND Boochana Klankamsorn and staff	Unavailable
A-10	OPERATIONAL CONSIDERATIONS FOR THE APPLICATION OF REMOTELY SENSED FOREST DATA FROM LANDSAT OR OTHER AIRBORNE PLATFORMS G. Robinson Barker and Terrance P. Feithe	115
A-11	TIMBER TYPE SEPARABILITY IN SOUTHEASTERN UNITED STATES ON LANDSAT-1 MSS DATA E. P. Kan and R. D. Dillman	135
A-12	MAPPING OF THE WILDLAND FUEL CHARACTERISTICS OF THE SANTA MONICA MOUNTAINS OF SOUTHERN CALIFORNIA J. D. Nichols	159
A-13	COMPUTER ANALYSIS AND MAPPING OF GYPSY MOTH DEFOLIATION LEVELS IN PENNSYLVANIA USING LANDSAT-1 DIGITAL DATA Darrel L. Williams	167
A-14	COMPUTER IMPLEMENTED CLASSIFICATION OF VEGETATION USING AIRCRAFT ACQUIRED MULTI-SPECTRAL SCANNER DATA William G. Cibula	183
A-15	THE USE OF SKYLAB DATA TO STUDY THE EARLY DETECTION OF INSECT INFESTATIONS AND DENSITY AND DISTRIBUTION OF HOST PLANTS W. G. Hart, S. J. Ingle, and M. R. Davis	203

Paper number		Page
A-16	AGRICULTURAL INVENTORY CAPABILITIES OF MACHINE PROCESSED LANDSAT DIGITAL DATA David L. Dietrich, Ronald E. Fries, and Dwight D. Egbert	221
A-17	AGRICULTURAL APPLICATIONS OF REMOTE SENSING – A TRUE LIFE ADVENTURE Earle S. Schaller	233
A-18	PRACTICAL APPLICATION OF REMOTE SENSING IN AGRICULTURE Richard A. Phelps	239
A-19	NEED FOR REMOTE SENSING IN AGRICULTURE Hosea S. Harkness	243
	Environment	
E-1	WILDLIFE MANAGEMENT BY HABITAT UNITS – A PRELIMINARY PLAN OF ACTION Carl D. Frentress and Roy G. Frye	245
E-2	AN OVERVIEW OF THE DEVELOPMENT OF REMOTE SENSING TECHNIQUES FOR THE SCREWWORM ERADICATION PROGRAM Charles M. Barnes and Frank C. Forsberg	263
E-3	THE RATIONALE FOR ATTEMPTING TO DEFINE SALT MARSH MOSQUITO-BREEDING AREAS IN GALVESTON COUNTY BY REMOTE SENSING THE ASSOCIATED VEGETATION Gerald K. Arp	289
E-4	PREDICTION OF HEALTH LEVELS BY REMOTE SENSING Marjorie Rush and Sally Vernon	301
E-5	MAPPING AND CLASSIFICATION OF STRIP MINES AND ACID MINE DRAINAGE THROUGH DIGITAL ANALYSIS OF LANDSAT-1 MULTISPECTRAL SCANNER DATA S. S. Alexander, D. Baumgardt, and J. Dein	Unavailable
E-6	APPLICATION OF EREP, LANDSAT, AND AIRCRAFT IMAGE DATA TO ENVIRONMENTAL PROBLEMS RELATED TO COAL MINING Roger V. Amato, Orville R. Russell, Kenneth R. Martin, and Charles E. Wier	309
E-7	LANDSAT INVENTORY OF SURFACE-MINED AREAS USING EXTENDIBLE DIGITAL TECHNIQUES Arthur T. Anderson, Dorothy T. Schultz, and Ned Buchman	329
E-8	REMOTELY-SENSED DATA USED TO DELINEATE LAND-WATER COVER IN COAL MINING REGIONS IN EASTERN TENNESSEE A. E. Coker, A. L. Higer, S. Sauer, and R. H. Rogers	Unavailable
E-9	QUANTITATIVE WATER QUALITY WITH LANDSAT AND SKYLAB Harold L. Yarger and James R. McCauley	347
E-10	LANDSAT-1 DATA AS IT HAS BEEN APPLIED FOR LAND USE AND WATER QUALITY DATA BY THE VIRGINIA STATE WATER CONTROL BOARD Peter L. Trexler and John L. Barker	371
E-11	THE LANDSAT-1 MULTISPECTRAL SCANNER AS A TOOL IN THE CLASSIFICATION OF INLAND LAKES D. H. P. Boland and Richard J. Blackwell	419
E-12	TROPHIC STATUS OF INLAND LAKES FROM LANDSAT Lawrence T. Fisher and Frank L. Scarpace	443
E-13	THE USE OF LANDSAT-1 IMAGERY FOR WATER QUALITY STUDIES IN SOUTHERN SCANDINAVIA Ulf Hellden	451

Paper number		Page
E-14	COMPARATIVE UTILITY OF LANDSAT-1 AND SKYLAB DATA FOR COASTAL WETLAND MAPPING AND ECOLOGICAL STUDIES Richard Anderson, Linda Alsid, and Virginia Carter	469
E-15	AUTOMATIC CATEGORIZATION OF LAND-WATER COVER TYPES OF THE GREEN SWAMP, FLORIDA, USING SKYLAB MULTISPECTRAL SCANNER (S-192) DATA A. E. Coker, A. L. Iliger, R. H. Rogers, N. J. Shah, L. Reed, and S. Walker	479
E-16	A COMPARATIVE INTERREGIONAL ANALYSIS OF SELECTED DATA FROM LANDSAT-1 AND EREP FOR THE INVENTORY AND MONITORING OF NATURAL ECOSYSTEMS Charles E. Poulton	507
E-17	REMOTE SENSING APPLICATIONS IN KANSAS B. G. Barr, Jerry C. Coiner, and Donald L. Williams	569
E-18	REMOTE SENSING APPLICATIONS IN THE INVENTORY AND ANALYSIS OF ENVIRONMENTAL PROBLEMS Gordon E. Howard, Jr., and C. Al Waters, Jr.	585

VOLUME I-B

Geology

G-1	SLAR RECONNAISSANCE, MIMIKA-EILANDEN BASIN, SOUTHERN TROUGH OF IRIAN JAYA R. S. Wing and J. C. Mueller	599
G-2	LANDSAT IMAGE STUDIES AS APPLIED TO PETROLEUM EXPLORATION IN KENYA John B. Miller	605
G-3	DETECTABILITY OF GEOTHERMAL AREAS USING SKYLAB X-5 DATA Barry S. Siegal, Anne B. Kahle, Alexander F. H. Goetz, Alan R. Gillespie, and Michael J. Abrams	625
G-4	GEOLOGIC AND RELATED APPLICATIONS OF REMOTE SENSING IN GEORGIA Sam M. Pickering, Jr.	Unavailable
G-5	THE ANATOMY OF AN ANOMALY Nicholas M. Short and Ronald W. Marrs	641
G-6	USE OF SPECTRAL REFLECTANCE MEASUREMENTS OF ALTERED AND UNALTERED ROCKS IN SOUTH-CENTRAL NEVADA AS A BASIS FOR ENHANCEMENT OF LANDSAT IMAGES Lawrence C. Rowan, Alexander F. H. Goetz, and Roger P. Ashley	Unavailable
G-7	APPLICATION OF SKYLAB IMAGERY TO RESOURCE EXPLORATION IN THE DEATH VALLEY REGION Ira C. Bechtold, John T. Reynolds, and C. Gregory Wagner	665
G-8	A GEOLOGICAL INVESTIGATION OF SOUTHEASTERN ARIZONA USING LANDSAT IMAGERY AND GEOPHYSICAL DATA Richard F. Pascucci	Unavailable
G-9	SUMMARY OF SPACE IMAGERY STUDIES IN UTAH AND NEVADA Mead LeRoy Jensen and Philip Laylander	673
G-10	GEOLOGIC SIGNIFICANCE OF FEATURES OBSERVED IN COLORADO FROM ORBITAL ALTITUDES Don L. Sawatzky, Gary Prost, Keenan Lee, and D. H. Knepper	713
G-11	THE APPLICATION OF RADAR IMAGERY TO SPECIFIC PROBLEMS OF INTERIOR ALASKA P. Jan Cannon	761

Paper number		Page
G-12	LANDSAT IMAGERY ANALYSIS AN AID FOR PREDICTING LANDSLIDE-PRONE AREAS FOR HIGHWAY CONSTRUCTION Harold C. MacDonald and Robert S. Grubbs	769
G-13	ACTIVE AND INACTIVE FAULTS IN SOUTHERN CALIFORNIA VIEWED FROM SKYLAB P. M. Merifield and D. L. Lamar	779
G-14	THE UTILIZATION OF LANDSAT IMAGERY IN NUCLEAR POWER PLANT SITING A. J. Eggenberger, D. Rowlands, and P. C. Rizzo	799
G-15	SMALL-SCALE IMAGERY: A USEFUL TOOL FOR MAPPING GEOLOGICAL FEATURES IN THE TEXAS GULF COASTAL PLAIN David L. Amsbury, Uel S. Clanton, and Von R. Frierson	833
G-16	APPLICATION OF SKYLAB IMAGERY TO SOME GEOLOGICAL AND ENVIRONMENTAL PROBLEMS IN ITALY R. Cassinis, G. M. Lechi, and A. M. Tonelli	851
G-17	SKYLAB PHOTOGRAPHY APPLIED TO GEOLOGIC MAPPING IN NORTHWESTERN CENTRAL AMERICA W. I. Rose, Jr., D. J. Johnson, G. A. Hahn, and G. W. Johns	869
G-18	IDENTIFICATION AND CORRELATION OF PRECAMBRIAN AND PHANEROZOIC ORTHOGONAL FAULT AND LINEAMENT SYSTEMS IN CENTRAL AND NORTHERN ARIZONA Donald P. Elston and William D. Dipaolo	Unavailable
G-19	QUANTIFICATION OF GEOLOGIC LINEAMENTS BY MANUAL AND MACHINE PROCESSING TECHNIQUES Melvin H. Podwysocki, Johannes G. Moik, and Walter C. Shoup	885
G-20	CREATING A SYSTEM FOR THE GEOLOGICAL EXPLOITATION OF SATELLITE IMAGES: AUTOMATIC MAPPING AND GEOPHYSICAL DATA COMPARISON S. Braconne, M. Cavalier, M. Dubesset, J. Guillemot, and M. Guy	905
G-21	APPLICATION OF SATELLITE PHOTOGRAPHIC AND MSS DATA TO SELECTED GEOLOGIC AND NATURAL RESOURCE PROBLEMS IN PENNSYLVANIA W. S. Kowalik, D. P. Gold, and M. Dennis Krohn	933
G-22	GEOLOGICAL MAPPING IN NORTHWESTERN SAUDI ARABIA USING LANDSAT MULTISPECTRAL TECHNIQUES H. W. Blodget, G. F. Brown, and J. G. Moik	971
G-23	NEAR-INFRARED REFLECTANCE ANOMALIES OF ANDESITE AND BASALT IN SOUTHERN CALIFORNIA AND NEVADA Howard A. Pohn	Unavailable
G-24	ENHANCEMENT OF LANDSAT IMAGERY BY COMBINATION OF MULTISPECTRAL CLASSIFICATION AND PRINCIPAL COMPONENT ANALYSIS A. Fontanel, C. Blanchet, and C. Lallemand	991
G-25	REMOTE SENSING FRACTURE STUDY - WESTERN VIRGINIA AND SOUTHEASTERN KENTUCKY Gordon L. Owens and William M. Ryan	Unavailable
G-26	A SEARCH FOR SULFIDE-BEARING AREAS USING LANDSAT-1 DATA AND DIGITAL IMAGE-PROCESSING TECHNIQUES R. G. Schmidt, B. B. Clark, and R. Bernstein	1013
G-27	REGIONAL INVENTORIES AND MAPPING OF LAND RESOURCES AND ENVIRONMENTAL GEOLOGY USING REMOTELY SENSED DATA E. G. Wermund, L. F. Brown, Jr., and W. L. Fisher	1029

Paper number		Page
G-28	MINERAL TARGET AREAS IN NEVADA FROM GEOLOGICAL ANALYSIS OF LANDSAT-1 IMAGERY Monem Abdel-Gawad and Linda Tubbesing	1059
G-29	ATTEMPT AT CORRELATING ITALIAN LONG LINEAMENTS FROM LANDSAT-1 SATELLITE IMAGES WITH SOME GEOLOGICAL PHENOMENA. POSSIBLE USE IN GEOTHERMAL ENERGY RESEARCH Enrico Barbier and Mario Fanelli	1079
	Information Systems and Services	
I-1	LAYERED CLASSIFICATION TECHNIQUES FOR REMOTE SENSING APPLICATIONS P. H. Swain, C. L. Wu, D. A. Landgrebe, and H. Hauska	1087
I-2	THE MIXTURE PROBLEM IN COMPUTER MAPPING OF TERRAIN: IMPROVED TECHNIQUES FOR ESTABLISHING SPECTRAL SIGNATURES, ATMOSPHERIC PATH RADIANCE, AND TRANSMITTANCE Harry W. Smedes, Roland L. Hulstrom, and K. Jon Ransow	1099
I-3	SECOND GENERATION DIGITAL TECHNIQUES FOR PROCESSING LANDSAT MSS DATA S. S. Rifman, K. W. Simon, and R. H. Caron	1161
I-4	THE SKYLAB CONCENTRATED ATMOSPHERIC RADIATION PROJECT Peter M. Kuhn, Victor S. Whitehead, and William E. Marlatt	1177
I-5	MARKING LANDSAT IMAGES WITH SMALL MIRROR REFLECTORS William E. Evans	1185
I-6	REMOTE SENSING -- A VALUABLE TOOL IN THE FOREST SERVICE DECISIONMAKING PROCESS Fleet L. Stanton	1197
I-7	SPACE TECHNOLOGY -- PUTTING IT IN THE EDUCATIONAL PERSPECTIVE Donna B. Hankins	1221
I-8	GROUND ZERO AND UP -- NEBRASKA'S RESOURCES AND LAND USE Donald M. Edwards and Roger Macklem	1225
I-9	AN UNSUPERVISED CLASSIFICATION OF MULTISPECTRAL SCANNER DATA USING CORRESPONDENCE ANALYSIS (CLAMS) J-M. Monget and P. Roux	1237
I-10	ADVANCES IN AUTOMATIC EXTRACTION OF EARTH RESOURCES INFORMATION FROM MULTISPECTRAL SCANNER DATA Jon D. Erickson	1245
I-11	IMAGE 100 – THE INTERACTIVE MULTISPECTRAL IMAGE PROCESSING SYSTEM Earle S. Schaller and Robert W. Towles	1275
I-12	GEOLOGIC ANALYSES OF LANDSAT-1 MULTISPECTRAL IMAGERY OF A POSSIBLE POWER PLANT SITE EMPLOYING DIGITAL AND ANALOG IMAGE PROCESSING Jon R. Lovegreen, William J. Prosser, and Richard A. Millet	1293
I-13	THE SCREWWORM ERADICATION DATA SYSTEM (SEDS) Matthew J. Quinn	1309
I-14	LANDSAT ACTIVITIES IN THE REPUBLIC OF ZAIRE Sendwe K. Ilunga	1313
I-15	REMOTE SENSING AS AN INNOVATION: HOW CAN WE IMPROVE ON ITS RATE OF ADOPTION? Buzz Sellman	1317

Paper number		Page
I-16	M-DAS – SYSTEM FOR MULTISPECTRAL DATA ANALYSIS Robert H. Johnson	1323
I-17	ERIPS – EARTH RESOURCE INTERACTIVE PROCESSING SYSTEM Matthew J. Quinn	1351
I-18	LOW-COST DATA ANALYSIS SYSTEMS FOR PROCESSING MULTISPECTRAL SCANNER DATA Sidney L. Whitley	1355
I-19	THE INTEGRATION OF MANUAL AND AUTOMATIC IMAGE ANALYSIS TECHNIQUES WITH SUPPORTING GROUND DATA IN A MULTISTAGE SAMPLING FRAMEWORK FOR TIMBER RESOURCE INVENTORIES: THREE EXAMPLES Michael J. Gialdini, Stephen Titus, James Nichols, and Randall W. Thomas	1377
I-20	DESIGN CRITERIA FOR A MULTIPLE INPUT LAND USE SYSTEM Frederic C. Billingsley and Nevin A. Bryant	1389
I-21	USER SERVICES AVAILABLE FROM USDA'S AERIAL PHOTOGRAPHY FIELD OFFICE Ronald A. Dickson	1397
I-22	THE TEXAS REMOTE SENSING TRAINING PROJECT John B. Wells	1403
I-23	INTERACTIVE DIGITAL IMAGE MANIPULATION SYSTEM (IDIMS) Janice Henze and R. DeZur	Unavailable
I-24	IMAGE ANIMATION FOR THEME ENHANCEMENT AND CHANGE DETECTION William E. Evans	1437
I-25	THE TOTAL EARTH RESOURCES SYSTEM OF THE 1980's: A VIEW OF THE FUTURE Charles E. Cheeseman and David W. Keller	1451
I-26	EARTH RESOURCES SURVEY AND THE SPACE SHUTTLE W. Kent Stow and Roman Andryczyk	1473
I-27	SENSOR EQUIPMENT OF THE GERMAN EARTH SCIENTIFIC AIRPLANE PROGRAM Peter Seige	1483

VOLUME I-C

Land Use

L-1	THE SOUTH DAKOTA COOPERATIVE LAND USE EFFORT: A STATE LEVEL REMOTE SENSING DEMONSTRATION PROJECT Paul A. Tessar, Dennis R. Hood, and William J. Todd	1499
L-2	AN EXAMINATION OF THE POTENTIAL APPLICATIONS OF AUTOMATIC CLASSIFICATION AND TECHNIQUES TO GEORGIA MANAGEMENT PROBLEMS Bruce Q. Rado	1525
L-3	OHIO'S STATEWIDE LAND USE INVENTORY: AN OPERATIONAL APPROACH FOR APPLYING LANDSAT DATA TO STATE, REGIONAL, AND LOCAL PLANNING PROBLEMS Paul E. Baldridge, Paul H. Goesling, Frank Leone, Charles Minshall, Robert H. Rodgers, and Carl L. Wilhelm	1541
L-4	ARIZONA LAND USE EXPERIMENT Carl C. Winikka and Herbert H. Schumann	1553

Paper number		Page
L-5	THE DESIGN, IMPLEMENTATION, AND USE OF A STATEWIDE LAND USE INVENTORY: THE NEW YORK EXPERIENCE Ernest E. Hardy	1573
L-6	ALASKAN RESOURCES, CURRENT DEVELOPMENT, TRADITIONAL CULTURE VALUES AND THE ROLE OF LANDSAT DATA IN CURRENT AND FUTURE LAND USE MANAGEMENT PLANNING Arthur LaPerriere	1603
L-7	THE NATIONAL LAND USE DATA PROGRAM OF THE U.S. GEOLOGICAL SURVEY James R. Anderson and Richard E. Witmer	1609
L-8	CASES IN THE RELATION OF RESEARCH ON REMOTE SENSING TO DECISIONMAKERS IN A STATE AGENCY James W. Jondrow	1617
L-9	COORDINATING APPLICATIONS OF REMOTE SENSING AT THE STATE LEVEL Marvin P. Carlson and James Barr	Unavailable
L-10	THE DEVELOPMENT OF A LAND USE INVENTORY FOR REGIONAL PLANNING USING SATELLITE IMAGERY A. H. Hessling and Timothy G. Mara	1631
L-11	LUMIS – A LAND USE MANAGEMENT INFORMATION SYSTEM FOR URBAN PLANNING Charles K. Paul	1637
L-12	THREE U.S. URBAN AREAS ANALYZED FROM AIRCRAFT, LANDSAT, AND SKYLAB SENSORS James R. Wray	Unavailable
L-13	SATELLITE INFORMATION ON ORLANDO, FLORIDA John W. Hannah, Garland L. Thomas, and Fernando Esparza	1665
L-14	LAND USE AND ENVIRONMENTAL ASSESSMENT IN THE CENTRAL ATLANTIC REGION Robert H. Alexander, Katherine Fitzpatrick, Harry F. Lins, Jr., and Herbert K. McGinty III	1683
L-15	REMOTE SENSING IMPACT ON CORRIDOR SELECTION AND PLACEMENT F. J. Thomson and A. N. Sellman	1729
L-16	IMPROVED RESOURCE USE DECISIONS AND ACTIONS THROUGH REMOTE SENSING R. Hill-Rowley, M. Boylan, W. Enslin, and R. Vlasin	1747
L-17	DEVELOPMENT OF USER APPLICATIONS FOR EARTH RESOURCES SURVEY DATA IN URBAN AND REGIONAL PLANNING IN THE PUGET SOUND AREA Frank V. Westerlund	1769
L-18	APPLICATION OF SATELLITE REMOTE-SENSING DATA TO LAND SELECTION AND MANAGEMENT W. J. Stringer, J. M. Miller, A. E. Belon, L. H. Shapiro, and J. H. Anderson	1785
L-19	THREE EXAMPLES OF APPLIED REMOTE SENSING OF VEGETATION J. W. Rouse, Jr., A. R. Benton, Jr., R. W. Toler, and R. H. Haas	1797
L-20	INTERACTIVE MULTI-SPECTRAL ANALYSIS OF MORE THAN ONE SONRAI VILLAGE IN NIGER, WEST AFRICA Priscilla Reining and Dwight Egbert	1811
L-21	USE OF LANDSAT-1 IMAGERY FOR BROAD LAND USE PLANNING IN THE NORTHERN PART OF THAILAND Manu Omakupt	Unavailable

Paper number		Page
L-22	PRESENT AND POTENTIAL LAND USE MAPPING IN MEXICO Hector Garduño, Ricardo García Lagos, and Fernando García Simo	1823
L-23	LAND USE CLASSIFICATION IN BOLIVIA Carlos E. Brockman and William G. Brooner	1841
L-24	THE BRAZILIAN REMOTE SENSING PROGRAM R. A. Novaes and F. de Mendonca	Unavailable
L-25	APPLICATION OF LANDSAT AND SKYLAB DATA FOR LAND USE MAPPING IN ITALY J. Bodechtel, J. Nithack, G. DiBernardo, K. Hiller, F. Jaskolla, and A. Smolka	1863
	Marine	
M-1	THE SIGNIFICANCE OF THE SKYLAB ALTIMETER EXPERIMENT – RESULTS AND POTENTIAL APPLICATIONS A. George Mourad, S. Gopalapillai, and M. Kuhner	1887
M-2	A COMPARISON OF SKYLAB S-193 AND AIRCRAFT VIEWS OF SURFACE ROUGHNESS AND A LOOK TOWARD SEASAT Duncan Ross	1911
M-3	SKYLAB S-193 RADSCAT MICROWAVE MEASUREMENTS OF SEA SURFACE WINDS R. K. Moore, A. K. Fung, J. Young, J. Claassen, H. Chan, M. Afarani, W. J. Pierson, V. J. Cardone, J. Hayes, W. Spring, C. Greenwood, and R. Salfi	1937
M-4	A PROCEDURE FOR ESTIMATION OF SEA-SURFACE TEMPERATURE FROM REMOTE MEASUREMENTS IN THE 10-13 μm SPECTRAL REGION David C. Anding	1953
M-5	SURFACE CIRCULATION IN THE GREAT LAKES AS OBSERVED BY LANDSAT-1 AUGUST 1972 TO DECEMBER 1973: SOUTHERN LAKE MICHIGAN Harry G. Stumpf and Alan E. Strong	1973
M-6	OCEAN COLOR IMAGERY – COASTAL ZONE COLOR SCANNER Warren A. Hovis	1989
M-7	SKYLAB INVESTIGATION OF THE UPWELLING OFF THE NORTHWEST COAST OF AFRICA Karl-Heinz Szekielda, Dennis J. Suszkowski, and Paul S. Tabor	2005
M-8	THE FEASIBILITY OF UTILIZING REMOTELY SENSED DATA TO ASSESS AND MONITOR OCEANIC GAMEFISH Kenneth J. Savastano and Thomas D. Leming	2023
M-9	LANDSAT DIGITAL DATA PROCESSING – A NEAR REAL-TIME APPLICATION John Barker, Charles Bohn, Locke Stuart, and John Hill	2063
M-10	NEARSHORE COASTAL MAPPING Fabian C. Polcyn and David R. Lyzenga	2075
M-11	QUANTITATIVE SUSPENDED SEDIMENT MAPPING USING AIRCRAFT REMOTELY SENSED MULTISPECTRAL DATA Robert W. Johnson	2087
M-12	REMOTE SENSING OF SALINITY Gary C. Thomann	2099

Paper number		Page
M-13	AUTOMATIC INTERFACE MEASUREMENT AND ANALYSIS Kenneth H. Faller	2127
M-14	THE MAPPING OF MARSH VEGETATION USING AIRCRAFT MULTISPECTRAL SCANNER DATA M. Kristine Butera	2147

VOLUME I-D

Water

W-1	THE USE OF SKYLAB AND LANDSAT IN A GEOHYDROLOGICAL STUDY OF THE PALEOZOIC SECTION, WEST-CENTRAL BIGHORN MOUNTAINS, WYOMING Barbara J. Tomes	2167
W-2	HYDROGEOLOGICAL INVESTIGATIONS IN THE PAMPA OF ARGENTINA Wolfgang Kruck and Wilfried Kantor	2183
W-3	HYDRO-MORPHOLOGICAL EVALUATION OF FALSE COLOR COMPOSITE MADE FROM MULTISPECTRAL IMAGERY FOR AREA BETWEEN THE GANGES AND JUMNA RIVERS, INDIA S. K. Sharma and S. C. Sharma	Unavailable
W-4	URBAN LAND USE: REMOTE SENSING OF GROUNDBASIN PERMEABILITY Larry R. Tinney, John R. Jensen, and John E. Estes	2199
W-5	MICROWAVE REMOTE SENSING OF SOIL MOISTURE Fawwaz T. Ulaby, Percy P. Batlivala, Josef Cihlar, and Thomas Schmugge	2207
W-6	SOIL MOISTURE DETECTION FROM SKYLAB Joe R. Eagleman and Wen C. Lin	2233
W-7	THE CORRELATION OF SKYLAB L-BAND BRIGHTNESS TEMPERATURE WITH ANTECEDENT PRECIPITATION Marshall J. McFarland	2243
W-8	FLOOD HAZARD STUDIES IN CENTRAL TEXAS USING ORBITAL AND SUBORBITAL REMOTE SENSING IMAGERY Victor R. Baker, Robert K. Holz, and Peter C. Patton	2253
W-9	AN INUNDATION STUDY OF THE LOWER MAGDALENA-CAUCA RIVER BASIN Eduard van Es, Hernán Gómez, and Robert Soeters	2295
W-10	REMOTE SENSING OF MISSISSIPPI RIVER CHARACTERISTICS J. F. Ruff, M. M. Skinner, B. R. Winkley, D. B. Simons, and D. E. Dorratcague	2299
W-11	APPLICATION OF THERMAL SCANNING TO THE STUDY OF TRANSVERSE MIXING IN RIVERS J. Wayland Eheart	2317
W-12	UTILIZATION OF LANDSAT DATA FOR WATER QUALITY SURVEYS IN THE CHOPTANK RIVER James M. Johnson, Philip Cressy, and William C. Dallam	2325
W-13	HYDROLOGIC LAND USE CLASSIFICATION OF THE PATUXENT RIVER WATERSHED USING REMOTELY SENSED DATA William C. Dallam, Albert Rango, and Lurie Shima	2351
W-14	LAND USE CLASSIFICATION FOR HYDROLOGIC MODELS USING INTERACTIVE MACHINE CLASSIFICATION OF LANDSAT DATA Thomas J. Jackson, Robert M. Ragan, and Richard M. McCuen	2365

Paper number		Page
W-15	REMOTE SENSING TECHNIQUES FOR PREDICTION OF WATERSHED RUNOFF Bruce J. Blanchard	2379
W-16	WATER-MANAGEMENT MODEL IN FLORIDA FROM LANDSAT-1 DATA A. L. Higer, E. H. Cordes, A. E. Coker, and R. H. Rogers	2407
W-17	THE USE OF LANDSAT DCS AND IMAGERY IN RESERVOIR MANAGEMENT AND OPERATION Saul Cooper, Paul Bock, Joseph Horowitz, and Dennis Foran	2443
W-18	THE APPLICATION OF REMOTE SENSING TECHNOLOGY TO THE INVENTORY OF PLAYA LAKES IN THE HIGH PLAINS OF TEXAS A. Wayne Wyatt, Michael L. Ellis, and Ann E. Bell	2523
W-19	REMOTE SENSING APPLICATIONS IN WATER RESOURCES MANAGEMENT BY THE CALIFORNIA DEPARTMENT OF WATER RESOURCES Barry Brown	2531
W-20	A COMPARATIVE STUDY OF MULTISPECTRAL SATELLITE DATA (SKYLAB, LANDSAT) FOR EUROPEAN APPLICATIONS J. Bodechtel, R. Dittel, and R. Haydn	Unavailable
W-21	EVALUATION OF THERMAL X/5 DETECTOR SKYLAB S-192 DATA FOR ESTIMATING EVAPO-TRANSPIRATION AND THERMAL PROPERTIES OF SOILS FOR IRRIGATION MANAGEMENT D. G. Moore, M. L. Horton, M. J. Russell, and V. I. Myers	2561
W-22	REMOTE SENSING INPUTS TO WATER DEMAND MODELING John R. Jensen, Larry R. Tinney, and Michael Rector	2585
W-23	AREAL EXTENT OF SNOW ESTIMATION IN THE NORTHERN SIERRA NEVADA MOUNTAINS USING LANDSAT-1 IMAGERY Edwin F. Katibah	2621
W-24	SNOW SURVEY FROM SPACE, WITH EMPHASIS ON THE RESULTS OF THE ANALYSIS OF SKYLAB EREP S-192 MULTISPECTRAL SCANNER DATA James C. Barnes and Michael D. Smallwood	2643
W-25	FACTORS AFFECTING SNOW ASSESSMENT FROM LANDSAT DATA David F. McGinnis, Jr., Michael C. McMillan, and Donald R. Wiesnet	2661
W-26	OPERATIONAL WATER MANAGEMENT APPLICATIONS OF SNOWCOVERED AREA OBSERVATIONS Albert Rango, Vincent V. Salomonson, and James L. Foster	2669

SLAR RECONNAISSANCE, MIMIKA-EILANDEN BASIN, SOUTHERN TROUGH OF IRIAN JAYA G-1

By R. S. Wing and J. C. Mueller, Advance Exploration Group, E.H.P.D., Continental Oil Company

N76-17502

ABSTRACT

The Mimika-Eilanden Basin is the Irian Jaya portion of the Southern Trough, an arcuate mobile-front foredeep that extends some 900 kms, from the Arafura Sea to the Gulf of Papua. The basin is assymetric with at least 3.7 kms of post-Triassic strata in the axial part. The prospective part of the Eilanden segment of the Trough is up to 160 kms wide and is largely included within two contract areas. This paper has to do with those geologic concepts that led to the acquisition in late 1971 of Conoco's 325 by 165 km contract area and, explicitly, with subsequent SLAR reconnaissance geologic mapping. The Eilanden Basin seems to have been simply a shelf and upper slope regime until Late Middle-Miocene time when the collision of the Australian plate with an oceanic island arc resulted in a tectonic style and framework now observable in the Irian Range. The suturing superimposed a compressive effect on the Eilanden strata. The present Eilanden Basin took form as a mobile-front foredeep, considerably south of the suture zone. This basin, immobilized against the buttress of the southern stable platform, underwent a southward compressive shove related to mountain building at the collision margin. The compressive effects are strongest and most complex in the belt flanking the folded and near-vertically-uplifted Paleozoic mountain core. The higher strongly-folded structures lie parallel to the Paleozoic mountain axis, whereas lower foothills structures farthest from the mountain axis are oblique to the axis by up to 20°. The oblique trend of these lower relief folds suggests a slightly later lateral component of movement, and this in turn suggests that some such surface folds might be rooted or at least be approximately coincident with their subsurface expressions.

The Kembelangan clastics of Late Jurassic and Cretaceous age comprise probably the most prospective part of the sedimentary wedge which was deposited along this margin during Phanerozoic time and is over 1.5 kms thick where measured in the Irian Mountains. Outer-shelf Kembelangan sandstones were found to contain large amounts of gas, with heavier hydrocarbons, in the Barikewa Anticline in Papua. Surface oil seeps from exposed Cretaceous clastics in NW Papua adjoining Irian Jaya are known to exist. In addition to Kembelangan clastics, the last pre-collision stratigraphic unit was a thickly deposited Middle Miocene coralline formation which is considered highly prospective and equivalent to productive reefal limestones in both Irian Jaya and Papua.

The SLAR was obtained in early April 1973 by Westinghouse for Conoco by means of an AN/APQ-97 K-band brute-force system. The flight strips are all north-look, with ground-range display, and 60% overlap. The interpretation was compiled on a 1/100,000-scale mosaic, but the actual mapping of contacts, dips, lineaments, and the like, was done on 1/100,000-scale stereo-strips. Initial regional mapping was intended as an aid in determining that part of the Southern Trough most likely to be underlain by relatively unmetamorphosed paralic Kembelangan sandstones ideally interdigitated with marine source and cap shales. SLAR reconnaissance mapping met a subsequent need to rapidly and inexpensively narrow the search to that part of the "fairway" coincident with a favorable structure. The SLAR mosaic clearly displays the Irian mountains, strongly and gently folded foothills belts, and the southern front of the fold belt south of which is a large complex of alluvial fans.

The mosaic also shows various drainage anomalies in the alluvial covered area south of the gently-folded belt. Some of these are coincident with hilly areas and are considered as possibly indicative of reef draping or deeper structure.

INTRODUCTION

The Mimika-Eilanden Basin is the Irian Jaya, Indonesia portion of the Southern Trough, an arcuate suture-deformed continental-margin sedimentary wedge on the island of New Guinea, convex to the north, that extends some 900 kms from the Arafura Sea to the Gulf of Papua. The basin is assymetric with at least 3.7 kms of post-Triassic strata in the axial part, along the northern margin, immediately south of the Irian Range. The prospective part of the basin is about 160 kms wide. The onshore part of the basin is largely included within two contract areas, one granted to Phillips Petroleum in 1968 and the other originally granted to Conoco in late 1971. This paper has to do, cursorily, with those geologic concepts that led to acquisition of Conoco's Contract area and, more explicitly, with subsequent SLAR reconnaissance mapping.

In January of 1973, Conoco farmed-out 50% of its interest in the Eilanden Contract Area to Amoseas, and the latter has since been operator. In early 1975, Conoco farmed-out a 25% interest to CFP. The results of hard data acquired by Amoseas, after the authors finished their 1972 preliminary SLAR mapping, are not included in this report. Data that is included was primarily derived from the late 1950's Shell work as reported by Visser and Hermes, 1962. The authors have examined SLAR coverage of most of the Southern Trough, but the SLAR on which this paper is based is necessarily restricted to coverage of the Eilanden Contract Area.

OBJECTIVES

Initial regional geologic mapping was intended as an aid in determining that part of the Southern Trough most likely to be underlain by relatively unmetamorphosed paralic Juro-Cretaceous Kembelangan sandstones, ideally interdigitated with marine source and cap shales. SLAR reconnaissance mapping was a subsequent need and this approach helped to further narrow the search to that part of the Kembelangan "fairway" coincident with a favorable structural setting.

Specifically, one of our two primary SLAR mapping goals was to locate that part of the known fold belt within which surface and subsurface expressions of individual anomalies might be approximately coincident and, within which, volcanic complications would likely be minimal or nonexistent. The second SLAR mapping goal was to identify any likely surface expression of possible Miocene hingelines that might have localized mid-Miocene reef growth.

It was also intended to use the SLAR as an aid in planning for accessibility and for the laying-out of initial seismic lines. The use of either SLAR or air photos was mandatory in order to compress the time necessary to localize prospects and leads and thus limit expensive seismic reconnaissance in what is among the most difficult of operating terrains in the world. The use of SLAR in preference to air photos was necessitated by the fact that the folded foothills belt receives 5+ meters of rain per annum and is largely cloud covered most of the time.

SLAR SPECIFICATIONS AND TECHNOLOGY

The Eilanden SLAR mosaic illustrates an area 370 kms east-west by 170 kms north-south. The component imagery strips were obtained for Conoco in early April, 1973 by Westinghouse and are the product of a high altitude AN/APQ 97 K-band, brute force SLAR system. **The mosaicking and other photographic rendering** of all SLAR modes were done in London by Hunting. The component flight strips are all north-look, with ground range display and 60% overlap. The north-look aspect was intended to minimize any possible shadowing of the foothills belt from the Irian Range, which has peaks as high as 5000 meters. It was also desired to maximize the known east-west fold grain by choosing an orthogonal look. The same-look aspect was necessitated by economics and by a desire for stereo-capability.

The contract area was divided into quadrants for SLAR imaging with no flight strip over 185 kms in length, thus ensuring greater accuracy in matching strips for the mosaic, besides ensuring fewer wipeouts. In the contract area there is no sharply defined dry season, and even with SLAR, wipeouts from intense rain cells were a problem; also, interference from the plane's necessary deicing equipment was a related problem, as was atmospheric turbulence. However, we found a "clear weather window" between 4 and 11 AM, after most of yesterday's storms and before most of todays. Even so, it was necessary to refly a number of strips from the standpoint of quality control. The imaging was monitored in-flight on a TV screen. A field mosaic was constructed day-by-day as imaging progressed. These practical measures were the basis for quality control and an on-site speculative first interpretation of results.

Ultimately, the interpretation was compiled on a 1/100,000-scale mosaic, but the actual mapping of contacts, dips, lineaments, and the like was done on 1/100,000-scale stereo-strips. A 5-minute latitude-longitude grid that was superimposed on the mosaic suggests that it is highly accurate, though we have few star fixes and accuracy is in fact relative to the accuracy of the topographic map from which the grid was derived. The 5-minute "squares" are approximately 9 kms per side.

REGIONAL STRATIGRAPHY

The Mimika-Eilanden Basin seems to have been simply a shelf and upper slope regime until late middle-Miocene time. That is to say, it was part of the northern continental margin of Australia during the Mesozoic, Paleogene, and early Neogene.

The Cambrian Kariem is comprised of metasediments. The Permo-Carboniferous Aifam is comprised of highly indurated clastics and marlstones. The Juro-Triassic Tipoema is comprised largely of clastics but with a carbonate facies. The subcrop of these strata represents economic basement and the source terrain gradually inundated by the transgressive Juro-Cretaceous Kembelangan Sea.

Of primary interest in hydrocarbon exploration are the Kembelangan clastic shelf facies, notably shallow-water and nearshore sandstones and shales. The Kembelangan is over 1.5 kms thick where measured in the Irian Mountains. Reservoir-type sandstones are well developed in the basal Cretaceous and Jurassic and in the upper half of the formation. Kembelangan clastics have been found to contain large amounts of gas and gas with condensate respectively, at depths of about 3500 meters, in the Iehi and Barikewa Anticlines in Papua. Within the uplifted Irian Range, there is generally some very low-grade metamorphism of Kembelangan strata.

At the end of the Cretaceous, deposition of the Kembelangan ended and a major unconformity is recorded which is approximately coincident in timing with the splitting-off of Australia from Antarctica. The Paleogene was represented by a carbonate sea restricted to the shelf edge and upper slope. By early Miocene time, a broad shallow carbonate sea had covered the entire north end of the Australian plate; shales were coincidently deposited on the slope. It is the Miocene New Guinea Limestone Group that has produced some gas in the Gulf of Papua and oil in the Vogelkop area from reef pinnacles. Reefal facies are a strong secondary objective within the Mimika-Eilanden Basin.

The late mid-Miocene suture-orogeny that created the Irian Range and the Southern Trough was followed by deposition in the down-warped Trough of what are now poorly consolidated marls, shales, siltstones, and sandstones. Quaternary debris obscures the southernmost lines of folding.

REGIONAL TECTONICS

The collision of the Australian plate with an oceanic island arc during late mid-Miocene thru Pliocene resulted in a tectonic style and framework manifested by the Irian Range. The suturing superimposed a compressive effect on the sedimentary wedge. The present Mimika-Eilanden Basin took form as a mobile-front foredeep considerably south of the suture zone. This basin, immobilized against the buttress of the southern stable platform, underwent a southward compressive shove related to mountain building at the collision margin. The compressive effects are strongest and most complex in the belt flanking the folded and near-vertically uplifted Paleozoic mountain core. The higher strongly-folded structures lie parallel to the Paleozoic mountain axis, whereas lower foothills structures farthest from the mountain axis are oblique to the axis by 10-20°. The oblique trend of these lower relief folds suggests a lateral component of movement, and this in turn suggests that some such surface folds might be rooted or at least be approximately coincident with their subsurface expressions.

SLAR INTERPRETATIONAL RESULTS

The various SLAR modes clearly display: the Irian Range detail, the strongly and gently-folded foothills belts, the southern front of the fold belt, large-scale alluvial and pyroclastic fans, and an area of Quaternary beach-bar complexes. The southern edge of the fan-complex is marked by ponds whereas the northern apex is clearly shown by braided stream patterns. There are also large-scale drainage anomalies in the alluvial-covered area south of the gently-folded foothills belt. Some of these are coincident with hilly areas and are considered as possibly indicative of underlying structure. The regional extent of the most major of these suggests that they may be reflecting a hingeline; and, if they are, they may manifest the most likely clue as to where mid-Miocene reefs will be found.

The pyroclastic fan complex is in the eastern part of the Contract Area and heads on the flank of a large volcanic cone. A number of volcanoes and plugs have been mapped and most, if not all, are in the eastern quarter of the Contract Area. The volcanic-pyroclastic area has obvious disadvantages from the hydrocarbon prospectors point of view, not the least of which is that foothills structure is obscured. Volcanic centers, when present, seem to be concentrated on fold axes and along bounding faults in the mountains to the north. This factor plus the excellent SLAR display of fault and fracture lineaments should be of interest to those concerned with sulfide mineralization.

The tell-tale karst topography of the New Guinea Limestone Group is at once apparent in the Karstens area, within the northeastern part of the Contract Area near the Papuan border. South of that, the Duguel-Timour Arch was mapped in the course of our work and it appears to be a giant closure expressed at the surface possibly by the New Guinea Limestone Group.

It is also readily apparent, from inspection of the SLAR, that the mountains and mountain front express a major trend change in the middle of the Contract Area and that the folds of the foothills belt are more sinuous east of this bend. It is the more gently-folded foothills anticlines to the west that may be especially prospective for hydrocarbons. It is our belief that the longer and more sinuous the foothills folds, the less likely they are to be rooted and the more likely that they have no pre-collision history.

From the relative dearth of obvious volcanic complications and from the morphology of the foothills folds, we were influenced to concentrate our attention on the western foothills folds, such as the giant Dusseldorph Anticline, 25 kms long and 6 kms wide. The east end of Dusseldorph is characterized by what appears to be massive land slides and there are a number of cross faults in evidence too. One can from inspection of the SLAR, spot feasible routes for potential seismic lines by using stereo-pairs. Though any such anticlinal crossings should be chosen so as to avoid, as much as possible, land slide terrain and topographic linears that likely reflect shears and tension fractures. It was thus possible to use the SLAR as an aid in planning for accessibility and for the laying-out of initial seismic lines, not only for the Dusseldorph area, but for the contract area as a whole.

The SLAR shows a great difference of style between the Dusseldorph Anticline and the Lorentz Anticline just north of it. Lorentz, which is over 50 kms long and generally less than 2 kms wide, is typical of the strongly-folded belt of decollement folds along the south side of the Irian Range Uplift. The gently-folded foothills anticlines such as Dusseldorph, are lower, broader, shorter, and trend 10-20° oblique to the mountain-front trend, suggesting a degree of left-lateral adjustment in their genesis. This is likely in view of the present left-lateral sense of motion on the Sorong fault and the oblique (SSW) convergence suggested by LePichon between the Australian and Pacific plates. Compression has clearly been generally southward and the present trend and bend of the mountains is primarily the result of this factor, plus the shape of the mid-Miocene continental margin. Nevertheless, a suggestion of secondary wrench effects is in evidence and such movements may have lessened the tendency for southward thrusting in the gently-folded belt of the western Eilanden Contract Area.

The Sabang Anticline mapped with SLAR is a large-scale fold, southwest of and adjacent to Dusseldorph. It is known from a 1959 Shell seismic line to be rooted and thus is part of the evidence supporting our belief in the presence of rooted folds in the gently folded belt. The late 1950's Shell survey depended much on drainage for access and data gathering. Turnovers and dip/strikes were gathered in abundance, but the fold axes were not always hooked together accurately when it came to piecing together isolated drainage surveys. It has been possible, using SLAR modes, plus the old Shell field data, to accurately map the full extent of a great many anticlines and to map alinements between anticlines such as between Dusseldorph and Sabang and between Dusseldorph and Sande (an anticline west of it). It has also been possible to map less obvious extension trends, such as the Rieger anticlinal lead just east of Dusseldorph.

A final word about SLAR stereo: In our case, it worked well for checking the fine points of the structural interpretation, for determining access routes, and hillocks in the alluvial area. The fact that we had much known ground control data from the old Shell survey allowed us to make the most of our stereo capability. Registry was a problem inasmuch as the area in stereo registry at any given time was relatively small. Vertical exaggeration was slight and in fact the degree of relief was not unlike what would have been seen from the plane at 20,000' with the naked eye.

CONCLUSION

SLAR for us was an available and relatively inexpensive tool for reconnaissance geologic mapping of a large area. It made possible the zeroing-in on numerous prospective targets with far-more-expensive seismic. We cannot say that it was better than aerial photography would have been, but it was the best mode available at the time and under the prevailing weather conditions. I could rehash the old arguments about synoptic views, better fracture resolution, etc., but will not. Let it suffice, that our Eilanden SLAR served our purpose well, and compressed by years the time it would otherwise have had to be expended in regional seismic reconnaissance.

ACKNOWLEDGMENTS

This paper was presented substantially in its present form at the Remote Sensing Research Conference, Space Technology Center, Lawrence, Kansas, February 18-20, 1975. We are indebted to Pertimena for permission to give this paper and show the SLAR on which is is based.

REFERENCES

Australian Petroleum Company Proprietary, 1961, Geological Results of Petroleum Exploration in Western Papua 1937-1961, Jour. of the Geol. Soc. of Australia, Vol. 8, Part I, p. 1-133.

Dow, B.B., 1968, A Geological Reconnaissance in the Nassau Range, West New Guinea, Geologie en Mijnbouw, Vol. 47 (1), p. 37-46.

LePicon, X., 1968, Sea Floor Spreading and Continental Drift, Jour. Geophysical Research, Vol. 73, p. 3661-3696.

Thompson, J.E., 1967, A Geological History of Eastern New Guinea, A.P.E.A. Jour., p. 83-93.

Visser, W.A. and Hermes, J.J., 1962, Geological Results of the Exploration for Oil in Netherlands New Guinea, Staatsdrukkern-en Vitceuerijbedrijf, p. 1-265, plus 21 enclosures (most important reference).

LANDSAT IMAGE STUDIES AS APPLIED TO PETROLEUM EXPLORATION IN KENYA*

G-2

By John B. Miller, Chevron Overseas Petroleum Inc.
San Francisco, California

N76-17503

ABSTRACT

The Chevron-Kenya oil license, acquired in 1972, covers an area at the north end of the Lamu Embayment. Immediately after acquisition, a photogeologic study of the area was made followed by a short field inspection. As geophysical work then got under way, an interpretation of LANDSAT-1 images as a separate attempt to improve geological knowledge was completed. This paper describes the method used in the image study, the multispectral characteristics of rock units and terrain, and the observed anomalous features as seen in the LANDSAT imagery.

The observed lineaments seem to be part of the regional fracture system associated with the East Africa rifting and crustal expansion. A trend intersection at the north end of the Lamu Embayment might be interpreted as a failed, immature triple junction, with one postulated arm opening into the Rudolf Trough, a second arm into the Ogaden Basin. The Lamu Embayment is viewed as a possible aulacogen.

A feature of some significance to the geologic interpretation is an early Quaternary depositional summit surface formed from merging alluvial fans. The surface is slightly entrenched along shallow modern valleys by erosion into the top part of Pliocene sedimentary deposits just beneath. An absence of a fan near the northeast license corner and a swampy area along the Ewaso N' Giro drainage suggests subsidence along what may be a structural trough or downwarp.

The postulated local trough along the Ewaso N'Giro is confirmed by the results of magnetometer and gravity surveys over the area and some early results of reflection seismic studies. The geophysical results also support certain predictions made from the photogeology and image studies relative to the basin boundaries and larger lineaments. For example, anomalies are found along the Lagh Choichuff, Lagh Bogal, Ewaso N'Giro and Hagadera-Liboi lineaments.

However, convincing geophysical evidence of the Habaswein-Wajir Bor lineament has failed to materialize. Postulated fault relief along the trend, down-dropped to the south, seems to be present relative to a structural block of basement rock at and west of Wajir, but is not apparent relative to the sedimentary units and underlying basement farther east, toward the Somali border. Something of a puzzle, in interpreting the geology of this northeast corner of the license area, is the fact that the sedimentary section north of the lineament as indicated from the preliminary geophysics is very much thicker than the section measured in surface exposures.

Anomaly "A", a large circular feature seen in the LANDSAT imagery, partly coincides with the apparent "basinal" (thick sedimentary) area east of Wajir. The real nature of this anomaly is not yet apparent.

The LANDSAT imagery yielded a surprising amount of information in this flat, relatively featureless area. The success obtained strongly supports LANDSAT studies as a

* Updated and slightly edited from a paper which was presented previously (Nov. 1974) at the Fourth Exploration Seminar, Egyptian General Petroleum Corporation, Cairo - and (Feb. 1975) at the Research Conference on Remote Sensing, University of Kansas, Lawrence.

valid exploration tool. Such image studies and photogeologic work nicely complement one another.

The study has helped to define the relationship of the Lamu Embayment and its internal structure with surrounding regional features, such as the East Africa rifting, the Rudolf Trough, the Bur Acaba structural ridge, and the Ogaden Basin.

INTRODUCTION

When LANDSAT-1 (ERTS-1: Earth Resources Technology Satellite-1) was launched by the National Aeronautics and Space Administration in July, 1972, a door was opened toward a new type of information, quick and inexpensive to use. Among many uses, the information can assist in exploring for oil, gas, and minerals.

The task of LANDSAT-1, also of LANDSAT-2 and future units is to provide an orderly array of pictorial images over what eventually may be most of the entire earth's surface. Already the coverage is large and in many instances repetitive through time and changing seasons, snow, flood, and drought.

Many geologists who have made serious and well informed efforts in the use of LANDSAT imagery have obtained good results. Also, they have recognized some of the limitations of such work. These things have been reported principally through the NASA ERTS-1 symposia, especially those of March and December 1973 (Ref.1).

Several things contribute to a rather unique value of the LANDSAT imagery as it applies to exploration. One is the coverage that is already great and promises to be all but worldwide. Also, the multispectral capability, supplementing what can be seen on conventional airphotos, helps the geologist to distinguish different types and combinations of rock, soil, and vegetation and to find anomalies. The orthographic exactness and scale uniformity of LANDSAT imagery is of special value. An important application of the data is to quickly provide useful planimetric and geologic maps in areas where information is sparse. Inaccuracies in existing maps can be corrected while posting the maps with additional new information visible on LANDSAT images.

The LANDSAT-1 imagery is of two types - MSS (the Multispectral Scanner data) and RBV (the Return Beam Vidicon data). However, the bulk of LANDSAT-1 data and all the Kenya imagery is MSS.

The LANDSAT imagery of Kenya was not obtained in time to be helpful in selecting the initial Chevron acreage. It was obtained soon afterwards, however, and was used in making an early appraisal of the area and in planning a work program. Also, it was part of the basis for filing later on a smaller additional optional block, not shown on the map, which adjoins the initial block at its northwest boundary and corner (Fig. 1).

GEOLOGIC BACKGROUND

The Chevron oil exploration license covers the northern part of the basinal feature of the Kenya Coast known as the Lamu Embayment. That much was known in 1972 when the exploration right was acquired. But not much was known about the exact basin shape, its limits, and structural nature.

Previously, British Petroleum-Shell had held an oil lease over a large part of the Lamu Embayment, including some of the ground taken by Chevron. Most of the BP-Shell rights had been relinquished, leaving only a relatively small area along the Kenya coast.

BP-Shell had explored extensively and drilled 16 "dry" wildcat wells in the Lamu Embayment. Only three of these - Meri-1, Waligero-1 and Wal Merer-1 - are on the Chevron tract. These were enough to demonstrate the presence of more than 12,000 feet (3660 meters,

approximately) of sedimentary rocks within the land acquired by Chevron. Several other wells of substantial depth were known to exist some distance to the east, in neighboring Somalia.

But while information on the embayment itself was sketchy, certain information on surrounding areas was well documented by the Geological Survey of Kenya. In the area west and north of Mombasa, Caswell (1953, 1956), Sanders (1959), Thompson (1956), and Williams (1962) - Refs. 2-6 - report a thick section of sedimentary rocks. This includes Karroo type red-beds (mainly continental sandstones, Permo-Carboniferous through Triassic), a section of marine shales and local shelf-type limestone (Jurassic and Cretaceous) and locally along the coast onlapping marine deposits of Tertiary age. The aggregate section of Karroo type beds totals about 22,000 feet (6700 m., approximately) The Jurassic section totals 6600 feet (2010 m.). The Cretaceous is incompletely represented in exposures by only about 300 feet (90 m.) of section.

In the area north of the license area, extending to the Ethiopia border, the stratigraphic column begins with Triassic strata and ranges through the Lower Cretaceous. These rocks have also been described by geologists of the Kenya Geological survey, particularly in reports by Thompson and Dodson (1958), Baker and Saggerson (1958), Saggerson and Miller (1957), and Matheson (1971) - Refs. 7-10. As compared with sediments at Mombasa, the thickness is much less and the lithology is somewhat changed. The Triassic again is a Karroo-type facies, but the exposed thickness is only 2000 feet (610 m.). The Jurassic strata, roughly 5500 feet (1680 m.) thick, are mainly dense, gray shelf-type limestones. About 2500 feet (760 m.) of Cretaceous section consists mostly of shallow-water sandstone and some interbedded marine shale.

Contrasts both in thickness and lithology are found when the stratigraphic units north of the license area are compared with those observed near Mombasa. However, it is not clear where and why the changes occur nor what may be their significance to the possible presence of commerical hydrocarbons.

Available maps show most of the surface in the license area as Quaternary alluvium. Jurassic limestones abut and enter the area east of Wajir, some late Tertiary volcanic rocks occur in the northwest corner, and Precambrian metamorphic rocks crop out in the southwest. Several small Jurassic exposures are reported just outside the area, north of Mado Gashi. Preliminary investigations have shown that, over much of the area, erosion has cut very shallow valleys into underlying clays considered as Pliocene. While the exact age of these is subject to question, the clays are mainly older than sands and soils found on the undissected summits, and older by yet another stage than the alluvium in the modern streamflats. They appear to be the top part of a fairly thick Mio-Pliocene section known in much of the Lamu Embayment.

A complex, sloping plateau rises from an altitude of about 1200 feet (370 m.) above the sea at the west margin of the Lamu embayment north of Garissa to a structural swell reaching a height of 6000 feet (1830 m.) or more along the Kenya (Gregory) Rift Valley. This is mainly an area of Pre-cambrian rocks, including a variety of metamorphics and intrusives, but there are also great areas of volcanic rocks and several large volcanic peaks. The more resistant crystalline masses stand as prominent inselbergs. Many belts of hills representing old topography occur within and between the valleys. In this terrain are well preserved parts of three planation surfaces, produced by denudation after principal stages of structural uplift associated with the African rift system. The plateau area was tilted seaward in late Cretaceous, middle Tertiary, and late Tertiary episodes of domal uplift (Saggerson and Baker, 1965; Matheson, 1971; Baker and Walenberg, 1971) - Refs. 11, 10, and 12.

Two geologic papers containing new, important information relative to the Lamu Embayment were published in 1973. One of these, by Walters and Linton of BP-Shell, (Ref. 13) provides subsurface information on the Lamu embayment. The other, by Gulf Oil geologists Beltrandi and Pyre (Ref.14) describes the geology of adjoining basinal areas

in Somalia. Although these add substantially to available knowledge, they provide incomplete answers about basinal structure, bounding limits, and stratigraphy.

GEOLOGICAL INTERPRETATION

Methods

To conduct this study, we (Chevron) purchased the 70 mm. positive transparencies of all four spectral bands of the required LANDSAT-1 imagery. These were composited into color, using an early model International Imaging System (I^2S) additive color viewer then available at the Chevron Oilfield Research Laboratories at La Habra, California. Several color arrays were recorded as 35 mm. color slides on Ektachrome high-speed film. For interpretation of the imagery, the 35 mm. slides and also the 70 mm. black and white images were projected to the wall of a darkened room. A sheet of white drafting paper fastened to the wall served as a projection screen and as a base for annotating the geology and other photographic detail.

Since completion of this work, Chevron Overseas has obtained, at its home office, an improved I^2S viewer. This eliminates a dependence on color slides, and makes it possible to annotate on a transparent medium directly over the screen of the compositor. This is done at a favorable scale of 1:500,000. During annotation, the image is examined with a binocular headpiece which provides 1-1/2 X and 2-1/2 X magnification.

Just prior to the LANDSAT study, even predating the availability of the LANDSAT imagery, I conducted a photogeologic study of our area and made a six-day trip into the field (airphoto scales partly 1:40,000; partly 1:80,000). This work extended from September into early November, 1972. As a prelude to the work on the LANDSAT photos, I regard this experience in Kenya as most fortunate. Of course, such experience is never amiss. As background toward evaluating a new and unfamiliar type of imagery, it proves to be especially helpful. It is a framework for judging the physiographic and geologic phenomena as registered by the LANDSAT sensors and for evaluating the usefulness of the data.

Used to illustrate this paper are two LANDSAT-image mosaics. These copy fourth-stage products from the 70 mm. positive transparencies acquired from the ERTS Data Center at Sioux Falls, South Dakota. The first step was to photographically enlarge the images into a set of negatives -- scale 1:1,000,000 -- produced on 9 x 9 inch film. Contact prints from these formed the original mosaic, which then was reproduced into a single mosaic negative and into photographic prints.

In the remainder of this paper, the objective is an appraisal of information recovered from the interpretation of the LANDSAT images. Comparisons will be made, from time to time, with detail as seen on airphotos and (occasionally) as seen on the ground.

Physiography

Much of the drainage pattern is seen on the LANDSAT images with remarkable clarity, even into the headwaters of relatively minor drainage courses. In viewing the LANDSAT images, this is almost the only evidence of relief. An impression of relief is better when there are ground shadows, but very few slopes in the area are steep enough to produce shadows. The exceptions are the cuestas of Triassic sandstones roughly 80 kilometers (50 miles) north of Wajir, several lava features west of Wajir, and local berg-like hills of basement. All of these hills are small, even at the scale used during the interpretation. At the reduced size of the present mosaics and maps (Figs. 2-5) they become all but invisible.

The drainages are gullies and wide, flood-washed channels in a semi-arid terrain. These are seen clearly in LANDSAT images and can be drawn accurately. The drainages that originate on the plateau and enter the region from the west have relatively wide stream

flats. The Tana River carries a good flow of water. Through the use of the infrared image (particularly) the dark, meandering line of this can be followed readily. The other streams are seasonal. The Ewaso N'Giro spreads and much of its flow is arrested at the Malka Galla swampy area north of Mado Gashi. Lush vegetation at the "swamp" produces high response in the infrared as compared to the green and red band response, so that a false color image registers flaming hues of red. Below this spot, the Ewaso N'Giro drainage channels become narrow and dispersed, and while borders of the streamflat are sharply defined, the channels within it are indistinct. The same is true for other similar streams. For example, a 15 kilometer segment of Lagh Katulo as sketched differs from the main streamcourse marked from airphotos, but the difference is inconsequential in small scale mapping amid shifting channels.

The relief, indeed, is low. Excepting for an escarpment along the Yamicha area lava bench, the only hills with substantial sloping profiles are either west or well to the north of our license. Although there is about 600 feet of slope in 140 miles (180 m. in 220 km.) from the west edge of our tract to the southeast corner, the horizon, as seen on the ground, is commonly flat. The most rugged ground generally consists of a gentle, faintly rilled slope into a shallow valley, a low cut bank, and then an equally gentle rise to a low, broad summit. In perhaps half of the tract, these slopes are so slight as to be imperceptible during ordinary stereoscopic study of airphotos. They are defined mainly by directions of rainwash and drainage rather than visible relief. Remarkably, much of the drainage of these insubstantial slopes is seen almost as clearly on LANDSAT images as on the airphotos.

Rock Signatures

Quite a number of boundaries between rock types can be traced on the LANDSAT images even though the nature of the lithology is not clear. To some degree, even the approximate nature of the lithology can be surmised. In this text, the visible characteristics of units will be reviewed in successive order of declining age. Many of the characteristics are not seen in Figs. 2 and 3 because these are much smaller than the images employed for interpretation.

The migmatitic character of the basement rocks seems to be subtly evident. A peculiarity of folia is that they show on many scales, which ranges from microscopic size into the outcrop and then to a textural grain seen on airphotos. Now, in the Kenya migmatites, some of the foliated grain is reproduced even in the LANDSAT images. It appears as faint, shadowy bands, probably representing rock and topography and interwoven layers of differing lithology. In places are berg-like erosional forms indicating resistant rock. A wide color range, from eggshell and flesh tones into green and gray very likely represent composition ranges from light-reflective bands of quartzose rocks and feldspar through rocks of intermediate composition, mantling residual material rich in iron oxides, into belts of relatively fresh rock containing unoxidized femic minerals, gray slate, and (locally) marble.

The Triassic conglomerate and sandstones north of Wajir stand out separately from the metamorphic complex mainly because of their sharp, arcuate- and irregular-shaped cuestas. The well-stratified and resistant character of the rocks is revealed by the erosional form of the ridges. The low dip present in the strata can be construed from down-dip expanse of the dip slopes.

A basal boundary of the Jurassic limestone can be followed only inexactly. The limestones image quite dark in bands 6 and 7, somewhat less dark in bands 4 and 5, and in the composite image show as dark gray partly flushed with red. The red is a response from a combination of thin soils and sparse vegetation.

Cretaceous sedimentary units show in the extreme northeast as sharply defined ridges and cuestas. The direction of dip is generally discernible.

Pliocene and Quaternary volcanic rocks, mainly basalts, are present in the northwesterly part of the area. In fresh outcrop, the e register darkest in all color bands, and in

the color composites they show as nearly black. There is a weathered surface and some soil across the basaltic mass at Yamicha, but in its southerly escarpment, which probably marks an original flow edge, the volcanic rocks are very fresh. Farther north, a virtually unweathered volcanic flow is defined both by its lobate form and nearly black color.

Of somewhat the same age range are the Plio-Pleistocene clastic deposits. These show the most varied color signatures of all -- a greater range than are accounted for by known differences in lithology. The Pliocene part can be locally divided into two parts. At the top and probably Quaternary in age is a depositional surface and duricrust.

The main unit, the Merti sands and clays named in Kenya geological literature, is regarded as late Pliocene. These sediments fill a late structural sag along the Lamu Embayment. The observed relationships strongly suggest faulting along the westerly basin margin, because the "End-Tertiary" erosion surface extends across basement rocks at elevations of 600 feet (182m.) or more west of Mado Gashi but drops beneath the Merti in the basin. As shown by the thickness of Merti beds in the Dera borehole, near the basement rock boundary (240 feet — 73m. — to top of basalt; 408 feet — 124m. — to base of volcanic debris: Matheson, Ref. 10 p. 19) the "End Tertiary" surface seems to drop structurally at least 250 feet (76m.) in crossing the basement boundary.

The boundary of the Merti deposits with basement rocks is plainly seen on LANDSAT-1 imagery at the Tana River. The basement appears banded. The adjoining Merti is finely rilled and, especially in band 7, has a lighter tone. Extrapolating from topographic maps, the thickness of Merti beds exposed in the valley slope near the basement boundary is about 600 feet (180 m.).

Above this, and within my knowledge recognized only on the LANDSAT-1 imagery, is a second unit. It begins at the basement boundary and thickens wedge-like into the basin. It is slightly darker in bands 5, 6 and 7, than the sediments beneath. I distinguish this wedge-shaped unit tentatively with the name "Upper Merti", but suppose it may not be readily separated from the underlying part of the Merti except in the Tana Valley. Saggerson and Baker (Ref. 11, p. 57) mention 300 feet (90 m.) of Merti sediments at Garissa. On the basis of the LANDSAT-1 image, at least 200 feet (61 m.) of these seem to belong to the "Upper Merti". Seemingly they will entirely overlie the estimated 600 feet (183 m.) of Merti beds exposed near the basement boundary.

The distinguishing tonal difference of the "Upper" Merti from underlying beds is clearly seen in the color image and in the longer wavelengths of bands 5, 6, and 7. It is seen hardly at all in band 4. The smaller sensitivity of shorter wavelengths to distinguish these lithic divisions may explain why the divisions were not recorded during work on convential airphotos. Coupled with this is another reason: The sediments are unconsolidated. They are intricately scored by rilled drainage, and small masses of the material have moved downslope through the action of crumbling and mudflow. The boundary, as seen on the airphoto, has probably been softened and blurred by this action. On the other hand, as seen in the overview of the LANDSAT image, the boundary is relatively sharp and conspicuous.

Above the Merti is a thin unit of sand, marl, and calcrete deposits or "caliche". This tends to form a duricrust with a thickness commonly ranging from a foot or two to perhaps 6 or 8 feet (about 2 or 3 meters at greatest). The top surface - I will guess its age as Pleistocene — is a thin layer of soil thinly mantled with sand. Near the town of Wajir, the Quaternary deposits — about half sand and shale, the top half mainly of calcrete — thicken to as much as 100 feet (30 m.) and contain a substantial amount of groundwater. Calcrete outcroppings in this area appear on the LANDSAT images as white patches.

The depositional surface of the Quaternary duricrust (mapped Qs) has been entrenched and partly destroyed by the modern system of streams. Nevertheless, there are numerous remaining patches. The distribution of these bears on several aspects of the geology, including the restoration of previous drainage and a definition of lineaments.

Remnants of the surface, as seen on airphotos, have a relatively dark gray cast and slight, benchland type rims. Commonly there is a pattern of widely spaced "pits" that appear to be subtle, periodically wet depressions. Where the surface has been destroyed are rilled slopes or an expansive surface of clay which is broken - probably along jointing - into prisms. Each prism has an almost imperceptible hummock and central cluster of brush (as confirmed on the surface) surrounded by bare clay and a wash of white sand.

The depositional surface stands out quite well on the LANDSAT imagery, although a color composite is needed for most effective mapping. It supports grass and significantly more trees than are found over most adjoining rock units. Consequently, in addition to a darker cast than most surrounding rock units except limestone and basalts, the false-color images rendered by the surface are distinctly reddish. A response that comes from grass and trees, the reddish tint is probably somewhat seasonal, dependent on rains.

Examination of the surface suggests two main parts, a sloping plain from the north-northwest, and what may be called the Tana fan from the southwest. Judged from valley entrenchment and airphoto stereoscopy, there is a definite easterly slope to the Tana fan. Also, the plain beyond the Ewaso N'Giro tends to undulate slightly across axes parallel with the present drainage. Destruction of some of the surface, e.g., the northwesterly part and a belt along the Ewaso N'Giro, as judged from the distribution seems to have started before development of the southerly part of the surface was complete.

Examination of the LANDSAT images reveals several elements within the plain that were not noticed on airphotos. Located between the Ewaso N'Giro and Lagh Bogal (see map) these can be effectively defined only on the color image. They show as four or possibly five differing arcuate bands of color. Their shapes suggest giant bedding structures. Preserved parts of the Quaternary depositional summit coincide with the associated arcuate forms, indicating these might be anchored by resistant layers among somewhat complex stratigraphic forms just beneath the surface. For example, they could mark the upper edges of several shallow, trough-shaped features related to erosion and depositional patterns. Although probably not sensitive to structural trends, these might be significant to the distribution of possible shallow ground water.

Lineaments

As used in this paper, the term lineament refers to apparently natural lines, bands, and anomalous zones generally more than 10 kilometers (6 miles) long. These lines and linear bands are associated variously with straight or slightly arcuate drainage courses, tonal lines, aligned erosional breaks in the Quaternary depositional surface, and occasionally other phenomena.

A set of linears aligned about N 50° - 60° E probably is paired with another set aligned N 45° - 60° W. Representatives of the northeasterly set are the Habaswein-Wajir Bor and Hagadera-Liboi lineaments. In the northwesterly set are trends along the Lagh Katulo, Lagh Bogal and a segment of the Ewaso N'Giro. Considered as conjugate directions, the intersection angles generally fall between 60° and 80°.

Another set of lineaments (e.g., Lagh Choichuff, Lagh Bor) commonly bears about N 10° W - N 20° W. Probably conjugate with this is the Lagh Bisika and several smaller trends bearing N 70° W. The intersection angle ranges between 50° and 65°.

A number of lineaments, accentuated in Fig. 4, are discussed below. Among the many linear features present, these seem to relate, as seen in Fig. 1, to geologic phenomena well beyond the Fig. 4 map boundary.

Habaswein-Wajir Bor Trend - This wide, subtly defined linear anomaly (lineament) crosses the license area at its middle west boundary and, east of Wajir, continues into Somalia. The anomaly forms a band distinguished in part by sparcity (a result of erosion) of the Quaternary duricrust.

The trend is defined by two bounding linear features comprised of separate, aligned but not quite continuous lineaments. Parts of these are formed by straight stream courses and other parts by tonal changes occurring, for example, along straight edges of remaining areas of the duricrust where fractures are probably a controlling factor in the erosion.

The dying topography and Jurassic limestone outcrops northeast of Wajir seem to be part of the tonal change along the Wajir Bor lineament east of Wajir. This suggests that the trend, in this sector, may be an expression of a fault that steps the limestones downward into the basin where they may then be overlaid by younger sediments.

An easterly extension of the Habaswein-Wajir Bor trend may play a part in an offset in basement rocks along the north flank of the Bur Acaba structural ridge in Somalia. This is mentioned further in later paragraphs.

In the southwesterly direction, the Habaswein-Wajir trend aligns toward distant Mt. Kenya, a major volcano.

Some 60 kilometers south of the Wajir Bor trend is a parallel LANDSAT lineament, mainly tonal. It is shown on the map, but not named. This feature plays a part in the tectonic scheme and will be mentioned again.

Hagadera-Liboi Lineament - About parallel with the Habaswein-Wajir Bor feature, the Hagadera-Liboi lineament crosses the southerly part of the license, then extends into Somalia. Much of it is defined by drainage along a southerly leg of the Ewaso N'Giro (locally called Lagh Dera) past the Liboi military post. Toward the west, it runs along lesser drainage courses and finally extends along the south margin of the Tana River Valley. In this segment, it partly outlines the edge of the preserved Quaternary surface.

As it is traced eastward on LANDSAT-1 imagery, the Hagadera-Liboi lineament aligns directly along the southerly edge of the Bur Acaba structural ridge. This ridge, in Somalia, is a major uplift exposing an area of granite and metamorphic basement. The local geology indicates that at least its southerly flank is faulted. The Habaswein-Wajir Bor and Hagadera-Liboi linear features were first defined through the Kenya photogeology. Their exact coincidence, when projected by means of LANDSAT imagery into Somalia, with the boundaries of the Bur Acaba structural ridge is considered as geologically significant.

Choichuff, Bisika, and Ewaso N'Giro lineaments - The Lagh Choichuff and its companion trend, Lagh Bor, trend southward across the license boundary along drainage courses bearing these names.

Just within the license, each is crossed by southeastward features -- the Lagh Bogal and Lagh Bisika lineaments. The Lagh Bor feature is not seen southward of its juncture with these features. The Choichuff trend meets with the valley of the Ewaso N'Giro and -- if structural aspects are continuous -- changes in trend from S20°E to a new direction of S25°-30°E.

The apparent bend along the Ewaso N'Giro apparently is caused by an interaction between trends and by structural slivering. When viewed with the aid of a regional map, the Choichuff lineament is found to align with a segment of seacoast north of Malindi and the lower streamcourse of the Tana River. This suggests a deeply rooted fracture nearly parallel with the fault which bounds the west margin of the basin.

Lagh Bogal and Lagh Bisika Lineaments - These two trends cross the northern part of the license area and intersect each other at a narrow angle. Some structural interference may occur where the two trends meet. There is a hint of left-lateral displacement of the Lagh Bogal feature, but exact placement of the lineaments and definition of offset is uncertain.

The Lagh Bogal lineament is about axial relative to a structural-morphologic feature

called the Rudolf Trough by Brock (1965, Ref. 15, p. 101-102). From a regional standpoint, it might be appropriate to name the lineament from North Island in Lake Rudolf because it can be traced this far to the northwest (Fig. 1) and probably is responsible for the North Island volcanic center. It is associated also with a concentration of volcanic craters northeast of Mount Marsabit. The Lagh Bisika feature also passes northwestward, but lies slightly askew to the trough. This trend flanks the south side of Mount Marsabit and merges with a bounding linear of the trough about at the south end of Lake Rudolf. Along the Kenya-Ethiopia border, linears flanking the north side of the Rudolf trough are seen on the LANDSAT imagery.

Lagh Katulo Fault - A fault displacement of Jurassic sediment along the Lagh Katulo can readily be detected both on LANDSAT imagery and on the Kenya airphotos. The displacement can be seen in the structural attitudes, also in the distribution and expanse of Mesozoic rock units. The faulted lineament can be traced northwestward into Ethiopia, also southeastward into Somalia.

Other Anomalies

Anomaly A. - This anomaly is partly within the license area. It centers east of the international border, in Somalia, and is a large anomaly of relatively pale tone and color, outlined by a circular drainage pattern. Its easterly edge is marked by a prominent deviation of the Lagh Katulo streamcourse. A northward boundary is the Wajir Bor lineament; a southward boundary is the Liboi lineament. The feature therefore may be related structurally to the Bur Acaba structural ridge which apparently develops astride this same trend and structural block, farther east.

In a fold regime, such an anomaly is suggestive of a domal uplift. Within this extension regime amid a strongly developed fracture system the domal implication becomes much less forceful. The stream systems seemingly are deflected across major fracture lines, then follow along polygons of fracturing. The anomaly as a whole is outlined by a rim-like margin of the preserved Quaternary duricrust, reduced by sapping action to a circular outline.

Whatever the difficulties in exact interpretation, the anomaly probably is related in one way or another to the conditions of subsurface structure.

Malka Galla area - The periodic collection of water over the Ewaso N'Giro streamflat is not strikingly abnormal at sites such as this where extensive drainage from highlands empty into arid plains. Yet it does suggest a break in the stream gradient and a possible structural sag.

Possibly more significant than the "swamps" is the apparent absence, in this sector, of any large alluvial fan coincident with the Ewaso N'Giro. The Quaternary duricrust developed mainly over fans entering from the southwest (Rio Tana sector) and north (Lagh Choichuff and Lagh Bor, and similar drainage).

The absence of a substantial fan on the Ewaso N' Giro may be construed as evidence of structural subsidence. Acting as a sediment trap, substantial subsidence would arrest the movement of sediment and minimize the growth of fans.

Construed in this way as a discrete structural sag filled with young clastic sediments, the area may be ideal for large, relatively shallow supplies of ground water.

Bur Wein - The Bur Wein anticline (Baker and Saggerson, Ref. 8) lies within Cretaceous outcrops about 40 kilometers south of El Wak. This feature, a sharply defined domal uplift, shows in the LANDSAT image as a unique feature. Its steep flanks, clearly visible, set it apart from all other recognized features. The characteristics of the Bur Wein anticline, as contrasted with the surrounding geology, suggest it as a diapiric feature possibly developed over an igneous plug.

Analytical Review

In the pattern of lineaments, four basic directions are described in the previous subchapter.

Three of the directions are coincident with major rift directions mapped in East Africa. The examples, classified roughly in terms of regional directional groups, are northward, parallel with the Gregory Rift Valley (Choichuff), northwestward (Lagh Bogal-Rudolf), and northeastward (Habaswein-Wajir Bor) -- the northwestward and northeastward systems parallel regionally with the Rukoban and Ruaha fracture sets in Tanzania. Except for local minor deviations, the directions are remarkably consistent. Not only the younger Cretaceous and post-Cretaceous rifts, but also the older basins filled with Karroo-phase sandstones as old as Permian, conform with this pattern. The rift and fracture system tends to divide the continental block into entire and partial hexagonal prisms.

The regional tectonics apparently are dominated by vertical movements and tensional stress. The Lamu embayment, which contains a succession of sedimentary rocks beginning with Karroo sandstones, is postulated as an extension basin of possible failed-arm type. Any compression-type structures within the embayment are probably of secondary importance.

Evidence of downfaulting of Pliocene sediments at the basement boundary west of Garissa is construed from the geometry of bedding and sedimentary infill (observed in the LANDSAT image) as these combine with known relief. The faulting suggests this line as a main, if not necessarily a unique westerly boundary to the basin, rather than as a less important line of sedimentary onlap and tilting.

The most logical northern limit of the Lamu embayment, east of Wajir, is a line of postulated fault relief across the Habaswein-Wajir Bor lineament. North of this, Triassic sandstones and Jurassic carbonates are found in outcrop, resting on metamorphic basement. South of it, one might expect a much thicker section, ranging to Tertiary age.

Westward from Wajir, the situation changes. It is possible to relate three separate phenomena, and conclude from them that an apex of the basin may extend into the northwest corner of the license area -- its margin staggered, perhaps, between several intersecting faults. The anomalous aspects of the northwest lease corner: 1) The semi-swamps of the Ewaso N' Giro, and 2) an absence of a clearly defined "Quaternary surface" fan. As previously discussed, these combine to indicate an active structural sag. 3) Jurassic outcrops reported in this area, stepped far to the west of the Jurassic boundary northeast of Wajir. These outcrops must be preserved in a downwarped or downdropped block, and suggest a major offset or displacement of the basin margin.

Construed from this evidence is the idea that a somewhat discrete trough or graben may extend to the northwest corner of the Chevron holding.

A number of lineaments converge within the northerly part of the tract. These may relate partly to the termination of the Lamu Embayment if the embayment is, in fact, an aulacogen or failed arm. The northerly trend of the Lamu embayment combined with two lesser branches may, in fact, form a triple junction. One of these, behaving as a carbonate shelf set behind the Bur Acaba Ridge, goes into the Ogaden Basin of Ethiopia and Somalia.

The other, the narrow graben-like trough toward Lake Rudolf, seemingly could have been a Mesozoic valley which directed Mesozoic river drainage into the Lamu Embayment. This could bring about major changes in sedimentary thickness and facies -- changes not yet known, but possibly important to oil occurrence -- within the Chevron holding. Possibly, also, the trough could have held a short-term arm of the sea.

Geophysical Program

During 1973, an airborne magnetometer survey and helicopter-mounted gravity survey

were made. These surveys were planned with the benefit of photogeologic knowledge. The work was already in progress during the LANDSAT study. A seismic program, which benefits from all previous work, is going forward in 1974 and 1975.

There is a limited amount of correlation between the geophysical results and the analysis made from LANDSAT images and the airphotos (Fig. 6). At this preliminary stage, neither the coincidence of anomalies where coincidence occurs, nor a lack of coincidence is very well understood. The best correlations are these:

1. A good magnetic definition, and a modest gravity definition closely matching the construed fault along the western basin boundary. The data does not suggest a single profound structural drop-off, but instead one that is stepped or, (most likely) involves an element of tilt as well as faulting.

2. Defined in all geophysical results including a preliminary seismic line is a trough-like feature in the northwest part of our license area, coincident with the inferred structural sag along the Ewaso N' Giro. A northeast and east boundary of this feature is evidently a fault. For a considerable distance, the fault lies along the Lagh Bogal lineament. About at the juncture of the Lagh Bor lineament it turns south through an area where there is no distinct, matching linear. It tends to die away near the center of the Chevron holding.

3. Rocks having high seismic velocities and the magnetic properties of basement project slightly into the license area in the Giriftu structural block, just east of the Lagh Bor lineament.

4. Shallow magnetic basement, probably igneous, lies along the Lagh Bogal and Lagh Bisika lineaments southeast of their juncture and about 80 kilometers southeast of Wajir. A tonal LANDSAT lineament parallel with the Wajir Bor lineament, midway between the Wajir Bor and Liboi lineaments, also crosses this point. As noted by geophysicist R. F. Flege, the coincident magnetic and gravity anomalies are triangular. Their shapes correspond with magnetic linearity in three directions about parallel with the Wajir Bor, Rudolf Trough and Lamu Embayment directions of structure. Conceivably, the magnetic anomaly may represent an igneous mass related to triple junction spreading.

5. The area north of this basement high, over anomaly "A" and the entire northeast corner of our license area, has a thick section of sediments. This relatively basinal feature is confirmed by early results of seismic work.

6. A general gravity high trend crosses the area along a line just north of the Hagadera-Liboi lineament. A magnetic high trend follows this in a general way. Basement along the crest of this feature, as compared to the flanks of the feature, appears relatively shallow.

Some differences and things yet unexplained are apparent also:

1. There appears to be no distinct downstepping of the basin from the carbonate shelf northeast of Wajir toward anomaly A. Also, the apparent depth to basement within and immediately adjacent to the Jurassic outcrops is at least twice what it should be as judged from the stratigraphic measurements of the surface sections reported by Thompson and Dodson (Ref. 7), Joubert (1963 - Ref. 16) and others. Why this is so is not yet clear.

2. No substantial geophysical anomaly has been found along the Habaswein-Wajir Bor lineament. The Giriftu basement block seems to end near the lineament probably through downfaulting. West of the Lagh Bor lineament, no geophysical anomaly at all seems to be associated with the Habaswein-Wajir lineament. East of the

town of Wajir, gravity data fail to detect the lineament and the magnetic data only faintly suggests its presence.

3. The northern flank of the transverse basement "high" aligned along the Hagadera-Liboi lineament seems to define the southerly extent of the Ewaso N'Giro (northeast license corner) structural trough.

4. Low velocity beds that seemingly would be Tertiary do not commence just southward of the Wajir Bor lineament, as predicted. Their first appearance is approximately at Lagh Bisika, some 70 or 80 kilometers farther south.

5. Although phenomena coinciding with many of the major imagery lineaments are seen in the geophysical data, the features generated along a single lineament are often highly varied. A substantial number of the individual elements among these are elongated in direction of the photo-lineament. Yet from the geophysical evidence alone, one generally would not integrate them as a structural trend.

The idea that the Lamu Embayment may have originated as an aulacogen, even though unproven, is partly supported by gravity data. Readings over the embayment are consistently higher than strongly negative readings generally obtained over the outcropping Precambrian rocks to the west. The readings are not anomalous to what is commonly regarded as a normal crustal thickness for continents. Significant, however, is a three-way alignment seen among the structural components of the basin.

CONCLUSIONS

The results of the LANDSAT image study are analyzed here as they fit within an evolving program of exploring for oil in Kenya. They start with a review of geological knowledge initially available, progress through a comparison of LANDSAT image analysis with photogeology, and finally compare the results with what has been learned during the beginning stages of geophysical exploration.

The LANDSAT information assists the geological program in two ways:

1. By helping to define an oil license area and the end of the Lamu Embayment relative to a regional geological setting, and

2. By improving the definition of anomalies and lineaments significant to interpreting structure and stratigraphy. The area provides a severe test of the use of LANDSAT data, because surface geological differences within the license area are few and the relief very low. Almost all the important basin geology is concealed by young, flat-lying Pliocene and Quaternary infill. Useful ideas have sprung from the information extracted, and this is counted as progress.

In addition, the LANDSAT studies contributed evidence for suspecting subsidence along the Ewaso N'Giro near Malka Galla and suggested a branching arm of the basin toward the Rudolf Trough. When supported by geophysical evidence, this led to filing on an option area adjoining the original Chevron license, thus extending the Chevron holdings.

Several of the anomalies are defined better on the LANDSAT images than on the airphotos. The Lagh Bisika lineament, as a distinct fracture direction, was defined only from LANDSAT data. On the airphotos it might be thought of simply as a sub-fracture parallel with the Lagh Bogal lineament. The Hagadera-Liboi lineament and the Lagh Katulo fault are defined more completely on LANDSAT images than on airphotos. Anomaly "A" was not covered completely in airphoto work and did not become apparent until the LANDSAT images were examined.

On the other hand, substantial evidence in support of the Habaswein-Wajir Bor trends comes from the pattern of smaller fractures observed only on airphotos. In the LANDSAT

imagery, this lineament - mainly seen as a tonal band - has its best expression northeast of Wajir extending into Somalia. Its coincidence with the north flank of the Bur Acaba structural ridge appears more than coincidental. I believe the lineament is an important, valid structural feature and do not understand why the geophysical data in Kenya do not show it clearly.

The coincidence found when many features of the LANDSAT and airphoto interpretation are compared with features shown by geophysics strongly suggests that most of the large anomalies and lineaments are structurally valid. However, the data generally indicate complex rather than simple geology, defying an early understanding.

During the LANDSAT image study, evidence was found of a previously unrecognized lithologic division within Pliocene deposits west of Garissa, also internal depositional structure within Plio-Pleistocene deposits along a summit east of the Ewaso N' Giro. These proved helpful in understanding structural and basinal depositional patterns and in reconstructing basin history. And significantly, they show how LANDSAT images can function as a separate source of information.

In the LANDSAT interpretation, I have used a modified form of the usual techniques and skills of photogeology. The LANDSAT studies give an overview predisposed to find regional anomalies, while airphotos more effectively look at local detail. The LANDSAT and airphoto work logically should go hand-in-hand, neither of them separately and alone, because each of them may lose the things most easily seen by the other. LANDSAT imagery adds multi-spectral data that is geologically useful. Most significant of all, LANDSAT studies have the advantage of very quick interpretation over new areas and regions. Such work saves time and money and gives a substantial basis for new ideas.

REFERENCES

1. National Aeronautics and Space Administration (1973) "Abstracts" and "Summary of Results" - Second and Third ERTS Symposia, Nasa-Goddard Space Flight Center, Greenbelt, Md.

2. Caswell, P. V. (1953) "Geology of the Mombasa-Kwale Area", Report No. 24, Geol. Survey of Kenya, Nairobi.

3. Caswell, P. B. (1956) "Geology of the Kilifi-Mazeras Area", Report No. 34, Geol. Survey of Kenya, Nairobi.

4. Sanders, D. L. (1959) "Geology of the mid-Galana Area", Report No. 46, Geol. Survey of Kenya, Nairobi.

5. Thompson, A. O. (1956) "Geology of the Malindi Area", Report No. 36, Geol. Survey of Kenya, Nairobi.

6. Williams, L. A. J. (1962) "Geology of the Hadu Fundi-Isa Area", Report No. 52, Geol. Survey of Kenya, Nairobi.

7. Thompson, A. O., and Dodson, R. G. (1958) "Geology of the Kerkali-Melka Murri Area", Report No. 43, Geol. Survey of Kenya, Nairobi.

8. Baker, B. H., and Saggerson, E. P. (1958) "Geology of the El Wak-Aus Mandula Area," Report No. 44, Geol. Survey of Kenya, Nairobi.

9. Saggerson, E. P., and Miller, J. M. (1957) "Geology of the Takabba-Wergudud Area", Report No. 40, Geol. Survey of Kenya, Nairobi.

10. Matheson, F. J. (1971) "Geology of the Garba Tula Area", Report No. 88, Geol. Survey of Kenya, Nairobi.

11. Saggerson, E. P. and Baker, B. H. (1965) "Post-Jurassic Erosion Surfaces in Eastern Kenya and Their Deformation in Relation to Rift Structure", Quart. Jour. Geol. Soc. London, V.121, p. 51-72.

12. Baker, B. H., and Walenberg, J. (1971) "Structure and Evolution of the Kenya Rift Valley", Nature, V. 229, p. 538-542.

13. Walters, R. and Linton, R. E. (1973) "The Sedimentary Basin of Coastal Kenya", in Sedimentary Basins of the African Coasts, Assoc. of African Geol. Surveys, p. 133-158.

14. Beltrandi, M. D., and Pyre, A. (1973) "Geological Evolution of Southwest Somali" in Sedimentary Basins of the African Coasts, Assoc. of African Geol. Surveys, Paris, p. 159-178.

15. Brock, B. B. (1965) "The Rift Valley Craton", in The World Rift System, International Upper Mantle Project, Geol. Survey of Canada, Paper 6614, p. 99123.

16. Joubert, P. (1963) "Geology of the Wajir-Bor Area", Report No. 57, Geol. Survey of Kenya, Nairobi.

ILLUSTRATIONS

Note relative to Figs. 2 and 3. These are mosaics from LANDSAT scenes 1190-07052 (upper left), 1189-06593, (upper right), 1190-07054, 1189-07000, 1190-07061 and 1153-07003. The lines where the images are matched show as sharp, straight boundaries -- one longitudinal and two transverse -- parallel and normal with the slant margins. The white flecks in the lower right hand scene and at extreme lower left are clouds. Scale 1: 2,500,000.

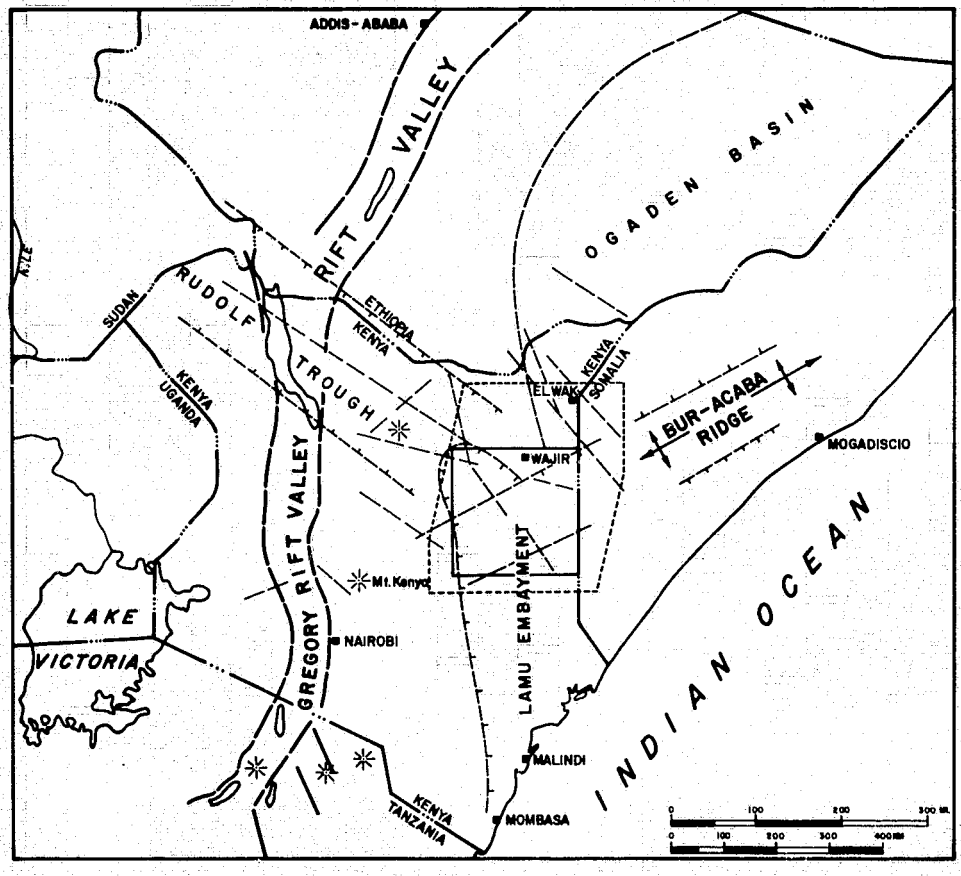
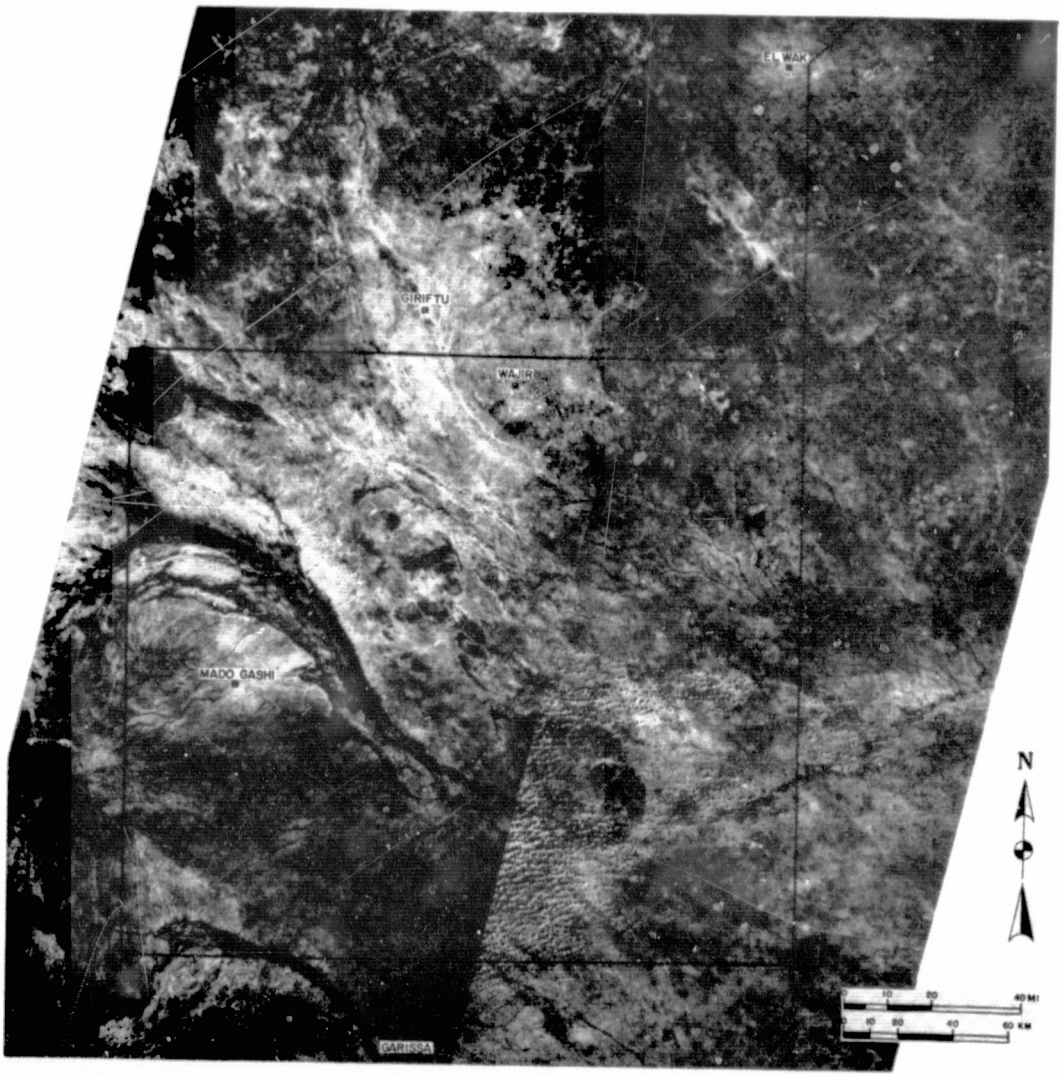


FIG. 1 **INDEX MAP**

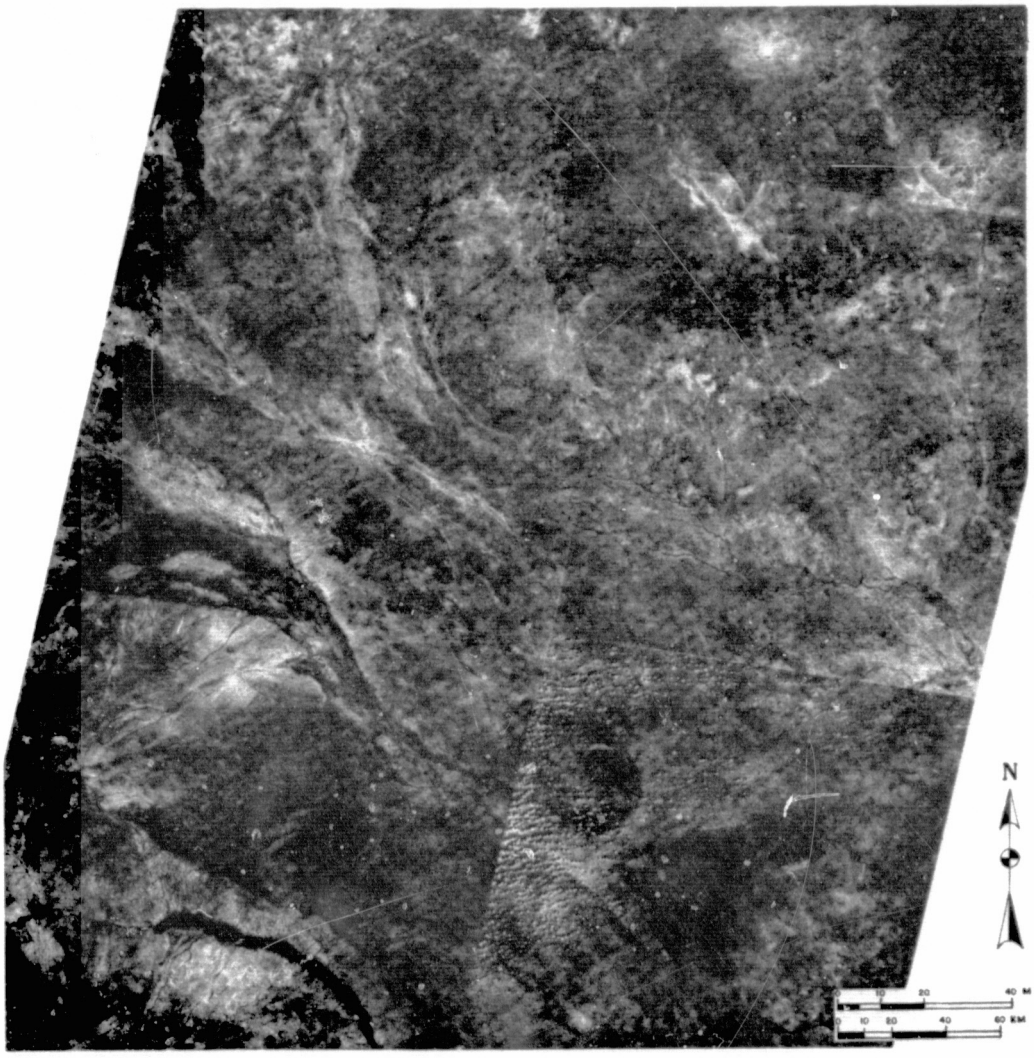


LANDSAT - IMAGE MOSAIC

GARISSA - WAJIR - EL WAK AREA

FIG. 2 KENYA BAND 7

REPRODUCIBILITY OF THE
ORIGINAL PAGE IS POOR



LANDSAT - IMAGE MOSAIC

GARISSA - WAJIR - EL WAK AREA

FIG. 3 KENYA BAND 5

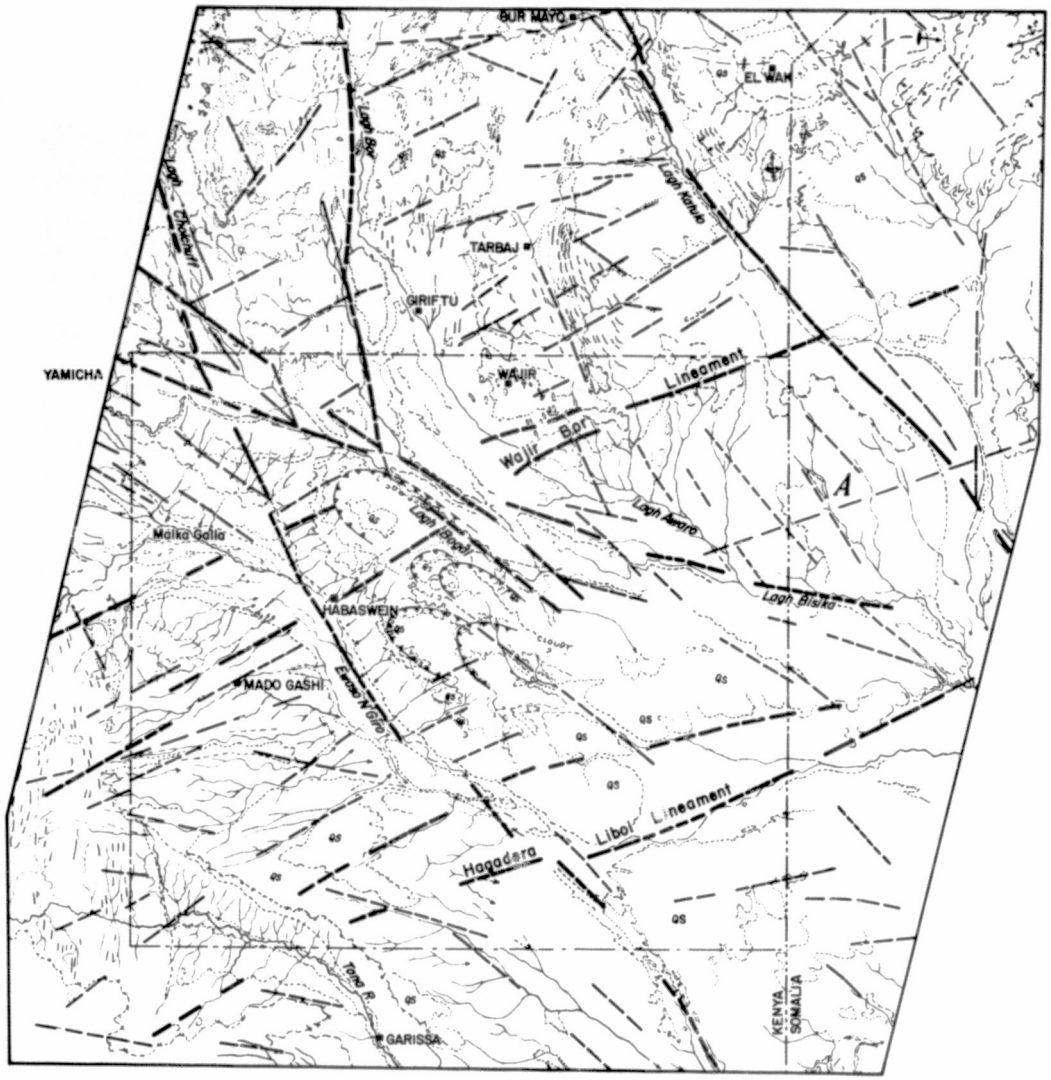
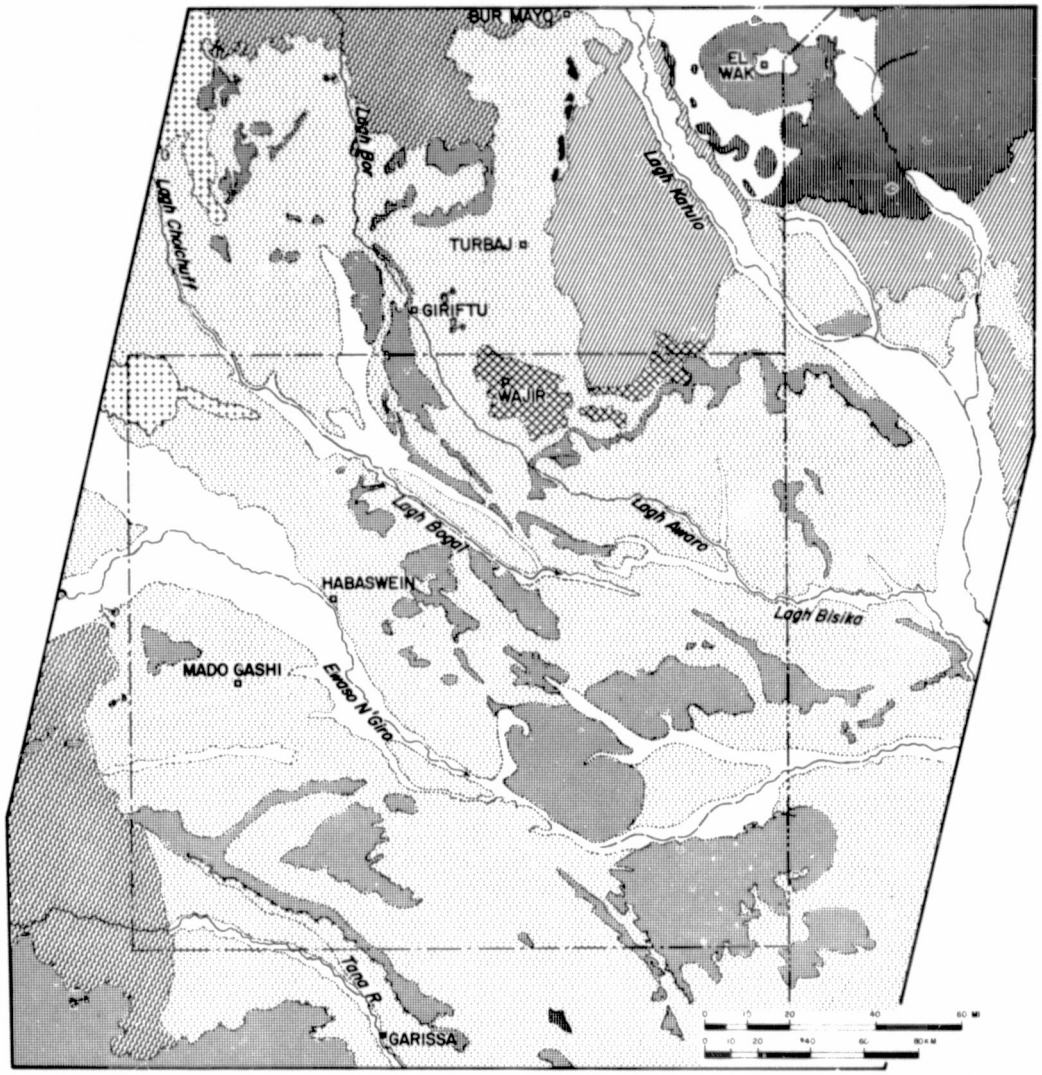


FIG. 4 LINEAMENTS, ROCK UNIT BOUNDARIES AND OTHER FEATURES AS INTERPRETED FROM THE LANDSAT IMAGERY



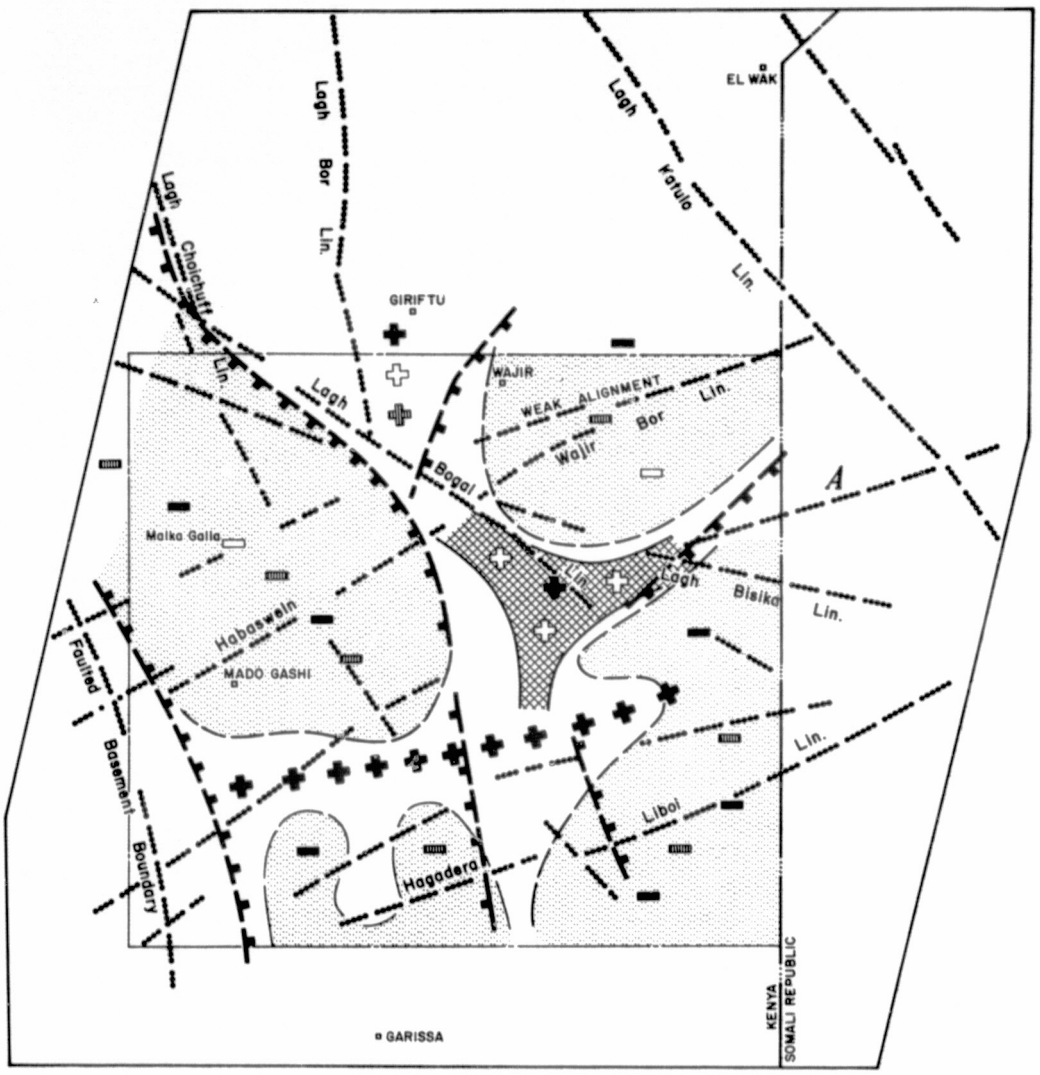
SEDIMENTARY

- RECENT ALLUVIUM & OUTWASH
- PLIO-PLEISTOCENE DEPOSITIONAL SURFACE
- CALCRETE
- PLIOCENE
- CRETACEOUS
- JURASSIC (J)
- TRIASSIC

METAMORPHIC & IGNEOUS

- TERTIARY & QUATERNARY VOLCANICS.
- PRE-CAMBRIAN METAMORPHIC (B) & IGNEOUS

FIG. 5 ROCK UNIT DISTRIBUTION, BROADLY DEFINED FROM LANDSAT IMAGERY AND OTHER SOURCES.



LEGEND

LINEAMENTS
LOW OR BASIN
INTRUSIVE HIGH
FAULT (GRAVITY OR MAGNETIC)
CHEVRON LEASE BOUNDARY

ANOMALIES AND AXES
(MAGNETIC) (GRAVITY) (SEISMIC)

HIGH
LOW
AS INTERPRETED STRUCTURALLY

FIG. 6- STRUCTURAL COMPARISON OF LANDSAT FEATURES WITH CRUDELY REPRESENTED GEOPHYSICAL DATA.

N76-17504

DETECTABILITY OF GEOTHERMAL AREAS USING SKYLAB X-5 DATA

By Barry S. Siegal*, Anne B. Kahle, Alexander F. H. Goetz,
Alan R. Gillespie, Michael J. Abrams, Jet Propulsion Laboratory,
California Institute of Technology, Pasadena, Calif.

ABSTRACT

This paper presents the results of a recent study which was undertaken to determine if data from a single near-noon pass of Skylab could be used to detect geothermal areas.

The size and temperature requirements for a geothermally heated area to be seen by Skylab S-192 MSS X-5 thermal sensor were calculated. This sensor obtained thermal data with the highest spatial resolution of any non-military satellite system. Only very large hot areas could be expected to be unambiguously recognized with a single data set from this instrument. For example, a 400 square meter area must have a temperature of 360°K or an area of 100 square meters must have a temperature of 480°K in order for one resolution element to appear to be 10° above the background temperature. The study area chosen was The Geysers geothermal field in Sonoma County, California, the only geothermal area of significant size scanned by Skylab. Unfortunately, 95% of the Skylab thermal channel data was acquired within 3 hours of local noon. For The Geysers area only daytime X-5 data were available.

An analysis of the thermal channel data (10.2 to 12.5 μm) revealed that ground temperatures determined by Skylab were normally distributed. No anomalous hot spots were apparent. Computer enhancement techniques were used to delineate the hottest 100 and 300 ground areas (pixel, 75 m by 75 m) within the study region. Without exception, the hottest areas occurred on south-facing sunlit slopes. Most of the slopes were barren or sparsely grass covered. A chi square test for association between the location of the hottest ground temperatures and bare areas revealed that the observed association would occur by chance less than once in a thousand. A plot of the cosine of the angle between the surface normal of 145 bare slopes, which in general appeared to have similar albedos on aerial photographs, and the ground temperature clearly demonstrated that the hot ground temperatures resulted from solar heating. None of the geologic units appeared to be identifiable based on temperature.

The sites of known geothermal features and related man-made structures were compared to the hottest areas indicated by Skylab. Only one geothermal site, the blowout feature at Thermal Well #4, coincided with any of these areas. This 30 by 15 m site of boiling surface waters and steaming ground is the only area which fulfilled the temperature-area product requirement for detection by the Skylab X-5 detector. Field reconnaissance indicated that the other hot areas measured by Skylab reflected local effects of topography, vegetation, and micrometeorological conditions.

Data from the north-facing, shaded slopes in the study area were analyzed in the hope of better detecting heat sources because of the lower average background temperature. Within the accuracy of individual pixel locations, the hottest areas appear to coincide with marginally sunlit peaks. No geothermal sources were detected.

In conclusion, and not surprisingly, the Skylab MSS with the X-5 thermal detector does not have sufficient spatial resolution to locate unambiguously from daytime data any but the largest and hottest convectively created geothermal features, which in general are prominent enough to have been previously recognized.

INTRODUCTION

With the continued demand for energy, speculation has arisen on the possible use of satellites for the detection of geothermal areas. However, not until the advent of

*National Research Council Resident Research Associate

Skylab has any non-military satellite had sufficiently high thermal or spatial resolution to have even the theoretical capability of detecting any but the most prominent areas.

The Skylab multispectral scanner (S-192) imaged the ground in 13 wavelength bands in the visible, reflective infrared and thermal infrared spectral regions, with an instantaneous field of view of approximately 75 by 75 meters. The thermal infrared portion of the spectrum in the region of 10.2 to 12.5 μm was measured during the Skylab missions at various times by one of two detectors. During the first two missions and part of the third, thermal infrared data were acquired by the Y-3 detector. This detector was exceptionally noisy and did not attain the expected theoretical NEΔT of 0.7°C. Consequently, the detector was replaced during the third mission with the X-5 detector which had a NEΔT of approximately 0.67°C.

Theoretically, if only one measurement can be made, the ideal times for detection of geothermal areas are either post-dawn or at sunset, since the effects of thermal inertia of surface materials are minimized at these times (1). Unfortunately, Skylab data acquisition times do not coincide with these optimal times. Over 95 percent of the thermal infrared data obtained with the X-5 detector was acquired during the day within three hours of local noon.

This paper presents the findings of a recent study which was undertaken to determine if data from a single Skylab near-noon pass could be used to detect warm ground in a known geothermal area.

DETECTABILITY OF GEOTHERMAL AREAS BY SATELLITE

The applicability of Skylab in detecting a known geothermal field can be determined, in part, from the spatial and thermal resolution of the detector and the size and temperature of surface geothermal features. Ground temperatures are determined by measuring the flux of ground infrared radiation which reaches the spacecraft sensors. The sensor integrates the flux over a resolution element and provides a signal corresponding to an area weighted average temperature after calibration.

The flux emitted by a surface of temperature T is $\varepsilon\sigma T^4$, where ε is the emissivity of the surface, which is assumed here to be 1.0, and σ is the Stefan-Boltzmann constant.

The Skylab thermal imaging system yields an average temperature over a ground area, A, of approximately 75 meters by 75 meters (a pixel). If a smaller area, a, at a hotter temperature, T_H, exists within the resolution element A, the measured value (T_s) will be the total flux from the various temperature sources

$$A \sigma T_s^4 = a \sigma T_H^4 + (A - a) \sigma T_g^4 \quad (1)$$

where T_g is the average temperature of the remainder of the pixel. Solving for a we have

$$a = \frac{A(T_s^4 - T_g^4)}{(T_H^4 - T_g^4)} \quad (2)$$

Equation 2, which ignores the effects of atmospheric absorption and the effect of restricting the spectral response of the detector to 10.2 to 12.5 μm, can be used to establish the size and temperature of an anomalously hot area which could be detected by Skylab sensors. This anomalously hot area must be hot enough and/or large enough to raise the integrated temperature T_s (which is based on the flux sensed by the satellite) significantly higher than the sensed temperature of the surrounding pixels. A background temperature, T_g, of 280°K is assumed for the normal temperature of the sensed pixel and its surroundings. The size and temperature relationship for detectability at various levels of T_s above the background temperature, T_g, are shown in Figure 1. As indicated, a hot area 16 meters by 16 meters at a temperature of 360°K would raise the sensed temperature, T_s, by 5° to

285°K. Clearly, geothermal areas must be hot and/or large to be unambiguously detected by Skylab sensors.

In a few localized geothermal areas, the heat flow is as high as 10,000 HFU (heat flow unit = 10^{-6} cal/cm^2 sec). This is in marked contrast to the normal terrestrial heat flow which is about one to two HFU. A rough "rule of thumb" is that a heat flow of 100 HFU will raise the affected surface area by approximately 1°C. The very large heat flow in some geothermal areas is generally due to steam and hot water convecting heat to or very near the surface. These areas are usually characterized by the presence of hot springs, hot pools, geysers, and steaming ground. As an example, Wairakei, New Zealand has areas as large as 1/2 km x 1/2 km with a heat flow of 10,000 HFU, within areas 10^3 km^2 that have an average heat flow of 50 HFU (2). On the other hand, since the surface material of the earth is a poor thermal conductor, when the heat is not convected to the surface, large geothermal reservoir regions may exhibit only very slightly elevated heat flows depending on source strength and depth of burial. The known geothermal areas in Larderello, Italy, the Salton Sea area of California, and The Geysers in California have surface heat flows of only about 15 HFU (3) or only about one order of magnitude above normal.

STUDY AREA

The study area chosen was The Geysers geothermal field in Sonoma County, California, which is one of the few producing geothermal fields in the world. This area has been studied extensively using both ground and aerial survey techniques, (see 4, 5, 6, 7, 8, 9, 10). This area was potentially suitable for study not only because of the extensive amount of "ground truth", but also because geothermal anomalies, although small, have been identified and delineated on day and night aerial thermal infrared images (7). These anomalies may result from the convective transport of hot fluids in naturally occurring hot springs or steam vents. At least one such area was known to exist in The Geysers geothermal field.

Description of the Site

A 15 by 12 km area in The Geysers geothermal field was chosen for study (Figure 2). The topography of this region is characterized by northwest trending valleys and ridges. Relief varies from 400 to 1100 meters. Drainage for the area is through Big Sulphur Creek, Squaw Creek, and Little Sulphur Creek, which all feed into the Russian River to the southwest. The climate is Mediterranean, and most of the precipitation occurs in the winter; summers are hot and dry. Vegetation consists of seasonal grasses, scrub bushes and some trees.

The main geothermal activity occurs in the valley occupied by Big Sulphur Creek and along Geyser Canyon, trending north from The Geysers Resort. The south-facing slopes along Big Sulphur Creek are barren or sparsely grass covered with occasional scrub brush and trees along drainages, whereas north-facing slopes are predominantly tree covered.

The Geysers area is underlain by the Jurassic-Cretaceous Franciscan Assemblage (see Figure 3), a complex eugeosynclinal sequence of chert, greenstone, graywacke and sedimentary breccia, and sedimentary and tectonic melange. The Franciscan Assemblage is overlain by Jurassic metamorphosed ultramafic rocks and serpentine.

Extrusive volcanic rocks of Pliocene-Pleistocene age occur near the study area. These include the Clear Lake series, which extends to within 8 km of The Geysers area, and rhyolite flows which cap Cobb Mountain just northeast of the area.

The area has undergone complex faulting, trending predominantly northwest, producing a series of horsts and graben. The individual horsts and graben are 2-3 km wide and extend for up to 15 km (Figure 3).

The Geysers is one of numerous thermal areas within one of these northwest-trending graben. McNitt's (6) interpretation indicates 4 km of vertical displacement along this graben. It is possible that this displacement has provided channels for the ascension of heated fluids, which could be the source for geothermal activity in the area.

Recent detailed geologic mapping of The Geysers region by McLaughlin (11) shows that the area is extensively covered by Quaternary landslide deposits. Hydrothermal alteration is prevalent, predominantly along fault zones, and transcends lithologic boundaries.

DATA ANALYSIS

Skylab digital data of The Geysers geothermal area was obtained from Johnson Space Center on computer compatible magnetic tapes. A geometric correction was applied to the digital data to compensate for skew caused by the earth's rotation during acquisition of the image. The image was then geometrically registered to 7-1/2' topographic base maps of The Geysers region (The Geysers and Asti, California quadrangles). Contrast in the rectified image was then increased to distribute measured brightness levels (DN) over the entire dynamic range of the photographic film used for display of the digital image. This process increases the investigator's ability to discern contrast variations in the picture.

As a first step in the recognition of the hottest ground areas within The Geysers region, a probability density function which describes the frequency of occurrence of DN within an image was produced of ground temperatures from the Skylab data. No anomalous hot spots were detected; rather, ground temperatures were normally distributed. If geothermal areas are to be distinguishable, their temperatures must be measurably higher than their surroundings. Nevertheless, in an effort to delineate the hottest 100 and 300 ground areas (pixels), computer enhancement techniques were used. These results are displayed in Figures 4 and 5. The hottest areas are black. The next lower temperatures are displayed as medium gray and decreasing ground temperatures are in diminishing shades of gray, the coolest areas are white. Although there appears to be an extreme contrast between the hot areas and their surroundings, this is due to the enhancement procedure; actual temperatures differ less than 1°C between the coolest of the black areas and the darkest gray regions. Stream channels and other pronounced physiographic features can be recognized and matched to the same features in the topographic map (Figure 2).

From inspection of Figures 4 and 5, it is apparent that all of the hottest areas occur on south-facing slopes. It is also apparent that the clusters of the top 300 pixels are primarily an expansion of the clusters of the top 100, indicating that these are probably true hot areas and not noise in the data.

The location and distribution of known geothermal areas and related man-made structures (Figures 6 and 7) were compared to the hottest ground areas indicated by Skylab. Only one cluster of pixels (cluster A on Figure 4) appeared to coincide with a known geothermal feature. This suggested that either unknown geothermal areas existed within The Geysers region, or more probably, that the hottest areas indicated by Skylab were those most favorably oriented to receive solar radiation and having a minimum amount of vegetative cover.

Recent aerial photographs of The Geysers region at a scale of 1:20,000 were examined and revealed that almost all of the south-facing slopes were barren or sparsely vegetated. To statistically test the association between bare areas and the clusters of pixels representing the hottest 100 ground temperatures, a 3 x 3 pixel grid was constructed and placed over the study area. The observed association between these variables was then tabulated in a contingency table and a chi square test was performed. The expected χ^2 value for 1 degree of freedom at $P_{.001}$ is 10.8, whereas the observed χ^2 value is 102.6. Consequently, it is concluded that the observed association between bare areas and hot spots would occur by chance much less than once in a thousand times.

The slope angle and azimuth for 145 barren and sparsely vegetated slopes, outlined

within the boundaries of the 3 x 3 pixel grid, were measured. The cosine of the angle between the normal to these slopes and incident solar radiation was plotted against the average DN values (Figure 8). Despite the large scatter of data, the expected relationship between temperatures and solar radiation is apparent. If areas with significant geothermal heating are present, their distribution of points on Figure 8 should lie above and to the left of the main distribution. The large scatter of data precludes unambiguous identification of any geothermally heated area in the study region. Furthermore, refinement by analyzing each geologic unit separately did not reduce the scatter.

Another possible explanation for the occurrence of anomalous hot areas is that geologic units may contrast thermally because of differences in reflectivity and thermal properties. To test this possibility, the locations of the top 100 and 300 pixels were compared to the most recent detailed geologic map of The Geysers region (Figure 3). The hot areas appeared to be independent of geologic unit. Thus, it appears that almost all of the hottest ground areas detected by Skylab resulted from solar heating of barren ground. However, at this point, it was not certain whether any geothermal areas within the study region were detectable in the Skylab data. Therefore, a field reconnaissance was undertaken.

FIELD RECONNAISSANCE

Field reconnaissance was undertaken in The Geysers region to try to determine the cause of the anomalous heating occurring at the location of the pixels representing the hottest temperatures. One cluster of these pixels (cluster A in Figure 4) coincided with the highest thermal anomaly seen by Moxham (7) in daytime and nighttime infrared images of The Geysers region. This area includes a large geothermal region of boiling surface waters and steaming ground about a blown-out steam well, Thermal Well #4. The highest temperature value within the cluster occurs at the well location.

The hottest ground temperatures within this region occur in a hydrothermally altered area approximately 15 by 30 meters in size. Although measurements of subsurface temperatures at a depth of a few centimeters were consistently near boiling, surface occurrences of boiling water and steam were patchy. Between these very hot areas, surface temperatures were only slightly to moderately elevated due to apparent evaporative cooling.

Several drilled vents in the immediate area are forcefully venting steam, which combined with the steaming ground, produced a large steam cloud to a height of about 100 meters over the entire area. Temperature of the venting steam at the smallest drilled hole was 125°C at the top of the well casing, decreasing to 70°C two meters above the well casing.

Although steam wells, small steam vents and minor surface springs were observed in the immediate surrounding areas corresponding to the remaining pixels in cluster A, it was impossible to determine if there was sufficient geothermal heat flow to enhance the surface temperature measurably. These regions are steep, barren or sparsely grass covered, have south-facing slopes, and receive substantial solar heating.

Based upon these field observations, it appears certain that the geothermal heating about Thermal Well #4 was detected by Skylab. The actual temperature measured by Skylab was 25°C for the pixel coinciding with Thermal Well #4, which is 4°C hotter than the next hottest pixels immediately adjacent. This temperature is reasonable in view of the effects of evaporative cooling, masking of the ground by steam clouds, and averaging of temperatures over an area larger than the anomalously hot region about Thermal Well #4.

An extensive network of steam pipes leads from the wells to power plants and cooling units in many parts of the study area. None of these structures are hot enough or large enough to be identified by Skylab.

The hottest temperature within The Geysers region seen on the Skylab images did not

occur near Thermal Well #4 nor near any other known geothermal site. It is located above Squaw Creek (cluster B in Figure 4) on a steep, barren, southeast-facing slope comprised of dark greenstone. Between outcrops, slopes were thinly covered with dry grass. No surface indications of geothermal activity were found.

Clusters C and D are located above Squaw Creek and also contained some of the hottest temperatures (Figure 4). They were similar in all respects to cluster B.

Cluster E is located on the northwest side of Cobb Creek (Figure 4). The southeast-facing slopes are more heavily grass covered, less steep, and have fewer rock outcrops than the Squaw Creek locations. The slopes are concave and form a sheltered valley. Therefore, local meteorological effects may also have added to the heating of this region. Minor occurrences of warm springs indicate geothermal activity in the general vicinity, which may also enhance the heating.

Cluster F on Figure 4 is located at the abandoned Cloverdale Mine. Although it does not include one of the highest 10 temperatures, this cluster was investigated because of the mapped occurrence of hydrothermally altered rocks, (Figure 3), and reports of H_2S gas. The slopes are steep, southeast facing and sparsely grass covered. Extensive mine dumps of chert mantle the slopes below the Cloverdale Mine. The hottest temperature in the cluster coincided with graywacke outcrops above the dumps. No geothermal activity was noted.

All the aforementioned locations except Thermal Well #4 had concave, sheltered slopes, though to a lesser degree than at Cobb Creek.

Areas of known but unpublished geothermal activity were investigated and no correlation could be found with the top 300 pixels on the Skylab image. All of these areas were either heavily vegetated or located on flat, west-facing or north-facing slopes.

In view of the preceding results, it appears clear that geothermal areas with surface features of the magnitude of The Geysers area cannot be unambiguously identified in areas undergoing solar heating.

ANALYSIS OF NORTH-FACING SLOPES

An attempt was made to make use of shadowed, steep slope areas as simulated nighttime images. Better detection of geothermal areas might be expected here because of lower average surface temperatures. The temperatures of the north-facing slopes within The Geysers region were extracted for the daytime X-5 thermal channel. The highest 100 temperatures within these regions were set to black and displayed in picture form (Figure 9). Within the accuracy of pixel location, the ground areas with highest temperatures coincided with marginally sunlit ridges or slopes. No thermal sources were detected in the shadowed areas.

CONCLUSION

While it may be impossible to detect small isolated hot surface features due to lack of spatial resolution, it may be possible to locate the large areas of often only moderate conductive heat flow which may be associated with potentially valuable geothermal resources. Watson (1) has shown that it may be theoretically possible to detect geothermal heat flow of only a few tens of HFU by remote sensing of the surface temperature at several carefully chosen times of the day, combined with computer modeling of the surface heating. However, this assumes that all the heating processes at the surface can be modeled with accuracy comparable to the size of the heat flow. Since radiative heating is of the order of 10,000 HFU, and the extremely variable meteorological heating terms can also be of this magnitude, any such detection of geothermal heat flow would require many measurements under ideal meteorological conditions, combined with a sophisticated surface heating model.

In summary, Skylab does not have sufficient spatial resolution to discern any but the largest and hottest, convectively created geothermal features, which in general are large enough to have been previously detected.

ACKNOWLEDGMENTS

We would like to thank Peter Paluzzi and George Baker of the Image Processing Laboratory, of JPL for computer processing of data; Shirley Hauser of USGS for invaluable aid in data reduction and Robert Ward of Johnson Space Center for producing and supplying color-coded Skylab data.

We also appreciate the courtesy extended to us by Burmah Oil Company and Union Oil Company for providing access to their lands and the assistance of their geologists Tom Box and Jim Moore.

Howard Pohn provided valuable assistance in the location and interpretation of anomalous areas during the initial stages of this investigation.

The paper is the result of research carried out at the Jet Propulsion Laboratory, California Institute of Technology, under Contract NAS7-100, sponsored by the National Aeronautics and Space Administration.

REFERENCES

1) Watson, K., 1975, Geologic applications of thermal infrared images; Proc. I.E.E.E., 63, 128-136.

2) Elder, J. W., 1965, Physical processes in geothermal areas; in Lee, W.H.K. (ed.), Terrestrial Heat Flow, Geophys. Monograph Series, #8, Amer. Geophys. Union.

3) McNitt, J. R., 1965, Review of geothermal resources; in Lee, W.H.K. (ed.), Terrestrial Heat Flow, Geophys. Monograph Series, #8, Amer. Geophys. Union.

4) Allan, E., and Day, A., 1927, Steam Wells and Other Thermal Activity at "The Geysers" California: Carnegie Inst. Washington pub. 378, 106 pp.

5) California Division of Mines and Geology, 1966, Gravity Map of Geysers Area, Mineral Information Service, Vol. 19, 148-149.

6) McNitt, J., 1968, Exploration and Development of Geothermal Power in California: California Division of Mines and Geology Special 75, pp. 1-44.

7) Moxham, R., 1969, Aerial Infrared Surveys at The Geysers Geothermal Steam Field, California: U.S.G.S. Professional Paper 650-C, pp. C106-C122.

8) Stanley, W. D., Jackson, D. B., and Hearn, B. C., 1973, Preliminary Results of Geoelectrical Investigations Near Clear Lake, Calif., U.S.G.S. Open File Rpt. #73-270.

9) U.S.G.S, 1973, Aeromagnetic Map of the Clear Lake Area, Lake, Sonoma, Napa and Mendocino County, Calif., Open File Rpt. #73-299.

10) Chapman, Rodger H., 1975, Geophysical Studies in the Clear Lake Region, Calif., Calif. Div. Mines and Geology, Special Rpt. #116, 23 p.

11) McLaughlin, R., 1974, Preliminary Geologic Map of The Geysers Steam Field and Vicinity, Sonoma County, California: U.S.G.S. open file map.

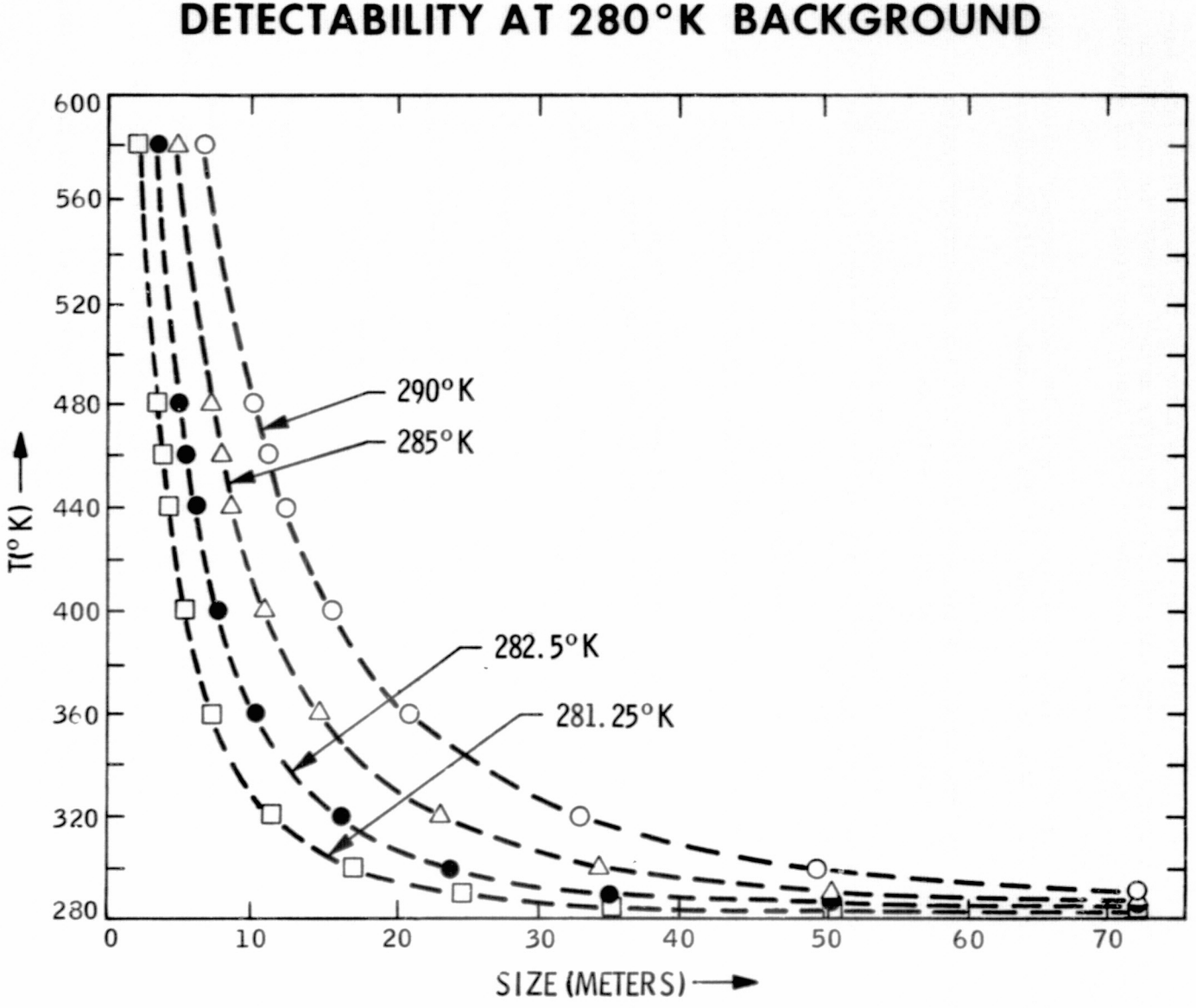


Figure 1. Detectability of thermal anomalies as a function of size and temperature.

REPRODUCIBILITY OF THE
ORIGINAL PAGE IS POOR

Figure 2. Topographic map of a portion of the Kelseyville 15' Quadrangle showing The Geysers geothermal region.

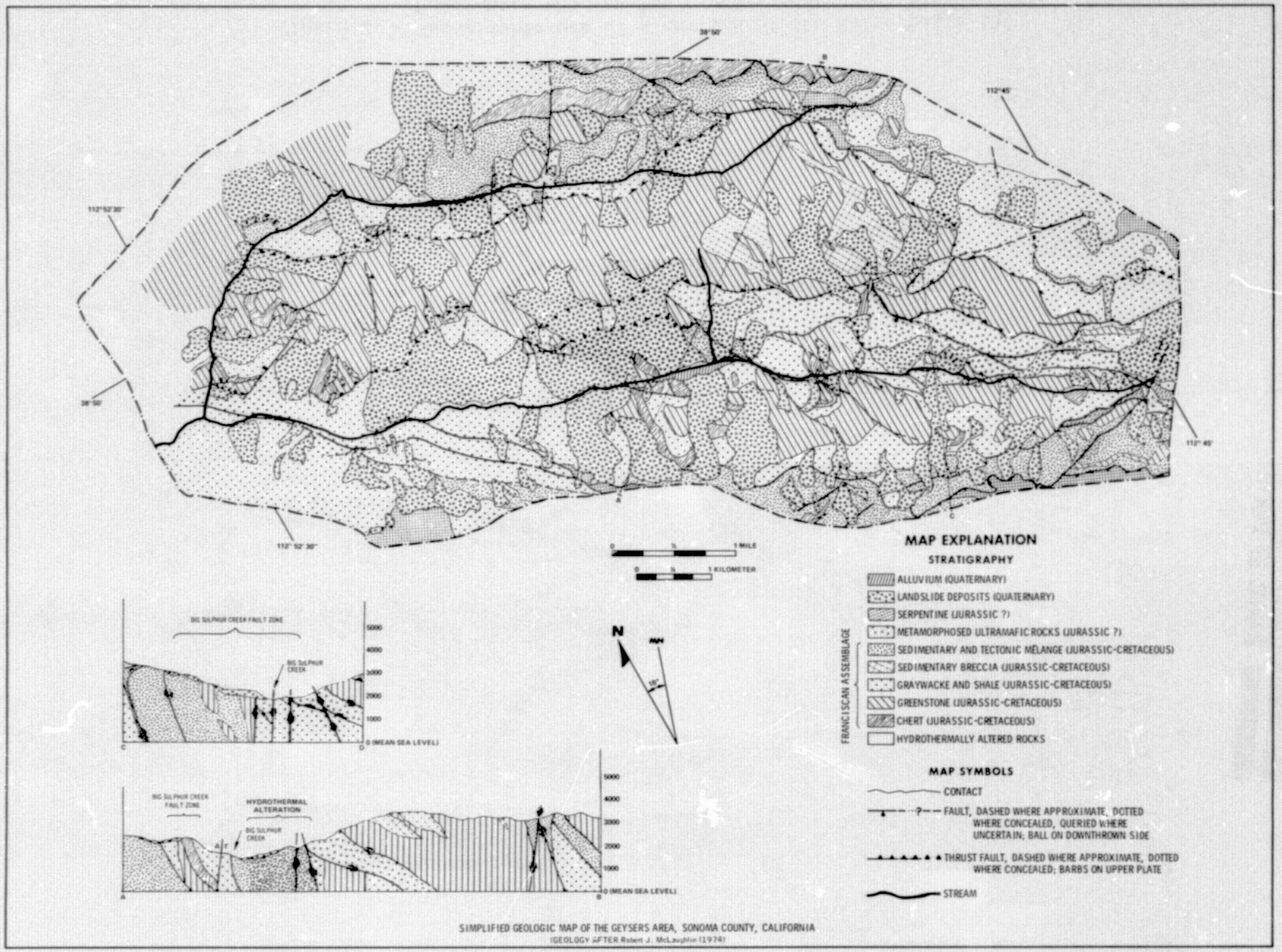


Figure 3. Generalized geologic map of The Geysers area after McLaughlin (11).

REPRODUCIBILITY OF THE
ORIGINAL PAGE IS POOR

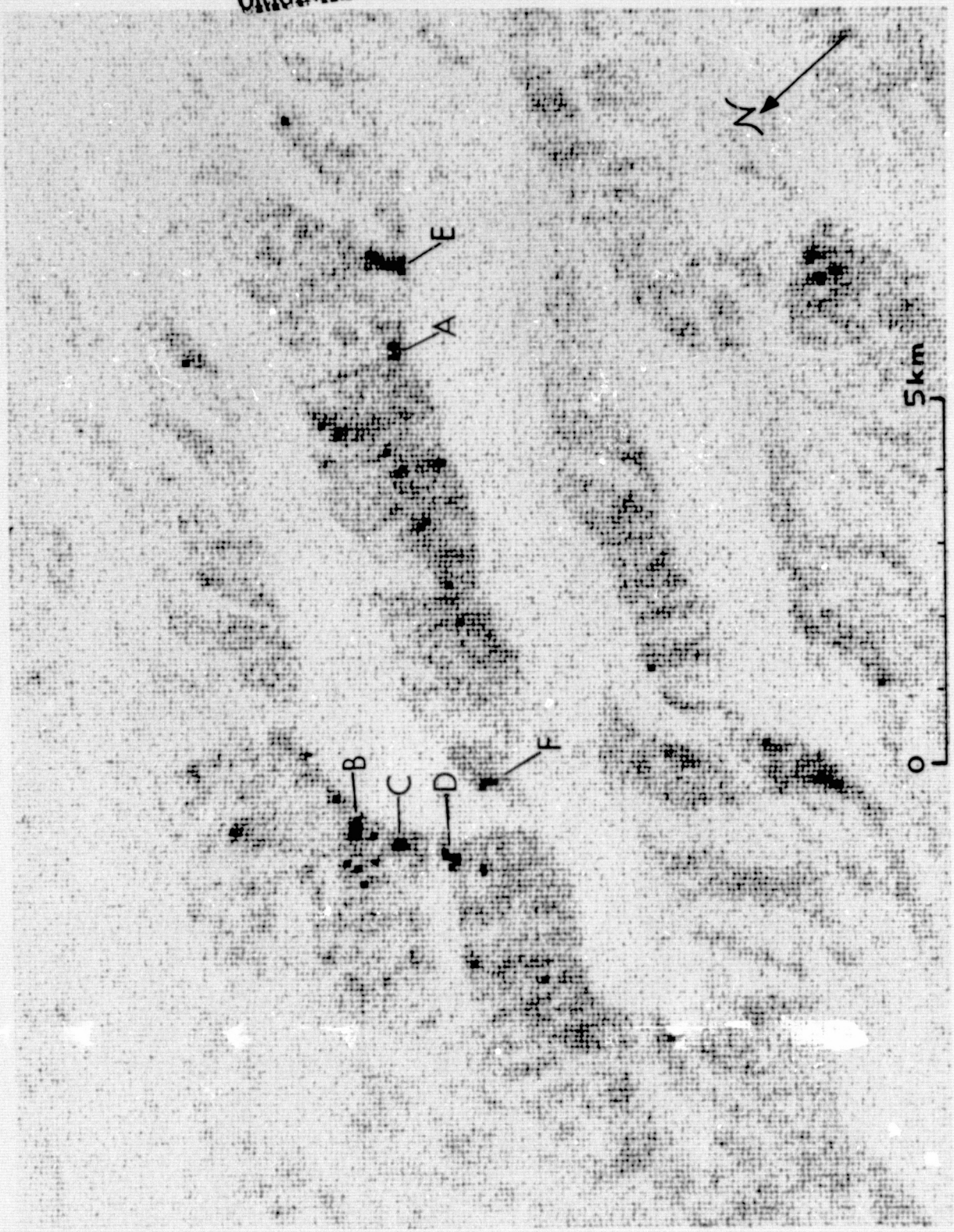


Figure 4. The Geysers region at 10.2-12.5 μm, computer enhanced to show the pixels representing the 100 hottest temperatures.



Figure 5. The Geysers region at 10.2-12.5 μm, computer enhanced to show the pixels representing the 300 hottest temperatures.

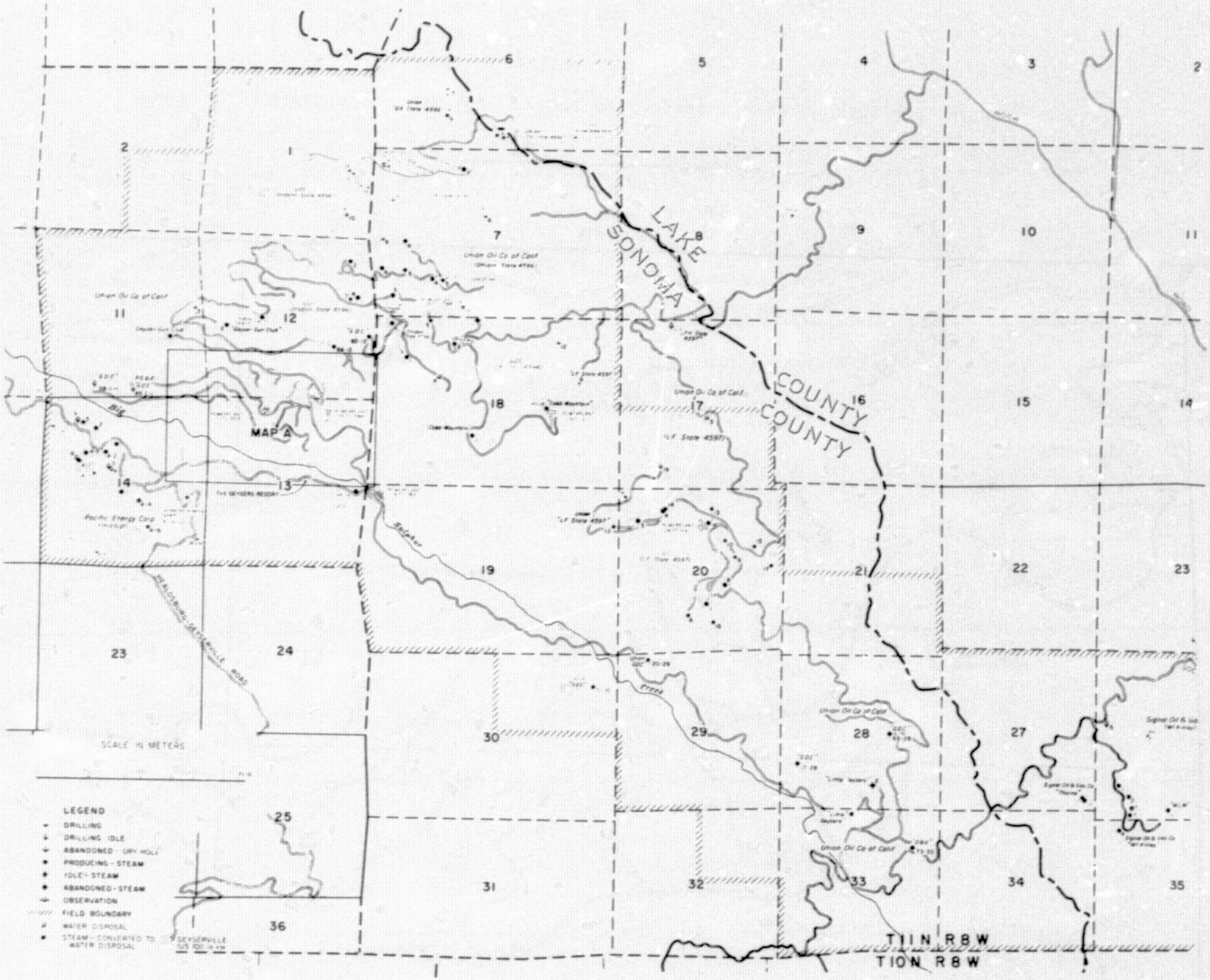


Figure 6. Location map of geothermal wells and power plants in The Geysers area. (After State of California Division of Oil and Gas, 1974.)

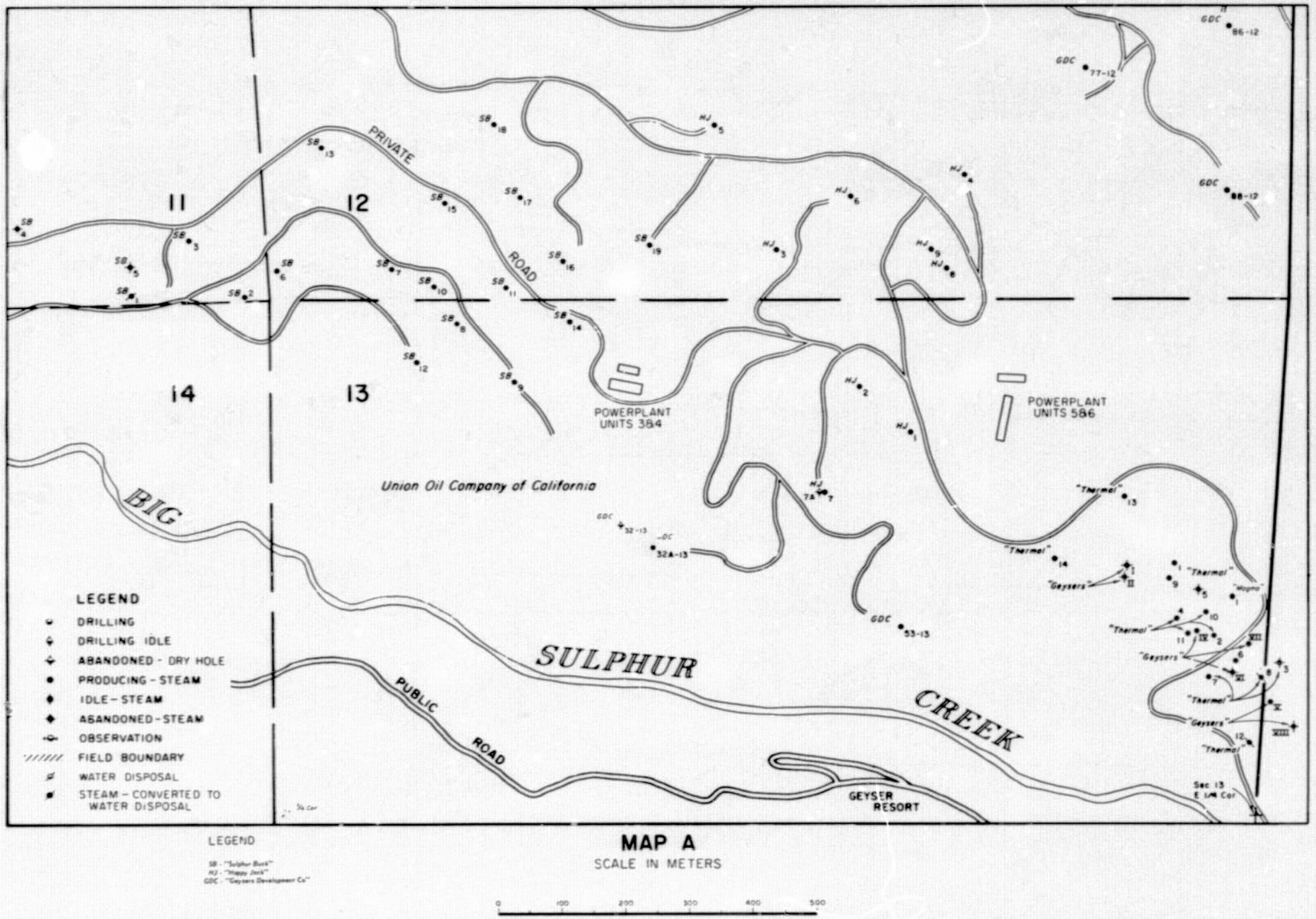


Figure 7. Detailed map of The Geysers and adjacent area showing locations of wells.

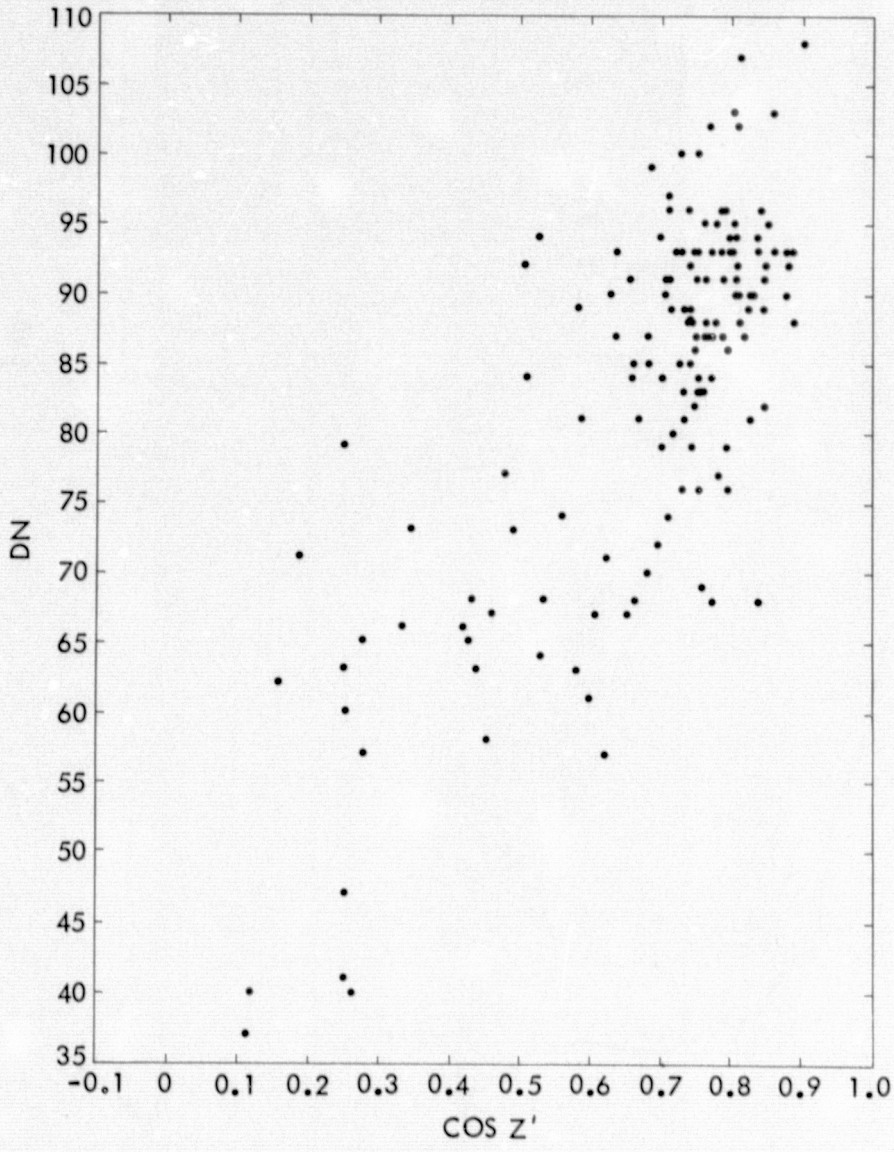


Figure 8. Graph of DN versus cosine of the angle between slope normal and sun (Z').

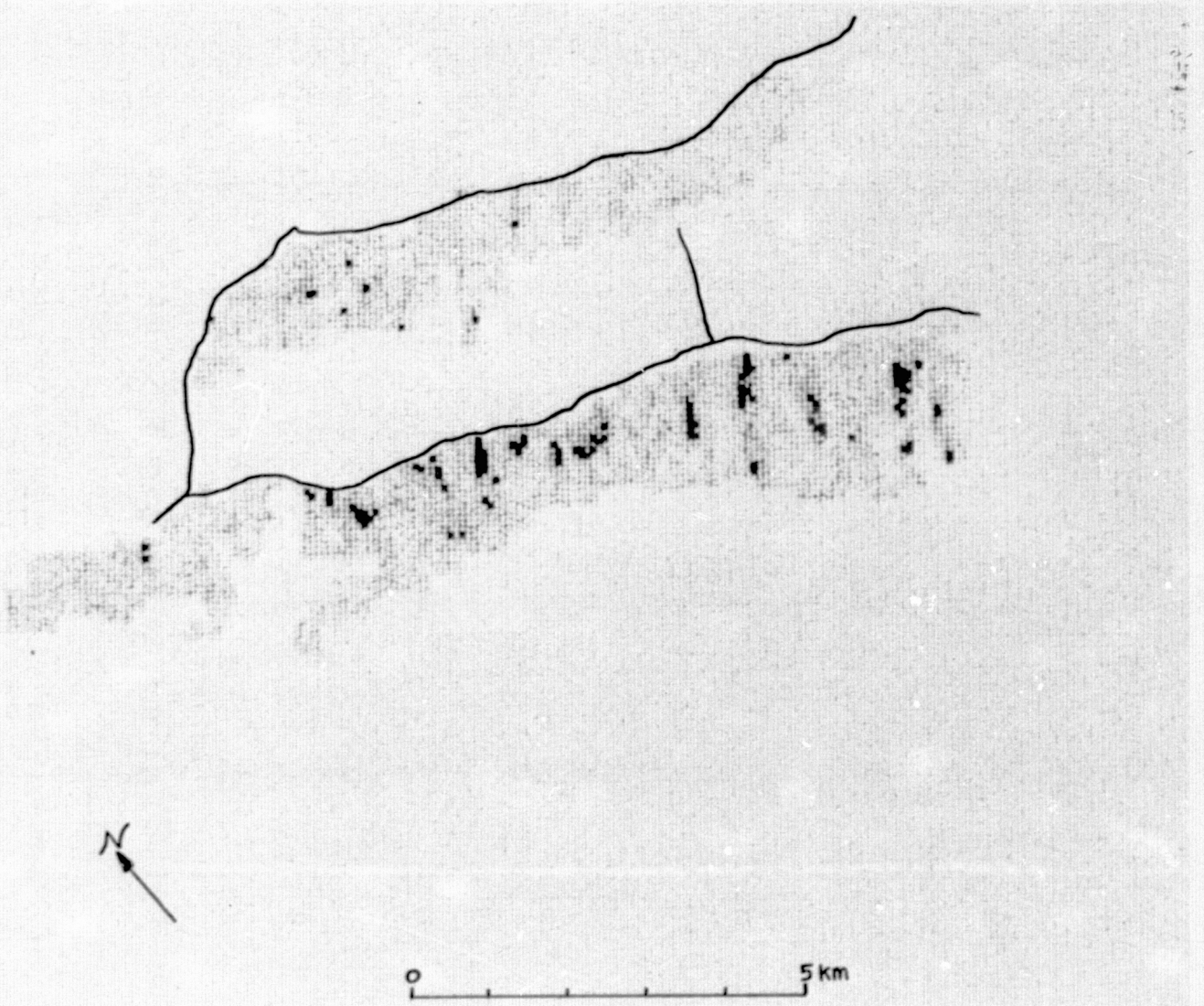


Figure 9. Extracted north-facing slopes of The Geysers region. The hottest ground areas are black.

THE ANATOMY OF AN ANOMALY

G-5

By Nicholas M. Short, Earth Resources Branch, Goddard Space Flight Center, Greenbelt, Maryland 20771 and Ronald W. Marrs, Department of Geology, University of Wyoming, Laramie, Wyoming 82071

N76-17505

ABSTRACT

An anomalous tonal pattern, apparently associated with the Beaver Creek Oil Field in central Wyoming, has been identified by R. K. Vincent using an MSS Band 5 to 4 ratio image made from digital LANDSAT data. He has attributed this pattern to an increase in iron with rocks and/or soils which might have resulted from escaping hydrocarbons.

The nature of this anomaly has been investigated by geologists at Goddard Space Flight Center and University of Wyoming by producing several different combinations of band ratios and by conducting appropriate field studies. The results indicate 1) the existence of a well-defined oval feature related to exposure of iron-cemented red sandstones in a badlands topography, 2) a broader iron-influenced anomaly surrounding this feature, and 3) a spectral response of the rocks, soils, and alluvium making up this iron-colored surface that is readily distinguishable from that of iron-rich reddish Chugwater siltstones exposed in nearby anticlines. The general pattern of the broad anomaly extending beyond the Beaver Creek Field is controlled by several factors including variations in vegetation (mainly sage and tall grasses), soil composition and moisture, and topography in addition to variations in iron content of the rock materials. From the available evidence, there is no provable correlation between the oval or the broad anomalies and the distribution of petroleum-producing structures or possible surface alteration effects related to uranium deposits known to occur within this region.

INTRODUCTION

Since the launch of the first LANDSAT, investigators have used the imagery and supporting data in two specific applications of direct value to mineral exploration.

The first takes advantage of the remarkable ability of LANDSAT images to highlight both localized and regional linear features of a geological nature. Some of these linears have subsequently been field-checked and prove to be previously unknown major fracture zones and/or faults. Because of the well-known role of large lineaments in the crust — especially where they intersect — in providing avenues of migration and emplacement of mineralizing solutions, these new discoveries offer many more targets for extensive exploration.

The second application seeks to look for evidence at the surface of alteration products associated mainly with (usually shallow) metallic ore bodies also indicative in some cases of other types of mineral deposits. Common alteration effects include hydrated iron oxides (gossans), colorful stains or blooms consisting of secondary minerals derived from copper, nickel, cobalt, uranium and other metals, and characteristic clay minerals formed from decomposition of host rocks. In a few instances, such alteration effects can be observed in standard black and white or color composite LANDSAT images. However, reprocessing through several computer-based techniques designed to enhance the images by manipulating spectral and radiometric differences among surface materials as sensed by the four MSS bands has proved successful in several studies. Contract stretching, or shifting the dynamic range of the grey levels recorded in black and white images, is a simple but effective means of bringing out subtle details from surfaces. Band ratioing is a more elaborate approach that involves pixel-by-pixel comparison of the relative radiances of any pair of MSS bands. This is accomplished by dividing the reflectance of any one pixel for one band by the reflectance measured for that pixel in any other band.

R. K. Vincent (1973) has applied this ratio technique for LANDSAT MSS bands 5/4 to discriminate red and yellow colors due to hematite and limonite in surface coatings or pervasively distributed through iron-rich rocks (e.g., cements in siltstones) from colors associated with rocks lacking significant amounts of these minerals. He demonstrated this technique by strongly emphasizing the surface expression of the Triassic Chugwater Formation as it outcrops within and adjacent to the Wind River Basin of central Wyoming. In the field and hand specimen, the Chugwater is a deep reddish-brown to reddish-orange. The beds tend to be uniquely defined in the usual false color composites of LANDSAT imagery by a distinctive mustard yellow tone. In a 5/4 ratio, the red color contributes a much higher reflectance value to Band 5 than is added to Band 4 by any associated green vegetation. A black and white print of a ratio image (using each ratioed pixel to produce the scene) displays the Chugwater as a very light grey against a much darker overall background. In principle, some tonal differences (shades of light grey) should be distinguishable between red Chugwater pigmented by hematite and several other iron-bearing sedimentary units in the Wyoming stratigraphic section that are colored lighter yellowish-brown (e.g., Nugget and Dakota Formations) to orange-brown (e.g., Phosphoria and some Nugget units).

A. F. H. Goetz and co-workers have extended the band ratio technique to allow combinations of several different ratio pairs (e.g., 7/4, 6/5, 5/4) to be expressed as ratio color composites. The image of each ratio pair is projected through a color filter as though it were a single band. This combination frequently leads to better enhancement and visual separation of small differences in surface coloration that can be tied to variations in soil and rock types. Using this technique, Rowan et al. (1974) have detected several types of alteration products in the Goldfield, Nevada mineral district and have also been able to discriminate between mafic basalts and andesites and felsic intrusive and extrusive igneous rocks in the same area. This multiple ratio compositing seems to work best for surfaces that show only moderate to slight contrasts in the standard composites and are dominated by rock materials with only minimal vegetation cover.

The band ratio technique is being employed by the Geology Group of the Earth Resources Branch at Goddard Space Flight Center in its investigation of the usefulness of LANDSAT imagery in exploring for oil and gas. One objective of this program is to search for any evidence detectable in LANDSAT of surface alteration owing to escaping hydrocarbons. The possibility that such alteration effects can produce significant changes in lithology (mainly color and composition) and soils and perhaps also vegetation is supported by observations of T. J. Donovan (1974) at the Cement and other petroleum-producing fields in the Anadarko Basin of Oklahoma-Texas. A joint study of similar surface manifestations above oil and gas fields in several intermontane basins of Wyoming, as displayed in LANDSAT-1, Skylab-EREP, and aircraft data, is now underway at the co-authors' institutions.

Recently, R. K. Vincent (1975) has published a report of a 5/4 ratio enhancement of LANDSAT imagery that discloses a strong anomaly seemingly associated with the Beaver Creek oil field about 12 miles south of Riverton, Wyoming near the southwestern edge of the Wind River basin. He postulates this anomaly to be a ferric iron alteration effect brought about by hydrocarbons leaking to the surface. The anomalous pattern in the ratio image is proximate to the Beaver Creek producing structure but does not clearly coincide with it.

Because of the promising nature of that anomaly as a further confirmation of the Donovan hypothesis, both Goddard and the University of Wyoming have produced their own enchanced LANDSAT images of the same area using somewhat more elaborate band ratio programs. The Goddard Geology group used LANDSAT image 1013-17294 (August 5, 1972), the same scene examined by Vincent, while Wyoming analyzed image 1373-17292 (July 31, 1973). Goddard computer-processed its scene through the VICAR program developed by the Jet Propulsion Laboratory whereas Wyoming employed the General Electric Image 100 system available at the Department of the Interior's EROS Data Facility. Both processing programs produce color versions of either single or combined band ratio images.

As described in the following sections, the results of these enhancements, coupled with supportive field work, have led to a greatly improved understanding of the nature of this type of anomaly, its potential value in exploration, and the cautions to be exercised in its application to practical problems.

DEFINITION OF THE ANOMALY

The area containing the anomaly identified by Vincent near the southwestern end of the Wind River Basin is outlined in the black and white rendition of LANDSAT-1 frame 1013-17294 (Figure 1). This area (about 33 miles E-W by 26 miles N-S) is shown in detail (Figure 2) in the enlargement of the scene produced by contrast stretching bands 4, 5, and 7 on the VICAR computer program* and combining as a color composite in the DICOMED color processor. In that version, a distinctive yellow tone near the middle of the composite defines a broad anomaly that covers about 100 square miles. The center of this broad anomaly is about 16 miles south-southeast of Riverton and 20 miles due east of Lander.

Most of the stratigraphic column from lower Paleozoic through upper Mesozoic is exposed in northeast-dipping beds along the southeast flank of the Wind River Mountains to the west. The specific area investigated at the Goddard Space Flight Center includes the oil-producing Derby and Dallas anticlines, along this flank, within which the oldest surface rocks are Pennsylvanian in age. East of the anomaly are three other producing fields — Sand Draw, Big Sand Draw, and Alkali Buttes — also expressed at the surface in units as old as Cambrian for the first-named field to upper Cretaceous for the last. In the false color image (Figure 2), the Triassic Chugwater Formation is rendered a characteristic yellowish tone, the Sundance, Morrison, and Dakota units appear in medium brown tones, and the Mowry-Thermopolis black shales (and, in places, the Cody shales) show up as a dark blue-grey to grey-brown. Other rock units between the top of the Pennsylvanian and the base of the Tertiary are indistinctly and ambiguously colored in this image.

Much of the area around the anomaly is surfaced by dissected, nearly horizontal units of the Tertiary Wind River Formation which lies unconformably on the structures listed above and on the flank beds. The Riverton and Beaver Creek fields occur north of the anomaly center but have no apparent surface expression. A number of oil well sites in the southern part of the Beaver Creek field are clustered within the northern third of the broad anomaly. Further south, younger Tertiary continental sediments form a flat-topped topographic bench some 500 feet higher than the rolling hillocks closer to Riverton; the receding escarpment marking the juncture between the lower Wind River and higher White River beds is known as the Beaver Divide. A granite outlier — part of the Sweetwater Mountains complex — lies within the area considered.

Most of this area is displayed in detail in the aerial photomosaic reproduced in Figure 3. This mosaic was prepared by Aero Service from hundreds of high resolution aerial photos obtained during the summer of 1952. The LANDSAT-1 Band 5 image equivalent of this same area as well as the region to the south and west considered in this study is enlarged as in Figure 4a. By comparing these two scenes with the photomosaic, it is evident that some of the lighter toned patterns in the Basin below the Divide coincide with "badlands" topography cut into the soft sediments of the Wind River Formation. Such topography appears brighter in the LANDSAT imagery because it 1) is underlain by fresher (less weathered or soil-covered) highly reflective sediments, 2) contains a large number of southeast-facing slopes that reflect more of the morning sun's rays to the spacecraft sensor, and 3) is generally less vegetated.

Neither the Bands 4 or 5 (Figure 4a) standard images of the area nor the contrast-stretched renditions of these bands (Figure 4b) reveal any unusual tonal patterns in the vicinity of Big Sand Draw as it enters Beaver Creek. However, a very distinct oval anomaly about 8 miles (E-W) by 4 miles (N-S) in dimension shows up in the contrast-stretched Bands 5/4 ratio (Figure 5) produced by VICAR computer-processing. A color rendition, made by assigning selected colors to grey levels in the

*This and other individual bands and band ratio images produced by VICAR for this study have not been corrected for vertical foreshortening or aspect.

ratio image; using the DICOMED system, displays this anomaly to best advantage (Figure 6). In the same ratio image, the approximate outcrop area of the Chugwater Formation in the Dallas, Derby, and Big Sand Draw anticlines is marked by the same light beige tone. There is no indication, however, of a separation in the 5/4 image between the darker reddish Chugwater beds from the adjacent orangish Phosphoria beds (lower) or yellowish-brown Nugget beds (higher).

The overall effect of this ratioing is to reduce the range and display of the various grey levels that form discrete, often recognizable patterns in either Band 4 or 5 images. Aside from the oval anomaly and nearby patches of the same beige color, the bulk of Figure 6 is colored either orange, purplish-red, or blue. In particular, a medium to darker blue (corresponding to some darker greyish-brown areas in Figure 2), seems to be associated with areas known to contain a higher density of vegetation dominated by sage brush. This vegetation is especially prominent along the flatlands above the Beaver Divide scarp, and along its northwest-facing escarpment, as well as on the slopes making up the flank of the Wind River Mountains. Very dark blue colors coincide with vegetation lining the Beaver Creek and the cultivated floodplain of the Popo Agie River near Riverton. This marks farmlands given over mainly to hay and alfalfa. Several lighter, greenish-blue areas just north of the Dallas and Derby anticlines correspond to the outcrop areas of the Mowry-Thermopolis and the Cody shales — but this color also shows up along the Beaver Divide flatlands where these rock units are absent.

A narrow blue band extends roughly east-west westward from the Beaver Creek just above the oval anomaly. This is another rendition of a dark strip seen in Figure 1. When first noticed the strip was postulated to be a soil moisture zone formed by a passing thunderstorm presumed to have occurred on the preceding day. That this is probably the case is supported by the absence of this dark pattern on any other LANDSAT image of the same area taken at different dates. It is interesting to note that the 5/4 image displays the rain shadow in the same grey or color tone as assigned to the sage. For this ratio pairing, the only contributing factor seems to be the darkness of the surface; the relative brightness of wet soil and heavy sage cover are sufficiently alike in Bands 4 and 5 to cause them to have similar spectral signatures when ratioed.

How then can these two different surface features be distinguished? The simple answer is to use Band 7 to separate them. Black and white ratio images for Bands 7/5 and 7/4 are shown in Figure 7a and b. In both, the blue areas of Figure 6 associated with the sage and the hayfields are expressed as very light grey tones. As expected, the rain shadow, however, is not similarly defined, since there is only a local contribution from normal, sparse vegetation to the high reflectance associated with Band 7.

Color coded versions of these 7/5 and 7/4 ratio pairs (Figure 8a and 8b) provide additional information. Much of the light grey tones become subdued and take on green and orange colors that persist over the image. Very heavily vegetated areas stand out in a cream-buff color. Note, too, that the cream-colored pattern is less extensive in the Derby anticline and almost absent in the Dallas anticline in the 7/5 color image relative to that of 7/4. A partial explanation is suggested by inspection of Figure 9. That ground view of the Red Canyon south of Lander reveals a vegetation-free escarpment of Chugwater beds overlying grass-covered Chugwater and Phosphoria red beds and colluvial soils in the adjacent valley. Applying this observation to the 7/4 ratio image, the strong reflectance for Band 7 from Chugwater rocks and soils (see Figure 10) and some associated grasses and a much smaller reflectance from Band 4, mainly from brownish grasses, produces a very light toned ratio that is expressed as the wide cream colored pattern within the anticlines. However, the Band 7/5 rendition highlights only the denser vegetation in nearby streams both because Band 5 reflectances from the Chugwater are not much lower than those of Band 7 outcrops and soils and because the stream-lining vegetation appears very dark in Band 4. The light area on the Beaver Creek Divide surface south of the Big Sand Draw no longer acts as typical vegetation, so that much of the reflectance contributing to the blue in that area in Figure 6 may actually result from darkish soils (in the field a rock pavement of lag gravels (?) was noted in parts of this area). In many places, the blue colors in Figures 8a and 8b coincide with dark areas in Figures 7a and 7b. These dark areas,

in turn, are generally the same as the lighter buff- and beige-colored areas seen in Figure 2. Those light areas are mainly associated with light-colored Tertiary rock units. Their darkness or blueness in Figures 7 and 8 respectively are merely a measure of very sparse vegetation — confirmed from field and aircraft checks discussed later. However, the blue colors also correspond to the areas underlain by Mowry-Thermopolis shales and part of the Cody outcrop area north of the Dallas and Derby anticlines.

Of special interest in the Band 7/5 color rendition (and less so in the black and white version) is the emphasis of the outline of the Alkali Butte structure by a narrow blue band. This band seems to coincide with the blackish Mowry and Thermopolis shales and to a lesser degree with the Cody grey shales. In this ratio rendition, the prime oval anomaly is again brought out (in dark blue) because of the absence of vegetation but its precise pattern is slightly different from that depicted in the 5/4 ratio image.

The University of Wyoming has utilized the Image 100 system to produce band ratios of a somewhat smaller area that includes the Beaver Creek structure but excludes the Dallas, Derby, and Big Sand Draw structures (thus omitting any display of Chugwater-type beds). A ratio made by subtracting and adding Band 5 reflectances to those of Band 4, i.e., $(4 - 5)/(4 + 5)$, causes the oval anomaly to stand out in black tones (arbitrarily selected in assigning colors) against a blue background (Figure 11). This version also discloses a crude arcuate anomaly west of Beaver Creek composed of black tones. The arcuate anomaly is roughly bisected by the Ninemile Hill anticlinal structure which has no evident surface expression. There is also an anomalous collection of light-toned spots northwest of the oval anomaly, which shows up as very dark grey levels in Figures 5 and 7 and as blue tones in Figures 6 and 8. This spotty anomaly is roughly coincident with the Riverton and northern Beaver Creek oil fields. The spots closely coincide with the beige tones in that immediate vicinity in Figure 2 and are probably related to bare or sage-deficient terrain. The black anomalies particularly are made more obvious by an enhancement which colors them straw yellow and superimposes them on an image made as a contrast-stretched color composite using Bands 4, 5, and 7 (Figure 12).

The distribution of anomaly patterns within the area selected by the University of Wyoming as defined by the 5/4 ratios of Goddard and of Vincent and in the $(4 - 5)/(4 + 5)$ ratio made by Wyoming have been compared in Figures 13a, b, and c.

Goddard has produced a color composite (Figure 14) from $(5 - 4)/(5 + 4)$ (red filter), Band 5 (green), and 7 (blue) which displays much new information. The Chugwater beds (and adjacent colluvial soils) are expressed as a red color within the Dallas, Derby, and Big Sand Draw anticlines. The oval feature is largely subdued but can be discerned within a 10 to 15 mile wide patch shown in shades of medium orangish-brown that is nearly identical in distribution to the yellow-toned broad anomaly seen in Figure 2. The area to the west appears in dark reddish-brown tones. The higher plains surface south of the Beaver Divide has been shown as a very dark burnt orange-black. Much of the remaining rolling country in the basin is colored bright blue in the image. The hay meadows in the valleys are a deep blue. Note that, while these fields are blue and red respectively in this and the Figure 2 composite, the areas of Chugwater outcrops and soils are generally red inside the three anticlines in both composite renditions.

This color pattern suggests two distinct and separable iron anomalies are being discriminated. The Chugwater outcrops and colluvial soils have low reflectances in both Bands 5 and 4 but 5 is relatively much brighter. The $(5 - 4)/(5 + 4)$ ratio values for the Chugwater are projected red (i.e., through the light grey of the black and white image) while Band 5 itself introduces almost no green and some vegetation reflectance from Band 7 adds a little blue; the resulting color is thus dominated by red but is best described as approaching magenta. The iron-rich surface around Beaver Creek is much more reflective. For that surface the $(5 - 4)/(5 + 4)$ ratio remains light-toned in the black and white input and the additional light tone for Band 5 alone allows much more green to be combined with the red from the ratio image to produce yellow, orange and brown shades in the color composite.

A multiple ratio color composite has been made by projecting 5/4 through a red filter, 7/5 through blue, and 7/4 through green (Figure 15). The result is similar to the previous ratio-single bands composite in most respects but shows several important differences. First, the area corresponding to the broad anomaly, shown in this version as brownish-orange, has expanded somewhat over that displayed in Figure 14. Most of the seeming increase is more apparent than real in that the color tone is more uniform in the Figure 15 version while the equivalent area on the west in Figure 14 is rather more brownish. Another major difference is the replacement of the dark orange-brown tones just south of the Beaver Divide and the Dallas-Derby anticlines in Figure 14 with blue tone in Figure 15. These tones now correspond to the blues assigned to the hay fields in Figure 15 which are a notably different dark blue relative to the orange-browns of Figure 14. They presumably therefore denote a sensitivity of this ratio combination to vegetation, which would contribute to high 7/5 and 7/4 ratios. Still a third difference are the very dark browns that match the outcrop patterns of the Mowry-Thermopolis shales and Cody shales north of the Dallas, Derby, and Big Sand Draw anticlines.

Two significant special observations have been extracted during analysis of various processed images. The first observation, already alluded to in several paragraphs, relates to the effects of topographic irregularities on the expected spectral reflectances of certain of the stratigraphic units exposed in the scene. As previously stated, the Chugwater red beds and the Mowry-Thermopolis and Cody shales appear to have unique spectral signatures that yield distinctive tones in standard false color composites. Inspection of Figure 10, which reproduces the reflectance spectra of many typical Wyoming rock types as obtained on a Cary 90 Reflectance Spectrometer at Goddard Space Flight Center, indicates some aspects of these signatures. The Thermopolis black shale should be a low reflector over full visible-near IR range sampled by the LANDSAT MSS. The Mowry shale has comparable low reflectances in Bands 4 and 5 but increasingly high ones on Bands 6 and 7. The Chugwater also has a low reflectance in Band 4, a sharply higher reflectance in Band 5, and a somewhat higher reflectance in Bands 6 and 7 than either of the shales (this pairing of high Band 5 and somewhat higher Band 7 reflectances from the Chugwater rocks accounts for the distinctive yellow color in the false color composite, which results when 5 is projected through a green filter and 7 through a red filter).

Wherever these three units outcrop in generally broad low surfaces, their expressions in the false color composite give rise to distinguishable and characteristic colors. However, careful matching of outcrop patterns as seen on the geological map of Wyoming and on aerial photos (see Figure 16) shows that the characteristic spectral response is very sensitive to slope angle. This is indicated to some extent by the Chugwater beds at the Big Sand Draw anticline. Where the slope is steep (Figure 16a), the characteristic yellow tone in Figure 2 tends to be lighter that that associated with the soils downslope in the valley. In part, this tonal difference depends on the strike (azimuth) of the slope as well as its inclination: e.g., northwest-facing slopes respond differently from those trending northeast. However, some of the difference is caused by the effects of vegetation in the valleys that reduce the overall reflectance but add some relative increase in Band 7.

A better illustration of slope angle effects is provided by the spectral response of the Mowry-Thermopolis units around the Big Sand Draw (Figure 16b). As shown in that figure, the Mowry-Thermopolis outcrops as a cuesta fronted by a steep scarp behind which the beds are exposed in a dissected but generally low-inclined slope. Where these beds occur in the nearly flat (undulating) terrain, they show up as grey-blue shades in Figures 1 and 2. In contrast, the beds outcropping along the scarps appear as much brighter tones (see arrow in Figure 2), particularly where the slopes face the southeast. Under these conditions, the Mowry-Thermopolis units act as effective reflectors of the morning sun, despite their low average reflectances in MSS Bands 4 - 7. Vegetation effects are minimal in this case since neither sage nor grasses flourish on these dark shales.

It is clear, then, that topographic variations can play a marked role in determining the average intensity of reflected light emanating from a particular rock unit. Fortunately, the intensity changes

tend to remain relatively proportional in the several MSS bands as slopes steepen. When ratios are taken between bands, the intensity-slope effect is greatly reduced. This is evident in Figure 14 (see arrow), where the bright linear pattern associated with the Mowry-Thermopolis scarp (in Figures 1 and 2) disappears and the entire shale outcrop pattern is rendered a uniform blue. Unless such ratioing is carried out, it may be necessary to correct for steep slope and other topographic effects in order to identify lithologies by spectral signature data.

The second observation, relevant to looking for alteration zones in iron-pigmented rocks overlying petroleum-bearing structures from which hydrocarbons might be escaping, can be first raised as a question: Is it possible to distinguish yellowish-brown from darker red rocks (a color difference noted by T. J. Donovan at the Cement Field in the Anadarko Basin and attributed by him to hydrocarbon-induced chemical reduction and bleaching of hematite-cemented Permian sandstones) using LANDSAT data? An approximate answer can be sought in the ratio results that include the Dallas and Derby anticlines in the images. It seems reasonable to expect some differences in grey levels and assigned colors associated with the outcrop patterns of the Nugget sandstone (which forms the cap and backslope of a hogback overlying the Chugwater as shown in Figure 9) and the Phosphoria (which forms part of the lowlands or valley within the breached anticlines) with respect to the intervening Chugwater beds. Where associated with gentle dip slopes, these outcrop patterns should consist of linear bands more than 80 meters wide. Inspection of the color and ratio color composites indicates no such differences to be defined. The impression is gained that these adjacent units have sufficiently similar radiometric responses over the Band 5 interval that they cannot be resolved spatially. Judging from this near-optimum case, it seems very unlikely that the color variations (which are areally smaller and more irregular) observed on the ground at the Cement Field can be recognized by any of the ratio enhancements tried to date.

INTERPRETATION OF THE ANOMALY

Both the oval feature and the broad anomaly around the Beaver Creek field have now been studied in high resolution photos (Figure 16a, b, c, and d) obtained from a NASA NP-3A aerial flight on September 10, 1971, from a recent light aircraft overflight, and during several ground reconnaissance trips (Figure 17 a, b, c, and d). From the information thus gained, the several major color differences noted in the ratio images are explained as follows:

(1) The oval feature results mainly from irregular exposure of a 25-foot thick red sandstone unit in the Wind River Formation within a local badlands topography on which vegetation cover is very sparse. Northeast-facing slopes within the badlands also contribute to the definition of the feature.

(2) The broader yellow (Figure 2) or orangish-brown area (in Figures 14 and 15) surrounding the oval feature is a barren (sporadic grasses and sage) area of light-toned sandstones, claystones, and bentonite beds, generally naturally colored in buff, yellow, to light red, exposed in gentle to locally steep slopes. Small dry playa lakes are intermixed with this topography. From the air, the surfaces tend to have a reddish- to yellowish-brown tone.

(3) The anomaly west of Beaver Creek encompassing Ninemile Hill is an area of reddish soils, supporting more grass and sage which reduce reflectances (hence darker tones). This area shows up as notably darker in both the black and white and color aerial photos (Figure 16) from the P-3A flight. The brighter region shown in the University of Wyoming 4 - 5/4 + 5 rendition corresponds to a less vegetated, topographically raised area dominated by buff-colored sandy soils.

(4) The plains above the Beaver Divide scarp show especially dark because of increased sage cover mixed with gravels and darker beds of the White River Formation.

(5) The bluish tones (Figure 14) coincide with areas of extensive Tertiary sediments or Mowry-Thermopolis and Cody shales (often covered by thin, bleached soils) that are variably covered with clumps of tall grass but relatively few sage bushes.

(6) In many lower areas north of the Beaver Divide scarp, the effects of iron coloration on surfaces underlain both by the Wind River Formation and by alluvium are probably widespread and general but stand out sharply in the ratio color composites only in those areas where the reflectance contribution from vegetation is minimal.

CONCLUSIONS

As initially defined in the pronounced oval feature and later shown as a more extensive, distinctive patch of bright orange-brown in Figures 14 and 15, the Beaver Creek anomaly promised much as an indicator of mineralization. However, no clear correlation with nearby oil fields has been proved; proximity and some overlap favor a relationship but differences in shape and trend argue against this. The alternate explanation that the anomaly (particularly the oval feature) is an indicator of iron deposition associated with uranium roll deposits (the rich Gas Hills uranium district is just 30 miles to the east) is apparently discounted by the low radiometric readings obtained in a controlled ground survey with a scintillometer.

The lesson gained from this study is simply that promising "anomalies" of interest in mineral exploration must also be examined in the field rather than through imagery alone in order to distinguish those defined or modified by topographic, soil, and vegetation influences from the few residual ones that reveal truly anomalous and meaningful geologic information. The corollary to this conclusion is that many anomaly patterns are in fact the direct outgrowth of the interplay between a prime cause, like red rock or soils, and such complicating factors as variations in vegetation density, topographic slopes, soil moisture, and other surface conditions. In that respect, only a careful analysis of these several contributing or modifying factors will lead to full recognition of the geologic information that is otherwise being misrepresented or masked.

REFERENCES

Donovan, T. J., Petroleum Seepage at Cement, Oklahoma: Evidence and Mechanism; Amer. Assoc. Petroleum Geol. Bull. v. 58, p. 429-446, 1974

Rowan, L. C., P. H. Wetlaufer, A. F. H. Goetz, F. C. Billingsley, and J. H. Stewart, Discrimination of Rock Types and Detection of Hydrothermally Altered Areas in South-central Nevada by the Use of Computer-Enhanced ERTS Images, U.S. Geological Survey Prof. Paper 883, 35 pp., 1974

Vincent, R. K., Ratio Maps of Iron Ore Deposits, Atlantic City District, Wyoming, NASA Symposium on Significant Results Obtained from the Earth Resources Technology Satellite-1, v. 1, section A, NASA SP-327, p. 379-386, 1973

. . . . . , Oil, Gas Exploration Tool-Composite Mapping of Earth Satellite Information, Oil and Gas J., v. 73, no. 7, p. 141-142, 1975

REPRODUCIBILITY OF THE
ORIGINAL PAGE IS POOR



Figure 1. – LANDSAT-1 frame 1013-17294 on which is outlined the area containing the iron-rich surface anomaly described in this paper. The Wind River Mountains appear at the lower left, the Owl Creek Mountains near the top, and the Rattlesnake Hills at the far right. The Wind River runs across the image; where it enters the Bighorn Basin (top), it is renamed the Bighorn River. The Chugwater and Nugget Formations appear mustard yellow where exposed (arrows) in a color rendition.

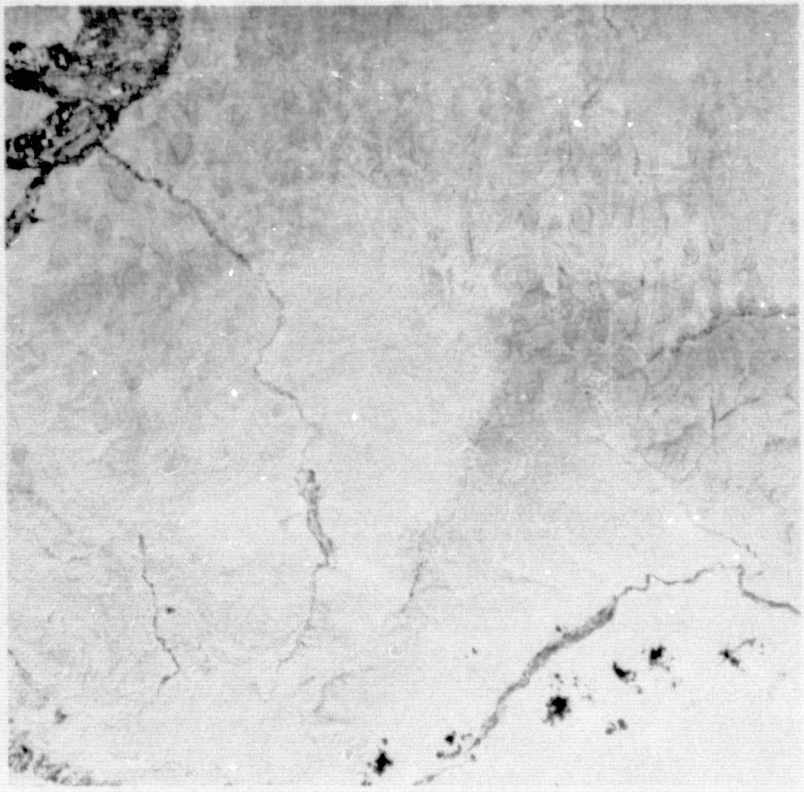
REPRODUCIBILITY OF THE
ORIGINAL PAGE IS POOR



Figure 2. - Contrast-stretched, computer-processed enlargement of the anomaly area shown in Figure 1. The anomaly along the Beaver Creek shows up in this version as strong yellow tones. Areas labelled A, B, and C are the Derby, Dallas, and Big Sand Draw structures. The Beaver Divide is marked by D. Left arrow points to a blue tone associated with Mowry-Thermopolis shales. Right arrow notes a SE-facing cliff composed of these shales as discussed in the text. Agricultural areas show up in valleys of Popo Agie River near Riverton (upper left corner) and Sweetwater River (lower right).



Figure 3. - Aerial photomosaic, prepared in 1952, covering essentially all the area considered in this paper. Arrow points to location of oval feature. Letters A through D identify features listed in Figure 2.



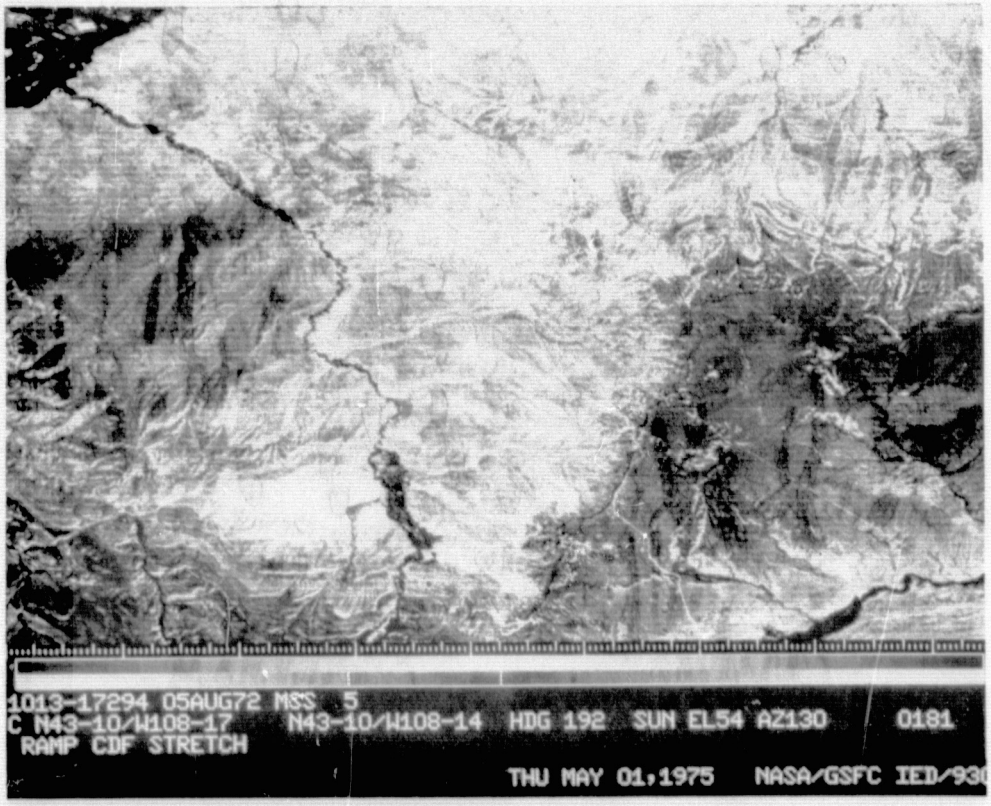


Figure 4. - (a) Enlargement of anomaly area as shown in a standard-processed Band 5 rendition from 1013-17294; (b) Same area as in a shown as a computer-produced, contrast-stretched version.



Figure 5. – Contrast-stretched Band 5/4 ratio image of the anomaly area reproduced in black and white. Arrow denotes location of oval feature near the Beaver Creek anticline. This feature is difficult to pick out in this version because of surrounding light grey tones.

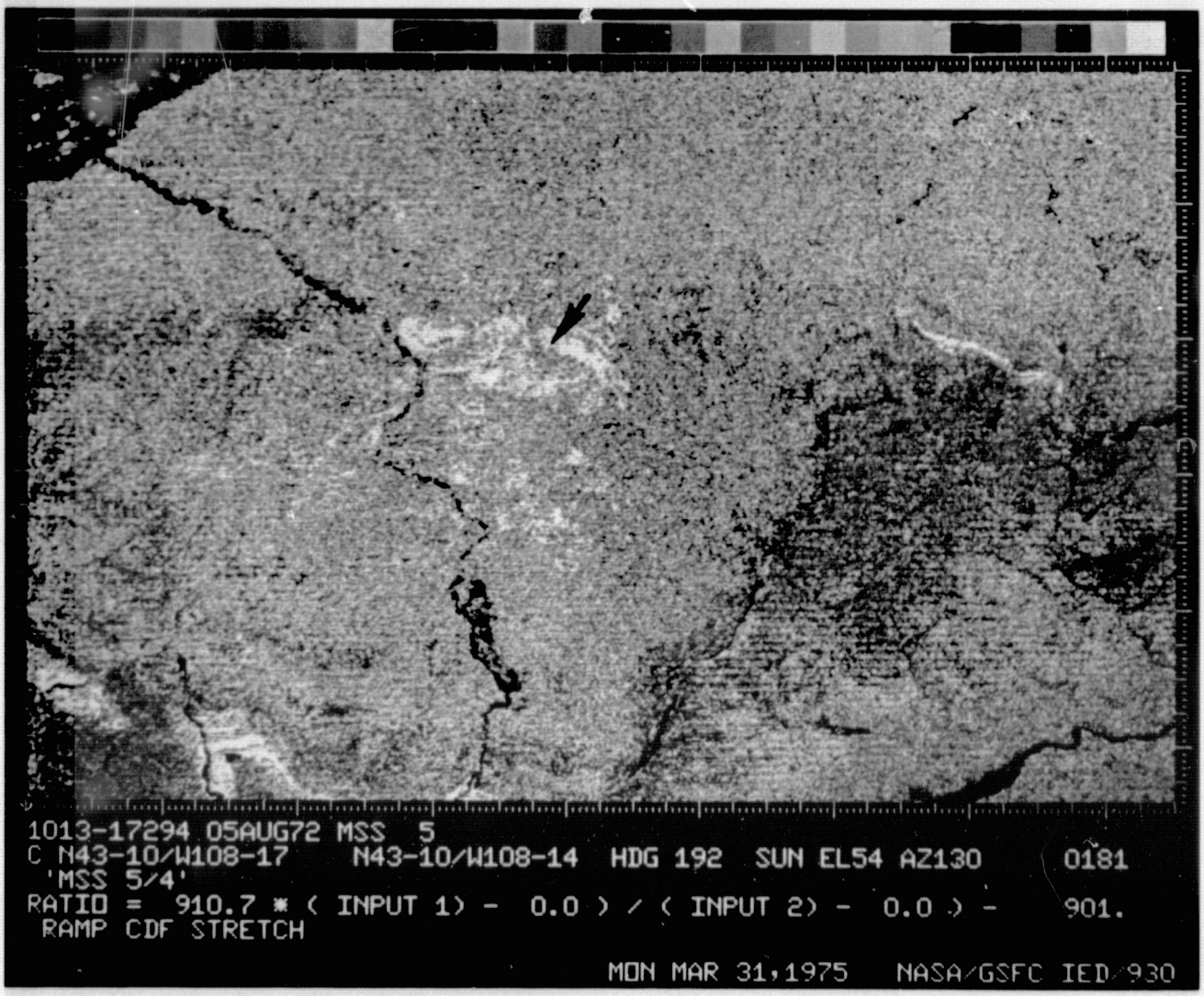


Figure 6. - Same scene as presented in Figure 5 but now processed through the DICOMED system which assigns a range of colors to the gray levels. The oval feature (arrow) stands out in a light beige tone, as do surfaces associated with the Chugwater Formation at the Dallas, Derby, and Big Sand Draw anticlines.

REPRODUCIBILITY OF THE
ORIGINAL PAGE IS POOR



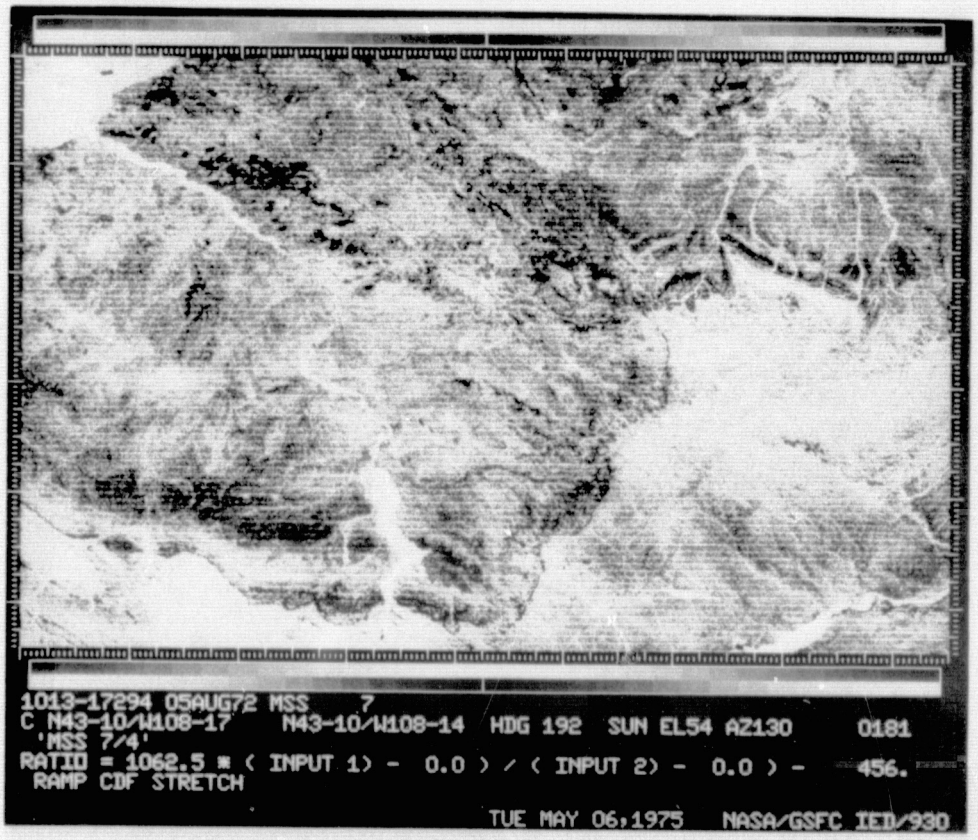


Figure 7. - Black and white contrast-stretched ratio images of the anomaly area made for (a) Bands 7/5 and (b) Bands 7/4.





Figure 8. - DICOMED color versions of the Bands 7/5 (a) and 7/4 (b) ratio images in Figure 7.

REPRODUCIBILITY OF THE
ORIGINAL PAGE IS POOR

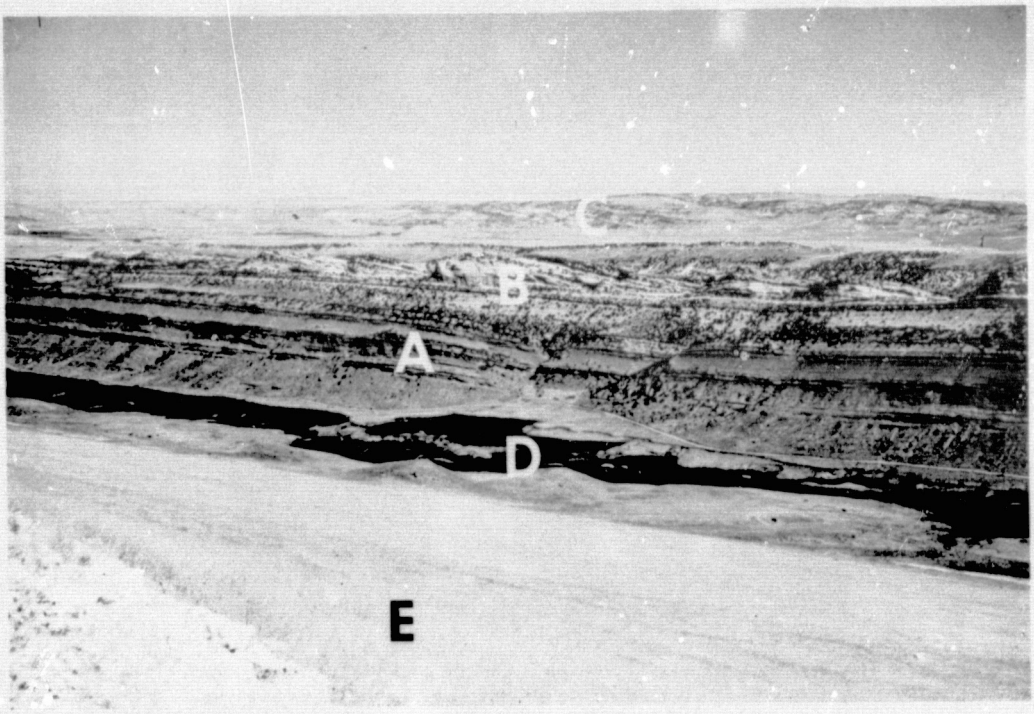


Figure 9. - View of cliffs along Red Canyon south of Lander, Wyoming. (A) Chugwater Formation (dark red in color print), (B) Nugget sandstone (yellow-brown), (C) Scarp of Frontier sandstone, (D) Hay fields along tributary to Little Popo Agie River; Phosphoria Formation outcrops in this valley, (E) Grass-covered dip slope formed by Tensleep Formation.

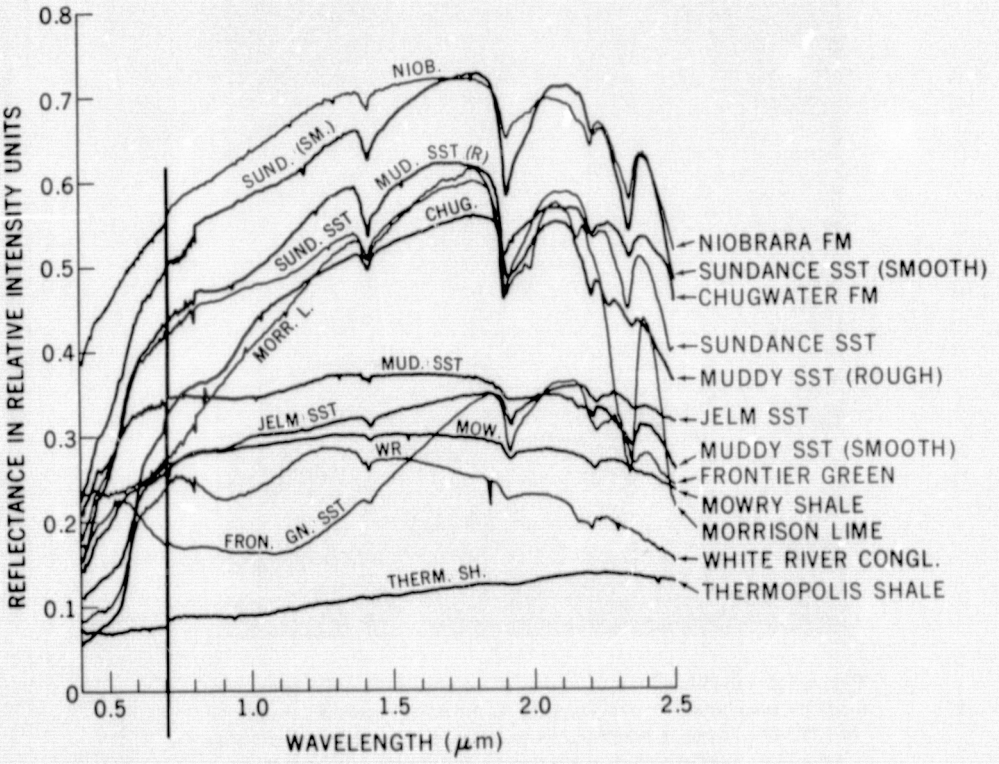


Figure 10. - Plots of reflectance spectra for a select group of Wyoming sedimentary rocks.



Figure 11. - Black and white version of a ratio color composite prepared on Image 100 by the University of Wyoming. The ratio combination used here is (4 - 5)/(4 + 5). The oval feature stands out in black tones (corresponding to bright beige tones in Figure 6 version) against a generally blue (medium-grey here) background. Similar black areas are expressed around the Ninemile Hill buried anticline to the west.



Figure 12. - Black and white version of another ratio color composite made by the University of Wyoming. In the color rendition the (4 - 5)/(4 + 5) ratio image is presented in straw yellow tones (very light grey here) and superimposed on a reconstructed false color composite made from Bands 4, 5, and 7.

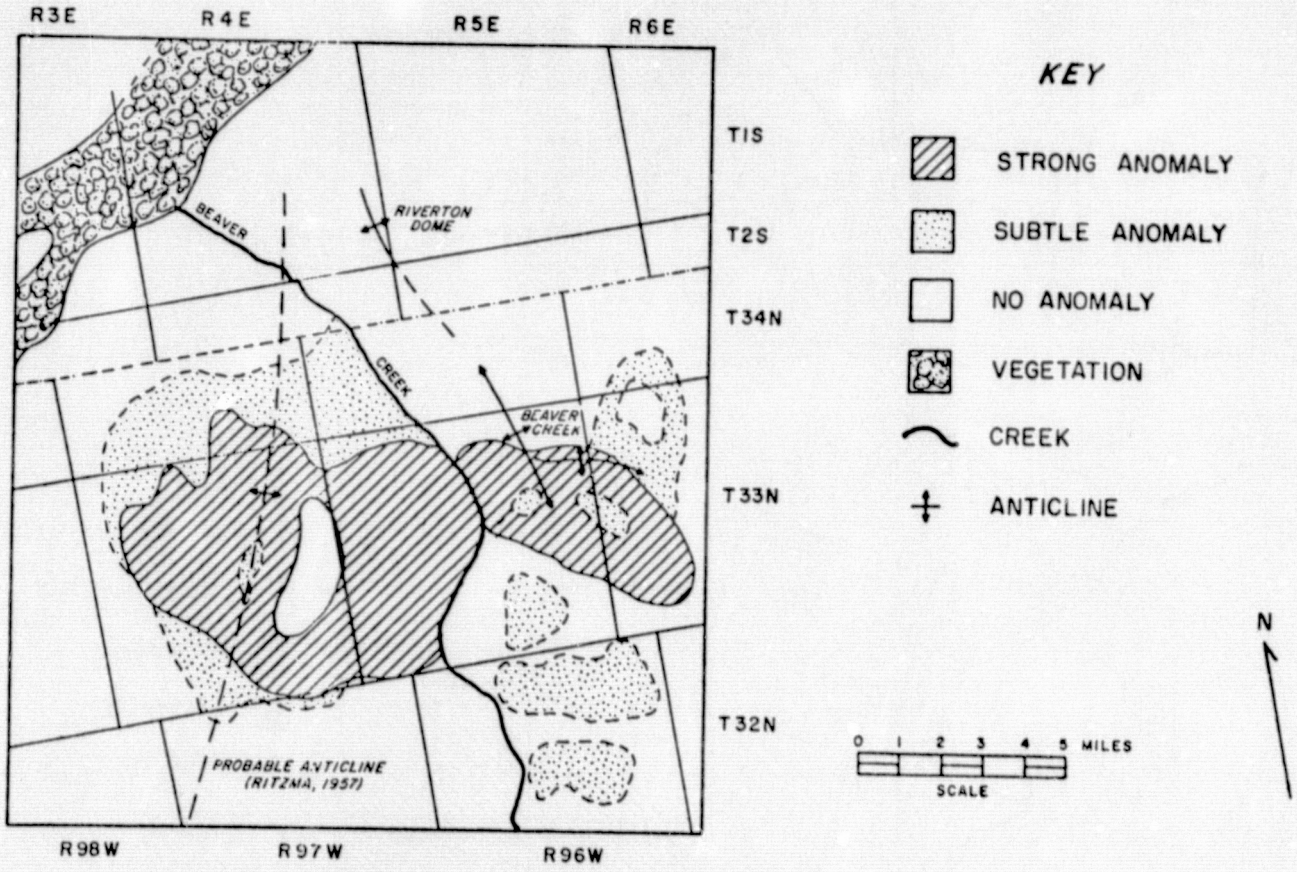


Figure 13a. – Map interpreted from (4 – 5)/(4 + 5) x 4 ratio (Figure 11) showing anomalies in relation to structural features.

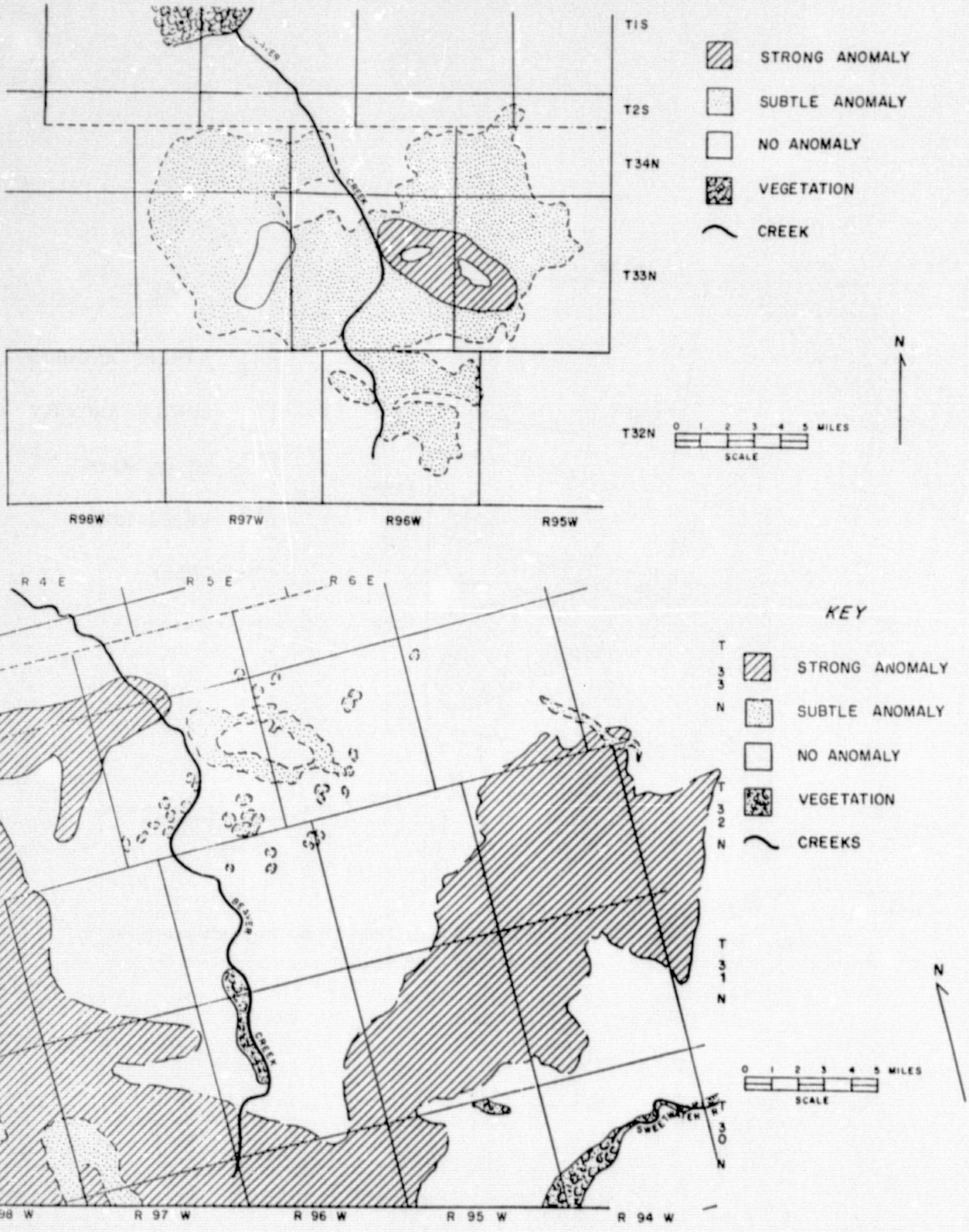


Figure 13. - (b) Light and dark anomalies detectable on R_5, 4 ratio generated by R. K. Vincent (as reproduced on p. 141 of the Oil and Gas Journal, v. 73, no. 7, 1975), (c) Map of light and dark anomalies from Bands 5/4 ratio produced at Goddard Space Flight Center.

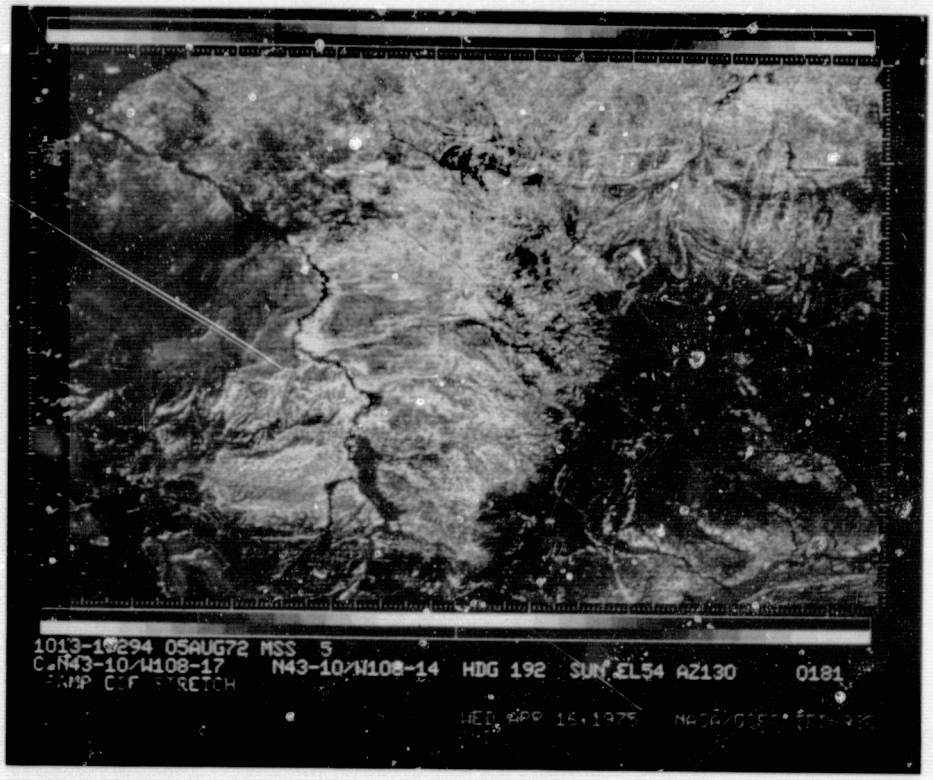


Figure 14. - DICOMED color composite of anomaly area produced by color-coding black and white renditions of Bands (5 - 4)/(5 + 4) (red), Band 5 (green), and Band 7 (blue).

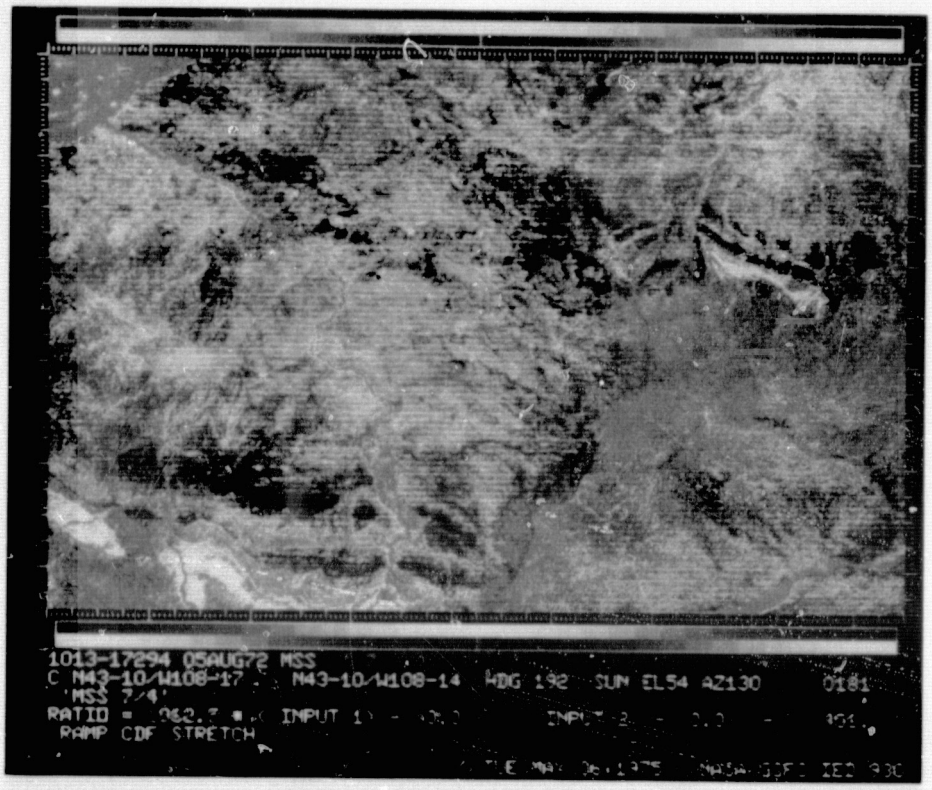


Figure 15. - Another DICOMED color composite of the anomaly area made from band ratios as follows: 5/4 (red), 7/5 (blue) and 7/4 (green).

REPRODUCIBILITY OF THE
ORIGINAL PAGE IS POOR

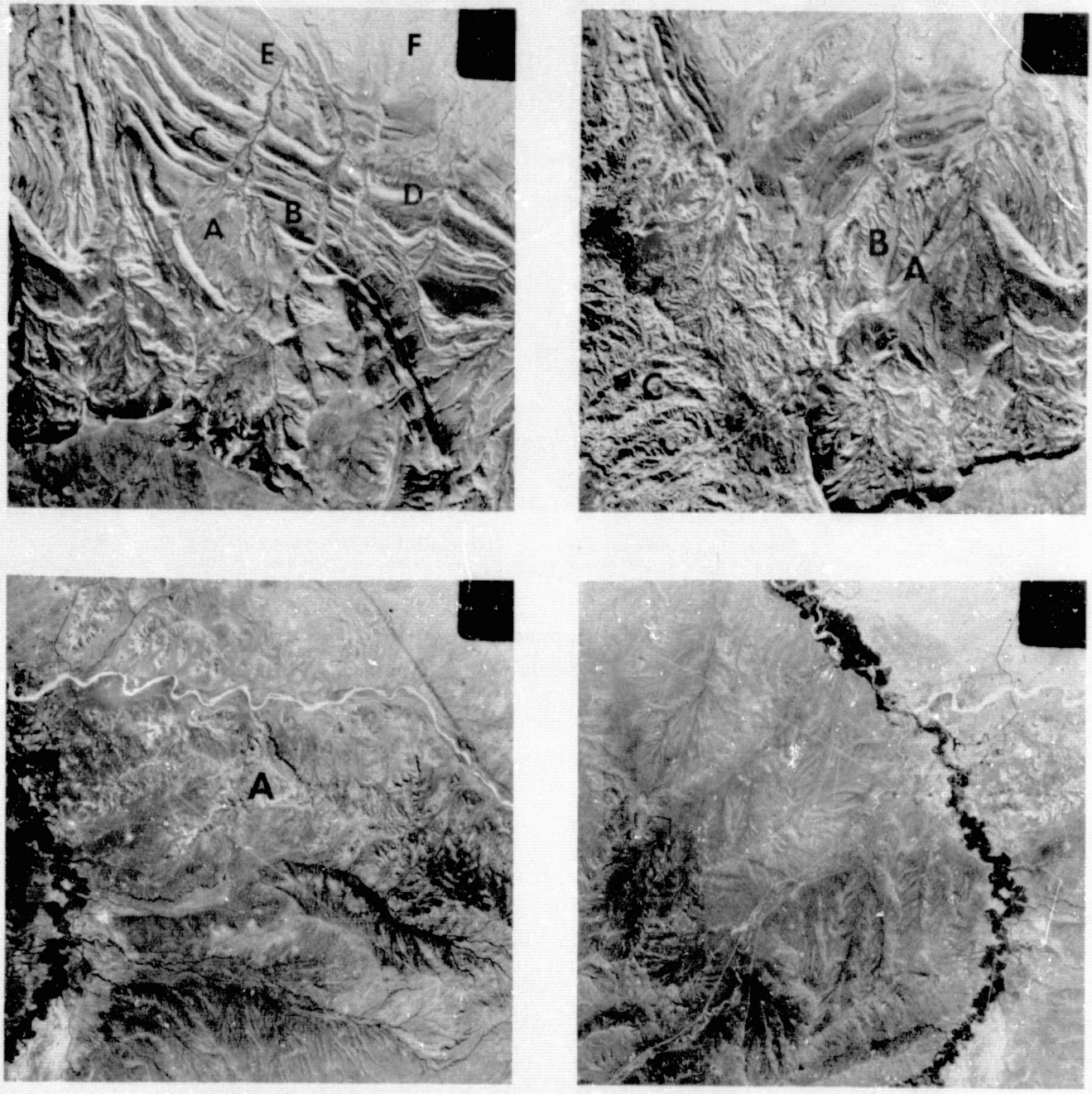
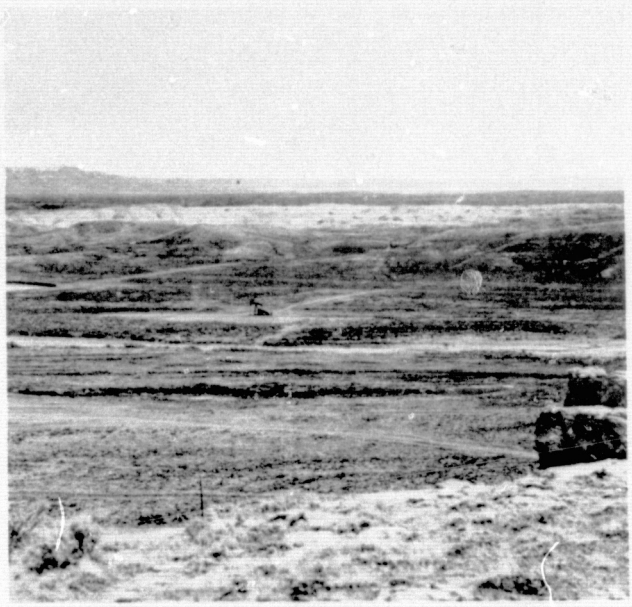


Figure 16. - Aerial photos obtained during a September 10, 1971 flight by the NASA NP-3A aircraft at an average altitude of 20,000 feet across the southwestern part of the Wind River Basin. The photos are recorded on Eastman-Kodak panchromatic film 2402 through a red filter. (a) Part of the Big Sand Draw structure (top is north in this and other photos in this figure) in which major stratigraphic units are identified as follows: A. Chugwater red beds in valley; B. Chugwater red beds in cliff; C. Sundance-Morrison units; D. Mowry-Thermopolis shales; E. Frontier sands; F. Cody shales; (b) Continuation of folded units west of Big Sand Draw. A. Southeast-facing cliff of Mowry-Thermopolis shales; B. Dip slope of dissected Mowry-Thermopolis shales; C. Dissected Eocene sediments; (c) Badlands topography, exposing reddish sandstone units of Wind River Formation at A, along the southern end of the Beaver Creek anticline; (d) Change in surface reflectances along Beaver Creek; units to the west of the creek are darker owing to increased proportion of sagebrush.

REPRODUCIBILITY OF THE
ORIGINAL PAGE IS POOR



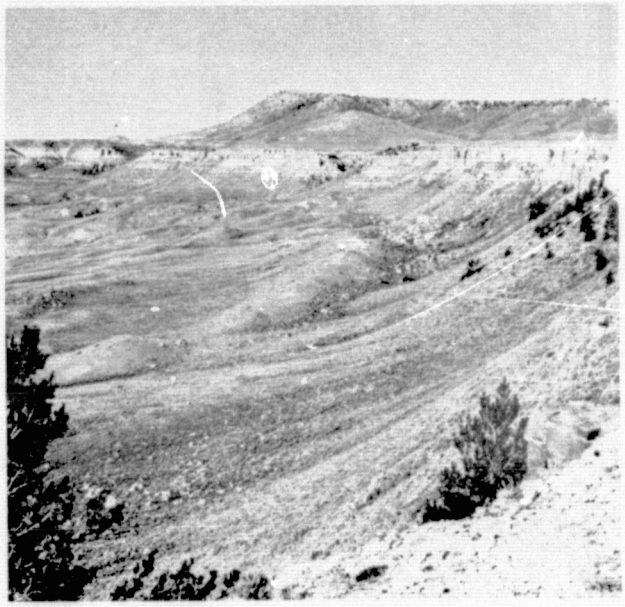






Figure 17. - Ground photos (taken during April of 1975) of selected scenes within the anomaly area: (a) View looking SSE of part of the area along the south end of the Beaver Creek oil field that includes the oval feature. The light-toned beds in the badlands (above oil pump) include the red sandstone and other reddish units of the Eocene Wind River Formation. The rim of the Beaver Divide appears in the distance; (b) Close-up of the cliffs of the Beaver Divide (looking NE) and the undulating, grass- and sage-covered slopes below; (c) The grass-covered surface, with occasional sagebrush, along the road leading to the Big Sand Draw oil field further east; (d) View southward from Ninemile Hill. Sage cover in foreground is typical of the region west of Beaver Creek.

REPRODUCIBILITY OF THE
ORIGINAL PAGE IS POOR

APPLICATION OF SKYLAB IMAGERY TO RESOURCE EXPLORATION IN THE DEATH VALLEY REGION

G-7

By Ira C. Bechtold, John T. Reynolds, C. Gregory Wagner
Bechtold Satellite Technology Corporation
City of Industry, California

N76-17506

ABSTRACT

The Hunter Mountain plateau in the northern Panamint Range, California, exhibits anomalous topographic, vegetative, color and structural features in Skylab and LANDSAT satellite images which have strong correlation with mineralized areas and should prove significant for future exploration. Data observed to date has been studied with reference to published geology and is interpreted in terms of greatest probability of ore mineralization. Further study in conjunction with space imagery analysis is recommended for location of potential mineral zones.

INTRODUCTION

Skylab photographic products have been found useful for all types of geologic investigations, and in many instances provide observations of previously unrecognized features. Such observations have been made specifically in a region on the western boundary of Death Valley National Monument in the northern Panamint Mountain Range, California. Regional as well as local structural, color, and reflectance differences have been plotted directly from satellite images and interpreted as highly significant in terms of mineral resource exploration. The correlations of identified photographic features with specific mineralized areas is tentative, as ground work has been very limited to date, and the study has not passed the reconnaissance stage of exploration. Satellite data has, however, exhibited the following valuable utilizations in this study:

1. Wide synoptic coverage assisting visualization of regional geologic structure and rock type relations.

2. Identification of abundant detail of culture and geography for location.

3. Ease of projecting transparencies to mappable scale for data transfer.

4. Location of subtle anomalies, especially those having high potential for mineralization.

5. Interpretation of some rock reflectance signatures as correlatable to mapped geologic units or zones of alteration.

6. Identification of regions probably not mapped accurately or in sufficient detail and of sites recommended for further investigation.

PRECEDING PAGE BLANK NOT FILMED

LOCATION

The study encompasses an area of approximately 500 square kilometers (200 square miles) in the northern Panamint Range, 50 km. (30 miles) due east of Lone Pine, California. Centered within the study area is Hunter Mountain, a high plateau between two major downfaulted valleys, Saline Valley to the northwest and Panamint Valley to the south (Figure 1). Death Valley lies beyond the mountains 30 km. to the east (Stovepipe Wells). The region is accessible almost solely by gravel road 30 km. north from California Highway 190 and from Ubehebe Crater at the northern end of Death Valley.

The Hunter Mountain plateau is approximately 1800 meters (6000 feet) in elevation, having steep canyons on all sides, with relief of as much as 900 meters (3000 feet) above the surrounding basin floors. All drainage is internal, principally into the three major valleys, thereby categorizing the region as part of the western edge of the Basin and Range province.

Hunter Mountain and the surrounding region is composed of large masses of granitic bodies in contact with older, deformed remnants of Paleozoic marine sedimentary rocks. The area is geographically near major mining areas, the Cerro Gordo mining district 25 km. due west, the Darwin mining district 30 km. due south. Additional activity has occurred throughout the Panamint Range to the southeast, and various operations are located to the north within the area studied. Geologic work done in the area is sparse, and virtually the only mapping done in the Ubehebe Peak quadrangle was by J. F. McAllister in 1956. Many of the surrounding quadrangles have been mapped more recently, but the Marble Canyon quadrangle, containing the eastern portion of Hunter Mountain, has remained virtually unmapped, primarily due to remoteness and rugged terrain.

PROCEDURE

Both LANDSAT and Skylab satellite imagery is available over the studied area; two scenes of Skylab were most important in the project, one S190B high resolution Ektachrome camera scene (SL4-94-013, Feb. 1974), and an S190A Ektachrome scene (SL2-04-189, June 1973). Additional useful scenes were SL4-76-222, LANDSAT 1287-17555, 1054-18001, 1090-18010. S190A data was projected in a viewer to a 1:250,000 scale, as were LANDSAT 70mm positive film chips. These were viewed as color composites utilizing various combinations of color filters in the spectral bands. The S190B data was viewed by mounting the film transparency so that the desired area appeared in the window originally made for 70mm frames and projecting to a scale of 1:62,500, the scale of a 15 minute topographic quadrangle. The data observed was compared to the geologic quadrangle mapped by J. F. McAllister (1956). Data transferred to the 1:250,000 scale was compared to the mapped geology on the Death Valley sheet of the Geologic Map of California series.

Data was gathered solely by visual means, and was transferred manually by acetate overlay to map scales. Interpretation primarily involved first hand observation of images, but also correlation with maps and geologic literature.

ANALYSIS AND INTERPRETATION

The initial feature observed is a large, nearly perfectly circular structure which appears strongly in the S190B high resolution camera image. The Hunter Mountain plateau is covered by a light snowfall, which evidently made possible the observation of the entire feature. In other images, this arcuate pattern is barely visible in the south and east, probably due to a subtle change in relief that appears only when enhanced by snow cover. The arc encompasses most of the topographic high named Hunter Mountain on the Ubehebe Peak quadrangle, over 8 km. in diameter, and is bounded on the southwest by a deep gorge, Grapevine Canyon (Figure 1). Northerly trending linears, interpreted as faults, form the western edge, along with light colored rock outcrops. Other numerous linears appear to strike tangentially to the arcuate edges. The entire arcuate structure lies within plutonic rock designated by McAllister (1955) as the Hunter Mountain quartz monzonite. The northern and northeastern edges are approximately at the contact of this igneous body and undifferentiated Paleozoic rocks (Death Valley sheet, Geologic Map of California), but the eastern and southern boundaries lie in a region of subdued topography within the mapped body which extends eastward to Death Valley.

Rock reflectances from the entire region are variable yet most of the gray-green and blue hues correspond to the Paleozoic sedimentary rocks, while the regions of mapped plutonic rock appear dark gray-green and brown in the S190A Ektachrome scene. Bright white regions occur immediately outside of the western, northern, and to a lesser extent, the northeastern margins of the arcuate structure. These areas correlate strongly with areas of exposed Paleozoic metasedimentary rocks, and apparently indicate the contact with the plutonic rock where deformation accompanied the intrusion. Anomalously bright reflectance is believed caused by fine clay materials, alteration likely by hydrothermal activity and by thermal metamorphism of the dominantly limestone and dolomite-bearing rocks. In the S190A Ektachrome image, an apparent color zoning appears east of the arcuate structure along the mapped contact of granitic and Paleozoic rocks. In this area, a brown zone parallels the contact for nearly 20 km. while a lighter gray-green reflecting zone appears to the south, toward the interior of the granitic body. This color zoning probably reflects rock type changes as yet unmapped in the Marble Canyon quadrangle; furthermore, lithology appears different from that within the arcuate area. The arcuate region appears much darker and appears to truncate the zoned region in the east, perhaps indicating it was a later intrusive phase.

McAllister (1955) describes the Hunter Mountain plutonic body as quartz monzonite intruding Paleozoic marine sedimentary rocks, with the majority of the mass light colored and containing less than 5% mafic minerals, but having various mafic border facies. In the adjoining region to the south, Hall (1971) indicates that biotite-hornblende quartz monzonite occurs as an extension of the Hunter Mountain body, and that centers of intrusive masses are predominantly more silicic quartz monzonite grading to quartz-poor monzonite or syenodiorite near the borders. McAllister's data agrees as he mapped the western portion of the Hunter Mountain body as a complex of mafic facies in contact with Paleozoic limestones, and he attributed the occurrence to mixing with the wallrock. He indicates pegmatite and aplite masses occur abundantly around Hunter Mountain, but did not consider them worthy of mapping. In the Darwin quadrangle, such small bodies are observed commonly at borders of quartz monzonite bodies and as thin dikes (Hall and MacKevett, 1958). Also he reports inclusions to be abundant in finer

grained rock in places especially on the southern part of Hunter Mountain. Knowledge of these minor intrusive facies could contribute greatly to the understanding of the histories and conditions of intrusive emplacement, definition of border zones, and relations of mineral deposits.

The intrusive events apparently took place after deposition of at least 4600 meters (15,000 feet) of Paleozoic marine sediments, and probably after the middle Mesozoic since similar intrusives are known to cut Triassic rocks in the Inyo Range to the west (Ross, 1969). Nearly all authors describing the surrounding regions consider the masses of quartz monzonite to have intruded generally in Jurassic to Cretaceous time. Very few age determinations have been made near Hunter Mountain; Ross (1969) reports an age of 190 million years on a zircon from the area and assigns the intrusive event to early Jurassic. Hall and MacKevett (1958) reported a zircon dated at 99 million years from the southeast part of Ubehebe Peak quadrangle. The accuracy of these dates is tenuous, but they may have been obtained from widely different ages of intrusives. More reliable ages of similar rocks yield a middle Jurassic age in the Argus Range to the south and a late Jurassic to early Cretaceous age in the Panamint Range to the north (Burchfiel, 1969). Various similar ages have been obtained in the Inyo Range to the west, indicating a range of intrusive dates. The Hunter Mountain body may be Jurassic in age or possibly younger, and appears younger than the neighboring granitic body in the east.

The fracture pattern and lineament trends observed in satellite images are complex. Linears have been plotted which lie tangential to most of the perimeter of the arc, especially from the S190B scene. The greatest concentrations of lineaments appear to be at the west and southwest boundaries, and on the northern margin. Additional lineaments strike through the structure, trending mainly N 70 W and N 30 E. This pair of trends occurs throughout the region and may represent an orthogonal joint set. Other minor trends occur throughout the region, and may prove important to interpretation of mineralized zones. A major mapped fault zone, Grapevine Canyon, strikes about N 60 W along the arcuate's southwest boundary, linking Saline Valley with Panamint Valley; this fault appears to be a relatively recent feature, and has probably been responsible for much of the later fracturing.

Fault control of mineralization in the region has long been recognized as important. The Ubehebe Mine to the far north exhibits N-S faults, and associated N 15 E trending faults are particularly characterized by mineralization. This small district which has produced lead, zinc, and silver, occurs very close to a syenite facies of a stock of the same Hunter Mountain quartz monzonite and within shattered dolomitic rocks. The altered and mineralized zone is readily apparent in satellite images as is that adjacent to two stocks nearer the Hunter Mountain body. The Lippincott Mine area which is located on the edge of the stock immediately northwest of Hunter Mountain produced lead and silver and some copper and tungsten from metamorphosed dolomite. The main controlling structures are apparently N 10 to 15 E and N 50 W. These trends are usually visible in detailed imagery, and in the Hunter Mountain region, the lineaments have been plotted and found to have a high correlation to known mineralized areas.

Small mine workings and prospects have been active around the margins of the Hunter Mountain body. Massive thermal metamorphism occurs along most of the northern and western margins, as is evident from the bright reflectances observed, and in many places metasomatic processes have

enriched the zone with local tactite and ore deposits. Mineralized areas having previous mining activity seem to have a correlation with the arcuate anomaly, and the structural, lithologic, and vegetative differences appear to be interrelated. Mining of ore deposits has occurred primarily in the Paleozoic rocks where closely adjacent to the intrusive bodies, and control by faults and fractures has been important according to many authors. To the west near Big Dodd Spring, copper, lead, and tungsten are the principal economical materials occurring in small bodies in fault zones. Here are seen abundant north-northeast trending lineaments as well as minor, discontinuous fractures at nearly 90 degrees. Old prospects were worked mainly for copper minerals in marble and calc-silicate rock in this area as well as to the northeast and to the south, following the western border of the arc. Near the southern edge of Hunter Mountain occur additional claims with copper silicates filling fractures and pegmatite trending N 70 W. This same trend is observed to be strong in the satellite images, particularly in this southerly area, and intersections with lesser northeast trending lineaments. In each of the mineralized areas, intersections of approximately N 70 W and N 30 E lineaments are observed. To the extreme north on the steep northern face below the plateau rim occurs a copper claim in a well-brecciated contact metamorphic zone where white marble contacts a mafic border facies of the Hunter Mountain quartz monzonite. In this region is observed a complex of lineaments which probably helped give rise to the large, bright altered zone visible, and the heavy mineral deposition.

In general, the faults which apparently help to control mineralization are more or less tangential to the plutonic contacts. This fact is of major significance to the location of new mineralized areas around the anomaly, especially with respect to copper which occurs mainly in deposits near the pluton margin. The well-known rich mining districts of Darwin and Cerro Gordo nearby to the south and west, exhibit many of the same relations of mafic border facies of quartz monzonite intrusives near limestone or dolomite contacts, in conjunction with complex control by faults and fractures.

The southern portion of the arcuate area appears darkest in the S190A Ektachrome frame. Compositing of the spectral bands into a false infrared color combination reveals this area to be one of the few densely vegetated regions in the scene. The vegetation appears isolated, however, and diminishes considerably to the north in the high plateau region. The primary explanation seems to be that the vegetation is restricted to areas of greatest water retention: the higher elevations and northern slopes. But, the entire northern portion and surrounding areas appear almost totally barren despite comparable elevations and abundant north-facing slopes. LANDSAT color compositing of enhanced 70mm frames also reveals relatively dense vegetation only in the southern region and virtually none in the adjacent plateau region, but immediately outside the arcuate appears widespread, fairly homogeneous vegetation. For these reasons, the arcuate region has been identified as containing a vegetation anomaly, as well as structural and coloration anomalies. These characteristics have been observed in Skylab imagery, and are supported by LANDSAT color composite scenes.

FIELD OBSERVATIONS

A reconnaissance field trip was made to briefly study the region where the arcuate structure was seen, and to visualize what was actually being observed in the images. As soon as the area of the southern arcuate boundary was reached, it was evident that abrupt changes in the vegetation

existed, all within the plutonic rock terranes. Juniper and pinyon pines occur above 1500 meters (5000 feet) elevation. Part of the northern border was also studied where a mafic border facies of the quartz monzonite contacted Paleozoic limestones, forming a wide zone of calc-silicate metamorphic rock with an associated tactite zone containing several percent of copper oxides. Pyrite and bornite occur disseminated in marble in the zone. Even from cursory examination, it was readily apparent that the large, bright-white area in the images corresponded with this thermally metamorphosed and mineralized zone. The dark region immediately adjacent to it apparently represents the mafic facies, and the contact appears linear, probably due to a fault, trending northeast. The local area appears in images to be complexly fractured, and this condition most likely provided the desired relations giving rise to mineralizing solutions near the contact.

FURTHER WORK RECOMMENDED

Beyond a more detailed study of lithologic and structural relations from satellite imagery, further work is suggested to support and complement the remote sensing investigation. Future study should include: sampling consistently across the arcuate structure to determine changes in lithology and minor mineral constituents, a geobotanical survey identifying any geochemical zoning, age dating of the plutonic bodies, investigation of color anomalies and determination of any possible remnants of Paleozoic rocks in the mass or near the arcuate edges, study of image lineaments and actual faults, joints and fractures and correlating them to mineralization, and a comprehensive mapping program in conjunction with imagery analysis. Few of the lineaments and subtle lithologic differences observed have been previously mapped, but the likely important associations of these with mineralized areas warrants detailed investigation of all features. We suspect that further work will indicate the arcuate region to be an intrusive sequence of slightly different composition and age, likely responsible for mineralizing the area.

CONCLUSION

Image analysis of the Hunter Mountain region has shown many interesting patterns deserving much more investigation on both regional and detailed scales. Mineralization of economic grade is known to occur throughout the region and has been mined for years. If attention is paid to the interrelationships of subtle lithologic differences, fracture patterns, vegetation anomalies and known mineralized areas, tremendous information about distribution of mineral resources could be gained, in particular utilizing all the methods and interpretations available with satellite remote sensing data. These various factors occurring in combination should continue to help delineate potentially valuable mineralized areas of Hunter Mountain and surrounding areas. Synthesis of previous data and present and future data applications will undoubtedly indicate recognizable patterns relating to mineralization in specific regions, and remote sensing techniques will be found invaluable as reliable and integrative tools for resource exploration.

BIBLIOGRAPHY

Burchfiel, B. C., 1969, Geology of the Dry Mountain Quadrangle, Inyo County, California: California Div. Mines and Geology Spec. Report 99.

Hall, Wayne E., 1971, Geology of the Panamint Butte Quadrangle, Inyo County, California: U.S. Geol. Survey Bull. 1299.

Hall, Wayne E. and MacKevett, E. M., 1958, Economic Geology of the Darwin Quadrangle, Inyo County, California: California Div. Mines and Geology Spec. Report 51.

Hall, Wayne E. and Stephens, Hal G., 1963, Economic Geology of the Panamint Butte Quadrangle and Modoc District, Inyo County, California: California Div. Mines and Geology Spec. Report 73.

Jennings, Charles W., 1959, Geologic Map of California, Death Valley Sheet: California Div. Mines and Geology, Scale 1:250,000.

McAllister, James F., 1952, Rocks and Structure of the Quartz Spring Area, Northern Panamint Range, California: California Div. Mines and Geology Spec. Report 25.

_____, 1955, Geology of Mineral Deposits in the Ubehebe Peak Quadrangle, Inyo County, California: California Div. Mines and Geology Spec. Report 42.

_____, 1956, Geology of the Ubehebe Peak Quadrangle: U.S. Geol. Survey Quadrangle Map GQ-95.

Merriam, C. W., 1963, Geology of the Cerro Gordo Mining District, Inyo County, California: U.S. Geol. Survey Prof. Paper 408.

NASA, 1972, EREP Investigator's Data Handbook: Manned Spacecraft Center, Houston, Texas.

Ross, Donald C., 1967, Generalized Geologic Map of the Inyo Mountains Region, California: U.S. Geol. Survey Misc. Geol. Investigations Map I-506.

_____, 1967, Geologic Map of Waucoba Wash Quadrangle, Inyo County, California: U.S. Geol. Survey Geologic Quadrangle Map GQ-612.

_____, 1969, Descriptive Petrography of Three Large Granitic Bodies in the Inyo Mountains, California: U.S. Geol. Survey Prof. Paper 601.

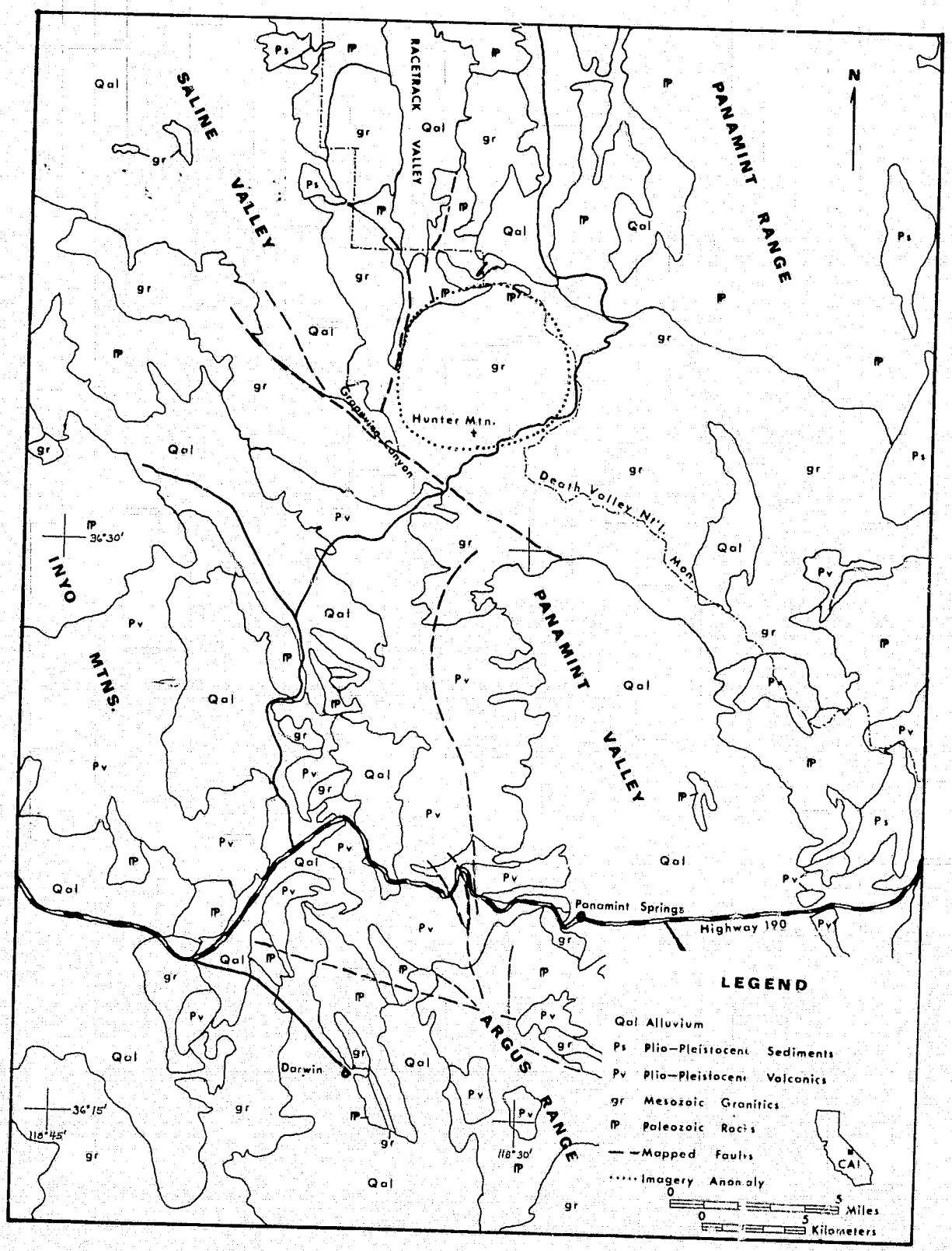


Figure 1 Location map and generalized geology of the Hunter Mountain region, California. Scale 1:275,000.

SUMMARY OF SPACE IMAGERY STUDIES IN UTAH AND NEVADA

G-9

By Mead LeRoy Jensen, University of Utah, Salt Lake City, Utah 84112, and
Philip Laylander, Consultant, 500 East 4800 South, Salt Lake City, Utah 84107.

N76-17507

ABSTRACT

Geologic Mapping.- LANDSAT-1, Skylab, and RB-57 imagery acquired within days of each other of the San Rafael swell have enabled geological mapping of individual formations of the southern portion of this broad anticlinal feature in eastern Utah. Mapping at a scale of 1/250,000 on an enhanced and enlarged S-190B image has resulted in a geological map showing correlative mappable features that are indicated on the Geological map of Utah at the same scale.

An enhanced enlargement of an S-190B color image at a scale of 1/19,200 of the Bingham Porphyry Copper deposit has allowed comparison of a geological map of the area with the space imagery map as fair for the intrusion boundaries and total lack of quality for mapping the sediments. Hydrothermal alteration is only slightly evident on space imagery at Bingham but in the Tintic Mining district and the volcanic piles of the Keg and Thomas ranges, Utah, hydrothermal alteration is readily mapped on color enlargements of S-190B (SL-3, T3-3N Tr-2).

Several sites of calderas have been recognized and new ones located on space imagery. Attempts to locate the boundaries of three previously suggested calderas in the Topaz, Desert, Drum, and Keg mountain area, Utah, have been made with limited success on an enlargement of (SL-3, S-190B, 02-3N, Tr-2) a color image. New calderas have been recognized and their boundaries have been readily located by space imagery in the Escalante area, Utah, and in the environs of Timber Mountain, Nevada.

Geomorphology.- As the search for hidden mineral deposits in the Basin-Range province extends into post-ore blankets of Quaternary alluvium or volcanics, there developed a need to select those pediment or valley sites where only a thin veneer of alluvial material existed. Such sites required recognition and study of pediments, alluvial fans, bajadas, and valleys with shallow alluvial fill. Some specific examples and applications are cited.

Instrumentation - Exploration Geology and Geothermal Studies.- One of the "tools" developed through this contract is a mercury soil-gas analyzer that is becoming of significant use as an aid in locating hidden mineralized zones which have been suggested from space imagery. In addition, this "tool" is a prime aid in locating and better delineating geothermal sites.

The collector consists of a hemisphere equipped with a battery powered fan. Filters are used to collect contaminants. Silver screen disks (180 mesh) are placed in the orifice of the fan which is operated for ten minutes. The screen is heated at 650°c in a portable flameless atomic absorption instrument and the released Hg content is measured with a precision of ± 2 ppb.

Known geothermal areas that have been tested have given background readings of between about 10-50 ppb of Hg with anomalous samples collected near and as far as one-half mile from geothermal and drill hole sites that have measured in excess of 1300 ppb of Hg.

Further specific examples of the successful use of this tool are:
(1) extending the trend of the Comstock lode vein into post-ore alluvial and volcanic areas that resulted in more successful exploration drilling results,
(2) detecting anomalous values over porphyry copper deposits in contrast to surrounding non-altered nor mineralized areas, and

(3) other specific areas.
A notable test site in the Robinson Mining district was selected after space imagery of both EREP and LANDSAT-1 imagery indicated an area of potential post-mineralization covered with Tertiary dacite. A major fault through the volcanics allowed rapid erosion of the west portion of the area resulting in small inliers of Permian limestone to be exposed. Large positive aeromagnetic anomalies occur over nearby mineralized areas and known large production mines as do similar anomalies over the volcanic area although it is not known if the volcanics or a speculative buried intrusive, mineralized or not, is the cause of the positive magnetic anomaly. An extensive Hg soil-gas study in selective portions of the volcanic area has resulted in detecting several Hg anomalies of more than 100 ppb with background values of less than 10 ppb that correlate with aeromagnetic anomalies. Highly speculative explorative drilling is planned for the near future on one or two of these anomalies.

INTRODUCTION

The application of Space Imagery to geological studies in Utah and Nevada was initiated with the LANDSAT-1 program on July 23, 1972. Prior to this time, no space imagery from space sensors located normal to the surface north of 37° latitude, the southern border of Utah, had been obtained. Some high altitude, fixed-wing aircraft imagery along with low-elevation airphotos were available.

In addition to LANDSAT-1 imagery of Utah and Nevada, EREP imagery was also acquired for the purposes of this remote sensing study that consisted of S-190A, S-190B, S-192 photography and imagery along with RB-57F photography acquired at elevations near 57,000 feet.

Although the prime objective of these studies using space imagery has been mineral exploration, application to other geological specialties could hardly be ignored.

Figure 1 is a photo of a map of Utah and Nevada on which is indicated all of the LANDSAT-1 imagery received along with the EREP (Skylab) paths. The LANDSAT-1 imagery nadir positions are indicated by colored pins, with the color indicating the cloud cover of this specific imagery along with tags indicating the date of the recording of the imagery in space.

LANDSAT false color composite and EREP imagery enlargements display anomalous color changes in rock units which are closely related to some known and potential mineral deposits. This simple and direct use of black and white and color anomalies for selection of mineralization targets has been profitable in many areas (Short and Lowman, 1973). Correlation of such imagery anomalies with larger scale multispectral photography, geologic maps, geophysical surveys, etc. is proving to be productive.

Our principal objective of the application of space imagery was to determine its value in the location of new major ore targets. In this study the LANDSAT and EREP imagery was used as color composites and black and white photographic enlargements with scales between 1:20,000 to 1:1,000,000. LANDSAT tapes, analyzed and correlated by digital computer processing is of increasing value for the exploration photogeologists. A prime example of such is some of the studies performed by personnel of the Jet Propulsion Laboratory in collaboration with U. S. Geological Survey personnel on the Goldfield Nevada area (Rowan, L. C., et. al., 1974).

In summary, therefore, the purpose of this paper is to report on the utilization, method of study, and the results of the application of space imagery to geology including mineral exploration in the states of Utah and Nevada.

STUDY OF IMAGERY

The examination and study of imagery was done essentially by visual study using light tables to which is attached a Mikkon binocular microscope of variable magnification up to 50X. Lately, some LANDSAT positive transparencies are being studied using Add Color viewers that allow more visual latitude than the ozalid false color process that we have used extensively.

Imagery features were correlated and compared to ground truth data consisting of geological and geophysical maps, especially magnetic maps. Quaternary features consisting of landslides, fan deposits, and fracture and joint patterns were readily recognized. In addition, Pleistocene lake shorelines, deltas, bars, etc. of Lakes Bonneville and Lahontan, hydrothermal alteration features of known and potentially unknown mineral deposits were studied.

Geologic Maps were made from the imagery for comparison to known geologic features and some of the maps delineated features such as calderas, faults, and potential mineralized areas that had not been previously recognized.

RESULTS OF GEOLOGICAL MAPPING

Oblique SL-3 Image of Utah.- An oblique color photograph of a large portion of Utah and portions of Arizona, Nevada, and Idaho is shown by Fig. 2. The dark portion is not space but the outline of the Apollo Spacecraft window. The contrasts of the reflectivity of water are remarkably well displayed with the light gray colored fresh water Utah Lake located slightly above and to the left of the center of the image. In contrast, the Great Salt Lake exhibits the two lakes separated by the Southern Pacific railroad earth filled causeway with the more saline lake reflecting lighter color and the less saline lake, where much more fresh water streams enter, reflecting a dark blue color. The differences in the colors of the Great Salt Lake are the result of different bacteria existing in the waters of different degrees of salinity.

Only a very few scattered clouds exist to the north or left portion of the image with all other white areas being snow. The Uinta mountains, the Wasatch Plateau, and the Wasatch mountains are all tipped with snow, as are the Rocky and East Humboldt ranges of Eastern Nevada as shown in the lower right corner of the image. In the west portion of the image, those ranges with snow in the higher elevations are the Schell Creek and Snake ranges, Nevada, with the latter two snow capped portions separated by Sacramento Pass. The snow tipped Deep Creek range in Utah is located farther north and on the edge of the Bonneville Salt Flats.

Lake Mead is visible near the right edge of the image as is Lake Powell in the upper center of the image. The San Rafael swell is well displayed in the upper left portion of the image.

Other vertical images of specific portions of this oblique photograph are dealt with in detail in this report.

San Rafael Swell, Utah.- LANDSAT-1, Skylab, and RB-57 imagery acquired within days of each other of the San Rafael swell have enabled geological mapping of individual formations of the southern portions of this broad anticlinal feature in eastern Utah. Mapping at a scale of 1/250,000 on an enhanced and enlarged S-190B image (Fig. 3) has resulted in a pre-

liminary geological map (Fig. 4) showing more detailed mappable features than are indicated on the Geological map of Utah at the same scale (Fig. 5). Attempts to map using S-190A and LANDSAT-1 images (Fig. 6) are much less satisfactory because of coarse-grained emulsion of the former and the telecon fuzziness of the latter.

Bingham Porphyry Copper Mine, Utah.- Using an enhanced enlargement of an S-190B color image at a scale of 1/19,200 of the Bingham Porphyry Copper deposit (Fig. 7) has resulted in poor mapping of part of the geological contact of the Bingham stock and intruded sediments exposed on the pit levels. Comparison of a geological map of the area with the space imagery map is fair for the intrusion boundaries within the pit but of little value for the sediments. Hydrothermal alteration is only slightly evident on space imagery at Bingham but in the Tintic Mining district, Utah, and the volcanic piles of the Keg and Thomas ranges, Utah, hydrothermal alteration is readily mapped on color enlargements of S-190B (SL-3, T3-3N Tr-2).

Calderas, Timber Mountain area Nevada, Escalante Desert, Utah, and Keg and Drum Mountains, Utah.

Several sites of calderas have been recognized and new ones located on space imagery. Attempts to locate the boundaries of three previously suggested calderas in the Topaz, Desert, Drum, and Keg mountain area, Utah, have been made with limited success. The suggested calderas are shown on Fig. 8 with a geologic map of part of the area Fig. 9. New calderas have been recognized and their boundaries have been readily located by LANDSAT space imagery in the Escalante area, Utah, (Fig. 10) (LANDSAT-E1447-17412-7) and in the environs of Timber Mountain, Nevada (Fig. 11) (Byers et.al., 1968; Byers, et.al., 1969). Other investigators have also recognized the additional calderas near Timber Mountain and the comparisons of independent mapping of such is remarkably similar (Verbal Comm. by N. Short).

GEOMORPHOLOGY

As the search for hidden mineral deposits in the Basin-Range province extends into post-ore blankets of Quaternary alluvium or volcanics, there developed a need to select those pediment or valley sites where only a thin veneer of alluvial material existed. Such sites required recognition and study of pediments, alluvial fans, bajadas, and valleys with shallow alluvial fill. Some specific examples and applications are:

Alluvial fans.- Image SL-2, 10-007, Tr 34, shows post Lake Bonneville (< 12,000 years BP) alluvial fans where only the fan heads are evident above the Bonneville level. Significantly, the new fans in this area have resulted from recent uplift of this range rejuvenating the source area. The uplift is either tectonic or isostatic rebound occurring after the disappearance of Lake Bonneville.

Bajadas.- Well developed bajadas of this area are interpreted as indicating a state of dynamic equilibrium. In the Snake Range of eastern Nevada, good correlations can be observed between the steepness of fans and the ruggedness of source drainage basins (S1-2, 04-012 to 015, Tr 34).

Death Valley, California.- The patterns of alluvial deposition are easily discernible in the Southern California-Nevada border on space images (SL-2, 04-186 to 192, Tr 6) where throughout the area, numerous observations have been made. This area sharply contrasts with the preceding one in respect to maturity and activity. In the north end of Death Valley, well developed fans are observable. Individual fans are more distinct on the southwest side than on the northeast side. The north end of the valley is being aggraded by alluvium entering from the northwest.

In the south end of Death Valley, areas of present and recent deposition can be easily distinguished from areas of desert pavement on the southwest fans. There is an absence of desert pavement at the toes of all these fans. The upper limit of this narrow

grey band parallels the fan-playa junction. This feature, along with the differences in size and morphology, are quite probably the result of tectonic activity. The general area is known to be tectonically active and Death Valley is tilting to the East. This tilting may explain the above observations. These interpretations have been done in our laboratory by Robert Rogers.

SEASONAL VARIATIONS OF IMAGERY

Although EREP imagery was acquired during different seasons of the years, LANDSAT imagery is considerably better in exhibition of seasonal ground variations not only because of snow cover, changes in the sun angle, and more closely spaced time intervals between overflight passes.

The differing views of an area provided by LANDSAT in the different seasons emphasize different geologic features and patterns. To illustrate seasonal changes in LANDSAT images and their effect on geologic analysis, the La Sal Mts. area in SE Utah is shown in three differing sets of spectral bands 5 and 7, together with a geologic map and an EREP high resolution photograph of the area (Fig. 12 and 13). In Fig. 12, MSS Band 5 is shown on the left side of the figure with MSS Band 7 on the right. Fig. 12 includes LANDSAT images and an EREP pass and a geological map with the LANDSAT imagery acquired on 9/28/72, and Fig. 13 includes images acquired on 10/29/73/ in the lower portion of the figures and 1/14/73/ in the upper portion of the figures. The contrasts are not strikingly different. This area is of interest for important known and potential uranium and copper ore deposits. The relationships between the La Sal intrusives and the copper and uranium mineralization, particularly on the Lisbon Anticline are most striking.

It is apparent that most of the large geologic units are well defined on the LANDSAT prints of this small scale. Snow cover and low sun angles emphasize some stratigraphic details and fracture zones and patterns which are obscure on the geologic map and even in the darker portions of the S-190B (Fig. 12) high resolution color photograph.

Two strikingly different LANDSAT images are shown by Figs. 14 and 15. Both cover essentially the same area but on the two different dates of 12/14/72/ (Fig. 14) (E-1144-18001-7) and 8/5/73/ (Fig. 15) (E-1378-17591-7). This area includes I-80 in the upper portion of the figure with Battle Mountain, Nevada, located slightly left of the upper center of the images. The major mineralized areas are in the Antler Peak range consisting of Copper Canyon and Copper Basin where two open pit operations are active. Both show some evidence on the images of hydrothermal alteration bleaching. Goat Window located to the left of the few cumulus clouds near the center of the summer scene (Fig. 15), is accentuated by the juniper trees that are more prevalent in the limestone window than in the surrounding upper plate allochthonous formations. Tertiary volcanic fields are readily recognized by their characteristic patterns in the upper and left portions of the images.

The winter scene (Fig. 14) exhibits relief exceptionally well along with fracture and fault locations, but offers little for recognition of lithologic changes. The elongate, dark trace in the upper portion of the image is close to I-80 and the major valley in that part of the image, but it does not follow the valley trace well at all and even continues along the east side of the Antler Peak range rather than the major Humboldt river path. Its exact significance is not yet known. The images also include Cortez and the Cedars mining districts.

HYDROLOGY - UTAH LAKE

Soon after LANDSAT-1 was launched, an enormous algal bloom, swirl pattern was noted in Utah Lake. This is a classic image as shown on Fig. 16. Wind patterns had created the patterns. The prior 18 day overpass on 8/25/72/ (Fig. 17) detected a slight beginning of this algal development that might have been ignored had it not been for the prominence of

the later full development. Interestingly enough, on Aug. 30, no evidence remained and no blooms have been detected since.

There are suggestions of the cause of this algal bloom. Similar but rare occurrences are known in Utah Lake. It is interesting to note that the bloom appears to originate on the west shore of the lake very close to an industrial plant where slurry explosives are developed and tested. There may be a possibility that diesel fuel, nitrates, or other energy sources spilled near the shore could have played a nutrient role in the development of this major algal bloom.

S192 IMAGERY

Cursory analysis of the 13 bands of the S-192 black and white imagery of Utah Lake and the Tintic mining district illustrates the utility of the numerous bands. All channels are located as follows:

	Fig. 19	Fig. 20	Fig. 21
NW Quadrant	2	6	10
NE Quadrant	3	7	11
SW Quadrant	4	8	12
SE Quadrant	5	9	13

Fig. 18 includes, according to the above order of quadrants, the following features:

Geologic map of the area of a scale of 1:550,000
Black and white print of Skylab S-190B
Color print of Skylab S-190B
Color enlargement of Skylab S-190B

The major feature of Utah Lake, a fresh water lake that drains into the Great Salt Lake located about 40 miles north, are quite variable on the S-192 precision imagery. The lake is most prominent in black reflectivity on channels 4, 5, 6, 7, 8, 10, 11, and 12. None show the details, however of EREP photos on Figure 18. Channel 13, the thermal IR band, indicates a signal to noise ratio of less than one. Geological structural features are well identified, especially in the upper portions of the images on channels 4, 6, 8 and 9. The city of Provo, east of the Lake, is displayed in varying degrees in all 12 channels. The major highway, I-15, is identified more readily on channels 6, 10 and 11. Lake Bonneville strand lines or shore lines are prominently on the mountain slopes in the north portion of the images on channels 5, 7, 8, 10, 11, and 12.

The large Tintic mining district is located in the southwest corner of all images. The EREP color images provide the most detail including the dark and white mottled area located most readily in the lower central portion of the SE enlarged color photo of Fig. 18. This area is the well-known East Tintic district where hydrothermal alteration studies (Lovering, 1949; Lovering, et.al., 1960) have been accomplished, and which led to the discovery of the Burgin Mine. The mottled effect is the result of darker relatively unaltered volcanics in contrast to the well-altered and bleached volcanics. Greater enlargements of this area, in color, would allow better delineation of the altered areas.

In contrast, EREP channels 2, 3, 4, 6, 8, 10 and 11 allow identification of the district but do not provide the detail as viewed on EREP, S-190B, color photos.

S-192 - THERMAL IR STUDIES

Band 13, S-192, is shown in the SE quadrant of Fig. 21. It is obvious that this thermal IR imagery is of low quality and of little use. Being aware of this difficulty, another thermal IR detector (w/X-5) was added to the SL-4 phase of Skylab. Fig. 22 shows the path of this predawn thermal IR track which intersects the California coast north of Los Angeles, covers the southern San Joachin valley, the Sierra Nevada, and crosses Nevada into Utah.

Fig. 23 (LANDSAT E-1015 17422-7) shows the position of two thermal IR images acquired with the w/X-5 detector carried on SL-4. Clouds cover portions of both thermal IR images and only one image is included in this report.

Detailed analysis of this IR data has not been completed but specific observations have been made. In the Fish Spring range, Utah, however, hot springs are abundant near the northeast edge of the range. The upper left hand corner of Fig. 24 shows the northward discharge or runoff from these springs as white paths flowing over light gray salt flats. The temperature of the springs average around 83°C and the runoff cools slowly over distances of several miles.

MINERAL EXPLORATION

In the Robinson mining district, White Pine County, Nevada, which includes the Ruth porphyry copper mines, three large positive aeromagnetic anomalies exist over the Ward Mountain area, the Ruth porphyry copper operations, and over a Tertiary volcanic area northwest of Ruth (Figs. 25 & 26). Prior studies of this area have suggested that the volcanics may or may not be the cause of the anomalies. Both LANDSAT-1 and Skylab S-190A imagery however, indicate possible outcrops in the volcanic area of the Paleozoic sediments. Field studies or ground truth have verified the existence of these inliers. Subsequent to our field study we were made aware of a USGS open file map (Hose and Blake, 1970, USGS open file) of White Pine County, a portion of which is shown as Fig. 27. This figure shows the inliers of Paleozoic carbonate formations overlain by the dacite volcanics. A few areas of Pliocene fresh water carbonate formations overlie the volcanics. Minor modifications have been made in the map and a major fault has been added based on the lack of exposures of rock older than the volcanics in the eastern portion of the area. On this same figure, areas A, B, and C are covered with standard contiguous lode mining claims based on the highly speculative potential of this area.

A magnetic map and gravimetric map (Carlson and Mabey, 1963) of the area is included as Figs. 26 and 28 respectively. Fig. 29 is an aeromagnetic map acquired at an elevation of 600 feet above the ground that shows the magnetic variations in detail and the areas covered by standard contiguous lode claims held by three different concerns.

Carlson and Mabey (1963) realized the suggested potential of the volcanic area of post-mineralization age of the Ruth area and are quoted as follows:

> Egan Range. A large magnetic high is centered over the southern edge of the Robinson mining district at Ruth where disseminated copper deposits occur in an east-trending zone of metamorphosed sedimentary rocks and altered monzonite porphyry. The near-surface igneous rocks associated with the copper deposits could produce part of the magnetic anomaly, but the major part is produced by a large, partly concealed, intrusive body.
>
> In the Egan Range northeast of Jakes Valley, Tertiary volcanic rocks are exposed in an area of moderate relief. The gravity values over this area are not markedly different from those on Paleozoic rock in adjoining areas and indicate either that the volcanic rocks are thin or have about the same density as the Paleozoic rocks. The volcanic rocks are covered on the magnetic map by an area of alternate high and lows. The cause of these local magnetic anomalies over the volcanic rocks is not known but the anomalies may be related to intrusive rocks near the surface or the eruptive centers.

The gravity values over the dacite volcanics are similar to those over the Ruth area where a large intrusive underlies the area. Certainly, of course, none of these data is conclusive in indicating a buried intrusive, mineralized or not, in the northern volcanic area.

Further studies are needed to prove or disprove its existence. It is interesting, however, that the structural trend of the Ruth ore bodies which is essentially east-west, does suggest a change to a more northerly trend that is overlapped by the volcanics as shown by a LANDSAT image (Fig. 25) and by an S-190B black and white image (Fig. 30). One further study consists of a mercury soil-gas analysis that has been done over part of the area.

Mercury soil-gas analysis.- Mercury is associated with mineralized zones as a trace element, but constantly escapes, ultimately to the surface because of its high vapor pressure. It can be collected readily as an amalgam and can be quantitatively measured by atomic absorption techniques with a precision of ±2 ppb.

The mercury soil-gas collectors designed under the NASA contracts have been used for almost two years in numerous environs. Measurable amounts of Hg have always been collected, the only exception noted to date is in heavily frozen ground, which appears to form an impenetrable barrier to the passage of soil-gas. Incidentally, soil samples have been collected at the same sites both before and after Hg soil-gas collecting. There is little if any correlation, presumably because Hg in the soil or rock is probably cinnabar of which the vapor pressure of Hg is nil in contrast to elemental Hg existing in the soil-gas. More detailed research needs to be done on this subject, however.

In practice, the collector cone is buried in the ground to a depth of about six inches and the loose soil that is removed from the hole is tamped down firmly around the outside of the cone. At least two small 1" discs of 180 mesh silver screen are placed in the orifice of the apparatus, and the fan is switched on for a period of ten minutes causing the soil-gas to move out of the soil under the cone and through the screen. Any mercury in the soil-gas is captured by the silver screens forming Ag-Hg amalgam. After collecting, each screen is then placed in a sealed glass vial and refrigerated until it is ready to be assayed in either the mobile trailer or motel room where the portable Lemaire model 500D mercury analyzer is located. The cold environment of storage is a precaution to prevent vaporization of the Hg from the silver amalgam. This procedure is not absolutely necessary, but it does guard against inadvertent exposure to high temperatures while in transit. Blank silver screens are also included after being exposed to air for about 10 seconds or so before being placed in the sealed vials. They usually pick up about zero to 10 ppb of Hg. This determines the contamination level measured in that particular area.

A portion of the results of a mercury soil-gas study of part of the volcanic covered area is shown on the low level aeromagnetic map, Fig. 29. With background measurements of about 10 - 30 ppb, a major anomaly exceeding 120 ppb was located as shown. Because of this anomaly and its location on the flank of the positive magnetic anomaly to the west, this site has been selected for an exploration drill hole test.

Mercury in Geothermal Areas.- The association of mercury with present or past hot spring and geothermal sites is well known. Sulfur Bank, California, for example was a mercury mine until the depth of open-pit mining reached temperatures unbearable to the miners, not to mention the health hazard through inhalation of mercury vapor. Monte Aimata, Italy, has a storage reservoir rock that apparently underwent post-volcanic collapse that fragmented the reservoir rock and the mercury deposits lie below an impermeable thrust sheet that confined and controlled the mercury mineralization. Very few geothermal sites lack mercury mineralization and the resulting escape of mercury vapor to the atmosphere.

This technique has been used in successful exploration for trends of hidden mineral deposits and it has been tested over known ore deposits during the past two years. Recently, however, the technique has been tested over four geothermal areas. Three of the four showed amazing correlation with known geothermal zones within the specific geothermal areas. The fourth area released too much H_2S to obtain valid results and a precipitator of H_2S before it reaches the Ag screen to form Ag_2S is now being developed as an addition to the soil-gas collector. A map of one of the areas is shown as Fig. 31 with the close

correlation of one of the anomalies with a successful geothermal drill hole.

It is apparent, therefore, that this comparatively low-cost exploration tool could be of considerable benefit to those concerns not only exploring for geothermal areas but of important use to better delineate further drilling targets within the area, all of which should be of increased significance to the national concern with geothermal energy resources.

The relationship between mercury mineralization, and hot-spring activity is observed at many geothermal fields throughout the world. In fact, when nuclear or conventional explosive techniques are used to enhance the output of geothermal wells, the danger of post-shot mercury toxicity to human beings will have to be considered, a subject that has received very little study to date.

REFERENCES

Short, N.M., and Lowman, P.D., 1973, Earth observations from space: Outlook for the geological sciences, NASA Goddard Space Flight Center publ. X-650-73-316, p. 1-115.

Rowan, L.C., Wellaufer, P.H., Goetz, A.F.H., Billingsley, F.C., and Stewart, J.C., 1974, Discrimination of rock types and detection of hydrothermally altered areas in south-central Nevada by the use of computer-enhanced ERTS images. U.S. Geol. Survey Professional Paper 883, p. 1-35.

Byers, F.M., Jr., Orkild, P.P., Carr, W.J., and Quinliran, W.D., 1968, Timber Mountain Tuff, southern Nevada, and its relation to cauldron subsidence, in Nevada Test Site, Geol. Soc. Amer. Mem. 110, p. 87-97.

Byers, F.M., Jr., Carr, W.J., and Orkild, P.P., 1969, Volcanotectonic history of south-western Nevada caldera campha, Symposium on volcanoes and their roots, Oxford, England, 1964 (Abst.). Internat. Assoc. Volcanology and Chemistry of the Earth's Interior, p. 84-86.

Lovering, T.S., 1949, Rock alteration as a guide to ore, East Tintic district, Utah, Econ. Geol. Monograph 1.

Lovering, T.S., et. al., 1960, Geologic and alteration maps of the East Tintic district, Utah, U.S. Geol. Surv. Mineral Investigations, Field Studies Map MF 230, 1/9, 600 (two sheets).

Carlson, J.E., and Mabey, D.R., 1963, Gravity and aeromagnetic maps of the Ely area, White Pine Co., Nevada, U.S. Geol. Surv. Geophysical Investigations, GP 392.

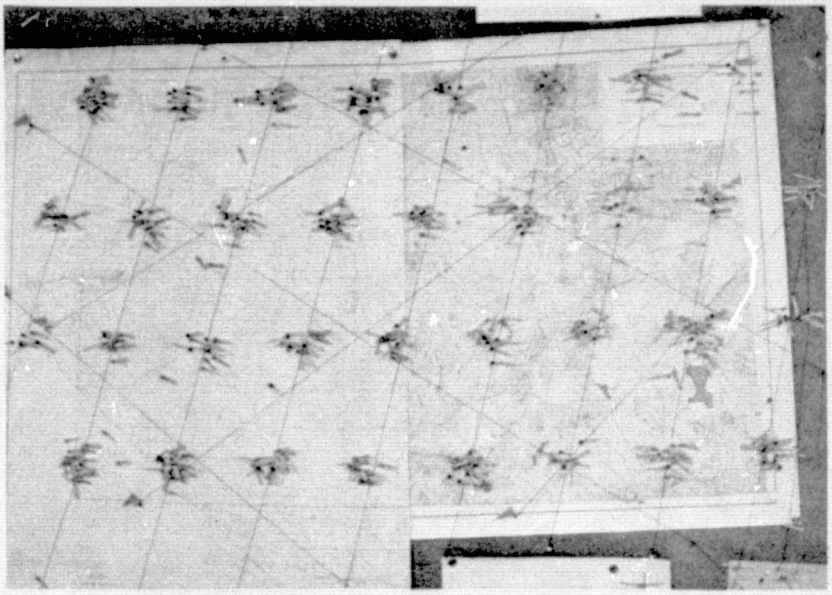


Fig. 1. Location of LANDSAT-1 images and EREP tracks in the states of Utah and Nevada. Colored pens were used on the maps to indicate percentage of cloud cover.

REPRODUCIBILITY OF THE
ORIGINAL PAGE IS POOR

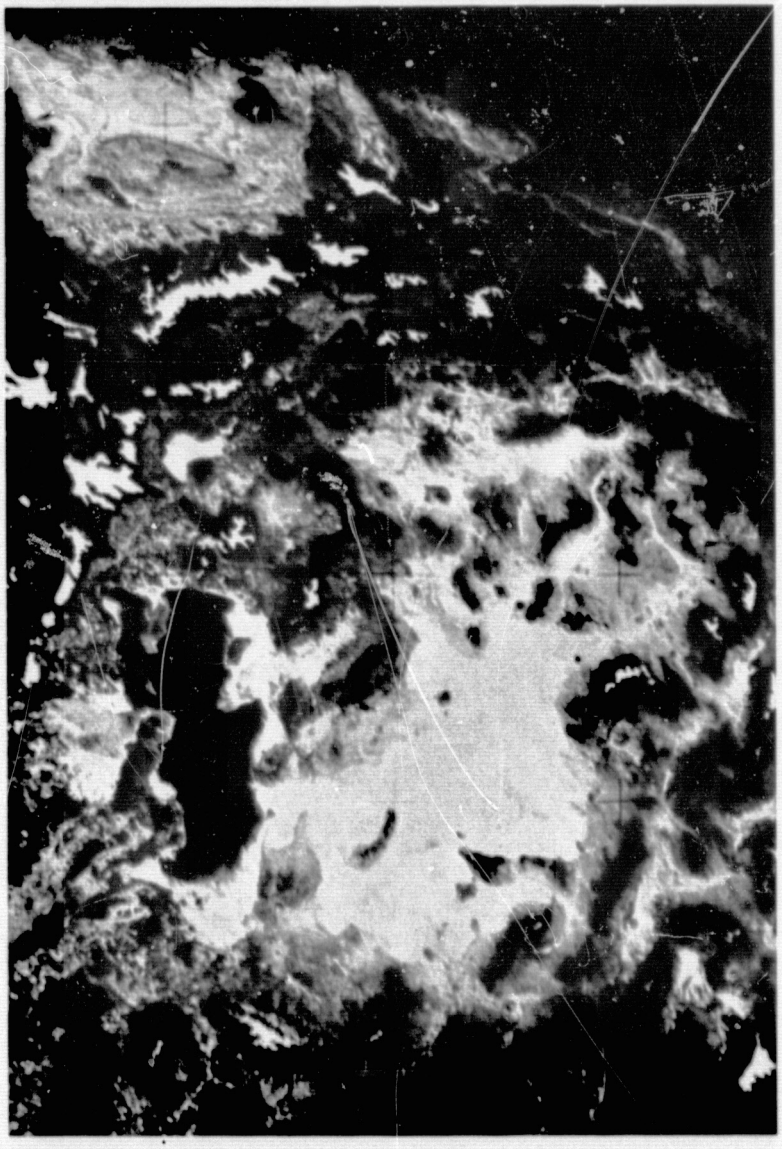


Fig. 2. Oblique color photograph from Apollo spacecraft of Great Salt Lake, Salt Flats, San Rafael Swell, Utah and Nevada.

REPRODUCIBILITY OF THE
ORIGINAL PAGE IS POOR

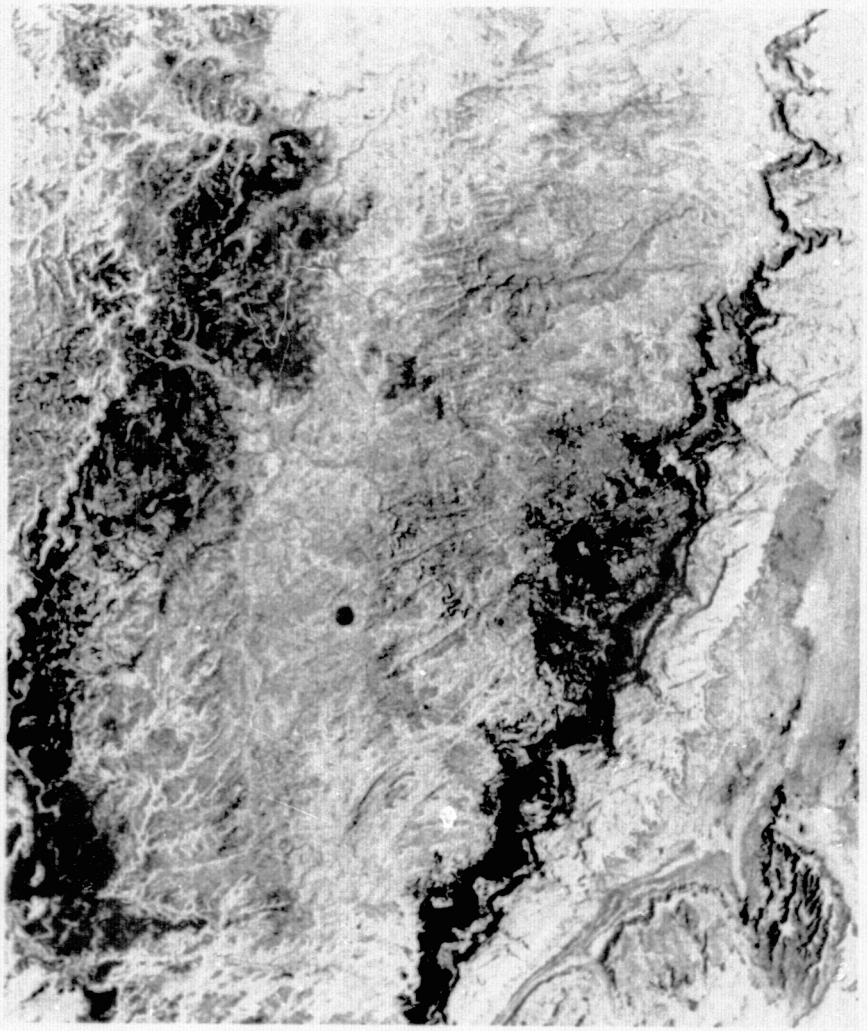


Fig. 3. S190B B&W photograph of the southern portion of the San Rafael swell which has been used for geological mapping at a scale of 1/250,000.



Fig. 4. Transparent overlay of geological features mapped from Fig. 3.

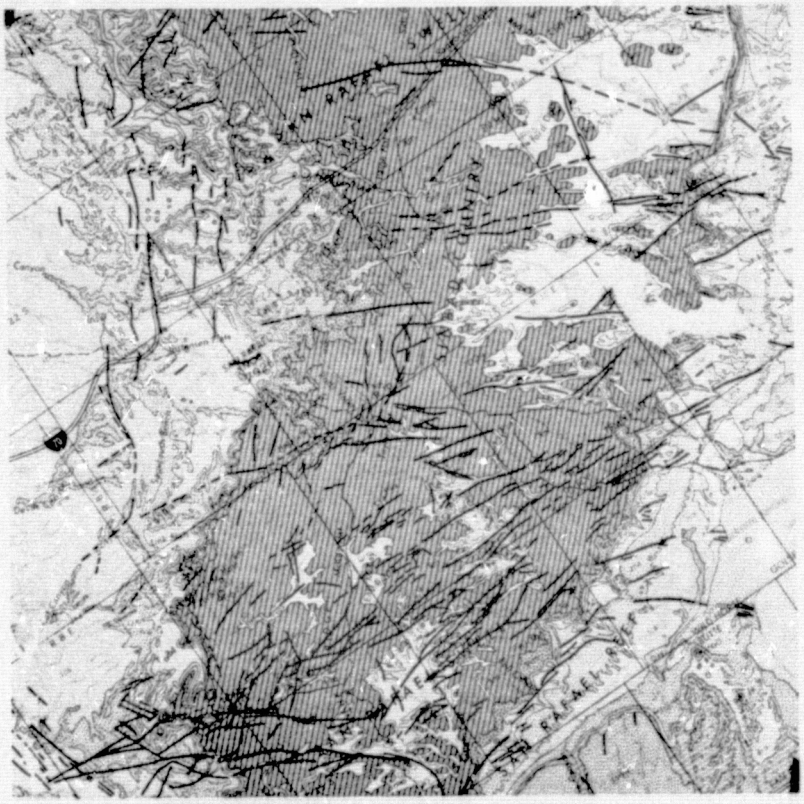


Fig. 5. Geological map of the southern portion of the San Rafael swell for comparison to Figs. 3 and 4.

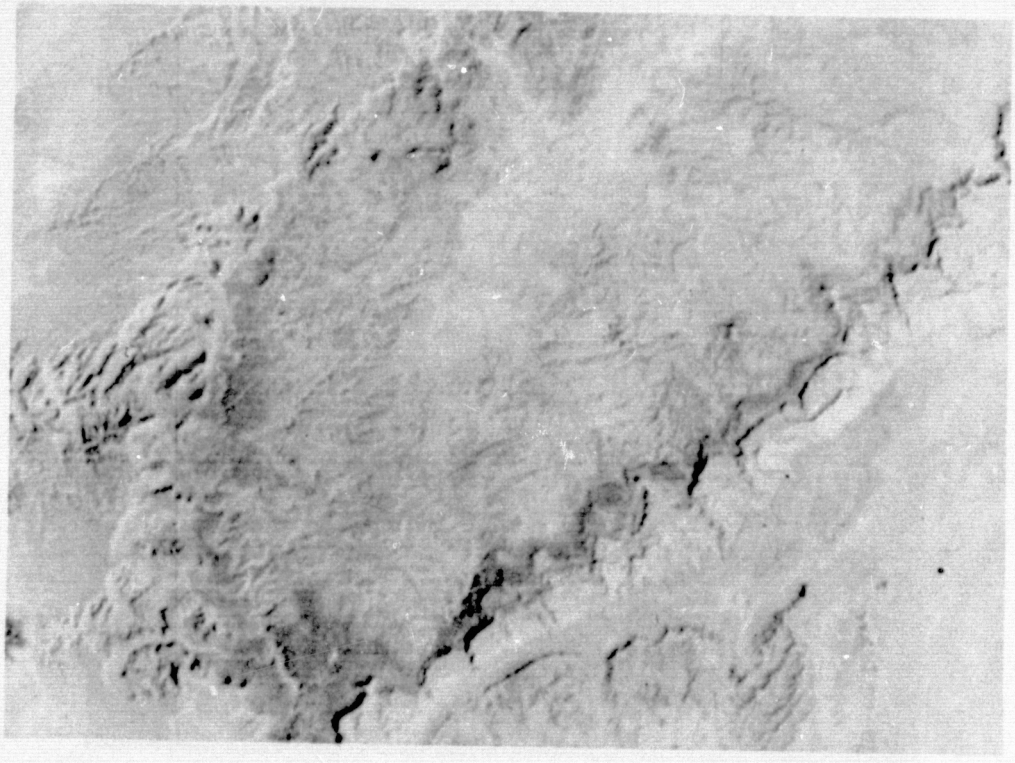


Fig. 6 LANDSAT-1 image of the southern portion of the San Rafael swell for comparison to Figs. 3 and 4.



Fig. 7. Color enlargement of the Bingham Porphyry copper pit. S190B image. Although sun shadows cause some darkening of the waste dumps, the darker eastern portion of the pit roughly indicates the position of the granite porphyry Bingham stock.

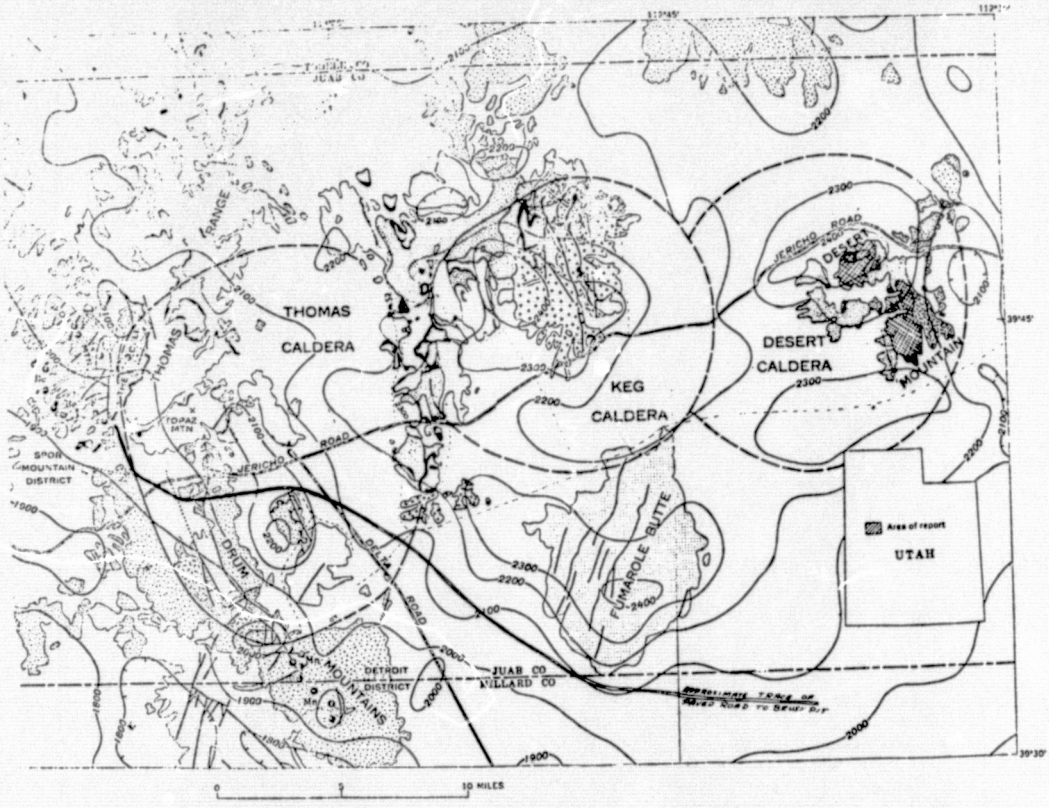


Fig. 8. Suggested outlines of three calderas located in west central Utah as indicated on the drawing. (After Shawe, Reese, and Staub.)

REPRODUCIBILITY OF THE
ORIGINAL PAGE IS POOR

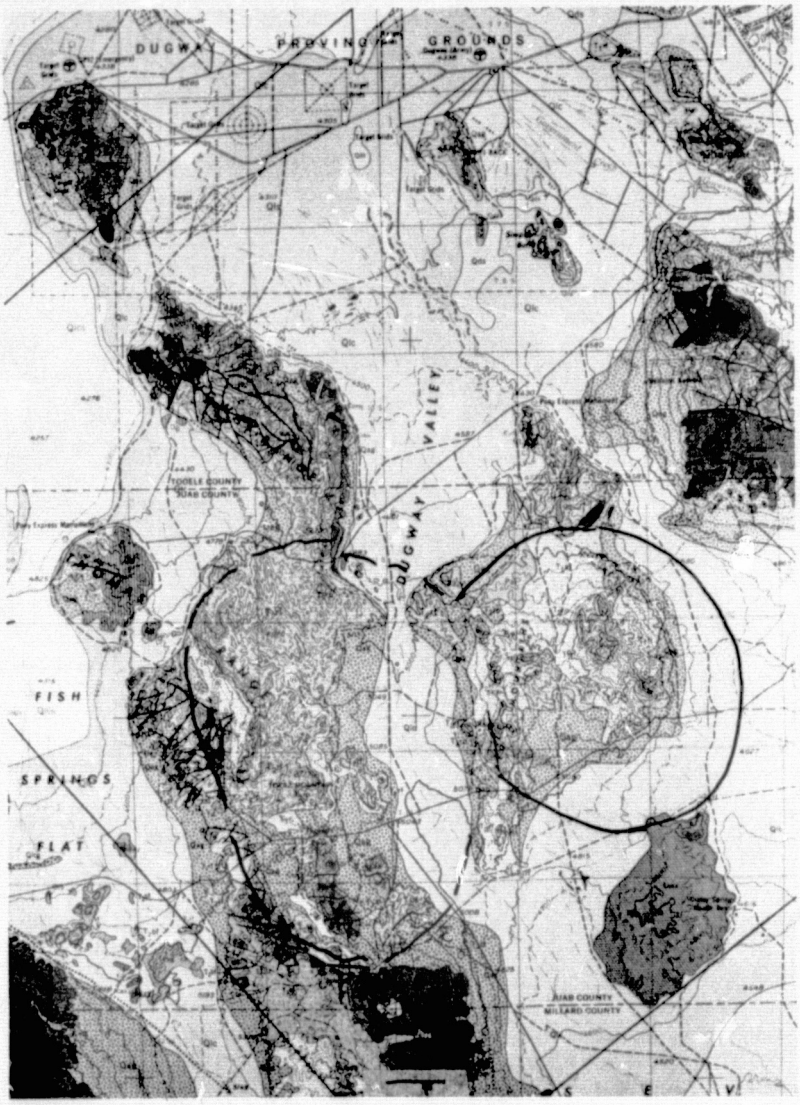


Fig. 9. Geologic map of two of the suggested calderas that are not well defined on space imagery.



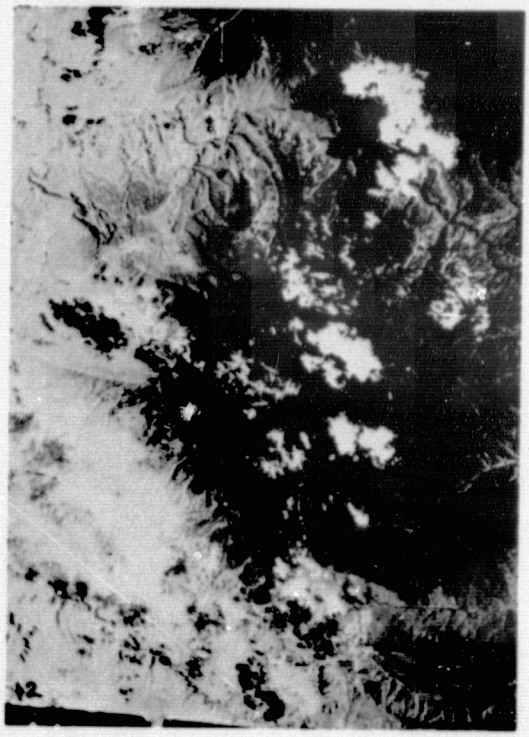
Fig. 10. Well defined Escalante Desert caldera on LANDSAT-1 image E-1447-17412-7.



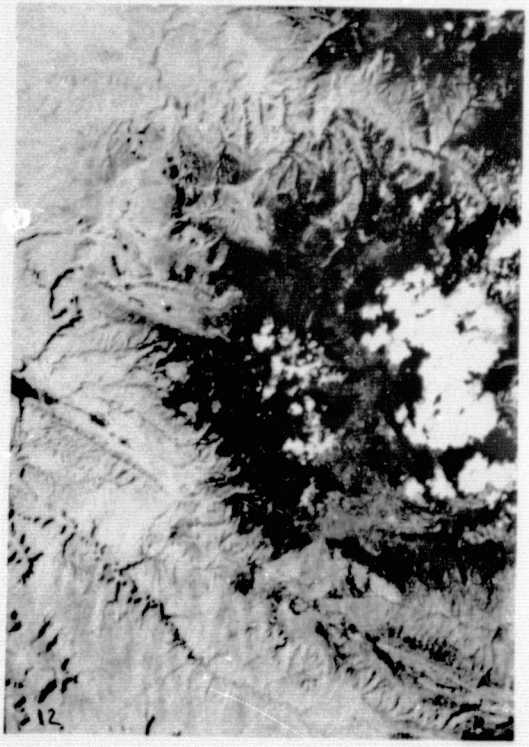
Fig. 11. Calderas of the Timber Mountain area with associated known and newly-identified calderas located on LANDSAT-1 images.



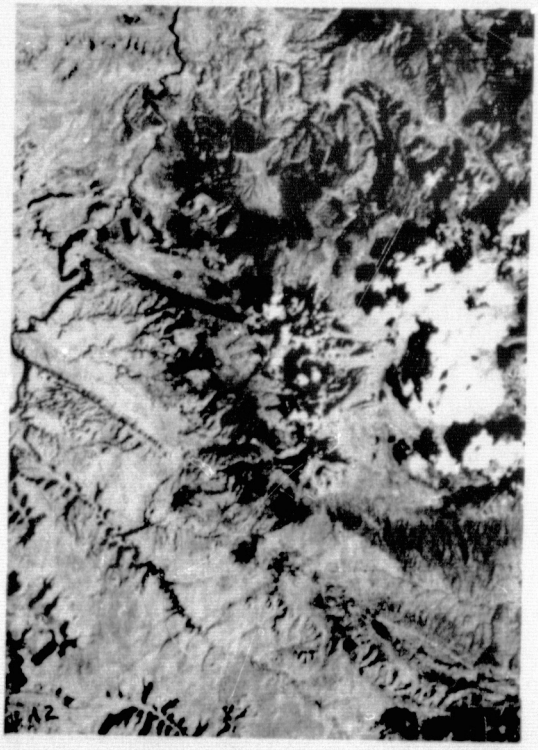
Geologic map



S190B color print



LANDSAT Band 5
Sept. 28, 1972



LANDSAT Band 7
Sept. 28, 1972

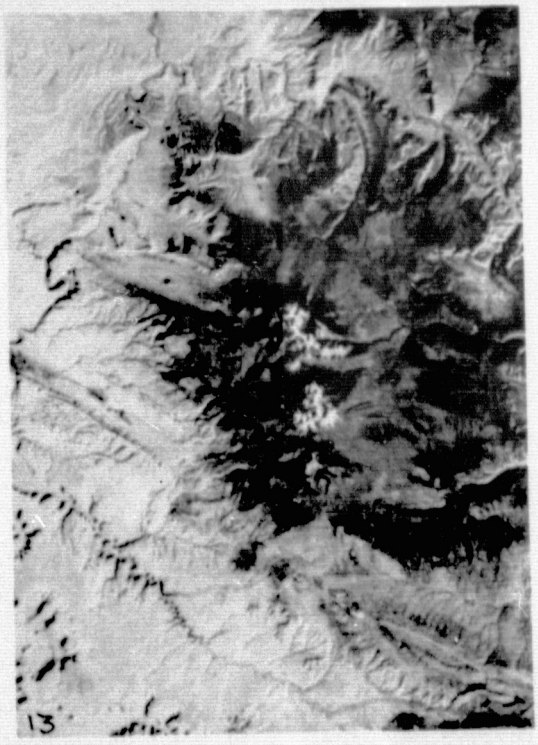
Fig. 12. Maps and images of part of the Colorado Plateau, Utah.



LANDSAT Band 5
Jan. 14, 1973



LANDSAT Band 7
Jan. 14, 1973



LANDSAT Band 5
Oct. 29, 1973



LANDSAT Band 7
Oct. 29, 1973

Fig. 13. Summer-winter scenes.



Fig. 14. Winter snow covered scene, Dec. 14, 1972, of LANDSAT E-1144-18001-7 image with sun declination angle of 22 degrees.



Fig. 15. Summer scene, Aug. 5, 1973, of LANDSAT E-1378-17591-7 with sun declination angle of 56 degrees. Compare to Fig. 14. Area is northern Lander County, Nevada.

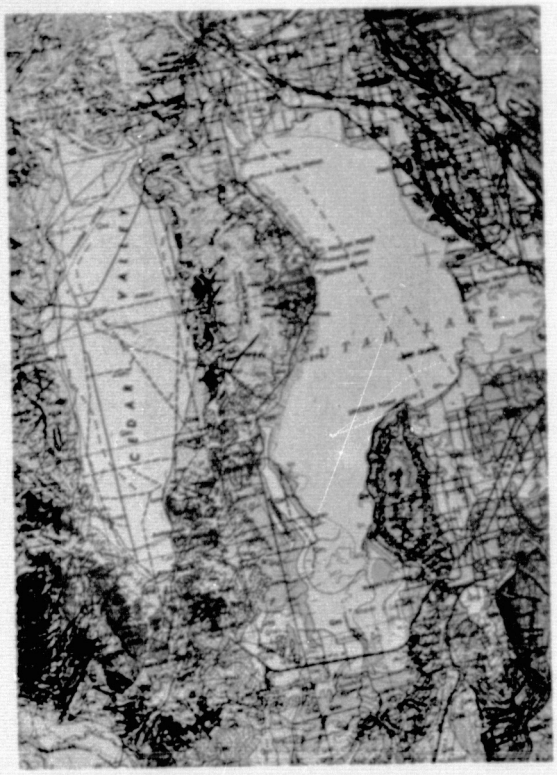
REPRODUCIBILITY OF THE
ORIGINAL PAGE IS POOR



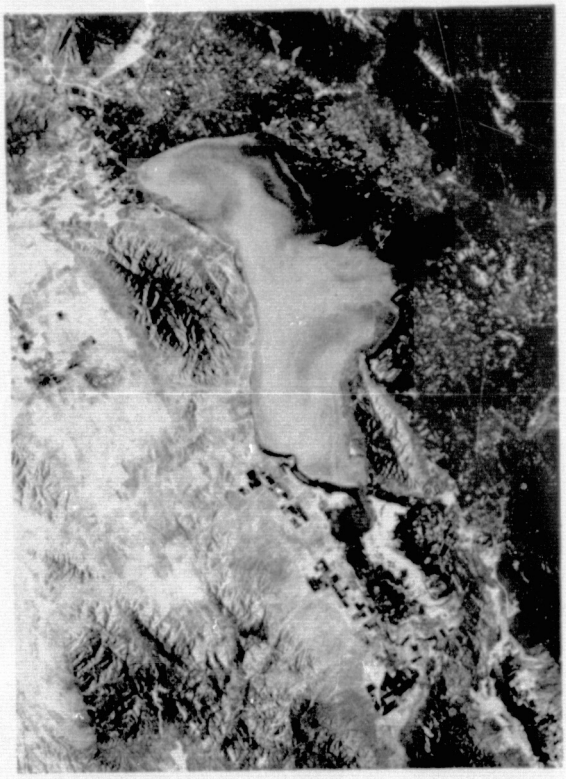
Fig. 16. Utah Lake algal bloom on LANDSAT image, Sept. 12, 1972.



Fig. 17. Utah Lake, beginning of algal bloom is light streak on LANDSAT image of Aug. 25, 1972. Compare to full bloom 18 days later, Fig. 16.



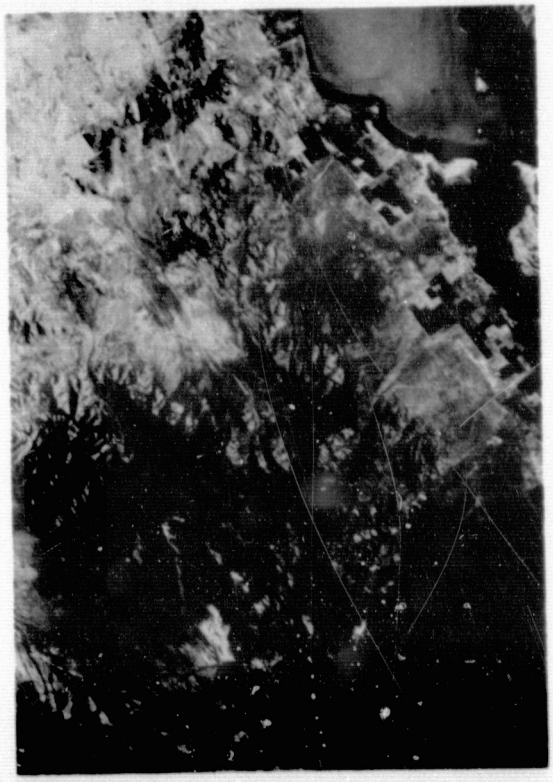
Geologic Map



S190B B&W



S190B Color



S190B Color
enlargement

Fig. 18. Utah Lake and Tintic Mining District.



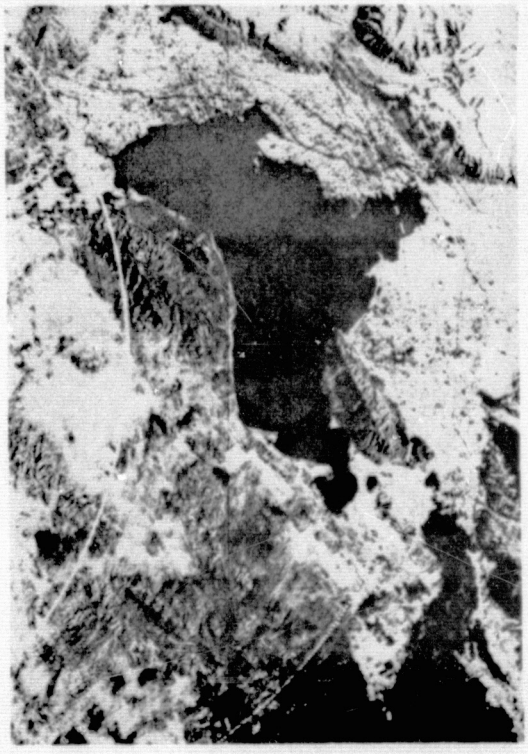
Channel 2



Channel 3



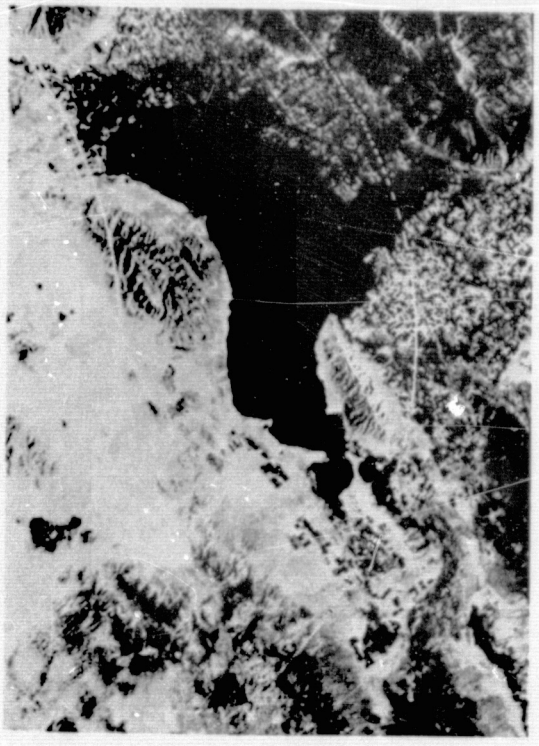
Channel 4



Channel 5

Fig. 19. S192 images of different channels.

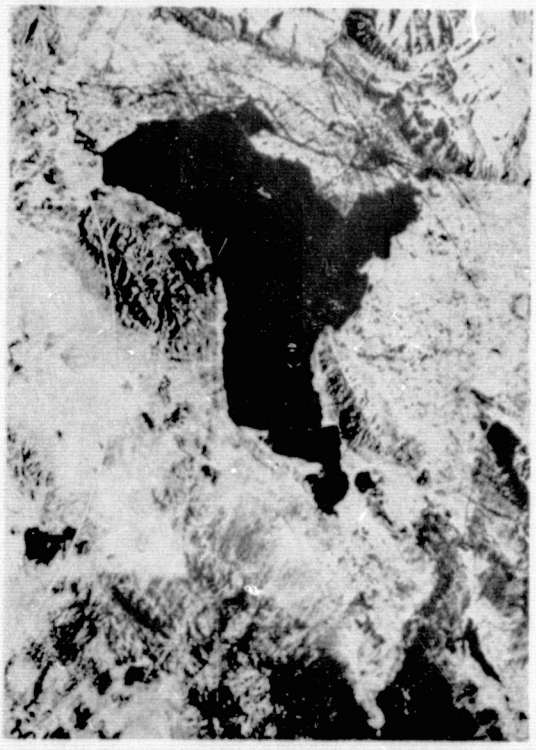
REPRODUCIBILITY OF THE
ORIGINAL PAGE IS POOR



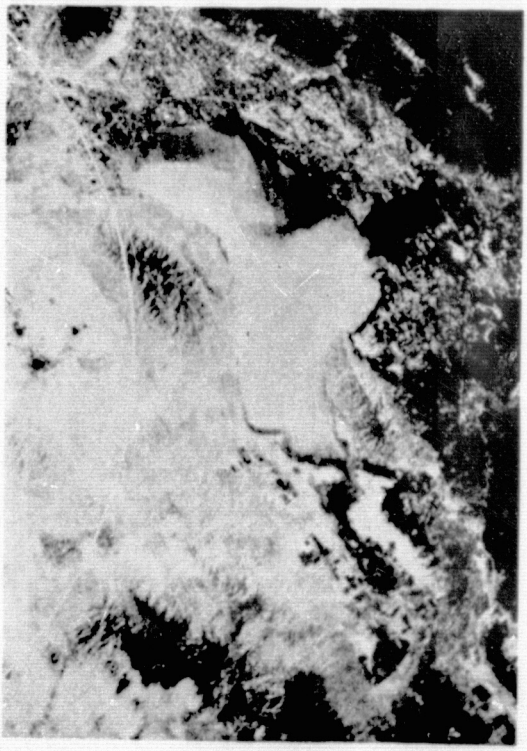
Channel 6



Channel 7



Channel 8



Channel 9

Fig. 20. S192 images of different channels.



Channel 10



Channel 11



Channel 12



Channel 13
Thermal IR channel

Fig. 21. S192 images of different channels.

S-192 W/X-5

Fig. 22.

REPRODUCIBILITY OF THE
ORIGINAL PAGE IS POOR

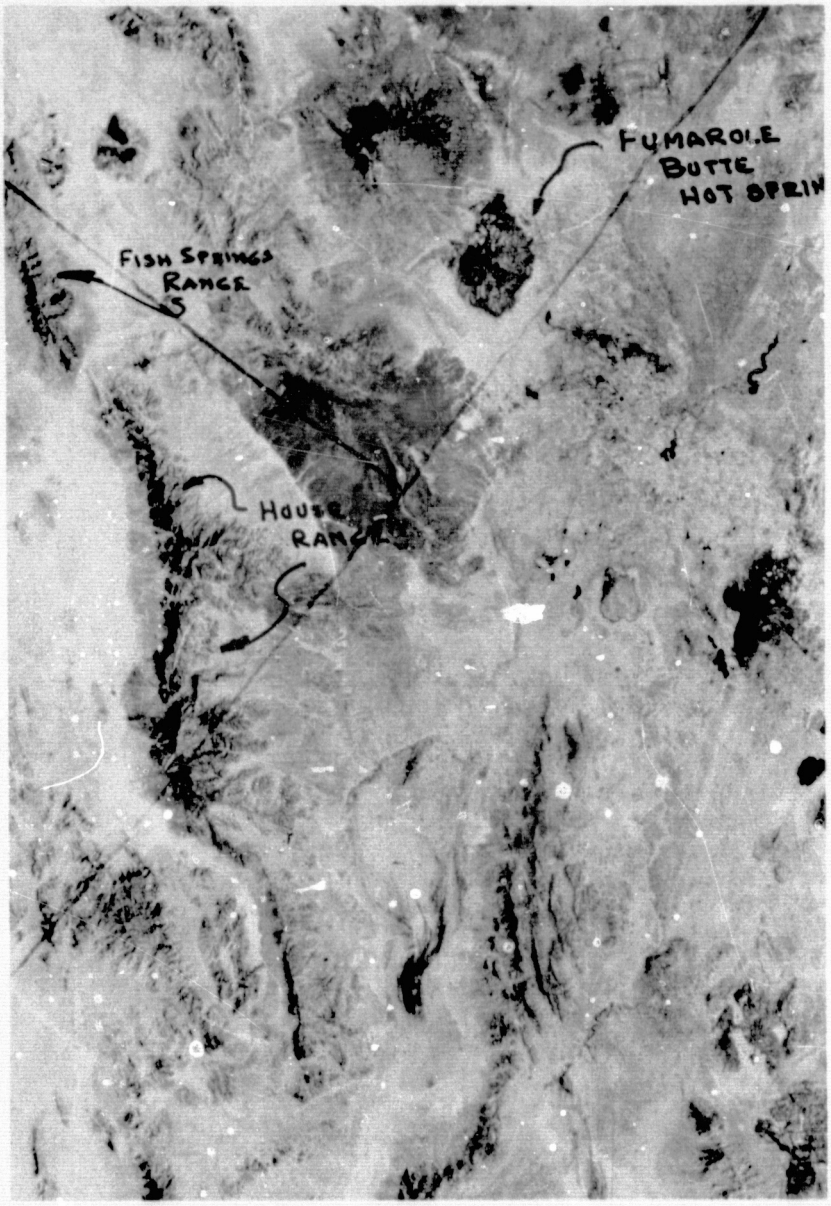


Fig. 23. LANDSAT image of west central Utah showing position of two precision S192 thermal IR images obtained with the w/X-5 detector. The north edge of the Fish Springs range has several hot springs at temperatures of abour 82 degrees C. Compare to Fig. 24.

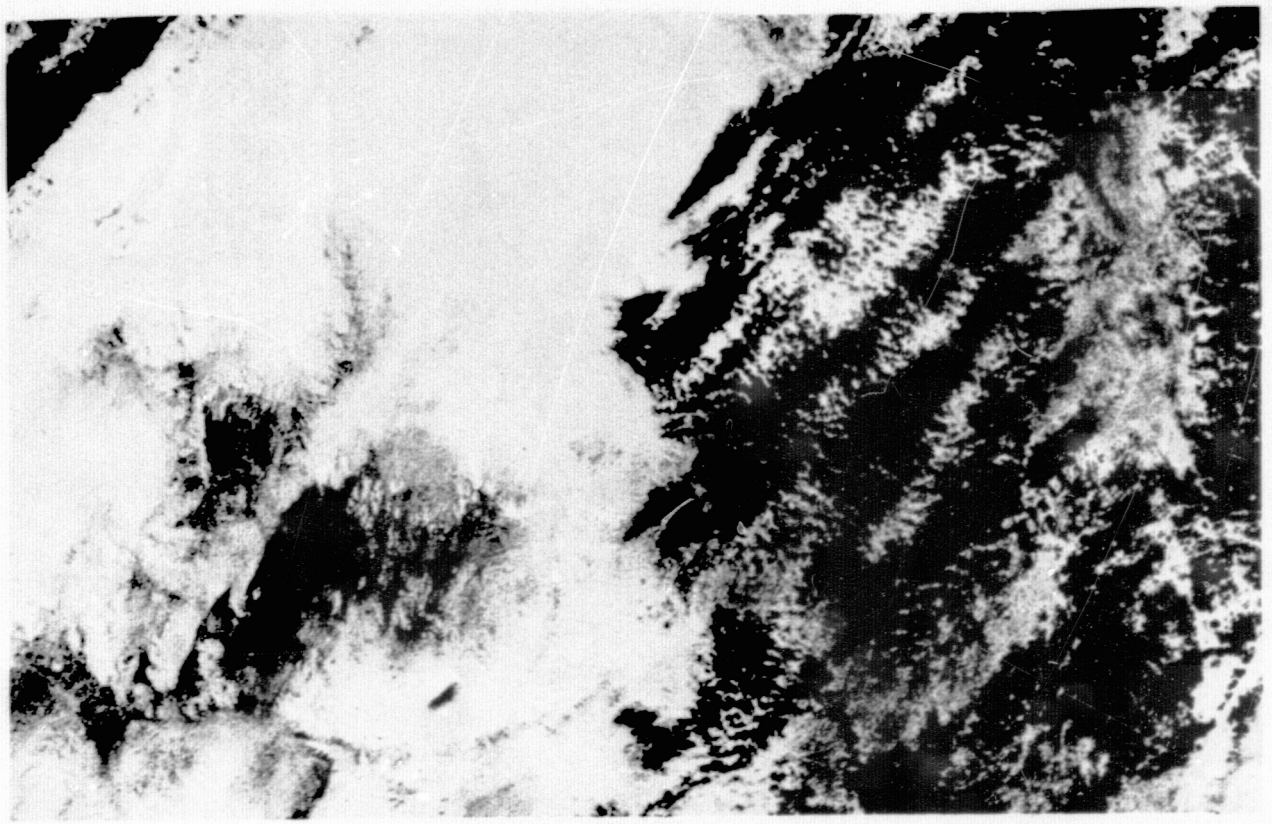


Fig. 24. Thermal IR image of S192, w/X-5 detector precision image. Overflow of hot water from Fish Springs is evident in two parallel discharges in the upper left hand corner of the image.

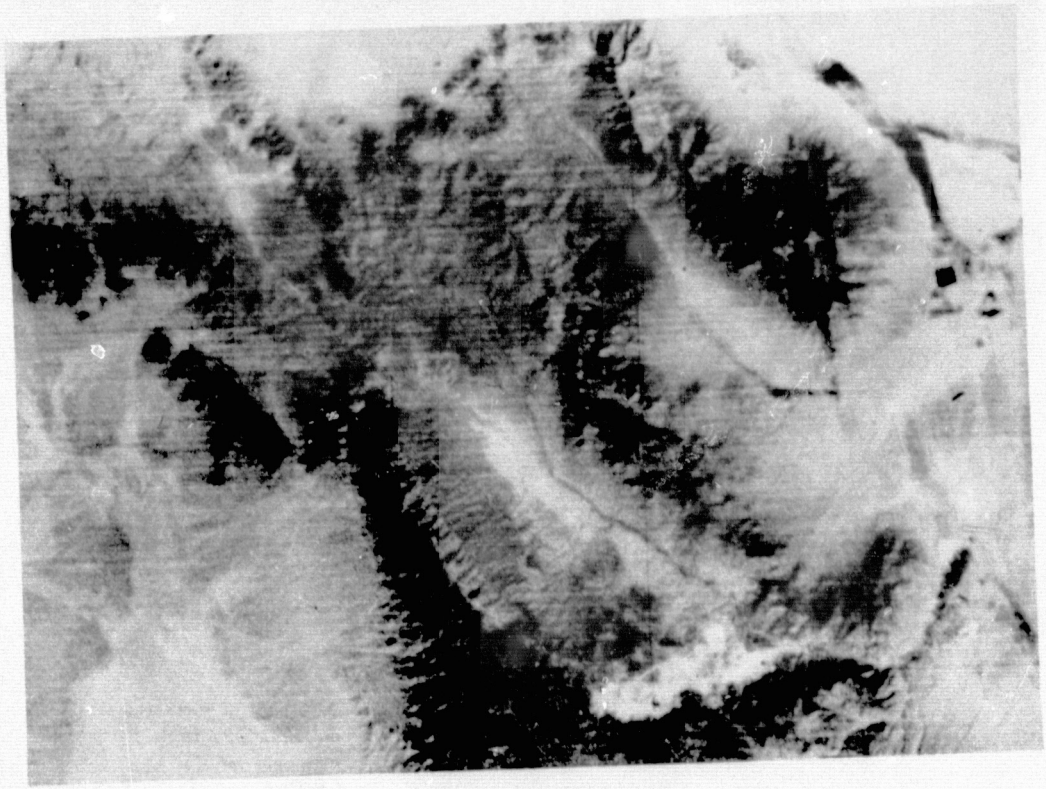
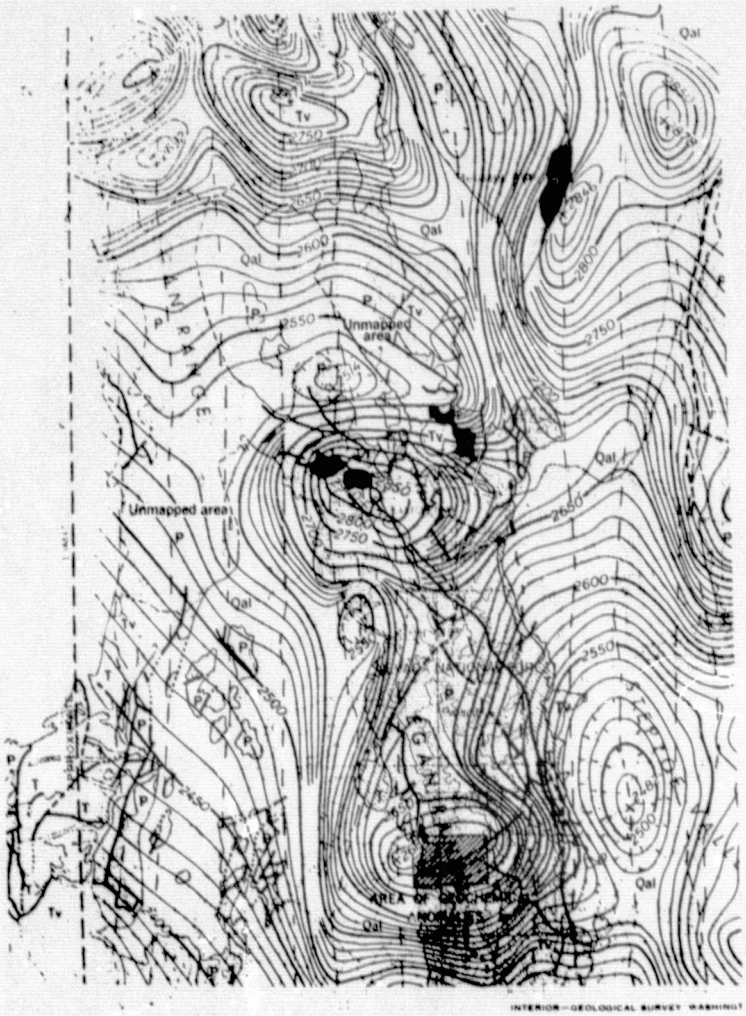


Fig. 25. LANDSAT image of Ruth porphyry copper pits, McGill tailings pond in upper right portion of image, and dacite volcanic area in upper portion of image where erosion has exposed outcrops of the underlying Permian limestone.



B. TOTAL INTENSITY AEROMAGNETIC MAP

Fig. 26. Total intensity aeromagnetic map of the Ruth area, White Pine County, Nevada showing large magnetic anomalies over the Ruth porphyry copper deposits, the Ward Mountain area of geolochemical anomalies in the southern part of the image, and the positive anomalies in the dacite volcanic area to the north.

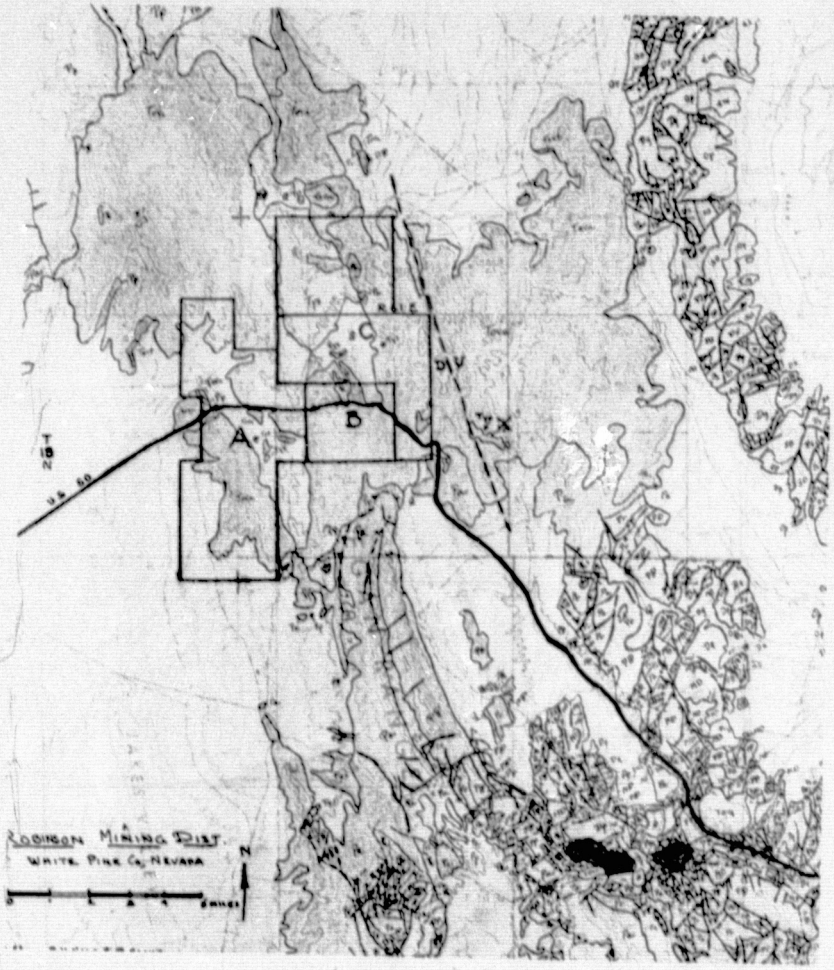
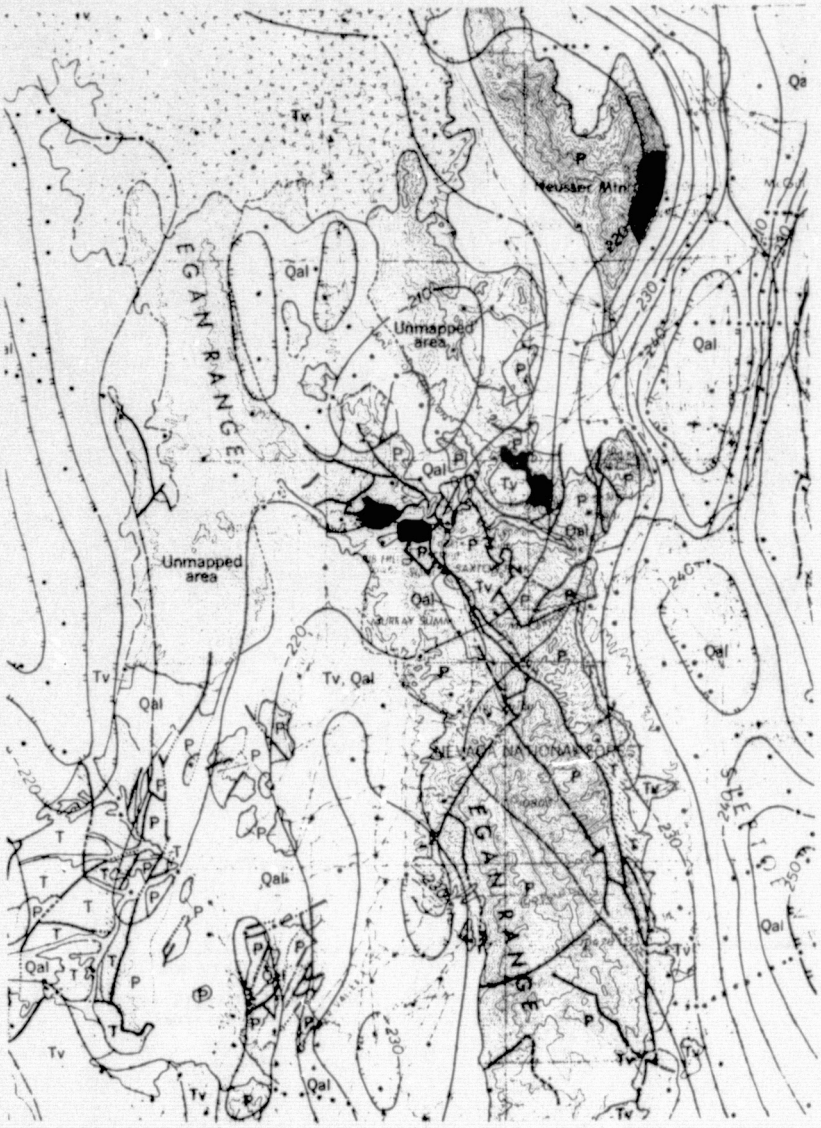


Fig. 27. Geologic map of the Robinson Summit area, White Pine County, Nevada. The Ruth Porphyry copper deposits are located in the southeast corner of the map. The lettered areas are covered with standard contiguous lode mining claims. (Geology by Hose and Blake, USGC, slightly modified by Jensen.)



A. BOUGUER GRAVITY ANOMALY MAP

Fig. 28. Bouguer gravity anomaly map of the Robinson and Ward Mountain mining districts.

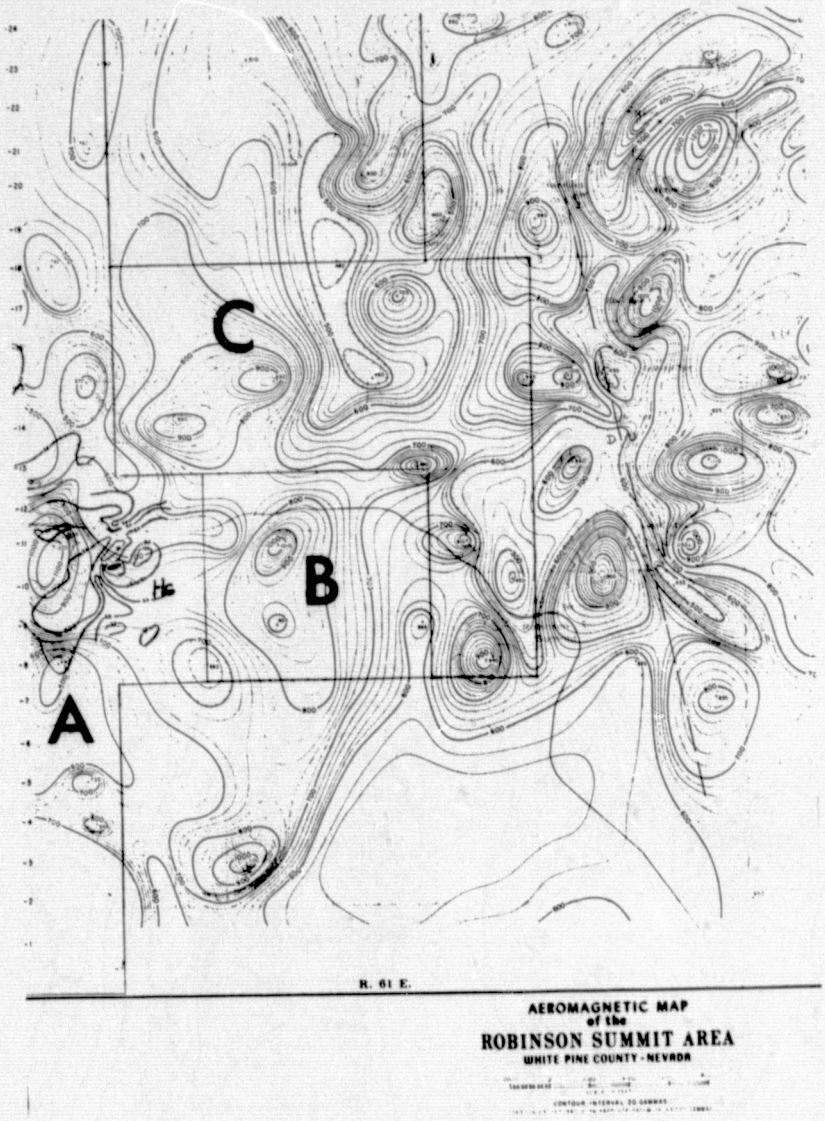


Fig. 29. Total intensity aeromagnetic map of the Robinson Summit area, White Pine County, Nevada. Lettered areas are covered with standard contiguous lode mining claims and the contours at the left edge of the figure indicate ppb of mercury collected as soil-gas.

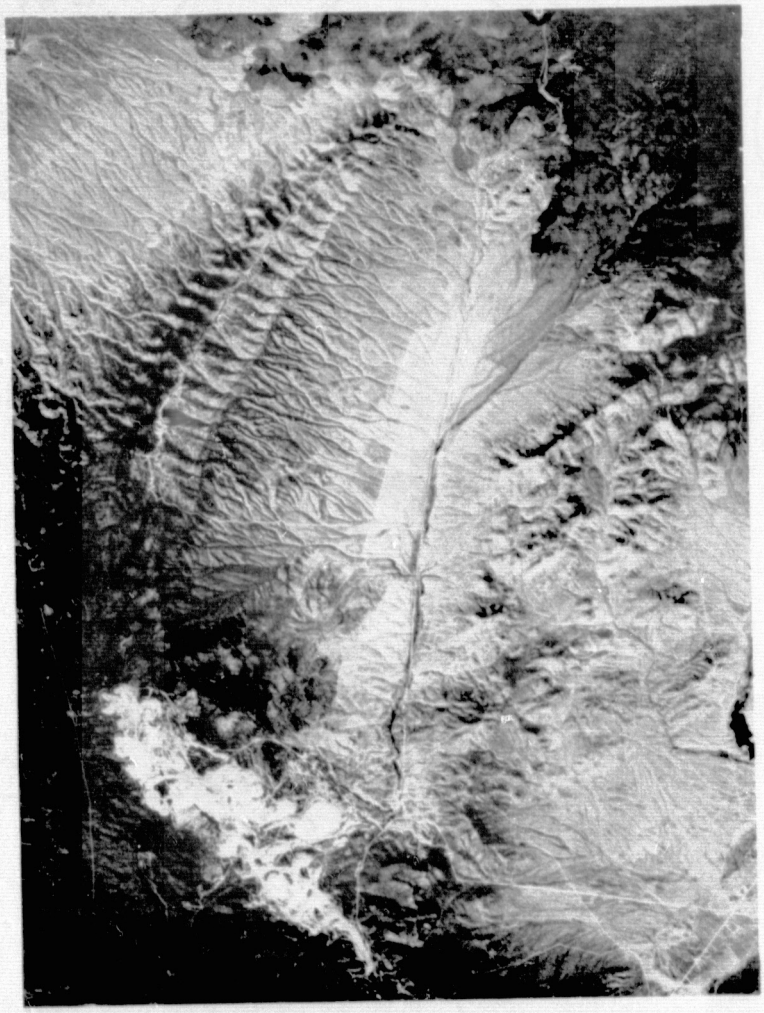


Fig. 30. Photograph from S190B of the Ruth Porphyry copper deposits and the structural trend toward the north of Paleozoic limestones to where the dacite volcanics cover the Paleozoic sediments.

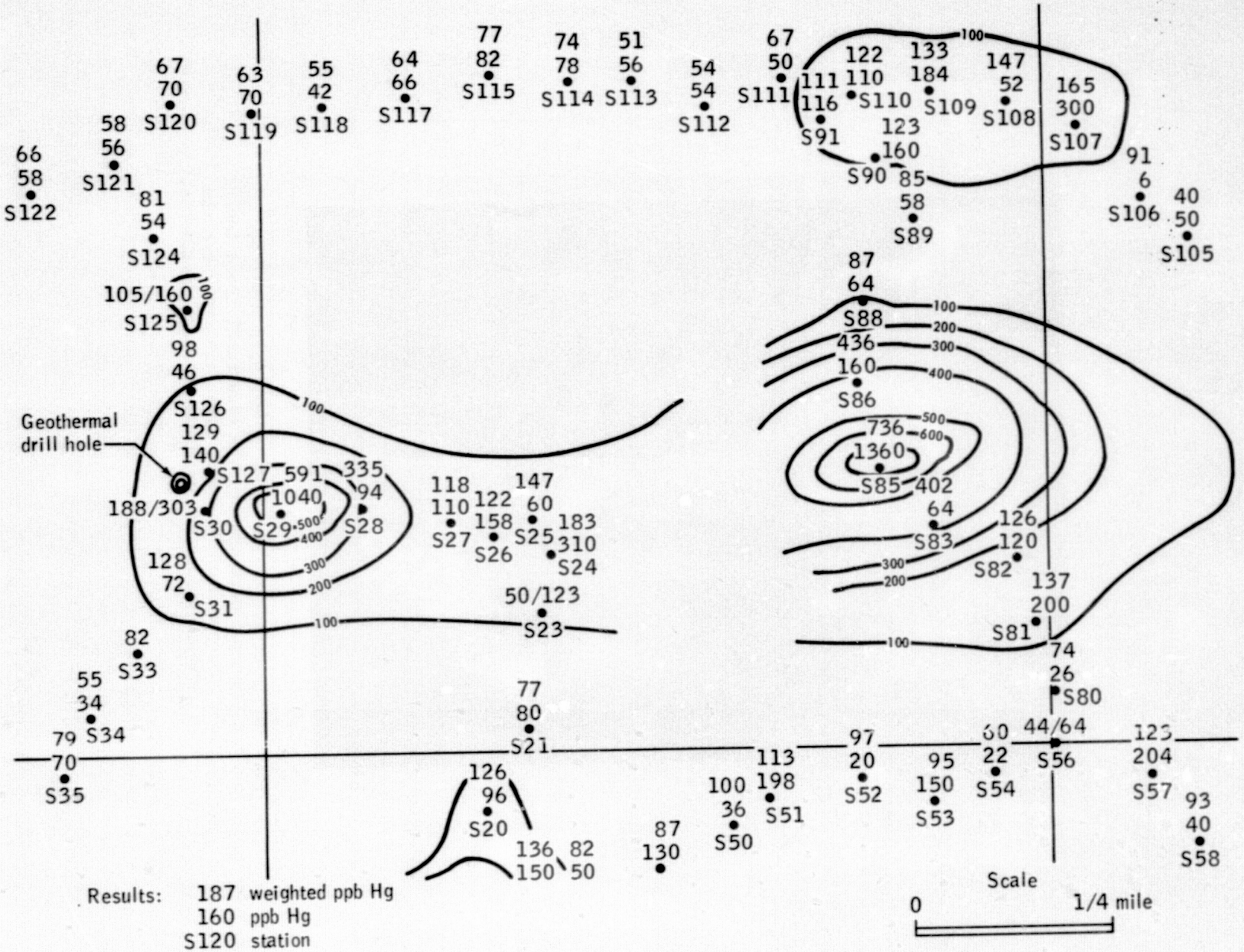


Fig. 31. Mercury soil-gas results.

GEOLOGICAL SIGNIFICANCE OF FEATURES OBSERVED IN COLORADO FROM ORBITAL ALTITUDES

G-10

N76-17508

Don L. Sawatzky, Gary Prost, Keenan Lee, and D.H. Knepper

Geology Department, Colorado School of Mines, Golden, Colorado

ABSTRACT

Three major investigations using LANDSAT and Skylab imagery were concerned with analyses of color anomalies and linear features of central Colorado.

Skylab S190A and S190B photographs over central Colorado, covering approximately 47,000 sq km of the Rocky Mountains, were analyzed to determine which features associated with known mining districts are recognizable on space images. This analysis indicates that visible features associated with mineralization include high densities of linears, complex linear intersections, red-ocher and light color (alteration) anomalies, and perhaps vegetation patterns unique to mineralized areas. It was assumed that linears designate ore-controlling fractures, and that color anomalies are gossans or hydrothermally-bleached intrusives.

The Skylab photographs were then studied to locate indicators of mineralization. Two target areas were chosen where several features coincide; a primary study area (32.5 sq km) at Weston Pass, and a secondary area (130 sq km) at Dome Rock. Ground truth, obtained at the primary target by geologic mapping at a scale of 1:12,000, was used to identify the features seen on photography and to evaluate orbital imagery as a tool in mineral exploration. The secondary target was briefly field-checked by identifying the indicators of mineralization in a reconnaissance fashion. The secondary site was evaluated to determine if indicators of mineralization are consistent throughout the region.

Field work indicates the original assumptions are incomplete. Red-ocher colors may result from features other than weathered sulfides, and light-colored units need not be intrusive sills. Linear patterns may not be unique to an area, nor are high densities and intersections of regional linears the only structural controls on mineralization. Distinctive vegetation patterns associated with mineralization were not observed because vegetation is influenced more by other factors.

Orbital imagery in itself is inadequate to fulfill exploration needs; it may, however, be a powerful tool when used in conjunction with aerial photography and field work.

The second investigation was concerned with the structural information available in a LANDSAT image of central Colorado and has revealed several

techniques that extract much of that information.

The techniques include selecting an image with maximum linear enhancement, preparation of a relatively unbiased linear map, measurement of lengths and azimuths of the linears, selection of all linears of supermodal length, generation of strike-frequency diagrams, and selection of significant structural trends.

A length-versus-frequency graph of the linears is prepared from which is determined the modal length. Azimuth-versus-frequency curves suggest that the short linears of less than modal length have a large part of the uniformly distributed azimuths. On the other hand, comparisons with structural trends indicate that linears greater than modal length contain most of the structural information. A length-weighted strike-frequency diagram of super-modal linears combines the two features and reveals structural information in close correlation to structural trends.

Four major trends are present in the LANDSAT imagery of the central Colorado test site. The test site contains sedimentary terrains (South Park, Denver Basin, and Canon City Embayment) surrounding the metamorphic and igneous terrains of the southern Front Range. In addition is a Tertiary volcanic terrain superposed on a metamorphic terrain south of South Park. A N.25W. trend is an important trend which is manifest as a pervasive fracture trend in the uplifted mountain block and as the trends of Laramide folds and faults in the sedimentary terrains. In the northern part of the test site these structures have the prominent N.0-10E. trend. The N.65E. trend is parallel to a fracture trend orthogonal to the other fracture trend. The fourth trend N.85E. appears only in the length-weighted analysis and occurs in the Tertiary volcanic terrain. It is a manifestation of long pre-volcanism drainage channels which have been enhanced by differential erosion.

The third investigation was concerned with those anomalous megalinears and their associated geologic lineaments that transect major tectonic features in central Colorado. They are anomalous relative to the major known lineaments that essentially bound and parallel the major features. These anomalous megalinears have not been studied extensively because a synoptic view has not been available heretofore.

The transecting megalinears are equally as detectable in an image as the more structurally consistent lineaments. Their associated lineaments are composites of anticlines, synclines, drag folds, monoclines, faults, crush zones, shear zones, and rock joints. The variability of structure types along the trend of a lineament is very dependent upon the lithologic terrains in which they are developed. It is this variability as well as the transecting nature of the lineaments that presents a somewhat confusing structural picture, and perhaps has slowed the recognition of these major anomalous structural features.

In LANDSAT and Skylab images the normal tectonic elements and their marginal structures are recognizable. In addition are four concentric features and several transecting megalinears. Of the concentric features, the most prominent one is the Pikes Peak intrusive center of the Pikes Peak batholith. Two volcanic centers, the Thirtynine Mile and one in Wet Mountain Valley, are also recognizable. Three transecting megalinears are in the Rampart Range portion of the Front Range, and three are in part of the Front Range south of Pikes Peak.

The structural evidence associated with the transecting megalinears of the Front Range uplift points to a more complex involvement of the crystalline basement in the regional tectonic deformations. These deformations consist not only of the familiar ones of uplifts decoupled from the basins along flank thrusts and monoclines but also independent or subsequent, continuous cross-cutting deformations that have the spatial unity of a lineament, yet are manifest in different structural features along that lineament. Further study of these features may add considerably to our knowledge of the tectonic histories and kinematics of regions.

INTRODUCTION

The results of three independent investigations of LANDSAT and SKYLAB imagery of central Colorado are reported in this paper in three sections. These studies are concerned with, through the use of extensive ground observations, the geological significance of spectral and spatial features on the images. The first investigation analyzed and evaluated color anomalies in SKYLAB photographs for locating indicators of mineralization. The second investigation determined the relationships of all linear features in a LANDSAT image to the rock joint systems and the detectable larger geologic structures and indicates techniques to extract that geologic information. The third investigation analyzed some anomalous megalinear features in LANDSAT and SKYLAB images that transect major structures and described their associated geologic features.

PART 1: LOCATING INDICATORS OF MINERALIZATION

Introduction

The objective of this research has been to evaluate and utilize Skylab EREP (Earth Resource Experiment Package) and, to a lesser extent, LANDSAT and aircraft imagery, for their value in locating indicators of mineralization in central Colorado. The reason for such a study is that it is economically more desirable to survey large areas for potential ore deposits by remote sensing than by conventional ground surveys. Advantages of satellite imagery, both photography and scanned imagery, include a synoptic view, repetitive coverage, accessibility to remote areas, and relatively low cost to the user. Despite the desirability of locating targets quickly and inexpensively, it must be stressed that field work is essential as verification. It is merely hoped that needless field work may be eliminated.

This research began with an evaluation of two mining districts considered typical of those in central Colorado. A literature study of the Leadville and Cripple Creek districts was undertaken to determine which geologic features are associated with mineralization. Satellite photos over these areas were studied and compared with published geologic maps. It was determined that color (alteration) anomalies and structural density and intersections were the most obvious indicators of mineralization in the two areas, and it was assumed these criteria would be valid for the central Colorado region.

Limited Skylab coverage over Colorado restricted research to the area outlined in figure 1. This area is covered by frame 17, track 48, Skylab 2 S190A taken on 11 June 1973; by frames 106 and 107, track 48, Skylab 3 S190A and frames 38 and 39, track 48, Skylab 3 S190B taken on 4 August 1973; by frames 181 and 182, track 48, Skylab 4 S190A and frames 57 and 58, track 48, Skylab 4 S190B taken on 30 January 1974. Skylab 4 photography was delivered too late to be used in target selection. The area is also covered by frame 1172-17141, LANDSAT imagery from 11 January 1973; by frame 1154-17143, LANDSAT imagery from 24 December 1972; and by several aircraft underflights, including NASA Missions 184, 211, and 235. The entire study area covers approximately 46,800 square kilometers (18,000 square miles) in central Colorado.

The central Colorado area was studied to locate indicators of mineralization. Structure targets were chosen in areas of high linear density or at complex linear intersections. Target areas were ranked from most to least favorable according to the degree of association of color anomalies (each a "color" target) with structure targets.

Evaluation of the primary target at Weston Pass consisted of mapping from satellite and aerial photography and in the field (scale 1:12,000) to determine the origin of color anomalies and linears, and to discern the relationship of these features to mineral deposits. The secondary test site, at Dome Rock, was briefly investigated in the field to identify the indicators of mineralization.

The relationship between satellite, aircraft, and field mapping was determined, and the usefulness of Skylab in locating indicators of mineralization in Colorado was evaluated.

Skylab Evaluation

Remote sensing studies have been conducted on various aspects of the geology over both the Weston Pass and Dome Rock targets. In a study of controls on mineralization in the Colorado mineral belt, (1) noted that "areas of high density of lineament intersections, associated with circular lineaments...are considered the most promising areas for exploration." Linear overlays of LANDSAT imagery led him to select ten targets in central Colorado. Five of these covered major mineral districts; the highest priority target that did not correspond to a major mining district covered the Weston Pass-Buffalo Peaks area.

Lineament studies over central Colorado using both LANDSAT (2) and Skylab (3) indicate linear trends correlate well with known regional joint sets and fault patterns. Linears are most abundant in areas of crystalline basement, and linears with greater relief (as in the Dome Rock area) are visible because erosion has exposed the otherwise buried basement.

Prior to field work, Skylab photography was compared to LANDSAT and aircraft imagery over central Colorado. The comparison indicates that LANDSAT multiband imagery is superior to Skylab S190A multiband photography in the photographic-infrared (photo-IR) range, and that LANDSAT imagery in the red and green bands is comparable in quality (contrast and resolution) to the Skylab red and green bands. In general, the simulated color on LANDSAT imagery is comparable to Skylab, but system resolution is inferior to Skylab.

Cloud-free LANDSAT images are available during various seasons, while cloud-free Skylab photography is not, due to lack of repetitive coverage. In all cases the Skylab S190B product is superior to LANDSAT and S190A because of its greater resolutions.

Advantages of Skylab photography over LANDSAT imagery include greater resolution, stereo coverage, and the availability of colored films (both true color and color infrared), eliminating the need for color composites. Disadvantages include the general lack of repetitive coverage, the time necessary to retrieve and process film, and a restricted ground track.

Aircraft photography has equal or lower system resolution but greater scale than Skylab photography. Therefore more detail, and consequently more geology, can be mapped.

Advantages of satellite over aircraft photography include the synoptic view, the ability to see regional linear features, easier access to remote areas, and relatively low cost to the user. Disadvantages include over-flight times that cannot be varied to take advantage of changing surface conditions (weather), slow film retrieval, and smaller scale. Surprisingly, the color rendition of the S190B film (SO-242) allowed detection of color anomalies that were not obvious on aircraft photography. Among airphotos, color film at a scale of 1:20,000 proved most useful for detailed photointerpretation.

The primary objective of field work was to obtain ground truth to determine the origin of anomalous colors, linear features, and vegetation patterns. A common surface indicator of ore at depth is the gossan, an outcrop of leached and oxidized iron sulfides (4). Where unobscured, the characteristic red-ocher color should be easily seen on color photography. In addition, intrusive rhyolite porphyries should be obvious as light-colored anomalies where intruded into darker sediments. Areas of complex structural intersection have also long been considered favorable to ore deposition. It is hoped that linear features seen on satellite photography are structures (faults, joints, shear zones). Many researchers have suggested that vegetation patterns near ore deposits should be influenced by unique soil characteristics (5, 6, 7, 8). It was assumed that such patterns should be easily seen on satellite and aircraft photography, providing an additional indicator of mineralization. The Weston Pass and Dome Rock study areas were evaluated with these indicators in mind.

Red-ocher color anomalies can be caused not only by a gossan, but also by red sedimentary rocks, such as the Maroon Formation, which are probably the most visible red features in central Colorado, and by microcline-rich crystalline rocks and grus, commonly found in Precambrian units. Rocks appearing red-ocher on satellite and aerial photography in the Weston Pass study area are exposed as talus or outcrops and contain microcline and/or iron oxides. The most obvious color anomaly, on the west slope of Weston Peak (fig. 2), contains both microcline- and hematite/limonite-rich granite talus. One less visible anomaly consists of microcline-rich granite outcrop and grus; another comprises limonite-stained dolomite talus overlying a white quartzite. The extensively limonitized ore horizons at Weston Pass were not visible on orbital photography because of limited outcrops and extensive vegetation and soil cover.

Outcrops, talus, and minimal soil and vegetation cover provide optimum visibility. This limits most anomalies in central Colorado to talus slopes or areas above timberline. Mapping indicates that color anomalies in the Precambrian units generally are due to greater than thirty percent 'pink minerals' (potassium feldspars and iron oxides) in outcrops, talus, or grus, regardless of unit (figs. 3,4,5,6). Red color is not obvious in every place these conditions are met; an explanation may be indirect illumination, or differences in films or processing.

Light color anomalies (none was seen on satellite images in the primary study area) may be caused by light sedimentary units such as the Sawatch Quartzite or quartz-rich pegmatites, as well as by light-colored, altered intrusives. Light-colored intrusives are visible on aircraft photography because of their color contrast with adjacent rocks. They have often been emplaced as sills between dark dolomites and shales, and sometimes there is a change in vegetation growing on the unit (this change in vegetation is inconsistent from place to place). It is not possible to distinguish the sills where there is a lack of contrast, such as within the Sawatch.

Photography at a scale of 1:20,000 was most useful for discriminating colors and attempting to determine their origins. Even at this scale, however, distinguishing between microcline-rich talus and limonitically-altered talus is difficult, and identification is a matter of speculation.

Regional lineaments were assumed to be the expression of structure, and lineament density and complex intersections were important criteria in target selection. Field work revealed that linear objects may be accidentally aligned or geologically aligned streams and saddles, ridges, vegetation alignments, cultural features such as fences, roads, powerlines, or airplane contrails, as well as geologic features such as dikes, contacts, shear zones, joints, and faults. Within the Weston Pass area, 22 lineaments were mapped from Skylab photography (fig. 7). A comparison with faults mapped by (9) (modified within the study area) shows that seven mapped lineaments, or 32%, correspond closely to known faults (Fig. 8). One lineament was correlated to a cultural feature (powerline), and the remainder are thought to be structurally-controlled drainage or vegetation alignments. A comparison of 53 linear drainage azimuths with 239 joint measurements suggests that one drainage trend is directly controlled by jointing, and that another trend is a consequence of drainages formed on dip slopes normal to fracturing.

The indicators of mineralization did lead to an old mining district at Weston Pass, where lead and zinc sulfides formed manto deposits in the Leadville Formation. The ore is thought to have originated either in nearby porphyry sills or in a batholith at depth, and to have migrated along fissures adjacent to large, regional, gouge-filled fractures such as the Weston fault.

Reconnaissance field work in the Dome Rock area indicates that lineaments and color anomalies mapped using Skylab 3 S190B photos (fig. 9) are generally related to geologic or geomorphic features. Lineaments were found to be the topographic expressions of weathering along faults, joints, lithologic contacts, folds, and paleovalleys (R.B. Taylor, oral comm., 1974). Major linear orientations do coincide with fault and fracture trends in the

Precambrian Pikes Peak granite, the dominant rock in the area (R.M. Hutchinson, oral comm., 1974). It has been suggested that the fracture pattern in the study area is not unique, but rather is a local exposure of the regional basement pattern. Comparison to fracture orientations throughout the region confirms this (10,11).

The color anomaly in the secondary test site is Pikes Peak granite and grus. The rock is a pink to red-brown biotite granite with associated aplite and pegmatite. Pink minerals compose approximately forty to sixty percent of the rock, and are dominantly microcline. The color is particularly obvious where it is vegetation-free (at Dome Rock, Balanced Rock, and Sheep Rock).

The main source of potentially economic minerals in the Pikes Peak batholith is pegmatite; minerals include feldspars, mica, beryl, topaz, cassiterite, and lithium minerals. The position, shape, and size of pegmatites are controlled by structure. Primary fractures, such as cross joints, longitudinal joints, diagonal joints, and flat-lying joints, as well as marginal fissures and fissure intersections, may be used by pegmatitic solutions escaping a magma, and may become filled with pegmatite. Pikes Peak pegmatites are tabular, lenticular, or highly irregular in shape, and range in size to one kilometer in length, and up to 60 meters in width (12). Pegmatites in the Pikes Peak region have been uneconomic.

Interpretation of Skylab photos identified no pegmatites, probably because they are vegetation- or soil-covered, or lack unique color or weathering characteristics.

Results of this study suggest the original assumptions are incomplete. Red-ocher colors in central Colorado may result from sedimentary red-beds, microcline-rich crystalline rock, iron-oxide alteration, or combinations of these. Light color anomalies were attributed to quartz-rich pegmatites, light-colored sedimentary units, as well as to altered intrusives.

Linear features have been identified as aligned or straight streams, ridges, vegetation, cultural features, and geologic features including faults, joints, shear zones, dikes, contacts, folds, and paleovalleys. Where a linear pattern is obviously structural, such as jointing in the Pikes Peak granite, what is seen may be just a local manifestation of a regional pattern, enhanced in the particular area by unique aspect angle, or weathering or erosional characteristics.

Intersections and high densities of regional lineaments are not the only structural controls on mineralization. Regional faults with large displacements may be filled with gouge. Relatively small auxiliary fractures are often equally important. Intrusive centers, sometimes related to "circular features," frequently supply metallizing fluids. Changes of foliation in crystalline rocks have been cited as controls on ore deposition. Identification of reactive units, such as the dolomites of central Colorado, would facilitate locating mineralized strata. Recognition that a reactive unit had been intruded would increase its prospects as a host. Many of these features, however, are not visible on satellite photos at available resolutions.

Vegetation assemblages in the two target areas were found to be influenced more by moisture, slope steepness and direction, season, and altitude than by composition of the substrata.

Conclusions

Skylab photography can cover large areas quickly and inexpensively, and there are some surface features in any given region that are indicators of mineralization. Photolineaments and color anomalies may be important indicators of mineralization in central Colorado, but positive identification of these features is not possible. A thorough evaluation of assumptions and detailed field work are mandatory. Also, areas that are extensively covered by soil, vegetation, clouds, or snow, no matter how favorable, are incapable of being evaluated. Areas where orbital photography would be most useful in the search for mineral deposits include desert mountains or snow-free alpine mountains. Orbital photography in itself is considered inadequate to fulfill exploration needs. It is useful in reducing the size of an exploration area to potentially favorable targets; like other remote sensing techniques, it is a powerful tool only when used in conjunction with detailed field work.

PART 2: LINEAR FEATURES IN LANDSAT IMAGERY

Two LANDSAT images of central Colorado, E-1172-17141 (Figure 10) and E-1154-17143, were selected for analysis of linear geologic structure information content. The two images were selected for their excellent expression of linear features. Their main attributes are low sun elevation and near maximum snow cover. Since a significant proportion of linears is the result of shadow enhancement of topographic features, the lowest sun elevation was selected; it was the minimum available nearest the winter solstice, approximately 23 degrees. This sun elevation is not the optimum for maximum shadow enhancement of the topography in central Colorado, because slopes less than this are not shadow enhanced. In addition to this restriction, there is selective shadow enhancement of linears as a function of deviation from the sun azimuth, which was approximately S.30W. (13). On the other hand, some linear features, especially those which are the margins of dark areas or are long linear dark areas, were enhanced by the snow cover. Snow cover enhances the dark-area margins (particularly between coniferous forests and dormant grassland) and shadow margins by increasing the contrast between the dark and light areas. Furthermore, the snow decreases the contrasts in illuminated areas and provides a uniform high reflectance in areas of otherwise variable reflectance. On the contrary, snow cover might obliterate some linears by smoothing low topographic features. All things considered, when imagery from other seasons was subjectively evaluated, information content and detectability of linears were found to be very much less, which discouraged further analysis for new information not available in snow-covered imagery.

The image that has the more widespread and deeper snow cover, E-1174-17141, also has the greater detectability. The reason seems to be in the greater contrasts as explained above. However, despite some cloud cover, E-1154-17143 has more information (more linears) compared to the other image.

Band 6 images seem to have the greatest detectability of all the LANDSAT bands. In these winter scenes, contrasts between vegetation types and

between vegetated and less vegetated areas are the least and are further diminished by snow cover. In addition, detectability is improved in Band 6 because shadows are darker because of low radiance in this bandwidth as compared to other bandwidths.

There is little doubt that the linear trends in images are not always a true representation of linear trends determined from fault maps and/or rock joint trend maps. Other studies have shown that less than half the linears in one photograph can be related to known structures. Not all geologic linears are represented as linears on the image, say, for example, as vegetation or topographic linears. This may be due to preferential enhancement of some trends by geomorphic processes. Some linears parallel to streams seem not to be controlled so much by lithology or structure, but by direction of drainage evolution, determinable by the line from the local headwaters to the local outflow area of the stream. It seems very probable that stream patterns contribute a great deal of randomness to strike frequency distributions, while structurally controlled trends provide less information. Thus, the "signal-to-noise" ratio is low. The detrimental effects of snow cover and sun attitude have already been discussed.

Strike-Frequency Analysis

The purpose of the strike-frequency analysis was to determine the dominant azimuthal trends of the linears measured on the imagery in order to study the geographical distributions of the trends and their geologic origins. Firstly, linears were marked and traced on a clear overlay of a 9 in. by 9 in. positive transparency (scale - 1:1,000,000) viewed in transmitted light (Figure 11). Only linears of obviously cultural origin were not entered into the analysis. As will be demonstrated, there may be some valid bases for being more selective of linears to be entered into the analyses and, thereby, the possibility of improving correlations between two or more data sets.

Following preparation of the overlay, the linears were hand digitized for length and azimuth to the nearest degree. When lengths of linears were measured, they were grouped into length classes of 0.254mm (0.1 inch) with a maximum of 5cm (2 inches) being found. Strike-frequency histograms of the azimuths of the linears and their length-weighted azimuths were made with the aid of a computer program developed for the study. Azimuthal trends were selected at those azimuths where maxima in the strike-frequency histogram occurred. In addition, to aid in the selection of trends, significance values were calculated for the frequency maxima.

Various degrees of smoothing of the frequency histograms were performed by the method of moving sums as even large data sets had very irregular histograms. Because of the loss of information in the summing process, various summing intervals were investigated for optimum enhancement of dominant trends. Maxima and minima of the histogram constitute an irregular wave form, and where two maxima or two minima are closer together than the summing interval, they are merged into one and some information is lost or filtered out (Figure 12). It should be noted that the summing interval for the original data set is 1 degree of azimuth.

In the discussion that follows, strike frequency histograms have significance values plotted on the ordinate and azimuths on the abscissa as in Figure 12. Relative frequency values determined by moving averages at each degree of azimuth were converted to significance values. Two smoothing intervals were selected for emphasizing the trends found in the histograms. An 18-degree interval (10% of azimuth half-circle) was selected to emphasize broader trends. A 5-degree trend (3%) was selected to emphasize trends of narrower azimuthal range.

Selection of trends was not easy nor entirely consistent because of the irregularity of the frequency histograms. However, the procedure of selecting trends was to associate them with significant maxima surrounded by significant minima. Thus, in the worst case, a trend or significant maxima might consist of numerous significant "spikes" surrounded by values of low significance. A study of some randomly generated linears indicated that such data sets have fewer maxima above the 90 percent significance value than real data sets. In this study, if a real data set fell short of producing 99-percent maxima then 90-percent maxima were used for trend selection.

It was found that the "signal-to-noise" ratio of the histogram is considerably increased by length weighting linears before entering them into the strike-frequency analysis. Thus, where any azimuth had a frequency value of one, in the unweighted analysis, this value became the value of the length class (increasing from 1 in steps of 1). This method provided no new trends over the non-length weighted analysis, but did enhance the trends; that is, increased the "signal-to-noise" and improved their significance values (Figure 13). While no new trends appeared as a result of length weighting, it is very possible for a few long linears to produce a trend in a length-weighted analysis, but none in an unweighted analysis.

Azimuth Trends in the Whole Images

Approximately 300 linears were measured in each of the two images studied. Strike-frequency histograms at unweighted azimuths for each image are shown in Figure 14 and for the combined images in Figure 15. The larger interval of smoothing (18 degrees) was used for Figure 14 and two intervals (5 and 18 degrees) in Figure 15. The trend in Figure 15a is a very broad and significant one ranging from N.40E. to N.35W. and corresponds to the major structural and topographic trends in central Colorado (Figure 16). Figure 15b reveals that at the smaller smoothing interval there may be 5 to 7 closely grouped trends constituting the broader trend. The trends are wholly in counterclockwise deviation to the sun azimuth of N.30W., indicating that there are relatively fewer slopes, as well as other linears, with trends in the west-northwest and east-northeast quadrants.

Areal Distributions of Trends

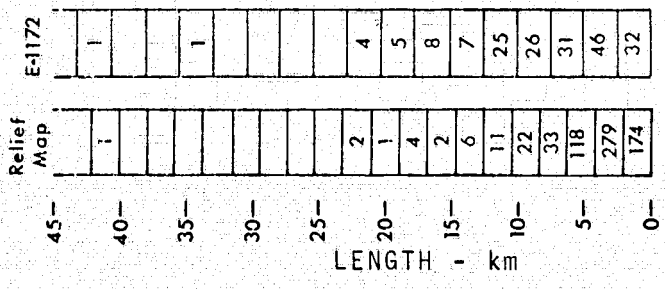
Inspection of the areal subdivisions of the linear map (Figure 11) indicates that each contains one or more distinct and easily detectable trends, more so than in the greater imaged area. Also, the trends in each subdivision are not part of image-wide trends but of trends localized to that subdivision and a few neighboring ones.

The local trends of each of the 10 subdivisions are plotted in Figure 17. The frequency of local trends for each 10 degree interval of azimuth for the combined images is shown in the histogram in the figure. The frequency histograms for each image are nearly the same. The result is that the local trends, while spread across the azimuth half-circle, do emphasize four major trends: N.20-40W., N.0-10E., N.20-50E., and N.60-70E. When the occurrence of the local trends within the major trends is plotted areally, as in Figure 18, a correspondence to the major structural features in Figure 16 can be made. The N.20-40W. and N.0-10E. trends are associated within the Cenozoic folds and faults of South Park and Canon City Embayment and in the older igneous and metamorphic terrains of the Front Range. The N.20-50E. trend is predominant in the southeast quarter of the area. The N.60-70E. trend is associated with the Cenozoic volcanic terrain and is also dominant in the Front Range in the north part of the image. In the volcanic terrain, there is a definite control of topography by volcano-depositional features (14). In the north, the area is of high relief associated with the Tarryall Mtns. and the North Fork of the South Platte River. Generally, local trends occur in no more than about 40 percent of the area.

Lengths of Linears

All linears of E-1172-17141 that lie within the area of the Pueblo, Colorado, Quadrangle plastic relief map (scale 1:250,000) were grouped by length. For comparison, a linear map of the relief map was made and the linears were also grouped by length. Frequency distributions of linear lengths in the two data sets are shown in Table 1.

TABLE 1. FREQUENCY OF LINEARS FOR EACH LENGTH CLASS CONVERTED TO KILOMETERS FOR LANDSAT IMAGE E-1172-17141 (IN AREA OF RELIEF MAP) AND FOR PUEBLO RELIEF MAP.



The LANDSAT linears consist of topographic and non-topographic linears illuminated at a sun elevation of 23° and azimuth of N.28W. in a heavily snow-covered scene. The Pueblo linears are essentially high-relief topographic linears illuminated at a sun elevation equivalent to 15 degrees

and accumulated at illuminations from four directions, S.45E., South, S.45W., and West. The relief map was painted white to remove tonal contrasts not due to illumination angle. Thus, the relief map linears were mapped under optimum conditions.

The scale of the LANDSAT image studied is 1:1,000,000 and that of the photograph of the Pueblo Relief Map is 1:800,000. Smaller features are detectable in the LANDSAT scene than in the relief map photograph because the resolution of the relief map itself is lower.

Over three times as many linears were extracted from the relief map as from the LANDSAT scene. While the modal and longest lengths are nearly the same between the two sources of data, the LANDSAT images yielded a greater average and median length (Table 2). It is believed that the higher

TABLE 2. STATISTICS OF LENGTHS OF LINEARS IN E-1172-17141 AND PUEBLO RELIEF MAP IN KILOMETERS.

Source	No.	Total Length	Average Length	Median Length	Modal Length	Longest
E-1172-17141	186	1417	7.6	6	3	42
Pueblo Relief Map	653	2561	3.9	3	3	42

resolution of the LANDSAT images permits the connection of what would be disconnected line segments on the relief map in the range greater than the modal length and less than the greatest length.

Length and Trend

The two data sets discussed in the previous section were analyzed for length preference as a function of azimuth. Length trends (of length-weighted azimuths) are shown in Figure 19b and 20b. Comparison of the length trends with the azimuthal trends in Figure 19a and 20a indicates that no new trends occur as a result of length-weighting of linears, but enhancement of the maxima and minima does occur. Figures 21a and 21b show the frequencies of length as a function of azimuth. In both data sets there is a preference of long linears (length greater than the modal values) in the range of N.10-40W. and a weaker preference at N.20E., N.60E. and N.85E. It is concluded that within a trend the frequencies at the modal length of the data are greater than in non-trend areas, and that lengths greater than the modal length occur much more frequently at azimuths within the major trends. Hypothetically, the best way to extract structural information from LANDSAT linears is to determine modal values from data sets of all linears and then determine structural trends by analyzing the trends of the linears of length greater than the modal length (super-modal linears).

A frequency analysis of the super-modal linears (length class greater than 2) of E-1172-17141 yields 4 significance trends: (I) N.20-40W.,

(II) N.5-20E., (III) N.40-50E., and (IV) N.85E.-N.70W. These trends are plotted for the image subdivisions in Figure 22. They are also extrapolated to subdivisions outside the area of the Pueblo relief map. They are further extrapolated to the local linear trends of E-1154-17143. Trends I and II are associated with the trends of the large folds and faults of the central Colorado area (Figure 16). Subdivisions 22, 32, 33, 34 are underlain mostly by Precambrian rocks which contain trends I and II. Subdivisions 23, 24 and 42 are underlain by younger sedimentary rocks folded at least by Cenozoic diastrophism. In subdivision 22 Cenozoic volcanic rocks lie upon Precambrian metamorphic rocks and Paleozoic and Mesozoic sedimentary rocks.

Subdivisions 22 and 32 also contain trend IV which is dominant in the Cenozoic volcanic terrains. This trend may be ascribed to non-topographic linears discussed in the following section. Trend IV is also found in subdivision 24 outside the area of the length-trend analysis. In this subdivision, the trend can be ascribed to deep topographic valleys in the Tarryall Mountains and the area of the North Fork of South Platte River

Topographic and Non-topographic Linears

Analysis of the Pueblo relief map was done primarily to evaluate the dominance of topographic linears in LANDSAT imagery over other linears. To make the trend sampling as complete as possible, and diminish the azimuthal filtering effect, linear azimuths and lengths from four illumination directions were collected. The results of the analyses of all linears and super-modal linears is shown in Figures 20 and 23. Trends I, II, III, IV appear in Figure 20a, though trend IV is weak. In the length-weighted data (Figure 20b), trend IV is not present, indicating that long linears are few in this trend. The same is true for the super-modal trends (Figure 23). Thus, trends I, II, and III contain much of the total length of linears while trend IV does not. A comparison of Figures 20b and 23 would indicate that trend IV contains a large proportion of linears of length 2 or less and few longer linears.

The non-length-weighted histogram of E-1172-17141 (Figure 19a) is similar to Figure 20a. The length-weighted trends (Figure 20b) are all strong. The enhancement of trends II and IV is due to length-weighting. Trend IV enhancement is due to length-weighting of a few long linears as further indicated by the super-modal trends in Figure 24.

Because the LANDSAT image records non-topographic linears (these will include topographic linears of low relief) as well as topographic linears (mostly moderate to high relief), comparison of LANDSAT and relief map trend analyses should indicate the relative proportions of the two types of linears in LANDSAT imagery. A hypothetical comparison will be given here as no corroboration by study of other sources of data has been done. Hypothetically then, LANDSAT trends IV could consist mainly of non-topographic linears. Trends I, II, and III could contain large numbers of topographic linears. The idea could be extended further to compare the trends of snow-free and snow-covered scenes of an area in the same season. The snow-covered scene would approximate the painted relief map in the enhancement of topographic linears.

Linears and Joints

Measurements of attitudes of joints from the area of subdivisions 32, 42, 33, 24, and 34 were also analyzed for trends. Many of the joints were provided by Dr. Robert M. Hutchinson of Colorado School of Mines from uncompleted research and were available only in synoptic form. The following discussion considers the correspondence of joints for the entire data set covering the five subdivisions and for a data set from the southern Front Range south of Pikes Peak.

Figure 25 shows that the dominant trends in the two groups of joints are N.0-30W. and N.55-90E; they are approximately orthogonal. In the southern Front Range, the LANDSAT trends are I, II, and III, (Figure 22a), but not IV since the area lies outside the Cenozoic volcanic terrain. The correspondence of the joints trends with the orthogonal LANDSAT trends I and III is the most favorable one but is 20 degrees out of register for both. Nevertheless, the tendency is to correlate the NNW joint trend with the major structural trend (Trend I) in favor of topographic control by joints. The ENE joint trend correlates with the major faults that transect the southern Front Range, again in favor of topographic control by joints.

The LANDSAT trends for the larger area of joint coverage are dominated by the local trends of the subdivisions, trends I and II (Figure 25b). The major structures parallel these trends, as does the NNW joint trend. However, the ENE joint trend does not seem to strongly affect topography and enhance or produce trend III. A joint analysis in the Devil's Head Quadrangle (1:24,000) is subdivision 34 by (15) indicates two strong trends: N-S and E-W. The latter trend does appear on E-1154-17143 in subdivision 34 (Figure 22). Three major faults in the Rampart Range parallel trend II and do have fault-line topography (Figure 16). It is entirely possible that in this area trend II contains a large percentage of topographic linears. Comparison of LANDSAT trends with relief map trends and length-weighted analyses could be done for this area as was done to the south.

Summary and Conclusions

Method of Analysis

1. Estimating azimuth data to nearest degree, smoothing over 15-20 degree moving intervals and plotting in strike frequency histograms is an effective way to determine azimuthal trends of linears.

2. The method used for determining significance values provides a measure of the likelihood of non-random origin of the frequency values in a trend.

3. Detectability of linears and trends in LANDSAT images varies greatly between image generations and depends on sun attitude and surficial tonal contrasts due to seasonal vegetation effects, snow cover, etc.

4. The high resolution of LANDSAT imagery allows detection and connection of longer linear features than is possible with relief maps or topographic maps.

5. Length-weighted linears produce more distinct trends, and can reveal trends based on a few, very long linears.

6. Short linears contribute a large number of random azimuths and, as a result, decrease the signal (trend)-to-noise ratio.

7. More distinct trends can be produced from length-weighted linears greater in length than the modal length.

Data Characteristics

1. The strike-frequency histogram of linears from the total imaged area is not isotropic, but contains one distinct broad trend.

2. In subsets of the imaged area based on geologic distinctions 4 trends exist.

3. Trends are localized to less than 50 percent of the total area and are related to large geologic features.

4. In small areas of the image, the existence of only one or two trends is typical.

Correspondence with Geologic Trends

1. The analysis was confined to a portion of the imaged area of two LANDSAT images of central Colorado and four linear trends were found.

2. An overall broad trend reflects a change from south to north of the trends in major geologic structures from N.40W. to N.10E.

3. All four linear trends have geologic trends associated with them.

4. Trend I (N.20-40W.) and II (N.5-20E.) correspond to the trends of the major geologic folds and faults as well as one regional joint set.

5. Trend III (N.40-50E.) corresponds to a second regional joint set (perpendicular to the other) and several major faults.

6. Trend IV (N.85E.-N.70W.) corresponds to a few long, linear depositional features in a volcanic terrain.

7. The localization of trends in smaller areas is strongly related to the underlying major lithologic terrains.

Speculations

1. Trends of linears of length greater than modal length may yield the most information about geologic trends.

2. All geologic trends are not expressed as linear trends in a given small area, but might be on opposite sides of the area. In other words, all geologic trends are expressed somewhere as linear trends.

3. Intersections of linear trends in an image do not necessarily indicate a localized or unique intersection of geologic trends.

4. The trends of geologic structures in younger sedimentary strata strongly parallel linear trends in older metamorphic and igneous terrains.

PART 3: MEGALINEARS AND LINEAMENTS

Linears are here defined as any essentially unidimensional straight or continuously curved features in an image. They are defined on combinations of infinitesimally small picture elements and not on the real things they represent. Megalinears are defined as features which are essentially unidimensional groups of linears that are parallel, en echelon, overlapping, or end-to-end. Lineaments are the groups of geologic structures, often diverse in type, that are associated with the linear elements of a megalinear. The lineaments of this section are those that have structural elements that appear only to have the same kinematic movement plan and subparallel trends.

Included in the discussion of linears are closed or open, curved or polygonal features. These often consist of concentric groupings of short linears. They are frequently associated with plutonic igneous or volcanic activity as well as other structural deformation. They will be called concentric features.

This investigation is concerned with those anomalous megalinears and their associated lineaments that transect major tectonic features in central Colorado. They are anomalous relative to the major known lineaments that essentially bound and parallel the tectonic features. These anomalous megalinears have not been studied extensively before now because a synoptic view has not been available. Furthermore, most earlier geologic investigations have been circumscribed by the margins of major tectonic features, and synoptic evaluations have been thus restricted.

Transecting megalinears are nearly as detectable in an image as the more structurally consistent lineaments. Their associated lineaments are composites of anticlines, synclines, drag folds, monoclines, faults, crush zones, shear zones, and rock joint sets. Structure type along the trend of a lineament is very dependent upon the lithologic terrains in which they are developed. It is this variability as well as the transecting nature of the lineaments that presents a somewhat confusing structural picture, and perhaps has slowed the recognition of these major anomalous structural features.

The anomalous transecting megalinears are part of a regional tectonic framework as follows. The major structural elements of the central Colorado test site (Figure 16) are the southern Front Range, a block mountain uplift bounded by typical mountain flank structures; the Denver Basin on the east;

South Park on the west; Canon City Embayment on the south; the Wet Mountains, a block mountain uplift; and Wet Mountain Valley. The basins are downfolded Cenozoic and older sedimentary rocks. The block mountains are Precambrian metamorphic and plutonic igneous rocks which also underlie the basins. Between South Park and Wet Mountain Valley, the Tertiary Thirtynine Mile volcanic field lies upon metamorphic rocks.

The flank structures of the block mountains consist of major high-angle thrust faults and associated monoclines (Figures 26, 27). The Rampart Range and Ute Pass thrusts lie along the eastern margin of the Front Range; the Elkhorn and Oil Creek thrusts along the western margin. The eastern margin of the Wet Mountains is bounded by the Wet Mountain thrust and monoclines.

In LANDSAT and Skylab images of central Colorado the normal tectonic elements and their marginal structures are recognizable. In addition, there are four concentric features and several of the transecting mega-linears (Figure 28). Of the concentric features the most prominent one is the Pikes Peak intrusive center of the Pikes Peak batholith. Two other centers of the batholith are not recognizable. The Lake George stock also is very prominent. Two volcanic centers, the Thirtynine-Mile and one in Wet Mountain Valley, are also recognizable (Figure 28).

Three transecting megalinears are in the Rampart Range portion of the Front Range and three are in part of the Front Range south of Pikes Peak.

In the Rampart Range (Figure 29), the Manitou Park megalinear is associated with the Ute Pass fault on the south, which passes into the Ute Pass thrust west of Manitou Park, and northward in Pikes Peak granite into the Bear Creek shear zone. The one singular feature of this lineament is that the fault zones have been intruded with sandstone dikes throughout the length of 125 kilometers. The Manitou Park "graben" of sedimentary rocks is bounded on three sides by this large crescent-shaped lineament.

East of this lineament is the Jackson Creek megalinear associated with the Jackson Creek fault which also has been intruded by sandstone dikes. This lineament transects the Rampart Range and offsets the flank structures on the east and passes into the flank structure of Manitou Park on the west. A third unnamed megalinear is associated with a long prominent escarpment that trends into the flank structure on the east and a shear zone in the flank structure of Manitou Park on the west.

The three large lineaments of the Rampart Range are continuations of or are involved with long known structural features. On the west, they are continuations of the major thrust fault and the monocline of the Manitou Park structures. These lineaments extend northward across the Range and become involved in the major thrust fault on the eastern side of the block uplift. The Rampart Range thrust is offset in the places where two of the megalinears pass into the flank structure. A new interpretation of this block uplift is that it consists of three giant imbricated plates with two thrust faults at the outer margins and two normal faults between the plates.

South of Pikes Peak (Figure 30), the Milsap Creek megalinear trends S.10W. from the Pikes Peak intrusive center across Garden Park syncline, Royal Gorge Arch and into the Wet Mountain Valley. The associated structures consist of mafic intruded crushed zones in the metamorphic terrain of the

Front Range, a major offset of the mountain flank structure on the western margin, a gentle drape fold in Garden Park, and Mikesell Gulch fault. The latter fault passes into intensely folded and fault sedimentary rocks west of Royal Gorge arch and southwestward into metamorphic rocks. The total length is 35 kilometers.

Two other megalinears are the Adelaide and Peck's Camp features. The latter is a mineralized mafic-intruded crushed zone. The Adelaide megalinear is associated with a major fault that transects the block mountain range and involves faulted sedimentary rocks in the flank structure on both margins of the range.

The structural evidence associated with the transecting megalinears of the Front Range uplift points to a more complex involvement of the crystalline basement in the regional tectonic deformations. These deformations consist not only of the familiar ones of uplifts decoupled from basins along flank thrusts and monoclines but also independent or subsequent, continuous cross-cutting deformations that have the spatial unity of a lineament, yet are manifest in different structural features along that lineament. Further study of these features may add considerably to our knowledge of tectonic history and kinematics of regions.

ACKNOWLEDGMENTS

These investigations were carried out at the Department of Geology at Colorado School of Mines under LANDSAT contract NAS5-21778 and Skylab contract NAS9-13394. Data collected under Bonanza Project contract NGL-06-001-015 were also used.

REFERENCES

1. Nicolais, S.M., 1974, Mineral exploration with ERTS imagery: in Third Earth Resource Technology Satellite-1 Symposium, v. 1, Sec. B, Goddard Space Flight Center, Washington, D.C., p. 785-796.

2. Knepper, D.H. (ed.), 1973, Geologic and mineral and water resources investigations in western Colorado using ERTS-1 data: Progress report 9: Colorado School Mines Remote Sensing Rept. 73-5, 53 p.

3. Lee, Keenan, Knepper, D.H., and Sawatzky, D.L., 1974, Geologic information from satellite images: Colorado School Mines Remote Sensing Rept. 74-3, 37 p.

4. Blanchard, Roland, 1968, Interpretation of leached outcrops: Nevada Bur. Mines, Bull. 66, p. 89-91.

5. Carlisle, Donald, and Cleveland, G.B., Plants as a guide to mineralization: California Div. Mines Spec. Rept. 50, 31 p.

6. Cannon, H.L., 1960, Botanical prospecting for ore deposits: Science, v. 132, p. 591-598.

7. _____ 1971, The use of plant indicators in ground water surveys, geologic mapping, and mineral prospecting: Taxon, v. 20, p. 227-256.

8. Canney, F.C., 1969, Remote detection of geochemical soil anomalies, in Second Annual Earth Resources Aircraft Program Status Review: NASA, v. 1, p. 7-1 to 7-8.

9. Tweto, O.L., 1974, Reconnaissance geologic map of the Fairplay West, Mount Sherman, South Peak, and Jones Hill 7½-minute quadrangles, Park, Lake, and Chaffee Counties, Colorado: U.S. Geol. Survey map MF-555, 1:62,500.

10. Sawatzky, D.L., 1973, Photolinears, in Knepper, D.H. (ed.), Geologic and mineral and water resources investigations in western Colorado using ERTS-1 data: Progress report 9: Colorado School Mines Remote Sensing Rept. 73-5, 53 p.

11. _____ 1974, Geologic structures, in Lee, Keenan (ed.), Geologic and mineral and water resource investigations in western Colorado using Skylab EREP data: Colorado School Mines Remote Sensing Rept. 74-6, p. 18-27.

12. Hanley, J.B., Heinrich, E.W., and Page, L.R., 1950, Pegmatite investigations in central Colorado, Wyoming, and Utah, 1942-1944: U.S. Geol. Survey Prof. Paper 227, 125 p.

13. Sawatzky, D.L., and Lee, Keenan, 1974, New uses of shadow enhancement. Remote Sensing of Earth Resources, v. 3, p. 1-18.

14. Epis, R.C., Scott, G.R., and Taylor, R.B., 1973, Petrologic, tectonic, and geomorphic history of central Colorado: Geol. Soc. America, Rocky Mtn. Section, Guidebook for Field Trip 8, 22 p.

15. Johnson, D.H., 1961, Geology of the Devil's Head quadrangle, Douglas County, Colorado: Unpublished Colorado School Mines D.S. Thesis.

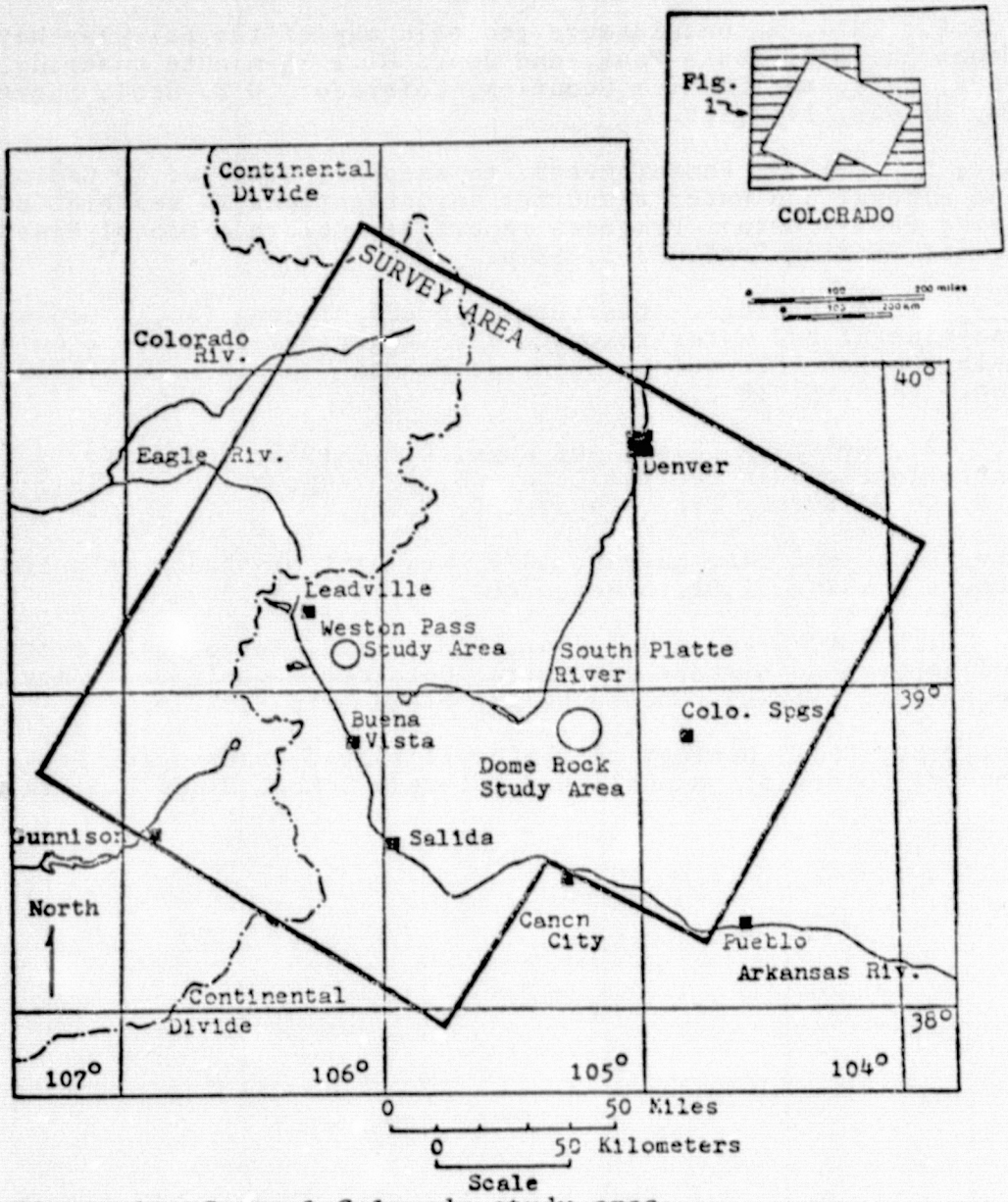


Figure 1: Central Colorado study area.

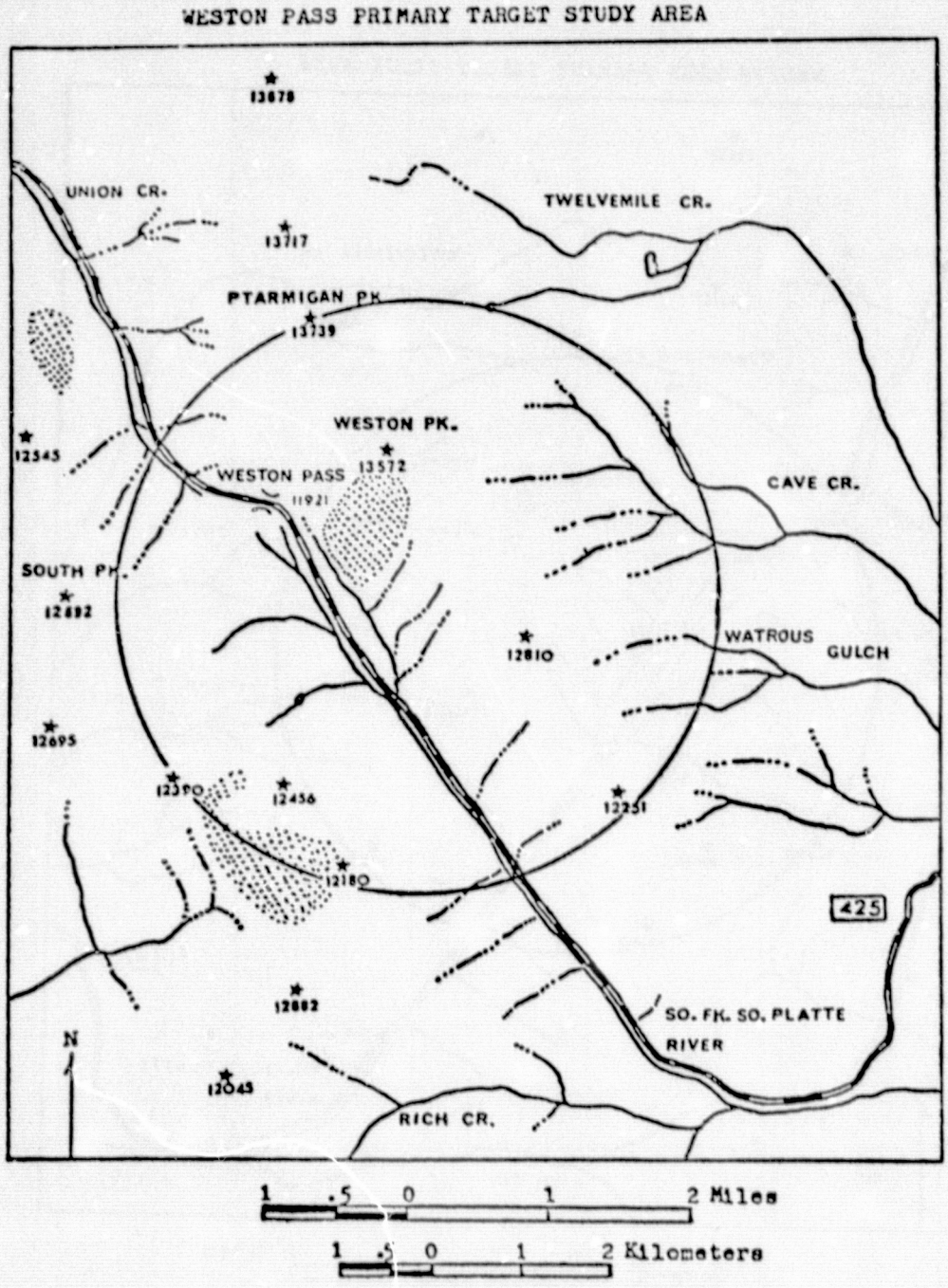


Figure 2 : Red-ocher color anomaly targets, mapped from Skylab 3 S190B, track 48, frame 38, 4 August 1973.

Anomalous colors.

WESTON PASS PRIMARY TARGET STUDY AREA

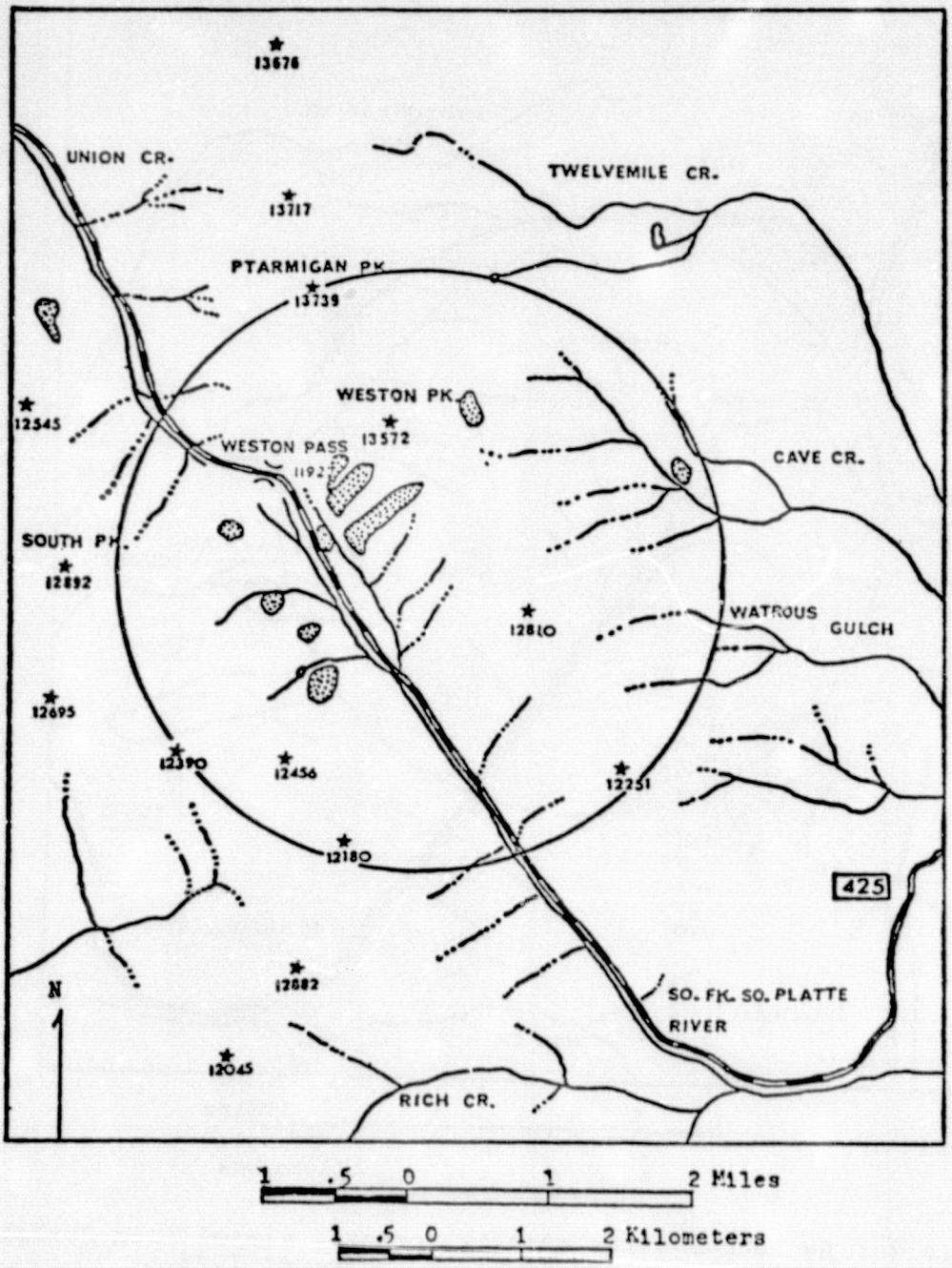


Figure 3: Distribution of limonitic alteration.

Limonitic alteration.

WESTON PASS PRIMARY TARGET STUDY AREA

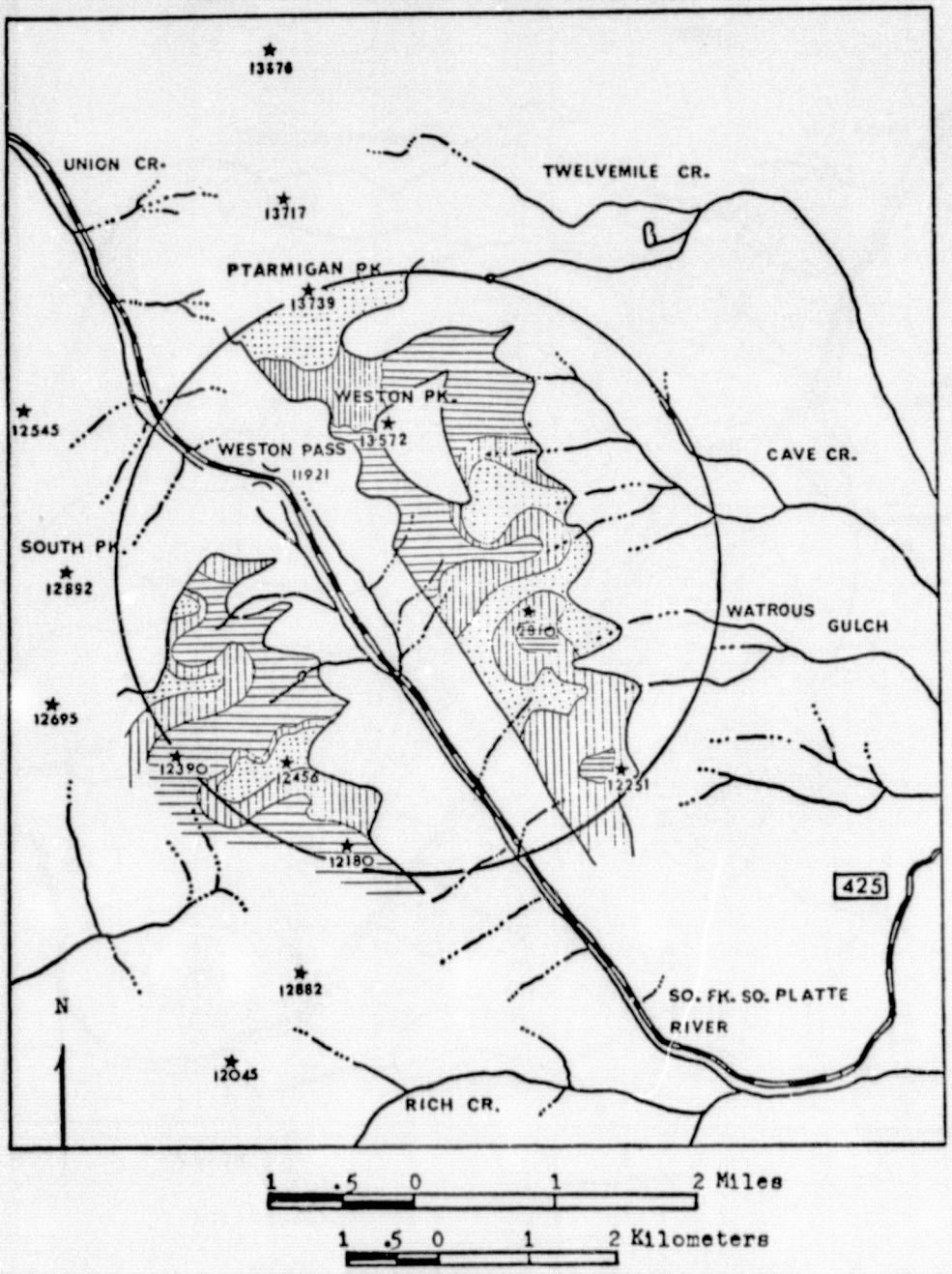


Figure 4: Distribution of 'pink minerals' (volume percent) in Precambrian units.

0-15% 16-30% greater than 30%

WESTON PASS PRIMARY TARGET STUDY AREA

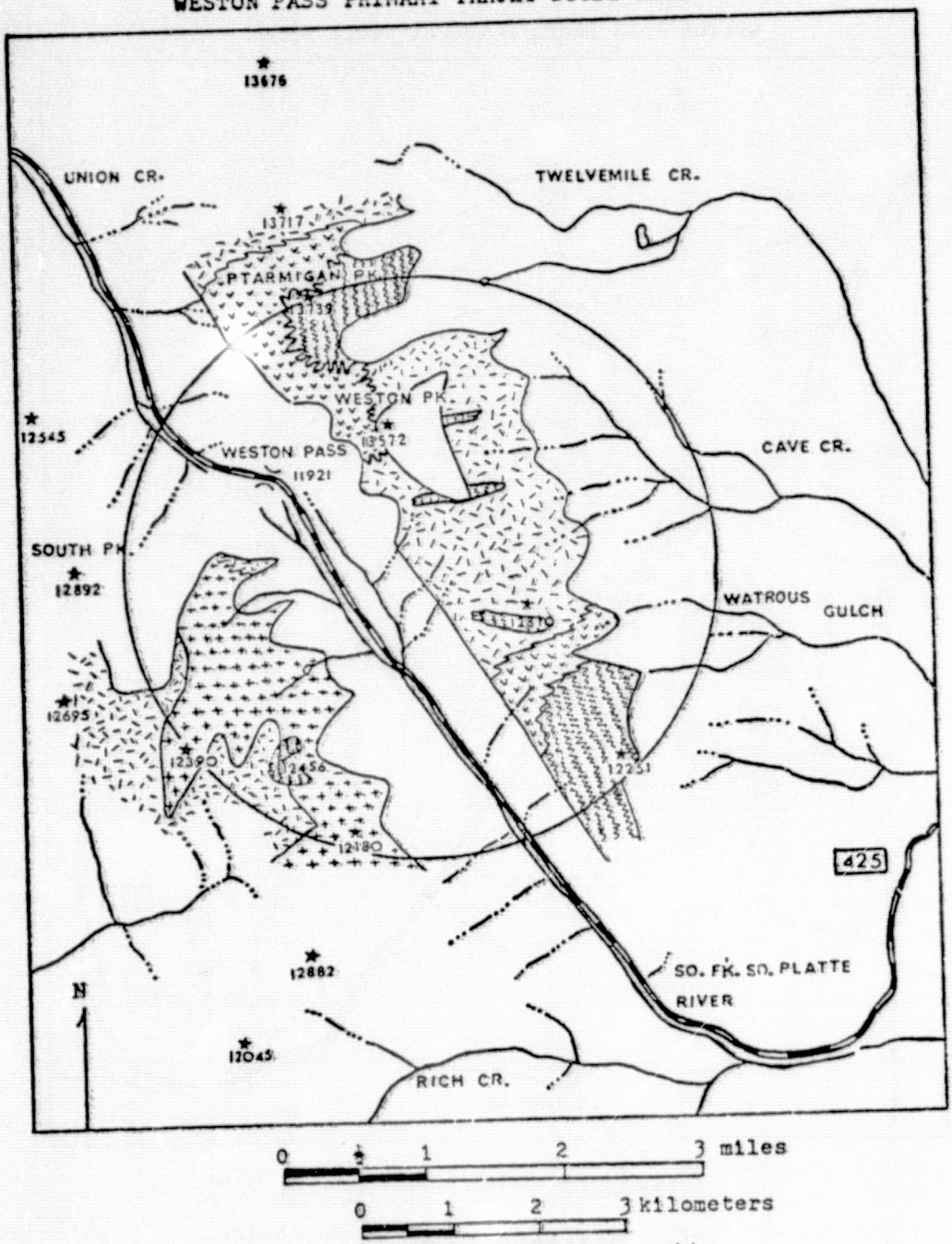


Figure 5: Distribution of Precambrian units.

Silver Plume-Type Granite

Biotite Gneiss

Trout Creek Augen Gneiss

Injection Gneiss

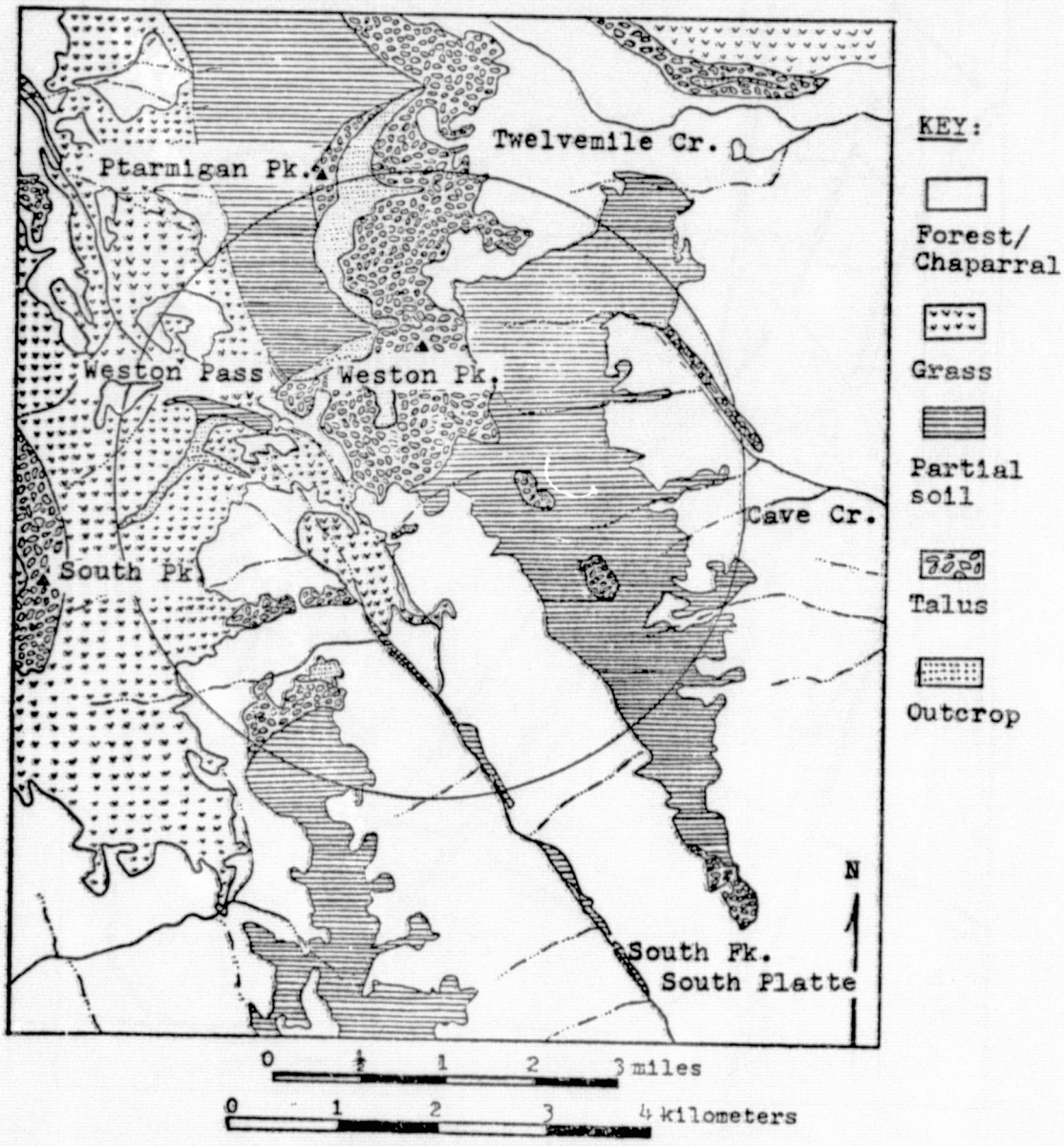


Figure 6: Ground cover map, Weston Pass and vicinity.

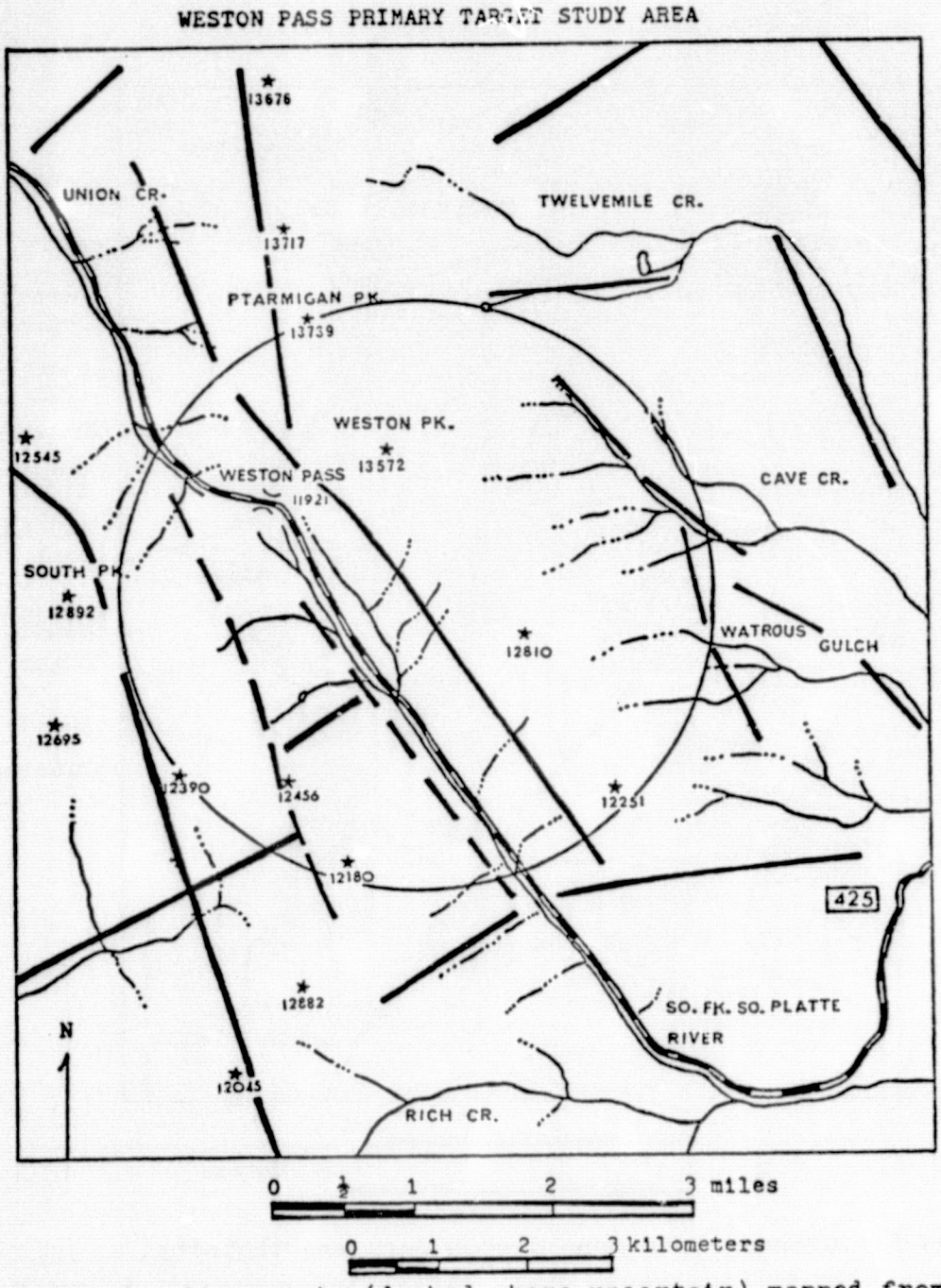


Figure 7: Lineaments (dashed where uncertain) mapped from Skylab 2 S190A, track 48 frame 17, 11 June 1973, and Skylab 3 S190A, track 48 frames 106 and 107, 4 August 1973.

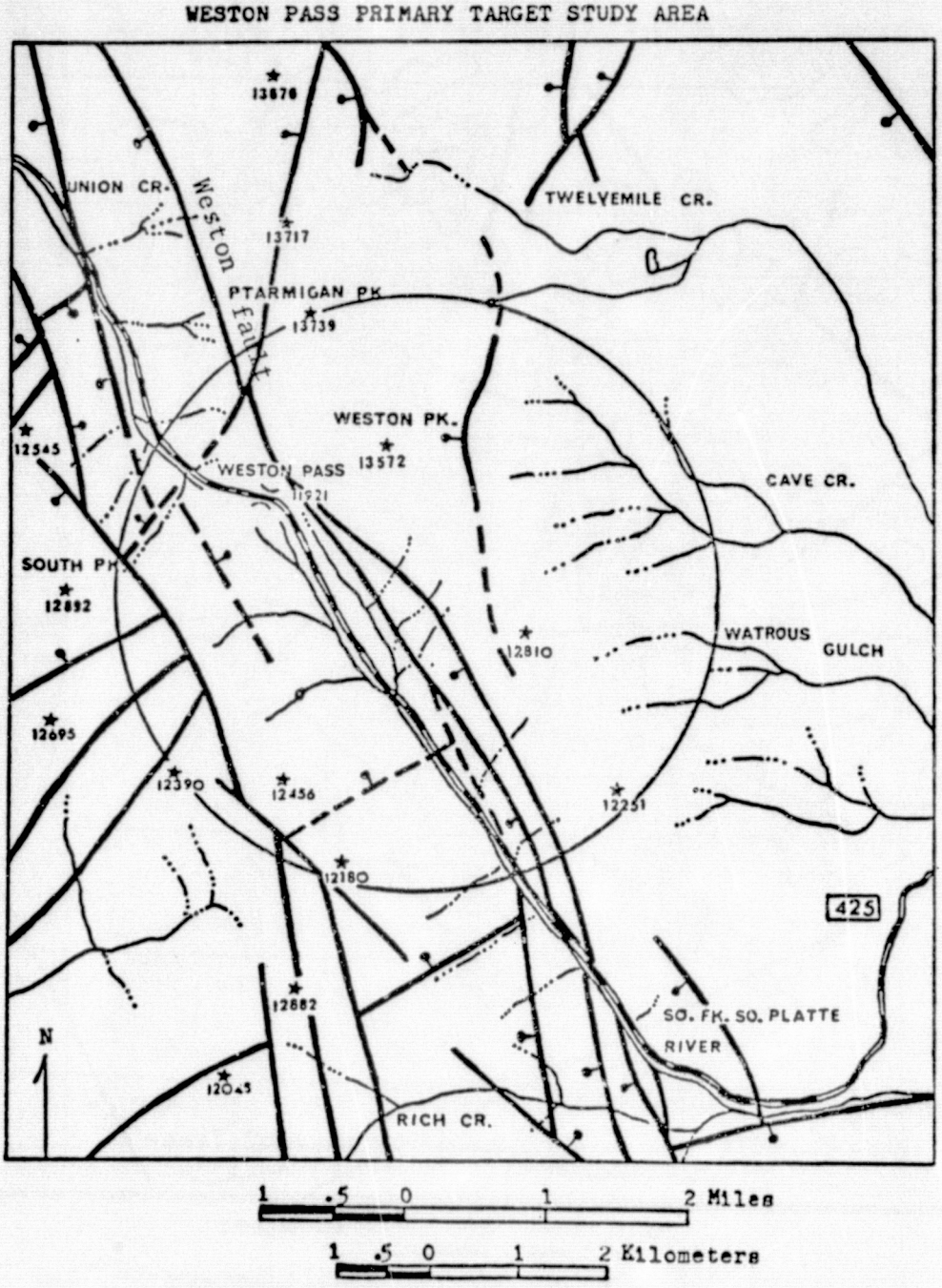


Figure 8: Regional structure, modified after Tweto, 1974. Bar and ball on downthrown side of fault.

REPRODUCIBILITY OF THE
ORIGINAL PAGE IS POOR

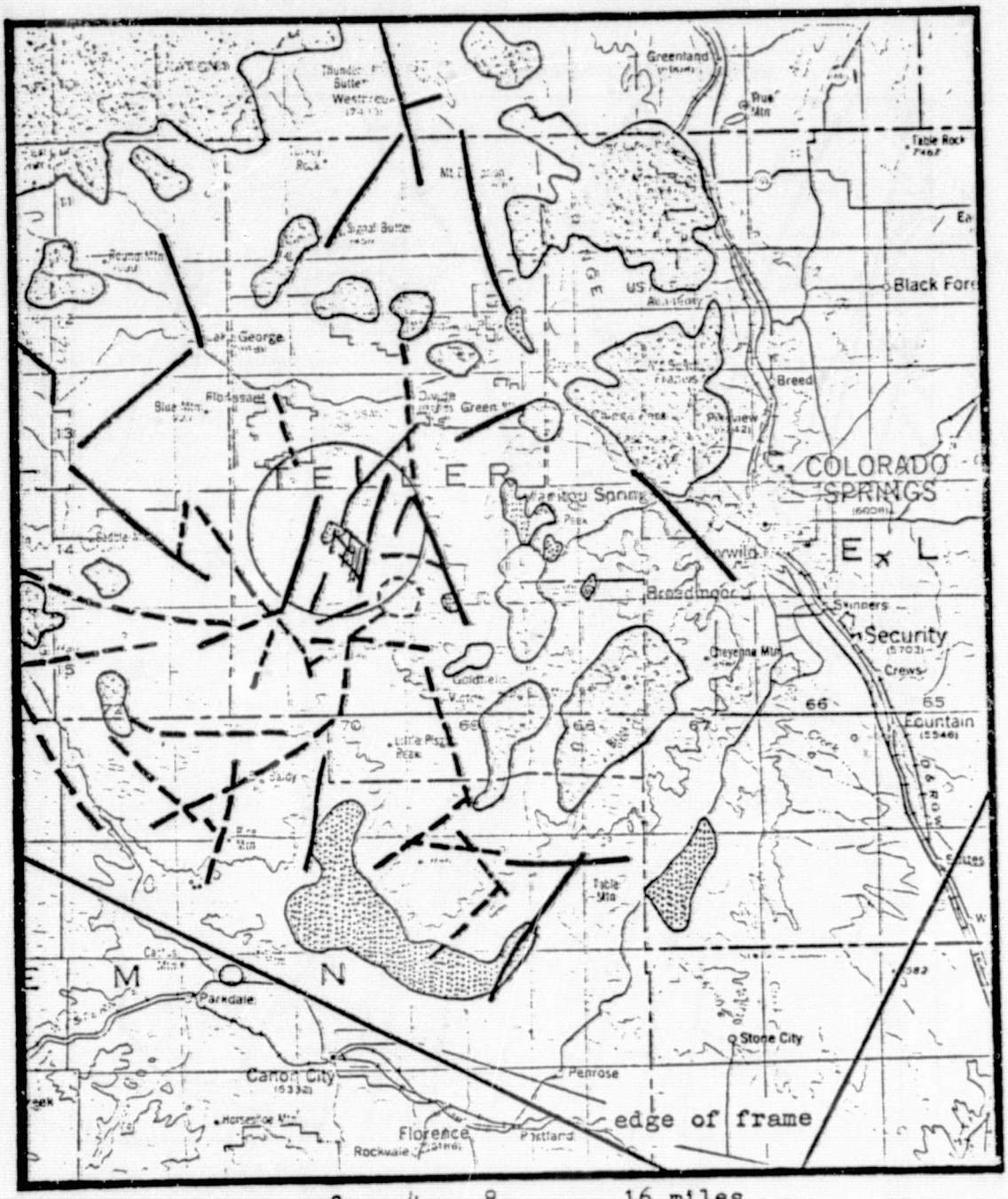


Figure 9: Linear diagram. Skylab 3 S190-B, track 48 frame 39, 4 August 1973. Study area at Dome Rock is circled.
——— — — Linears, dashed where existence questioned.
Color anomalies.
Clouds.

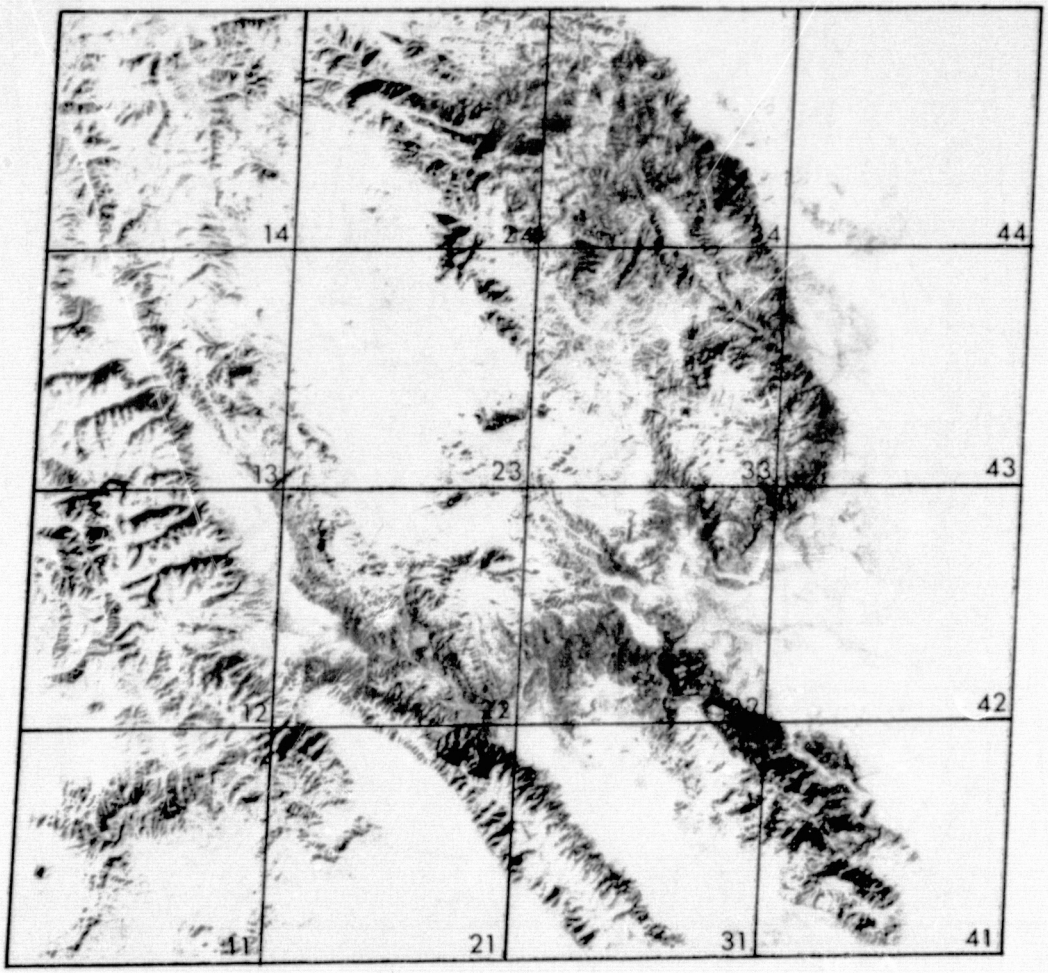


Figure 10. LANDSAT image, E-1172-17141, of central Colorado. Date January 11, 1973, sun elevation is 23 degrees, sun azimuth is 150 degrees. Grid subdivisions will be referred to in the text.

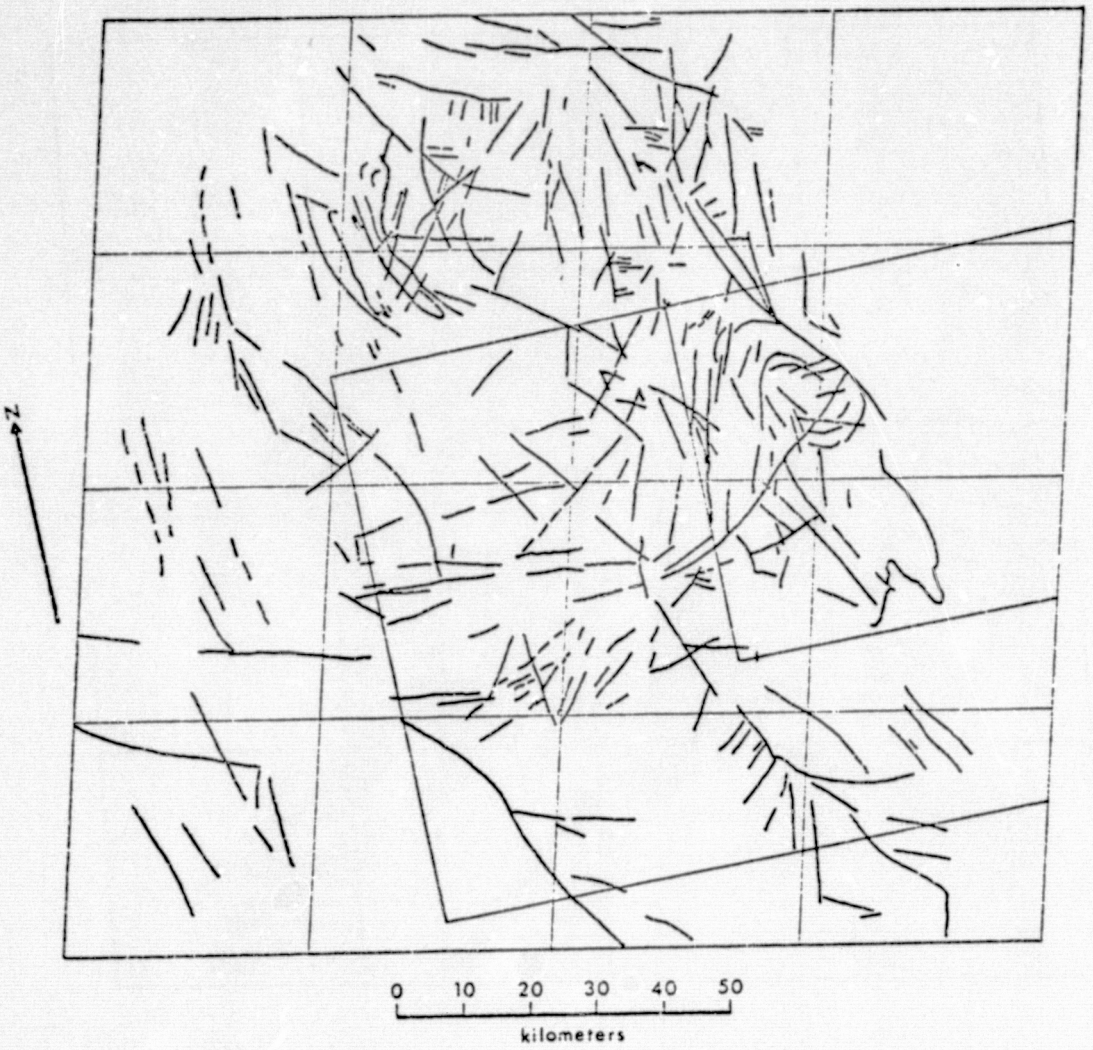
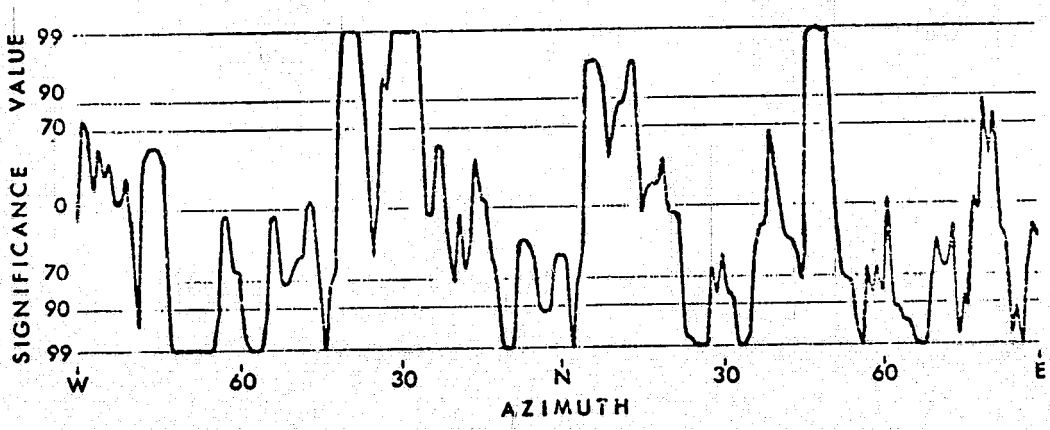
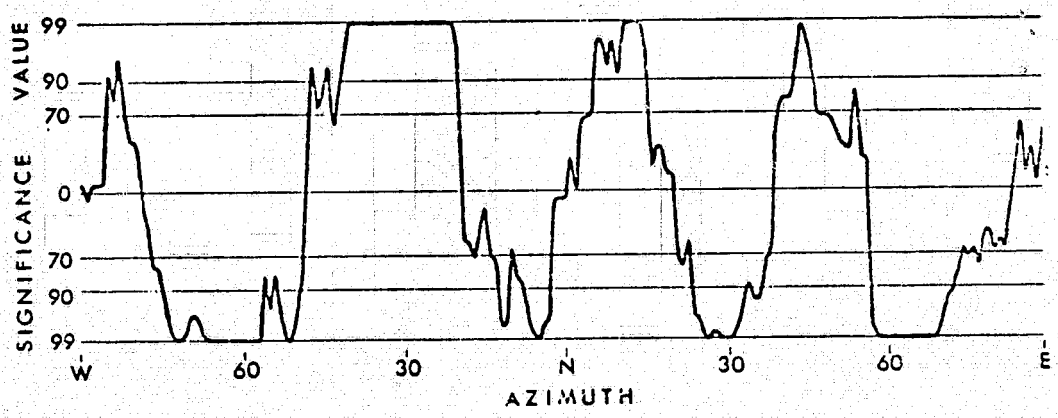


Figure 11. Linears traced from LANDSAT image E-1172-17141. Gridded areas are as in Figure 10. Larger rectangular subarea is of the Pueblo relief map. Smaller subarea is of the Southern Front Range.

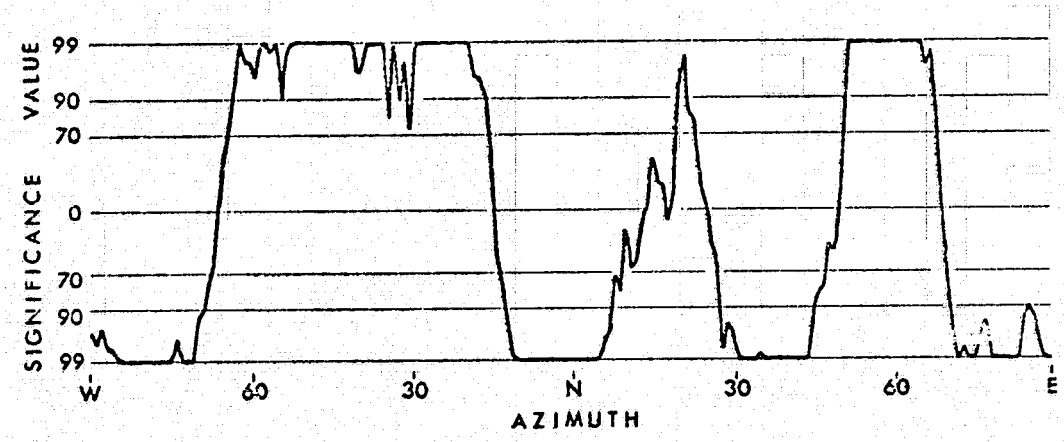


(a) Smoothing interval is 5 degrees of azimuth.

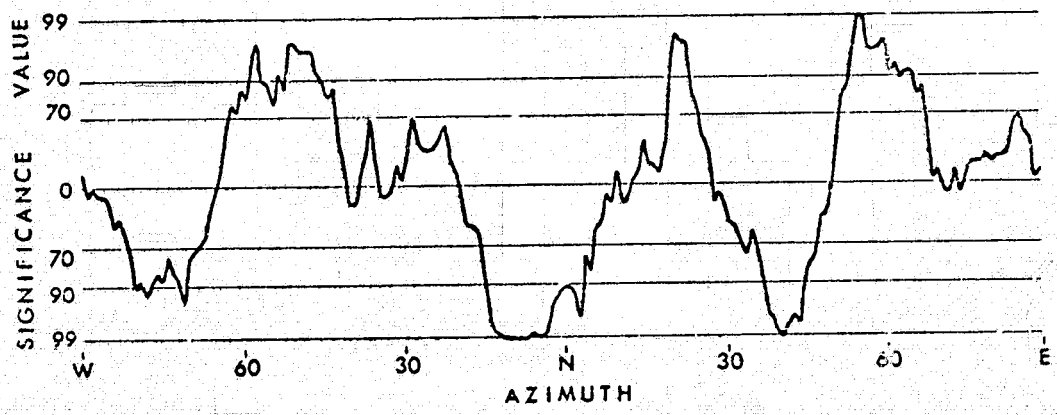


(b) Smoothing interval is 18 degrees of azimuth

Figure 12. Example of merging of narrow maxima and minima by increasing the azimuthal summing or smoothing interval.

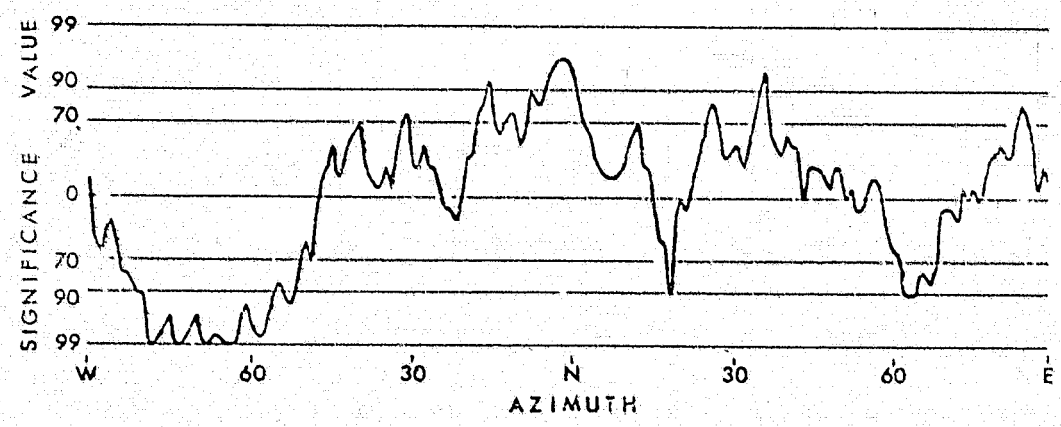


(a) Length-weighted azimuthal data

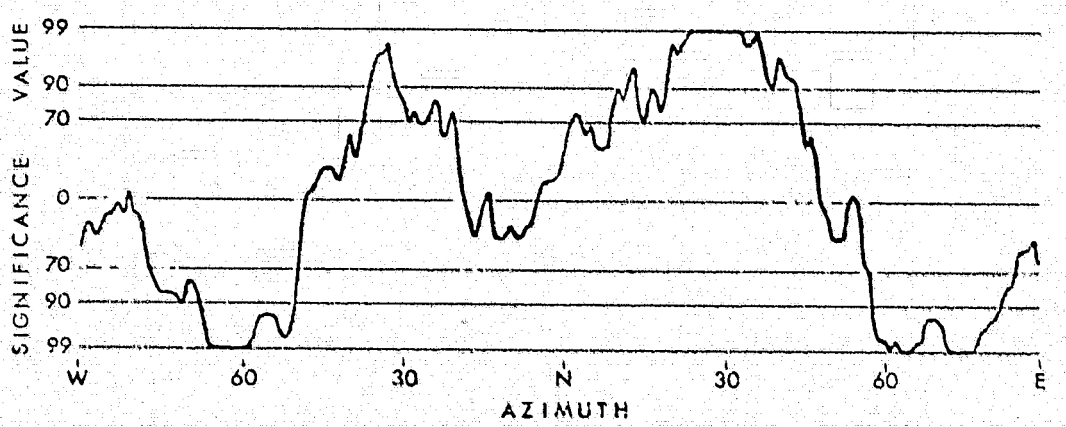


(b) Unweighted azimuthal data

Figure 13. Illustration of effect of length-weighting on significance of trends in strike-frequency histograms, 18-degree smoothing.

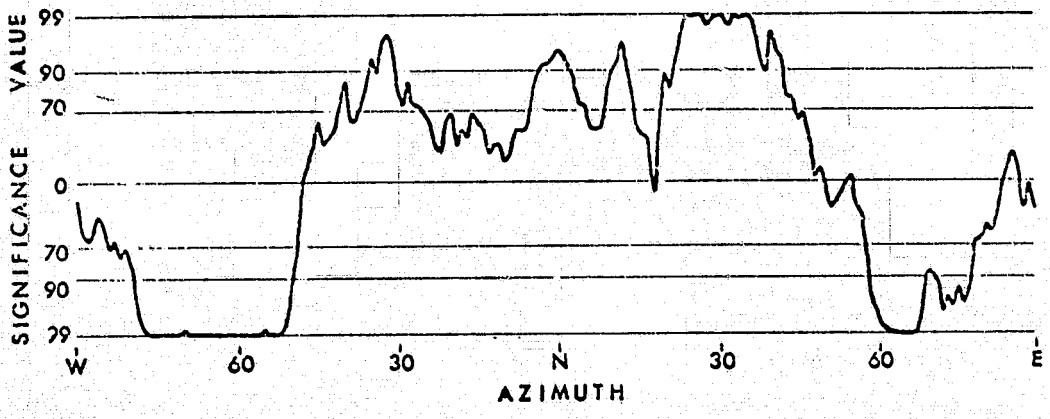


(a) E-1154-17143

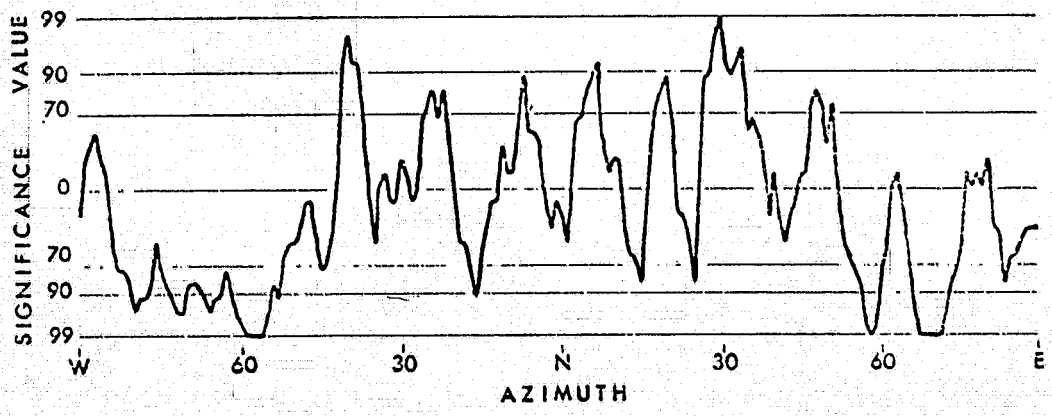


(b) E-1172-17141

Figure 14. Strike-frequency histograms of linears in two LANDSAT images of central Colorado. The area covered is shown in Figures 2 and 7.



(a) Smoothing interval is 18 degrees



(b) Smoothing interval is 5 degrees.

Figure 15. Strike-frequency histograms of linears combined from both LANDSAT images, E-1154-17143 and E-1172-17141.

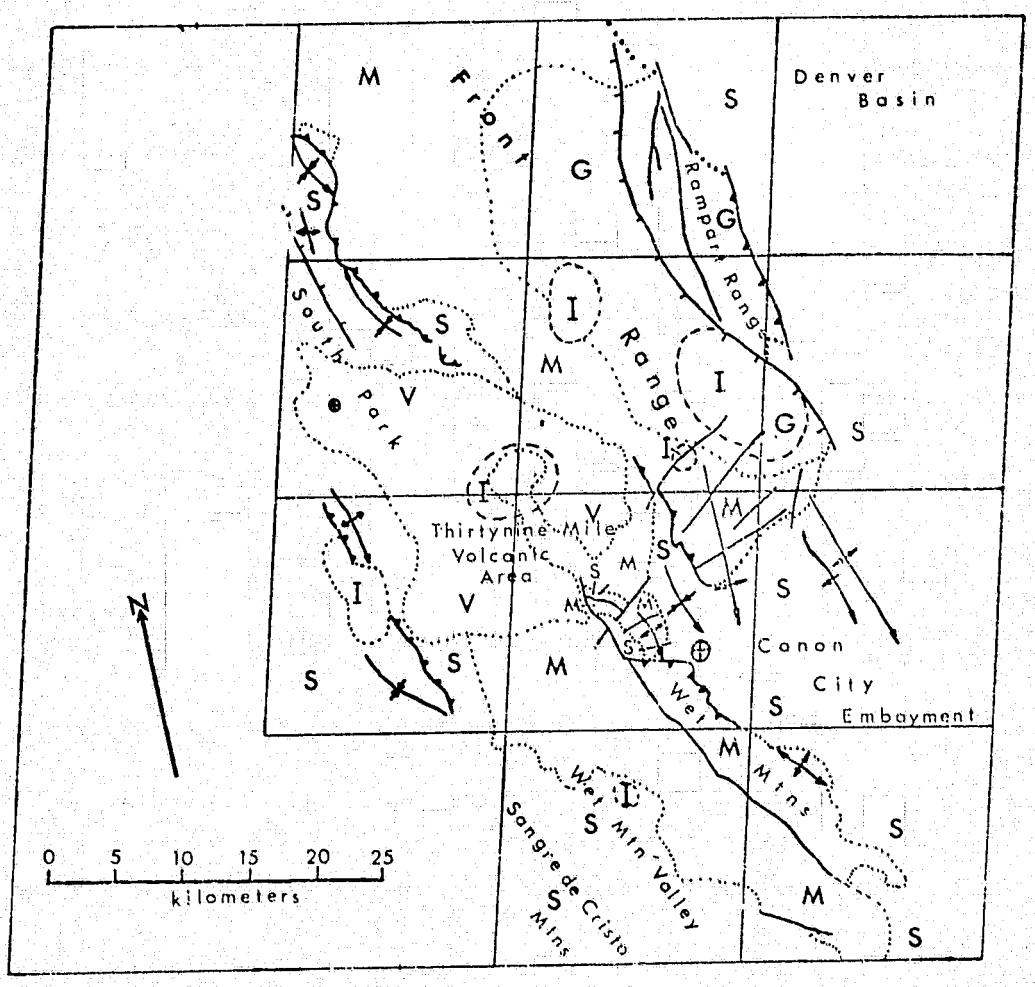


Figure 16. Geologic map of imaged area showing major faults and folds and gross lithologic terrains. Plain, hachured, and toothed lines are faults. Hachures indicate reverse faults, teeth indicate thrust faults. Lines with arrows are folds. Lithologic terrains are defined by dotted lines and are sedimentary (S), metamorphic (M), granitic igneous (G), volcanic (V), igneous or volcanic intrusive centers (I).

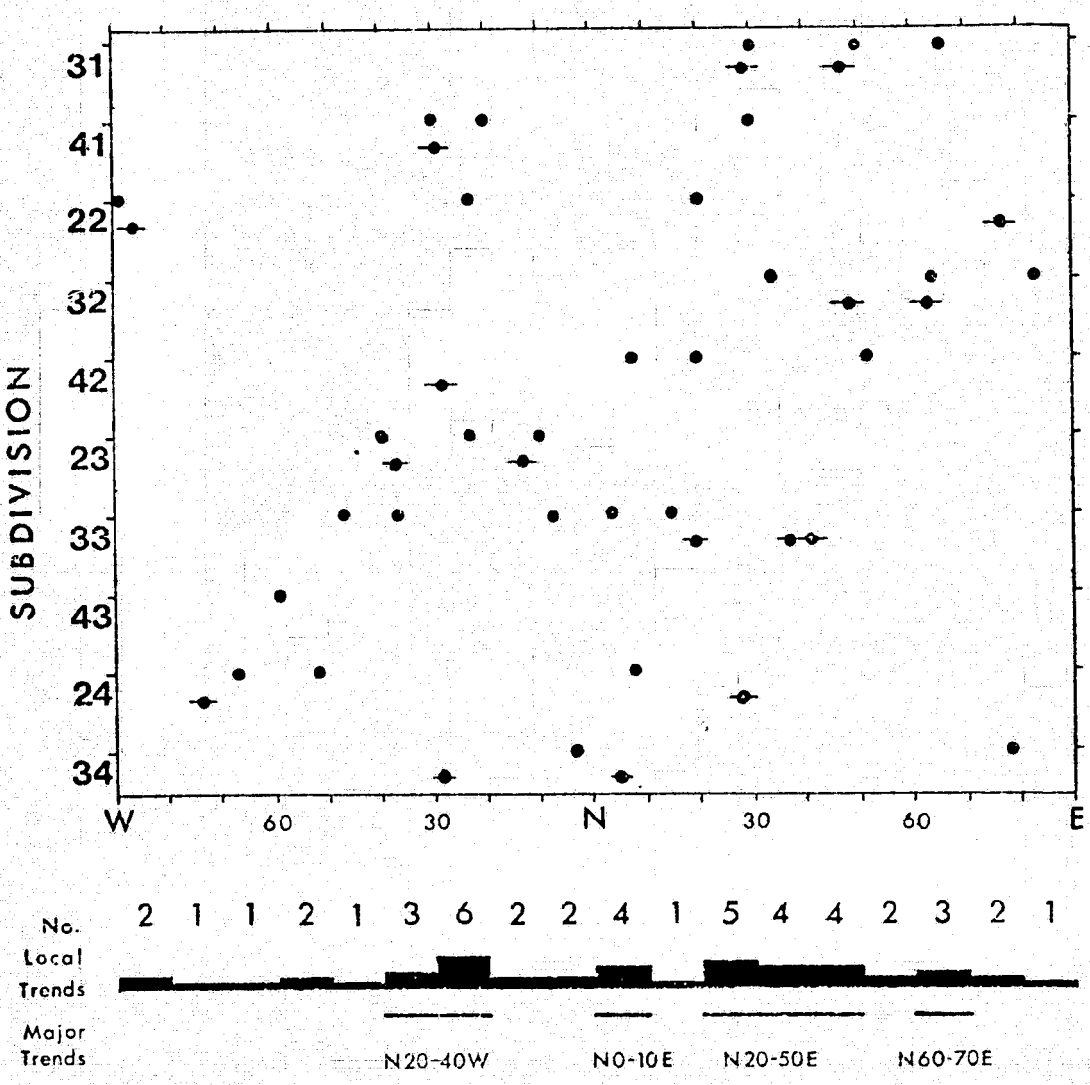


Figure 17. Areal distribution of local trends in 10 subdivisions of E-1172-17141 (barred dots) and E-1154-17143 (plain dots). Histogram shows number of trends for both images per 10 degree sector of azimuth. Heavy lines below histogram indicate 4 prominent trends for total area of all subdivisions.

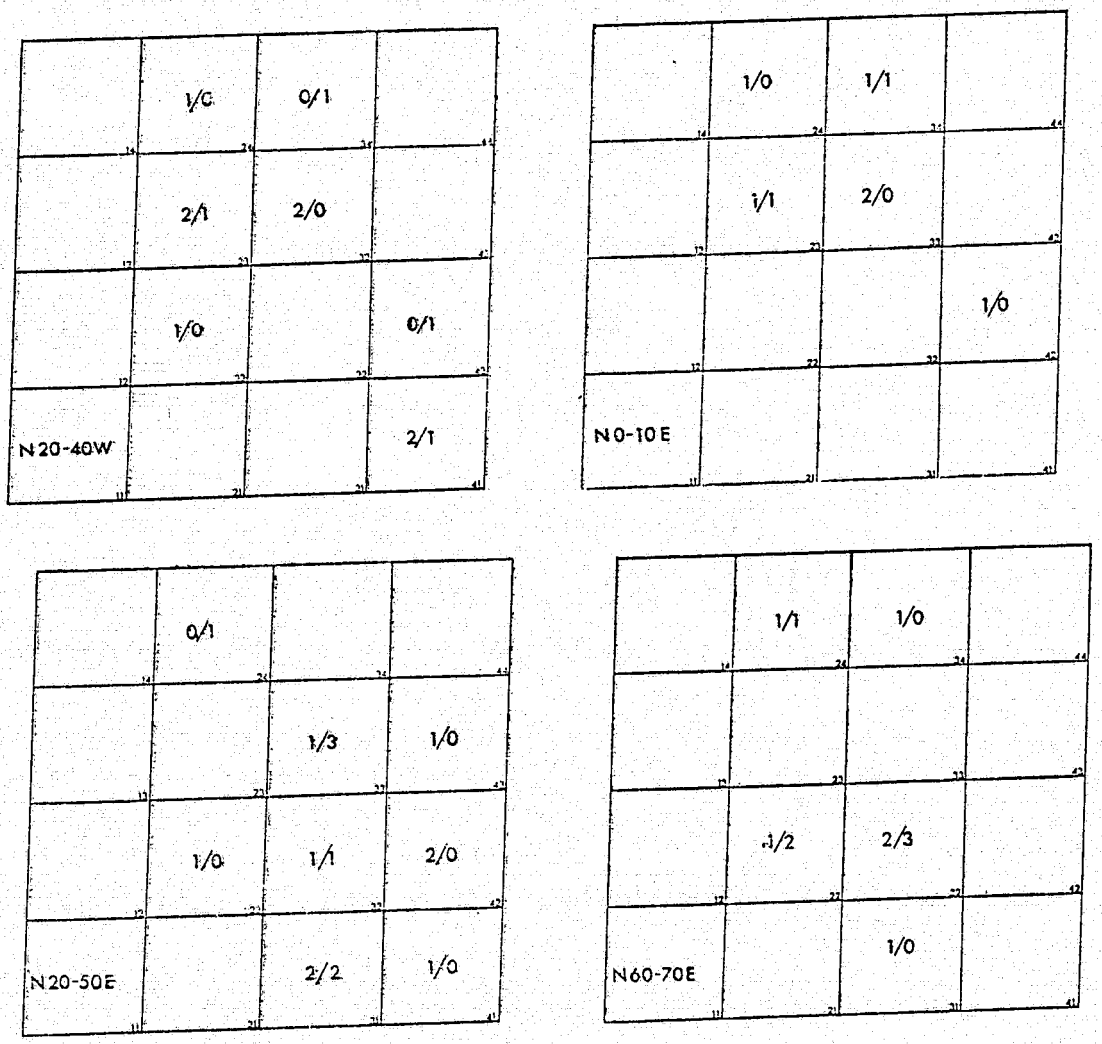
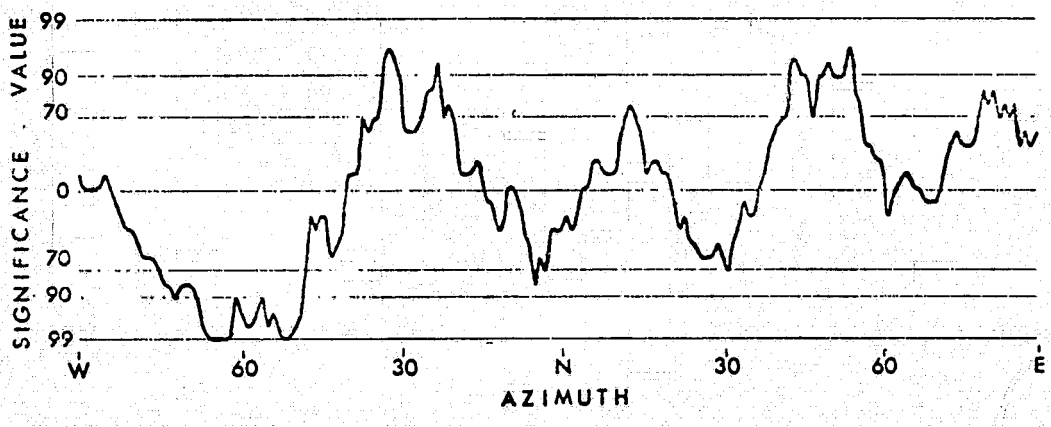
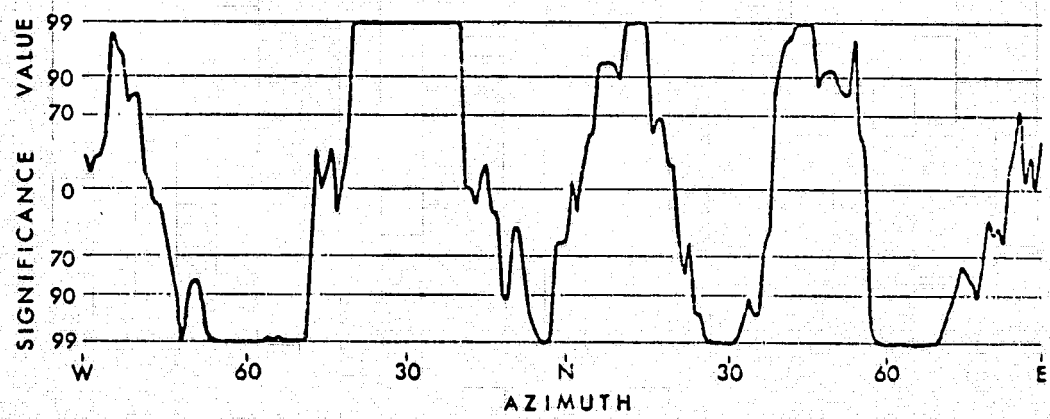


Figure 18. Number of local trends within each subdivision that falls within the four major trends of Figure 8. Numerator is for E-1154-17143 and denominator is for E-1172-17141.

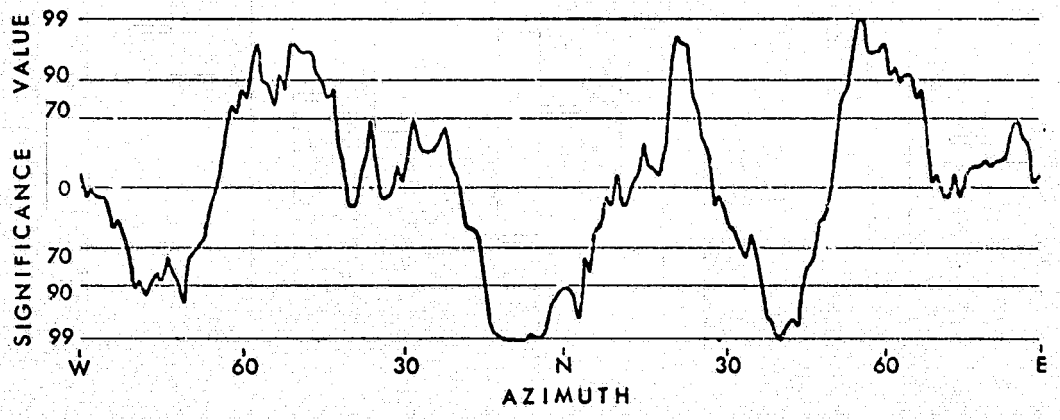


(a) unweighted azimuthal trends

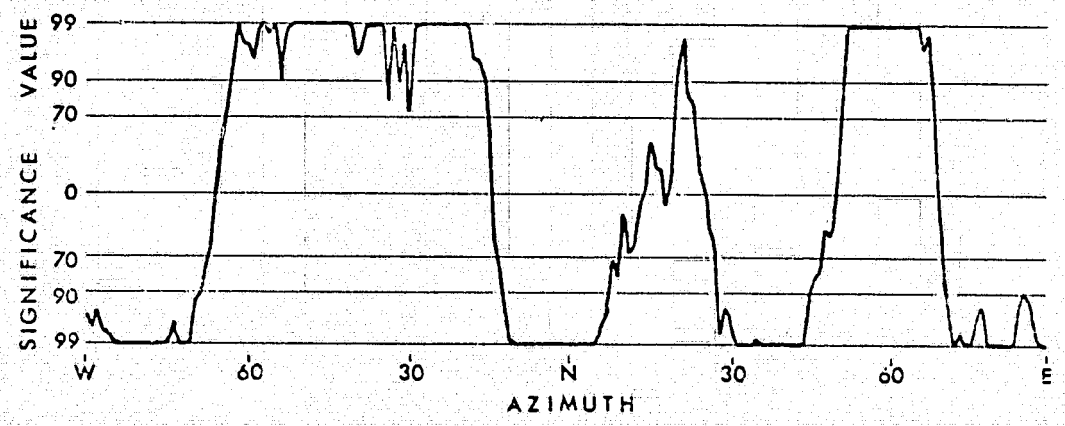


(b) length-weighted azimuthal trends

Figure 19. Linear trends in LANDSAT image E-1172-17141 for area of Pueblo relief map as outlined in Figure 2, 18 degree smoothing.

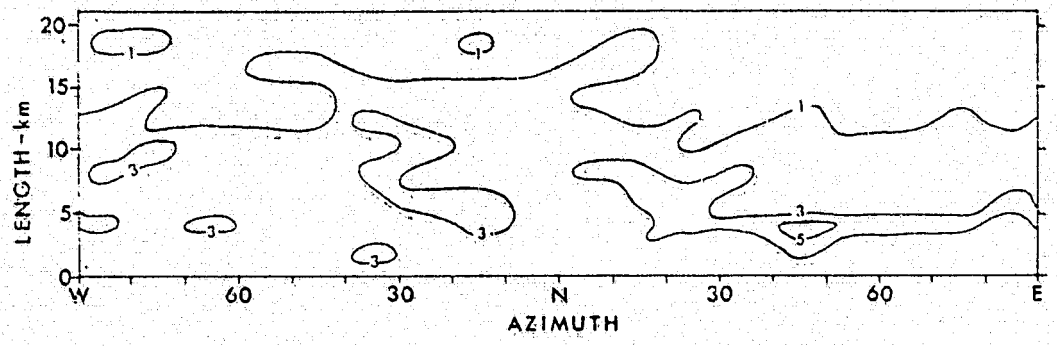


(a) Unweighted azimuthal trends

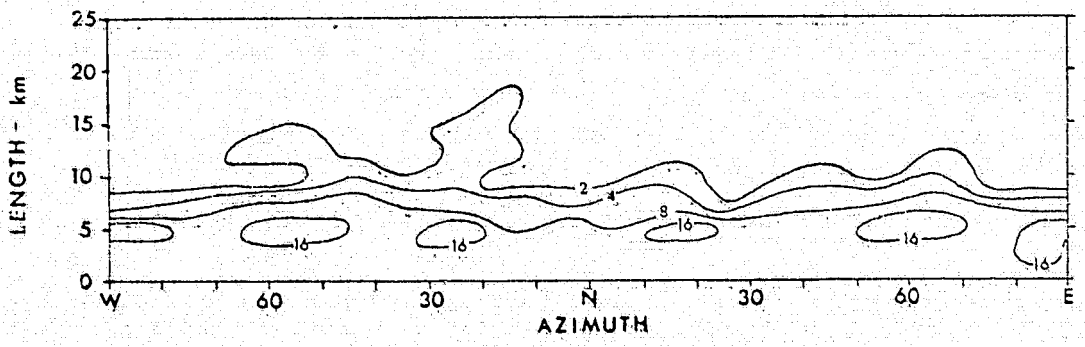


(b) Length-weighted azimuthal trends

Figure 20. Histograms of linears in Pueblo relief map as outlined in Figure 2, 18 degree smoothing.

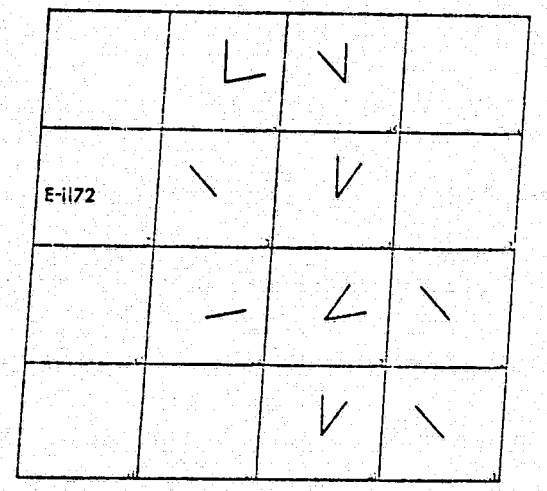


(a) E-1172-17141 image

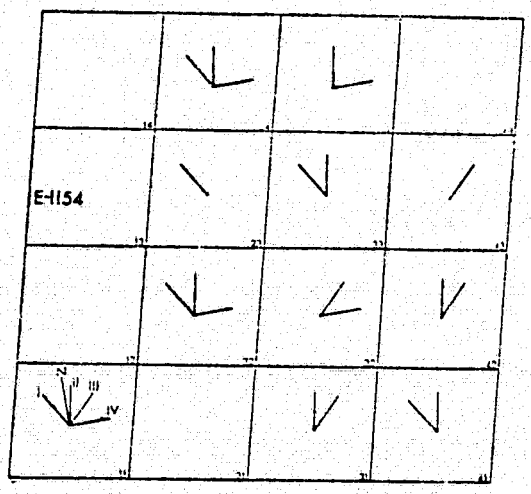


(b) Pueblo relief map

Figure 21. Graphs of frequencies of linears for given length and azimuth for 10 degree intervals.



(a) LANDSAT image E-1172-17141



(b) LANDSAT image E-1154-17154

Figure 22. Occurrence in areal subdivisions of four supermodal trends of length-weighted linears

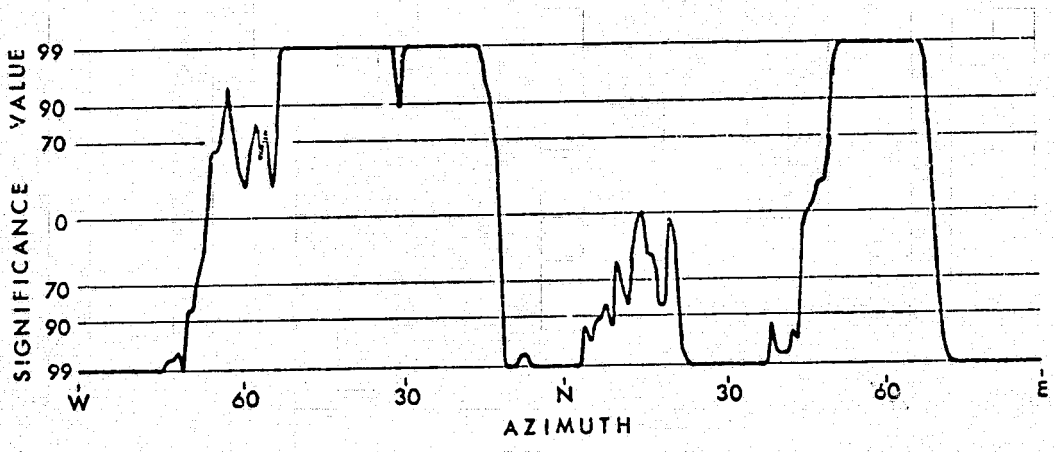


Figure 23. Length-weighted, super-modal linear trends in Pueblo relief map.

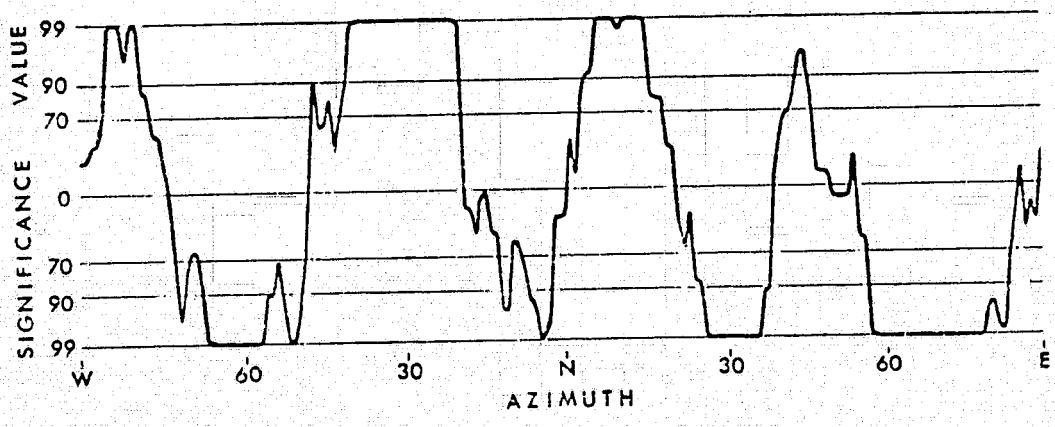
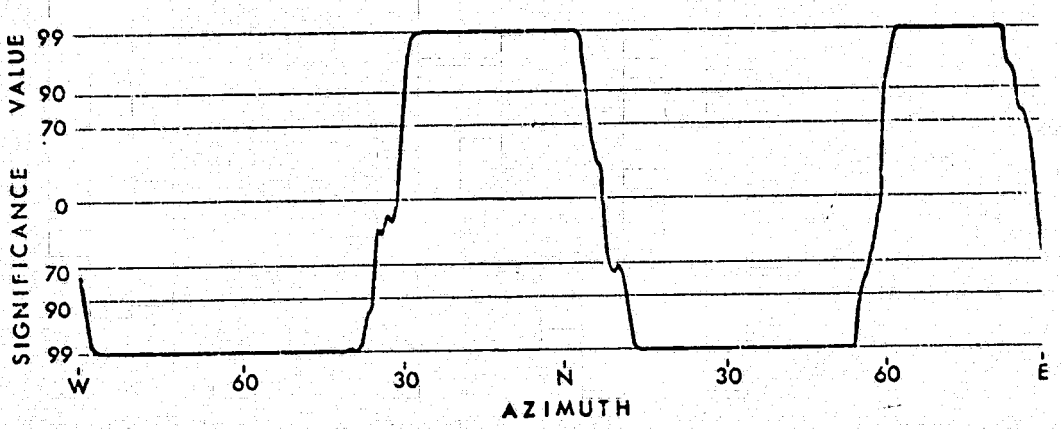
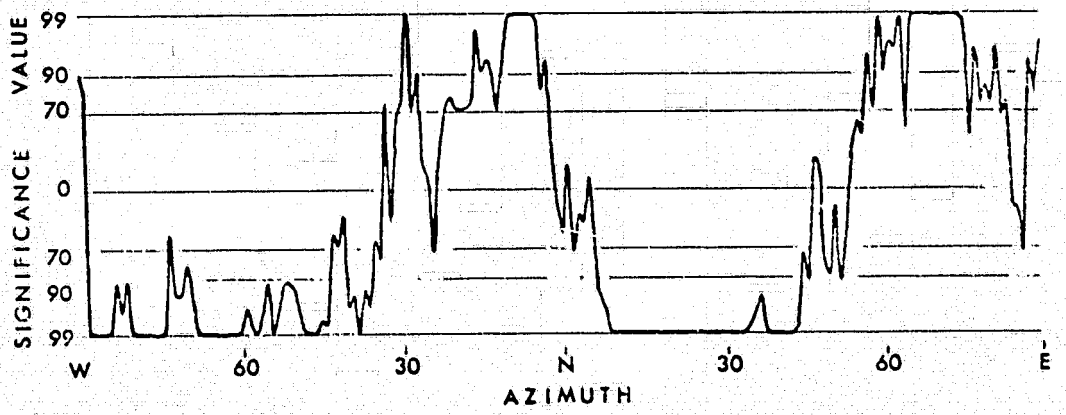


Figure 24. Length-weighted, super-modal linear trends in E-1172-17141 for area of Pueblo relief map.



(a) Southern Front Range south of Pikes Peak, 18 degree smoothing



(b) Subdivisions 32, 42, 33, 24, and 34 of imaged area of E-1172-17141, 5 degree smoothing.

Figure 25. Azimuth trends of joints in area of central Colorado.

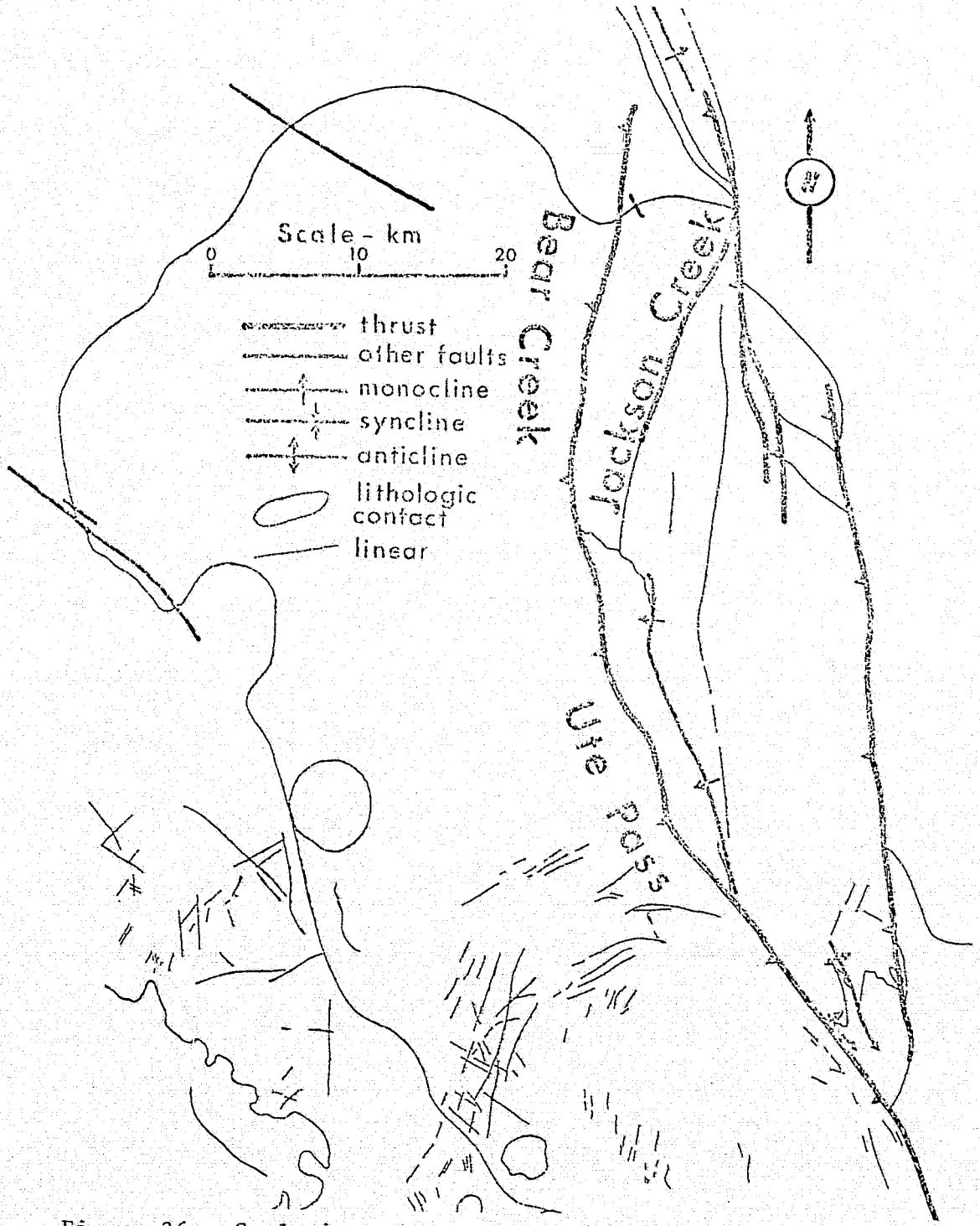


Figure 26. Geologic structure map of Rampart Range, central Colorado, showing named anomalous megalinears.

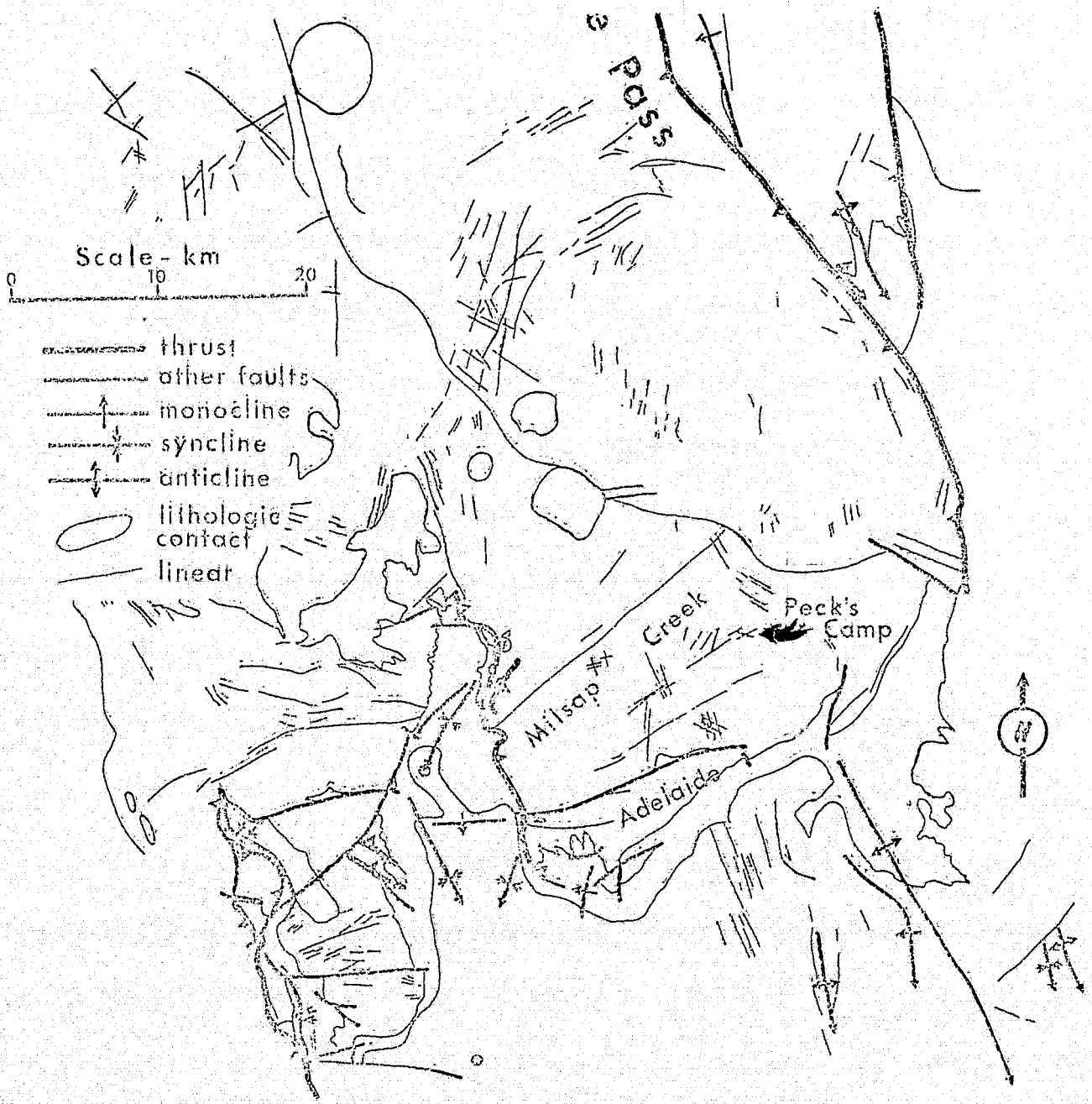


Figure 27. Geologic structure map of southernmost Front Range, central Colorado, showing named anomalous megalinears.



Figure 28. Concentric features in LANDSAT image E-1172-17141 described in Figure 10. 1-Pikes Peak intrusive center of Pikes Peak batholith, 2-Lake George stock, 3-Thirtynine Mile volcanic field, 4-Wet Mountain Valley volcanic field.

REPRODUCIBILITY OF THE ORIGINAL PAGE IS POOR

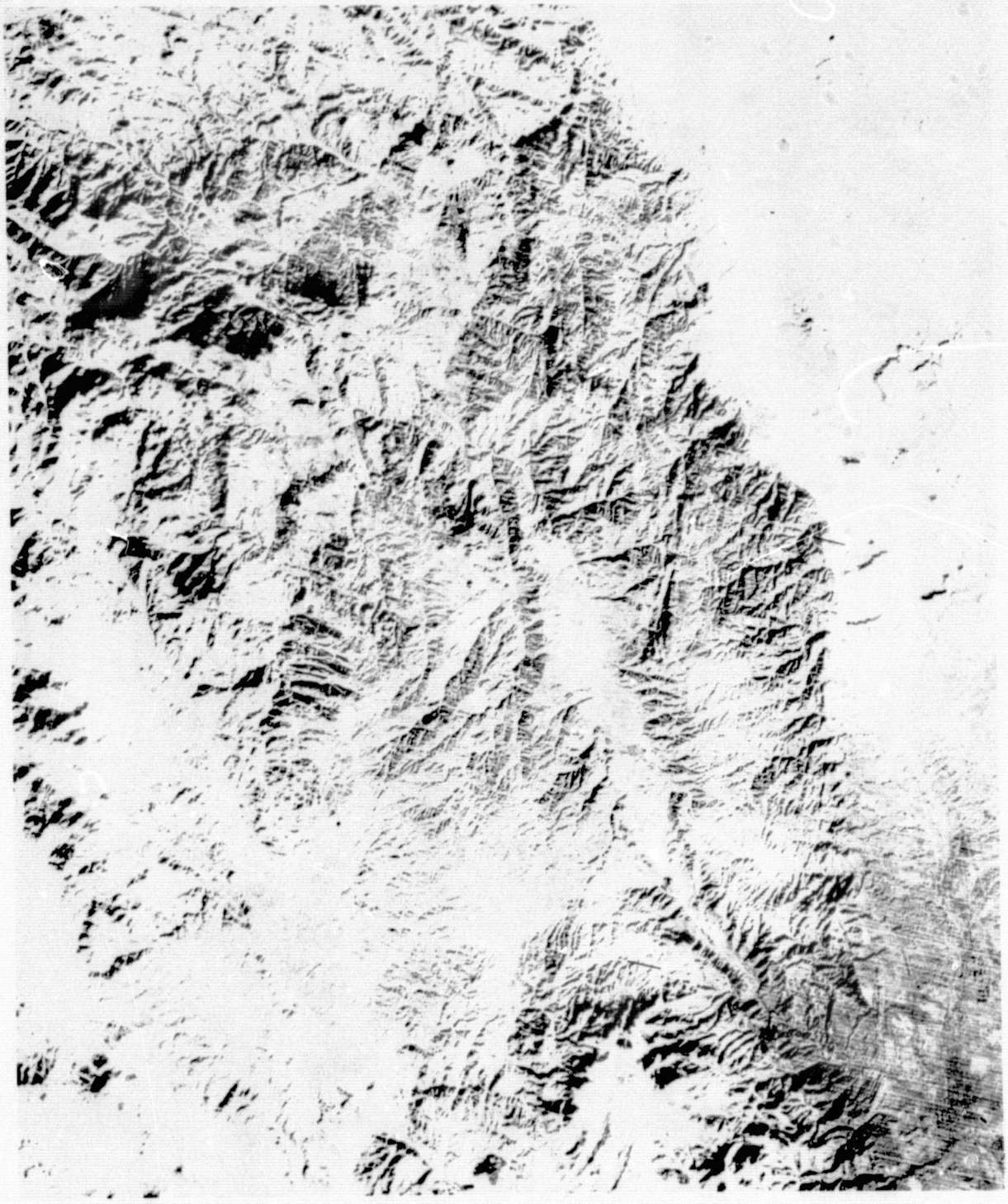


Figure 29. Linear features of the Rampart Range in snow-enhanced LANDSAT image E-1550-17102. Sun azimuth is 147. Sun elevation is 25. Date is January 24, 1974. Scale is same as Figure 26.

REPRODUCIBILITY OF THE
ORIGINAL PAGE IS POOR



Figure 30. Linear features of the southernmost Front Range in LANDSAT image E-1550-17102 described in Figure 29. Scale is same as Figure 27.

REPRODUCIBILITY OF THE
ORIGINAL PAGE IS POOR

THE APPLICATION OF RADAR IMAGERY TO SPECIFIC PROBLEMS OF INTERIOR ALASKA G-11

By P. Jan Cannon, University of Alaska, Fairbanks, Alaska

N76-17509

INTRODUCTION

The purpose of this paper is to present an indication of the possible applications of side-looking airborne radar (SLAR) imagery to specific geomorphic and environmental geologic problems in Interior Alaska. The radar imagery described in this paper was acquired in July, 1972, by the NASA NP3A aircraft, as part of Mission 209 of the Earth Resources Aircraft Project (ERAP). The frequency of the radar energy that was transmitted and recorded by the radar system was 16.5 Gigahertz. Therefore, the wavelength of the radiant energy was about 1.8 centimeters. The radar system operated in both the real aperture and synthetic aperture modes simultaneously.

Interior Alaska has what is termed an "extreme continental climate" (Thornbury, 1965, p. 567). The greatest range of temperatures in Alaska occur here with both the record high and the record low having been recorded in this region. The official high is 38°C (100°F) above zero, and the record low is 60°C (76°F) below zero. Although winter temperatures and conditions are severe in the Arctic region of Alaska, they are not so extreme as in the Interior.

The normal yearly precipitation of thirty centimeters of water may seem low, but over half of that thirty centimeters occurs as snow which averages in total about 154.9 centimeters of snow per year (Rieger and others, 1963, pp. 3-4). The fact that the snow remains on the ground until the end of April and that the evaporation rates in the summer months are low, the area has what would be termed a constantly-moist climate (Wolff and Haring, 1967, p. 17).

Snow remains on the ground from the first of October until the end of April. This and the low sunlight conditions of the near-Arctic winter make the acquisition of aerial photographs difficult, if not impossible, during these seven months of winter. The cloudy conditions that exist during the month of August cut the total time of obtaining useful aerial photographs to only four months out of the year.

Interior Alaska is bounded by the Brooks Range on the north and by the lofty mountains of the Alaska Range on the south. Interior Alaska is characterized by broad flatlands and low-rolling mountains (Wahrhaftig, 1965, pp. 18-33). The flatlands are drained by braided-meandering streams. The low-rolling mountains have a moderate local relief of about 150 to 600 meters. The flatlands are mostly less than 200 meters above sea level and the rounded peaks of the low-rolling mountains range from about 600 to 1,600 meters above sea level.

GLACIAL LANDFORMS

Radar imagery of an area provides a unique spatial presentation of that area with an enhancement of the relief. Because of this, landforms can be recognized and identified more rapidly using radar imagery than with any other means; that includes topographic maps and aerial photographs (Cannon, 1974, p. 1983). Radar imagery of a region 24 kilometers southeast of Livengood, Alaska (Figures 1 and 2) indicated the presence of some glacial landforms between the Talalina River and O'Brien Creek. The landforms are ice-scour features which indicate movement of glacial ice from the south towards north. This type of glacial landform had not been previously recognized in this area (Hunt, 1967, p. 423;

Flint, 1971, p. 470). The shape of the landforms is so subtle that the landforms would not be noticed on aerial photography of the area unless the investigator is aware of the possible existence of the landforms. Due to the scale of the available topographic maps of the area, the landforms cannot be recognized on the topographic maps. The landforms indicate a greater northern advance of the Early Pleistocene glaciers of the Alaska Range, than previously recognized. This small amount of geomorphic information will greatly change the interpretation of the Quaternary history of Alaska. These features were initially recognized on the radar imagery shown in Figures 1 and 2.

YUKON RIVER FLOODPLAIN

Radar imagery of the valley along the Yukon River (Figure 3) from the village of Rampart, northward to Point No-point, revealed the existence of geomorphic features that are formed by large magnitude floods. These geomorphic features are flood-scour, elongate ridges and lakes which occur in a belt four to five miles wide along the Yukon River. It is near this area where a bridge is being constructed across the Yukon River for the crossing of the Trans-Alaska Pipeline. This bridge appears to span only a high frequency, low magnitude floodplain. The level of this floodplain is about 70 meters below the high water level indicated by the large flood-scour features. The Yukon River has a drainage area (watershed) of 613,590 square kilometers (Iseri and Langbein, 1974). This ranks the Yukon River second in drainage area for all the rivers which cross the United States and empty into the oceans directly. Of the same class of rivers, the Yukon River is the second longest, nearly 3,000 kilometers, and fourth in average discharge. However, there exists less than 20 years of continuous discharge data for the Yukon River. Therefore, it should be noted that the discharge data for the Yukon is inadequate for engineering studies. It appears that these floodplain features were not recognized previously or were misinterpreted, because no other remote sensing technique can provide the unique view which is displayed on the radar imagery. The greater area of display coupled with the enhancement of the low-relief features is unique.

ENVIRONMENTAL GEOLOGY

The use of radar imagery in lower latitudes for environmental geologic mapping has been extensively explored (Cannon, 1974). Actually, environmental geologic mapping of Interior Alaska is simplified because of the small number of indigenous species of vegetation (Reiger and others, 1963, p. 4). Radar imagery of a portion of the Tanana River (Figures 4 and 5) demonstrates the possible applications to environmental geologic mapping in Alaska. The region shown in Figures 4 and 5 is halfway between Fairbanks and Nenana, where Whiskey Island and Hot Slough are located. The most obvious feature on the radar imagery is the main channel and anabranches of the Tanana River. The main channel and the anabranches indicate the areas flooded during high frequency - low magnitude flooding events which occur annually. The broad flat area, extending from where cliffs that have been undercut by stream action are apparent, across the river and many abandoned stream meanders, to an area beyond the edge of the imagery, is the floodplain of low frequency - high magnitude flooding events (Childers and Mechel, 1967). The real aperture radar imagery of Figure 4 shows best the differences in returns from the spruce and the broad leaf deciduous trees. The differences are greatest during summer months when the broad leaves of the deciduous trees return a greater amount of radiant energy. Floodplains, channels, channel features, hillslopes and vegetation can all be mapped for environmental projects easily and rapidly using the radar imagery.

CLEAR CREEK FAULT

Radar imagery of an area 40 kilometers south of Fairbanks, Alaska, (Figure 6) revealed some significant information about geologic structure. The area is physiographically referred to as the Tanana Flats and is included in a military bombing and gunnery range. The Tanana Flats are composed of broad sheets of glacial and fluvial deposits, which are

Pleistocene and Recent in geologic age (Pewe and others, 1966). One of the most conspicuous features displayed on the radar imagery of the area is the scarp of a recent fault. The fault cuts across Clear Creek and has been given the name of "Clear Creek Fault" for the purpose of location and identification. The total vertical displacement along the scarp is about 10 meters. The plane of the fault is nearly vertical and the upthrown block is to the south of the fault. The extent of the Clear Creek Fault was poorly represented in previous geologic mapping of the area (Pewe and others, 1966). The extent of the fault is quite clearly shown on the radar imagery and an accurate map of its extensions around the hills surrounding the Blair Lakes can be made (Figure 6). The mapping of such structures is important both economically and environmentally. Regardless of the future uses that are planned for the Tanana Flats, the structure of the area should be remapped using radar imagery.

CONCLUSION

Based on the all-weather characteristics of radar imagery and its unique enhancement effects, extensive mapping programs using radar imagery are in progress throughout the State of Alaska. These mapping programs include: land-use evaluations, geomorphic studies, environmental assessments, and exploration. The vastness and remoteness of Alaska will continually demand the practical application of radar imagery both in initial regional studies and in the continuous monitoring of projects and environmental conditions.

REFERENCES CITED

Cannon, P. J., 1974, Application of radar imagery to environmental geologic mapping of Texas, in Proceedings of the ninth international symposium on remote sensing of environment, April, 1974: Willow Run Lab. of the Environmental Research Institute of Michigan, Report No. 107000-1-X, the University of Michigan, Ann Arbor, pp. 1981-1988.

Childers, J. M., and Meckel, J. P., 1967, Flood of August 1967 at Fairbanks, Alaska: U.S. Geol. Survey Hydrol. Inv. Atlas HA-294.

Flint, R. F., 1971, Glacial and Quaternary Geology: New York, John Wiley & Sons, Inc., 892 p.

Hunt, C. B., 1967, Physiography of the United States: San Francisco, W. H. Freeman and Co., 480 p.

Iseri, K. T., and Langbein, W. B., 1974, Large rivers of the United States: U.S. Geol. Survey Circ. 686, 10 p.

Pewe, T. L., Wahrhaftig, C., and Weber, F., 1966, Geologic map of the Fairbanks Quad., Alaska: U.S. Geol. Survey Misc. Geol. Inv. Map I-455, scale 1:250,000.

Reiger, S., Dement, J. A., and Sanders, D., 1963, Soil survey, Fairbanks area, Alaska: U.S. Dept. Agriculture, Soil Survey Series 1959, no. 15, 41 p.

Thornbury, W. D., 1965, Regional geomorphology of the United States: New York, John Wiley & Sons, Inc., 609 p.

Wahrhaftig, C., 1965, Physiographic divisions of Alaska: U.S. Geol. Survey Prof. Paper 482, 52 p.

Wolff, E., and Haring, R. C., 1967, Natural resource base of the Fairbanks North Star Borough, Alaska: College, Alaska, Mineral Industries Research Lab., 127 p.

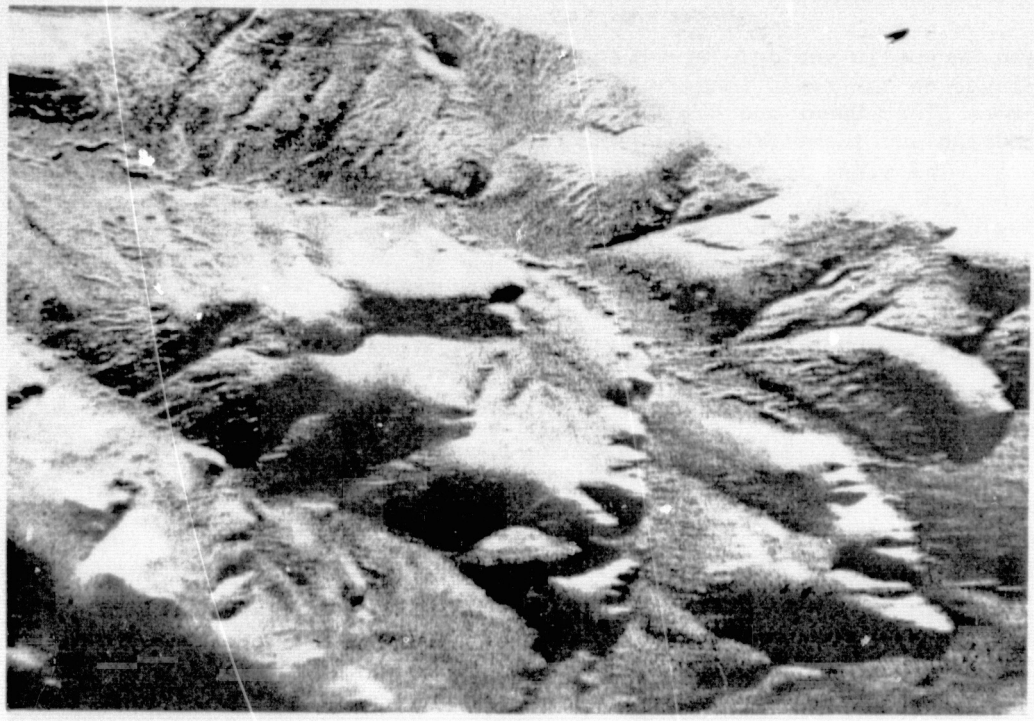


Figure 1. Real aperture, K-band, radar imagery of an area of Interior Alaska, showing glacial, ice-scour features. North is to the right of the figure and the movement of the glacial ice was from the upper left to the lower right. The area shown in this figure is about eleven by sixteen kilometers.

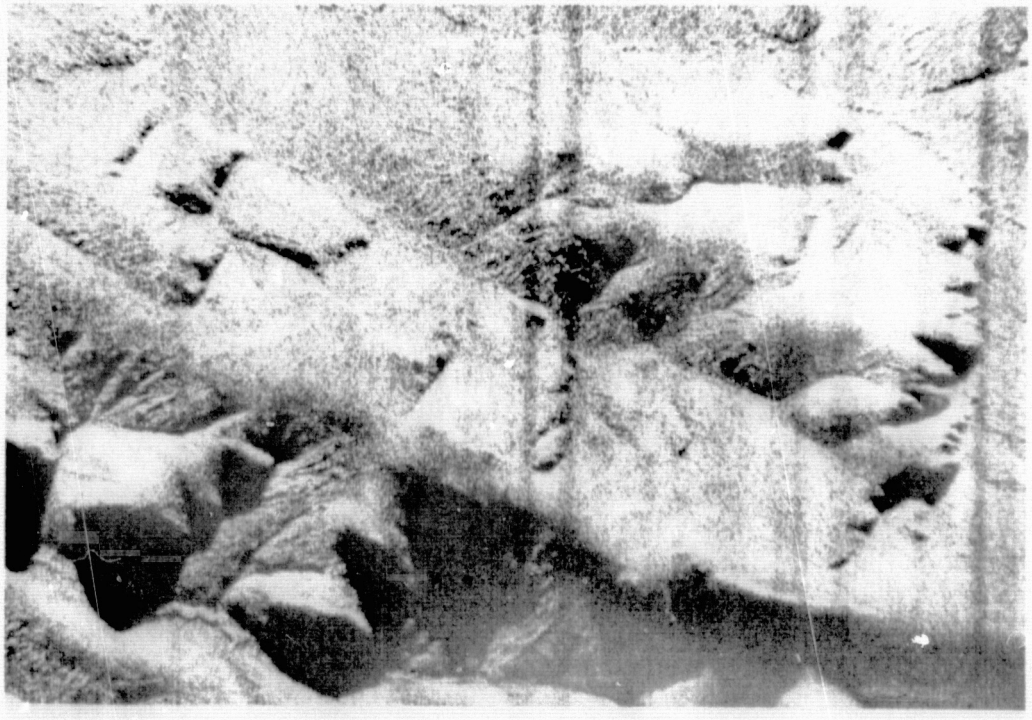


Figure 2. Synthetic aperture, K-band, radar imagery of nearly the same area shown in Figure 1. The orientation and scale of the imagery is the same as in Figure 1.

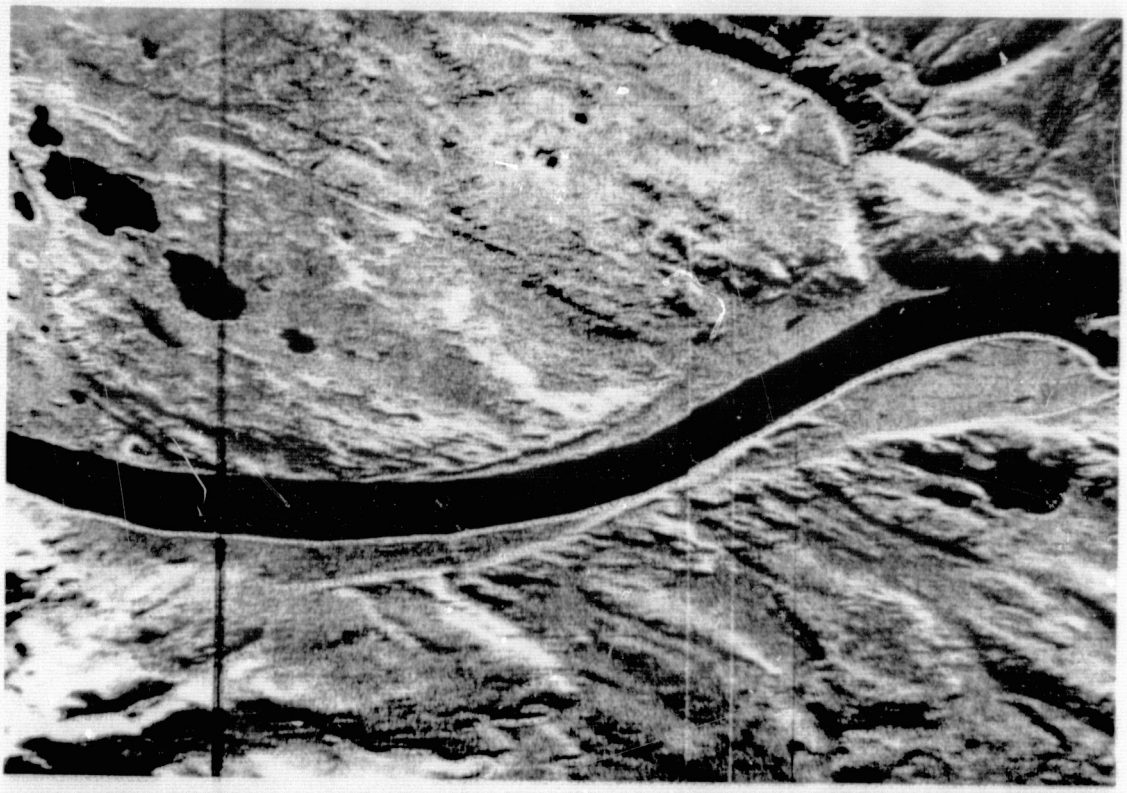


Figure 3. Real aperture, K-band, radar imagery of an area (10.5 by 13.0 kilometers in size) along the Yukon River north of Rampart, Alaska. The elongate features, oriented in a direction from upper left to lower right, were formed by high magnitude, low frequency flooding events. North is to the left of the figure and the flow of water is from left to right.

REPRODUCIBILITY OF THE
ORIGINAL PAGE IS POOR



Figure 4: Real aperture, K-band, radar imagery of part of the Tanana River between Fairbanks, and Nenana, Alaska. The size of the area shown is 7.6 by 10.3 kilometers and south is at the top of the figure. This piece of imagery demonstrates the usefulness of radar imagery in environmental geologic mapping. The longest island is Whiskey Island and the channel below it is Hot Slough.

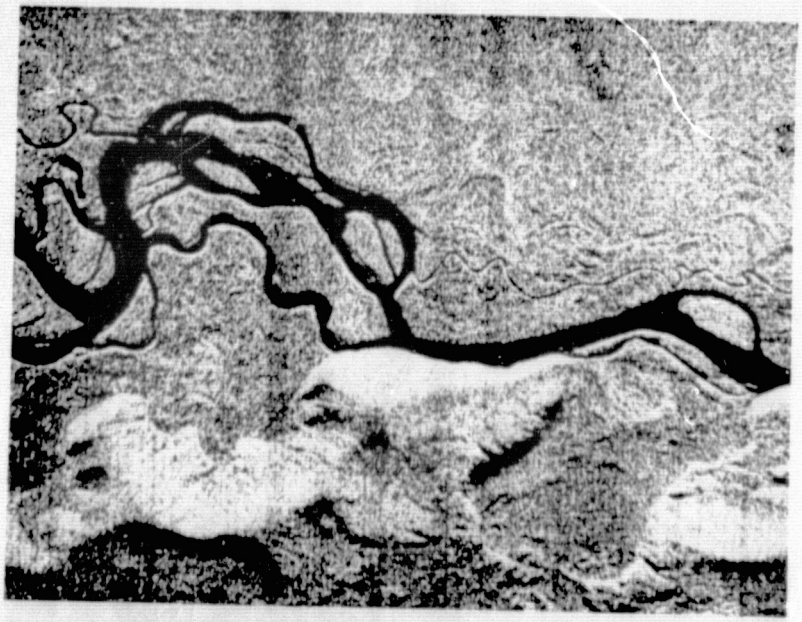


Figure 5. Synthetic aperture, K-band, radar imagery of the same area shown in Figure 4. Although the terrain is emphasized better on this imagery, there is more information from vegetation displayed in Figure 4.

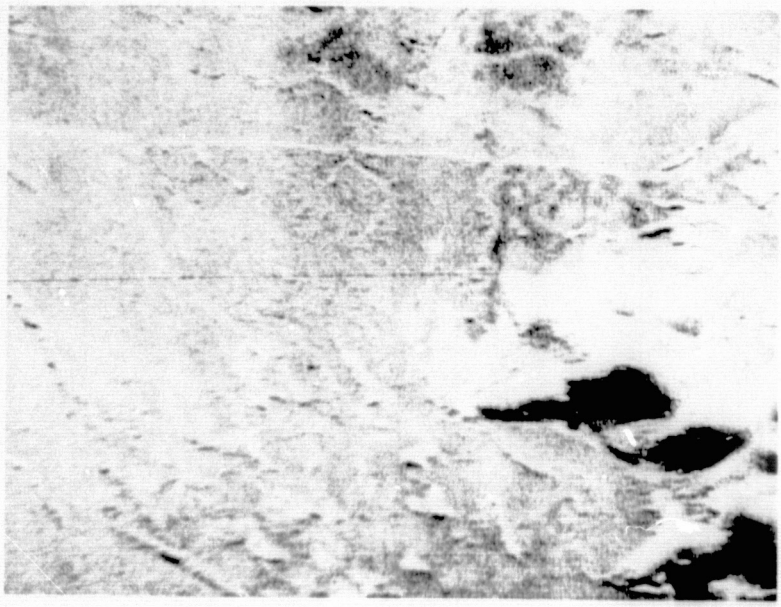


Figure 6. Real aperture, K-band, radar imagery of the Clear Creek Fault in the Tanana Flats. North is towards the upper left and the area covered by the figure is 7.5 by 9.8 kilometers. The fault scarp is the bright line that goes from left to right in the upper third of the figure. The fault can be traced eastward around the hills on the upper right.

LANDSAT IMAGERY ANALYSIS - AN AID FOR PREDICTING LANDSLIDE-PRONE AREAS FOR HIGHWAY CONSTRUCTION

By Harold C. MacDonald, and Robert S. Grubbs,
Department of Geology, University of Arkansas,
Fayetteville, Arkansas 72701

N76-17510

ABSTRACT

Perhaps the most obvious landform features of geologic significance revealed on LANDSAT imagery have been linear trends or lineaments. These ubiquitous trends have been found to correspond, at least to a large degree, with unmapped faults or complex fracture zones. In many cases, especially in Arkansas, these gross linear trends were unmapped and first recognized on LANDSAT imagery. The primary objective of many LANDSAT investigations has been an attempt to correlate these anomalous trends with zones of mineralization to define potential economic significance. Within a major part of Arkansas however, analysis of LANDSAT linear trends appears to provide less glamorous but economically significant practicality. LANDSAT imagery analysis in northern Arkansas has revealed a lineament complex which provides a remarkable correlation with landslide-prone areas along major highway routes. The weathering properties of various rock types, which are considered in designing stable cut slopes and drainage structures, appear to be adversely influenced by the location and trends of LANDSAT defined lineaments. Geologic interpretation of LANDSAT imagery, where applicable and utilized effectively, should provide the highway engineer with a new tool for predicting and evaluating landslide-prone areas.

INTRODUCTION

The utilization of sophisticated remote sensors for terrain analyses in Arkansas was initiated in the mid-1960's. The sensor information used at that time consisted of relatively small scale (approximately 1:1,000,000) radar imagery which revealed a series of north trending linears on the southern flank of the maturely dissected plateau surface of the Boston Mountains. These linear trends were believed to be zones of fault and fracture concentration generally represented by surface drainage channels ranging in magnitude from minor tributaries to major river valleys. During this time, speculation was made as to the structural significance of recognizing such linear features in the terrain; however, because of very limited areal coverage, additional applications could not be pursued. The 1972 launch of LANDSAT-1 provided the first extensive small-scale, synoptic imagery coverage for the State of Arkansas, and revived interest in determining the origin and geologic significance of linears or lineaments. LANDSAT imagery afforded the interpreter with the capability of viewing large areas of terrain in a small format, permitting the integration of seemingly isolated features into a regional picture.

Previous geologic investigations conducted throughout the world have shown that lineaments are ubiquitous features corresponding at least to a large degree, with unmapped faults or complex fracture zones. In many cases, especially in Arkansas, many of these gross linear trends were first recognized and mapped from LANDSAT imagery. During the past two years, the primary objective of many LANDSAT-oriented, geological investigations has been an attempt to correlate these newly recognized trends with zones of mineralization in an attempt to define their economic significance. While

PRECEDING PAGE BLANK NOT FILMED

the mineralization aspect has not been ignored in Arkansas, analysis of LANDSAT derived linear trends appears to provide a less glamorous but economically significant aspect. In northern Arkansas where a residual soil mantle is usually developed, zones of fracture concentration can represent zones of groundwater discharge or zones of surface water absorption. In either case, a water exchange zone allows acceleration of weathering processes with the consequent development of topographic expression. Not only would we expect the fracture zones or lineaments to exert a strong influence on the pattern and orientation of terrain features, but the weathering properties of various rock types which should be considered in designing stable cut slopes also appear to be adversely affected by the location of LANDSAT defined trends. Imagery interpretation of northern Arkansas terrain has revealed a lineament complex which provides a remarkable correlation with landslide-prone areas along major highway routes.

PHYSIOGRAPHY AND GEOLOGIC SETTING

Parts of two major physiographic regions of the southern United States are contained within the boundaries of Arkansas; the Gulf Coastal Plain, which covers the southern and eastern sections of the state, and the Interior Highlands encompassing the northern and western part (Figure 1). The Interior Highlands can be further subdivided into the Ozark Plateaus Region, also known as the Ozark Highlands and the Ouachita Province. Of particular concern to this study are the Ozark Plateaus which comprises three well defined sections: the Salem Plateau, the Springfield Plateau, and the Boston Mountains (Figure 2). These features form three step-like surfaces occupying a 65 mile wide belt extending eastward from the Oklahoma border to the Gulf Coastal Plain.

Most of Arkansas' major landslides occur in the rugged topography of the Boston Mountains. The area is characterized by steep valley walls and higher ridges with the relative relief generally ranging from 500 to 1,500 feet. The nearly horizontal strata of the Boston Mountains consist mainly of Early and Middle Pennsylvanian age sandstones and shales, with minor amounts of carbonate rock. The engineering properties of the exposed rock are extremely poor, especially with regard to slope stability. Compaction type shale units contain a large percentage of carbonaceous matter, and these shales tend to weather rapidly to the original clay size particles. At the landslide sites, the sliding mass is usually composed of silty clay or clay soils which are intermixed with other rock fragments[1].

The number of major landslides occurring in the Springfield and Salem Plateaus is considerably less than the Boston Mountains. Two factors could account for fewer landslides; 1) these plateaus are characterized by a somewhat more subdued topography and relative relief, and 2) in a northerly traverse across the Springfield and Salem Plateaus, the percentage of carbonate rocks in the stratigraphic section increases markedly, while the shale content decreases.

IMAGERY ANALYSIS

The use of sophisticated remote sensors for terrain analyses in Arkansas was initiated in the mid-1960's. The information used was small scale, side-looking radar imagery. Figure 3 illustrates two swaths of radar imagery taken from an altitude of approximately 40,000 feet (X-band, AN/APQ-69). While the most obvious features on the radar imagery are the contrasting structure and physiography between the Ozark Highlands to the north and the Ouachita Province to the south, a pattern of north trending linears (arrows shown on Figure 3) was first recognized on the southern flank of the maturely

dissected plateau surface of the Boston Mountains[2]. These same linear trends also appeared in a much more subtle fashion on larger scale radar imagery of the same area [3]. The linears were believed to be zones of fracture concentration or faults which were generally expressed on the surface as natural drainage channels ranging in magnitude from minor tributaries to major river valleys. On the ground a plot of major joint and fracture patterns generally supported this premise[4]

The appearance and detectability of the linears on the radar imagery was related to the areal coverage, relatively coarse resolution, uniformity in gray-scale, and oblique angle of terrain illumination[3]. Because of these unique microwave characteristics, the interpreter was able to integrate subtle topographic differences over long distances, thus combining seemingly isolated features into a regional picture; a capability not previously provided by any remote sensor. During this time speculation was made as to the structural significance of recognizing such linear features in the terrain configuration; however, because of the lack of extensive small scale, areal coverage, further application studies were not pursued.

The July 1972 launch of the LANDSAT-1 satellite provided the areal coverage that had not been previously available. As LANDSAT imagery became available to geologists, the synoptic or broad overview of the terrain was immediately recognized as a geologic advantage, so that updating and modification of geologic maps was initiated. Of particular interest to geologists throughout the world were the linears or lineaments, or fracture zones which had not been previously recognized.

Satellite imagery of Arkansas proved to be of special significance to geologists. The LANDSAT-1, multispectral scanner (MSS) imagery of northwestern Arkansas (Figure 3) was recorded on December 15, 1972. On this image, the pattern of linears or lineaments which were previously recognized on the radar were detectable (Figure 4, area A), but the most obvious features were the through-going lineaments trending for tens of miles in a northeasterly direction (Figure 4; B-C, D-E, F-G, H-I). Two of these linear trends were, at least in part, coincident with previously mapped faults (Fayetteville and Drakes Creek; B-C, D-E respectively); however, two other equally spectacular trends (F-G, H-I) had not been previously recognized. The essentially parallel nature of the newly recognized trends with mapped fault zones suggests a similar origin and history of these features. The lineaments detected on the imagery are of such length and width that their origin might be attributed to either fault or shear zones widened by weathering of soluble surface rocks. Certainly where fractured or faulted limestone strata crop out in northern Arkansas, accelerated solutioning is a common phenomenon. Gold et al.,[5] have suggested that stratigraphic separation of a few feet can be sufficient to concentrate water flow along a fracture, thus promoting solutioning and weathering within a fault zone.

In addition to the very obvious lineaments shown on Figure 4, a number of more subtle (previously unmapped) lineaments were also recognized on this same LANDSAT-MSS image. One might suggest a number of reasons as to why many of these lineaments had not been recognized prior to the acquisition of the LANDSAT data. First, their lack of detection could be attributed to the sparsity of detailed geologic mapping in the area. Another reason could be that the lineaments actually represent zones of shear or strike-slip faulting rather than the normal type of faulting, and consequently the displaced strata would probably not be easily recognized during ground surveys. Finally, because the major lineaments (Figure 4) are represented geomorphically by relatively straight but discontinuous stream valleys (up to one half mile in width), recognizing the landform expression of such features in the field would be extremely difficult. Contrasting with the terrain characteristics which contribute to nondetectability of lineaments are those system-terrain parameters which allow enhancement of the same features from a satellite. For example, perhaps one of the major factors contributing to the recognition of these linears on the particular LANDSAT image of Figure 4 is that the terrain was partially snow covered at the time of imaging. Wobber and Martin[6] have shown that snow cover may actually be utilized as a photogeological tool to identify fracture

traces and faults. This indeed has proven to be the case in northern Arkansas where the combination of snow cover and the relatively low sun angle provided the enhancement of linear trends. The snow cover tends to not only reduce the background gray tones of land use patterns, but also enhances forest boundaries. In addition, the low sun angle at the time of imaging provides a highlighting and shadowing effect similar to that provided by side-looking airborne radars. Analysis of other LANDSAT imagery from the same area in northern Arkansas, taken during different seasons, confirms the fact that lineaments are much more obvious and relatively easy to detect on the snow-covered image.

APPLICATION

If the LANDSAT-defined lineaments are expressed in the rock units as fault or shear zones, or areas of fracture concentration; the obvious question to ask is do these factors influence slope stability? To answer this question, the major landslides and most conspicuous lineaments were plotted on a highway base map of northern Arkansas (Figure 5). The correlation between sites of landslides and the lineament trends (or their extension) is quite remarkable. Although not obvious on either Figure 4 or 5, a number of those landslides which are not coincident with major lineaments do indeed correlate with the more subtle trends which can be mapped by detailed imagery interpretation. Systematic analysis of the LANDSAT imagery (Figure 4) will provide the reader with evidence that numerous lineaments (most less than 10 miles in length) crisscross the entire region.

If we consider the geological environment where lineaments and landslide zones coincide, the reason for their marked correlation becomes apparent. In those regions where a residual soil mantle has developed, the linear trends probably represent fracture zones of groundwater discharge or zones of surface water absorption. In either case, a water exchange zone is developed which accelerates weathering locally, with the consequent development of a characteristic topography. It is these resultant landforms which have been enhanced on the LANDSAT-MSS imagery. The major factors contributing to poor slope stability appear to be a combination of the accelerated weathering processes of compaction shales which are in close proximity to zones of increased porosity and permeability. This observation would be consistent with the findings of Parizek and Voight[7], who have shown that fracture traces could be used in geotechnical investigations to predict zones of increased weathering in advance of foundation exploration; areas of potential roof collapse and excess water in mining and tunneling operations; and leakage beneath dams into excavations within bedrock.

While the majority of major landslides in northern Arkansas are coincident with LANDSAT-mapped lineaments, there are also slides that have no association with these linear trends. Obviously, wherever there are slopes there will also be processes of mass movement. With the right geologic conditions, especially in mountainous terrain, we can expect landslides. Because there is no way our highway systems can avoid mountains, we have to accept the fact given the right conditions, landslides will occur; however, with proper planning the worst slide-prone areas can be avoided.

CONCLUSIONS

Prevention of landslides is directly related to recognition of slide-prone areas, and ability to recognize such areas is essential to the engineering geologist or location engineer. Because the usual slide preventative measures will frequently cost much less than the corrective action after failure, we would recommend using the new tool of LANDSAT imagery to help plan new highway routes in order to avoid or anticipate the worst slide-prone areas. Certainly satellite imagery used in concert with a back-

log of geologic and engineering data now appears to offer the highway engineer with a predictive technique that could ultimately reduce the number and seriousness of highway landslides.

REFERENCES

1. Bissett, J.R. (Principal Investigator), and others, 1964, Landslide Studies Highway Research Project 14, Final Report: Civil Engineering Department, University of Arkansas in Cooperation with Arkansas Highway Department and Department of Commerce Bureau of Public Roads, May 1964, 30 p.

2. Dellwig, L.F., H.C. MacDonald, and J.N. Kirk, 1968, The Potential of Radar in Geological Exploration: Proc. 5th Symp. Remote Sensing of Environment, University of Michigan, Ann Arbor, p. 747-764.

3. MacDonald, H.C., J.N. Kirk, L.F. Dellwig, and A.J. Lewis, 1969, The Influence of Radar Look-Direction on the Detection of Selected Geological Features: Proc 6th Symp. Remote Sensing of Environment, University of Michigan, Ann Arbor, p. 637-650.

4. Kirk, J.N. 1971, A Regional Study of Radar Lineament Patterns in the Ouachita Mountains, McAlister Basin-Arkansas Valley, and Ozark Regions of Oklahoma and Arkansas, CRES Tech Rept. 177-4, University of Kansas, Lawrence, Kansas, 61 .

5. Gold, D.P., R.R. Parizek, and S.A. Alexander, 1973, Analysis and Applications of ERTS-1 Data for Regional Geological Mapping: Symposium on Significant Results Obtained from the Earth Resources Technology Satellite-1, vol. 1, sec. A, p. 231-246.

6. Wobber, F.J., and Martin, K.R., 1973, Exploitation of ERTS-1 Imagery Utilizing Snow Enhancement Techniques: Symposium on Significant Results Obtained from the Earth Resources Technology Satellite-1, vol. 1, sec. A, p. 345-351.

7. Parizek, R.R., and B. Voight, 1970, Question 37: On Remote Sensing Investigations for Dam and Reservoir Construction in Karst Terranes: Commission Internationale des Grands Barrages, Montreal, G.R.Q. 37, Trans, 10th Internat'l Congress on Large Dams, vol. VI, p. 538-546.

8. Croneis, C., 1930, Geology of The Arkansas Paleozoic Area: Arkansas Geol. Survey Bull. 3, 457 p.

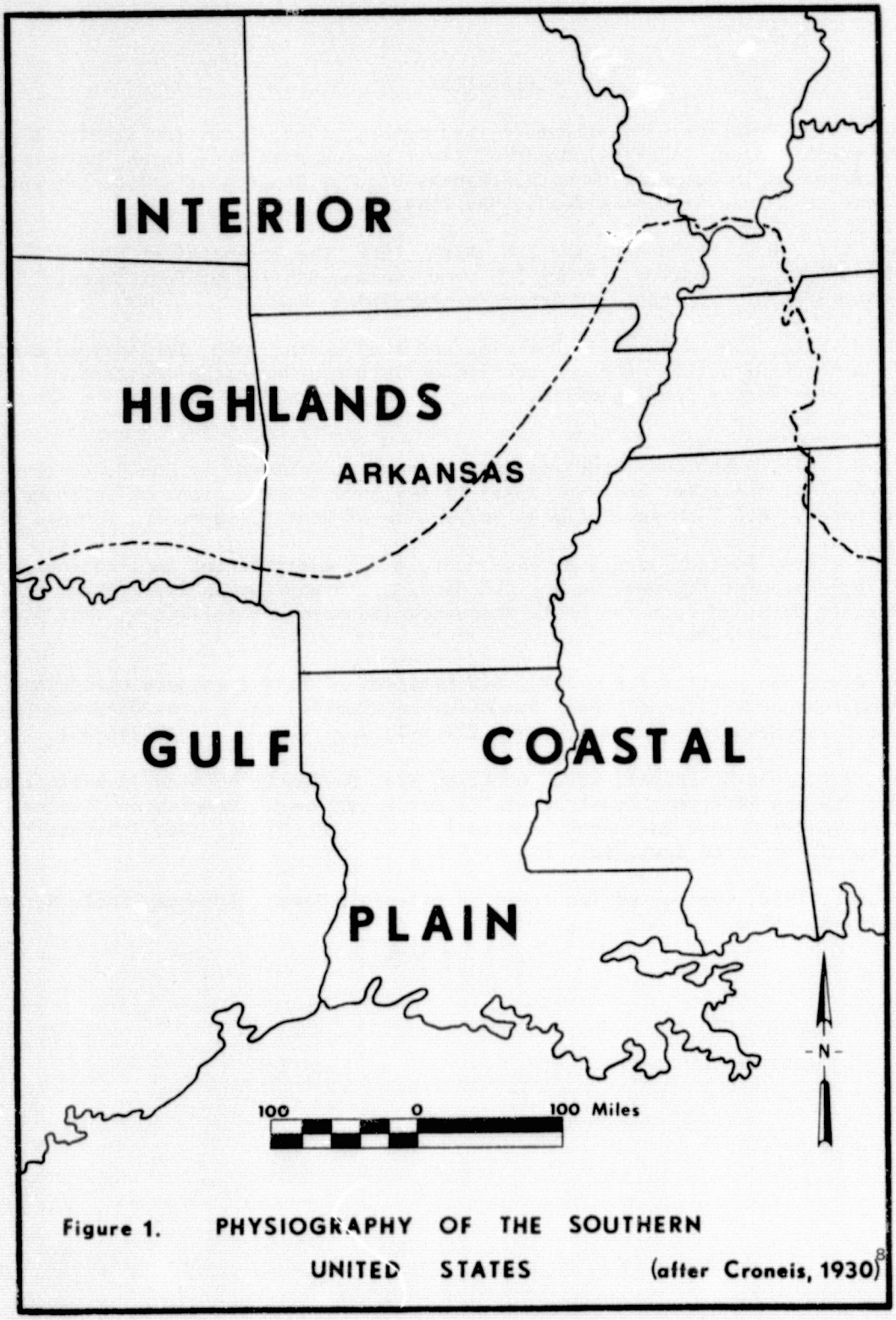


Figure 1. PHYSIOGRAPHY OF THE SOUTHERN UNITED STATES (after Croneis, 1930)[8]

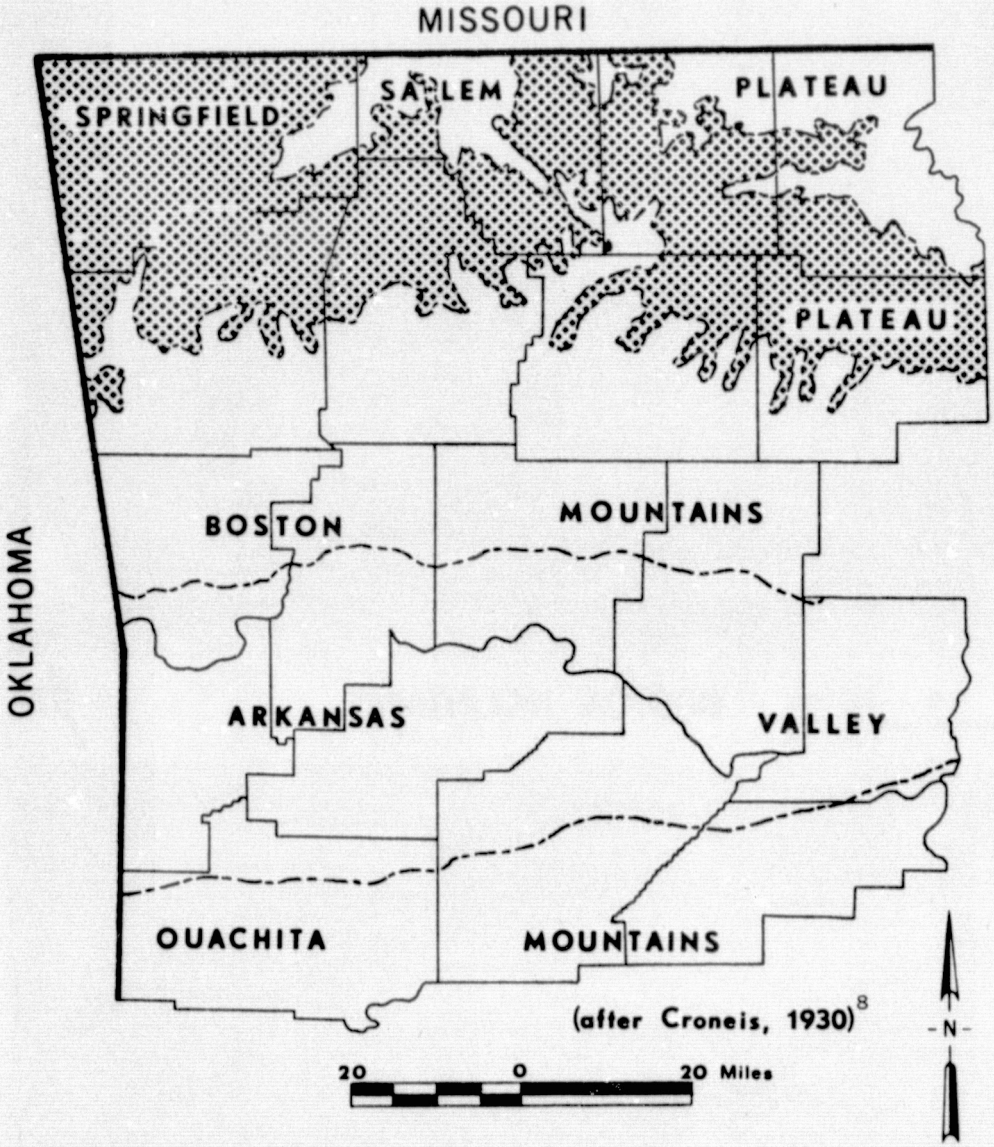


Figure 2. PHYSIOGRAPHIC PROVINCES OF NORTHWEST ARKANSAS

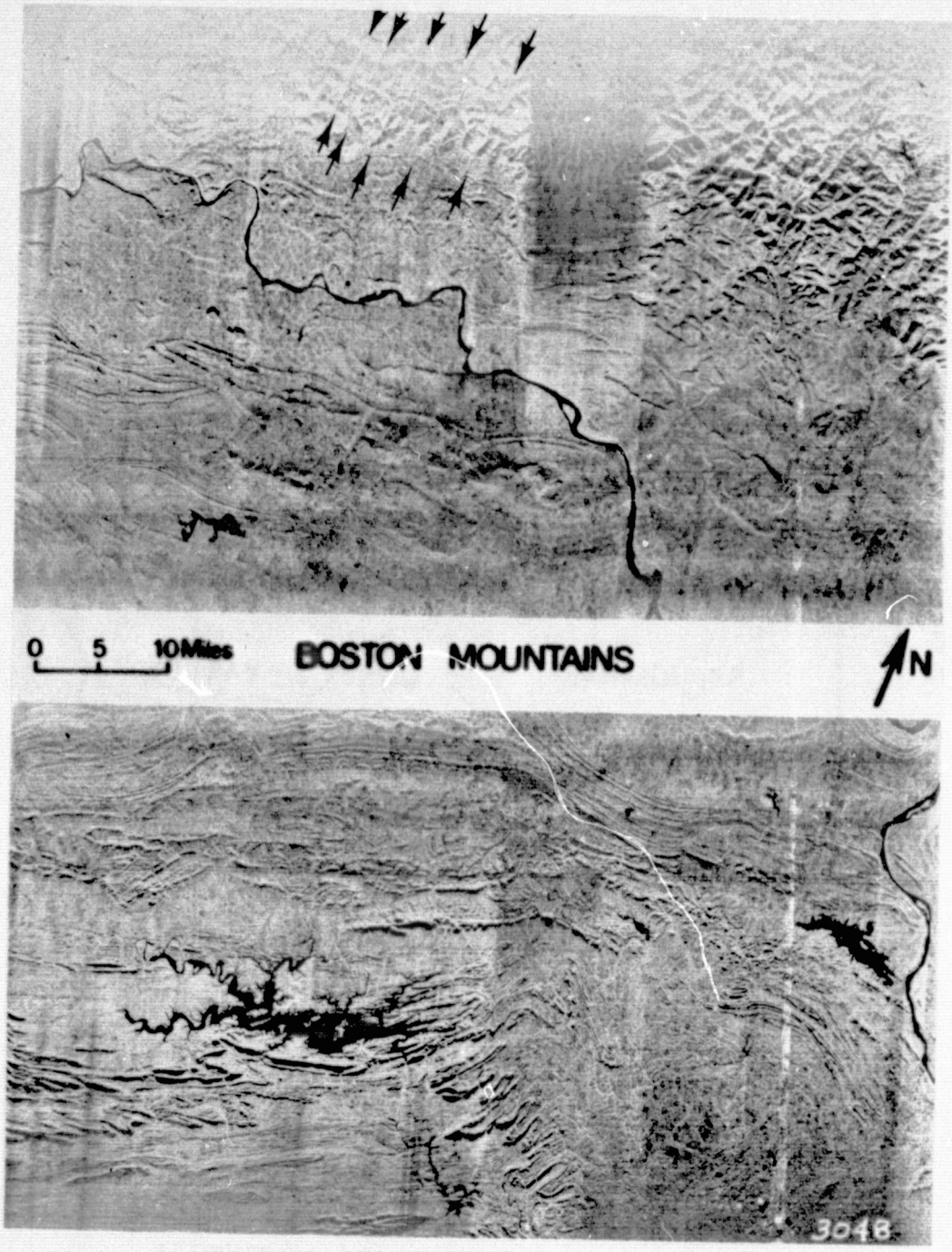


Figure 3. Side-looking airborne radar (SLAR) of the southern Ozark Highlands (Boston Mountains to the north), and Ouachita Province.

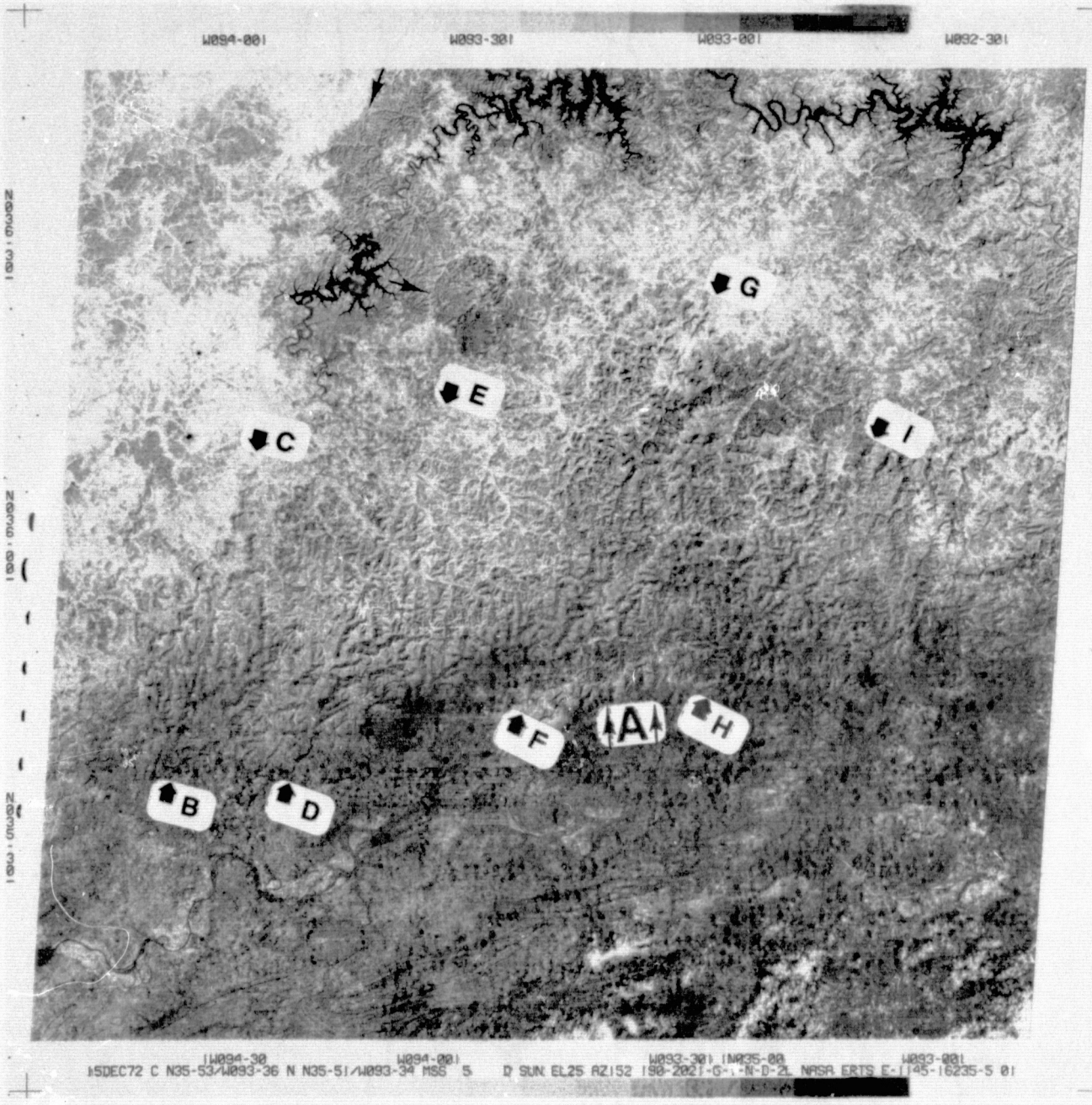


Figure 4. LANDSAT-MSS image (band 5) of northwestern Arkansas showing regional lineament trends.

REPRODUCIBILITY OF THE
ORIGINAL PAGE IS POOR

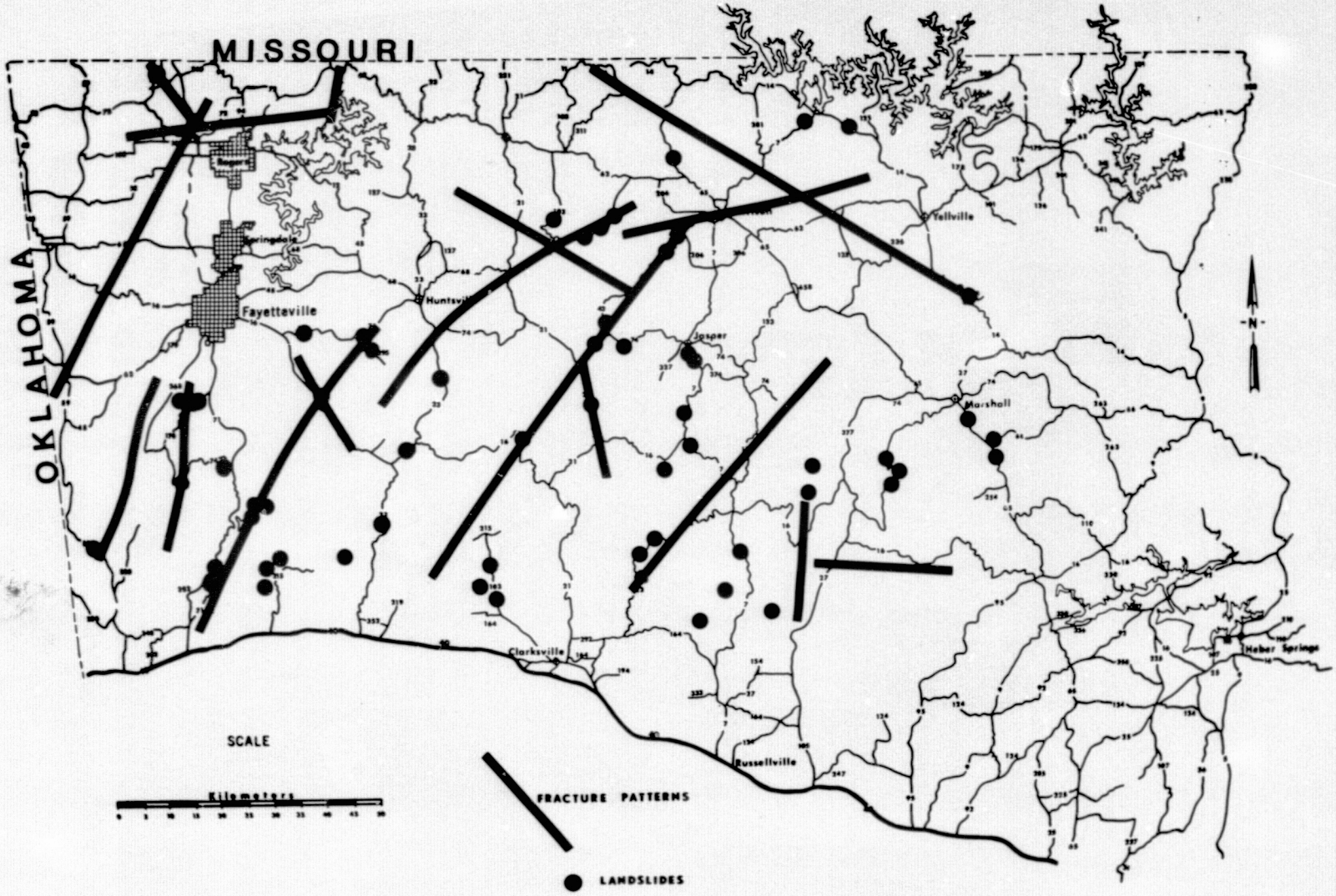


Figure 5. Plot of major lineaments or fracture trends from LANDSAT imagery. Location of major landslides for northwestern Arkansas also shown.

ACTIVE AND INACTIVE FAULTS IN SOUTHERN CALIFORNIA VIEWED FROM SKYLAB G-13

By P. M. Merifield and D. L. Lamar, California Earth Science Corporation, 1318 Second Street, Suite 27, Santa Monica, California 90401

N76-17511

ABSTRACT

Repeated movement along active high-angle faults results in distinctive topographic features such as scarps, offset drainage, and depressions, and also impoundage of ground water. Many of these features are identifiable in Skylab photography of arid regions of southern California. The 190B camera is superior to the 190A camera for distinguishing active from inactive faults because the majority of the topographic features have a scale of meters to tens of meters requiring high resolution. A northwestern extension of a fault in the San Andreas set, indicated by recent geophysical surveys in northwest Sonora, is postulated by the regional alignment of possible fault-controlled features. The suspected fault is covered by Holocene deposits, principally windblown sand, and therefore subsurface exploration would be necessary to verify its existence. A northwest trending tonal change in cultivated fields across Mexicali Valley is visible on Skylab photos. No surface evidence for faulting was observed; however, the linear may be caused by differences in soil conditions along an extension of a segment of the San Jacinto fault zone.

A number of prominent linears in basement terrane of the Peninsular Ranges appear on Skylab images. In most cases they are represented by straight or gently curved valleys; however, detailed field investigations have shown that several of these linears mark previously unmapped faults which form two distinct fault sets: one set trends northeast, the other west-northwest. No indications of recent movement are present on these faults which are truncated by seismically active, northwest trending fault zones such as the Elsinore and San Jacinto. Right-lateral separation is demonstrable on the northeast trending set. Left-lateral separation is possible but not definitely established on the west-northwest trending set. The two sets may represent conjugate shears that formed in response to an earlier stress system involving west-southwest, east-northeast crustal shortening. Field investigations have proven that a number of other linears are not due to faulting. They resulted from erosion along foliation or close-spaced joint sets, or are produced by the coincidental alignment of linear segments of diverse origin. The combination of the synoptic view and the high resolution of Skylab images has proved valuable in regional fault studies. Information on faults resulting from our investigation is applicable to land-use planning and the siting of engineered structures in southern California.

INTRODUCTION

Knowledge of the location and earthquake potential of faults is an essential input to land-use planning and the siting of critical engineered structures, such as nuclear power plants, dams, hospitals and schools. Earthquake damage to structures is related to earthquake magnitude, distance to the hypocenter, and local geologic conditions. A rough correlation between earthquake magnitude and fault length can be used to estimate the maximum credible earthquake, and the possibility of future movement can be predicted to some degree from the past history of movements. The human historic record is too short for estimating earthquake recurrence intervals for large earthquakes on active faults in California; therefore, the recent geologic history of movement should also be used. Inactive faults, as well as active faults, are unsuitable sites for dams and reservoirs and constitute a hazard to tunneling operations. Fault gouge and breccia are poor foundation materials, and fault zones commonly provide the passageway for large volumes of subsurface water.

In an accelerating effort to introduce geologic information into the land-use planning process, Federal and state geologic agencies, in cooperation with universities and engineering-geologic consulting firms, are preparing fault maps of California. Faults are being classified on the basis of their geologic history of movement (e.g. Jennings, 1973; Ziony et al, 1974). This paper describes the application of Skylab imagery, in conjunction with larger scale photography and field investigations, to the preparation of these maps. Specifically, the images are being utilized to assist in 1) distinguishing active from inactive faults (by recognizing indications of recent displacement), 2) determining the length of potentially active faults, 3) identifying previously unmapped faults (inactive as well as active), and 4) gaining additional information on regional tectonic history.

DETERMINATION OF FAULT ACTIVITY

It is generally assumed that future movement will occur on faults that have been active in the recent past. Movement in Holocene time (past 11,000 years) is a commonly accepted criterion for classifying a fault as active although faults showing displacement since late Quaternary time should probably also be considered active for some purposes (Wentworth and Yerkes, 1971). In addition to the historic record and stratigraphic relationships, certain topographic features are useful indicators of recent movement. These include scarps, benches, linear ridges, shutter ridges, linear valleys (in recent sediments), undrained depressions, ponded alluvium and offset drainage (Vedder and Wallace, 1970). Although their preservation will vary depending on climatic conditions and rock type, at most locations these features probably would be obliterated by erosion or deposition in 11,000 years. They need to be evaluated with care in order to differentiate them from fault-line scarps, linear valleys, notches and apparent offset streams (trellis drainage), all of which could have been formed along ancient faults by differential erosion.

Blockage of ground water in alluvial deposits by fault displacement can cause spring alignments, oases and linear differences in vegetation or land use along or on opposite sides of a fault. Such features are useful in tracing faults through alluvium where other surface indications are absent. Alluvial deposits are commonly not well dated, but the uppermost layers of alluvium are usually considered to have been deposited in Holocene time; thus, surface evidence of ground water blockage is evidence that the fault is active.

The ability of the Skylab 190B camera to resolve these indicators is examined along the section of the Garlock fault shown on the index map (Fig. 1). Although movement on the Garlock fault has not occurred in historic time, it should be considered active because of physiographic evidence of recent displacement. The following features previously described by Clark (1973) are visible on the enlarged Skylab image (Fig. 2): depressions, linear valleys, linear ridges, shutter ridges and faceted ridges. Other features with relief on the order of one meter are not visible. Comparison with Clark's map indicates that scarps and ridges down to perhaps 5 meters or less in height can be seen when aided by shadow. Topographic indicators of recent faulting possess a wide range in scale; depressions may be measured in kilometers and scarps in centimeters. But a large proportion of them fall into the range of meters to tens of meters and are, therefore, resolved by the 190B camera with an estimated spatial resolution of about 10 meters (ca. 30 feet). The 190A camera with a resolution of around 30 meters (ca. 100 feet) resolves a large percentage of these features, but is less suitable for this purpose.

Fig. 3 covers a segment of the Mesquite Lake fault, which is part of a northwest trending zone extending from the southern edge of the Mojave Desert almost to the Garlock fault (Hope, 1966). Bassett and Kupfer (1964) inferred right-slip on this fault from the orientation of drag folds in Pleistocene (?) sediments. Vegetation grows only on the

southwest side of the fault where ground water has been impounded; a change in vegetation along the fault trace is clearly visible north of the town of Twentynine Palms (Fig. 4).

Segments of the Pinto Mountain fault are visible in the same image (Fig. 3). The east trending Pinto Mountain fault stretches over 50 kilometers (30 miles) from the San Andreas fault to Twentynine Palms, where it meets the Mesquite Lake fault in a structurally complex area (Hope, 1966). Recent activity is indicated by scarps across alluvial fans and a stand of palms growing along the fault at the Oasis of Mara; the seeps are produced by ground water blockage (Bassett and Kupfer, 1964).

The foregoing examples are high-angle faults with straight or gently curved traces. Repeated movements have produced large, distinctive topographic features. Thrust or reverse faults have more irregular traces, and mass movements on the upthrown block commonly obscure their traces. Such faults are not easily recognized on Skylab photos or even in conventional aerial photography.

SALTON TROUGH AREA

Photos of the Salton Trough between the Gulf of California and the Salton Sea taken from Skylab provide a remarkable overview which aids in the interpretation of the regional relationship between structural features. The structure of the Salton Trough is of considerable interest because of its geothermal resources, a proposed nuclear desalination plant near Yuma, Arizona, and a controversy concerning the southeastern extension of the San Andreas fault beyond the southeast end of the Salton Sea. Linears and other features which appear on the Skylab images southeast of the San Andreas fault, and strands of the San Jacinto fault, have been investigated. The areas covered by the individual Skylab images studied are outlined on Fig. 5, and the images are reproduced as Figs. 6 and 7.

San Andreas Fault

The San Andreas fault, the major tectonic feature of California, extends for nearly 1000 kilometers (600 miles) southeasterly from the Pacific Ocean near Point Arena to at least a point approximately midway along the eastern shore of the Salton Sea (Fig. 1). Southeast of the Salton Sea, surface evidence of faulting in late Quaternary sediments and seismic activity are lacking, and on the basis of subsurface investigations, Biehler et al (1964) conclude that a southeastern extension of the San Andreas fault can not be justified. Allen et al (1972) have suggested that the San Andreas fault is a right-lateral transform fault and that activity at the southeast end may terminate at a spreading center. The spreading center could lie between the San Andreas and San Jacinto faults beneath Quaternary volcanic rocks and geothermal anomalies on the southeast shore of the Salton Sea (Elders et al, 1972). According to this hypothesis, extensions of the fault to the southeast would have little or no horizontal displacement but would bring crust of different age and character into juxtaposition. Thus, abrupt differences in depth to basement could occur across southeastern extensions of the San Andreas fault zone. The eastern edge of the Salton Trough sedimentary basin is possibly delineated by such faults.

East of the Salton Trough, deposits similar or correlative to the Imperial Formation (Pliocene) are exposed at an altitude of about 320 meters (1050 feet). Near the center of Imperial Valley, these deposits were not penetrated in a well bottoming at a depth of 4098 meters (13,443 feet) (Dutcher et al, 1972). The required vertical offset could be explained by a fault interpreted from geophysical surveys near the eastern margin of the Sand Hills (Kovach et al, 1962). The Sand Hills fault has been aligned with the Algadones fault southeast of Yuma, Arizona (Mattick et al, 1973). However, the Algadones fault cannot delineate the eastern margin of the Salton Trough in Sonora, Mexico, because a southeastern extension would lie east of exposures of basement rocks of possible Precambrian age in Sierra del Rosario (R. Merriam, personal communication).

Gravity and aeromagnetic data suggest 3 kilometers (2 miles) vertical separation at the top of basement rocks along a fault between sediments of the Salton Trough and basement rock exposed to the northeast in Sierra del Rosario (Sumner, 1972). Between the Salton Sea and Gulf of California, shifting sands and river flood plain deposits obscure any direct surface indications of faulting along the northeast edge of the Salton Trough. However, physiographic features appearing on Skylab imagery may be indicative of faulting along this trend. A prominent dark spot appears on the Skylab image (Fig. 6) on the approximate surface trace of the fault identified by Sumner. The dark spot is a lake (R. Merriam, personal communication) which, in this arid region, could be due to impoundage of ground water on the northeast side of a fault.

To the northwest, a remarkably straight tonal difference is located near the edge of the Sand Hills. The slightly darker tone on the northeast side is the result of denser vegetation which may be due to impoundage of ground water on the upthrown side of a fault. We are unaware of any water well data which could test this hypothesis. A fault is suspected on the basis of a well drilled on the southwest margin of the dune field (S. L. Werner, personal communication). The well was drilled on a geothermal anomaly by the California Department of Water Resources, and silicified recent basin deposits were encountered (Werner and Olson, 1970). The relatively straight dune edge may be primarily wind controlled (Norris and Norris, 1961). However, the linear change in vegetation may contribute to the straightness, as the western edge of the dune field is much straighter than the eastern edge.

Approximately half way along the western edge of the Sand Hills, the dune field overlaps the line of vegetation. To the northwest, the suspected fault is aligned with the Hot Springs fault; however, it could join the Sand Hills fault as shown by Jennings (1973). Between the north end of the vegetation break and the Hot Springs fault, surficial evidence of faulting would be obscured by cultivated fields and leakage along the Coachella Branch of the All American Canal. The overview provided by the Skylab images therefore aided in the interpretation of a possible fault in the San Andreas set by showing the regional alignment of fault indicators at an appropriate scale.

San Jacinto Fault Zone

The San Jacinto fault zone extends from near the San Andreas fault in the San Gabriel Mountains and continues southeast approximately 500 kilometers (300 miles) to the Gulf of California as a zone of sub-parallel and branching faults up to 20 kilometers (12 miles) wide (Fig. 1). Two prominent linears appear on the Skylab images of the Colorado Delta area (Fig. 6). The western linear in recent deltaic deposits corresponds to the segment of the San Jacinto fault believed to have been active in 1934 (Allen et al, 1965). The eastern linear appears as a straight, sharp boundary between deltaic deposits on the west and dune sand on the east. Merriam (1965) indicates that the southeast end of this linear is a fault and describes extensions of the San Jacinto fault zone to the southeast in Sonora.

To the northwest in Mexicali Valley, the fault traces are obscured by cultivated fields. However, an inferred northwest extension of the western linear passes through the Cerro Prieto geothermal field (De Anda and Parides, 1964); it is reasonable to assume that the geothermal activity is related to the fault zone. Northwest of the geothermal area, faint differences in the tone of cultivated fields south of Mexicali can be seen across a line along the same trend (Figs. 5 and 7). No additional evidence concerning the origin of this linear was found during a field reconnaissance, but variations in the tone of the cultivated fields could be related to subtle differences in the soil. The lake sediments beneath Mexicali Valley are primarily interbedded silt and clay. Because of better drainage, silt is preferable for crops. Silt and clay juxtaposed along a fault could be reflected in different crops or land use.

The tonal difference cannot be traced northwest of a point 6 kilometers (4 miles) south of the international border, but a continuation of the same trend lines up with a fairly straight segment of the New River. Exposures along the New River north of the border were examined, but no evidence of faulting was observed. If a fault along this trend curves slightly and is situated west of the New River, it would be aligned with a queried fault in the San Jacinto fault zone shown by Jennings (1973).

PREVIOUSLY UNMAPPED FAULTS IN BASEMENT TERRANE OF THE PENINSULAR RANGES

The crystalline basement terrane of the Peninsular Ranges in southwestern California is composed of late Mesozoic plutonic rocks and associated roof pendants of metamorphosed Paleozoic and Mesozoic rocks (Jahns, 1954). Northwest trending faults of the San Andreas set (Hill, 1965), notably the San Jacinto and Elsinore fault zones, dominate the structure of the Peninsular Ranges. Recently acquired small-scale images from Skylab and LANDSAT spacecraft, as well as larger scale color aerial photos from RB-57 and U-2 aircraft, have provided a new look at this region. Lowman (1969) originally pointed out that unmapped northeast trending linears, expressed primarily by persistent valleys, are prominent on Gemini and Apollo photographs of the Peninsular Ranges of southwestern California. These features and the San Jacinto, Elsinore and other northwest trending faults are apparent in the Skylab image reproduced in Fig. 8. A number of west-northwest linears and one north-south linear are also visible. As shown on Fig. 9, some of these linears have been previously mapped as faults, but many others have not.

The mapping and compilations of Merriam (1955, 1958), Larsen (1948), Everhart (1951), Rogers (1965), Strand (1962), Gastil et al (1971), Weber (1963), and Jennings (1973) have been invaluable in our studies. However, most of the previous mapping has been at reconnaissance scales (1:62,500 or smaller) and earlier studies were without the benefit of aerial photography. Consequently, it is not surprising that some of the faults recognized in our investigation are not shown on existing geologic maps.

Using the perspective provided by small-scale imagery from the Skylab and LANDSAT spacecraft, attention was focused on persistent linears which were heretofore unmapped because they were not obvious in larger scale photography or on the ground. Aided by large-scale aerial photos, field investigations were accomplished to determine the nature of the linears not explained by previous geologic mapping (see Merifield and Lamar, 1974). Several of the features have been identified as faults by displaced contacts and well-developed breccia zones and slickensided shear surfaces parallel to the linear. Field work is hampered by the dense growth of chaparral which denies access to large areas. Moreover, displacements within the basement terrane are difficult to establish owing to gradational contacts and zones of mixed rocks.

The northeast trending San Ysidro Creek fault was first recognized as a prominent 7 kilometer (4 mile) long linear on satellite images by Lowman (1969). Discovery of exposures of gouge up to 7 meters (20 feet) wide with striated shear surfaces parallel to the linear demonstrates the existence of the fault. Data are insufficient to determine the slip direction on the San Ysidro Creek fault, but striations on shear surfaces suggest predominantly horizontal (strike-slip) movement. The ends of the San Ysidro Creek fault appear to terminate against northwest trending faults.

The northeast trending San Diego River Valley southwest of the Elsinore fault forms a 30 kilometer (20 mile) long linear separated 10 kilometers (6 miles) from the southwest end of the San Ysidro Creek fault. Although the San Diego River linear and San Ysidro Creek fault are approximately aligned, Skylab imagery, as well as larger scale air photographs, clearly show that these features do not connect. The northeast end of the San Diego River linear appears to abut the Elsinore fault.

Some previous maps (Sauer, 1929; Miller, 1935; California Department of Water Resources, 1967; Jennings 1973) show a fault or inferred fault along The San Diego River, while others (Everhart, 1951; Merriam, 1958; Strand, 1962; Rogers, 1965; Fitzurka, 1968) do not. None of the previous maps or reports which indicate a fault describe any field observations of fault zone exposures or offset rock contacts.

In a detailed study along a segment of the river, Fitzurka (1968) found a right-separation of contacts between Julian Schist and plutonic rocks of 300 to 600 meters (1000 to 2000 feet). A fault along the river in the area mapped by Fitzurka would be obscured by alluvium, and he reported no direct evidence of faulting. Our field work substantiated the apparent separation observed by Fitzurka and also revealed a probable 420 meter (1400 foot) right-separation of a schist body within quartz diorite along the same trend to the northeast. An en echelon pattern of zones of sheared and altered breccias and alignments of straight canyon segments, saddles and benches was also discovered along the river valley. The orientation of the en echelon pattern is consistent with right-slip along a shear zone.

One of the most prominent linears seen on satellite imagery stretches for 20 kilometers (12 miles) in a north-northeast direction through Thing Valley in southeastern San Diego County. Breccia, fault gouge and slickensided shear surfaces were discovered along the linear. One hundred meters (330 feet) of right separation was measured on the fault at the southwest end of Thing Valley, and field work and study of large-scale air photos suggest as much as 1 kilometer (0.6 mile) of right-separation of mixed metamorphic and igneous rocks at the northeast end of Thing Valley. The latter separation, however, may be explained at least in part by contacts curving nearly parallel into the fault.

Although the exact relationships are obscured by alluvium, the north end of the Thing Valley fault south of Agua Caliente Hot Springs appears to be displaced 700-1300 meters (2300-4300 feet) in a right-lateral sense by the south branch of the Elsinore fault, as mapped by Merriam (1955) and Buttram (1962). It is impossible to prove that the Thing Valley fault was ever continuous across the Elsinore fault, but previous alignment is suggested by similar attitudes of the fault segments (Merifield and Lamar, 1974). The north end of the Thing Valley fault abuts the north branch of the Elsinore fault at Agua Caliente Hot Springs; a concentration of breccia at the fault intersection may provide a conduit for the hot water.

In addition to northeast trending faults, several west-northwest to east-west faults have been identified. The most prominent of these was mapped by Weber (1963) over 40 kilometers (24 miles) in a west-northwest direction from El Cajon to Campo (shown as Barrett Lake fault on Figs. 8 and 9). Our attention was drawn to additional linears of this trend by studies of Skylab, LANDSAT and RB-57 photos. Fault breccia and slickensided shear surfaces have been found along two of these linears which have been referred to as the Potrero and Ramona faults (Merifield and Lamar, 1974). Because of the lack of distinctive contacts between rock units, the amount and sense of displacement on these faults is indeterminant. An apparent 120 meter (370 foot) left-separation of 40° northeast dipping flows in the Santiago Peak volcanics was observed at the eastern end of the east-west trending Otay Mountain linear. The exposures are not adequate to prove that the separation is due to faulting, and no other evidence of faulting was observed along this linear.

A north-south trending linear was studied and named the Chariot Canyon fault by Allison (1974a, 1974b), who reports 8 kilometers (5 miles) of right-separation based on the distribution of Julian Schist and plutonic rocks. Our examination of a number of exposures in Chariot Canyon did not reveal a single fault separating Julian Schist on the west from granitic rocks on the east, but a broad shear zone appears to occupy the width of the canyon. Steeply dipping slickensided shear surfaces were observed to strike between north-south and N30°W. The foliation in schist and gneiss is locally undulatory, but has a general strike conformable with the shear surfaces and the trend of the canyon.

Several other linears which show no evidence of faulting were investigated and are indicated on Fig. 9. In some cases, the exposures were sufficient to make us reasonably certain that the linear is due to erosion along foliation (Henderson Canyon linear) or joints (Sutherland Reservoir linear). Intrusive contacts along the Sweetwater River in Cuyamaca Rancho Park curve to the right as they cross the river valley, and no distinct break is evident. Thus, the Sweetwater River linear (Fig. 9) corresponds to the axis of a small flexure or perhaps shear (slip) fold. The Witch Creek linear is shown as a fault by Jennings (1973); our study indicates that a contact in basement rock is not displaced along this feature, and no evidence of faulting was found. The origin of other linears could not be established with certainty because of the lack of exposures and mappable contacts.

Of particular interest is the relationship of the northeast and west-northwest trending faults which we investigated, to the northwest trending faults of the San Andreas set. If the northeast trending faults form a conjugate shear system with the presently active northwest trending right-slip faults, the northeast trending faults would have to be left-slip. However, a right-slip component is probable on the Thing Valley and San Diego River faults. Also, the northeast and west-northwest trending faults are restricted to pre-Tertiary rocks and nowhere cut the northwest set.

It is possible that the northeast and west-northwest sets were formed by an older stress system, unrelated to the presently active system. East-northeast, west-southwest crustal shortening is consistent with the fault pattern and probable right-separation on the Thing Valley and San Diego River faults. No conclusive evidence of the slip direction on the west-northwest trending faults has been found, although left separation on the east trending Otay Mountain linear is possible. Data concerning slip directions on the faults studied, therefore, are not adequate to prove this hypothesis. However, on the basis of north-south trending thrust faults and mylonitic zones, Sharp (1968) has also suggested an earlier period (Middle Cretaceous to Eocene ?) of east-west crustal shortening in the eastern Peninsular Ranges. The plate tectonic model of a subduction zone parallel to the continental margin during the Mesozoic (Hamilton, 1969; Hill, 1971) is also consistent with earlier east-west crustal shortening.

CONCLUSIONS

The following conclusions are indicated from our study: (1) In areas such as the basement terrane of the Peninsular Ranges, where most of the mapping has been reconnaissance or accomplished decades ago without the aid of aerial photography, Skylab imagery provides an efficient means of focusing on potential faults and planning larger scale surveys. Several unreported faults have been found during our investigation. (2) Prominent photo linears result from erosion along foliation and jointing as well as faults. The coincidental alignment of unrelated features may also give the appearance of faults. Detailed field investigations are required to establish the origin of any linears. (3) Topographic indicators of movement on recently active, high-angle faults are resolved by the 190B camera, which is superior to the 190A camera for this purpose. The somewhat smaller coverage of the 190B camera is not a serious drawback. The critical indicators of faulting are topographic, and the multispectral capability of the 190A camera has not played a significant role in these investigations. (4) The perspective afforded by Skylab enables fault patterns to be viewed in a single image; this is useful in understanding regional relationships. The truncation of the east-west and northeast trending fault sets by the active northwest trending right-slip faults in the Peninsular Ranges is evident in Skylab photos. This broad perspective has also led to hypotheses for an extension of the San Jacinto fault across Mexicali Valley and the continuation of a fault forming the northeastern border of the Salton Trough.

REFERENCES

Allen, C. R., St. Amand, P., Richter, C. F. and Nordquist, J. M., 1965, Relationship between seismicity and geologic structure in the southern California region: Bull. Seism, Soc. Am., v. 55, p. 753-797.

Allen, C. R., Wyss, M., Brune, J. N., Grantz, A., and Wallace, R. E., 1972, Displacements on the Imperial, Superstition Hills, and San Andreas faults triggered by the Borrego Mountain earthquakes: in The Borrego Mountain earthquake of April 9, 1968; U.S. Geol. Survey Prof. Paper 787, p. 87-104.

Allison, M. L., 1974a, Geophysical studies along the southern portion of the Elsinore fault: M.S. thesis, San Diego State University, 229 p.

Allison, M. L., 1974b, Tectonic relationship of the Elsinore fault zone and the Chariot Canyon fault, San Diego County, California: Abstracts with program, Geol. Soc. Am., Cordilleran Section, p. 138.

Bassett, A. M. and Kupfer, D. H., 1964, A geologic reconnaissance in the southeastern Mojave Desert, California: Calif. Div. Mines and Geol., Special Rpt. 83, 43 p.

Biehler, S., Kovach, R. L., and Allen, C. R., 1964, Geophysical framework of northern end of Gulf of California structural province: Am. Assoc. Petroleum Geologists, Mem. 3, p. 126-143.

Buttram, G. N., 1962, The geology of the Agua Caliente Quadrangle, California: M.S. thesis, Univ. of Southern Calif.

California Department of Water Resources, 1967, Ground water occurrence and quality, San Diego Region: Calif. Dept. of Water Res. Bull. 106-2, 233 p.

Clark, M. M., 1973, Map showing recently active breaks along the Garlock and associated faults, California: U.S. Geol. Survey Misc. Inv. Map I-741.

De Anda, L. F. and Parides, E., 1964, La falla de San Jacinto y su influencia sobre la actividad geothermica en el valle de Mexicali, B.C., Mexico: Boletin de la associacion Mexicana de Geologos Petroleros, v. XVI, No. 7-8, p. 179-181.

Dutcher, L. C., Hardt, W. F. and Moyle, W. R., Jr., 1972, Preliminary appraisal of ground water in storage with references to geothermal resources in the Imperial Valley area, California: U.S. Geol. Survey Circular 649, 59 p.

Elders, W. A., Rex, R. W., Meidev, T., Robinson, P. T. and Biehler, S., 1972, Crustal spreading in southern California: Science, v. 178, p. 15-24.

Everhart, D. L., 1951, Geology of the Cuyamaca Peak Quadrangle, San Diego County, California: Calif. Div. Mines and Geol., Bull. 159, p. 51-115.

Fitzurka, M., 1968, Geology of a portion of the San Diego River Valley, California: Senior thesis, San Diego State Univ.

Gastil, R. G., Phillips, R. P., and Allison, E. C., 1971, Reconnaissance Geologic Map of the State of Baja California: Geol. Soc. Am., scale 1:250,000.

Hamilton, W., 1969, Mesozoic California and the underflow of Pacific mantle: Geol. Soc. Am., Bull., v. 80, p. 2409-2430.

Hill, M. L., 1965, The San Andreas rift system, California and Mexico; in The world rift system: Canada Geol. Survey Paper 66-14.

Hill, M. L., 1971, Newport-Inglewood zone and Mesozoic subduction, California: Geol. Soc. Am., Bull., v. 82, p. 2957-2962.

Hope, R. A., 1966, Geology and structural setting of the eastern Transverse Ranges, southern California: Univ. California, Los Angeles, Ph.D. thesis, 201 p.

Jahns, R. H., 1954, Geology of the Peninsular Ranges Province, southern California and Baja California: in Calif. Div. Mines and Geol., Bull. 170, Ch. 2, p. 29-52.

Jennings, C. W., 1973, State of California, preliminary fault and geologic map, scale 1:750,000: Calif. Div. Mines and Geol., Preliminary Report 13.

Kovach, R. L., Allen, C. R., and Press, F., 1962, Geophysical investigations in the Colorado Delta Region: J. Geophys. Res., v. 67, p. 2845-2871.

Larsen, E. S., Jr., 1948, Batholith and associated rocks of Corona, Elsinore, and San Luis Rey Quadrangles, southern California: Geol. Soc. Am. Memoir 29.

Lowman, P. D., 1969, Apollo 9 multispectral photography; Geologic analysis: NASA Goddard Space Flight Center, Greenbelt, Md., X-644-69-423.

Mattick, R. E., Olmstead, F. H., and Zohdy, A. A. R., 1973, Geophysical studies in the Yuma area, Arizona and California: U.S. Geol. Survey Prof. Paper 726-D, 36 p.

Merifield, P. M., and Lamar, D. L., 1974, Lineaments in basement terrain of the Peninsular Ranges, southern California: presented at First International Conference on New Basement Tectonics, in press in Proceedings volume.

Merriam, R., 1955, Geologic map of Cuyapaipe Quadrangle, California, scale 1:62,500: unpublished map (Cuyapaipe Quad. presently designated Mt. Laguna Quad.).

Merriam, R., 1958, Geology and mineral resources of Santa Ysabel Quadrangle, San Diego County, California: Calif. Div. Mines and Geol., Bull. 177, 42 p.

Merriam, R., 1965, San Jacinto fault in northwestern Sonora, Mexico: Geol. Soc. Am., Bull. v. 76, p. 1051-1054.

Miller, W. J., 1935, Geomorphology of the southern Peninsular Ranges of California: Geol. Soc. Am. Bull., v. 46, p. 1535-1562.

Norris, R. M. and Norris, K. S., 1961, Algadones dunes in southeastern California: Geol. Soc. Am. Bull., v. 72, p. 605-620.

Proctor, R. J., 1973, Map showing major earthquakes and recently active faults in the southern California region: in Geology, Seismicity and Environmental Impact; Assoc. Eng. Geol., Special Publ.

Rogers, T. H., 1965, Geologic map of California, Santa Ana Sheet: Calif. Div. of Mines and Geol.

Sauer, C., 1929, Land forms in the Peninsular Ranges of California as developed about Warner's Hot Springs and Mesa Grande: Univ. Calif., Pubs. in Geography, v. 3, p. 199-290.

Sharp, R. V., 1968, The San Andreas fault system and contrasting pre-San Andreas structures in the Peninsular Ranges of southern California: in Proc. Conf. on Geologic Problems of the San Andreas Fault System, Stanford Univ. Publ., Geol. Sci., v. XI, p. 292-293.

Strand, R. G., 1962, Geologic map of California, San Diego-El Centro Sheet: Calif. Div. of Mines and Geol.

Sumner, J. R., 1972, Tectonic significance of gravity and aeromagnetic investigations at the head of the Gulf of California: Geol. Soc., Am. Bull., v. 83, p. 3103-3120.

Vedder, J. G. and Wallace, R. E., 1970, Map showing recently active breaks along the San Andreas and related faults between Cholame Valley and Tejon Pass, California: U.S. Geol. Survey, Misc. Inv. Map I-574.

Weber, F. H., 1963, Geology and mineral resources of San Diego County, California: Calif. Div. Mines and Geol. County Report 3, 309 p.

Wentworth, L. M. and Yerkes, R. F., 1971, Geologic setting and activity of faults in the San Fernando area, California: in The San Fernando, California earthquake of February 9, 1971; U.S. Geol. Survey Prof. Paper 733, p. 6-16.

Werner, S. L. and Olson, L. J., 1970, Geothermal wastes and the water resources of the Salton Sea area: Calif. Dept. of Water Resources Bull. No. 143-7, 123 p.

Ziony, J. I., Wentworth, C. M., Buchanan-Banks, J. M., and Wagner, H. C., 1974, Preliminary map showing recency of fault movement in coastal southern California: U.S. Geol. Survey, Misc. Inv. Map MF-585.

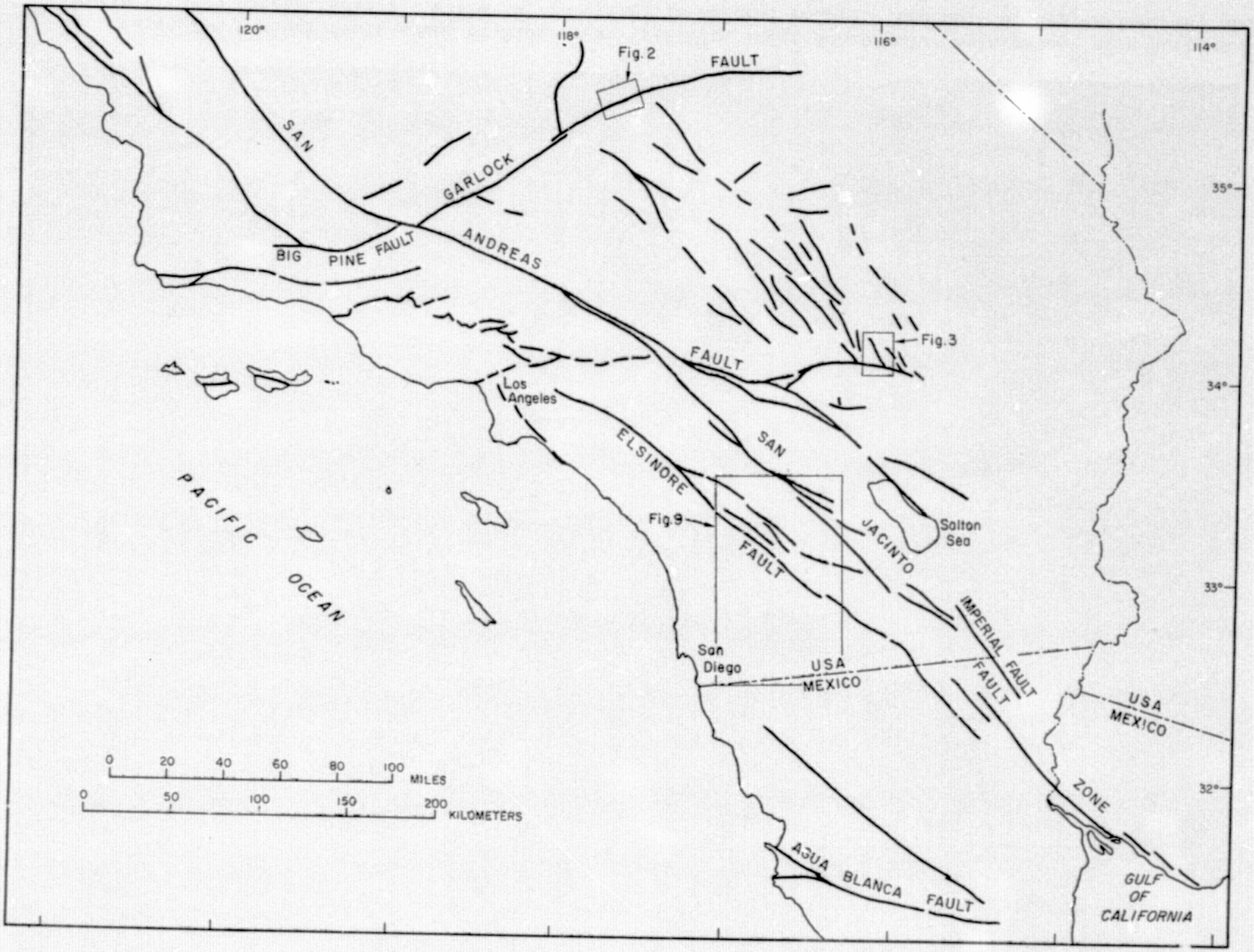


Fig. 1 - Index map showing major faults and areas studied, redrawn from Proctor (1973).

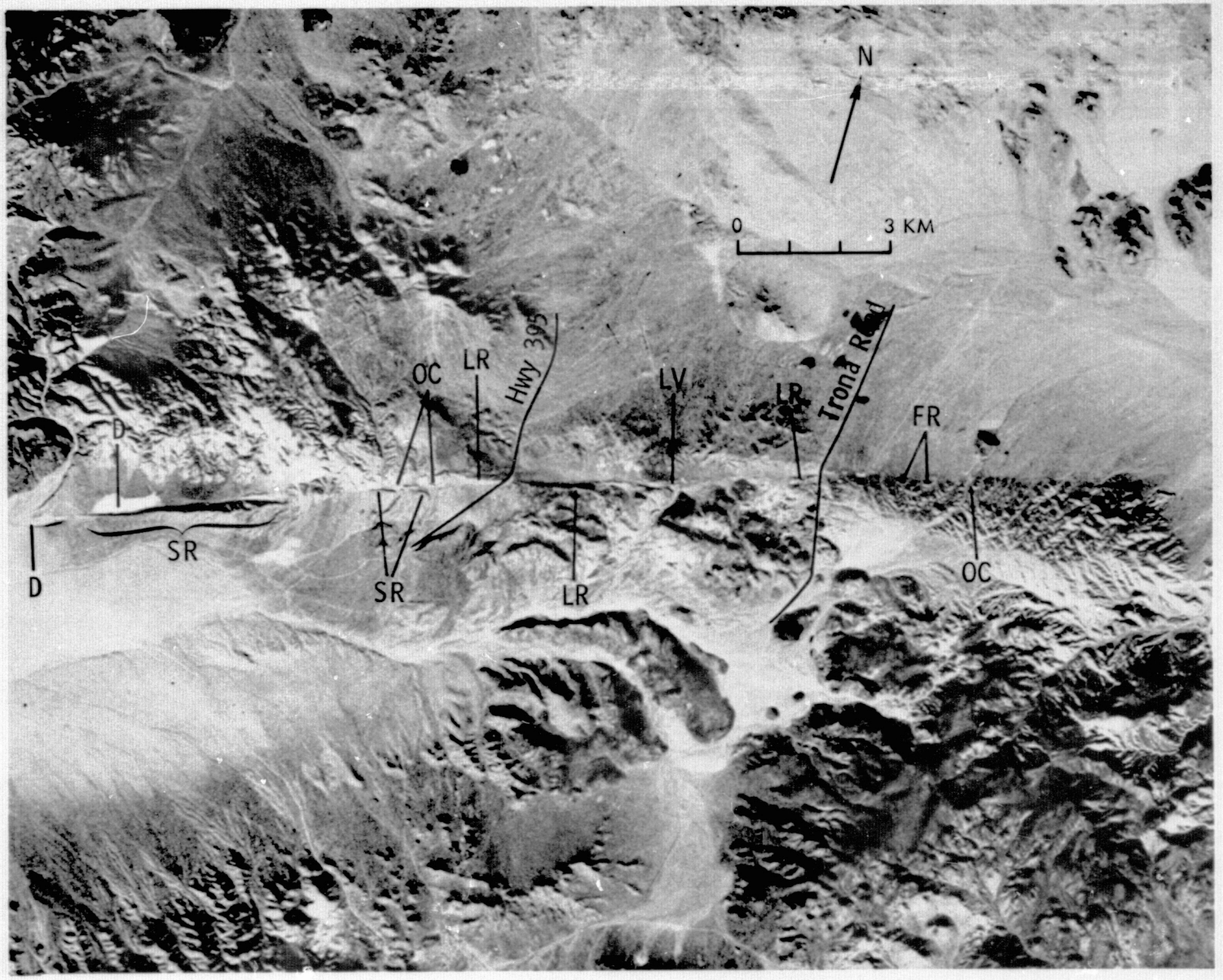


Fig. 2 - Section of the Garlock fault south of Ridgecrest (see Fig. 1 for location). Enlargement of a portion of Skylab 4, 190B camera, Roll 92, Frame 347 (original in natural color). Legend: D, depression; SR, shutter ridge; OC, offset channel; LR, linear ridge; LV, linear valley; FR, faceted ridges.

REPRODUCIBILITY OF THE ORIGINAL PAGE IS POOR

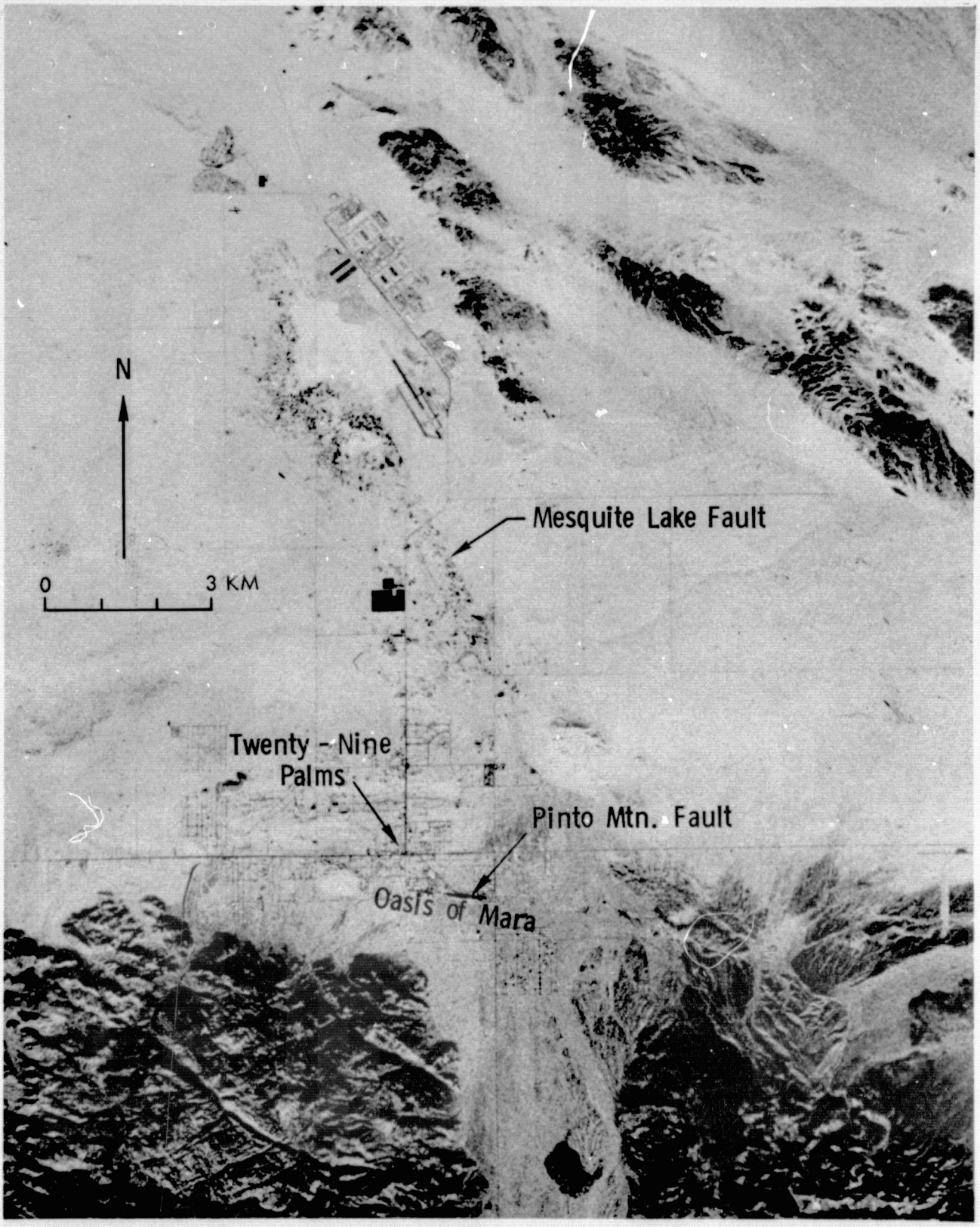


Fig. 3 - Mesquite Lake and Pinto Mountain faults near Twentynine Palms (see Fig. 1 for location). Enlargement of a portion of Skylab 4, 190B camera, Roll 92, Frame 351 (original in natural color).

REPRODUCIBILITY OF THE
ORIGINAL PAGE IS POOR

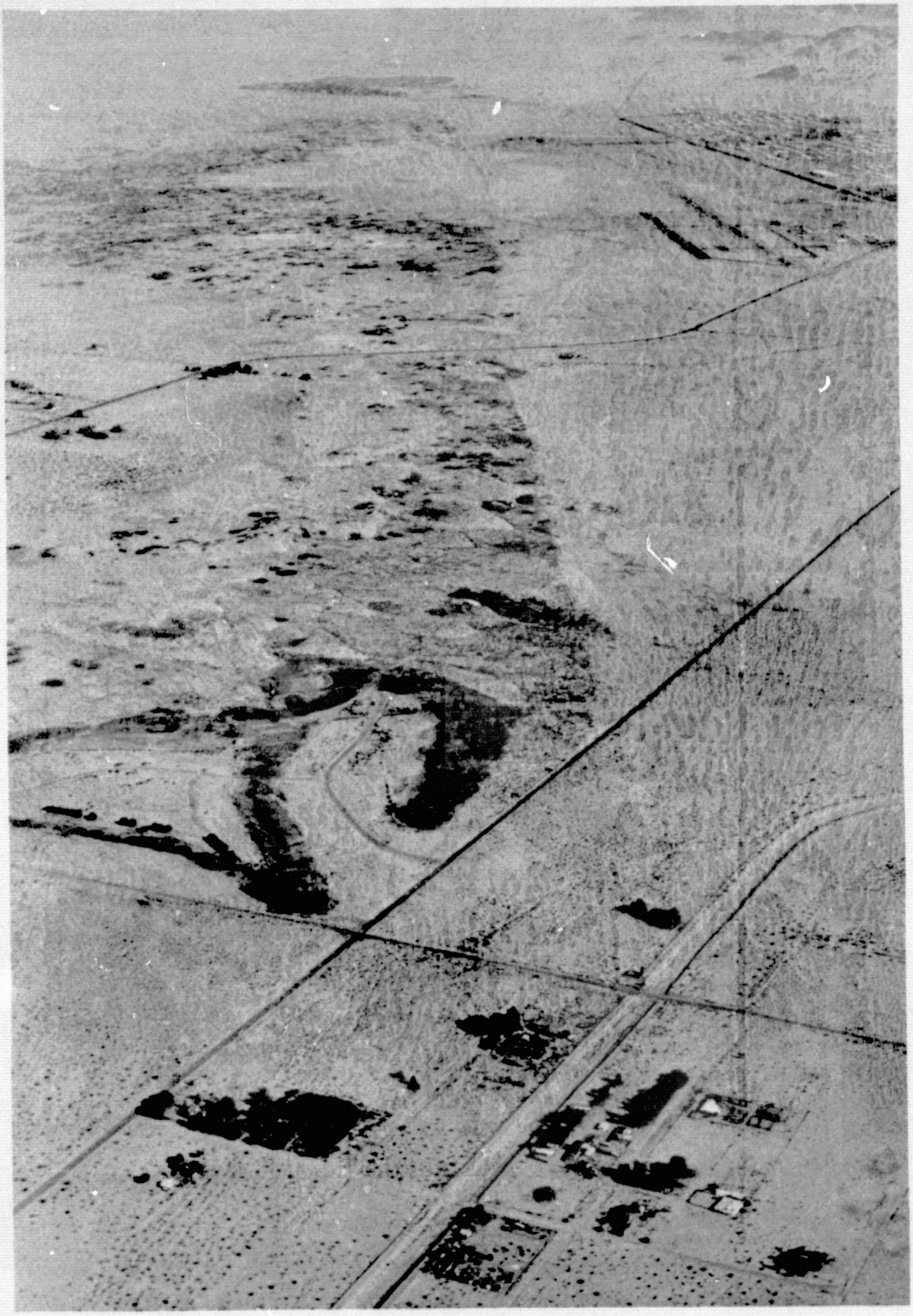


Fig. 4 - Low-altitude aerial view looking northwest along the Mesquite Lake fault.

REPRODUCIBILITY OF THE
ORIGINAL PAGE IS POOR

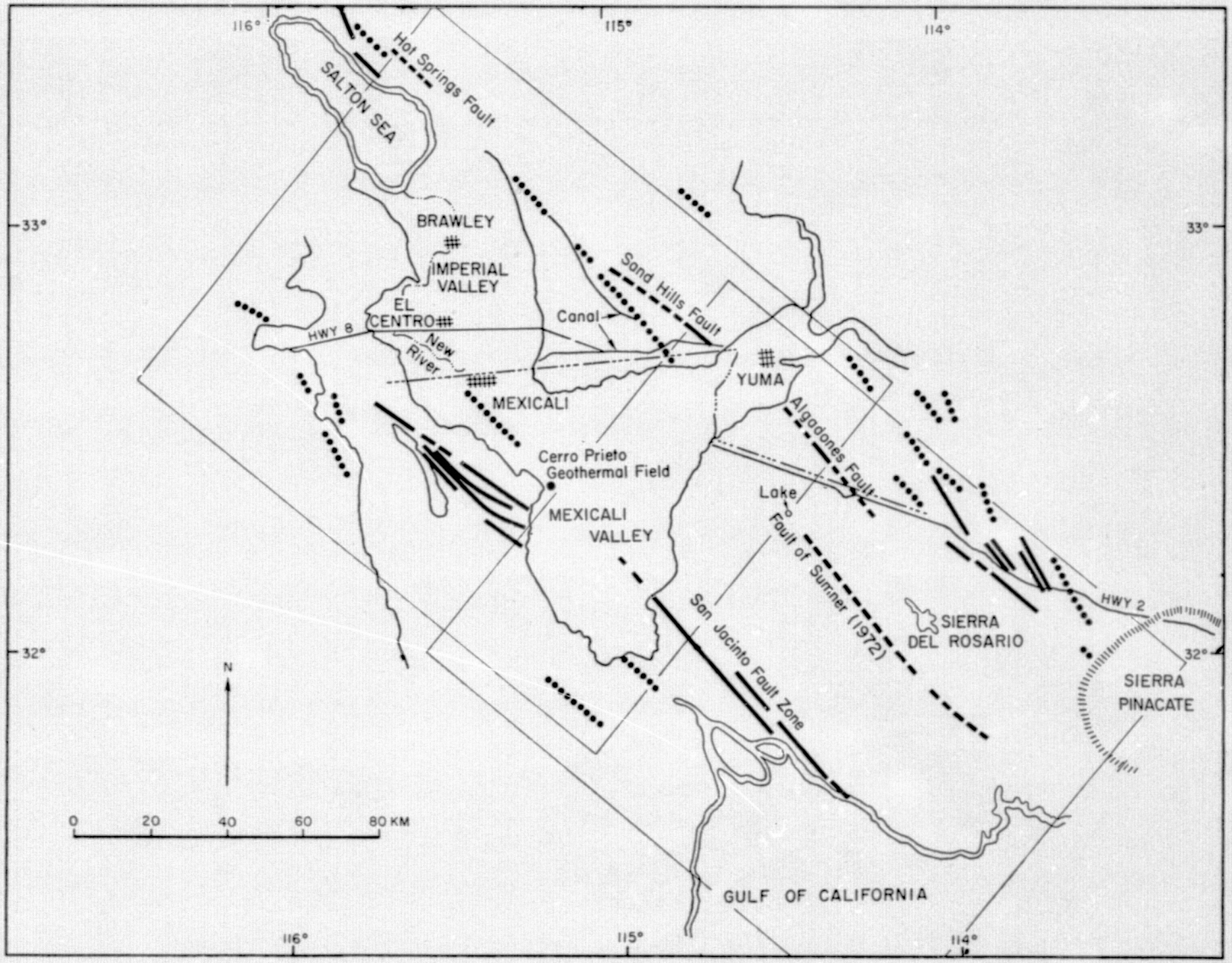


Fig. 5 - Location map, Salton Trough and vicinity. Legend: Heavy solid lines, mapped faults visible in Skylab photos; heavy short dashes, covered faults located primarily by geophysical surveys; dotted lines, photo linears of unknown origin.



Fig. 6 - Colorado River Delta, Skylab 2, 190A camera, Roll 2, Frame 135 (original in natural color).

REPRODUCIBILITY OF THE
ORIGINAL PAGE IS POOR

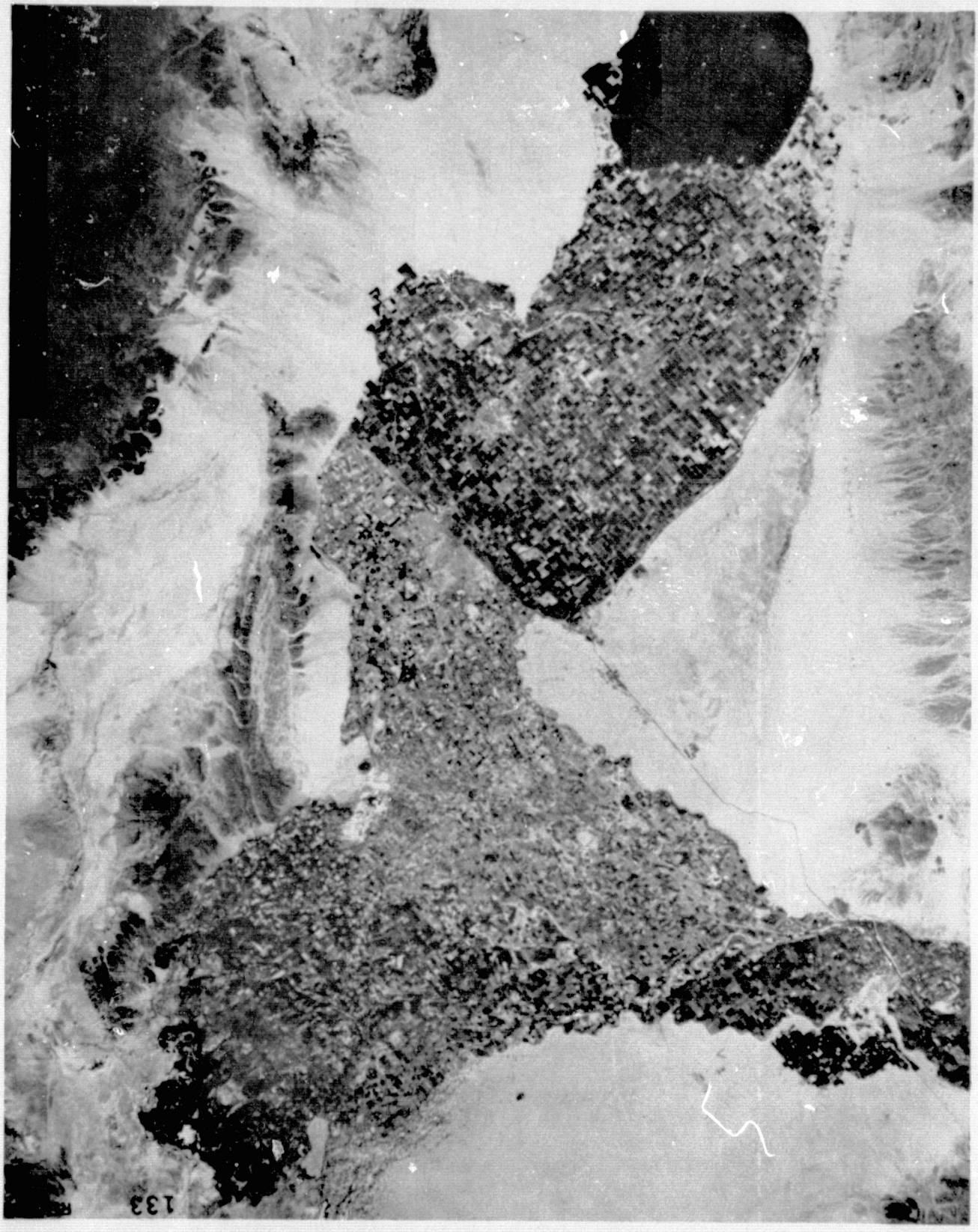


Fig. 7 - Eastern edge of Salton Trough, California and Sonora, Mexico, Skylab 2, 190A camera, Roll 4, Frame 133 (original in natural color).

REPRODUCIBILITY OF THE
ORIGINAL PAGE IS POOR

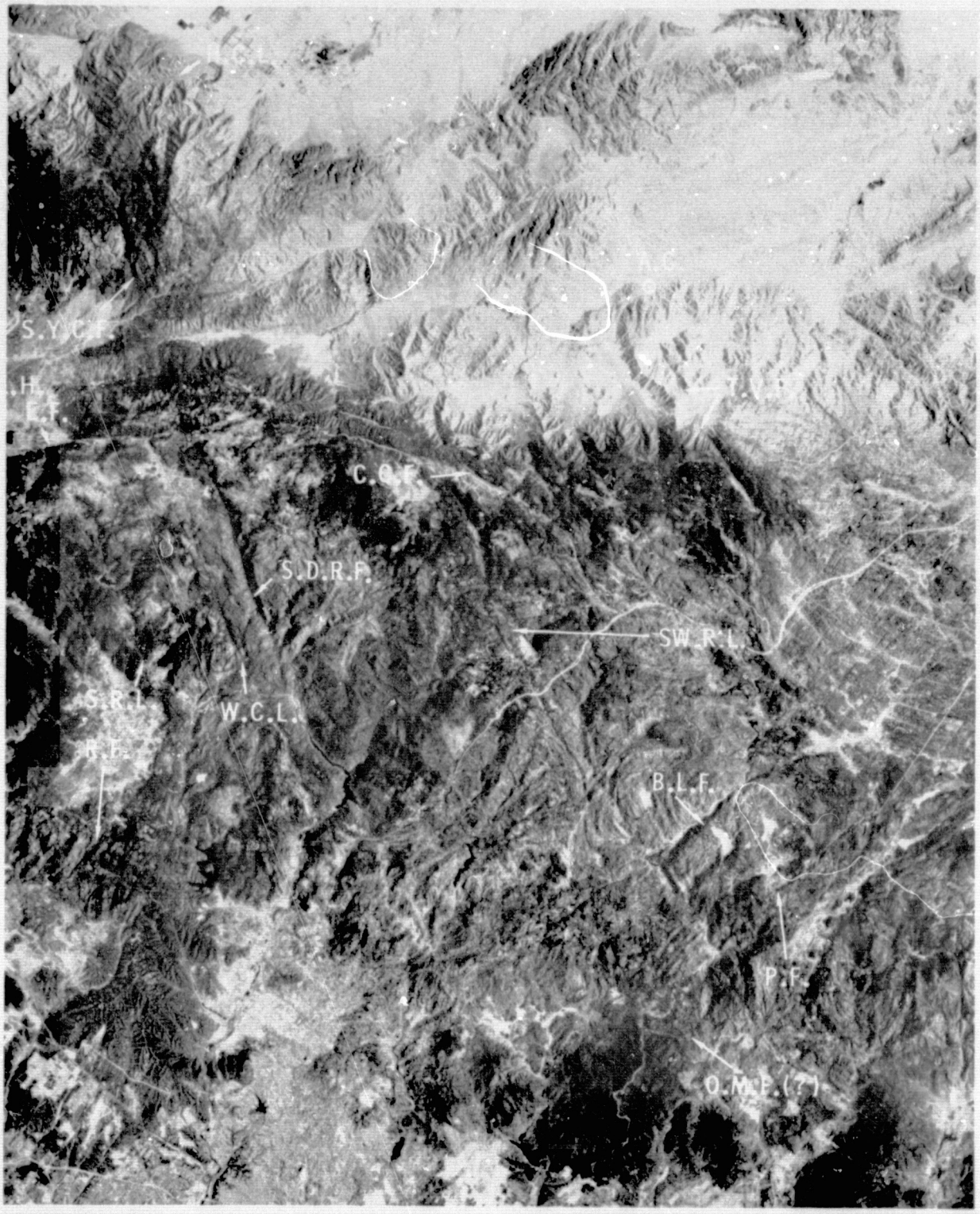


Fig. 3 - Peninsular Ranges, southwestern California, portion of Skylab 3, 190B camera, Roll 87, Frame 111. See Fig. 9 for location of individual features. Abbreviations: A.C., Agua Caliente Hot Springs; B.L.F., Barrett Lake fault; C.C.F., Chariot Canyon fault; E.F., Elsinore fault; H.C.L., Henderson Canyon linear; L.H., Lake Henshaw; O.M.F. (?), Otay Mountain fault; P.F., Potrero fault; S.D.R.F., San Diego River fault; S.R.L. Sutherland Reservoir linear; SW.R.L., Sweetwater River linear; S.Y.C.F., San Ysidro Creek fault; T.V.F., Thing Valley fault.

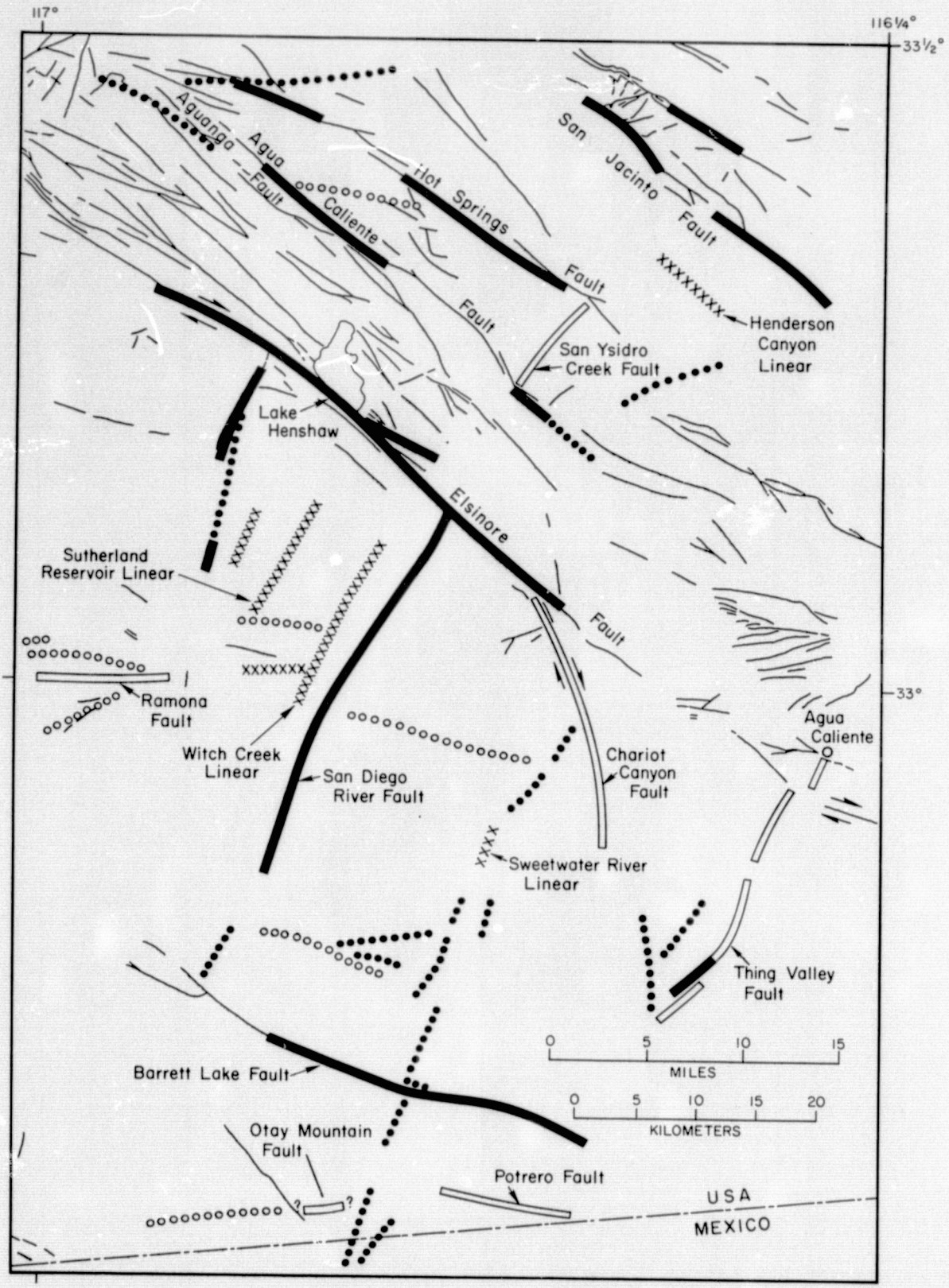


Fig. 9 - Faults and linears visible on Skylab photo in Fig. 8, southwestern California. Solid lines, faults shown by Strand (1962), Rogers (1965), or Jennings (1973); heavy lines, faults visible on satellite images; light lines, faults not visible; open lines, previously unmapped faults. Dotted lines, linears of unknown character; solid dots, no field investigation; open dots, field investigation but exposures not adequate to determine origin, XXXX, linears not due to faulting.

THE UTILIZATION OF LANDSAT IMAGERY IN NUCLEAR POWER PLANT SITING

G-14

A. J. Eggenberger, D. Rowlands, and P. C. Rizzo
E. D'Appolonia Consulting Engineers, Inc.
Pittsburgh, Pennsylvania

N76-17512

ABSTRACT

Imagery derived from the Earth Resources Technology Satellite (LANDSAT) is being used to aid in the evaluation of sites for Nuclear Power Plants in the United States and foreign countries. This imagery has been used primarily to map geologic features such as lineaments, linears, faults, and other major geologic structures which affect site selection for a Nuclear Power Plant.

INTRODUCTION

The United States Nuclear Regulatory Commission (USNRC) has established regulations for seismic and geologic considerations which determine the suitability of proposed sites for nuclear power plants. The suitability of the plant design basis is established in consideration of the seismic and geologic characteristics of the proposed site in order to provide reasonable assurance that the nuclear power plant can be constructed and operated at a proposed site without undue risk to the health and safety of the public.(1) A great many of the governments outside the United States have adopted the USNRC reactor site criteria per se or the philosophy implied by these criteria. The design basis for the vibratory ground motion is determined through an evaluation of seismology, geology, and the seismic and geologic history of the site and the region surrounding the site.

The design basis for vibratory ground motion is the earthquake which could cause the maximum vibratory ground motion at the site and is designated as the Safe Shutdown Earthquake (SSE). The SSE is identified by a thorough evaluation of seismic and geologic information. The most severe earthquakes associated with tectonic structures or tectonic provinces in the site region are identified and if capable faults are in the site region, the most severe earthquakes associated with these faults are identified.

A tectonic province is defined as a region characterized by a relative consistency of the geologic features contained within and a tectonic structure is a large scale dislocation or distortion within the earth's crust and is usually measured in miles. Alternately, when earthquake epicenters cannot be reasonably correlated with tectonic structure or with known faults, they may be identified with a seismotectonic province. The seismotectonic province is a region characterized by like geologic structural features and equipotential seismicity. The seismotectonic province is identified by boundaries determined by an analysis of the geologic and tectonic environments and the seismic history. The assumption is made that any historical earthquakes which have occurred in the seismotectonic province can occur anywhere in the province. Figure 1 is an example of a tectonic map and Figure 2 is a seismotectonic map.(2)

PRECEDING PAGE BLANK NOT FILMED

The vibratory ground motion at the site is then determined by assuming that the epicenters or locations of the highest historical Intensity of the earthquakes are situated at the point on the tectonic structures and tectonic or seismotectonic provinces nearest the site. The associated site Intensity then determines the Safe Shutdown Earthquake.

Site selection for a nuclear power plant is usually determined in one of two methods depending on the scope and depth of previous investigations. One method is to evaluate an entire region such as a service area for an individual electric utility. The other method is to evaluate a group of candidate site locations. A primary purpose of the evaluation process is to recognize aspects of a particular site or site area which would essentially abort a site or require a large investment of capital to make a site feasible for use. The overall siting process addresses basic factors such as hydrology, geology, demography/land use, meteorology, ecological sensitivity, geography/topography, and general overall acceptability. Other factors such as accessibility may be important depending upon location.

This paper is concerned with the geologic factor and more specific the geologic factor as it relates to the determination of vibratory ground motion at a particular site.

The field investigations used to evaluate a potential nuclear power plant site require a period of time on the order of a year and an expenditure of considerable capital. It is desirable, when alternate siting locations exist, to evaluate a site in a short period of time with minimum capital outlay. The use of satellite derived imagery along with ground truth has, in many cases, reduced the time and the expenditures required to complete site selection studies as well as aiding in the establishment of the relationship between local and regional conditions with respect to geology and seismology.

The imagery has been used by the authors on both reconnaissance and detailed levels. On the reconnaissance level the LANDSAT imagery enables the investigator to independently compile regional geologic and tectonic maps. In areas of detailed geologic mapping, the LANDSAT derived maps are used to evaluate the quality of mapping and to pinpoint areas where more detailed studies may be required. In areas where sufficiently detailed geologic maps are not available or where geologic mapping has not been conducted, the LANDSAT imagery provides an excellent base for the initiation of regional geologic studies and provides clear evidence for large scale structures. These large scale structures are further studied by conventional aerial photography and by standard geologic field methods.

Detailed studies by the authors have utilized methods of fracture trace analysis to statistically relate surface geologic features to linears detected on LANDSAT imagery. A study of this type in the southern Piedmont concluded that LANDSAT linears correspond quite well with trends of minor geologic structures and has aided in the establishment of the relationship between linears and seismic potential and historical earthquake activity.

LANDSAT imagery is being used in Europe to evaluate potential nuclear power plant sites. Analyses of the imagery has led to the possible extension of an existing fault along which earthquake activity has been associated. A potential site, which lies on this extension has been recommended to be withdrawn from consideration as a potential candidate site on this basis and known ground truth

existing in the technical literature. Similar studies are also being conducted in Asia to evaluate specific areas as to their desirability as a potential nuclear power plant site.

REGIONAL STUDY

Pakistan

The region of Pakistan is dominated by the tectonic activity associated with the Himalayan Mountains. This mountain system is considered by most to be the prototype area for continent-continent plate tectonic interaction where the two primary plates involved are the Indian Plate and the Eurasian Plate,[3] although some authors feel that the presence of additional, smaller plates are needed to satisfy small irregularities in relative motions indicated by focal mechanism solution. Generally, the Indian Plate is moving northward and colliding with the Eurasian Plate. Estimates of cumulative thrusting along this plate margin are 450 km for the area near Assam and 370 km in the Punjab-Hindu Kush region.[4] The plate tectonic configuration for this region is shown in Figure 3.

Studies of focal mechanism solutions for Himalayan earthquakes indicate that most earthquakes are being generated by horizontal compressive stresses that result in the formation of large scale, low angle thrust faults. It appears that most of the motion between these plates is taken up by movement along the Himalayan Thrust and the Hazara Thrust. Although these are the most prominent thrust faults in the region, it should be expected that movement along additional thrust faults would be likely. The rate of convergence has been estimated by LePichon to be approximately 5.6 cm/year.[5]

The eastern and western borders of the Indian Plate are not well defined. Very little research has been concentrated along the eastern region of the Indian Plate and no definite conclusions can be reached regarding the relationship of the Indian Plate to the Asian Plate and Burmese Arc.[6] The western border of the Indian Plate and The Baluchistan Arc, has been studied more extensively in terms of plate tectonics.[3,7] Focal mechanism solutions along the Kirthar-Sulaiman fault zone in Pakistan shows consistent left lateral strike-slip motion along a fault plane that strikes north-south. This type of movement agrees with field evidence, as well as observed displacements during earthquakes, and indicates a northward movement of the Indian subcontinent with respect to Afghanistan. The entire area can be considered to be moving northward, with the Indian Plate moving at a more rapid rate than the remainder of southwest Asia and the Middle East. The exact relationship of the Kirthar-Sulaiman fault zone to the spreading centers in the Indian Ocean has not been conclusively demonstrated.

The geology of the Baluchistan Arc is very complex. The area in general represents a bend, or syntaxis, of the east-west trend of the Himalayas to a north-south orientation. This north-south trend remains relatively consistent for a distance of approximately 1,000 km before taking another east-west bend in the Makran Mountains of southeastern Iran. Even the north-south segment is characterized by several smaller syntaxial bends, the largest of which is near the seismically active area of Quetta, another is west of the town of Mianwali, and a third is northwest of Tank in the Bhittani Mountains.

The structure of the Baluchistan Arc is dominated by thrust faults, mainly from the northwest and west toward the Indian Platform, and tight folds with axes essentially north-south, parallel to the general trend of the arc.(7) The pattern of mountain ranges, and the structural characteristics of each range, however, do not fit a simple model for the plate tectonic evolution of this region, nor does the pattern of thrust faults within the north-south or east-west oriented ranges fit into a simple model of the structural evolution of the region. A considerable amount of work is still needed to adequately define the tectonic setting as well as the tectonic evolution of this complex area.

Two areas in Pakistan have been studied in regard to utilization of LANDSAT Imagery to obtain geologic information. One area, as shown on Figures 4A, 5A and 6A, is dominated by the flood plain of the Indus River and the Thal desert of central Pakistan. It is bordered on the north by the Salt Ranges and on the west by the Khisor Range. The other area, along the Pakistan-Afghanistan border is within the Baluchistan Arc.

The first area is the region being considered for an industrial site. The Indus Valley and much of the Thal desert is covered by surficial deposits of Quaternary age which includes alluvium and sand dunes. The slopes of the ranges are generally covered by alluvial fans, bahadas, and unconsolidated detritus. Some older, possibly early Tertiary, terrace deposits are found in the foothills of the Sulaiman Range. Some of these are well cemented and attain thickness in excess of 250 feet.(8)

The Salt Range and the Khisor Range are dominated by thrust faults and salt tectonics. The Salt Range has apparently been formed by tectonic transport along a Precambrian-Cambrian formation composed of salt and gypsum. The range extends for several hundred kilometers in an east-west direction from Kalabagh to near the Kashmir border. The frontal area of this range has been mapped as a thrust fault along its entire length. There is, in addition, evidence for salt tectonics such as large salt domes near Kalabagh and small salt intrusions throughout the entire range.

The Khisor Range trends north-south and is perpendicular to the trend of the Salt Range. They are indirectly related by the poorly mapped Mianwali Re-entrant. This range is also dominated by thrust fault tectonics, however, there apparently has been no salt mapped as is the case with the Salt Range. The frontal region of this range has been mapped as a continuous thrust,(8,9) but it is nowhere exposed. Folding along this frontal range, however, may be indicative of drag folding associated with large scale thrusting.

The LANDSAT imagery is used in the analysis of this area to define areas where large linears are present in the mountain ranges, and to determine if they are traceable into the alluvial deposits adjacent the mountain ranges. Once these areas are identified they can be studied in more detail on conventional aerial photography and eventually by a team of field geologists. This, therefore, enables one to pinpoint areas of interest in regard to capable faults over an extensive area through a relatively inexpensive, but thorough analysis of linears. It has great advantages over conventional aerial photography in regard to man-hours as well as availability of imagery and cost. This is especially true for Pakistan since the military controls all aerial photographic coverage and it may take several months to get access to conventional aerial photography.

The area shown on Figures 4A, 5A and 6A was analyzed for linears prior to a brief field reconnaissance by one of the authors. It was, therefore, possible to define the areas of most significance to the site including the area of the Mianwali Re-entrant between the Salt Range and the Khisor Range, and the frontal regions of both the Salt Range and the Khisor Range. As seen on Figures 4B, 5B and 6B, the area of the Mianwali Re-entrant is dominated by several long linears, the longest of which crosses the Salt Range where it intersects the Indus River. This region (Figures 4A and 4B) was examined in the field and it was found that the linear corresponds to a fault of relatively large displacement that has been extensively eroded to form a major valley tributary to the Indus Valley. In addition, several other faults, with parallel orientations were found within a kilometer of the larger fault. This area has been chosen as one needing additional field work to determine the relationship between the faulting and the alluvial deposits.

The frontal portion of the Khisor Range was examined in some detail. The slopes, as well as the plain immediately below the slopes, are covered in most places by alluvial fans and river terrace deposits. All of the alluvial fans appear to end at the same distance from the range and several of the fans have sharp, steep scarps. It has been decided that these deposits should be studied in greater detail to determine if these features are a result of surface faulting, or if they are related to erosion of the alluvium by the meandering Indus River.

An additional area examined on the LANDSAT imagery and in the field, but not shown on the Figures is in the Bhittani Range, west of the Khisor Range. The structural style is similar to the Khisor and Salt Ranges. This range trends east-west and marks another small syntaxial bend in the mountain chain. The central portion of this range is marked by a large fault. It has been mapped as a strike-slip fault,(8) however, strike-slip movement appears to be inconsistent with the overall structure of the range. This fault may represent a large scale thrust along which there has been a considerable amount of erosion. Additional field work is planned to clarify the nature of this fault.

Much of the mountainous regions of Pakistan are inaccessible, especially the mountainous regions along the border with Afghanistan. It is, therefore, difficult to evaluate large scale geologic and tectonic maps or to assess the nature of faulting. This is again, complicated by the relative inavailability of conventional aerial photography, which is especially true along this disputed border region. We have found that LANDSAT Imagery is very valuable for this purpose, especially in areas of rugged relief and little vegetation. Figure 7A is the LANDSAT Imagery for a region along the Pakistan-Afghanistan border which clearly shows the major structural features. Figure 7B is a regional tectonic map derived from this LANDSAT Imagery. This area is being analyzed for evidence of large scale strike-slip displacement associated with the Kirthar-Sulaiman fault zone discussed earlier in this paper. Additional areas to the north, south, and east of this area are being examined to determine the distribution and interrelationships between faults along this suspected plate boundary. This LANDSAT analysis will aid the evaluation of available geologic and tectonic maps, as well as assisting in defining areas of capable faulting.

In general, analysis of LANDSAT Imagery has enabled the initiating of large scale tectonic and structural studies as well as helping to define areas of structural complexity and areas of potential surface faulting hazards to industrial sites in Pakistan.

RECONNAISSANCE STUDY

Huelva, Spain

LANDSAT Imagery has been used extensively in Spain to aid in the initial tectonic analysis of approximately 20 power plant sites. Most of Spain has been mapped in relatively good detail (1:50,000) and the LANDSAT analysis has been used primarily to check the location of large tectonic features and to determine the presence of other tectonic features that have not been identified by conventional geologic studies. In one instance, analysis of this nature has resulted in the recommendation to reject a site from any further consideration.

The LANDSAT Imagery for the region investigated is shown on Figure 8, and represents an area of southwest Spain along the Atlantic Ocean, and near the city of Sevilla. The geology of the region is relatively simple. A long prominent linear divides the imagery into two regions. North of the linear lies Hercynian metamorphic rocks, while to the south the area is composed of sediments of the Guadalquivir Basin, as shown on Figure 9. This linear has often been mapped as a fault, although recent evidence indicates that it is a monoclinal flexure within the Hercynian rocks of the basement complex. This linear is well known and was anticipated during the analysis. What was not expected, however, was a second long linear within the Guadalquivir Basin. This northeast-southwest linear passes through the city of Sevilla and continues to the coast. It passes very near to the town of Huelva, where the power plant site was being considered.

The Guadalquivir Basin is generally considered to be a downwarped section of the Hercynian Shield. Geologic evidence indicates that subsidence began during the Miocene and accumulated at least 3,310 meters of sediments. Basement faults have been identified beneath these sediments near the axis of the basin,[10] however, no faults have been mapped in the Tertiary deposits. There is some evidence that indicates that the basin subsidence may be continuing at present. Archeological evidence indicates at least several meters of subsidence during historic time. In addition, the area south of the recently identified linear is generally swampy, while the area to the north is well drained. In addition to subsidence, this last information may be indicative of normal faulting along this linear. Recent mapping along the Guadalquivir River, shown on Figure 10, near Sevilla indicates the presence of several small faults which either coincide with this linear or have similar trends. The interpretation of the linear features and the locations of faults are shown on Figure 11.

Although earthquake frequency is not high in this region of Spain, several earthquake epicenters are located along this linear. These include the 1504 Carmona Earthquake which had an estimated epicentral Intensity of XI (Modified Mercalli).

Using the combination of available literature, LANDSAT Imagery analysis, and earthquake data it was possible to perform a rapid analysis of this particular site. No definitive evidence was found for recent faulting, such as Quaternary offsets, however, sufficient information existed that indicates a probability of faulting. Since this was part of a multiple site selection study it was decided that large capital outlay would be required to prove the absence, or non capability of faulting in this region and the site was abandoned in favor of other sites.

DETAILED STUDY

South Carolina Piedmont

A detailed analysis of LANDSAT linears was conducted for a nuclear facility in South Carolina in 1973. This study included a statistical analysis of LANDSAT linears and their relationship to geologic features, both major and minor, in a part of the Piedmont Province of the Appalachian Orogenic Belt, as shown on Figure 12. Although the imagery includes a portion of the Blue Ridge Province, no detailed field work was done in the Blue Ridge, and hence it will not be treated in this paper.

The Piedmont Province lies between the Coastal Plain to the southeast and the Brevard Zone to the west and extends for the entire length of the Appalachian. Typically the Piedmont Province is a broad plateau sloping gently seaward from the front of the Brevard Zone and the Blue Ridge to the Coastal Plain. Bedrock exposures in the province are scant and poor since rock is covered with a residual mantle of thoroughly weathered material (saprolite) of varying thickness. Because rock exposure is poor, the geology of the province has not been fully investigated and the regional interpretation is inferred from a few locations where details are known.

The Piedmont in North Carolina, South Carolina and Georgia consists mainly of a complex of contorted gneisses, schists, phyllites and slates, containing granite plutons and small ultrabasic intrusives. The metamorphic grade generally increases toward the west and then decreases again in the Blue Ridge. The last high temperature metamorphism and plutonic emplacement is thought to have been at the end of the Paleozoic era.

The Piedmont Province can be divided into five zones as shown on Figure 12, which are elongated parallel to the Appalachian structural trends. These belts are: the Chauga Belt, the Mobilized Inner Piedmont, the Charlotte Belt, the Kings Mountain (Lowndesville) Belt and the Carolina Slate Belt.(11)

The Chauga Belt forms the westernmost subdivision of the Piedmont Province, and is bounded on the northwest by the Brevard Zone. The belt contains two formations, the Chauga River Formation, consisting primarily of phyllites with some impure marble and the quartzo-feldspathic Henderson Gneiss.

The Mobilized Inner Piedmont Belt contains rocks of the highest metamorphic grade formed in the Southern Appalachian Piedmont. These rocks include both volcanic and sedimentary series that have been metamorphosed to the staurolite-kyanite and sillimanite-almandine subfacies of the almandine-amphibolite facies.(11) Griffin(12) states that the rocks in the core of the Inner Piedmont are of a higher grade than either the northwest or southeast flanks. Griffin(12) has also observed that the Inner Piedmont is marked by undulatory foliation with a predominance of very gentle dips that are most likely the result of a gentle folding of a previously deformed foliation.

The Kings Mountain Belt (Lowndesville Belt) of South Carolina and North Carolina has been studied extensively by Overstreet and Bell,[13] Overstreet,[14] Butler,[15] and Griffin.[12] Overstreet and Bell[13] believe that field evidence indicates that the Kings Mountain Belt represents a metamorphosed sedimentary sequence which is in part the age equivalent of similar lithologies in the Inner Piedmont, Charlotte Belt and Carolina Slate Belt. They also indicate that the apparent physical differentiation between the Kings Mountain Belt and other belts in the Piedmont is a result of a change in metamorphic grade rather than the result of faulting. More recently Griffin[16] and Hatcher[11] indicate that the northwest boundary of the Kings Mountain Belt is a fault contact.

The Carolina Slate Belt, the easternmost belt in the Piedmont and the one with the lowest grade of metamorphic rocks, can be followed almost continuously from Virginia, 30 kilometers north of the North Carolina border, well into Georgia. The stratigraphic section within the Slate Belt is composed of metasedimentary and metavolcanic rocks. The metasediments are mudstones, argillites and greywackes, which are poorly sorted and contain bedding that ranges from fine laminations to thick, graded beds. All of the fine grained rocks in the section show slaty cleavage. Quartzites, conglomerates and carbonates occur in this belt but are not major constituents. The interbedded metavolcanic rocks are tuff, breccia and mafic and felsic volcanic flows.

The Charlotte Belt extends from eastern Alabama through South and North Carolina and into Virginia. Rocks similar to those found in the Charlotte Belt also crop out in the eastern area of the Carolina Slate Belt. The rocks of the Charlotte Belt are predominantly medium grade gneiss, schist and amphibolite that were intruded by many pre-metamorphic and post-metamorphic plutons. Overstreet and Bell[13] found that granitic textures are common in the rocks of the Piedmont and that the belt includes a large number of plutons. They found that the granitic rock has strong compositional banding resulting from the metamorphism of sedimentary and volcanic rocks. This granitic rock is often a fine-grained gneiss and migmatite of the albite-epidote-amphibolite subfacies, the highest of temperature subfacies of the green-schist facies. In places, metamorphic grade rises to staurolite-kyanite subfacies and near plutons, it even rises to sillimanite-almandine subfacies; both subfacies of the almandine-amphibolite facies. Thus the Charlotte Belt represents an area of moderate grade metamorphism between two areas of lower grade metamorphism.

The LANDSAT Imagery used for this study is presented in Figure 13 and a map of linears on this imagery is presented as Figure 14. Visual comparison of the linear map and LANDSAT Imagery to the map of geologic subdivision shows only two features common to both. These are the Blue Ridge Province and the Brevard Zone, which separates the Blue Ridge from the Piedmont.

The most prominent linear feature, which is sufficiently long to be considered a lineament, is associated with the Brevard Zone. This zone is characterized throughout its length by both faulting (possibly several periods of movement) and a distinctive stratigraphy consisting of the Chauga River Formation[11] and the Henderson Gneiss. With the exception of the Brevard Zone and the Chauga Belt with which it is associated, no other geologic subdivision within the Piedmont can be discerned on the imagery.

Considering the regional lithologic and structural variations within these subdivisions it would be expected that at least the northwest boundary of the Kings

Mountain Belt (Lowndesville Belt) would be represented by a pronounced photo linear, especially since it is considered to be bounded by a fault that extends well into Georgia.[11,16] This lack of a distinct linear feature may indicate that the northwest border of the Kings Mountain Belt is not fault controlled, or that faulting along this boundary may be of only minor importance in the regional tectonic setting.

The most interesting of the remaining linears that have been detected in this study is located north of the Greenville-Spartanburg area of South Carolina and passes near the town of Tigerville. This east-west oriented linear extends from the Brevard Zone in the west, to within 20-30 miles of the North Carolina state line in the east. This linear has not been studied in detail, however, it is tentatively suggested that this may represent a large fault within the Piedmont Province. However, no faults have been mapped along this trend. This linear appears to be marked by a distinct change in topography, with the northern area having a rugged topography more similar to the Blue Ridge than to the gentle topography of the remaining portion of the South Carolina and North Carolina Piedmont.

It is difficult and time consuming to field check each linear mapped on LANDSAT Imagery. It was decided that the most efficient way to analyze the results of a large areal linear study was to perform a statistical analysis of linear orientations and determine their relationship to minor geologic structures. The area of the LANDSAT Imagery was subdivided into two domains based on gross geologic features; the Blue Ridge, and the Piedmont. The Blue Ridge was not of immediate concern in regard to the site being evaluated and subsequently no additional work was conducted there. The orientations of the LANDSAT linears within the Piedmont Province were then measured and plotted on a rose diagram, shown on Figure 15. The orientations are listed in Table I.

In order to evaluate these orientations in terms of geologic structure, a reconnaissance level joint study was undertaken. Three areas were defined for collection of data based on geologic and geographic distribution. The area near Lake Hartwell (Area 1 on Figure 16) was chosen because of its proximity to the proposed site. The area near Hendersonville, North Carolina (Area 2) was chosen because of the differences in topographic character with the remaining portion of the piedmont being studied. The area northwest of Columbia, South Carolina (Area 3) was chosen because of the difference in geologic features between the Slate Belt and the Inner Piedmont. Joints were measured in each of these areas and plotted on rose diagrams. These are shown on Figure 17, and presented in tabular form in Table I.

It is evident from the comparison of orientation data in Table I that most of the LANDSAT linears correspond quite well with the orientations of joints distributed throughout the Piedmont. This is particularly the case with the N2E, N43W, and N68W orientations, which may represent primary fracture trends in the Piedmont Province. Wielchowsky and Drakovsal(17) have indicated that a N47W orientation is one of the dominant LANDSAT linear trends in the Dora-Sylvan Springs Area of Alabama. Comparison with other areas cannot be made because there is very little published information on joint orientations within the Piedmont Province.

Each of the other LANDSAT linear orientations has at least one area within the study region that has joint orientations with similar, or identical trends. The only exception to this is the N53W trend on the LANDSAT Imagery. Additional work is in progress to determine the relationship of this trend to the regional

structural setting. It is tentatively suggested however, that this trend corresponds with one of the predominant northwest trends of Triassic diabase dikes which are distributed throughout the Piedmont.

This study has shown the usefulness of LANDSAT analysis to the study of major and minor linear geologic structures within the Piedmont Province of the Appalachians. Large scale geologic features such as the Brevard Zone are very evident and easy to distinguish on this type of Imagery. The statistical treatment of small linears on LANDSAT Imagery coupled with reconnaissance studies of minor geologic structures such as joints has proven to be a valuable technique in the evaluation of geologic hazards for power plant siting.

CONCLUSIONS

This study emphasizes the usefulness of LANDSAT Imagery interpretation in the selection processes for industrial and power plant sites. It has proved useful for the delineation of linear geologic or geographic features that may represent traces of faults. These areas can then be examined in more detail by conventional aerial photography and eventually by geologic field mapping. LANDSAT Imagery has also been of particular use in the analysis of regional tectonics as a check on maps that are currently available and as a base on which to begin tectonic studies in areas that have insufficient geologic control.

ACKNOWLEDGMENTS

The authors would like to express their gratitude to E. D'Appolonia Consulting Engineers, Inc. for providing financial support for the preparation of the text and figures.

BIBLIOGRAPHY

1. United States Nuclear Regulatory Commission, Part 100-Reactor Site Criteria, Federal Register, Vol. 38, No. 218, Washington, D. C., November 13, 1973.

2. Hadley, Jarvis B. and James F. Devine, "Seismotectonic Map of the Eastern United States," U. S. Geological Survey, Miscellaneous Field Studies, MF-620, 1974.

3. Nowroozi, A. A., "Focal Mechanisms of Earthquakes in Persia, Turkey, West Pakistan, and Afghanistan and Plate Tectonics of the Middle East, Bull. Seis. Soc. Amer., Vol. 62, No. 3, pp. 823-850, June 1972.

4. Seeber, L., K. H. Jacob, and J. Armbruster, "Microseismic Study, Tarbela Dam Project, Hazara, Pakistan," Lamont-Doherty Geological Observatory, Palisades, New York, April 1974.

5. LePichon, X., "Sea Floor Spreading and Continental Drift," Jour. Geophys. Research, Vol. 73, pp. 3661-3697, 1968.

6. Fitch, T. J., "Earthquake Mechanisms in the Himalayan, Burmese, and Andaman Regions and Continental Tectonics in Central Asia," Journal Geophysical Research, Vol. 75, No. 14, 1970.

7. Abdel-Gawad, Monem, "Wrench Movements in the Baluchistan Arc and Relation to Himalayan-Indian Ocean Tectonics," Geological Society of America Bull., Vol. 82, pp. 1235-1250, 1971.

8. Hemphill, W. R., and A. H. Kidwai, "Stratigraphy of the Bannu and Dera Ismail Khan Areas Pakistan," U. S. Geol. Survey, Professional Paper, 716-B, 1973.

9. Geological Survey of Pakistan, Geological Map of Pakistan, Islamabad, 1964.

10. "Mapa Tectonico de la Peninsula Iberica y Baleares," Instituto Geologico y Minero de Espana, Madrid, 1972.

11. Hatcher, R. D., Jr., "Developmental Model for the Southern Appalachians," Geol. Soc. of America, Bull., Vol. 83, pp. 2735-2760, 1972.

12. Griffin, V. S., Jr., "Inner Piedmont Belt of the Southern Crystalline Appalachians," Geol. Soc. of America, Bull. Vol. 82, 1971.

13. Overstreet, W. C., AND H. Bell, III, "The Crystalline Rocks of South Carolina," U. S. Geol. Survey Bull. 1183, 1965.

14. Overstreet, W.C., "The Piedmont in South Carolina," in Studies of Appalachian Geology Central and Southern, Interscience Publishers, New York, 1970.

15. Butler, J. R., "Structure of the Charlotte Belt and Adjacent Belts in York County, South Carolina," South Carolina Division of Geology, Geologic Notes, Vol. 15, pp. 49-62, 1971.

16. Griffin, V. S., Jr., "Position of the Kings Mountain Belt in Abbeville County, South Carolina," Southeastern Geology, Vol. 12, 1970.

17. Wielchowsky, C. C., and J. A. Drakovsal, "A Comparison of Lineaments and Fracture Traces to Jointing in the Appalachian Plateau of Alabama - Dora - Sylvan Springs Area, abs," Geol. Soc. America, Annual Mtg. November, 1974.

TABLE I. - SUMMARY OF ORIENTATION DATA

LANDSAT Linears (Piedmont Area)	Joints Anderson Area, S. C.	Joints Hendersonville Area, N. C.	Joints Columbia Area, S. C.
N63E		N62E	
N52E	N52E		N57E
N32E	N37E	N30E	
N16E	N15E	N17E	
N2 E	N2 E	N2 E	N8 E
N8 W			N12W
N22W	N17W		
N43W	N42W	N47W	N42W
N53W			
N68W	N62W	N62W	N68W
N82W	N82W	N88W	
	N82E	N80E	
		N42E	
	N32W		N32W
	N72W		

REPRODUCIBILITY OF THE
ORIGINAL PAGE IS POOR



A, TECTONIC MAP

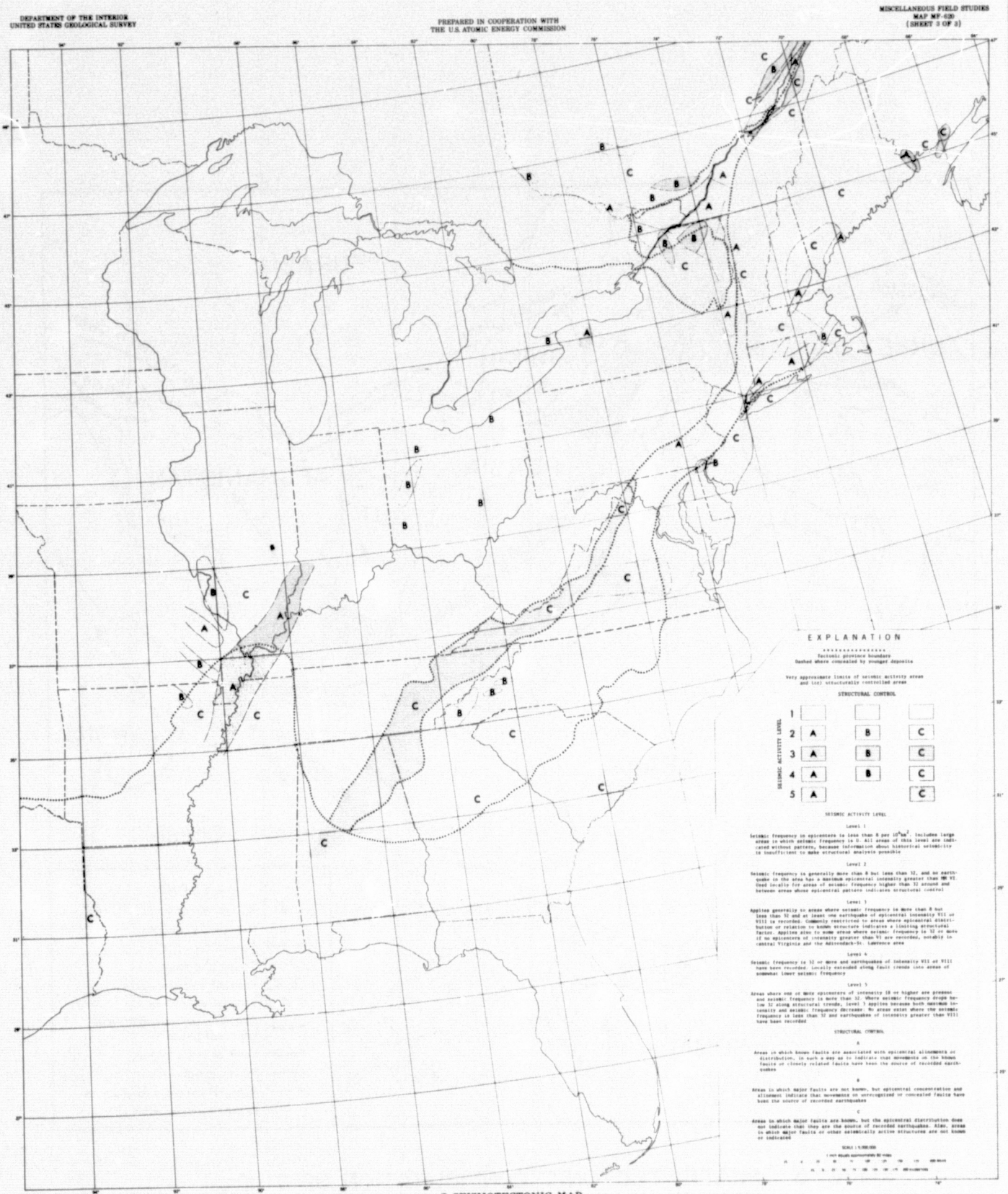
SEISMOTECTONIC MAP OF THE EASTERN UNITED STATES

By

Jarvis B. Hadley and James F. Devine

1974

FIG. 1 EXAMPLE OF A TECTONIC MAP



C, SEISMOTECTONIC MAP

SEISMOTECTONIC MAP OF THE EASTERN UNITED STATES

By

Jarvis B. Hadley and James F. Devine

1974

FIG. 2 EXAMPLE OF A SEISMOTECTONIC MAP

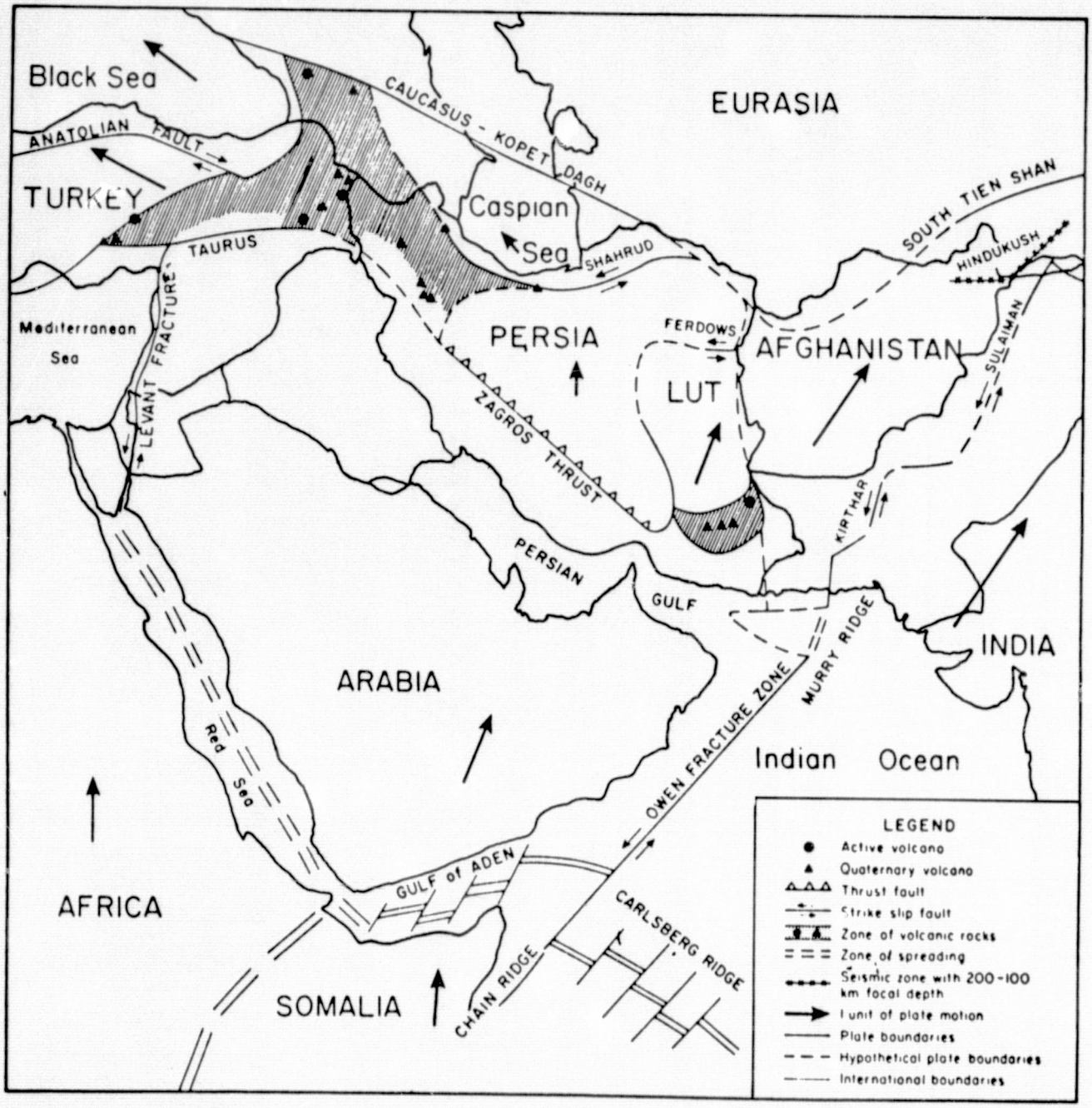


FIG. 3 PLATE TECTONIC CONFIGURATION OF THE MIDDLE EAST (FROM NOWROOZI, 1972)

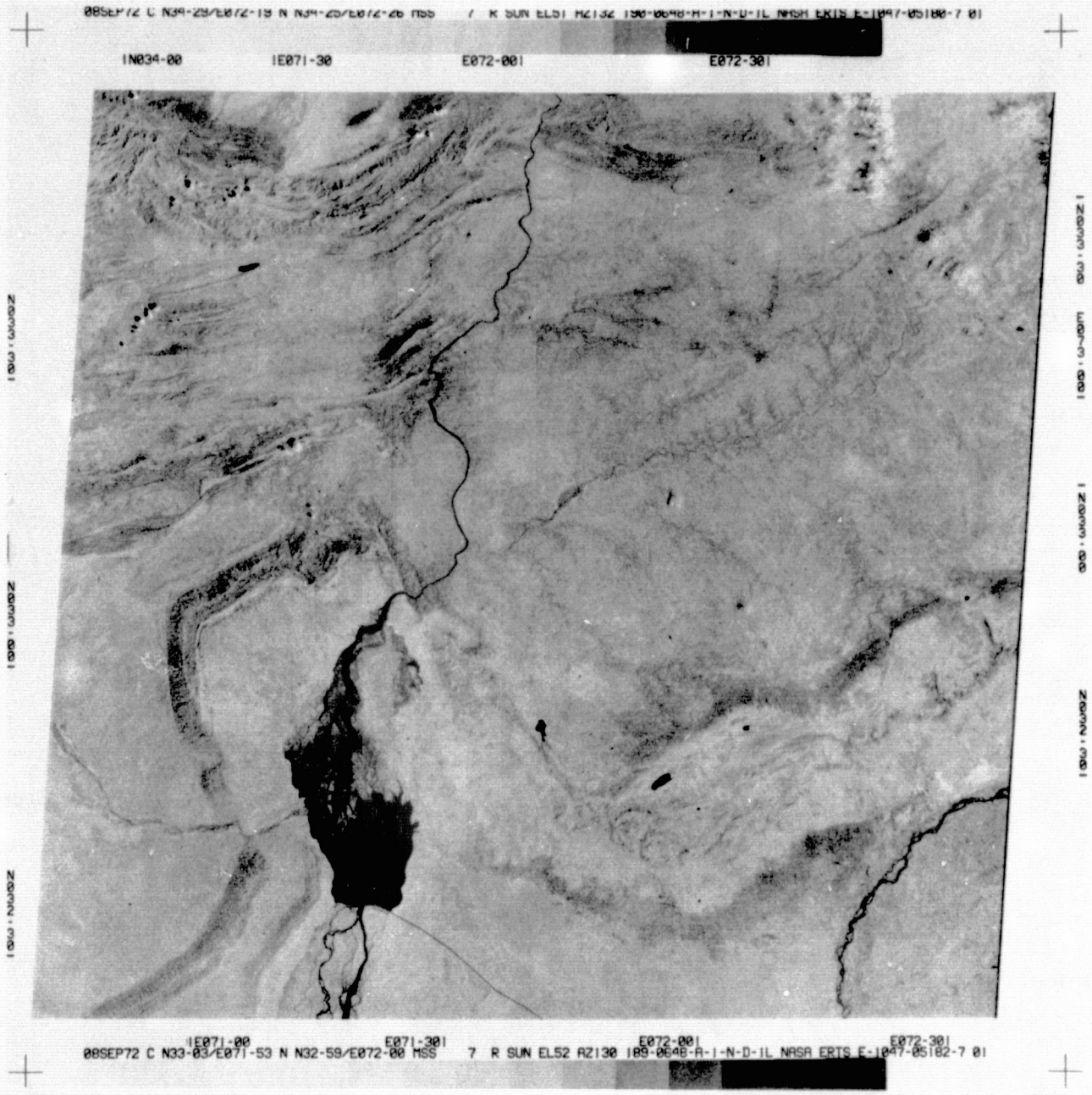


FIG. 4A LANDSAT IMAGERY OF A PART OF THE INDUS RIVER VALLEY, SALT RANGE, KHISOR RANGE, AND MIANWALI RE-ENTRANT

REPRODUCIBILITY OF THE ORIGINAL PAGE IS POOR

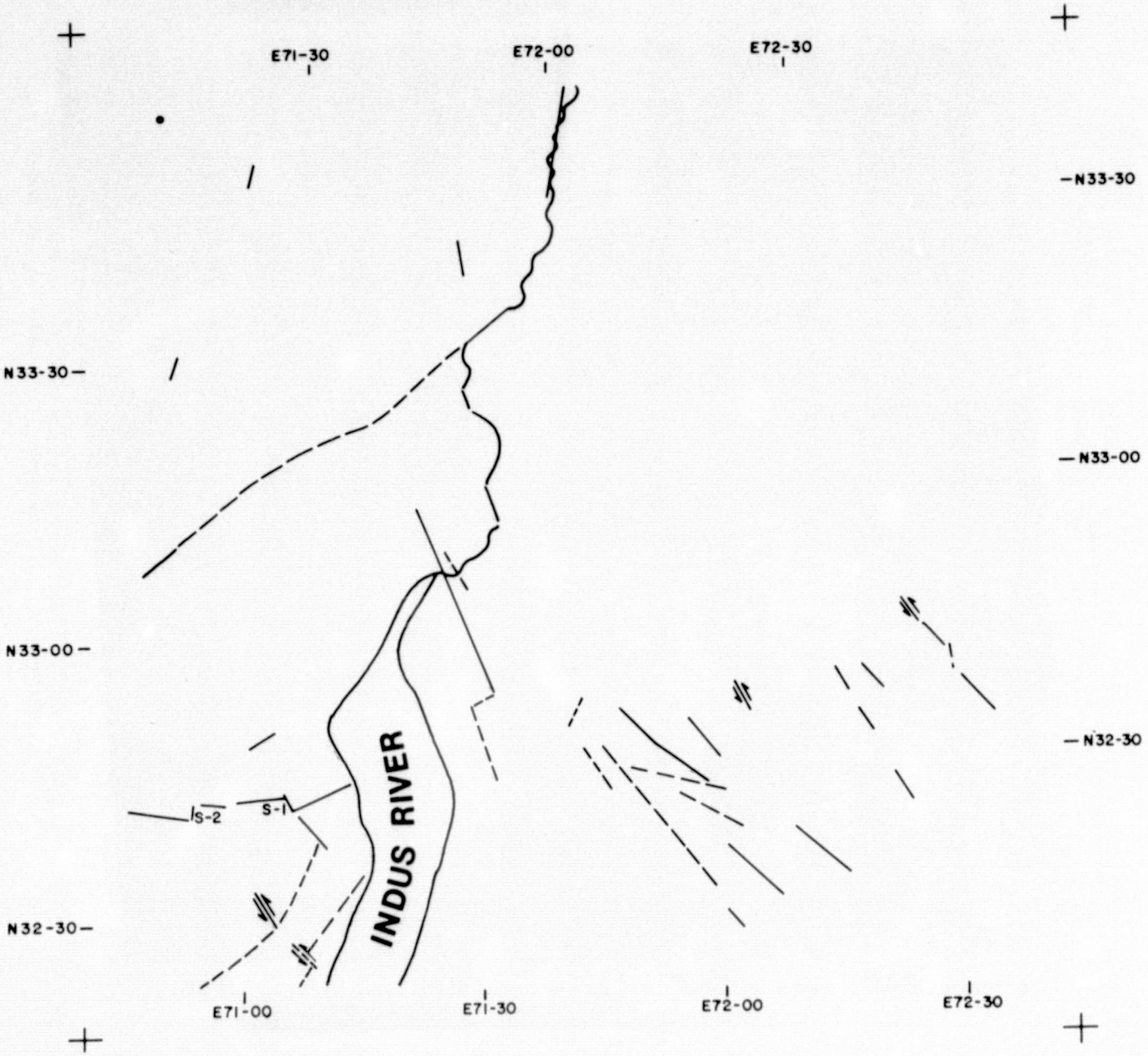


FIG. 4B INTERPRETATION OF LINEAR FEATURES ON FIGURE 4A

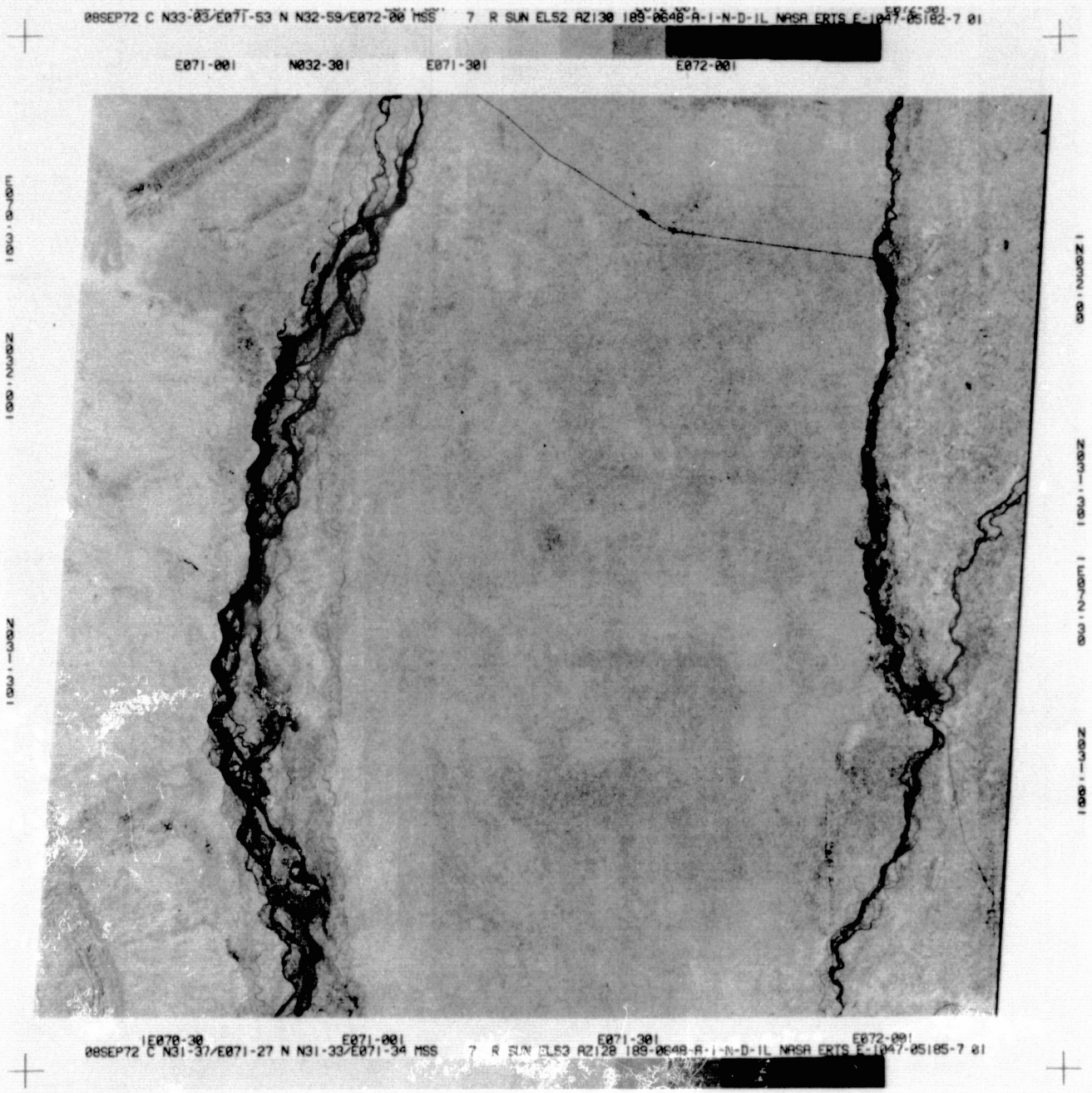


FIG. 5A LANDSAT IMAGERY OF THE INDUS RIVER VALLEY SOUTH OF FIGURE 4A

REPRODUCIBILITY OF THE ORIGINAL PAGE IS POOR

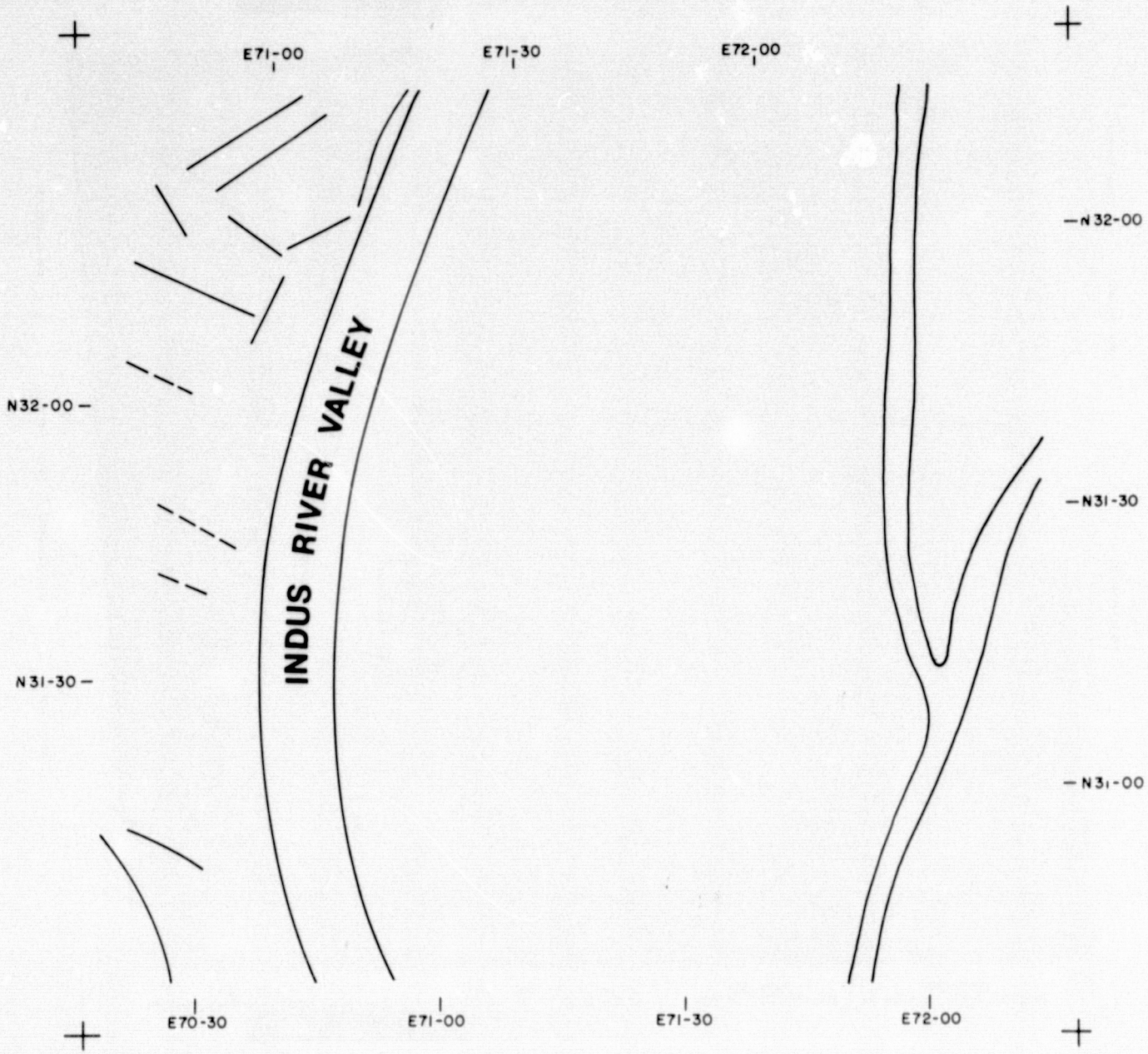


FIG. 5B INTERPRETATION OF LINEAR FEATURES ON FIG. 5A



FIG. 6A LANDSAT IMAGERY OF THE INDUS RIVER EAST OF FIGURE 4A SHOWING THE TOPOGRAPHY OF THE SALT RANGE

REPRODUCIBILITY OF THE ORIGINAL PAGE IS POOR

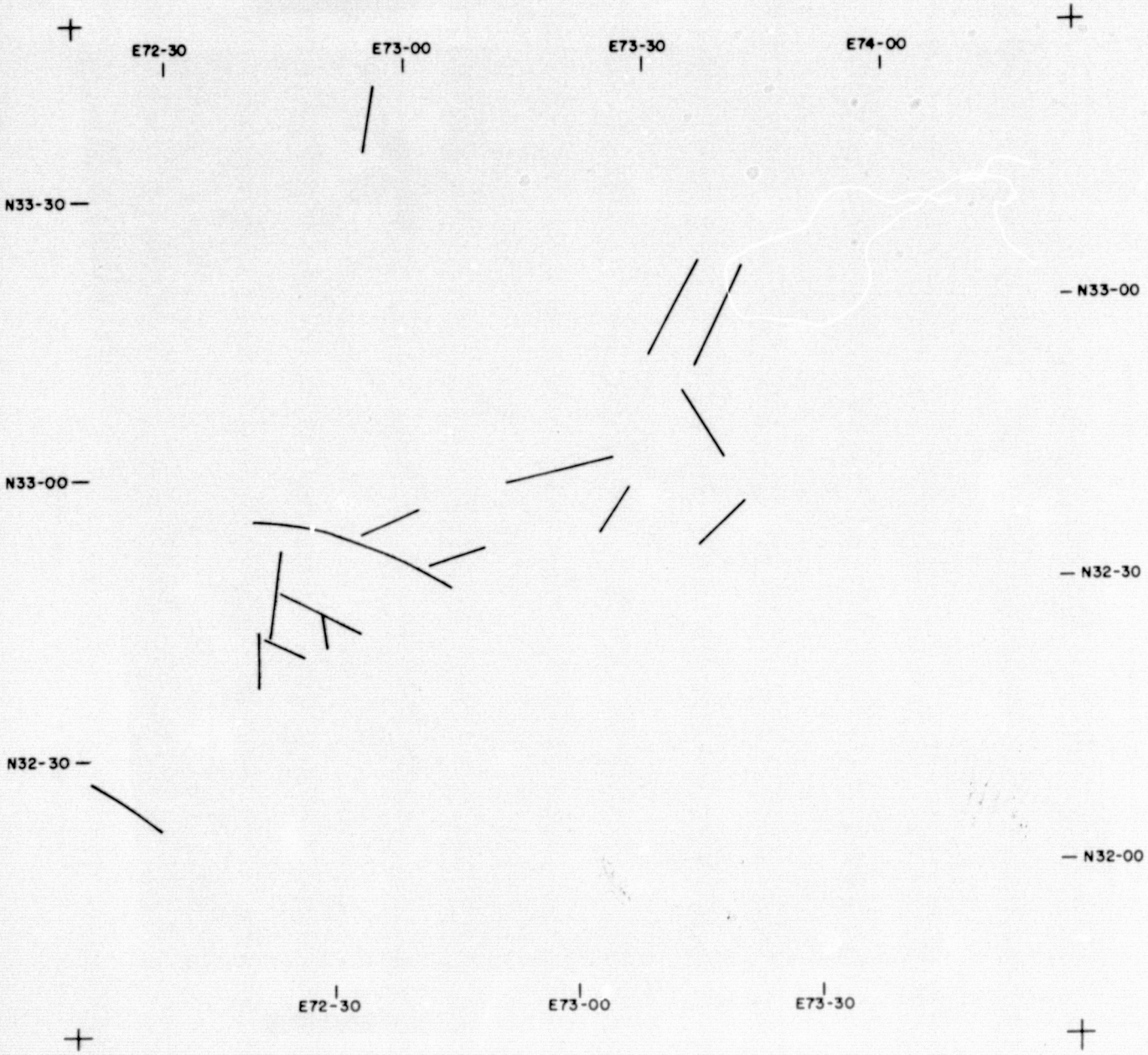


FIG. 6B INTERPRETATION OF LINEAR FEATURES ON FIGURE 6A

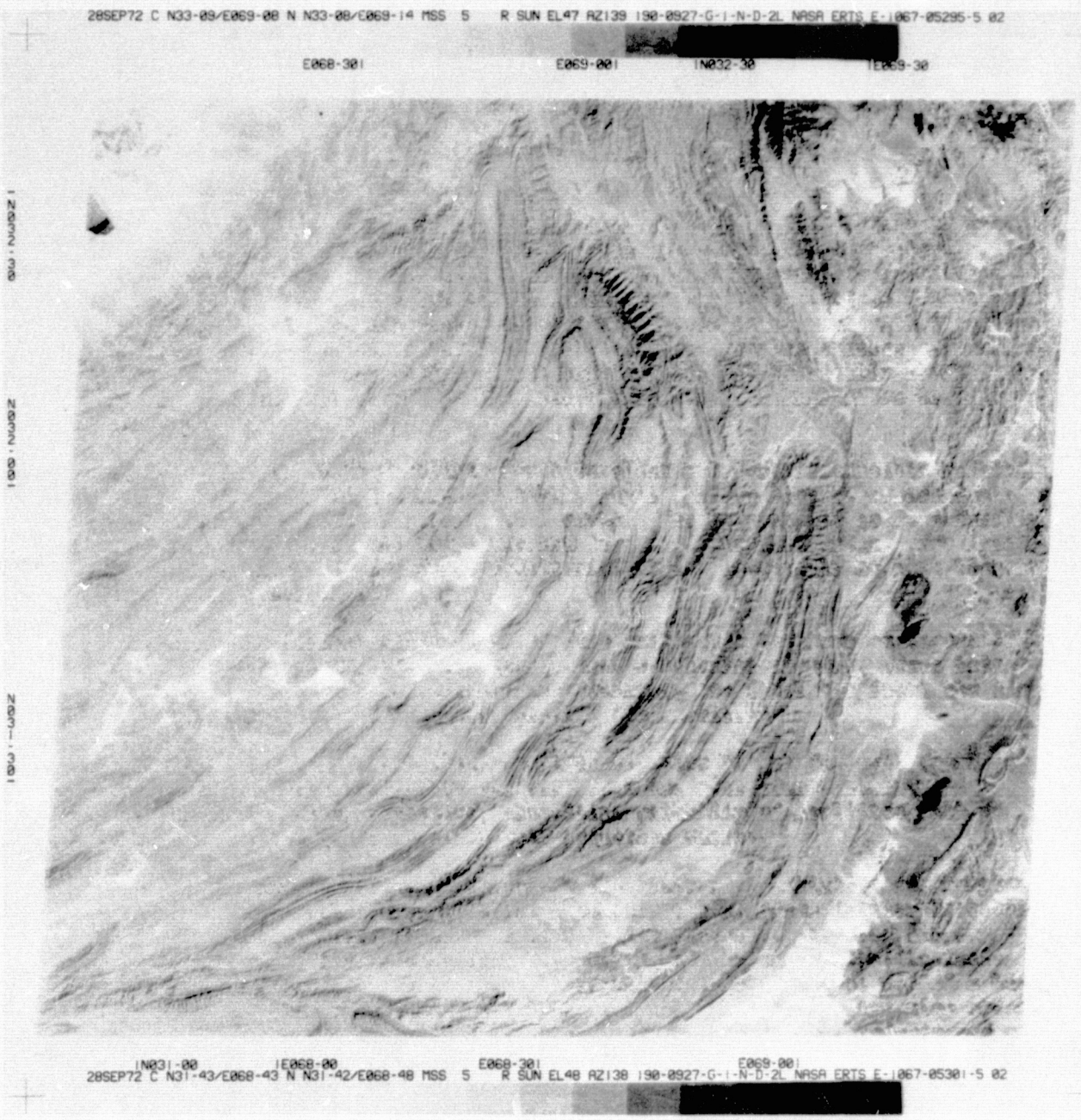


FIG. 7A LANDSAT IMAGERY OF PART OF THE BALUCHISTAN ARC ALONG THE PAKISTAN-AFGHANISTAN BORDER

REPRODUCIBILITY OF THE ORIGINAL PAGE IS POOR

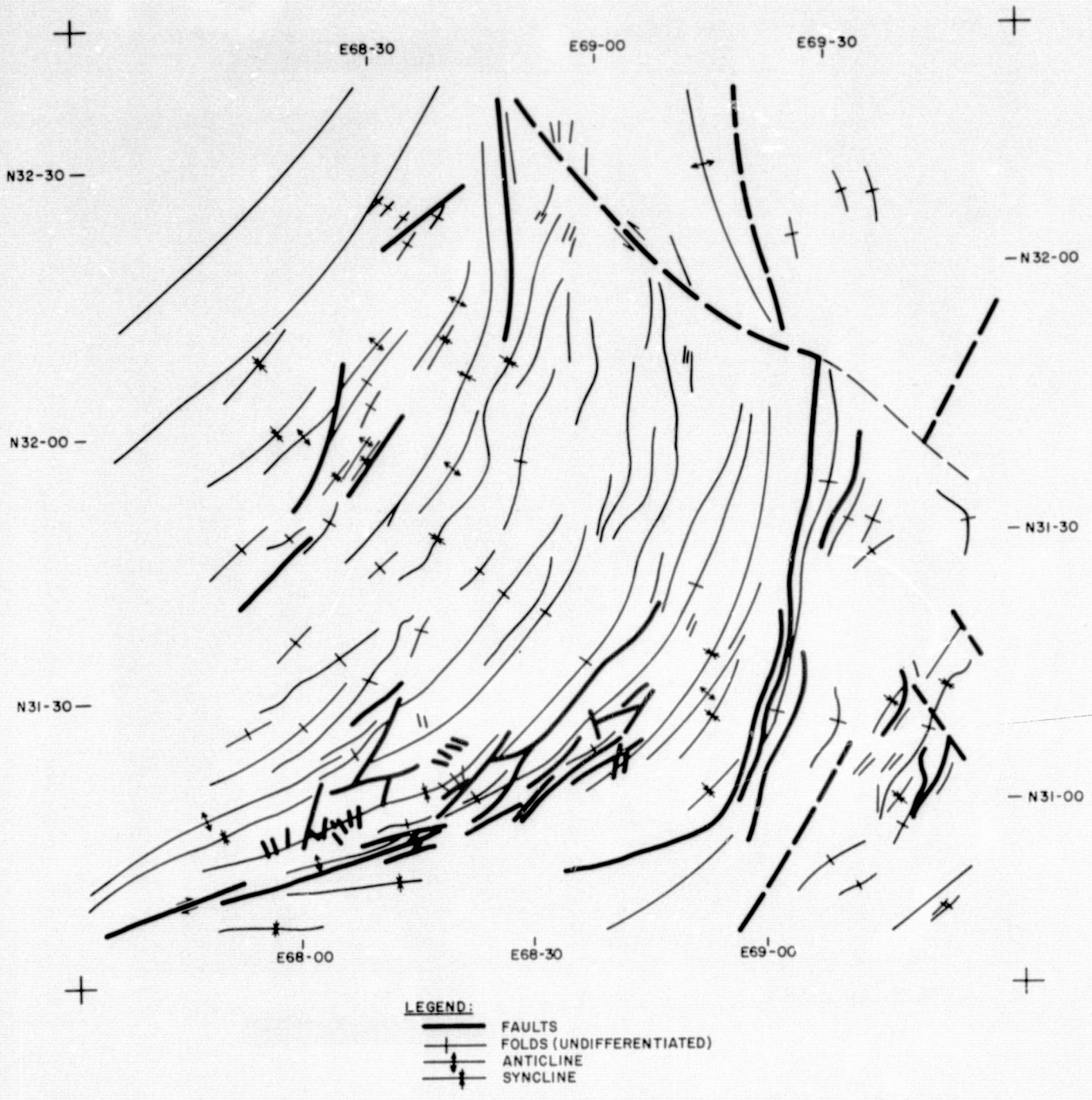


FIG. 7B TECTONIC MAP DERIVED FROM AN ANALYSIS OF GEOLOGIC FEATURES SHOWN ON FIGURE 7A

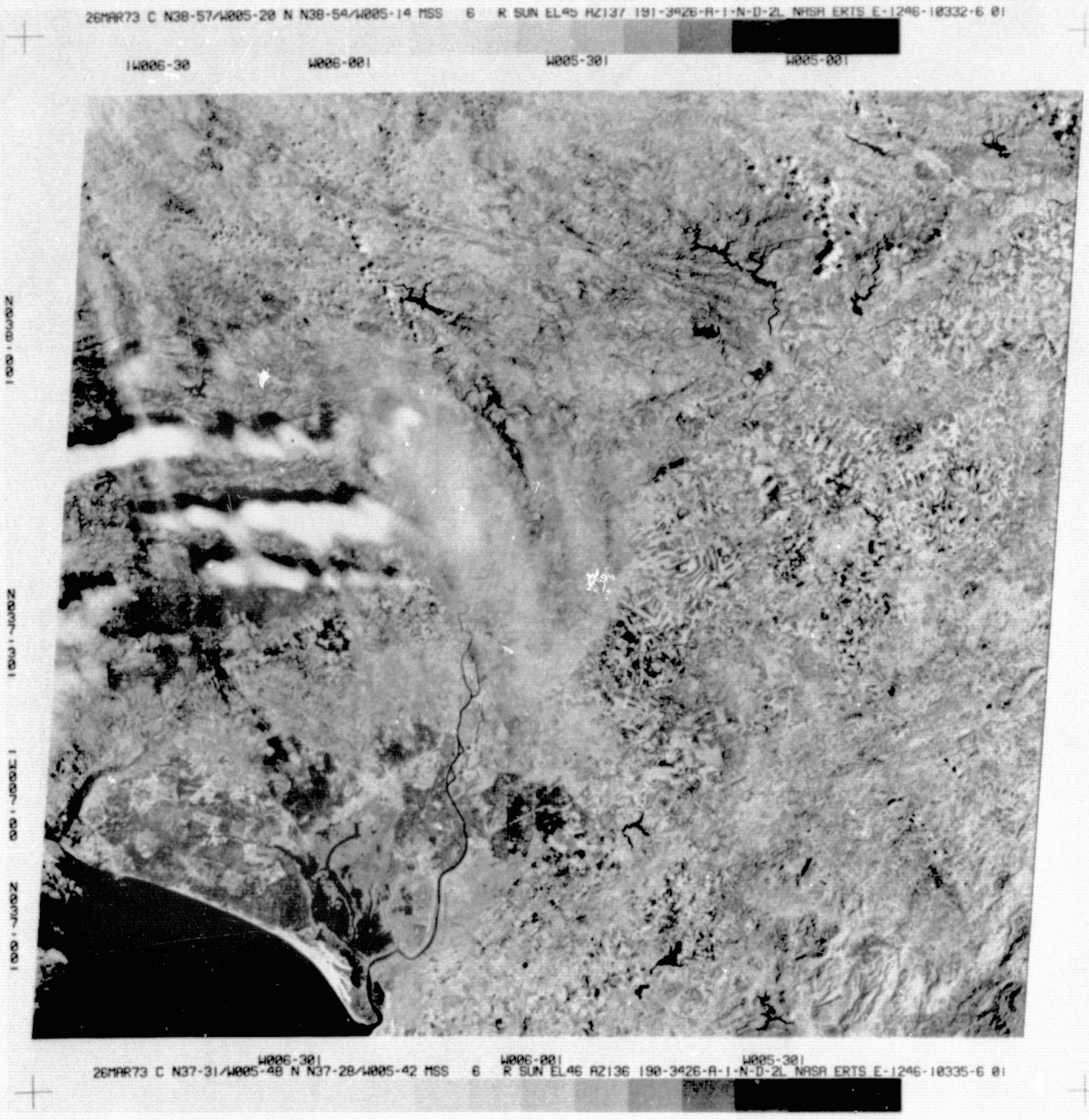
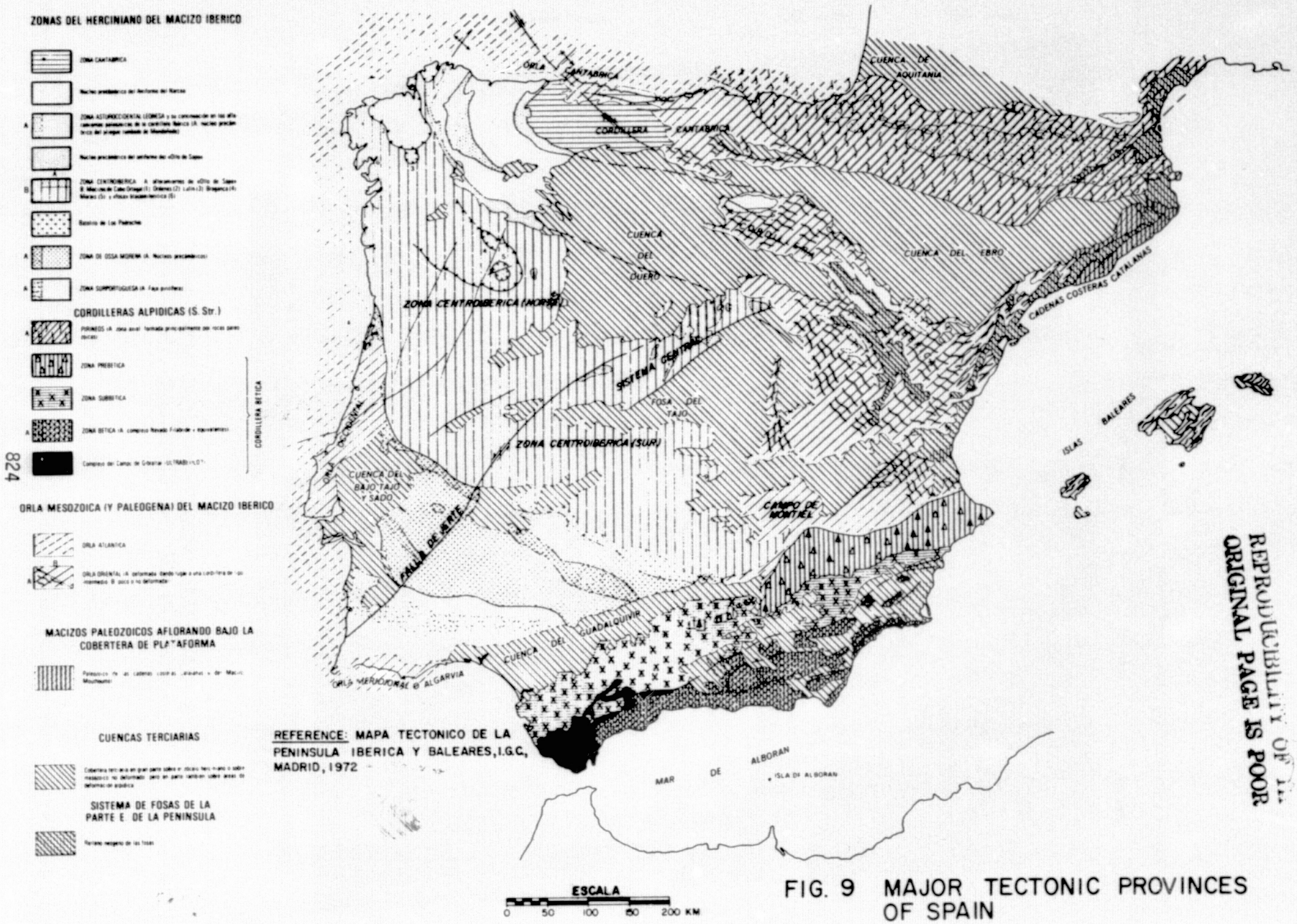


FIG. 8 LANDSAT IMAGERY OF THE NORTHWEST PORTION OF THE GUADALQUIVIR BASIN, SPAIN

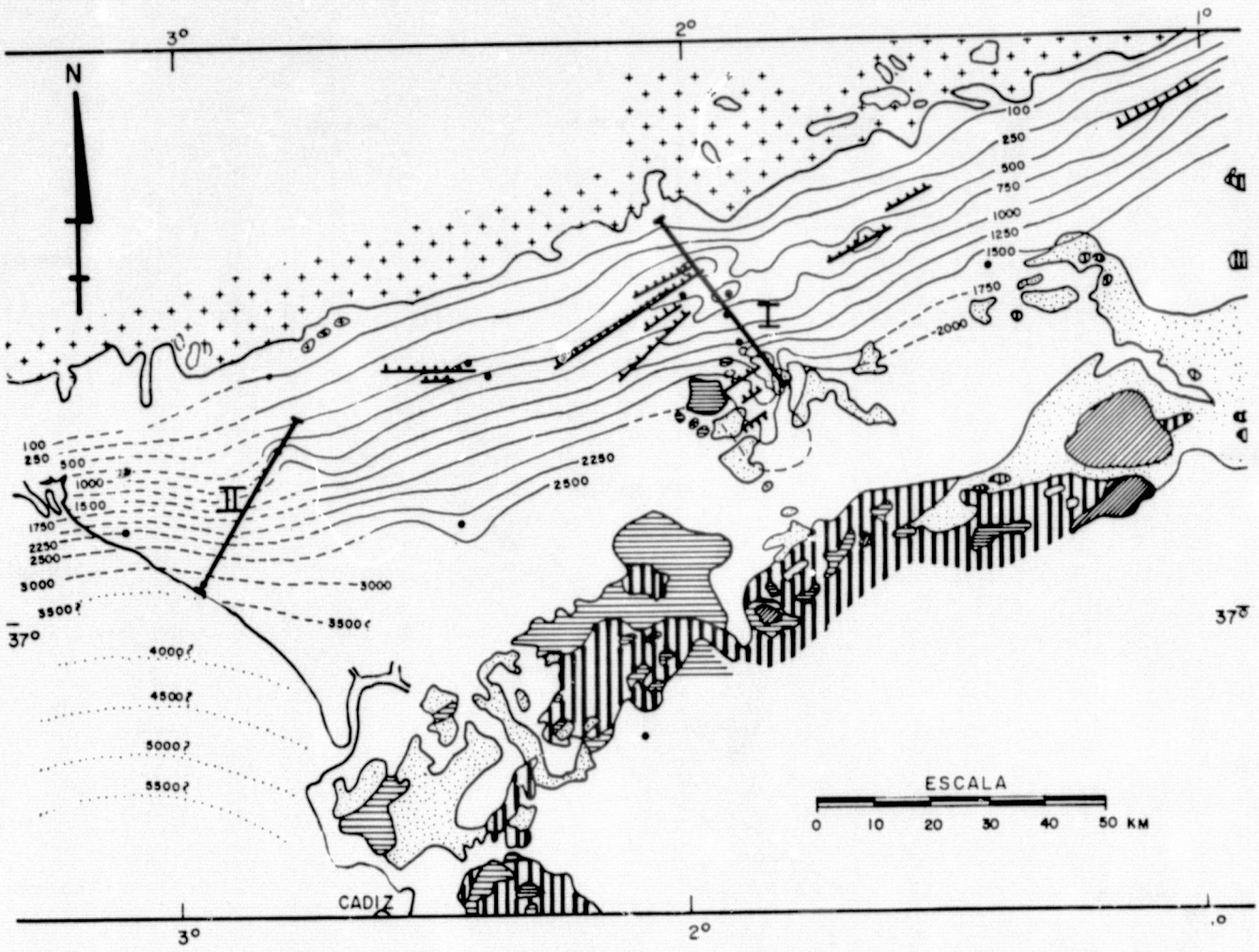
REPRODUCIBILITY OF THE ORIGINAL PAGE IS POOR



REFERENCE: MAPA TECTONICO DE LA PENINSULA IBERICA Y BALEARES, I.G.C., MADRID, 1972

FIG. 9 MAJOR TECTONIC PROVINCES OF SPAIN

REPRODUCIBILITY OF THE ORIGINAL PAGE IS POOR



LEGEND

- NEOGENE / QUATERNARY
- "ALBARIZAS" (LOWER MIOCENE)
- UPPER CRETACEOUS/PALEOGENE
- JURASSIC/LOWER CRETACEOUS
- TRIASSIC (MARLS AND GYPSUM)
- PALEOZOIC
- BORINGS
- 250 BEDROCK ISOBATHS (DEPTH BELOW SEA LEVEL)
- FAULTS
- BASEMENT CONTOURS (AFTER DRAKE ET. AL.)

NOTE: LONGITUDE BASED ON MADRID = 0°

ISOBATHS AND BASEMENT CONTOURS REFER TO THE TOP OF THE PALEOZOIC.

REFERENCE:
DURAND-DELGA, 1960-1963.

FIG. 10 GEOLOGIC MAP OF THE GUADALQUIVIR BASIN

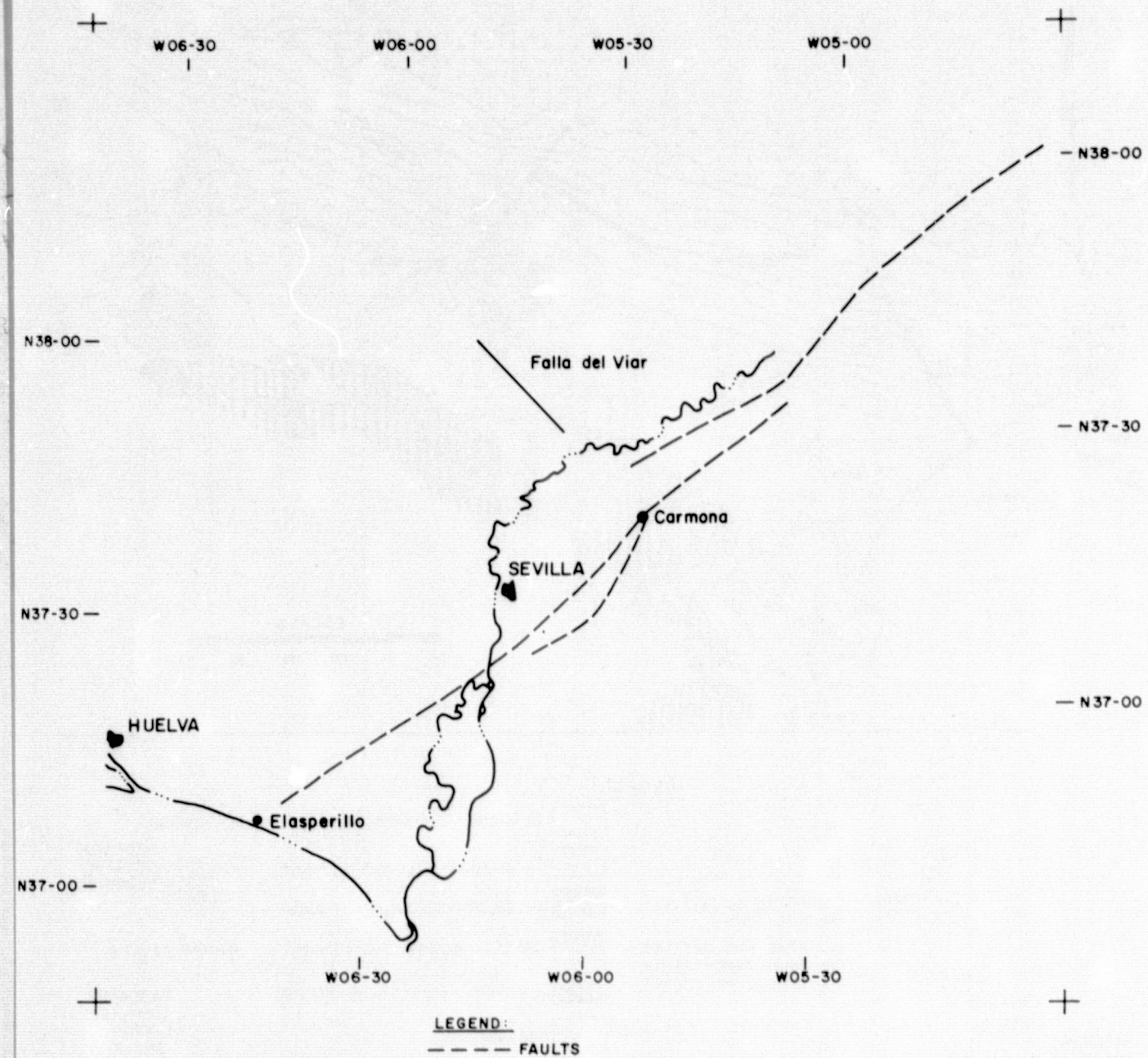


FIG. 11 INTERPRETATION OF LINEAR FEATURES SHOWN ON FIGURE 8

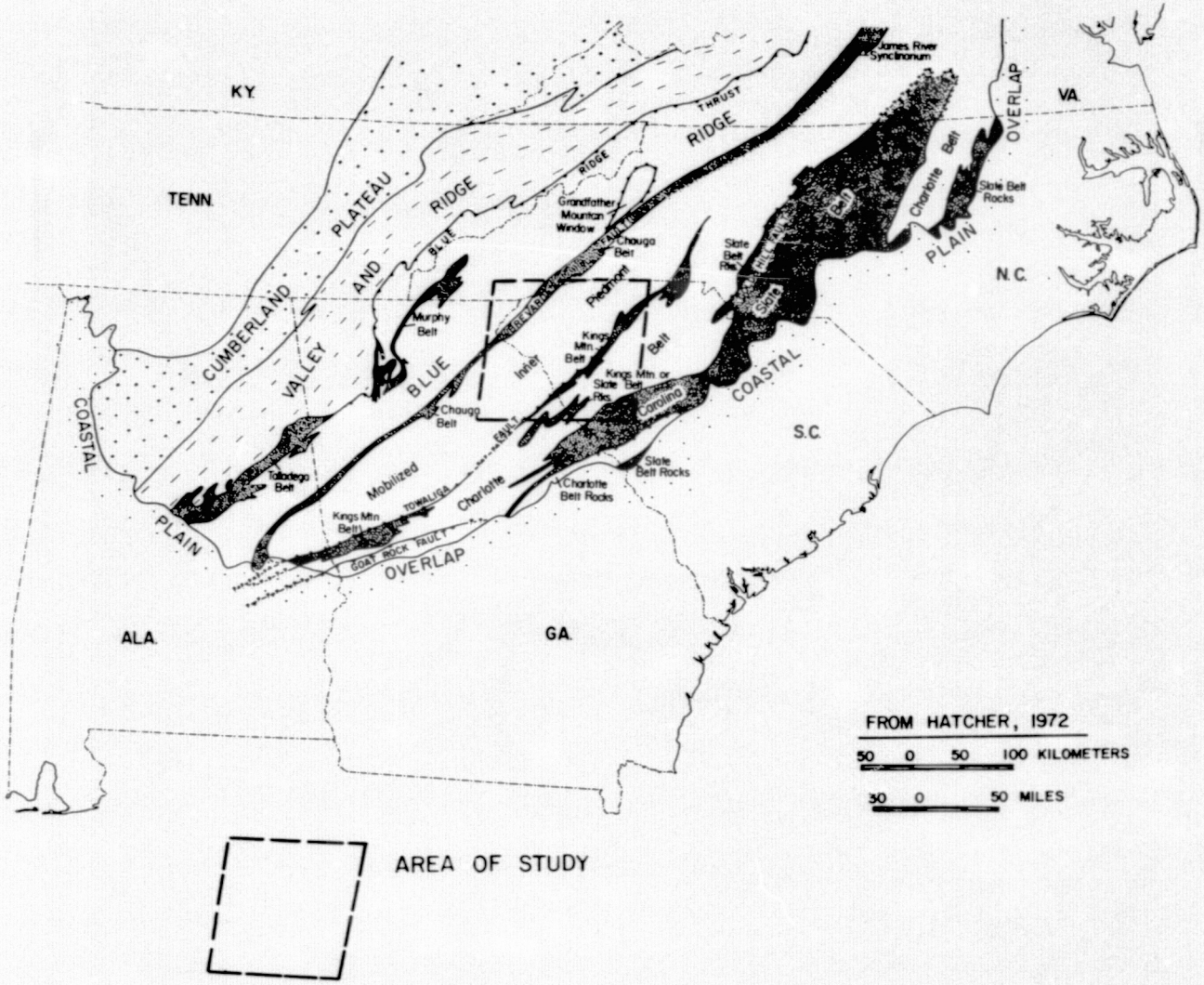


FIG. 12 GENERALIZED GEOLOGIC MAP OF SOUTHERN APPLACHIANS SHOWING AREA OF STUDY

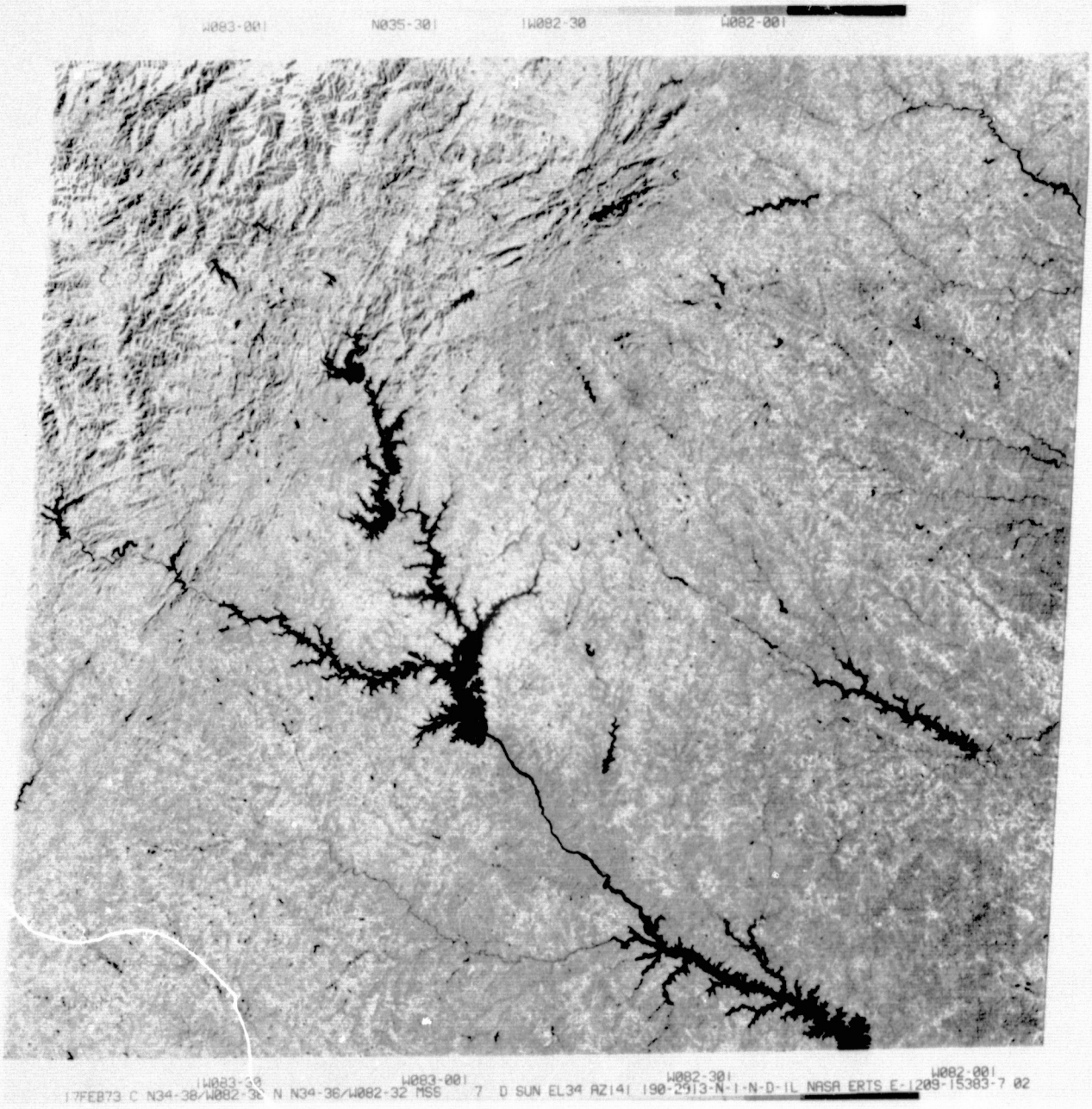


FIG. 13 LANDSAT IMAGERY OF THE PIEDMONT AND BLUE RIDGE PROVINCES OF SOUTH CAROLINA, NORTH CAROLINA AND GEORGIA

REPRODUCIBILITY OF THE ORIGINAL PAGE IS POOR

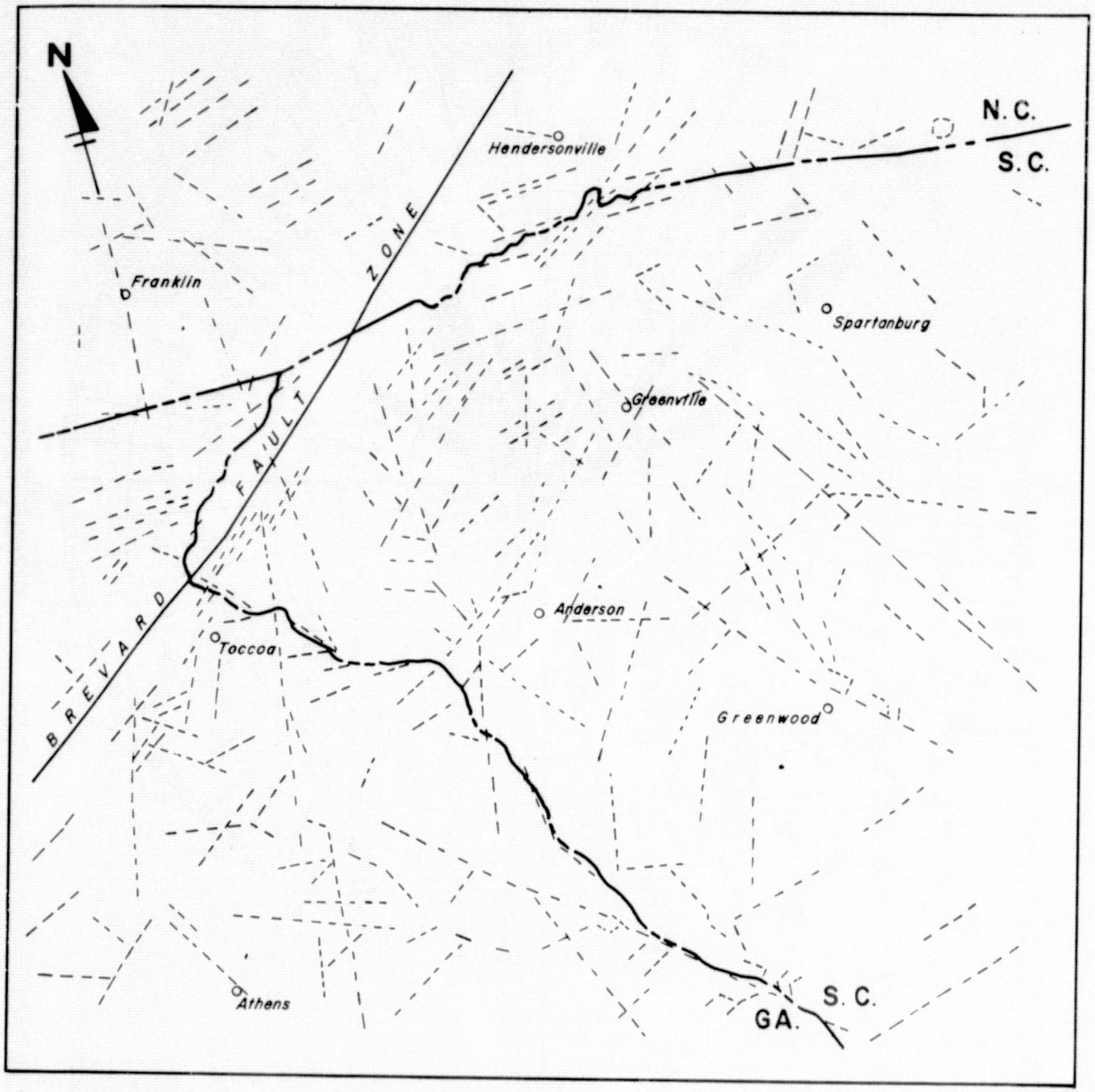
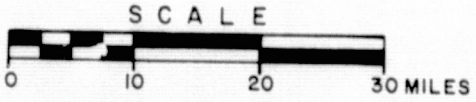
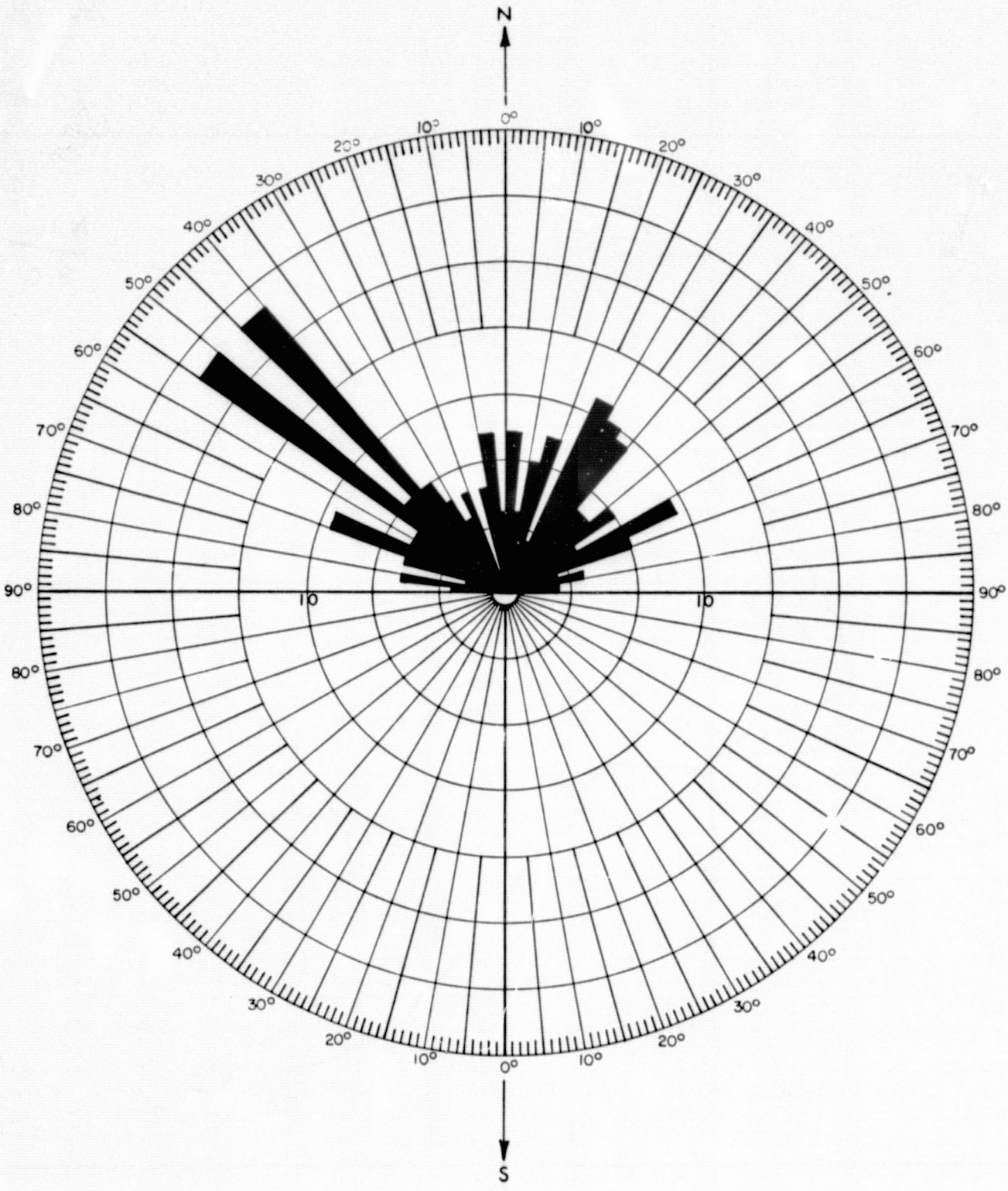


FIG. 14 MAP OF LINEAR FEATURES IN THE AREA OF FIGURE 13





178 LINEARS
LANDSAT PHOTO
PIEDMONT - ANDERSON
NORTH CAROLINA

FIG. 15 DIAGRAM SHOWING DISTRIBUTION OF LINEARS MAPPED FROM FIGURE 11

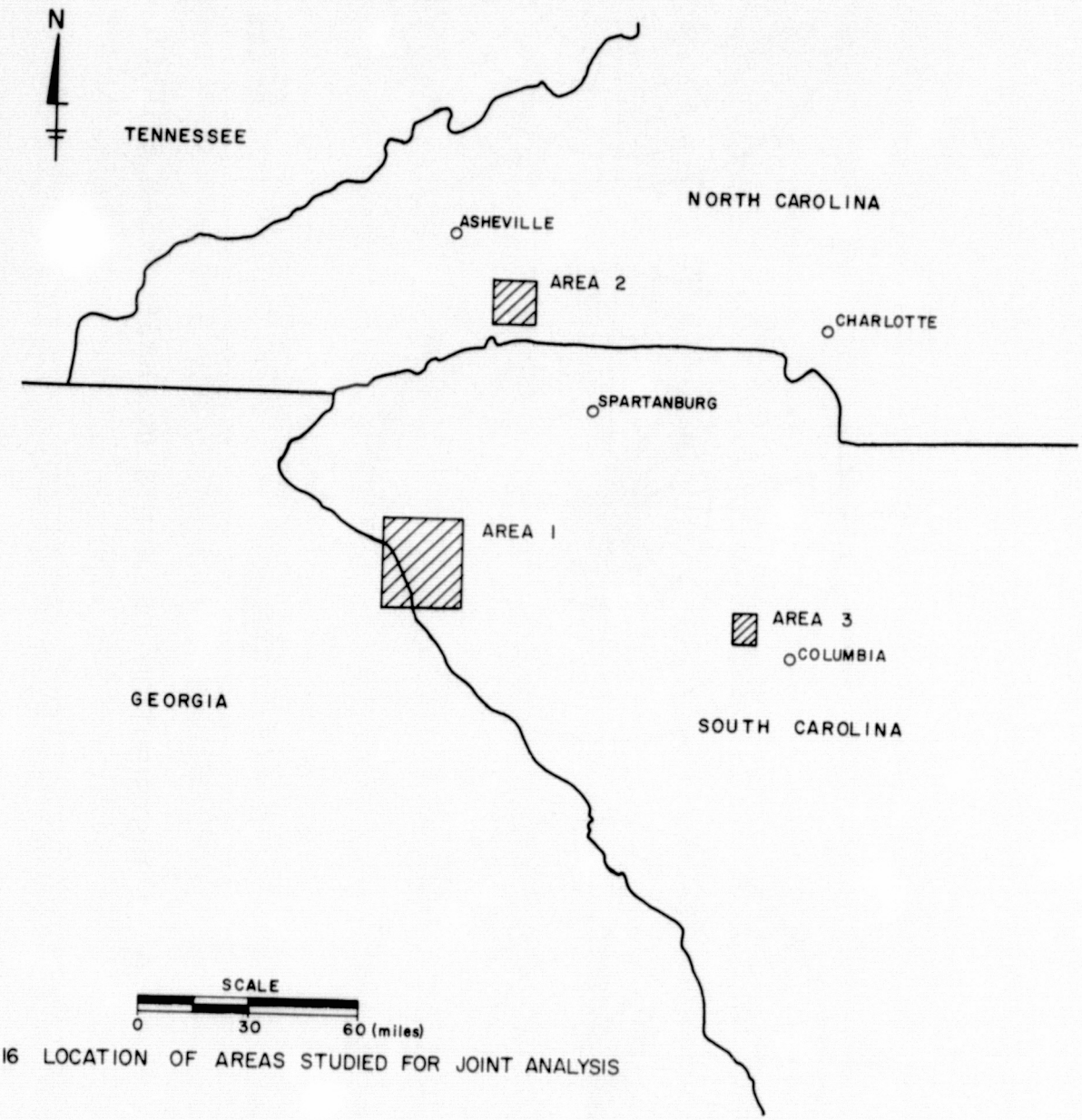


FIG. 16 LOCATION OF AREAS STUDIED FOR JOINT ANALYSIS

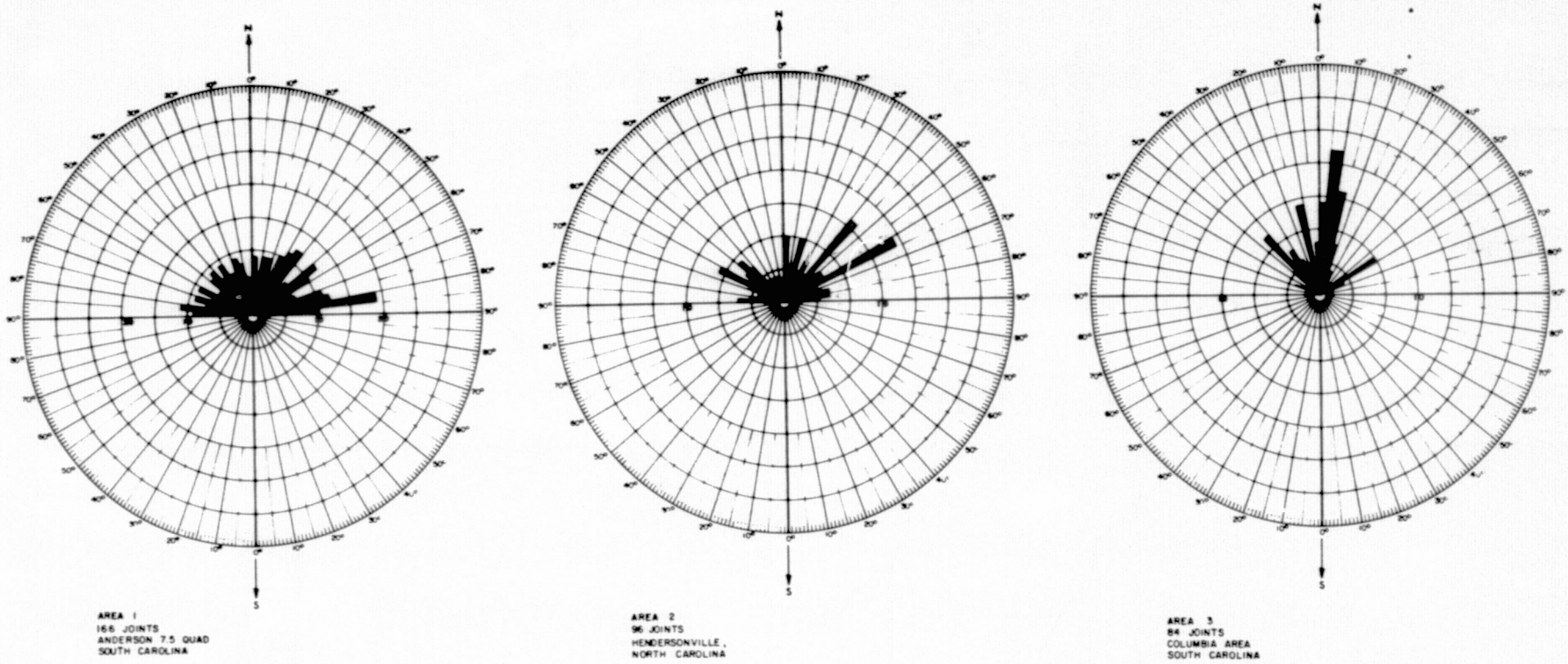


FIG. 17 DISTRIBUTION OF JOINTS IN THREE AREAS STUDIED

SMALL-SCALE IMAGERY: A USEFUL TOOL FOR MAPPING GEOLOGICAL FEATURES IN THE TEXAS GULF COASTAL PLAIN

N76-17513

David L. Amsbury
Principal Investigator Office, Earth Observations Division
Uel S. Clanton
Geology and Geophysics Branch, Lunar and Planetary Sciences Division
Von R. Frierson
Lockheed Electronics Corporation
NASA Johnson Space Center, Houston, TX 77058

ABSTRACT

Imagery taken from altitudes of 150 to 500 km with high-resolution cameras offers the exploration geologists a reconnaissance tool at a new scale and very reasonable costs. Most of the United States and portions of the rest of the world have been imaged recently by NASA spacecraft. In addition, large portions of the United States have been photographed by NASA aircraft from altitudes of 15 to 18 km.

A sample of this imagery includes photographs and multispectral scanner imagery from the Apollo, LANDSAT, and Skylab spacecraft over an area west of Houston, Texas. Large circular features and lineaments can readily be mapped. One of the circular features identified by drainage, vegetation, and soil-tone anomalies, occurs in Fort Bend County, Texas, and covers an area about 25 miles in diameter. Another circular feature lies to the north, immediately west of Houston, and is about 15 miles in diameter. These features may represent the surface expression of deeply-buried positive structures.

A photolinear expressed in drainage and vegetation patterns extends from Matagorda on the Gulf Coast toward the north along the Colorado, Brazos, and Navasota Rivers. This lineament and others possibly mark surface traces of old, deep-seated fractures that would extend approximately at right angles to the coastline and to mapped growth faults.

The geologic causes, if any, for the very large photo anomalies have not been determined, but similar, smaller photo anomalies can be identified as the surface traces of geological structures. Photolinears are readily mapped on small-scale, color-infrared, aerial photographs in the Houston area. Some of these linears coincide with surface traces of previously-known, active faults. Others coincide with faults mapped during this investigation.

A complex graben southeast of Houston, Texas, and 5 km north of the Johnson Space Center can be traced from the Friendswood-Webster oil field and Interstate Highway 45, eastward through Ellington Air Force Base, northeastward through a new residential subdivision, into the Clear Lake oil field, and on toward LaPorte, Texas, a distance of 20 km. Some of the faults in this graben system are known to have been active for decades and are represented by scarps several feet high in the deltaic deposits of the Pleistocene Beaumont formation. Another fault system appears to control the shoreline configuration of Clear Lake and the courses of streams tributary to the lake.

Explorationists should consider the advantages of synoptic imagery when studying well-developed areas as well as frontier areas. It might be very fruitful to reinterpret existing subsurface and geophysical data in the context of regional geological features that can be mapped using space imagery. In addition, this imagery is excellent for planning phases of exploitation, and will be indispensable in monitoring the environmental effects of man's exploitation of energy sources.

Introduction

The perspective from space provides a tool for a new insight into some regional geologic problems. Earth-orbiting satellites have been returning geologically-useful small-scale imagery for more than a decade (Short and Lowman, 1973; Amsbury, 1969). Most geologists agree that space photographs and high-altitude (10,000 m) aerial photographs are useful for geological reconnaisance in arid or unmapped portions of the world. However, a review of the available data indicates that small-scale imagery is not only useful but may be indispensable for gaining an understanding of the regional geology in any locality. As an example, analyses of space data have shown that some unknown or poorly-recognized linear and circular features exist even in the "mature petroleum province" of the Texas Gulf Coastal Plain. If these features are the surface traces of geological structures, a new interpretation of subsurface and geophysical data will be in order.

Regional geological studies, whether surface, subsurface or geophysical, should begin by using image analysis to map the surface geology, in the writers' opinion. It is important to obtain not only large-scale coverage of the specific area of interest but also small-scale coverage for a more regional overview. Although oil-well and water-well data may provide a great deal of detail, the information may apply only to a zone a few meters in diameter around the bore hole. Well control and geophysical survey lines are separated by hundreds of meters to many kilometers; an evaluation of surficial geology using photointerpretation techniques allows one to extrapolate subsurface data with more confidence. In addition, imagery may suggest the existence of geological features between subsurface and geophysical data points, areas that may hold a high potential for production.

Apollo Photography

A systematic effort was made during the Apollo 9 mission to photograph selected sites in the United States using a cluster of multiband cameras (Colwell, 1972). The four cameras contained color-infrared film, panchromatic film filtered to image the green band, panchromatic film filtered to image the red band, and black-and-white infrared film. In the southwestern United States, the red band appears to be the best for geological interpretation; for the Texas Gulf Coast, color-infrared and black-and-white infrared are more useful because of the greater tonal contrast between different types of vegetation and soils.

Figure 1 is a black-and-white infrared photograph from the Apollo 9 mission; figure 2 is a geological interpretation with geographic annotations. Large scale, circular-elliptical and linear features are visible on this photograph. The largest elliptical feature, partially outlined by the Brazos River, is the Ft. Bend Anomaly. Seven known salt domes occur around the periphery of this feature; Hickey, et al. (1972) suggest that this area is domed on a regional scale.

A north-south zone of photolinears is visible in figure 1; a comparison with figure 2 may aid in the interpretation. The linears show up as tonal variations which are caused primarily by differences in vegetation. The general trend of the major rivers on the Gulf Coast appears to be controlled by this linear pattern; figures 1 and 2 illustrate that the overall drainage pattern of the Brazos and Colorado Rivers coincide with the N-S and E-W linear systems. This linear pattern coincides with the western edge of the Houston Embayment Salt Basin and the eastern flank of the San Marcos Arch. The linears may represent surface traces of old, deep-seated structural systems. The E-W linears are aligned with the Wharton Fault as mapped at a scale of 1:1 million by Hickey, et al. (1972).

Skylab Photography

Figure 3 is a mosaic of three photographs that were taken with the S-190B camera (45-cm focal length lens) in January 1974, during the third manned Skylab mission. The tonal contrasts between different types of vegetation are less for color film than for infrared film; consequently some geological features are not enhanced by color film. However, the increased resolution of the S-190B camera system allows one to map short, straight stream segments as well as circular tonal anomalies (Figure 4). The straight stream segments may be controlled by a fracture-joint system or by faulting; some of the circular anomalies appear to be surface traces of salt domes or deep-seated, nonpiercement domes.

A multispectral, 70-mm camera system (S-190A) was also used to photograph the Earth during the Skylab missions. Figure 5 illustrates red-filtered panchromatic photographs, and figure 6 the near-infrared. Interpretations shown in figures 5 and 6 were made by the same interpreter; and although similar they are not identical. From experience, it is evident that no two interpreters will agree exactly on which features are significant. We recommend the use of interpretations such as these as guides to further work, not as depictions of the geology of an area.

Aerial Photography

Photographs from high-altitude aircraft form an important link between field observations, low-altitude photography and imagery from Earth-orbiting satellites. Large portions of the United States have been photographed from high-altitude (above 10,000 m) aircraft using color, color-infrared, and multiband black-and-white film at scales of 1:60,000, 1:120,000, and 1:400,000.

Figure 7 is an example of some of the color-infrared photography taken from an altitude of 20,000 m near Houston, Texas. Although the relief is low, stereoscopic viewing has been found to be an asset in interpreting the photographs. Some photolinears coincide with surface traces of active faults that were mapped by Van Siclen (1967), Sheets (1971), and Reid (1973). Field work by Clanton and Amsbury (1973, 1975) demonstrated that most of the photolinears have some surface expression either as a topographic scarp, vegetation boundary or soil boundary (figure 8). Figure 9 is a map of this area prepared by photointerpretation of high-altitude photographs and about 2 man-weeks of field checking. The solid lines indicate the location of photolinears associated with structural damage, e.g., the failure of streets, runways, and buildings (figure 10). The dashed lines indicate the location of photolinears associated with topographic scarps that are not associated with structural damage. Some of the dashed lines may represent active faults but because of the lack of structural damage, data are insufficient to prove it.

This study demonstrates that the use of high-altitude photographs can materially shorten the time required to investigate an area for geological information. Perhaps more importantly, photointerpretation may reveal some evidence that would otherwise be overlooked; field checking increases the level of confidence of the conclusions drawn from the photointerpretation.

Summary

All of the United States has been photographed at a scale of 1:60,000 to prepare the 1:250,000 Army Map Service topographic sheets; for many areas, multiple governmental and commercial coverage is available. Most of the continental United States has been imaged during different seasons by the multiband scanner on-board LANDSAT I or LANDSAT II, and has been photographed by high-resolution cameras on-board Skylab. NASA aircraft (RB-57 and U-2) have also photographed large areas using color, color-infrared, and multiband black-and-white film.

It is recommended that regional geological studies begin with photo-interpretations of high-altitude aircraft and synoptic space imagery. Space imagery provides the synoptic view of rapid evaluation of large-scale features, and, at enlarged scales, the resolution required for detailed study of selected areas or structures. The photointerpreter is also required to aid in synthesis of the surface and subsurface, and geophysical data, for two reasons: (1) a regional image analysis is the best and quickest way to learn the geography and geology of an area, and (2) there is a continual need for interaction between image analysis and the synthesis of surface, subsurface, and geophysical data.

REFERENCES CITED

Amsbury, D. L. 1969, Geological Comparision of Spacecraft and Aircraft Photographs of the Potrillo Mountains, New Mexico and the Franklin Mountains, Texas: Univ. Michigan, Proc. 6th Symp. on Remote Sensing of Env., p. 394-515.

Clanton, U. S., and Amsbury, D. L., 1975, Active Faults in Southeastern Harris County, Texas: Environmental Geology, in press.

Colwell, R. N., 1972, Monitoring Earth Resources from Aircraft and Spacecraft: NASA SP-275, U. S. Govt. Printing Office.

Hickey, H. N., et al., 1972, Tectonic Map of Gulf Coast Region USA: Am. Assoc. Petroleum Geologists, Tulsa, Oklahoma.

Reid, W. M., 1973, Active Faults in Houston, Texas: Dissertation, The University of Texas at Austin, Texas.

Sheets, M. M., 1971, Active Surface Faulting in the Houston Area, Texas: Houston Geol. Soc. Bull., vol. 13, p. 24-33.

Short, N. M., and Lowman, P. D., Jr., 1973, Earth Observations From Space: Outlook for the Geological Sciences: NASA Goddard Space Flight Center Document X-650-73-316.

Van Siclen, D.. 1967, The Houston Fault Problem: Proc. 3rd Annual Mtg., Texas Section Inst. Prof. Geol., p. 9-31.

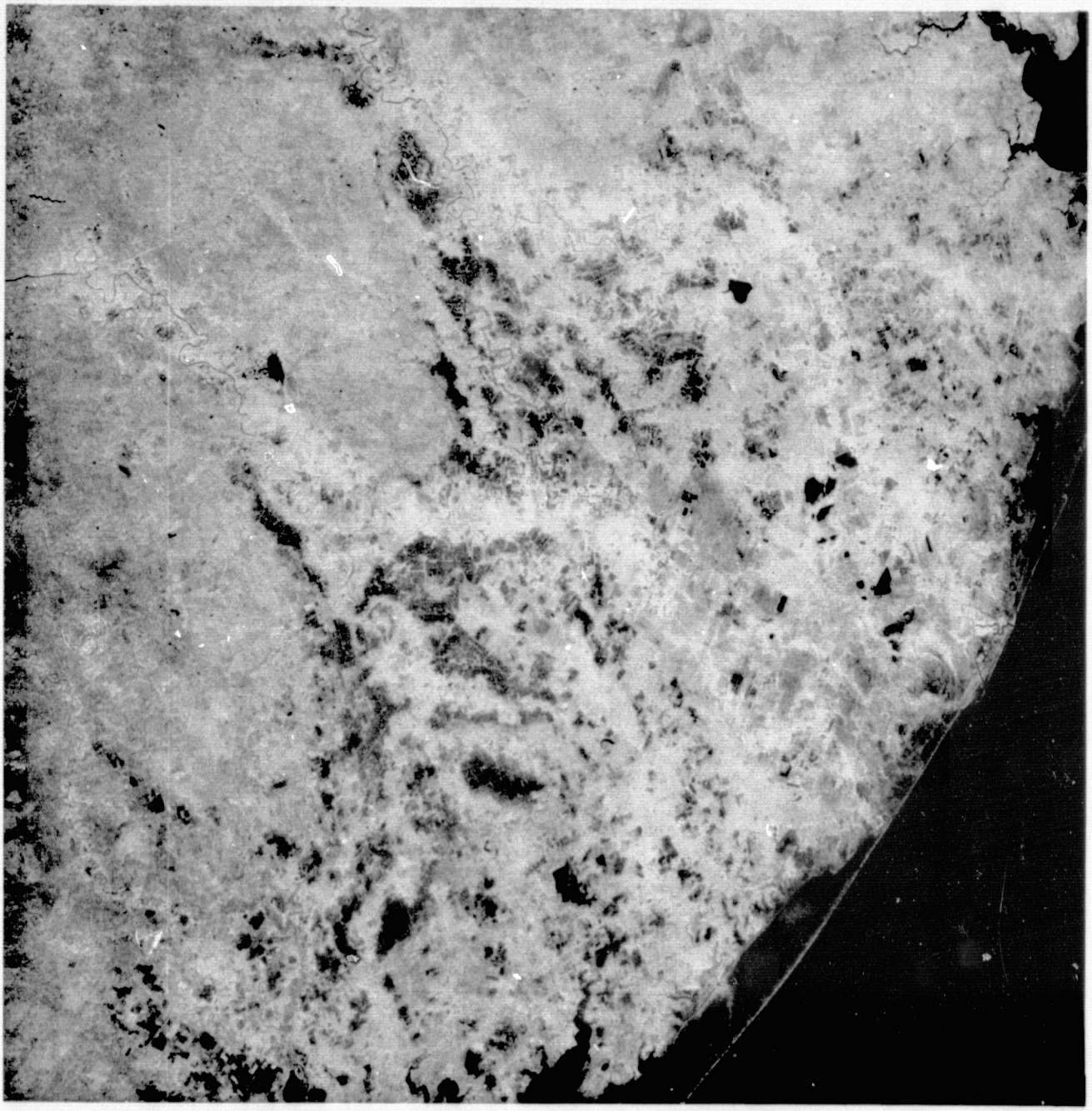


Figure 1: Black-and-white infrared photograph (AS9-26C-3727C) from the S-065 experiment on the Apollo 9 mission. The scale of the original negative is about 1:4,000,000; the area shown covers about 10,000 square miles of southeastern Texas.

REPRODUCIBILITY OF THE
ORIGINAL PAGE IS POOR

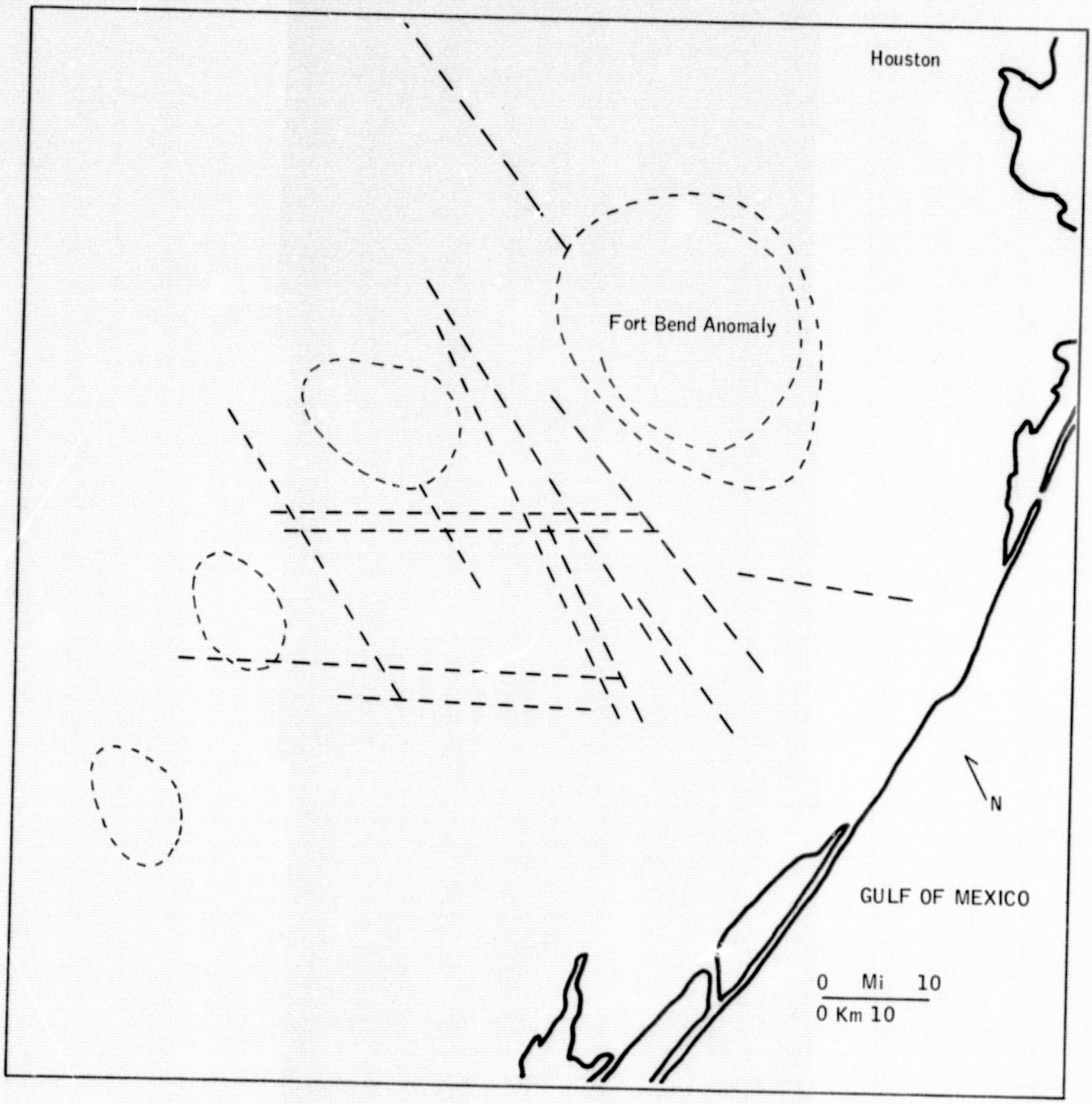


Figure 2: Sketch map of figure 1 showing geographic features, photolinears, and elliptical drainage and tonal anomalies.

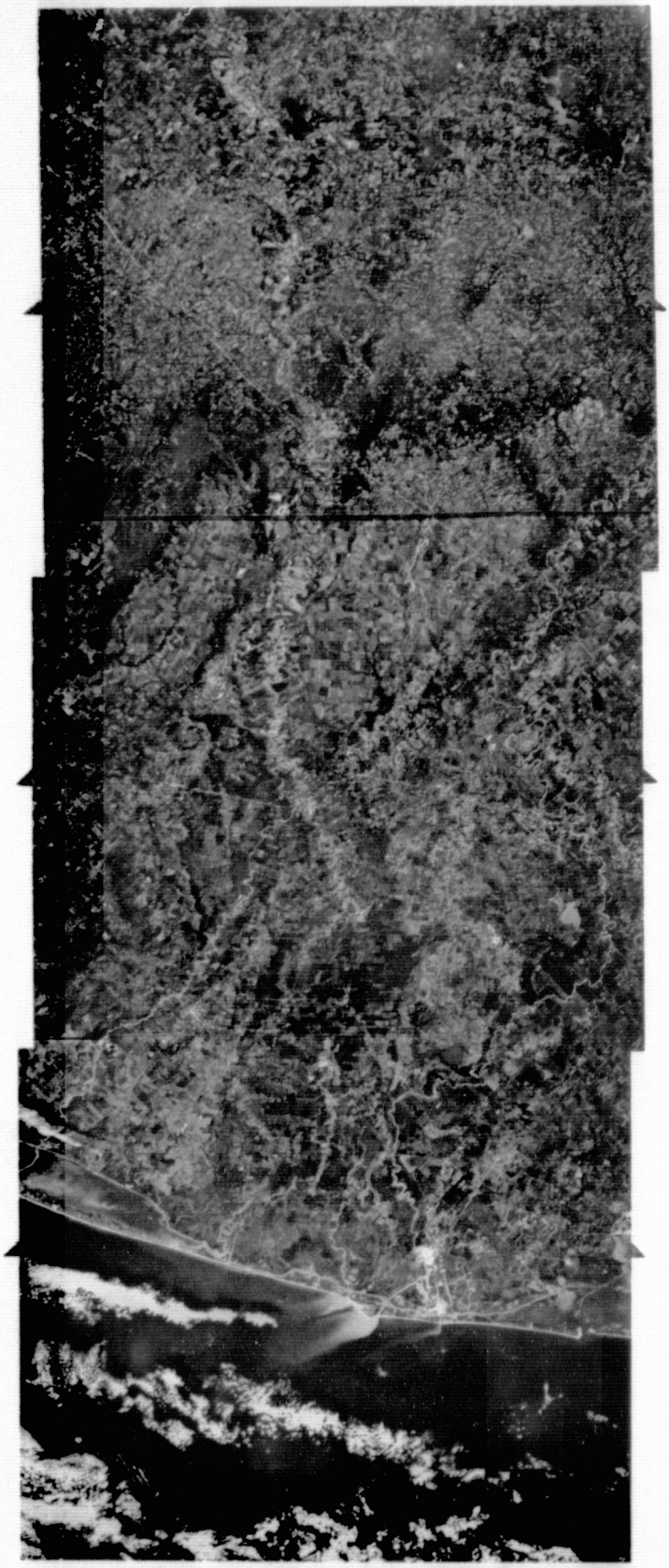


Figure 3: Print from an original color-transparency taken during the Skylab 4 mission (SL-4-94-126, -128, and -130). The scale of the original is about 1:1,000,000.

REPRODUCIBILITY OF THE
ORIGINAL PAGE IS POOR

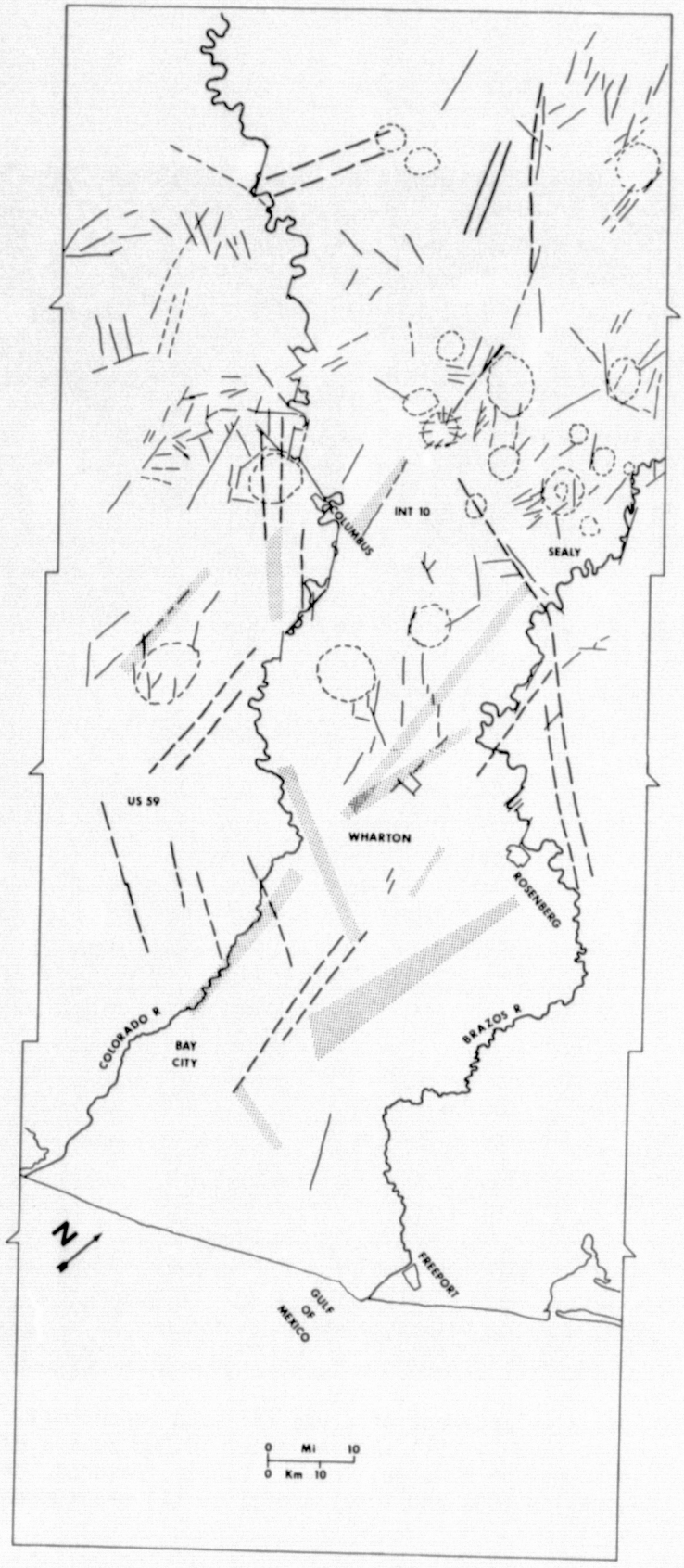
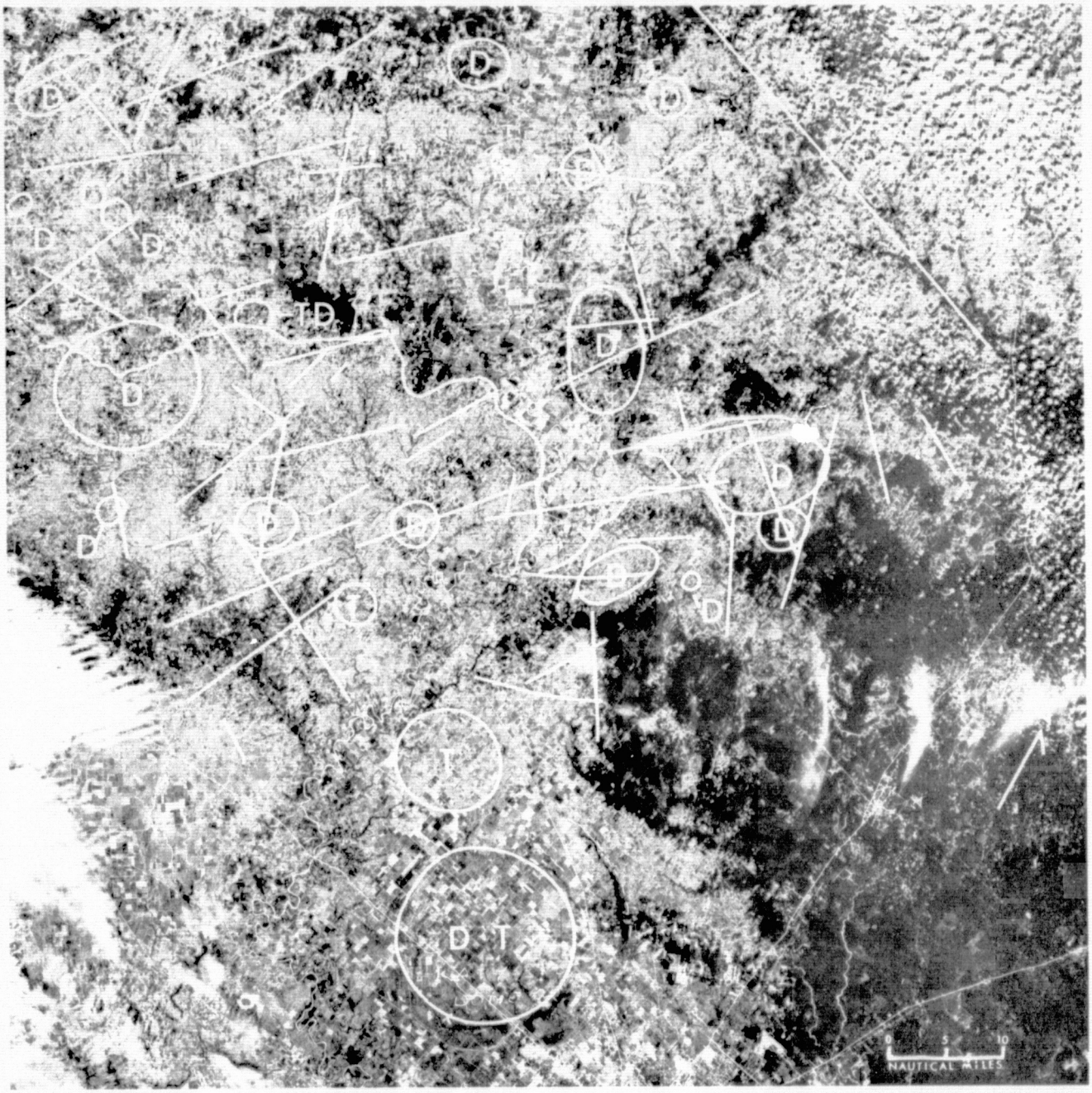


Figure 4: Sketch map of figure 3 showing linear zones (pattern), straight stream segments, and elliptical anomalies.


D
D
D

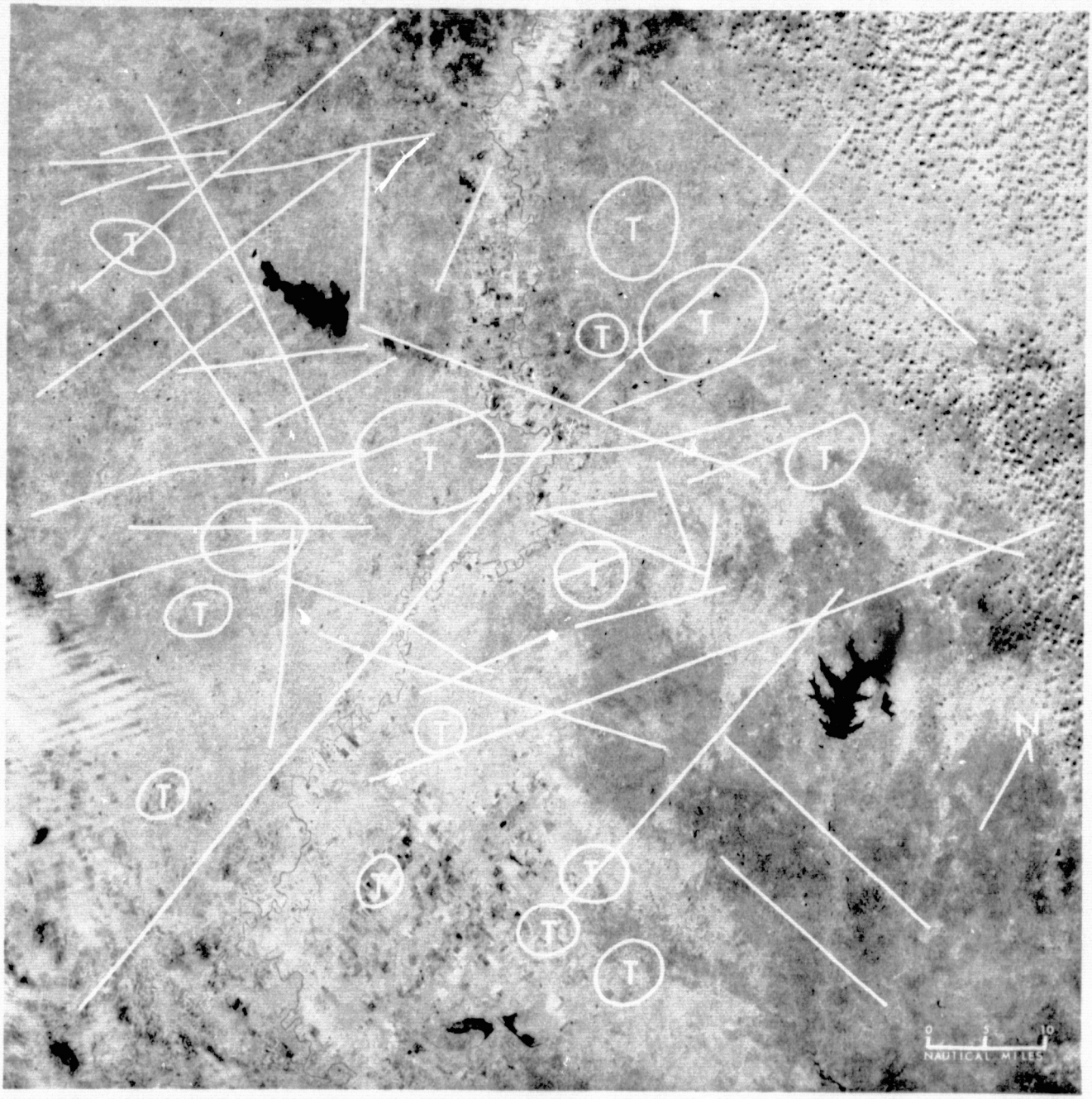


Figure 6: Four X enlargement of an infrared-filtered black-and-white photograph (SL3-38-291) taken at the same time as figure 5, with an interpretation of photo anomalies.

REPRODUCIBILITY OF THE
ORIGINAL PAGE IS POOR



Figure 7: Contact print from a positive transparency, color infrared film, of frame 148, roll 69, RB-57F Mission 145 on November 3, 1970. The scale of the original is 1:120,000; the area shown covers about 68 square miles.

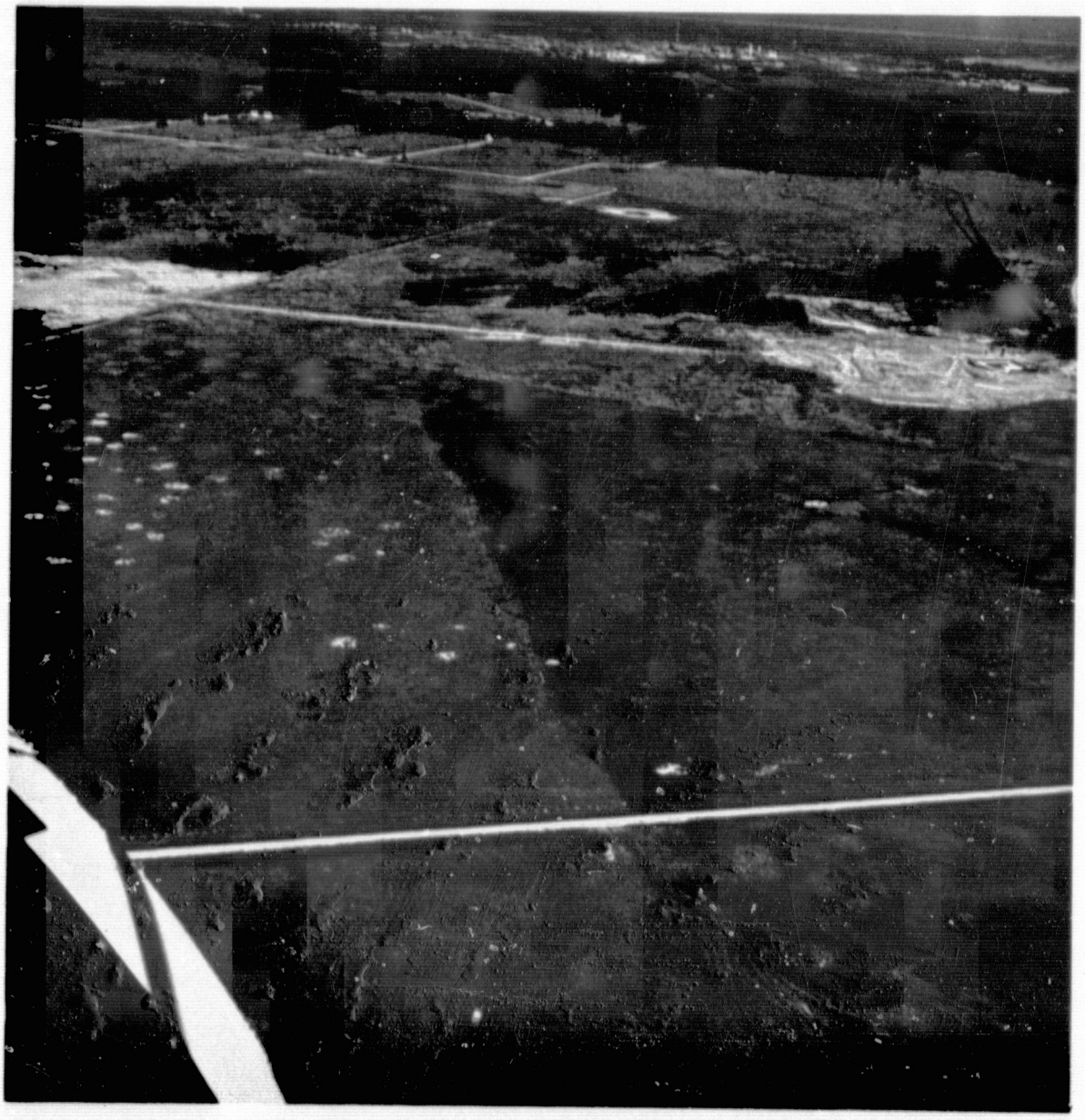


Figure 8: Print from a color infrared transparency taken from an altitude of about 300 m. The upthrown side of the fault is typically lighter in color. The more luxuriant vegetation, wet ground and occasional sag pond give the downthrown side a darker color. The abrupt "termination" at the fence line is an illusion caused by a difference in land use; the fault can be traced for another kilometer.

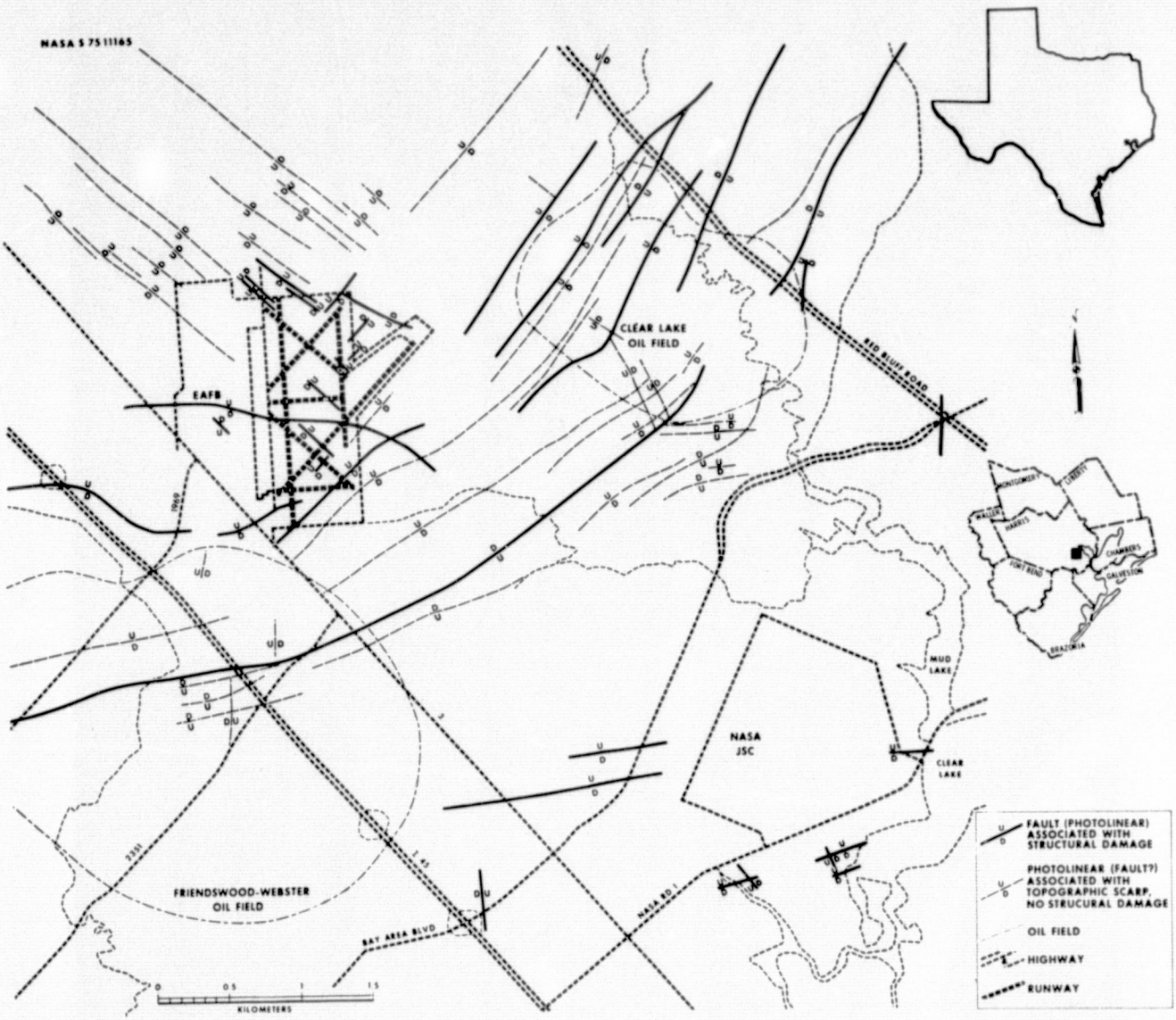


Figure 9: Map of the Ellington Air Force Base - NASA Johnson Space Center, showing active faults (heavy lines) and photo-linears having topographic expression (light dashed lines). This map was prepared as an overlay on color-infrared photographs whose original scale was 1:60,000, enlarged to 1:20,000 scale.

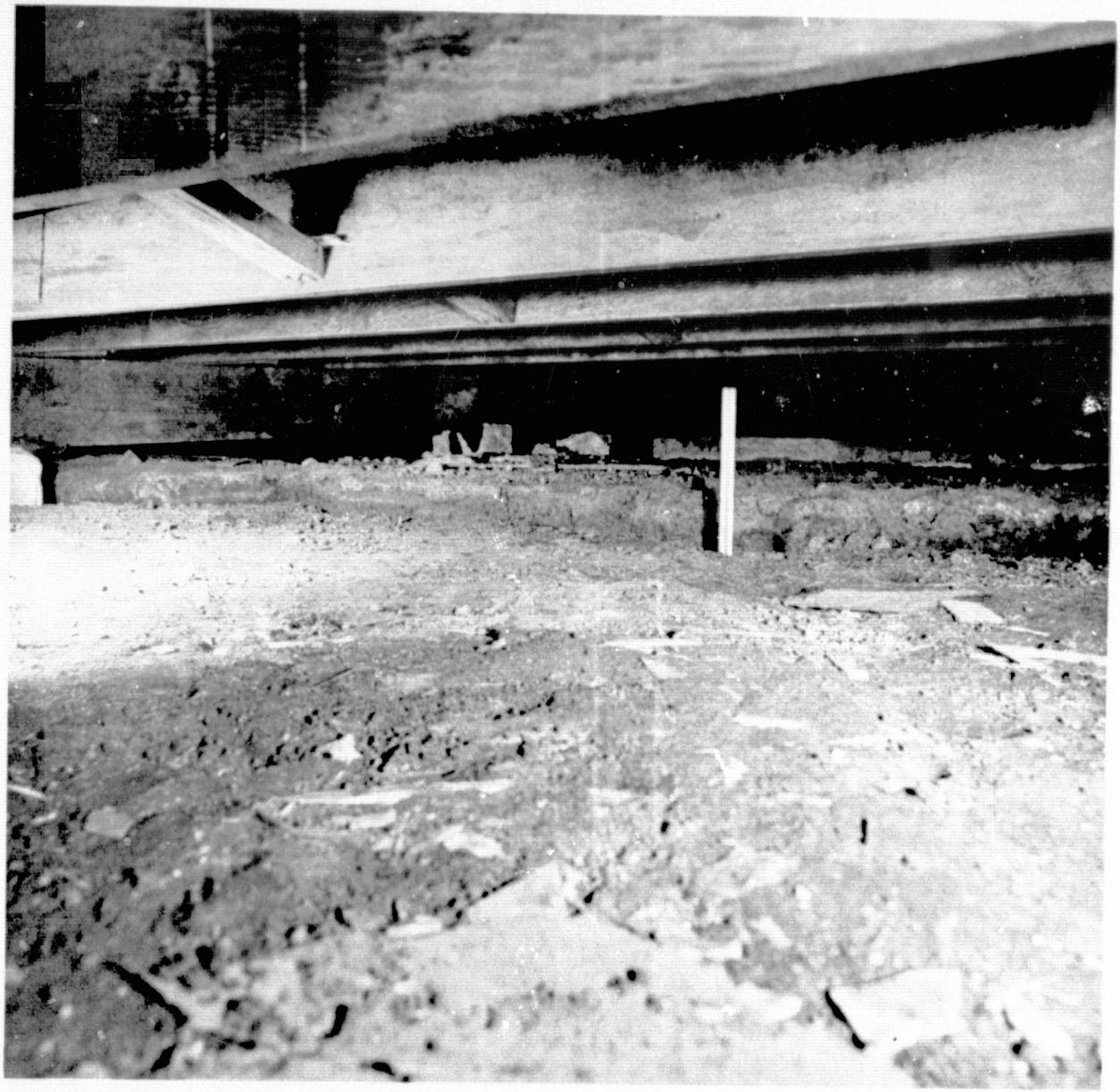


Figure 10: Open fracture protected from erosion and slumping by a building at Ellington Air Force Base. About 0.5 m of movement on this fault is visible as a topographic fault, with about 0.2 m of movement since the building was constructed in the early 1940's.

APPLICATION OF SKYLAB IMAGERY TO SOME GEOLOGICAL AND ENVIRONMENTAL PROBLEMS IN ITALY

By R. Cassinis, G. M. Lechi, and A. M. Tonelli,
Laboratorio per la Geofisica della Litosfera-C.N.R.,
Via Mario Bianco, 9 Milan, Italy

N76-17514

ABSTRACT

This paper summarizes the results obtained from various studies of geology and the environment in Italy. Four topics are considered: regional geology of Sicily, volcanic surveillance in southern Italy, hydrogeology (with special regard given to the discovery and mapping of paleoriverbeds) and crop investigation. Although some aspects of research are not yet complete, the first results are very promising. The discovery of unknown lineaments and structures in Sicily will contribute to the geological knowledge of this region and in particular to the mechanical phenomena involving the upper part of the crust.

An attempt was made to relate the status of vegetation surrounding Etna volcano to the magmatic gas escapes filtering through the soil. False-color Skylab images were used to analyze the vigor of the Etnean forestal belt vegetation canopy in order to map possible gas-vent ways as well as the "active" microfractures.

In northern Italy, buried channels were mapped in the Venetian Plain, and a tentative cost-benefit evaluation has been done in the field of vegetational studies, both disease detection and species inventory have been performed in the Po River Delta and in northwestern Italy.

INTRODUCTION

LANDSAT-1 and Skylab (SL-3) multispectral imagery has been applied to areas of geological and environmental interest in Italy. The main test site for experimental investigation was the Island of Sicily, where both regional geology and the volcanic environment of Mount Etna were studied.

REGIONAL GEOLOGY OF SICILY

The regional linears and the main geological features observed by the space platforms were compared with the known structures. Ground and airborne truth was used to check the potential of space imagery and to explain the new features. According to the plate tectonics theory, Sicily is a marginal part of the African plate. Only the southeastern Ragusa carbonatic platform seems to be an undisturbed portion of the Continental plate, whereas the northern belt is a folding system produced by the overthrusting along the margin. The central part and, to some extent, the western part, are subsidence areas filled by a variable thickness (as much as 10 kilometers in the center) of resedimentation material (flysch) of different lithology deposited by submarine slides coming from the northeast primarily during the

PRECEDING PAGE BLANK NOT FILMED

Miocene Epoch. Because of the lithology (plastic shales) and the chaotic deposition, long fracture lines are not present in the central part of the island, although there are many reported faults which have been determined by surface geology and by geophysical methods on the regions where "rigid" formations outcrop. The physiographic subdivisions of Sicily are clearly shown by LANDSAT-1 original imagery (band 7) or by a false-color composite of two or three bands. The composition of bands 4, 5, and 7 (November, 1972) gave the best single account because of the seasonal illumination and weather conditions. Many new lineaments, some of which cross the entire island, were observed.

The SL-3 imagery (September, 1973) gave little information about this field. Shown in figure 1 is an enhancement: the false-color density slicing of the ratio of LANDSAT bands 7 and 5. This image represents quite clearly the main soil classes and, owing to the strict dependence of vegetation on lithology, is similar to a geological map. In figure 2, the linears observed on the LANDSAT imagery and the gravity (Bouguer) anomalies were plotted. The number of linears discovered is equal to or smaller than the known faults on rigid formation exposures (Ragusan southeastern carbonatic horst, northern belt, Peloritani Mountains). Conversely, in central area (Mio-Pliocenic Basin), where the outcropping formations are mainly plastic, the new linears greatly outnumber the known ones. At the same time, one can see that on rigid formations, the continuity of the linears is high, but their total length is generally not very large. The linears appear as very sharp cuts. In the central basin, the appearance of linears is broader and the continuity lower, but the total length is generally greater. Rose diagrams show that the main trends are remarkably different in the southeastern plateau and in central Sicily.

An attempt was made to compare the linears with the seismicity (figure 3). Although the epicenters are plotted with very low accuracy (± kilometers), their pattern suggests active lines in north-northeast and northeast directions rather than along the Tyrrenian and Ionian coasts as generally believed. A detailed analysis of a group of lineaments in Central Sicily was carried out using a strip of stereopairs for comparison. The original scale of the aerial survey (figure 4) was 1:33,000; the results of space imagery were plotted in 1:250,000 scale. The known faults are indicated on the map. In figure 5, the linears found on all available space images are plotted using several band combinations. The corresponding rose diagrams show substantial agreement, but the map derived from the space images looks "filtered" and, therefore, contains only regional information. In figure 6, only the linears which were observed in all images (LANDSAT, SL-3) and band combinations are shown. The lineaments observed in central Sicily, crossing the subsidence basin, appear to be produced by the correlation of straight fragments generally of morphological origin (drainage pattern, lithological contacts, fragments of rigid material floating on the plastic chaotic shales). These fragments (Pliocene sand, gypsum, or limestone of the evaporitic formations) appear to be aligned along the linears, owing to the synopsis of the space observation. These remarks seem to suggest that the long lineaments crossing the island are of different origin than the shorter and sharper linears on rigid formations. The latter frequently corresponds to actual fracturing reaching the surface and are enhanced by the effect of the erosion; the former can be indicators of very deep movements. Because the lineaments cross formations of different ages and lithology, it seems that they could correspond to very recent, if not present, stress. Further ground and geophysical investigation is required to understand the direction and the amount of the stress.

The pattern of morphology seen on the LANDSAT imagery (figure 7) would suggest a transcurrency. A more detailed study was made on a relatively short linear

discovered on the product of bands 5 and 7. This linear was found to correspond to a fault found several years ago by a seismic reflection survey for the sulphur-bearing limestone of upper Miocene (figure 8). In figure 9, the results of some seismic line crossing the shallow fault is shown. The airborne and ground survey showed that the linear is probably enhanced by morphological and lithological factors. This result demonstrates that a careful examination of space images also can be effectively used to plan detailed ground geophysical surveys.

VOLCANIC SURVEILLANCE

In the domain of active-volcano surveillance, Skylab imagery was used to build a map of fractures on the lava blanket of Mount Etna. The map was based mainly on the false-color infrared frame and was integrated by IR false-color airborne photographs. The fracture length ranges from 100 to 2000 meters. An attempt also has been made to study the correlation between side eruptions on the slope of the volcano and the nodal points of fractures.

Another possible study concerns forecasting side eruptions at lower elevations along the slope of the cone where a vegetation blanket covers the lavas. Such a study would investigate the anomalies in the status of vegetation produced by volcanic gases escaping from lava fractures. The working hypothesis consists of considering plants as an integrative system and of changing the spectral response (output) of their leaves with the accumulation of the chemical effect of gases. The examination of the Skylab images taken over Sicily in September 1973 leads to the conclusion that a reflectivity variation occurs in the conifer belt, where four months later, the paroxysmal phenomenon took place. Fractures can also be classified from the behavior of the vegetation canopy; in fact, where the so-called "active fractures" occur, an escape of volcanic gases can be localized. Although some correlation was found, a direct approach to the forecasting is not yet possible. Nevertheless, this trend in the field of volcanic surveillance appears to be very promising and the airborne and ground surveys will continue.

HYDROGEOLOGY

Another application of Skylab imagery was made in the field of hydrogeology; this application concerned surveys of building material in the Venetian Plain in northern Italy. Different treatments were applied to the multispectral images to extract the surficial features of some paleoriverbeds and to determine the position and extension of the so-called "freshwater-spring line." For the first problem (paleoriverbeds), the employed criterion was to increase the contrast between the different soils with special regard to the moisture content. The ratio of bands seems to be the best means of emphasizing this difference; in fact, in such a manner it is possible to dispose of the relative reflection of one band as compared to another. With suitable ground truth, it was possible to classify different kinds of soil and vegetation. To determine the pattern of the paleoriverbeds in the Venetian Plain, the most useful band ratio was red/orange. The additive synthesis (false-color composition) was also useful as well as the product of bands. The product was employed particularly for emphasis of the freshwater-spring line. The results of this research include the discovery of several unknown buried channels and the actual pattern and continuity of the ones only partly mapped. The cost-benefit ratio in this case is very low because, with just one image, it is possible to discover a great volume of building material.

In figure 10, the map of buried channels is shown after the photo-geological and geophysical surveys; in figure 11, the map of buried channels is shown after the Skylab space imagery. Resistivity profiles and boreholes give a clear account of the ground and underground truth. In this case, a rough evaluation of the benefits of remote sensing from space platforms is already possible. To follow the patterns of the buried channels and to calculate the gravel and sand volume, it would be necessary to establish a network of electrical resistivity profiles having a density of at least 10 per square kilometer; one or two boreholes per square kilometer also are needed. The cost of these operations is about $500/km^2$. Using the space imagery, the ground control can be reduced at least to one-tenth. Long-term benefits include the possibility of managing the aquifers to avoid the pollution of underground water.

CROP INVESTIGATION

A valuable application of remote sensing techniques was provided in Italy in 1974 in the area of crop analysis. Some of the results obtained are discussed in the following paragraphs.

a) Rice inventory. In the area of the Po River Delta a satisfactory correlation has been found between the official maps of the rice fields and the same cultivations observed from the Skylab platform. Analog techniques were employed for this investigation because of low cost, quick response, and sufficient accuracy. During the phase of analog treatment, some difficulties arose when separating the signature of rice from that of alfalfa by means of the ratio of contiguous bands. For the purpose of rice inventory, the best method is to compare surveys performed in June and July by employing the multispectral combination 5 + 7 (LANDSAT code). It is possible in these two seasons to dispose of two very different ground situations, bare soil and irrigated soil; the fields thus affected are easy to detect and to map.

b) Relationship between the vegetative growth (biomass) and production of rice. It seems possible to correlate the evaluation of the spectral signature with time; thus, the biomass (which is proportional to the volume of yield) can be predicted one month, or earlier, before the maturation time. For this purpose, an Exotech radiometer ranging in the 4 LANDSAT bands was employed from a high position, and 10 different rice fields were surveyed regularly each week from May through October. The evaluation of the ratio 5/7 bands with the time seems to be the parameter which best describes the real canopy's biomass. The biomass is strictly related to the total yield, so the total yield was controlled through the 5/7 ratio (in the frame of AGRESTE project).

c) Poplar plantations. Now under investigation is the possibility of using satellite images to map the areas of poplar plantations. Although previous mapping has been accomplished by aircraft survey, in the near future, it will be attempted by satellite. The experiments conducted thus far indicate very promising results.

REFERENCES

Cassinis, R.; Lechi, G. M.; and Tonelli, A. M. (1974): "Contribution of space platforms to the ground and airborne remote sensing programme over the Italian active volcanoes," Symposium on European Resources Satellite Experiments, Frascati.

Cassinis, R.; Marino, C. M.; and Tonelli, A. M. (1971): "Evaluation of thermal I. R. imagery on Italian volcanic areas. Ground and airborne surveys," Proceedings of the Seventh International Symposium on Remote Sensing of Environment. Ann Arbor, Michigan.

Cassinis, R.; Marino, C. M.; and Tonelli, A. M. (1970): "Ground and airborne thermal imagery on Italian Volcanic areas," U.N. Symposium on the Development and Utilization of Geothermal Resources, Pisa. Geothermics, Vol. 2, Part 1, Special Issue 2.

De Carolis, C.; and Lechi, G. M. (1974): "Rilievi da terra e dall'aereo nell'infrarosso fotografico e termico su campi di riso affetti da 'giallume'," Il Riso, N. I. Anno XXIII.

Lechi, G. M. (1973): "Potenza irradiata da una pianura coltivata e da un centro abitato adiacente: confronto fra le fisionomie termiche dei due sistemi," Bollettino di Geofisica Teorica ed Applicata, Vol. XV, N. 58.

Lechi, G. M. (1975): "Problemi connessi con le immagini da telesensori: le derivate e gli integrali approssimati," Proceedings of XV Convegno Internazionale Tecnico Scientifico sullo Spazio, Roma, 17-20 March 1975.

Lechi, G. M. (1974): "Tecniche di elaborazione analogica applicate allo studio di immagini multispettrali," Associazione Elettrotecnica ed Elettronica Italiana.

Lechi, G. M.; and De Caroli, C. (1974): "Rilievi da terra e dall'aereo nell' infrarosso fotografico e termico su campi di riso affetti da 'giallume'," Il Riso. N.2. Anno XXIII.

Lechi, G. M.; Marino, C. M.; and Tonelli, A. M. (1974): "Analog techniques of data enhancement applied in the study of geologic and geothermal features of test-sites in the Italian region (Central Alps and Volcanic areas) illustrated by the images from ERTS-1 and other remote sensing platforms," Symposium held at Banff, Alberta, 7-11 October 1974.

Lechi, G. M.; Marino, C. M.; and Tonelli, A. M. (1972): "Geological applications of remote sensing surveys in Italy with special reference to their utilization on the volcanic areas," Proceedings of 24th International Geological Congress. Ottawa, Section 9. Canada.

Lechi, G. M.; and Tonelli, A. M. (1974): "Rilevamenti sulle aree vulcaniche del Sud-Italia per mezzo di scanners aerotrasportati operanti nell'infrarosso termico: confronto tra i diversi rilievi effettuati e possibilita future offerte dalle piattaforme spaziali," Proceedings of XIV Convegno Internazionale Tecnico-Scientifico sullo Spazio. Roma, Italy.

Lo Giudice, E.; Marino, C. M.; and Tonelli, A. M. (1974): "Le Tecniche di

ripresa all'infrarosso termico applicate ai rilievi aerei dell'Isola di Vulcano. Analisi dei risultati in rapporto alla situazione geovulcanologica locale," In press in Bollettino di Geofisica Teorica ed Applicata, Triestse

Lo Giudice, E.; Marino, C. M.; and Tonelli, A. M. (1974): "Lo studio delle aree vulcaniche con la metodologia del remote sensing: rilievi all d'infrarosso termico," Bollettino di Geofisica Teorica ed Applicata, Vol. XVI, N. 64, Trieste.

Marcolongo, B.; Lechi, G. M.; and Tonelli, A. M. (1974): Applicazioni delle immagini multispettrali da satellite alla individuazione di materiali da costruzione nella Pianura Veneta," In press in the Proceedings of I Covegno Internazionale sulla Coltivazione di Pietre e Minerali Litoidi. Associazione Mineraria Subalpina. Torino, Italy.

Marino, C. M. (1975): "Applicazione delle teleosservazioni (I.R. termico e riprese multispettrali) nel campo delle risorse idriche in Italia," Proceedings of XV Convegno Internazionale Tecnico Scientifico sullo Spazio, Roma, 17-20 March 1975.

Tonelli, A. M. (1975): "Contribution of ERTS-1 and SKYLAB missions to regional studies in Italy," In press in Proceedings of British Interplanetary Society, April 1975, London.

Tonelli, A. M. (1975): "L'impiego dei metodi di teleosservazione per l'analisi di fenomeni non esclusivamente superficiali," Proceedings of XV Convegno Internazionale Tecnico Scientifico sullo Spazio, Roma, 17-2 March 1975.

Tonnelli, A. M. (1972): "Termografie all'infrarosso da stazioni da terra e dall'aereo," La Ricerca Scientifica. N.83 Special Issue on Philegrean Bradisism. Consiglio Nazionale delle Ricerche.

Tonelli, A. M. (1974): "Trattamento analogico di informazioni provenienti da telesensori termici," Associazione Elettrotecnica ed Elettronica Italiana.

Tonelli, A. M.; Carli, L.; Ferretti, O.; and Nicolli, C. (1974): "Applicazione del 'Remote Sensing' in alcune zone agricole del Trentino-Alto Adige," Economia Trentina. N.I. Trento, Italy.

Figure 1.- False-color enhancement of LANDSAT imagery of the island of Sicily.

REPRODUCIBILITY OF THE ORIGINAL PAGE IS POOR

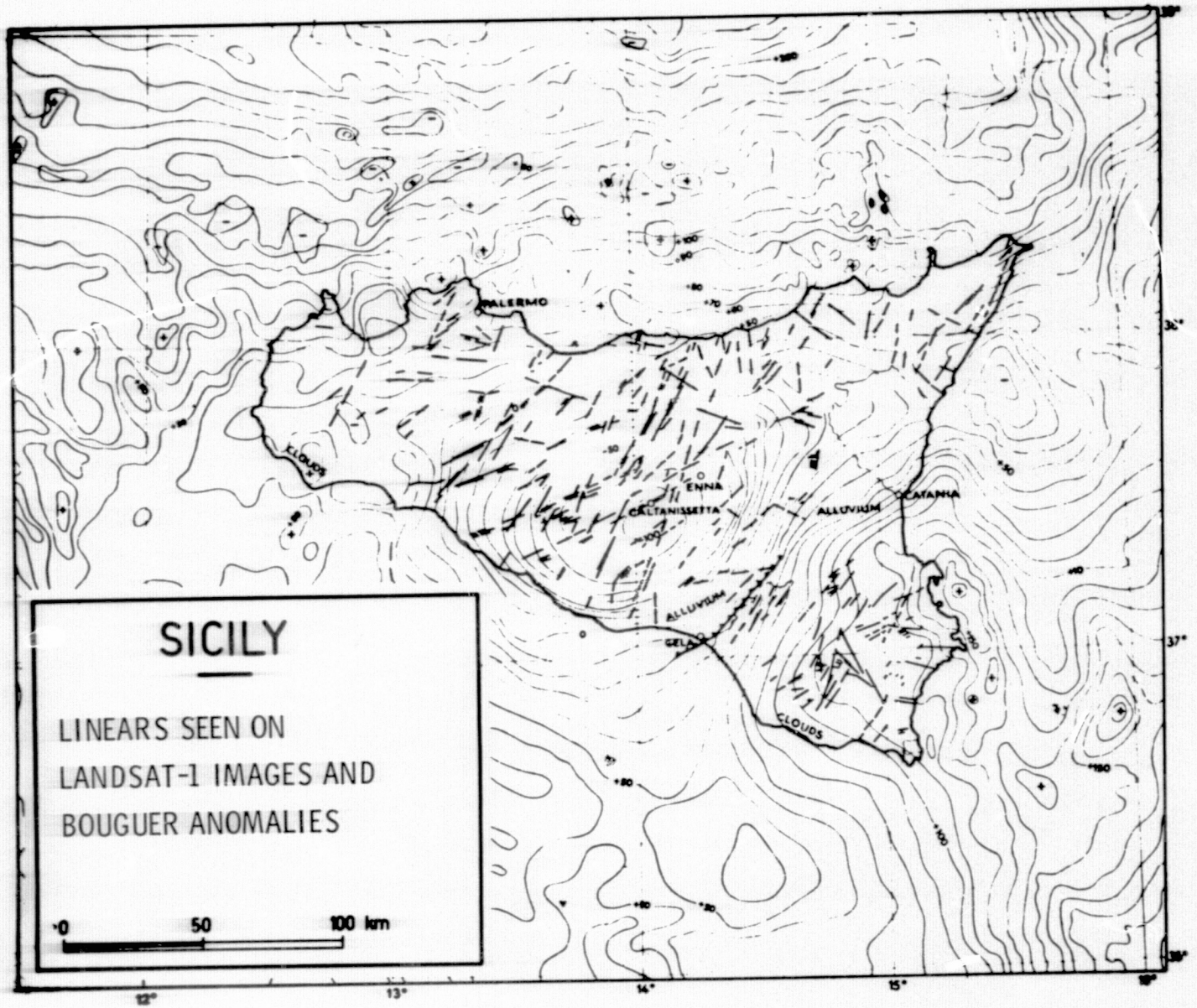


Figure 2.- Linears on Sicily plotted from both LANDSAT imagery and gravity anomalies.

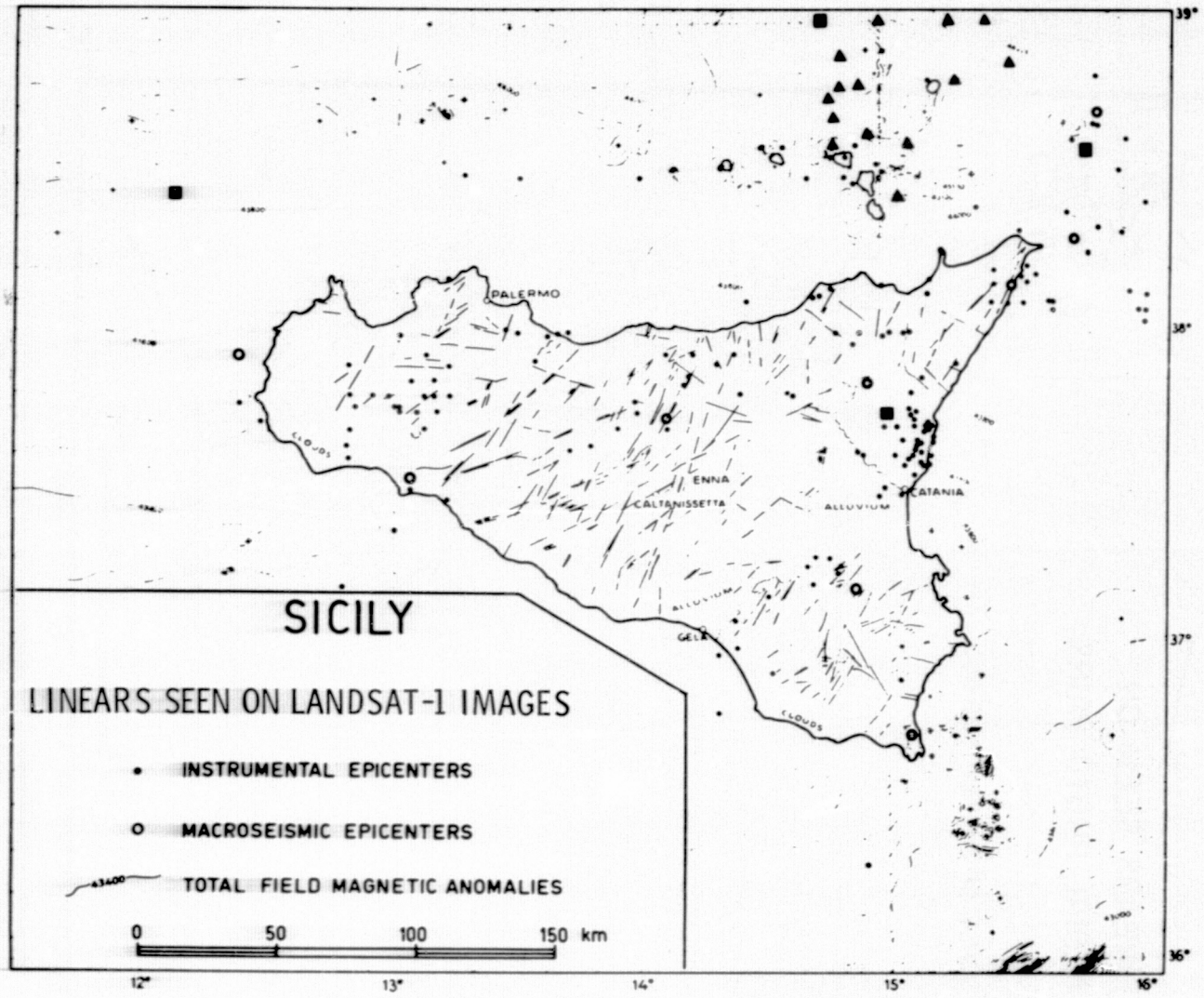


Figure 3.- LANDSAT linears on Sicily compared to seismicity.

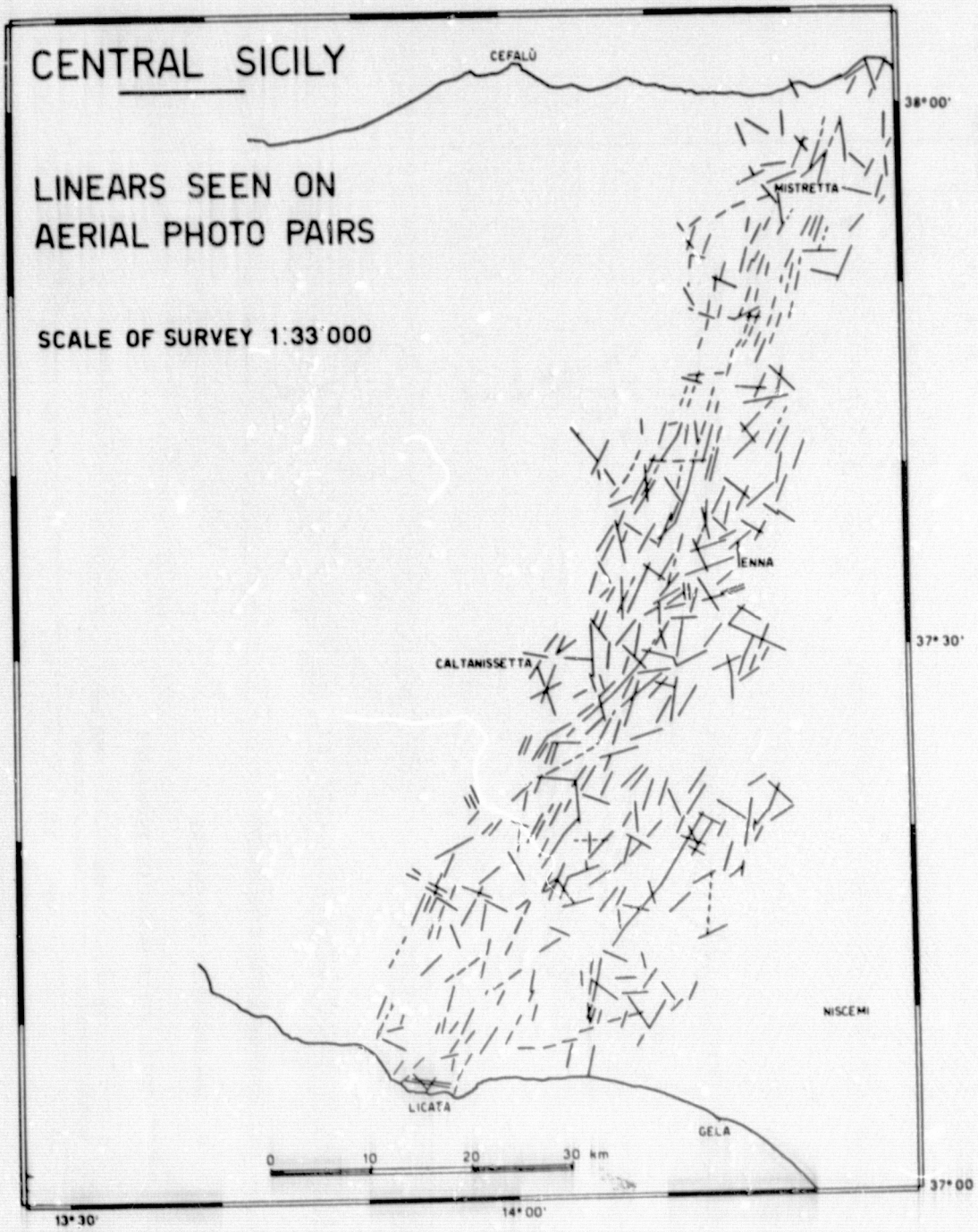


Figure 4.- Detailed analysis of linears in central Sicily derived from aerial imagery.

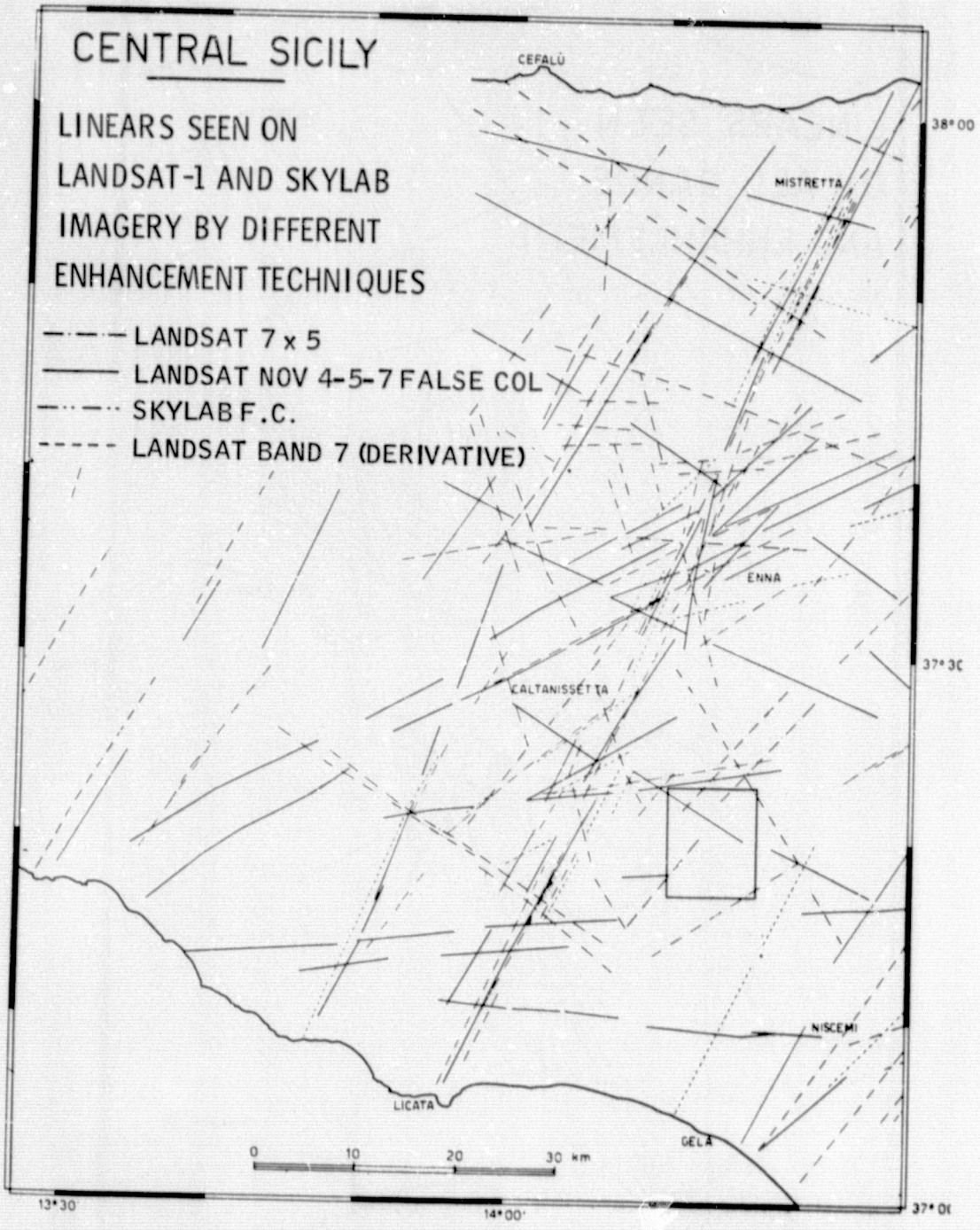


Figure 5.- Linears of central Sicily derived from LANDSAT and Skylab imagery.

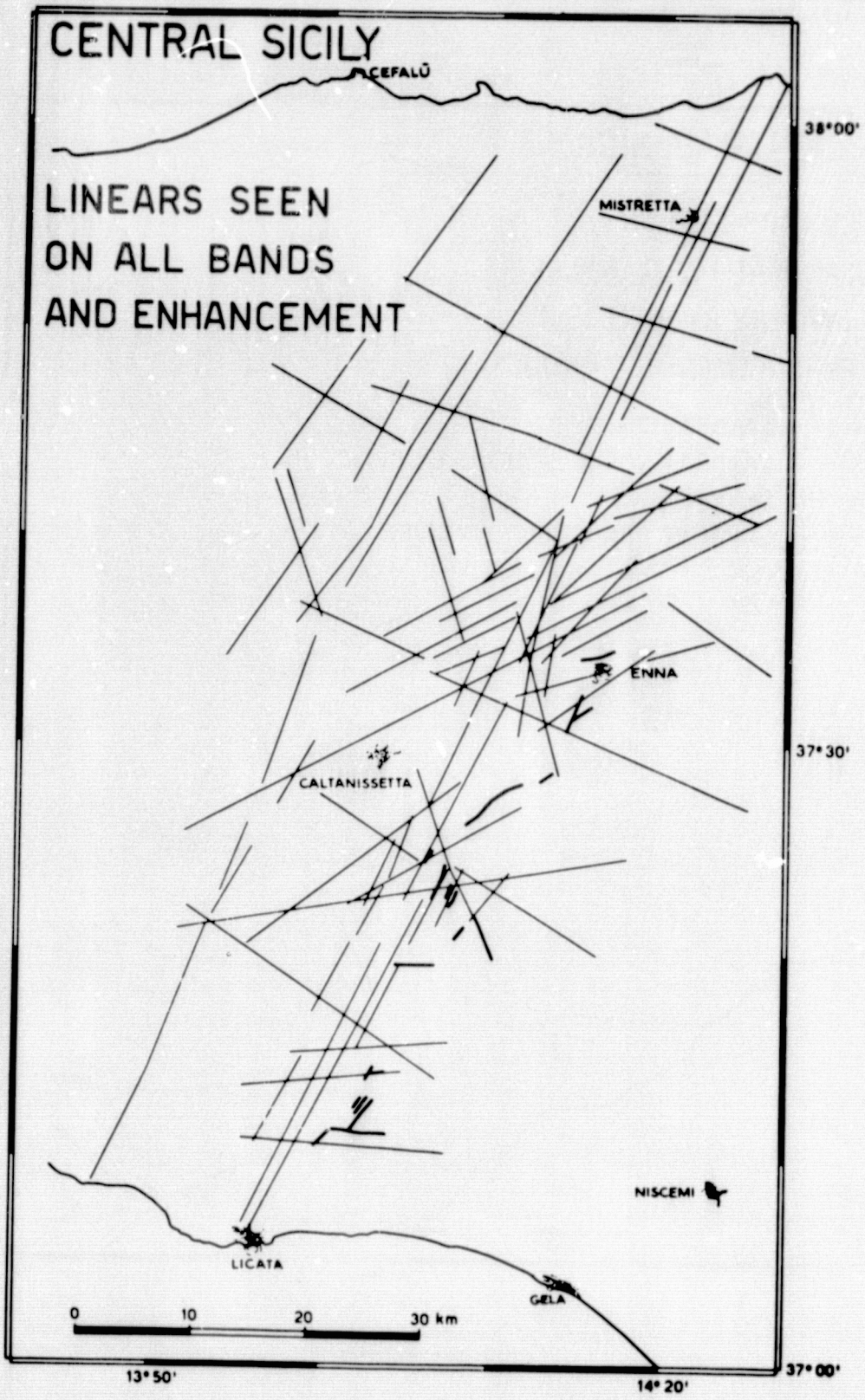


Figure 6.- Plot of central Sicily showing only those linears visible on all imagery.

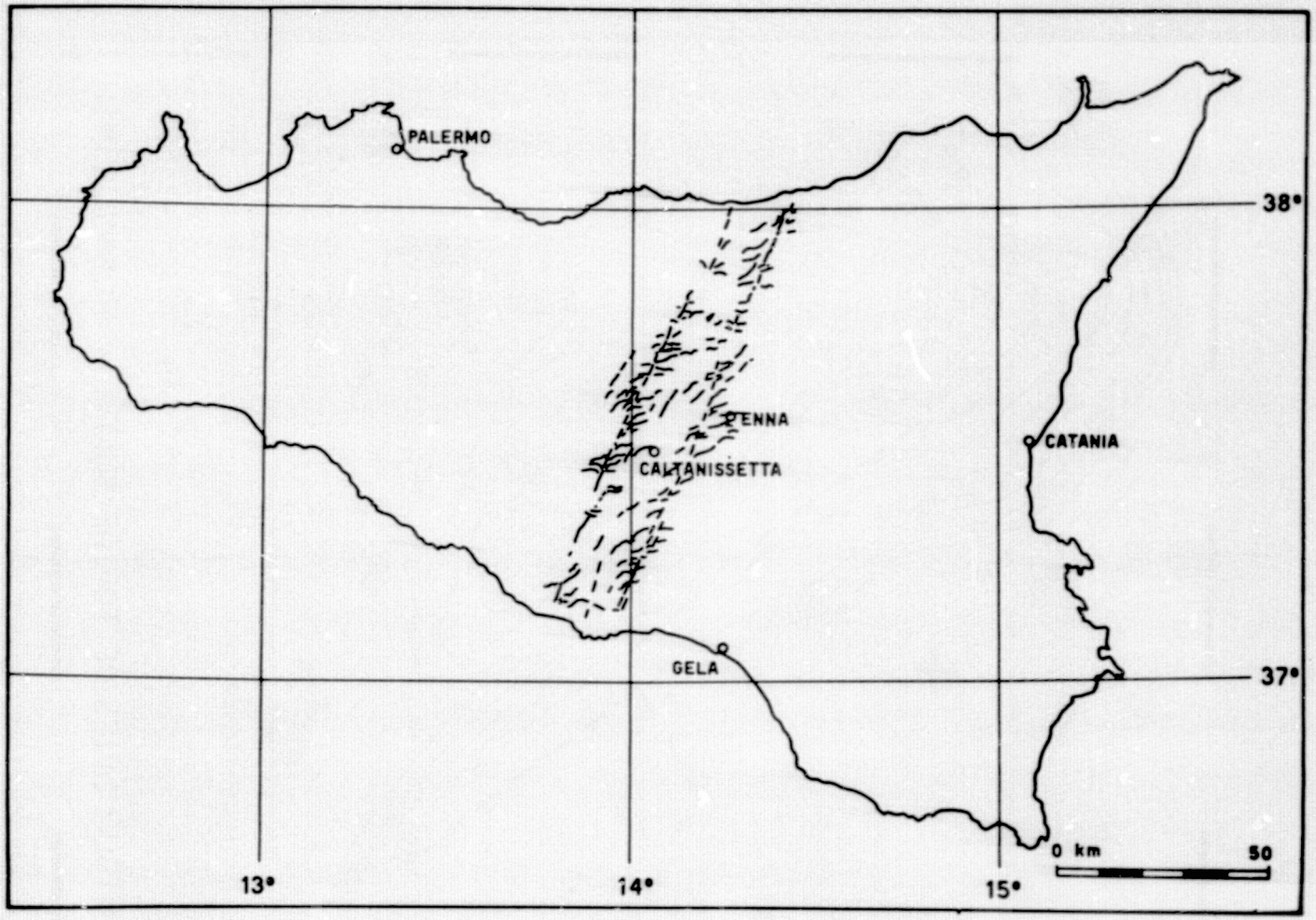


Figure 7.- Pattern of morphology drawn from LANDSAT imagery.

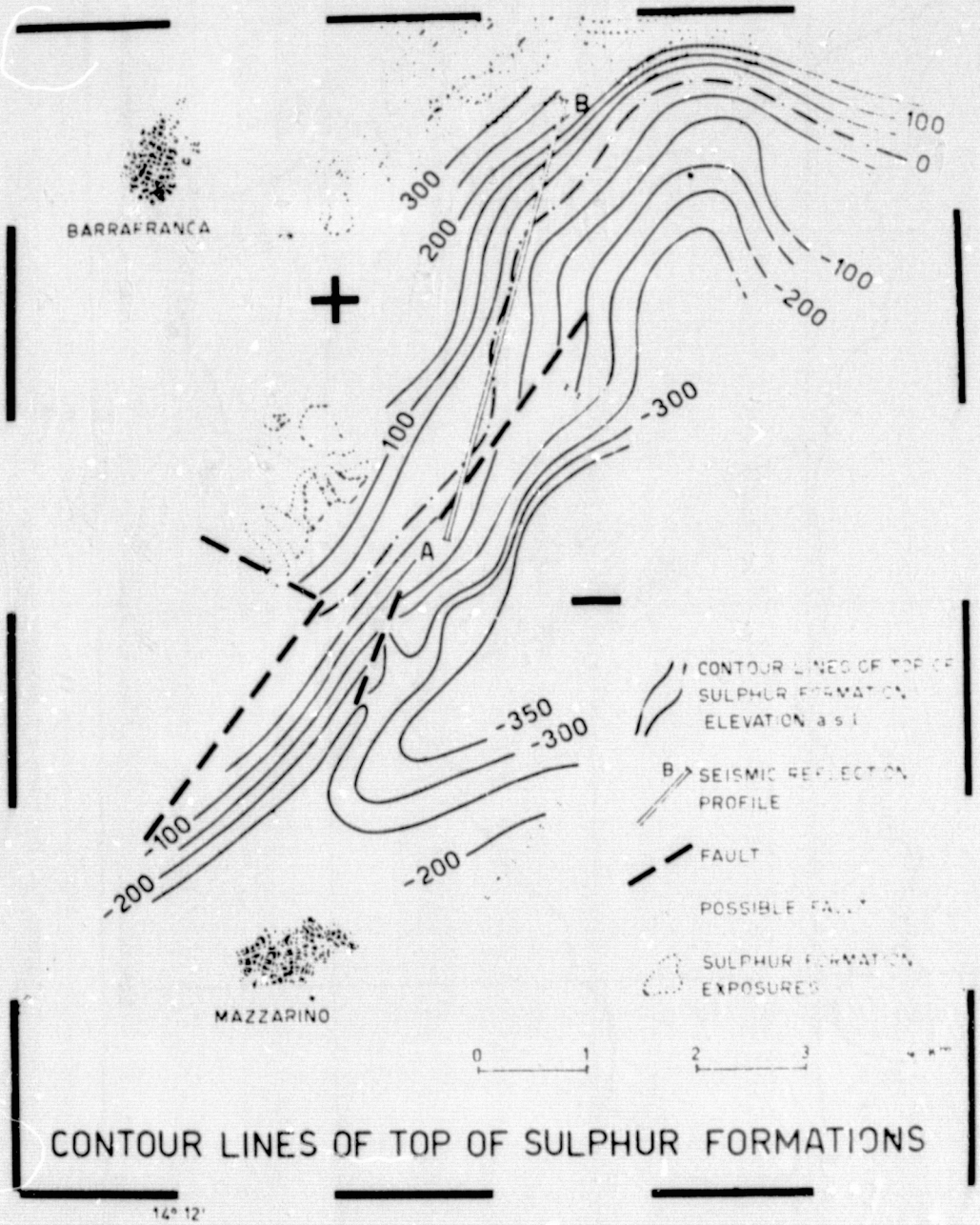


Figure 8.- Linear observed on LANDSAT imagery corresponds to known fault.

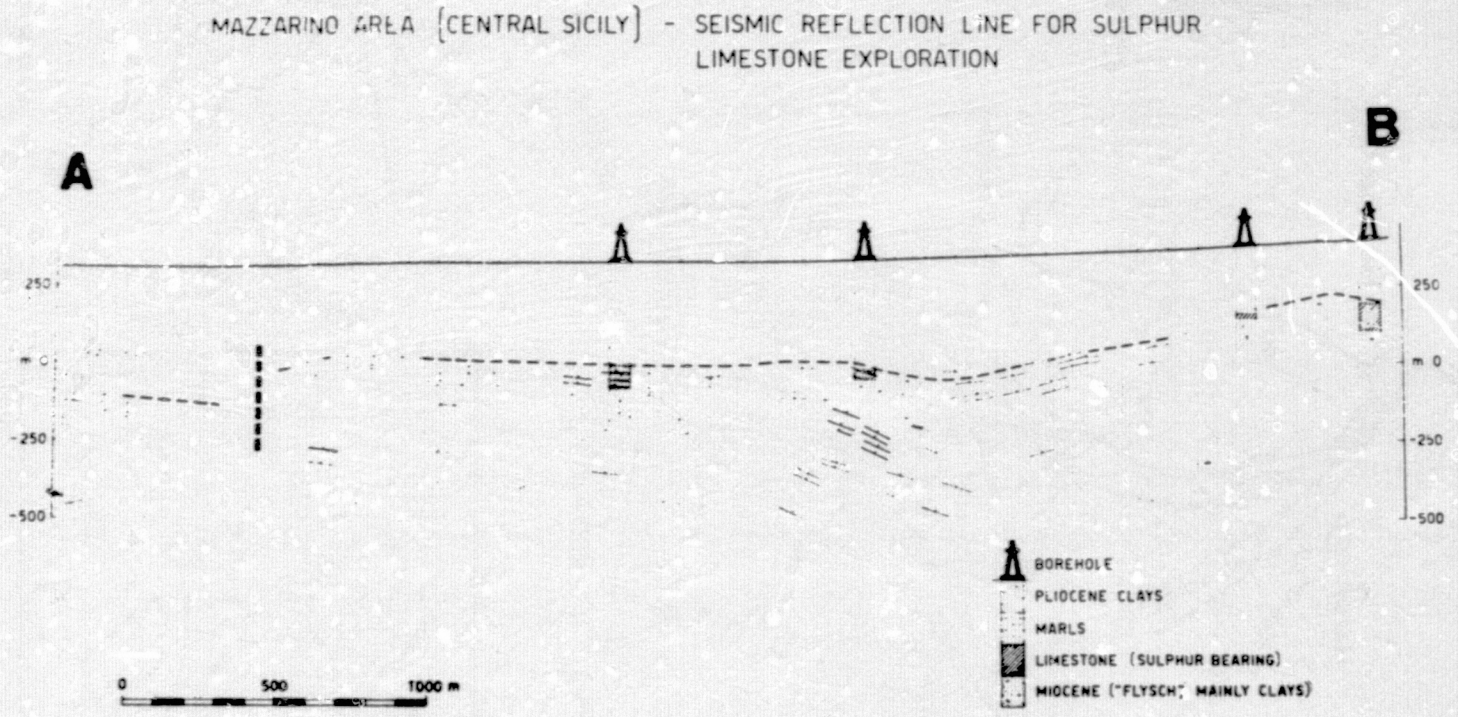


Figure 9.- Cross-section of an area where a seismic line crosses a shallow fault.

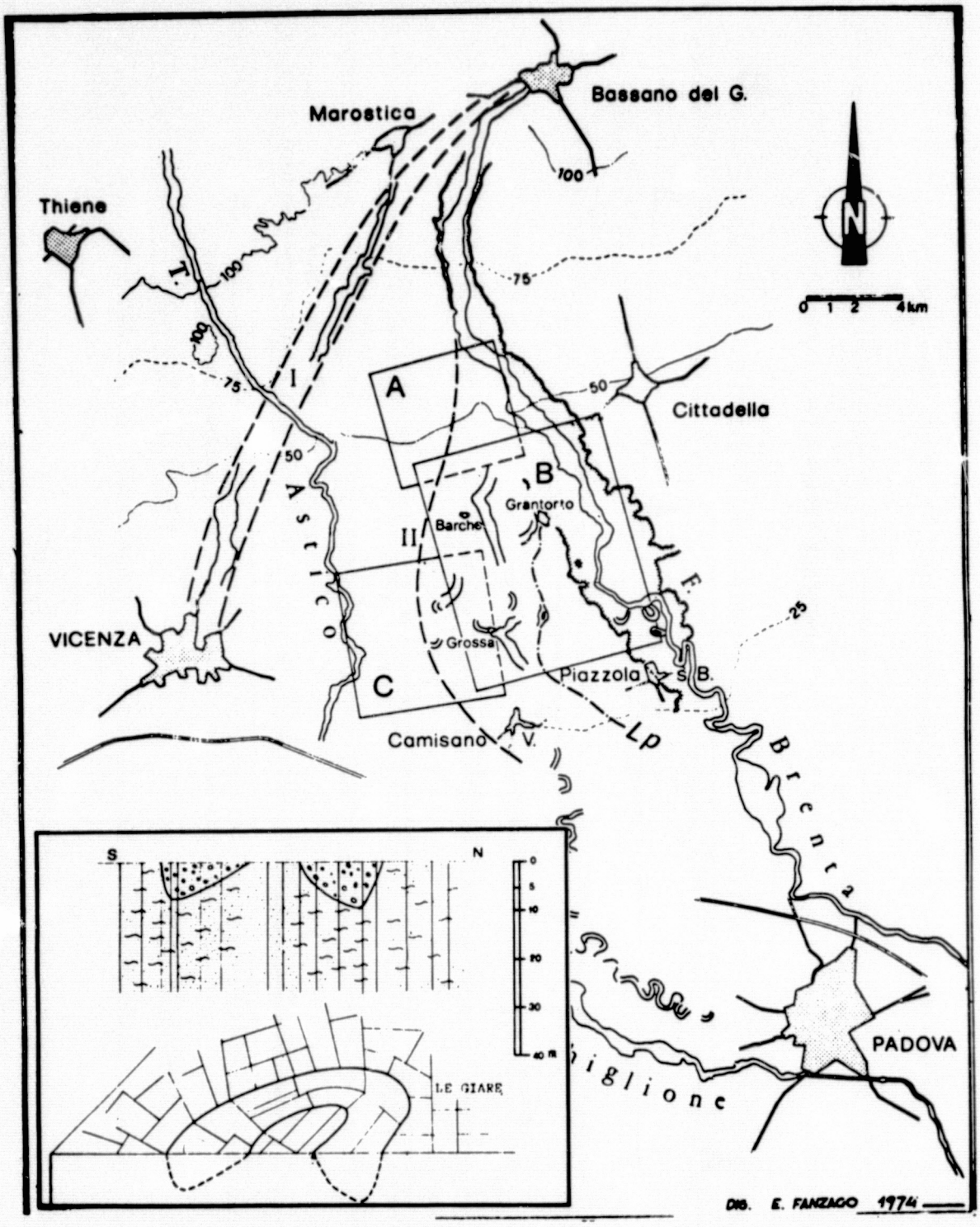


Figure 10.- Buried channels mapped from photo-geological and geophysical surveys.

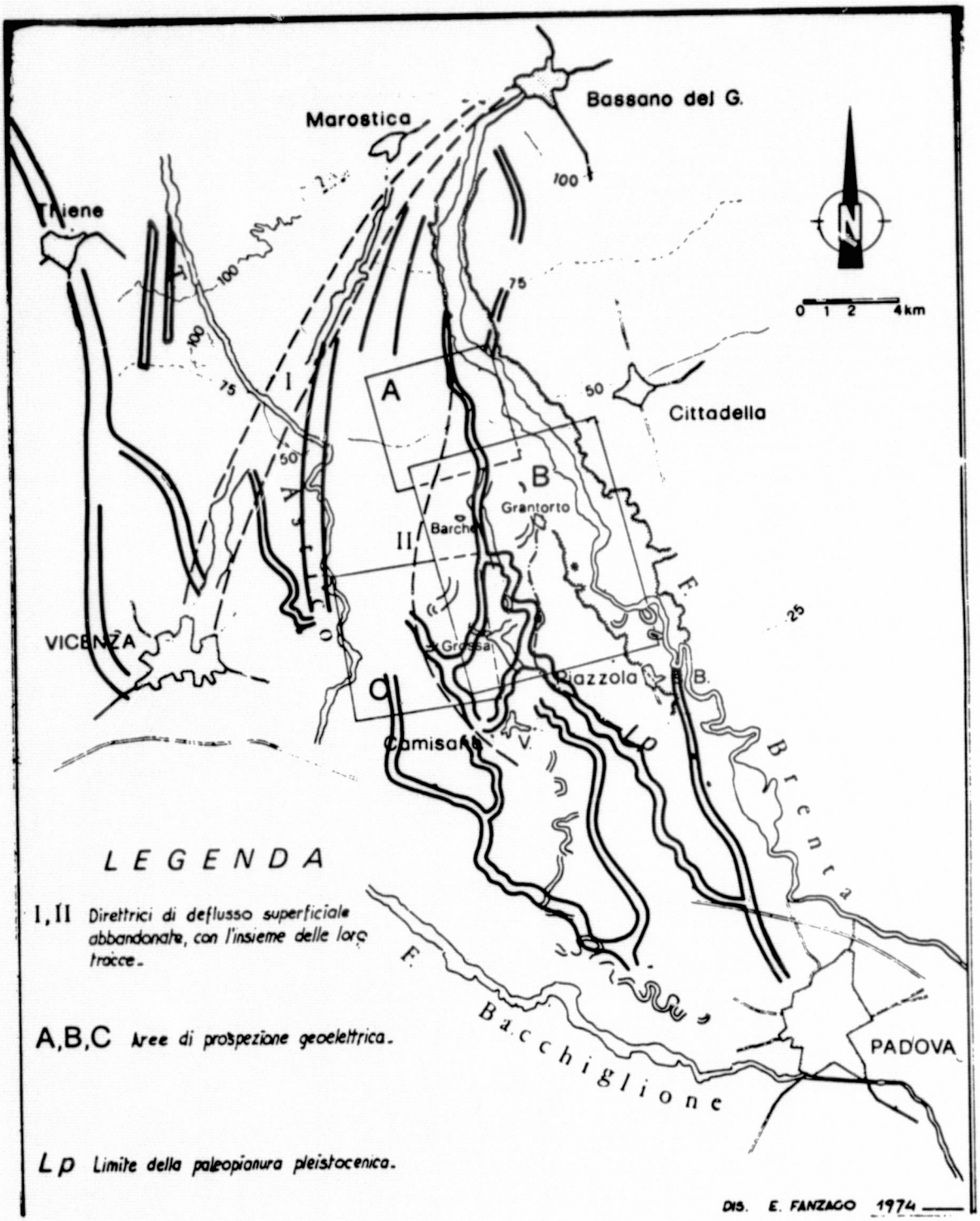


Figure 11.- Buried channels mapped with the help of Skylab imagery.

SKYLAB PHOTOGRAPHY APPLIED TO GEOLOGIC MAPPING IN NORTHWESTERN CENTRAL AMERICA

G-17

By W. I. Rose, Jr., D. J. Johnson, G. A. Hahn, and G. W. Johns,
Michigan Technological University, Houghton, Michigan

N76-17515

ABSTRACT

Two photolineation maps of southwestern Guatemala and Chiapas have been made from S190 photographs along a ground track from Acajutla, El Salvador to San Cristobal de las Casas, Mexico. The maps document a great structural complexity spanning the presumed triple junction of the Cocos, Americas and Caribbean plates. The Polochic fault zone, supposedly the Americas-Caribbean plate boundary, is a sharply delineated feature across western Guatemala. Westward of the Mexican border it splays into a large number of faults with NW to SW trends. The structural pattern is quite different to the north (Americas plate) and to the south (Caribbean plate) of the Polochic fault, though both areas are dominated by NW-trending lineations.

Within the Central American volcanic chain the lineation patterns support the segmented model of the Benioff Zone, by showing a concentration of transverse lineations in the predicted locations, most notably NE-trending elements near Quezaltenango, Guatemala. Compilation of circular and arcuate lineations within the Guatemalan Highlands offers new information about the nature and distribution of Early Quaternary and Tertiary volcanic vents.

The structural pattern obtained from the new maps are compared to patterns described on recently published maps of more southerly parts of Central America, to begin a synthesis of the structure of the convergent plate boundary.

INTRODUCTION

In this study a series of Skylab S190A and S190B photographs taken in February 1974, along a northwest-trending ground track extending from Acajutla, El Salvador to San Cristobal de las Casas, Mexico (Figure 1), have been interpreted for geologic structures and other features. The area is about 150 by 500 km, and is of particular interest for two reasons. First it crosses the presumed Americas-Caribbean plate boundary, which is thought to be marked by the Polochic fault, at a point near the triple junction of these plates with the underthrusting Cocos Plate. The dramatic expression of the Caribbean-Americas plate boundary traversing Guatemala has been already shown in Skylab imagery by Muehlberger and Ritchie (1975). Secondly, this area has not been mapped in detail, and so structural information was very limited. Thus, the possibility of producing a useful geologic contribution was enhanced.

Recently several new geologic maps of parts of Central America have been published (Bonis, et al., 1970; Carr, 1974; Anderson, et al., 1973; Wiesemann, 1974; Martinez, 1973). The area mapped in this study complements these other maps to provide more detailed structural patterns along the Central

PRECEDING PAGE BLANK NOT FILMED

American Pacific Coast from Chiapas to Costa Rica.

The existence of new data allows reflection upon several previous structural interpretations of Central America (Dengo, et al., 1970; Kesler, 1971; Malfait and Dinkelman, 1972; Stoiber and Carr, 1973).

METHODS

The photographs used in constructing the maps were chiefly of three types, all from the S190 camera system. Aerial color photographs were used most extensively. These were judged particularly effective for mapping during the Central American dry season, when much of the foliage is absent. The best set of images we had to study were taken in February 1974 (SL4 RL4B FEB74 102-113). Another excellent set of photographs along a nearly identical ground track is available for September 1973. Because of the dry season timing and because of better cloud conditions, we selected the February 1974 photographs. Black and white infrared and color infrared photos taken simultaneously proved useful for special purposes in our mapping and were used supplemental to the aerial color photographs. The infrared photos did not show any lineations not observed in the other photographs. High resolution aerial color (S190B) pictures were used exclusively in one of the maps (Figure 2).

All photographs were studied as stereoscopic pairs, this approach greatly enhancing many of the structures mapped.

The first new map produced is a compilation of photolineations and miscellaneous other geologic features (Figure 3). A total of 786 photolineations were mapped, with 3/4 of these lying to the north of the Polochic fault zone. Except for the detailed work of Anderson, et al. (1973), previous maps have shown a low fault density in the studied area, a fact more attributable to the reconnaissance nature of the mapping than to structural simplicity.

The map has three weights of lines. Heavy solid lines correspond to lineations that have great topographic expression. The Polochic fault is the longest of these, and shows up to 1500 m of topographic expression. Other heavy lines correspond to scarps and linear river valleys. Thinner solid lines represent lineations that are readily observable (i.e. reproducible by a second interpreter), but judged less prominent than the major set. Dashed lines represent mapped lineations that are most subject to personal interpretation. All of the lineations were scrutinized for possible non-geologic origin and some lineations were rejected on these grounds. High resolution photographs (S190B) were useful in demonstrating cultural or vegetational lineations. Thus we believe a high percentage of the mapped features have real geologic significance, and together represent the structural pattern of the area.

The cloud cover over the map area varies from 0 to 100%. Four arbitrary divisions are made on the map (see Figure 3). Lineations drawn in cloud covered areas were drawn with extreme care; no lineations could be drawn in areas with heavy cloud cover. Thus, some lineations that terminate at cloud cover boundaries on the map probably continue.

INTERPRETATION

The Plate Boundary and the Polochic Fault Zone

The Polochic fault (name taken to include the Cuilco-Chixoy-Polochic system of faults) is the single dominant structural feature of the area. The fault does not obviously extend westward beyond the Sierra Madre Mountains with the clear identity it shows to the east. This observation was made prior to study with satellite photography (Kesler, 1972). From the new map, it seems likely that movement along this plate boundary becomes more complex, and is absorbed in a "horsetail" system of mainly parallel E-W trending structures shown to the north of the Polochic trace. The break in identity of the Polochic structure occurs before the fault reaches either the cloud-covered area of the photographs or the alluvial coastal plain, so we believe that this observation is significant.

Movement along the Polochic system supposedly has a left lateral strike-slip component. In view of this, it is surprising that only one of the lineations mapped crossing this structure in Figure 3 shows left-lateral offset. At distances of 20 to 30 km north of the Polochic, some lineations appear to be bent in a left lateral sense, however. This may also support the idea that some of the strike-slip movement of the Polochic system has occurred north of the principal fault trace. Malfait and Dinkelman (1972, p. 259, 261) have proposed that an increased rate of underthrusting at the Middle America trench after the late Miocene caused compression along the Motagua and Polochic systems and thereby inhibited strike-slip movement. This would be especially effective at stopping movement to the west along these faults, since the trends of the faults curve to be more nearly perpendicular to the assumed convergence of about N30°E. Thus, it seems plausible that increased underthrusting rates have caused the left-lateral displacements, which fit the plate tectonic model in this area, to move further to the north. The previous northward progression of movement along en echelon left lateral shears is suggested by the configuration of the Jocotán-Chamelecon, Motagua and Polochic systems (Figure 1).

Muehlberger and Ritchie (1975) suggest that the Polochic fault bifurcates into NW and NE trending forks at the Sierra Madre; the NE-trending branch they believe to reflect the plate boundary. We do not wholeheartedly agree with this interpretation for several reasons: 1) The prominence of this fault is not at all comparable to the eastern extension of the Polochic. 2) We could not trace this feature across the coastal plain. 3) This fault parallels numerous other NE-trending structures that occur transverse to the volcanic chain at several places in Guatemala, and we suggest that the origin of this westernmost structure is analogous to the others, rather than having a unique explanation. Our own explanation fits concepts of segmented underthrusting which we discuss further below.

Predominance of Northwesterly Structures

We have compared the patterns of faulting of the area south of the Polochic fault to the area north of this structure. To show the general faulting patterns of both areas we constructed rose diagrams (orientation-frequency diagrams) for both these areas (Figure 3). Both rose diagrams show a predominance of northwest-trending structural elements. This direction is roughly parallel to the coastline and the offshore Middle America trench. The predominance of northwesterly faulting is a feature of Central American geology from Mexico to Panama, as shown by previous small scale map compilation (Dengo and Levy, 1970) and must be closely related to plate convergence. Though they are the dominant fault directions, we are not at all

certain of the nature of the offset along these structures. Idealized models of zones of plate convergence show that normal faulting as a result of geanticlinal uplift might parallel the offshore trench in certain situations (Dickenson, 1972). Dengo and others (1970) favor this explanation for Central America, citing the Nicaragua graben as an obvious example of the predominately normal faulting. Some or many of the NW-trending structures may be right-lateral shears, analogous to the Jalpatagua fault (Williams and others, 1964). Indeed, recent geologic mapping in Nicaragua has suggested that the Nicaragua graben may have opened with some right lateral shearing component (Williams, 1972). New evidence of this type of interpretation is becoming available from the work of Carr (1974, and in press) in southeastern Guatemala and western El Salvador.

We took advantage of the availability of new structural information along the length of Central America to begin a structural comparison along the volcanic belt (Figure 4). Rose diagrams were constructed from new geologic maps available from the work of Carr, 1974 (Area 4), Wiesemann, 1974 (Areas 5 and 6) and Martinez, 1973 (Areas 7, 8 and 9). Together the data represent a series of similar size areas from north to south (1-9). Such a comparison is meant only as a first superficial look at structural patterns and all conclusions are general and tentative.

In all but one of the areas tested (Figure 4) northwesterly faults predominate, and in all of the areas northwest-trending structures are very numerous. The parallelism of the strike of Middle America trench and the seismic zone with these structures points to a direct association. In more detail, the association is not perfect, for the more westerly (N75°W) trend of the Middle America trench south of El Salvador is not accompanied by a discernible westerly shift of the northwest-trending structures in the El Salvador segments (Areas 5 and 6). We do not know the reason for this, but do not feel it negates the general association of the strike of underthrusting and the attitudes of the predominant faults along the volcanic axis.

Kesler (1971) has proposed, on the basis of structural trends in Mexico and South America, that the pre-Mesozoic structural grain in nuclear Central America trends northwesterly. We cannot say to what extent a pre-existing structural grain influences the northwesterly dominance. We are quite confident that there is no significant decrease in the relative dominance of northwesterly structures from north to south along the Central American volcanic axis. This suggests that underlying continental crust, which is known in Guatemala and unknown (and probably absent) in Nicaragua, cannot alone account for a uniform northwesterly fault concentration.

Comparing the predominately NW-trending structures of Areas 1 and 3 (Figure 4), the slightly more westerly orientation of area 1 lineations is observed. This difference may be due to the slight differences in the interactions between the Cocos-Americas plates (Area 1) and the Cocos-Caribbean plates (Area 3). Following this speculation, if convergence of the Cocos-Americas plate is N30°E, perpendicular to the predominant structural elements, then convergence of the Cocos-Caribbean plate might be indicated as slightly more nearly easterly, perhaps N50-60°E.

It is very important to any real understanding of the structure of Central America (and presumably other convergent plate boundaries) that field work which better describes the significance and nature of this predominant NW-trending set of structures be completed.

"Transverse" NE Faulting

South of the Polochic fault, NE-trending faults make up a large relative proportion of structures on our photolineation map (Figure 3). The map shows that faults of this orientation are concentrated at several restricted portions of the area. The most obvious concentration of NE structures occurs at Quezaltenango, in western Guatemala, with a series of lineations paralleling the Zuñil Fault. The position of this and the other NE lineation groups support the model of segmented underthrusting for Central America (Stoiber and Carr, 1973; Carr and others, 1974) since they coincide very well with the proposed discontinuities in the seismic zone. These discontinuities were originally postulated and located on the basis of differences in the strikes and positions of volcanic lineaments of the historically active volcanoes and supported by seismic data. In addition to the obvious concentration of NE lineaments at Quezaltenango, there are also suggested concentrations east of Pacaya volcano and at Tacaná volcano. The lineations appear to denote zones of about 20 km in width. The most westerly zone of transverse structures (at Tacaná) is that proposed by Muehlberger and Ritchie as the Americas-Caribbean plate boundary extension. We propose it to be analogous to the Quezaltenango and Pacaya zones, having the same strike and width, and occurring in the spot predicted by the Stoiber-Carr model. It should be noted that all three of these transverse fault zones are associated with noticeable submarine canyons offshore in Guatemala (see Stoiber and Carr, 1973, p. 306). If these transverse zones represent left-lateral shears (see below), offset along the Tacaná zone is in the same sense as the Polochic fault, and thus at least some of the plate boundary movement could be absorbed by this transverse zone, as suggested by Muehlberger and Ritchie (1975).

North of the Polochic fault NE-trending faulting is less prominent. This is shown by the rose diagrams of Figure 3. A small part of this northern section of the study area has been mapped in some detail by Anderson and others (1973). The area covered is entirely in Guatemala and is outlined as Area "2" in Figure 4. The rose diagram for Area 2 shows that NE-trending structures are a very important fraction in this area. On consulting the geologic map it is clear that these faults are generally much shorter than faults of other orientation, indeed they are generally shorter (2-4 km) than any of the photolineations mapped in Figure 3. This, we believe, explains the only notable difference in the rose diagrams of Areas 1 and 2. This does not detract from the observation that through-going northeasterly structures are more important south of the Polochic fault system.

NE-trending faults show noticeable population peaks in all but one of the areas tested (Figure 4). In general, there appears a tendency for the relative proportions of NE-trending structures to increase southward. This observation may not be significant, however. The northeasterly faults might be expected to be underrepresented in maps prepared from satellite photographs (i.E. Areas 1 and 3) because they are not as long as other faults.

On the geologic maps used in preparation of Figure 4, we cannot observe obvious concentrations of NE-trending structures within zones transverse to the volcanic axis within El Salvador and Nicaragua. This could be because: 1) Such concentrations do not occur. If true, this appears to negate the support given the Stoiber-Carr model of segmented underthrusting by the new photolineation map. 2) Satellite-prepared maps, which tend to emphasize through-going structural elements, are better suited to demonstrate these concentrations. 3) Such concentrations are masked by changes in the locations of segment boundary zones during the Neogene. Alternative 2 can be tested by study of new satellite photos covering El Salvador and Nicaragua.

The proposal of left-lateral shearing along these transverse faults given by Stoiber and Carr (1973) is consistent with the plate convergence model, since as these authors show, underthrusting rates should be increasing from north to south in Central America. Segments to the south are, therefore, underthrusting continually more rapidly and their boundaries should show left-lateral shear. Dramatic recent evidence supporting this interpretation exists with the study of the pattern of faulting responsible for the Managua earthquake of December 1972 (Brown and others, 1973). Four en echelon northeast-trending faults showed clear left lateral offsets. Managua is located along one of the transverse segment boundaries proposed in the Stoiber-Carr model.

Along the Zunil Fault in western Guatemala, Johns (1975) has determined that movement is at least in part normal faulting while geophysical work has suggested left-lateral offset along parallel faults near Totonicapán, Guatemala (M. J. Whims, personal communication). M. J. Carr (in preparation) is at present completing a careful structural field study in southeastern Guatemala which should further clarify the nature of NE-trending faults.

N-S Trending Structures

Data of Figure 4 suggests that N-S trending structures are more prominent within El Salvador and Eastern Guatemala than in areas to the northwest or southeast along the volcanic axis. N-S trending structures in these areas may be associated with grabens, such as the Guatemala City graben and the Comayagua graben. Thus, E-W extension may be especially important within Areas 4, 5, and 6. Extension along N-S features in these areas is explained by Malfait and Dinkelman (1972, pp. 259-261) by temporary pinning of southern Guatemala and western Honduras to the North American plate. The result of such pinning would be to produce the most pronounced extension exactly where it is observed. Extension could be expected to decrease to the southeast with decreased proximity to the plate boundary. It would be also expected to decrease in intensity northwestward, since the Polochic fault (representing the plate boundary) curves to a more nearly E-W orientation. Pinning of the fault would be progressively more effective to the west since the fault is more nearly perpendicular to the underthrusting. N-S extension is also compatible with the idea of NE left-lateral shearing and the association of these structural elements in the Managua area is pointed out by Stoiber and Carr (1973, p. 320-321). We can anticipate further interpretation of all of the structural elements of Area 4 (where N-S faulting is most important) from M. J. Carr (1974 and in preparation).

Relationship of Structural Patterns with Ore Deposits

In order to compare the results with the general structural synthesis, we compiled information on the attitudes of veins and fractures associated with various types of mineral deposits in Central America (Roberts and Irving, 1957). Figure 5 shows the results, and demonstrates noticeable NW and NE concentrations. This pattern correlates well with the general structural pattern defined in Figure 4.

Miscellaneous Features Observed with the Study Area

Because the photographs used were taken in the dry season, ground color was observable in most of the study area. We noticed areas of anomalously blue-grey color which seemed to correlate with serpentinite bodies along the

Polochic fault (Figure 3). Most, but not all of these areas were previously mapped as serpentinites.

Areas of anomalously red-orange colored ground were mapped as "possible gossans" (Figure 3). Field examination would be necessary to verify the cause of abnormal coloration.

In the northwestern part of the map area, the outlines of several small possible intrusive bodies are shown. These are delineated based on topographic, geomorphologic and coloration criteria. Again, these features await field verification.

Large lobate geologic units are delineated on infrared photographs on the Guatemalan coastal plain south of Guatemala City and Cuilapa (see Figure 3). The explanation of these features is still unknown, but geologic mapping by University of Missouri geologists headed by D. K. Davies is now in progress. Infrared photography shows these units as diffuse dark areas. In this respect they are somewhat similar to young lava flow units. Both units are found down slope from river valleys which flow onto the coastal plain. This suggests they may be laharic in origin.

Circular Features in the Tertiary Volcanic Belt of Guatemala

During preparation of the photolineation map (Figure 3) we noticed a distinct concentration of circular and arcuate structural elements within the volcanic belt of Guatemala. We used the S190B photographs to prepare a separate map of these features (Figure 2). A few of the features mapped (labeled by name on the map) are Quaternary cones and domes. To the north of this WNW-trending line of Quaternary volcanoes, correlating with the extent of Tertiary volcanic rocks, is the area where the greatest density of arcuate and circular features (mainly topographic depressions) are found. Their shapes and the close association of these features with the volcanic belt suggests a volcanic origin. We believe they represent Tertiary volcanic centers.

The Tertiary volcanic belt in Guatemala is not well described and very little is known about the volcanoes which produced these rocks. Existing descriptions (Williams, 1960; Bonis, 1965; Lamarre and others, 1971) seem to emphasize the flat-lying character of Tertiary rock units and suggest fissure vent origin for the eruptions. This style of volcanism contrasts with Quaternary events, which seem to center on steep, composite cones. The description of this contrast is made less certain by the recognition (McBirney, 1975) that volcanism is episodic in Central America and a significant period of quiescence separates the Quaternary activity from Tertiary volcanism. This means that erosion has had a much longer time to obscure Tertiary volcanic features.

Nonetheless, circular volcanic features within the Tertiary of Guatemala have been recognized before, west of Sansur in the San José Pinula Quadrangle (Lamarre and others, 1971). These probably represent eroded Tertiary cones and/or caldera-like structures. In Figure 2, the abundance of these circular structures increased to the southeast, from Volcán Tacaná to Quezaltenango. This change correlates with a general change in lithology within the Tertiary, from a dominance of basaltic andesite flows in southwestern Guatemala (Bonis, 1965) to more siliceous ash flow dominance within the central Guatemalan Highlands (Williams, 1960). Thus, the circular features may be more particularly associated with siliceous volcanism. We believe the map also suggests that the number of circular features may be

most abundant around the proposed boundary of the segmented Benioff Zone that passes northeastward through Quezaltenango. This suggestion must be corroborated by other examples before we can say whether these proposed transverse structural elements have significance in the Tertiary record.

CONCLUSIONS

1. S190 photographs proved a useful basis for structural mapping in northern Central America, permitting the delineation of a high density of photolineations, and the recognition of circular features.

2. The structural geology of northwestern Central America, and to some degree of the remainder of the volcanic chain is dominated by NW trending faults. These structures parallel and are related to the active seismic zone, but are not well understood in detail.

3. NE-trending faults are also of general importance all along the volcanic axis of Central America. In Guatemala, concentrations of NE-trending faults occur in areas where transverse segmentation of the volcanic chain and the seismic zone have been postulated.

4. The Polochic fault system "horsetails" into a complex series of faults, striking NW to SW, westward of the Mexican border. The plate boundary, which seems so well defined in western Guatemala, consists of a whole system of shears in southern Chiapas.

5. The Tertiary volcanic province of Guatemala is characterized by an abundance of circular structural features, which reflect old volcanic centers. The existence of these underlines a fundamental difference in the style of volcanism in the Tertiary and Quaternary.

ACKNOWLEDGMENTS

Financial support for this work came from NASA contract NAS-9-13311. Peter Ostlender drafted all maps and figures.

REFERENCES

Anderson, T.H., B. Burkart, R. Clemons, O. Bohnenberger and D. Blount, 1973, Geology of the Western Altos Cuchumatanes, Northwestern Guatemala, Geol. Soc. Amer. Bull. 84, 805-826.

Bonis, S.B., 1965, Geología del area de Quezaltenango, Guatemala, Inst. Geográf. Nacional (Guatemala) Geol. Bull. No. 1, 84 p.

Bonis, S.B., O.H. Bohnenberger and G. Dengo, 1970, Mapa Geológicc de la Republica de Guatemala, Inst. Geográf. Nacional (Guatemala).

Brown, R.D., P.L. Ward and G. Plafker, 1973, Geologic and Seismologic Aspects of the Managua Nicaragua earthquakes of December 23, 1972, U.S. Geol. Surv. Prof. Paper 838.

Carr, J.J., 1974, Tectonics of the Pacific Margin of Northern Central America, Ph.D. Dissert., Dartmouth College, Hanover, N.H., 159 p.

Carr, M.J., R.E. Stoiber and C.L. Drake, 1974, The Segmented Nature of Some Converging Plate Margins, in Geology of Continental Margins, ed. by C.A. Burk Hamburg, Springer-Verlag, 105-114.

Dengo, G. and E. Levy, 1970, Mapa Metalogenetico de America Central, Publ. Geol. del ICAITI (Guatemala), No. 3.

Dengo, G., O. Bohnenberger and S.B. Bonis, 1970, Tectonics and Volcanism along the Pacific Marginal Zone of Central America, Geol. Rundschau, 59, 1215-1232.

Dickenson, W.R., 1972, Evidence for Plate-Tectonic Regimes in the Rock Record, Am. Jour. Sci., 272, 551-576.

Johns, G.W., 1975, Geology of the Cerro Quemado Volcanic Dome Complex, Guatemala, M.S. thesis, Michigan Technological University, Houghton, 124 p.

Kesler, S.E., 1971, Nature of Ancestral Orogenic Zone in Nuclear Central America, Am. Assoc. Pet. Geol. Bull. 55, 2116-2129.

_____, 1972, Western Extension of the Northern Side of the Caribbean Plate, Int. Geol. Congress (Montreal) Sect. 3, 238-244.

Lamarre, A.L. and 11 other authors, 1971, The Geology of the San José Pinula Quadrangle, Guatemala, Inst. Geográf. Nacional (Guatemala) Geologic Quadrangle Map.

Malfait, B.T. and M.G. Dinkelman, 1972, Circum Caribbean Tectonic and Igneous Activity and the Evolution of the Caribbean Plate, Geol. Soc. Amer. Bull. 83, 251-272.

Martinez, M., 1973, Mapa Geológico Preliminar, Instituto Geográfico Nacional and Servicio Geológico Nacional (Nicaragua).

McBirney, A.R., 1975, Geologic Constraints on Models for Wet Melting of Calc-Alkaline Magmas, Geol. Soc. Amer. Abst. Prog. 7, 817.

Muehlberger, W.R. and A.W. Ritchie, 1975, Caribbean-Americas Plate boundary in Guatemala and Southern Mexico as seen in Skylab IV Orbital Photography, Geology, 3, 232-235.

Roberts, R.J. and E.M. Irving, 1957, Mineral Deposits of Central America, U.S. Geol. Surv. Bull. 1034.

Stoiber, R.E. and M.J. Carr, 1973, Quaternary Volcanic and Tectonic Segmentation of Central America, Bull. Volcanol. 37, 304-325.

Wiesemann, G., 1974, Geologic Map of El Salvador, in press.

Williams, H., 1960, Volcanic History of the Guatemalan Highlands, Univ. Calif. Publ. Geol. Sci. 38, 1-86.

Williams, H., A.R. McBirney and G. Dengo, 1964, Geologic Reconnaissance of Southeastern Guatemala, Univ. Calif. Publ. Geol. Sci., 50, 1-66.

Williams, R.L., 1972, The Geology of Western Nicaragua; Final Technical Report Vol. IV, Managua.

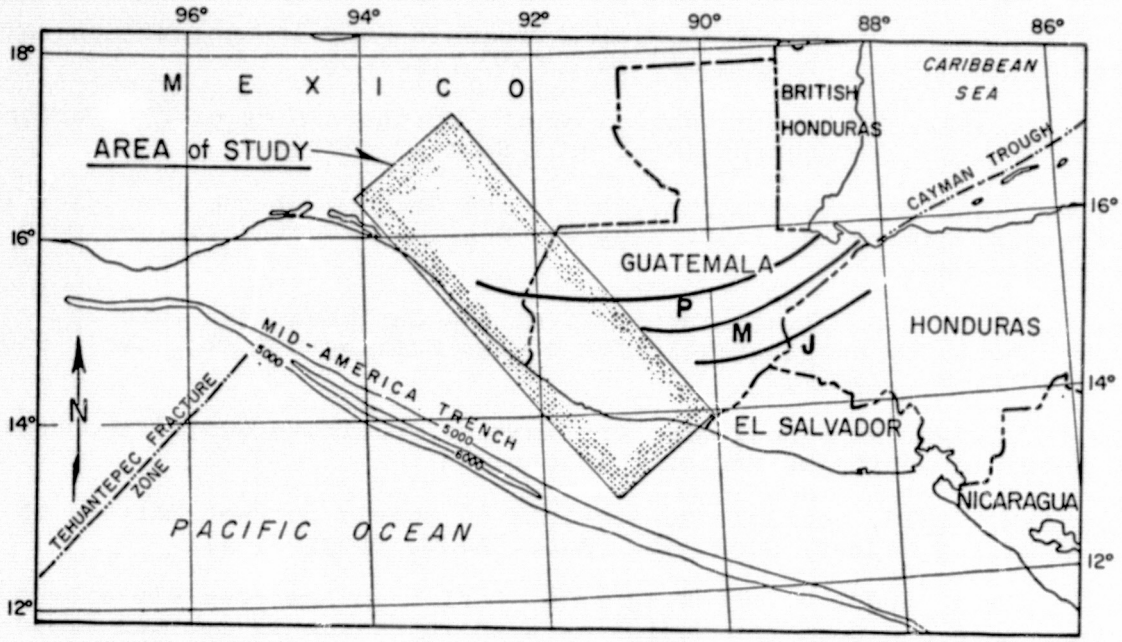


Figure 1: Map showing location of area mapped in Figure 3. Lines labeled P, M and J are the approximate locations of the Polochic, Motagua and Jocotán fault systems, respectively.

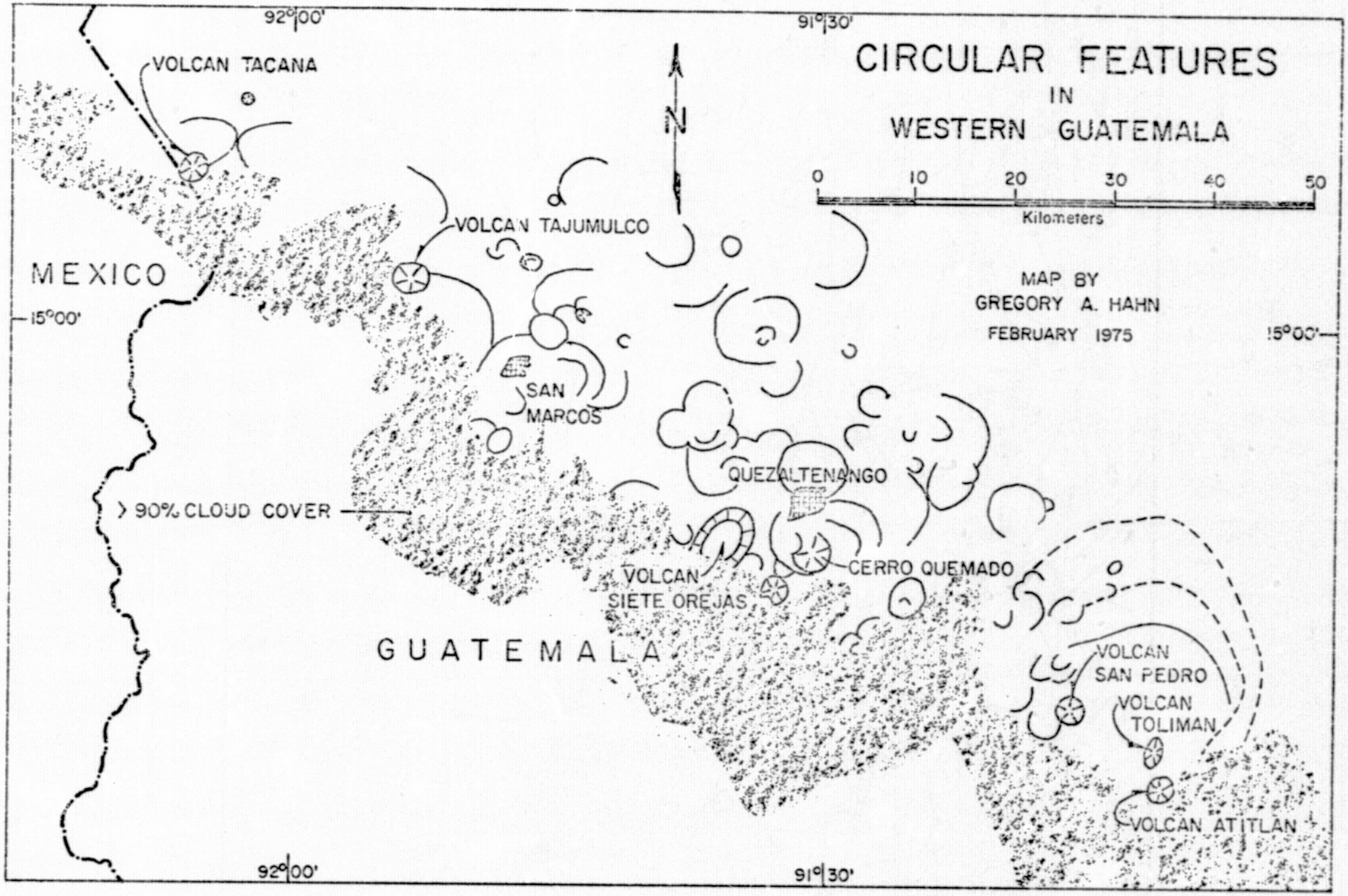


Figure 2: Map of arcuate and circular features within the western volcanic highlands of Guatemala. Prepared from S190B color photographs.

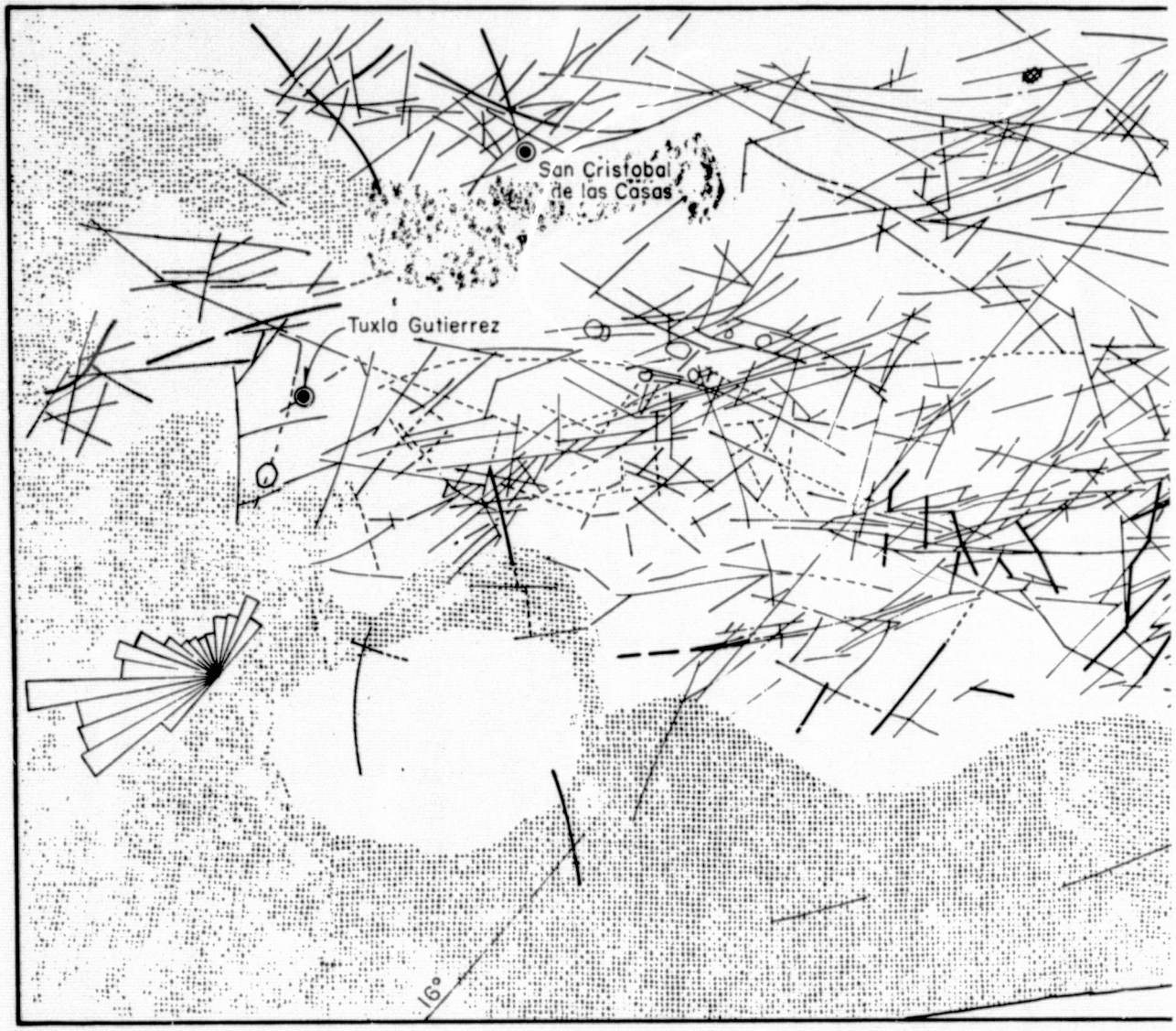


Figure 3: Photolineation map of a portion of southern Mexico and southwestern Guatemala.

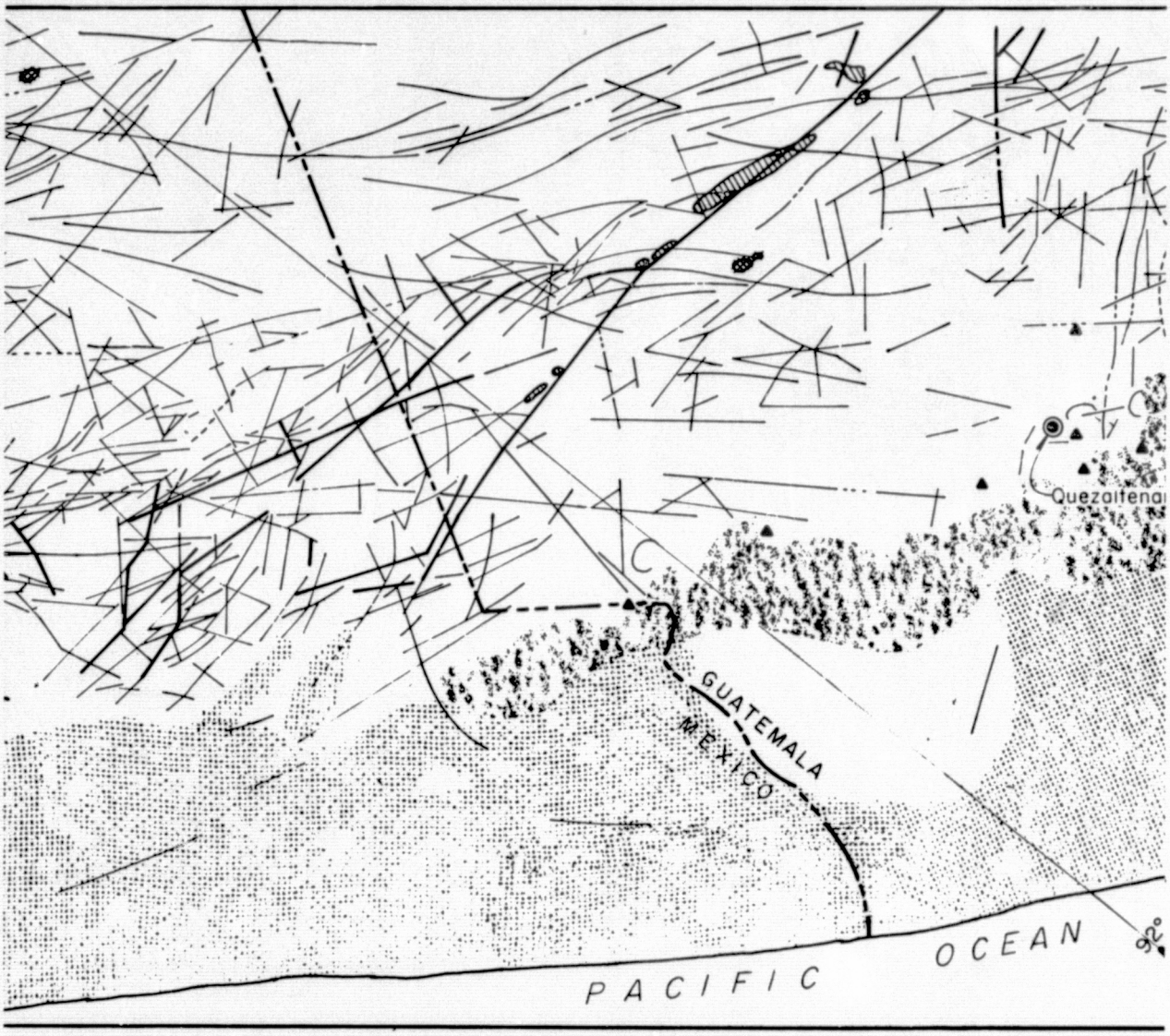


Figure 3: Continued.

REPRODUCIBILITY OF THE
ORIGINAL PAGE IS POOR

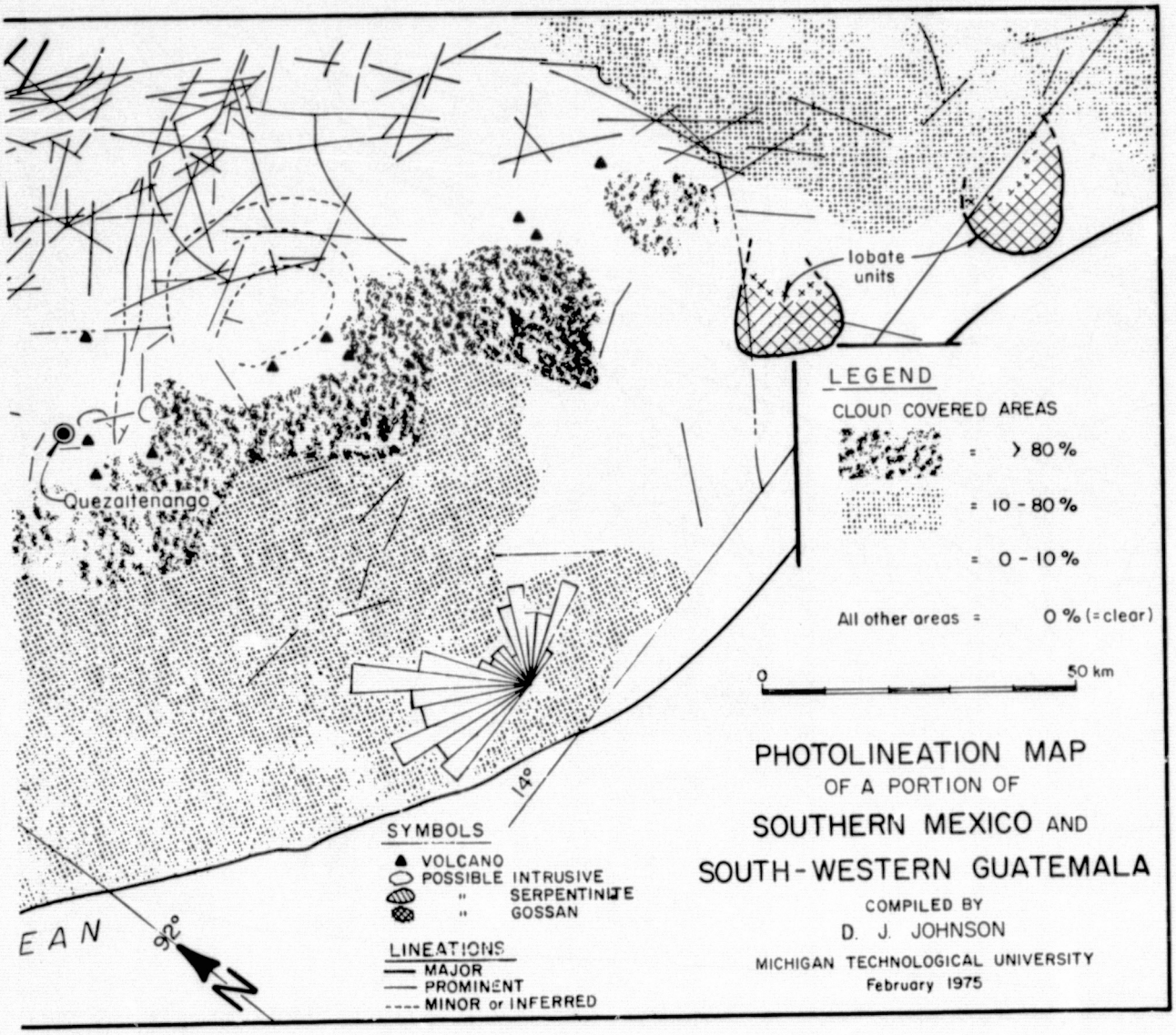


Figure 3: Concluded.

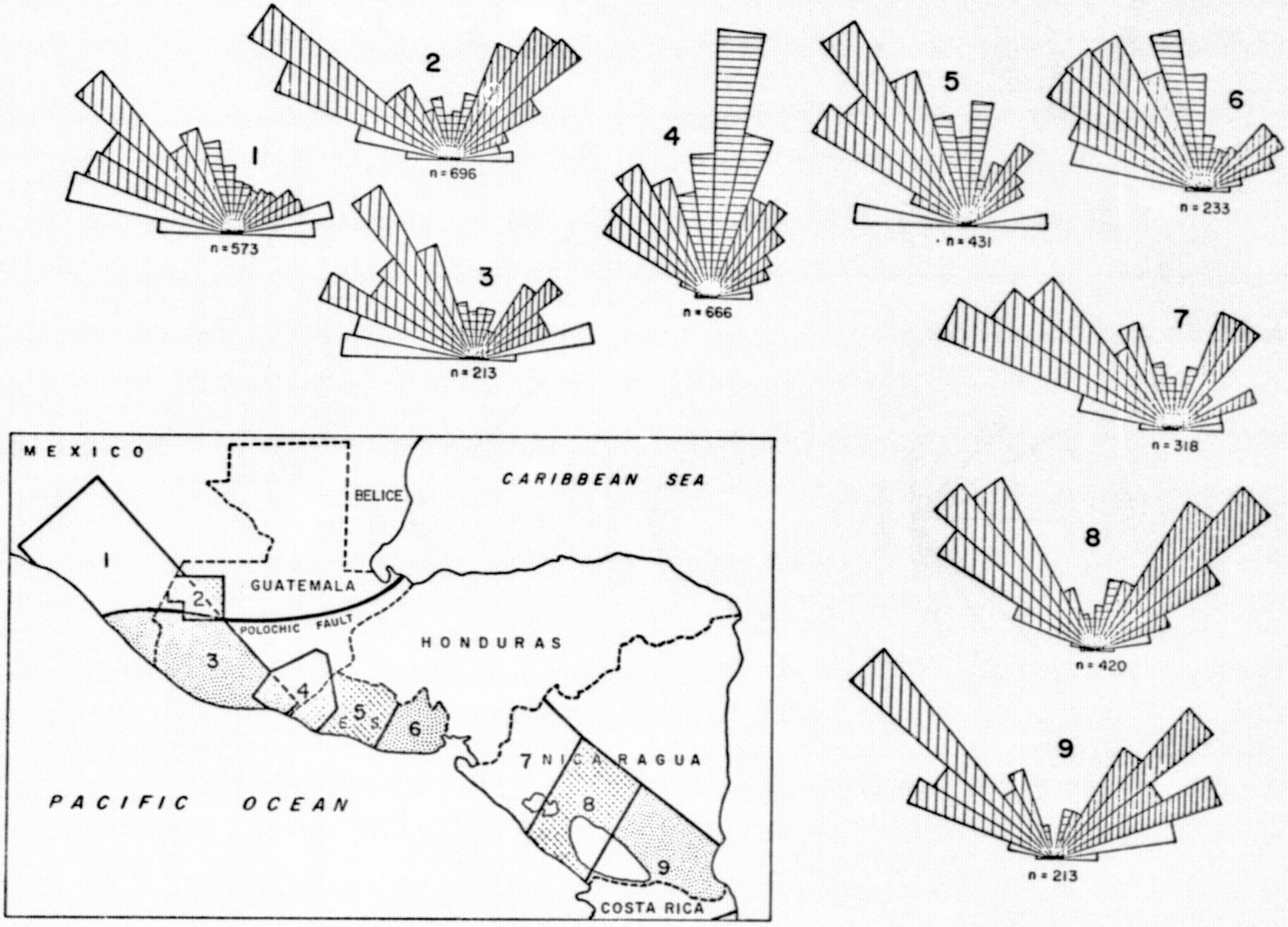


Figure 4: Rose diagrams of structural features from along the Central American volcanic axis. Numbered rose diagrams are keyed to areas numbered on the map. Sources of data are given in the text. The number of structures on which the rose diagram is based is given under each.

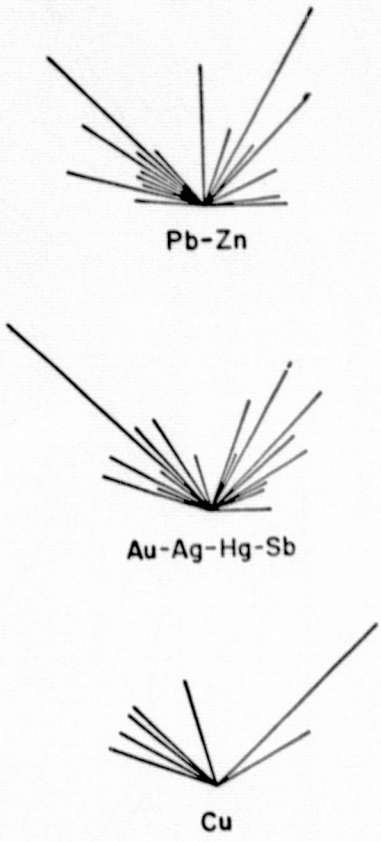


Figure 5: Rose diagrams of trends of veins and fractures associated with different types of Central American mineral deposits. Data on which the diagram is based comes from Roberts and Irving (1957). Trends of veins and fractures were plotted in 5° intervals.

QUANTIFICATION OF GEOLOGIC LINEAMENTS BY MANUAL AND MACHINE PROCESSING TECHNIQUES

BY

Melvin H. Podwysocki, NASA - Goddard Space Flight Center, Greenbelt, Md.,
Johannes G. Moik, Computer Sciences Corp., Silver Spring, Md., and
Walter C. Shoup, Computer Sciences Corp., Silver Spring, Md.

N76-17516

ABSTRACT

An on-going study is being carried out at Goddard Space Flight Center to study the effect of operator variability and subjectivity in lineament mapping and to examine methods to minimize or eliminate these problems by use of several machine preprocessing methods. LANDSAT scenes from the Anadarko Basin of Oklahoma and the Colorado Plateau were analyzed as test cases.

Four geologists mapped lineaments on an Anadarko Basin scene, using transparencies of MSS bands 4-7 and their results were compared statistically. The total number of fractures mapped by the operators and their average lengths varied considerably, although comparison of lineament directions revealed some consensus. A summary map (785 linears) produced by overlaying the maps generated by the four operators showed that only 0.4% were recognized by all four operators, 4.7% by three, 17.8% by two and 77% by one operator. Similar results were obtained in comparing these results with another independent group. This large amount of variability suggests a need for the standardization of mapping techniques, which might be accomplished by a machine aided procedure.

Two methods of machine aided mapping were tested, both simulating directional filters. One consists of computer (digital) processing of CCTs using edge enhancement algorithms. The other employs a television (analog) scanning of an image transparency which superimposes the original image and one offset in the direction of the scan line. Both methods created similar products, producing many more linear features than were observed by the geologists in the original work. This suggested some processing artifacts may have been introduced either in the machine processing or the original LANDSAT image. Various tests were performed which downgraded the possibility of artifacts.

Comparison with published data for the Colorado Plateau indicates that numerous directions of the edge enhanced linears do correspond with known directions of jointing and airphoto linears. Further study is required to determine the implications of these machine methods of fracture mapping before operator interpretations and automated machine mapping may be attempted.

INTRODUCTION

As part of an ongoing research program at Goddard Space Flight Center into the evaluation of linears as observed on satellite and aerial photograph images, the geologists of the Earth Resources Branch (EBR) have analyzed in detail a LANDSAT-1 image of a portion of the Anadarko Basin, Oklahoma, an area studied by the Eason Oil Co. in its LANDSAT-1 investigations. Their study attempted to evaluate the usefulness of space imagery for petroleum exploration through morphotectonic and fracture analysis. For this reason ERB chose the same scene for the purposes of 1) further investigation of anomalous structural features by spectral enhancement techniques, 2) extraction and classification of lineaments, and 3) comparison of results of the two independent groups. In addition, this same scene, as well as one of the Colorado Plateau of New Mexico, was processed by several automatic methods in order to determine the feasibility of linears enhancement. These processes will be discussed in detail later.

This paper has two purposes: 1) To point out the subjectivity and variability involved in mapping linear features by different interpreters, particularly in low relief terrains, and 2) to propose some automatic enhancement techniques, which with some reservations, may aid in eliminating some of this operator variability.

Lineaments are naturally occurring linear features observed on small scale remote sensing imagery. They are manifest in the imagery as various combinations of stream, tonal, vegetational and topographic alignments. Lineaments may be either continuous or discontinuous in nature, and can vary from several to several hundreds of kilometers in length. They are usually regarded as the surface manifestations of fault and fracture zones, or with zones of increased jointing, have been linked in one fashion or another with local or regional tectonics, and have been used on occasion as a tool for oil, gas (1-3) and minerals exploration.

The features discussed in this paper are unverified in the field and some are inevitably related to anthropogenic activity. Consequently, the more general terms "linears" or "linear features" will be used, however, it should be noted that a good many of these features would fall into the category of lineaments.

ANALYSIS OF OPERATOR VARIABILITY

Four geologists of the ERB mapped lineaments on MSS bands 4 - 7 over a period of several days in order to minimize mapping fatigue. A maximum of six hours was spent by individuals in examining the scene. Each geologist, within the constraints of the definition, mapped what he determined to be a lineament, and it was agreed that cultural features should be ignored. A lack of communications resulted in only 3 of the 4 operators ignoring the cultural features. This will be evident in the ensuing illustrations.

All four MSS bands were analyzed, beginning with 5 and 7, followed by the two remaining bands. Composite maps of linears were generated for each operator, summarizing each individual's results for all four bands onto one overlay. A summary map was then created, comparing the results of all four operators by overlaying their results and checking for coincidence of linears. All linears which fell within approximately one km (1 mm on the 9 x 9 inch LANDSAT image) of each other and deviated by no more than approximately 3 degrees were considered contiguous. Where two linears overlapped by more than half their length, they were considered to be coincident.

Figure 1 illustrated the Anadarko Basin scene, an area underlain mainly by gently dipping (less than 2 degrees) sedimentary rocks of Pennsylvanian and Permian ages. Figure 2 illustrates the results of the individual mapping efforts by the four operators. Very little information was added to the analysis by the use of MSS bands 4 and 6, so that they were not included in the analysis. Furthermore, if a linear feature was noted in one band, it could usually be found on the other, but some of the linears were more apparent on one.

A wide disparity in the number of linears mapped and their average lengths is noted in Figure 3 which is a frequency (number of linears)/azimuth class and density (summed length of linears)/azimuth class plot for each of the four operators. There was a tendency for the operators to map linears of differing average lengths as well as total numbers. Moreover, some operators, in varying degrees, mapped features which were associated with the north-south and east-west boundaries of the midwestern land-grid system. This is particularly evident in the results of operator 4. Operator 2 picked very few linear features in the northwesterly directions. This may be partially the result of unfamiliarity with these features and because of the sun's southeasterly position, which preferentially enhances the northeasterly trending linear features.

Variability due to illumination is not discussed in this paper, but is noted by Wise (4) and Siegal (5), and is another major factor to be considered. Generally, the northeast and northwest directions, corresponding to Sonder's "regmatic shear" (6) are found by the majority of operators. Operators 1 and 3 show the closest correspondence. This result may be attributed to the fact that they both had considerable prior industrial and/or academic experience in lineament mapping. A Chi Square test (4 operators x 18 azimuth classes contingency table) shows that the operators did not map the same directions based on a .01 level of rejection. Elimination of operator 2 (3 x 18 contingency table) produced results which show no cause to reject the hypothesis that the remaining three operators picked the same directions based on a .05 rejection level.

A comparison of the linears picked by the 4 operators is summarized in Figure 4. It can be seen that only a very minor amount of the total was seen by all four operators. Only 22.9% was seen by at least 2 operators. In defense of the operators in this test, it should be stated that the area chosen was less than ideal for this type of test, because of 1) the dominating effect of man's activities and 2) the relatively low relief of the terrain. Analysis of more rugged terrain would likely show better agreement.

A comparison of the work performed by the Eason Oil Co. (7) with the ERB geologists (Figure 5) shows only 20% of the linears were seen by both groups, using the combined linears map of the ERB group. This lack of coincidence is further reinforced in the Eason Oil study, where their comparison of Skylab and LANDSAT mapping resulted in only a 30% agreement between the two sets of imagery (7). Figure 6 illustrates the frequency/azimuth and density/azimuth histograms for the Eason Oil and ERB groups. Besides those linear features which are in agreement, a Chi Square test (2 x 18 contingency table) comparing linears directions seen by each of the two groups, gives no reason to reject the hypothesis that they are mapping the same directions, even though the individual linear features do not agree.

The above comparisons show that selection of individual linears is highly subjective, but that with training, a regional pattern suitable for tectonic interpretation may be possible, particularly within a closely knit group of geologists. However, any attempt to reach agreement among the members of the whole geologic community would prove more difficult, as interpretations of lineaments will vary.

AUTOMATED PROCESSING FOR LINEARS EXTRACTION

It therefore seems imperative that in order to minimize differences both between operators and between institutions, some truly objective standardization criteria are

required. This is particularly important when analysis is made to define minor changes in lineament density, a factor which some have claimed as a geologic exploration tool for structures suitable for petroleum accumulation (1,8,9).

Several philosophies exist, two of which are discussed here. One would entail rigorous training of operators to pick the same features and might prove successful at least within one or several closely cooperating institutions. This technique, unfortunately, does not eliminate other factors such as changes in operator acuity due to fatigue or mental attitude. Another approach is through machine processing: one involving either a completely automated procedure of pattern recognition and mapping or a semi-automated one in which linears are enhanced for ease of operator interpretation. Machine methods still require some interaction to eliminate cultural effects. Goetz (pers. comm.) found that a fully automated method requires an inordinate amount of computer processing of the image and would still not produce an accurate map devoid of cultural effects.

Several methods for semi-automated mapping of linear features are presently available. One involves the use of an analog television system, which scans an image with a vidicon camera, electronically producing a positive and negative version of the image offset from each other by a minute amount along the scan line direction. This is analogous to a masking technique discussed by Wier and Wobber (10), where positive and negative transparencies are superposed to produce a product from which linears could be mapped. A single image developed by this electronic offsetting gives only part of the information, as the technique selectively enhances only certain directions. However, the problem is easily circumvented by a stepwise rotation of the image through 180 degrees, thus enhancing all possible directions of linears. A final product would involve creating a composite of a number of these images, taken at different rotations to the television scan lines. The method is advantageous, because it allows for a rapid inspection of the image, but it produces a somewhat spatially degraded result.

The second method uses digital image processing techniques. High pass digital filtering is used to enhance linear features employing an interactive variant of the Jet Propulsion Laboratory VICAR system implemented at Goddard Space Flight Center. Both directional and non-directional filters were tested. Thus far, most success has been achieved with the directional filters and these will be discussed herein. Although this system does not have the real-time quick image rotation and display, it excells in giving the best possible resolution and variety of filter possibilities.

Both systems produced many more linears for a given direction than had previously been detected by the unaided eye. Consequently, many of the features became suspect as machine artifacts.

Both systems enhanced those linear features which were inclined at a relatively low angle either to the television scan line or filter direction in the digital case. Figure 7 shows the results of edge enhancing a star test pattern on the analog system. It can be seen that the finest lines which are preferentially enhanced are inclined at small angles (15°-30°) to the horizontal or scan line direction of the system.

Rotation of a LANDSAT image on the television system produced sets of linears which were enhanced when brought within this critical angle, which would rotate with continued image rotation, and would then disappear as these features passed out of the critical angular field. Thus, the television image was not continuously occupied by linears, but only when a set would come into the critical field, suggesting that the features were real.

The possibility of an electronic "ringing" (i.e., spurious linears generated when a set of linears fell within the critical angle) induced by the techniques was examined for the analog system. This would be manifested as a repetition of a pattern on the screen beyond the actual confines of the pattern. A grid of progressively closer spaced lines was examined on the television system, and no ringing effects were noted.

It was also suggested that the digital LANDSAT data or its resultant image might have some systematic processing or electronic artifact unrelated to the sensed image. However, examination of Skylab S-190B photography, free of digital processing, produced similar patterns of linears directions when processed with the television system.

A comparison between the LANDSAT digitally processed data and the high resolution S-190B photography showed that in many instances, linears could be correlated between the two, although some were of obvious man-made origin. This observation is exemplified in Figure 8. These features have yet to be field-checked to determine their origin.

In order to determine if these detected linears processed from LANDSAT imagery could be related to lineaments, a comparison was made with the detailed lineament mapping of Kelley and Clinton (11) for a portion of the Colorado Plateau of New Mexico. Both analog and digital techniques were investigated and the enhanced images were qualitatively compared using an optical transferring device. The processed LANDSAT images reveals coincident lineament directions, but again, many more features can be isolated from the image compared to the map. Figures 9 and 10 illustrate the comparisons.

CONCLUSIONS

Studies of operator variability in the mapping of fracture patterns and lineaments has shown that:

1) Operators have differing concents as to the average lengths of lineaments..
2) There is little reproducibility between operators or groups in the selection of individual linears, although with some training, they may pick the same directions.

Processing of imagery by both digital and analog methods indicates that:

1) There are many more linear features than are detected by the unaided eye.
2) There is agreement between the two processing techniques, and the features seen are related to linear features on the ground; in some cases they are of obvious man-made origin.
3) A comparison of a processed LANDSAT image and a map of lineaments created from relatively large-scale photography indicates a concurrence in directions of individual lineaments, although many more features are seen by the enhancement.
4) The analog television system allows a reconaissance inspection of the imagery, but suffers from degraded resolution. Ultimate detail and greater processing flexibility can be achieved by using digital processing of the LANDSAT computer compatible tapes. The effect of filter size, direction, and shape must be investigated to determine optimum criteria for quantification. These factors are being investigated at this time.
5) The data must still be interpreted by the operator to eliminate cultural effects. Although the large number of linear features enhanced will most likely lead to operator variability, it may fall within more tolerable limits.
6) Ultimately, automatic recognition techniques must be developed to allow complete quantification.

REFERENCES

(1) Blanchet, P.H., 1957, Development of fracture analysis as an exploration method; Bull. Amer. Assoc. Petrol. Geol., V. 41, No. 8, p. 1748-1759.

(2) Podwysocki, M.H., 1974, An analysis of fracture trace patterns in areas of flat-lying sedimentary rocks for the detection of buried geologic structure; NASA-Goddard Space Flight Center Document X-923-74-200, 77 p.

(3) Podwysocki, M.H. and Gold, D.P., 1974, The surface geometry of inherited joint and fracture trace patterns resulting from active and passive deformation; NASA-Goddard Space Flight Center Document X-923-74-222, 37 p.

(4) Wise, D.U., 1968, Regional and sub-continental sized fracture systems detectable by topographic shadow techniques; in Conf. on Research in Tectonics (Kink Bands and Brittle Deformation), (Baer, A.J. and Norris, D.K., eds.), Geol. Surv. Canada Paper 68-52, p. 175-199.

(5) Siegal, B.S., 1975, Significance of operator variation and the angle of illumination in lineament analysis on synoptic images; paper in preparation, Jet Propulsion Labs., Calif. Inst. Technol., Pasadena, Calif.

(6) Sonder, R.A., 1947, Discussion of "Shear patterns of the earth's crust" by F.A. Vening Meinesz; Trans. Amer. Geophys. Union, V. 28, No. 1, p. 1-61.

(7) Collins, R.J. and Everett, J.R., 1975, Evaluation of the suitability of Skylab data for the purpose of petroleum exploration; Eason Oil Corp. Quart. Report, NASA contract NAS9-13297, March, 1975, 22 p.

(8) Gol'braikh, I.G., Zabaluyev, V.V., Lastochkin, A.N., Mirkin, G.R., and Reinin, I.V., 1968, Morfostrukturnye metody izucheniya tektoniki zakrytykh platformennykh neftegazonosnykh oblastei (Morphostructural methods for the study of tectonics in covered platform oil and gas bearing regions), NEDRA, 151 p.

(9) Gol'braikh, I.G., Zabaluyev, V.V., and Mirkin, G.R., 1968, Tectonic analysis of megajointing: a promising method of investigating covered territories; Internat. Geol. Rev., V. 8, No. 9, p. 1009-1016.

(10) Wier, C.E. and Wobber, F.J., 1975, Application of ERTS-A (LANDSAT-1) imagery to fracture related mine safety hazards in the coal mining industry; IBM Corp., Civil/Space Systems, Gaithersburg, Md., 125 p.

(11) Kelley, V.C. and Clinton, N.J., 1960, Fracture systems and tectonic elements of the Colorado Plateau; Univ. of New Mexico Publ. in Geology, No. 6, 104 p.

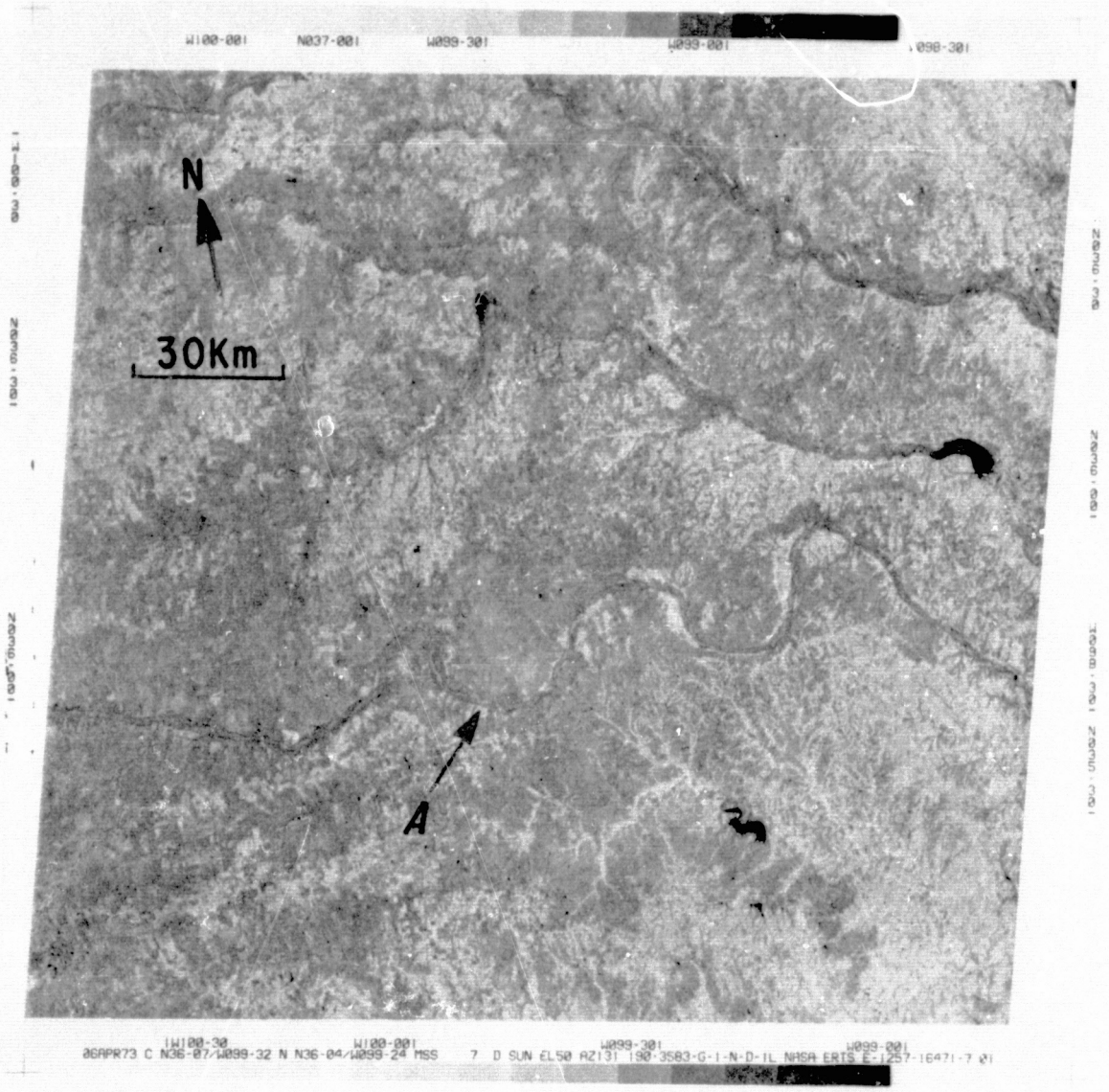


FIGURE 1

MSS Band 5 rendition of a LANDSAT-1 image of a portion of the Anadarko Basin, Oklahoma. The meander of the South Canadian River (labeled A) will be illustrated in later figures.

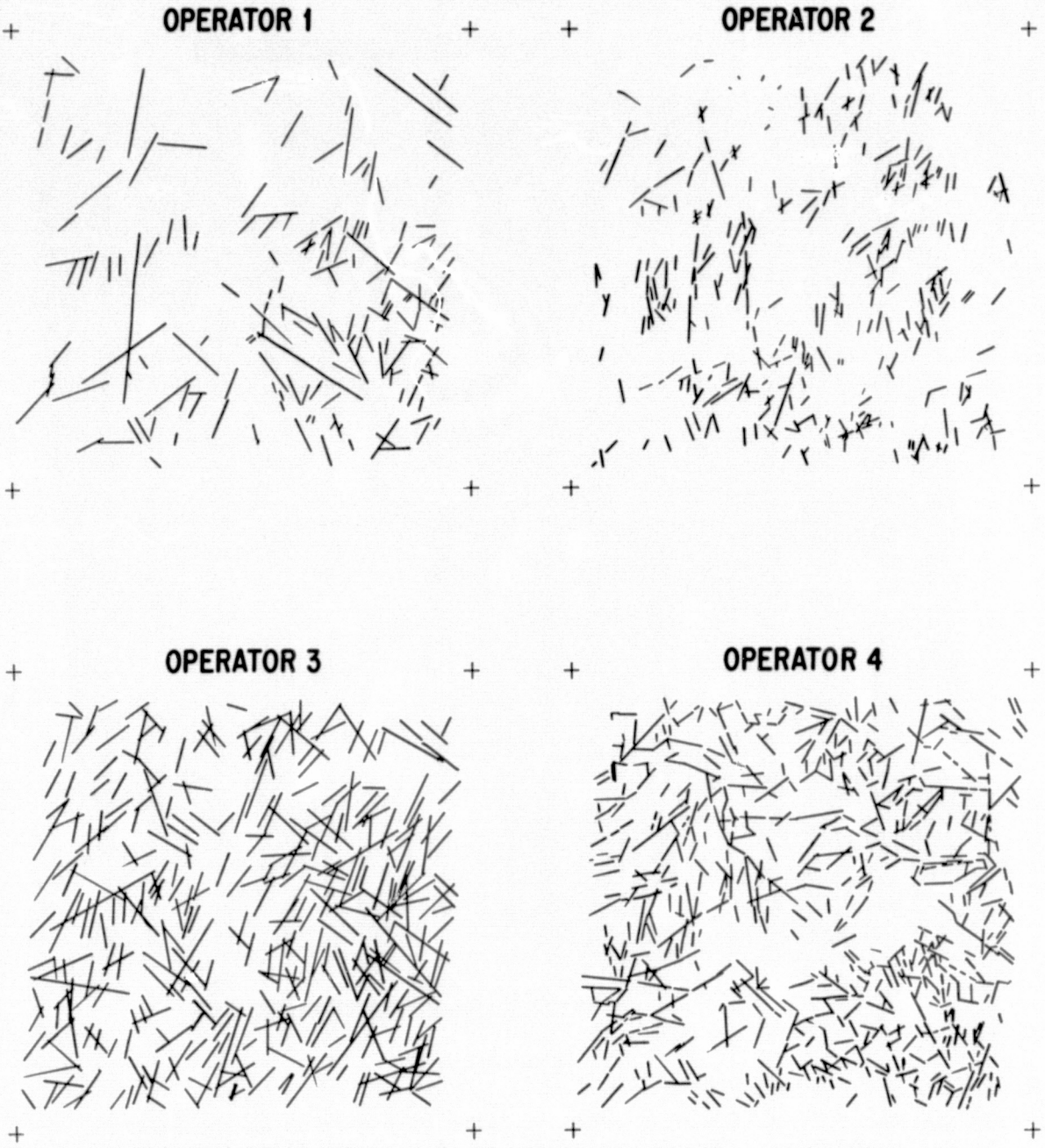
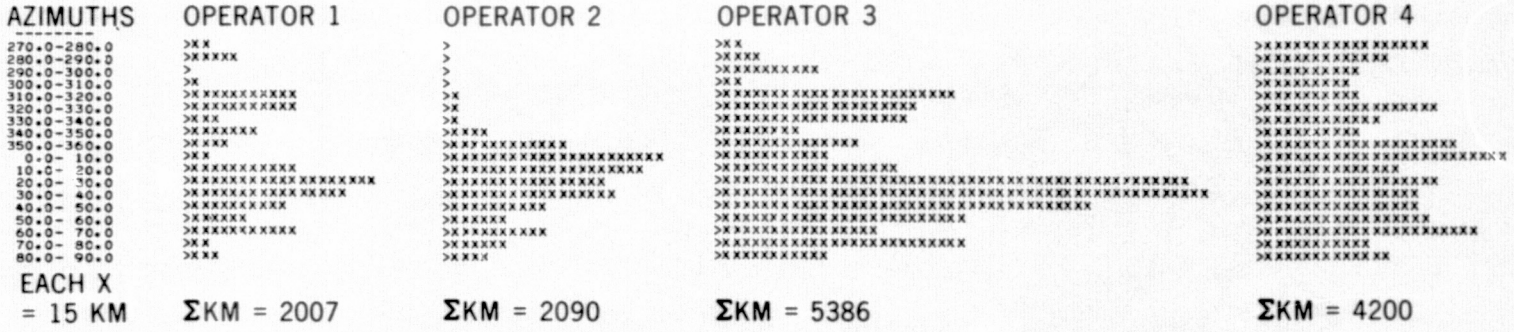


FIGURE 2

A comparison of linear features mapped by the four operators. MSS Bands 5 and 7 are included in this composite. The tic marks correspond with the registration marks on the LANDSAT image.

EVALUATION OF OPERATOR VARIABILITY IN LINEARS SELECTION, ANADARKO BASIN

LINEARS SUMMED AS LENGTH/AZIMUTH CLASS



LINEARS SUMMED AS NUMBER/AZIMUTH CLASS

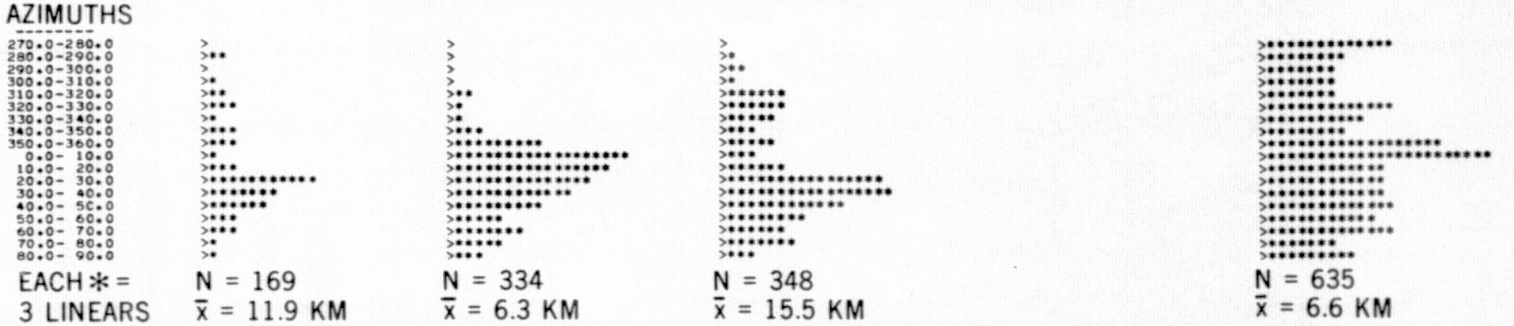


FIGURE 3

A comparison of density (total length of linears mapped) and frequency (number of linears mapped) per azimuth class for each of the operators. A Chi Square contingency table (4 x 18) showed that the operators were not mapping the same population of linears based on a .01 level of rejection. Removal of operator 2 from the analysis indicates that there is no reason not to believe the remaining 3 operators were mapping the same population based on a .05 level of rejection.

REPRODUCIBILITY OF THE
ORIGINAL PAGE IS POOR



FIGURE 4

Composite map of coincident linears for the four ERB geologists. Only 3 (0.4%, shown in black) of the total 785 linears were seen by all four operators, 37 (4.7%, in green) by three, 140 (17.8%, in purple) by two and the remainder (in brown) by one of the four.

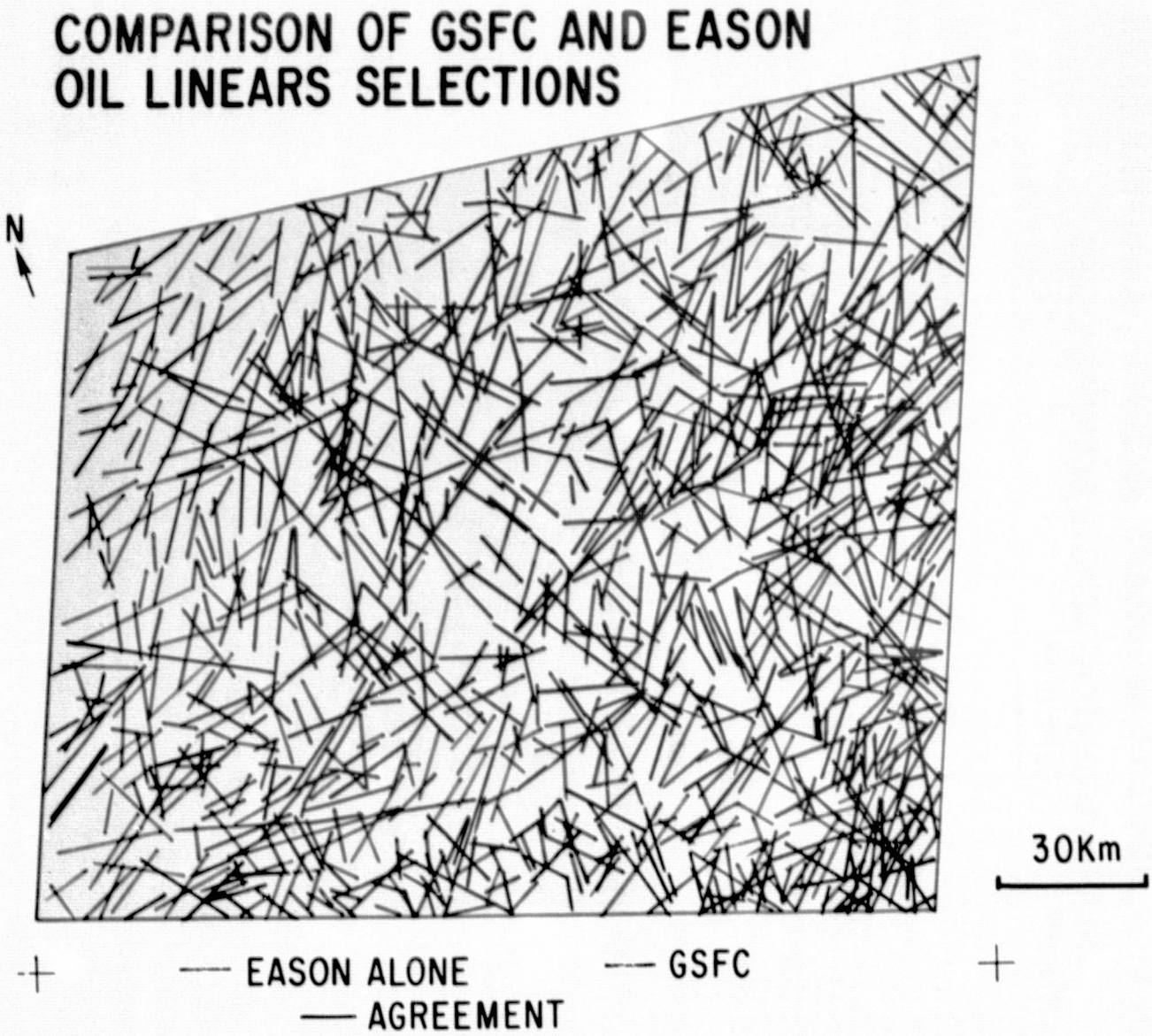


FIGURE 5

Comparison of coincident linears between Eason Oil and Earth Resources Branch maps for a portion of the same Anadarko Basin area. Only 20% (shown in black) agreement was found between the two groups, 50% by ERB (in brown) and 30% (in green) by Eason Oil. The Eason efforts were based on several images, whereas the ERB results were the result of analysis of one image.

EVALUATION OF VARIABILITY IN LINEARS SELECTION, ANADARKO BASIN

LINEARS SUMMED AS LENGTH/AZIMUTH CLASS



LINEARS SUMMED AS NUMBER/AZIMUTH CLASS

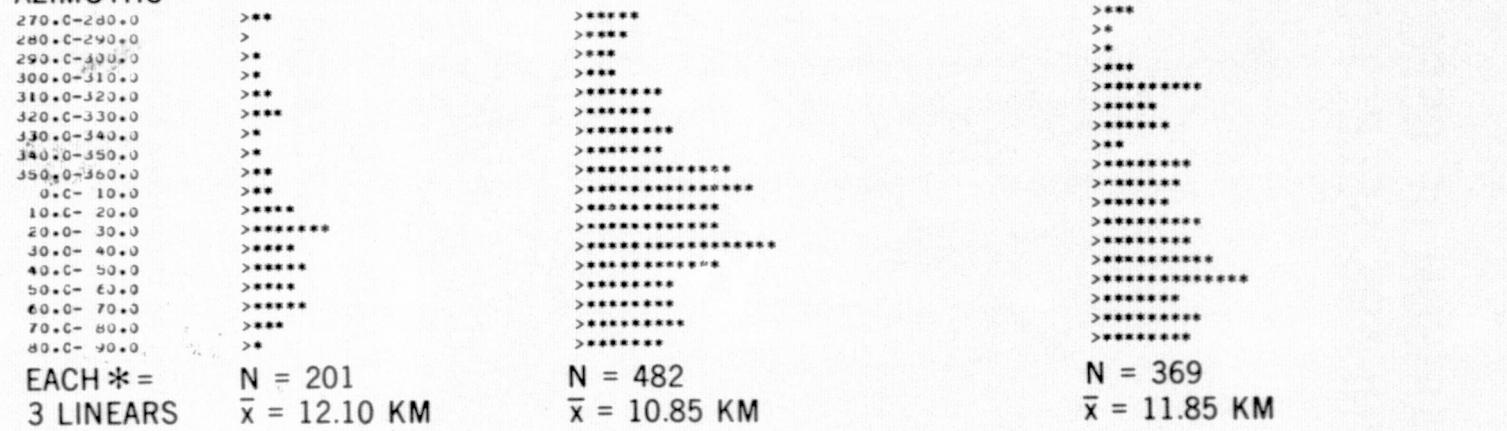


FIGURE 6

A comparison of density and frequency per azimuth class for the Eason Oil and ERB (4 operators) maps of linear features. Although only 20% of the linears were in agreement, a Chi Square test of those mapped by the two organizations and not in coincidence (2 x 18 contingency table), gave no reason to reject the hypothesis that the two groups were mapping the same directions of features based on a .05 level of rejection.

REPRODUCIBILITY OF THE ORIGINAL PAGE IS POOR

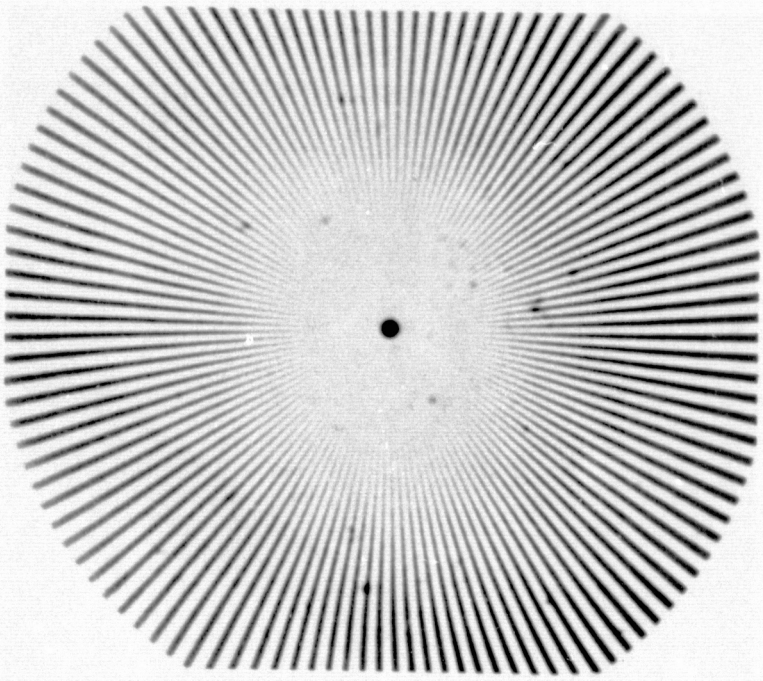


FIGURE 7a

Unenhanced version of the star test pattern as viewed on the television screen (analog process). Note that as the lines become finer towards the center of the pattern, they become less distinguishable.

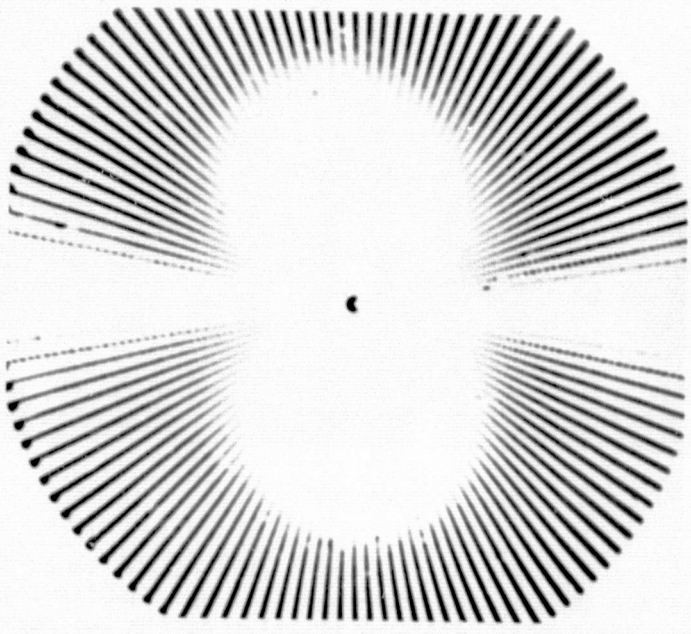


FIGURE 7b

Enhanced version of the same pattern. The lines are preferentially enhanced (their fine detail is seen closer to the center of the pattern) in the area inclined at a relatively shallow angle (15°-30°) to the horizontal scan line. Note also that those lines parallel to the scan line direction are not visible.

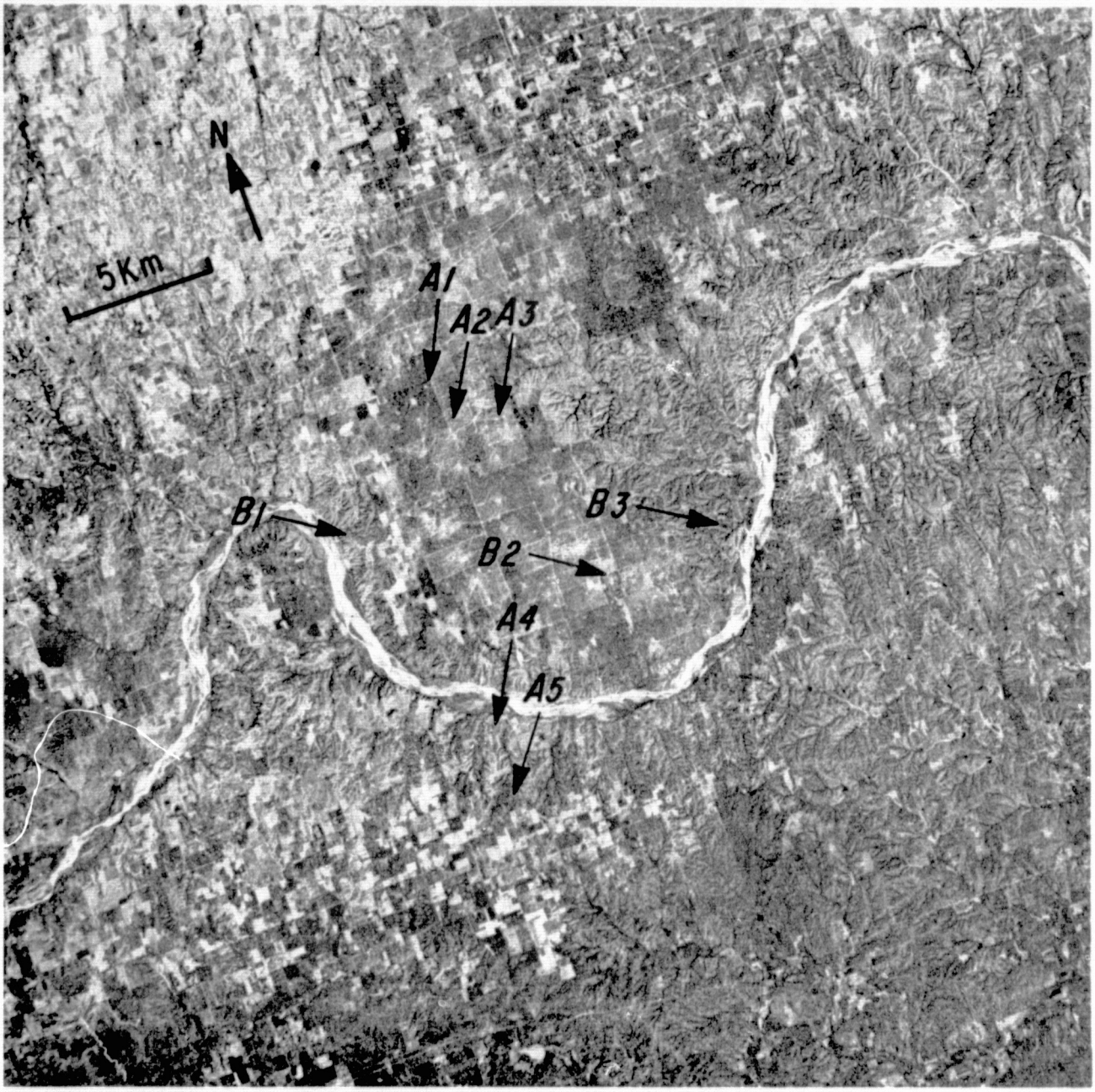
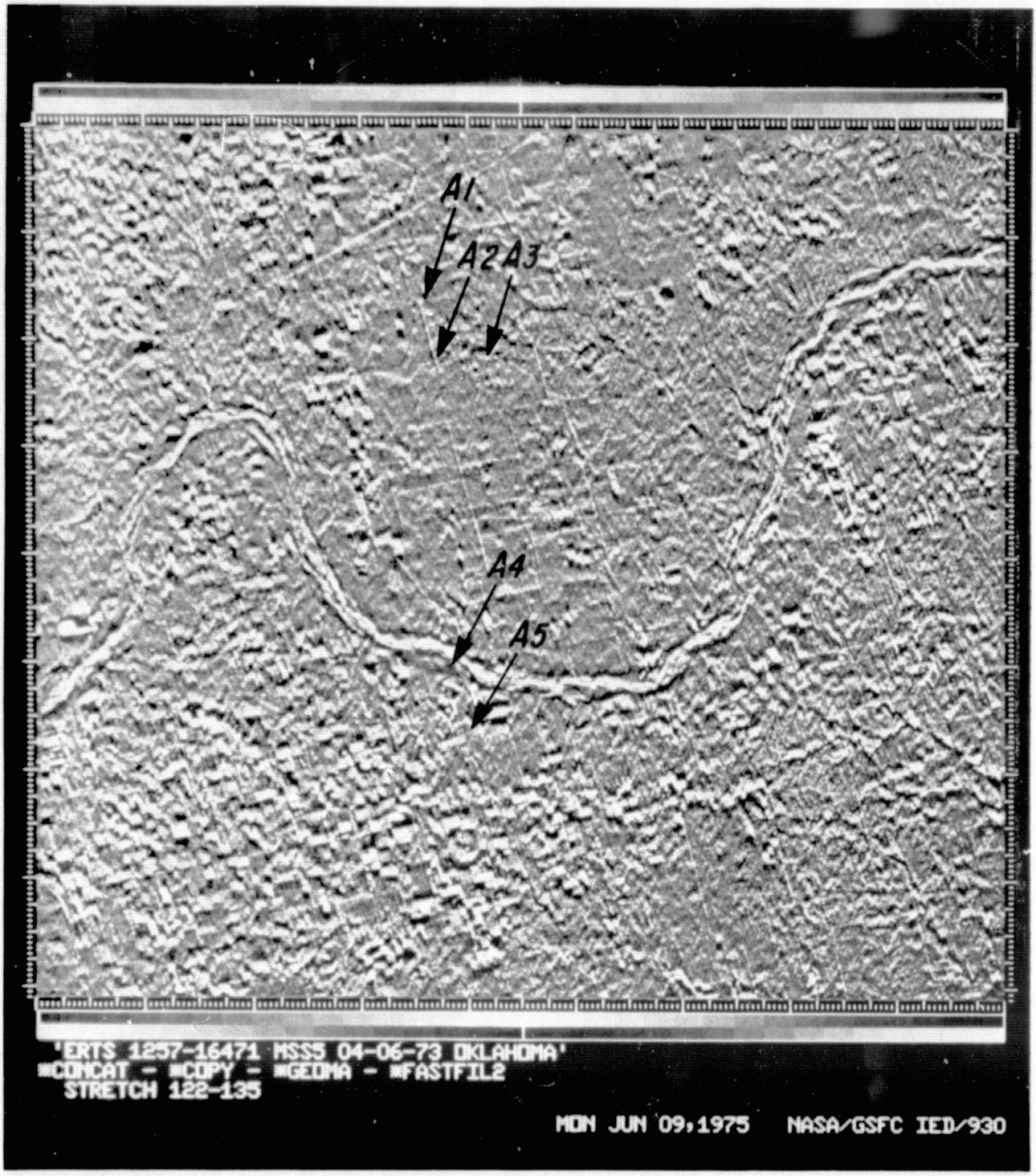


FIGURE 8a

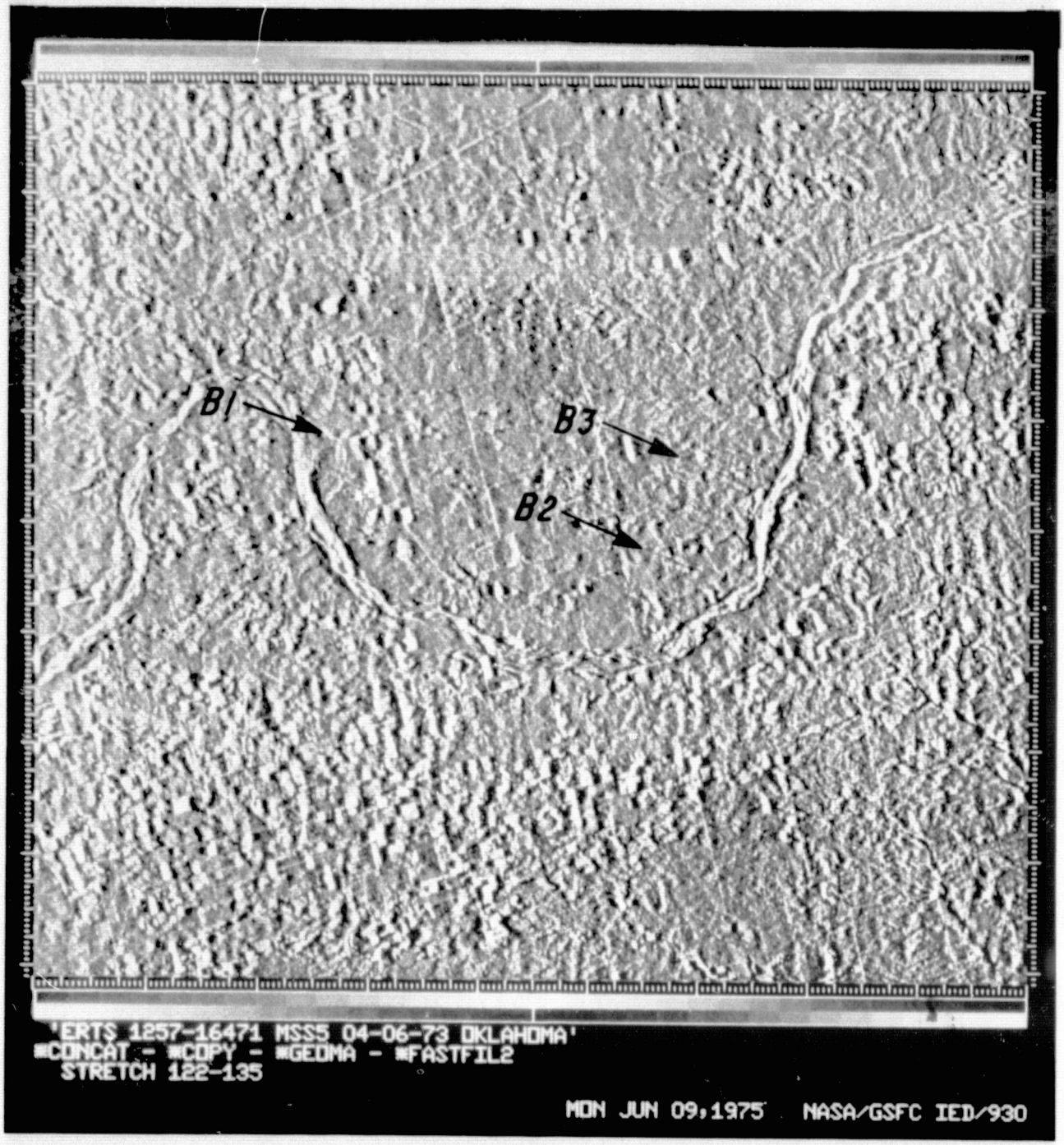
Comparison of a Skylab S-190B photograph (8a) of the South Canadian River meander and the digital high-pass filtered LANDSAT-1 images for the same areas (8b & 8c). A filter oriented nearly due north (perpendicular to the MSS scan line direction) was applied in Figure 8b. Arrows marked A1-A5 (Fig. 8a & b) mark the northern extent of representative linear features observable on the Skylab photograph. Linear A1 is most likely due to culture. A filter oriented parallel to the MSS scan line was applied to the image illustrated in Figure 8c. Arrows B1-B3 mark the westernmost extent of representative linear features in Figures 8a & c.

REPRODUCIBILITY OF THE
ORIGINAL PAGE IS POOR



8b

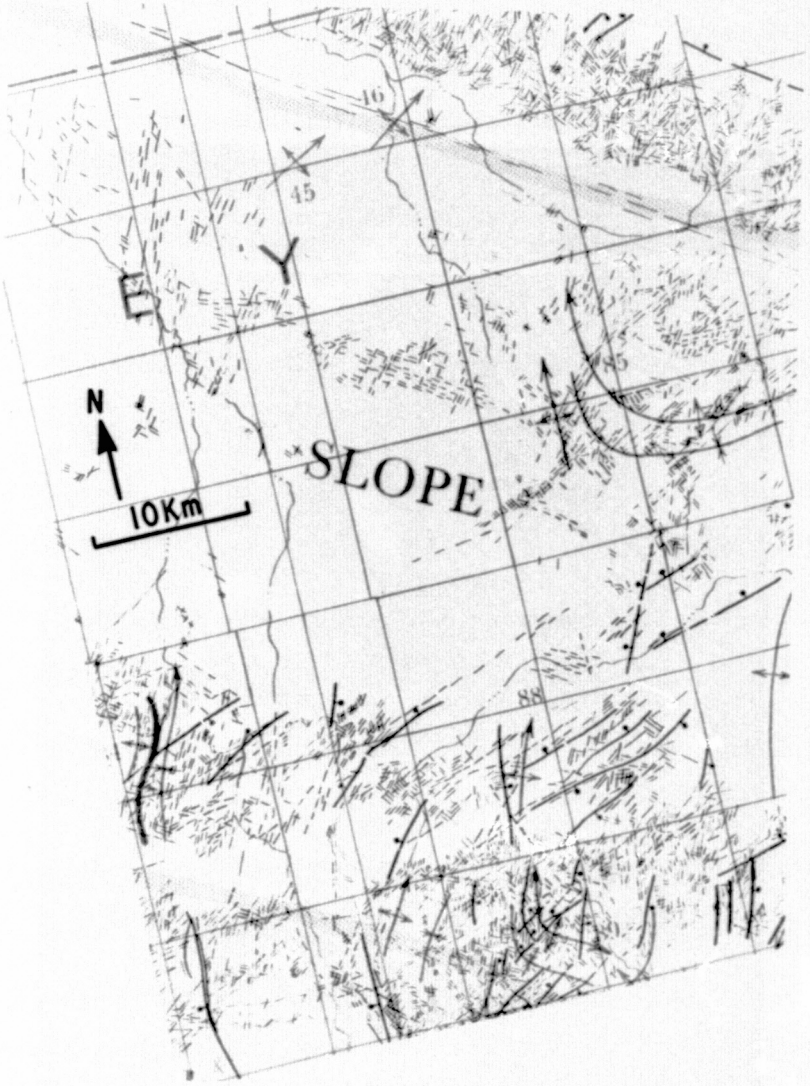
REPRODUCIBILITY OF THE
ORIGINAL PAGE IS POOR


B1
B3
B2
'ERTS 1257-16471 MSS5 04-06-73 OKLAHOMA'
#CONCAT - #COPY - #GEOMA - #FASTFIL2
STRETCH 122-135
MON JUN 09,1975 NASA/GSFC IED/930

8c

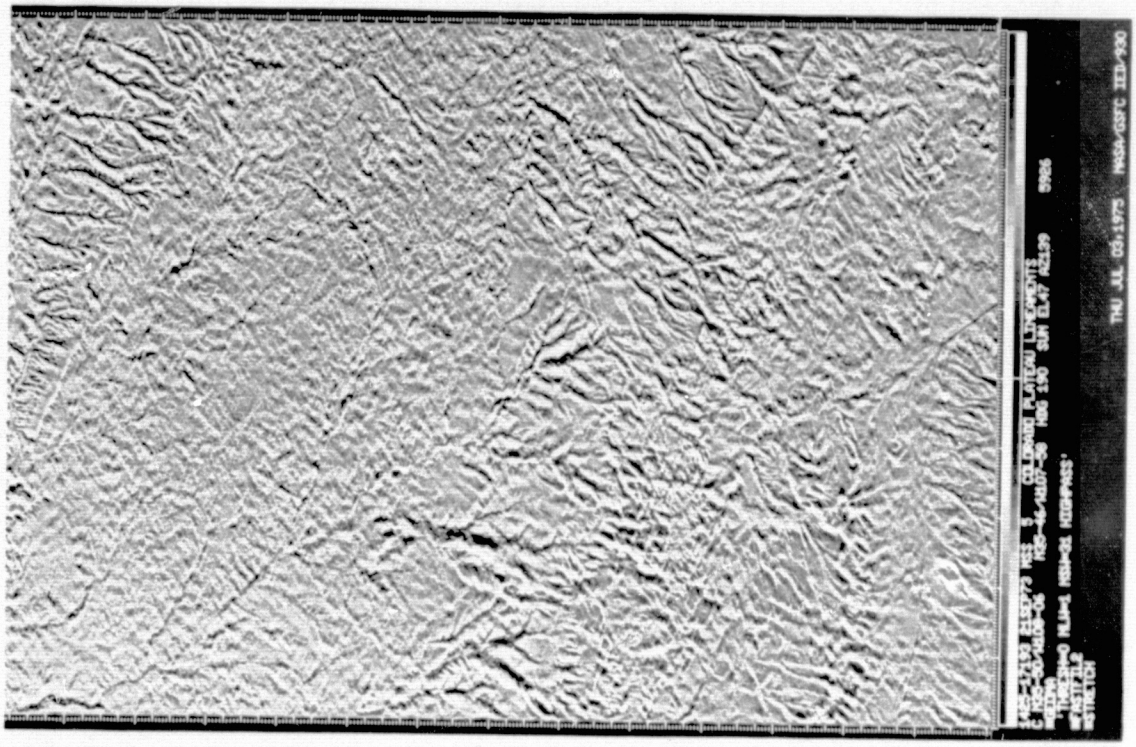


9a

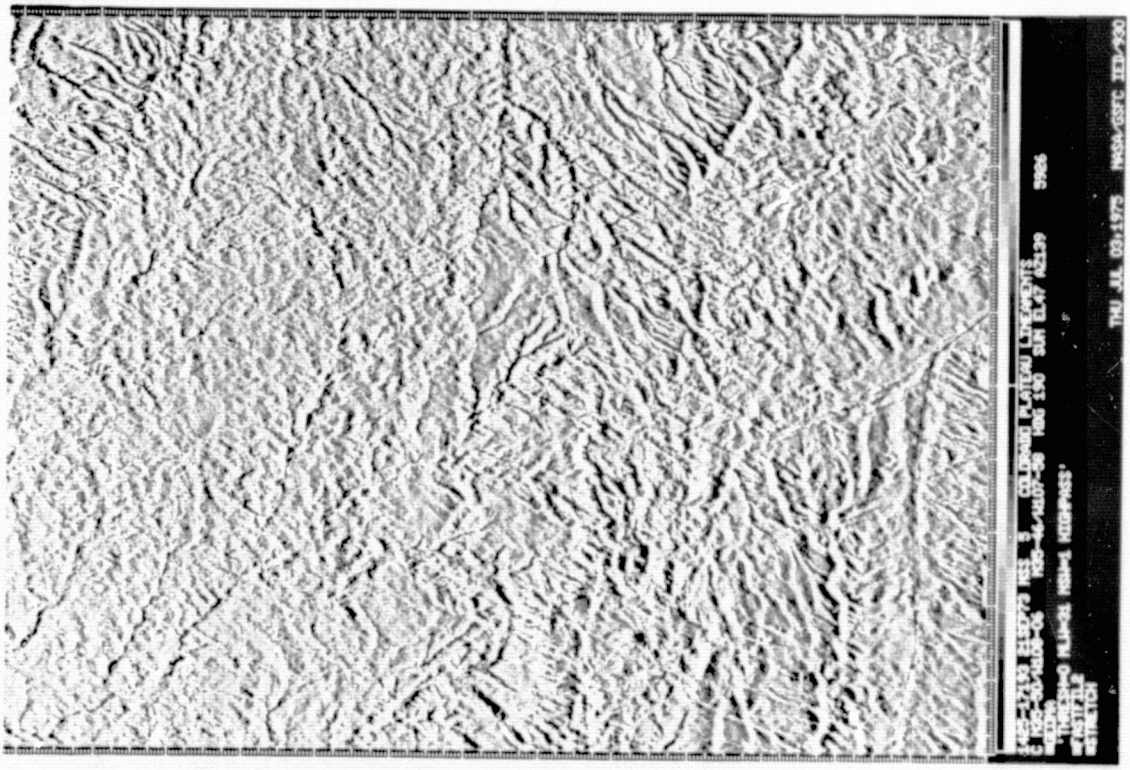


9b

FIGURE 9 A non-enhanced version of MSS Band 5 of a portion of the Colorado Plateau test area (Figure 9a) and its corresponding part from the fracture map of Kelley and Clinton (11) (Figure 9b). Figures 9c and 9d represent high pass digital line filters respectively oriented normal and parallel to the scan line direction.

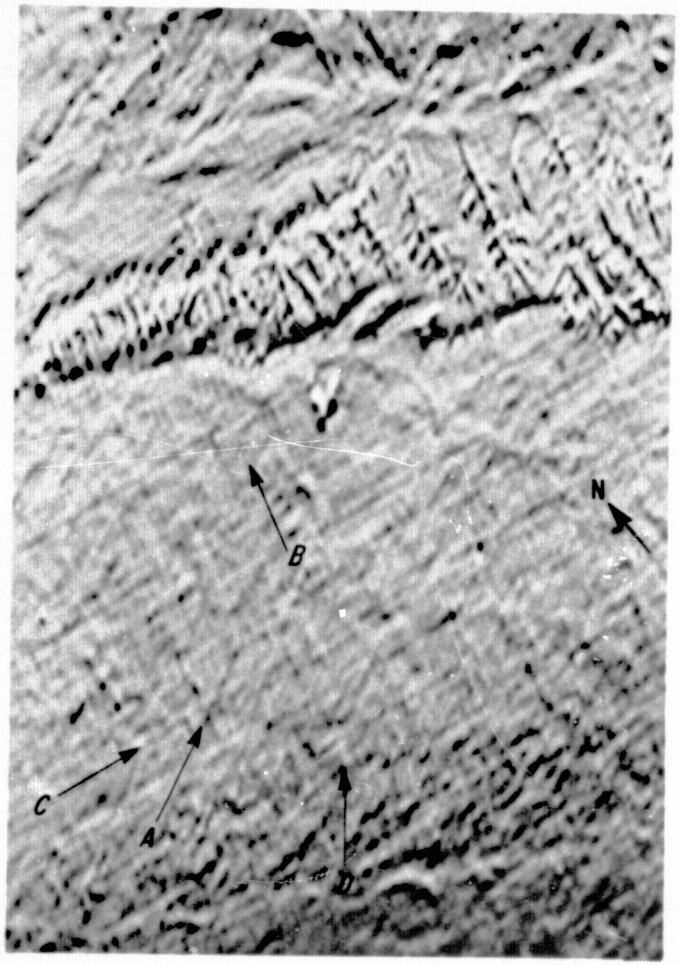


9d

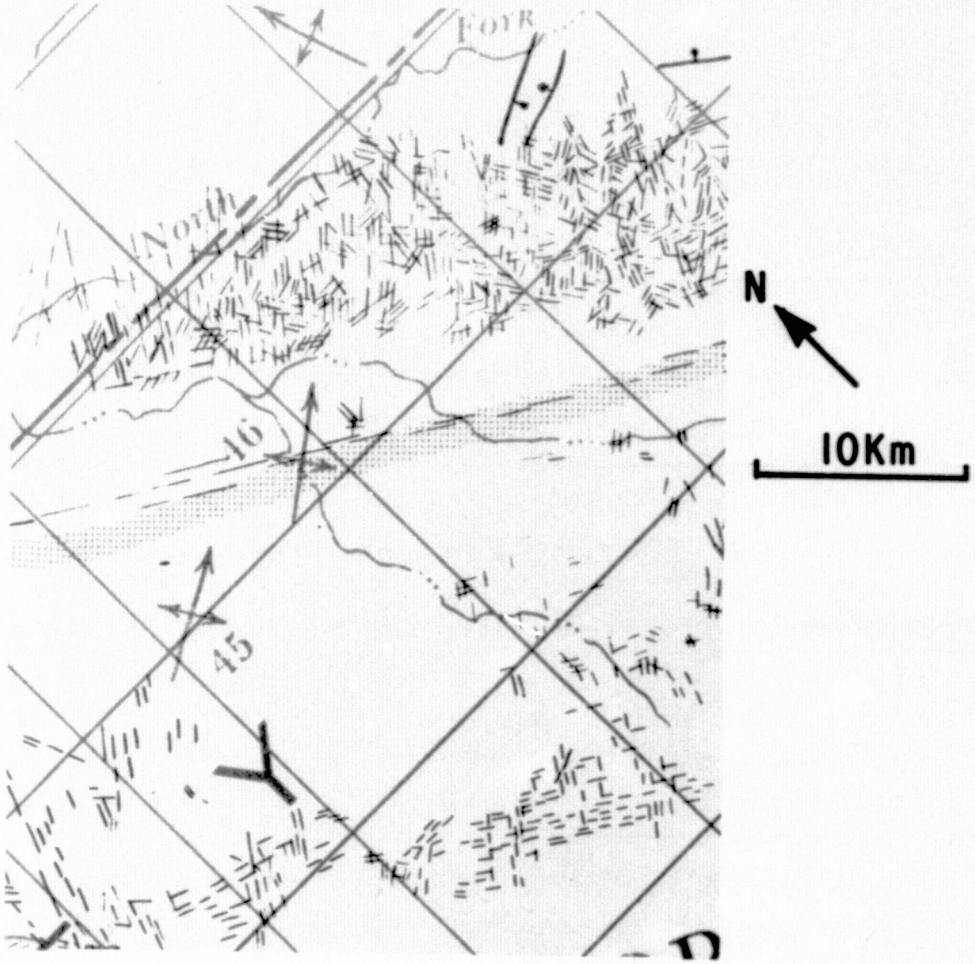


9c

REPRODUCIBILITY OF THE
ORIGINAL PAGE IS POOR



10a



10b

FIGURE 10 A television (analog) enhancement of a portion of the area covered in Figure 9a (Figure 10b). Arrows labeled A and B in Figure 10a are representative of the directions of enhanced linear features. Arrow C is the direction of the MSS scan lines whereas D represents the television scan line direction.

CREATING A SYSTEM FOR THE GEOLOGICAL EXPLOITATION OF SATELLITE IMAGES: AUTOMATIC MAPPING AND GEOPHYSICAL DATA COMPARISON

G-20

By S. Braconne, M. Cavalier, M. Dubesset, J. Guillemot and M. Guy,
Institut Francais du Petrole, 92502 Rueil Malmaison, France

N76-17517

ABSTRACT

A conventional detailed analysis of images cannot become sufficiently detached from known geological facts to provide new viewpoints in investigating clues showing tectonic relationships on satellite images.

An original way is described that attempts to totally integrate satellite images into a geophysical data interpretation system.

The less conventional aspects are:

i. An attempt to automatically interpret images by structural, mainly topological, methods for the mapping of geological contours.

ii. An analysis of the position relation of the contours gives a skeleton stratigraphy (order of succession).

iii. A system combining some of the extracted elements with geographic data to make an objective search for an interpretation hypothesis.

Only part of this system is operational at present. Some examples are presented.

INTRODUCTION

The target of the Pyralp project was to investigate clues showing tectonic relationships between the Pyrenees and the Alps (1)*. From the very beginning it became apparent that a conventional detailed analysis of images could not become sufficiently detached from known geological facts to provide frankly new viewpoints as suggested by the major lineaments detected.

Indeed, the path of the lineaments often coincided with known geological objects that were very different in their nature, structural meaning and age. For example (2), the most extensive of the lineaments detected between the Ligurian Alps and the southern Cantabrian Pyrenees, going via Languedoc and cutting through the Pyrenees south of Pau, proved on the ground to be a transcurrent fault in the Mercantour Massif, the northern boundary of a complex fold system with a "Provencal" trend (NE-SW), the alignment of a valley in the recent Valensole formations, the overlapping frontal fault toward the south of the Luberon anticline, the S-shaped folds north of Montpellier which overlap toward the north, etc.

---

*Digits refer to the list of references.

PRECEDING PAGE BLANK NOT FILMED

Since the same evidence can be found with regard to most of the lineaments detected, it might seem that field geology merely detects epiphenomena that must be linked to causes having a rather vast geographic extension and a relatively long lifetime and that are located sufficiently deeply to appear under various geological aspects on the surface.

The search for these deep-lying phenomena linked to lineaments must be done by making a systematic analysis of the relations the lineaments have with numerous geological or geophysical facts of varying kinds. The lineaments that can be traced are themselves very numerous, and experience has shown that each geologist tends to detect them more or less in keeping with his tectonic notions. So it is tempting to have recourse to computer data processing both for discovering "interesting objects" and for analyzing the correspondences between them and the geophysical data.

As a result, the operational exploitation of images supplied by satellites (LANDSAT, Skylab, NOAA, etc.) for geological prospecting and petroleum exploration can be done in two ways:

i. One way follows traditional photointerpretation methods and uses satellite images as very small-scale aerial photos. The interpreter-geologist can be helped out by overall image enhancements or by highlighting various characteristic features (filtering).

ii. The other way, whose inception and initial application are described here, seeks to make a total integration of satellite images into a geophysical data interpretation system. Its aim is to supply geologists with automatically pre-interpreted documents such as photogeological maps with or without the elimination of surface formations, maps of lineaments reduced to basic features, and surveys of differing-origin anomaly coincidences (earthquakes, mineral concentrations, gravimetric anomalies, etc.).

The different parts making up the system are compiled simultaneously by several scientists, each in an order that is not the one perceived by future users, but rather that of the logical difficulty.

Likewise, in this methodological phase, the data used may be either unprocessed data from a satellite image, when comparison with the results of a manual interpretation so requires, or else data from a digitized image. In some cases, and this will be the general case in the future, the initial textures are the result of preprocessing and classification of multispectral data analyzed elsewhere (3).

Some links in the chain are still missing but the examples we describe show that the construction of such an automatic interpretation system is possible within a reasonable length of time.

Part of the method is entirely classic. This is a file containing image references and processed by short programs and printouts or the cartographic plotting of selected images. It can also be used to plot interpretations. However, scale changes led us to write an original contour generalization program. An example is given of generalization in order to reduce the scale of a base map.

The other two parts are less conventional. One is an attempt to automatically interpret images for the sake of automatic geological mapping. The interpretation process is based on conventional concepts of texture analysis and classification,

then on the structural analysis and interpretation of the positions occupied by the elements of the texture classes. The structures used are mainly topological. In this way it is possible to determine regularized texture zones that can be assimilated with "color patches" on a map.

Examples are presented to illustrate this method. The first one involves the automatic plotting of "geological" contours from a digitized aerial photo of the In Salah region in the Algerian Sahara. These contours are compared with two manual interpretations by geologists.

The following example is the application of a similar but simpler method of plotting contours by regularizing the results of a LANDSAT-1 multispectral data classification. A comparison with geological and vegetation maps shows that the contours obtained are a blend of the two maps and that it is thus not possible to avoid a structural analysis.

If contours have a geological value, the position relations of the "terrains" they delimit can be analyzed in an attempt to find a stratigraphic order, if one exists. An example will show that a stratigraphic order can be found automatically, that discordant "filiform" layers such as alluvia can be detected, that such layers can be eliminated, and that a geological "cutaway" can be obtained.

A step now being studied is not described in the following but makes up an essential articulation in the system. It involves the location, in the paths obtained by previous interpretations, of narrow zones where bunched "geological contours are aligned, where there are anomalies in the analyzed theoretical stratigraphy, or where there are other morphological features such as straight stream beds. These are the "lineaments" that will be interpreted by the last part of the system.

This part is not designed to analyze images but to search for coincidences between geophysical data of different origins, because remote sensing is only one among various geophysical methods. The two systems presented are complementary. One consists in analyzing the coincidence of the lineaments detected on satellite images with different geophysical phenomena. The example described is a program to search for lineaments that coincide sufficiently with earthquake alignments. The same program can be used to investigate the coincidence of other natural phenomena such as mineral concentrations and magnetic or gravimetric anomalies. The other system consists in taking advantage of the experience and intuition of the photointerpreter to analyze geophysical documents by transforming recordings into images that can be combined with the lineaments revealed by LANDSAT which is now being done.

After describing the several parts of this system that have already been established, in conclusion we will see that the contribution of remote sensing to geological investigations must certainly lead to a very thorough transformation in the spirit and methods of these sciences.

FILE AND AUTOMATIC PLOTTING WITH CONTOUR GENERALIZATION

The large number of satellite images in the area covered by the Pyralp project required the creation of an automatic file. With this file, sorting could be done according to the most important elements in the images, i.e. the coordinates of the

center, the date of photography and the geographic location (given by the names of countries, cities, rivers, etc.). Other elements such as the quality of each band, the cloud covering, the position of the sun, etc., were not retained as classification criteria.

The extremely simple sorting subroutines give automatic printouts of lists of images so that a quick search can be made. The images thus selected can be represented on a digitized geographic map by their center or their four corners (Fig. 1). The four corners of each image are determined in longitude and latitude by knowing the plot of the satellite trajectory (given by the coordinates of the centers of two successive images) and by knowing the geometry of an image.

Once these four points are known by their geographic coordinates, they are also known in the map projection system being considered. Hence, it becomes possible to calculate the affine transformation making all points in the image of the magnetic tape correspond to one another, i.e. a line and column number to a point on the map. In this way, image elements or interpretations, such as contours obtained by digital analysis, can be automatically plotted on a map.

However, if the scale is reduced, the elements must be modified so that the drawing does not become overloaded. A quick and relatively inexpensive method was adopted for these scale-change generalization problems. It bears some similarity to the principle of the separating power of the eye at a given distance from a map. Making a reduction in scale thus means, to a certain extent, moving away from the map that is being looked at. The processing algorithm considers a grid pattern on the map, and so then the size of the elementary square can be increased. In each square, the initial number of digitized points is reduced to a single point (its barycenter), sometimes two. In addition, some points are assigned a weight on the basis of a certain logic of vicinity designed to maintain the complex nature of the pattern in the zone. If the weight is very great, the point will be kept intact; if the weight tends toward zero, the point may be eliminated. Generalization algorithms are known, but the originality of this one is in the suppression of the "non-significant at this scale" points.

The method proves to be very fast. One defect that has not yet been corrected is the appearance of a "point-of-reflection" effect in the case where certain coastal accidents disappear. However, an effort was made to take various psychological effects into consideration during a reduction. For example, a strait has to be artificially widened so that the two edges do not appear to touch each other at a small scale. Likewise, an island must be "enlarged" so as not to disappear, no matter what the scale reduction may be (Fig. 2).

This process has the defect of not preserving the exact geometric position, but it does preserve the "visual" nature which is essential for geologist.

The two examples of scale reduction presented here (Fig. 2) are drawn on the same scale so that they can be compared. The actual scale is given by the dotted-line frame that would contain the map. The phenomenon of island enlarging can be seen when the reduction goes from 1 : 1 to 1 : 6, after which the size of the islands becomes constant . If the islands were represented on their true scale, they would be reduced to a simple closed contour whose shape would be of little importance. On the other hand, the cutting up of the coast is less and less accentuated, and the phenomenon does not become stabilized.

AUTOMATIC CONTOUR PLOTTING

Automatic interpretation methods can be sought by using the spectral signatures of objects within the topic being investigated (e.g. here, calcareous layers, sandstone layers, etc.) or by recognizing shapes. Previous theoretical investigations (4, 5) led us to use a quite different method based on the use of topological structures applied to sets of data defined as the positions where textures are located. After a review of theoretical concepts described elsewhere (4, 6, 7), two examples are commented on.

1. Theoretical Aspects (cf. Ref. 4, 6, 7).- The thematic mapmaking method described here stems from the formalization of a theoretical photointerpretation method. We will begin by reviewing its three basis intuitive postulates.

   a. Principles

   On an aerial image:

   (1) We are capable of isolating shapes by distinguishing them in any way.

   (2) Each shape is recognizable and may be repeated, thus implying an overall definition for each class of shapes thus created.

   (3) The classes of shapes will be organized.

   Hence we are led to make three fundamental definitions:

   (1) Textural elements: shapes discernable among one another and regroupable by classes according to their colors, sizes, etc.

   (2) Textures: these are the classes in question.

   (3) Structures: any characteristic property of the organization of textural elements or textures.

   Therefore:

   The first postulate (shapes can be isolated by being distinguished in any way) consists in assuming a set in the mathematical sense of the term. Here it is the elements (shapes) that are perfectly defined (distinguished in any way but non-ambiguously).

   The second postulate (each form may be repeated and is recognizable, thus implying an overall definition for each class of elements) corresponds to the existence of an equivalency relation for the previously defined set, with each class having a sufficiently numerous population.

   The third postulate (classes of elements may be organized) corresponds to the existence of a structure. This structure will be identified with the set of elements it holds. Hence it is a subset of the set of textural elements.

This gives us the following three stages:

(1) Texturation: obtaining elementary shapes from the digitized image making up a set (in the mathematical sense of the term) on which we will base our reasoning.

(2) Structuration: studying the relations between the previously defined elements, and especially the topological relations of their positions.

(3) Characterization of the theme: once a theme has been designated, it corresponds to certain boundaries characterized by topological structures (modeling).

2. Applications to digitized images

We will consider here only digitized images defined as the application of a set of positions within a set of characteristics. The examples dealt with will be such that the set of positions (P) is a grid with square meshes and the set of textural elements (T) is a set of luminous intensities, i.e. a subset of the set of integers (N). If the image is multispectral $T\ N^r$ (with $r = 4$ in the case of LANDSAT images).

In general, such an unprocessed digitized image cannot be taken as a set of textural elements. It requires a regrouping of the gray shades (monospectral case) or a more sophisticated classification, e.g. by a discriminant analysis for multispectral images (3, 7). But any improvement of an image or any generation of a derivative image can likewise be considered as valid (8). Nonetheless, most of the time, regroupings are necessary (so that each texture has a sufficiently numerous population).

The first basic structure encountered is the concept of neighborhood. We have used neighborhoods with 5 or 9 elements as usually defined in the literature (9). But we have chosen to define them within a more general setting, namely by a reflective and symmetrical relation (similarity) between the elements in a set. In this way, other than the neighborhoods of positions already mentioned (nonetheless in staying free of any geometric or algebraic consideration), we can consider neighborhoods of textures or textural elements. Indeed, when we speak of neighboring textures, we are actually referring to resembling textures, and the definition of neighborhoods by a similarity is perfectly justified.

The initial structure can be used to define another, probably more basic one, i.e. connectivity. Here again we did not follow the usual procedure, i.e. to characterize a subset by its number of components and its number of holes. This type of property was mainly used in problems of recognizing letters, figures, chromosomes, etc. However, the images we were considering were much more complex, and we were actually interested mainly in connected components forming a new set of textural elements that could be easily characterized by so-called standard structural properties for each component, i.e. ratios of population of the interior/total population; population of the periphery (edge)/ total population; number of points of articulation/population of periphery (with a point of articulation being a point which, when withdrawn from a component, disconnects it).

Nevertheless, to facilitate the structural analysis, the image is made to undergo treatment called "regularization," whose aim is to make connected components more regular. The texture of a textural element is changed if a similar texture can be found in its neighborhood where it is represented a sufficient number of times (i.e. if this number is higher than a given level). Reiterating is done until no further change is possible. This treatment also brings about (with a suitable choice of regularization level) a welcome improvement of the image.

In this way, once a set of textural elements has been obtained from a digitized image, we know how to build another one, i.e. the set of connected components. These components may be characterized by a certain number of standard structures. And so now we can go on to the thematic analysis.

3. Thematic Analysis

The thematic analysis makes various "physical" properties of the area being examined correspond to various structrues that can be defined in the set of textural elements, i.e. having a thematic significance. The set of such structures thus makes up a model of the theme (4, 6, 7). Given a set of textural elements, an analysis of the structures in the model can be used to produce a thematic map.

Just as a digitized image considered as a set of textural elements was defined as a set of textures $t \varepsilon T$ having positions $p \varepsilon P$, a map m will be defined as a set of signs $s \varepsilon S$ having positions $p \varepsilon P$. We will designate these signs by s1, s2, ... sN in a descriptive list used as the caption for the map. This leads us to define a thematic map as an application of $m = P \rightarrow S$, in which:

$$m = \{(P, S) \varepsilon P \times S \mid m(P) = S\} \text{ and } m \subset P \times S$$

It then becomes obvious that a one-to-one relation exists between a map m and a set of textural elements from the moment these latter are defined in the same set of positions P.

In practice, such maps correspond to what is commonly called printout display. A final step is the automatic drawing on a pen plotter. But the technical difficulties in this are far from negligible, although do not appear insurmountable. Two examples will be given later on.

In general, a specialized photointerpreter has memorized the characteristics of a theme, both on conventional aerial photos and on existing thematic maps, and he can intuitively explain the characteristics he sees there. An initial working hypothesis is that these characteristics will coincide, with more or less obliteration, with the topological structures that can be defined in the set of textural elements. Let us illustrate this procedure by two very roughly simplified examples.

a. Let us assume that the theme being analyzed is "cultivated areas" (6) and that a specialist has proposed the following characterization: (i) homogeneous zones, (ii) relatively large interior and (iii) with rectilinear edges. The translation in terms of topological structures could then be: (i) connected component, (ii) a cardinal-of-the-interior/cardinal-of-the-component ratio higher than a certain level, and (iii)

without any point of articulation and a regular outside edge. It should be pointed out that the latter structure expresses merely the idea of "regularity" for the "rectilinear" term because it alone has a topological nature.

b. In the more delicate case of the "geology" theme, the specialist tells us that the geological layers are distributed throughout the image according to a well established order and that any local non-respecting of this order corresponds to faults, unconformities, etc. This idea of the ordered distribution of layers can be translated in terms of neighborhoods. The elements of a given structure (bearing in mind that a structure is a family of subsets of the set of textural elements) are always neighbor to those of another structure; in other words, the probability of the transition from a given type of structure to another one is close to 1. (Let us note in passing that the structures in question correspond to the different layers). An unconformity then becomes an aberrant boundary.

This hypothesis enables a rough model to be built, defined by a certain number of topological structures. Corresponding to it is an initial thematic map that will enable us to test the model. The resulting thematic map contains errors, and the structures already chosen have to be completed on it and restrictive measures must be taken to reduce them.

Therefore, in the example on cultivated areas (6), we found that it was useful to take the component density into consideration (number of components per unit of area). As a result, the level that the cardinal-of-the-interior/cardinal-of the-component ratio must surpass in order to belong to the theme is proportional to this density. Actually, a cultivated area is characterized by a great many components (homogeneous patches), and hence has a low density. On the contrary, isolated fields are sparse. In order to be recognized, such fields must thus have good regularity and size properties. In this way, we obtain a second model and a second map, and we can begin over again until we obtain a model felt to be satisfactory. When this is done, we consider this model to be an operational one.

Once an operational model has been obtained, we still have to see to what extent it is capable of producing reliable maps. A theme is modeled under well defined conditions of scale, geographic context and textural elements used. At the same time, the context may hide or obliterate a part of the structure. These problems have already been written about at length in conventional photo-interpretation, and it is obvious that if we apply the "cultivated areas" model defined from 1:25,000 digitized photos to a 1:1,000,000 satellite image, the map obtained will be false. The models should be applied to images with fairly similar characteristics, or they should be adapted to the types of images used.

4. Example of Contour Plotting from a Digitized Image (In Salah, Algeria)

The photo is a 1:50,000th IGN photo, format 16 x 16 cm, digitized by microdensitometry, with a step of 50μ. We examined a restricted zone with 100 x 300 elements, using only one point out of four in the digitizing.

It can be seen on the image that the "spots" that the interpreter considered as belonging to a single terrain take on values in 6 of the 7 gray shades, These gray shades thus cannot be taken as significant textural elements in the

theme, and we have to try to reestablish what the eye does, i.e. to search for a model that makes certain structures in the image correspond to those that we use implicitly. Some spots are made up by a set of components that should be reconnected. Yet a structural property that appears from the examination of the image of these components shows that they all have their interior empty. This gave us the idea of using the standard IPR*(cardinal-of-the-interior/cardinal-of-the-component ratio) for texturing. In this way, 11 textural classes were extracted, and an effort was made to define the geological boundaries on the basis of the boundaries of the new components obtained by taking the IPR image as a set of significant textural elements in the theme.

An initial regularization (REGUL) with the lowest permitted regularization level (i.e. 5 in the case of a 9-element neighborhood) did not produce satisfactory boundaries because of the small number of textures. On the contrary, a regularization, i.e. an elimination of the weak population components and of the points of articulation capable of creating an absurdity in the automatic drawing by the plotter.

The boundaries produced by this automatic interpretation, drawn with a Benson plotter, are given in Figure 3. The two maps on the left are geological maps that had previously been hand drawn (10) and stem from two interpretations made from a different standpoint. The ones on the right were compiled by computer processing.

Map (a) on the left is a photogeological "sketch" indicating the geomorphological details that will guide geologists in their field work. It includes layerhead talus slopes, dips, alignments, etc. The other (b) is a more cartographic interpretation in which a great many morphological details have been eliminated but in which the succession of stratigraphic units has been made more readable.

The drawing on the right (d) is the unprocessed document obtained automatically by the plotter, while (c) is the same map in which the boundaries have been reinforced differently so as to provide elements for comparison with maps (a) and (b) (df. caption of Fig. 3). Two aberrant boundaries were also found. The first (x) is a valley that the photointerpreter would have neglected. For the second (y), there is a connection between a zone having geological significance (G) and an alluvia zone (H). Nonetheless, it can be seen that most of the boundaries shown on the preceding maps are reproduced and that the new ones are mainly localized in the alluvia. Some of them can be eliminated (not because they are aberrant, but because they are not of interest to us) at the level of the plotting orders. In this way, the first map obtained is similar to map (a), i.e., a sketch intended to guide geologists.

A choice of textural elements that are more representative of the theme, e.g. more complex texturings (7-8), performed by a geologist interactively using a display console, along with a more thorough structural analysis, leads to an interpretation quite close to (b).

---

*One of the subroutines in the topological analysis system.

5. Geology and Multispectral Classification

At this point, the question arises whether it is necessary to manufacture textures by means of spatial structuration and whether the textural elements resulting from a classification by discriminant analysis of multispectral data could reflect the geology of the area in question. The example comes from a LANDSAT-1 image of the Avignon region, in France.

The computerized display on the drawing board is that of the texture contours resulting from a classification after a "second order" regularization had been made.

Figure 4 shows, from top to bottom, the contours recopied on the geological map, then on the vegetation map, followed by those obtained with the computer plotting. Among these latter, after comparison with the other two maps, we distinguished the contours that were more geological from those corresponding rather to vegetation boundaries (sometimes with a correlation between the two types). Some contours remain uninterpreted because they cannot be identified on either of the two reference maps.

One immediate conclusion is that the textures do not, in general, correspond to geological terrains but rather to a vegetation-geology imbrication in which it is difficult to disassociate the two. Hence it is absolutely necessary to use all the structural criteria at the same time (e.g. topological) in order to determine interpretable textures.

6. Stratigraphy and Transition Probabilities

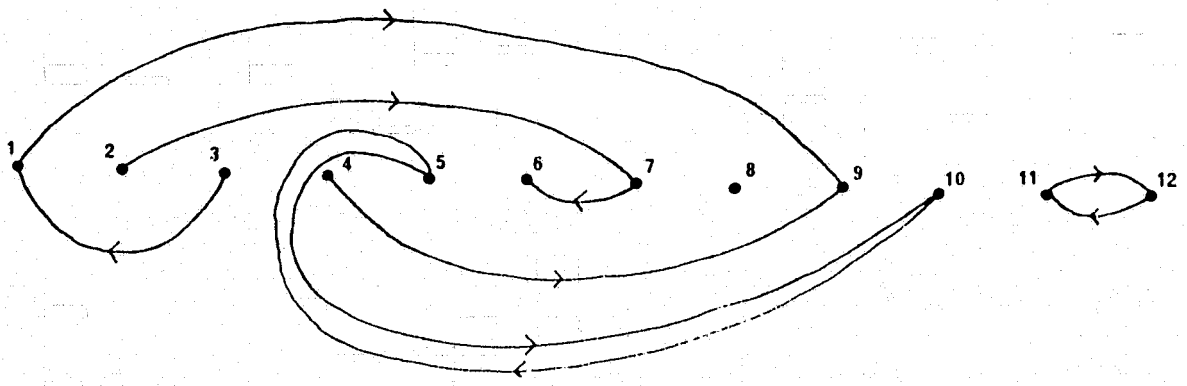
Because stratigraphy is based on a chronological order, it needs to be checked in the field (taking samples so as to date layers). Nevertheless, a relative order can be determined by considering the relative position of layers among one another (i.e. their topology) and the trend of dips. Without any relief, it is not possible to determine this trend, but it is always possible to determine the topology. Therefore, we will examine the role of the topology in the stratigraphy.

One idea is to make use of the fact that a geological map (with or without faults) can be assimilated with a topological planar graph. Then the dual graphy expresses the neighborhood relations between the components of the different layers. But this graph takes all the relations into consideration, no matter what the importance of the contact between the layers may be. The use of transition probabilities enables contacts of slight importance to be neglected. In addition, they indicate the neighborhood relations between subsets of components (layers) and not merely components (outcrops).

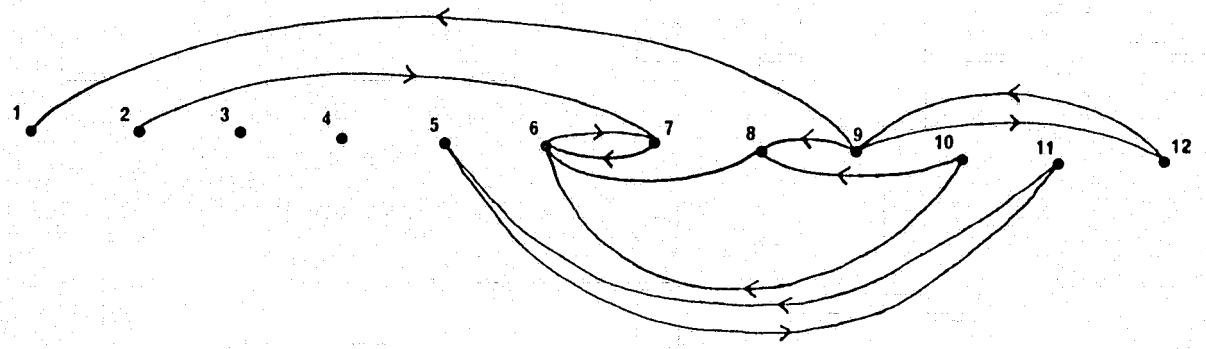
The image taken as an example (Fig. 5) comes from the digitizing of a photogeological pattern determined by photointerpretation. The set, P, contains 76 x 120 positions, while 12 layers have been differentiated. The matrices of the populations encountered and the transition probabilities as well as the proposed order are given in Table 1.

If we take $\alpha = 0,50$ and $\beta = 0.25$ as the upper and lower probability levels, an analysis of the transition probability matrix shows that an order is effectively created, with the upper probability being often surpassed. So

as not to obtain too crowded a figure, we have plotted, below, the graphs obtained by considering, respectively, the upper arcs* and the lower arcs. For the same reasons, the transition probabilities are not shown this time.



(a) Graph obtained by taking only the upper arcs into consideration.



(b) Graph obtained by taking only the lower arcs into consideration.

Graphs (a) and (b) must be considered as subgraphs of the same overall graph.

We can see that each vertex is the origin of an upper arc, except for 7 and 8 which both are the origin of a lower arc. In addition, peak 8 stands out by being the end of three upper arcs and two lower arcs. By neglecting the lower arc with origin 8 and end 6, and by using either upper or lower arcs, it is possible to begin at any vertex and to arrive at 8 (and stay there).

7. Geological Application and Obtaining a New Image

About Fig. 5, questions may be asked about the nature of this texture 8. It corresponds, on the image, to alluvia characterized by their treelike

---

*upper arc = upper transition probability level arc

structure and their numerous points of articulation. Yet, in geology, alluvia create a singularity in the stratigraphy by appearing unconformable on the different layers. This explains the particular role of the vertex 8 on the graph of the transition probabilities. Since the first job is to establish a stratigraphy, we will assume the attitude of a geologist by not taking the alluvia into consideration (while still considering them as the most superficial layer). Therefore, a spec 1 subroutine will eliminate this texture on the image and recreate "for the best" the positions of the underlying terrains (Fig. 5, bottom view). This is the operation that geologist call making a geological cutaway. The stratigraphy can then be studied without the alluvia so as to determine the stratigraphic order of the geological order of the geological layers in the strict sense of the word.

8. Detection of Geological Anomalies and Lineaments

It is easy to see on the geological cutaway of Figure 5 (bottom) that some components, if taken separately, have not the same transition probabilities as the subset of components to which they belong. More often they have particular topological properties, such as to have a cardinal of the interior/cardinal of the component ratio lower than the ratio of the other components of the same textural subset, i.e. they are "elongated" or "linear" (see A, in Fig. 5, bottom).

Then, we can write algorithms to extract the subset of positions which are the boundaries or the "articulation points" of such "anomalous in their context" components, i.e. pinpoint the faults or lineaments.

Now, this part of the system is not yet completed and writing of the algorithms just begins. But, as this was only a matter of time because the theoretical way was clear, we have begun to make the third part of the system whose aim is to indicate a working hypothesis to the geologist by searching coincidences between satellite image lineaments and some other geophysical data.

COMPARISON OF REMOTE SENSING DATA AND GEOPHYSICAL DATA

Two methods are examined. One consists in systematically testing the coincidences of pinpoint phenomena and geographic anomalies of the lineament type, circular structures, etc. The example described has to do with what was immediately the most obvious to us, i.e. the relation between the position of earthquakes and certain lineament trends. The other method consists in using the reverse procedure and in considering as a whole the relatively dense and regularly distributed data as "textural elements" in a remote sensing image, hence in applying the same interpretation methods to it, beginning with good old stereoscopic photointerpretation! This idea is illustrated by an example of gravimetric data processing.

1. Searching for Coincidences Between Earthquakes and Lineaments or Groups of Lineaments (Fig. 6 and 7)

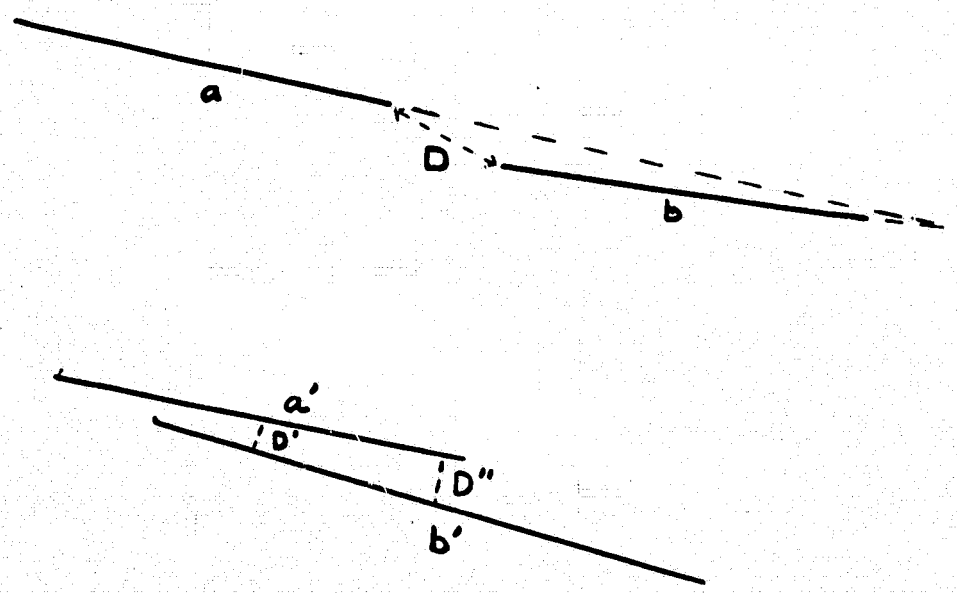
Once the lineaments have been determined in any old way, their relation with seismicity can be studied by a very simple and quick method. Since France is a region with little seismic activity, the process worked out does not involve the searching for possible earthquake alignments, but, by using previously

determined lineaments, it seeks to delimit a zone of influence around each lineament. This zone of influence is defined as a strip with a specific width on either side of the path of the lineament. The program allows this width to be varied. The width can be made to depend on the precision of the position of earthquakes (one tenth of a degree here). Likewise, the width can be made to depend on the width of the lineament on the satellite image if so desired. If more than one earthquake exists in the "zone of influence" of the lineament, the mean straight line running through these earthquakes is calculated. If the straight line thus calculated coincides sufficiently well with the lineament, it can be considered to correspond to an earthquake zone, and it is plotted on the map (Fig. 6). With this algorithm, it becomes evident that very few lineaments can be considered as fracture zones, but that they are lineaments having a great extension. In the region we are looking at they are mainly the ones trending E-W (80° N).

In the beginning, the way of interpreting and drawing the lineaments must play an important part. When the entire system becomes operational, these lineaments will be determined automatically. Up to now, the only ones used have been the lineaments that are visible to the eye on 1:1,000,000 LANDSAT-1 images. Considering the dispersions of the drawings that can be made and the dispersion of the lineaments detected, it seems reasonable to group the ones that are aligned or those that are more or less parallel and quite close together. The program can thus link strips of influence of the lineaments detected according to the following two criteria:

i. That of "being in the alignment of";

ii. That of "being parallel to" but "in the immediate vicinity of."



We chose to join two lineaments that are in the prolongation of each other, e.g, (a) and (b) if, on the one hand, the concept of prolongation is verified, i.e. if angle (a, b) is sufficiently small (in practice less than 15°), and if, on the other hand, the distance (D) between the two lineaments (a) and (b) is sufficiently slight (several tests have been made with a different threshold D).

Two lineaments parallel to each other, i.e. (a') and (b'), are joined if, on the one hand, the concept to parallelism is verified (if the angle between the two lineaments is sufficiently small), and if, on the other hand, the distance (D' and D") between the two lineaments is underneath the threshold chosen. (D') is the distance from the middle point of (a') to the lineament (b') and (D") is the distance from the middle point of (b') to lineament (a').

Therefore, three thresholds have to be set for: (i) the angle between two lineaments, (ii) the distance of separation (D), and (iii) the distance of parallelism (D') and (D"). The separation threshold may either be fairly great in the beginning, in which case the group of lineaments is quite large, or else it may be narrow and the group is determined by successive iterations.

This algorithm enables a bunch of lineaments to be grouped into a single format as well as into a megalineament. They are represented on the map by a trace that is distinct from the originals. On the basis of these megalineaments, the algorithm of coincidences is applied to obtain fracture zones of greater extent than those obtained before grouping.

The first example of cartographic printouts (Fig. 6) shows, a search for a coincidence between lineaments and earthquake positions, with the width of the "zone of influence" being 5 kilometers.

On the original, the earthquake alignments are marked in red and the lineaments in black. When a single earthquake coincides with an alignment, it is framed and given the number of this alignment. Then, Figure 7 shows the result given by a grouping followed by a search for coincidence on the "megalineaments" resulting from the grouping. In this case, the width of the zone of influence was set at 7 km.

Between the two maps, lineament 262, 282, 283, was grouped, and a remarkable coincidence was found between the "megalineament" and the mean straight line of the five or six earthquakes located in its zone of influence. At this stage, however, alignment 237 and earthquakes 17, 24, 61, 29 have not been merged as they will be in the subsequent grouping-coincidence iteration. When the procedure converges very quickly, i.e. if after two or three iterations almost all the earthquakes have been attributed to very few grouped lineaments, it can be affirmed that a relation has been shown between the two phenomena.

These algorithms, and others resembling them which take other types of structures into consideration (circular, vortex, etc.), will be extremely effective ways of providing geologists with objective hypotheses.

2. Processing Geophysical Data Such as Remote Sensing Images (Fig. 8)

As part of the Pyralp project whose problems resulted in the creation of this generalized interpretation system, it was quickly seen that a study of the seismicity would not entirely solve the problem of the nature of the

lineaments. It would have to be combined with an analysis of other geophysical findings. A process was sought that would enable a non-specialized photointerpreter to analyze geophysical documents and to compare them with remote sensing. For this, it was decided to transform the data (e.g. gravimetric) into images having levels of gray and relief that would be deduced by texture functions as is done in other remote sensing methods, including aerial photography. The basic documents that are used are isovalue-curve gravimetric maps. By digitizing them and then interpolating to obtain a network of square-base points, it thus becomes possible to impose any type of digital processing on the values of gravity, and in particular filtering and derivatives. Before any processing, a stereoscopic pair can be created to represent the actual value of gravity in gray shades and also in relief. This document gives good interpretation results, and the same trends are found as those obtained from satellite images, although there is an offset. The fastest and most advantageous processing consists in calculating the value and direction of the horizontal gradient for the plane $z = 0$. A stereoscopic pair of pseudophotos will be created with a gray shade representing the direction of the gradient and having a relief conforming to the value of the gradient. As the darkest gray shade, any desired direction can be chosen, thus obtaining several images. A high relief is equivalent to a large value of the gradient, hence to a considerable difference in gravity. A photointerpreter has no trouble in sketching in the peaks and hollows that may well represent faults if these peaks and hollows also correspond to the same gray shade.

The example given in Figure 8 shows a synthetic stereoscopic pair from computer processing of gravimetric data. Right bottom view is a sketch of lineaments from manual satellite image interpretation, and left bottom is the conventional Bouguer gravimetric anomaly.

It is easy to see lineament (AA) as a white straight crest in the stereopair. Some other features have comparable shape (mainly by their orientation) on the two views.

The next step of this processing, which is under development, will be a superimposition, with stereoscopic effect, of satellite and geophysical data.

CONCLUSIONS

The system for the geological exploitation of earth resources satellite data presented here is far from being complete. The aim of this paper is simply to indicate an original way of research, showing at the same time that it is not absurd or unworkable.

Now, at this step of development we think we have shown that, with regard to cartography:

i) It is possible to write algorithms and computer programs for image interpretation, giving "geological" cartographic contours as good as conventional photogeological sketchmapping would give (e.g. Fig. 3).

ii) This work demands the use of spatial texturation methods because multispectral data analysis, even if very sophisticated, gives mixed contours of various meanings (e.g. Fig. 4).

iii) For making textural sets useful for a certain theme, as well as for making better cartographic contours, topological structures are very suitable (e.g. Fig. 2, 3, 4, 5).

iiii) We can write algorithms for finding order structures among the contours, i.e. to analyze a stratigraphy if present (e.g. Fig. 5).

More, while exploring the field of geological and geophysical interpretation, we are beginning to feel that we are becoming able to make up as a whole remote sensing, geophysical and geological data in a general interactive interpretation process.

i) If looking at all the data as equivalent ones (or in another way, as "neutral" or "meaningless" against interpretation to come), but significant only by the structure of their relative spatial positions, then, we are able to write algorithms for the simulation of some "intelligent" behavior of the geologist (e.g. Fig. 7). These programs may be used to suggest working hypotheses.

ii) In the opposite way, we may transform geophysical data into images to make use of the intuitive bahavior of an experimenter photogeolgoist (e.g. Fig. 8).

All this is only a beginning, suggesting that bringing remote sensing computerized interpretation in earth sciences will result in a great change, not only a quantitative one (more data to take into account) but also a qualitative one, leading to a change in the way of acting and thinking of geologists and geophysicists.

REFERENCES

A. Fontanel, J. Guillemot, M. Guy (1973), First ERTS 1 results in Southeastern France: geology, sedimentology, pollution at sea. Symposium on significant results obtained ERTS 1, NASA Goddard Space Flight Center, 5-9 Mar. 1973.

J. Guillemot, M. Guy, M. Lobjoit (1973), Un systeme coherent d'alignements structuraux commun aux Alpes et aux Pyrenees mis en evidence par le satellite ERTS 1. C. R. Academie des Sciences, Paris, t. 277, serie D., p. 481-484.

C. Blanchet, A. Fontanel, C. Lallemand (1975), Enhancement of ERTS imagery by combination of multispectral classification and principal components analysis. Earth resources survey symposium, Houston, June 1975.

M. Guy (1970), Traitement des images et methodes d'exploitation., Geoforum, 3, p. 47-62.

M. Guy (1967), Quelques principes et quelques experiences sur la methodologie de la photo-interpretation. Actes du 2eme Symposium de Photo-Interpretation. Paris, Technip, 1967, groupe I, pp. 21, 41.

S. Braconne (1974), Structures topologiques et cartographie thematique automatique. Bul. Soc. Franc. Photogram. (a paraitre).

S. Braconne, A. Fontanel, M. Guy, C. Lallemand (1974), Cartographie thematique automatique: principes et realisation partielle d'un systeme. 4eme Symposium de Photo-Interpretation, (Commission VII de la S.I.P.), Banff, Oct. 1974 (a paraitre).

R. M. Haralick, K. S. Shanmugam (1974), Combined Spectral and Spatial Processing of ERTS Imagery data, in Remote Sensing of environment 3, 3-13, 1974.

A. Rosenfeld (1969), Picture Processing by Computer, Academic Press, New York, London, 1969.

J. J. Hausknecht (1962), Revue Photo-Interpretation n°2 - 1962, exemple n°6.

TABLE I. - STUDY OF BOUNDARIES BETWEEN TEXTURES
ÉTUDE DES FRONTIERES ENTRE TEXTURES

MATRICE DES POPULATIONS RENCONTREES
(Matrix of the populations encountered)

	1	2	3	4	5	6	7	8	9	10	11	12	
TEXTURE NO 1	0	0	0	0	0	0	0	1	144	0	0	10	TOTAL= 155.
TEXTURE NO 2	0	0	0	0	0	0	63	97	0	0	0	0	TOTAL= 160.
TEXTURE NO 3	33	0	0	0	0	0	0	0	0	0	0	0	TOTAL= 33.
TEXTURE NO 4	0	0	0	0	0	0	0	31	10	0	0	0	TOTAL= 41.
TEXTURE NO 5	0	0	0	0	0	2	0	298	0	88	175	7	TOTAL= 570.
TEXTURE NO 6	0	0	0	0	0	0	145	47	0	225	1	0	TOTAL= 418.
TEXTURE NO 7	0	65	0	0	0	146	0	138	0	0	0	0	TOTAL= 349.
TEXTURE NO 8	0	95	0	0	311	47	145	0	214	124	11	32	TOTAL= 979.
TEXTURE NO 9	147	0	0	12	0	0	0	157	0	0	0	147	TOTAL= 463.
TEXTURE NO 10	0	0	0	0	90	188	0	121	0	0	0	0	TOTAL= 399.
TEXTURE NO 11	0	0	0	0	175	2	0	10	0	0	0	250	TOTAL= 437.
TEXTURE NO 12	10	0	0	0	7	0	0	33	151	0	248	0	TOTAL= 449.

MATRICE DES PROBABILITES DE PASSAGE
(Matrix of the transition probabilities)

	1	2	3	4	5	6	7	8	9	10	11	12
TEXTURE NO 1	0.000	0.000	0.000	0.000	0.000	0.000	0.000	.006	.929	0.000	0.000	.065
TEXTURE NO 2	0.000	0.000	0.000	0.000	0.000	0.000	.394	.606	0.000	0.000	0.000	0.000
TEXTURE NO 3	1.000	0.000	0.000	0.000	0.000	0.000	0.000	0.000	0.000	0.000	0.000	0.000
TEXTURE NO 4	0.000	0.000	0.000	0.000	0.000	0.000	0.000	.756	.244	0.000	0.000	0.000
TEXTURE NO 5	0.000	0.000	0.000	0.000	0.000	.004	0.000	.323	0.000	.154	.307	.012
TEXTURE NO 6	0.000	0.000	0.000	0.000	0.000	0.000	.347	.112	0.000	.538	.002	0.000
TEXTURE NO 7	0.000	.186	0.000	0.000	0.000	.418	0.000	.395	0.000	0.000	0.000	0.000
TEXTURE NO 8	0.000	.007	0.000	0.000	.318	.046	.148	0.000	.219	.127	.011	.033
TEXTURE NO 9	.317	0.000	0.000	.026	0.000	0.000	0.000	.339	0.000	0.000	0.000	.317
TEXTURE NO 10	0.000	0.000	0.000	0.000	.226	.471	0.000	.303	0.000	0.000	0.000	.572
TEXTURE NO 11	0.000	0.000	1.000	0.000	.400	.005	0.000	.023	0.000	0.000	0.000	0.000
TEXTURE NO 12	.022	0.000	0.000	0.000	.016	0.000	0.000	.073	.336	0.000	.552	0.000

ORDRE PROPOSE
(Proposed order) (Probability of transition to the next texture)

ORDRE NO 1	TEXTURE= 3	PROBABILITE DE PASSAGE A LA TEXTURE SUIVANTE	=1.000
ORDRE NO 2	TEXTURE= 1	PROBABILITE DE PASSAGE A LA TEXTURE SUIVANTE	= .929
ORDRE NO 3	TEXTURE= 9	PROBABILITE DE PASSAGE A LA TEXTURE SUIVANTE	= .339
ORDRE NO 4	TEXTURE= 8	PROBABILITE DE PASSAGE A LA TEXTURE SUIVANTE	= .318
ORDRE NO 5	TEXTURE= 5	PROBABILITE DE PASSAGE A LA TEXTURE SUIVANTE	= .307
ORDRE NO 6	TEXTURE= 11	PROBABILITE DE PASSAGE A LA TEXTURE SUIVANTE	= .572
ORDRE NO 7	TEXTURE= 12	PROBABILITE DE PASSAGE A LA TEXTURE SUIVANTE	=0.000
ORDRE NO 8	TEXTURE= 0	PROBABILITE DE PASSAGE A LA TEXTURE SUIVANTE	=0.000
ORDRE NO 9	TEXTURE= 0	PROBABILITE DE PASSAGE A LA TEXTURE SUIVANTE	=0.000
ORDRE NO 10	TEXTURE= 0	PROBABILITE DE PASSAGE A LA TEXTURE SUIVANTE	=0.000
ORDRE NO 11	TEXTURE= 0	PROBABILITE DE PASSAGE A LA TEXTURE SUIVANTE	=0.000
ORDRE NO 12	TEXTURE= 0	PROBABILITE DE PASSAGE A LA TEXTURE SUIVANTE	=0.000

REPRODUCIBILITY OF THE ORIGINAL PAGE IS POOR

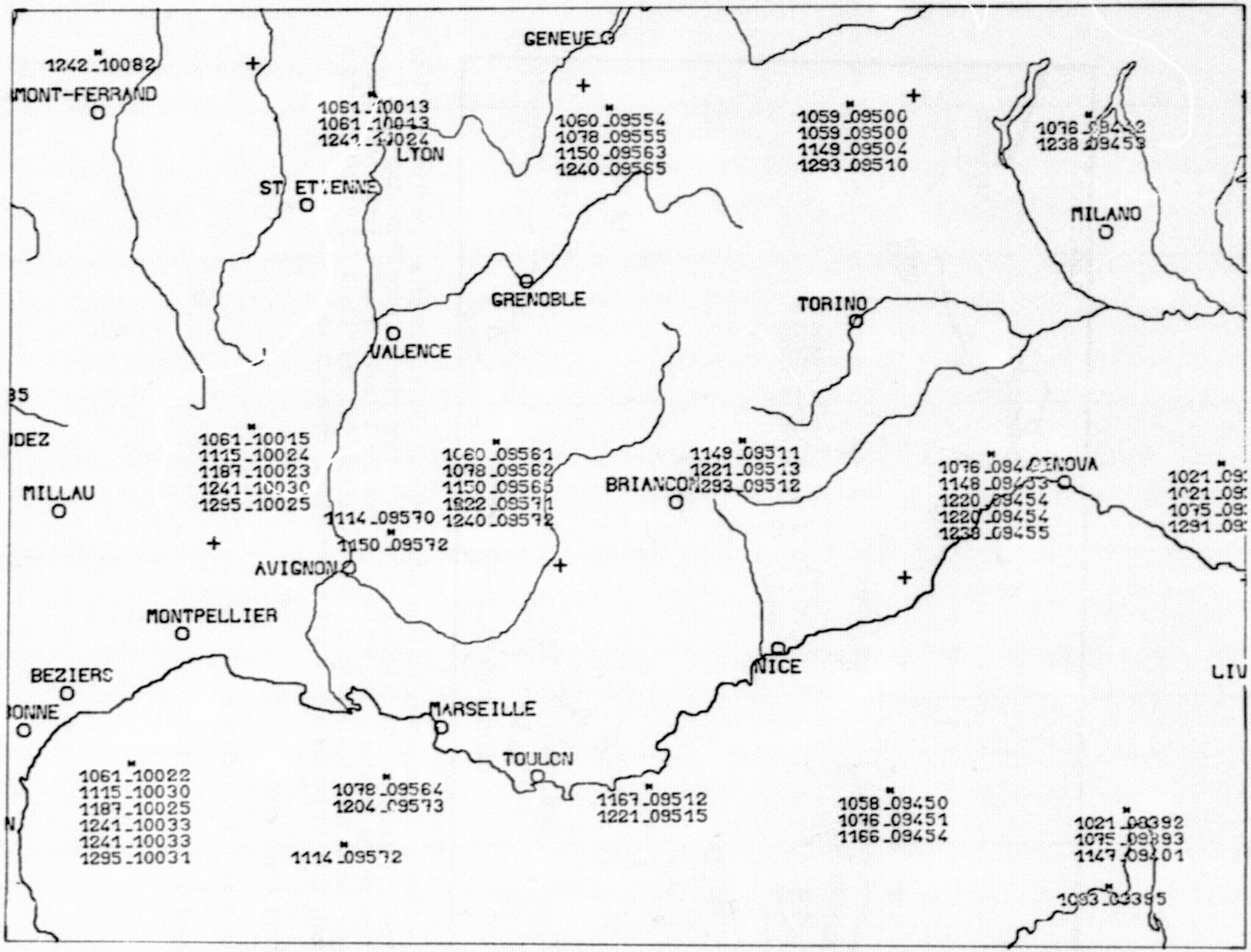


Figure 1.- Sample of the localization map drawn by the Benson Plotter as a readout of the file. Crosses (+) are Longitude - Latitude marks. Diabolos (⋆) are the centers of the images. Map scale: 1/2:500,000

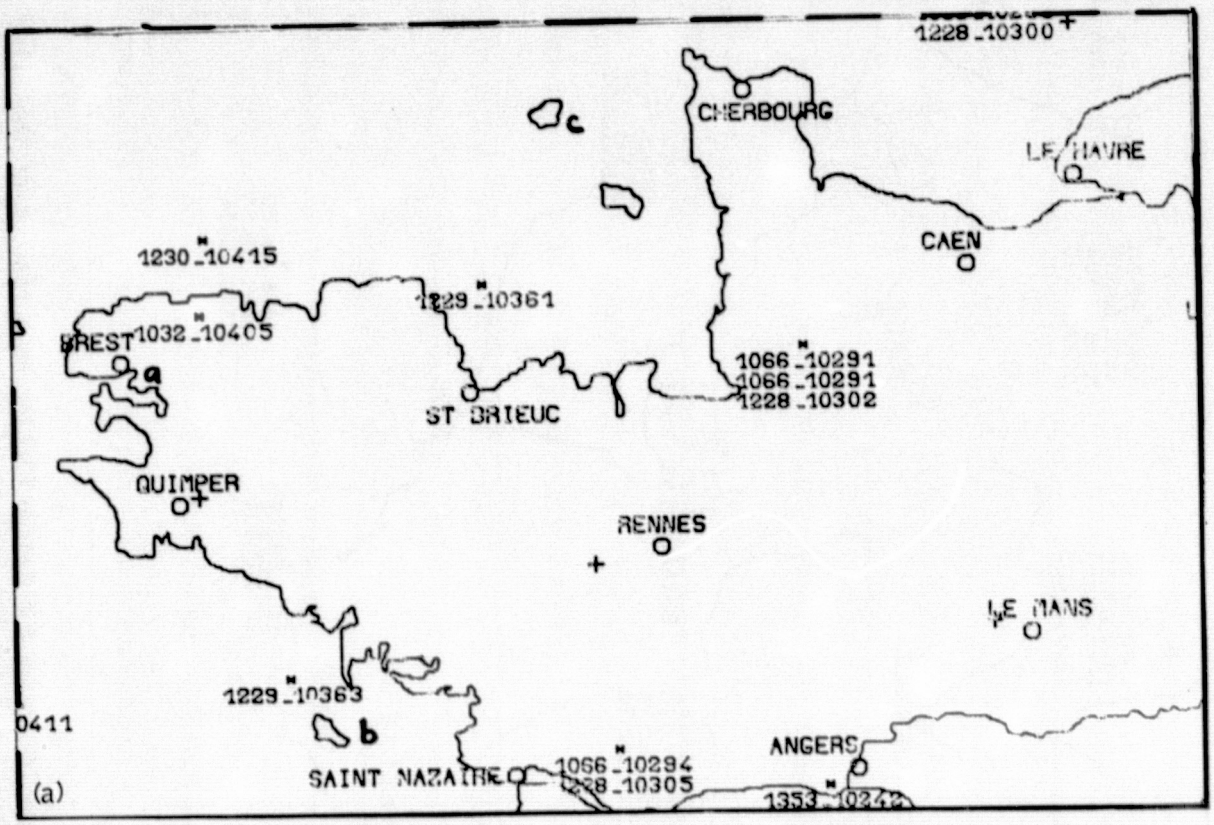


Figure 2.- Effect of the generalization subroutine on the aspect of a shoreline for 1 to 3 and 1 to 6 reduction of the original contour - bottom right window shows the actual dimensions of the drawing - the estuary (a) and the island (b) are slightly enlarged by the algorithm to be visible with the 1/6 reduction; but the island (c) is reduced to a line; now, this is on the way to being corrected. From top to bottom:

(a) Scene being used.

(b) Scene at 1/3 reduction.

(c) Scene at 1/6 reduction.

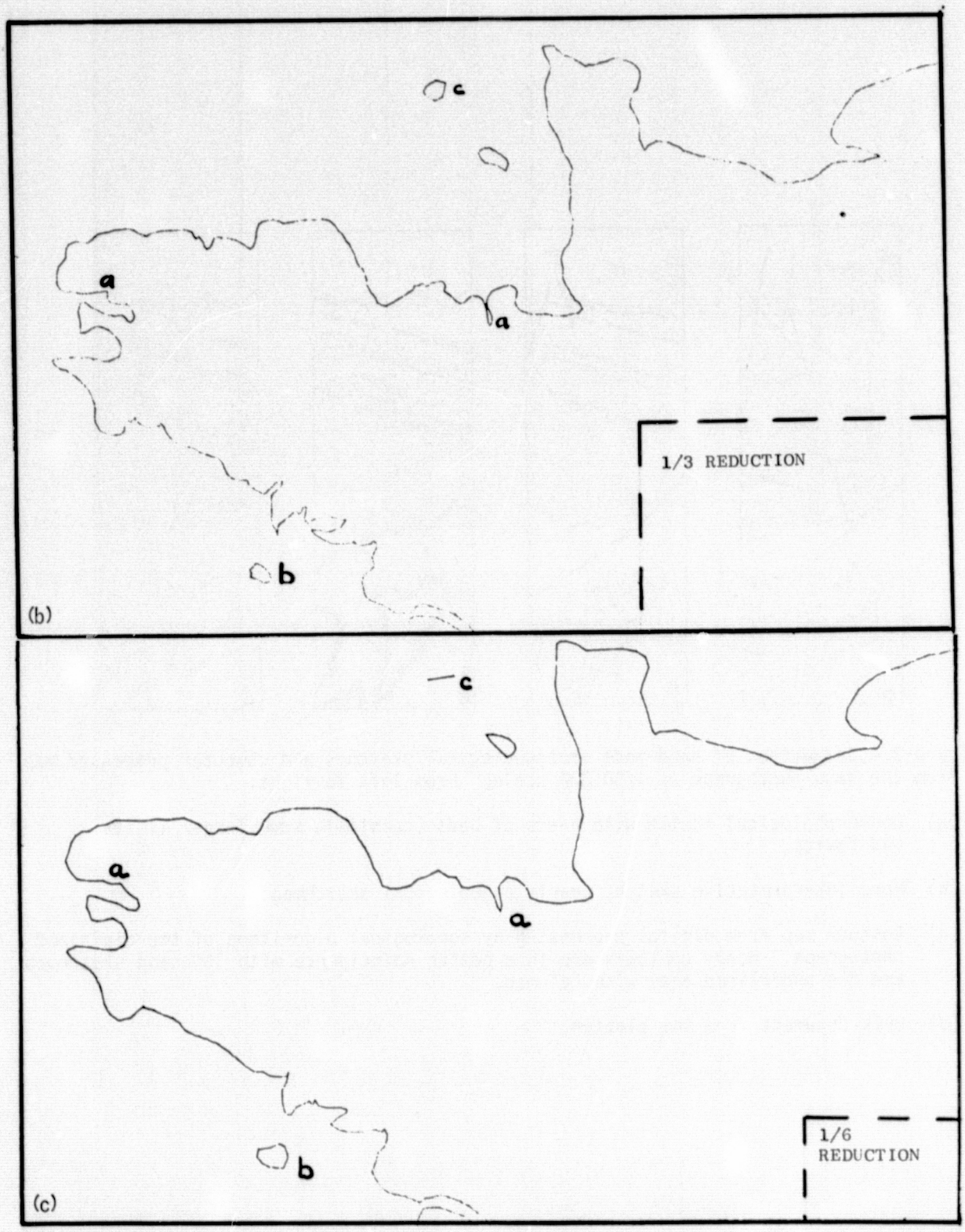


Figure 2.- Concluded.

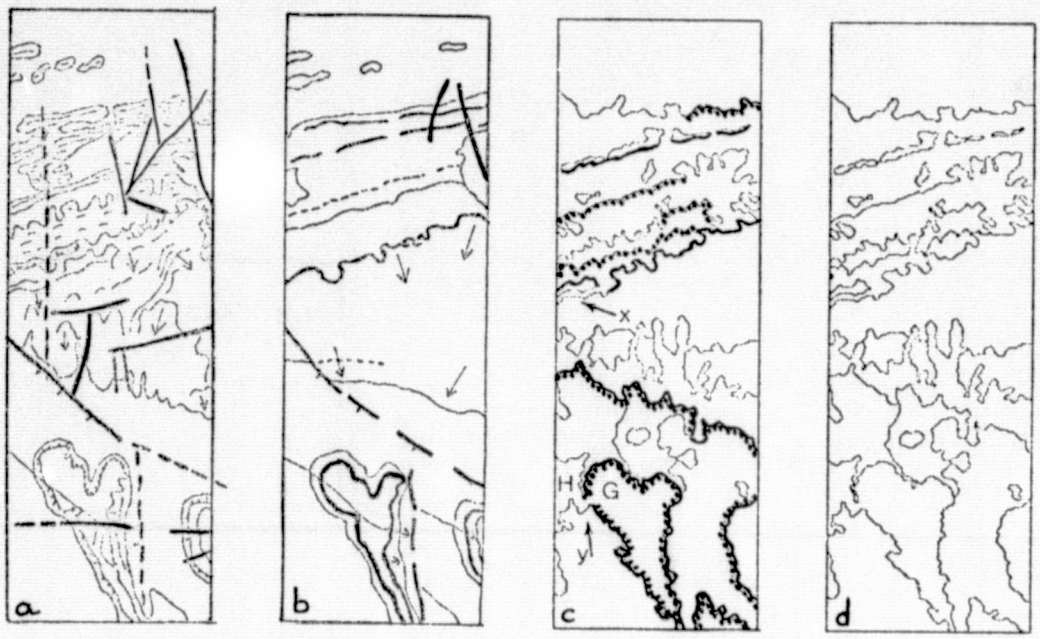


Figure 3.- Comparison of hand-made photogeological sketches and computer processed map from the same photograph at 1/50.000 scale. From left to right:

(a) Geomorphological sketch with heads of beds (cuestas), some larger limits and faults.

(b) More interpretative sketch, nearly a geological sketchmap.

(c) Contour map from digital processing by topological algorithms of the digitized photograph. Heavy contours are in a better coincidence with "b" hand sketchmap and dot underlined ones with "a" map.

(d) Bulk document from the plotter.

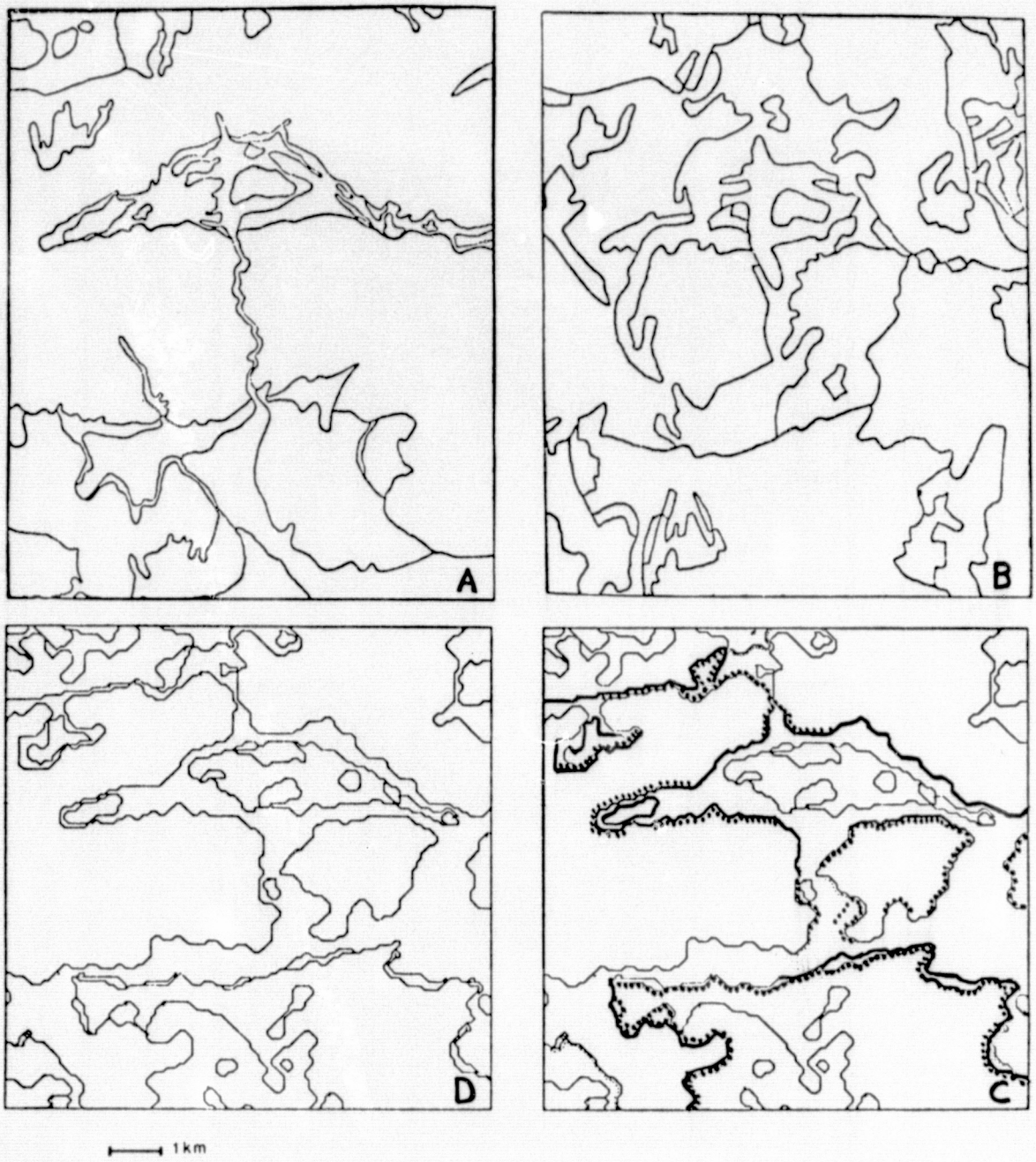


Figure 4.- Comparison between ground map contours of geology and vegetation and computer processed contours from a multispectral classification of the four LANDSAT-1 - MSS bands.

(a) Geological contours from 1/50 000 map reduced at approximately 1/100 000 scale.

(b) Vegetation map contours enlarged at 1/100 000 from 1/200 000 map.

(c) Comparison of A, B, and D maps. (The projection of "D" map is free and the scale is only very approximately 1/100 000). Heavy lines are in coincidence with geological contours and dot lines with vegetation contours.

(d) Rough contour map from the plotter. Processing is a multi-spectral classification without spatial structural analysis. (A regularization has been made before plotting but only for drawing convenience and not as an interpretative process).

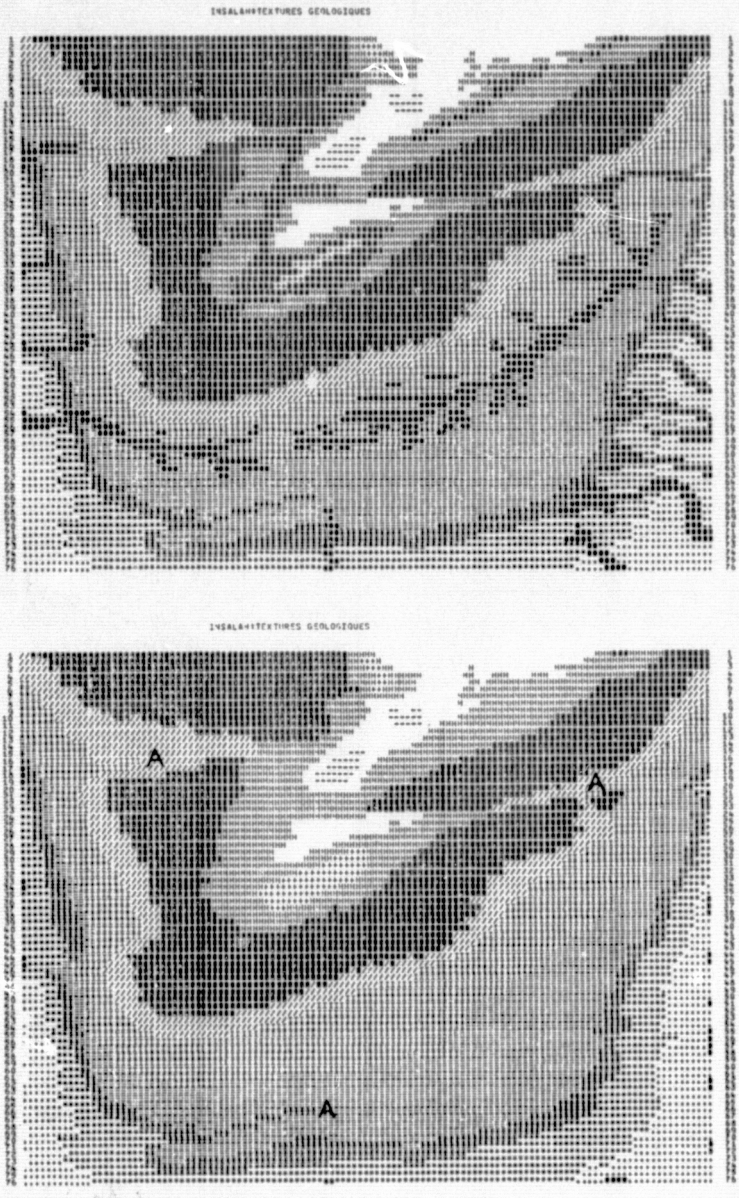


Figure 5.- The upper view is a linea-printer sketch map of geological texture with tree shaped bands of alluvium. By using probabilities of crossing frontiers between connex subsets of textures an algorithm can recognize if a texture is "unconformable" i.e. is "alluvium" (see Table 1 and text).

Then, another subroutine has to eliminate elements of the textural subset of alluvium and replace them by the best texture, in a topological meaning. Resulting map is the bottom listing.

One can see that, by analyzing some other topological properties of anomalous frontiers, faults or "lineaments" may be detected (A).

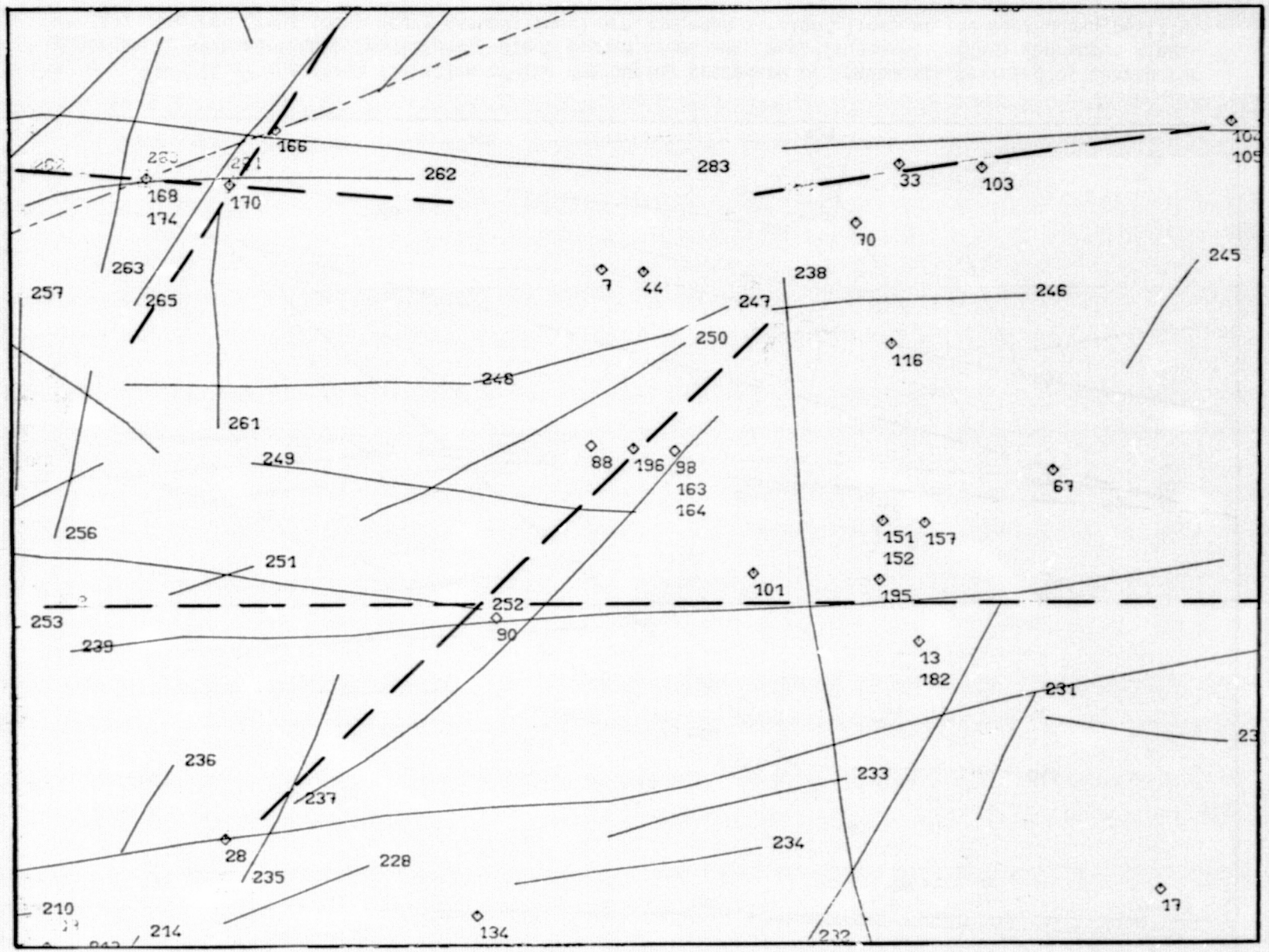


Figure 6.- Search for coincidence between lineaments and earthquake positions. The diamond shaped dots are the earthquake locations with reference number. If more than one earthquake exists near a lineament, the mean straight line running through them is indicated by a red line (here dashed line).

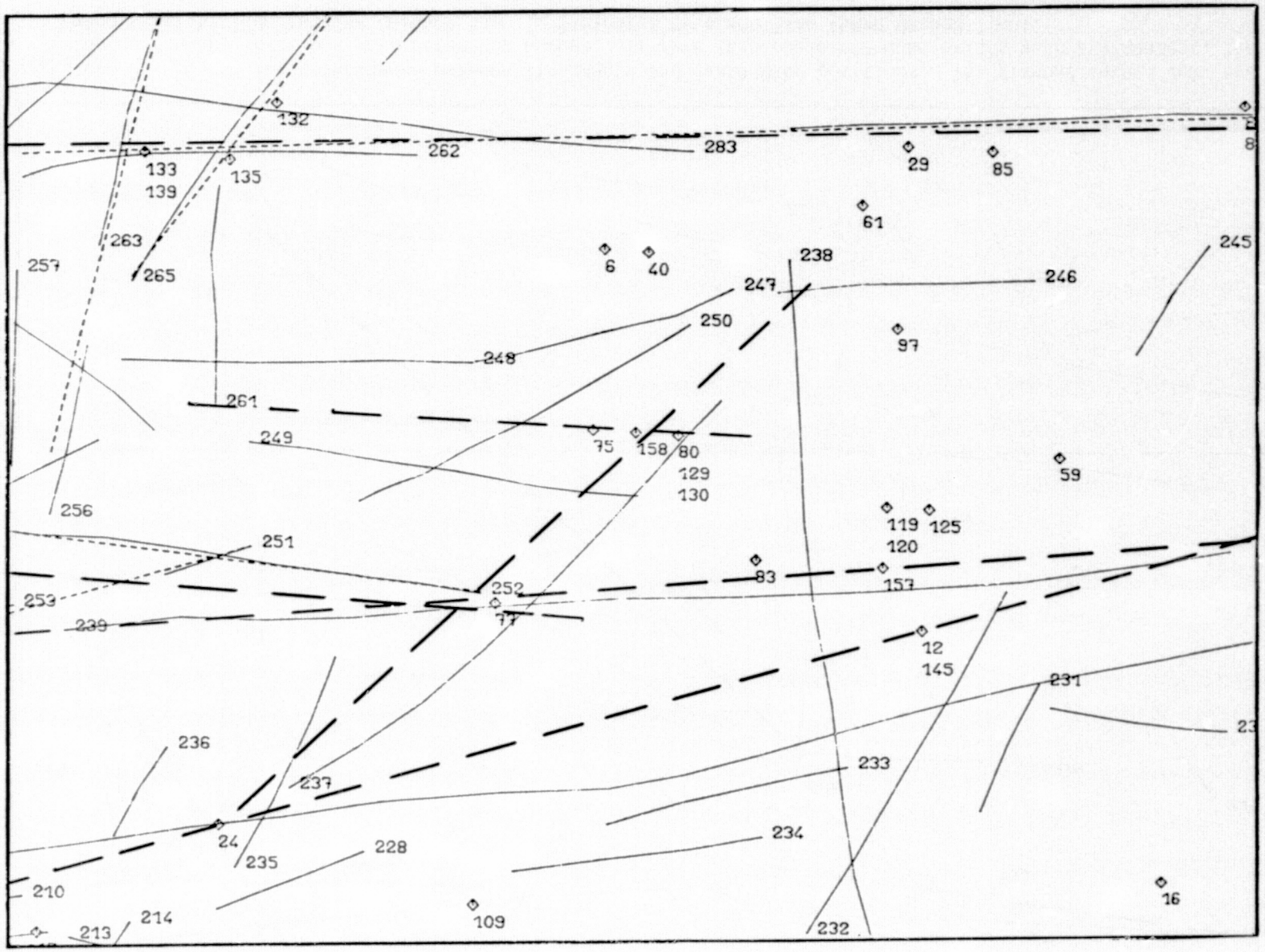


Figure 7.- Result of the first iteration of the regrouping procedure of lineaments followed by search for coincidence with earthquake positions. Black dashed lines are "mega lineaments" (i.e. regrouped lineaments). The red lines (here heavy dashed lines) are the mean straight lines of the earthquake positions.

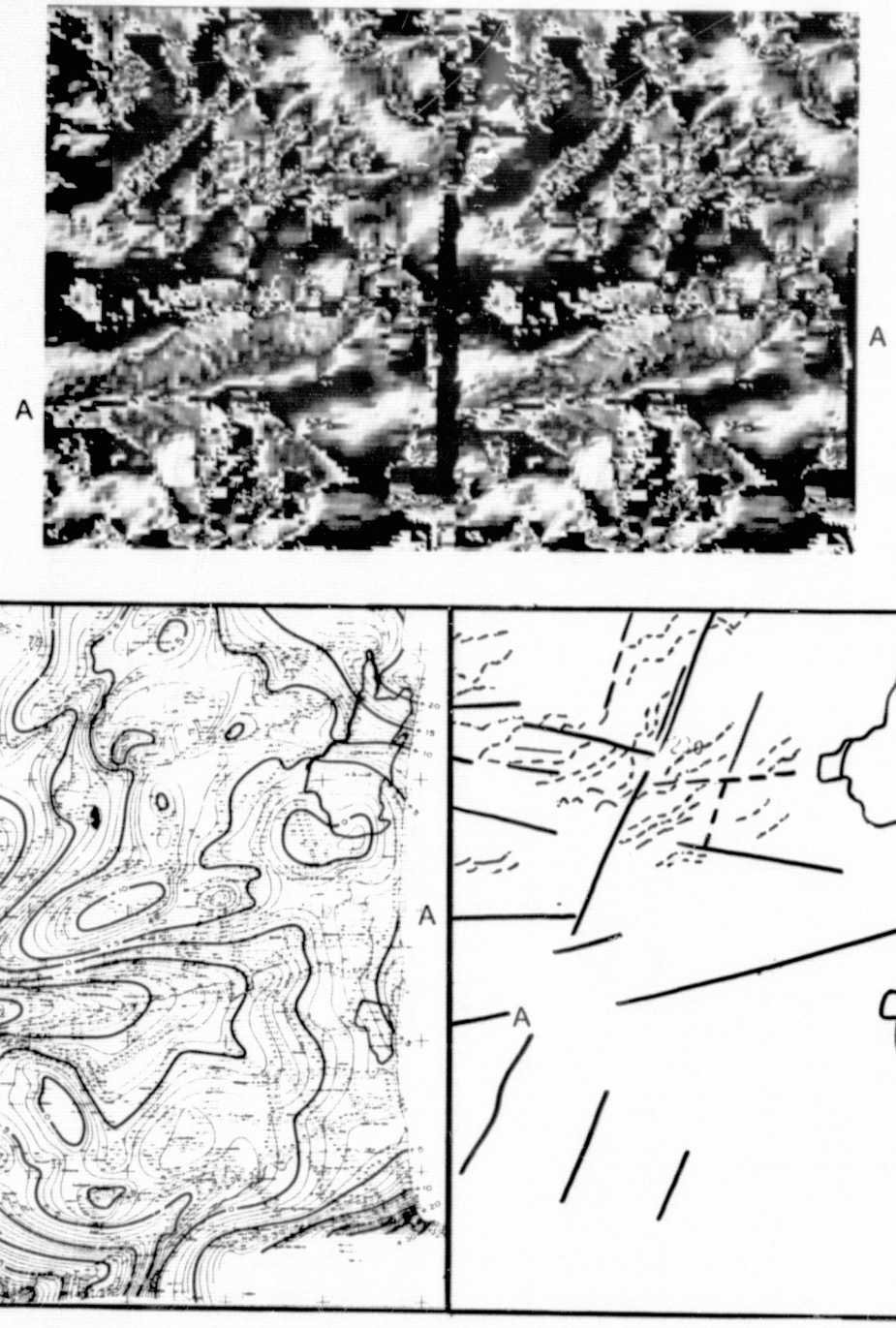


Figure 8.- The upper view is a synthetic stereo-pair made from computer processed Bouguer anomaly. Grey tones are gradient orientation from N 80° (black) to N 170° (white). Heights are slopes i.e. absolute values of the gradient. Bottom right is an interpretative sketch of satellite image of the same area (see ref. 3). Lineament AA, is clearly visible on the stereo pair as a straight white crest; but it may be confused, on Bouguer map, with the northern slope of an elongated nose trending N 60 E, although it is on the southern slope. Some other features have similar shape on the stereo pair and on the satellite sketch, but they seem to belong to the "cuestas" of sedimentary beds. (B)

REPRODUCIBILITY OF THE
ORIGINAL PAGE IS POOR

APPLICATION OF SATELLITE PHOTOGRAPHIC AND MSS DATA TO SELECTED GEOLOGIC AND NATURAL RESOURCE PROBLEMS IN PENNSYLVANIA* G-21

I.- LINEAMENTS AND MINERAL OCCURRENCES IN PENNSYLVANIA

W. S. Kowalik and D. P. Gold

N76-17518

Office for Remote Sensing of Earth Resources
Pennsylvania State University

Lineaments are naturally occurring linear topographic and tonal features greater than 1 mile in length (Lattman, 1958). Lineaments, similar to shorter linear features known as fracture traces (Lattman and Nickelson, 1958; Lattman and Matzke, 1961; Kiem, 1962; Lattman and Parizek, 1964; Wobber, 1967; Siddiqui and Parizek, 1971, Parizek, 1975) appear to be surface manifestation of nearly vertical zones of fracturing or faulting in the underlying bedrock (Wier, et al., 1973; Gold et al., 1973; Gold et al., 1974). As fractured zones, lineaments may act as zones of increased permeability, channeling fluids in the crust. Smith et al. (1971) and Drahovzal (1973), as well as Krohn and Gold (see part II of this paper), have cited possible genetic associations of lineaments and mineral occurrences in the Appalachians. Other workers have noted an association between increased density of lineament intersections and major mining districts in Nevada and Colorado (Levandowski et al., 1973; Jensen, 1973; and Nicolais, 1973).

This paper reports those metallic mineral occurrences in Pennsylvania which lie near lineaments mapped from LANDSAT-1 satellite imagery (Kowalik and Gold, 1975) and verified from Skylab photography (see part III) where available. The lineaments were categorized by degree of expression and type of expression; the mineral occurrences were classified by host rock age, mineralization type, and value. The accompanying tables and figure document the mineral occurrences geographically associated with lineaments and serve as a base for a mineral exploration model.

The Lineament Map

Figure 1 represents a conservative compilation of lineaments interpreted from the best LANDSAT-1 infrared (channel 7, 0.8-1.1 μ) positive transparent images (Kowalik and Gold, 1975). Where available, Skylab S190B photography was used to verify these plots. During interpretation, each lineament was rated on two different ordinal scales, a scale of degree of

*Support for this work was provided by NASA contract NAS 5-23133 as part of the LANDSAT-1 program. Work reported in part I and III was also supported by NASA contract NAS 9-13406 as part of the Skylab EREP program.

PRECEDING PAGE BLANK NOT FILMED

definition and a scale of the nature of the expression. The most well defined lineaments were classified as 3, those of intermediate definition were classified as 2, and the least well defined were classified as 1. This classification of definition is represented on the figure by solid, dashed, and dotted lines, respectively. Class 3 lineaments are visually more reliable than class 1 lineaments and class 3 lineaments show less interoperator variability. These lineaments are possibly younger or lie over zones of greater disturbance or dislocation at the surface than do class 1 lineaments. However, the degree of expression also appears to depend on artificial factors present during data collection, such as sun illumination azimuth and elevation angle, amount of foliage, and atmospheric conditions. The degree of expression is, therefore, a considerably less reliable criterion for defining relative disturbance at the surface than might otherwise be the case.

The second classification used on the figure describes each lineament as, A) alignments of major stream segments (streams in which water is visible on LANDSAT imagery); B) alignments of minor stream segments; or C) alignments of tonal features not classifiable as A or B. Although not precise, this classification provides the map user with an indication of the criteria used in mapping a particular lineament.

Procedure

The lineament map was interpreted on LANDSAT-1 channel 7 transparancies at the nominal image scale (1:989,000) using standard photogeologic techniques, after which the lineaments were digitized for computer processing. Two FORTRAN IV programs were written to sort the data by lineament length, degree of expression and type and to provide Calcomp plotter colored line maps at desired scales. The map was enlarged by means of the Calcomp plotter, to the scale of the Stream Map of Pennsylvania[1] (1:380,160) on which 11 known metallic mineral localities, mineral prospects, and abandoned and working mines had been plotted. During interpretation, few lineaments were drawn parallel to strike in order to aviod recording erosional differences between lithologies. Recognized cultural linear features were filtered out.

Most of the mineral occurrences were taken from the Mineral Atlas compiled by Rose (1970). These were updated with data from the Pennsylvania Geological Survey Open File Reports (1972 and No Date) and from theses by Hsu (1973) and Krohn (1975). The mineral classification scheme is based on host rock age after Rose (1970). (See Tables 1 through 3.)

[1]Published in 1965 by the College of agriculture, The Pennsylvania State University.

Typical widths and the subsurface nature of lineaments are poorly known or understood. Recent sampling by Krohn and Gold (part III) along the crest of Bald Eagle Mountain suggests that lineaments transecting the ridge are underlain by a disturbed zone with anamalous faulting, jointing, and brecciation averaging 1 km wide and ranging from 0.65 to 2 km in width. Assuming this applies to the valleys as well as to the quartzite ridge crest, and to the remainder of the State as well as to Bald Eagle Mountain, the 1 km wide zone is accepted here as a practical working width for the anomalous bedrock fracturing of a lineament. This width is used here in deciding whether a particular mineral occurrence is on or off a lineament.

Lineaments are approximated on the figure by straight lines and mineral occurrences are represented by points on the map. In reality, lineaments may vary in linearity (when viewed at larger scales), in width, in origin, and in the type and intensity of fracturing. Similarly, the shape of the mineral occurrences varies from their generalized form given here. Despite these approximations, this lineament - mineral occurrence comparison provides a first order measure of the association of mineralized areas with the lineaments mapped.

Tables 4 through 7 list, by host rock age, mineral occurrences lying on 1 km wide lineaments. Each table lists the lineament class and type, the type of mineralization, the county-number identification code devised by Rose (1970), the name of the occurrence, and the known value of the occurrence. Map users will require Rose's (1970) Plate I to locate individual mineral occurrences for comparison with the lineaments numbered on the figure here. Lineaments with associated mineralization are numbered on the figure according to their listing in Tables 4 through 7.

Discussion

The lists of metallic mineral occurrences coincident with lineaments do not necessarily imply they are genetically related, for the large numbers of lineaments and mineral occurrences makes chance associations inevitable. Of 383 known mineral occurrences, 116 show a geographical association with lineaments, and another 25 lie at intersections of two lineaments. We suggest that genetic relationships must be present, particularly where large numbers of mineral occurrences lie on a single lineament.

One possible factor relating mineral occurrences to lineaments is outcrop availability. Lineaments lying along major valleys which typically provide outcrop, especially on the Allegheny Plateau, probably bias the discovery of mineralization. Although many of the listed associations may be a result of such bias, it is not possible to identify them at this stage.

Two lineaments in Pennsylvania are notable here. The Tyrone - Mount Union lineament (Gold, et al., 1973; Krohn, 1975) in central Pennsylvania passes through three major water gaps along the Little Juniata River in crossing the Valley and Ridge Province from the southeast toward the Allegheny Plateau, where its trace coincides with a strike slip fault (Gray, et al., 1960). Previously mined Pb-Zn veins in Ordovician limestones lie on its trace at the town of Birmingham. Five Pb-Zn occurrences lie on lesser lineaments adjacent to the main lineament along the northwest trending zone described by Smith, et al. (1971). The Perkiomen Creek lineament trends north across the Triassic Basin in southeastern Pennsylvania. Nine Cu-Fe mineralized areas are distributed along its length. Sanders (1963) noted a period of late Triassic northeast and north trending fracturing accompanied by the main Triassic mineralization. The Perkiomen Creek lineament may be the surface expression of a major zone of Late Triassic fractures and may have controlled the locations of the mineralization at that time.

Conclusions

It is hoped that the tables and figure presented will provide users with clues to possible controls of metallic mineralization which will be of value in prospecting in Pennsylvania. The Tyrone - Mount Union lineament complex and the Perkiomen Creek lineament are the most strongly associated with mineralization in Pennsylvania. Other un-named lineaments listed in Tables 4 through 7 are geographically associated with 3, 4, and 5 mineral occurrences each. (See lineaments 1, 2, 10, 12, 15, 29, 47, 58, 60, 65, 83, 88, and 95.)

Further work with surface and subsurface structural expression of lineaments will be necessary to define and separate lineaments genetically, and to sort out those most likely to be mineralized. The present study will hopefully encourage further field study of lineaments in varied terrains across the State.

REFERENCES

Drahovzal, J. A. (1973) Significance of Selected Lineaments in Alabama. Technical Presentations, 3rd Earth Resources Technology Satellite-1 Symposium. 1:897-918.

Gold, D. P., S. S. Alexander, and R. R. Parizek (1974) Applications of Remote Sensing to Natural Resource and Environmental Problems in Pennsylvania. Earth and Mineral Sciences. The Pennsylvania State University. 43(7):49-53.

Gold, D. P., R. R. Parizek, and S. S. Alexander (1973) Analysis and Applications of ERTS-1 Data for Regional Geological Mapping. Technical Presentations, Symposium on Significant Results Obtained from the Earth Resources Technology Satellite-1. 1(A):231-246.

Gray, C., et al. (1960) Geologic Map of Pennsylvania. Scale of 1:250,000. Pennsylvania Geological Survey, 4th Series.

Hsu, Fu-Tzu (1973) Geochemical Exploration in the Nittany Valley Area, Centre County, Pennsylvania. Unpublished M.S. Thesis, Department of Geosciences, The Pennsylvania State University.

Jensen, M. L. (1973) Geology of Utah and Nevada by ERTS-1 Imagery. Technical Presentations, Symposium on Significant Results Obtained from the Earth Resources Technology Satellite-1. 1(A):247-257.

Kiem, J. W. (1962) Study of Photogeologic Fracture Traces Over the Bisbee Quadrangle, Arizona. Unpublished M.S. Thesis, Department of Geology, The Pennsylvania State University.

Kowalik, W. S. and D. P. Gold (1975) Lineament Map of Pennsylvania. ORSER-SSEL Technical Report 5-75. The Pennsylvania State University.

Krohn, M. D. (1975) The Relation of Lineaments to Gossans and Geochemical Anomalies Along Bald Eagle Mountain, Centre, Blair, and Huntingdon Counties, Pennsylvania. Unpublished M.S. Thesis, Department of Geosciences, The Pennsylvania State University.

Lattman, L. H. (1958) Technique of Mapping Geologic Fracture Traces and Lineaments on Aerial Photographs. Photogrammetric Engineering. 24(4):568-576.

Lattman, L. H. and R. H. Matzke (1961) Geologic Significance of Fracture Traces. Photogrammetric Engineering. 27(3):435-438.

Lattman, L. H. and R. P. Nickelson (1958) Photogeologic Fracture Trace Mapping in Appalachian Plateau. Assoc. Am. Pet. Geol. Bulletin. 42(9):2238-2245.

Lattman, L. H. and R. R. Parizek (1964) Relationship Between Fracture Traces and the Occurrence of Groundwater in Carbonate Rocks. Jour. Hydrology. 2(1):73-91.

Levandowski, D. W., T. V. Jennings, and W. T. Lehman (1973) Applications of ERTS-1 Imagery to Mapping Lineaments Favorable to the Localization of Ore Deposits in North Central Nevada. LARS Information Note 101073. Laboratory for Applications of Remote Sensing, Purdue University.

Nicolais, S. M. (1973) Mineral Exploration with ERTS Imagery. Technical Presentations, 3rd Earth Resources Technology Satellite-1 Symposium. 1:785-789.

Parizek, R. R. (1975) On the Nature and Significance of Fracture Traces and Lineaments in Carbonate Terranes. Paper presented to the Bilateral United States - Yugoslavian Seminar in Karst Hydrology and Water Resources, Dubronvik, Yugoslavia.

Pennsylvania Geological Survey (1972) Open File Report: Knisley Quarry, Blair County.

Pennsylvania Geological Survey (No Date) Open File Report: U.S. 22 Roadcut, Mapleton, Huntingdon County.

Rose, A. W. (1970; reprinted 1973) Atlas of Pennsylvania's Mineral Resources. Part 3: Metal Mines and Occurrences in Pennsylvania. Bulletin M50. Pennsylvania Geological Survey, 4th Series.

Sanders, J. E. (1963) Late Triassic Tectonic History of Northeastern United States. Am. Jour. Science. 261:501-524.

Siddiqui, S. H. and R. R. Parizek (1971) Hydrogeologic Factors Influencing Well Yields in Folded and Faulted Carbonate Rocks in Central Pennsylvania. Water Resources Research. 7(5):1295-1312.

Smith, R. C., III, D. C. Herrick, A. W. Rose, and J. M. McNeal (1971) Zn-Pb Occurrences Near Mapleton, Huntingdon Co., Pennsylvania. Earth and Mineral Sciences Experiment Stateion Circular 83. The Pennsylvania State University.

Wier, C. E., F. J. Wobber, O. R. Russell, R. V. Amata, and T. V. Leshendok (1973) Relationship of Roof Falls in Underground Coal Mines to Fractures Mapped on ERTS-1 Imagery. Technical Presentations, 3rd Earth Resources Technology Satellite-1 Symposium. 1(A):825-844.

Wobber, F. J. (1967) Fracture Traces in Illinois. Photogrammetric Engineering. 33(5):499-506.

Table 1: Key to Deposit Types*

Host Rocks	Type	Description
PreCambrian and Piedmont	A	Cr with minor Ni, Cu, and Fe, associated with ultramafic rocks.
	B	Ni and Cu sulfides with mafic to ultramafic rocks (Gap Nickel).
	C	Mo, Cu, U and other elements in pegmatites, or associated with pegmatites.
	D	Cu and other elements in gneiss, schist, metagabbro and related rock.
	E	Native Cu and Cu sulfides in metabasalt (Lake Superior Type).
Paleozoic	F	Appalachian-type Zn-Pb deposits in Cambro-Ordovician Ls.
	G	An-Pb sulfides in Helderberg-Tonoloway Limestones.
	H	Other Zn-Pb in sedimentary rocks.
	I	Barite in limestone.
	J	Zn-Pb-Cu sulfides as fracture fillings and veins in ls.
	K	Wurtzite and other sulfides in nodules.
	L	Sandstone-type Cu-U, U, and Cu deposits.
Triassic	M	Cu, Au, and other elements in Triassic diabase.
	N	Cornwall-type magnetite-Cu deposits.
	O	Cu in Triassic sediments adjacent to diabase, and related deposits.
	P	Cu in Triassic sediments distant from diabase.
	Q	Zn-Pb-Cu in quartz veins cutting Triassic and Precambrian rocks (Phoenixville Type).
	R	U in Triassic sediments.
Unclassified	S	Other Cu.
	T	Other Ni.
	U	Other Barite.
	W	Miscellaneous.

*From Rose (1970), Table 2.

Table 2: Approximate Production of Deposit Types at 1968 Prices*

Type	Description	Value (dollars)
A	Chromite	5 million
B	Gap Nickel	7 million
E	Copper in metabasalt	10 thousand
F	Appalachian zinc	50 million
G	Silurian lead-zinc	110 thousand
L	Sandstone copper-uranium	10 thousand
N	Cornwall-type magnetite	1 billion
O	Copper adjacent to diabase	1 thousand
P	Copper in Triassic Red Beds	1 thousand
Q	Phoenixville Type	1 million

*From Rose (1970), Table 1.

Table 3: Symbols Used in Tables 4 through 7*

Symbol	Production Class
M	Mineral locality
P	Mineral prospect
L	Production less than 1 million dollars
H	Production greater than 1 million dollars

*From Rose (1970), Table 2.

Table 4: Precambrian and Piedmont Host Rock Mineral Occurrences Associated with Lineaments[a]

LINEAMENT			ASSOCIATED MINERALIZATION[b]			
Number	Class	Type	Type	County Code[c]	Name	Production Class
1	2	B	I	Franklin 4	Near Waynesboro	M
			E	Adams 22*	Bingham (Cu Furnace) Mine	L
			E	Adams 23*	Red Hill Mine	L?
2	1	B	E	Adams 22*	Bingham (Cu Furnace) Mine	L
			E	Adams 23*	Reed Hill Mine	L?
			O	Adams 17	Fairfield South West	P
3	1	B	E	Adams 26*	Culp (Deshler) Shaft	P
			E	Adams 25*	Bechtel Shaft	P
4	3	B	E	Adams 25*	Bechtel Shaft	P
			E	Adams 26*	Culp (Deshler) Shaft	P
5	1	B	A	Lancaster 22	Newbold Mine	L
			A	Chester 33	Hillside Mine	L
6	3	B	A	Lancaster 20	Carter (Texas) Mine	L
			A	Lancaster 21	Wood Mine	H
7	1	C	D	Chester 9*	Keystone Quarry (Cornog)	M
8	2	B	C	Delaware 19*	Upland Station	M
9	1	B	C	Delaware 19*	Upland Station	M
10	1	B	C	Delaware 12	Franklin's Paper Mill	M
			C	Delaware 15	Leiper's Quarry	M
			C	Delaware 17	Deshong Quarry	M

(Continued)

[a] Lineaments with associated occurrences of different host rock ages are listed under the host rock.

[b] From Rose (1970) unless noted otherwise. See Tables 1, 2 and 3 of this report.

[c] A single asterisk indicates location on the intersection of 2 lineaments. A double asterisk indicates location on the intersection of 3 lineaments. For localities with more than one mineral occurrence, not all of these may occur on one lineament — some may occur on one and others on another.

Table 4 (continued)

LINEAMENT			ASSOCIATED MINERALIZATION			
Number	Class	Type	Type	County Code	Name	Production Class
11	2	B	A	Delaware 3	Worrell	M
			A	Delaware 4	Blue Hill	M
12	1	C	D	Philadelphia 17	George's Hill	M
			Q	Philadelphia 18	Falls of Schuylkill	M
			C	Philadelphia 19	Pennsylvania Ave	M
13	3	A	D,I	Montgomery 37	Mogeetown	M
			D	Montgomery 39	Gladwyne	M
14	2	B	D	Montgomery 44	Paper Mills Station	M
15	3	C	W	Montgomery 41	Smith's Quarry	M
			C	Montgomery 42	Heacock's Quarry	M
			D	Montgomery 43	Ogontz	M
16	1	B	C	Berks 8	Pricetown	M
17	1	B	C	Northampton 5	Hellertown	M
18	1	B	E	Franklin 1	Hayes Creek	P
19	2	C	D	Chester 9*	Keystone Quarry (Cornog)	M
20	2	B	D	Philadelphia 1	Bells Mill Road and Wissahickon Valley	M

Table 5: Paleozoic Host Rock Mineral Occurrences Associated with Lineaments[a]

LINEAMENT			ASSOCIATED MINERALIZATION			
Number	Class	Type	Type	County Code	Name	Production Class
21	3	C	I	Franklin 5	Near Waynesboro	M
22	1	B	J	York 4	York Valley Line	M
23	1	C	F	Lancaster 10	Bamford Mine	H?
24	2	C	F	Lancaster 11	Herr's Mine	L?
			F	Lancaster 12	Flory's Mill Quarry	M
25	1	C	F	Lehigh 6	Friedensville	H
26	2	A	F	Lehigh 3	Allentown	P
27	3	A	H	Lehigh 1	Lehigh Gap	M
28	1	B	H	Monroe 1	Middle Smithfield Township	P
29	3	A	L	Carbon 2	Penn Haven Junction	P?
			L	Carbon 3	Penn Haven Junction	P
			L	Carbon 4	Butcher Hollow	P
30	2	B	L	Wyoming 1	Nicholson Township	M
31	2	C	L	Wyoming 2	Forkstown	P
32	1	C	L	Luzerne 3	Laurel School	M
33	2	B	L	Schuylkill 2	Hecla	M
34	1	C	H	Schuylkill 3*	Adamsdale	M

(Continued)

[a]See footnotes to Table 4.

Table 5 (continued)

LINEAMENT			ASSOCIATED MINERALIZATION			Production
Number	Class	Type	Type	County Code	Name	Class
35	2	B	H	Schuylkill 3*	Adamsdale	M
36	1	B	H	Schuylkill 1	Pottsville	M
37	1	A	G	Northumberland-1	Doughty Mine	L
38	3	B	L	Montour 1	Near Roaring Creek	P
39	1	B	L	Columbia 1	Grassmere Area (8 occurrences)	P
40	1	B	L	Columbia 1	Grassmere Area (8 occurrences)	P
41	1	B	L	Lycoming 3*	Beaver Lake (5 localities)	P
42	1	B	L	Lycoming 3*	Beaver Lake (5 localities)	P
43	1	B	L	Lycoming 3	Beaver Lake (5 localities)	P
			L	Lycoming 2	Hughesville (3 localities)	P
44	2	B	L	Sullivan 5	West of Beech Glen (4 localities)	P
45	3	B	L	Sullivan 3*	Dushore	P
46	2	B	L	Sullivan 3*	Dushore	P
47	2	B	L	Bradford 1*	Carpenter Mine	L
			L	Bradford 2*	Near New Albany	P
			L	Bradford 6*	Near New Albany	L
			L	Bradford 3*	Near New Albany	P
48	1	C	L	Bradford 5	Near New Albany	P
49	3	B	H	Sullivan 1	Millview	M

(Continued)

Table 5 (continued)

LINEAMENT			ASSOCIATED MINERALIZATION			Production Class
Number	Class	Type	Type	County Code	Name	
50	3	C	L	Bedford 2	Near Breezewood	M
51	3	B	L	Huntingdon 4	Brownsville	P
52	3	B	L	Huntingdon 6	Mapleton (4 localities)	M
			H	Huntingdon 6	Mapleton Roadcut	P
53	2	A	F	Blair 1	Birmingham	L
54	2	B	G	Blair[b]	Knisley Quarry (NE Sproul)	M
55	2	B	H	Centre 1	Milesburg Gap	P
56	1	C	H	Armstrong 1	North Vandergrift	M
57	1	C	K	Allegheny 3*	Glassmere	M
			K	Allegheny 4*	Creighton	M
58	1	A	K	Allegheny 3*	Glassmere	M
			K	Allegheny 4*	Creighton	M
			K	Allegheny 2	Springdale	M
59	1	C	K	Allegheny 5	Witmer	M
60	3	B	K	Allegheny 1	Abers Creek	M
			K	Westmoreland 1	Un-named	M
			K	Westmoreland 2	Murraysville	M
61	1	C	L	Beaver 1	Darlington	M
62	1	C	K	Butler 1	Butler	M
63	1	B	H	Butler 2	West of Parker	M

(Continued)

[b]From the Pennsylvania Geological Survey Report.

Table 5 (continued)

LINEAMENT			ASSOCIATED MINERALIZATION			Production
Number	Class	Type	Type	County Code	Name	Class
64	3	B	L	Bradford 8	Canton	P
65	2	B	L	Bradford 6*	Near New Albany	L
			L	Bradford 2*	Near New Albany	P
			L	Bradford 1*	Carpenter Mine	L
			L	Bradford 3*	Near New Albany	P
66	1	B	L	Lycoming 3*	Beaver Lake (5 localities)	P
67	1	B	L	Lycoming 3*	Beaver Lake (5 localities)	P
68	1	B	L	Lycoming 2	Hughesville (3 localities)	P
69	1	A	L	Union 3	Opposite Northumberland	P
70	2	B	L	Huntingdon 6	Mapleton (4 localities)	M
71	1	C	F	Lancaster 14	Lancaster	M
72	3	B	H	Pike 1	Westfall Township	M
73	3	B	U	Centre[c]	Near Coleville	M
74	1	C	U	Centre[c]	Lambs Gap	M
75	2	C	F	Blair	Near Arch Spring	M
76	2	B	F	Blair*	Near Waterstreet	M
77	2	B	F	Blair*	Near Waterstreet	M

[c]From Hsu, 1973

[d]from R. C. Smith, personal communication.

Table 6: Triassic Host Mineral Occurrences Associated with Lineaments[a]

LINEAMENT			ASSOCIATED MINERALIZATION[b]			
Number	Class	Type	Type	County Code[c]	Name	Production Class
78	2	C	N	Adams 13	Orrtana	M
			N	Adams 14	Carr Hill	P
79	3	C	O	Adams 2*	Teeter's Quarry	M
			O	Adams 3	Gettysburg	M
80	1	C	O	Adams 2*	Teeter's Quarry	M
81	2	C	P	Adams 1	Bonneaughtown	M
82	1	C	O	Adams 5	Near Heidlersburg	P
83	1	C	N	York 24	Bender and vicinity	L
			N	York 26	Dillsburg North	P
			N	York 25	Franklintown Area (4 localities)	P
84	1	C	N	York 25	Franklintown Area (4 localities)	P
			N	York 23*	Dillsburg (3 localities)	H
85	1	C	N	York 23*	Dillsburg (3 localities)	H
			N	York 21	Wellsville North East (2 localities)	P
86	1	C	P	York 6	LeCrons Copper Mine	P
87	2	C	N	Chester 7*	French Creek Mines	H
			N	Chester 8	Knauertown	P
88	2	C	N	Chester 7*	French Creek Mines	H
			N	Chester 6	Southeast of Hopeville	L?

[a]See footnotes to Table 4.

(Continued)

Table 6 (continued)

LINEAMENT			ASSOCIATED MINERALIZATION			Production
Number	Class	Type	Type	County Code	Name	Class
			Q	Chester 16	Wheatly, Phoenix, Brockdale, and Chester County Mines	L
			Q	Chester 17	Napoleon Mine	P
			Q	Chester 12	Morris Copper Mine	L?
89	2	B	Q	Montgomery 27*	Arcola	M
90	2	A	Q	Montgomery 27*	Arcola	M
			Q	Montgomery 28	Perkiomen Mine	L
			Q	Montgomery 29*	Ecton Mine	L
			Q	Montgomery 30	Wetherill Mine	L?
			P	Montgomery 25	Grater's Ford	M
			O	Montgomery 4	Kibblehouse Quarry	M
			P	Montgomery 26	Collegeville Station	M
			O	Montgomery 6	Hendricks Station	P
			O	Montgomery 21**	Schwencksville	P
91	2	A	O	Montgomery 21**	Schwencksville	P
			O	Montgomery 3	Young's Mine	L?
92	3	C	O	Montgomery 20	Old Perkiomen Mine	L
			O	Montgomery 21**	Schwencksville	P
93	1	B	Q	Montgomery 29*	Ecton Mine	L
94	1	B	N	Berks 3	Boyertown	H
95	3	A	O	Bucks 20	New Hope	M
			R	Bucks 19	Un-named	P

(Continued)

Table 6 (continued)

LINEAMENT			ASSOCIATED MINERALIZATION			Production
Number	Class	Type	Type	County Code	Name	Class
			R	Bucks 16	2.7 miles northeast of Point Pleasant	M
			R	Bucks 17	Delaware Quarry	M
96	1	B	O	Bucks 5*	Ferndale	M
			O	Bucks 4*	Kintnersville	M
97	2	C	O	Bucks 4*	Kintnersville	M
			O	Bucks 5*	Ferndale	M
98	2	C	R	Bucks 15	1.5 miles northeast of Pipersville	M
			R	Bucks 18	0.33 miles northeast of Point Pleasant	M
99	2	A	N	Berks 16	Frity Island Mine	H
			N	Berks 17	Raudenbush Mine	L
100	1	C	N	Berks 22	Grace Mine	H
			N	Berks 23	Byler's Mine	H?
101	1	C	N	Berks 18	Wheatfield Mine	H
			N	Berks 19	Ruth Mine	L
102	1	C	N	Adams 16	McNair Farm	P

Table 7: Miscellaneous Mineral Occurrences Associated with Lineaments.[a]

LINEAMENT			ASSOCIATED MINERALIZATION			Production
Number	Class	Type	Type	County Code	Name	Class
103	2	B	S	Bucks 28	Vanartedalen's Quarry	M
104	1	C	W	Berks 7	Flint Hill	M

[a]See footnotes to Table 4.

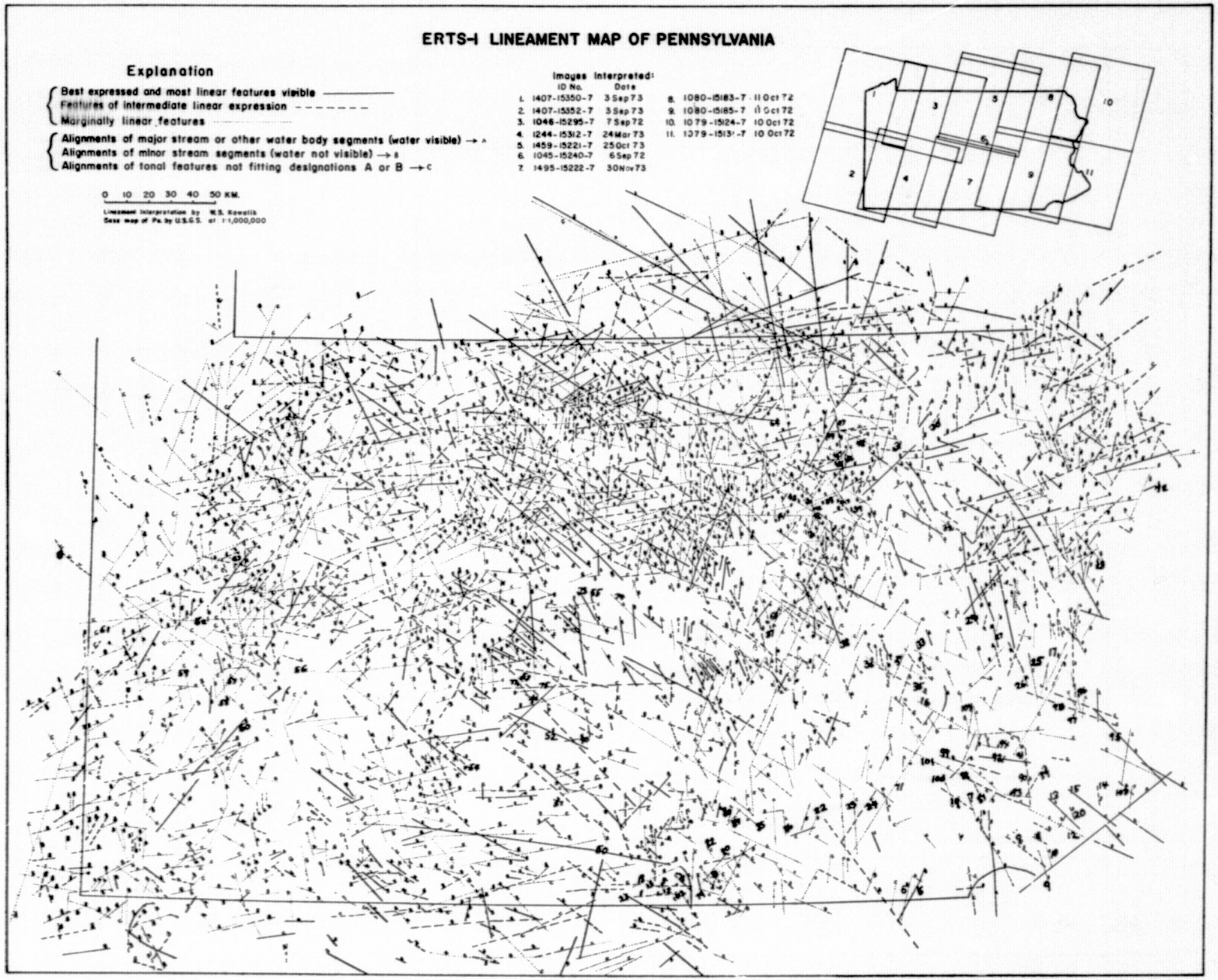


Figure 1: Lineament map of Pennsylvania drawn from LANDSAT imagery.

REPRODUCIBILITY OF THE ORIGINAL PAGE IS POOR

II.- RELATION OF LINEAMENTS TO SULFIDE DEPOSITS: BALD EAGLE MOUNTAIN, CENTRE COUNTY, PENNSYLVANIA

M. Dennis Krohn and D. P. Gold

Office for Remote Sensing of Earth Resources,
Pennsylvania State University

The results of recent mineral exploration in central Pennsylvania suggest that the megascopic fracture pattern of the Appalachian Mountain system may have a controlling influence on the location of metallic sulfide occurrences. The Tyrone - Mount Union lineament (Gold, et al., 1973), a marked topographic linear feature over 160 kilometers long, is the locus of seven lead-zinc occurrences within three separate host lithologies, plus one copper occurrence and at least 3 known fault zones (Smith, et al., 1971); Rose, 1970). With the release of LANDSAT-1 imagery for Pennsylvania in the autumn of 1972, many previously unknown lineaments were detected and offered potential new sites to search for lead-zinc mineralization. The objectives of this LANDSAT experiment was to attempt a ground verification for the newly-detected LANDSAT lineaments and to determine whether mineralized sites are significantly more numerous in the vicinity of lineaments than in areas characterized by the absence of lineaments.

Procedures

The test area encompasses a 60 kilometer section of Bald Eagle Mountain extending from two kilometers southwest of Tyrone, Pennsylvania (N40°39'/W78°15') to Lamb's Gap near Mount Eagle, Pennsylvania (N40°58'/W77°42'). The area includes one well-documented lead-zinc locality (Butts, 1939), plus four barite localities and several localities with anomalous heavy metal content which were discovered in an extensive geochemical survey of the stream network draining Bald Eagle Mountain (Hsu, 1973). Other advantages of the test site were that it was easily discernible on LANDSAT imagery and that it was one of the areas designated by ORSER for repetitive underflight coverage by C130, U2, and RB57 aircraft.

A sampling and mapping traverse was made of the entire 60 kilometer length of the test area along the geologic contact of the Tuscarora Formation (an erosionally resistant white quartzose sandstone that is the principal ridge-forming lithology) and the Juniata Formation (a less erosionally resistant sequence of red siltstones and sandstones). In order to numerically estimate the mineralized population, integer counts of the sandstone float[1] were made at each sample locality along four cross-traverses,

[1]Float is defined as a general term for those rock fragments in the superficial cover material (soil) that are essentially in situ with respect to their original bedrock position.

60 meters long and 18 meters apart, perpendicular to the ridge axis. The presence and abundance of the following eight features that might indicate fracturing or mineralization were noted: sulfides (sphalerite, galena, and pyrite), barite, limonite gossans, druzy rocks, breccia, slickenslides, quartz-veins, and iron-staining. Sample localities were spaced at 0.4 kilometer intervals and ultimately came to a total of 148 for the entire test area.

Prior to the field work, lineaments were plotted on a 25 x 30 centimeter enlargment of the LANDSAT infrared (0.8-1.1 microns) image, E-1243-15253-7 of 23 March 1973, at a scale of 1:280,000. Sixteen lineaments were found to pass through the test area (Figure 1) and all lineament positions were verified on U2 and RB57 color infrared transparencies at a scale of 1:130,000 and 1:61,500, respectively.

Results

Seventeen mineralized localities are found in this section of Bald Eagle Mountain; three localities have sphalerite and/or galena, seven localities have barite, and 12 localities have limonite gossans. Most of the barite is found near stream gaps on slickenslided fracture surfaces or as fracture fillings; whereas, the limonite gossans are usually found in a brecciated quartzite matrix near the crest of the ridge. Crushed rock geochemical analyses of the limon.te gossans show that all but one of the gossans contain anomalous concentrations of trace elements, notably lead, zinc, and arsenic; one gossan sample contained 0.62% lead. The limonite gossan fragments frequently are found surrounded by a zone of brecciated or fractured float. Other such zones of brecciation are apparent along the ridge and have an average width of 1 kilometer with a range from 0.4 to 1.6 kilometers.

Continuous exposures in a 1.6 kilometer long silica brick quarry near Port Matilda, Pennsylvania, offer an opportunity to observe the subsurface nature of the zones of brecciated float. Five fracture zones -- thin ribbon-like structures of iron-stained, finely-fractured material, 0.15 to 1.0 meters in width -- are observed to vertically transgress bedding throughout the entire 20 meter quarry face. These five fracture zones in outcrop could all be linked to areas of brecciated float at the lip of the quarry face supporting the concept that the areas of brecciated float represent fracture-zones with subvertical dips.

The breccia data from the length of the test area were compiled into a frequency histogram to further test whether discrete populations of fracturing do exist on a scale comparable to the LANDSAT imagery (Figure 2). The observed discrete distribution was compared to three calculated distributions, the positive binomial, the Poisson, and the negative binomial distribution, using a chi-square goodness-of-fit test (Griffiths, 1967). Only the negative binomial distribution (Figure 3) was not significantly different from the observed frequency distribution, yielding a chi-square value of 18.755 with 18 degrees of freedom. A negative binomial result is

interpreted to signify that the trials are not independent, so that the presence of one event increases the chances that another event will occur, or that the probability does not remain constant from trial to trial (Griffiths, 1967). Hence the negative binomial supports the concept of discrete zones of intensified fracturing which are a separate population from the minor amounts of fracturing associated with the bulk of the ridge.

Lineament Correlations

Only four of the 17 fractured and mineralized float zones were symmetrically aligned with the lineament positions derived from the LANDSAT imagery. Inspection of Figure 2 indicates that many lineaments are marginal to the mineralized localities. To test whether the lineaments of Bald Eagle Mountain might be systematically offset from the mineralized zones, a 2 x 2 contigency table was constructed for three different lineament configurations (Siegal, 1956). The correlation index improved if lineaments were defined assymetrically to one side of their original LANDSAT-defined location.

Sampling bias is a possible explanation for this apparent systematic offset of the mineralized zones of the lineaments. Taking samples of float places an inherent bias on the data from the stream gaps because mass wasting has altered the float population in comparison to the other portions of the ridge. The common alignment of lineaments with stream gaps would lead to correlation with float minima, resulting in a net lower correlation.

Relative erosional resistance of the mineralized areas is a second possibility for the offset. The silicified material in a mineralized area would tend to remain topographically higher than the nonminerialized rocks, especially in fractured areas. This process should result in a resistant mineralized zone symmetrically bounded by a pair of lineaments. Lineaments A & B, J & K, and M & N, might be lineament pairs exemplifying such a process.

Conclusions

Discrete areas of finely-fractured and brecciated sandstone float are present along the crest of Bald Eagle Mountain and are commonly sites of sulfide mineralization, as evidenced by the presence of barite and limonite gossans. The frequency distributions of the brecciated float as the negative binomial distribution supports the interpretation of a separate population of intensely fractured material. Such zones of concentrated breccia float have an average width of one kilometer with a range from 0.4 to 1.6 kilometers and were observed in a quarry face to have subvertical dips. Direct spatial correlation of the LANDSAT-derived lineaments to the fractured areas on the ridge is low; however, the mineralized and fracture zones are commonly assymmetrical to the lineament positions. Such a systematic dislocation might result from an inherent bias in the float population or could be the product of the relative erosional resistance of the silicified material in the mineralized areas in relation to the erosionally weak material at the stream gaps. Hence lineaments, like other physical phenomena associated with basement rocks (e.g., magnetic intensity), need not always have a precise spatial correlative at the earth surface. Because of the subsequent erosional history, it might be necessary to interpret lineaments as broad, ill-defined features.

REFERENCES

Butts, Charles, et al. (1939) Tyrone quadrange. Atlas 96. Pa. Topo. & Geol. Survey, 4th series.

Gold, D. P., R. R. Parizek, and S. S. Alexander (1973) Analysis and applications of ERTS-1 data for regional geologic mapping. Interdisciplinary Applications and Interpretations of the Susquehanna River Basin: NASA Type II Annual Report -- June 1, 1972 - May 30, 1973. ORSER-SSEL Technical Report 9-73. pp. 120-134.

Griffiths, J. C. (1967) Scientific Method in the Analysis of Sediments. McGraw-Hill, New York.

Hsu, F. T. (1973) Geochemical exploration in the Nittany Valley area, Centre Co., Pa. Unpublished M.S. thesis. Department of Geosciences, The Pennsylvania State University.

Rose, Arthur W. (1970) Metal mines and occurrences in Pennsylvania. Bulletin M-50, Part 3. Pa. Geological Survey.

Siegal, S. (1956) Nonparametric Statistics for the Behavioral Sciences. McGraw-Hill, New York.

Smith, R. C. II, D. C. Herrick, A. W. Rose, and J. M. McNeal (1971) Zinc-lead occurrences near Mapleton, Huntingdon Co., Pa. Circular #83. Earth & Mineral Sciences Experiment Station. The Pennsylvania State University.

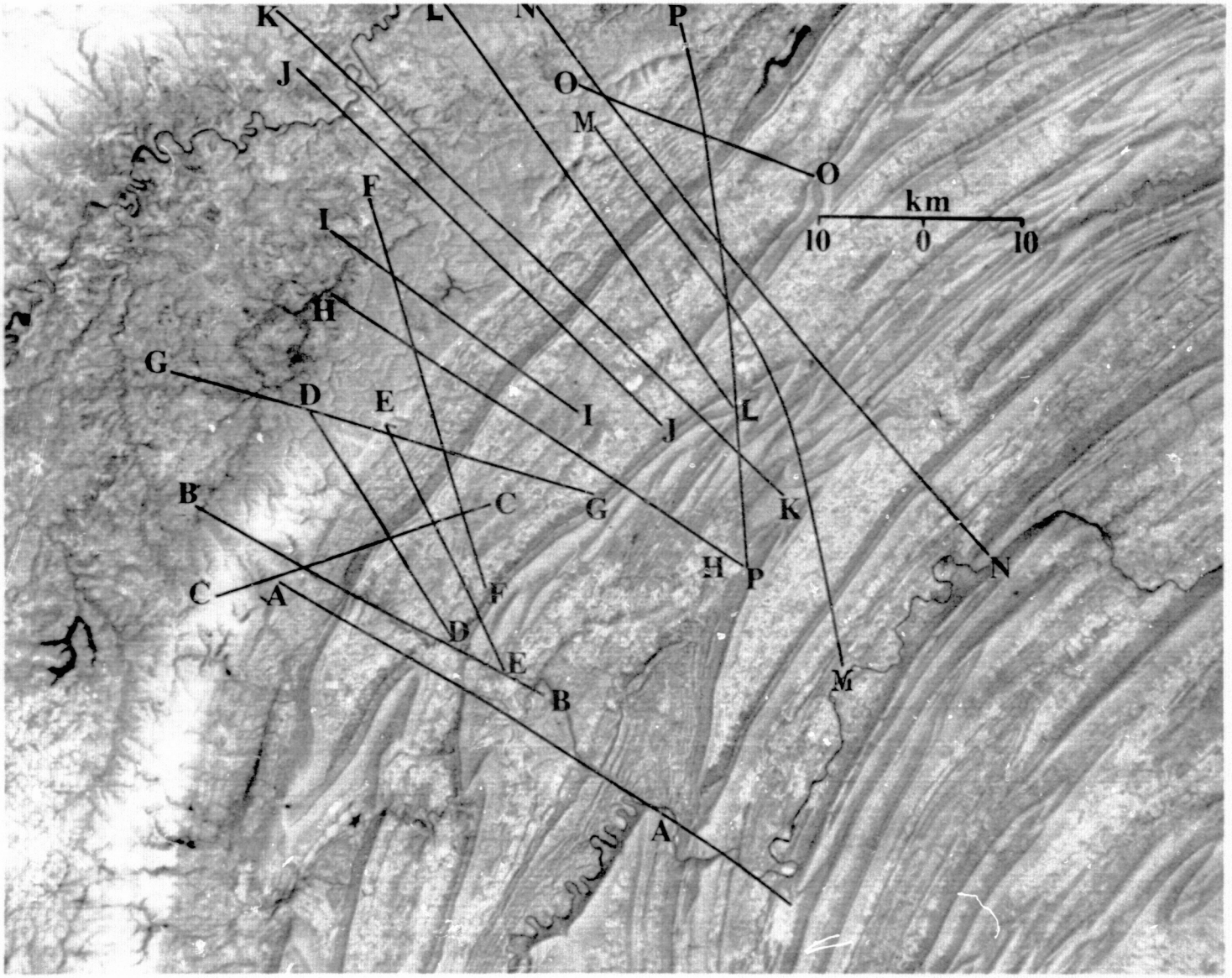


Figure 1: Enlargement of LANDSAT-1 image 1243-15253-7 of 23 March 1973 showing 16 lineaments found within the test area of Bald Eagle Mountain. Lineament B is the Tyrone-Mount Union Lineament; the silica brick quarry at Port Matilda lies between lineaments H and I.

REPRODUCIBILITY OF THE ORIGINAL PAGE IS POOR

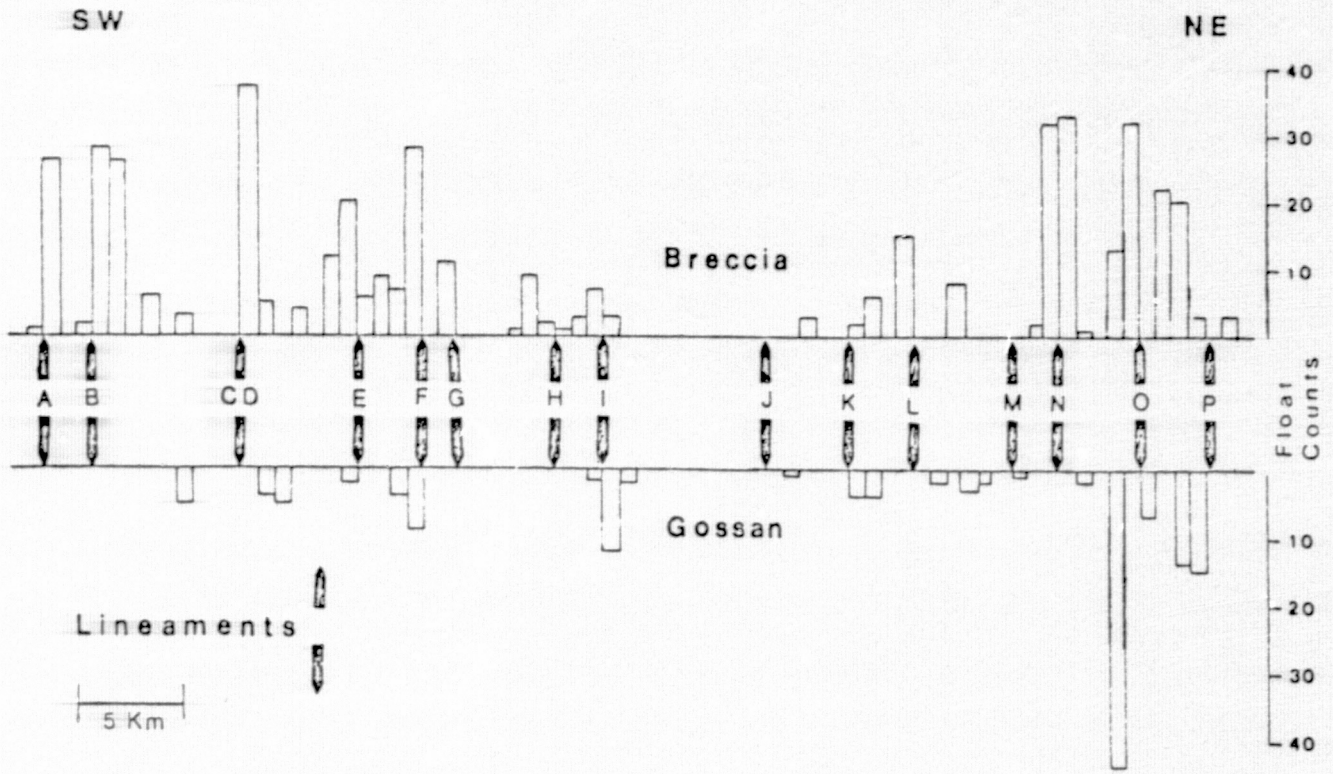


Figure 2: Histogram showing spatial relations of breccia and gossan float to the position of lineaments defined from LANDSAT imagery. Each bar represents the sum of two sample localities and is equivalent to 0.8 km along the ridge crest. Lineament C-D represents the intersection of two lineaments at the ridge crest.

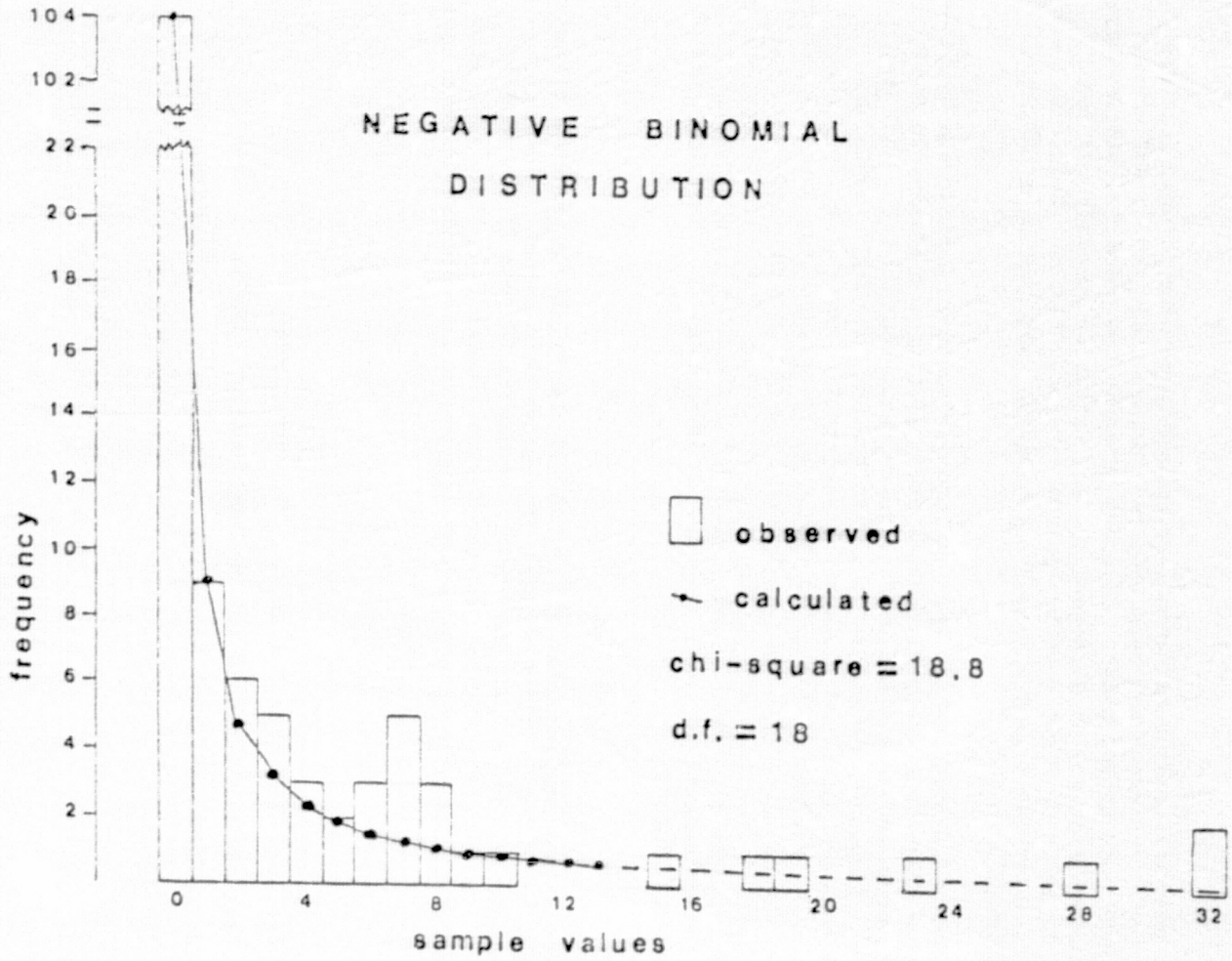


Figure 3: Frequency histogram comparing the observed distribution of integer sample counts for the breccia float to the expected distribution of the negative binomial. Note the break in scale along the ordinate. (d.f. = degrees of freedom.)

III.- COMPARISON OF SKYLAB AND LANDSAT LINEAMENTS WITH JOINT ORIENTATIONS IN NORTHCENTRAL PENNSYLVANIA

W. S. Kowalik

Office for Remote Sensing of Earth Resources
Pennsylvania State University

A geometric and/or mechanical relationship between joints, fracture traces[1], and lineaments[2] has been inferred (Gold, et al., 1973; Gol'braikh, et al., 1968; and Haman, 1964). In order to study the possible relationships between linear features at different scales, linear topographic and tonal features in parts of eight counties on the Allegheny Plateau (Figure 1) were mapped and interpreted from a Skylab-4 photograph[3] and part of a LANDSAT-1 infrared image[4].

Immediately adjacent to the area considered here, Lattman and Nickelsen (1958) have shown that joint directions are typically subparallel to the fracture traces and that the fracture traces peak from N20°W to N45°W near Houtzdale. Elsewhere, in similarly undeformed strata, Hough (1960) and Boyer and McQueen (1964) have shown that joints lie subparallel to fracture traces; while Isachsen (1973) noted that many lineaments also parallel joint trends on the Allegheny Plateau. Lineaments in the area studied here also lie subparallel to joints and to the fracture traces identified by Lattman and Nickelsen (1958). This subparallel orientation of joints, fracture traces, and lineaments suggests a genetic relationship for these features on the Allegheny Plateau.

Procedure

Positive transparencies of the LANDSAT and Skylab images were viewed on a light table and relatively short lineaments were mapped. The length distributions of the LANDSAT and Skylab lineaments (Figure 2) are similar except for the larger number of shorter Skylab lineaments. This indicates that essentially the same population of lineaments were sampled in each case.

[1]Linear features less than 1.5 km long (Lattman, 1958).

[2]Linear features greater than 1.5 km long (Lattman, 1958).

[3]S190B, 4 Jan 1974, Roll 91, Frame 324, color positive, 1:517,000 scale.

[4]Scene 1459-15221, 25 Oct 1973, Channel 7, 1:989,000 scale.

The lineaments were rated on a three-class ordinal scale of degree of expression, and on a purely descriptive three-level classification of lineament type (major streams, minor streams, or tonal lineaments). The majority of lineaments are mapped from alignments of stream channel segments. Orientation of lineaments were summarized using modified versions of Podwysocki's (1974) programs.

Biased Sampling

Wise (1968) has noted the lineament sampling bias caused by illumination from a point source. He showed that maximum enhancement of lineaments occurred when the incident light completely illuminates one valley wall and just grazes the opposite wall. The enhancement of any lineament is thus a function of valley wall slope and the orientation of the lineament with respect to the illumination azimuth and vertical illumination angle. The conditions for maximum enhancement are illustrated in Figure 3. Note that if the inclination angle exceeds the valley slope, no shadow enhancement occurs.

The steepest valley walls in the area considered here are close to 32°. Outcrops of the resistance Pocono and Pottsville units approach 90° for a few tens of feet in valley walls. It is doubtful that these cliffs cause much shadowing. The lineaments enhanced to maximum visibility on the Skylab photograph (20° sun elevation) therefore, should theoretically be oriented between 40° and 90° to the illumination direction. On the LANDSAT image (32° sun elevation), maximum enhancement should occur for lineaments oriented approximately 90° to the illumination direction. Conversely, lineaments should be relatively obscured at angles from 0° (parallel) and up to about 40° to the sun azimuth on the Skylab photograph and at nearly all angles -- but especially parallel to the sun azimuth -- on the Landsat image.

Figure 4 presents the total length versus orientation histograms for the Skylab and LANDSAT lineaments interpreted in the area. The LANDSAT histogram shows a double NW peak and the Skylab histogram shows a single broad peak at that position. The double LANDSAT peak appears to be primarily a function of the lack of lineaments parallel to the sun azimuth. The Skylab histogram also shows a decrease of lineaments near its sun azimuth.

The direction of maximum enhancement to the LANDSAT lineaments lies near the bedrock strike direction, near which lineaments were purposefully not drawn. The major N-NW Skylab peak lies within the zone of optimum enhancement of lineaments on the Skylab photograph. It appears that this peak is real because the Skylab histogram does not show a symmetrical peak to the East of the mean strike direction where one one might also be expected as a result of lineament enhancement.

Current research by this author suggests there is a bias against detecting lineaments parallel to the scan lines on LANDSAT images. The Skylab photograph, which lacks scan lines, also shows a decrease parallel

to the LANDSAT scan line direction (N77°W), however, suggesting that the decrease in lineaments detected on LANDSAT images is not necessarily artifically introduced.

Sorting of lineaments by degree of expression showed that the straightest and best expressed lineaments lie between N40°W and N60°W on the LANDSAT image and between N10°W and N50°W on the Skylab photograph (Figure 5). This difference may be a result of the scale difference between Landsat and Skylab images, but the position of the respective sun azimuths suggests that more well expressed LANDSAT lineaments may lie in the general trend of N30°W as they do in the Skylab photograph.

It appears that if the illumination and strike biases were eliminated, the orientations would be much less peaked. However, the peak of the best expressed LANDSAT lineaments (Figure 5) near the sun azimuth where lineaments should be relatively obscured must indicate an actual perferred orientation.

Comparison with Orientations of Joints

The major shale joint and coal cleat orientations in the Snowshoe and Renova West Quadrangles (Nickelsen and Hough, 1967) are drawn on lineament histograms of the area in Figure 6. A shale joint peak at N35°W and a coal cleat peak at N25°W, both nearly perpendicular to bedrock strike, correspond with the peak of the Skylab lineaments in that direction. A poorer relationship exists between LANDSAT lineaments and joints. This is thought to be due to a significant illumination bias and the small sample of LANDSAT lineaments within the area covered by the 15 minute quadrangle maps. The histogram of all LANDSAT lineaments within the area (Figure 4) shows the major peak near the main joint trends of N35°-45°W over the entire area studied. (One may postulate that the LANDSAT NW peak should broaden northward and be similar to the Skylab peak if the LANDSAT illumination bias were not present.)

This agreement reflects the long observed and typical similarity of stream channel orientations (here largely forming the lineaments) and joint trends in undisturbed sedimentary rock (Van Hise, 1895; Hobbs, 1905; Stone, 1964; and Thornbury, 1966). Because of the great scale difference between joints and lineaments, and because many lineaments cross drainage divides, the structural significance of lineaments must be more significant than simple parallelism with joints and reduced erosion resistance in the joint direction.

Discussion

A second order relationship between lineaments of the size detected here and joints of lower order as envisioned by Gold, et al. (1973) would require changes in strike of 20° to 60°. Instead, joint directions tend to coincide with the strike of fracture traces and lineaments rather than lying in symmetrical peaks at acute angles to the linear topographic and tonal features. It seems likely that in undisturbed strata, joints and lineaments are differently scaled affects of a continuous range of natural linears of similar origin. It is notable that body forces have been invoked to explain the origin of joints (Hodgson, 1961), as well as of fracture traces

(Blanchet, 1957) and of lineaments (Blanchet, 1957; Gold, et al., 1974). Price (1966) pointed out that several workers have noted an inverse relationship between joint frequency and bed thickness, holding other factors such as lithology and degree of tectonic deformation constant. Lineaments may be produced by body forces acting on mega-layers of the earth's crust in much the same fashion that fracture traces may be produced in structurally coherent thicknesses of strata. These same forces, at much higher frequencies, may also provide joints parallel to the larger lineaments in individual lithologic units.

Summary

The histogram peaks of lineaments mapped from the Skylab photograph at a scale of 1:517, 000, lie subparallel, within 20°, to major shale joints and coal cleats on the part of the Allegheny Plateau considered here. The LANDSAT lineaments, mapped at 1:989,000 are biased by illumination and scan line directions. While there is an illumination bias in the Skylab photograph, its direction does not coincide with the main transverse lineament trend, thus providing an independent assessment of the illumination direction bias. The coincidence in direction regardless of scale of the linear features, in the area considered here, suggests a mechanical relationship between joints, fracture traces and lineaments which is more consistent with a tensional model than a shear model of origin.

REFERENCES

Blanchet, P. H. (1957) Development of Fracture Analyses as Exploration Methods. Bull. Am. Assoc. Petrol. Geologists. 41:1748-1759.

Boyer, R. E. and J. E. McQueen (1964) Comparison of Mapped Rock Fractures and Airphoto Linear Features. Photogram. Engineering. 30:630-635.

Gol'braikh, I. G., V. V. Zabaluyev, and G. R. Mirkin (1968) Tectonic Analyses of Megajointing: A Promising Method of Investigating Covered Territories. Internat. Geol. Review. 8(9):1009-1016.

Gold, D. P., R. R. Parizek, and S. S. Alexander (1973) Analysis and Application of ERTS-1 Data for Regional Geological Mapping. Symposium on Significant Results Obtained from the Earth Resources Technology Satellite - 1. 1:231-246.

Gold, D. P., S. S. Alexander, and R. R. Parizek (1974) Application of Remote Sensing to Natural Resources and Environmental Problems in Pennsylvania. Earth and Mineral Sciences. 43(7):49-53.

Haman, P. J. (1964) Geomechanics Applied to Fracture Analysis on Aerial Photographs. Western Canadian Research Publication of Geology and Related Sciences, Serial No. 2.

Hobbs, W. H. (1905) Examples of Joint Controlled Drainage from Wisconsin and New York. Jour. Geology. 13:363-374.

Hodgson, R. A. (1961) Regional Study of Jointing in the Comb Ridge - Navajo Mountain Area, Arizona and Utah. Bull. Am. Assoc. Petrol. Geologists. 45:1-38.

Hough, V. N. D. (1960) Photogeologic Techniques Applied to the Mapping of Rock Joints. West Va. Geol. and Econ. Survey Report of Investigation 19.

Isachsen, Y. W. (1973) Spectral Geological Content of ERTS-1 Imagery Over a Variety of Geological Terranes in New York State. Proceedings of Symposium on Management and Utilization of Remote Sensing Data, Sioux Falls, October 29 - November 1. pp. 342-363.

Lattman, L. H. (1958) Technique of Mapping Geologic Fracture Traces and Lineaments on Aerial Photographs. Photogram. Engineering. 24(4):568-576.

Lattman, L. H. and R. P. Nickelsen (1958) Photogeologic Fracture Trace Mapping in Appalachian Plateau. Bull. Am. Assoc. Petrol. Geologists. 42:2238-2245.

Nicklesen, R. P. and V. N. D. Hough (1967) Jointing in the Appalachian Plateau of Pennsylvania. Bull. Geol. Soc. America. 78:609-629.

Podwysocki, M. H. (1974) Fortran IV Programs for Summarization and Analysis of Fracture Trace and Lineament Patterns. NASA - Goddard Space Flight Center Document X-644-74-3.

Price, N. J. (1966) Fault and Joint Development in Brittle and Semi-Brittle Rock. The Commonwealth and International Library, Pergamon Press, Oxford.

Stone, J. E. (1964) Drainage Patterns Controlled by Systematic Joints in Glacial Drift. Geol. Soc. Am. Special Paper 76. pp. 159-160.

Thornbury, W. D. (1966) Principles of Geomorphology. J. Wiley and Sons, N. Y.

Van Hise, C. R. (1895) Origin of Dells of Wisconsin. Transactions of Wisconsin Academy of Science, Arts, Letters. 10:556-560.

Wise, D. U. (1968) Regional and Sub-Continental Size Fracture Systems Detectable by Topographic Shadow Techniques. Geol. Surv. Canada Paper 68-72. pp. 175-199.

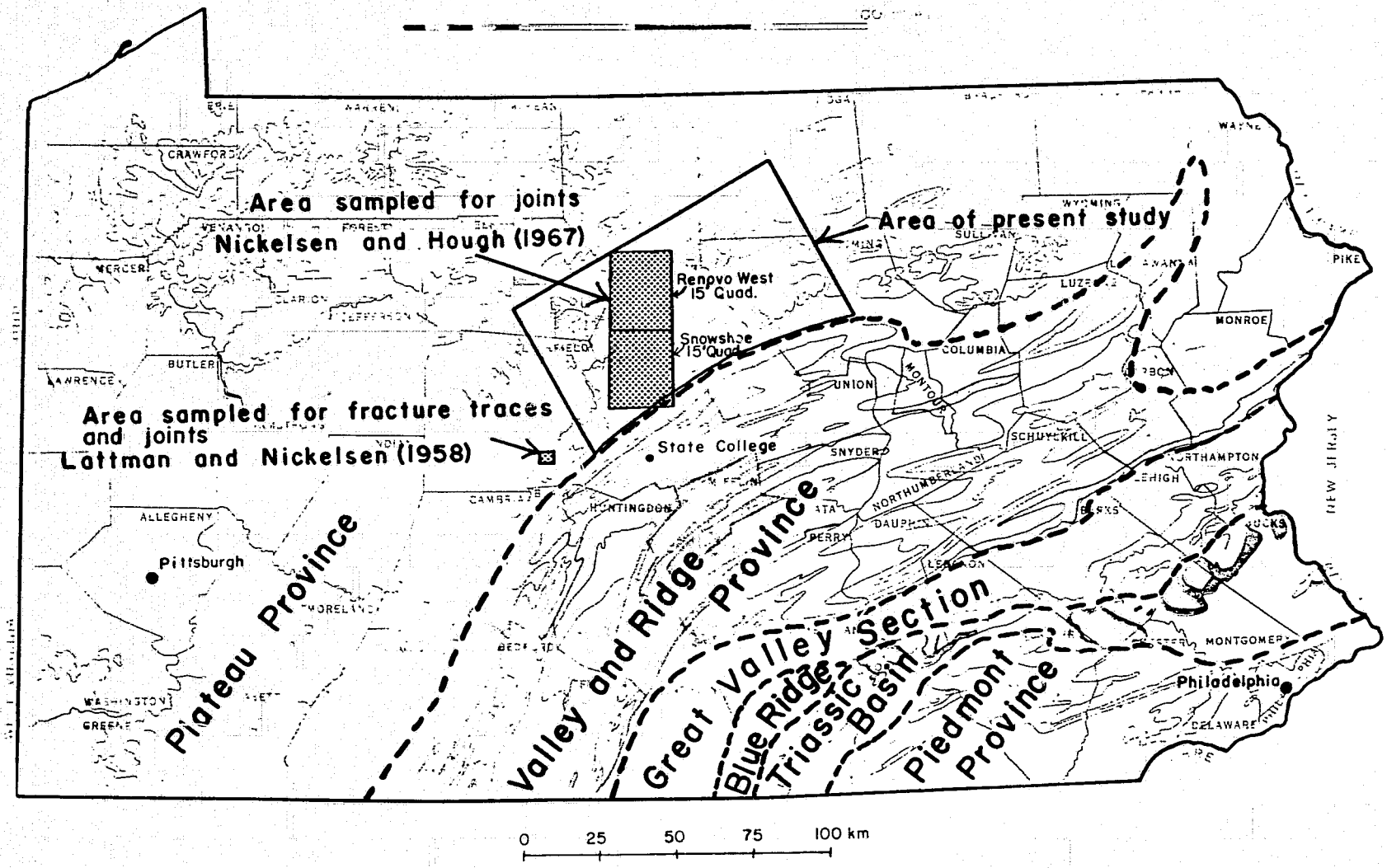


Figure 1: Location of areas in central Pennsylvania referred to in this report. The base map is the geologic map of Pennsylvania.

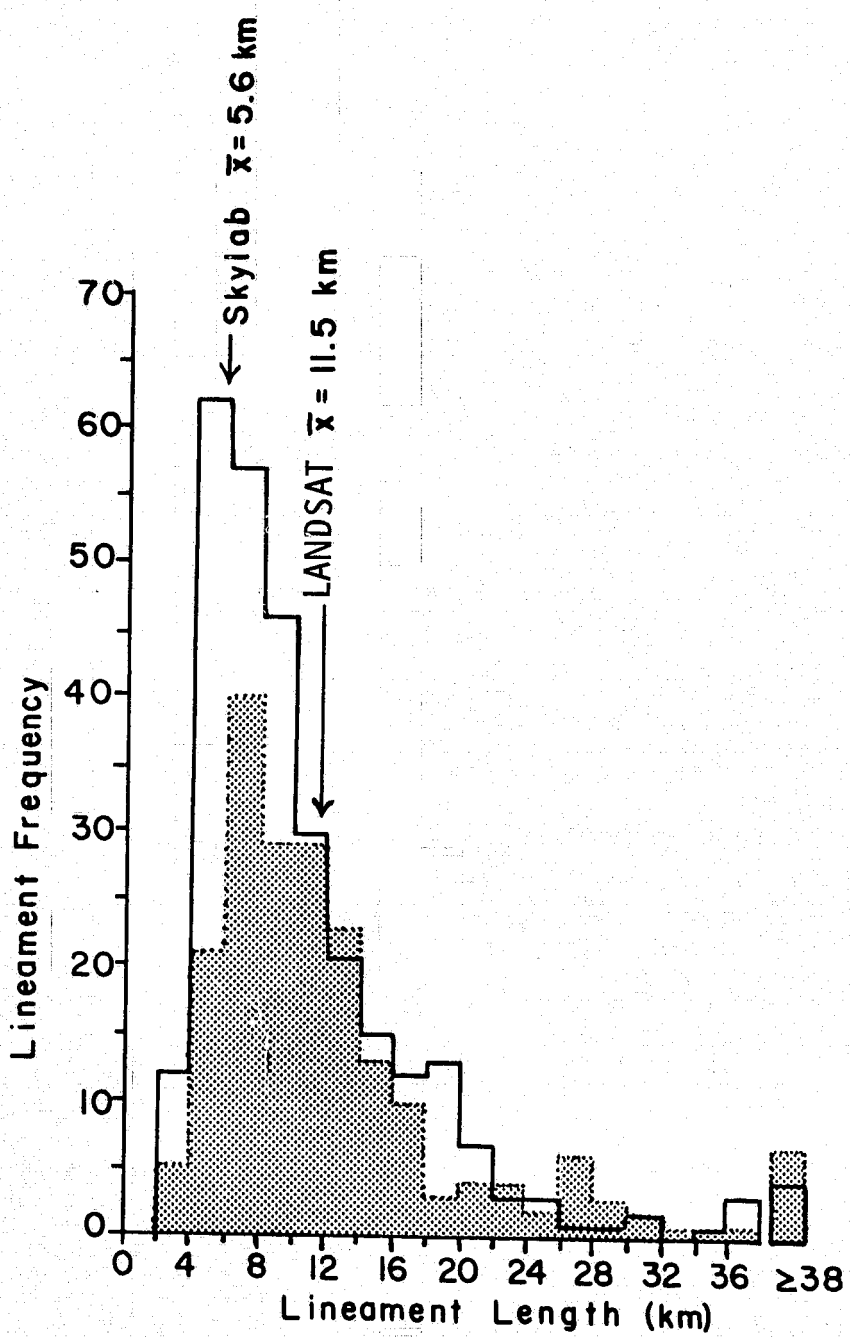


Figure 2: Lineament length distributions intrepreted from Skylab and LANDSAT images in the study area shown in Figure 1. The shaded distributions are for the LANDSAT lineaments.

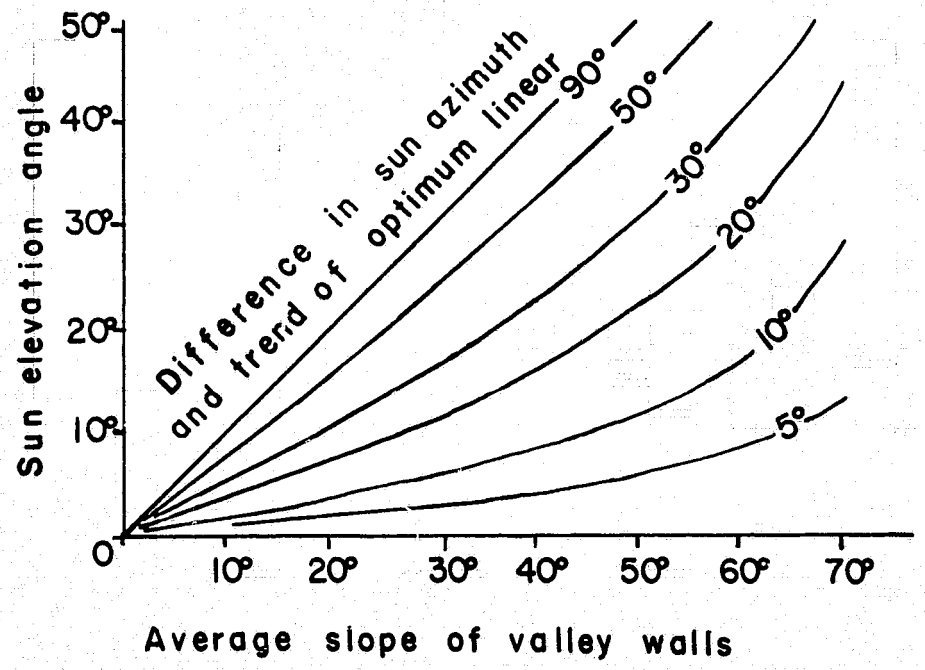


Figure 3: Conditions for maximum enhancement of a topographic linear by shadow techniques. (After Wise, 1968)

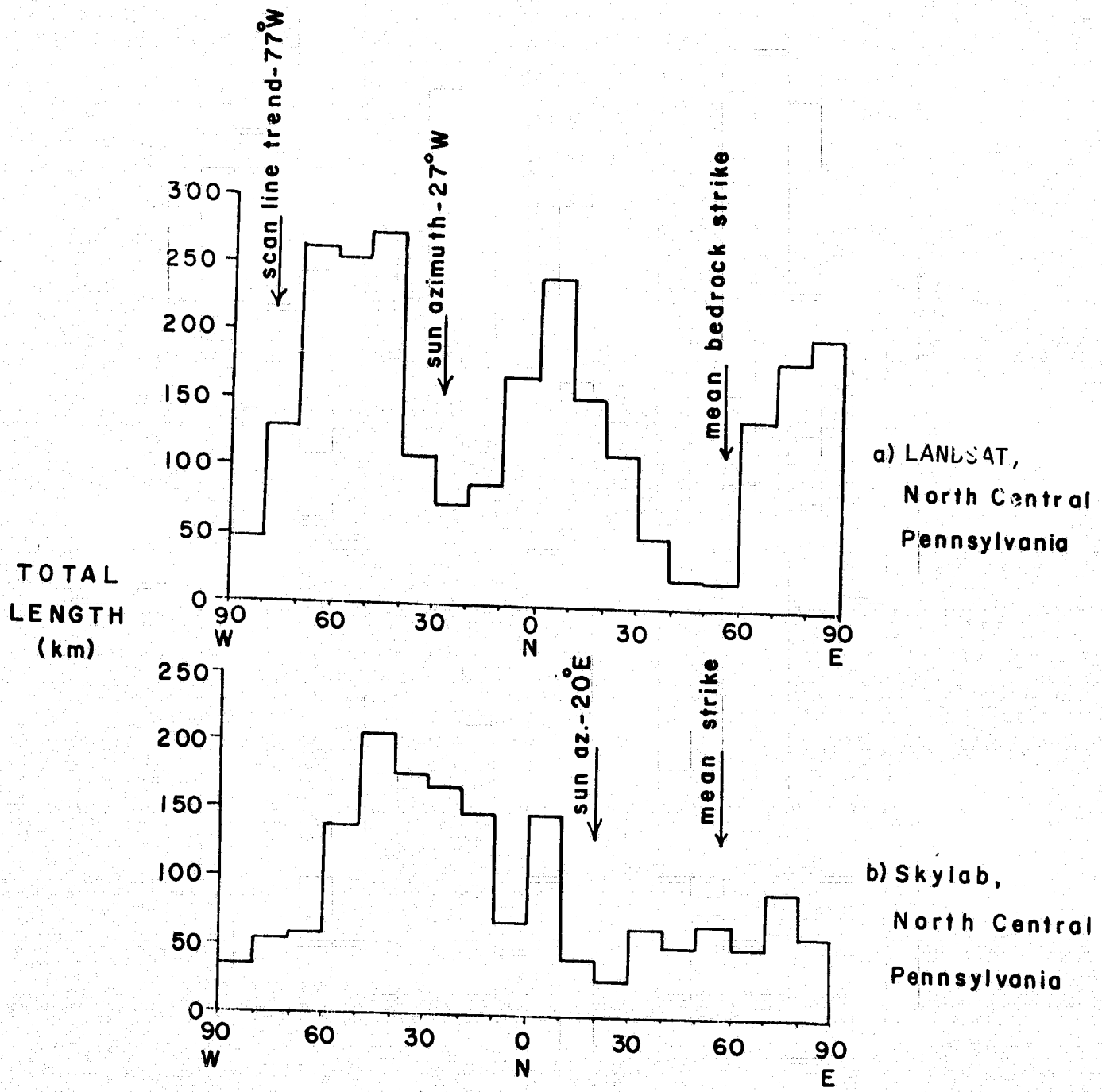


Figure 4: Summed length versus orientation histograms for LANDSAT (a) and Skylab (b) lineament interpretations.

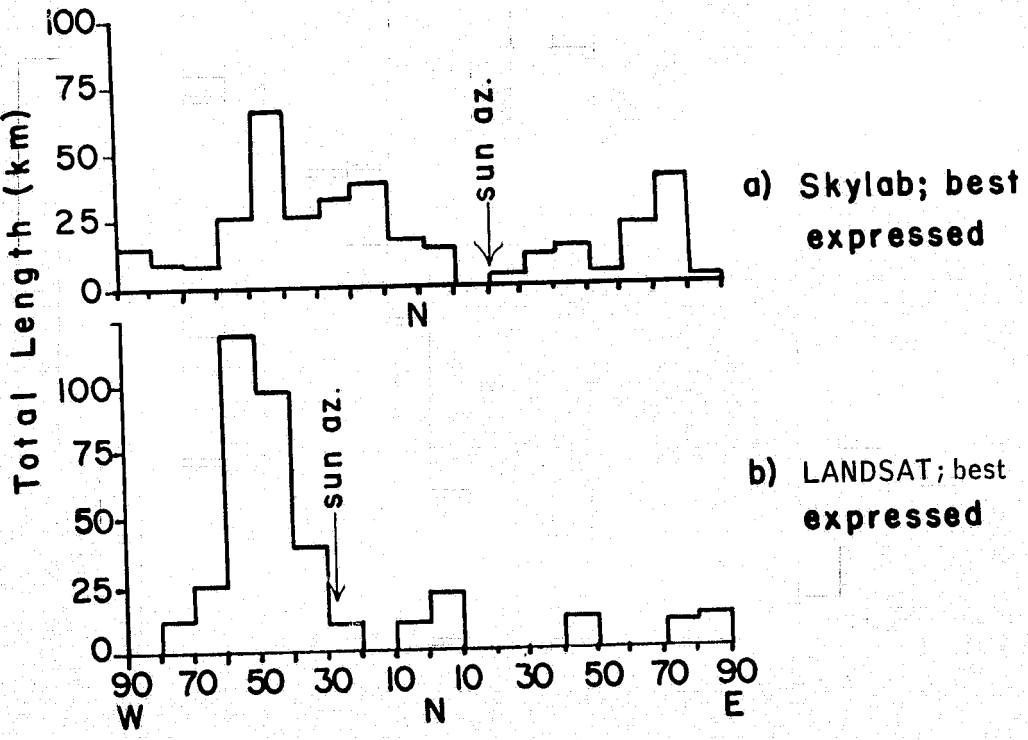


Figure 5: Summed length versus orientation histograms for the most linear and best expressed Skylab (a) and LANDSAT (b) lineament.

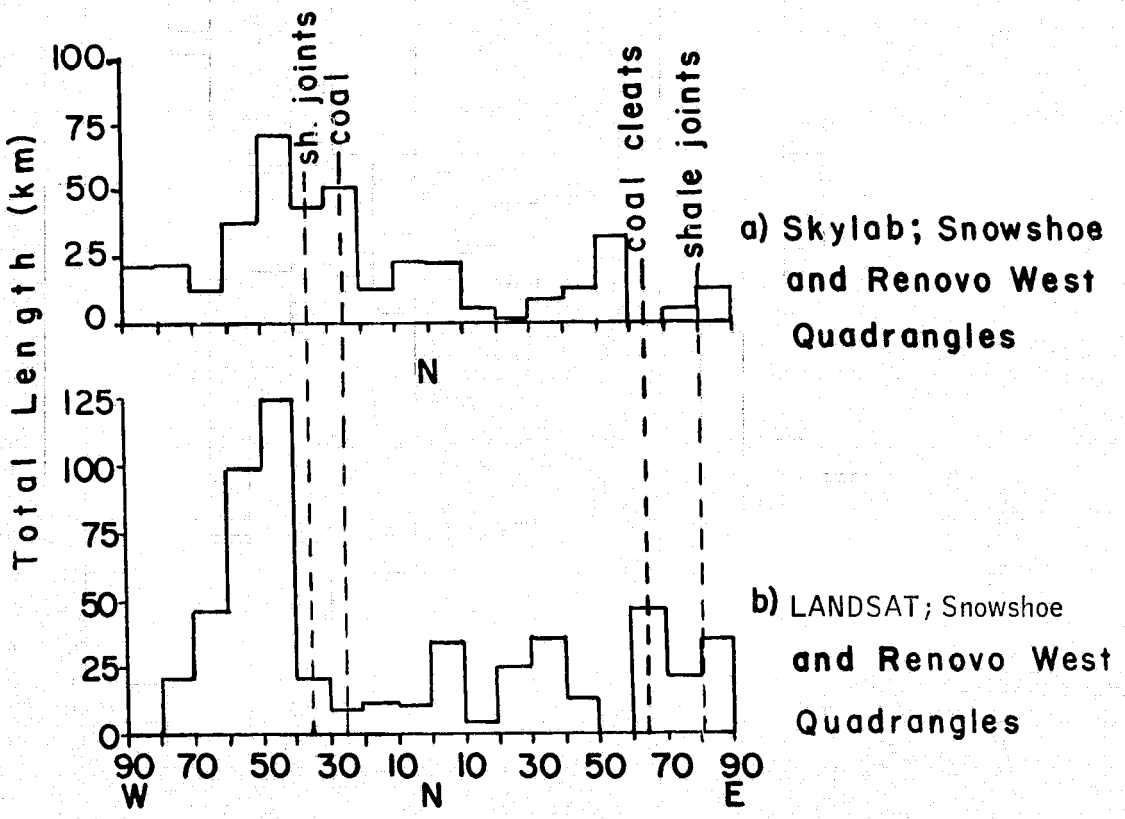


Figure 6: Summed length versus orientation histograms for lineaments in the Snowshoe and Renova West 15-minute quadrangles for Skylab (a) and LANDSAT (b) data. (Joint and cleat orientations are from Nickelsen and Hough, 1967.)

GEOLOGICAL MAPPING IN NORTHWESTERN SAUDI ARABIA USING LANDSAT MULTISPECTRAL TECHNIQUES

H. W. Blodget, NASA Goddard Space Flight Center, Greenbelt, Md.
G. F. Brown, U.S. Geological Survey, Reston, Va.
J. G. Moik, Computer Sciences Corp., Silver Spring, Md.

N76-17519

ABSTRACT

Various computer enhancement and data extraction systems using LANDSAT data have been assessed and used to complement a continuing geologic mapping program. Interactive digital classification techniques using both the maximum-likelihood and thresholding statistical approaches achieve very limited success in areas of highly dissected terrain. Computer enhanced imagery developed by color compositing stretched MSS ratio data has been constructed for a test site in northwestern Saudi Arabia. Initial results indicate that several igneous and sedimentary rock-types can be discriminated.

INTRODUCTION

During the past 25 years, the Saudi Arabian Ministry of Petroleum and Mineral Resources, in cooperation with the U.S. Geological Survey, has actively engaged in the geologic mapping of the Precambrian areas of the Arabian Peninsula. Initial field mapping efforts have contributed to the publication of preliminary geologic maps at 1:500,000 and 1:2,000,000 (1963) scale for the entire peninsula, as well as a tectonic map at 1:4,000,000 (Brown, 1972).

Present geologic goals include mapping the entire shield at 1:100,000 scale. The first few maps in this series have been published during the past several years, but a monumental task is still required to complete this ambitious project.

Various approaches using LANDSAT data are currently being assessed and used to complement the continuing mapping program in this 600,000 km^2 area. The capacity of discrimination of some of the lithologic units appears to be particularly promising.

Figure 1 is a reduction made from a 1:1,000,000 mosaic constructed from 137 LANDSAT frames. The entire Arabian shield is included in this regional coverage, and its approximate eastern margin is delineated by the solid black line. The basement rocks, in general, are seen as varying shades of dark gray. The very dark areas, however, are most commonly the poorly reflective flood basalts of Tertiary or younger age. The flow identified on the figure provides an example of this poorly reflective rock class. The Precambrian outcrops extend approximately 2000 kilometers from the Gulf of Aqaba on the north, southward to the Gulf of Aden, and attain a maximum width of 700 kilometers, at approximately 23 degrees north latitude.

Figure 2, an enlargement of the northern section of the mosaic, includes the present area of interest. The test site, located just east of the Red Sea coast in northwestern Saudi Arabia, is shown within the outline.

Only limited and very generalized distinctions are possible in attempting rock-type identification based on photo interpretation of the various LANDSAT photographic formats alone. Several very generalized lithologic groupings can be distinguished on the basis of tonal, textural and distribution characteristics. These include: (1) highly reflective alluvium and aeolian deposits, (2) poorly reflective, extensive basalt extrusions, (3) regionally homogeneous sedimentary strata and (4) coarse textured (at LANDSAT scale) massifs. Within the latter unit, sub-circular, highly reflective intrusions are common in the Red Sea area, and these, where maps are available, are generally designated as

PRECEDING PAGE BLANK NOT FILMED

being of granitic composition. The high spectral reflectivity associated with these intrusions does not generally appear to be directly related to their discrete mineralogic composition, but rather is an indirect indication of their topographic expression. Using the limited side-lap stereographic available coverage on LANDSAT imagery, light areas associated with these rocks are shown to be topographically low. This would suggest that the intrusions are subject to more rapid mechanical weathering than their respective host rocks. The topographic depressions caused by such differential weathering appear now to be partially filled with highly reflective aeolian and/or alluvial sediments.

Identification of generalized rock-types such as these discussed above, however, are not generally adequate for most geologic mapping objectives. To improve on this discrimination capability, the use of LANDSAT digital data was evaluated using various computer enhancement techniques.

The frame selected for the initial test site is shown in Figure 3. This particular scene was selected because it includes two of the areas mapped at 1:100,000 scale which are already published. Thus we have some larger scale geological mapping for interim "ground truth" for about 20 percent of the scene. Figure 4 is made up of portions of the 1:500,000 published geologic maps of the northwestern Hijaz and northeastern Hijaz which correspond to the test site.

The geology included in the scene consists predominantly of complex Precambrian metamorphic assemblages intruded by plutonic rocks varying in composition from gabbro to granite. On the north, the Precambrian is overlain by northeasterly-dipping sandstone of Cambrian (Cs) age. Quaternary/ Tertiary flood basalts (QTb) make up the dark, less dissected areas in the west and southeast. Several small volcanic flows extend northward at the left side of the bottom margin. Because of the generally low spectral reflectivity and poor tonal contrast, individual igneous and metamorphic units are difficult to distinguish in standard image formats.

Figure 5 is a reproduction of the 1:100,000 Sahl al Matran map, which is entirely within the test site. The area included is enclosed by the upper box in Figure 3. The additional detail provided by the larger scale is, of course, immediately recognized. In particular, it should be noted that the generalized granite units shown at 1:500,000 scale, have been mapped as granite/granodiorite (ggd) on the south, and as two hornblende-biotite quartz monzonites intrusions (hbqm) on the north. These units will subsequently be discussed in some detail.

APPROACH

In order to determine the applicability of computer classification and/or image enhancement for rock identification in this test area, the several programs available to us at the Goddard Space Flight Center were assessed. These included interactive, multispectral classification systems, using both the "maximum likelihood" and "thresholding" classification techniques and digital image enhancement using the SMIPS-VICAR System* (Moik, 1973). None of the systems have been exhaustively studied, but several preliminary conclusions can be projected.

COMPUTER CLASSIFICATION

Based on our admittedly limited studies of lithology discrimination within the test site, the more successful results to date, using interactive digital classification techniques, were attained with the maximum likelihood approach incorporated into the Bendix M-DAS system. The most positive results attained with this system are shown on Figure 6.

*Small Interactive Image Processing System, an interactive version of the Jet Propulsion Laboratory VICAR System.

Training sites were selected for ten lithology classes, which fell into three general categories. These included: 1) Rocks mapped at 1:100,000 scale which did not appear distinctive in the color composite imagery. In this category, training sites were selected within the Halaban group (hjm) and older greenstones (gd) mapped near the base of the Sahl al Matran Quadrangle in order to determine if these units could be separated on the basis of their spectral differences. 2) Rocks somewhat distinctive on the composite imagery that correspond with field mapped units. These units included flood basalts (QTb) mapped on the Northwestern Hijaj Quadrangle and a granite/granodiorite (ggd) mapped at 1:100,000 on the Sahl al Matran Quadrangle. 3) Sediment units that appear to be distinctive on the composite imagery but have not been subdivided during 1:100,000 mapping. The six training sites selected in this category were established in alluvium having different tonal characteristics on standard LANDSAT imagery. In some cases, it appears that discrete alluvial units can be in part related to their specific source rocks.

Clearly, the units defined in red (basalt), purple, yellow and dark blue (tonal alluvial units), correlate best with the geologic maps and the original MSS imagery. The granite/granodiorite (ggd) though not uniquely distinctive, does appear to be off-white, and its related alluvium depicted in dark blue, defines the general outcrop area mapped on Figure 5.

On the other hand, no obvious discrimination can be made in the highly dissected metamorphic and igneous terrains. It is important to note here that the more consistently correct classification is associated with the more homogeneous, near-horizontal beds formed by the flood basalts (red) and alluvium (purple, yellow and dark blue).

Figure 7 and 8 are computer enlargements of portions of the basalt and granite/granodiorite classes defined in Figure 6. The small boxes within each unit designate the training sites selected for classification. In both figures, the generally poor definition of the class-unit margins, in comparison with the equivalent mapped formations shown on Figures 4 and 5 respectively, is emphasized.

Based on our preliminary assessment of classification systems in this test site, it is concluded that the multispectral classification techniques appear to be severely limited for lithology mapping. One prime reason for this is the extreme difficulty encountered in defining adequate training sites in areas of highly dissected terrain.

COMPUTER ENHANCEMENT

Of the various rock discrimination approaches tested to date, a technique using color composites constructed from enhanced ratio data has proven to be most successful at this particular test site. An excellent summary of this method is provided by Rowan, et al. (1974).

In simplified form, the procedure consists of three fundamental steps:

1. Selected MSS bands are ratioed pixel by pixel.

2. The ratio images are contrast stretched to enhance spectral differences. In the ratioing procedure, alternative ratio combinations are used to enhance specific rock classes in different areas. The 4/5, 5/6, and 6/7 combinations have provided the greatest amount of discriminative data for both the Saudi Arabia test site and the Nevada test site of Rowan. In the Sahl al Matran area, however, other ratio combinations have successfully provided identification of additional rock classes. At present no general rule exists for selecting optimum ratio combinations that provide the greatest discrimination capability over a wide range of climatic and/or topographic conditions. Goetz and associates (1975, II-1 to II-20, and Goetz and Rowan, 1975) are currently conducting field studies using a portable field

reflectance spectrometer to better define the optimum spectral and ratio combinations for specific applications.

Both linear and non-linear stretch processes can be alternatively used to increase scene contrast optimally over the dynamic range of the output product. Linear stretching increases the scene contrast uniformally over the dynamic range while non-linear stretching can be used to increase local scene contrast in dark areas at the expense of the brightest areas. In our test area, an Histogram equalization stretch generally provided maximum contrast. Here again, as with the selection of ratio combinations, there are no general rules that can be applied to all images to determine the optimum stretch parameters for a given set of conditions.

3. Stretched data of three ratio combinations are combined into color composite imagery using various combinations of light filters and intensities.

We have been using a rotating drum film recorder (OPTRONICS) to construct black and white photo transparencies from the digital images. The various combinations thus constructed are then combined in a color-additive viewer to rapidly determine the more significant combinations in regard to rock discrimination capability. Once these combinations are defined, they are processed through a CRT film recorder (DICOMED) to produce hard copy with a better registration than that attained on the color-additive viewer.

All digital enhancements were performed using an interactive image processing system of IBM/360-75 or -91 computers.

The resultant composite provides the distinct advantage of displaying a single type of material as being similar or the same regardless of the local variation due to albedo and topography. Conversely, however, very dissimilar materials easily separable on a standard composite image may become inseparable on a ratio image where spectral reflectively slopes are similar. Thus, optimum rock-type discrimination must be accomplished in several combinations of different ratio combinations.

Figure 9 is a DICOMED color ratio-composite where the MSS band 4/5 ratio image is projected with a blue filter, 5/6 image with a green filter, and 6/7 image with a red filter. Note in this presentation that the monzonites (hbqm) mapped on the Sahl al Matran Quadrangle are a dark green while the granite/granodiorite (ggd) and alluvium around the granites are ocher in hue. Outside the Matran map area, at the right margin, a dark green triangular body has also been mapped as a hornblende-biotite quartz monzonite on the 1:100,000 Wayban Quadrangle. In addition the ocher-brown body immediately to the west of the monzonite is mapped as riebeckite granite. There is no 1:100,000 coverage of the ocher-colored area to the north, but it is also shown as granite on the 1:500,000 Northwestern Hijaz Quadrangle.

The brilliant blue unit on the composite, of course, corresponds to the basalt flows (QTb) discussed earlier. It can be seen very clearly here that the margins of the basalt are much more clearly defined than they were using a computer classification system (Figure 7). Several smaller basalt flows are seen near the eastern margin, while several discrete cinder cone fields are visible across the wadi from the large flow. This enhancement has been used to aid in distinguishing small cinder cones of basaltic composition from ultramafic rocks in the 1:100,000 map compilation for the area south of the Sahl al Matran Quadrangle.

The tan-colored outcrops in this enhancement are largely comprised of complex metamorphic assemblages. Our ability to distinguish between metamorphic units mapped in the field has been poor to date.

Figures 10 and 11 were photographed from a color additive viewer screen. Some resolution degradation caused by the poor registration of the different ratio images data caused the slight blurring effect. The points of reference, however, can still be readily distinguished.

The Figure 10 image was made from a combination using MSS band ratios 4/7 with blue filter, 7/4 with a green filter, and 6/5 with a red filter. In this rendition, the Siq sandstone (Cs) in the upper right is a bright yellow. This is not unique to the scene, however, for granites (G) to the south are of the same hue. It is thus not possible to distinguish between the two different lithologic units on the basis of this particular ratio enhancement alone. When the MSS 6/5 band ratio image is replaced by 7/6 image using a red filter, however, tonal changes occur as shown in Figure 11. In this second ratio composite, the Siq sandstone remains a bright yellow, but the granites (G) that were yellow in Figure 10 are now a pale yellow-green hue. Conversly, the monzonite (hbqm), that is pale yellow-green in Figure 10, is yellow on Figure 11 with the new ratio combination. The use of a pair of ratio combinations, thus, seems adequate in this case to define the Siq sandstone within this particular scene; at the same time, differences in the spectral characteristics between granites and monzonites are reemphasized.

Figure 12 is a DISCOMED ratio-enhancement that overlaps the area shown in Figure 9, on the south. This color ratio-composite was made using MSS 5/4 ratio with a blue filter, 6/5 with a green filter, and 7/6 with red filter, or just the inverted ratio combinations used in the construction of Figure 9. The several volcanic flows that extend northward from the left side of the bottom margin of the test site (Figure 3) are shown in two colors in this ratio-enhancement. Based on field confirmation, the geologically recent flows correlate with the areas shown in ocher while the flows of historic age are shown as black (the most recent eruptions in the area were recorded in 1280 A.D.). The flood basalts (QTb) that were blue in Figure 9 are a bright yellow in Figure 12. There is, thus, a strong suggestion that the progression of color tonal differences from black to ocher to yellow among the basalts can be at least crudely related to age. Difference in chemical composition of the respective flows could provide an explanation for the color differences. Field data, however, suggest that the compositional differences are not sufficient to significantly alter the spectral response between the different volcanic units. Changes in reflectance due to a varying degree of weathering, on the other hand, can better explain the observed difference of spectral response, and this would also relate to age.

In addition to the mapped extrusives discussed above, there appears to be a distinct lithologic class defined in pale yellow in the southeast corner of Figure 12. The entire lithologic suite in this quadrant has been mapped as schist at small scale (see Figure 4). The enhanced imagery was compared with a 1:100,000 orthophoto mosaic of the area which had been constructed from reduced 1:30,000 aircraft photography.

The pale-yellow spectral unit defined on the ratio-enhanced image correlated extremely well with a clearly defined, dark, "botryoidal"-textured unit on the mosaic. It is anticipated that this unit will be investigated in the field to determine if the pale-yellow unit does indeed define a specific metavolcanic sequence.

Most of the western one-fourth of the scene shown in Figure 12 is included within the area to be covered by the 1:100,000 Dhaylan Quadrangle. The lithology change across the well-defined north-south trending fault (A-A') is especially well displayed on the south where there is an abrupt change from purple on the west to a dark-brownish-green on the east. The southern part of the pale green sinuous body (g) is designated as granite on the preliminary geologic map. On the same map, however, this granite is shown to terminate at a secondary fault extending between B and B' on Figure 12. The ratio composite data, however, strongly suggest that the granite continues in a northwesterly direction as a discrete unit, and terminates at the major north-south fault. This area must be further investigated in the field to determine the true extent of the granite body.

In addition to the spectral-lithologic relationships discussed above, special attention was placed on the areas immediately adjacent to the three ancient mine workings described by Hadley (1973). Each area was studied in detail using a variety of ratio/filter and stretch combinations in order to identify any hydrothermal alteration that might be associated with the mineralization. No anomalies were recognized in association with the mineralized areas, but this could very well be due either to the absence of alteration products or the small areal extent of mineralized areas. Plans are presently being formulated to study several well-developed hydrothermal alteration zones known to exist in association with massive sulfide deposits near the Yemen border.

CONCLUSIONS

The ability to identify lithologic classes using LANDSAT multispectral techniques appears to be possible, at least to a limited degree. The various classification techniques that have been so successful in a variety of agriculture, land use and environmental studies appear to be severely limited in rock-type discrimination, especially in areas of highly dissected terrain. This is not necessarily the result of the inadequacy of the various statistical approaches used in classification, but rather, the extreme difficulty encountered in defining adequate training sites in areas of highly dissected terrain.

A technique of image enhancement using stretched ratio-composite data uses slope difference as the basis for discrimination rather than absolute reflectance values. By using this approach, the effects of local variation of terrain and albedo are minimized.

Preliminary studies, using images constructed using this technique, indicate that several rock-types can be distinguished. These include basalts, monzonites, and certain granites. Efforts to distinguish between different metamorphic lithologies have been unsuccessful.

Computer enhanced LANDSAT imagery continues to be used in selected test sites to complement traditional mapping techniques in Saudi Arabia. The initial promising work is being refined and expanded to form a base from which we can expand and refine our present capabilities.

REFERENCES

Brown, G. F., 1972, Tectonic map of the Arabian Peninsula: Ministry of Petroleum and Mineral Affairs map AP-2.

Brown, G. F., Jackson, R. O., Bogue, R. G., and Elberg, E. L., Jr., 1963, Geologic map of the northwestern Hijaz Quadrangle, Kingdom of Saudi Arabia: U.S. Geological Survey Misc. Geol. Inv. map I-204A.

Brown, G. F., Layne, N., Goudzarzi, G. H., and MacLean, W. H., 1963, Geologic map of the northeastern Hijaz Quadrangle, Kingdom of Saudi Arabia: U.S. Geological Survey Misc. Geol. Inv. map I-205A.

Goetz, A. F. H., 1975, Use of ERTS and other correlative data: in Goetz, A. F. H., Billingsley, F. C., Elston, D. P., Lucchitta, I., Shoemaker, E. M., Abrams, M. J., Gillespie, A. R., and Squires, R. L., 1975, Application of ERTS images and image processing to regional geologic problems and geologic mapping in northern Arizona: Final Report ERTS (LANDSAT) investigation MMC-308.

Goetz, A. F. H., and Rowan, L. C., 1975, The realities of using satellite spectral data for lithologic identification: Presented at Annual Mtg. of the Am. Soc. of Photogrammetry, Washington, D.C. Mar 9-14.

Hadley, D. G., 1973, Geology of the Sahl al Matran Quadrangle, northwestern Hijaz, Kingdom of Saudi Arabia: Ministry of Petroleum and Mineral Resources map GM-6.

Hadley, D. G., 1974, Geologic map of the Wayban Quadrangle, Kingdom of Saudi Arabia: Ministry of Petroleum and Mineral Resources map GM-7.

Moik, J. G., 1973, Small interactive Image Processing System, User's Manual: NASA/GSFC X-650-73-283, 61 p.

Rowan, L. C., Wetlaufer, Goetz, A. F. H., Billingsley, F. C., and Stewart, J. H., 1974, Discrimination of rock types and altered areas in Nevada by use of ERTS images: U.S. Geol. Prof. paper 883, 35p.

U.S. Geological Survey-Arabian American Oil Company, 1963, Geologic Map of the Arabian Peninsula: U.S. Geological Survey Misc. Geol. Inv. map I-270A.

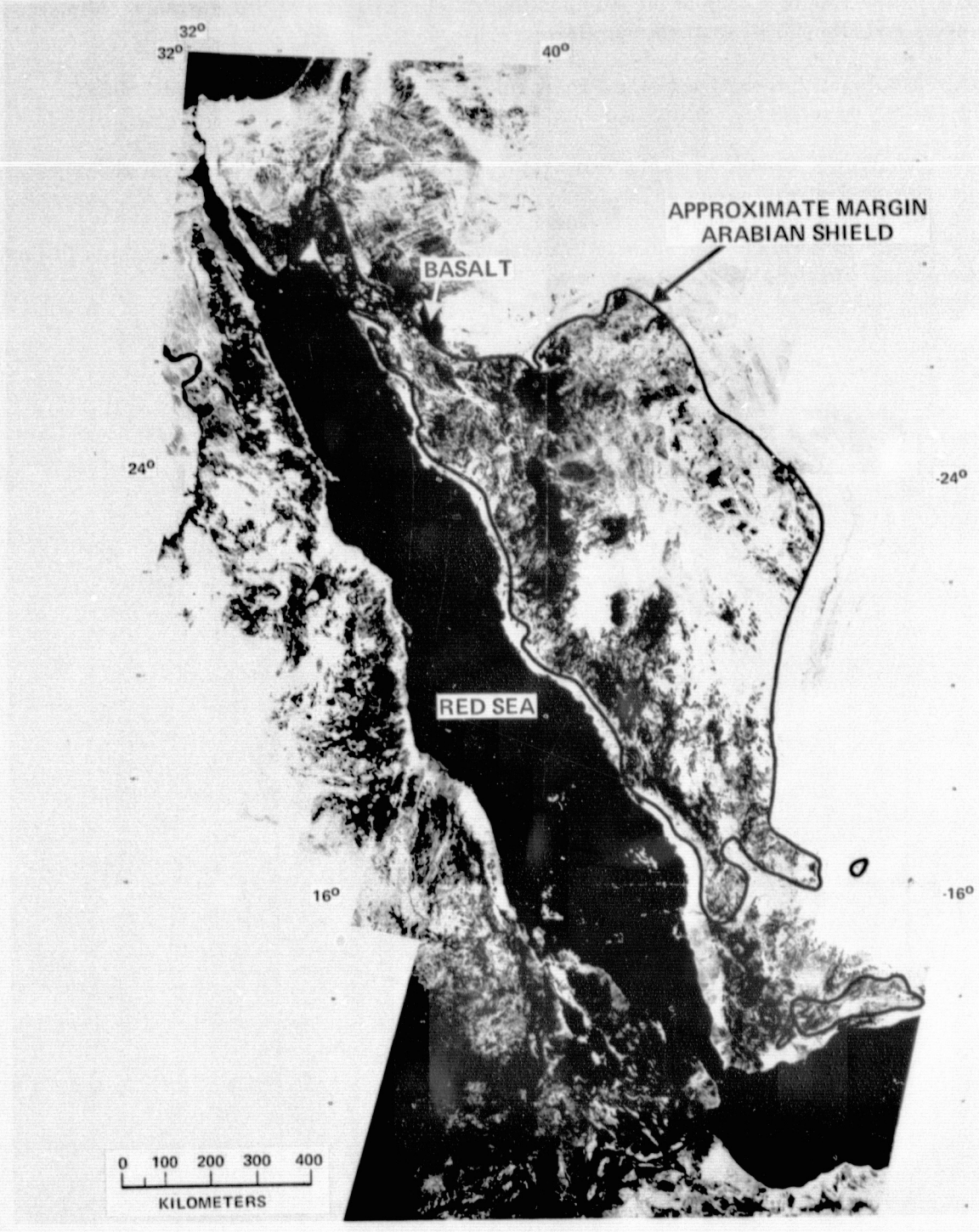


Figure 1. Semi-controlled mosaic of the Red Sea and adjacent Precambrian basement.



Figure 2. Mosaic of northern Red Sea and adjacent terrestrial areas.

REPRODUCIBILITY OF THE
ORIGINAL PAGE IS POOR

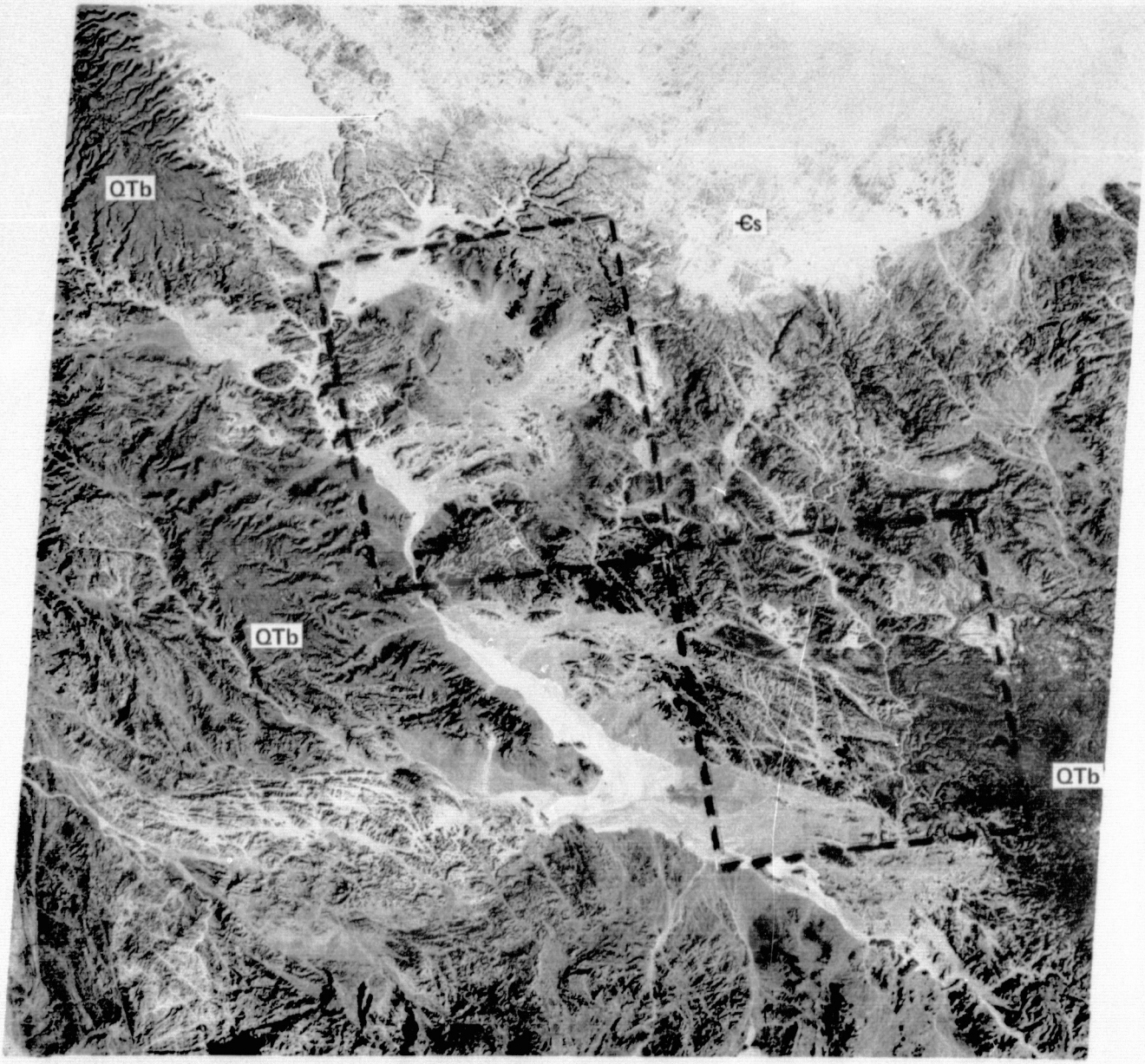


Figure 3. Northwestern Saudi Arabia test site. Areas included on Sahl al Matran (1973) and Wayban (1974) geologic maps are indicated by the northwest and southeast insets respectively.

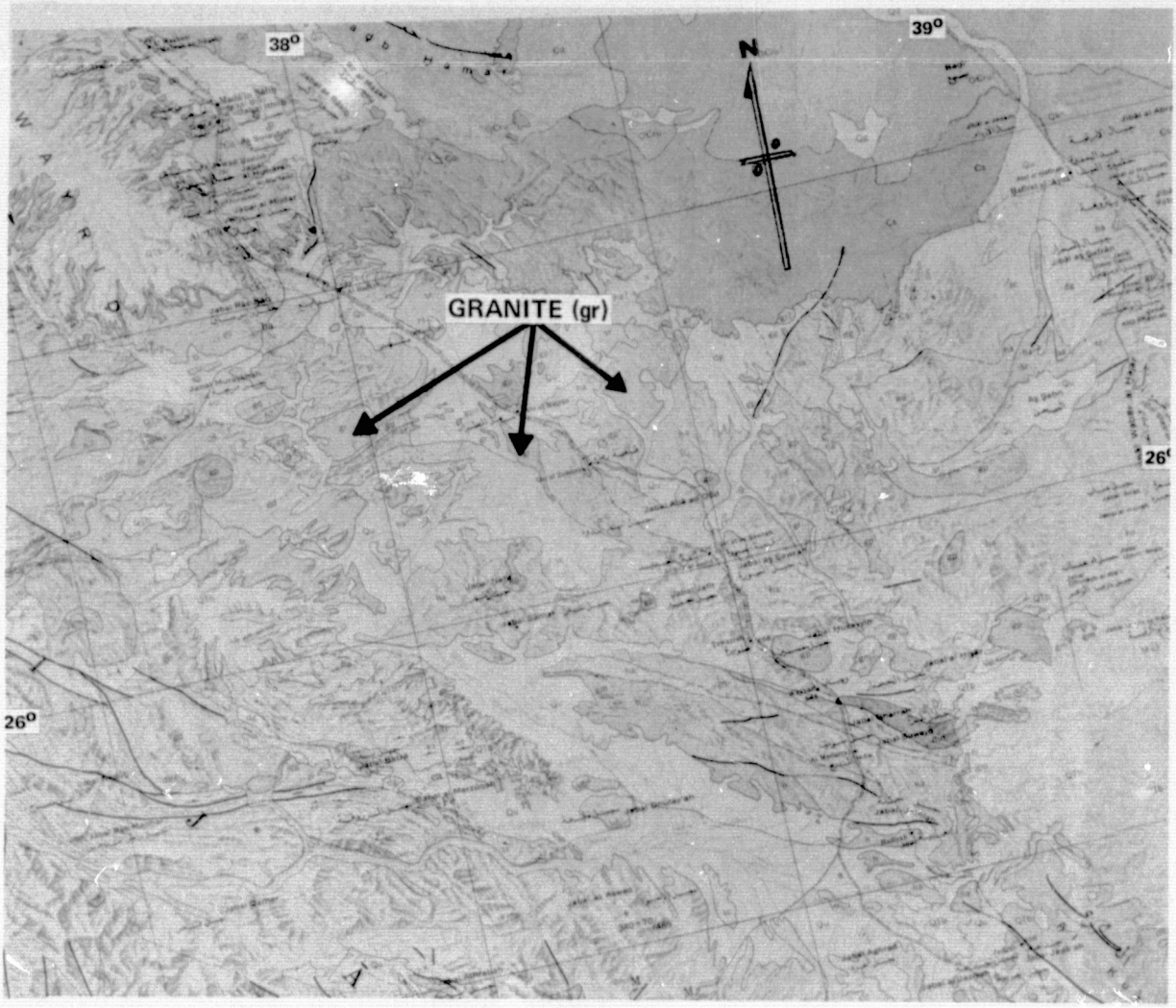


Figure 4. Northwest Saudi Arabia test site geological map, after Brown, Jackson, et al. (1963) and Brown, Layne, et al. (1963). Original at 1:500,000 scale.

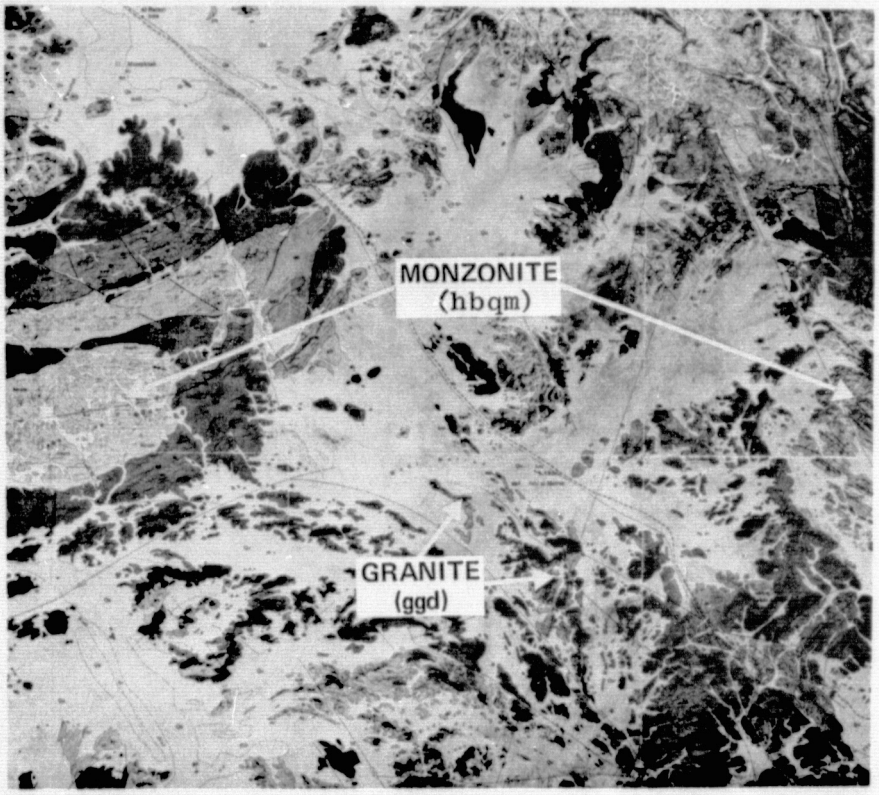


Figure 5. Geologic map of Sahl al Matran quadrangle, after Hadley (1973). Original at 1:100,000 scale.

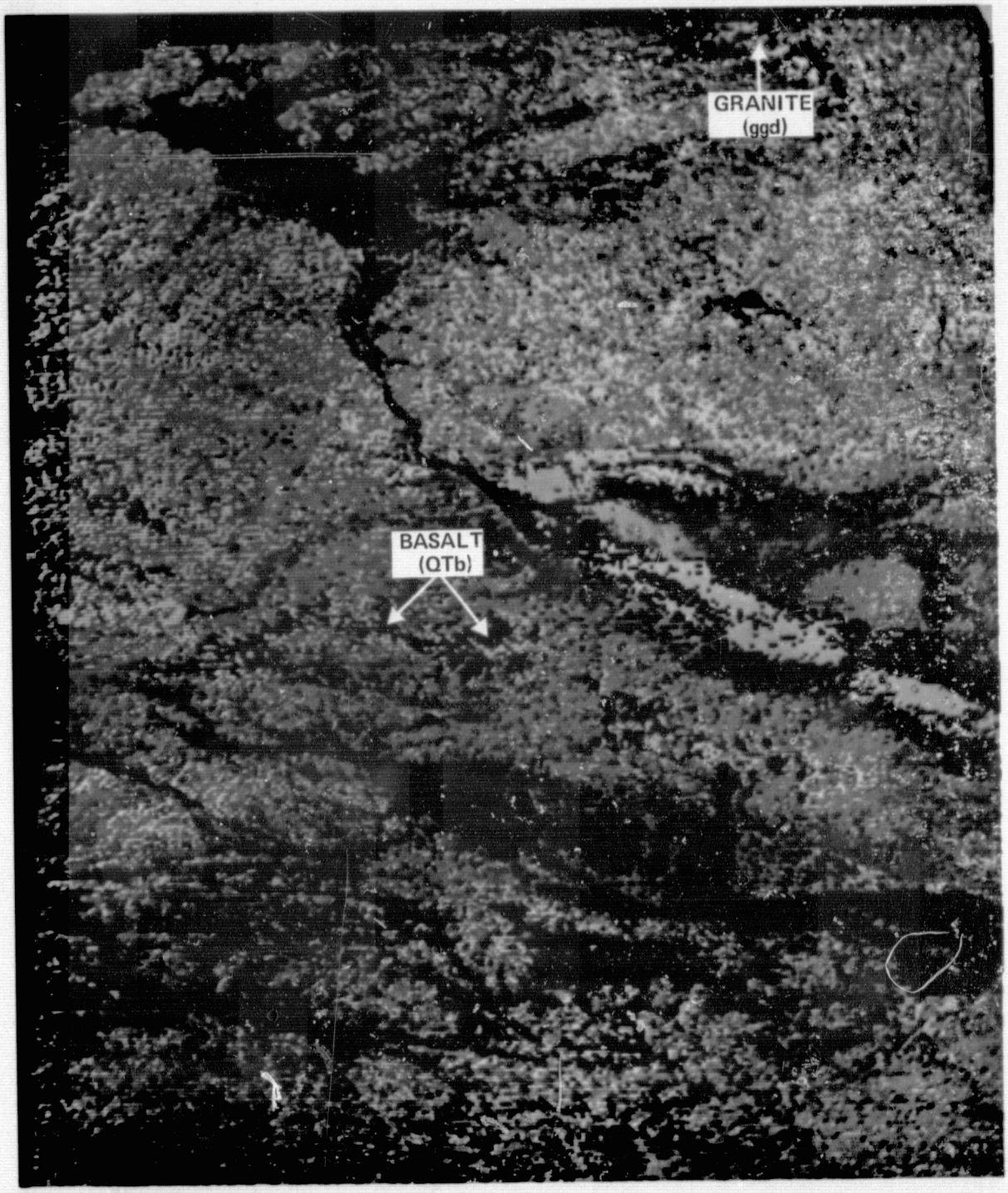


Figure 6. Classification of part of the northwest Saudi Arabia test site using the maximum likelihood approach.

REPRODUCIBILITY OF THE
ORIGINAL PAGE IS POOR

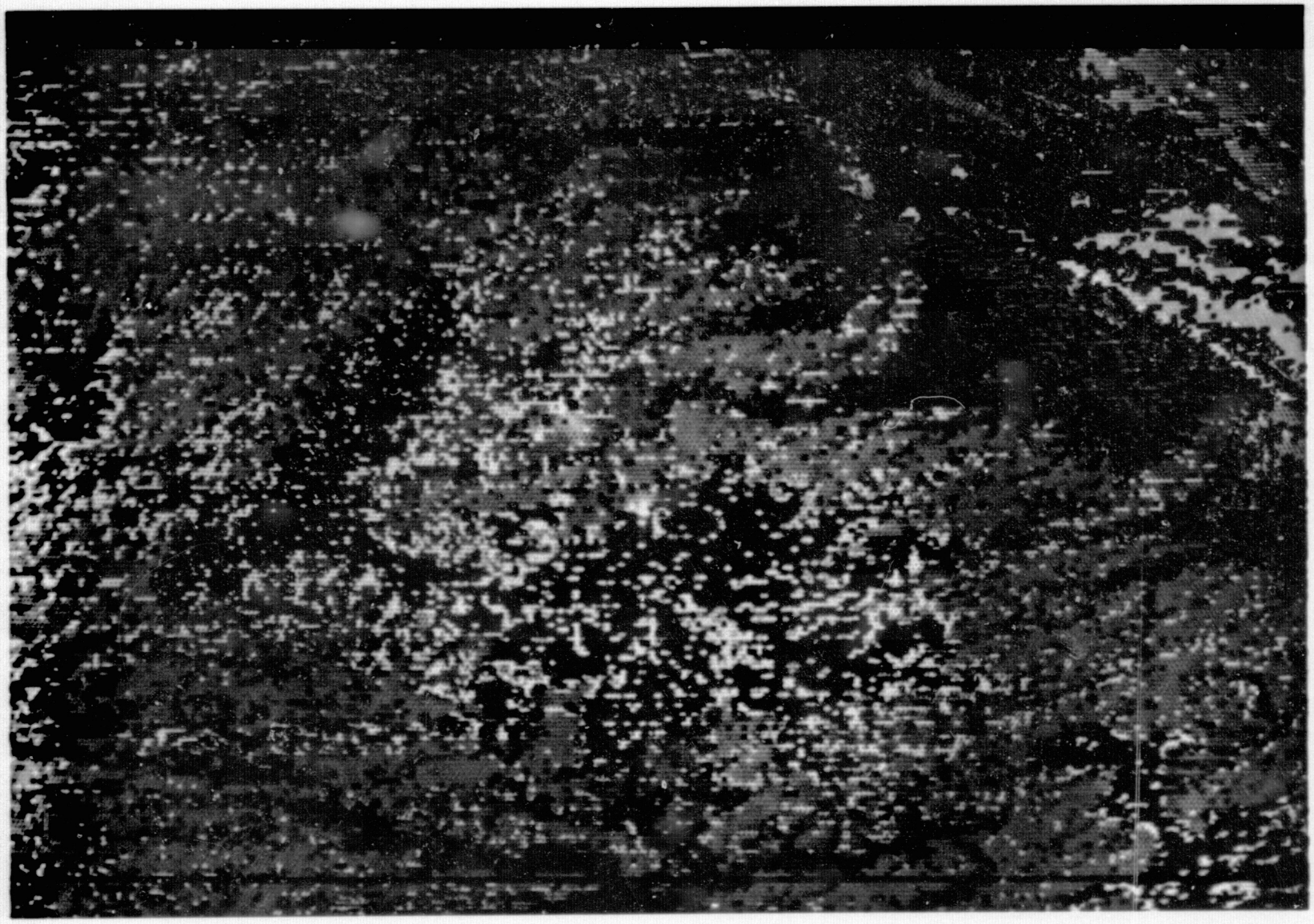


Figure 7. Computer enlargement of basalt (QTb) class using maximum-likelihood classification. Angular box is training site for this class.



Figure 8. Computer enlargement of granite (ggd) class using maximum-likelihood classification. Rectangular box is training site for this class.

REPRODUCIBILITY OF THE
ORIGINAL PAGE IS POOR

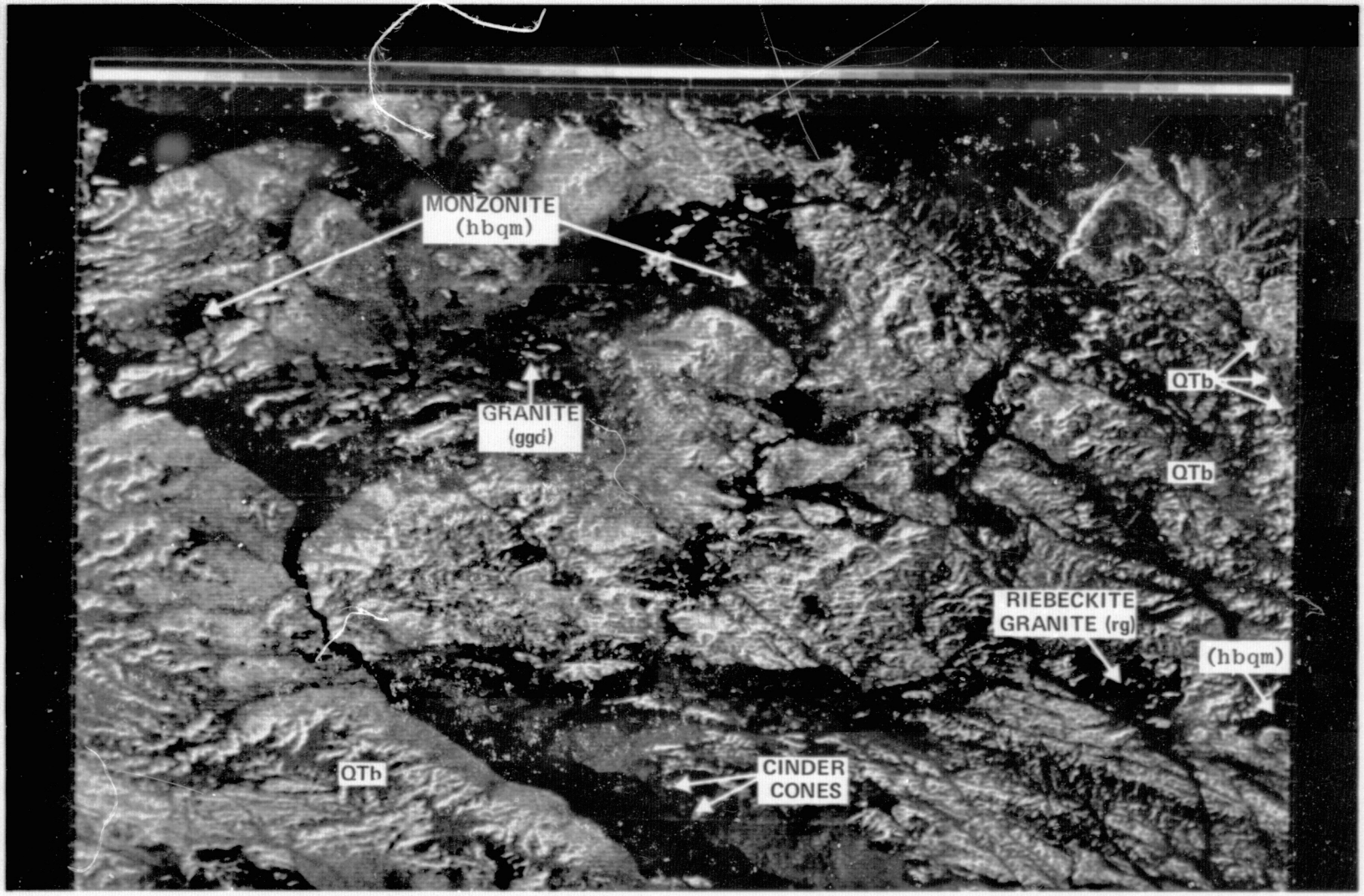


Figure 9. DICOMED color ratio-composite of a part of the northwest Saudi Arabia test site. Constructed from MSS 4/5 ratio data projected through a blue filter, MSS 5/6 data through a green filter and MSS 6/7 data through a red filter.

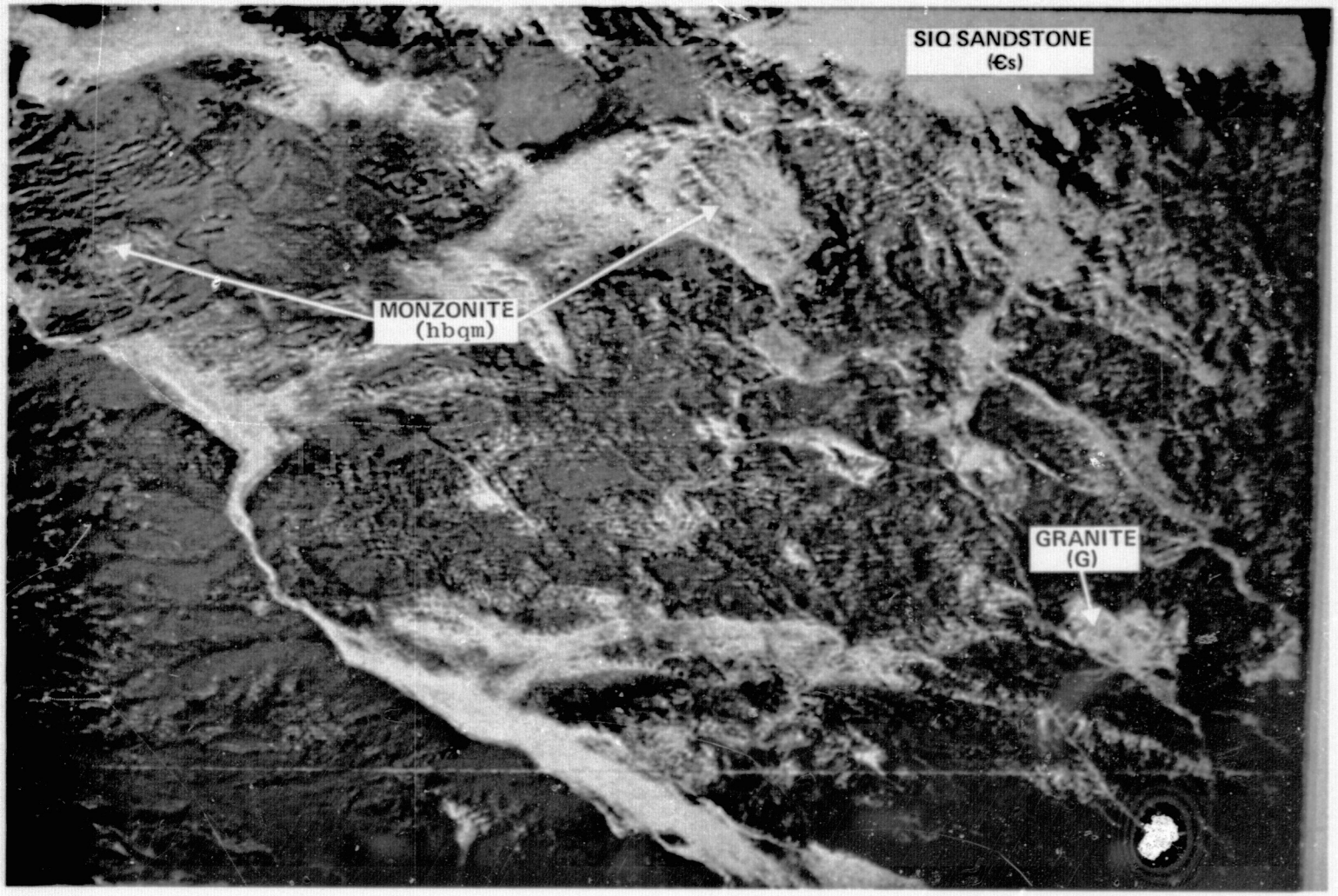


Figure 10. Ratio-composite enhancement photographed from a color additive viewer screen. Composite is constructed from MSS 4/7 ratio data projected through a blue filter, MSS 7/4 data through a green filter and MSS 6/5 data through a red filter.

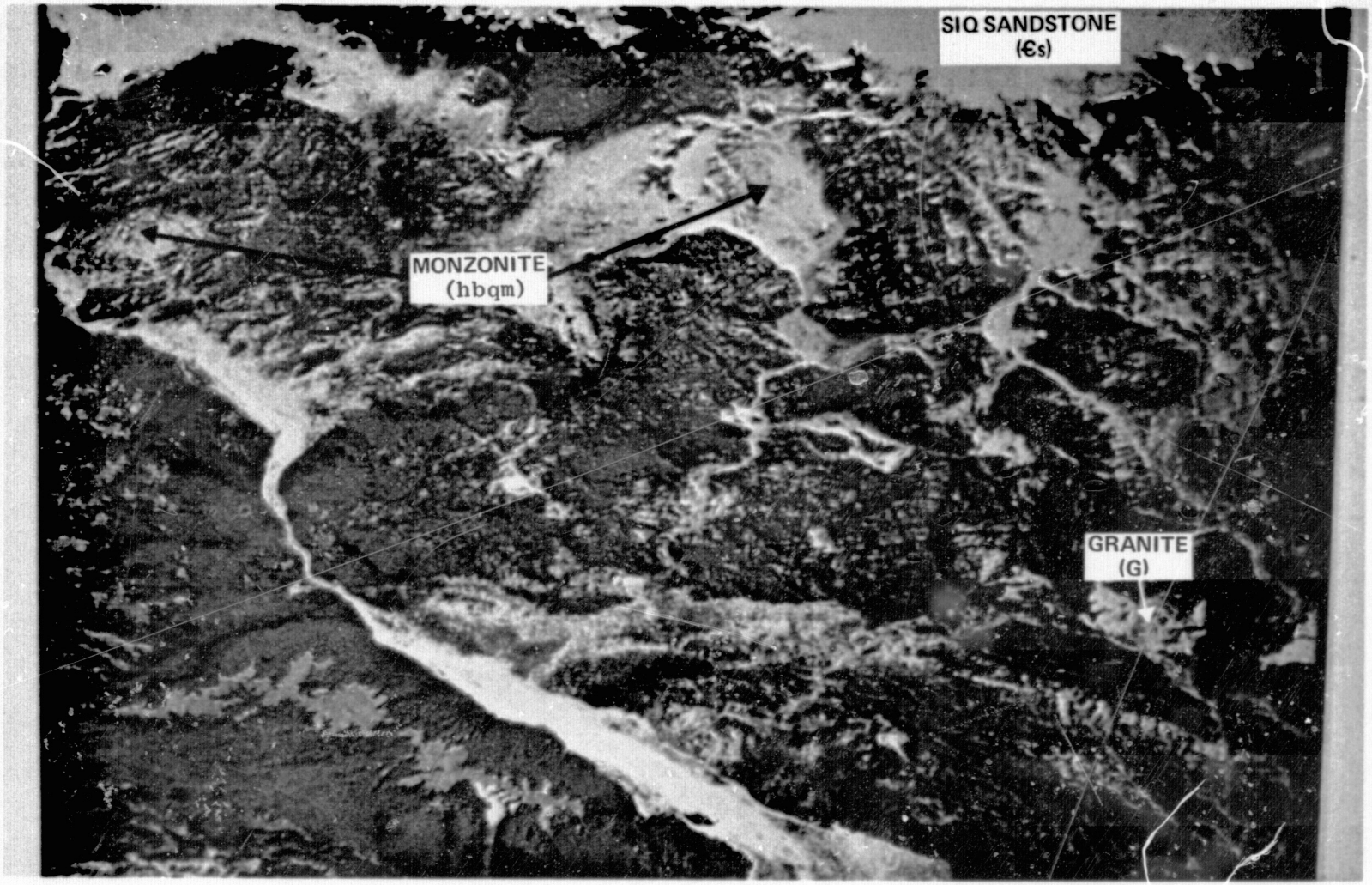


Figure 11. Ratio-composite enhancement photographed from a color-additive viewer screen. Composite is constructed from MSS 4/7 ratio data projected through a blue filter, MSS 7/4 data through a green filter and MSS 7/6 data through a red filter.

REPRODUCIBILITY OF THE ORIGINAL PAGE IS POOR

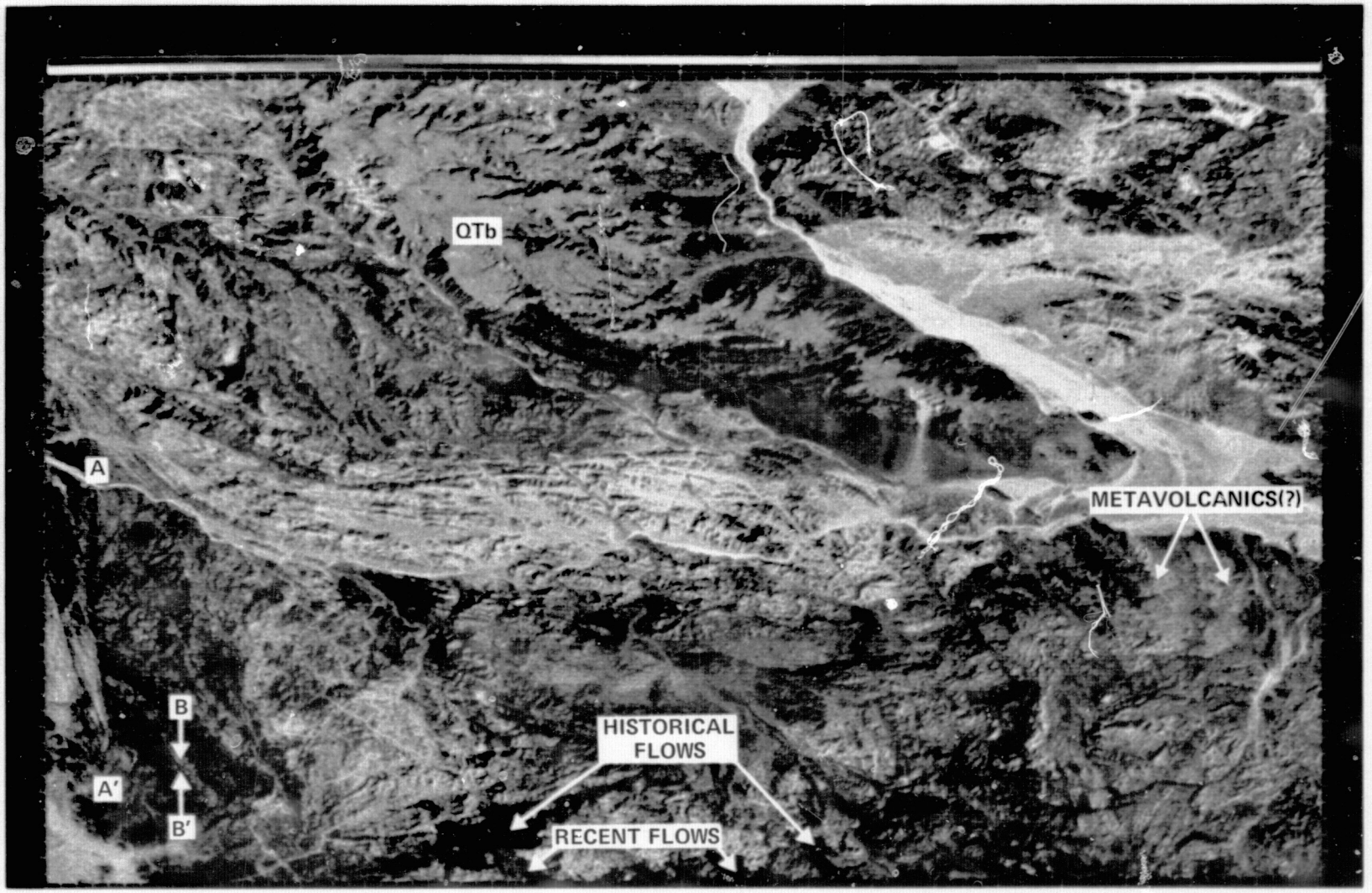


Figure 12. DICOMED color ratio-composite of a part of the northwest Saudi Arabia test site. Constructed from MSS 5/4 ratio data projected through a blue filter, MSS 6/5 data projected through a green filter and MSS 7/6 data through a red filter.

ENHANCEMENT OF LANDSAT IMAGERY BY COMBINATION OF MULTISPECTRAL CLASSIFICATION AND PRINCIPAL COMPONENT ANALYSIS

By A. Fontanel, C. Blanchet, C. Lallemand,
Institut Français du Pétrole, 92502 Rueil-Malmaison, France

N76-17520

ABSTRACT

Digital enhancement of LANDSAT imagery can be obtained by application of principal component analysis separately on each of the classes previously determined in a multispectral classification step. Each part of the image is thus greatly enhanced whatever its spectral signature may be. Furthermore a document is obtained which is a synthesis between a conventional image and an ordinary computerized classification. The interpreter can, at the same time, take into account not only the classification but also other features such as context and structure. An example is discussed with the help of geological interpretation.

INTRODUCTION

Two aspects of computer processing of LANDSAT images have generally been developed. One is multispectral classification which enables thematic maps to be obtained in some specific applications such as land use, forestry, agriculture, water quality, etc. The other is the optimization of images through the use of various numerical techniques.

In some applications such as geology, automatic thematic mapping is generally not sufficiently accurate. In general this is due to the inherent complexity of the geologic setting and in particular to a low degree of correlation between vegetation and geology.

For this reason the interpreter usually prefers to study the image itself rather than a computerized classification, so as to be sure not to leave out any significant data.

In some cases, visual study of original LANDSAT images may be disappointing, because of a low contrast between objects present on the image or of inherent recording defects. This is the reason why various numerical techniques have been used to enhance LANDSAT data: stretching, ratioing, filtering, principal component analysis, etc. Good results are generally obtained with this last method combined with a composite color display of the two principal components. The technique described in this paper makes use of principal component analysis. This analysis is not applied to the original data but to the result of a multispectral classification, in order to obtain a better enhancement of each part of the image under study.

The eigenvalues used in the principal component analysis are generally determined using either all the pixels in the image or only a given set of samples. It is well known that the eigenvalues are different depending on which samples have been selected. If all the pixels of the image are taken into account, only a "mean" enhancement can be obtained which is not optimum for any part of the image. If the samples are located in a given area, only this part of the image, or similar areas showing the same spectral signature, are correctly enhanced. But if the analysis is applied separately on each multispectral class, a better enhancement can be obtained for each part of the image whatever its spectral signature may be. On the other hand a document can be thus obtained that is a synthesis between a conventional image and an ordinary computerized classification.

PRECEDING PAGE BLANK NOT FILMED

DESCRIPTION OF THE METHOD

In a first step a multispectral classification is made in order to separate the different classes of terrain (ref. 1). An unsupervised classification program is used in order to save time by not having to determine training areas.

The eigenvalues are determined separately for each class of terrain, and principal component analysis is then applied separately in each area showing the same spectral signature. Then weighting factors can be applied to each class in order to bring out the boundaries between classes on the enhanced image.

Multispectral Classification

The classification method (ref. 2) makes use of statistical analysis. It consists in classifying samples according to various distribution laws that are deduced from the image itself. It has generally been observed that the different samples of a homogeneous multispectral class can be associated in a Gaussian distribution. Each distribution can be characterized by the vector of its center of gravity and its covariance matrix. The method consists in clustering the pixels of the image under study into various Gaussian distributions. This is achieved through an iterative process. During each iteration, each pixel not previously associated with a given cluster is successively taken into account. The center of gravity and the covariance matrix of each class is modified each time a new pixel is aggregated into the corresponding cluster.

The probability density function of a class i corresponding to a Gaussian distribution can be expressed for a given pixel X by the expression:

$$d_i(X) = \frac{1}{(2\pi)^2} \cdot \left[\text{Det. } (V_i)\right]^{-\frac{1}{2}} \cdot e^{-0.5(X-G_i)^T V_i^{-1}(X-G_i)}$$

$d_i(X)$ = probability density function.

X = vector corresponding to the point to be classified.

V_i = covariance matrix of class i.

Det (V_i) = determinant of V_i.

G_i = vector corresponding to the center of gravity of class i.

Pixel X is classified in class i if the value of p(X/i) is maximum and higher than a given threshold p', with:

$$p(X/i) = d_i(X) / \sum_j d_j(X) \ .$$

$\sum_j d_j(X)$ = sum of the probability density functions for all classes found in the image.

The threshold p' can for example be equal to 80% at the first iteration and 70% at the second iteration.

New classes are generally obtained up to the third or fourth iteration. Then the procedure is stable and no more classes are obtained. A new class is considered as valid only if its center of gravity is sufficiently distinct from the centers of gravity of classes obtained during previous iterations. Furthermore a neighborhood analysis is made on each class at each iteration step, in order to define a compacity index and to keep away classes corresponding only to "isolated" pixels. This compacity index represents, for a given class, the mean number of pixels of the

same class surrounding the pixel under study.

Fig. 1 shows LANDSAT-1 image No. E 1187-10025, Band 5, taken in the southern part of France, along the Mediterranean Sea. The area studied is indicated on this image. The Pyrenees mountains lie in the lower part of this area and Massif des Corbières in the upper left corner.

Fig. 2 shows the multispectral classification obtained on this area including 353,858 pixels. Six different classes have been found, and 10,015 pixels (class 7) are unclassified. Class 1 correspond to sea-water, Class 2 to fresh water (Etang de Leucate and Etang de Carret). Classes 3, 4, 5, 6 correspond to various types of terrain. Fig. 2 was obtained with a drum plotter by coding each class with a given gray level. Many sub-classes could be defined in this area, but it is only necessary in this application to separate the main classes present in the image.

Table I gives the following characteristics for each class: number of pixels, center of gravity and compacity index.

TABLE I.- GENERAL CHARACTERISTICS OF THE MULTISPECTRAL CLASSES

	Number of pixels	Center of gravity				Compacity index	Nature
		λ4	λ5	λ6	λ7		
Class 1	17,730	16.84	7.91	3.78	0.45	6.98	Sea-water
Class 2	14,759	20.16	10.89	4.60	0.69	4.79	Fresh-water
Class 3	125,587	19.27	14.91	17.14	8.00	4.76	Recent } alluvial
Class 4	72,159	21.82	14.99	20.55	9.00	4.77	Ancient } deposits
Class 5	46,097	23.43	21.32	24.48	11.84	2.87	Undifferentiated terrains
Class 6	67,581	15.24	8.78	11.80	5.56	5.60	Outcrops
Class 7	10,015	-	-	-	-	-	Unclassified

It must be noted that the centers of gravity of the different classes are relatively far from each other.Values in Table I correspond to coordinates.

Table II indicates the standard deviation and the correlation coefficient between spectral bands for Class 1 (seawater), Class 3 (alluvial deposits) and Class 7 (unclassified samples). It can be observed that for Class 1 there is a very low degree of correlation between the different spectral bands and that the corresponding samples are strongly clustered in the multispectral space (low value for the standard deviation). On the other hand, samples in Class 7 correspond, in the multispectral space, to a very elongated "cloud" where samples are highly scattered. Furthermore, the correlation degree between the responses in the four spectral bands is very strong.

The corresponding values found for Class 3 are intermediate between those of Class 1 and Class 7.

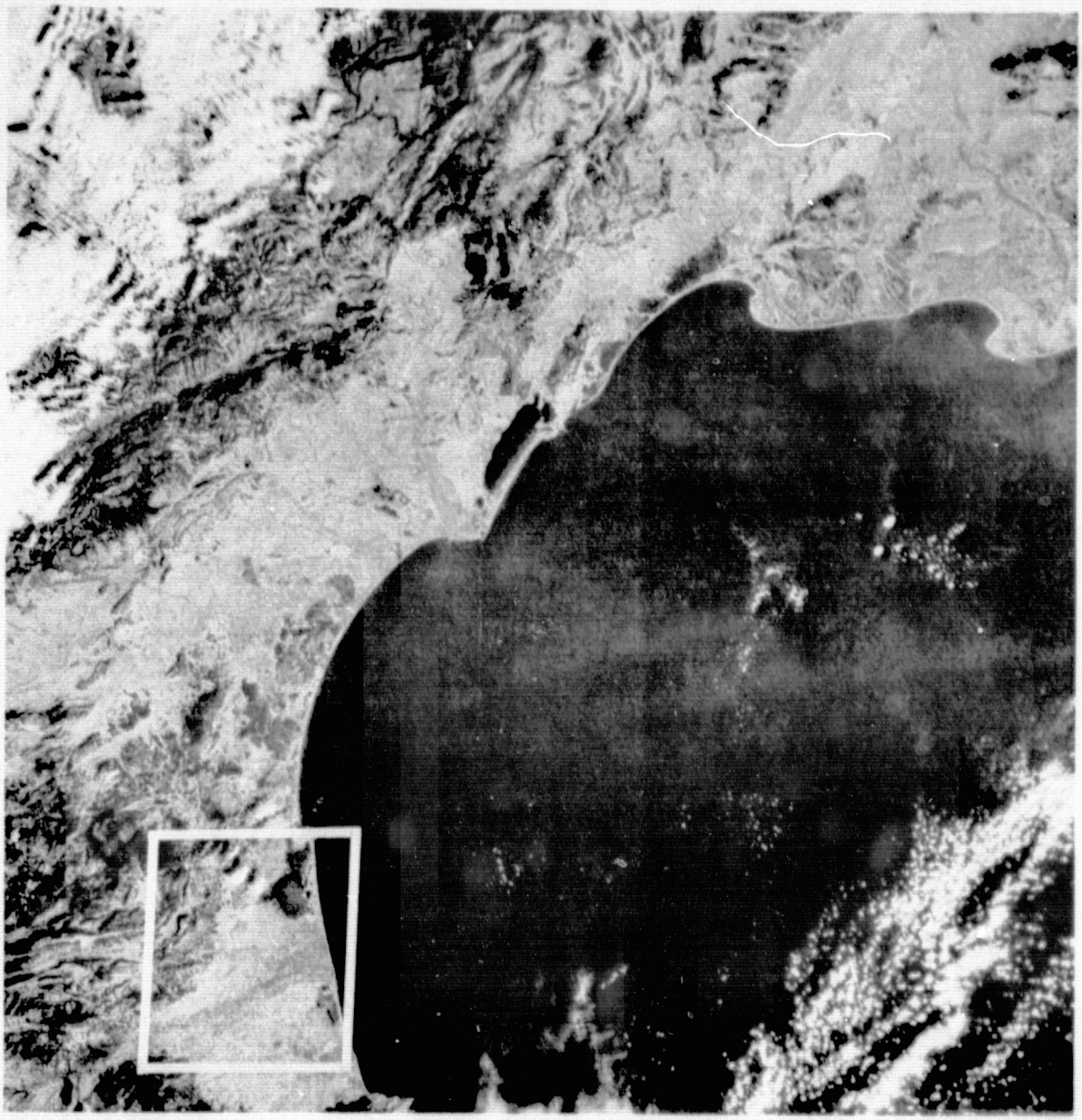


Figure 1.- Original LANDSAT I Image
(band 5) - E - 1187 - 10025

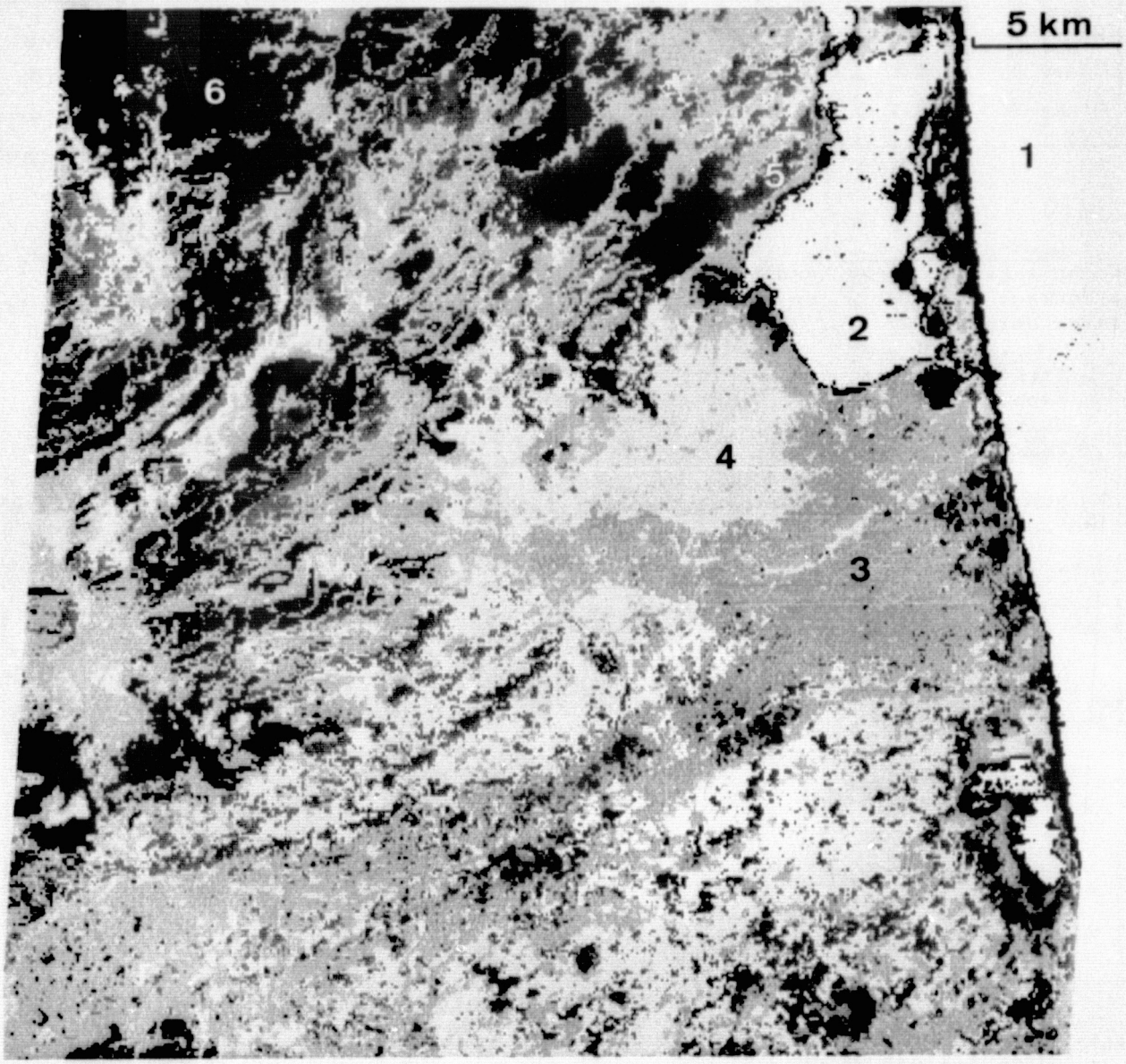


Figure 2.- Unsupervised Multispectral Classification of Fig. 1.
6 classes have been determined and are represented with arbitrary gray levels. From white to black:

Class 1 = sea water - Class 2 = fresh water -
Class 3 = recent alluvial deposits - Class 4 = ancient alluvial deposits -
Class 5 = undifferentiated terrains - class 6 = outcrops

REPRODUCIBILITY OF THE
ORIGINAL PAGE IS POOR

TABLE II.- STATISTICAL CHARACTERISTICS OF THE CLASSES

	Standard deviation				Correlation coefficient					
	λ4	λ5	λ6	λ7	λ4/λ5	λ4/λ6	λ4/λ7	λ5/λ6	λ5/λ7	λ6/λ7
Class 1	0.9	0.6	0.7	0.5	0.24	0.15	0.04	0.17	0.14	0.10
Class 3	2.0	2.9	3.6	2.2	0.84	0.57	0.38	0.56	0.36	0.88
Class 7	14.2	16.3	16.2	8.00	0.98	0.91	0.80	0.93	0.86	0.98

Principal Component Analysis (P.C.A.)

Conventional P.C.A. (ref. 3).- P.C.A. was done with the conventional method, i.e by taking into account all the 353,858 pixels of the image under study. The percentage of inertia (or information content) explained by the four components is listed below:

First component	80%
Second "	16%
Third "	3%
Fourth "	1%

96% of the total information content can be represented with the first two principal components.

Figures 3 a and 3 b represent the images that can be obtained respectively with the first and second components. These images are usually combined in order to obtain a composite color (fig. 3 c).

P.C.A. after Multispectral Classification.- P.C.A. was done separately on each class, as previously explained. The information content of each component for the various classes is listed below:

TABLE III.- INFORMATION CONTENT OF PRINCIPAL COMPONENTS

Principal components / Classes	1	2	3	4
	%	%	%	%
1 sea water	42	25	18	15
2 fresh water	56	25	12	7
3 }	78	18	3	1
4 }	70	24	4	2
5 } terrains	61	24	10	5
6 }	78	16	4	2
7 unclassified	94	6	0	0

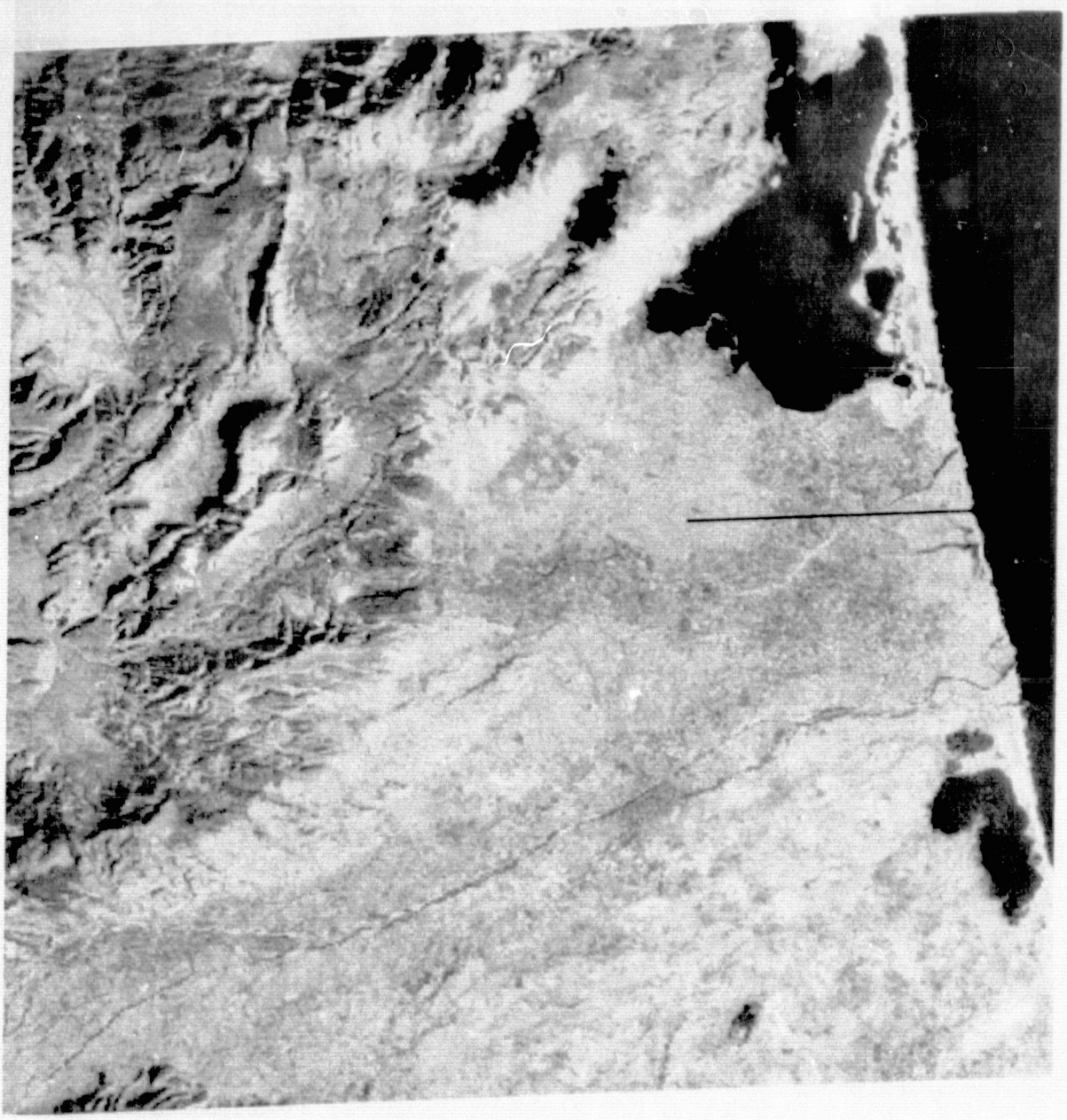


Figure 3 a.- Conventional Principal Component Analysis.
Display of the first component.



Figure 3 b.- Conventional Principal Component Analysis.
Display of the second component.

REPRODUCIBILITY OF THE
ORIGINAL PAGE IS POOR

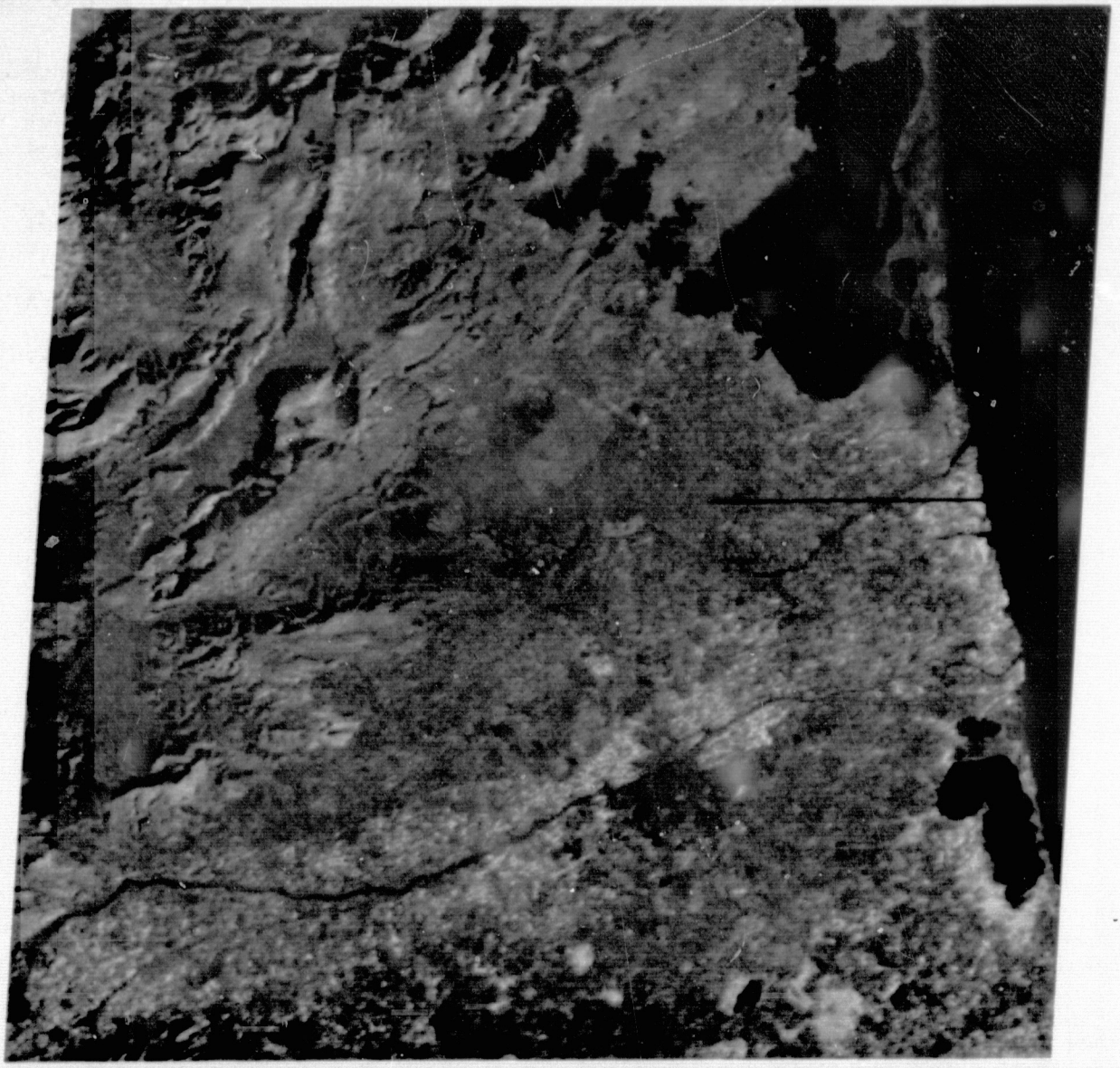


Figure 3 c.- Color combination of the first two principal components shown in Figs. 3 a and 3 b.
(First component in red, second component in yellow)

REPRODUCIBILITY OF THE
ORIGINAL PAGE IS POOR

It should be noted that for seawater (Class 1) the first two components represent only 67% of the information content. For land, the two principal components represent 92% of the information content; with conventional P.C.A. the value of 96% was obtained. This can be explained since in conventional P.C.A. all the pixels are taken into account, including unclassified samples for which all the information is contained in the first two components.

Fig. 4 a shows the image representing the first principal component obtained with P.C.A. after multispectral classification.

A comparison of Figs. 4 a and 3 a clearly shows that each detail of the image has been greatly enhanced in Fig. 4 a. However the mean contrast between the different zones is reduced in Fig. 4 a. A geological interpretation of the area studied will be discussed further, but it is obvious that in mountainous areas (upper part of the image) many lineaments appear quite clearly in Fig. 4 a. This is quite imimportant for geological applications. In the same manner, a great many details (cultivated fields, etc.) are brought out in alluvial deposits in the central part of this image. All along the seashore, coastal water can continuously be delineated in Fig. 4 a. A plume appears at sea offshore from the mouth of Agly River. Different gray tones can be seen on lakes, mainly because of differences in water depth and algae concentrations. A very long period phenomenon can be observed at sea which has not been detected elsewhere. This phenomenon has not yet been interpreted.

It should be noted that, in Fig. 4 a, certain terrain features can be detected through the clouds present NW of the main lake. This result was not obtained with stretching or with classical P.C.A.

Comparison of Figs.4 b and 3 b (second component) is not as clear as for Fig. 4 a and 3 a except for open waters. However Fig. 4 b seems to be more contrasted than Fig. 3 b. Banding has not been removed from original data and a high level of noise appears at sea in Fig. 4 b.

The images of Figs.4 a and 4 b can as usual (ref. 4) be combined in color. The corresponding colored image is shown in Fig. 4 c.

Furthermore, the technique which has been described gives another presentation of the final product which synthesizes the image itself and the multispectral classification.

As a matter of fact, after P.C.A. has been done on each class of terrain, it is possible to shift the values corresponding to each class by a constant, in order to bring out the boundaries of the classes. This constant is different for each class and may, for example, be equal to the mean value of the corresponding pixels in the original image. In this way the interpreter can conduct his interpretation by taking into account, at the same time and on the same display, a computerized classification and the whole information content of the original image.

Fig. 5 a shows such an image obtained from Fig. 4 a by shifting the values obtained in each class by a constant equal to five times the mean value of the original Band 5 for the corresponding pixels. Thus, Fig. 5 a synthesizes the results obtained in Fig. 2 and Fig. 4 a.

As usual, a color composite (Fig. 5 c) can be obtained by combining the images of Fig. 5 a (first component) and Fig. 5 b (second component).

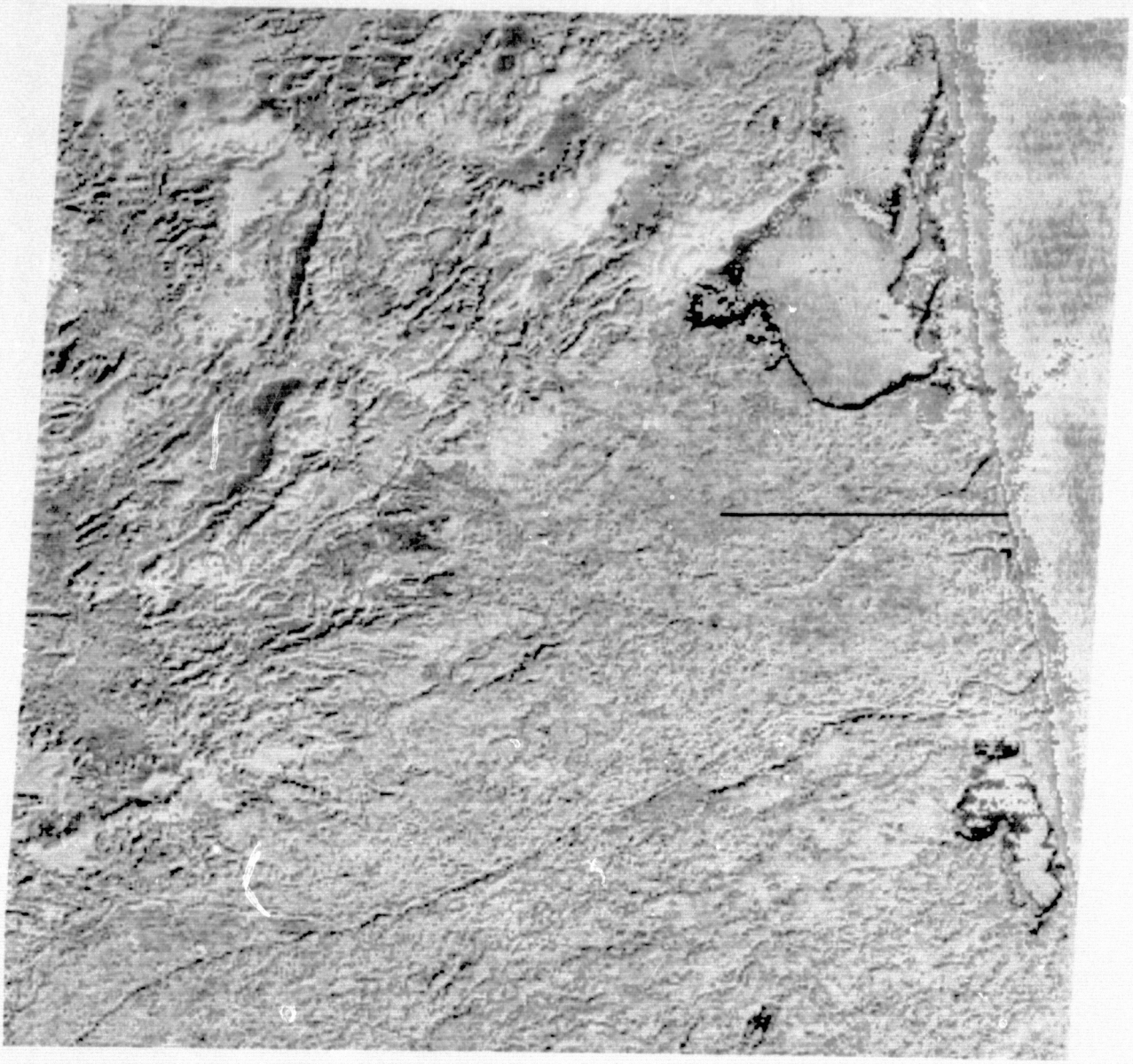


Figure 4 a.- Principal Component Analysis after multispectral classification. Display of the first component.

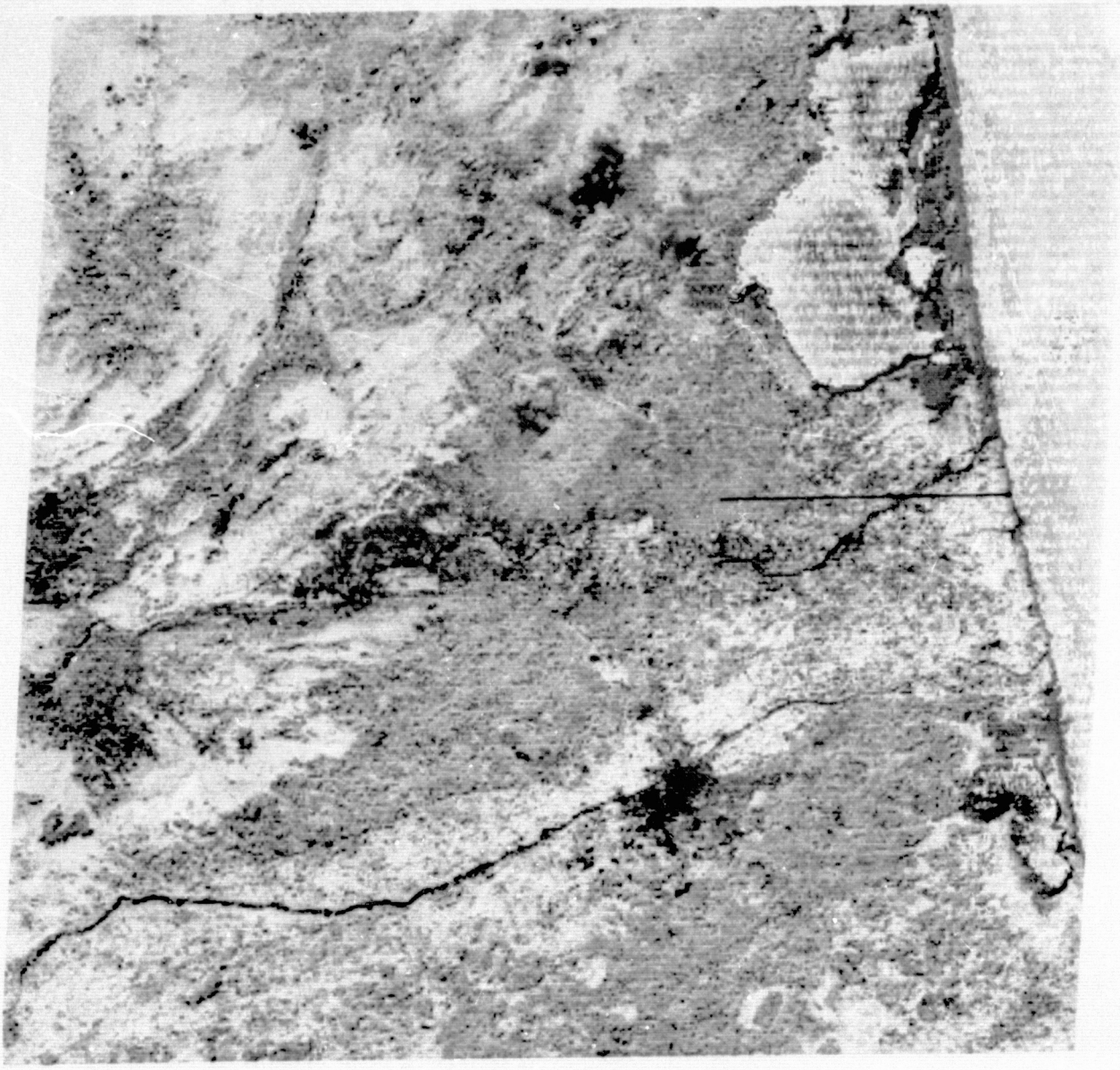


Figure 4 b.- Principal Component Analysis after multispectral classification. Display of the second component.

REPRODUCIBILITY OF THE ORIGINAL PAGE IS POOR

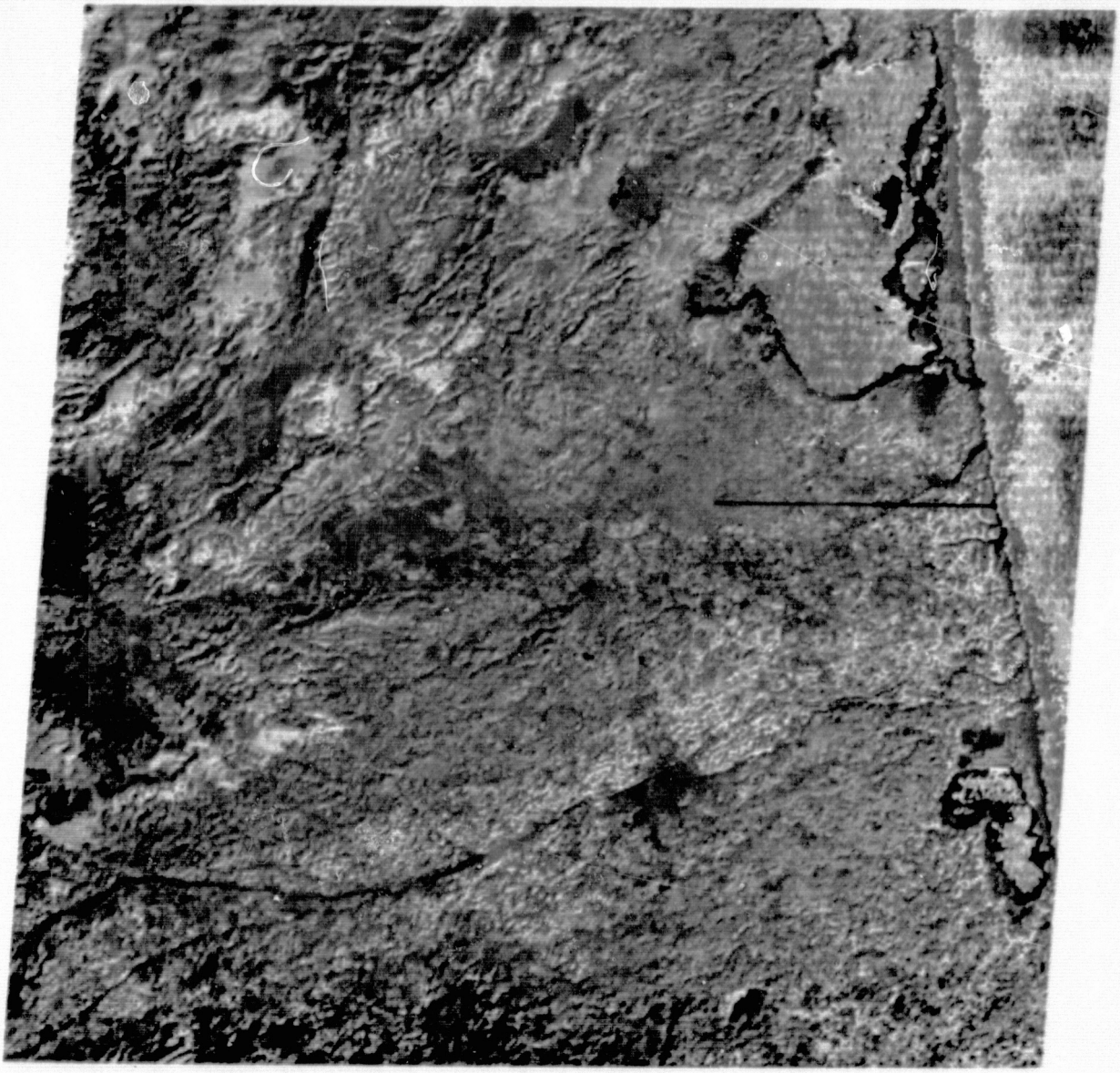


Figure 4 c.- Color Combination of the first two principal components shown in Figs. 4 a and 4 b. (First component in red, second component in yellow)

REPRODUCIBILITY OF THE ORIGINAL PAGE IS POOR

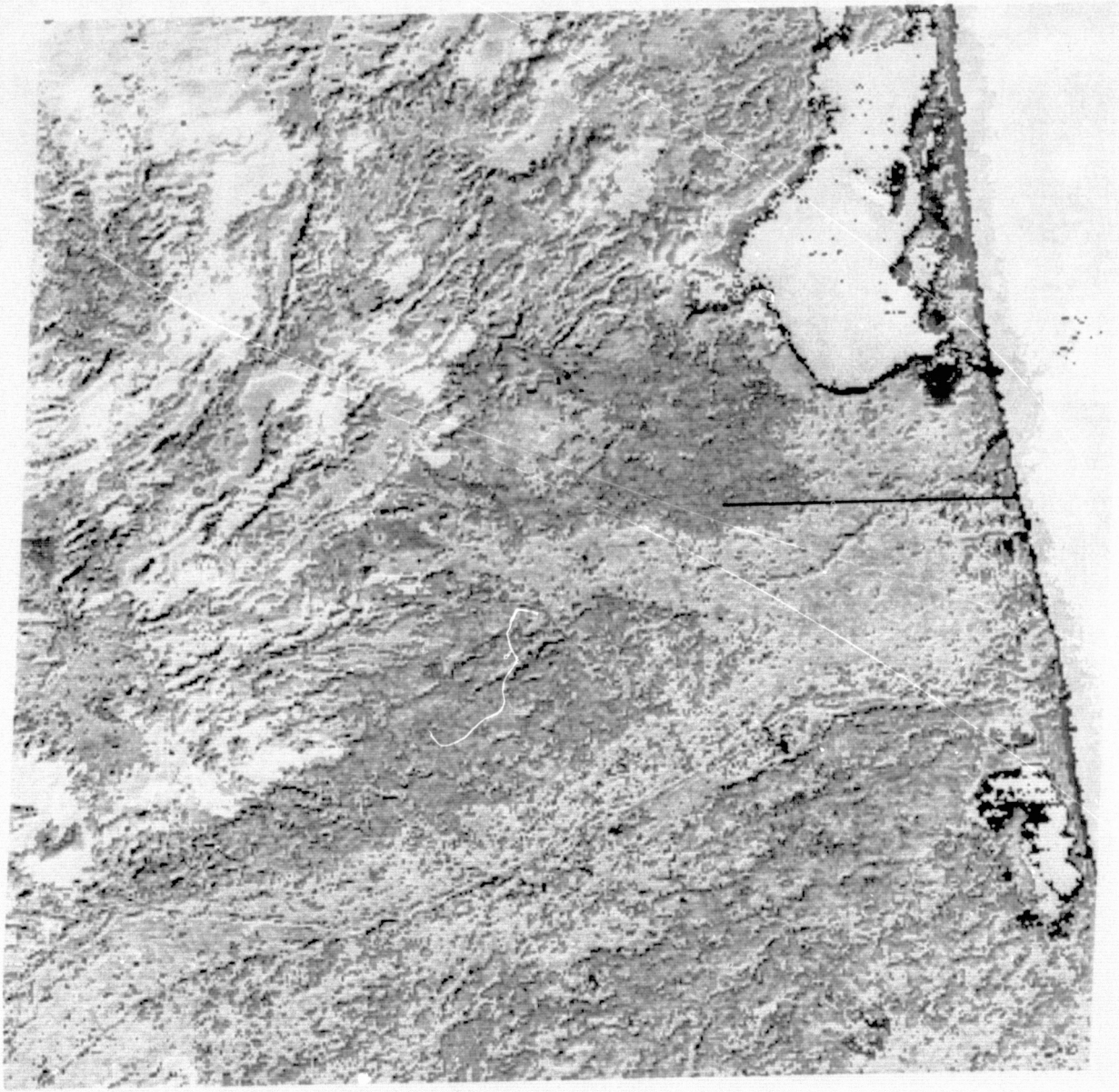


Figure 5 a.- Principal Component Analysis performed after multispectral classification. Display of the first component. The mean value of each class has been shifted by a given constant.

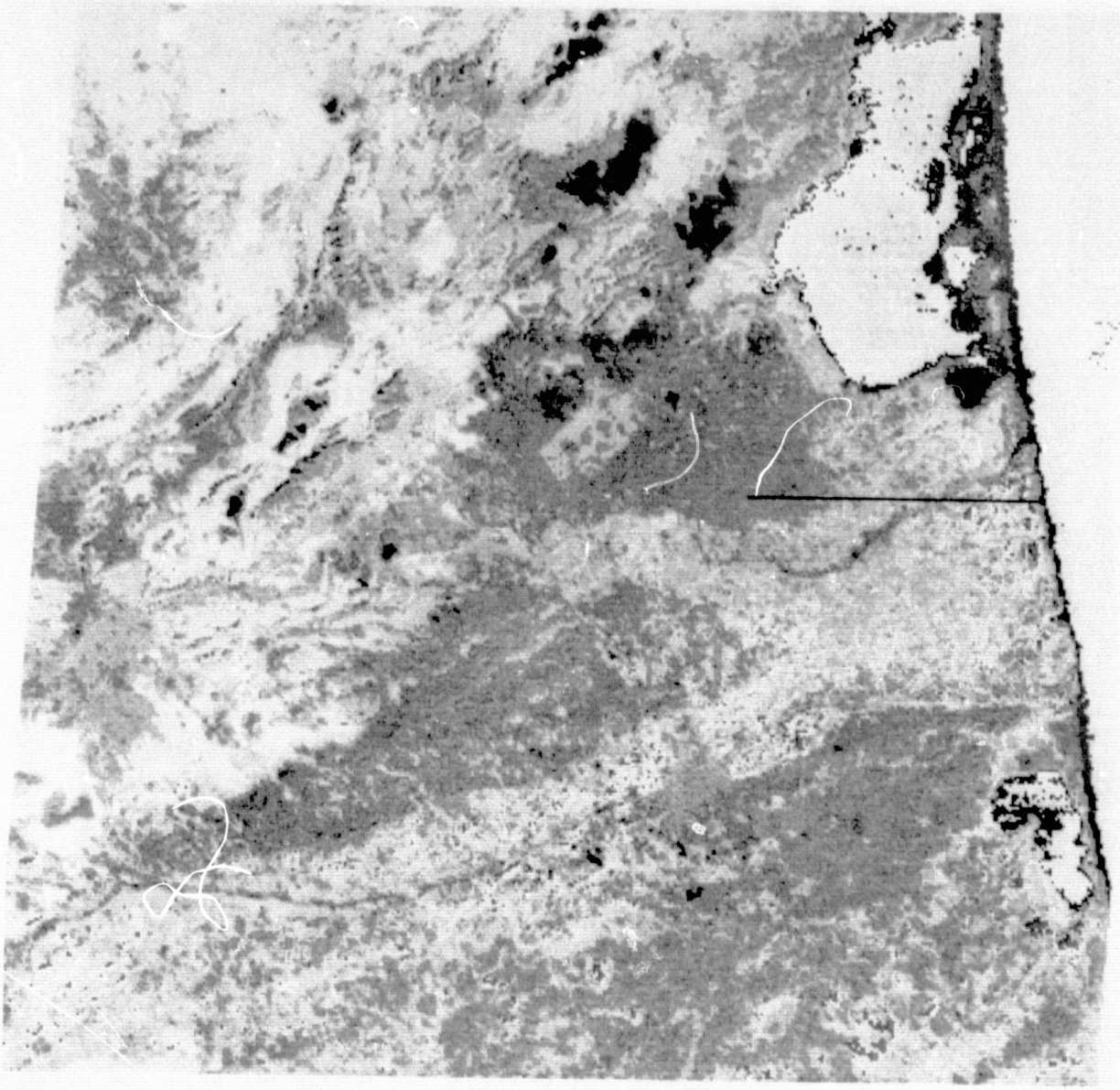


Figure 5 b.- Principal component analysis after multispectral classification. Display of the second component. The mean value of each class has been shifted by a given constant.

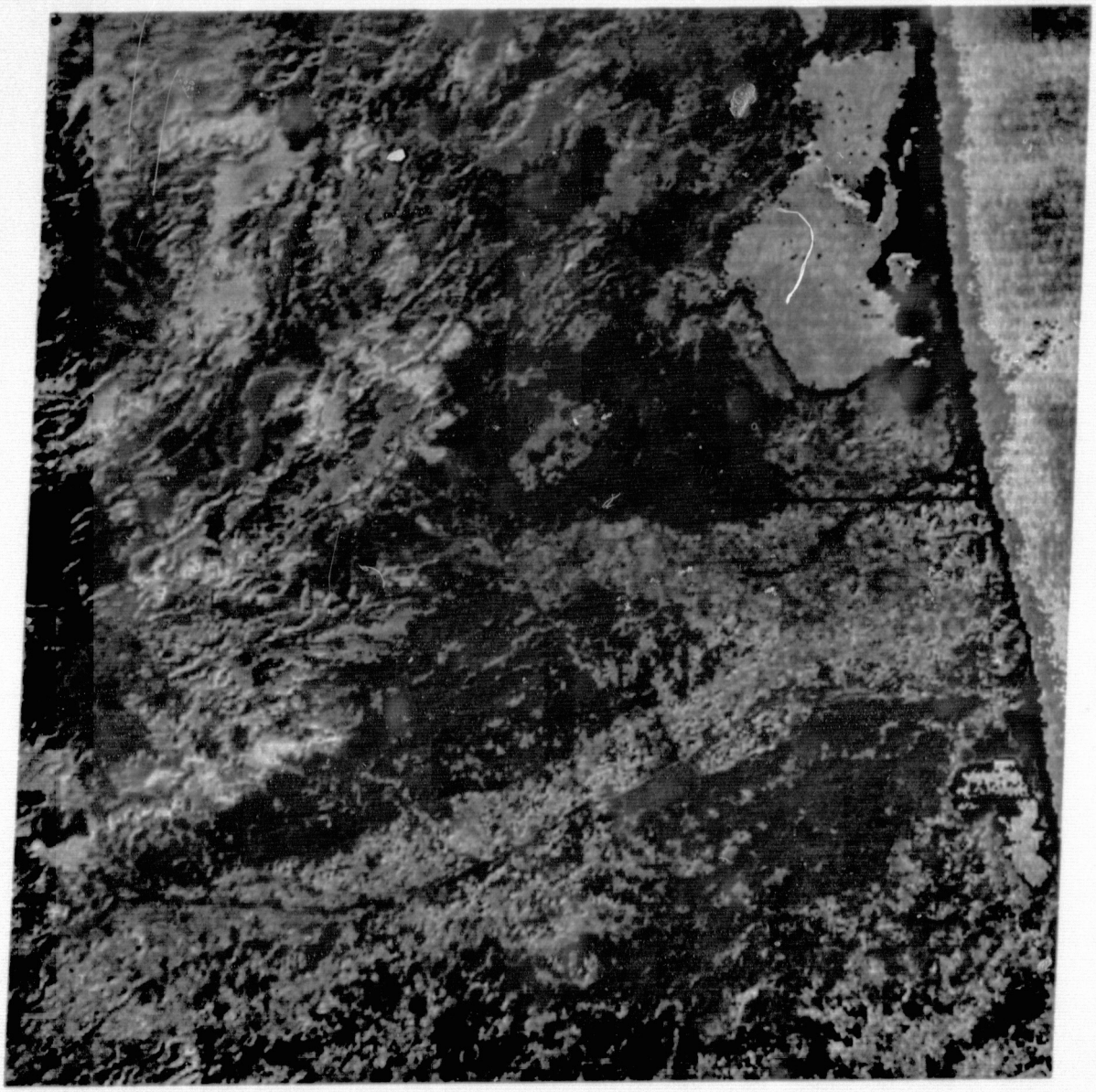


Figure 5 c.- Color combination of Figs. 5 a and 5 b.
This image is a synthesis of the multispectral classification
of Fig. 2 and of the composite color of Fig. 4 c.
(First component in red, second component in yellow)

REPRODUCIBILITY OF THE
ORIGINAL PAGE IS POOR

DISCUSSION OF RESULTS

The three enhanced images, Figs. 3 c, 4 c and 5 c will be compared in connection with their geological interpretation. These images correspond to the color composites obtained by coding the first component in red and the second component in yellow. Other color combinations can be used but this particular combination has been found to be well adapted. The same color code has been used in this paper for all the colors composite.

Three main units will be considered in this area: a mountainous area (upper part of the image), alluvial deposits (central and lower part of the image) and open waters (sea and coastal lakes).

Figures 6, 7, and 8 represent a photointerpretation of the three images. The interpretation consisted only in underlining marker beds in the mountainous area (R) and in delineating the different alluvial deposits. Faults and lineaments have been plotted in each unit. The reference document was the geological map at the scale of 1:80,000.

The first unit (R) corresponds to Massif des Corbières, which consists mainly of Jurassic and Cretaceous limestones and sandstones, strongly folded and faulted. Paleozoic terrains (Massif du Monthoumet) appear in the upper left corner.

Altitude in this mountainous zone lies between 150 meters and 500 meters.

Yellowish zones in Fig. 3 c correspond to scrub and reddish zones to cultivated areas (mainly vineyards). Few marker beds have been plotted in the yellowish part of Fig. 3 c. These beds are oriented NE-SW. A few major accidents running NS appear on this image. They correspond to well known left lateral strike-slip faults.

The boundary between unit R and the alluvial deposits is perhaps less visible on Fig. 4 c than on Fig. 3 c. In any part of the image many more marker beds have been plotted in Fig. 7 than in Fig. 6, especially in the Northeastern corner which corresponds to limestones of Aptian age. On the same manner, many more lineaments appear on Fig. 7. It must be noted that two of these lineaments can be followed through the two small clouds located North West of main lake. Furthermore, a new set of lineaments running East-West can be picked in Fig. 7. They correspond to strongly folded geological structures.

The lineaments running NW-SE in Fig. 7 have only been detected with ERTS imagery. Their interpretation is yet subject to question.

The same marker beds appear on 7 and 8. But, owing to the fact that the boundaries between the different classes of terrain have been brought out in Fig. 5 c by digital processing, more lineaments appear in this last image, especially a very large lineament located in the upper part of the image and running North 70° East. It corresponds to the prolongation towards the East of a major accident running North of the Paleozoic oldland Massif du Monthoumet.

The second unit corresponds to alluvial deposits of Quaternary and Pliocene age covered mainly with vineyards and cultivated fields. Sand occurs along the shoreline and marshlands exist around the lakes. The studied LANDSAT image having been taken in January, the differentiation corresponds mainly to pedology.

Six sub-units A1, A2, ... A6 can be delineated in the alluvial deposits.

A1 : damp areas around the lakes.
A2 : sand along the shoreline.
A3 : ancient alluvial deposits.

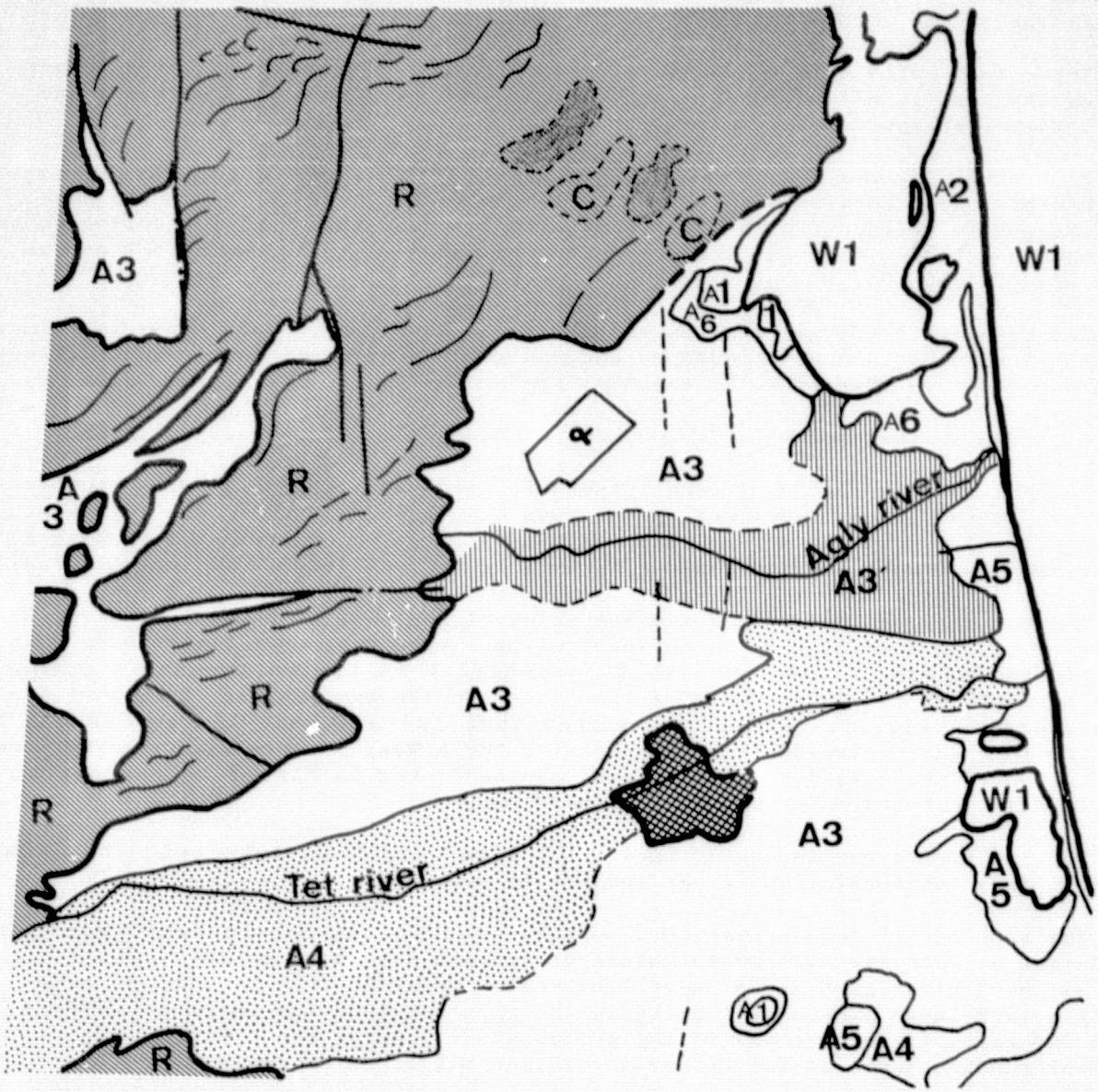


Figure 6.- Photo-interpretation of fig. 3 c.

R	outcrops	∼	marker beds
A_1.... A_6	alluvial deposits	— --	lineaments
W_1.... W_8	water qualities		

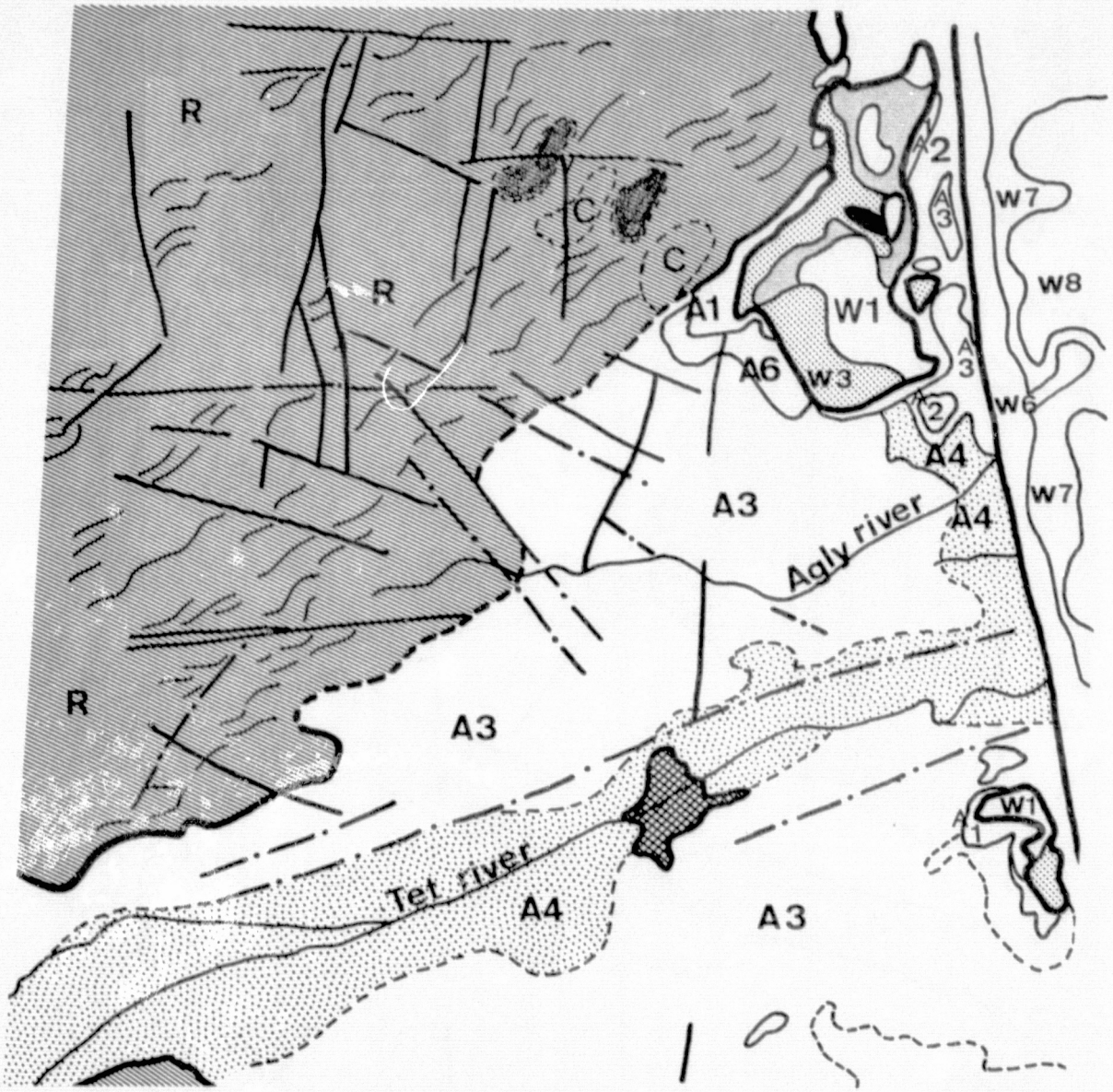


Figure 7.- Photo-interpretation of fig. 4 c.

R	outcrops	~	marker beds
A_1 .... A_6	alluvial deposits	— - -	lineaments
W_1 .... W_8	water qualities		



Figure 8.- Photo-interpretation of fig. 5 c.

R outcrops
A_1 .... A_6 alluvial deposits
W_1 .... W_8 water qualities

marker beds
lineaments

A4 : recent alluvial deposits with frequent irrigation
A5)
A6) : photogeological differentiations in recent deposits, (∝ corresponds to a military camp).

Many more details appear on Fig. 4 c than on Fig. 3 c but it is generally more difficult to delineate the various sub-units on 4 c. On the other hand, lineaments appear more clearly on 4 c, especially NS lineaments running parallel to faults which are well known in the outcrops west of the image.

Lineaments detected in the first unit on Fig. 4 c can generally be followed in the second unit.

The various sub-units in the alluvial deposits appear clearly on Fig. 5 c, especially the most important sub-units A3 and A4 which correspond respectively to ancient and recent deposits.

All the lineaments picked on Fig. 4 c appear on Fig. 5 c but other lineaments can be detected in this last image because multispectral classification and the weighting factors used for the display strongly bring out the boundaries between terrains of different nature.

The third unit corresponds to open waters. No water classes can be detected in Fig. 3 c and eight water classes appear on Figs. 4 c and 5 c (cf. W1 ... W8 sub-units in Figs. 7 and 8). Coastal waters (W6) can be followed all along the shoreline. The outflow of River Agly can be detected offshore in the last two images.

CONCLUSION

A technique has been described which allows a combination of an enhanced image and its corresponding multispectral classification to be obtained. Examples described in this paper show that each detail of the original image being greatly enhanced this technique can help the interpreter to gain a clearer view of targets against their background. Marker beds and lineaments are more clearly visible on the processed image than either on the original image or on the conventional principal component analysis color display. Furthermore it allows the interpreter to take into account at the same time not only the image itself but also the corresponding computerized classification which can be of great value in mapping certain lineaments or geologic boundaries.

ACKNOWLEDGMENTS

Authors acknowledge the assistance of J. Prud'homme for the color composites.

REFERENCES

1 - David Landgrebe, 1973, Systems Approach to the Use of Remote Sensing, La Télédétection des Ressources Terrestres, Ecole d'Eté, C.N.E.S., Paris, p. 163-192.

2 - F. Brun, A. Fontanel, C. Lallemand, G. Legendre, J.C. Rivereau, G. Thomas, 1974, Comparaison de différentes techniques numériques servant à la classification des données multispectrales in European Earth Resources Satellite Experiments, Proc. Symp. ESRO, Frascatti, 28 Jan., 1 Feb., p. 303-316.

3 - Patrick J. Ready, Paul A. Wintz, 1973, Information Extraction, SNR Improvement and Data Compression in Multispectral Imagery, IEEE, Trans. on Com., vol. Com - 21, No. 10, p. 1123-1131.

4 - V. Ralph Algazi, 1973, Multispectral Combination and Display of ERTS I Data, Third ERTS Symp., Dec. 10-14, Washington D.C., p. 1709-1717.

N76-17521

A SEARCH FOR SULFIDE-BEARING AREAS USING LANDSAT-1 DATA AND DIGITAL IMAGE-PROCESSING TECHNIQUES

G-26

By R. G. Schmidt, U. S. Geological Survey, Reston, Virginia and
B. B. Clark and R. Bernstein, International Business Machines
Corporation, Federal Systems Division, Gaithersburg, Maryland

ABSTRACT

Two experiments were conducted using LANDSAT-1 multispectral scanner (MSS) data to identify ground features that are indicators of sulfide-bearing rock. A nearby known sulfide deposit was used as a control. In the first experiment, false-color composites were examined visually to locate possible favorable areas; in the second, favorable areas were classified by digital-computer processing.

For the first experiment, false-color composites were made using three bulk-processed MSS images of three scenes over a very arid and vegetation-free part of the western Chagai District, Pakistan. Later, a color composite was also prepared from MSS bands 4, 5, and 7 by using imagery that had been digitally system-corrected and radiometrically adjusted for recording on a film recorder. These composites were examined for tonal features resembling the known porphyry copper deposit at Saindak. Seven areas were selected for prospecting, and three of these were field checked. None of the three contained significant mineralization.

In the second experiment, digital multispectral classification was performed using reformatted computer-compatible tapes of one scene. The IBM Digital Image Processing Facility was used for image correction, image enhancement, and multispectral classification. A 55 km^2 area in the Saindak vicinity was extracted and displayed in photographic form using the imagery printer, and a test area was selected which included the known porphyry deposits. Data points representing specific rock types were identified, and their data values were extracted for bands 4, 5, 6 and 7. Classification tables were postulated corresponding to geological features; each table was used to classify the test area, and the tables were modified upon comparison of these results with the known geology. The cycle was repeated five times until the final classification table was selected.

The final classification table was then used to evaluate 2100 km^2 in the western Chagai Hills, east of the test area, and a partial field check of the results was conducted. By evaluating the digital classification map, 23 prospecting targets were selected as being similar to the Saindak altered rock, and 19 of these were visited in the field. Of these 19, five localities constituting a total area of 4.7 km^2 contain hydrothermally altered rock that is mostly quartz feldspar porphyry. The rock is generally silicified, has argillic and sericitic alteration, and contains 5-10 percent pyrite. The pyritic rock may possibly represent the pyrite zones of porphyry copper-type deposits. The presence of copper or other valuable metals beyond trace amounts has been established at only one locality.

The results of the experiment show that outcrops of hydrothermally altered and mineralized rock can be identified from LANDSAT-1 data under favorable conditions. The empirical method of digital-computer classification of the multispectral scanner data was relatively unrefined and rapid. The five mineralized prospecting sites identified are in locations that the geologist (Schmidt) would not have selected as favorable on the basis of geologic knowledge or photogeologic interpretation at the time of the investigation.

INTRODUCTION

Mapping and mineral prospecting were undertaken at Saindak, Pakistan (fig. 1) in 1962 because the locality was considered one of the more favorable prospecting localities in the Chagai District. In 1962, after discovery of the disseminated copper sulfide deposit

at Saindak, it was reasoned that tonal changes and topographic expression related to hydrothermal alteration might be detected by optical remote sensing.

Two investigations concerned with direct detection of sulfide mineralization and hydrothermal alteration using LANDSAT-1 multispectral scanner data have used the porphyry copper deposit at Saindak as a test site because the deposit is large, has well-developed alteration zones, little vegetation, is well mapped, well exposed and undisturbed, and because the senior author was familiar with the deposit and region. Both investigations used image ID-1125-05545 (Nov. 25, 1972).

The first investigation (Schmidt, 1974) involved visual examination of false-color composite images to select light-toned areas that might be related to hydrothermal alteration. Relatively few areas were selected for field checking, and none checked proved to be mineralized. Later analysis of the results indicated that the method must be considerably modified for greatest effectiveness in mineral exploration.

In the second investigation, digital-computer processing was used to classify data from the four multispectral scanner bands (MSS bands 4, 5, 6, and 7), in order to remotely identify the material at the surface. In 1973, experimental work was undertaken by Ralph Bernstein and Bruce Clark of the Federal Systems Center, IBM Corporation, on digital processing of LANDSAT-1 data as a method of locating mineral deposits, using the Saindak area, as suggested by Schmidt. Later, the experiment was resumed by the IBM Corporation on behalf of the U. S. Geological Survey.

Clark extracted numeric data for the four MSS bands for each pixel from small test areas chosen to represent single rock types and single rock-alteration types. The classification tables for the area of the known deposit at Saindak were revised and tested five times. The final table was used for the mineral evaluation of 2100 km^2 (810 mi^2) of the Chagai District, which was considered to have a good potential for porphyry copper deposits, but in which widely distributed eolian sand made visual analysis of colored composites particularly troublesome (application area, fig. 2).

Following completion of digital-classification maps of the application area, a field check was made during October 13-31, 1974, of some of the prospecting sites selected in the two studies, and five mineralized areas were found. Data were collected that were useful for evaluating and improving the methods used. In 1975, further changes were made in the style of the classification tables, and the new tables were tested in the same parts of the Chagai District, Pakistan.

In the experiment leading to the field check in October, 1974, a direct, simple, and inexpensive application of LANDSAT-1 data to mineral exploration was tested in one particular geologic environment. Few revisions of classification tables, no ground checks prior to application, and no incorporation of ground-collected quantitative reflectance data into the study achieved simplicity and held down costs.

ACKNOWLEDGMENTS

The original color composite experiment conducted by the U. S. Geological Survey was partly supported by the National Aeronautics and Space Administration. Financial support for the digital-processing experiment and for the travel expenses of the field checking was provided by the EROS Office, and logistical support in the field was furnished by the Resource Development Corporation, a Pakistan Government corporation. The extraction of reflectance data for the Saindak area and for various sites in the application area performed in 1975 by Jon D. Dykstra, Department of Earth Sciences, Dartmouth College, is gratefully acknowledged.

REGIONAL GEOLOGY

The Mirjawa ranges, where Saindak is located, and the Mashki Chah region where the classification method was applied, have somewhat different regional geological aspects.

The rocks of both areas are Cretaceous to Quaternary in age. The Mirjawa range area has mostly folded (along northwest trends) and much faulted sedimentary and volcanic-sedimentary strata and relatively small amounts of intrusive and extrusive igneous rock. The detailed geology of the Saindak area (Ahmed, Khan, and Schmidt, 1972) is fairly representative of the geology of the more extensive border region. Cretaceous sedimentary rocks represent a wide variety of marine and continental depositional environments; lower Tertiary rocks are mostly shallow marine, and upper Tertiary-Quaternary strata are largely of continental origin.

In the Mashki Chah region, in a western section of the Chagai Hills, gently folded pre-Cretaceous and undeformed Tertiary volcanic rocks with low dips (probably initial) are common and widespread, and intrusive rocks are more abundant than in the Mirjawa Ranges. Faults are also present. The folding lacks the strong linear pattern characteristic of the Mirjawa Range. Recently dried or still weakly flowing sinter-depositing saline springs, plus a few fumaroles on the volcano Koh-i-Sultan indicate that there is still hydrothermal activity.

For all of the western part of Pakistan, 1:253,440 photogeologic reconnaissance maps (Hunting Survey Corporation, Ltd., 1960) are available, but probably less than 1 percent of the Chagai District has been mapped in detail.

ECONOMIC GEOLOGY

Mineral reconnaissance in the Chagai District has been spotty and mostly for high-grade deposits. If a porphyry copper deposit had been noticed during early investigations, it might have been passed over as too low grade for consideration at that time. Several large areas of the Chagai District containing abundant volcanic rocks of intermediate and felsic composition, and small bodies of hypabyssal intrusive rocks of Cretaceous through Pleistocene age may be considered to have a good potential for large sulfide deposits of the porphyry copper type.

At Saindak, a group of small copper-bearing porphyritic quartz diorite stocks cut northward across the folded lower Tertiary stratigraphic section (Ahmed, Khan, and Schmidt, 1972). The stocks may be cupolas on a single barely exposed granitic body 8 km (5 mi) long and as much as 1.5 km (1 mi) wide, or separate but related intrusive bodies. The group of stocks is surrounded by zones of contact metamorphism and hydrothermal alteration. The stocks are enclosed in a sulfide-rich zone that contains as much as 15 volume percent pyrite; the sulfide-rich zone in turn is surrounded by a zone of propylitic alteration in which pyroclastic rocks in particular are altered to a hard, dark epidote-rich hornfels. Descriptions of the alteration zonation in the central part of the deposit have not been published, but there are areas of much quartz-sericitic alteration and areas of potassic alteration, some of which contain much hydrothermal biotite.

The well-developed pattern of hydrothermal-alteration zones and the general characteristics of the copper sulfide mineralization are similar to the simple ideal model of porphyry deposits described by Lowell and Guilbert (1970), but only detailed geological mapping plus extensive exploration drilling, such as the program now underway by the Government of Pakistan, can establish whether the deposit is of economic significance.

The sulfide-rich zone including both the intrusive porphyry stocks and the adjacent pyrite-rich country rock has been eroded to form a valley in which the colors of surficial materials are light-toned. Desert soils associated with many porphyry copper deposits the world over have distinct red and orange color anomalies, and this is true at Saindak as well, where the mineral natrojarosite ($NaFe_3(SO_4)_2(OH)_6$) has been identified in the pigmented material. In the central valley at Saindak, however, alluvial and windblown grains of sand dilute or cover part of the colored soil.

In plan view, this valley is encircled by a symmetrical rim of hills more rugged and darker in tone than the surrounding region (Ahmed, Khan, and Schmidt, 1972, fig. 2). These hills, generally corresponding to an erosion-resistant zone of hornfels and propylitic alteration, form the outer boundary of the whole exploration target.

COMPUTER-AIDED INFORMATION-EXTRACTION EXPERIMENTS

Computer-aided information-extraction experiments were conducted to identify potential sulfide ore-bearing localities. The experimental approach is summarized on figure 3. Shown here are the source data used, the digital processing applied to the source data, the products generated, the analysis conducted, and the final products. By a combination of digital image processing and information extraction, and manual analysis and evaluation, three processing operations were performed: digital image generation, support data generation and analysis, and multispectral classification.

Digital image generation.--The uncorrected LANDSAT multispectral scanner sensor (MSS) data were reformatted into 185 km x 185 km areas, and each band was radiometrically (intensity) adjusted and systematically geometrically corrected (Bernstein, 1974). The resulting computer-compatible tapes (CCT) were then recorded on film from which black and white and color prints were made. These prints were used as aids in the selection of the field prospecting sites during the evaluation of the classification results and also during the field checking. Figure 4 shows band 5 of the processed Pakistan scene.

Support data generation and analysis.--The formatted but uncorrected CCT's were used for analysis prior to the multispectral classification operation. Shade prints (computer printouts providing the reflectance sensed in each spectral band) for selected areas were prepared and used as maps for precise location of individual data rectangles (pixels) relative to known ground features and known rock types. Numeric data for the 4 MSS bands were extracted for each pixel in the known areas, and maximum and minimum sensed-reflectance limits were chosen for each rock type. A known copper sulfide-bearing deposit at Saindak was the source of data used to prepare the classification tables. Five revisions were made and tested, and one alternate classification table was tried, resulting finally in the classification table shown on Table 1. Table 1 shows three general types of materials: 1) Mineralized rock, including intensely hydrothermally altered (quartz-sericite zone) quartz diorite, and pyritic rock; 2) Alluvial and eolian materials, recently moved dry-wash alluvium and eolian sand being the materials most likely to be confused with the first group; and 3) A loose category of dark surfaces that includes both hornfels-type bedrock and many areas of desert-varnished lag gravels (especially in class 10). These tables of reflectance limits were then used on an interactive basis to classify a nearby region within the same LANDSAT scene in which copper sulfide-bearing areas were suspected but in which no deposits were known (application area).

Multispectral classification and analysis.--A spectral-intensity discrimination program was used for multispectral classification on the application area using the tables prepared for the Saindak deposit. The program tested the reflectance of each picture element within the application area against the maximum and minimum reflectance limits in the table and determined into which surface class (rock type) the picture element belonged. The symbol for that class was printed on a computer listing as part of a classification map. When the observed values fit more than one class (when classes were set up with overlapping limiting values), a pixel was placed in the class that was considered first in the search sequence.

The classification table resulting from five revisions was used to evaluate an adjacent area of 2100 km^2 considered to have good potential for porphyry copper deposits in the western Chagai Hills (fig. 2). The results were printed-out in 13 computer-generated vertical strip maps. These maps were examined for groups of pixels

classified as mineralized quartz diorite and pyritic rock, and about 50 groups or concentrations were identified. Each was then evaluated for probability of correct classification, relationship to concentrations of other classes, and comparison with known rock types and occurrences of hydrothermal mineralization. From this examination, 30 localities most deserving reconnaissance checking in the field were chosen. The locations of these targets were marked on an enlarged (1:250,000) digitally enhanced image of MSS band 5 in order to simplify location on aerial photographs and in the field.

As part of the field check, all anomalous areas were first examined on stereoscopic pairs of 1:40,000-scale aerial photographs. At this point, it was possible to reject seven areas as related to windblown sand. Nineteen sites were examined in the field, and four desirable sites were not reached in the field checks. Five sites were found to be extensive outcrops of hydrothermally altered sulfide-rich rock. Two additional sites contain altered rock with some sulfide but seem less attractive for prospecting at this time.

Evaluation of results.--Mineralized rock is believed to have been generally identified correctly, but much other light-toned surface was also classified as mineralized. Alluvium was mostly classified accurately. Perhaps only 25 percent of dune sand was correctly identified by means of table 1, most sand having been classified as mineralized rock. Classification of areas of dark rock outcrops and several types of lag gravels yielded different combinations of classes 10, 11, and 12 and made it possible to differentiate between these materials.

In Table 1, four of the main surface types are each represented by a high and a low reliability class. The high reliability or more restrictive class has reflectance limits in at least one band that make it exclusive from all other high reliability classes; the secondary class has reflectance limits that overlap the limits of at least one other class. The classes of two reliability levels have not been used in later tables. The classification map made by using Table 1 is compared with a geologic map (fig. 5).

In building Table 1, as the acceptable reflectance limits of a class were narrowed, fewer matches were found. In classes 1 and 2 (mineralized quartz diorite Table 1), for example, if we chose limits that include most pixels in the training areas and also many pixels in all the areas of known mineralization, we also got false classifications in dry-wash material. The limits were subjectively adjusted wider or narrower so that enough points were classified correctly in the areas of known mineralization to call attention to those areas, and the false classifications were reduced to an acceptable level. Because revisions to the tables are time-consuming and successive revisions generally achieve diminishing improvement, the final tables used in this experiment have been revised only a few times.

The three dark-surface classes were established on the basis of small samples of particular rock formations in training areas, but the classes were very unsatisfactory in discriminating between the three formations. The classes would have been abandoned except that various combinations of the three classes delineate areas of dark rock outcrops and lag gravels. The printout of class 11 (symbol #) in particular resulted in abundant pixel groups just inside the perimeter of the propylitic zone at Saindak.

The data collected in the field check made it possible to evaluate the accuracy of identification of all of the surface types, not the mineralized rock alone, and to revise the tables to improve accuracy. A new style of table was adopted, having several relatively narrow classes spanning the expected albedo range for each rock type, but having no high and low reliability classes (Table 2). The limiting values for each class span relatively narrower ranges than those in Table 1, and more classes are required. The use of several classes for a range in albedo from similar surface types is designed as a simple way to compensate for variations in reflectance angles, especially those caused by southeast- and northwest-facing slopes.

THE NEWLY IDENTIFIED AREAS OF MINERALIZATION

Four of the areas of mineralization newly discovered in this investigation are in the central core area of the eroded remnant of a large stratovolcano (fig. 2 and 6). A fifth is about 15 km to the east. Sites 5d, 6d, and 6e may be parts of a single large mineralized body as the bedrock between them is covered by Holocene alluvium. Site 5c seems to be a separate mineralized area nearby. Site 8a (fig. 2), 15 km east of 5d, is well outside the core of the stratovolcano, although it may be within the flank of the old volcanic edifice.

The areas of mineralization comprise a total of 4.7 km^2 of hydrothermally altered rock, generally containing 5-10 percent total sulfide. Traces of copper mineralization were seen in many places, but significant mineralization is hard to identify because of pervasive thorough leaching of the rocks near the surface. Most of the rock in the mineralized areas is quartz-feldspar porphyry, but some is probably tuff and sandstone or tuffaceous sandstone. Alteration is silicic and sericitic and locally argillic. The sulfide was present as disseminated grains in part of the areas, now indicated by limonite stains and sulfide casts, and as abundant veinlets forming stockworks. Unleached sulfide at site 6d, part disseminated and part in veinlets, is not as rare as at the other sites. Several places have traces of oxidized minerals. Weathered sulfide and rather common copper carbonate stains were found at one locality. Analysis of one sample of the fresh rock showed 0.3 percent copper. Jarositic and gypsum-rich soils, in which the sulfate has been derived from the weathering of sulfides, are common at all sites.

These mineralized areas of the porphyry copper type have the potential of being important deposits, but only through evaluation, including exploration drilling, can it be determined whether they are exploitable ore bodies.

SUMMARY

Visual evaluation of false color composites and a relatively simple method of digital classification were tested as aids to mineral exploration by using areas of known hydrothermal alteration and mineralized and altered intrusive stock as control areas. Both methods are shown to be useful exploration tools, and greatest advantage is probably gained by using them together. The simple classification method was applied to evaluate 2100 km^2 of area regarded as having a high potential for deposits of the porphyry copper type, leading to the discovery of 5 sizable areas of hydrothermally altered rock containing abundant sulfide, disseminated or in stockwork veins. Although the classification method used was relatively simple and unrefined, and 14 prospecting targets proved to be false leads, the number of sulfide-bearing areas identified was outstanding, and the falsely classified areas were not so many as to require an unreasonable amount of field checking. Further experimentation indicates that better discrimination of mineralized areas than we used in the field test can be achieved. Our study indicates that simple methods of digital classification of LANDSAT data can be a powerful supplement to standard methods of mineral exploration, especially in desert terrains.

REFERENCES CITED

Ahmed, Waheeduddin, Khan, S. N. and Schmidt, R. G., 1972, Geology and copper mineralization of the Saindak quadrangle, Chagai District, West Pakistan: U. S. Geol. Survey Prof. Paper 716-A, 21 p.

Bernstein Ralph, 1974, Scene correction (precision processing) of ERTS sensor data using digital image processing techniques: Third Earth Resources Technology Satellite-1 Symposium, v. 1: Technical Presentations Section B, NASA SP-351, Dec. 10-14, 1973, p. 1909-1928.

Hunting Survey Corporation, Ltd., 1960, Reconnaissance geology of part of West Pakistan; a Colombo Plan Cooperative Project: Toronto, 550 p. (Report published by Government of Canada for the Government of Pakistan).

Khan, S. N., 1972, Interim report on copper deposit of Saindak, Chagai District (Baluchistan), Pakistan: Pakistan Geol. Survey, Saindak copper report no. 1.

Lowell, J. D., and Guilbert, J. M., 1970, Lateral and vertical alteration-mineralization zoning in porphyry ore deposits: Econ. Geology, v. 65, no. 4, p. 373-408.

Schmidt, R. G., 1974, The use of ERTS-1 images in the search for large sulfide deposits in the Chagai District, Pakistan: U. S. Dept. of Commerce, Nat. Tech. Inf. Service, E74-10726, 38 p.

TABLE 1. DIGITAL CLASSIFICATION TABLE USED IN 1974 MINERAL EVALUATION IN THE CHAGAI DISTRICT, PAKISTAN

Class number	Rock type			Symbol	Multispectral scanner bands			
					4	5	6	7
1	Mineralized rock	Quartz diorite	High reliability	●	46-50	52-60	50-60	18-22
2			Low reliability	Ø	44-45	52-60	45-49	18-19
3		Pyritic rock	High reliability	⋇	41-45	47-54	39-44	16-17
4			Low reliability	X	41-45	47-54	39-44	16-19
5	Dry wash alluvium		High reliability	=	39-46	39-46	35-44	14-17
6			Low reliability	-	41-45	46-51	42-49	18-19
7	Boulder fan			+	33-40	39-46	30-35	9-16
8	Eolian sand		High reliability	·	38-44	46-54	42-51	18-22
9			Low reliability	'	45	46-127	42-127	18-63
10	Various dark surfaces including hornfelsic rock outcrops, desert-varnished lag gravels, and detrital black sand			1	33-36	28-38	29-35	11-15
11				#	24-35	19-27	20-32	8-12
12				H	29-36	28-38	20-28	9-14

TABLE 2. REVISED CLASSIFICATION TABLE PREPARED IN APRIL 1975

Class number	Rock type	Symbol	Multispectral scanner bands			
			4	5	6	7
1	Detrital black sand	,	27-30	26-28	23-26	9
2		,	28-32	27-31	25-27	10
3	Dry wash alluvium	-	38-44	39-44	35-38	13-16
4		=	43-48	44-48	38-43	15-18
5	Eolian sand	.	49-54	59-66	54-62	23-27
6		.	43-48	50-58	46-55	19-24
7		.	37-43	41-50	38-47	15-20
8		.	33-38	35-42	32-39	12-16
9	Mineralized rock	0	39-42	41-45	33-38	14-16
10		θ	41-44	44-48	37-41	16-18
11		⊖	43-46	47-51	41-45	17-20
12		⊕	44-46	50-53	45-48	18-20
13		⊠	46-49	53-56	48-51	19-21
14		●	49-52	56-59	51-54	20-22
15	Dark surfaces, except detrital black sand	I	33-36	28-38	29-35	11-15
16		#	24-35	19-27	20-32	8-12
17		H	29-36	28-38	20-28	9-14

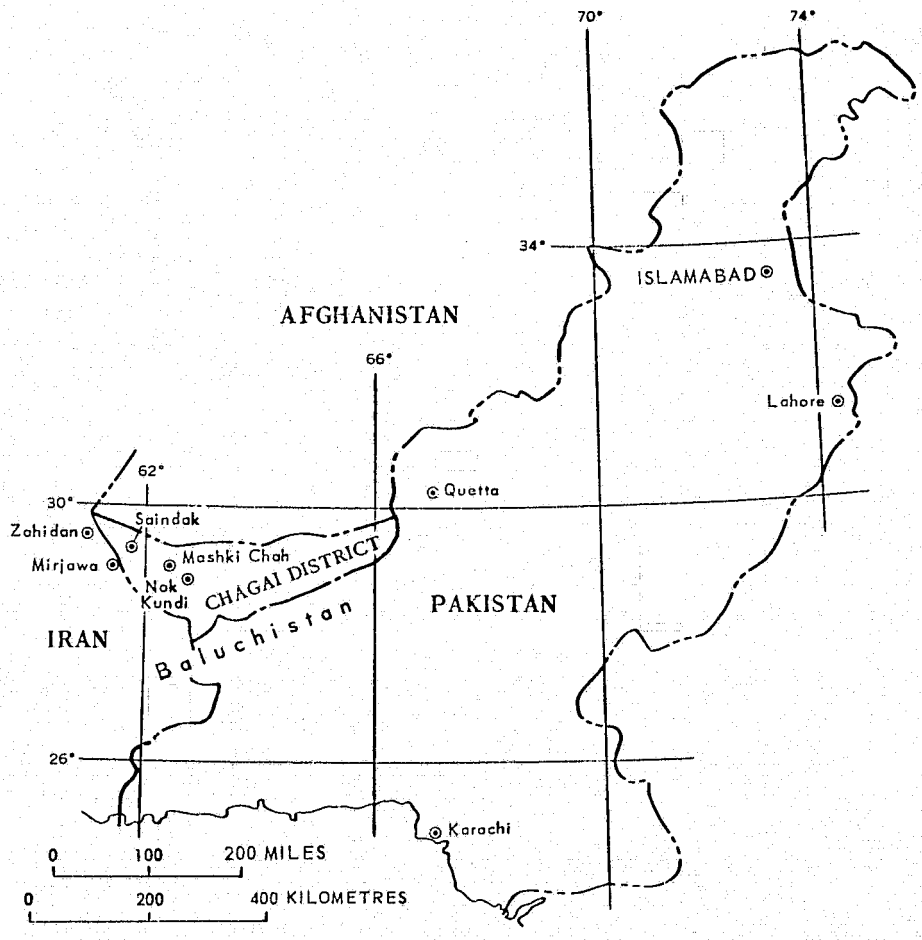


Figure 1. Index map showing the Chagai District and Saindak, Pakistan

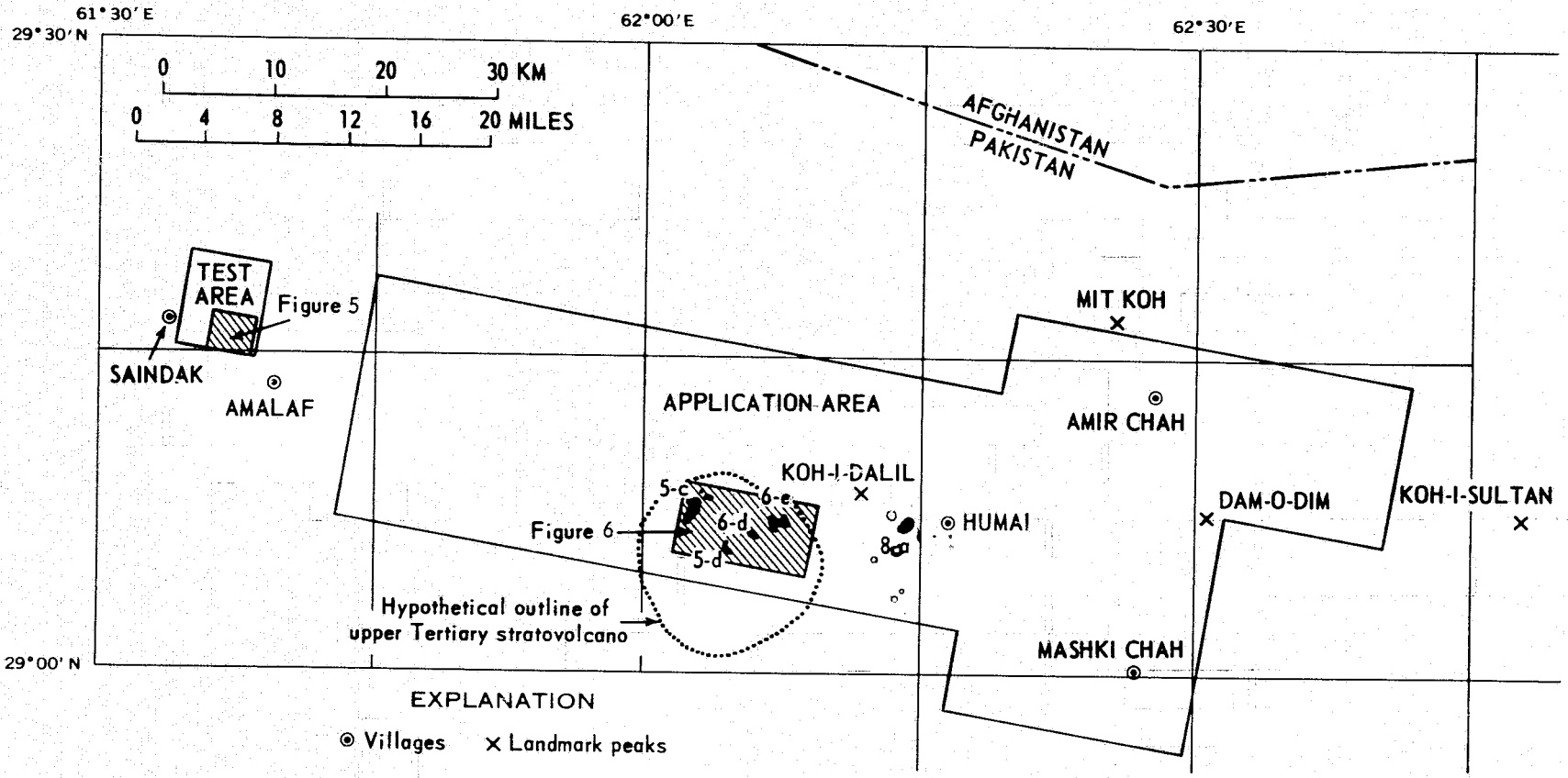


Figure 2. The Saindak-Mashki Chah area of the western Chagai District, Pakistan, showing the control area near Saindak and the area where the digital-classification method was applied. The numbered locations are mineralized prospect sites described in the text.

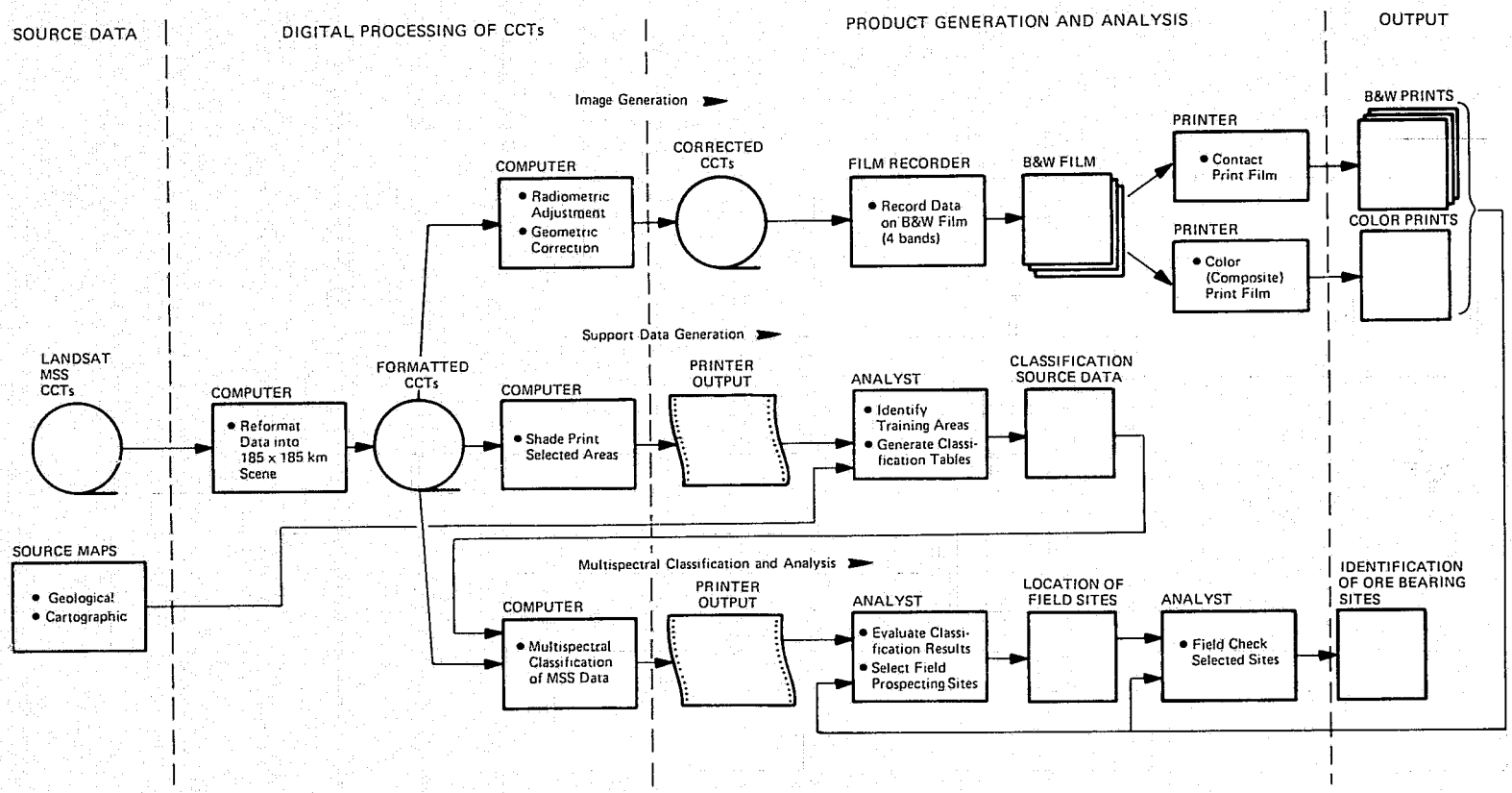


Figure 3. Graphic summary of digital processing and data analysis performed in the experiment

Figure 4. Digitally enhanced LANDSAT MSS band 5 image ID 1125-05545 of Pakistan and Iran. The areas studied in the experiments are in the northern quarter of the image.

ORIGINAL PAGE IS POOR

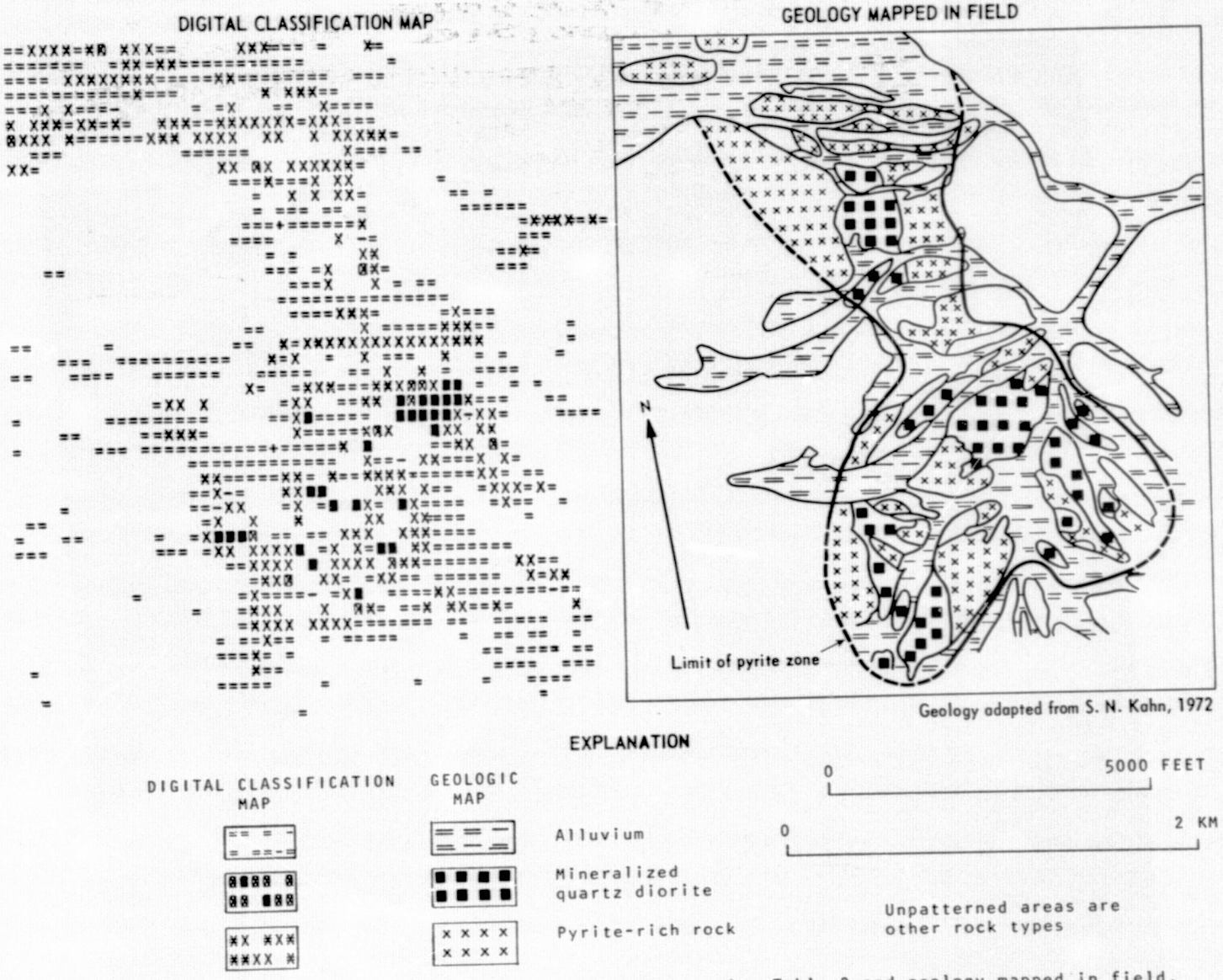


Figure 5. Comparison of digital-classification map made by using Table 2 and geology mapped in field, Saindak porphyry copper deposit, Pakistan

REPRODUCIBILITY OF TH
ORIGINAL PAGE IS POOR

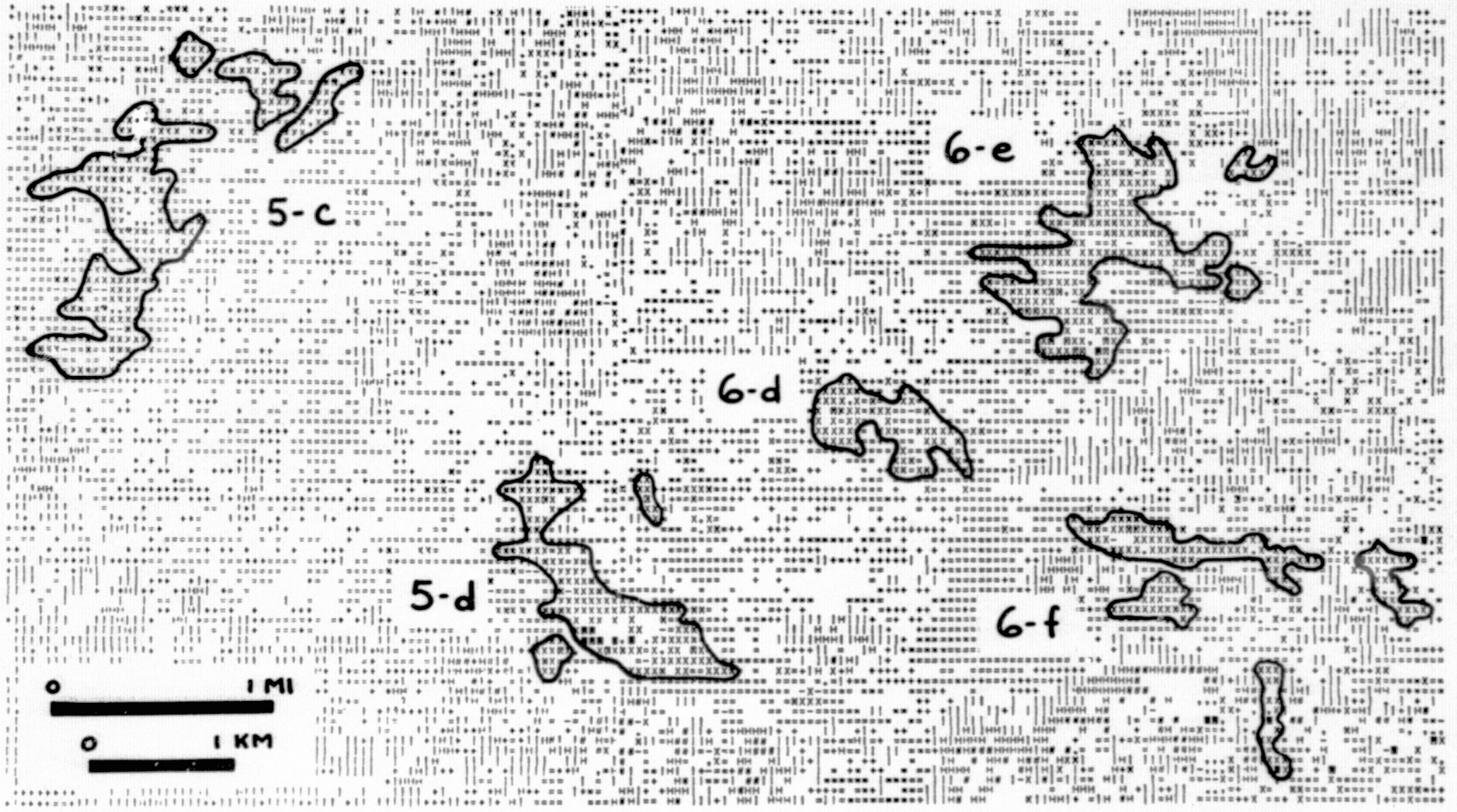


Figure 6. Classification map of an area west of Koh-i-Dalil (fig. 2) showing five areas classed as "mineralized". Reconnaissance field checks showed that some hydrothermal alteration and sulfide mineralization is present in each area. Area 6-d seems the most promising for further study. The northeast end of 5-c, the west end of 6-f, and the northeast end of 6-e were not adequately field checked. The east end of 6-f is mostly dune sand.

REGIONAL INVENTORIES AND MAPPING OF LAND RESOURCES AND ENVIRONMENTAL GEOLOGY USING REMOTELY SENSED DATA*

By E. G. Wermund, L. F. Brown, Jr., and W. L. Fisher,[1]
Bureau of Economic Geology, The University of Texas at Austin 78712

N76-17522

ABSTRACT

The Bureau of Economic Geology through its associated Land Resources Laboratory has inventoried land resources and mapped environmental geology using remotely sensed data for all 267,339 square miles of Texas. Seventy-eight statewide land and water resource units are presented at a scale of 1:500,000; six statewide land use units are mapped and presented at a scale of 1:250,000.

Mapping of the Texas Coastal Zone, an area covering 20,000 square miles, is complete; the product includes a suite of maps of environmental geology (69 units compiled at 1:125,000) as well as maps of physical properties, physical processes, biologic assemblages, economic resources, and land use (at 1:250,000 presentation scale). Resource capability maps are complete for (1) the Coastal Bend Council of Government, COG (43 units at 1:250,000), (2) Houston-Galveston COG (45 units at 1:125,000), (3) the Corpus Christi area (40 units at 1:125,000), and (4) parts of Mustang and northern Padre Islands (16 units at 1:24,000). In addition, both environmental geology and physical properties maps are available for the Capital City COG (33 units at 1:250,000), and the Lake Travis vicinity (7 units at 1:96,000). The environmental geologic mapping of both Austin and San Antonio has been completed. Land resource mapping is nearly completed for the Nueces, San Antonio, and Guadalupe River basins (33,000 square miles) and has been initiated in the East Texas lignite belt.

Black-and-white stereoscopic aerial photographs at a scale of 1:20,000, 1:40,000, and 1:65,000 and controlled aerial photo mosaics at a scale of 1:24,000 have been the basic data utilized for most mapping. Color and color infrared aerial photography (1:20,000) was employed to map the barrier islands, and color infrared photography (1:120,000) was used to map sand and mud units of the coastal plain north of Houston. LANDSAT-1 imagery in Bands 4, 5, and 7 (1:250,000) has been utilized to examine land use and certain resource units statewide. Side scanning radar (SLAR) and LANDSAT imagery were studied experimentally toward mapping land suitability units in carbonate terranes with high relief and certain other terranes.

Large-scale color and color infrared aerial stereoscopic photographs supply the most information for regional mapping. Black-and-white photography is the most practical data for mapping because of scale, complete coverage, availability, and relatively low cost.

INTRODUCTION

During basic geological mapping of the Texas Coastal Zone in the late 1960's, Fisher and others (1972) perceived the valuable potential of their fundamental geological interpretations for governmental planners and private

* Published by permission of the Director, Bureau of Economic Geology.

[1] Now Deputy Assistant Secretary for Energy, Department of Interior.

PRECEDING PAGE BLANK NOT FILMED

consultants. Map units clearly had significant environmental implications in a critical area of the State. Early in their work, resource capability units were defined by Brown and others (1971): "A resource capability unit is an environmental entity--land, water, area of active process, or biota--defined in terms of the nature, degree of activity or use it can sustain without losing an acceptable level of environmental quality."

The above definition was derived entirely from mapping and inventories of the Coastal Zone. One application which followed was concerned with siting sanitary landfills (Brown and others, 1972).

Basic concepts and mapping criteria recognized in this early work in the Coastal Zone have since been expanded toward mapping the entire State. Presently the mapping emphasizes land and water resource units which have been recently defined by St. Clair and others (in preparation) as "...mappable entities, either natural or man-made, that are defined by physical, chemical, and biological characteristics and processes which govern the type or degree of use that is consistent both with the natural quality and productive utilization."

Two important aspects are emphasized in this latest definition. One is the fact that man has frequently made a wide choice of land use already, especially in the areas of farming and ranching. Second is the emphasis on a map as a means of presentation. It is important that the units be mappable and moreover, that the resource or capability or environmental units are mappable in a regional sense. This approach is different from related kinds of geological mapping described in the literature because there is a real concern with regional problems--mapping continuously identifiable units in large areas. For example, the largest area mapped (fig 1) as an environmental study is the State of Texas--267,339 square miles (692,149 square kilometers); the smallest area mapped is Austin and vicinity, 712 square miles (1,844 sq km). Most areas mapped to date exceed 2,500 square miles (6,475 sq km).

Providing data for regional planners necessitates that large areas be mapped. Mapping of these large areas requires the work of only a few people within a clear-cut time schedule. It is never possible to take time to see the entire area or region on the ground, nor is all the needed information on the ground. Therefore, most of the environmental information that is mapped is collected from remote sensing data and supplemented by periodic field checks. The remote sensing data must be available and applicable for immediate use. There is rarely time for experimental study of selected areas, but practical applied studies must be selected for use throughout a region. Additional data supporting interpretations include published geology and biology, weather and climatological reports, maps and charts of topography and bathymetry, soil descriptions, and maps and assessments of economic resources.

Although abundant and variable supplementary data sources are investigated during mapping and inventorying of land and water resources, only the remote sensing interpretations are emphasized in the following report. Although land and water resources have been inventoried in more than ten areas, only results from three areas are reported here as examples. The three areas are the low-lying Coastal Zone, the rolling sand and mud terrane of the interior coastal plain, and the highly dissected thick carbonate of the southern Edwards Plateau (fig 1). They were chosen to represent mapping of diversified geologic provinces.

Acknowledgments.--We are grateful for financial support to NASA for work in the interior coastal plain in the Houston Area Test Site. Work in the southern Edwards Plateau carbonate terrane was supported in part by the

Texas Water Development Board. Peer review has been provided by R. A. Morton and T. Gustavson. Preliminary drafting of the text with initial editorial comments was provided by Mrs. Elizabeth T. Moore and her staff. Drafting was under the direction of James Macon, Chief Cartographer. Final editing was by Kelley Kennedy.

METHODOLOGY

Interpretation

To date, computer analysis of digital data has not been applied to environmental geologic mapping nor inventorying of land resources and water; all the results described herein are based on imagery interpretation--dominantly standard photographic interpretation of geology and biology. For those unfamiliar with standard aerial photographic interpretation, the method is briefly described. Interpretations depend on recognition of four variables: tone, fabric, geometry, and relief. Tone refers to the density of gray on black-and-white photography and to the color and hue from either color or color infrared photography. In either medium, darker tone surfaces are frequently finer grained sediments or soils which commonly retain more moisture than do lighter toned surfaces. Fabric concerns patterns resulting from juxtaposed or contiguous tonal variations, for example the alternation of darker tones in furrows and lighter tones on hillocks of a plowed field. Geometry relates to a kind of automatic recognition of known shapes, like a meandering stream or a tributary junction or a delta. Relief concerns topographic expression and can best be seen in stereographic aerial photography. In certain geologic interpretations, stereographic imagery is essential.

Superposed on the basic interpretive data is the geologist's experience. Interpretation requires a systematic mental picture or three-dimensional model (or system) of what the earth's surface looks like. The more experienced or more knowledgeable the geologist, then the more accurate is the model or system or framework within which he interprets imagery. Later, it will be known that a different system of geologic presentation or a concept of varied models are the bases of interpreting environmental geology for various areas. Moreover, the more sophisticated systems of particularly stratigraphic interpretation developed in recent years by researchers has greatly expanded the ability to interpret environmental geology.

The selection of what type of remote sensing imagery to be interpreted depends on several factors. There are always economic constraints in a tightly budgeted project. Of course, black-and-white aerial photography is commonly available and the least expensive. For other remote sensing data, several questions in addition to cost and availability are significant. They are (1) what information can be interpreted, and (2) is this interpretation capability sustained continuously over an extensive region. It is rarely worthwhile to interpret isolated phenomena unless the objective is site specific. Instead, regional planners need documentation of continuous variations of geologic or soil or other kinds of data in a regional perspective.

So far, environmental geology and land resources inventories have been mapped by interpretation of black-and-white aerial photography. In one pilot study, regional interpretation of color and color infrared photography proved better than interpretation of comparable black-and-white aerial photography. An experiment using SLAR demonstrated a capability to map certain scattered highlighted features. LANDSAT imagery has not been used enough to evaluate completely its potential. In the next 18 months, LANDSAT imagery will be evaluated for mapping in the Coastal Zone; more interpretations need to be made in various other geological areas in order to define

the limits of regional mapping using ERTS imagery.

Scale and Coordination

In addition to the kinds of features to be mapped and the kind of remote sensing data available, the nature and quality of available base maps also influences strongly the final results. Scale of base maps and of available remote sensing data then becomes a critical factor. U.S. Geological Survey 7.5-minute quadrangle topographic maps (1:24,000) are not always available. If a 1:24,000 scale base map is required, it may be possible to supplement missing topographic base maps with commercially available controlled black-and-white aerial mosaics at a scale of 1:24,000. If there are no available base data at a 1:24,000 scale, then standard 15-minute quadrangle topographic maps (1:62,500) generally can be acquired. Unfortunately, the latter may be very old, and the base map is consequently out of date.

The scale of available remote sensing data may also vary greatly. Photography at scales of 1:24,000, 1:40,000, 1:60,000, and 1:120,000 have been used for Bureau projects. The variability of scales of base maps and remote sensing data brings up another major problem that involves the coordination of the interpreters.

Large regional projects with a rigid time schedule frequently require several interpreters. Four to six people may divide up large regions, usually on some natural basis such as a river basin, in order that simultaneous mapping of the entire region can be undertaken. Excellent base maps may be available in one area, but poor data may exist elsewhere in the region. Some interpreters may have large-scale remote sensing data whereas others have small-scale topography or imagery. Coordination is achieved by scheduled regional trips to compare field variables and scheduled work sessions to compare imagery interpretation. By this means, a consistent interpretation is achieved.

Presentation

As mentioned previously, the principal purpose of regional environmental geologic mapping and inventorying of land resources is to provide information for regional planners. Some of the remote sensing interpretations, for example those at a scale of 1:24,000, are more nearly site specific. As with most original work, the environmental interpretations on the base maps are in preliminary form. Therefore, it has been a standard procedure to compile the final land resource information on base maps of smaller scales in order to reduce the significance of minor mapping errors. Compilation is achieved by using a pantograph to reduce the basic scale of mapping interpretation. The most common scales used to present regional data are 1:125,000, 1:250,000, and 1:500,000 (table 1).

For purposes of publication and to achieve clarity in presentation, multicolor maps are normally prepared. Therefore, an extensive detailed cartographic procedure of color separation and finally color printing is an essential part of the program. Finally, after publication the interpreters serve as ad hoc consultants to the users of our data.

RESULTS

Results available from mapping the environmental geology and inventorying the land and water resources in extensive and varied regions of Texas are shown on table 1. Results are available for: flat, rolling, and steep slopes; igneous-metamorphic, carbonate, and sandstone-mudstone bedrocks; coastal, fluvial, eolian, and ground-water recharge processes; arid,

semiarid, humid, and subtropic climates; desert, prairie, forest, and wetland floras; cities, seaports, and rural areas; forests, mining, and recreation land uses; and others. This experience has produced a broad spectrum of philosophies, concepts, experiences, procedures, and kinds of presentations of inventorying environmental variables of many different settings.

The ultimate goal of map utilization by regional planners is being realized in certain areas. Publications on the Coastal Zone are presently incorporated into the Coastal Zone management effort of the General Land Office of Texas. Mapping in the southern Edwards Plateau has influenced both the task force of the San Antonio City Council and the Alamo Council of Governments where they are both concerned with protecting the recharge zone of the subartesian Edwards aquifer. The Houston-Galveston area council has used preliminary results of the inventory of land and water resources in that area. Various reports and information have been included in decisions of the Division of Planning Coordination in the Office of the Governor. There has also been private sector use of published mapping of the Coastal Zone.

In the recent two biennium sessions of the Legislature, results of both environmental geologic mapping and inventorying of land and water resources have been presented by request to committees acting on bills concerned with regional planning in Texas.

DISCUSSION

In this paper, three regions are presented as examples of remote sensing interpretation of land and water resources. They are the Texas Coastal Zone, the interior coastal plain in the Houston Area Test Site, and the southern Edwards Plateau. These regions were selected to represent different terrains, substrates, processes, and biota.

Texas Coastal Zone

The Texas Coastal Zone (fig 1) is marked by diversity in geography, resources, climate, and industry. It is richly endowed with extensive petroleum reserves, sulfur and salt, deepwater ports, intracoastal waterways, mild climate, good water supplies, abundant wildlife, commercial fishing resources, unusual recreational potential, and large tracts of uncrowded land. At the same time, it is plagued by natural hazards including frequent hurricanes with heavy wind and water damage, a retreating coastline, large areas of subsidence related to ground-water withdrawal, and local zones of active faults. The Coastal Zone is a vast area of about 20,000 square miles, including approximately 2,100 square miles of bays and estuaries, 375 miles of Gulf coastline, and 1,425 miles of bay-estuary and lagoon shoreline. About one-quarter of the State's population and one-third of its economic resources are concentrated in the Coastal Zone, an area including about 6 percent of the total area of the State.

The guidelines for proper and prudent management of the Texas Coastal Zone depends upon adequate knowledge of the nature and distribution of natural environments, land and water capability, and man's impact on the Coastal Zone. The development, exploitation, and industrialization practices should be compatible with the natural limitations imposed on the region by its physical, chemical, and biologic setting. Any fair system of management must be based upon the concept of natural local and regional variation of environments; correspondingly, flexible guidelines should be firmly based upon these variations and properties, composition, and behavior under various land uses. Environmental geologic maps provide the fundamental data needed to create

such a system of resource management.

As mentioned previously, remote sensing interpretation is best developed within a proper geologic model or understanding of a clear natural system as a guide for recognizing discrete or particular units. The Texas Coastal Zone is composed of several active, natural systems of environments--fluvial and deltaic systems, marine barrier-strandplain-chenier systems, and bay-estuary-lagoon systems, as well as an eolian (wind) system in South Texas and marsh-swamp systems in the more humid middle and upper coastal regions (fig 2). The natural systems, whether ancient or modern, were deposited by the same natural processes that are active in shaping the present coastline--for example, longshore drift, beach swash, wind deflation and deposition, tidal currents, wind-generated waves and currents, delta outbuilding, and river point bar and flood deposition. It is the recognition of natural systems which are the summation of the individual units deposited by particular processes that gives rise to a systematic classification of the environmental geologic unit as shown in table 2.

Remote sensing interpretation.--An example of remote sensing interpretation from 1:24,000 black-and-white controlled aerial photographic mosaics is shown in figure 3. The particular or discrete units recognized are units that have substrates dominated by variations of mud or sand. In general, the sands have a higher reflectivity, lighter tone, and smoother texture than do the muds. Another key to the identification of the sands and the muds depends upon recognition of the major natural (or depositional) systems to which the particular units belong, as shown in the following.

Interpretations on a black-and-white 1:24,000 controlled aerial mosaic (fig 4) show that the appearance of one lithic unit varies in different depositional systems (fig 3). Mud is present (1) as a modern mud-filled channel, (2) as overbank muds of a Pleistocene fluvial system, and (3) as interdistributary mud, silt, and clay in a Pleistocene delta system. The characteristics of muds in different systems are not exactly the same. In the northern part of the aerial photograph, the overbank mud of the Pleistocene fluvial system carries a different vegetation and therefore has a different tone and a different contrast, much darker in fact than the muds that are interdistributary muds of the Pleistocene delta system. Without recognizing different geological systems, one would fail to interpret that the same mud substrate can have dissimilar tone and texture.

It may be possible to recognize some of the major systems of the Coastal Zone from study of 1:250,000 black-and-white LANDSAT imagery (fig 5). The LANDSAT imagery (fig 5) includes the area outlined in figure 3. Any interpretation of depositional systems from LANDSAT imagery at this time has to be considered tentative. To date, no systematic regional mapping of the Coastal Zone with LANDSAT imagery has been attempted; for remote sensing interpretation of environmental geology to be of use to regional planners, it is essential that any imagery interpretation have continuity throughout.

Houston Area Test Site

The Houston Area Test Site, including the Houston-Galveston area council, represents one of the most rapidly growing areas of the State of Texas (fig 1). The region contains the largest concentration of population, one of three major seashore resorts, valuable commercial fishing grounds, a major seaport, extensive industrial concentrations, valuable rangelands and croplands of rice and sorghum grain, and parts of the Texas lumber region. It is a dynamic region of great natural wealth and large capitalization by man, and is also subjected to the many natural hazards that occur in the Coastal Zone. Regional planners, recognizing their need for a natural information base, have independently invested in an inventory of land and water

resources for the region.

The physiography of this region includes a flat, level, coastal prairie near the city of Houston and hilly uplands of dense forests and savannas north of Houston. Elevations range from less than 50 feet on the coastal plain to over 500 feet in the northern forested areas. Northward of the Texas Coastal Zone, the combination of increasing relief and denser stands of vegetation complicate interpretation of remote sensing imagery and decrease the accuracy of interpretation. In the northern part of the HATS area, there are portions of the Tertiary system which are predominantly fluvial. The outcrop of Tertiary fluvial and in part deltaic systems differs from the outcrops of similar systems described earlier in the Coastal Zone because this area has considerable relief. Therefore, the sands and muds of fluvial-deltaic systems are being broken up by fairly steep slopes locally and have less continuity--as seen in remote sensing imagery.

South of the Tertiary system, there is a large alluvial fan system probably of Pleistocene age. The fan system also has some major slope elements in it, again giving rise to more difficult interpretation of remote sensing data examined only in a planar view. Because simple exposures of lithic types have less continuity, understanding of a geologic model or of a sedimentary system remains requisite in order to adequately identify particular lithic units that define environmental or land suitability. The important geologic systems noteworthy in the HATS zone distinctive from the Texas Coastal Zone are shown in figure 6.

South of the alluvial fan system of Pleistocene age, there are series of systems of fluvial and deltaic deposits. They are like the systems described earlier in considering the Texas Coastal Zone. Where they occur, there is somewhat more relief present and there is also somewhat more vegetation present. The region will be discussed in terms of remote sensing interpretation.

Remote sensing interpretation.--For interpreting the environmental geology and land resource units at the Houston Area Test Site, Proctor and Hall (1974) found the use of multispectral aerial photography to be definitely advantageous. There were black-and-white, color, and color infrared aerial photography at a scale of 1:120,000 available for the entire region. The definitive character of the land resource units was readily identified on color infrared photography as shown in figure 7. In the upper part of the photograph (fig 7) to the north above the irregular dashed line, there is a system that is dominated by fluvial sand. South of that line, the units are distributary channel sand bodies lying within overbank muds which make up more than 70 percent of the land area south of the previously described fluvial sand system. The difference between the system to the north and the system to the south is that the northernmost system was deposited higher up on the delta in the area where most of the mature streams were flowing. On the other hand, the system to the south, which makes up the bulk of the photograph, is lower on a deltaic plain, consequently it is finer grained and is composed principally of overbank muds. The overbank muds exhibit a speckled pattern suggesting a whole series of dotted playa areas retaining surface moisture in a clayey terrain. In the overbank mud area, land use is such that cultivated fields are quite large in extent. Comparatively, the sandstone units are brighter in hue than the muds. The land is also cultivated, but the fields are small and relatively narrow. Within the overbank muds, there are also residual oxbow lakes somewhat darker in tone as if they had been filled dominantly by clay. In the lower left corner of the illustration is a system dominated by a modern meandering stream which frequently floods.

Proctor and Hall (1974) found a very distinct advantage in using color

and color infrared remote sensing data, if available, rather than standard black-and-white remote sensing photography. For example, they could clearly recognize and map elongate sandstones on color photography (fig 8).

From the recognition of the environmental geologic units or land resource units that have been identified from remote sensing in the previous discussion, there is additional interpretation of great use to planners. This is the conversion of land resource units into what may be called either resource capability or land suitability units. It is possible to suggest the qualitative engineering properties for varied activities that might be conducted in the environmental units as shown in table 3. Capability or suitability evaluations are qualitative and do not involve consideration of a variety of engineering and technical data that can improve the use potential of a unit.

Southern Edwards Plateau

The southern Edwards Plateau (north of line CC in fig 9) is an area of approximately 8,000 square miles located in the headwaters of the Nueces, San Antonio, and Guadalupe River basins. It is important as the infiltration region and area of ground-water production from the subterranean Edwards Limestone aquifer. This subsurface aquifer is the sole source of potable water for San Antonio and its suburban area, which has a total population of nearly 850,000 people. An additional 150,000 people in smaller cities through the region depend on the same aquifer for water. Beyond the requirements for potable water, the aquifer also supplies water for more than 1,000 square miles of irrigated croplands.

The southern Edwards Plateau is also a major resort area. A large migrant summer population utilizes the region for dude ranches, swimming, canoeing, camping, and general sightseeing. It is also an area of considerable physical beauty. In the fall and winter, is is a major hunting preserve in Texas. Recently new development as a retirement center has impacted the region.

The area has about 1,500 feet of relief. At the divide to the north, the plateau is about 2,300 feet maximum elevation. In the plains and stream valleys in the south, the minimum elevation is about 800 feet. The plateau is deeply dissected by headward-eroding streams with very steep slopes in the north. There is a very clear break between the elevations of the plateau surface to the north (the dissected area), and the plains to the south (a lower area). The break generally coincides with an escarpment formed by the Balcones fault zone (line CC in fig 9).

The plateau area north of the Balcones fault zone is underlain by a thick section of carbonate rock. The lower portion of the section includes about 360 feet of alternating beds of limestone, dolomite and a marly limestone; about 60 percent of the section consists of soft limestones. Conversely, the upper part of the thick carbonate section is underlain by hard limestones and dolomites; limestone predominates over dolomite about four to one. The hard carbonate section forms a caprock in the upper part of the plateau, then the same vertical section is repeated in the downfaulted area of the Balcones fault zone. The alternating beds of limestone, dolomite, and very soft limestones containing a minimal amount of clay form a moderately rolling low terrain, locally stairstepped.

South of the major Balcones faulting and south of the limiting Edwards outcrop, there is a marked change in terrain. Maximum relief is about 100 feet in low rolling hills. The two types of outcrop that occur are (1) the normal succession of upper Cretaceous rocks including the Austin, Taylor, and Navarro Groups made up mostly of chalks and terrigenous mud rocks, and (2) broad, extensive gravel and sand that form fan plains just downdip of the Balcones faulting. At the base of the escarpment of the Edwards Plateau,

these fans extend southward and eastward as broad and elongate plains of clastics on which are developed a rich, well-drained loamy soil.

It is apparent in the description of the geology that there are two systems present. They are defined by geomorphology not sedimentary deposition or stratigraphy. One is the highly dissected carbonate terrane of the Edwards Plateau and the other is the rolling, low-relief terrain of plains south of the major faulting. The major zone of infiltration for the Edwards Limestone aquifer occurs in the plateau area; the area of production or withdrawal of ground water occurs in the low-relief southern plains. Only the dissected plateau system which contains thick carbonates and is the major area of ground-water infiltration, will be emphasized in this paper.

The general elements of the plateau system which are important in an environmental sense and relate to infiltration processes are shown in figure 9, after Morton (1974). Variables affecting infiltration and recharge rates are: (1) rock composition, (2) conduits reflecting porosity, permeability, and transmissivity of ground water, (3) soil and vegetation cover, (4) slope, and (5) the attitude of bedrock. These five variables are primary factors, and the mapping methodology is a secondary influence determining the derivation of the plateau environmental units. Where the rocks are limestone or dolomite, slope is probably the dominant property affecting recharge in the region. Variation in the development of soil and vegetation depends upon the slope; this factor remains constant over different calcareous rocks, regardless of their attitude. Limestone and dolomite behave similarly as soluble, dense fractured rocks; they can only be delineated by means of detailed ground mapping, not by remote sensing. It is essential that the remote sensing method used in this region permits the mapping of the relief and slope.

Remote sensing interpretation.--Remote sensing products available in the southern Edwards Plateau include 1:24,000 controlled black-and-white aerial photographic mosaics, 1:20,000 and 1:40,000 black-and-white stereoscopic aerial photography, one strip of SLAR imagery, and LANDSAT-1 imagery. The 1:24,000 controlled mosaics were not useful because neither slopes nor rock types could be distinguished. Rarely karstic terrane was apparent. However, the mosaics have proved valuable for studies of fracture zones--a separate study aimed at delineating variations in the vertical permeability of the aquifer.

Interpreters of environmental geology were totally dependent upon stereographic black-and-white aerial photography. An example is shown in figure 10. Even with stereographic aerial photography, it is not possible to differentiate between limestones and dolomites; slope variations, however, are well defined. From slope definition, it is possible to recognize areas that are dominated by runoff such as the deeply dissected terrain. Further, it is possible to clearly define nearly flat-lying carbonate beds that display karstic features, as for example, the karstic table land. Finally, the varied characteristics of fluvial deposits are readily separated one from another. Results of remote sensing interpretation of stereographic aerial photography are shown in two other forms. Figure 11 shows the results of slope mapping as compared to the topography and terrain which, in turn, are compared to the environmental interpretations that come directly from remote sensing imagery. Table 4 shows the derivation of both environmental geologic units and resource capability units with all of the inherent properties as recognizable from remote sensing.

Experimentation with SLAR imagery in the southern Edwards Plateau (Cannon, 1974) suggests its potential use in mapping carbonate terranes. However, to date only isolated environmental units have been illustrated. Regional continuity expressed by interpreting contiguous environmental

geologic units using SLAR has not been demonstrated. Experimentation with LANDSAT-1 imagery has not yet reached the point where it can be applied to mapping land suitability in carbonate terranes (fig 12). A major problem is the lack of topographic definition--an essential criterion for defining land suitability in carbonate terranes.

CONCLUSIONS

1. Stereographic black-and-white aerial photography is the most flexible, widely available, and least expensive remote sensing product from which one may readily interpret environmental geologic units or inventory land and water resources.

2. Color or color infrared stereoscopic aerial photography has the potential to replace black-and-white aerial photography in the future if it becomes less expensive.

3. Controlled black-and-white aerial photographic mosaics are adequate for either mapping flat terrain or mapping fracture zones.

4. The value of SLAR and LANDSAT imagery has yet to be demonstrated. Results to date suggest that it would be worthwhile to critically test both of these remote sensing products.

5. Numerical analysis of LANDSAT digital data presents an interesting challenge for automatically defining environmental geologic units and inventorying land and water resources.

REFERENCES

Brown, L. F., Jr., Fisher, W. L., Erxleben, A. W., and McGowen, J. H., 1971, Resource capability units--their utility in land- and water-use management with examples from the Texas Coastal Zone: Univ. Texas, Austin, Bur. Econ. Geology Geol. Circ. 71-1, 22 p.

_____, Fisher, W. L., and Malina, J. F., Jr., 1972, Evaluation of sanitary landfill sites, Texas Coastal Zone--Geologic and engineering criteria: Univ. Texas, Austin, Bur. Econ. Geology Geol. Circ. 72-3, 18 p.

_____, and Fisher, W. L., 1974, Environmental Geologic Atlas of the Texas Coastal Zone, in Approaches to Environmental Geology, E. G. Wermund (ed.): Univ. Texas, Austin, Bur. Econ. Geology Rept. Inv. 81, p. 25-51.

Cannon, P.J., 1974, The application of radar imagery to environmental geologic mapping, in Approaches to Environmental Geology, E. G. Wermund (ed): Univ. Texas, Austin, Bur. Econ. Geology Rept. Inv. 81, p. 229-235.

Fisher, W. L., McGowen, J. H., Brown, L. F., Jr., and Groat, C. G., 1972, Environmental geologic atlas of the Texas Coastal Zone--Galveston-Houston area: Univ. Texas, Austin, Bur. Econ. Geology, 91 p.

_____, Brown, L. F., Jr., McGowen, J. H., and Groat, C. G., 1973, Environmental geologic atlas of the Texas Coastal Zone--Beaumont-Port Arthur area: Univ. Texas, Austin, Bur. Econ. Geology, 93 p.

Morton, R. A., 1974, Delineation and environmental application of active processes mapped in recharge area of the Edwards aquifer, in Approaches to Environmental Geology, E. G. Wermund (ed.): Univ. Texas, Austin, Bur. Econ. Geology Rept. Inv. 81, p. 204-219.

Proctor, C. V., Jr., and Hall, W. D., 1974, Environmental geology of the greater Houston area, in Approaches to Environmental Geology, E. G. Wermund (ed.): Univ. Texas, Austin, Bur. Econ. Geology Rept. Inv. 81, p. 123-134.

St. Clair, Ann, Brown, L. F., Jr., Proctor, C. V., Jr., and Wermund, E. G., in preparation, Land and water resources in the Houston-Galveston area council: Univ. Texas, Austin, Bur. Econ. Geology, Map Series on Land and Water Resources.

Wermund, E. G., 1974, Environmental units in carbonate terranes as developed from a case study of the southern Edwards Plateau and adjacent interior Coastal Plain, in Approaches to Environmental Geology, E. G. Wermund (ed.): Univ. Texas, Austin, Bur. Econ. Geology Rept. Inv. 81, p. 52-78.

Table 1. Results of mapping and inventorying land resources and environmental geology.

Area	Square Miles	Map Type	Number of Features	Mapping Scale	Presentation Scale	Status
Texas (statewide)	267,339	Land and water resources	78	1:250,000	1:500,000	Hand colored, in color separation
Texas (statewide)	267,339	Land use	8	1:250,000	1:250,000	Completed, inc. patterns, open file
Coastal Zone Atlas	20,000	Environmental geology	69	1:24,000	1:125,000	Printed in color; described by text; 8 derivative maps at 1:250,000; Physical Properties, Active Processes, Biologic Assemblages, Economic Resources, Land Use, Man-Made Features, Topography and Bathymetry
Coastal Hazard Atlas	20,000	Active processes	13	1:24,000	1:250,000	Printed in two colors with text
Coastal Bend COG	12,195	Land and water resources	43	1:24,000	1:125,000	Printed in color
Houston-Galveston COG	12,444	Land and water resources	45	1:24,000 1:120,000	1:125,000	In color separation, to be printed by July 1, 1975
Capital City COG	5,710	Environmental geology	33	1:40,000	1:125,000	Hand colored, in manuscript
Corpus Christi — 4 counties	2,575	Land and water resources	40	1:20,000	1:125,000	Printed in color
Padre-Mustang Island complex	50	Land and water resources	16	1:2000	1:24,000	Black-and-white patterns; in press
Lake Travis vicinity	135	Environmental geology	7	1:20,000	1:96,000	2 colors, in press
Austin vicinity	712	Environmental geology		1:24,000	1:96,000	Color separation, plus maps of economic resources, physical materials, land use, and slopes
Nueces, San Antonio, Guadalupe River basins	33,000	Environmental geology	103	1:24,000	1:125,000	Scribing and first hand color out
East Texas lignite belt	3,000	Environmental geology	15	1:24,000	1:125,000	First year of work in progress as of 1/1/75
Inner coastal plain	22,000	Environmental geology	62	1:24,000	1:125,000	Colored out; basic maps of three unpublished dissertations

REPRODUCIBILITY OF THE ORIGINAL PAGE IS POOR

Table 2. Environmental geology map units, Texas Coastal Zone, after Brown and Fisher (1974).

HOLOCENE-MODERN SYSTEMS

Fluvial-Deltaic Systems

Meanderbelt sand, tree-covered, inactive, entrenched stream
Meanderbelt sand, prominent grain, inactive, non-entrenched stream
Fluvial sand and flood-basin mud, undifferentiated, inactive, non-entrenched stream
Meanderbelt sand and silt, sparsely grass- and shrub-covered, inactive within an entrenched stream
Interdistributary silt and mud, locally includes bay, lacustrine and crevasse splay
Flood basin, overbank mud and abandoned channel, mud-filled, inactive, within entrenched stream
Levee deposits, fresh-water, marsh-covered
Levee and crevasse splay deposits, silt, sand and mud, grass-covered
Levee and crevasse splay deposits, silt, sand and mud, tree-covered
Delta-plain mud and sand, sparsely grass-covered
Delta-plain mud and sand, grass covered
*Delta front and channel-mouth bar sand shoal (active and abandoned)
*Prodelta mud and silt
Point bar, sand, tree-covered, along active streams
Point bar, sand, bare or sparsely vegetative, along active streams
*Abandoned channel and course, mud-filled
*Abandoned channel and course, swamp-covered, mud-filled
*Abandoned channel and course, fresh-water, marsh-covered, mud-filled
*Marsh, salt-water, mud and locally sand substrate
*Marsh, fresh- to brackish-water, mud and locally sand substrate
*Marsh, fresh-water, mud and locally sand substrate
*Swamp, mud and locally sand substrate
*Tidal creek, fresh- to brackish-water, marsh-covered, mud-filled
*Tidal creek, mud-filled
*Wind-tidal flat, sand and mud, transitional between bay and stream
Small active, headward-eroding stream, tree-covered to barren
*Berm and beach ridge, abandoned, sand and shell
*Fan and fan delta, sand, subaerial

Barrier-Strandplain-Chenier and Offshore Systems

Shelf mud and sand, mottled
Shoreface, mud, burrowed
Shoreface, sand and muddy sand, burrowed
Coastal mudflat, subject to tidal inundation
Beach, sand and shell
Barrier flat, sand and shell, very sparse grass
Beach ridge and barrier or strandplain flat, grass-covered, sand and shell
Sandflats and/or coppice sand-dune fields, active
Fore-island blowout dunes and back-island dunes, sand, active
Fore-island dune ridge, sand
Chenier beach ridge, sand, grass-covered
Chenier flat, sand and shell, grass-covered
Strandplain-barrier oak motte
Stabilized blowout dune complex, sand, grass-covered, hummocky
Washover channel, sand-filled, inactive
Washover channel, sand, active
Washover fan, sand, subaerial, vegetated
Washover fan, distal, sand, subaerial, barren, active
Ebb-tidal delta, mud and sand, subaqueous
Ebb-tidal delta, sand, subaqueous, proximal to channel
Ebb-tidal delta, mud and sand, subaqueous, distal to channel
Flood-tidal delta, mud, subaqueous
Flood-tidal delta, mud and sand, subaqueous, distal to channel
Flood-tidal delta, sand, subaqueous, proximal to channel
*Tidal channel, mud and some sand, active
Tidal channel, sand, active
Tidal channel, mud- and sand-filled, inactive
Inlet-related shoal, sand, accretionary in passes
Wind-tidal flat, subaerial, burrowed
Tidal flat, sand
*Swale between beach ridges, mud-filled
*Swale between beach ridges, fresh- to brackish-water, marsh-covered, mud-filled
*Marsh, salt-water, mud and locally sand substrate
Back-island sandflats with small migrating dunes, unvegetated
Wind-deflation trough and storm runnel on barrier flat, sand

Marsh-Swamp System

*Marsh, salt-water, mud and locally sand substrate
*Marsh, brackish-water, closed system, mud and locally sand substrate
*Marsh, fresh- to brackish-water, mud and locally sand substrate
*Coastal lake or pond, partially or completely mud-filled
*Marsh, fresh-water, and poorly drained depressions, mud and locally sand substrate
*Swamp, mud and locally sand substrate

Bay-Estuary-Lagoon System

*Fan and fan delta, sand, subaerial, along bay margin
*Berm or beach ridge, abandoned, sand and shell (P/M)
Bay- or lagoon-margin sand, locally with mud and shell, subaqueous
Bay- or lagoon-margin sand and mud; shell berms, beaches and spits, active, subaerial
Bay-margin oolites and quartz sand
Bay-margin quartz sand and calcite-coated grains
Sand shoal with some oolites
Bay and bay-margin sandy mud, mottled, some shell
Grassflat, muddy sand with shell
Bay sand with mixed shell
Bay and lagoon mud, mottled, some mixed shell
Bay sand with oyster shell
Bay mud with oyster shell
Bay sand
Bay mud and silt
Bay and lagoon sand, muddy
Bay mud, laminated, rare shell
Bay sand and muddy sand, locally with oyster shell
*Prodelta mud and silt
*Delta front and channel-mouth bar sand shoal (abandoned and active)
Oyster reef
Oyster reef flank, sand or mud, abundant shell
Interreef mud with oyster shell
Serpulid reefs and related shell-rich sand and beach rock
Wind-tidal flat, sand, loose, rarely flooded
*Wind-tidal flat, sand and mud, extensive algal mats, alternately emergent-submergent
Wind-tidal flat, mud and sand, algal-bound mud, gypsiferous, firm
Wind-tidal flat, mud and sand, algal mats, depressed relief, wet and soft

REPRODUCIBILITY OF THE
ORIGINAL PAGE IS POOR

Table 2. Environmental geology map units, Texas Coastal Zone, after Brown and Fisher (1974) - concluded.

Wind-tidal flat, sand and mud, barren to sparsely vegetated, subaerial
Marginal residual sand apron on windward side of rincons and potreros, wind-deflation lag deposit
Eolian accretionary bars and ridges, sand and clay, on wind-tidal flats
Transitional zone, wind-tidal flat to eolian sand sheet, wind deflation

Eolian System

Active dune complex, sand, commonly banner dunes with small barchans
Active dune blowout areas, sand, local depressed relief, eolian grain prominent
Sand sheet with strong relict grain of base-leveled dunes
Sand and loess (silt) sheet with no relict grain
Moderately stabilized dunes, sand and loess (silt) sheet, brush-covered
Well-stabilized dune sands, live oak-covered
Sand and loess (silt) sheet deflation area, active
*Clay-sand dunes, accretionary, active
*Clay-sand dune complexes, inactive (H/M)
*Loess sheet, thin, silty, overlies calichified Pleistocene fluvial sand (H/M)
*Loess sheet, thin, discontinuous, silty, overlies Pleistocene deltaic mud and calichified sand (H/M)

Other Map Units

Point bar (fluvial) accretion grain
Beach ridge (barrier-strandplain-chenier) accretion grain
Spoil heap or mound, subaerial
Reworked spoil, subaerial
Spoil, subaqueous
Made land
Barchan dune orientation in banner dune complex
Longitudinal dune orientation in back-island dune field
Beach ridges, accretionary, relict (barrier-strandplain)
Wind accretion ridges, rincons and potreros
Serpulid reefs

PLEISTOCENE SYSTEMS

Fluvial-Deltaic Systems

Meanderbelt sand
Flood-plain mud
Flood-plain mud veneer over meanderbelt sand
Distributary sand and silt
Interdistributary mud
Interdistributary mud with sand veneer
Delta-front mud and sand, veneered by thin mud
Delta-front mud and sand
*Abandoned channel and course, mud-filled (P/M)
*Abandoned channel and course, swamp-covered (M)
*Abandoned channel and course, fresh-water, marsh-covered (P/M)
*Tidal creek, fresh- to brackish-water, marsh-covered (M)
*Tidal creek, unvegetated, mud-filled (M)
*Tidal creek, fresh-water, marsh-covered (M)
*Tidal creek, grass-covered, mud-filled (P/M)
*Marsh, fresh-water, and poorly drained depressions, mud and sand
*Upland oak motte
*Loess sheet, thin, overlies Pleistocene fluvial sand (M)
*Loess sheet, thin, discontinuous, overlies Pleistocene mud and sand (M)
Circular to irregular depressions on distributary/fluvial sand (P/M)
*Clay-sand dunes, active (M)
*Clay-sand dunes, inactive (H/M)
Lakes and ponds, coastal, mud and sandy mud-filled (P/M)
*Beach ridge and berm, margin of lakes, shell (P/M)
*Swale between beach ridges, margin of inland lakes, mud-filled (P/M)

Barrier-Strandplain Systems

Barrier-strandplain sand, tree-covered
Barrier-strandplain sand, grass-covered
Live oak-covered beach ridge, relict
Swale between beach ridges, unvegetated, mud-filled (P/M)
Swale between beach ridges, grass-covered, mud-filled (P/M)
Sheet sand, locally mud-veneered, back side of Pleistocene strandplain
Well-stabilized dune sand, dense live oak mottes (M)
*Marsh, fresh-water and poorly drained swales, mud- and sand-filled (M)

* Unit may occur within more than one system
M Modern
P/M Pleistocene to Modern
H/M Holocene and Modern

Table 3. Resource capability units -- use and capability. Evaluations are based on natural capability which can be improved by engineering. Blank areas represent either no problem or the use is not applicable on the particular resource capability unit. x = undesirable; will require special planning and engineering. o = possible problem(s). After Proctor and Hall, 1974.

RESOURCE CAPABILITY UNITS		ACTIVITIES	Liquid Waste Disposal			Solid Waste Disposal	Inland Construction										
			Surface Disposal of Untreated Liquid Wastes	Disposal of Untreated Liquid Wastes, Subsurface, Shallow	Maintenance of Feed Lots	Disposal of Solid Waste Materials	Placement of Pipelines and/or Subsurface Cables	Light Construction	Construction of Highways	Heavy Construction	Flooding (through dam construction)	Dredging of Canals and Channels, and Spoil Disposal	Excavation (includes extraction of natural materials)	Filling for Development	Draining of Wetlands	Well Development	Devegetation	Use of Herbicides, Pesticides, Insecticides
FLOOD-PLAIN UNITS	I_1	Active, headward-eroding stream valleys	x	x	x	x	o	x	o	o		o	o	x		o	x	x
	I_2	Meanderbelt sands	x	x	x	x		x		o		o		x		o	x	x
	I_3	Overbank mud and silt	x	x	x	x	o	x	o	o	o	o		x		o		o
	I_4	Meanderbelt sand and overbank mud, undifferentiated	x	x	x	x	o	x	o	o	o	o		o		o	x	x
	I_5	Terrace sands	x	x	x	x			o		o	o					x	x
WETLANDS	II_1	Marsh, swamp, and local abandoned channels within major flood-plain systems	x		x	x	o	x	x	x	x	o	x	x	x	o	x	x
GEOHYDROLOGIC UNITS	III_1	Highly permeable recharge sands	x	x	x	x					o	o				o		
	III_2	Elongate recharge sands	x	x	x	x						o				o	x	x
	III_3	Moderately permeable recharge sands and clayey sands	x	x	x	x						o				o	x	x
PHYSICAL UNITS	IV_1	Unstable sandy clay, marginal croplands	x	o			o	o	o	o						o		o
	IV_2	Unstable clay, good cropland	o				o	o	o	o						o		
	IV_3	Unstable clay, poor cropland	o				o	o	o	o						o	x	o
SUBSTRATE UNITS	V_1	Siliceous gravel and sand	x	x	x	x		o		o	o	o				o	x	x
	V_2	Glauconite-ironstone sandy clay	x				o	o		o							o	
	V_3	Mixed sandy clay and lignite	o				o	o	o	o	o						o	o
	V_4	Tuffaceous sand and sandy clay	x	x	x	x	o	o	o		o					o		x
OTHER UNITS	VI_1	Steep slopes and alluvial fans	x	o	x	x			o	o	o		x				x	x
	VI_2	Water bodies	x			x						x						x

REPRODUCIBILITY OF THE ORIGINAL PAGE IS POOR

Table 4. Properties and characteristics of environmental units and resource capability units derived from remote sensing and field study in the southern Edwards Plateau, after Wermund, 1974.

Unit	Karstic tableland	Karstic lowland	Deeply dissected	Moderately dissected	Upland rolling
Bedrock	Limestone Dolomite	Limestone Dolomite	Limestone Dolomite	Limestone Dolomite	Limestone Dolomite
Maximum relief (ft.)	40	100	800	100	40
Slopes	<5%	5-15%	>15%	5-15%	<5%
Soil	Dark, mildly alkaline clay	Dark, mildly alkaline clay. Thick in solution pits	Very thin dark clay	Stable alkaline clay	Dark clay of variable thickness
Vegetation	Grassy prairie Live oak mottes	Grassy prairie Live oak mottes	Sparse scrub juniper and live oak	Scrub juniper and live oak locally dense. Some open grass	Prairie
Structure Morphology	Joints with solution effects	Joints with strong solution evidence	Rock pavements Strongly jointed	Jointed	Some rock pavements
Man altered	Often root plowed	Some chaining and root plowing	None	Rare chaining Quarrying	Chained
Remarks	Sinkholes, shallow and often old	Both old and young sinkholes	Many cliffs of bare rock	Concave slopes	Flats are deeply dissected
Dominant Process	Recharge	Recharge	Runoff	Runoff Recharge	Recharge
Resource Capability Units	Recharge Carbonate Rangeland	Recharge Carbonate Rangeland	Rugged Carbonate Scenic	Recharge Carbonate Rangeland	Recharge Carbonate Rangeland

Table 4 (continued) –

Low rolling	Flood plain	Terrace	Alluvial fan	Colluvial	Mixed Alluvial-Colluvial
Limestone Alternating beds	Rounded gravel to mud-size clasts	Rounded gravel to mud-size clasts; may be caliche cemented	Subrounded gravel to mud; tough deep caliche cement to depths of 8 feet	Angular clasts of carbonate—caliche cemented	Angular and rounded clasts of carbonate from cobble to silt
20, often dip slope	20 where incised	20	60	100	40 to >100
<5%	<5%	<5%	5-15%	>10%	5 to >15%
Dark clay thicker on alternating beds	Calcareous, friable loam	Light, calcareous, friable, gravelly loam	None to thin, dark alkaline clay over thick caliche	Rubble area caliche	Barren in steeper colluvium to thick arable loam in high terrace
Juniper and live oak	Cypress	Dense to moderate stands of pecan and walnut	Sparse cedar and live oak	Generally barren	Prairie grass to oak-juniper stands
Some rock pavements	Jointed bedrocks	Torrential cross-bedding exposed in borrow pits	Creep scars of soil mass wasting over caliche	None	Creep scars and shallow fluvial gulleys
Tilled	Rare borrow pits	Caliche and gravel borrow pits	Caliche borrow pits	None	Lower part plowed; borrow pits
Some intermixed colluvium	Underfit streamflow in alluvium on bedrock floor	Sometimes cultivated. Prime housing site	Ubiquitous caliche. Often incised by a stream	Thick caliche, usually with incised streams	Always deep caliche. Individual alluvial units impossible to resolve
Recharge	Recharge	Recharge	Runoff	Colluviation	Runoff Recharge
Recharge Carbonate Arable Rangeland	Nonpermanent Recreational Flood plain	Arable Rangeland Gravelly loam	Sheetwash Caliche Gravel Rangeland	Colluvial Sheetflood Barren Caliche	Mixed alluvial-colluvial Rangeland

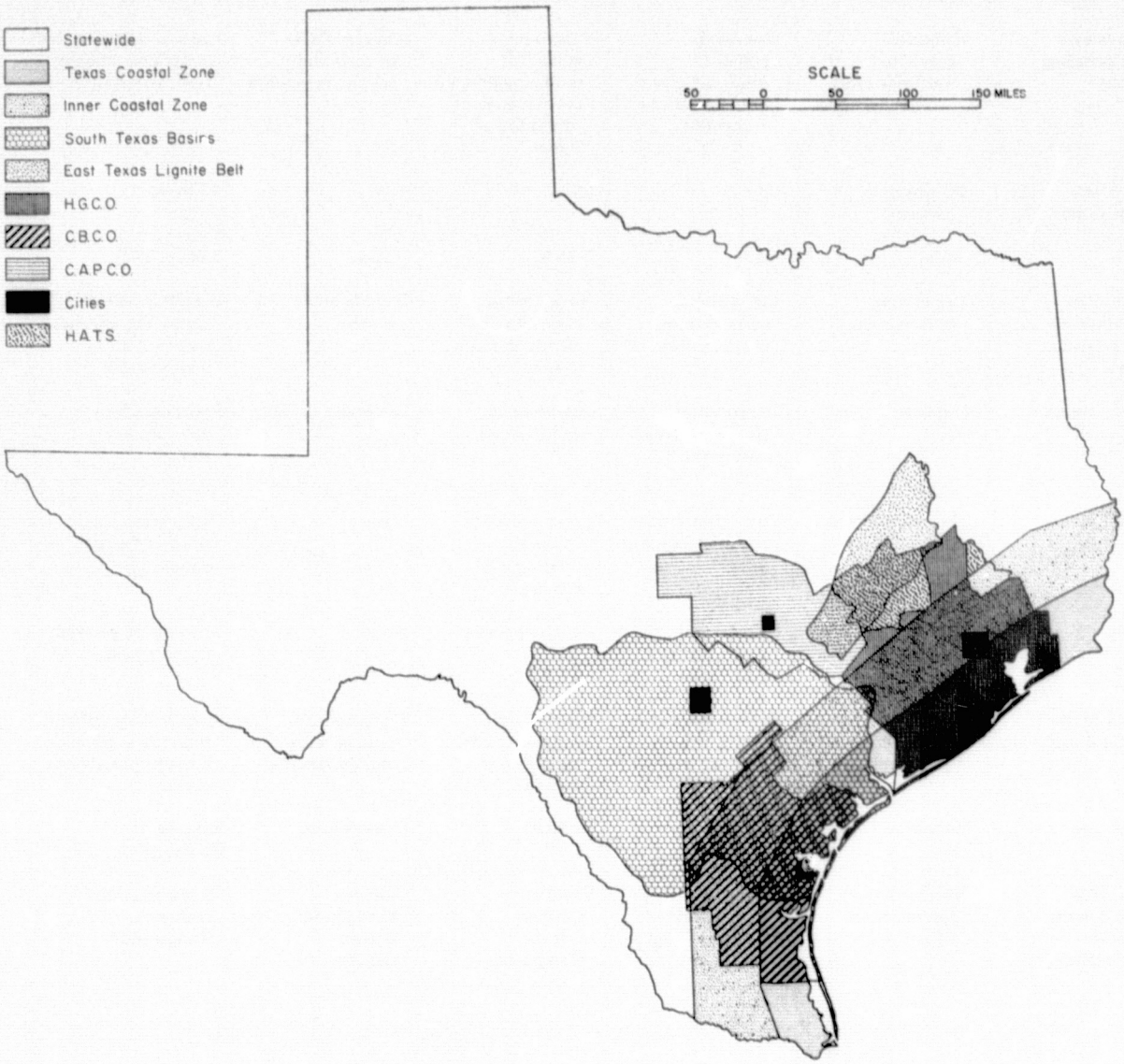


Fig. 1. Areas for which the Bureau of Economic Geology inventoried land and water resources by means of environmental geologic mapping using remote sensing.

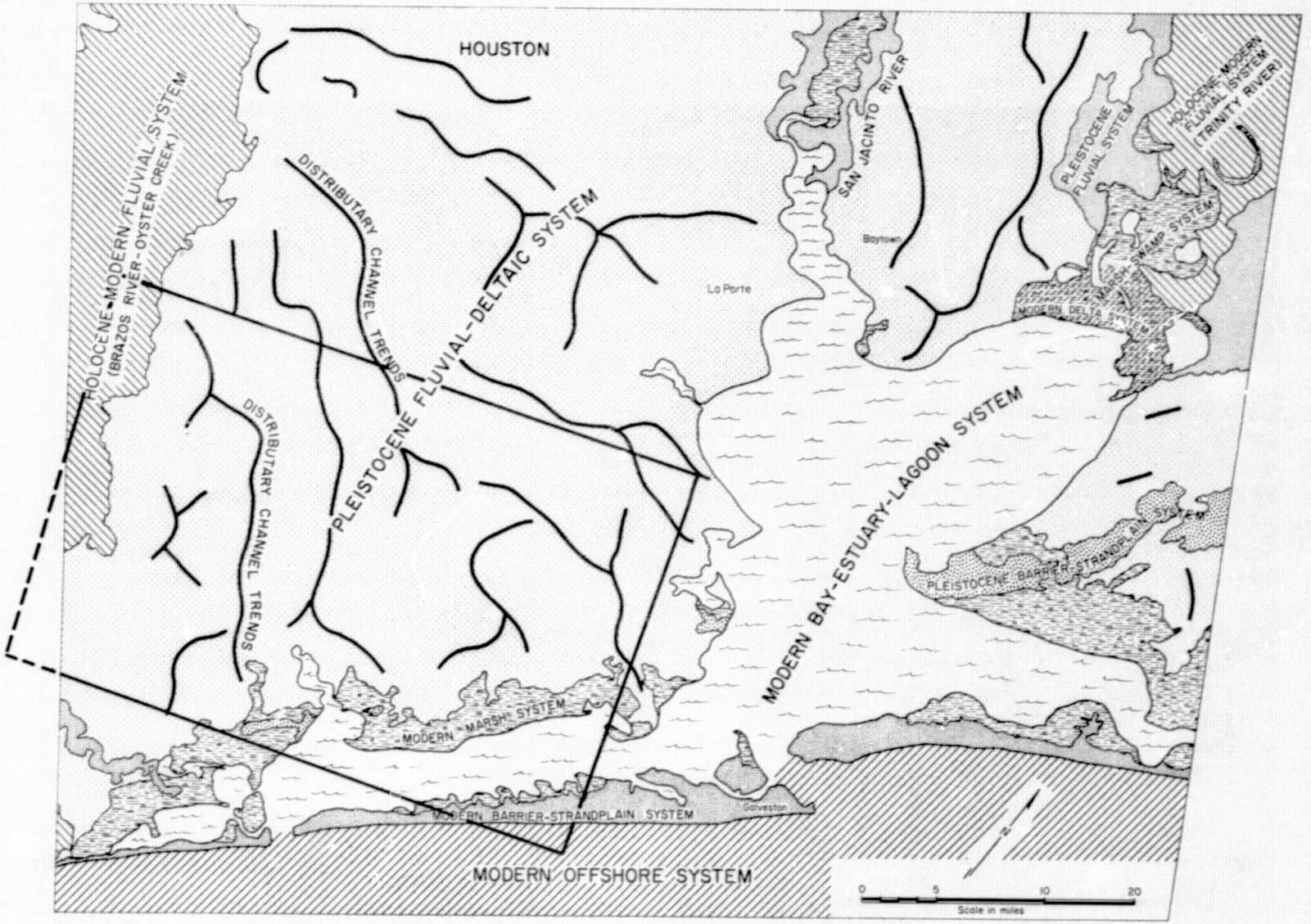


Fig. 2. Natural systems defined by environmental mapping in the Galveston-Houston area. These systems are composed of genetically related environments, sedimentary substrates, biologic assemblages, areas of significant physical processes, and man-made features. Simplified from the Environmental Geology Map of the Atlas. After Fisher and others, 1972.



Fig. 3. A portion of a 1:24,000 black-and-white controlled aerial photographic mosaic on which environmental geologic units were recognized from variations in tone, texture, fabric, and geometry. The units relate to a Pleistocene fluvial-deltaic system shown in figure 4.

REPRODUCIBILITY OF THE
ORIGINAL PAGE IS POOR

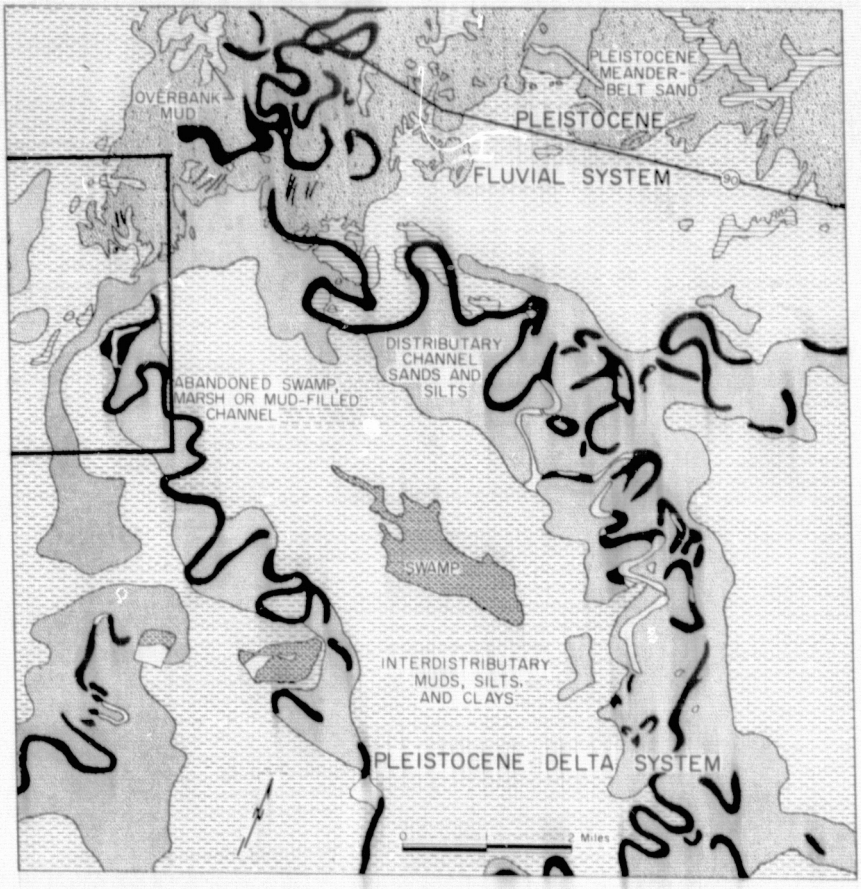


Fig. 4. Pleistocene fluvial-deltaic facies, coastal uplands in vicinity of Devers, Beaumont-Port Arthur area. Meanderbelt sands appear to grade coastward into elongate bands of sand and silt that were deposited principally during delta building. Area of figure 3 is outlined in upper left portion. After Fisher and others, 1973.

ORIGINAL PAGE IS POOR
REPRODUCIBILITY OF THE

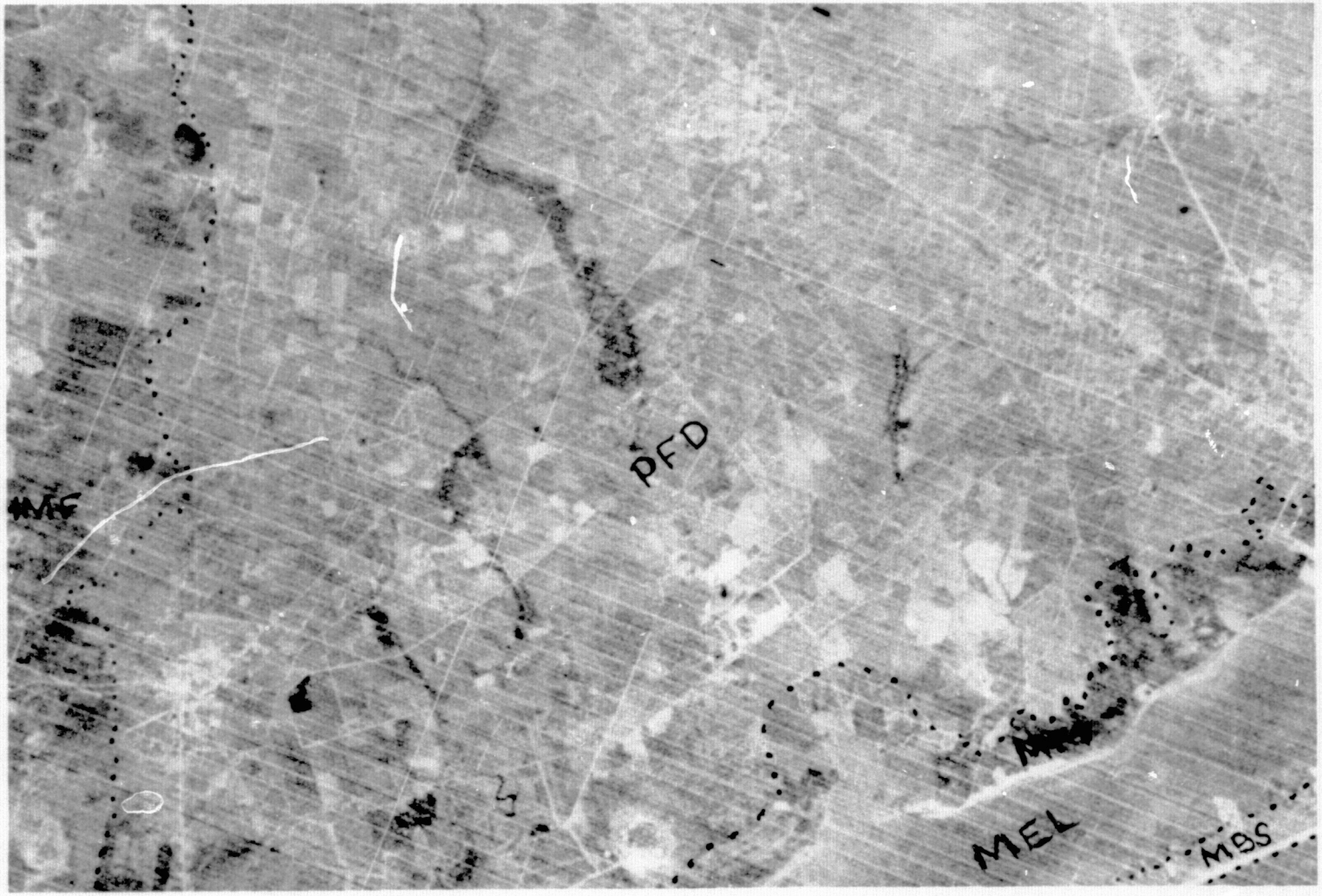


Fig. 5. LANDSAT-1 imagery of band 4, 1:250,000, showing an area of the natural systems outlined in figure 2. Dotted lines suggest boundaries among HMF, Holocene-Modern Fluvial System; PFD, Pleistocene Fluvial-Deltaic System; MM, Modern Marsh System; MEL, Modern Bay-Estuary-Lagoon System; and MBS, Modern Barrier-Strandplain System.

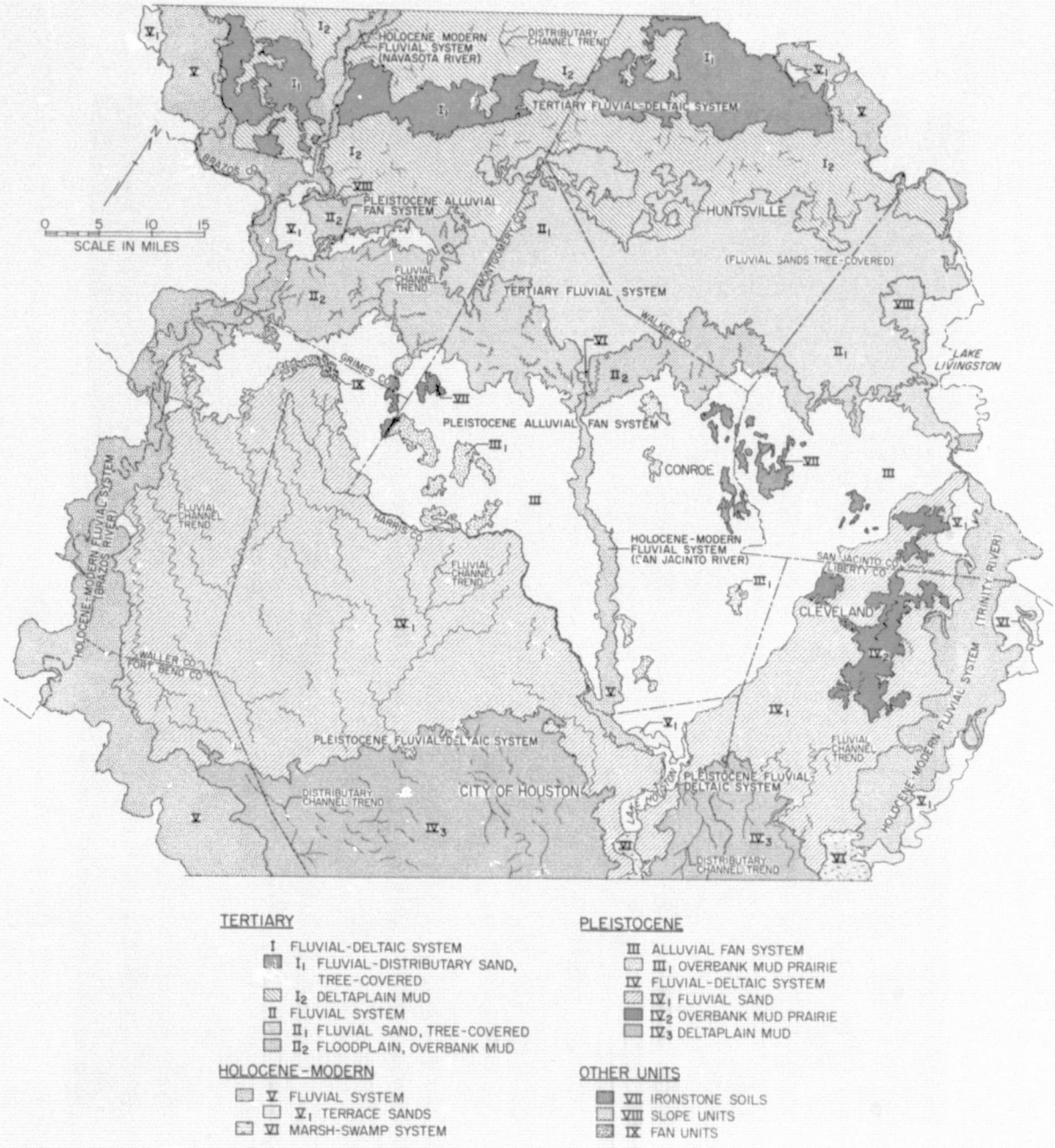
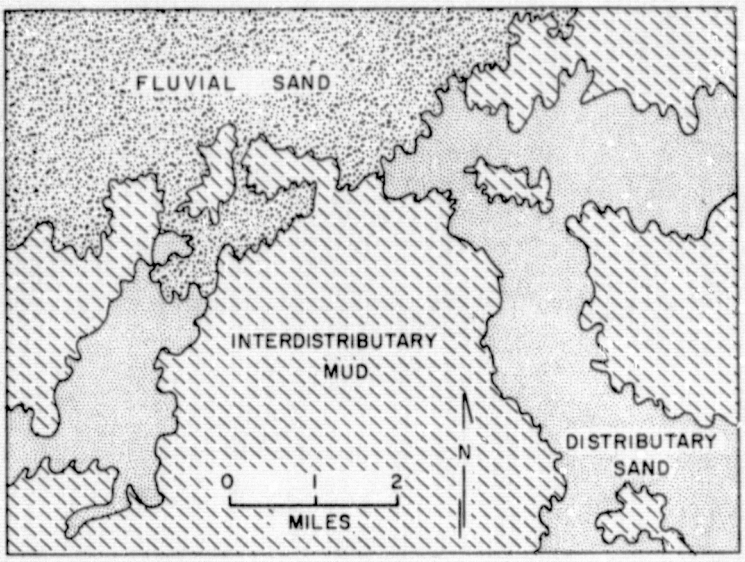


Fig. 6. Natural systems defined by environmental geologic mapping in the Greater Houston Area. After Proctor and Hall, 1974. Black square shows location of photography in figure 7.

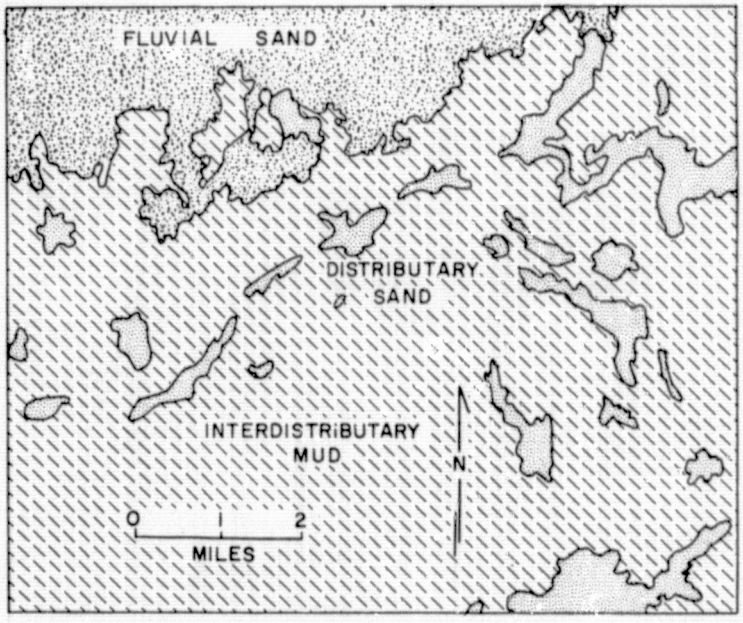


Fig. 7. A portion of a 1:120,000 infrared color aerial photograph on which resource capability units were recognized from variations in color, tone, texture, fabric, and geometry. In the northern part, the system is a fluvial sand high upstream on a delta plain, whereas in the southern 90 percent of the photograph, the system lies near the delta mouth on the distal deltaic plain. F, fluvial sand; S, sand; OM, overbank mud; and M, modern.

REPRODUCIBILITY OF THE
ORIGINAL PAGE IS POOR



A.



B.

Fig. 8. Sand trends interpreted in a high-mud deltaic system of the Greater Houston area. A was interpreted on 1:120,000 color infrared stereo aerial photography, whereas B was interpreted on 1:60,000 black-and-white stereo aerial photography. After Proctor and Hall, 1974.

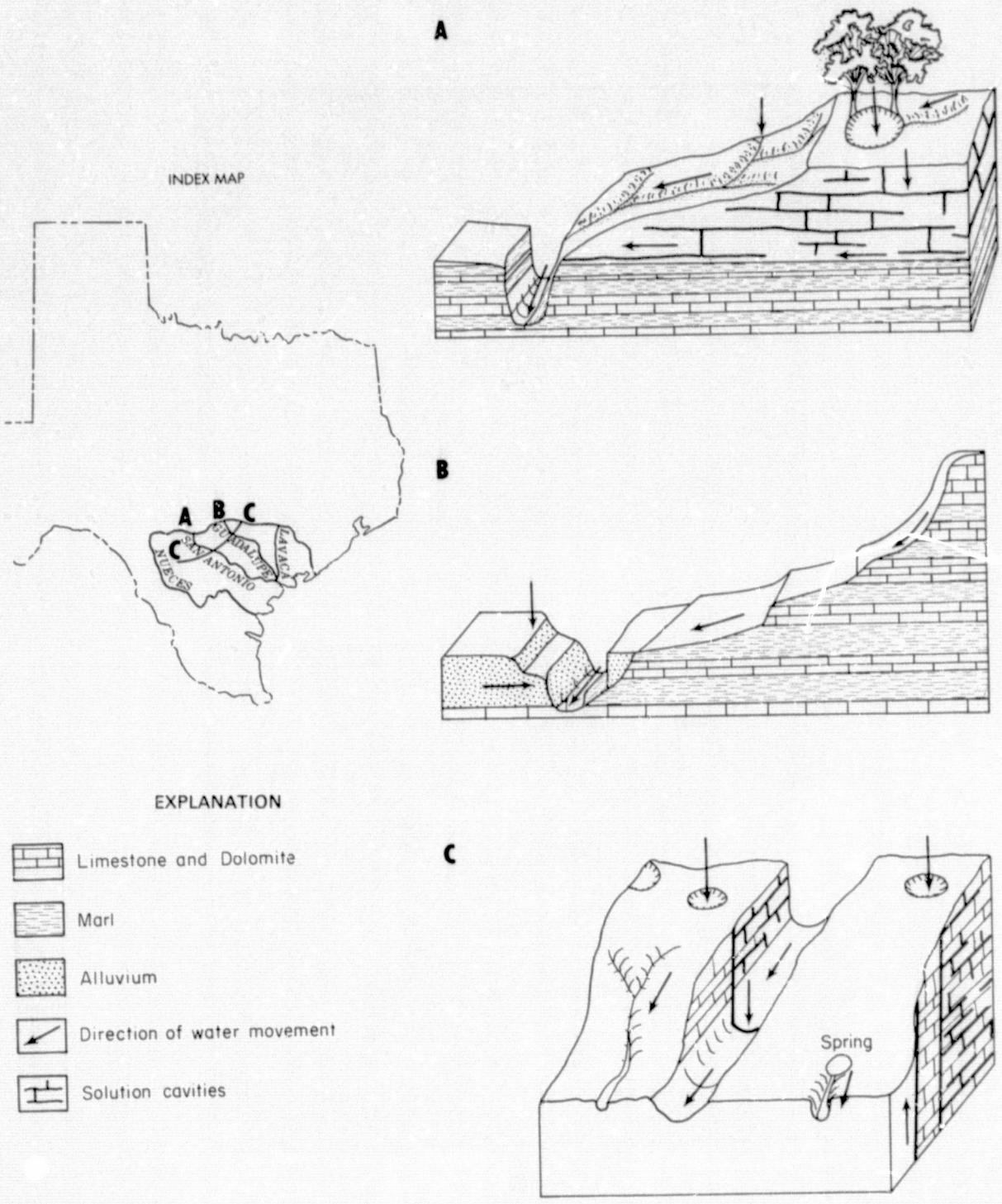


Fig. 9. Schematic diagram of recharge and ground-water movement in the southern Edwards Plateau. Major controls for recharge are slope, soil cover, vegetative cover, and rock type. After Morton, 1974.

REPRODUCIBILITY OF THE
ORIGINAL PAGE IS POOR

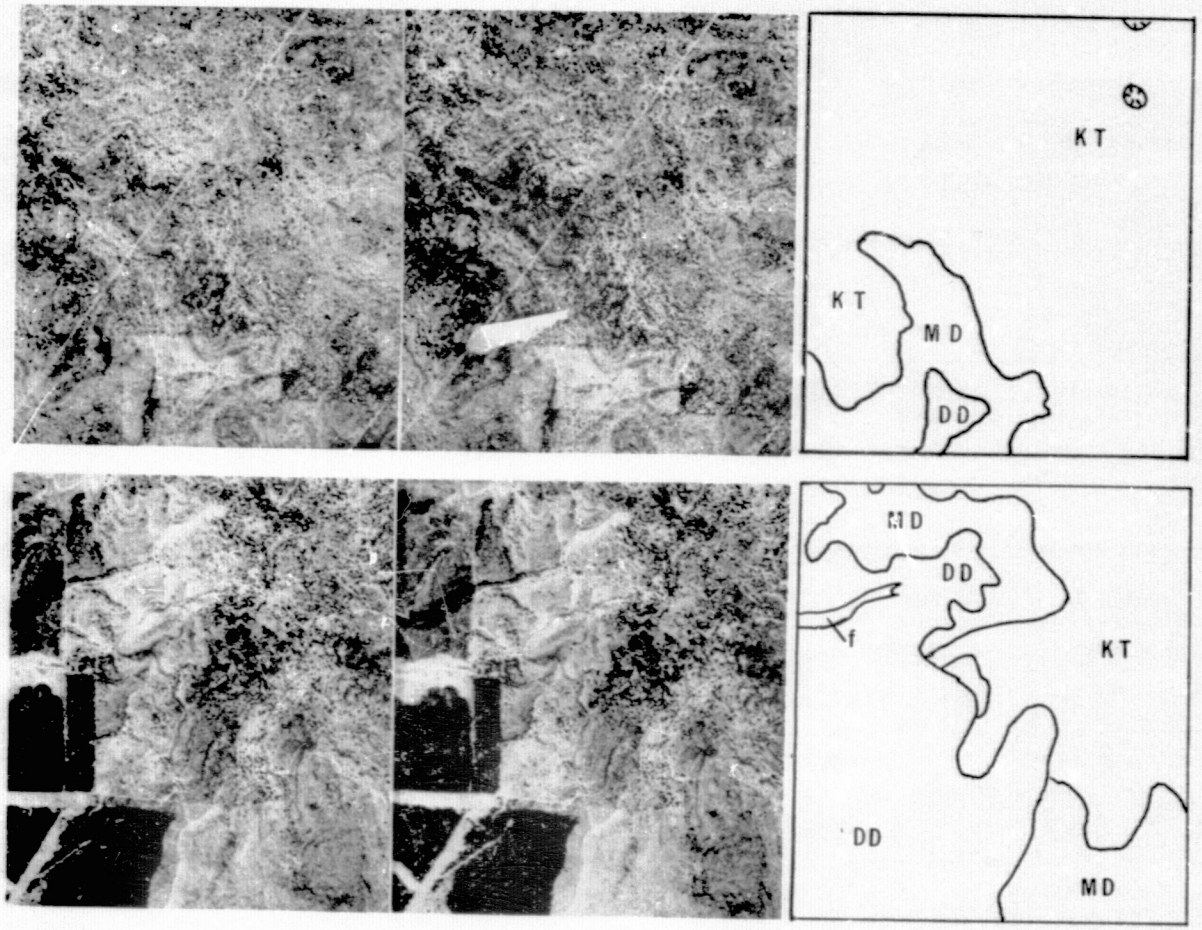


Fig. 10. Black-and-white stereo aerial photographs and an environmental geologic map illustrating the following environmental geologic units: KT, karstic tableland; MD, moderately dissected carbonate; DD, deeply dissected carbonate; and f, fluvial deposits.

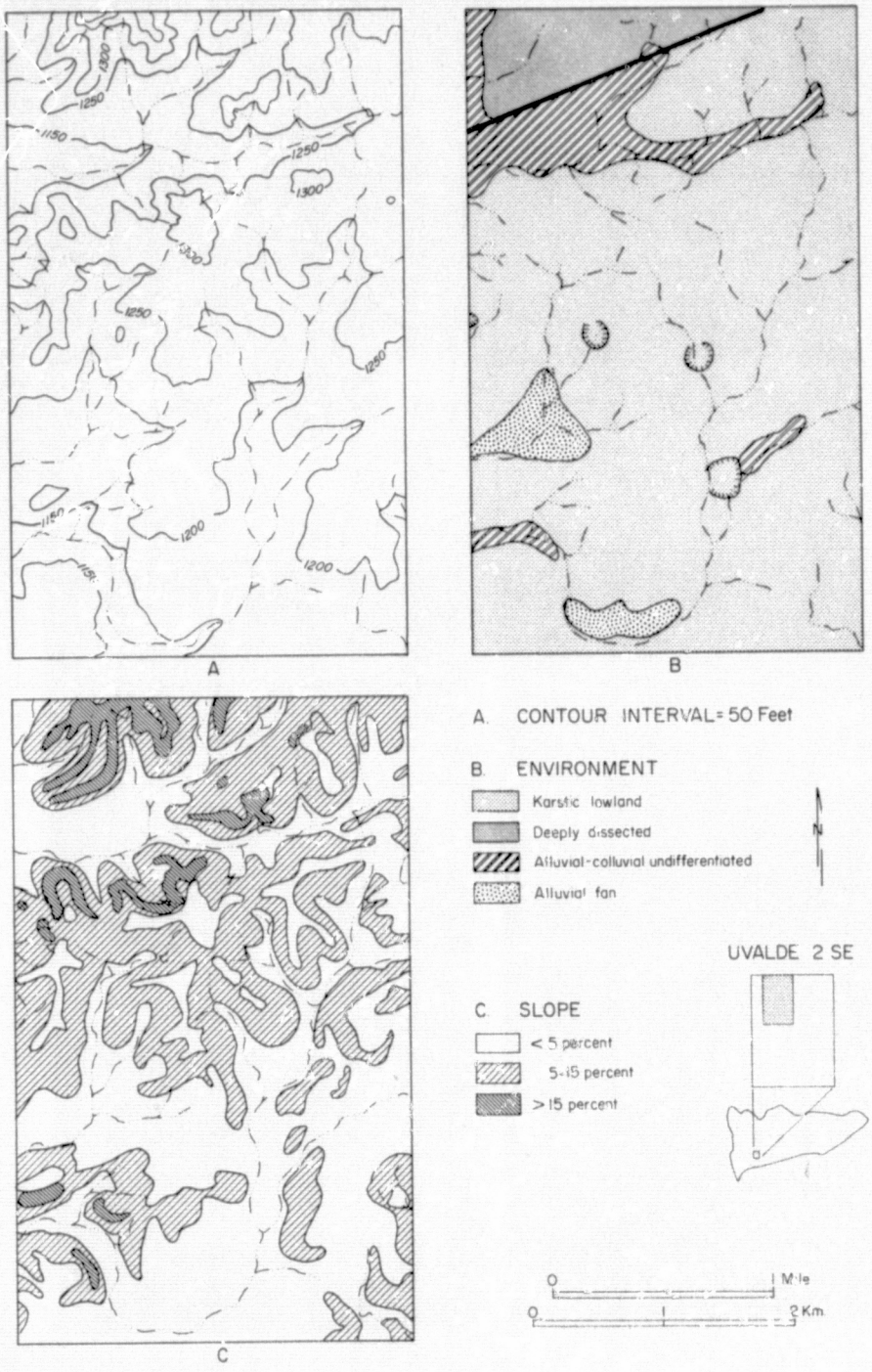


Fig. 11. A portion of the Balcones fault zone of the southern Edwards Plateau showing interrelation of A, topography; B, environmental; and C, slope units. After Wermund, 1974.

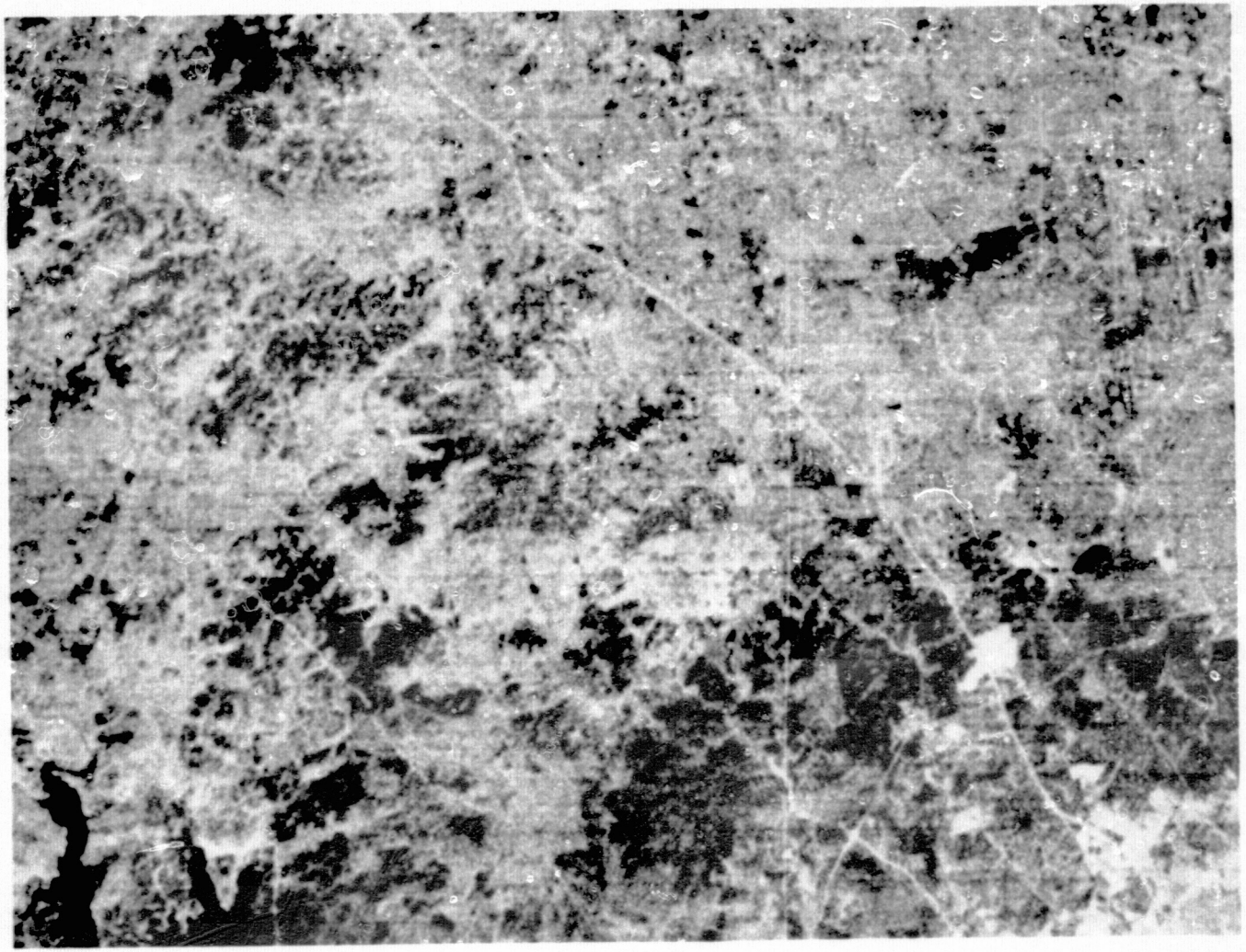


Fig. 12. A portion of a 1:250,000 frame of LANDSAT-1 imagery, Band 5, showing the area immediately north and west of San Antonio. The black arms of Lake Medina are apparent in the lower left. The dark gray dissected terrain is underlain by Edwards limestone. The pale areas are underlain by alternating beds of Glen Rose limestone.

Page intentionally left blank

MINERAL TARGET AREAS IN NEVADA FROM GEOLOGICAL ANALYSIS OF LANDSAT-1 IMAGERY

G-28

Monem Abdel-Gawad and Linda Tubbesing
Rockwell International Science Center
Thousand Oaks, California 91360

N76-17523

ABSTRACT

Geological analysis of LANDSAT-1 Scene MSS 1053-17540 suggests that certain known mineral districts in east-central Nevada frequently occur near faults or at faults or lineament intersections and areas of complex deformation and flexures. Seventeen (17) areas of analogous characteristics were identified as favorable targets for mineral exploration. During reconnaissance field trips we visited eleven areas. In three areas we found evidence of mining and/or prospecting not known before the field trips. In four areas we observed favorable structural and alteration features which call for more detailed field studies. In one of the four areas limonitic iron oxide samples were found in the regolith of a brecciated dolomite ridge. This area contains quartz veins, granitic and volcanic rocks and lies near the intersection of two linear fault structures identified in the LANDSAT-1 imagery. Semiquantitative spectroscopic analysis of selected portions of the samples showed abnormal contents of arsenic, molybdenum, copper, lead, zinc, and silver. These limonitic samples found were not *in situ* and further field studies are required to assess their source and significance.

PREFACE

Over the past four years, the Rockwell International Science Center has been pursuing research on the applications of space photography in the discipline of geology. In addition to the Rockwell International supported effort, the Science Center has been under contract to NASA Goddard Space Flight Center (LANDSAT-1 Contract #NAS5-21767) and Johnson Space Center (Skylab Contract #NAS2-7523) to perform investigations related to the identification and interpretation of regional geological structures from space imagery and to attempt to correlate known mineral deposits with these observed geological structures.(Abdel-Gawad and Tubbesing, 1974, 1975a, 1975b). As part of the Rockwell funded application of this technology, the Science Center has carried out an IR&D project for establishing the feasibility of utilizing space imagery to locate favorable target areas for future mineral exploration. The space imagery used in this study were taken by the NASA Resources Technology Satellite LANDSAT-1. This report presents a summary of the results of the IR&D project.

INTRODUCTION

One of the objectives of our research project funded by Rockwell International Science Center (CFY 1974) was to investigate the application of space imagery for identifying targets for mineral exploration and to carry out field studies in order to check our observations in the field. This special report describes significant results obtained from analysis of LANDSAT-1 Scene No. 1053-17540 over east-central Nevada.

BACKGROUND

Research on the utilization of space imagery as a tool for mineral exploration is based on the assumption that sites of hydrothermal mineral concentrations may have characteristics which can either be directly observed in the imagery or more likely to be indirectly derived from a combination of geological indicators. The assumption is generally valid because mineral deposits do not occur at random and are often associated with ore guides. Although each mineral district has some unique characteristics, occurrences in a given metallogenic province often have in common distinctive similarities in their modes of occurrence such as a favorable host rock, type of structural control, the mineral assemblage and alteration features. Global factors, which control the distribution and type of metallogenic provinces, are caused by deep seated tectonic and magmatic processes within the earth's crust and are reflected in an intimate relation between metallogenic and petrographic provinces. On

a regional scale, many geologists have presented persuasive arguments that clusters of mineral deposits tend to occur at the intersections of tectonic belts. An example is the porphyry copper districts in southern Arizona which lie at the intersection of Jerome and Texas tectonic belts. Individual lineaments and their intersections have also been noted to control the location of mineral districts and even an individual large mine. On the local scale of an individual mine detailed geological studies have frequently revealed that ore bodies are structurally controlled. In cases, the ore body may occur along a specific structure such as a shear zone, a fault, a breccia pipe, etc.

If these structures could be identified, satellite imagery could be utilized in mineral exploration. It has become very well known that linear structures such as faults, fractures and shear zones are among the most prominent features observed in satellite imagery and are the easiest to map. It is also true that some "lineaments" recognized by researchers are subtle and are not recognized by all. Subjectivity of interpretation no doubt complicates lineament analysis of imagery and detracts from the basic validity of this potentially useful approach.

Area of Investigation

One area selected for this study is in the Basin and Range province in east-central Nevada. The space imagery used is LANDSAT-1 Scene No. 1053-17540 (Fig. 1).

Selection of this particular scene for detailed study was based upon several geological factors:

1. From regional stratigraphic considerations, the area lies mainly in the eastern Nevada province which is underlain largely by Precambrian metamorphic and sedimentary rocks and particularly by Paleozoic carbonate rocks in contradistinction to the western province characterized by Paleozoic and Mesozoic clastic rocks (Nolan 1943, 1962). The significance of this distinction is that the carbonate strata particularly the dolomites of Cambrian age have been known to be favorable host rocks for emplacement of mineral deposits where intruded by the Laramide granitic stocks.

2. Most of this area lies east of the leading edge of the Roberts Mountain thrust which brought the western clastic Paleozoic section on top of the carbonate section (Fig. 2). Farther west, within the domain of this major thrust many mineral deposits probably occur concealed beneath the upper clastic plate; several major mineral districts occur in erosional windows where the carbonate section is uncovered.

3. Although large areas have not been geologically mapped in detail, many Laramide granitic intrusives are known to occur.

4. Besides the carbonates as favorable host rocks, Tertiary acidic volcanic tuffs and rhyolites which are known to be good host rocks for precious metals are widespread and are exposed in many places from beneath the generally barren volcanic flows.

5. The area lies within the eastern Nevada metallogenic province characterized by major lead and zinc deposits with associated gold and silver. The western province is known for gold and silver, tungsten, antimony, mercury and iron. Two northwest-trending mineral belts or

metallogenic lineaments cross the area: Ely, Battle Mountain-Eureka. The Lovelock-Austin and Fallon-Manhattan belts may also project southeastward (Figs. 2 and 3).

6. The scene includes three major mining districts: Eureka, Mount Hamilton, and Ruth: major producers of silver, gold, lead, zinc, copper and molybdenum. In addition, many smaller mining districts and individual mines are present.

Analysis of the structural pattern in relation to those known occurrences was made in order to gain some insights which may help us identify structurally analogous areas.

Approach

The basic approach in conducting this investigation was to: 1) analyze the structural pattern inferred from the imagery in relation to known mineral districts and relevant geological data, and 2) apply this analysis in identifying favorable sites for detailed mineral exploration in the field. In order to attain our objectives we performed the following tasks:

1. Assembled and plotted on overlays relevant data from the literature. These included: a) Basic geographic and geomorphologic data. b) The locations of known mineral districts classified by type and relative size of production, as well as many individual mines. c) Major structural elements, lineaments or mineral belts published in the literature. d) Basic geological information on the distribution of major time-stratigraphic or rock units.

2. Identified and mapped significant structures which include: a) Linears such as inferred faults, shear zones or fractures. b) Structural trends showing bends, flexures, oroclines, discontinuities.

3. Analyzed all pertinent data in relation to the distribution of known mineral districts.

4. Identified candidate targets for exploration on the basis of a) Location within the structural pattern such as intersections, flexures, re-entrants and areas of complex deformation. b) Areas showing color and textured characteristics similar to those observed in known mining districts.

5. Identified priorities for field checking mainly on the basis of easy access from major transportation routes and probable presence of favorable host rocks.

6. Carried out reconnaissance field observations for obtaining ground truth data.

PROGRESS

The area selected for this investigation covered approximately 26,000 km^2 in the Basin and Range province of east-central Nevada (Fig. 1).

In order to apply the concept that analogous metallogenic districts often show similarities in their structural settings, we plotted known mineral districts on imagery overlays showing the elements produced and their relative size of production. Figure 4 shows the known mineral

districts and occurrences in relation to geological structures inferred from LANDSAT-1 imagery. Figures 2 and 3 show the axes or trends of major mineral belts which cross or project into the area taken from Roberts (1964). The leading edge of the Roberts Mountain thrust was also approximately located. The mineral belts suggested by Roberts are: Ely, Battle Mountain-Eureka, Lovelock-Austin and Fallon-Manhattan, all trending northwest and Pioche which trends east-west.

The LANDSAT-1 image was analyzed to identify and map significant structural linears, fault zones, fracture lines and major flexures or structural bends. Figures 4 and 5 show the structural pattern corresponding to Fig. 1.

Some of our linears appear to coincide with or are parallel to Ely, Battle Mountain-Eureka and Pioche mineral belts. The structural expressions of Lovelock-Austin, and Fallon-Manhattan mineral belts are either vague or absent. However, we noted that many mineral deposits tend to occur along faults or linears and particularly at their intersections (Fig. 4). Examples of these are the Eureka mining district which was a major producer of silver, gold, lead, zinc and copper. This district lies at the intersection of north and northwest and northeast trending fault systems and a structural flexure. The Ruth district, which is a major producer of copper, silver, gold, molybdenum, lead and zinc, lies at a structural flexure where north and northwest trending fault zones converge. Mount Hamilton district is known mainly for silver and gold production together with tungsten, molybdenum and copper. This district appears to be controlled by north and northwest fault systems.

From observations on the structural control of known mining areas, as well as color, tonal and textural characteristics which reflect rock properties, we have identified a number of target areas judged to be favorable for exploration.

Study of the target areas on geological maps resulted in the selection of 17 high priority targets for ground truth field investigation. The high priority target areas (Fig. 5) were selected mainly on the basis of the presence of rocks of geochemical composition favorable for mineralization. Examples of these are Paleozoic dolomites, limestones and Tertiary rhyolitic intrusives, flows and tuffs.

SUMMARY OF FIELD OBSERVATIONS

During reconnaissance field trips we visited 11 sites. In ten sites we were able to identify the structural and lithologic features observed in the imagery. Table 1 lists a summary of the most pertinent field observations. Sites 17, 18, and 19 were found to have mining areas not known to us before the field trips. Sites 4, 23, 25, and 32 show favorable structural and alteration features which call for more detailed field studies.

AREA OF LIMONITIC IRON OXIDE

Area No. 4 lies in the Hot Creek Range, Morey Peak Quadrangle, Nye County, Nevada. Since available topographic maps show that section corners have not been established in much of that quadrangle, the precise location within section corners has not yet been established.

Table 1. Summary of Field Observations

Site	Location	Field Structures	Country Rocks	Evidence of Mineralization
1	Monitor Range	NW trending fault	Volcanic tuffs	Limonitic alteration, placer magnetite
2	Monitor Range	ENE fractures	Tertiary volcanics	None
4	Hot Creek Range	N-S and NE fault intersection	Dolomite, granite quartz veins, volcanic rocks	Gossan samples found in float
17	Horse Range, Elson Creek Area	NW topographic linears	Tertiary volcanics	Hematitic alteration old mining areas
18	Horse Range, White Pine Range	NE fracture zone	Tuffs, volcanic flows	Alteration, prospecting pits
19	Horse Range, Currant Summit	Extremely deformed rocks	White tuffs, Paleozoic rocks	Prospecting pits, mining in vicinity
22	Schell Creek Range	Subtle, uncertain	Paleozoic rocks	None
23	Schell Creek Range	Highly deformed	Quartzites, dolomite basalt	Secondary copper minerals in basalt
24	South Egan Range, Shingle Pass	NE anticline	Intrusive granites, dolomite, quartz veins	None visible
25	Schell Creek Range	NE fracture zone	Tertiary volcanics	Widespread rock alteration
32	Quinn Canyon Range	NW, NE faults	Volcanic tuffs	Alteration, pyrite in green tuffs

During reconnaissance field work within target area No. 4 (Fig. 5), chunks of limonitic iron oxide samples were found in the regolith of a dolomite ridge. The area lies at the intersection of a northeast-trending fault zone with a north-trending regional fault zone which aligns with the Eureka mining district. The latter zone is approximately parallel to the leading edge of the Roberts Mountain thrust. The country rock consists of dolomite, a favorable host rock for sulfide mineralization, cut by quartz veins and intrusive granite (Fig. 6). We have not located any of this limonitic material in situ and further detailed field work and geophysical measurements are needed to establish the source of the float and its economic significance.

Table 2, columns 2, 3, and 4 show semiquantitative emission spectroscopic analyses of limonitic material scraped from three distinctively different color regions in the samples. A large number of semiquantitative x-ray fluorescence analyses done in our scanning electron microscope showed that in addition to the major elements, potassium at about the one percent level and arsenic at less than one percent were generally distributed through these samples. On a scale varying from centimeters to micrometers no significant localization of important elements could be found.

Gray dolomite samples collected from the regolith and a brecciated outcrop are veined with calcite. Spectroscopic analysis of white, fluorescent encrustations shows trace amounts of lead, copper, and silver, Table 2, column 5.

Table 2. Semiquantitative Analysis* of Samples Found in Hot Creek Range, Nevada

	Red	Yellow-Orange	Black	White	Best, Red
Fe-	55.%	56.%	65.%	0.57%	35.%
Si-	5.4	5.5	2.3	2.1	4.0
Al-	1.3	1.1	0.36	0.50	4.4
As-	0.74	0.76	0.69	-	17.
Ca-	3.5	1.7	0.33	29.	2.6
B-	0.016	ND<0.003----------		TR<0.005	0.22
Sb-	-	ND<0.05----------		-	0.95
Mg-	0.22	0.49	0.22	6.1	0.40
Mn-	0.042	0.20	0.14	0.013	0.12
Pb-	0.091	TR<0.02----------		0.016	0.63
Mo-	0.082	0.086	0.034	-	0.28
V-	0.0051	0.0063	0.0034	-	0.0090
Cu-	0.017	0.027	0.023	0.00041	0.18
Ag-	0.0010	TR<0.0002----------		TR<0.002	0.0045
Zn-	0.064	0.26	0.073	-	0.86
Ti-	0.085	0.027	0.0096	0.027	0.049
Ni-	0.0026	0.0038	0.0016	TR<0.002	0.017
K-	-	ND<0.50----------		-	TR<0.50
Cr-	TR<0.0005	0.0058	TR<0.002	0.00075	TR<0.002
Other Elements		nil	nil		nil

*Pacific Spectrochemical Laboratory, Inc., Los Angeles, California

Our first spectroscopic analysis of red limonitic material showed concentrations of arsenic, antimony, lead, and zinc much higher than a subsequent analysis of similar but not identical material taken for verification. These initial results are listed in Table 2, column 6. Flakes from all identifiable red areas in the remaining samples have been examined in the scanning electron microscope. No region with arsenic, lead, or zinc concentrations approaching those in column 6 could be found. Therefore, it is certain that even if the high analysis is correct, it probably represents a small fraction of the material in the samples.

Examination of polished sections indicate the presence of goethite, lepidocrocite and secondary banded hematite. Available evidence seems consistent with the possibility that these samples are a gossan derived from the weathering of a massive sulfide vein, although other possible modes of origin certainly cannot be ruled out without additional work.

SUMMARY AND CONCLUSIONS

Geologic and structural analysis of a LANDSAT-1 scene in east-central Nevada in relation to known mineral districts resulted in the selection of 17 target areas for mineral exploration. During reconnaissance field observations three areas were found to show evidence of mining and prospecting not known before these areas were visited. Four areas showed structural as well as alteration features which appear to be favorable for detailed geological and geophysical exploration. In one area in the Hot Creek Range we found limonitic iron oxide samples in the regolith of a dolomite ridge containing abnormal contents of several economic elements. These limonitic samples found were not in situ, and further field exploration is needed to assess their source and significance.

REFERENCES

Abdel-Gawad, M. and L. Tubbesing, 1975a, Analysis of Tectonic Features in U.S. Southwest from Skylab Photographs: Final Report SC5007.16FR Rockwell International Science Center, Thousand Oaks, CA, prepared for NASA Johnson Space Center, Houston, TX, 94 p.

Abdel-Gawad, M. and L. Tubbesing, 1975b, Identification and Interpretation of Tectonic Features from Landsat-1 Imagery - Southwestern North America and The Red Sea Area : Landsat-1 Investigation Final Report SC543.16FR Rockwell International Science Center, Thousand Oaks, CA, prepared for NASA Goddard Space Flight Center, Greenbelt, MD, 118 p.

Abdel-Gawad, M. and L. Tubbesing, 1974, Transverse Shear for Southwestern North America - A Tectonic Analysis: Fist International Conf. on the New Basement Tectonics, June 3-7, 1974, Salt Lake City, UT Geological Assoc., (in press).

Nolan, T. B., 1943, The Basin and Range Province in Utah, Nevada and California; U.S. Geol. Survey Prof. Paper 197-D, p. 141-196.

Nolan, T. B., 1962, The Eureka Mining District, Nevada; U.S. Geol. Survey Prof. Paper 406, p. 78.

Roberts, R. J., 1964, Economic Geology in Mineral and Water Resources of Nevada; Nevada Bureau of Mines Bull. 65, p. 39-45.

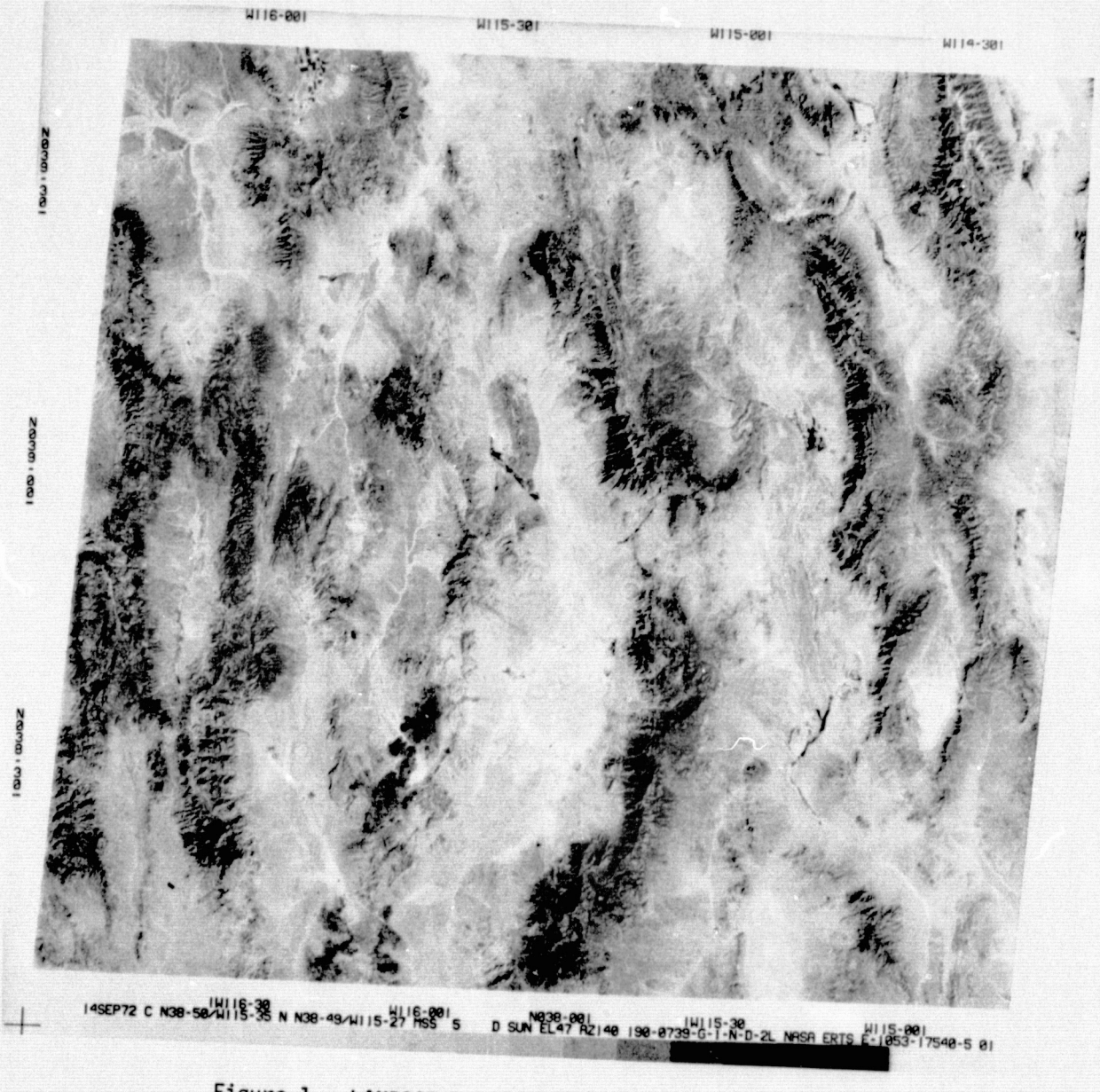


Figure 1 - LANDSAT-1 Scene MSS 1053-17540, Band 5

REPRODUCIBILITY OF THE
ORIGINAL PAGE IS POOR

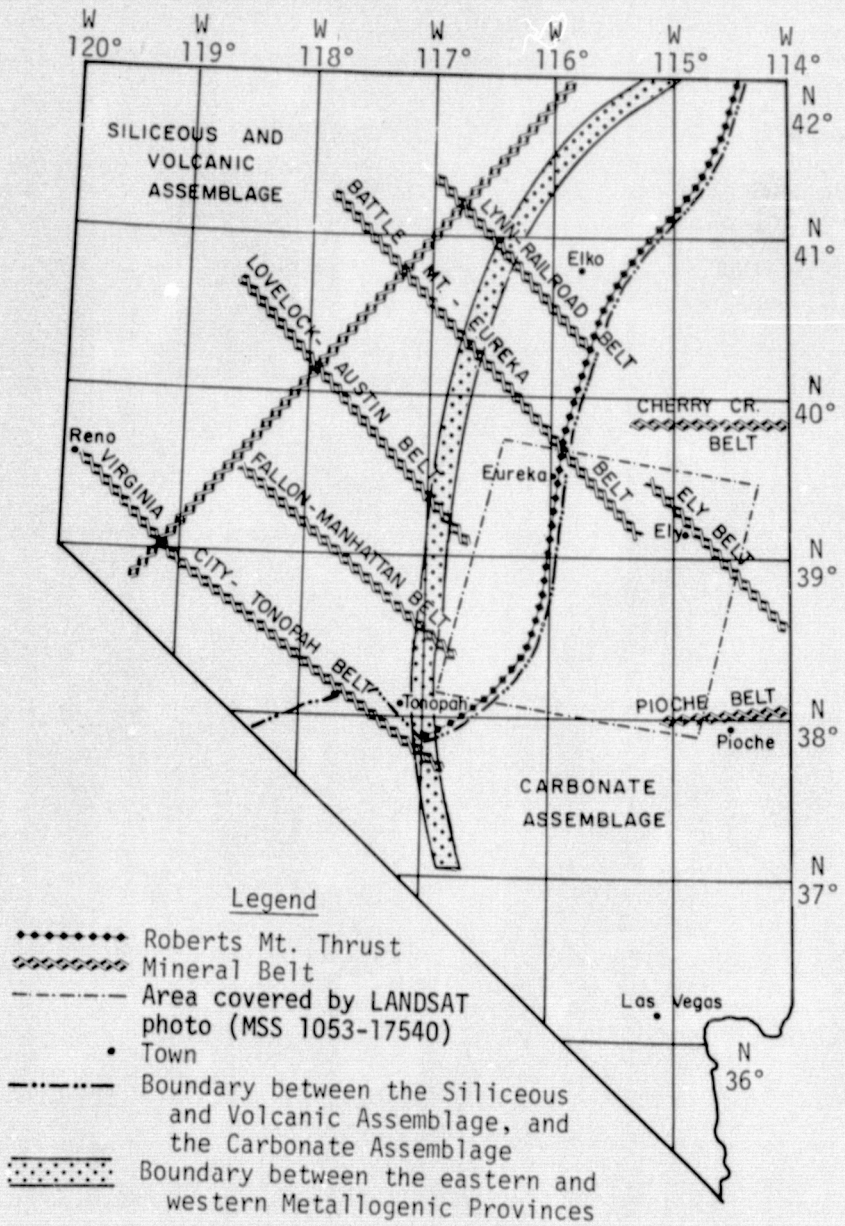


Figure 2 - Mineral Belts of Nevada (After: R. J. Roberts, 1964)

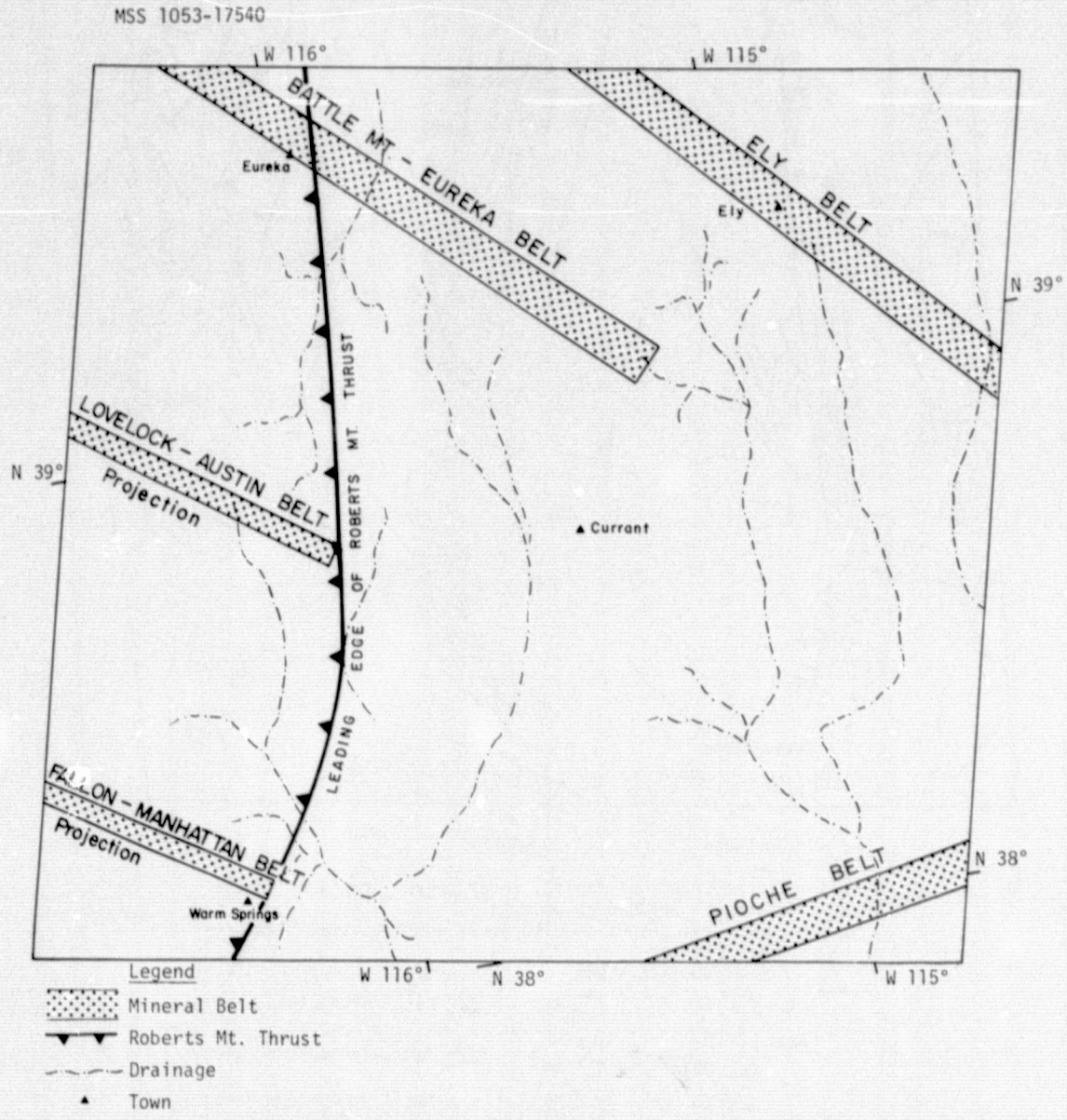


Figure 3 - Mineral Belts Projected on LANDSAT-1 Scene MSS 1053-17540

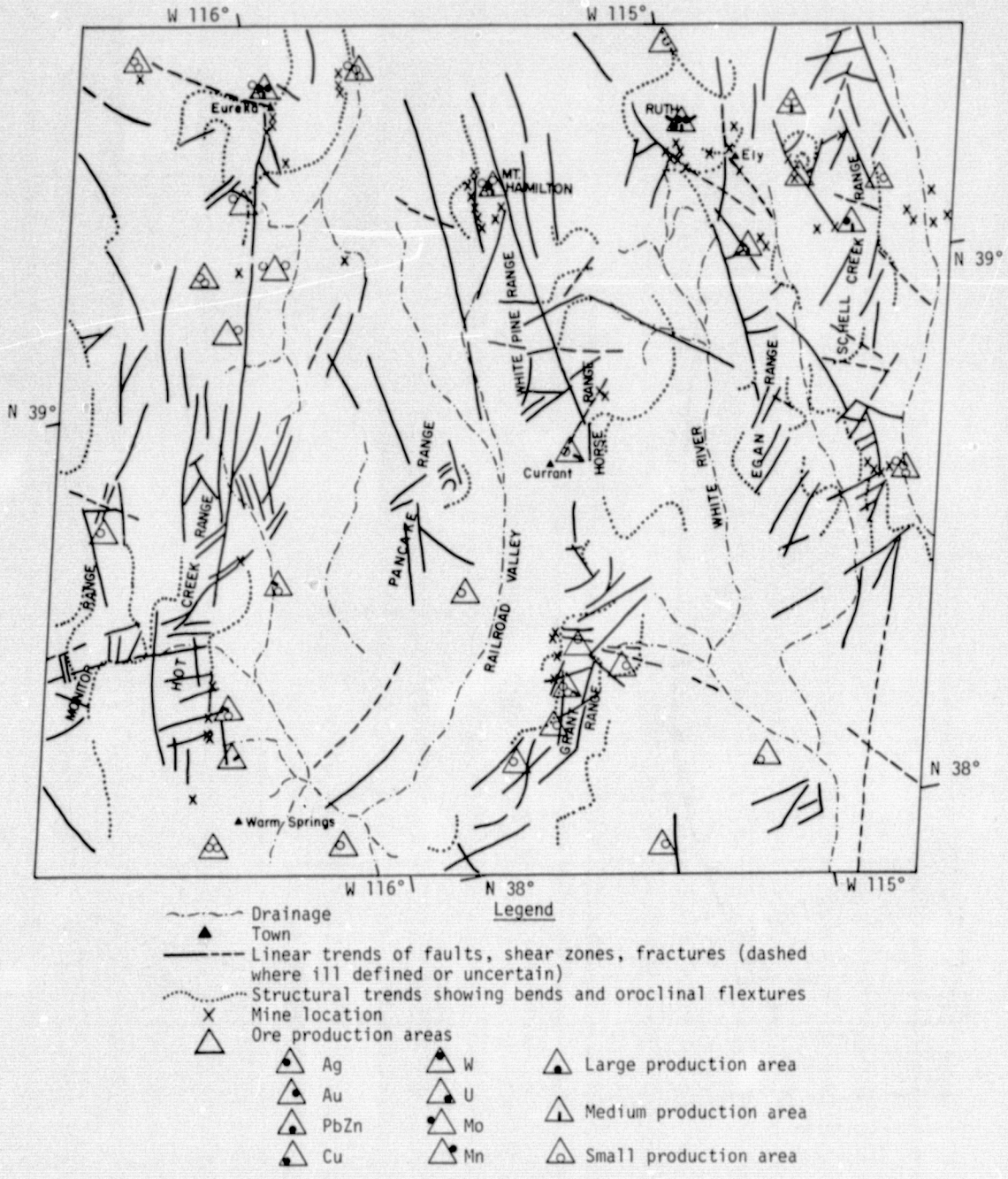


Figure 4 - Structures Inferred from LANDSAT-1 Imagery and Mineral Districts

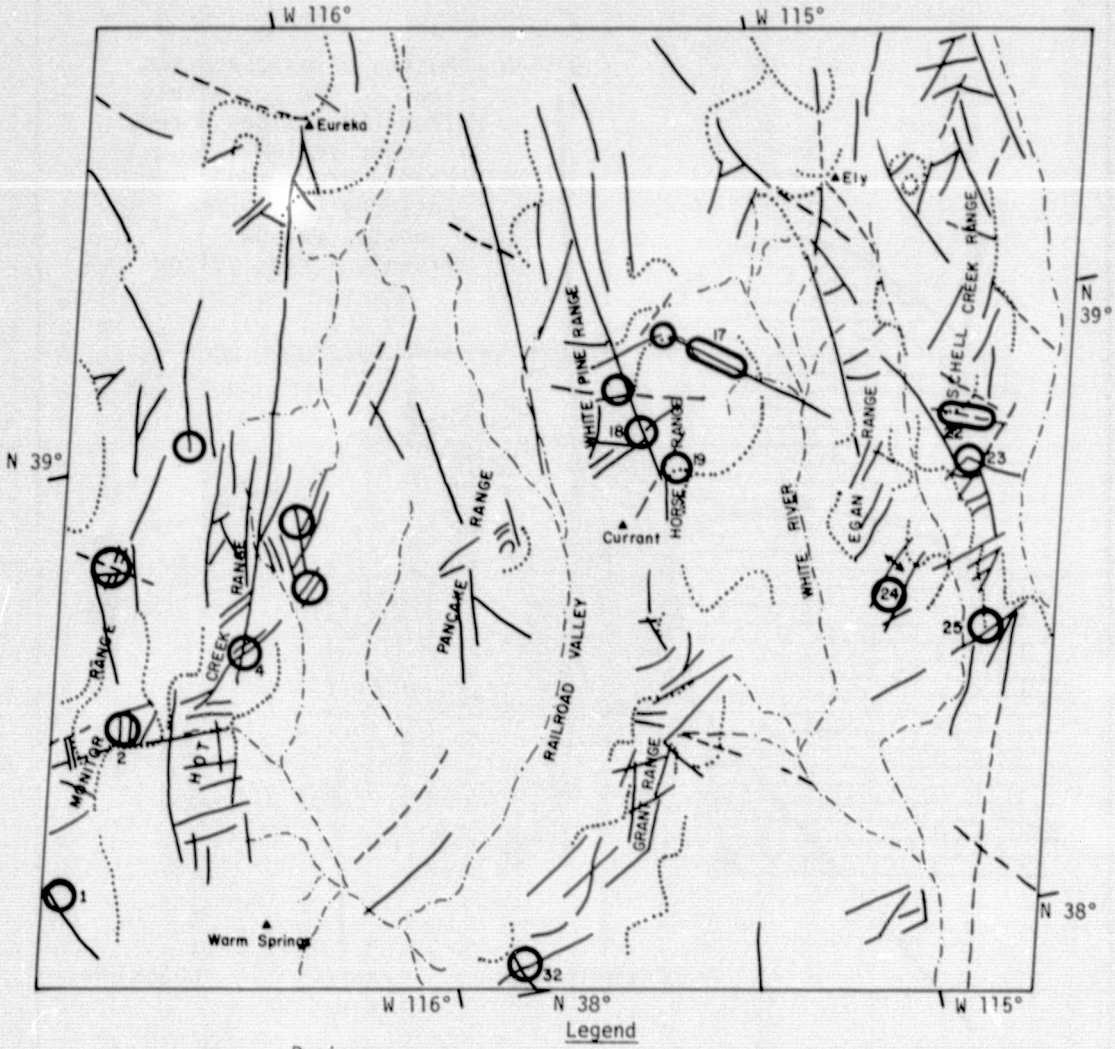


Figure 5 - High Priority Targets Identified on LANDSAT-1 Imagery Scene MSS 1053-17540

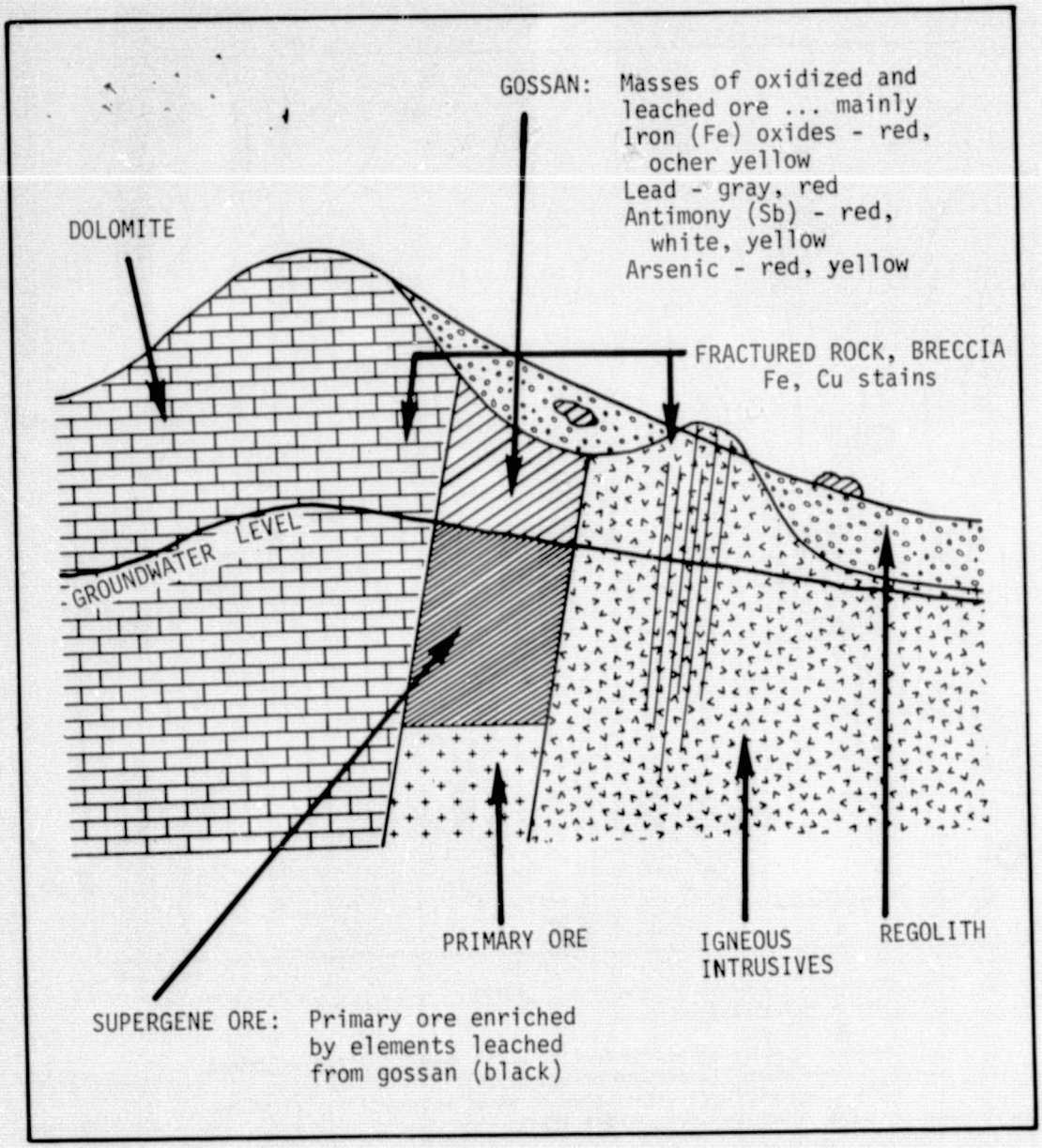


Figure 6 - Hypothetical Cross-Section of Vein Type Deposit.

ATTEMPT AT CORRELATING ITALIAN LONG LINEAMENTS FROM LANDSAT-1 SATELLITE IMAGES WITH SOME GEOLOGICAL PHENOMENA. POSSIBLE USE IN GEOTHERMAL ENERGY RESEARCH

By Enrico Barbier and Mario Fanelli, National Research Council
International Institute for Geothermal Research, Lungarno
Pacinotti 55, 56100 Pisa, Italy

N76-17524

ABSTRACT

By utilizing the images from the American satellite LANDSAT-1, in the spectral band 0.8-1.1 μm (near infrared), a photomosaic was obtained of Italian territory. From this mosaic the field of long lineaments was drawn, corresponding to fractures of the earth crust more than 100 km long. The authors have therefore verified the relationship between lineaments, hot springs, volcanic areas and earthquake epicenters. There is a clear connection between long lineaments and hot springs: 78% of the springs are located on one or more lineaments, and the existence of "hot lineaments" was observed. A slightly weaker, but still significant, connection exists between the Pliocene-Quaternary volcanic areas and long lineaments. The relationship between earthquakes and long lineaments can only be verified in some cases. The lineaments which can be related to earthquakes have little or no connection with the other phenomena. Results obtained by the authors could widen the possibility of using satellite images in the field of applied research.

INTRODUCTION

Recently images of LANDSAT-1 satellite on band 7 ("near infrared" 0.8-1.1 μm) of Italian territory were available to us. These images have been utilized to make a mosaic of the Italian territory (Fig. 1a).

One of the geological-structural features best revealed by the satellite images is that of the long lineaments, generally main fractures of the earth's crust. That is, those features which have the common characteristic of intersecting a horizontal plane along a nearly straight line. The basic assumption of this fact is that the high speed deformations of the crust, as opposed to the low speed ones, have almost rectilinear paths. These linear features are the evidence of structural deformations which probably affect great thicknesses of rock under the surface and which can with time reach the surface through thicknesses of more recent sediments.

As we are utilizing the satellite images where the geological phenomena can only be studied on a very regional scale, we must consider every recognized lineament not as a single fracture, but as representing the general trend of a system of smaller fractures or belt of fractures.

Having this new survey method which offers, for the first time, the possibility of studying Italian territory from a global view, we decided to check the possible

connection between long lineaments (more than 100 km) and some particular geological phenomena. Among the latter we considered the thermal springs, the recent volcanic areas (from Pliocene to the present day) and the earthquake epicenters (Figure 1b). It may seem obvious that there is a connection between geological phenomena of this type and lineaments, which reveal the bands of weaknesses of the earth's crust, but, for Italy at least, this connection could not be checked up to now. Furthermore, we think it interesting to draw attention in particular to those lineaments which, more than the others, are associated with the above-mentioned phenomena; this may also be of use in applied research.

From the total field of lineaments recognized on the mosaic formed by the LANDSAT images, for clarity of design we have removed those lineaments which did not seem to be connected with the above-mentioned geological phenomena. Of course not only the lineaments described but all those seen on the LANDSAT images have a precise geological significance. This can be seen by transferring the lineaments onto a structural map of Italy. However, this is not our objective here. The lineaments described in this paper, that is, those along which there are thermal springs, volcanic areas and earthquakes, although not representing the total field of lineaments, do give, nevertheless, a reasonably exact idea of its pattern.

CORRELATIONS BETWEEN LINEAMENTS AND THERMAL SPRINGS

In Italy there are 214 thermal areas, with one or more hot water springs. Taken individually these springs are about 700. About 80% have a low temperature (20°-45°C) and the remaining 20% consists of springs between 45° and 100°C.

In Figure 1b the scale prevented our including all the thermal areas, so that one symbol, where necessary, may also indicate different nearby areas. We have also added the travertine deposits which, when they are not associated with still active hot springs, are the proof of now extinct hot springs.

More than 60% of the hot springs, and the majority of the travertines, are however concentrated over a "hot belt" running down the whole western side of the peninsula as far as Sicily. This distribution is connected with the geological structures of the country which is such as to permit, especially on the western side, the formation of hydrothermal circuits. It is on this side, furthermore, that we can find the Pliocene-Quaternary volcanism, the exploited geothermal fields of Larderello, and Travale (B), and Monte Amiata (C), and the highest terrestrial heat flow values.

The hot springs are clearly related to the lineaments already described. In fact, 78% of the springs are marked on the map, and the majority of the travertine deposits, are found where there are one or more lineaments. Such a high percentage clearly excludes the possibility of a haphazard distribution. It should also be noted that a part of the remaining 22% of the springs could probably be associated with lineaments, but this was either uncertain or impossible due to the low quality images of some areas (certain zones of central-southern Italy and of Sardinia).

It would not seem that the hot springs are found on lineaments with one particular trend rather than another. It must, however, be noted that there are some lineaments which could be called "hot lineaments," where there is a greater density

of hot springs. These are in the eastern part of lineaments no. 6, in nos. 1, 7, 8, 9, 10, 11, 13, 16, 18, 19 and 20. Let us now examine the most interesting of these:

- lineament No. 6 contains the important group of springs of the Colli Euganei (A), corresponding to a Eocene-Oligocene volcanic complex, and is about 600 km long. It marks the boundary where the Alpine massifs disappear under the Pliocene-Quaternary sediments of the Padana Plain (Po valley), crosses the Alpine arc and ends in the French Burgundy area;

- lineament No. 1, which we were able to follow in the mosaic for 1200 km from Sicily to the Alps but which most probably continues further north, contains 8 thermal areas, marks the eastern boundary of the belt of Tyrrhenian springs and the volcanic flows of central Italy and includes the volcanic area of Ischia island (F). It may be deduced by bathymetry that it continues into the Tyrrhenian sea, including the active volcano Stromboli (G) and reaches the strongly seismic area in the northern corner of Sicily;

- lineament No. 7 has a visible length of about 400 km, and, judging by the isobath trend in the Tyrrhenian sea, probably continues southwards. Fourteen groups of hot springs can be directly connected with this lineament along with, what is especially worth noting, the geothermal field of Larderello (B), which produces superheated steam. It would seem that this lineament, which in its southern part can be associated with several Quaternary volcanic centers, is the most propitious to the circulation of hot fluids;

- lineament No. 8, which lies perpendicular to No. 7, although it may be associated with only five groups of thermal springs, is of interest for two reasons. It touches on the geothermal field of Larderello (B), which lies on the intersection of this lineament and the previous one (No. 7), and includes the geothermal field of Travale (B). These two lineaments, Nos. 7 and 8, could be of particular importance in regard to applied research on geothermal fluids;

- lineament No. 13, length 400 km, contains eight groups of hot springs and the Quaternary volcano of Vulture (D);

- lineament No. 18 and No. 19, in Sardinia, reveal the particularly linear distribution of the springs;

- lineament No. 20, on a N-S trend, which separates the Paleozoic volcanites from the Tertiary-Quaternary ones, contains five groups of hot springs along with four volcanic areas.

Finally, special note should be taken of the area in central Italy enclosed to the north by lineament No. 3, to the east by No. 1, to the south by No. 12 and to the west by the Tyrrhenian coast. In this relatively small zone, equal to about 9% of the whole surface of Italy, there are 35% of the Italian thermal areas, wide travertine deposits, the three geothermal fields under exploitation (Larderello, Travale, Monte Amiata) and several Plio-Quaternary volcanic centers. This area corresponds more or less to that which Marinelli (1974) called the "Etruscan swelling" in that it is a recently uplifted zone, shown by the Neogene sediments 200-300 m above sea level. The western part of this swelling, whose axis of symmetry seems to be formed by lineament No. 7, is partly submerged in the Tyrrhenian sea as a result of Plio-Pleistocenic direct faults running NW-SE direction (lineament No. 9, for example). The swelling area corresponds to an important heat flow anomaly (more than 3 $\mu cal/cm^2$ sec) (Loddo, Mongelli 1974), which is also confirmed

by previously described phenomena and by widespread hydrothermal mineralizations and a high surficial concentration in mercury.

AREAS OF VOLCANIC ACTIVITY

The areas with Plio-Quaternary volcanic activity--one or more volcanic centers--have an areal distribution very similar to that of the hot springs. That is, they lie on the western side of the Italian peninsula and in the islands of Sicily and Sardinia. Sixty-five percent of these areas can be associated with long lineaments and about one half of this percentage lie on the intersection of two or more lineaments.

Furthermore, of the volcanoes now active in Italy, Vesuvius (E) and Etna (I) are of the intersection of easily identifiable lineaments, while Stromboli (G) and Vulcano (H) are on the intersection, under the sea, of lineaments which can be seen on the earth and deduced on the sea bottom by the bathymetric contours.

The linear trend of the volcanic areas in correspondence with long lineaments is not as clear as in the case of the hot springs. However, the volcanic areas are quite easily seen on lineaments Nos. 7, 15 and 20. The volcanic areas on lineament No. 7, which as we have already said represents the axis of symmetry of the "Etruscan swelling," have very similar magmatic characteristics, with sialic magmas of anatectic origin. The heat flow anomaly associated with the swelling could be due to the higher temperature of the intracrustal magmas in this region, and there is convincing petrological proof of this phenomenon (Marinelli 1974).

Lineament No. 15, on the other hand, can be connected to the volcanic areas with typically potassic magma, which are usually younger than those of the "Etruscan swelling" and run from the southern part of the latter as far as Vesuvius (E). This Tyrrhenian volcanism is less than one million years old and is still active in its southernmost part (Vesuvius); it is also connected to a recent tension tectonics, with considerable sinking of crustal blocks (Marinelli 1974).

EARTHQUAKES

We have considered the earthquakes with intensity from the VI degree upwards on the Mercalli-Sieberg scale, which were recorded in Italy from 1893 to 1965. The epicenters of these earthquakes, whose foci are never deeper than 40 kilometers, cannot be clearly related to the long lineaments. In some cases only, this association is noticeable or may be assumed. This is true for lineaments Nos. 2, 3, 4, 5, and 17 and is especially evident in the case of lineament No. 14.

- lineament No. 3, in its western part, forms the northern boundary of the previously mentioned Etruscan swelling. There are three earthquake epicenters with a degree above the 9th and the volcanic area of Colli Euganei (A) all along this lineament;

- lineaments Nos. 4 and 5 form, in their eastern part, the boundary between the Alpine chain and the plain; in this area there is a certain densening of earthquake occurrences especially in correspondence with the previously mentioned lineament No. 3;

- lineament No. 14 corresponds to an important fault of that area.

CONCLUSION

There is undoubtedly a connection between long lineaments (more than 100 km) and hot springs. A slightly weaker connection, but still significant, exists between the Pliocene-Quaternary volcanic areas and these lineaments. The relationship between earthquake distribution and long lineaments can only be seen in some cases. The lineaments described as "hot," because of the considerable number of hot springs which can be associated with them, are often the same lineaments which cross the volcanic areas (No. 7, for example).

The lineaments which may be associated with earthquakes have little or no relation to the other two phenomena.

The close relationship between long lineaments, hot springs and volcanic centers, observed in the LANDSAT images, can make an interesting contribution to the research on exploitable natural hot fluids for energy production.

It is particularly useful in the first stage of exploration, to be able to individuate as rapidly as possible the areas designated for later more detailed surveys. The results obtained in this paper show that the satellite images can play an important role in this regard. In fact, the very regional view provided by these images allow us to recognize the large lineaments and fracture fields associated with the areas of weakness of the earth crust. It is in these areas, where permeability is higher, that high temperature water circuits of clear energetic value can more easily form.

REFERENCES

Barbier E., Condedera C., Dainelli P. - Aspetti geologici e morfologici del territorio nazionale dalle immagini del satellite LANDSAT. Universo, v.53, pp. 867-879.

Cloos E. - Lineation. Geological Society of America, Memoir 18, 5 May 1946, reprinted 1952.

Fanelli M. - Le acque calde italiane. CNR, Istituto Internazionale per le Ricerche Geotermiche, Pisa. Unpublished report, 195 pp., 1972.

Iaccarino E. - Attivita sismica in Italia dal 1893 al 1965. Com. Naz. Energia Nucleare, RT/GEO(68)14, Rome, 1968.

Loddo M., Mongelli F. - Tentativo di una mappa del flusso geotermico in Italia, In: "L'Italia, In: "L'Italia nell'ambito del l'evoluzione del Mediterraneo," 67th Congr. Soc. geol. ital., Parma, 1974, 12 pp.

Manfredini M. - Tentativo di correlazione tra distribuzione degli epicentri sismici e strutture tettoniche nel settore appennino dell'orogeno alpino. Congr. Soc. geol.ital., Parma, 1974, 12 pp.

Marinelli G. - Magma evolution. In "Geology of Italy," Petroleum Exploration Society of Libya, Tripoli (in press). 1974.

Ryan W. B. F., Stanley D. J., Hersey J. B., Fahlquist D. A. and Allan T. D. - The tectonics and geology of the Mediterranean Sea. In: "The Sea," v.4, pt. II, pp. 387-492, John Wiley & Sons, 1971.



Figure 1a.- Italy from the LANDSAT-1 satellite, band 7, 0.8-1.1 μm.

REPRODUCIBILITY OF TH
ORIGINAL PAGE IS POOR

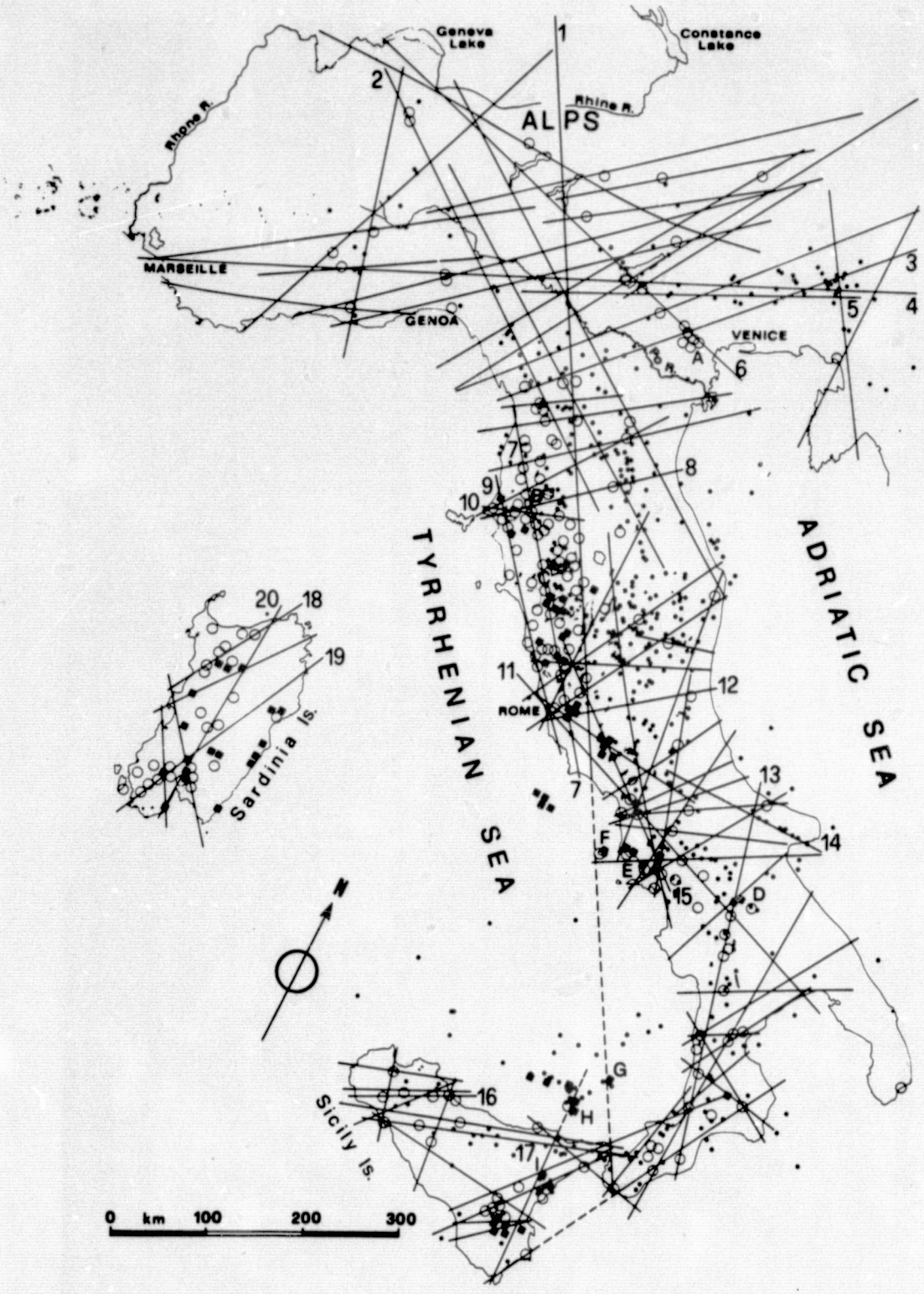


Figure 1b.- Long lineaments, thermal spring areas (blank circles), volcanic areas (black squares), earthquake epicenters (dots), travertine deposits (light dashed areas), geothermal steamfields (blank rhombs). A - thermal area of Colli Euganei; B - Larderello and Travale geothermal steamfields; C - Monte Amiata geothermal steamfield; D - Monte Vulture volcanic area; E - Vesuvius volcano; F - Island of Ischia; G - Stromboli volcano; H - Vulcano volcano; and I - Etna volcano.

LAYERED CLASSIFICATION TECHNIQUES FOR REMOTE SENSING APPLICATIONS

P. H. Swain, C. L. Wu, D. A. Landgrebe, and H. Hauska
Laboratory for Applications of Remote Sensing,
Purdue University, West Lafayette, Indiana*

N76-17525

ABSTRACT

Layered classification offers several advantages over the very familiar single-stage approach. The single-stage method of pattern classification utilizes all available features in a single test which assigns the "unknown" to a category according to a specific decision strategy (such as the maximum likelihood strategy). The layered classifier classifies the "unknown" through a sequence of tests, each of which may be dependent on the outcome of previous tests. Although the layered classifier was originally investigated as a means of improving classification accuracy and efficiency, it has become apparent that in the context of remote sensing data analysis, other advantages also accrue due to many of the special characteristics of both the data and the applications pursued. This paper outlines the layered classifier method and discusses several of the diverse applications to which this approach is well suited.

INTRODUCTION

The pattern classifiers commonly implemented in remote sensing data processing systems have an elementary logical structure like that shown in Figure 1. To classify each "unknown," the decision process is applied to a fixed set of features (usually spectral measurements) to select one of the candidate pattern classes. For some remote sensing problems encountered in practice, however, this simple structure is less than ideal and may even be inadequate. A structure like that suggested by Figure 2, a "decision tree" or "layered classifier," can be put to good use. The following cases illustrate this fact.

In regions characterized by highly variable topography, spectral response may depend significantly on topographic variables such as slope and aspect [1]. With the digital data bases and the data registration facilities which are now available, it is possible to overlay, say, satellite multispectral scanner (MSS) data and topographic data. Thus, it is feasible to use the topographic data in the classification process - except that the topographic data cannot be handled as simply an additional variable (or variables). Ideally, one might wish to use the topographic variable(s) to stratify the multispectral data analysis problem, and then apply a multivariate maximum likelihood procedure to the stratified data. This can be accomplished with a layered decision procedure, in which the data is stratified in the first layer and the classification is accomplished in one or more succeeding layers.

---

* Dr. Wu is now with the Jet Propulsion Laboratory, Pasadena, California; Dr. Hauska is an ESRO Research Fellow, at Purdue University on leave from Luleå University of Technology, Luleå, Sweden.

Another case in which a kind of stratification is of use is in detection of diseased crops. The spectral bands which are optimal for disease detection are not necessarily the bands optimal for crop species discrimination. Rather than use all of these bands jointly for every classification, which may be prohibitively expensive in terms of computational load, it would be preferable to use the "disease detection bands" only when the crop species of concern has been detected. Again, a multilevel decision procedure can be used.

Another class of problems for which layered classification is helpful is that characterized by very limited size training sets. Under such limitations, it may be necessary to restrict the dimensionality (number of features) of any decision procedure used in order to avoid the "dimensionality problem;" i.e., the phenomenon which, when the number of training samples is small, decreases classification accuracy when new pattern features are added [2,3]. This problem can often be circumvented by substituting multiple decisions with low dimensionality for a single decision having high dimensionality, which can be accomplished using layered decision logic.

Many other examples could be cited. In general they involve one or more of three factors: (1) compatibility of the scene variables with each other and with the analysis process; (2) the desire to maximize classification accuracy; (3) the desire to minimize classification cost (usually measured in terms of computer time). The challenge is to devise a systematic and effective procedure for determining the optimal decision logic.

APPROACH

For generality, we shall state the problem as follows:

Assume there is a set of classes $C = \{c_1, c_2, \ldots c_m\}$, a set of measurements or features $F = \{f_1, f_2, \ldots, f_n\}$ with which to discriminate between the classes, and a set of decision procedures $P = \{p_1, p_2, \ldots, p_k\}$ which can be applied to the features to achieve the required discriminations. Formally, a "decision tree" is a tree-like structure of connected nodes, such as shown in Figure 3, which defines a logical decision (classification) procedure. Each node (junction point) in the tree is labelled by a triple of the form $\{C_i, F_i, p_i\}$, where C_i is a subset of C, F_i is a subset of F, and P_i is a single element from P. Thus each triple defines a step in the decision process for classifying any given data observation. The uppermost or root node in the tree is always labelled with C; the lowest or terminal nodes in the tree are often, but not always, labelled with individual elements of C.

The problem is to select from the set of all possible decision trees a tree which (1) at every node uses a decision procedure compatible with the available data features, and (2) maximizes the overall classification accuracy while (3) minimizing the classification cost. Conditions (2) and (3) must be met in terms of an "optimal" trade-off. For almost any practical problem, the specifications for some of the nodes in the tree will follow naturally from the problem itself. But there may be a very large number of possibilities for the remainder of the nodes. Designing an "optimal" decision tree requires first a criterion for evaluating any given tree, and then a strategy for searching for the optimal tree among the possibilities. In the remainder

of this section we shall describe briefly a design approach we have been developing. The details may be found elsewhere [2].

Optimality Criterion

For a given data processing system, the computation time required to analyze the data of interest reflects the relative "cost" of the analysis. For instance, the time increases with the complexity of the decision procedure and the number of pattern features used. On the other hand, it is usually possible, up to a point, to "buy" analysis accuracy by paying the cost of a more complex decision procedure and/or adding more features.

The optimality of a given decision tree is expressed in terms of both the time required by the classifier to process the data and the error rate achieved. Since, up to a point, one of these factors can be traded for the other, the relative importance of these factors must be specified for the problem at hand. The optimality criterion is expressed as an "evaluation function" E:

$$E = -(T + K \cdot \varepsilon) \tag{1}$$

where T is the time required for classification and ε is the resulting error rate. The constant K expresses the relative importance of computation cost (time) and classification error. We have chosen to use the negative expression so that achieving optimality corresponds to maximizing the evaluation function.

Searching for an Optimal Tree

For any given problem, it would be theoretically possible to enumerate (make an ordered exhaustive list of) all possible decision trees and evaluate them one by one using eq. (1) to find the best possible tree. But for almost any nontrivial problem encountered in practice, this is infeasible because of the enormous number of possible trees. To get this problem down to manageable proportions, a strategy has been adopted which we refer to as "guided search with forward pruning" [2]. Essentially, the strategy is to construct the tree a node at a time, estimating the suitability of all candidate structures for the node under consideration, and discarding all but the most promising candidate "subtree."

The "guided search with forward pruning" strategy requires a means for evaluating each node. For each candidate structure following node d_i the evaluation is computed as follows:

$$E(d_i) = -T(d_i) - K \cdot \varepsilon(d_i) + \sum_{j=1}^{n_i} E(d_{i+j}) \tag{2}$$

where $T(d_i)$ and $\varepsilon(d_i)$ express the efficiency and accuracy of the node d_i and the summation is an estimate of the evaluation functions of the descendant nodes of d_i (which are n_i in number). A lower bound is used to form this estimate, which is the evaluation of a conventional single-stage classifier applied at that point.

Constructing the decision tree in this sequential fashion cannot guarantee that the optimal tree will be obtained, because, unfortunately, the optimal choice at any level in the tree is not necessarily independent of choices at later stages. However, improvement over conventional single-stage classifiers is generally achievable, a fact amply demonstrated by the empirical results obtained to date [2,4].

Estimation of Classification Accuracy

Use of eq. (2) requires computation of classifier error in order to evaluate any candidate subtree. However, even under the simplifying assumption that all classes to be recognized have multivariate Gaussian statistics, direct calculation of classifier error is not feasible [5]. Instead it is necessary to use an indicator function which provides a measure of the statistical separability of the pattern classes for any given subset of the pattern features. Several such functions have been investigated for this purpose, a transformation of the Bhattacharyya distance having proved most suitable so far [2,4,5].

Alternative Decision Tree Design Procedures

The search strategy discussed above provides an analytical tool for designing decision trees based on the statistical relationships between the pattern classes. In some instances, however, the appropriate design criteria may not be of a statistical nature. In such cases, a more user-interactive, less automatic procedure may be followed. Typically, the user will specify those nodes of the decision tree which can be specified from consideration of the problem characteristics and then use the optimal search method to determine the remainder of the tree. A good example is the approach for overcoming cloud problems, which is described in the next section.

APPLICATIONS

In the Introduction, we cited two potential applications and an entire class of problems for which layered classifiers are useful. Several more applications are listed in Table I. We will now describe a number of instances where this method has actually been used experimentally.

Water Temperature Mapping

It was desired to map the surface temperature of a river for which a multispectral scanner data set was available including a calibrated thermal channel [6]. To accomplish the desired mapping, it was first necessary to locate the river using the visible and reflective infrared scanner channels. The temperature of the water was then determined from the thermal infrared channel.

Figure 4 shows a simple decision tree structure used to accomplish the desired result. The design was simple enough to perform manually, without the use of the optimal search procedure.

Avoiding the Clouds

The classification of agricultural crops from satellite multispectral data promises to be one of the major applications of remote sensing. However, at many of the latitudes where important cropland is found, the remote sensing

data is often cloudy. A layered classifier used in conjunction with data from multiple satellite passes over the same area can alleviate this problem to a substantial degree.

In an experiment which demonstrated this capability, LANDSAT data collected over Livingston County, Illinois on June 29 and July 16, 1973, were geometrically registered. It was desired to determine, using the data from the June 29 pass, the acreage of corn and soybeans planted in the county. However, ten percent of the county was obscured by clouds and cloud shadows. Training statistics were determined for both dates, and the decision logic shown in Figure 5 was used to classify the data. Again, as in the previous case, the decision tree was determined by the problem logic, without resorting to the optimal search procedure.

As shown in Figure 5, the layered classifier was used simply to eliminate the effects of clouds in the earlier data set. More complex logic could have been developed. For example, at points where neither data set had clouds or shadows, all eight data channels could have been used for classification with the aim of improving the classification accuracy.

Optimization of Accuracy and Efficiency

A number of applications examples are described in [2] which involve designing layered classifiers so as to optimize accuracy and efficiency. In one fairly typical case it was desired to identify the classes "coniferous forest," "deciduous forest," "agriculture," "water," and "bare rock." In the analysis process, twenty-six spectrally distinct subclasses were identified, and the optimal search procedure was used to derive an appropriate decision tree, which is shown in Figure 6. (A simplified notation has been used in this figure to specify the tree. All nodes use maximum likelihood as the decision criterion.) This tree is fairly typical in several respects, including its breadth and depth. Efficiency of the classification process is gained through the fact that many of the decisions involve a small number of features (for the classification algorithm used, the time required is roughly proportional to the square of the number of features). Accuracy is gained by using an optimal subset of features for each decision, which is generally a subset determined by the specific classes to be discriminated in that decision.

SUMMARY

We have described here a flexible method for classification of remote sensing data. This method can be applied to a wide range of problems and varieties of data not conveniently handled by conventional classifiers. It also provides a means of maximizing classification accuracy and efficiency by optimizing the number and selection of features used in each decision.

The "decision tree" approach allows the user to take advantage of special characteristics of the problem at hand by manually specifying parts of the decision tree. Where the problem is one of choosing among a vast number of alternative tree structures, a programmed "optimal search procedure" is available. Often a hybrid of the manual and optimal search procedures provides the most suitable decision tree structure for a practical problem.

For problems involving large numbers of pattern classes and features, the "optimal search procedure" described here cannot guarantee that the resulting decision tree is truly the optimal tree. Future research using

heuristic search procedures and mathematical programming techniques is expected to improve on the design tools now available.

ACKNOWLEDGMENT

The research reported in this paper was supported by NASA Grant NGL 15-005-112 and NASA Contract No. NAS 9-14016.

REFERENCES

1. R. M. Hoffer, M. D. Flemming, and P. V. Krebs, "Use of Computer-Aided Analysis Techniques for Cover Type Mapping in Areas of Mountainous Terrain," Information Note 091274, Laboratory for Applications of Remote Sensing (LARS), Purdue University, West Lafayette, Indiana 47907; September 1974.

2. C. L. Wu, D. A. Landgrebe, and P. H. Swain, "The Decision Tree Approach to Classification," Information Note 090174, Laboratory for Applications of Remote Sensing (LARS), Purdue University, West Lafayette, Indiana 47907; May 1975.

3. G. F. Hughes, "On the Mean Accuracy of Statistical Pattern Recognizers," IEEE Transactions on Information Theory, volume IT-14, no. 1, pp. 55-63, January, 1968.

4. H. Hauska and P. H. Swain, "The Decision Tree Classifier: Design and Potential," Proceedings Purdue Symposium on Machine Processing of Remotely Sensed Data, Purdue University, West Lafayette, Indiana, June 1975.

5. P. H. Swain and R. C. King, "Two Effective Feature Selection Criteria for Multispectral Remote Sensing," Proceedings International Joint Conference on Pattern Recognition, Washington, D. C., November 1973.

6. L. A. Bartolucci, R. M. Hoffer, and T. R. West, "Automatic Data Processing of Remotely Sensed Data for Temperature Mapping of Surface Water," Information Note 042373, Laboratory for Applications of Remote Sensing (LARS), Purdue University, West Lafayette, Indiana 47907; August 1973.

Table I. SOME APPLICATIONS OF LAYERED CLASSIFIERS

General Application	Example
Change Detection	Snow pack variation Water level variation (e.g., reservoirs) "Urban sprawl" Logging practices
Use of Mixed Feature Types	Texture Topography Geophysical data (e.g., aeromagnetic)
Class-specific Properties	Crop disease detection Forest type mapping Water quality mapping Water temperature mapping (see text)
Other	Avoidance of cloud effects (see text) Minimization of data dimensionality

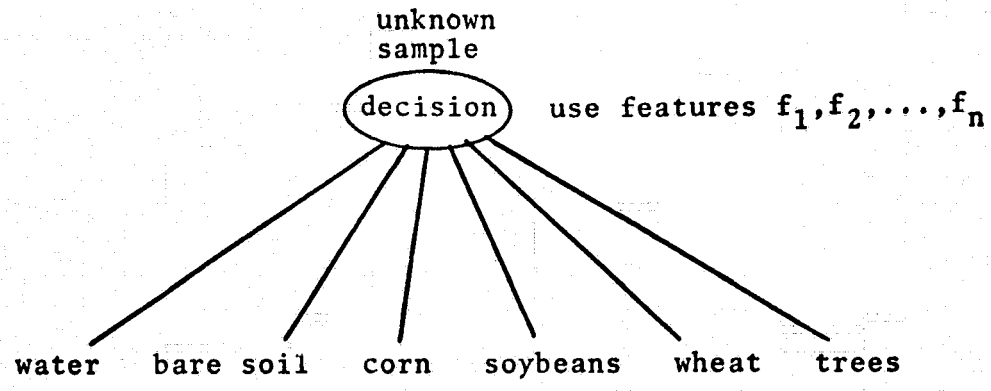


Figure 1.- Common single-stage classifier.

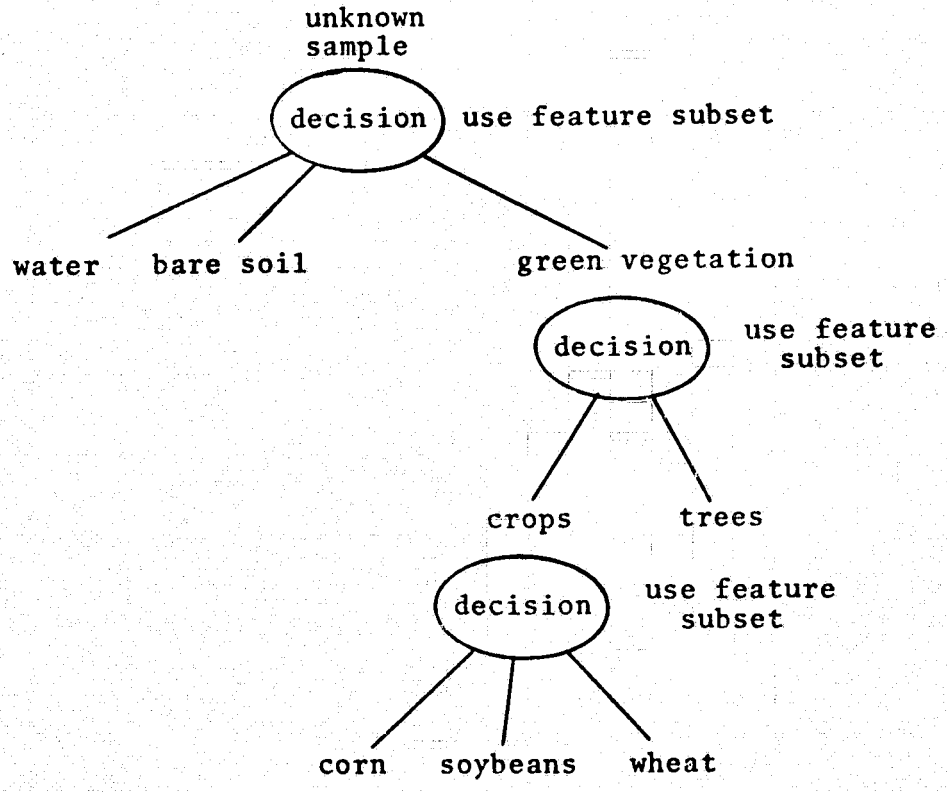


Figure 2.- A layered classifier.

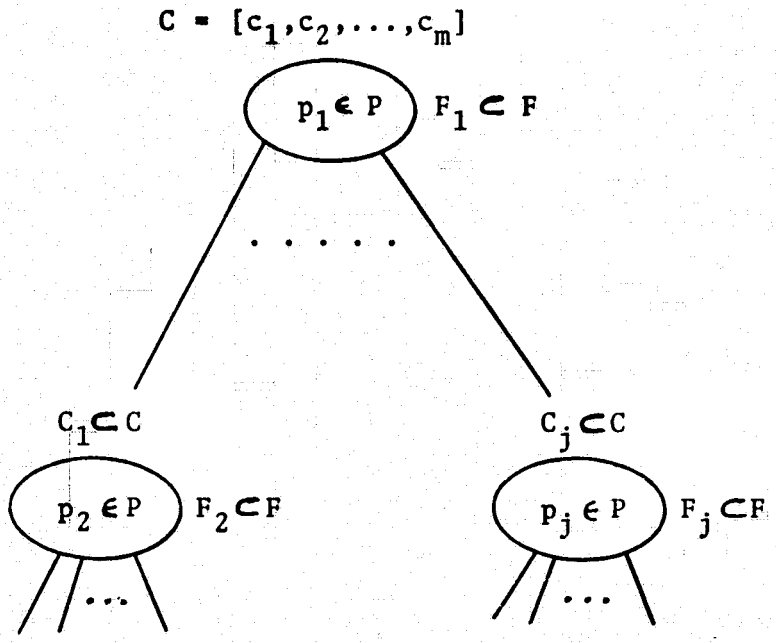


Figure 3.- General form of the decision tree.

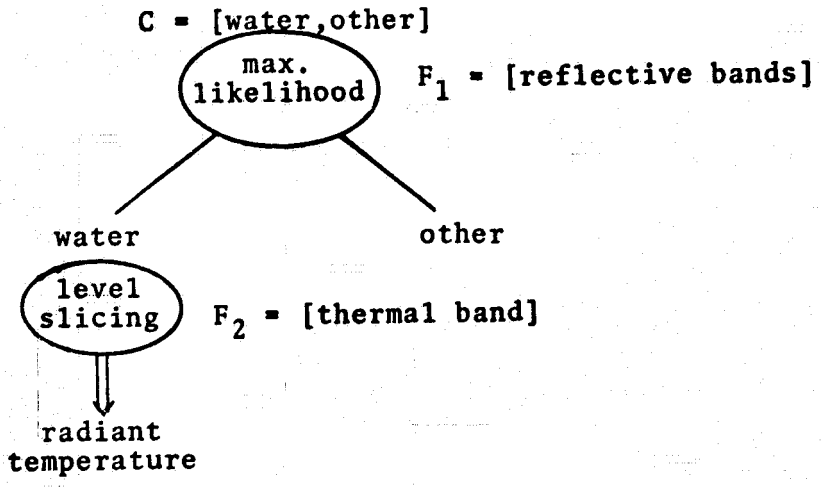


Figure 4.- A layered classifier for water temperature mapping.

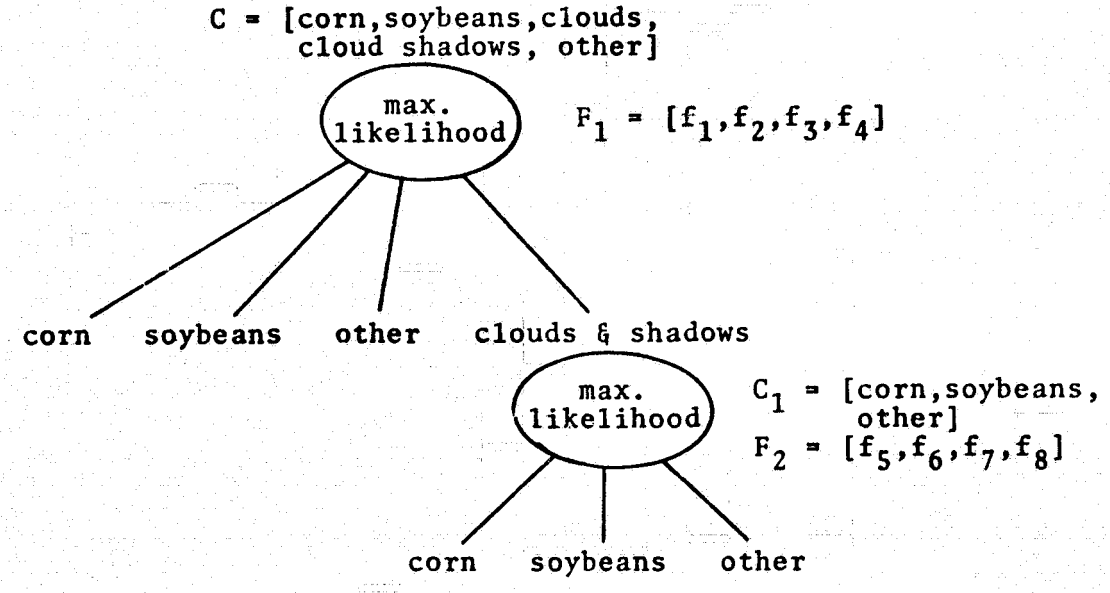
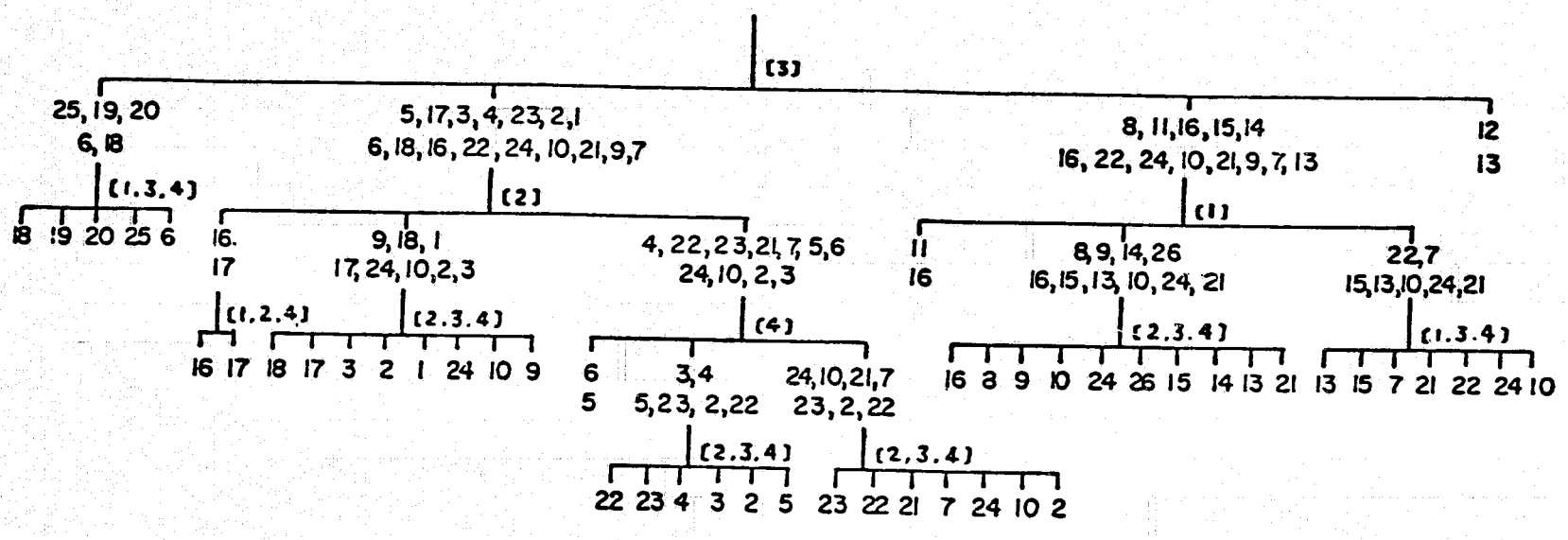


Figure 5.- Agricultural classification in the presence of clouds.



1. All decisions are maximum likelihood.

2. [ ] indicates features used.

3. Conifer: classes 1,2,3,4,5,6,23,25.
   Deciduous: classes 7,8,9,10,24,26.
   Agriculture: classes 11,12,13,14,15.
   Bare rock: class 17.
   Water: classes 18,19,20.

Figure 6. A layered classifier designed for accuracy and efficiency.

THE MIXTURE PROBLEM IN COMPUTER MAPPING OF TERRAIN: IMPROVED TECHNIQUES FOR ESTABLISHING SPECTRAL SIGNATURES, ATMOSPHERIC PATH RADIANCE, AND TRANSMITTANCE

By Harry W. Smedes, U.S. Geological Survey, Denver, Colorado,
Roland L. Hulstrom, Martin Marietta Aerospace Corporation, Denver, Colorado, and
K. Jon Ranson, Colorado State University, Fort Collins, Colorado

N76-17526

ABSTRACT

Among the results of our LANDSAT and Skylab research programs on the effects of the atmosphere on computer mapping of terrain, we emphasize the following: (1) The concept of a ground "truth" map needs to be drastically revised; (2) the concept of training areas and test areas is not as simple as generally thought because of the problem of pixels that represent a mixture of terrain classes; (3) this mixture problem needs to be more widely recognized and dealt with by techniques of calculating spectral signatures of mixed classes, such as those we used, or by other methods; (4) atmospheric effects should be considered in computer mapping of terrain and in monitoring changes; and (5) terrain features may be used as calibration panels on the ground, from which atmospheric conditions can be determined and monitored.

The natural terrain comprises a mixture of diverse classes, including combinations of such things as tree, grass, and other vegetative-cover species, different types of soil and rock, and water bodies of different size, depth, and clarity. Because the terrain features generally are small compared to the ground resolution element (= pixel) from multispectral scanner data, it is unusual for very many contiguous pixels to consist of a single terrain class. Commonly, each pixel is a mixture of two or more classes.

It has been shown that the spectral signature (radiance) of a mixture of terrain classes is not representative of any of the component classes composing the mixture. Automatic recognition processors may therefore misclassify mixture-containing pixels, which often leads to an underestimation of the amount of component classes present in the area scanned.

Even a single class may have a range in spectral signature depending on such things as size of pixel (sample size), solar aspect, orientation, and atmospheric conditions.

Because of this problem of mixtures in pixels, we at first attempted to compile ground control maps whose classes were designated by different increments of the more widely occurring mixtures and to train the computer to recognize them by selecting specific TRAINING AREAS of known proportions of classes. Not only was this a monumental task, loaded with subjective judgements and difficult to calibrate, but the TESTING of accuracy of the resulting computer-derived map proved to be equally monumental. After much effort we concluded that--if not impossible--it was certainly not at all feasible to prepare a truly accurate ground control map. In fact, while checking for errors in the computer map, the ground control or so-called ground "truth" map continually had to be upgraded. A serious problem that needs to be faced is: "what constitutes the ground truth?" Our first major conclusion was that, if properly trained on end-member and mixed classes, the computer made a more accurate map of terrain cover than we were able to compile as control data.

However, it is very difficult to measure precise proportions of mixtures and to locate those areas in terms of LANDSAT MSS, Skylab S-192, or other scanner pixels, especially in areas of mountainous terrain. This difficulty and the resulting uncertainty and imprecision led us to experiment with techniques to calculate mixes from data for end members and to use those calculated signatures in lieu of training areas for the mix classes. Previous research in this problem has largely been confined to classes of crops in flat agricultural fields. Our data and techniques will apply equally well to conditions ranging from croplands to wilderness.

PRECEDING PAGE BLANK NOT FILMED

Inasmuch as the radiance from a pixel is integrated over the entire area of the pixel (the instantaneous field of view of the scanner), mixture-class signatures can be determined from the known mean vectors and covariance matrices of the component classes and the proportional areas occupied by each component in the pixel. Signatures for mixed classes were calculated using spectral radiance from on-site measurements. In addition, several experiments were conducted with simulated LANDSAT MSS-type data to show the expected improvement in accuracy of automatic classification using simulated mixture-class signatures. We also studied methods for determining component class signatures when there were insufficient data points for conventional signature extraction.

Results are presented of a test area in mountainous terrain of south-central Colorado for which an initial classification was made using simulated mixture-class spectral signatures and actual LANDSAT-1 MSS data.

Not only are these techniques highly successful in terms of shorter preparation time and higher accuracy, but the calculated signatures also afford insights into what the appropriate increments of mixes and what the optimum wavelength bands are for the most accurate discrimination among specific classes.

Atmospheric effects must be known in order to combine spectral signatures derived directly from LANDSAT or Skylab scanner tapedata with those measured on-site and from aircraft. A few large homogeneous sites such as a large body of deep clear water, a large expanse of bare rock, dense forest, large nonvegetated dry lake bed or desert sand, and snow may serve as known natural calibration panels on the ground. These would be visible from spacecraft, from which the atmospheric path radiance and transmittance can be derived for each data set (mission or flight). This calculated path radiance and transmittance can then be applied to correct the tape data for true radiance values of the terrain classes. Used in another sense, this technique can serve as a useful means of monitoring atmospheric quality from spacecraft or aircraft, as atmospheric path radiance and transmittance are measures of air quality.

INTRODUCTION

Multispectral scanner data from satellites are used as input to computers for automatically mapping terrain classes of ground cover. Some major problems faced in this remote-sensing task include 1) the effect of mixtures of classes and, primarily because of mixtures, the problem of what constitutes ground "truth"; and 2) effects of the atmosphere on spectral signatures. This paper presents the fundamental principles of these problems and some of the results of our studies of them for a test site in Colorado, using LANDSAT-1 data.

The test site (figure 1) comprises about 2280 sq. km (880 sq. mi) of generally wildland terrain in south-central Colorado. It includes such landmarks as Pikes Peak, the Cripple Creek mining district, and Canon City. Altitudes range from 1525 to 4300 m. The terrain is highly varied and includes a diversity of rock types, soil, and vegetative cover, over a wide range of angle and aspect of slope.

The research was carried out as an integral part of LANDSAT and Skylab EREP projects funded by NASA, and by in-house research supported by the Martin Marietta Aerospace Corporation. Computer support was provided by Colorado State University and a computer-derived map was made by the Environmental Research Institute of Michigan (ERIM) as their part of a separate but coordinated LANDSAT project funded by NASA. This map provided further insights into the nature of the mixtures problem. This research effort was conceived, initiated and coordinated by Smedes. Hulstrom measured atmospheric properties and studied their effects, made on-site measurements of spectral signatures, and used these data in a computer program to calculate signatures of mixtures. Ranson studied the effects of mixtures using simulated LANDSAT data as part of a dissertation for an advanced degree at Colorado State University.

THE MIXTURE PROBLEM

The natural terrain is composed of mixtures of classes. This is true regardless of the size of the ground resolution element (= pixel) of the sensor system, and holds for satellite

data with resolution on the order of 100 sq. meters, to that of the microscope with resolution of the order of a sq. micron or less. By tradition, each discipline of the natural sciences has accommodated this mixtures problem by means of graded orders or hierarchies of classifications. We thus have, in order of decreasing size of resolution element, such classes as galaxies; stars and planets; continents and oceans; mountains, ridges, valleys, plains and deserts; woodlands, meadows, bare rock, and soil; spruce, aspen, bunchgrass, granite, and quartz veins; bark, needles, leaves stems, quartz, feldspar, and mica grains; petioles, chloroplasts, mitochondria; perthite, albite with fluid inclusions , and magnetite inclusions in biotite. Because we are dealing with current satellite scanners, the resolution element or pixel size we are concerned with is 65-80 m square. This results in high likelihood that any given pixel will contain two or more of such classes as woodlands, meadow, bare rock, and soil. If a recognition processor (computer) is trained to recognize only the homogeneous component classes (trees, grass, rock, etc.) the overall consequences of a mixture of these classes occurring within a pixel is a misclassified or unclassified pixel, which tends to make estimates of the area covered by a terrain class lower than actually present (ref. 1). Errors in classifications due to the mixture problem alone will be 25 to 30 percent (ref. 2 and 3).

There are two basic kinds of mixtures. One is due to the boundary or edge effect, where a pixel encompasses the interface of two or more homogeneous end-member component classes, such as water and dense coniferous forest. The resulting spectral signature would not be representative of a pixel that contained only one of these classes. The other mixture is represented by pixels which contain homogeneous mixtures of such things as forest canopy and grass, rock, or soil understory. In the first case, only the pixels along the interface will be misclassified. In the second case, large clusters of pixels throughout the forest will be misclassified if only the component classes were used to train the computer (ref. 4, 5, 6).

Variations in the amount of vegetative cover will result in corresponding mixtures of the vegetation and underlying material. Consequently, if the computer is trained to recognize only one vegetation density, then misclassifications would occur for densities above or below that of the training class, within the constraint of some response threshold. These misclassifications occur because when a mixture of terrain classes is contained within the instantaneous field of view (IFOV) of a scanner, the spectral response obtained is unlike that of any of the component class signatures (ref. 7). To illustrate this concept, three terrain classes were identified on graymaps of August 20, 1972 (frame no. 1028-17135) LANDSAT-1 MSS data that appeared representative of grassland (A), dense forest assumed to be 100% cover (B) and a class representing an assumed 50-50 mixture (C) of classes A and B and located on the interface between them. Spectral signatures were extracted with 21 data points sampled for Class A, 72 for class B and 24 for class C. The mean spectral response curves for the three classes are shown in figure 2. Note that the spectral response for the mixture class C is uncharacteristic of either of its component classes (A and B) but that the response curves falls between the two components' curves. Researchers investigating this phenomenon have found that the relationship of a mixture and the signatures of the component classes may be approximated as a function of the area of the pixel occupied by each component terrain class and their respective spectral signatures.

Because of this problem of mixtures in pixels, we at first attempted to compile ground control maps whose classes were designated by different increments of the more widely occurring mixtures and to train the computer to recognize them by selecting specific training areas of known proportions of classes. This method, described in detail in ref. 6 and 8, is extremely time-consuming, loaded with subjective judgements, and very difficult to calibrate. Testing the accuracy of the resulting computer-derived map is even more time-consuming.

Our conclusion, supported by other work (such as reported in ref. 6, 8, and 9), was that if the computer is properly trained on end-member components and on commonly-occurring mixtures, it could make a more accurate map of the terrain cover than we were able to compile as control data. This casts serious doubt upon and calls for reconsideration of what constitutes the ground "truth".

However, it is very difficult to measure precise proportions of mixtures and to locate

those areas in terms of LANDSAT MSS, Skylab S-192, or other scanner pixels, especially in areas of mountainous terrain. This difficulty and the resulting uncertainty and imprecision led us to experiment with techniques to calculate mixes from data for end members and to use those calculated signatures in lieu of training areas for the mix classes. Previous research in this problem has largely been confined to classes of crops in flat agricultural fields. Our data and techniques will apply equally well to conditions ranging from croplands to wilderness.

Inasmuch as the radiance from a pixel is integrated over the entire area of the pixel (the instantaneous field of view of the scanner), mixture-class signatures can be determined from the known mean vectors and covariance matrices of the component classes and the proportional areas occupied by each component in the pixel.

Two approaches were taken. One was to measure the reflectivity of pure end-member components on site and then calculate signatures of various mixtures. The other was to use the satellite data itself to extract the radiance signatures of known end-member targets and then calculate radiance signatures for various mixtures. Simulated LANDSAT MSS-type data were used. They show the expected improvement in accuracy of automatic classification using simulated mixture-class signatures. In addition, methods have been developed for determining component class signatures from mixtures when there were insufficient data points for conventional signature extraction of the end-member components.

CALCULATED SPECTRAL SIGNATURES FOR MIXTURES

Basic Concept

The basic problem of correctly identifying ground resolution elements that contain mixtures of terrain classes with simulated mixture signatures is obtaining representative signatures for the component classes. A component class can be defined as a homogeneous or non-homogeneous group of materials that make up a discrete mapping class or terrain type. A discrete mapping class may or may not be found in combination with other discrete classes as mixtures. For example, in an area where there is a sparse covering of grass with bare soil showing through, the grass and soil may be considered as two discrete mapping classes. With the 0.4 ha resolution of LANDSAT, the scene would be viewed as a mixture of grass and bare soil so these two classes would most likely be combined into one component class for analysis. If another class were identified as dense forest, then any time enough trees existed on the grass-soil unit to affect the response of a pixel, then a mixture of these two classes (forest and the grass-soil association) would exist. Discrete mapping class determinations can usually be considered a function of the natural associations, the objectives of the user, spectral radiance, and the limitations of the MSS data.

When selecting component classes for mapping mixtures, care must be taken to avoid situations where the data for a class form a multimodal distribution. Multimodal distributions occur where the response data for a class are affected by variables such as slope and aspect, vegetation vigor, underlying soil spectra, and sensor scan angle effects. The standard method for dealing with this problem is to divide the multimodal class distribution into subclasses as a function of slope, etc., classify the data and then combine the results for each subclass (ref. 10, 11) for final display.

Calculations From On-site Measurements

Mixtures.- For on-site and near-surface measurements (negligible atmospheric transmission and path radiance) the radiance, N_t of a pure target end-member can be given as

$$N_t = \frac{H\rho}{\pi} \tag{1}$$

Where H is the total solar irradiance and ρ is the target reflectivity. The radiance from a mixture of targets, N_m, can be given as

$$N_m = \frac{H}{\pi}(\rho_1 A_1 + \rho_2 A_2 + \rho_3 A_3 + \cdots \rho_n A_n) \tag{2}$$

where ρ_1, ρ_2, etc. are the reflectivity signatures of each component target, and A_1, A_2, etc. are the fractional proportions of the pixel that each component target occupies. The assumption is made that none of the component targets have strong specular reflectivities.

Note that even for the near-surface conditions, there are atmospheric effects to be considered (H, in equations 1 and 2, above).

In order to simulate mixed target radiance signatures, a knowledge of the total incoming solar irradiance (H), the pure target reflectivity signatures, and the fractional area of each target need to be known. In this study the spectral distribution and magnitude of the incoming solar irradiance is measured for various sun angles and atmospheric conditions; and the pure target reflectivities are measured on site and from a helicopter. The fractional area occupied by each target is simply varied to simulate various combinations of mixtures.

The first mixture problem addressed was that of Pikes Peak Granite and Coniferous Forest. This represents a very simple and common mixture. The reflectivity for the Pikes Peak Granite and the total incident solar irradiance were measured on site (as discussed in the following sections) while the reflectivity signature for Coniferous Forest was taken from ref. 12. Figure 3 shows all three of the parameters. The resultant simulations of component and mixture signatures for the LANDSAT bands and for the continuous spectral region from 500 to 1100 nm are shown in figures 4 and 5. It is interesting to note that (as shown in fig. 4 and 5) for a 50-50 mixture of rock and trees, the resultant mixture radiance signature no longer contains the characteristic chlorophyll absorption feature. The resultant radiance signature would most likely be interpreted as a grayish, low-albedo rock.

Spectral contrast.- In addition to computer simulations of pure and mixed target radiance signatures, the spectral inherent contrast of various targets and their background can be calculated. The inherent contrast, C, of a target versus its background is

$$C = \frac{N_T - N_B}{N_B} \qquad (3)$$

where N_T is the radiance signature of the target and N_B is the radiance signature of the background. The target and/or background can be any pure target or mixture of targets.

Spectral contrast was calculated in order to determine if there existed any particular spectral region or band that gave a better contrast than other spectral regions or bands. The goal of these spectral contrast calculations is not to exclusively attempt to determine if "optimum" bands existed for the discrimination of rock types, vegetation types, etc. Rather, the goal is to determine "optimum" bands for maximum spectral contrast between a selected target(s) and its background; because, for the natural terrain existing in the Colorado test site, this goal is in line with the actual terrain conditions. For example, two rock types rarely exist side-by-side with good exposure; instead, a given rock type is exposed and surrounded by a background made up of a complex mixture of other terrain. If the rock types do exist side-by-side they usually do not fill the entire field of view of the sensor. This is due to the fact that they occur as small outcrops and/or they exist in layers exposed on extremely steep slopes or cliffs.

An example of the computer spectral contrast calculations is shown in figure 6. The pure target is Pikes Peak Granite, and the background consists of mixtures of granite and coniferous forest. It is obvious that there are "optimum" spectral regions; and, if the background comprises a mixture, the contrast is reduced tremendously. The same case, only applied to the broader bands of LANDSAT, is shown in figure 7. As can be seen, "optimum" bands still exist; however, the overall contrast is reduced because of the broader bands.

The computer calculations of spectral contrast are not limited to the LANDSAT spectral resolution, but can be used to determine spectral contrast for any selected wavelength resolution or band width. The resolution is only limited by the resolution of the instrument used to measure solar irradiance and reflectivity. Such computer simulations of radiance signatures and spectral contrast would be a very useful tool for planning aircraft multi-

spectral remote sensing missions. A combination of a few selected measurements of solar irradiance and reflectivities, and the subsequent computer calculations of spectral contrast could be used to select film/filter combinations that would yield the highest contrast. This method would eliminate costly flights and subsequent data reduction performed in hopes of empirically determining optimum bands.

Calculations From LANDSAT Data

Modeling of spectral signatures of mixture.- Two approaches for modeling were used in this study. The first is a widely reported method that describes a mixture class signature in terms of weighted combinations of component class mean vectors and covariance matrices (refs. 1, 2, 7, and 13). The model describes the mean spectral response from a ground resolution element as:

$$M_{P_i} = \sum_{i=1}^{N} P_i M_i \tag{4}$$

where M_{P_i} = Mean response vector for a mixture of N component classes;

P = Relative amount (proportion) of class i;

M_i = Mean response vector for the ith component class.

The above relationship assumes statistical independence of normally distributed data points belonging to class i.

Assuming statistical independence for variables associated with elements from different object classes, the relationship for a mixture class covariance matrix can be written as:

$$C_P = \sum_{i}^{N} P_i C_i \tag{5}$$

where C_P = Covariance matrix for a mixture of N component classes;

P = Relative amount (proportion) of class i;

C_i = Covariance matrix describing the distribution of the ith component class.

Equations (4) and (5) represent the model used for automatic classification of mixtures of classes with a maximum likelihood processing algorithm. For supervised learning recognition processors, component class mean vectors and covariance matrices must be determined and proportions for each possible mixture must be specified. The approach presented here is based on modeling the spectral response within a single pixel and should be applicable to recognition processing with the RECOG (ref. 10, 14, 15) maximum likelihood algorithm (GLIKE) since classification is point by point.

Most of the work reported in the literature utilizing this modeling technique required sophisticated algorithms that calculate various mixture class signatures and select the one that gives the closest approximation of the response from a given pixel. In our study, however, we used the model to obtain a set of spectral signatures for specified mixtures of component terrain classes that are used by the RECOG pattern recognition routines to identify all MSS data points that exhibit that response. The value of this method lies in its straightforward applicability to the existing RECOG processing sequence, thus eliminating the need to develop new processing algorithms.

Equation 4 was used to simulate the spectral response expected from a mixture of the two component classes (A and B) whose extracted mean vectors were shown in Figure 2. Figure 8 shows the resulting simulated mean vector (D) for a 50% mixture of the two classes ie.

$P_A = P_B = 0.5$. A likely explanation for the difference between curves C and D is the difficulty of accurately estimating cover densities from high altitude aerial photographs used as ground control (in this case Mission 205, NASA RB-57 photographs with an approximate scale of 1:100,000) and the difficulty of locating non-homogeneous (mixture) training sets on graymaps (ref. 16).

When a set of representative component terrain class signatures are obtained then the signature of any mixture of these component classes may be determined using Equations 4 and 5. A computer program MIX was written to take two component class signatures and two proportion vectors and calculate the spectral response of any combination. The method involves scaling the mean vector and covariance matrix of a component class by a proportion factor and adding the result to the scaled mean vector and covariance matrix of another component class. The proportion factors P must be within the set $0 \leq P \leq 1$ and $P_j = 1$. The resulting spectral signature may then be used to classify all pixels in a set of LANDSAT MSS data that exhibit a similar spectral response.

The second modeling technique used linear regression to predict the spectral response of a mixture-containing pixel based on the mean response vectors for known mixtures of terrain classes. The regression model for a two-component mixture takes the form:

$$Y_i = C + B(X) \tag{6}$$

where Y = estimated mixture response in wavelength band i;

C = constant (Y intercept);

B = coefficient (slope of regression line);

X = proportion of one component of the mixture in the pixel scene.

Mead (ref. 5) indicated that this method may be useful in estimating the spectral response for varying densities of ponderosa pine, but also noted that the mean spectral response may be affected by the arrangement or distribution of ponderosa pine within a training set as described by the standard deviation.

The methods presented below, with the exception of signature extraction, were developed for mixtures of two component classes. The following is a synopsis of the techniques used to obtain component- and mixture-class spectral signatures for automatic analysis of MSS data:

METHOD	TECHNIQUE	COMPUTER PROGRAM
Signature Extraction	Statistical sampling of MSS data points	RECOG (Phase 2, Appendix A, B) (see ref. 14 & 15)
Component Signature Estimation	Solving simultaneous equations	SIGCALC
	Linear regression	STAT38R
Mixture Signature Simulation	Addition of weighted mean vectors and covariance matrices	MIX

Signature Extraction.- When areas on the ground have been satisfactorily identified as containing a known terrain class or mixture of terrain classes and the graymap coordinates have been determined, then spectral signatures may be obtained by statistically sampling these points. This process is known as signature extraction and represents the conventional mode for obtaining signatures that are assumed to characterize a class of objects. The designated data points known to contain a terrain class are sampled and the overall mean is determined for each channel of MSS data. These means, four in the case of LANDSAT-1, are

collectively known as the mean vector. Because of the inherent variability found in natural objects an additional set of statistics is obtained that characterizes the population distribution of the sampled data points. This set of statistics is the class covariance matrix and describes the within-channel and between-channels variation of the data. The technique used in this work is contained in the RECOG routines, specifically Phase 2 (Appendix A). The formulas used in these routines are described in Appendix B.

Estimating component-class spectral signatures.- One method for estimating component class signatures from known mixture class signatures involves solving two equations with two unknowns. The spectral signatures for unknown mixture classes are assumed to be related and can be described in equation form in the following manner:

$$P_a(MSR_a)_i + P_b(MSR_b)_i = M_{p_i} \tag{7}$$

where P_a, P_b = Proportions of classes A and B in the training set, respectively.

$(MSR_a)_i$,$(MSR_b)_i$ = Mean spectral responses of the component classes A and B, respectively in wavelength band i.

M_{p_i} = Mean spectral response recorded at the scanner for the mixture of classes A and B in wavelength band i.

The terms P_a, P_b, and M_p are known for each training set, leaving the mean spectral responses of the component classes A and B to be determined. If there exist two sets of spectral signatures describing training sets with similar components but of different proportions, then it is possible to calculate the two component classes by solving the two equations simultaneously. A general solution for the two-component class case takes the form:

$$MSR_{bi} = \frac{M_{p_{1i}} P_{a_2} - M_{p_{2i}} P_{a_1}}{P_{a_2} P_{b_1} - P_{b_2} P_{a_1}} \tag{8}$$

Equation 8 produces the mean spectral response for class B. To derive the mean spectral response for class A, the result can be substituted into equation 7 which can be rewritten as

$$MSR_{a_i} = \frac{MP_i - P_b MSR_{bi}}{P_a} \tag{9}$$

If the elements of the covariance matrix for a terrain class spectral signature behave in a similar fashion, then this method could be used to obtain a calculated covariance matrix for a component terrain class. The covariance matrix for a four-channel case such as LANDSAT-1 can be treated as a 10 element array to simplify the calculations. This can be done since the off-diagonal elements of the covariance matrix are mirror images of each other.

A computer program called SIGCALC was written to take two extracted mixture terrain-class spectral signatures and calculate the mean vector and covariance matrix for the component classes. In addition, the proportions of the component classes in the training set determined from ground truth must be specified. Situations where $P_{a_2} P_{b_1} = P_{b_2} P_{a_1}$ must be avoided since the denominator of equation 8 cannot equal zero.

The above method for determining component class spectral signatures should provide reliable results if the proportion estimates for the component classes are accurate. However, it is often difficult to measure the proportions of component classes with the accuracy needed to estimate representative component class signatures. Also, due to the variability of spectral responses for component classes found in nature it was decided to use another method that estimates the component-class spectral signatures from more than two mixture-

class signatures. This method involves using a stepwise linear regression analysis.

The stepwise linear regression analysis used is an applications program available at Colorado State University called STAT38R (ref. 14, 15). This program was used to develop a regression model that estimates the spectral response of a terrain class, either a component or mixture, given a set of mixture-class spectral signatures and the proportions of the component classes.

Simulations of LANDSAT data.- In order to examine the applicability of modeling mixture-class spectral signatures for automatic classification of LANDSAT-1 MSS data, a series of experiments was performed with simulated data. They include: identifying the expected improvement of automatic classification using modeled mixture terrain-class signatures versus conventional component class analysis, comparing modeled and extracted mixture-class mean vectors and covariance matrices, and analyzing the signature calculation technique.

Creation of simulated data fields: The automatic classification procedure conducted for these experiments approximates that of conventional RECOG LANDSAT-1 MSS analysis (ref. 10, 14, 15) with the exception of using modeled mixture class signatures and simulated LANDSAT-1 data. The steps are: 1) Examine control data on site to establish locations of representative training sets, determining the line and column numbers of the training sets on graymaps and extracting the mean vectors and covariance matrices from the data. 2) Simulate mixture signatures with the component class signatures obtained in Step 1 using Program MIX. MIX requires the mean vectors and covariance matrices of the component classes as input, as well as the mixture proportions desired for each mixture class. The simulated mean vectors and covariance matrices are punched on computer cards by MIX for future use. 3) Generate a random-normal data field for each class in RECOG format with program DTAFILE. This program uses a random-number generator that selects points as belonging to a given class based on the mean spectral response in each LANDSAT-1 MSS band and the appropriate covariance matrix, all within a normal Gaussian distribution. The overlying assumption here is that wildland terrain classes are normally distributed, which conforms to the assumptions imposed on the mixture modeling method (ref. 7) and the maximum likelihood pattern recognition algorithm (GLIKE) of RECOG (ref. 10). DTAFILE was designed to create simulated data fields of specified size for each class described by a mean vector and covariance matrix. The generated data points are written on a permanent file and stored for later use by any routine that uses data in a RECOG format.

The simulated data fields for each of the component and mixture classes were generated to contain 1000 spectral response values in each wavelength band, with each point being described by four variables (spectral response in each wavelength band).

The data fields as generated by DTAFILE represent LANDSAT-1 MSS data with the added advantage of "absolute" ground truth information. With these fields it is possible to analyze the accuracy of automatic classification using the conventional RECOG maximum likelihood routine and the mixture terrain-class modeling method. An example data field is shown in figure 9 as a graymap of a nine-class field. The class fields can be seen as horizontal bands 100 points across and 10 points down.

Classification of component classes: The initial experiment performed involved using a classification of simulated data that contained fields of two component classes and three mixture classes modeled from these components. Two component classes, Grassland (denoted by the symbol, G) and Forest (F), were identified on NASA RB-57 (scale 1:100,000) color IR aerial photographs and located on a graymap of August 20, 1972 LANDSAT-1 MSS (Frame no. 1028-17135) data over south-central Colorado. Signatures were extracted and then used to obtain mixture class signatures with program MIX. The mixture classes were simulated with a specified proportion increment of 0.25, producing three mixture classes of 75% Grassland - 25% Forest (C), 50% Grassland - 50% Forest (D), and 25% Grassland - 75% Forest (E). The mean spectral-response curves for the five classes are shown in figure 10.

The simulated data fields were then treated as actual LANDSAT-1 MSS data for purposes of classification. Component-class signatures were extracted from those fields created with

component-class signatures (top 3 rows, fig. 9) and used to classify the entire set of simulated data. The classification display is shown in figure 11 with the Grassland field at the top and the Forest field at the bottom. The mixture class fields are located between the components with C nearest the Grassland field, D in the middle and E nearest the Forest field. Note the number of unclassified points (seen as blanks in the display) in each of the mixture-class fields. These points were thresholded out at the 11.100 percentile as not belonging to either of the component classes. Misclassifications of the mixture-class fields occur only in fields C and E, with points being misclassified as the component class which has the highest proportion in the mixture.

The absolute classification accuracies were determined for each class. Since each data point was created as a specified class, a point was considered misclassified if it was classified as any class other than that specified. The results are summarized in the following classification confusion matrix (CCM) listing each class, the number of points that were classified correctly, and the number of points misclassified as other classes.

CLASS	F	E	D	C	G
FOREST (F)	1000				
25% GRASSLAND - 75% FOREST (E)	148				
50% GRASSLAND - 50% FOREST (D)					
75% GRASSLAND - 25% FOREST (C)					376
GRASSLAND (G)					1000

The table is read with the true class name and symbol on the left and the symbols of classes that a point was classified as across the top. The diagonal elements of the matrix represent accurate classifications. The off-diagonal elements represent either Type I or Type II errors, defined as follows.

Decision	True Classification	
	X belongs to A	X Does Not Belong to A
Classify AS A	Correct Decision	Type I Error
Do Not Classify AS A	Type II Error	Correct Decision

The overall accuracy of this classification was only 40.0% which in most LANDSAT-1 applications should be considered quite poor even though the component classes were classified perfectly.

Classification of two component and three mixture classes: The objectives of the study presented in this section were twofold. The first was to verify that the mixture-class spectral-signature modeling technique produces signatures that can be used by RECOG to classify pixels that contain mixtures. The second, assuming the first to be satisfied, was to determine the increase in information acquired using modeled mixture-class signatures over classification conducted with only component-class signatures.

The same data-field generated for the analysis of component classes was used for this experiment. Treating the data file as actual LANDSAT-1 MSS data, component-class mean vectors and covariance matrices were extracted. Signatures for the mixture-class fields were not

extracted from the data, but instead were modeled from the component-class mean vectors and covariance matrices. This procedure follows that which could be used with actual LANDSAT-1 data since representative mixture-class training sets are usually difficult to locate in natural situations. The two extracted component and three modeled mixture-class signatures were used to classify the simulated data file.

At this point it was desirable to compare modeled and extracted mean vectors and covariance matrices. The signatures of the mixture classes were extracted from the simulated data and compared with those that were modeled from the two component classes, as follows:

	Extracted				Simulated			
CLASS	GRASS							
BAND	1	2	3	4				
MEAN	32.45	34.13	39.10	19.40				
STD. DEV.	1.07	1.82	1.54	.88				
CLASS	75% GRASS-25% FOREST							
BAND	1	2	3	4	1	2	3	4
MEAN	28.57	28.48	34.40	17.26	28.57	28.46	34.35	17.21
STD. DEV.	1.06	1.80	1.65	1.01	1.04	1.72	1.66	.99
CLASS	50% GRASS-50% FOREST							
BAND	1	2	3	4	1	2	3	4
MEAN	24.71	22.86	29.62	15.04	24.68	22.78	29.61	15.01
STD. DEV.	1.05	1.54	1.74	1.11	1.00	1.54	1.76	1.09
CLASS	25% GRASS-75% FOREST							
BAND	1	2	3	4	1	2	3	4
MEAN	20.84	17.14	24.93	12.91	20.80	17.11	24.86	12.82
STD. DEV.	.99	1.42	1.87	1.21	.97	1.35	1.86	1.18
CLASS	FOREST							
BAND	1	2	3	4				
MEAN	16.92	11.44	20.12	10.63				
STD. DEV.	.95	1.12	1.96	1.26				

The results indicate that the extracted and modeled mean and standard deviation vectors vary, at most, by less than 0.1 of one standard deviation unit, which can be considered as quite adequate for this analysis. Figure 12 shows the classification display of the results. A classification confusion matrix (CCM) was also compiled for this analysis. It is a comparison of extracted and modeled mean and standard deviation errors. The standard deviations shown represent the square root of diagonal covariance elements. The results are as follows:

CLASS	F	E	D	C	G
FOREST (F)	997	3			
25% GRASSLAND - 75% FOREST (E)	9	977	14		
50% GRASSLAND - 50% FOREST (D)		8	967	25	
75% GRASSLAND - 25% FOREST (C)			12	970	18
GRASSLAND (G)				8	992

The classification results indicate that simulated mixture-class spectral signatures can be used to classify MSS data using the RECOG program. The classification information and accuracy were also greatly increased by the use of mixture signatures. The overall classification accuracy using this technique increased to over 98%, with only a slight decrease in the accuracies of component classes. It should be noted here that automatic classification of generated data fields will normally produce high classification accuracies due to the lack of "alien objects" which are often found in real life situations (ref. 3). The accuracies produced here should, instead, be considered a measure of the effectiveness of the classification technique. These results do indicate that given a pixel containing a mixture, it should be possible to accurately identify it with this method.

Classification of three component and six mixture classes: The successful results obtained with the five-class analysis warranted further study, so an additional component class was added to the signature set. A mean vector and covariance matrix for Water (W) was extracted from August 20, 1972 LANDSAT-1 MSS data. Mixture signatures were modeled from the Grassland component class and the new Water class with a proportion increment of C.25. The resulting three mixture classes and the component class combined with the original signature set bring the total number of signatures used to nine. Figure 13 shows the mean spectral response curves for the Grassland-Water mixture classes. The separation of these classes was adequate in all bands. The mean spectral response curves for all nine classes are illustrated in figure 14.

The classification procedure followed that of all previous experiments with a new data field being generated to include all nine classes. The classification display is shown in figure 15. A classification confusion matrix (CCM) for the 9-class analysis is as follows:

CLASS	F	E	D	C	G	Q	R	S	W
FOREST (F)	997	3							
25% GRASSLAND - 75% FOREST (E)	8	982	10						
50% GRASSLAND - 50% FOREST (D)		8	962	22		8			
75% GRASSLAND - 25% FOREST (C)			10	954	12	24			
GRASSLAND (G)				14	986				
75% GRASSLAND - 25% WATER (Q)			6	18		976			
50% GRASSLAND - 50% WATER (R)							999		
25% GRASSLAND - 75% WATER (S)								996	
WATER (W)									962

These results show a good classification accuracy for all the classes, with an average classification accuracy of 98%. Note that the greatest confusion exists between mixture classes that have the same proportion factor for a given component class, i.e., 75% Grassland-25% Forest and 75% Grassland-25% Water. This is probably the result of masking of the lesser components by the Grassland response.

REPRODUCIBILITY OF THE ORIGINAL PAGE IS POOR

The following comparison of the modeled and extracted mean and standard deviations was made as an additional check of the mixture modeling method:

	Extracted				Simulated			
CLASS	GRASSLAND							
BAND	1	2	3	4				
MEAN	32.49	34.19	39.09	19.46				
STD. DEV.	1.11	1.91	1.49	.92				
CLASS	FOREST							
BAND	1	2	3	4				
MEAN	16.95	11.48	20.19	10.67				
STD. DEV.	.92	1.15	1.95	1.26				
CLASS	WATER							
BAND	1	2	3	4				
MEAN	16.72	8.13	3.98	.24				
STD. DEV.	.55	.74	.63	.44				
CLASS	75% GRASSLAND-25% FOREST							
BAND	1	2	3	4	1	2	3	4
MEAN	28.57	28.48	34.40	17.26	28.60	28.51	34.36	17.56
STD. DEV.	1.06	1.80	1.65	1.01	1.06	1.75	1.62	1.00
CLASS	50% GRASSLAND-50% FOREST							
BAND	1	2	3	4	1	2	3	4
MEAN	24.68	22.81	29.61	15.01	24.72	22.84	29.64	15.06
STD. DEV.	1.00	1.52	1.77	1.08	1.02	1.57	1.73	1.10
CLASS	25% GRASSLAND-75% FOREST							
BAND	1	2	3	4	1	2	3	4
MEAN	20.83	17.10	24.82	12.83	20.84	17.16	24.91	12.87
STD. DEV.	1.01	1.33	1.82	1.17	.98	1.38	1.84	1.18
CLASS	75% GRASSLAND-25% WATER							
BAND	1	2	3	4	1	2	3	4
MEAN	28.49	27.62	30.30	14.59	28.55	27.67	30.31	14.65
STD. DEV.	1.01	1.62	1.35	.83	1.00	1.69	1.33	.82
CLASS	50% GRASSLAND-50% WATER							
BAND	1	2	3	4	1	2	3	4
MEAN	24.55	21.04	21.47	9.77	24.61	21.16	21.53	9.85
STD. DEV.	.85	1.39	1.20	.76	.87	1.44	1.14	.71
CLASS	25% GRASSLAND-75% WATER							
BAND	1	2	3	4	1	2	3	4
MEAN	20.67	14.63	12.75	5.00	20.66	14.64	12.76	5.04
STD. DEV.	.71	1.11	.91	.68	.73	1.14	.92	.59

As in the case of the five-class classification, the simulated mixture signatures closely approximate those extracted from the generated datafields. These results imply that if a representative set of component signatures can be found, then mixtures of these classes may be successfully modeled and used to classify pixels containing those mixtures.

Test of signature estimation technique: In wildland areas where large areas of homogeneous terrain classes are difficult to locate, it becomes necessary to obtain representative spectral signatures from a relatively small number of pixels. In some areas it is even diffi-

cult to find any pixels that contain only one terrain class (ref. 16). Consequently, methods to obtain component terrain-class signatures from pixels containing mixtures of terrain classes in known proportions have been investigated (for example, see ref. 17). The method involves solving a set of linear equations assuming that the data is from a Gaussian distribution and each signature has a common covariance matrix. Our study used a similar, but much simplified technique to attempt to acquire component-class spectral signatures from training-set data of terrain classes of known mixtures. A test of the method to obtain component-class spectral signatures using equations 8 and 9 was conducted using simulated data fields created in the same manner as the preceding experiments. The specific objectives of this test were: 1) to verify that this method could be used to determine component class signatures suitable for automatic mapping of LANDSAT-1 type MSS data when only mixture terrain classes were available for signature extraction, and 2) find out the type of classification accuracies that can be expected when implementing these estimated signatures as input into the model and RECOG.

The initial test used the random-normal data fields for the nine-class analysis described above. Spectral signatures were extracted from the data for mixture classes 75% Grassland-25% Forest (C), 50% Grassland-50% Forest (D), 75% Grassland-25% Water (Q), and 50% Grassland-50% Water (R). The pairs of extracted signatures and their corresponding proportion factors were input into SIGCALC and the component signatures for Grassland, Forest and Water were calculated.

Comparison between component class mean and standard deviation vectors extracted from the data set and those calculated with SIGCALC is as follows:

	Extracted				Calculated			
CLASS	GRASS							
BAND	1	2	3	4	1	2	3	4
MEAN	31.93	33.64	38.58	18.89	32.05	33.70	38.62	19.05
STD. DEV.	1.14	1.91	1.53	.92	1.30	1.97	1.48	.97
CLASS	FOREST							
BAND	1	2	3	4	1	2	3	4
MEAN	16.43	10.93	19.69	10.13	16.41	10.94	19.58	9.95
STD. DEV.	.92	1.19	1.99	.96	1.05	1.21	1.98	1.31
CLASS	WATER							
BAND	1	2	3	4	1	2	3	4
MEAN	16.21	7.61	3.50	.04	16.17	7.70	3.64	.00
STD. DEV.	.63	.80	.66	.19	.61	.82	.76	.52

The calculated component class signatures closely approximate the extracted with the average deviation being 0.08 for mean vectors and 0.15 for standard deviations.

In order to compare the effectiveness of estimated signatures with extracted signatures, the nine-class data field was classified by the computer. The class signatures used as input included the three estimated component signatures and six mixture-class signatures modeled from the estimated signatures. The classification accuracy obtained was approximately 2% less than that obtained when using extracted component signatures. The classification map

is shown in figure 16. The classification confusion matrix (CCM) of this data set is as follows:

CLASS	F	E	D	C	G	Q	R	S	W
FOREST (F)	984	13							
25% GRASSLAND - 75% FOREST (E)	17	973	10						
50% GRASSLAND - 50% FOREST (D)		20	964	11		4	1		
75% GRASSLAND - 25% FOREST (C)			27	876	25	65			
GRASSLAND (G)				59	907				
75% GRASSLAND - 25% WATER (Q)			28	24	2				
50% GRASSLAND - 50% WATER (R)							1000		
25% GRASSLAND - 75% WATER (S)								1000	
WATER (W)									1000

An overall classification accuracy of 96.1% was obtained, indicating that good classification results can be expected using this method.

The simulated data fields that contained the mixture-class signatures used to calculate the component classes represent uniform data. That is, each data point (pixel) represents a similar class of objects. Because this situation is sometimes difficult to find in natural situations, the technique was tested for mixture signatures extracted from non-uniform data or training sets. Non-uniform training sets can be defined as areas that contain a mixture of component classes with single pixels containing various proportions of the components. If the non-uniform training set is considered in its entirety the mean spectral response should approximate that from a uniform training set with the same proportions of component classes. The concept of uniform and non-uniform data is illustrated in figure 17 as two 20-pixel training sets, one containing a uniform mixture of two component classes (white and shaded) (a) and one containing a non-uniform mixture (b), but both with identical overall proportions of component classes. In the uniform training set each pixel (outlined by heavy black lines) contains a 50% mixture of two component classes, producing a 50% mixture within the entire training set. Since the spectral response from a pixel is integrated at the scanner optics, the within-cell distribution of the components does not affect the between-cell variance of the training set. The non-uniform training set is composed of some pixels containing 100% of one class, some containing 100% of the other class and some that contain various mixtures of the two components. The overall mixture proportion averaged over the entire training set is 50% of each component class. Referring to the equation 28 (Appendix B) it can be easily deduced that the mean vectors obtained from each training set should equal each other assuming constant illumination and no within-class variability. By equation 30 (Appendix B) however, it can be seen that covariance matrices will most likely vary due to the between-pixel variability existing in the non-uniform training set.

To verify these statements, mixture-class signatures from simulated non-uniform data were extracted and compared with those extracted from uniform data created with the same input

signatures. A comparison of extracted and calculated mean and standard deviation vectors of the component classes for uniform and non-uniform(*) data are as follows:

	Extracted				Calculated			
CLASS	GRASS							
BAND	1	2	3	4	1	2	3	4
MEAN	32.02	33.68	38.60	18.97	31.81	33.69	38.67	18.77
STD. DEV.	1.16	1.97	1.52	.96	1.08	1.36	1.64	1.00
CLASS	GRASS*							
BAND	1	2	3	4	1	2	3	4
MEAN	32.02	33.68	38.60	18.97	31.98	33.67	38.61	18.95
STD. DEV.	1.16	1.97	1.52	.96	5.17	8.59	11.15	6.09
CLASS	FOREST							
BAND	1	2	3	4	1	2	3	4
MEAN	16.43	10.93	19.69	10.13	16.53	10.93	19.55	10.13
STD. DEV.	.92	1.19	1.99	1.29	1.04	1.21	.88	1.31
CLASS	FOREST*							
BAND	1	2	3	4	1	2	3	4
MEAN	16.43	10.93	19.69	10.13	16.47	10.93	19.75	10.18
STD. DEV.	.92	1.19	1.99	1.29	5.02	7.32	6.33	4.35
CLASS	WATER							
BAND	1	2	3	4	1	2	3	4
MEAN	16.23	7.62	3.47	0.03	16.27	7.71	3.53	0.00
STD. DEV.	.63	.79	.67	.17	.63	.84	.56	.47
CLASS	WATER*							
BAND	1	2	3	4	1	2	3	4
MEAN	16.23	7.62	3.47	0.03	16.28	7.71	3.47	0.09
STD. DEV.	.63	.79	.67	.17	10.10	16.50	22.20	12.10

Note the close agreement of means and standard deviations from the uniform data and the close agreement of means but non-agreement of standard deviations calculated from the non-uniform data.

The consequence of using such large covariance matrices obtained from the non-uniform data is illustrated in Figure 18. The nine-class simulated data fields were classified with the calculated component signatures listed above. The first classification map (fig. 18a) was obtained using signatures calculated from uniform training sets and the second (fig. 18b) was obtained using signatures calculated from non-uniform training sets. The classification accuracy of component classes obtained for the uniform case was 99.1% whereas the accuracy obtained for the same classes in the non-uniform case was only 33.3%. The latter figure is misleading in that the nine-class data set was classified as 97.9% Grassland, 1.7% and .4% water. These figures indicate that the class distribution for Grassland was improperly defined by the covariance matrix.

The above study, coupled with the frequent lack of uniform mixture-class training sets in natural situations, lends itself to implementing an artificial covariance matrix for describing distributions of component classes. The use of a covariance matrix common to each class was discussed (ref. 7)for another, more sophisticated, signature calculation technique. Mean vectors for component classes can be successfully calculated from non-uniform mixture-class training sets. If a common covariance matrix that describes the proper distribution can be found, then with the calculated mean vectors, the signature should be representative of its respective class. To verify this, the component-class mean vectors calculated from

non-uniform mixture class training sets and various common covariance matrices were used to classify the simulated nine-class data fields.

The first classification utilized a covariance matrix with diagonal elements (σ^2_{ii}) of (1,3,3,1) and off-diagonal elements of 0.5. The determinations for the covariance elements were made by a priori inspection of covariance matrices for component and mixture classes extracted from simulated uniform data. The standard deviations in each band represent an estimate of the average standard deviations for all classes. The off-diagonal elements were established to be 0.5 as an estimated average of the correlation values for all of the 9-class correlation matrices.

The classification procedure followed that of all earlier runs with the mixture class mean vectors being modeled from the component class mean vectors calculated from non-uniform data. The classification map is shown in figure 19; its corresponding CCM is as follows:

CLASS	F	E	D	C	G	Q	R	S	W
FOREST (F)	993	5							
25% GRASSLAND - 75% FOREST (E)	13	975	11				1		
50% GRASSLAND - 50% FOREST (D)		17	959	15		9	2		
75% GRASSLAND - 25% FOREST (C)			19	897	21	63			
GRASSLAND (G)				26	974				
75% GRASSLAND - 25% WATER (Q)			20	23		956			
50% GRASSLAND - 50% WATER (R)							1000		
25% GRASSLAND - 75% WATER (S)								1000	
WATER (W)									1000

The acceptable level of classification accuracy obtained (97.3%) indicated that utilizing a common covariance matrix may help solve the problem of establishing representative spectral signatures for component classes when there exist insufficient points for conventional signature extraction.

An additional classification was conducted with the same class mean vectors as the above analysis, but with a common covariance matrix with the same diagonal elements and off-diagonal elements set to 0.0. The purpose of this run was to establish the expected classification accuracy for 0.0 correlations between channels. The classification results were again promising,with the average accuracy obtained being 96.5%. The classification map is shown in fig. 20; its corresponding CCM is as follows:

CLASS	F	E	D	C	G	Q	R	S	W
FOREST (F)	970	25							
25% GRASSLAND - 75% FOREST (E)	26	939	35						
50% GRASSLAND - 50% FOREST (D)		20	942	13		20	5		
75% GRASSLAND - 25% FOREST (C)			13	896	25	66			
GRASSLAND (G)				15	983				
75% GRASSLAND - 25% WATER (Q)			20	22		958			
50% GRASSLAND - 50% WATER (R)							1000		
25% GRASSLAND - 75% WATER (S)								1000	
WATER (W)									1000

One additional common covariance matrix was calculated, and tested as suggested by Nalepka and others (ref. 7, p. 17). This matrix consisted of an average of the covariance matrices of their signature set. One immediately recognizable disadvantage of this method is that a set of representative covariance matrices must be obtained from the MSS data which have small values such as those expected from component class covariance matrices extracted from uniform data. The results of using this technique for calculating the diagonal elements, but setting the off-diagonal elements to 0.0 are shown in figure 21. The corresponding CCM is as follows:

CLASS	F	E	D	C	G	Q	R	S	W
FOREST (F)	960	23							
25% GRASSLAND - 75% FOREST (E)	25	939	35						
50% GRASSLAND - 50% FOREST (D)		20	941	13		22	4		
75% GRASSLAND - 25% FOREST (C)			10	893	26	70			
GRASSLAND (G)				18	977				
75% GRASSLAND - 25% WATER (Q)			23	25		952			
50% GRASSLAND - 50% WATER (R)							1000		
25% GRASSLAND - 75% WATER (S)								1000	
WATER (W)									1000

Note that the 9-class data classification results are slightly less (95.0%) than those obtained using an estimated average of the diagonal elements and setting the off-diagonal elements to 0.0.

The overall results obtained from using common covariances appear promising for classifying LANDSAT-1 type MSS data when signatures must be obtained from non-uniform mixture class training sets. This technique applied to automatic classification of actual wildland data, is described in the next chapter.

Tests using LANDSAT-1 MSS data.- Experiments similar to those performed with simulated MSS data were conducted with actual LANDSAT-1 MSS data. An initial experiment was performed using extracted assumed "pure" component-class spectral signatures and mixture-class spectral signatures simulated from these component classes to classify an area designated as the 11-Mile study area. An additional experiment using estimated component signatures and simulated mixture signatures was performed using several plots located in the Manitou study area where ground control data were more detailed. Both of these experiments utilize methods described above. The objective of these experiments was to relate the concepts just presented to a real-world application. Hopefully, this will provide insight as to how well these techniques work to improve classification accuracies and/or what other factors may need to be considered to obtain optimum results.

LANDSAT-1 MSS data acquisition and description: The set of LANDSAT-1 MSS data analyzed is from an August 15, 1973 (frame number 1388-17134) overpass of the test site. The data set was provided by Dr. Richard S. Driscoll, Remote Sensing Project Leader at the U.S. Forest Services Rocky Mountain Forest and Range Experiment Station located in Fort Collins, Colorado. The data were geometrically corrected (deskewed) by the Laboratory for Applications of Remote Sensing (LARS) located at Purdue University, West Lafayette, Indiana (ref. 5, 18). The advantage of the deskewed data is its better conformity to aerial photographs, especially when displayed as a microfilm graymap or recognition map. A large section of this LANDSAT-1 frame was also studied by Heller and others (ref. 4) and Fleming (ref. 19).

Two areas from this frame were selected for study. They are referred to below as the Elevenmile Canyon Reservoir Study Area and the Manitou Study Area.

Experiments were conducted in these study areas using extracted component class and simulated mixture-class spectral signatures to classify a portion of LANDSAT-1 MSS data. The steps involved in the classifications are: (1) selecting component classes, (2) extracting representative spectral signatures, (3) simulating specified mixture-class spectral signatures, (4) classifying the data with a maximum likelihood processor, and (5) analyzing the results.

Elevenmile Canyon Reservoir Study Area: This area was selected because it is representative of the diversity of topography, geology, and vegetative cover throughout much of the total test site; and because of the availability of LANDSAT-1 MSS tape data. The location of the site is shown in figure 1. Elevations range from 2500 to 3020 m. The site is at the southwest margin of South Park: it includes the eastern part of Elevenmile Canyon Reservoir. Mountainous terrain lies to the north and east; a wide rolling grassland area lies primarily to the south of the reservoir. Wet meadows occur primarily along stream courses.

Two principal types of rocks occur; volcanic rock and granodiorites. The most commonly found volcanics are upper and lower andesite members of the Thirty-nine Mile volcanic field. The upper member is generally associated with high flat-topped mountains and the lower with the low rolling hills characteristic of South Park.

The granodiorite found in the site is dark gray, medium to coarsely crystalline and contains gneiss. It is correlated with the precambrian Boulder Creek Granodiorite of the central front range of the Rocky Mountains. It is found mainly in the northern portion of the test area where it forms high steep mountains. Several outcrops can be found to the east of Elevenmile Canyon Reservoir and on both sides of Elevenmile Canyon, but their areal extent is limited. Elsewhere, most of the bedrock is covered by some form of vegetation.

The vegetation in the area consists of a variety of forests and grasslands. The forests, which cover approximately one-third of the test site, include: (1) ponderosa pine, (2) Douglas-fir, (3) spruce fir, subalpine fir, and (4) Aspen. According to Heller and others (ref. 4), these forest species occur as "pure" types, but in many places there are various mixtures of species. There also exists a wide range of tree canopy densities, from very open to so dense that crowns nearly touch. In open stands of trees enough sunlight exists to allow the development of extensive herbaceous and/or shrubby understory, but under conditions of dense tree cover, little understory cover has developed.

The principle understory vegetation associated with Ponderosa pine forest includes Arizona fescue and mountain muhly. At higher elevations these species give way to Idaho fescue and Thurber fescue and oatgrass.

Approximately one-third of the study site consists of low rolling hills covered with vegetation characteristic of the short-grass prairie found throughout South Park. The principle species are blue grama and slim stem muhly. Mountain bunchgrass communities can also be found at the interface between grassland and forest.

Also occurring in the area are wet meadow and stream bank communities. These communities occur along the shore of Elevenmile Canyon Reservoir and along streams. Various species of sedges, rushes, and bulrush occur either as monospecific or mixed stands in the moist areas. In drier areas, blue grass and tufted hairgrass are found in mixed communities. The prominent shrubby communities consists of willow and shrubby cinquefoil. Although they occur sparsely throughout the study area, these communities are generally found associated with the wet meadows.

Five component classes were selected for use in this study area. They are Forest, Grassland, Water, Mountain Grassland and Wet Meadow. These classes were selected because of their importance in the area and also because mixtures of these various types occur. The Forest class is composed of several types of trees with a minimal amount of understory vegetation showing through the canopy. The Grassland class is characteristic of the short grass prairie community found throughout South Park and usually has much bare soil associated with it. The Water class is representative of the water of the reservoir. The Mountain Grassland class represents grassland communities found at higher elevations and at the interface between Forest and Grassland. The Wet Meadow class was selected to represent irrigated meadow areas and stream bank communities.

Homogeneous areas representative of each class were delineated on aerial photographs. These areas (training sets) were then transferred to LANDSAT graymaps and the line and point coordinates were determined. Figure 22 shows the microfilm graymap of MSS BAND 5 for the study site. Some modification of the photo locations were made on the graymaps as dictated by the graylevels associated with each training set. In this way, anomalous data points were avoided before signatures were extracted. A number of training sets were located for each class to provide statistically representative signatures. The number of points used to calculate each class signature were: Forest (75), Grassland (28), Mountain Grassland (20), Wet Meadow (20), and Water (96). The number of points for Grassland, Mountain Grassland and Wet Meadow was small due to difficulties encountered in locating training sets on computer graymaps, but are assumed representative for this study.

Mean vectors and covariance matrices were extracted for each training set for each class. The mean vectors for a class were compared with one another and the eigenvalues and eigenvectors of each class training set were determined and analyzed. Those training sets exhibiting dissimilar mean vectors and eigenvector plots were discarded so that final signatures obtained were as representative as possible.

The final component-class signatures were then used to classify the area. The resulting classification map is shown in Figure 23 as a microfilm display. As a check of how well the signatures identify their respective classes, the number of correct classifications in each training set was determined. All of the classes had training-set classification accuracies of 100% except Water which had 99%. A total of 60.5% of the test area was classified as one of the component classes, indicating that for a conventional analysis such as this, more classes

need to be added in order to classify the entire area. To satisfy this need, the following mixture classes were selected:

1. Grassland-Forest--selected to identify pixels covering areas with trees growing over Grassland areas and interfaces between the two communities.
2. Grassland-Wet Meadow--selected to identify pixels falling on the interface of the grass covered areas and irrigated meadows and stream bank communities.
3. Forest-Mountain Grassland--selected to identify pixels covering the interfaces between the two communities and locate areas of Mountain Grassland that appear as openings in the Forest which are smaller than the resolution of the LANDSAT-1 MSS scanner.

A proportion increment of 0.25 was selected for each combination of classes, and mixture-class spectral signatures were simulated with program MIX. The final signature set used to classify the test area included the five extracted component classes and nine intermediate mixture classes. The microfilm classification map at the 11.100 Chi-Square threshold level is shown in Figure 24. An increase in the number of classified points resulted in 86.35% of the area being classified, rather than 60.5%. Most of the unclassified points are associated with the interface between Grassland and Water since no spectral signatures characteristic of these mixtures were used in the classification. Classification of Grassland-Wet Meadow and Forest-Mountain Grassland mixtures appear reasonable. Grassland-Forest mixtures of 50% Grassland-50% Forest and 25% Grassland-75% Forest also appear to be classified well. The 75% Grassland-25% Forest mixture class contained a large amount of obvious misclassifications in areas where no Forest was present.

To investigate the source of these misclassifications, spectral signatures were extracted from the data for areas classified as the 75% Grassland-25% Forest class. A comparison of the mean and standard deviation vectors for the extracted signature and the simulated mixture signature showed them to be almost identical, as shown below:

	Extracted				Simulated			
MSS BAND	1	2	3	4	1	2	3	4
Mean	29.42	28.79	37.34	19.21	28.97	28.87	37.19	19.09
Std. Dev.	.94	1.66	1.51	1.00	1.62	2.02	2.10	1.15

This indicates that the material that is being classified as a Grassland-Forest Mixture has a vegetation or soil type that produces a response similar to that calculated for the mixture. The consequences of such a misclassification are an overestimation of the amount of Forest in the scene and an underestimation of Grassland. Because of the difficulties encountered in establishing mixture densities from high altitude aerial photographs no quantitative accuracy analysis was obtained for this experiment.

Because of the gross misclassifications of the 75% Grassland-25% Forest class, the proportion increment used to simulate mixture class signatures was changed to 0.33 and new signatures were simulated. The resulting signature set included the five component classes and ten two-component mixture classes. Combinations of Grassland and Water and Water and Wet Meadow were made as an attempt to identify those pixels left unclassified around the reservoir in the previous experiment.

A classification was made, producing the microfilm display shown in figure 25. The results indicated that the areas previously misclassified as 75% Grassland-25% Forest were still being incorrectly identified. A number of points along the shoreline of the reservoir were identified as either 67% Grassland- 33% Water or 33% Grassland-67% Water. There appeared to be some confusion of 67% Wet Meadow-33% Water and 33% Wet Meadow-67% Forest as the component class with the greatest amount occurring in the mixture. The other mixture classes appear to be classified correctly since they appeared where mixtures would logically exist.

Manitou study area: The Manitou study area is located to the northeast of the Elevenmile Canyon Reservoir area in and around the U.S. Forest Service Manitou Experimental Forest. Only

REPRODUCIBILITY OF THE
ORIGINAL PAGE IS POOR

a few selected plots identified by Mead (ref. 5) were studied in this work.

The plots lie within an area located between 38° 52' 30" and 39° 22' 30" north latitude and 105° 00" and 105° 37' 30" west longitude, along and just north of the area shown in fig. 1. The area typifies the mountainous part of the east slope of the Rocky Mountains, with a large variation of slopes and aspects. The topography is dominated by mountains and valleys with a north-south orientation due to extensive faulting that occurred during the Pliocene epoch and earlier.

For the most part, geologic materials in the area are covered with vegetation. The principal materials are pinkish to reddish soils developed from Pikes Peak granite. The underlying geologic unit is the Fountain Formation, but exposures are limited.

Variations in topography in the area have resulted in a complex mixing of plant communities generally aligned with the topography. For the most part, the plant communities are similar to those described for the forested hillslopes, mountains, and wet meadow areas of the Elevenmile Canyon Reservoir study area.

In this study area, experiments were performed to classify LANDSAT-1 MSS data with component class signatures estimated by solving simultaneous equations and linear regressions. Both of these techniques require data where the component classes and their respective proportions of the scene are known.

Several plots located in the Manitou study area and identified by Mead (ref. 5) were analyzed to obtain a number of plots suitable for signature estimation. Mead was specifically interested in the percent cover of ponderosa pine of the plots so it was a logical choice for one of the component classes. The second component class was identified as the other materials in the scene and denoted as Background. The Background class is actually a mixture in itself of soil, bare rock, and understory vegetation. Use of this Background class necessitated using only those plots which contained similar species occurring in the same relative amounts. It was also necessary to identify plots with similar slopes and aspects to avoid the signature variability associated with these factors. In summary, the criteria used for selecting the plots used for signature estimation were:

1. The plots must have known percent covers of ponderosa pine. (The Background percent cover was determined by subtracting the ponderosa percent cover from 100).

2. The plots must contain similar background materials such as vegetation, rocks and bare soil.

3. The plots must have similar orientation as determined by slope and aspect.

The first criterion was met by analysis of aerial photography by five photo interpreters from the U.S. Forest Service. The second was accomplished by field studies by Mead using a line-transect method to establish the materials present in each plot as well as their frequency of occurrence. The third was met by locating the plots on topographic maps and determining slopes and aspects by a computer program called TOPOGO (Mead, ref. 5; Sharpnack and Akin, ref. 20).

Analyzing all of the plots with these criteria produced a small subset of only six plots representing 120 total LANDSAT-1 MSS data points. The plots are as follows:

PLOT NUMBER	MEAD'S PLOT NUMBER (ref. 5)	PONDEROSA PINE PERCENT COVER	SLOPE (%)	ASPECT	FREQUENTLY OCCURRING BACKGROUND VEGETATION (see species list, below)
1	1	46	7.9	96	J, B, M, P, Q, D
2	2	74	17.0	53	B, J, M, P, D
3	3	76	6.9	108	J, B, M, Q, P, D
4	6	64	5.0	59	B, M, J, Q, F, D
5	14	22	8.1	77	B, M, F, P, B
6	17	16	9.9	134	M, AF, P, Q, BB

SPECIES LIST

ABBREVIATION	NAME
F	fringed sagebrush (Artemisia frigida Willd)
B	bear berry (Arctostaphylos uva-ursi (L.) Spreng.)
AF	Arizona fescue (Festuca arizonica Vasey)
J	common juniper (Juniperus communis (L.))
P	prairie junegrass (Koelaria cristata (L.) Pers.)
M	mountain muhly (Muhlenbergia montana (Nutt.) Hitch.)
Q	quaking aspen (Populus tremuloides Michx.)
D	Douglas-Fir (Pseudotsuga menziesii var. glauca (Beissn.) Franco)
BB	bottlebrush squirreltail (Sitanion hystrix (Nutt.) J.G.Sm.)

Spectral signatures for the six mixture plots were extracted from the LANDSAT-1 MSS data. The mean spectral response curves for the six plots are shown in Figure 26. Several pairs of signatures along with their respective mixture proportions of ponderosa pine and background were used as input for program SIGCALC. The results showed a wide variation in the estimated mean vectors for both of the component classes. In addition, the estimated covariance matrices contained very unrealistic values including negative variances. Consequently, this method was found to be unreliable for estimating component class spectral signatures for this case. Since results obtained with simulated data described above were acceptable, the error was probably due to inaccurate estimates of percent cover and variations of materials associated with the Background class. Since no representative spectral signatures could be obtained, no modeling of mixture class signatures or classification of MSS data was attempted.

Since the signature estimation technique used in the above study uses only data for two mixture training sets, slight errors in percent cover estimates will result in large errors for the calculated signature values. Also, the signatures, if successfully estimated, may only be representative of the material found in the specific training areas. To compensate for this all of the mixture training sets were used to determine component class signatures by means of linear regression techniques.

The method used for estimating component-class signatures with linear regression was discussed above. The necessary input data were the mean spectral response recorded from each of the plots in each wavelength band and the proportions of the two component classes, ponderosa pine and Background. Models were developed for each wavelength band as follows:

MSS BAND	Regression Model
.5-.6 μm	MSR=24.07-5.98(P_p)
.6-.7 μm	MSR=20.92-7.60(P_p)
.7-.8 μm	MSR=32.05-7.44(P_p)
.8-1.1 μm	--

where MSR=Estimated mean spectral response
P_p-Proportion of ponderosa pine in the scene

No regression model could be developed for the .8-1.1 μm wavelength band so a review of estimates of percent cover for the plots was made. It was found that for some plots, the cover estimates made by the five photo interpreters varied by as much as 30%. The standard deviations for the mean cover estimates ranged from 5.4 to 13.0 for the six plots. Additional cover estimates were then made using a dot grid superimposed on enlarged photos of the six plots. For these estimates no species determinations were made, but all trees were counted as belonging to a Forest class and all non-tree materials were counted as Background. New regression models were developed as follows:

MSS Band	Regression Model
.5-.6 μm	MSR=25.70-10.28(F_p)
.6-.7 μm	MSR=23.46-14.03(F_p)
.7-.8 μm	MSR=32.24-13.83(F_p)
.8-1.1 μm	MSR=19.55-8.73 (F_p)

where MSR=Estimated mean spectral response
F_p=Proportion of Forest in the scene

High R^2 values indicate that the grid estimates for the plots are reasonable values for the amounts of Forest and Background. Since only six plots were used in developing the regression models they may only be applicable for analysis of these plots. Component-class signature estimates can be determined from the models by setting the Forest proportion (F_p) to 1.0 and calculating the MSR's in each band to determine the Forest signature and setting F_p to determine the Background signature. The mean spectral response curves for the estimated Forest and Background Signatures are shown along with the extracted mixture curves for each of the plots in Fig. 26.

The estimated mean vectors for the Forest and Background classes were input into program MIX and mixture class signatures were simulated. The proportion increment used was set at 0.25, producing three intermediate mixture signatures. No covariance matrices for the component-class signatures were estimated by the regression models due to the non-uniformity of the mixture plots, so a common covariance matrix with diagonal elements of 1.0, 3.0, 3.0, 1.0 and off-diagonal elements of 0.0 was used for each of the classes.

The six plots selected for the study were classified with a maximum likelihood pattern recognition processor. Initially, only the estimated signatures for Forest and Background were used to classify the plots. The total number of points classified as these classes was only five of 120, or approximately 4%, illustrating the need to account for pixels that contain mixtures. A second classification was conducted with the two component class signatures plus the three simulated mixture class signatures. The number of classified points increased

to 112, or approximately 93%, with implementation of the mixture-class signatures.

The total amount of each component class in the plots was determined by summing the number of points classified as a class and multiplying by the proportion of each component class. A comparison of the percent cover estimates for Forest for each plot as determined by the dot-grid method and the classification map are as follows:

PLOT	GRID COVER ESTIMATE(%)	CLASSIFICATION COVER ESTIMATE (%)
1	55.0	63.75
2	65.0	71.25
3	60.0	71.25
4	40.0	48.75
5	20.0	28.75
6	30.0	37.50

If the dot-grid cover estimates can be assumed accurate then the amount of Forest occurring in the six plots was over-estimated by 11.5%.

EFFECT OF THE ATMOSPHERE ON SPECTRAL REFLECTANCE

Remote Sensing of Target Signatures

The signature of a target, as viewed from a satellite remote sensor (LANDSAT, Skylab EREP), is a radiance signature, N_s, given by

$$N_s = \frac{\rho HT}{\pi} + N_p \qquad (10)$$

where H is the total (180°, global) incoming solar irradiance, T is the beam transmittance (either the reflected target beam or the solar beam) of the atmosphere, N_p is path (between the satellite sensor and the target) radiance introduced by atmospheric scattering of sunlight, and ρ is the target reflectivity. This target reflectivity, ρ, is the true signature of the target. As can be seen in equation (10), the target's radiance signature is made up of three parameters other than the true target reflectivity signature. These parameters are the total incoming solar irradiance-H, the atmospheric beam transmittance-T, and the atmospheric path radiance-N_p. They will be discussed in the following section, where all three will be referred to as atmospheric effects. The wavelength region considered in this paper is the solar reflective region from 400 to 1300 nanometers(nm). This region includes the LANDSAT bands (500-600, 600-700, 700-800, and 800-1100 nm) and most of the Skylab EREP S-192 scanner bands.

Because the target radiance signature is dependent upon atmospheric effects, one goal of this program is to correct the satellite data for these atmospheric effects. Comparisons can then be made concerning what improvements can be realized in automatic terrain mapping by computer by using algorithms for correcting for atmospheric effects.

It is not within the scope of this paper to discuss each of these parameters in great detail in terms of atmospheric physics (radiative transfer); instead, the following subsections discuss them in sufficient detail to relate them to remote sensing.

Atmospheric Beam Transmittance

Atmospheric beam transmittance, T, can be given by the following expression (Beers, Lambert's, or Bouguer's law)

$$T = e^{-\tau l_p} \qquad (11)$$

where l_p is the path length, relative to the vertical path length of the beam, and τ is the atmospheric optical depth. The atmospheric path length is given by sec θ_o or sec θ, where θ_o is the solar zenith angle, sec θ_o is the path length of the solar beam, θ is the nadir angle of observation, and sec θ is the path length of the target reflected beam (see fig. 27). At low sun angles or oblique observation angles, θ_o or $\theta > 70°$, the path length needs to be corrected for atmospheric refraction (ref. 21). The atmospheric optical depth is wavelength - dependent (λ) and made up of three components: molecular (Rayleigh) scattering, τ_m; particle (Mie) scattering, τ_p; and, selective gaseous absorption, τ_a. Hence, the total optical depth is given as

$$\tau = \tau_m + \tau_p + \tau_a \tag{12}$$

The molecular-scattering optical-depth is proportional to λ^{-4}. This accounts for the blue sky, since the short wavelengths are scattered much more than the longer wavelengths. The wavelength-dependence of particle scattering is proportional to $\lambda^{-\alpha}$, where α is dependent upon particle size. For extremely small particles, α approaches 4.0 (as in Rayleigh scattering) and for large particles (clouds, fog, etc.) α approaches 0.0, which indicates gray scattering. The gaseous absorption optical depth is highly wavelength-selective, depending on the location of the various absorption bands of atmospheric constituents. Figure 28 illustrates the general nature of atmospheric beam transmittance of solar radiation.

Total Incoming Solar Irradiance

The total solar irradiance, H, is the sum of the direct-beam solar irradiance, on a horizontal surface, and the diffuse skylight, S; hence,

$$H = I \cos\theta_o + S \tag{13}$$

where I is the normal incident direct beam. This normal incident direct beam can be given, in terms of atmospheric effects, as

$$I = I_o e^{-\tau \sec\theta_o} \tag{14}$$

where I_o is the extraterrestrial solar irradiance, commonly referred to as the "solar constant". For "clear" days the diffuse skylight is normally bluish, which is indicative of the dominance of molecular (Rayleigh) scattering. However, the magnitude and spectral distribution of the diffuse skylight is a complex function of particle size, density, solar elevation and azimuth, optical depth, ground albedo, particle scattering phase function, particle albedo, and index of refraction. For representative measurements of total and diffuse irradiance see reference 22.

The diffuse skylight is also strongly influenced by clouds. Generally, clouds increase the skylight and change its spectral distribution from blue to white. Clouds can also strongly reflect solar radiation and cause "bright spots" (as opposed to shadows) on the ground, which can very significantly affect remote sensing of ground targets (ref. 23).

The total incident solar irradiance is very strongly influenced by the solar zenith angle cos θ_o (equation 13). Since the solar zenith angle is that angle between the target's normal and its planar surface, topography plays a significant role. For example mountainous terrane has very complex topography comprising north-, south-, east-, and west-facing slopes of various inclinations.

Atmospheric Path Radiance

Atmospheric path radiance results from molecules and large particles scattering sunlight in the field of view of the sensor. The magnitude and spectral distribution of path radiance is determined by all the variables that were given for diffuse skylight.

Atmospheric path radiance presents a special problem because it cannot be directly measured with ground-based instruments. Currently there are three techniques for deriving path

radiance:

(1) Calculations using radiative transfer models
(2) indirect ground-based measurements
(3) combination of model calculations and ground-based measurements

Radiative-transfer models have been the subject of considerable research. A review and discussion of such models is given in reference 12. Models are useful for parametric studies of the influence of the atmosphere, given hypothetical situations. However, for specific conditions they are difficult to apply because, without measurements, one simply cannot confidently choose a "representative" atmospheric state. This is due to the fact that atmospheric aerosols and water vapor are known to be extremely variable as a function of geographical locations, altitude, and local conditions.

Indirect ground-based measurements of path radiance have been employed by Duntley (ref. 24) and Rogers, (ref. 25). This technique uses ground-based measurements of downward scattered sky radiance at a geometry (sun-sensor) similar to the satellite-sun-target geometry. The measured sky radiance is then extrapolated to yield a path radiance for the satellite sensor (see ref.'s 24 and 25).

The third technique was used recently by Hulstrom (ref. 22) to analyze the performance of the Skylab EREP sensors (S-190 A, S-191, and S-192). This technique uses ground-based measurements of optical depth/transmittance, target reflectivity, ground albedo, and total solar irradiance (see equation 10); then, the optical depth and ground albedo measurements are used as inputs for a radiative-transfer computer model that calculates path radiance. This technique eliminates uncertainties in atmospheric state, optical depth, and total (direct plus diffuse) irradiance. However, values for the particle scattering, phase function, and albedo have to be assumed.

A fourth technique of deriving path radiance is being attempted in this program. This technique employs the satellite data itself and helicopter measurements of selected ground targets. If one plots equation 10, as shown in Figure 29, it can be seen that the y intercept is the path radiance and the slope is equal to the product HT/π . The natural target reflectivities are measured from a helicopter platform. This is performed by having nearly identical spectral radiometers measure the target radiance, N_t , from the helicopter; and, the other radiometer measure the total incoming solar irradiance, H. The target reflectivity can then be determined by

$$\rho_t = \frac{\pi N_t}{H} \quad \text{(assumes Lambertian target)} \tag{15}$$

Hence, one can determine the path radiance and the product HT/π . Therefore the reflectivity signatures of other (unknown) targets can be derived by

$$\rho = (N_s - N_p) \times \pi/HT \tag{16}$$

The advantages of this technique are

(1) it measures path radiance as "seen" from the satellite sensor

(2) it measures the combined atmospheric effects of total solar irradiance, H, and atmospheric transmittance, T.

(3) if the selected natural ground target reflectivities remain nearly constant over periods of time (as was found to be valid for this test site) numerous simultaneous ground-based measurements are not required in order to calibrate atmospheric effects.

The possible short-comings of this technique are

(1) It assumes fairly uniform atmospheric conditions of the surface area within which the natural target "calibration" sites are located.

(2) The accuracy of the technique depends on the accuracy and repeatability of the measurements of natural target reflectivity, and radiances measured by sensors in the satellite.

(3) It assumes that the sun angle with respect to the targets, both natural "calibration" and unknown targets, are similar. This is apparent when one considers the sun angle dependence, $\cos\theta_o$ of the total solar irradiance and the product $H\uparrow/\pi$.

Initially, during the summer and fall of 1975, this technique will be employed for LANDSAT data.

Four techniques of deriving atmospheric path radiance and atmospheric effects have been presented. Each has its advantages and shortcomings. Unfortunately, almost no data or experiments exist for checking and comparing the accuracy and validity of these techniques. All four techniques will be attempted during this program, and such comparisons subsequently made.

FIELD MEASUREMENTS OF ATMOSPHERIC EFFECTS AND TARGET REFLECTIVITY

Brief descriptions of the techniques and instrumentation used to measure atmospheric effects and target reflectivity are given. For a more detailed description see Hulstrom (ref. 22).

Atmospheric Effects

Atmospheric effects that are directly measureable by ground-based instruments are the total solar irradiance, H, and the beam transmittance, T.

The total solar irradiance was measured with an I.S.C.O. (Instrumentation Specialties Company) model SR (spectroradiometer) equipped with a SRR (spectroradiometer recorder) unit. This instrument consists of the SR and SRR units and a 6 ft fiber-optics bundle that has a flat teflon diffuser, 180° F.O.V., aperture at the end of the bundle. Light travels through the diffuser, through the fiber-optics bundle into the SR unit, where it is passed through a chopper, slit, and monochromator. The monochromator is a wedge interference filter. The wavelength of the instrument is varied by lengthwise movement of the wedge interference filter between the slit and the sensor. The wavelength region from 380 to 750 nm is measured with a silicon-junction photocell; and, the region from 750 to 1350 nm is measured with a germanium-junction photocell. The 1/2 bandwidth is 15 nm from 380 to 750 nm, and 30 nm from 750 to 1350 nm. The total solar irradiance was measured by positioning the flat teflon diffuser so that it was horizontal/level. Hence, the 180°F.O.V. diffuser was exposed to the total irradiance (direct + diffuse). The diffuse skylight can be measured by simply shading the diffuser from the direct sunlight. A complete spectral scan, from 380 to 1350 nm, requires about 3 minutes. During this time interval, the total broadband irradiance (400-1100 nm) was continuously monitored with a Y.S.I. (Yellow Springs Instrument Co.) model 68 pyranometer. This was done in order to assure that stable conditions existed during the I.S.C.O. spectral scan.

The complete I.S.C.O. unit was calibrated with an I.S.C.O. S.R.C. (Spectroradiometer Calibrator) unit, which uses a ribbon-filament tungsten lamp, and a N.B.S., coil filament type lamp (1963 standard No. E.P.I. 1523). These standards were used to derive an absolute calibration factor, C.F., for the I.S.C.O. unit. This is derived by viewing the standard irradiance, I_{STD}, and recording a raw intensity I_r. The calibration factor is then

$$C.F. = I_{STD}/I_r \qquad (17)$$

The raw field measurement, I_r, is then multiplied by the calibration factor in order to obtain absolute quantities. However, this calibration factor is only valid for measurements of normal-incident (to the diffuser) irradiance. For measurements of total solar irradiance, where the sun is at various zenith angles (angles off of the normal to the diffuser),

the cosine response of the diffuser has to be considered. This is evident from equation 13, i.e., I cos θ_o. If a diffuser has a true cosine response, the intensity of a constant parallel source as measured at a 60° angle to the source, I (60°), would be 1/2 (cos 60°) that measured on normal incidence (0°). In more general terms,

$$I(\phi) = I(\phi = o) \cos \phi \tag{18}$$

where ϕ is the angle between the source and the normal to the diffuser. In the case of solar irradiance, $\phi = \theta_o$. In order to determine the actual cosine response of the I.S.C.O. diffuser, extensive measurements of collimated light were made over a range of incident angles. This resulted in a cosine correction factor, C.C.F.,

$$C.C.F. = \frac{I(\phi=o) \cos \phi}{I(\phi)} \tag{19}$$

Examples of the cosine correction factors are shown in Figure 30. As can be seen the cosine response in the visible region is fairly true, while that in the infrared deviates by as much as 500%. The absolute total solar irradiance, H_{ABS}, is obtained by

$$H_{ABS} = (H_{raw})\ (C.F.)\ (C.C.F.) \tag{20}$$

Investigators have used the I.S.C.O. unit to measure target spectral albedo by pointing the diffuser up to measure the total incoming irradiance, $H\downarrow$, then pointing the diffuser down to measure the total outgoing irradiance, $H\uparrow$. The target's global albedo, p (180°),

$$p\ (180°) = \frac{H\uparrow}{H\downarrow} \tag{21}$$

If the diffuser's cosine response is not considered in this calculation, large errors (up to 500%) will result, especially in the infrared wavelengths, because the incoming irradiance has to be corrected for the cosine response (because the incoming irradiance is directional), while the outgoing irradiance is generally not directional, requiring no cosine correction.

In addition to the I.S.C.O. unit, Exotech Model 100 radiometers are also used for making total solar irradiance measurements in the specific LANDSAT wavelength bands. These units are calibrated in the same manner as discussed for the I.S.C.O. unit. At the time of this writing, no cosine response has been determined for these units.

The beam transmittance of the atmosphere was/is determined by using the Langley method. This method determines atmospheric optical depth by peforming several measurements of the solar direct-beam irradiance as it varies with relative air mass. Equation 14 can be rewritten to give

$$\ln I = -\tau \sec \theta_o + \ln I_o \tag{22}$$

In order to derive τ, a plot of the various measurements of I versus relative airmass-sec θ_o is made. The y-intercept is I_o, hence τ can be calculated knowing I, I_o, and sec θ_o. If the meter reading of the instrument, M, is linear with respect to I, then I can be replaced with M and I_o by M_o. M_o is the extraterrestrial meter reading of the instrument. For the measurements of direct solar irradiance, the ISCO unit was equipped with a 3° collimator. This resulted in beam transmittance for 27 wavelength measurements from 400 to 1300 nm. An example is shown in figure 31, where the four transmittance curves are for four sites located within and near the Colorado test site. Simultaneous measurements of beam transmittance reveal the uniformity of the atmosphere over the region. For the day shown in Figure 31, the atmosphere was fairly uniform.

Target Reflectivity

Both the I.S.C.O. and EXOTECH units were used to measure target reflectivity. The I.S.C.O. is modified with a 30° F.O.V. baffled collimator.

REPRODUCIBILITY OF THE
ORIGINAL PAGE IS POOR

For ground measurements of target reflectivity, standard "gray" and standard "white" reflectance panels are used to determine target reflectivity. These panels are accurately calibrated with a Beckman DK-2A/Gier-Dunkle Integrating Sphere. Field measurements consist of the radiance of the "gray" card, N_{gc}, the radiance of the target, N_t, and the radiance of the "white" card, N_{wc}. The target reflectivity can then be derived by

$$\rho_t = \frac{N_t}{N_{gc}} \times \rho_{gc} \tag{23}$$

and

$$\rho_t = \frac{N_t}{N_{wc}} \times \rho_{wc} \tag{24}$$

where ρ_{gc} and ρ_{wc} are the reflectivities of the "gray" and "white" cards. The two derived target reflectivities are then averaged. This technique was verified by plotting radiance, N_{gc} and N_{wc}, versus reflectivity, ρ_{gc} and ρ_{wc}, and extrapolating this plot to zero radiance and reflectivity. If the card calibrations are accurate and if the field measurements are accurate, the plot should go through the origin. Several of these verifications revealed the technique and measurements to be consistent to within 1 to 2% reflectivity. Examples of absolute reflectivity for 15 targets and their backgrounds are listed below:

Target Description	Identification Number
Pikes Peak Granite	1
Lichen Rock Cover	2
Soil/Grass Background for Pikes Peak Granite	3
Cripple Creek Granite	4
Soil/Grass Background for Cripple Creek Granite	5
Volcanic Fine-Grain Mafic	6
Soil/Grass Background for Volcanic Mafic	7
Meadow Grass	8
Volcanic Crystal Tuff	9
Yellow Grass Background	10
Volcanic Andesite	11
Background Soil for Volcanic Andesite	12
Background Grass for Volcanic Andesite	13
Background Soil at Cameron Mountain	14
Background Soil/Grass at Cameron Mountain	15

Target No.	Percent Reflectance			
	0.5 to 0.6	0.6 to 0.7	0.7 to 0.8	0.8 to 1.1 m
1	14.0	18.4	22.6	25.6
2	23.6	28.5	36.1	35.2
3	12.7	14.8	20.7	23.4
4	17.3	22.6	24.5	25.6
5	11.1	13.6	19.3	22.6
6	11.7	14.5	19.1	19.4
7	10.8	16.8	19.5	26.0
8	5.8	5.4	30.8	42.5
9	27.5	31.8	35.8	40.4
10	11.8	13.6	19.1	18.9
11	14.5	17.7	19.8	20.9
12	9.3	13.3	18.0	18.7
13	6.5	8.5	12.7	17.3
14	10.8	16.3	19.2	23.2
15	9.6	12.8	19.8	24.1

In order to measure signatures from mixtures and for areas that are on the same order of size as the satellite sensors, helicopter measurements are employed. Helicopter measurements consist of using one EXOTECH radiometer, with a 1° FOV, in the helicopter to measure the target radiance, N_t and one EXOTECH radiometer located on the ground to measure total incoming solar irradiance, H. The reflectivity, ρ is then

$$\rho = \frac{\pi N_t}{H} \tag{25}$$

In addition, the helicopter measurements of N_t will be compared with the computer simulations of the radiance signature.

SUMMARY AND CONCLUSIONS

Methods have been discussed for simulating spectral signatures of mixtures of two terrain classes for automatic analysis of LANDSAT-1 MSS data using on-site measurements, simulated LANDSAT data, and actual LANDSAT-1 data. Tests of the methods for estimating component-class spectral signatures and simulating two component-class mixture signatures with simulated MSS data indicated that improvements in classification results over conventional component class analysis are possible using these techniques. Applying these techniques to actual LANDSAT-1 MSS data of wildland areas showed an increase in classification information over conventional analysis, but no quantitative accuracy analysis could be made due to difficulties of estimating mixture proportions from the control or "ground truth" data.

It was found that misclassification of pixels as mixtures can occur when the simulated spectral signatures approximate those of component classes or other mixtures in the scene. There was also evidence of misclassifications due to more than two component classes existing within a single pixel. Within-class variability, slope and aspect variability, and the sensitivity of the scanner in detecting changes in mixture proportions may also contribute to degrading the classification performance using these methods.

These techniques may prove valuable in areas where vegetation masks the characteristic spectral response of the underlying geologic material, and future work should include an examination of this application. Emphasis should also be placed on methods of acquiring better "ground truth" information upon which the spectral signature estimation and simulation techniques are based.

Properties of the atmosphere play an important role in affecting the spectral radiance received at the satellite by the scanner. Some atmospheric properties can be measured on site. Others must be determined by comparing satellite data with the on-site measurements. Once their signatures have been determined, it may be possible for some large natural terrain features to serve as calibration panels from which atmospheric properties can be calculated by the satellite data. When the desired remote sensor product is an image having only rough spectral information, atmospheric effects can be ignored. However, when quantitative spectral information is required, atmospheric effects cannot be neglected.

REFERENCES

1. Horwitz, H. M., R. F. Nalepka, P. D. Hyde and J. P. Morgenstern, 1971, Estimating the Proportions of Objects Within a Single Resolution Element of a Multispectral Scanner: Proceedings of the Seventh International Symposium on Remote Sensing of the Environment. Ann Arbor, Michigan. p. 1307-1320.
2. Pace, W. H. and D. M. Detchmendy, 1972, A Fast Algorithm for the Decomposing of Multispectral Data into Mixtures: University of Tennessee Space Institute, Volume II, Tullahoma, Tennessee, p. 831-848.
3. Horwitz, H. M., P. D. Hyde and W. Richardson, 1974, Improvements in Estimating Proportions of Objects from Multispectral Data: Environmental Research Institute of Michigan. ERIM 190100-25-T.
4. Heller, R. C., R. C. Aldrich, R. S. Driscoll, R. E. Francis and F. P. Weber, 1974, Evaluation of ERTS-1 Data for Inventory of Forest and Range Land and Detection of Forest Stress: Final Technical Report to NASA. Contract No. S-70251-AG. 218 p.
5. Mead, R. A., 1974, Factors Affecting Computer Recognition of Ponderosa Pine from ERTS-1 Imagery: Master's Thesis, Dept. of Earth Resources, Colorado State University, Fort Collins, Colorado, 85 p.
6. Root, R. R., 1974, Computerized Terrain Mapping of Yellowstone National Park: Ph.D. dissertation, Dept. of Earth Resources, Colorado State University, Fort Collins, Colorado 242 p.
7. Nalepka, R. F., H. M. Horwitz, and P. D. Hyde, 1972, Estimating Proportions of Objects From Multispectral Data: Environmental Research Institute of Michigan. ERIM 31650-73-T.
8. Root, R. R., H. W. Smedes, N. E. G. Roller, and D. Despain, 1974, Color Terrain Map of Yellowstone National Park, Computer-derived from ERTS MSS Data: Proc. Ninth International Symposium on Remote Sensing of Environment, Ann Arbor, Mich., v. II, p. 1369-1398.
9. Malila, W. A., D. P. Rice, and R. C. Cicone, 1975, Final Report on the CITARS Effort by the Environmental Research Institute of Michigan: Report No. NASA-CR-ERIM 109600-12-F, NASA Scientific and Technical Reports Facility, College Park, Md., 127 p.
10. Smith, J. A., L. D. Miller and T. Ells, 1972, Pattern Recognition Routines for Graduate Training in the Automatic Analysis of Remote Sensing Imagery-RECOG: Colorado State University Science Series No. 3A, Fort Collins, Colorado, 85 p.
11. Smedes, H. W., 1971, Automatic Computer Mapping of Terrain: International Workshop on Earth Resources Survey Systems, Government Printing Office, Wash., D.C., v. II, p. 345-406.
12. Malila, W. A., R. B. Crane, C. A. Omarzu, and R. E. Turner, 1971, Studies of Spectral Discriminators: Report No. NASA-CR-WRL 31650-22-T, NASA Manned Spacecraft Center, Houston, Texas.
13. Nalepka, R. F. and P. D. Hyde, 1973, Estimating Crop Acreages From Space Simulated Multispectral Scanner Data: Environmental Research Institute of Michigan, ERIM 31650-148-T.
14. Ells, T., L. D. Miller and J. A. Smith, 1972a, Programmer's Manual for RECOG (Pattern RECOGnition Programs): Colorado State University Science Series No. 3C, Fort Collins, Colorado, 216 p.
15. _____1972b. User's Manual for RECOG (Pattern RECOGnition Programs): Colorado State University Science Series 3B. Fort Collins, Colorado, 85 p.
16. Maxwell, E. L. and G. R. Johnson, 1974, A Remote Rangeland Analysis System: United States Geologic Survey. Report No. 1885-F, Colorado State University, Fort Collins, Colorado.
17. Crane, R. B. and P. D. Hyde, 1972, Signature Estimation from Satellite Multispectral Scanner Data: Proceedings of the Eighth International Symposium on Remote Sensing of Environment. Ann Arbor, Michigan, p. 765-773.

18. Anuta, P. E., 1973, Geometric Corrections of ERTS-1 Digital Multispectral Scanner Data: The Laboratory for Application of Remote Sensing (LARS), Purdue University, West Lafayette, Ind., 23 p.
19. Fleming, M. D., 1974, Analysis of USFS Site 226C Colorado: The Laboratory for Application of Remote Sensing (LARS), Purdue University, West Lafayette, Ind., 53 p.
20. Sharpnack, D. A. and G. Akin, 1969, An Algorithm for Computing Slope and Aspect from Elevations: Photogramm. Eng., v. 35, p. 247-248.
21. Bemporad, A., 1907, Saggio Di Una Nuova Formola Empirica per Rappresentare il Modo di Zoriare Della Radiazione Solare Col Variare Dello Spessore Atmosferico Attrazersato Dai Raggi: Fisica Terrestre, in Rend. Accademia Lincei, Roma, Ser. 5, vol. 16, p. 66-71.
22. Hulstrom, R. L., 1974, Spectral Measurements and Analyses of Atmospheric Effects on Remote Sensor Data: Proc. Soc. Photo-Optical Engineer, v. 51, p. 90-100.
23. _____1973, The Cloud Bright Spot: Jour. Photogrammetric Engineering, v. 39, p. 370-376.
24. Gordon, Jacqueline I., Harris, James L. Sr., and Duntley, Seibert Q., 1973, Measuring Earth-to-Space Contrast Transmittance from Ground Stations: Applied Optics, June, p. 1317-1324.
25. Rogers, R. and K. Peacock, 1973, A Technique for Correcting ERTS Data for Solar and Atmospheric Effects: Symposium on Significant Results of ERTS-1, NASA Spec. Paper 5P-327, p. 1115-1122.

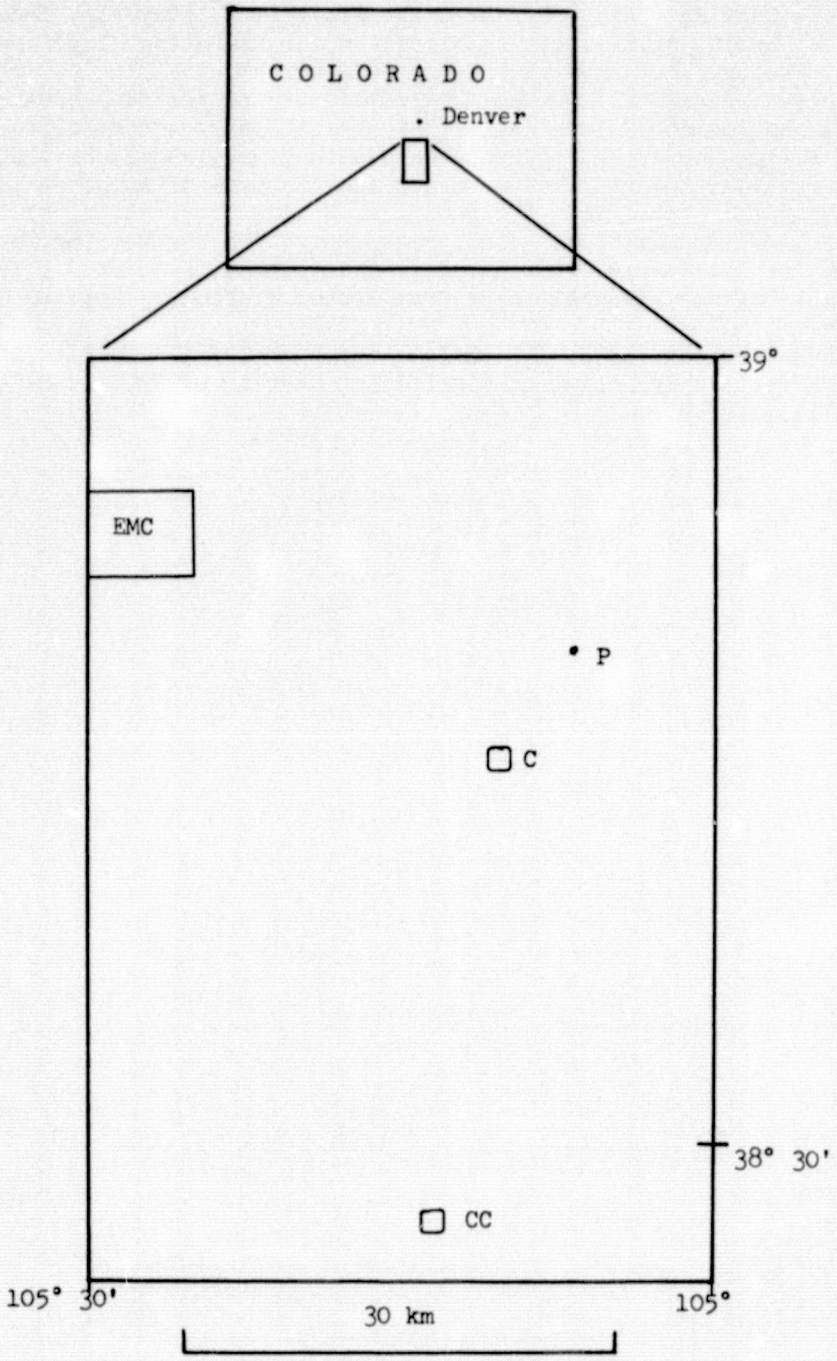


Figure 1.-Location of test site. EMC=Elevenmile Canyon Reservoir Study Area, P=Pikes Peak, C=Cripple Creek, CC=Canon City.

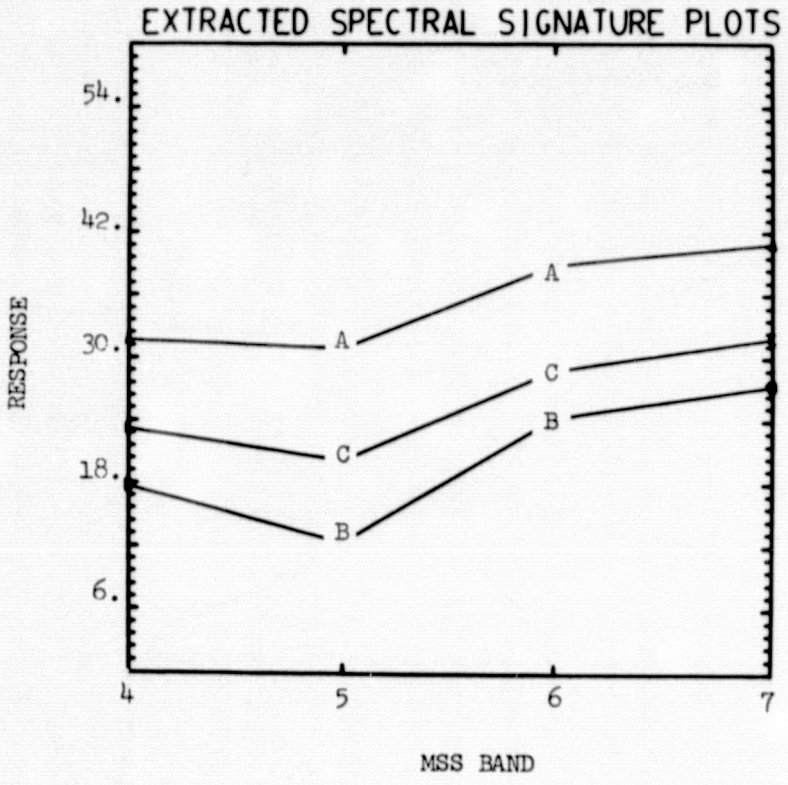


Figure 2.-Spectral response of two component terrain classes (A,B) and a mixture of them (C) extracted from LANDSAT-1 MSS data.

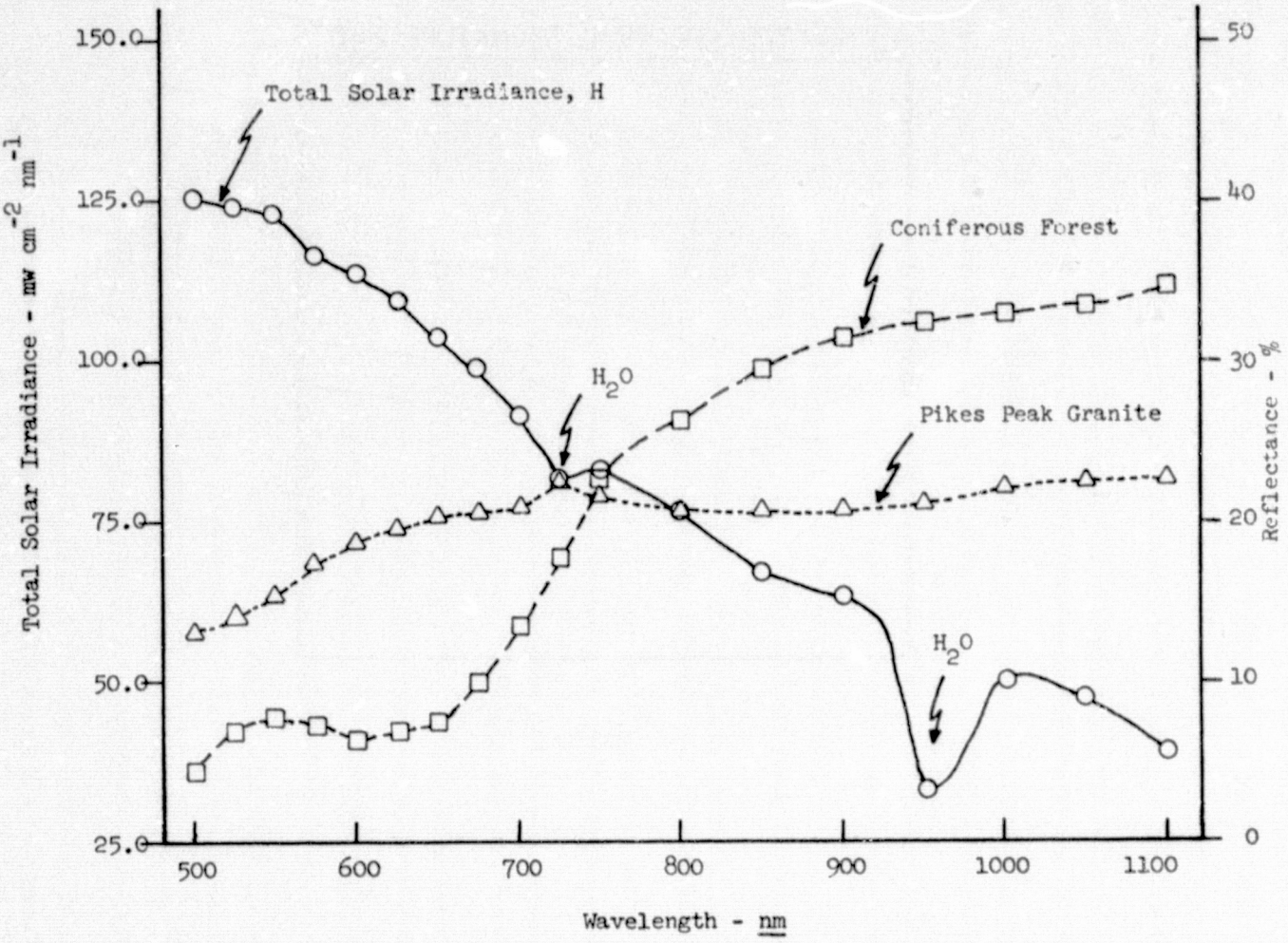


Figure 3.-Comparison of total solar irradiance and reflectivity of coniferous forest and Pikes Peak Granite.

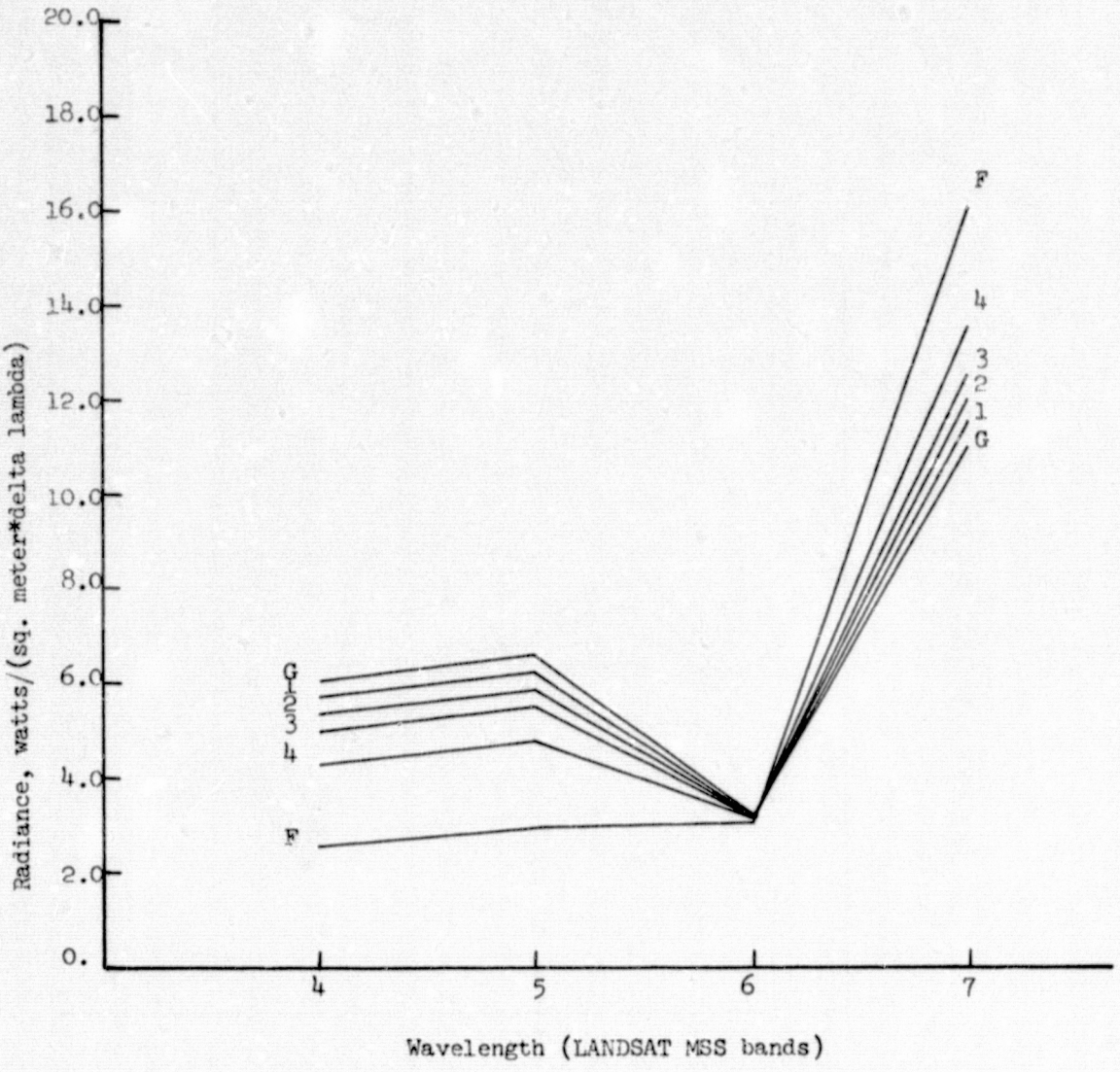


Figure 4.-Radiance signatures of Pikes Peak Granite, coniferous forest and mixtures of the two. Curves: G=100% Pikes Peak Granite, F=100% coniferous forest, 1=90% G 10% F, 2=80% G 20% F, 3=70% G 30% F, 4=50% G 50% F. Data from May 29, 1974; lat. 38.83° N, long. 105.26° W, solar elevation 64.51°, solar azimuth 126.62°, time 10:30 AM MST. Curves traced from computer printout.

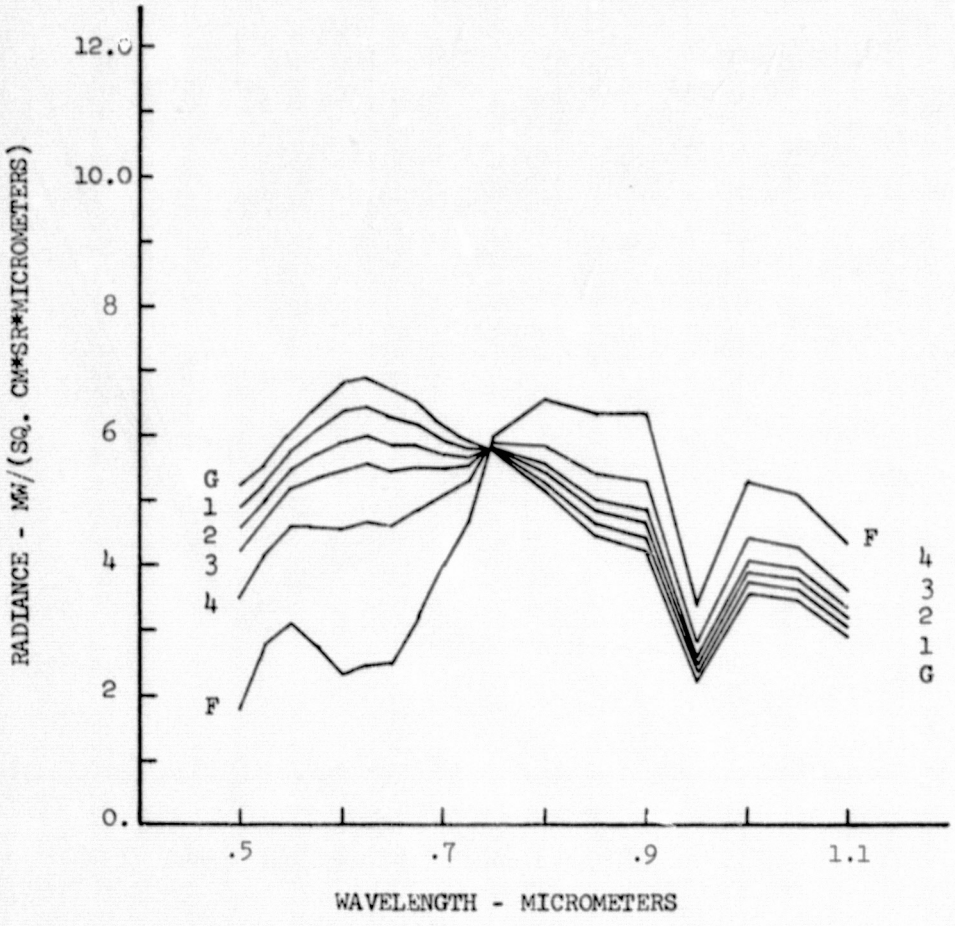


Figure 5.-Spectral radiance of Pikes Peak Granite, coniferous forest, and mixtures of the two. Curves, date, time, and other documentation same as in fig. 4.

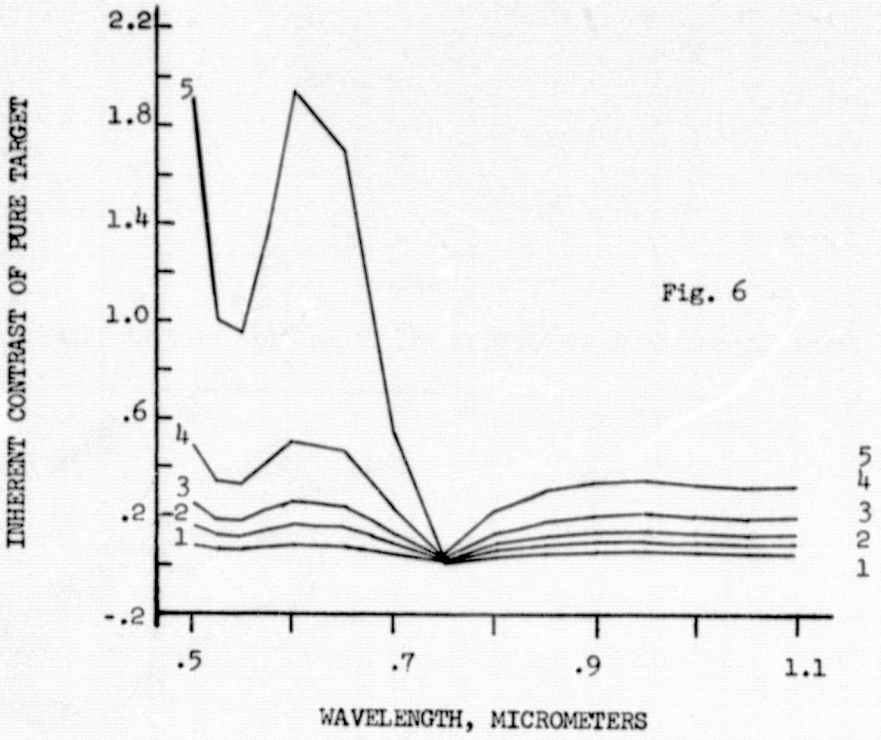


Fig. 6

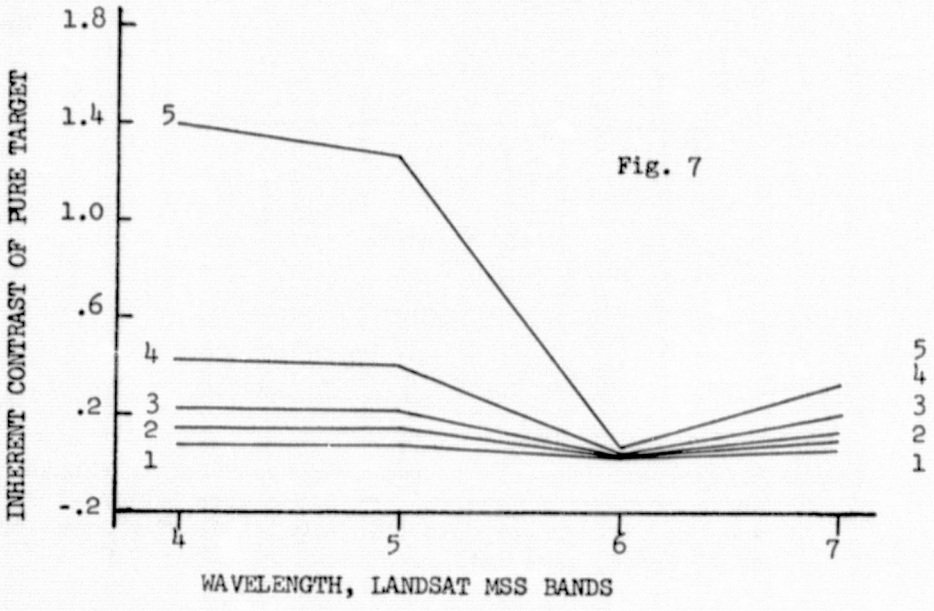


Fig. 7

Figures 6 and 7.-Spectral inherent contrast of Pikes Peak Granite (G) target with background of Coniferous Forest (F), and mixtures of granite and forest. Curves: 1=90% G 10% F, 2=80% G 20% F, 3=70% G 30% F, 4=50% G 50% F, 5=100% F.

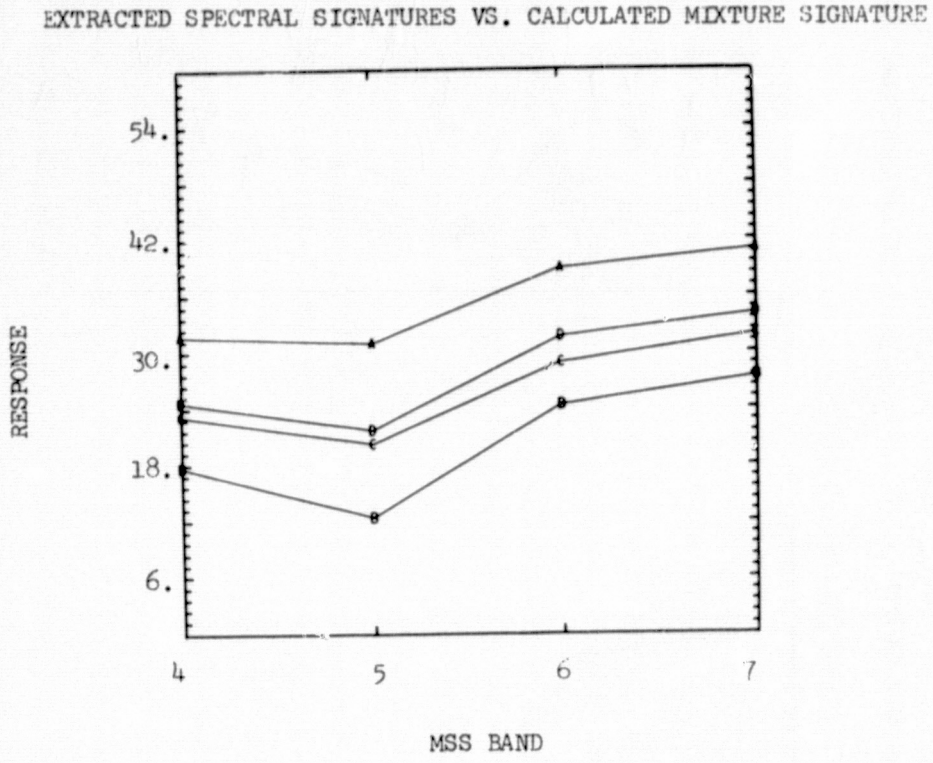


Figure 8.-Spectral response of two component terrain classes (A,B) and a mixture of them (C) extracted from LANDSAT-1 MSS data, and the mixture response (D) calculated using equation 4. A, B, and C, same data as in fig. 2.

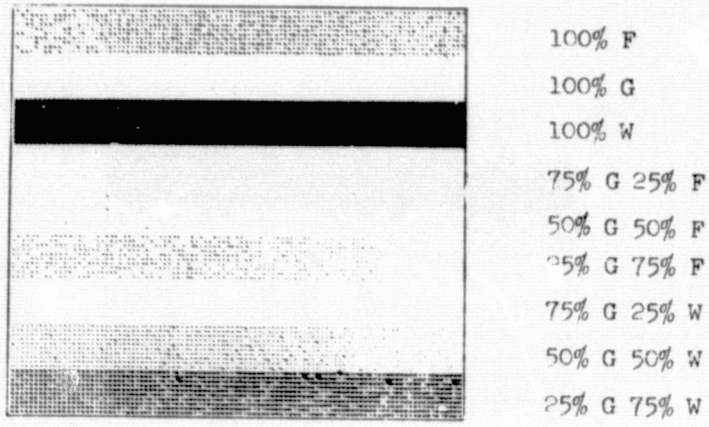


Figure 9.-Microfilm graymap of 9-class simulated data set. Each horizontal band represents a field of simulated data for a given class, as labelled. F=Coniferous forest, G=grassland, W=water.

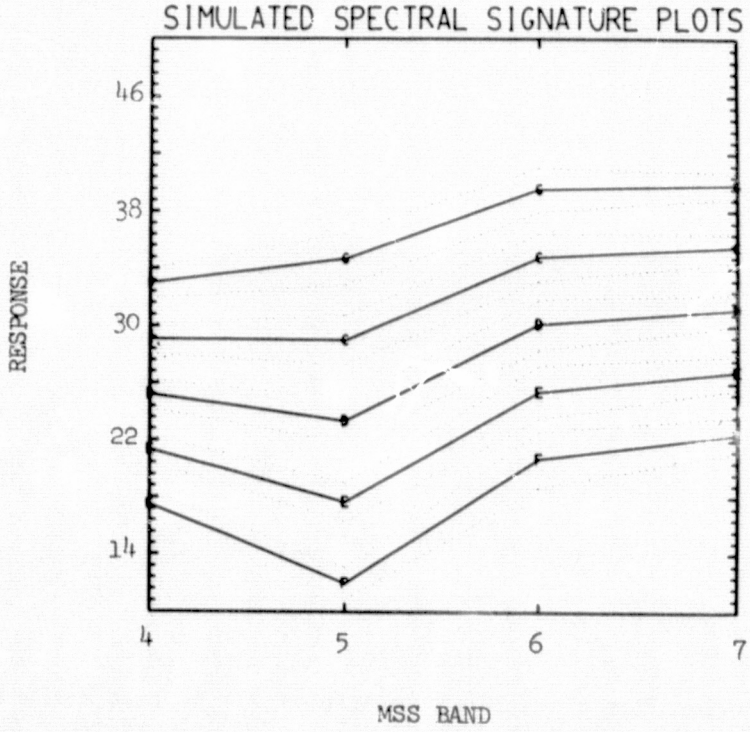


Figure 10.-Mean spectral response for two component classes and modeled mixture classes. Curves: G=100% grassland, F=100% forest, C=75% G 25% F, D=50% G 50% F, E=25% G 75% F. Dotted lines represent standard deviations.

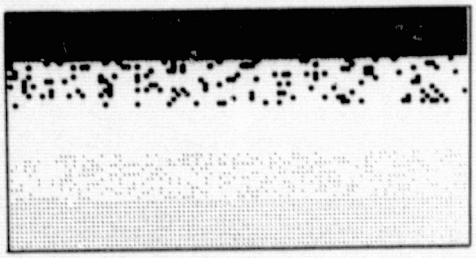


Figure 11.-Microfilm classification display for component-class analysis. Blanks denote unclassified points. Symbols are: • =grassland(G), .=forest(F). C,D,E same as in fig. 10.



Figure 12.-Microfilm classification display for 5-class analysis. Symbols are: • =G, ▲=C, \=D, ·=E, .=F. Letters refer to classes and mixtures as in fig. 10.

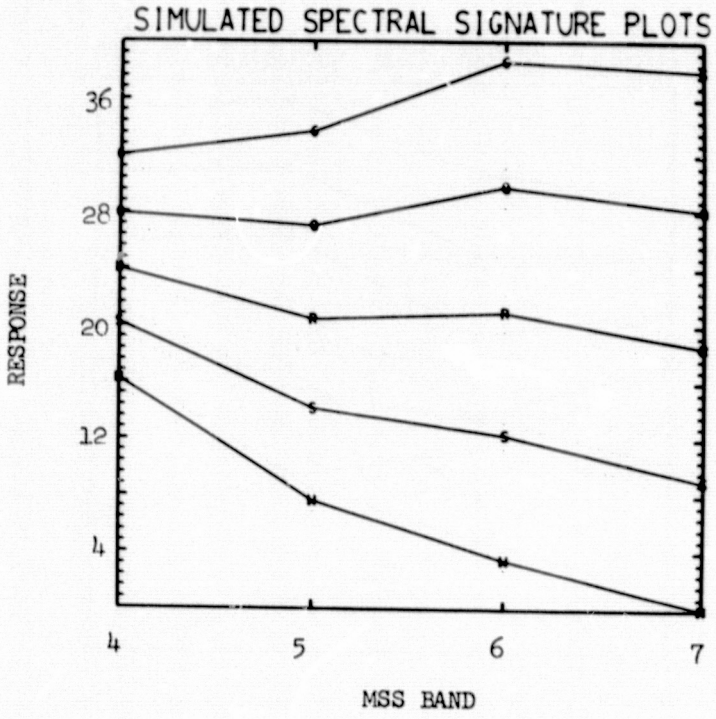


Figure 13.-Mean spectral response curves for simulated Grassland-Water mixtures. Dotted lines indicate standard deviations. Letter symbols are same as in 9-class classification confusion matrix in text.

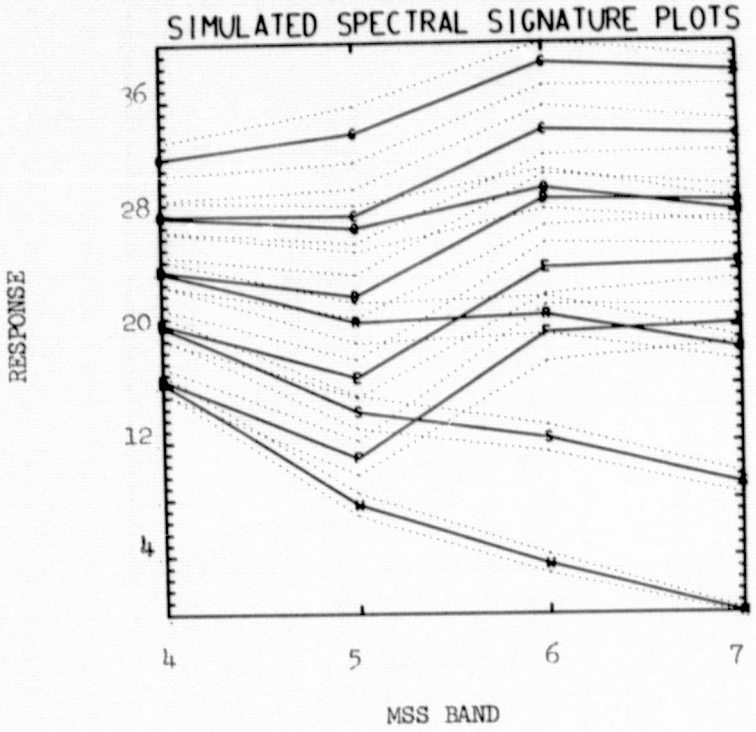


Figure 14.-Mean spectral response curves for component and mixture class signatures used for 9-class analysis. Dotted lines indicate standard deviations. Letter symbols are same as in 9-class CCM in text.

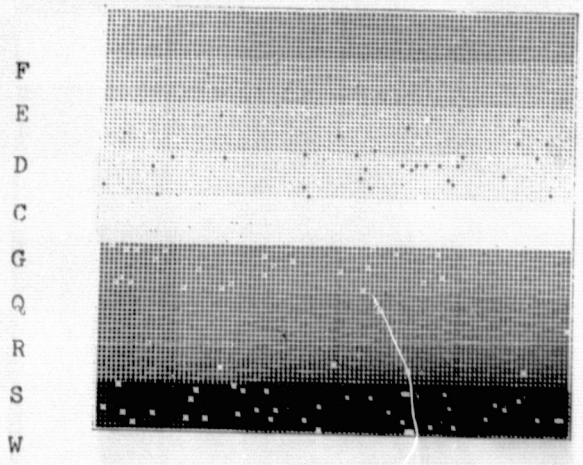


Figure 15.-Microfilm classification display of 9-class analysis. True class field symbols noted at left of display are same as in 9-class CCM in text.

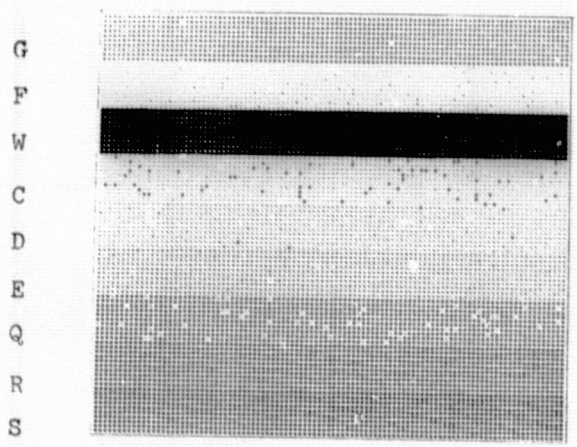
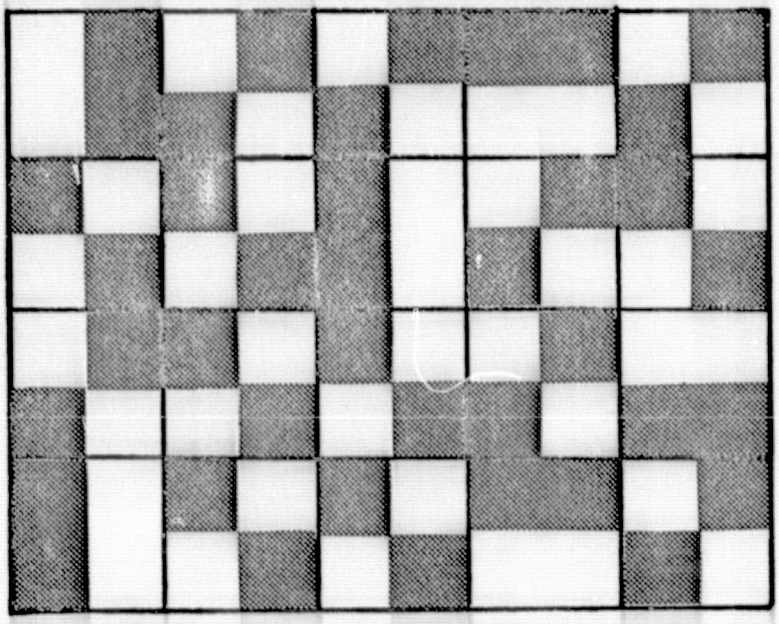


Figure 16.-Microfilm classification display for 9-class analysis with calculated component class signatures from uniform data. True class field symbols noted at left of display are same as in 9-class CCM in text.

a.



b.

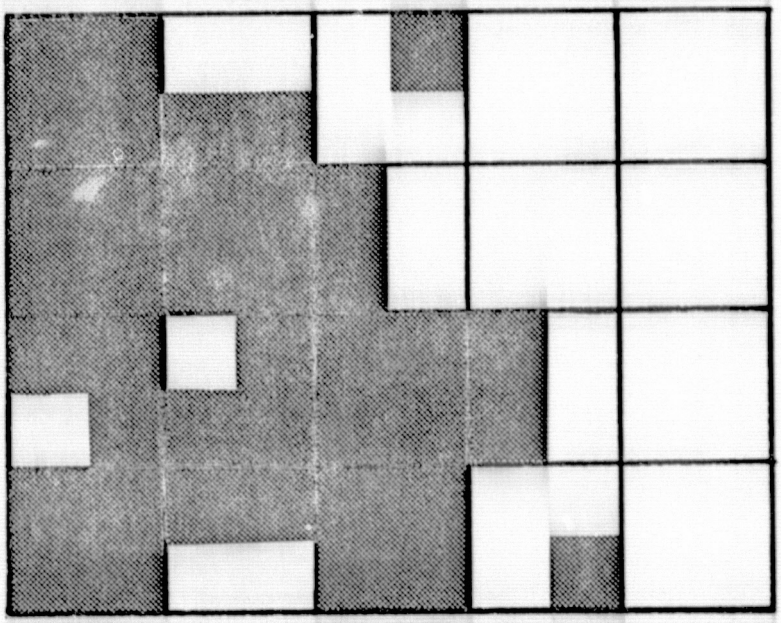
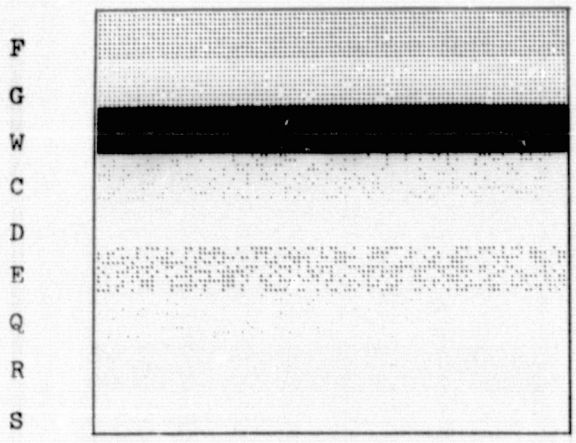


Figure 17.-Graphical representation of uniform and non-uniform training sets. a). Uniform mixture of 50% White - 50% Shaded. b). Non-uniform mixture of 50% White - 50% Shaded.

a.



b.

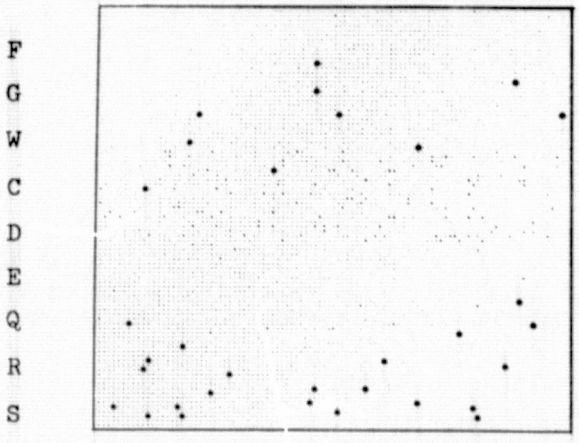


Figure 18.-Microfilm classification displays for component-class analysis using estimated mean vectors and covariance matrices. a) Spectral signatures estimated from uniform training sets. b) Spectral signatures estimated from non-uniform training sets. Symbols are: · =Grassland, \ =Forest, ° =Water. True field classes noted at left of displays have same symbols as in 9-class CCM in text.

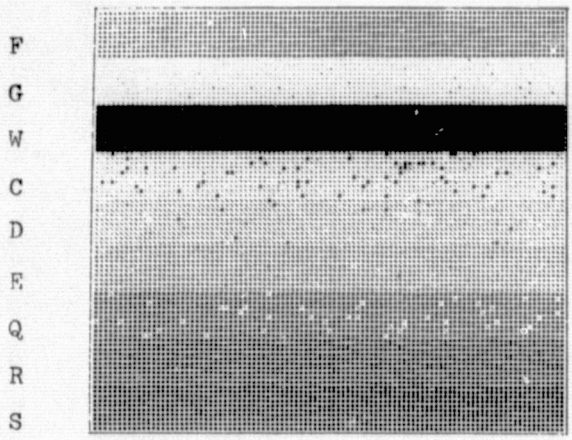


Figure 19.-Microfilm classification display of 9-class analysis using calculated component class mean vectors and common covariance matrix. Trueclass field symbols noted to left of display are same as in 9-class CCM in text.

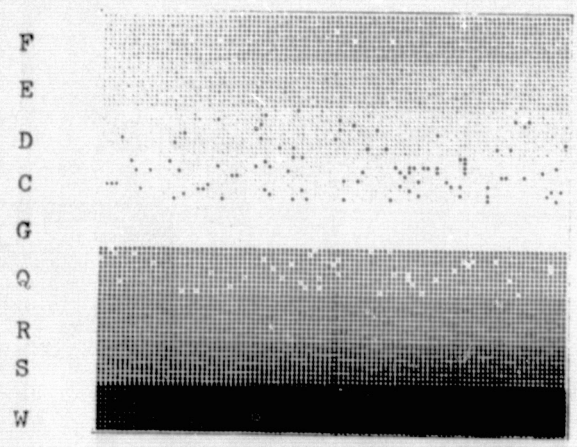


Figure 20.-Microfilm classification display of 9-class analysis using calculated mean vectors and common covariance matrix. True field class symbols noted at left of display are same as in 9-class CCM in text.

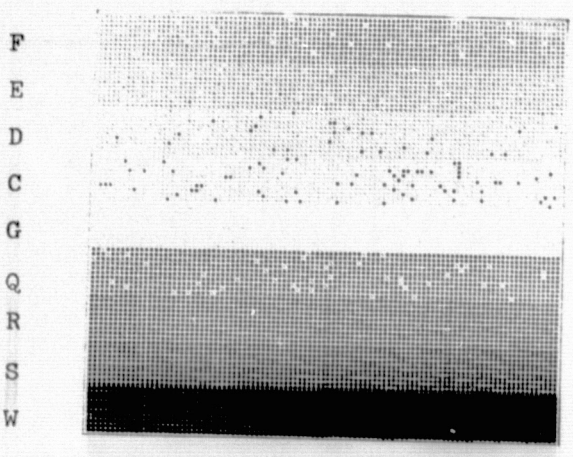


Figure 21.-Microfilm classification display for 9-class analysis using calculated mean vectors and averaged common covariance matrix. True class fields noted at left of display are same as in 9-class CCM in text.

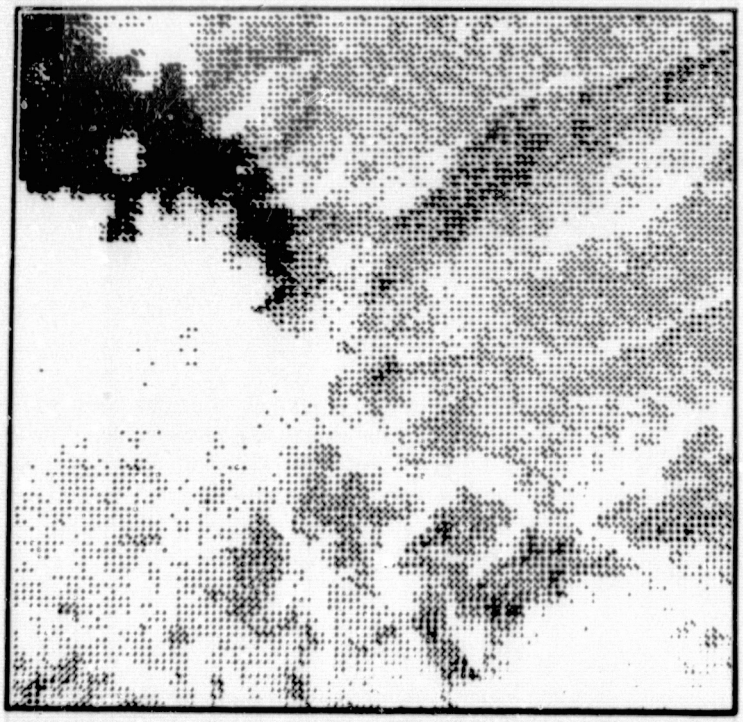


Figure 22.-Microfilm graymap of MSS Band 5 of the Elevenmile Canyon Reservoir Study Area.

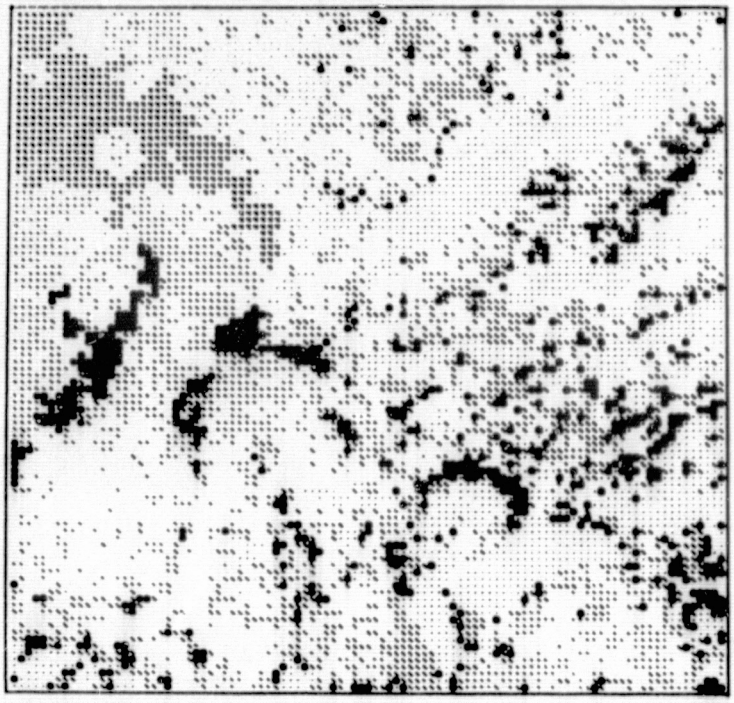


Figure 23.-Microfilm classification display of Elevenmile Canyon Reservoir Test Area with 5 Component Classes. Symbols are: • =Forest, ` =Grassland, ' =Water, \ =Mountain Grassland, ◦ =Wet Meadow, Blank Unclassified.

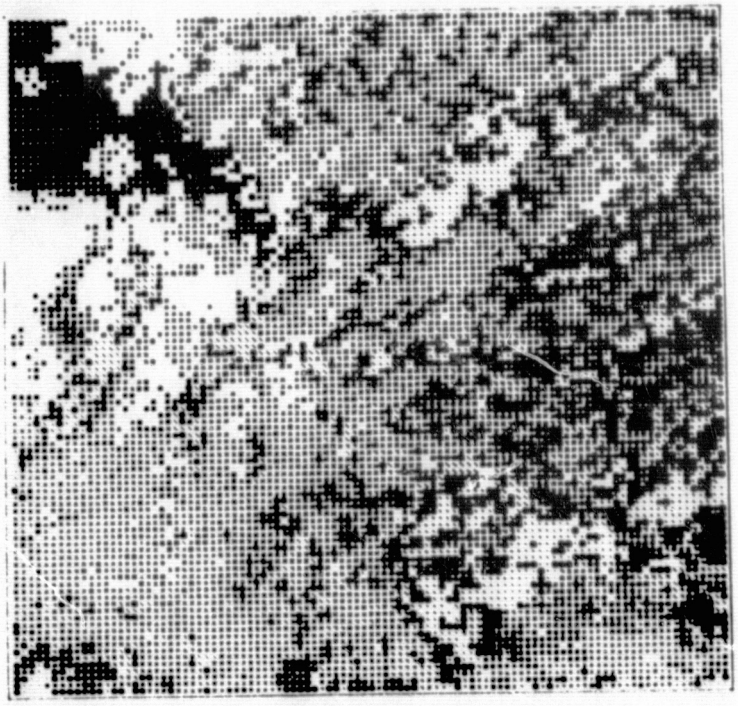


Figure 24.-Microfilm classification map of Elevenmile Canyon Reservoir study area with 5 component classes and 9 mixture classes. Because of limitations of the microfilm display, separate symbols could not be shown for the mixtures; however, for study purposes they were printed separately by a conventional line-printer.
Component classes:

, Grassland (G)
\ Forest (F)
' Mountain Grassland (MG)
\ Wet Meadow (WM)
o Water (W)

Mixture classes:

X = 75% G 25% F, 50% G 50% F, 25% G 75% F,
75% G 25% WM, 50% G 50% WM, 25% G 75% WM,
75% F 25% MG, 50% F 50% MG, 25% F 75% MG

Blank, unclassified

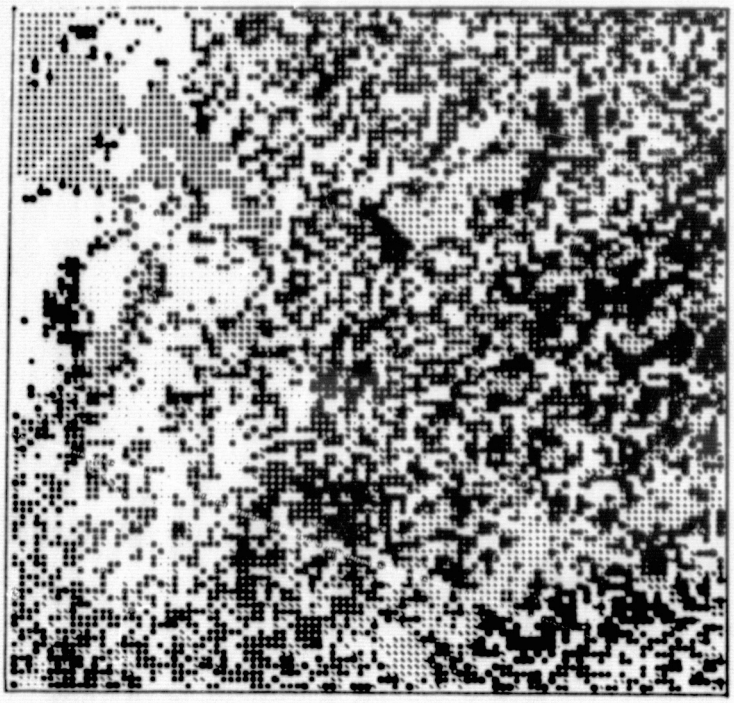


Figure 25.-Microfilm classification map of Elevenmile Canyon Reservoir study area with 5 component classes and 10 mixture classes. Because of limitations of the microfilm display, separate symbols could not be shown for the mixtures; however, for study purposes they were printed separately by a conventional line printer.
Component classes:

◦ Grassland (G)
\ Forest (F)
◣ Mountain Grassland (MG)
◥ Wet Meadow (WM)
✖ Water (W)

Mixture classes:

■ 67% G 33% F
• 67% G 33% W

X = 67% WM 33% W, 33% WM 67% W, 33% G 67% F,
33% G 67% W, 67% F 33% MG, 33% F 67% MG
67% G 67% WM, 33% G 67% WM

Blank, unclassified

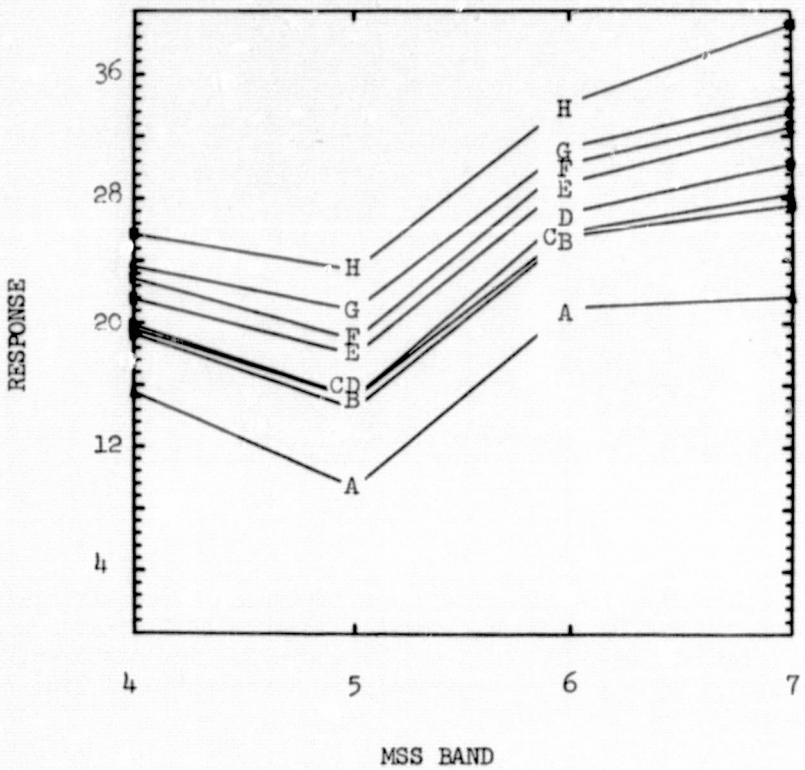


Figure 26.-Mean Spectral Response Curves for Manitou Study Plots and Estimated Component Classes. Symbols are: A=Estimated Forest Curve, B=Plot #2, C=Plot #3, D=Plot #1, E=Plot #4, F=Plot #6, G=Plot #5, H=Estimated Background Curve.

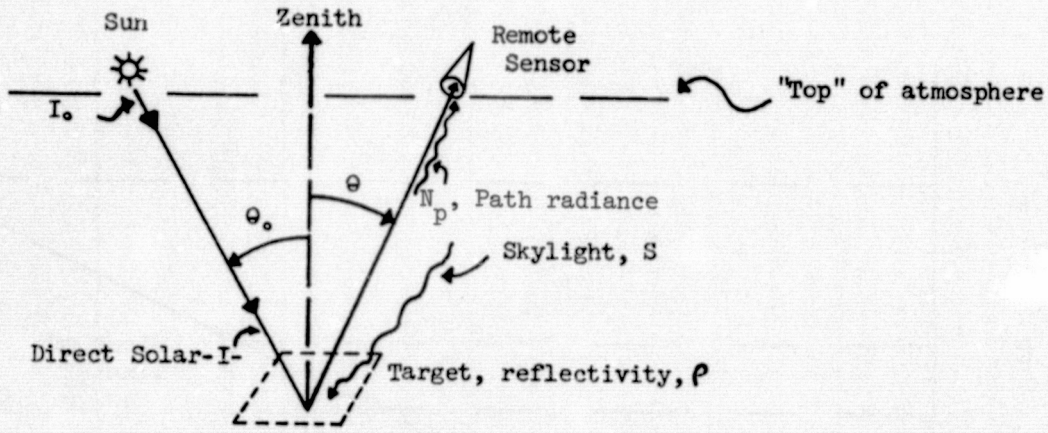


Figure 27.-Satellite remote sensing of target on the ground.

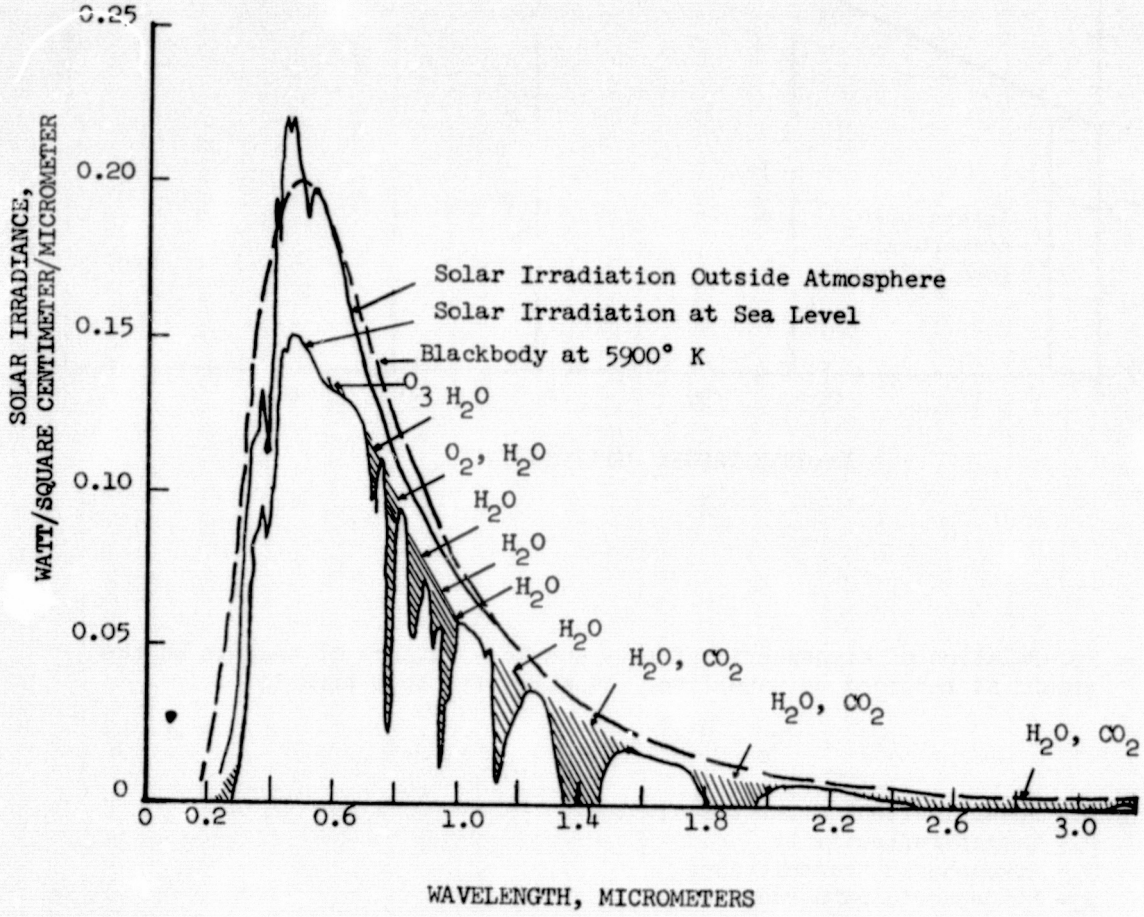


Figure 28.-Typical spectrum of solar energy reaching the surface of the earth. From Handbook of Geophysics and Space Environment, S. L. Valley, Editor (New York: McGraw-Hill Book Company, Inc.), p. 16.2

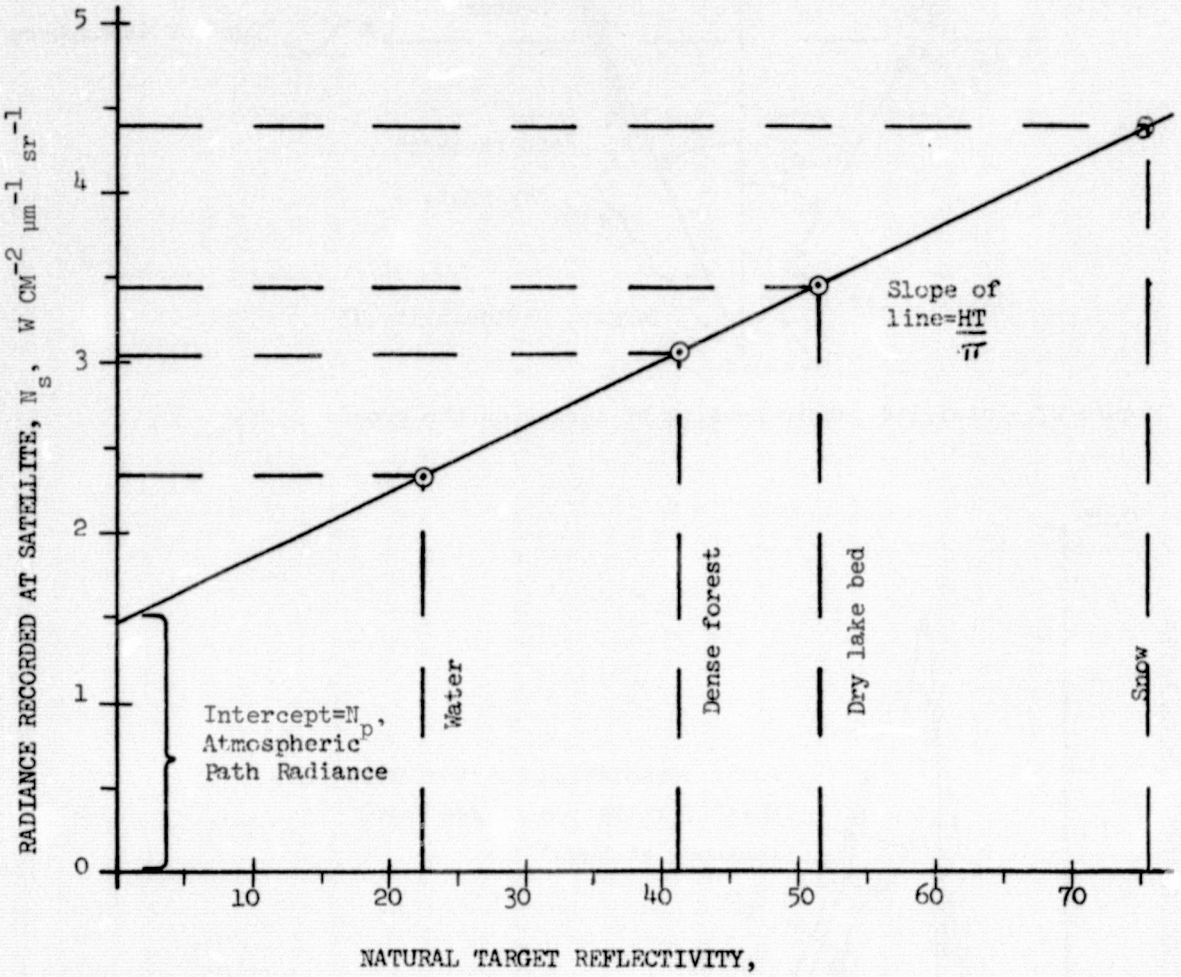


Figure 29.-Relation of atmospheric effects and the radiance of targets on the ground as recorded by satellite. Equation for this plot is:

$$N_s = \frac{H \rho T}{\pi} + N_p$$

H = Total incident solar irradiance
ρ = Target reflectivity
T = Atmospheric transmittance
N_p = Atmospheric path radiance

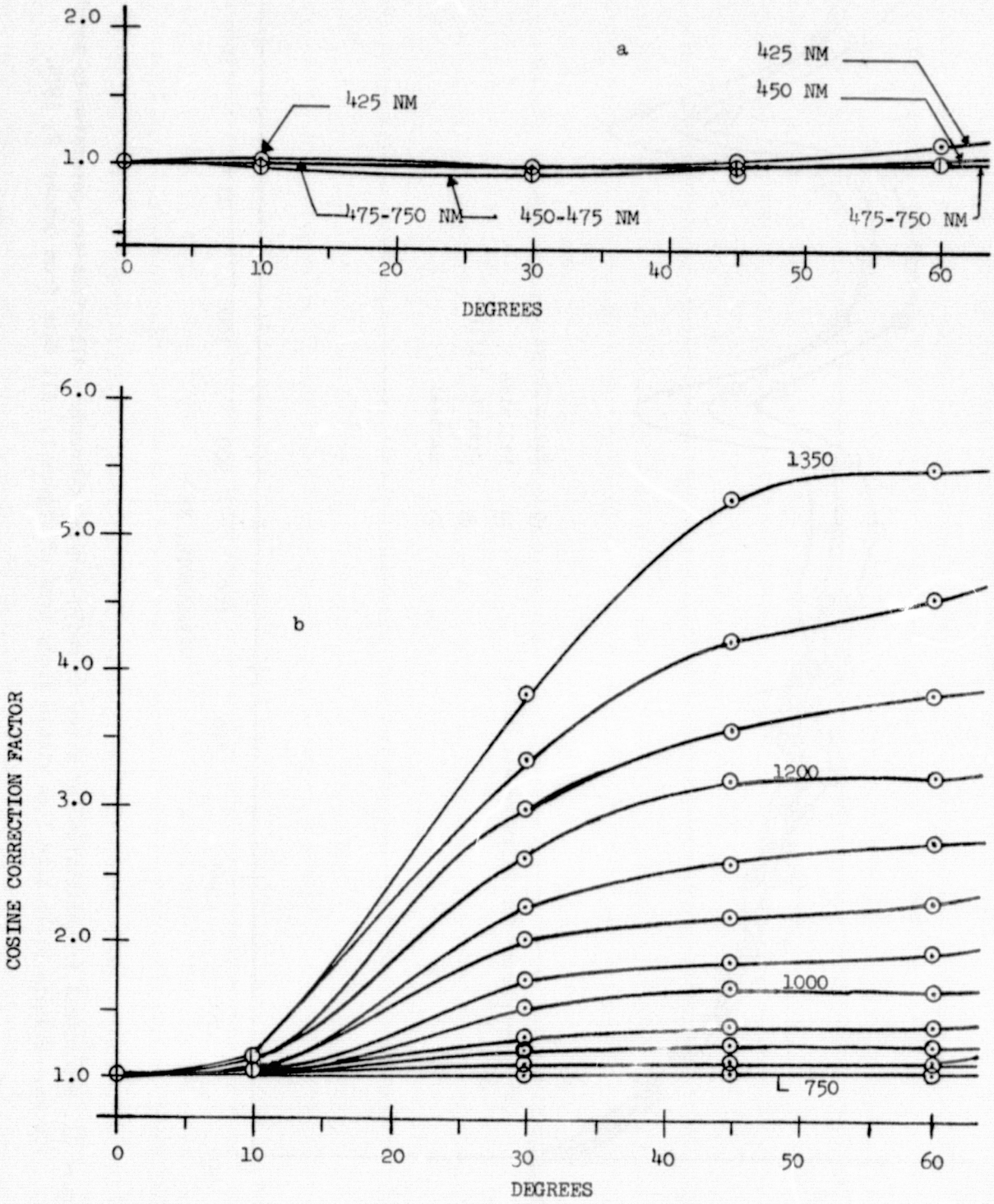


Figure 30.-Cosine correction factors for ISCO diffuser in the visible (a) and near-infrared (b) spectrum. I.S.C.O. 30109 using six-foot fiber optics probe. In b, each curve represents a wavelength from 1350 N.M. (top) to 750 N.M. (bottom).

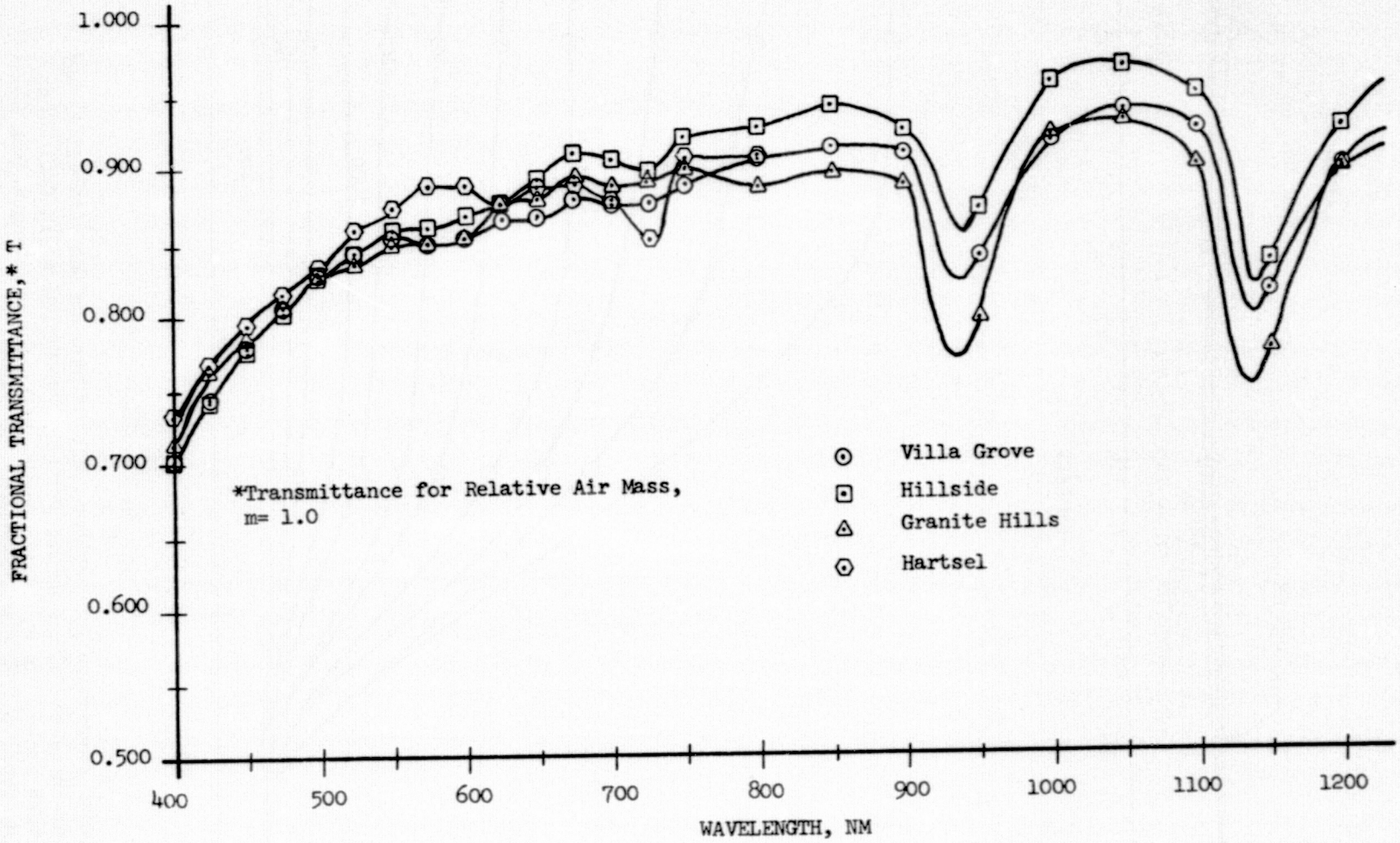


Figure 31.-Fractional transmittance for sites in south-central Colorado. All sites are separated by about 80 km. Granite Hills site lies within study area of figure 1. All data from October 2, 1974.

APPENDIX A

RECOG Computer Program Blocks

At Colorado State University, conventional automatic analysis of MSS data is accomplished through the use of a series of pattern recognition programs called RECOG. RECOG consists of six program blocks which are a modification of an original version, called LARSYS, developed at Purdue University (ref. 10). These programs provide a logical procedure for processing MSS data using supervised learning techniques. A brief description of each program block or phase is presented here.

Phase 1

Phase 1 is a display routine that provides the user with a computer line-printer or microfilm representation of the scene that is to be automatically analyzed. The MSS data are displayed as a graymap representing the radiation response from each pixel. A range of radiation responses (either specified or default) are coded as a symbol and displayed for a selected wavelength band. This display provides a pictorial representation of the MSS data from which the user may delineate field boundaries of terrain classes that he may wish to map.

Phase 2

The fields identified on the Phase 1 graymaps are used as training sets from which the mean spectral response and standard deviation vectors and correlation and covariance matrices are determined by Phase 2. The mean spectral response vector and covariance matrix provide a statistical spectral signature for a terrain class that is used in a later Phase to automatically classify each point in the MSS data set.

Phase 3

When the multispectral scanner has a large number of channels available, processing the data using all of the information becomes quite expensive. Phase 3 is designed to select a subset of optimum channels for identifying all of the terrain classes utilizing divergence criteria.

Phase 4

The spectral signatures obtained for each terrain class from Phase 2 can be analyzed as to how well they represent the class by selecting a subset of the MSS data and classifying it with Phase 4. Phase 4 is designed as an instructional mode and allows classification of the data set with three algorithms: LEVELS, a level-slicing routine; EUCLID, a Euclidian-distance routine; and GLIKE, a maximum-likelihood routine. GLIKE is the algorithm used to classify the data in the next Phase so it is valid to test the representativeness of the signature set with it. This allows refinement of each spectral signature by redefining the training set to discard any point that would tend to make a signature unrepresentative of its respective terrain class.

Phase 5

Phase 5 is the actual classification mode for the RECOG pattern recognition sequence. The mean vector and covariance matrix for each terrain class are used with the maximum likelihood decision rule GLIKE to classify each pixel in the specified MSS data set. As the classification results are generated they are written onto a magnetic tape and stored as a permanent file.

Phase 6

The final step in the processing scheme, Phase 6, displays the results generated by Phase 5. The user is given the option to specify a threshold level which sets a confidence limit for the classified data points. This is designed to eliminate false classifications of data

which do not fit any of the terrain classes. Current display modes available with Phase 6 include a thematic map produced on the computer line-printer and/or microfilm similar to those produced by Phase 1, except each pixel is identified by a symbol or intensity level (line printer and microfilm respectively) representing a terrain class. A more detailed description of RECOG can be found in refs. 14 and 15.

APPENDIX B

EQUATIONS

The mean vector and covariance matrix that describe the spectral response of a terrain class are determined from a set of MSS data points known to contain that class. The statistical equations used to compute them are discussed below.

Since the radiation response from a ground resolution element sensed by a multispectral scanner can be described by the column vector

$$X^A = \begin{pmatrix} x_1 \\ x_2 \\ x_3 \\ x_4 \end{pmatrix} \tag{26}$$

where each x component represents the radiance recorded in a spectral channel, we can find expressions for M^A and C^A in terms of the radiation responses X^A. (ref. 10)

The mean vector M^A is given by the column vector

$$M^A = \begin{pmatrix} m_1 \\ m_2 \\ m_3 \\ m_4 \end{pmatrix} \tag{27}$$

where m_i is the mean spectral response in wavelength band i (for LANDSAT-1 i=1,....,4) given by

$$m_i = \frac{1}{n^A} \sum_{k=1}^{n^A} Xik \tag{28}$$

where n^A is the number of pixels (sample points) in the training set describing terrain class A, and k is the sample point index.

The covariance matrix which indicates how the radiation response in one MSS channel varies with the response in the other channels can be described as

$$C^A = \begin{pmatrix} \sigma_{11}^2 & \sigma_{12}^2 & \cdots & \sigma_{14}^2 \\ \sigma_{21}^2 & & & \\ \vdots & & & \\ \sigma_{41}^2 & & & \sigma_{44}^2 \end{pmatrix} \tag{29}$$

where σ_{ij}^2 is the covariance between channels i and j given by

$$\sigma_{ij}^2 = \frac{1}{n^A} \sum_{k=1}^{n^A} (x_{ik} - m_i)(x_{jk} - m_j) \tag{30}$$

The standard deviation for channel i in class A is σ, and the correlation coefficient r_{ij} between channel i and channel j for class A is given by

$$r_{ij} = \frac{\sigma_{ij}^2}{\sigma_i \sigma_j} \tag{31}$$

SECOND GENERATION DIGITAL TECHNIQUES FOR PROCESSING LANDSAT MSS DATA

S.S. Rifman, TRW Systems Group, Redondo Beach, California
K. W. Simon, TRW Systems Group, Redondo Beach, California
R. H. Caron, TRW Systems Group, Redondo Beach, California

N76-17527

ABSTRACT

In order to fully exploit the potential value of LANDSAT synoptic data collected at least 20 times each year at any point in the spacecraft's coverage pattern, one must utilize not only the multispectral, but also the multitemporal nature of such data. Automatic (computer) analyses of vegetation growth, the estimation of potential runoff from melting snow cover, the mapping of the impact on the environment of natural disasters, etc., become feasible if bulk digital LANDSAT data for a given site is registered to high accuracy.

Results are reported in this paper for precision corrected LANDSAT MSS full scene registration of better than 0.5 picture element (rms), utilizing all digital methods. Examples of such registered full scene images are presented and evaluated by two methods: (1) change detection imagery which represents pixel by pixel the difference of corresponding pixel values in the registered data; and (2) direct measurement of registration errors throughout the imagery by means of a highly accurate cross correlation algorithm. Subscene image details illustrate the impact on registration accuracy of two interpolation algorithms.

I. INTRODUCTION

Many investigators have come to understand and prefer the benefits of LANDSAT data processed by all-digital methods over conventional photographically generated products. The advantages of precision, repeatability, permanence, and control over the data that characterize digital methods have been found useful in the areas of correction of bulk digital data (References (1) and (2)), contrast enhancement and spectral ratioing (Reference (3)), multispectral classification (Reference (4)), and magnification (Reference (5)). All of these digital techniques can be implemented in low cost minicomputer-based processing systems. Some such systems utilize hardwired algorithms to implement various algorithms at very high speed.

As useful as the current digital approaches are, however, further progress in advancing the state of the art in utilizing the existing hardware and software systems requires an extension of the capability to make use of the data base generated by LANDSAT-1, now being augmented by LANDSAT-2. In other words, in order to fully exploit the potential value of data collected at least once every 18 days at a given point on the earth's surface within the spacecraft's ground coverage pattern, use must be made of the multitemporal, as well as multispectral character of such data. Multitemporal data makes possible dynamic studies of vegetation growth (crops, forestry, etc.), the monitoring of man's impact on the environment (strip mining, water pollution, etc.), the mapping of the impact of natural disasters (flood, fire, etc.), and a host of other studies. Improved multispectral classification results can also be expected from multitemporal-multispectral data (Reference (6)).

In order to facilitate automatic (computer) processing of multitemporal data, it is first necessary to bring the data into spatial registration. That is, picture element (pixel) by pixel the processed digital data recorded on computer compatible tape (CCT) must correspond to a particular point on the earth's surface, irrespective of the date the data was collected. This registration requirement calls for a new generation of processing

PRECEDING PAGE BLANK NOT FILMED

techniques that go beyond the first generation single scene requirement for geometric correction (rectification) and gridding of bulk data.

An additional benefit is derived implicitly from the second generation techniques for LANDSAT scene/scene registration. That is, if each new scene is registered to some reference scene which has been precision rectified previously, then all such scenes will be rectified to the same accuracy as the reference scene, providing the registration error is sufficiently small.

This paper briefly outlines the nature of the LANDSAT MSS multitemporal registration problem and then describes two methods utilized to evaluate full scene registered data, processed by all-digital methods. Examples of fully corrected full scene MSS images are shown, along with details extracted therefrom, in order to illustrate the impact on registration quality of two widely known digital interpolation techniques.

II. THE LANDSAT MSS REGISTRATION PROBLEM

The LANDSAT Multispectral Scanner (MSS) scans cross track swaths of 185 Km width, imaging six scan lines along track in each of four spectral bands simultaneously. The object plane of the sensor is scanned by means of oscillating flat mirror, with an 11.56 degree cross track field of view. The instantaneous field of view (IFOV) of each individual detector subtends an earth-area square 79 meters on a side. Along track separation of IFOVs is approximately the same, but the center-to-center separation across track is approximately 56 meters. The mirror oscillation frequency is such that the spacecraft's nadir position on the earth's surface advances 474 meters along track during one mirror scan and retrace cycle, equal to the distance on the ground subtended by the six along track detectors in each spectral band. During 390 mirror cycles, a ground track swath 185 Km in length is imaged.

During the 28.6 seconds it takes for the MSS to collect data for an area 185 Km x 185 Km on the ground, the spacecraft's attitude (roll, pitch and yaw) varies in a nonlinear fashion. This attitude motion produces principally an image offset, but also produces higher order image distortions traceable to the attitude rate, acceleration, etc. If not compensated, these attitude errors will spoil attempts to rectify and register MSS scenes to fractional pixel accuracy, inasmuch as attitude changes with time during a scene and is naturally different from one scene to the next. Unfortunately, the spacecraft attitude data in the downlinked telemetry is not sufficiently accurate to permit correction of attitude errors, and use must be made of information in each scene (features called control points) to make this correction.

Other factors which must be taken into account in order to rectify and register MSS scenes are due to spacecraft altitude and altitude rate errors and spacecraft ephemeris deviations (position and heading) as a function of time from the nominal orbit, due to long term orbital drift induced by the solar wind and atmospheric drag. Tracking data inaccuracies compound the problem.

Sensor related geometric distortions are essentially systematic, and are due to the mirror scan nonlinearities and detector commutation time offset. The latter results from a small time delay between samples collected from each of the six detectors in a given spectral band which causes a small sawtooth appearance in otherwise linear features ("Golden Gate Effect"). The number of samples collected in one active mirror scan is subject to some small variation with time, inasmuch as the mechanical motion of the mirror is subject to slight rate variabilities.

Finally, the effect of earth rotation and shape must be taken into account before a corrected MSS scene can be represented in map coordinates. Two popular mapping systems are Universal Transverse Mercator (UTM) and Space Oblique Mercator (Reference (7)).

In order to produce MSS image data free of the distortions outlined above, it is first necessary to determine the geometrical distortions, and then implement the correction by means of an image resampling (interpolation) technique. The techniques utilized to determine geometric distortion for the rectification problem have been outlined previously (References (1), (2), (8), and (9)). The techniques utilized to determine the registration distortion will be the subject of a forthcoming paper.

The technique for computing corrected image pixel values from bulk (uncorrected) image values is called image resampling, or interpolation. Various techniques for resampling the image data have been discussed previously (References (8) and (10)), and apply to both the rectification problem and the registration problem. For the purposes of this paper, two specific resampling techniques will be considered, namely, TRW Cubic Convolution and nearest-neighbor interpolation. The former is a high-order interpolation method which yields performance very near the ideal; whereas the latter is a very simple (low-order) algorithm.

III. REGISTRATION RESULTS

Figure 1 shows the full scene 1062-15190-5 of the Chesapeake Bay region, derived from precision corrected bulk data using all-digital methods. This UTM-projected image is geometrically corrected for all the sources of error discussed in Section II with the help of ground control points (image features the geodetic locations of which are known to high accuracy). Figure 2 shows the full scene 1080-15192-5, which has been digitally registered to the scene of Figure 1. The scene of Figure 2, which was imaged 18 days (one LANDSAT cycle) after that of Figure 1, shows the effects of a rainstorm: increased sedimentation in the Potomac (more reflective in Figure 2 than in Figure 1) and a general absence of cloud cover and atmospheric haze.

Graphic illustration of the full scene registration accuracy is shown in Figure 3, the change detection image for Figures 1 and 2. Each pixel of Figure 3 was computed as the difference of the corresponding normalized pixel values of Figures 1 and 2.[1] Neutral gray is representative of no significant difference (change) between corresponding pixel values in Figures 1 and 2; light areas are indicative of bright features in Figure 2, not present in Figure 1; and dark areas represent bright features in Figure 1, not present in Figure 2. Note for example, that the sedimentation change appears clearly as a bright area in the river; clouds in Figure 1, including the jet contrail in the lower right, show up as dark features in Figure 3. Note in particular, the significant changes in the agricultural area on the eastern shore of Maryland, in the right of Figure 3.

Figure 4 shows the precision-corrected full scene 1411-17381-6 of an area in Saskatchewan, Canada. Figure 5 shows scene 1339-17391-6, registered to the scene of Figure 4. The corresponding change detection image for the 72-day temporal separation appears in Figure 6.

In order to illustrate more clearly the effects of two interpolation algorithms, image details from Figures 1 and 3 are shown respectively in Figures 7-a and 7-b, for data generated by means of the TRW Cubic Convolution Process. Imagery corresponding to Figure 7, derived from nearest-neighbor resampled data, is shown in Figure 8. Note in particular, the blocky appearance of Figure 8-a compared to Figure 7-a. Note also the increased structure in the change detection image of Figure 8-b, relative to Figure 7-b. This structure, which can complicate analyses of multitemporal data, is strictly an artifact of the nearest-neighbor resampling process, and is evident for data processed in otherwise identical fashion.

[1] The image of Figure 3 is greatly contrast-enhanced to bring out details. The pixel values in the interval 24 to 41 (out of a potential range from 0 to 127) have been stretched over the full black-white interval. No other images in this paper have been enhanced in this manner.

A comprehensive treatment of the various interpolation algorithms is given in References (8) and (10). However, as can be seen in Figures 7 and 8, and as underscored in the two references, the important conclusion to be drawn for second generation processing systems is that even if scene data is registered to high accuracy (discussed below), the use of a low order interpolation algorithm (e.g., nearest neighbor) will produce artifacts which can significantly impact the performance of algorithms utilizing registered multitemporal scene data. High order interpolation (e.g., cubic convolution) reduces the artifacts to a minimum, and makes feasible multitemporal scene studies (Reference (6)).

Figure 9 illustrates results obtained when scenes are not registration processed, but are independently precision corrected (rectified) such that there is no lateral displacement or rotational misalignment. That is, the second scene is centered and rotated to exactly the same parameters as used for the first scene, but otherwise processed independently. Figure 9-a shows the reference image detail from Figure 1; Figure 9-b shows the change detection image for this detail, derived from Figure 3; Figure 9-c shows the change detection image for this detail when the second scene is corrected independently of the first, but centered and rotated to the same values as the reference image. The TRW Cubic Convolution process has been utilized for all images in Figure 9, which have not been contrast-enhanced.

Accuracy of the full scene MSS registration process has been evaluated quantitatively by measuring to high precision the relative positions of image features in the two scenes. To do so, a regular grid of points (16 x 16) is defined at uniform intervals in the reference (precision rectified) scene. Precisely, the same grid of points is defined in the registered scene. Image chips centered at the corresponding positions in the two scenes are then cross-correlated against one another using a small search area ($\pm$ 2 lines, $\pm$ 2 pixels). By fitting a biquadratic polynomial to the integer values of relative chip displacement it is possible to achieve correlation measurement accuracies of 1/10 pixel.

Registration errors for the two scenes shown in Figures 1 and 2 are plotted in Figure 10. The scale of errors is indicated at the left of the figure. Circles indicate grid points where correlation peaks were not found; dashed arrows indicate grid points where correlation peaks were less than 75%. Most of the circled grid points, where no correlation peaks were found, lie in the image areas of homogeneous content, such as the Chesapeake Bay and Potomac River, or else regions of no image overlap.

All errors plotted in Figure 10 are less than 1 pixel in magnitude (1 pixel = 57 meters). The rms error in the along-track direction (i.e., the direction of spacecraft motion) is $\sim$ 1/3 pixel, and the rms error in the across-track direction is $\sim$ 1/4 pixel. Errors are smallest where image registration features (control points) were utilized to determine geometric warp, but registration performance is uniformly good throughout the scene. Results for the images of Figures 4 and 5 are very similar to the results shown in Figure 10.

IV. CONCLUSIONS

Full scene LANDSAT MSS bulk digital data has been precision corrected (rectified) and precision registered utilizing all-digital techniques. Qualitative evaluations using change detection imagery demonstrate the quality of the registered data. Subareas derived from the full scene data processed by TRW's Cubic Convolution Process have been visually compared with data processed by nearest neighbor interpolation. It is clear from these comparisons that the low-order (nearest neighbor) resampled data contains a number of artifacts which can degrade change detection studies. Such artifacts are absent from cubic convolution processed data.

Numerical measurements of full scene registration accuracy have been performed directly with the corrected and registered digital data. Registration accuracies of less than .5 pixel rms (1 pixel, worst case) have been measured by direct cross-correlation of image subareas located throughout the full scene.

In summary, registration processing of bulk digital MSS data has been demonstrated to fractional pixel accuracy. This capability extends the presently accepted advantages of digital processing techniques to the multitemporal as well as the multispectral environment. Thus, the full potential of repeat LANDSAT coverage over the earth's surface can now be exploited.

ACKNOWLEDGMENT

Portions of the results reported in this paper were obtained during performance of Contract NAS5-20085 with NASA/Goddard Space Flight Center.

REFERENCES

(1) S.S. Rifman, "Digital Rectification of ERTS Multispectral Imagery," Symposium on Significant Results Obtained from the Earth Resources Technology Satellite-1, New Carrolton, Md., NASA SP-327, p. 1131 (March 5-9, 1973).

(2) S.S. Rifman, "Evaluation of Digitally Corrected ERTS Imagery," Symposium on Management and Utilization of Remote Sensing Data, Sioux Falls, South Dakota, p. 284 (October 29-November 1, 1973).

(3) F.C. Billingsley, "Some Digital Techniques for Enhancing ERTS Imagery," Symposium on Management and Utilization of Remote Sensing Data, Sioux Falls, South Dakota, p. 284 (October 29-November 1, 1973).

(4) Third Earth Resources Technology Satellite-1 Symposium, Washington, D.C., NASA SP-351, (December 10-14, 1973).

(5) J.E. Taber, "Evaluation of Digitally Corrected Images," Third Earth Resources Technology Satellite-1 Symposium, Washington, D.C., NASA SP-351, p.1837 (December 10-14, 1973).

(6) R.H. Caron, "Evaluation of Full-Scene Registered ERTS MSS Imagery Using a Multitemporal/Multispectral Bayes Supervised Classifier," Proceedings of Fourth Annual Remote Sensing of Earth Resources Conference, University of Tennessee Space Institute, Tullahoma, (March 24-26, 1975).

(7) A.P. Colvocoresses, "Space Oblique Mercator -- A New Map Projection of the Earth," Photogrammetric Engineering 40, p. 921 (August 1974).

(8) R.H. Caron, S.S. Rifman, and K.W. Simon, "Application of Advanced Signal Processing Techniques to the Rectification and Registration of Spaceborne Imagery," Proceedings of the First Houston Technology Transfer Conference, p. 245 (September 1974).

(9) R.H. Caron and K.W. Simon, "Attitude Time-Series Estimator for Rectification of Spaceborne Imagery," Journal of Spacecraft and Rockets 12, p. 27 (January 1975).

(10) K.W. Simon, "Digital Image Reconstruction and Resampling for Geometric Manipulation," Symposium on Machine Processing of Remotely Sensed Data, West Lafayette, Indiana (June 3-5, 1975).

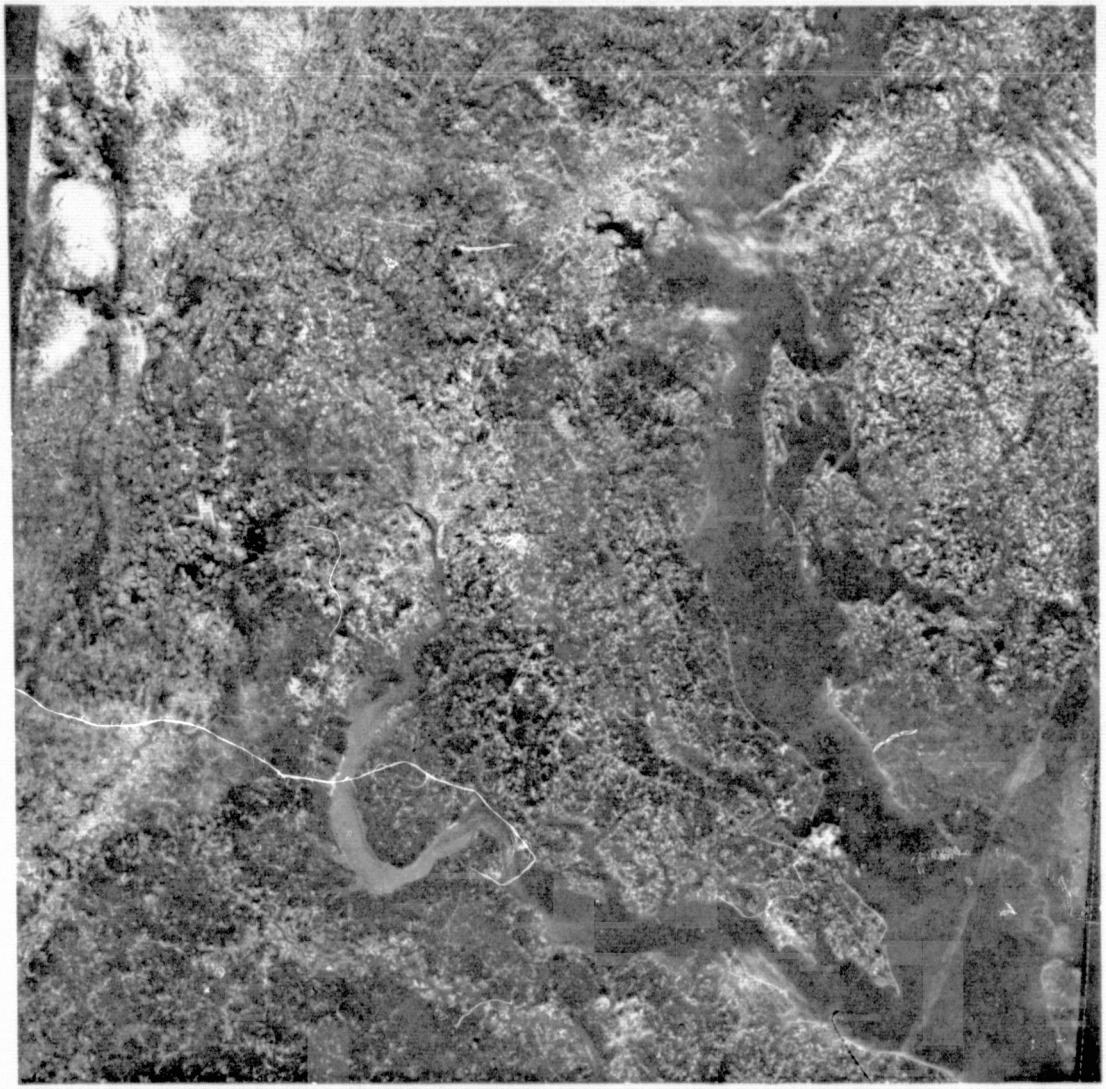


Figure 1. Precision Corrected Full Scene 1062-15190-5.
This image of the Chesapeake Bay Area was produced from digitally corrected bulk digital data.

REPRODUCIBILITY OF TH
ORIGINAL PAGE IS POOR

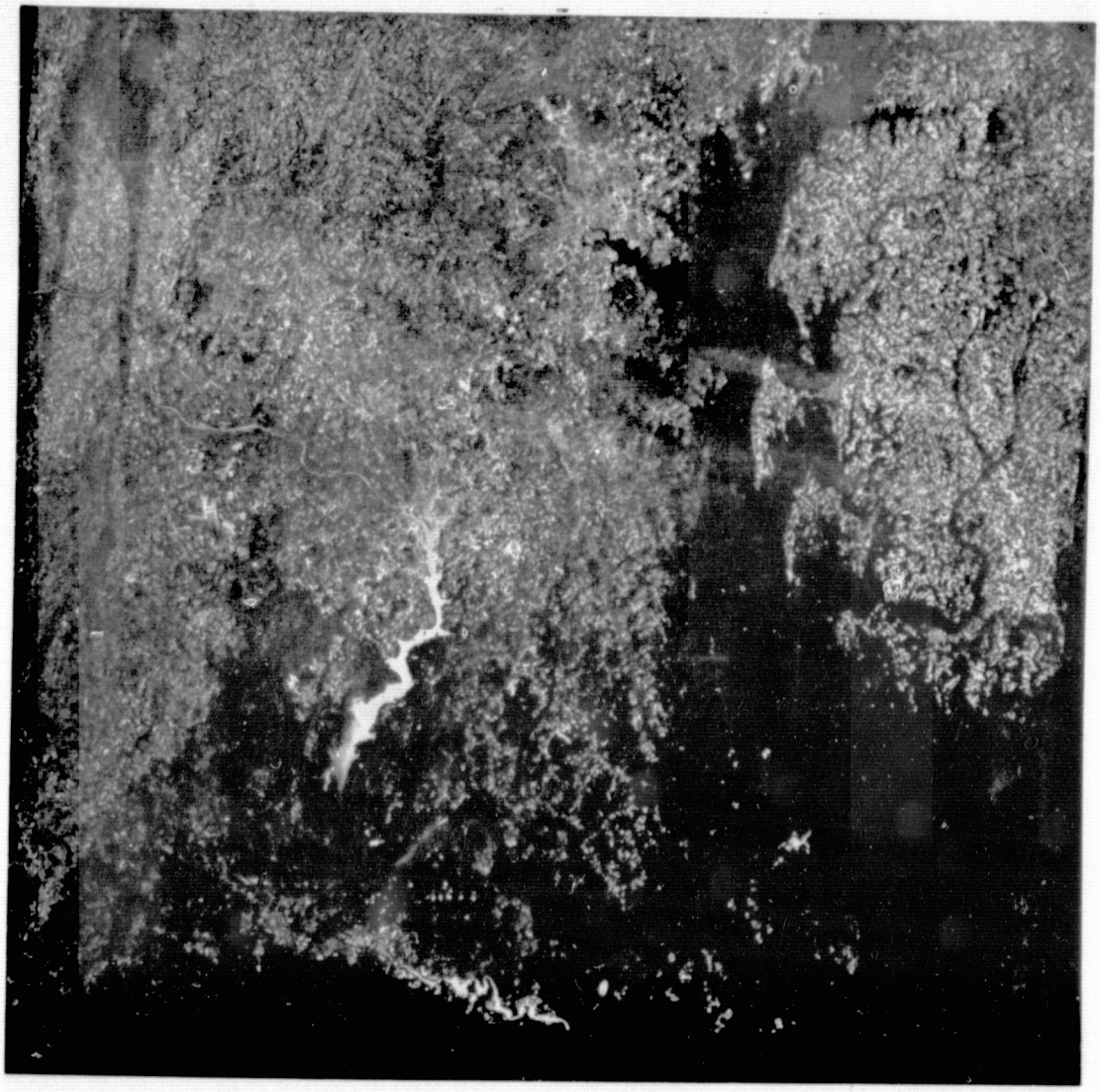


Figure 2. Precision Corrected and Registered Full Scene 1080-15192-5. This image was produced from digitally corrected bulk data, 18 days removed in time from the data of Figure 1.

REPRODUCIBILITY OF THE
ORIGINAL PAGE IS POOR

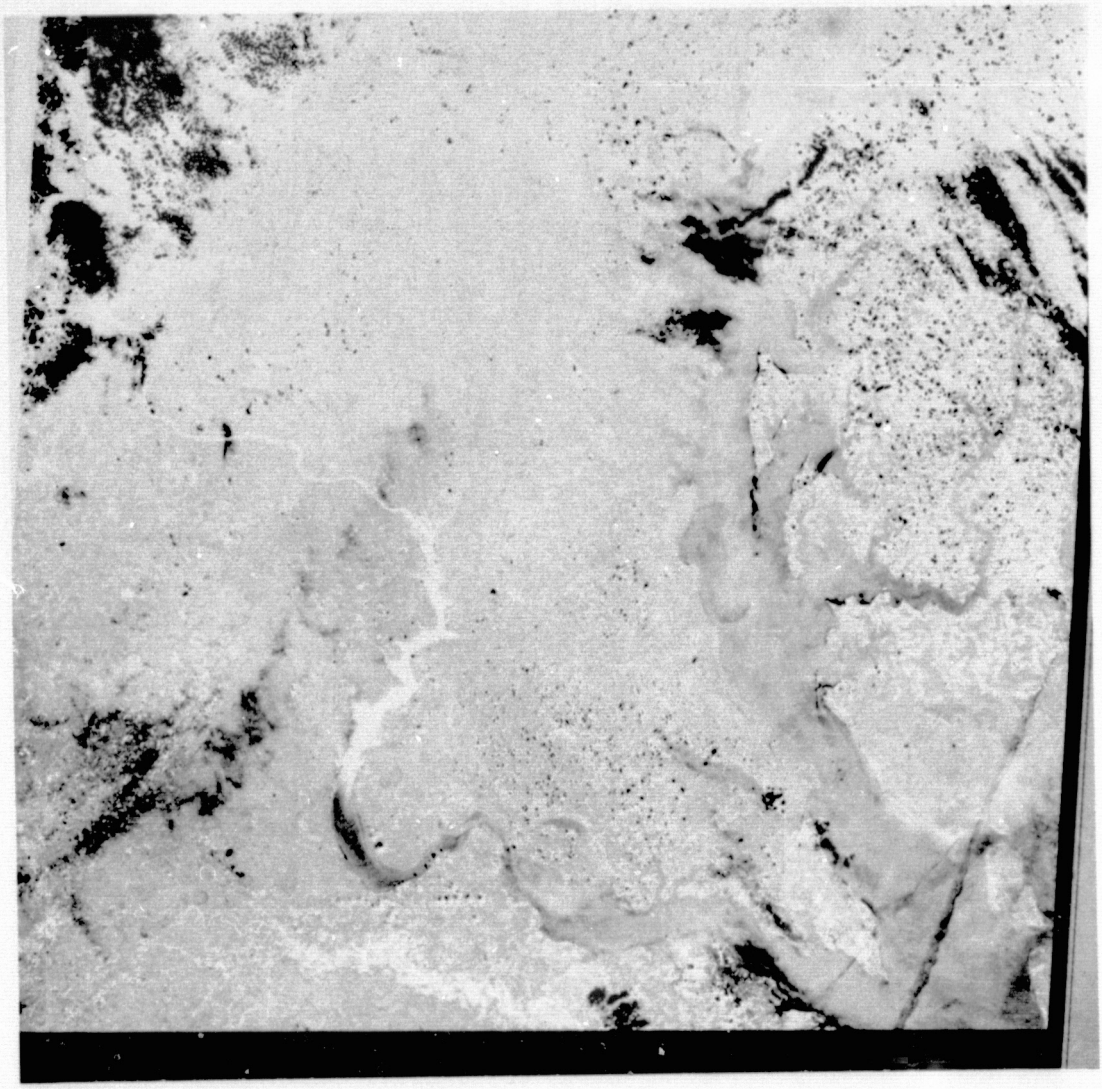


Figure 3. Change Detection Image for Scenes 1062-15190-5 and 1080-15192-5. Every pixel is computed as the difference of corresponding normalized pixels from registered scene data. Neutral gray represents no change; light and dark patches represent positive and negative changes, respectively.

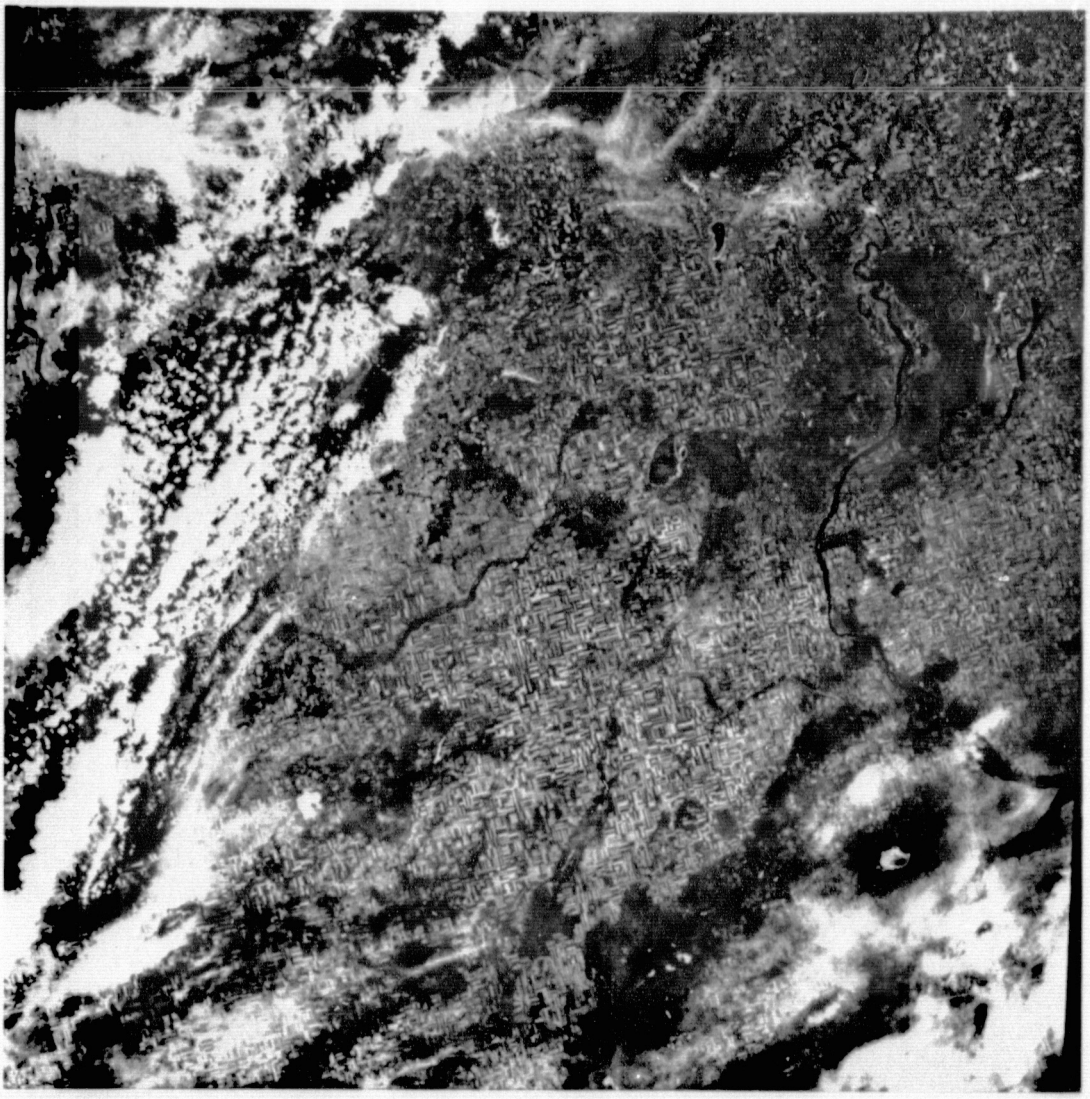


Figure 4. Precision Corrected Full Scene 1411-17381-6.
This image of an area in Saskatchewan, Canada was produced from digitally corrected bulk digital data.



Figure 5. Precision Corrected and Registered Full Scene 1339-17391-6. This image was produced from digitally corrected bulk data, 72 days removed in time from the data of Figure 4.

REPRODUCIBILITY OF THE
ORIGINAL PAGE IS POOR

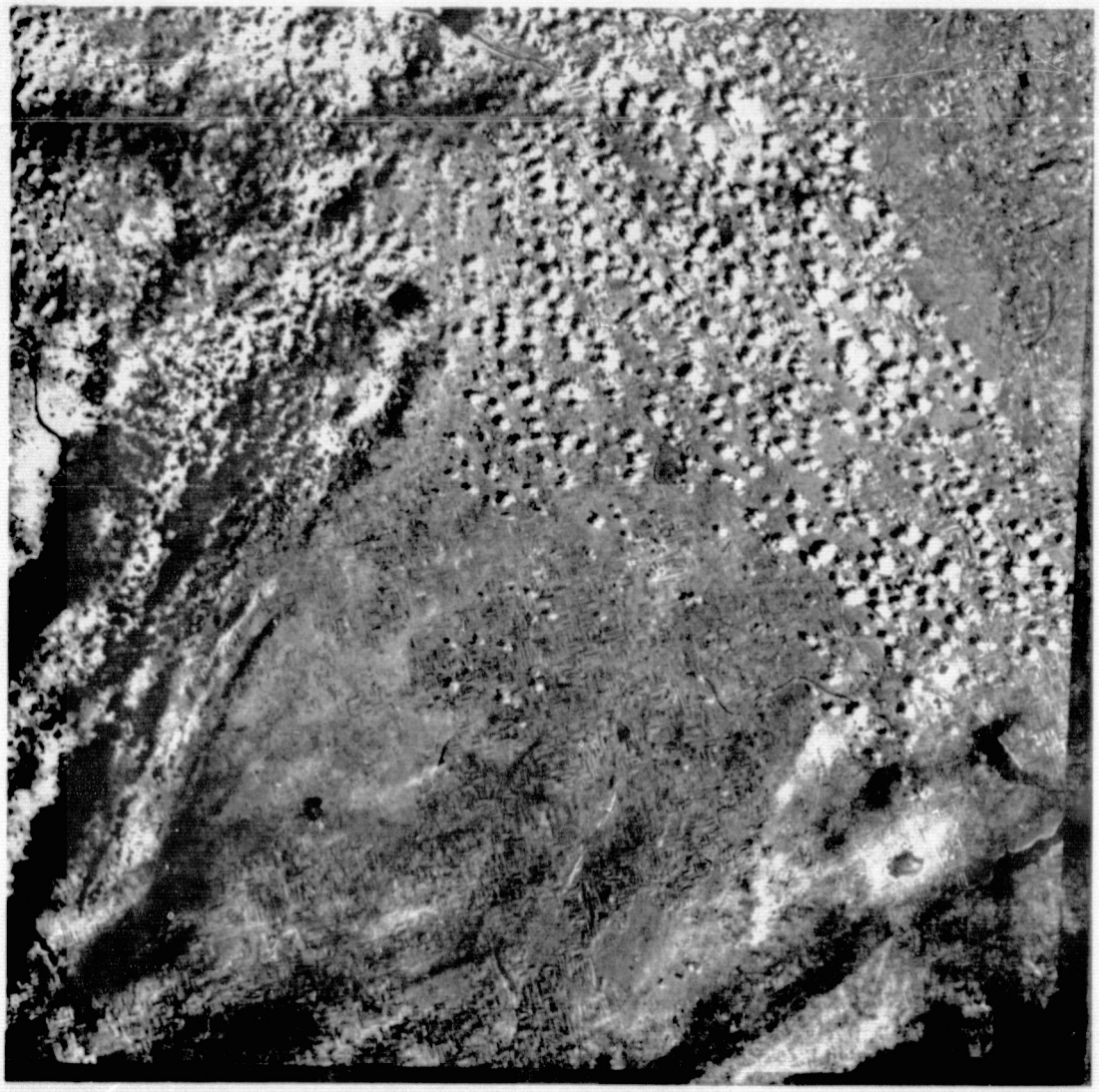
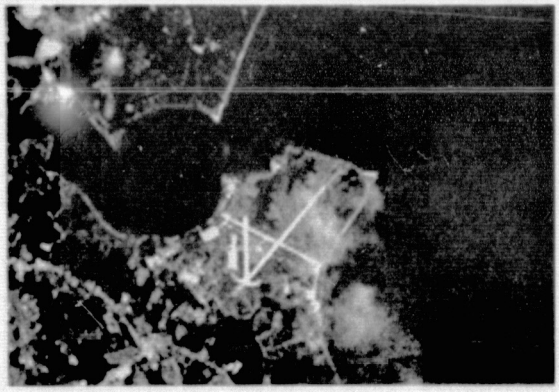
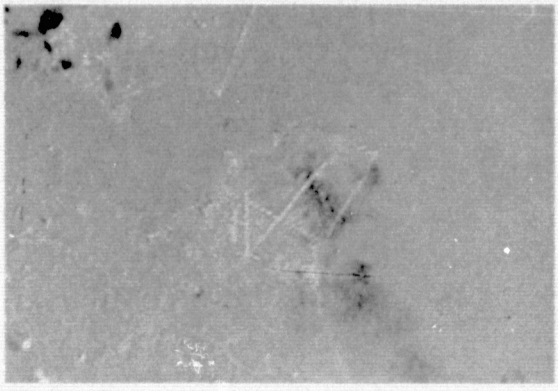


Figure 6. Change Detection Image for Scenes 1411-17381-6 and 1339-17391-6 Every pixel is computed as the difference of normalized, registered scene data. Neutral gray represents no change; light and dark patches represent positive and negative changes; respectively.



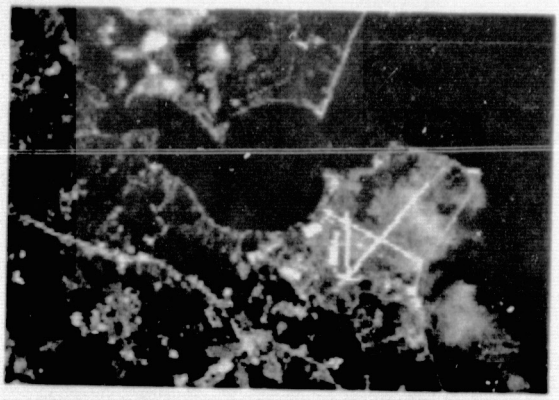
(a)



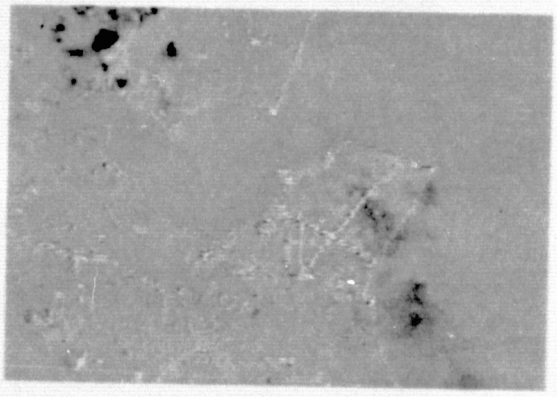
(b)

Figure 7. Details from Data Processed by Cubic Convolution Process These details (29.2KM wide) were derived from Figure 1 and Figure 3, respectively, in the area including the Naval Air Station.

REPRODUCIBILITY OF THE
ORIGINAL PAGE IS POOR



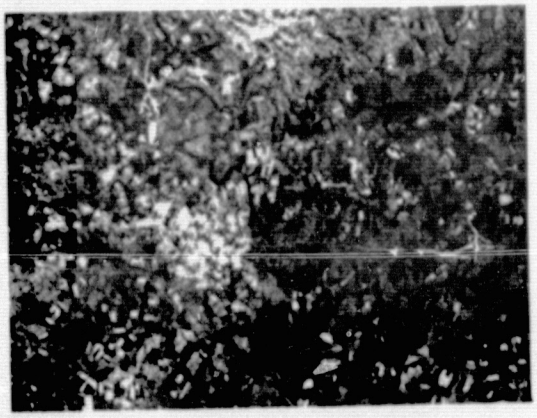
(a)



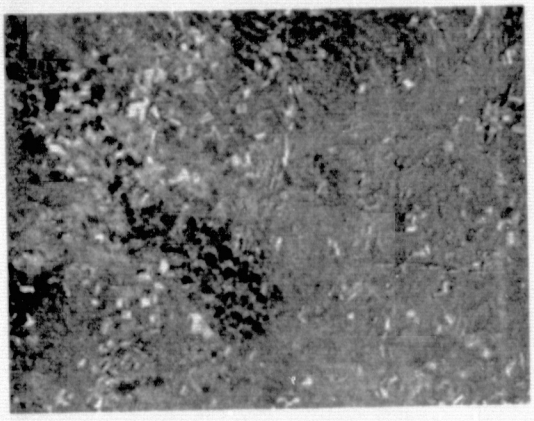
(b)

Figure 8. Details from Data Processed by Nearest Neighbor Interpolation These details (29.2KM wide) were derived from data processed in the same manner as in Figure 7, but with the exception of utilizing nearest neighbor interpolation. Full scene nearest neighbor resampled data would appear indistinguishable from Figure 1, in this half-tone reproduction.

(a)



(b)



(c)

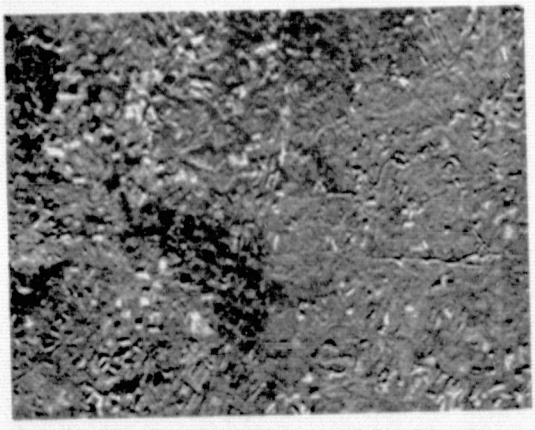


Figure 9. Comparison of Precision Registration Data with Independently Precision Processed Data
(a) Detail from precision corrected full scene 1062-15190-5; (b) Detail from change detection image produced from precision registered full scene data; (c) Detail from change detection image produced from full scene data precision corrected independently, but with the same center and orientations.

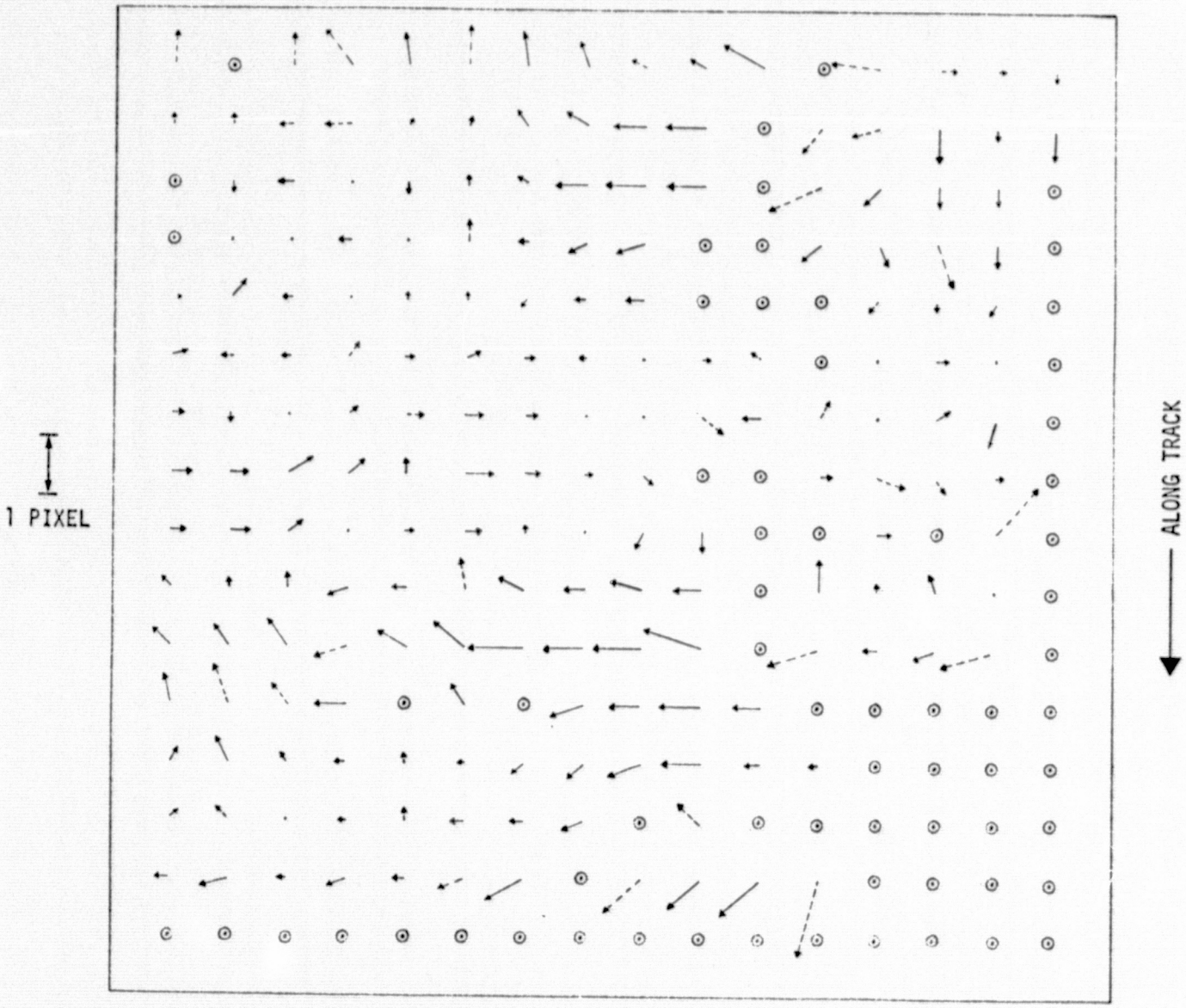


Figure 10. Registration Errors for Precision Registration of Two Full Scenes
The solid lines correspond to the measured registration errors for the full scene data of Figures 1 and 2. The scale of a registration error of 1 pixel is indicated on the left. Circled dots are positions for which no correlation peaks were found. Dotted lines correspond to correlation peaks under 75%.

By Peter M. Kuhn, National Oceanic & Atmospheric Administration, Boulder, Colorado
Victor S. Whitehead, NASA Johnson Space Center, Houston, Texas and
William E. Marlatt, Colorado State University, Fort Collins, Colorado

N76-17528

ABSTRACT

The Skylab field phase in June, August and September of 1973 for the SCARP (Skylab Concentrated Atmospheric Radiation Project) provided a unique opportunity to conduct infrared and solar observations and subsequent calculations beneath the orbiting space vehicle during EREP overpasses. Infrared and solar transmission and absorption properties observed within the atmosphere were compared with EREP experiments, notably the S-191 and S-192. These same observations were later employed in the development and comparison of various atmospheric infrared and solar radiative transfer approximations. Solar radiation observations and calculations in the scattering atmosphere included the 0.4 to 1.1μm spectral range while infrared observations and calculations covered the spectral band and portions thereof within the 5.0 to 40.0μm region. Principal conclusions drawn from the solar radiation research are:

1. More sophisticated models yield more accurate results when compared with observations.
2. The models, on the whole, overestimate the actual surface albedo.

Principal results of the infrared radiation research are:

1. Semimaritime atmospheres (Houston) haze transmission ranges from 0.80 to 0.95 with a "bulk" absorption coefficient for the spectral interval, 870 to 1050 cm^{-1}, averaging 0.04 km^{-1} (-0.009 km^{-1}).
2. Cooling due to infrared radiation divergence or convergence in the haze layer averages only 0.009C hr^{-1} with an rms error of one third to one half of this value.
3. Infrared transfer models tend to over-compute atmospheric attenuation.
4. Transfer of radiation in the water vapor continuum developed by Bignell resulted in more attenuation than was actually observed.
5. Total infrared extinction coefficients for the Phoenix and surrounding desert areas were observed to be 0.30 km^{-1} and 0.052 km^{-1}, respectively.

INTRODUCTION

The purpose of the research described was and is during its final compilation to arrive at a more complete description of radiative transfer within the atmosphere with emphasis on the contribution of aerosols to this transfer both in the

PRECEDING PAGE BLANK NOT FILMED

infrared and solar spectral regions. It was further a defined objective to determine the accuracy and applicability of a variety of models of radiative transfer through air masses of differing characteristics including varying amounts of wet and dry aerosols.

TECHNIQUES

Radiative data were collected primarily by onboard aircraft radiometric sensors, balloon-borne radiometric sensors and ground based sensors observing both radiation and aerosol properties of the atmosphere. At Phoenix, helicopters were employed to profile radiation and aerosol content of the atmosphere from the surface to 2.7 km above sea level reference. In all instances EREP S-191, S-192 and S-190 data were integrated into the evaluation of the various models when possible.

The formulas employed in the research in the development of the various transfer models are given by Kuhn, Weickmann and Stearns (1975), Renne and Marlatt (1974), Reeser and Marlatt (1974) and by Pueschel and Kuhn (1975).

RESULTS

Figure 1 symbolizes the atmospheric infrared radiative transfer in a non-scattering atmosphere. Figure 2 presents an average set of values for the haze transmission and total extinction calculated from data observed in the Phoenix area. The expression for this calculation is given by,

$$\tau = N_2\uparrow - N_c\uparrow - \rho(N_2\downarrow - N_c)/(N_{22}\uparrow - N_c).$$

The formula is valid for the spectral interval 870 - 1050 cm^{-1} and should be referred to Figure 1. Figure 3 typifies cooling in haze.

It is evident from Figures 4 through 8, which show comparisons between observed and calculated radiation (infrared) profiles that better agreement was achieved between observation and models for some test sites than for others. Two major factors contribute to a failure of agreement--the thermal nonuniformity of the test sites, where the surface observation of the interface temperature may not be representative of the site, and changes of the surface or interface temperature with time due to changes in the intensity of solar radiation and cloud cover. One should recall that at least one third of the upwelling radiation at levels above the surface by some 3 to 10 kilometers is due to transfer in the atmospheric window region.

In Figure 9, typical results determined with the doubling solar transfer model for White Sands, N.M., aerosol data are shown. To determine the target albedo, only the solar zenith angle and the planet albedo are required. For many situations the albedo determined can be substituted for spectral reflectivity. Figure 10 shows the calculated target albedo vs. planet albedo curves. These are the expected extremes between the different models as far as sophistication is concerned. Figure 11 provides the aerosol size distribution for Phoenix, Arizona, and vicinity on September 6, 1973.

REFERENCES

1. Kuhn, P. M., H. K. Weickmann and L. P. Stearns: Radiative effects of the Harmattan haze. Accepted for publication, JGR, Oceans & Atmospheres, 1975.

2. Renne, D. S. and W. E. Marlatt: A comparison of several atmospheric infrared radiation transfer models, Sixth Conference on Aerospace and Aeronautical Meteorology, American Meteorological Society, Boston, Mass., Nov., 1974.

3. Reeser, W. K. and W. E. Marlatt: A test and comparison of radiation transfer models through scattering atmospheres, Sixth Conference on Aerospace and Aeronautical Meteorology, American Meteorological Society, Boston, Mass., Nov., 1974.

4. Pueschel, R. F. and P. M. Kuhn: Planetary radiation budget: Effects of urban aerosols. Accepted for publication, JGR, Oceans & Atmospheres, 1975.

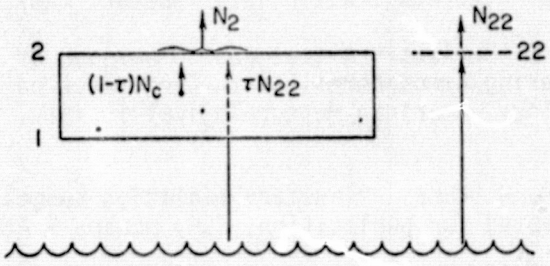


Figure 1. Symbolic atmoopheric haze layers with arrows depicting upwelling IR radiance.

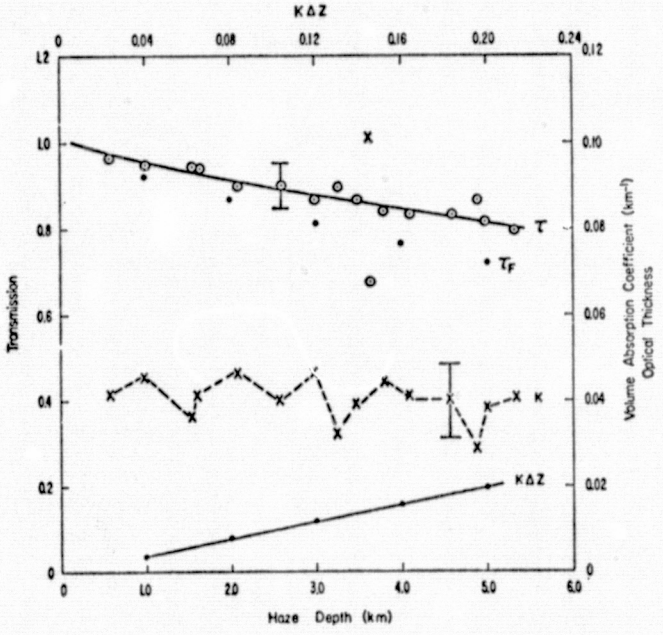


Figure 2. Haze transmission, volume absorption coefficient relative to haze depth and optical depth using White Sands, New Mexico, 11, 12 August 1973.

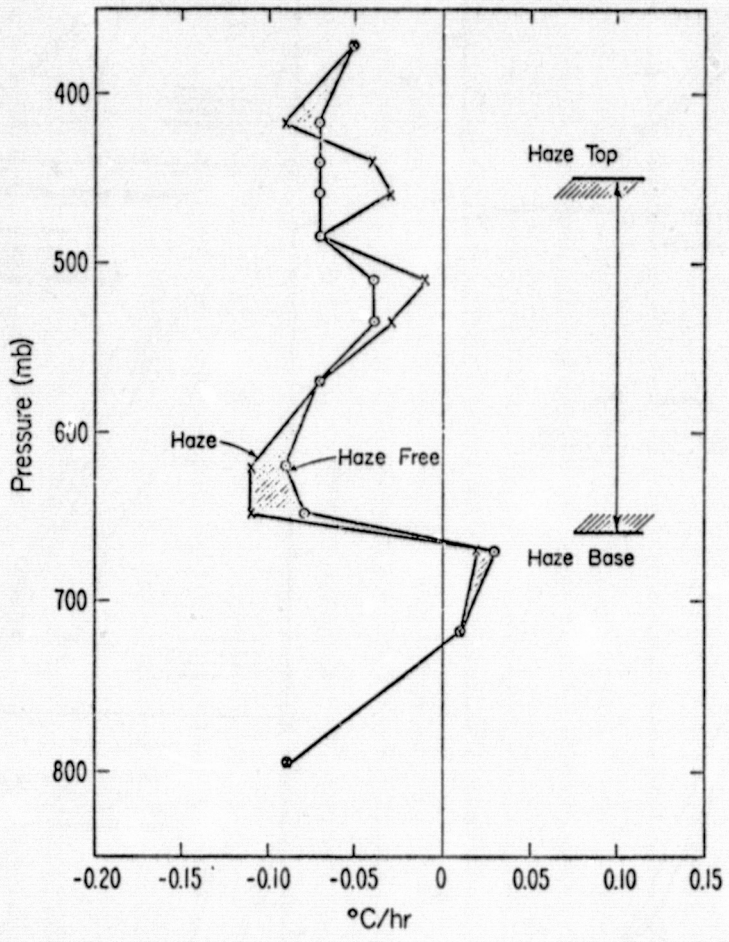
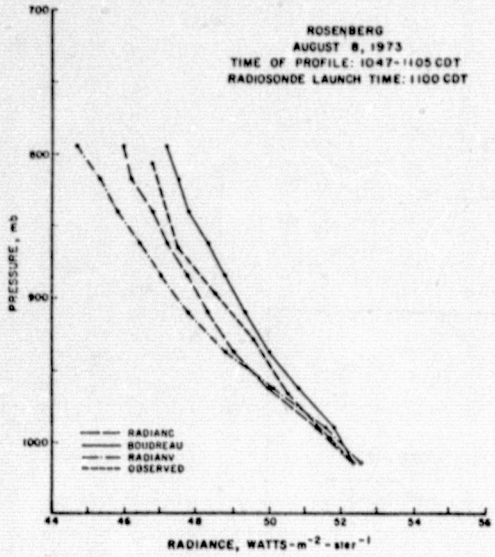
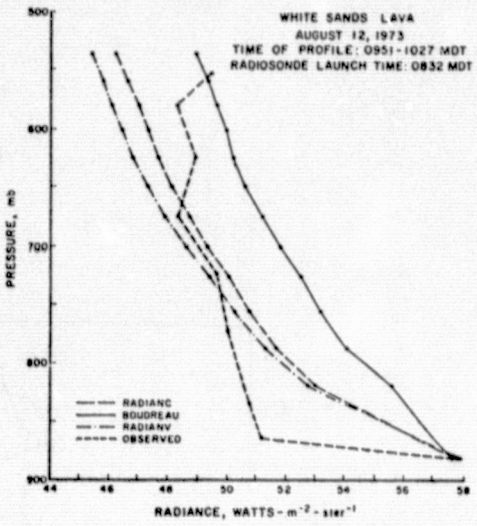
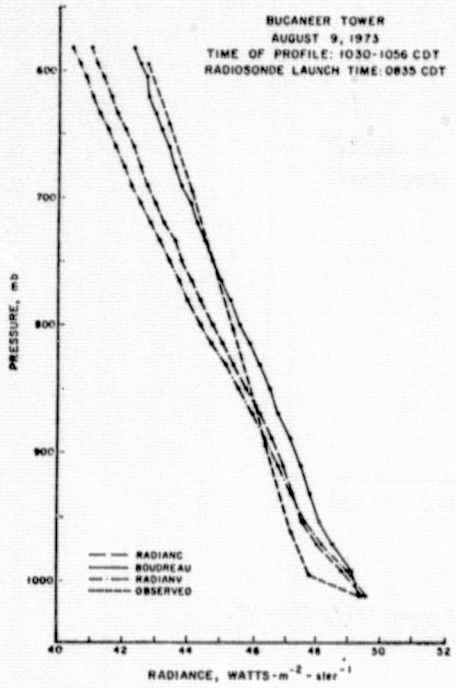
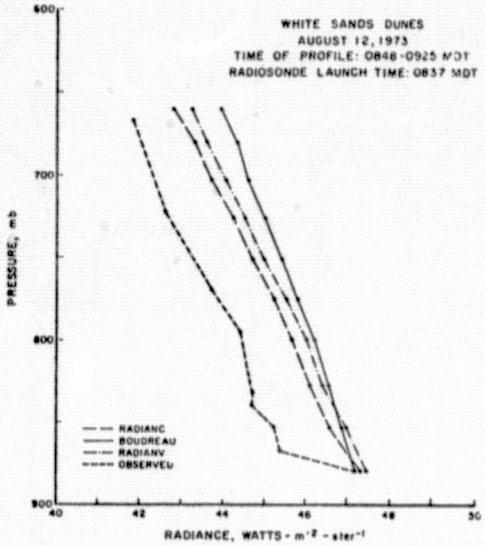


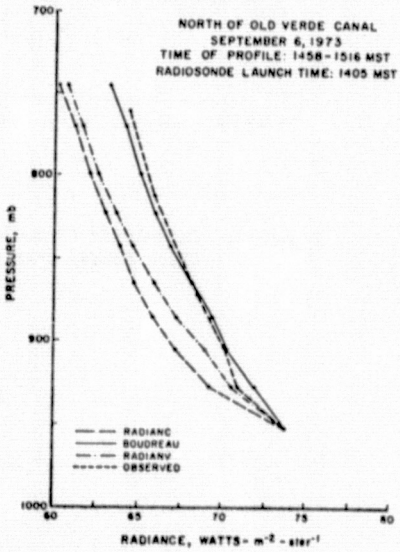
Figure 3. Calculated IR cooling in haze, 11 August 1973, 2130 UT, White Sands, over sand dunes, New Mexico.











Figures 4 through 8,
Upper left to lower right

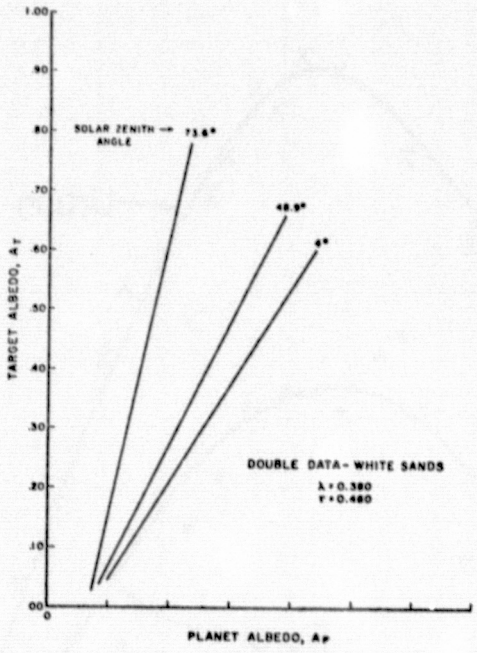


Figure 9

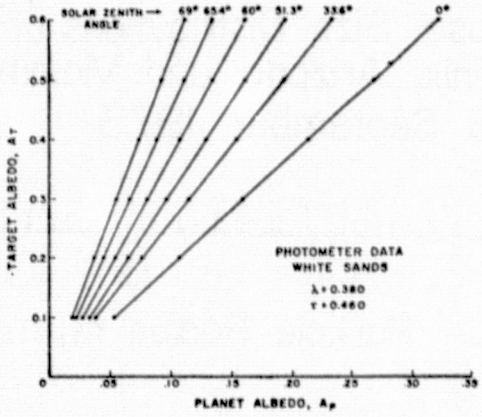


Figure 10

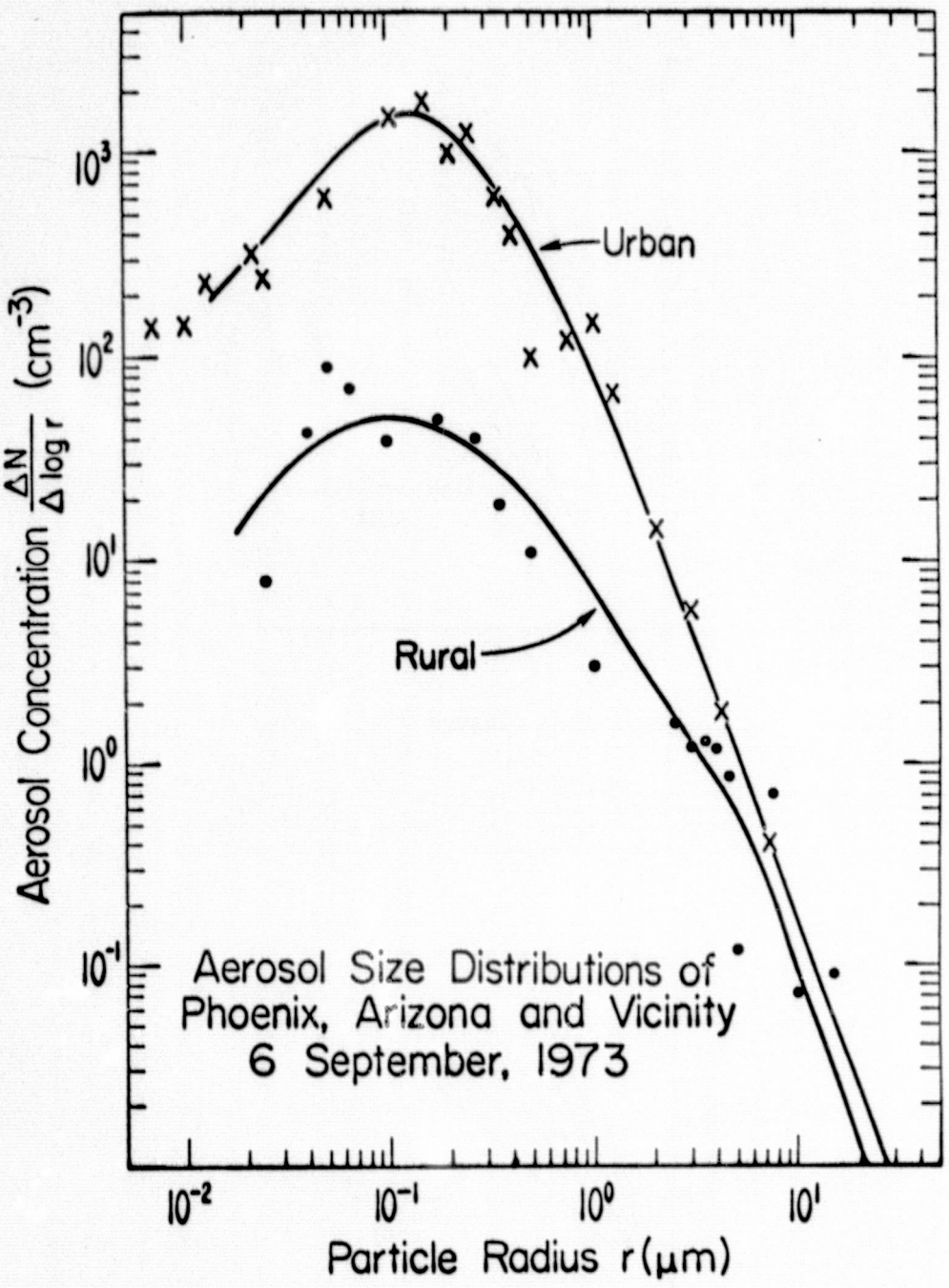

Aerosol Concentration $\frac{\Delta N}{\Delta \log r}$ (cm^{-3})
10^3
10^2
10^1
10^0
10^{-1}
Urban
Rural
Aerosol Size Distributions of
Phoenix, Arizona and Vicinity
6 September, 1973
10^{-2}
10^{-1}
10^0
10^1
Particle Radius r(μm)

Figure 11

MARKING LANDSAT IMAGES WITH SMALL MIRROR REFLECTORS

Wm. E. Evans, SRI, Menlo Park, California

N76-17529

ABSTRACT

Uniquely identifiable artificial "landmarks" have been generated in LANDSAT imagery by making use of specular solar reflection from small, easily transportable mirrors. The results are most impressive in well-registered color composite enlargements, where the mirror returns appear as bright white spots. The signatures are unique enough that returns can be readily located in the computer compatible tape records either manually or by machine search. As embodied in experiments to date, the system is entirely passive. Mirrors must be carefully positioned prior to each satellite pass, but the required angle calculations are simple enough to be made on a hand calculator and the required input data are relatively easily available.

Possible applications of the technique include providing site identification and geodetic control in remote regions of the earth, enhancement of small targets such as offshore oil derricks, providing atmospheric transmission data coincident with other LANDSAT experiments, and providing a nearly perfect optical "point source" for overall system checkout.

INTRODUCTION

Useful data can be added to LANDSAT imagery by employing a modern-day version of a fact familiar to many generations of signalmen and small boys--that the specular solar reflection from a small mirror can be detected at great distances.

The procedure, briefly, is to predict the time and location of the satellite for the single approximately 10-microsecond period during each eighteen day orbital cycle when the multispectral scanner will be viewing the mirror site. Directions toward the satellite and toward the sun are then computed and the mirror is positioned so that its normal bisects the angle between these two directions. The order of precision required is a few tens of seconds in time and a few tenths of a degree in angle.

INITIAL EXPERIMENTS IN CALIFORNIA

First results were obtained early in the life of LANDSAT-1 on a purely amateur basis using a 22-inch slightly convex mirror in the author's backyard and using satellite position and timing data projected from images obtained from the Sioux Falls data bank via the normal public access route. The uncertainties inherent in this approach required that the reflected beam be diverged appreciably (by a curved mirror) in order to achieve a reasonable probability of illuminating the satellite sensor at the proper time.

Initial calculation[1] indicated that with perfect pointing accuracy and average atmospheric conditions a 40.6-cm (16-inch) diameter plane mirror should provide a saturation signal at the satellite for all four spectral bands. Use of a plane mirror implies

operation with a reflected beam divergence of 0.5 degrees--the angular width of the sun as viewed from earth. To relax the required pointing precision, it was decided to diverge the beam slightly more and to partially compensate for the resulting lower energy density at the satellite by increasing the mirror area.

The early experiments used a 56-cm (22-inch) diameter round mirror, bowed slightly to produce a reflected beam divergence of 1 to 1.5 degrees. This divergence resulted in a spot size at a satellite altitude that covered only about half of the width of the 37-km orbital corridor within which NASA promised to navigate the satellite. The expected 50 percent probability of obtaining a "hit" appeared to be confirmed when identifiable returns were obtained on four occasions out of six attempts during 1972-73.

Figures 1 through 4 show the diverging mirror set-up and a sample signal return obtained from the Los Altos backyard site. As can be seen from the computer-compatible digital tape printout of Figure 4, the single-pixel return exhibits a contrast of better than 2:1 with the average surrounding area in all four spectral bands. Since full-scale response for the system is 127 for MSS bands 4, 5, and 6, and is 63 for band 7, the mirror-reflected energy added about 20 percent of full-scale response to all bands.

While the results were discernible in all photographic products, they were most convincing when displayed in a well-registered color composite image where the spot shows up as a small white dot.

THREE-MIRROR TEST AT RESTON, VIRGINIA

In the fall of 1974, an invitation to demonstrate the technique to cartographers at the USGS National Center in Reston, Virginia provided an opportunity to run the experiment with a degree of control that had not been essayed on an amateur basis.

The NASA satellite control center at Goddard provided accurate (to about ± .5 km and ± 5 seconds) predictions of the satellite location and transit times. Experienced surveyors were on hand with theodolites to check the mirror pointing directions.

While several unpredictable factors (e.g. satellite yaw) can still affect the required pointing angles by a few tenths of a degree, the probability of success with plane mirrors seemed high enough that they were tried at two locations. At the third location, the same diverging mirror that had been used in the California experiments was used for control. Figure 5 is an aerial photograph of the Reston site with the three-mirror locations marked.

RESULTS

Figure 6 shows the photographic results, and indexes the location of the site within the Washington, D. C. area LANDSAT-1 frame. Figure 7 is the pertinent section of the computer printout for the scene data.

Returns from the two plane mirrors were clearly discernible in all four bands in the photographic products. There was a suggestion of the signal from the diverging mirror in bands 4 and 5, but the background return from the relatively light-colored surrounding rooftop made identification difficult. The printout of the corresponding data from the computer-compatible tape reveals a saturation signal in all four bands for one of the plane mirrors (site 2), 75 to 85 percent of full-scale for the second plane mirror, and an increase of approximately 12 percent of full-scale increase above background for the diverging mirror.

Our results indicate that the effective geometric resolution of LANDSAT-1 is somewhat less in the horizontal or cross-track direction than it is in the vertical or in-track direction. While mirror responses in the in-track direction nearly always have been confined to just one line, responses in the cross-track direction have been recorded in two or more horizontally adjacent pixels for 14 of the 16 cases where the tape records have been examined. The bar graphs of Figure 8(a) and (b) illustrate this effect for the strong return from the plane mirror at site 2. Note that while the signal level from the average landscape is much less uniform than one would like for such an evaluation, it seems clear that mirror energy is being reported for at least four horizontally adjacent samples in bands 5 and 6 (Figure 8b) while no such spreading is evident in the north-south direction (Figure 8a).

The extent of horizontal smearing appears to be greater than can be completely accounted for by the quantizing effect of sampling the video signal at a spatial period less than the optical beamwidth. The generally unsymmetrical nature of the spreading indicates that it results from some system bandwidth effect rather than from optical or atmospheric conditions. Whatever the source, the horizontal spreading effect appears to be real and perhaps should be investigated further since it can affect small-area classifications made by computer image processing and also degrade the horizontal definition possible in the photographic images.

For cartographic applications, it would be desirable to know that equal response in adjacent pixels would indicate that a mirror or other small feature was located on the interpixel boundary. This would facilitate measuring locations with appreciably less than the ±40 meter uncertainty that one might intuitively associate with the LANDSAT 80-meter pixel size. A multiple mirror array, with spacings intentionally chosen to maximize the number of pixel boundary situations, should provide the near ultimate procedure for precisely locating ground points in LANDSAT imagery.

OTHER MIRROR SIZES

The results indicate that where extreme portability is important, plane mirrors with areas on the order of 0.1 square meter (one square foot) should be feasible as beacons. Such units could be mounted and pointed reliably using fixtures adapted from surveying instruments.

Since larger-than-saturation signals are not useful and might even be harmful to the satellite sensors, the only reason to consider mirrors larger than those reported here for LANDSAT would be to permit diverging the beam in order to relax the pointing requirements.

Tests are currently under way with a 0.6- by 1.8-meter (2- by 6-foot) mirror bowed in the long dimension to give a 2.8 degree fan-shaped beam intended to cover the full gamut of probable cross-track orbital deviations. However, the mounting, rigidity, and wind-loading problems multiply rapidly with larger structures, and a closely spaced array of smaller mirrors might be a more desirable alternative for controlling the pattern of the reflected beam.

CONCLUSIONS

It has been demonstrated that through the use of solar reflections from small, transportable mirror beacons uniquely identifiable artificial landmarks can be generated in LANDSAT imagery with very modest cost and effort.

The relative simplicity of the method makes it a candidate for consideration where the need exists for identifying specific ground points. It also provides an effective point source for post-launch performance checks of satellite sensor systems.

ACKNOWLEDGMENTS

The California experiments were initiated and performed as an unfunded hobby project, but benefited from the author's work at SRI for the NASA LANDSAT-1 program. The interest and encouragement of Dr. W. A. Fischer and Col. A. P. Colvocoresses of the Cartographic Division of the U.S. Geological Survey, and the support of that agency for the Reston demonstration and subsequent work now in progress is gratefully appreciated.

REFERENCE

1. Evans, Wm. E., "Marking ERTS Images with a Small Mirror Reflector," Photogrammetric Engineering, Vol. XL, No. 6, pp. 665-671, June 1974.



Figure 1. A 22-inch mirror in position for satellite pass.
Stable platform is oil drum partially filled with water.



Figure 2. Close-up view of mounting frame used in Reston, Virginia experiments.
Elevation angle is being checked with bubble level on adjustable protractor.
Azimuth setting circle is clamped to top of oil drum.
Leveling screws are on front of channel.
Identical frames were used to hold the rectangular plane mirrors of 1/4-inch plate glass.

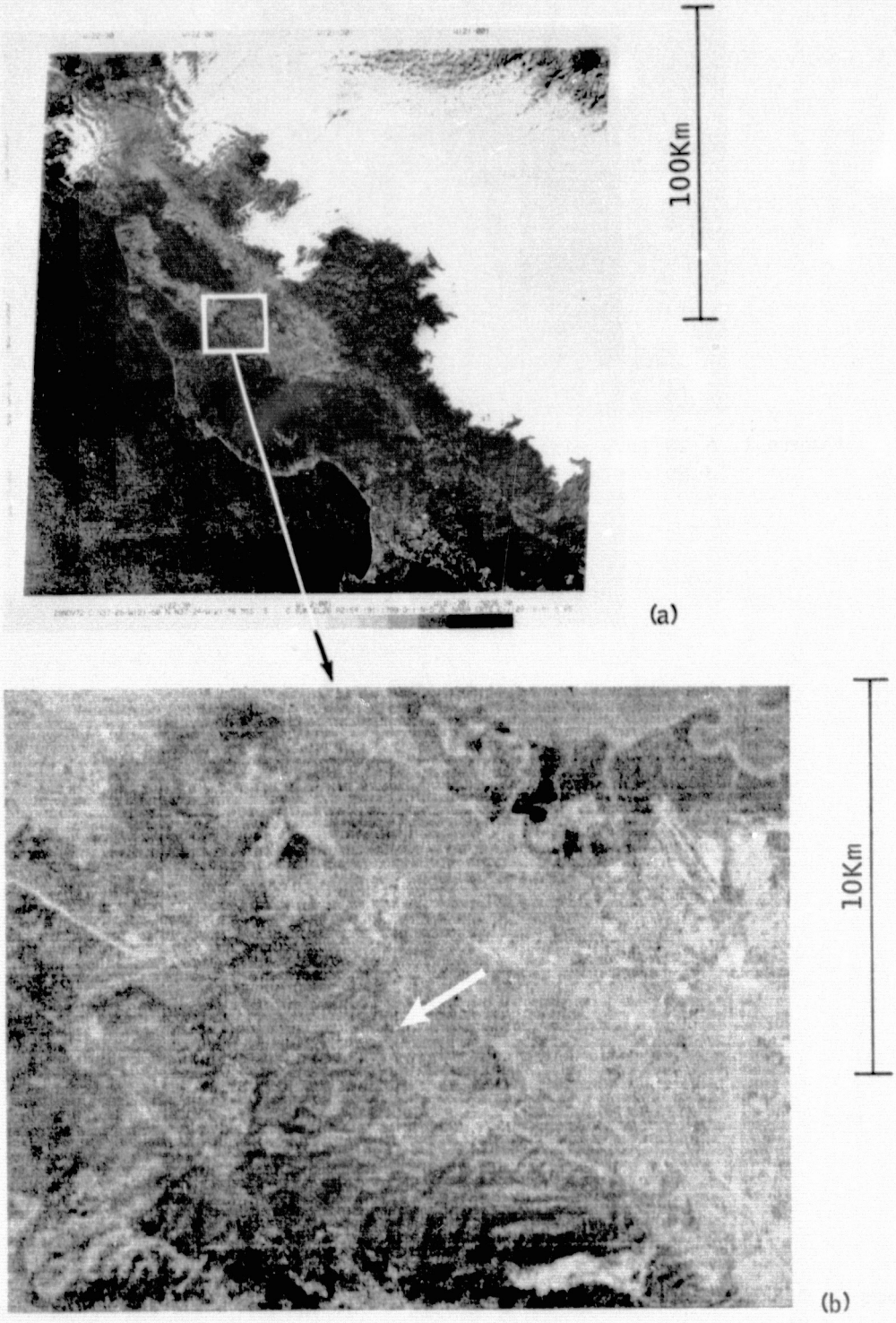


Figure 3. LANDSAT-1 image No. 1129-18181-5 of San Francisco Bay region for 29 November 1972;(a) Full frame;(b)Enlarged section. Arrow points to specular reflection from mirror of Figure 1.

DIGITAL PRINTOUT OF EHTS IMAGE 1129-18181 TAPE 2 OF 4 WITH INITIAL COORDINATES (1257, 349).

X / B / Y	349				354				359				364				369				374				379			
1257 B4	20	2	21	21	21	21	18	20	21	20	18	21	21	21	20	20	21	21	20	20	21	21	24	20	20	20	20	20	20	20	21	20	20
B5	13	11	13	15	15	15	13	13	13	10	11	14	11	14	14	14	14	14	13	11	14	16	15	15	14	14	13	14	13	13	14	14	11
B6	29	25	25	30	36	29	21	27	30	19	24	29	29	27	29	29	24	25	25	27	27	19	24	25	21	22	22	24	24	24	24	27	34
B7	16	14	14	16	20	17	11	15	17	9	13	16	16	15	16	14	12	13	14	15	12	10	12	13	11	11	12	13	13	12	12	14	20
1258 B4	19	22	22	22	20	19	19	20	19	19	20	21	22	19	19	20	20	19	20	22	20	23	22	20	20	22	22	19	20	20	20	20	20
B5	12	14	14	14	13	12	13	13	13	12	13	14	13	13	13	13	13	14	14	13	15	16	16	14	13	14	14	14	13	13	13	13	13
B6	30	44	46	42	32	22	32	40	33	25	37	37	34	23	18	23	25	23	26	34	29	26	29	30	29	26	26	23	25	23	29	34	32
B7	15	22	23	22	16	8	16	21	11	11	19	18	16	11	7	10	11	11	13	16	13	12	13	14	13	11	12	10	10	11	14	16	16
1259 B4	20	21	20	20	19	20	21	20	18	20	20	21	20	20	20	21	21	20	20	20	21	21	20	20	21	23	20	20	21	21	20	20	20
B5	13	14	12	12	12	13	13	13	12	12	13	13	14	13	13	15	15	14	13	13	14	15	14	14	14	15	14	14	14	14	14	14	14
B6	33	35	28	28	21	26	30	25	25	30	33	35	31	19	23	25	19	21	25	23	21	23	21	25	19	21	23	21	21	21	25	23	25
B7	20	21	16	16	19	16	17	14	14	18	19	20	15	11	14	12	10	11	13	12	11	13	12	13	11	11	12	12	12	13	12	13	14
1260 B4	20	2	22	18	17	18	18	20	20	20	20	22	20	20	18	18	20	20	20	22	22	20	22	22	22	22	22	20	22	20	20	20	20
B5	14	13	13	12	12	12	12	12	13	13	14	14	14	14	10	13	14	14	13	14	15	14	14	13	14	15	14	15	14	14	13	13	14
B6	46	35	26	20	18	26	24	23	26	33	33	32	27	19	15	18	23	23	24	23	26	29	26	24	23	23	21	21	23	25	26	23	26
B7	24	14	14	10	10	14	13	11	15	19	18	19	14	8	7	9	12	12	12	12	14	16	15	14	12	12	11	11	12	14	14	12	12
1261 B4	20	2	19	20	20	19	19	20	20	20	20	22	20	19	19	18	18	18	20	24	24	20	22	22	22	21	22	24	24	22	22	20	22
B5	12	12	11	12	12	12	11	12	14	11	12	14	14	12	12	10	11	12	15	18	16	15	16	15	15	15	16	20	20	18	15	16	15
B6	44	35	32	36	30	23	28	36	32	32	37	36	28	23	20	18	17	20	23	23	23	20	22	23	25	22	23	22	23	23	25	23	25
B7	26	14	18	21	17	12	16	20	18	17	21	22	16	12	9	8	8	11	12	11	11	11	11	12	13	11	11	11	11	11	13	14	14
1262 B4	20	2	21	21	20	21	21	20	19	20	20	20	20	20	20	19	19	20	20	38	36	20	20	21	20	20	20	24	24	25	24	21	24
B5	12	13	14	14	14	14	14	13	13	13	13	13	13	12	13	12	12	13	14	41	28	14	14	14	14	14	14	18	19	19	17	17	18
B6	32	34	42	42	36	34	36	34	26	29	26	26	31	22	18	15	17	22	25	50	38	26	29	22	18	20	22	25	29	29	23	25	26
B7	19	21	24	24	26	20	21	19	15	15	15	15	17	10	10	7	9	11	14	26	19	15	16	11	10	10	11	11	16	15	12	11	12
1263 B4	21	21	21	21	24	24	24	24	24	24	21	21	21	20	18	20	21	20	21	24	21	18	18	18	20	21	21	21	20	19	21	21	21
B5	14	14	15	14	14	17	16	15	14	14	14	14	14	13	13	14	15	14	15	15	13	11	10	11	14	16	16	13	13	13	15	15	15
B6	38	4	40	34	38	36	41	43	40	42	40	36	36	24	21	22	25	25	25	30	24	21	22	18	21	21	22	22	21	24	22	22	24
B7	23	21	22	21	20	21	23	24	24	24	21	20	19	13	10	11	13	13	13	15	15	11	11	9	11	11	11	12	12	13	11	12	12
1264 B4	23	20	26	26	26	26	26	26	26	23	22	22	20	20	20	20	19	20	22	22	20	19	20	20	20	20	20	20	20	22	22	22	22
B5	19	2	20	20	20	21	20	20	19	16	16	16	15	14	13	13	12	14	15	14	13	14	14	14	15	14	14	13	14	15	15	14	15
B6	26	26	26	26	30	30	30	32	37	44	44	42	35	20	25	23	25	30	32	28	21	25	28	32	32	25	22	22	23	25	25	22	22
B7	12	11	12	12	12	13	13	16	19	23	23	22	18	11	11	10	10	13	16	13	9	11	13	16	16	11	10	9	11	11	10	9	10
1265 B4	21	2	20	20	20	21	21	23	23	25	23	23	23	21	20	20	20	23	21	21	23	23	20	20	20	18	20	20	20	21	21	21	20
B5	15	14	14	14	14	14	15	15	16	20	18	15	15	15	14	12	13	14	15	15	16	15	13	12	12	12	13	14	15	15	16	15	15
B6	18	17	16	14	16	19	21	21	25	26	28	31	26	23	21	25	30	39	37	23	21	23	21	18	19	18	16	19	23	19	16	14	18
B7	8	8	7	6	8	9	10	11	11	12	16	16	14	11	12	13	18	22	19	11	11	12	12	11	10	10	9	11	13	11	10	9	9

Figure 4. Computer printout of section of digital tape record for 29 November 1972. The mirror return is marked on scan line 1262.

REPRODUCIBILITY OF THE ORIGINAL PAGE IS POOR

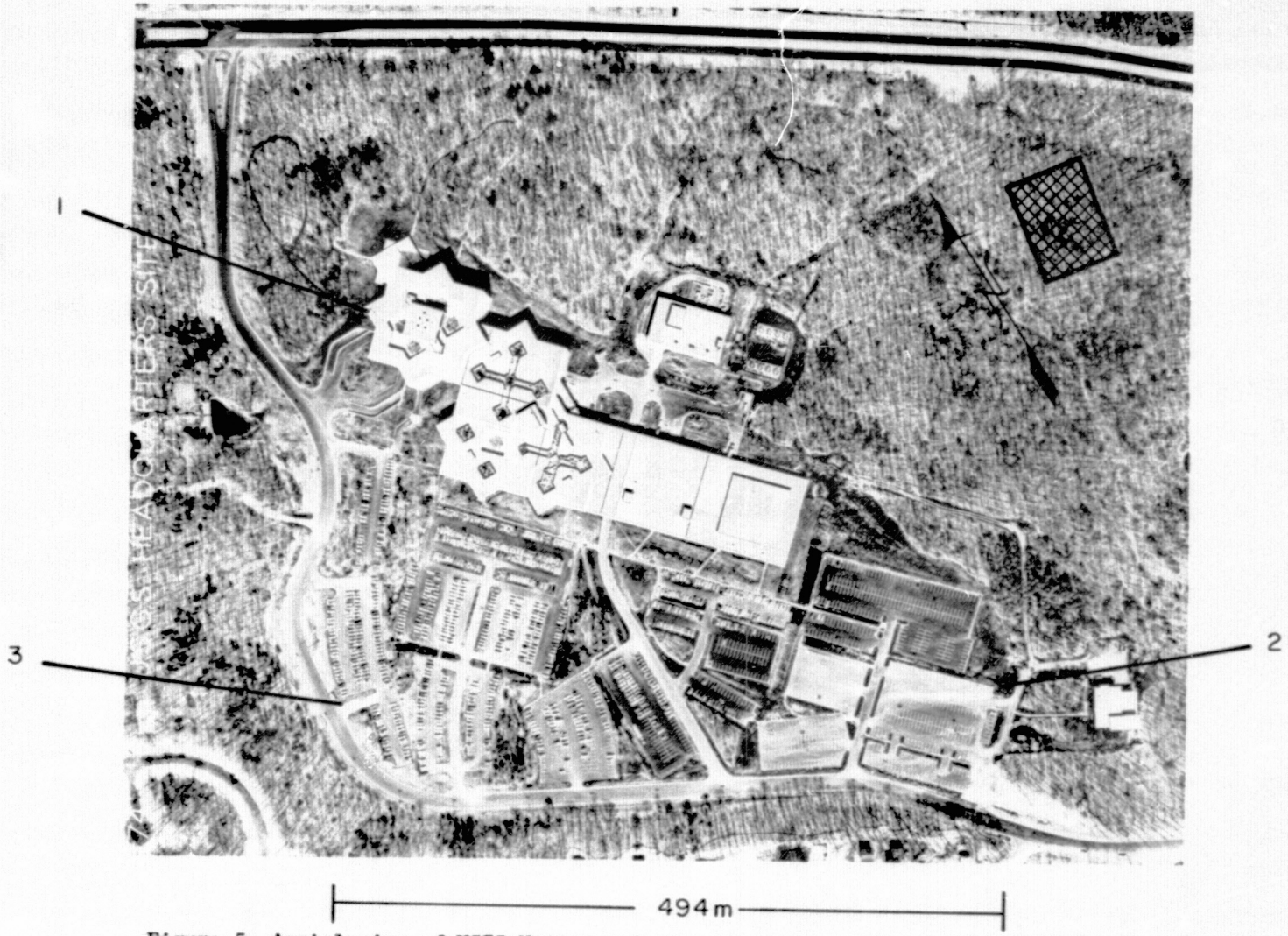
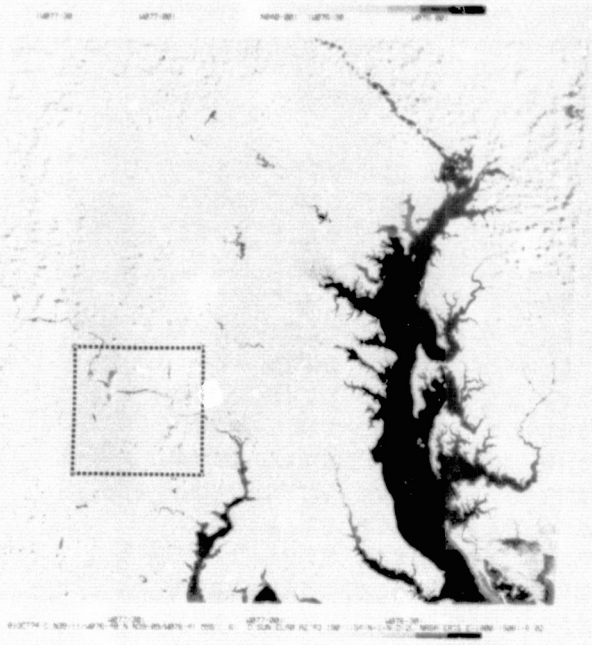
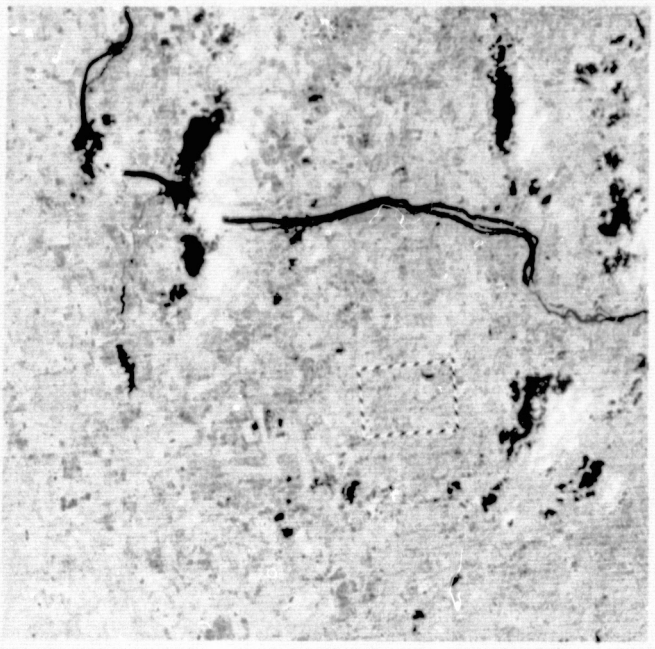


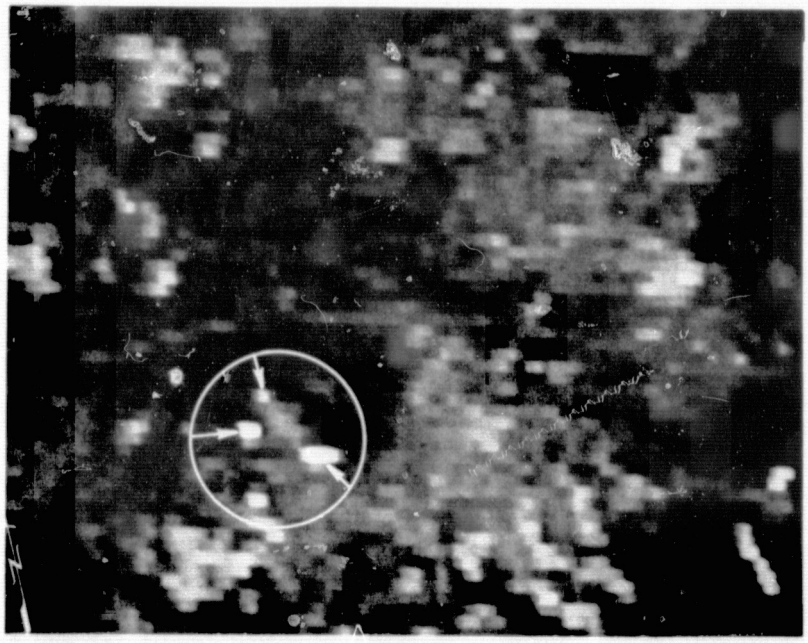
Figure 5. Aerial view of USGS National Center facility at Reston, Virginia. The round diverging mirror was located on the building roof at (1). Rectangular plane mirrors were located in the parking lot at (2) and (3). The rectangular patch indicates the size and orientation of a single LANDSAT pixel.



(a) Full frame, MSS-6
Chesapeake Bay at right.
Potomac river at lower left.
Reston, Virginia centered in insert.



(b) A 5X enlargement of region marked in (a).



(c) A 9X enlargement of region marked in (b)
Arrow point to responses from the three mirrors
Derived from CCT display of MSS-5 and MSS-6
Dulles Airport access road runs horizontally through center of picture

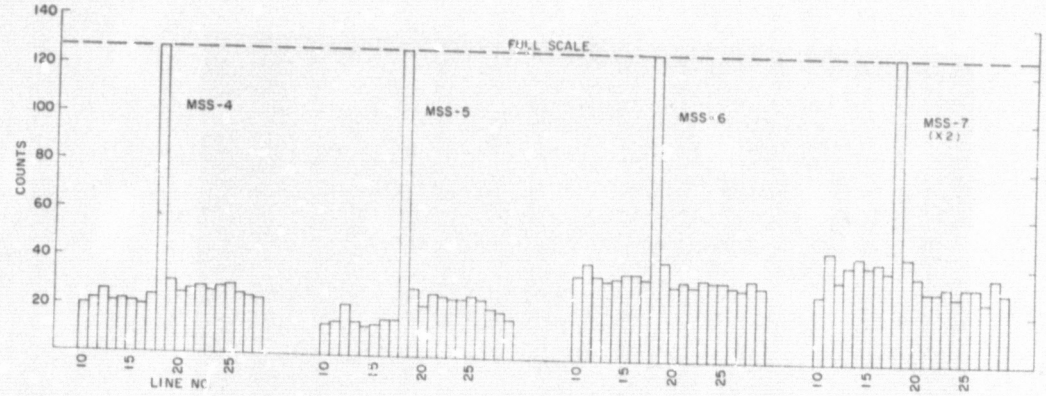
Figure 6. Mirror spots on Washington-Baltimore frame for 1 October, 1974.

DIGITAL PRINTOUT OF ERTS IMAGE 1800-15081 TAPE 2 OF 4 WITH INITIAL COORDINATES (1610, 51).

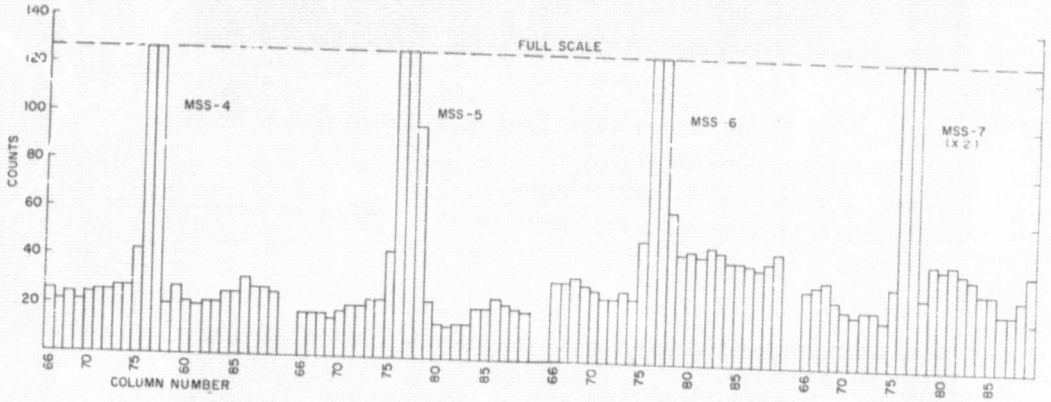
X / B / Y		51				56				61				66				71				76				81				86			
1610	B4	26	26	24	24	23	20	19	20	20	20	20	20	20	20	20	20	20	20	24	23	20	19	20	20	20	20	20	20	20	20	20	20	20	20	23	26	31	30
	B5	22	21	19	17	15	13	12	13	16	15	15	13	13	13	13	13	12	16	17	15	13	13	13	13	13	13	13	13	13	13	12	12	12	15	22	28	28	
	B6	34	33	31	31	31	36	36	38	34	31	30	30	34	36	36	36	34	31	31	34	36	38	34	36	36	34	36	36	38	38	36	36	36	38	38	38	38	31	31	40
	B7	17	16	16	17	18	19	20	23	19	18	17	17	20	20	21	20	20	20	17	20	21	21	20	20	21	19	19	21	22	21	20	21	22	23	23	22	22	16	13	20
1611	B4	23	22	22	19	22	22	22	19	22	22	22	22	22	22	22	19	19	19	22	22	23	22	23	23	23	23	23	22	22	22	22	22	22	22	22	22	22	24	29	31	29
	B5	16	14	12	12	12	12	14	14	14	15	15	14	14	12	12	14	14	15	16	14	16	16	16	14	14	14	14	14	12	12	14	12	12	12	12	12	17	25	28	24
	B6	36	31	32	32	32	32	38	40	32	34	31	34	36	36	34	34	36	36	29	31	34	31	32	38	40	40	38	34	38	36	36	38	38	38	40	38	31	32	38	
	B7	19	18	19	19	20	19	22	23	19	18	18	20	21	21	20	20	21	19	14	16	17	17	19	22	23	23	23	21	22	21	22	22	22	22	22	23	20	12	15	21
1612	B4	21	19	19	22	21	21	19	21	21	19	19	21	21	19	19	21	21	21	21	22	21	19	19	22	25	26	25	22	19	21	21	21	21	19	19	21	28	33	32	26
	B5	14	14	12	12	14	14	12	14	15	14	14	14	14	12	12	14	12	14	14	14	14	12	14	15	19	21	19	16	12	12	14	14	14	12	12	12	21	29	26	19
	B6	37	35	33	33	33	32	37	35	35	35	35	35	37	37	37	39	39	35	35	39	35	37	35	32	33	35	41	44	37	39	39	41	41	37	37	39	37	35	39	46
	B7	19	18	18	18	17	18	20	19	18	18	19	20	19	20	20	22	21	18	18	21	20	19	17	16	16	17	21	22	20	21	22	23	22	22	22	22	17	15	18	24
1613	B4	22	21	19	21	21	21	22	22	21	21	21	21	21	22	22	22	22	24	28	46	28	19	21	21	21	21	22	24	24	22	21	21	21	21	21	22	27	28	28	27
	B5	16	14	14	15	15	15	16	14	15	14	15	14	12	14	15	15	16	16	25	44	22	14	14	12	12	14	16	19	17	15	14	14	14	14	14	15	22	29	25	17
	B6	35	31	29	31	31	31	31	35	33	29	33	35	35	35	39	39	37	33	39	47	35	37	37	33	35	33	33	33	33	39	37	35	37	39	39	42	39	42	35	41
	B7	22	18	18	18	18	19	20	21	20	20	22	22	21	22	23	24	24	19	22	21	20	23	21	21	23	20	19	18	20	23	24	23	23	24	24	23	21	21	19	24
1614	B4	22	22	22	20	22	22	24	22	22	20	20	22	22	22	20	20	22	26	30	32	36	32	30	26	22	22	22	22	22	22	25	24	24	24	24	24	24	26	28	28
	B5	16	18	16	14	14	16	20	16	14	14	13	14	14	14	14	13	14	20	24	27	31	26	24	21	13	12	13	13	13	15	18	18	16	14	14	18	18	22	24	21
	B6	31	31	30	30	31	31	31	34	30	31	38	36	34	31	34	34	31	34	30	28	31	38	31	34	34	34	36	38	34	31	30	31	36	38	38	38	36	38	36	45
	B7	19	18	17	16	17	19	17	19	18	19	22	21	20	19	20	20	19	17	15	13	16	20	17	19	22	22	22	22	21	18	16	18	21	23	23	22	23	19	20	27
1615	B4	21	22	22	25	27	28	25	22	22	21	21	22	21	20	21	20	21	22	25	28	34	36	34	27	21	21	21	20	20	20	20	20	20	21	21	25	27	28	27	27
	B5	16	17	17	17	22	24	21	16	20	15	16	17	16	13	13	13	13	15	20	22	29	34	29	21	13	13	13	12	13	12	12	13	13	17	17	21	21	22	22	22
	B6	34	34	36	34	36	37	32	34	34	29	34	33	34	34	34	36	37	36	30	30	32	34	34	29	29	36	36	32	36	37	34	34	33	33	33	33	33	32	32	
	B7	19	18	18	18	18	19	17	18	16	16	18	17	18	21	20	20	22	19	15	15	13	13	14	14	15	20	22	20	22	23	20	19	17	16	16	16	16	15	15	15
1616	B4	23	24	24	31	37	31	23	23	23	23	30	27	24	24	26	24	23	107	81	24	33	30	33	33	27	20	20	20	20	20	20	20	20	23	23	24	26	27	27	27
	B5	17	19	22	30	39	30	17	15	15	17	28	25	21	21	21	17	19	111	70	22	28	28	30	30	21	15	13	13	13	12	12	13	13	15	15	21	21	24	22	21
	B6	31	36	34	38	44	42	34	38	30	36	36	28	30	34	36	36	40	96	56	23	28	34	34	34	36	36	36	31	34	36	36	34	36	36	36	36	31	30	38	47
	B7	17	19	18	17	18	18	18	22	16	19	16	13	16	18	19	19	21	33	15	11	12	16	15	15	19	21	20	22	21	22	20	19	21	21	21	18	15	13	19	27
1617	B4	23	24	25	28	29	25	22	22	22	22	23	24	25	25	23	23	24	29	31	28	29	28	29	29	28	24	23	23	19	22	22	22	22	22	22	28	28	25	25	25
	B5	17	17	21	24	28	19	14	14	14	15	15	19	21	17	15	15	17	29	29	24	24	24	25	28	21	15	12	12	14	14	14	12	12	16	16	23	23	23	23	19
	B6	32	38	40	44	44	32	34	34	32	38	32	32	31	36	32	34	36	44	32	27	31	27	29	32	29	34	38	38	36	38	36	38	40	36	36	32	29	31	36	44
	B7	18	20	22	22	21	16	21	19	18	20	18	16	15	19	18	17	20	23	14	12	12	11	12	15	14	19	23	24	20	22	22	21	22	20	20	14	13	14	19	26
1618	B4	22	22	25	22	22	19	19	21	21	22	25	26	25	22	25	26	22	25	22	25	26	26	28	28	43	127	127	21	28	22	21	22	22	26	26	32	28	28	26	26
	B5	18	16	19	19	16	14	12	12	14	15	16	21	18	16	18	18	18	18	16	19	21	21	24	24	44	127	127	96	24	15	14	15	15	22	22	26	24	22	21	19
	B6	32	33	37	37	30	32	37	35	37	37	37	33	30	37	35	33	33	35	32	30	27	27	30	27	51	127	127	63	46	37	35	39	37	33	33	32	30	33	37	47
	B7	16	17	19	19	16	18	20	19	20	18	19	16	15	17	17	16	17	18	14	12	11	12	12	10	17	63	63	15	22	21	22	20	19	16	16	12	12	15	20	25
1619	B4	22	22	22	22	21	21	22	21	21	22	27	27	28	28	27	24	24	24	28	30	28	28	28	27	28	30	28	22	21	21	24	24	27	28	28	28	28	28	28	27
	B5	19	19	17	17	15	14	15	12	14	16	21	22	25	24	22	19	19	22	25	28	25	24	24	24	25	28	24	16	14	15	19	17	21	25	25	25	22	25	24	21
	B6	31	31	33	31	29	35	35	37	35	37	31	29	37	41	39	35	35	35	33	35	39	37	35	31	29	41	41	39	41	41	35	29	33	31	31	28	29	29	35	44
	B7	19	18	19	18	18	21	21	24	23	22	16	16	19	22	21	20	20	17	17	19	19	20	18	15	14	22	21	25	24	25	19	15	18	14	14	12	13	16	18	26
1620	B4	24	25	24	24	22	22	20	22	22	24	26	28	30	25	24	28	26	25	25	24	28	30	30	28	26	25	25	25	25	25	26	25	26	25	25	26	26	25	25	32
	B5	16	18	20	18	14	14	13	13	13	16	22	26	27	22	16	26	22	16	18	16	24	27	24	24	20	21	18	18	20	20	22	20	21	21	21	21	24	21	22	33
	B6	34	36	31	30	30	34	36	38	38	31	31	31	31	30	36	34	28	36	31	31	36	34	31	31	30	31	38	40	36	30	26	28	31	30	30	30	28	30	36	42
	B7	19	19	18	17	19	21	22	23	22	19	15	14	16	15	18	17	15	20	18	17	17	15	16	15	16	18	22	24	20	16	14	15	16	16	16	15	15	16	18	20
1621	B4	25	25	22	21	21	20	20	20	21	21	22	25	25	25	25	25	28	27	22	28	28	25	22	25	25	27	27	28	27	27	27	25	27	25	29	29	29	27	27	27	27
	B5	20	20	16	16	13	12	13	13	13	15	20	21	21	20	17	26	21	17	26	22	16	17	22	21	24	26	28	22	24	21	21	22	20	28	28	29	22	21	22	26
	B6	37	34	32	32	32	34	36	37	36	36	33	30	32	29	34	34	27	33	37	37	34	36	33	29	30	33	33	33	30	32	30	30	33	32	32	32	32	32	30	34
	B7	19	19	18	17	17	20	21	22	21	20	17	14	14	15	18	16	13	17	19	19	19	18	16	14	14	15	15	14	15	14	14	13	16	15	15	14	14	16	14	16

Figure 7. Computer printout of section of digital tape record for three-mirror experiment at Reston, Virginia. Marked pixels correspond to mirror sites identified in Figure 5. Portions of this data are plotted in Figure 8.

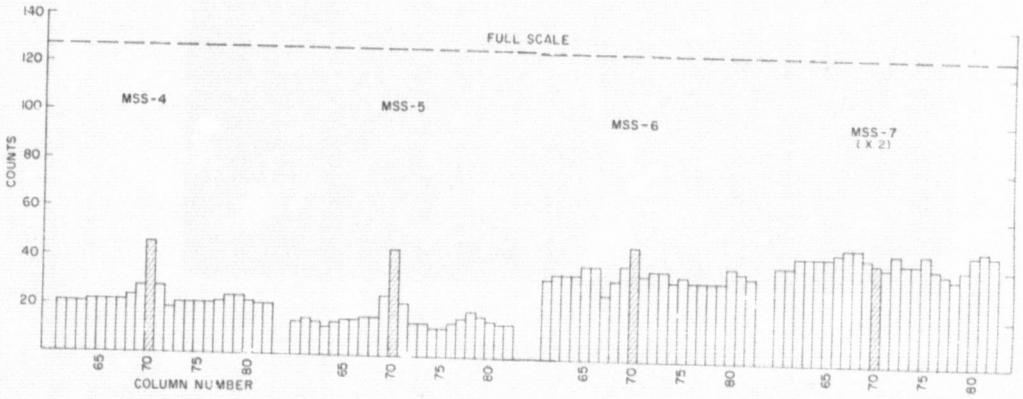
REPRODUCIBILITY OF THE ORIGINAL PAGE IS POOR



(a) In-track (column) response from mirror No. 2 (22- x 24-inch plane). Note that major effect is clearly confined within a single 79-meter scan swath.

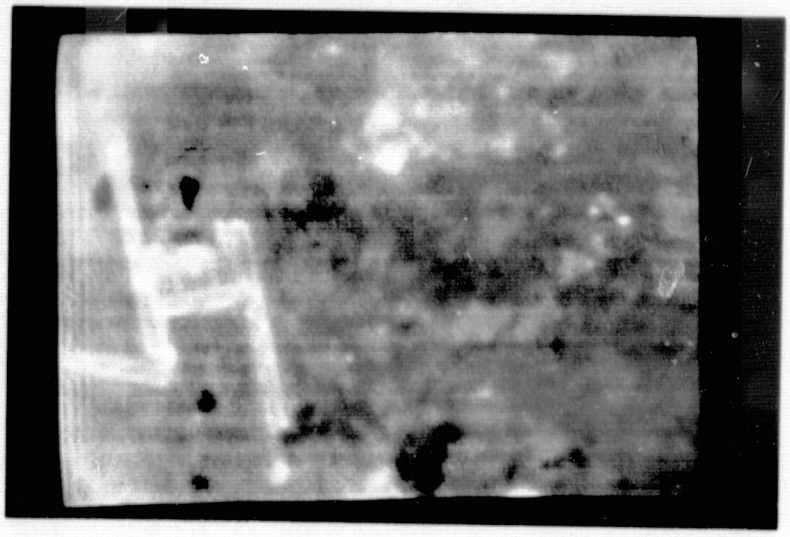


(b) Cross-track (row) response from mirror No. 2 (22- x 24-inch plane). Saturation signal reported for two adjacent samples (59-meter spacing). Noticeable effect over at least four samples.

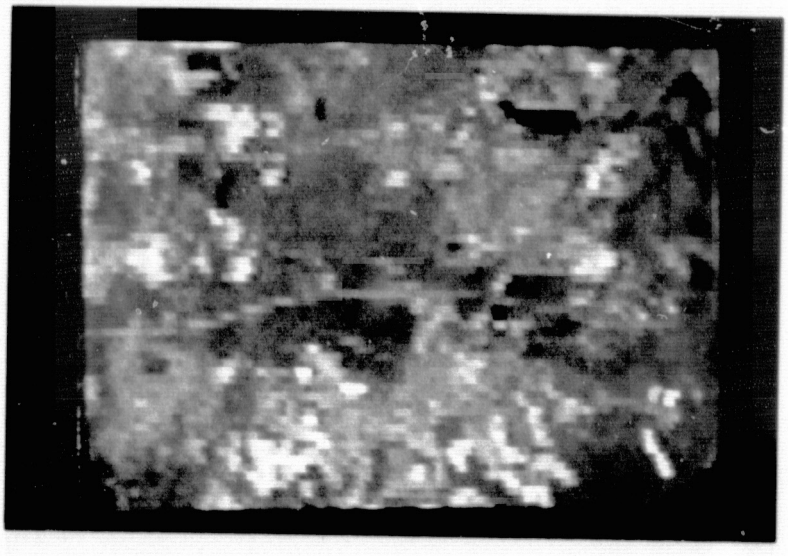


(c) Cross-track (row) response from mirror No. 1 (22-inch round, diverging). Weak signal but still useful as part of an array.

Figure 8. Graph plots of selected data from Figure 7 (Reston, Virginia, 1 November 1974).



(a) Produced by TV displays from photographic transparencies.
Picture height covers 9.6 km.
Dulles airport is at left center.
Reston mirror returns are three white dots at right center.



(b) Produced by TV display from digital tape.
Picture height covers 5.5 km.
Triangle of white dots at left center (just below Dulles access road) is from mirror array at USGS National Center at Reston, Virginia.

Figure 9. Color composite of MSS bands 5 and 6 for portions of the image shown in Figure 6.

REMOTE SENSING - A VALUABLE TOOL IN THE FOREST SERVICE DECISIONMAKING PROCESS

By Fleet L. Stanton, Geometronics Engineer
Forest Service, Ogden, Utah

N76-17530

ABSTRACT

Forest Service studies for integrating remotely sensed data into existing information systems highlight a need to: 1) re-examine present methods of collecting and organizing data, 2) develop an integrated information system for rapidly processing and interpreting data, 3) apply existing technological tools in new ways, and 4) provide accurate and timely information for making right management decisions. To meet these needs, the Forest Service is attempting to find out what tools and processes are in existence today and how they can be applied.

Concerned people are striving to develop faster, cheaper, and more accurate means of collecting data. Remote sensing applications are proving to be the most valuable and will allow people with critical skills to be relieved from time-consuming manual tasks.

Also, tools and processes are available to convert collected data from source to digital format for storage on magnetic tapes. In addition, computer hardware and software programs are being developed to retrieve data from magnetic tapes, synthesize data for interpretation, and generate and array alternatives to be evaluated for management decisions.

The Forest Service, in cooperation with U.S. Department of Agriculture, Forest Service, Surface Environmental and Mining Program (SEAM), is presently developing an integrated information system using remote sensors, micro-densitometers, computer hardware and software, and interactive accessories. Their efforts are substantially reducing the time it takes for collecting and processing data.

INTRODUCTION

For integrating remotely sensed data into existing information systems the Forest Service recognizes a need to: 1) determine how this data is presently being collected, organized, generated, and displayed, 2) identify minimum generic data requirements, and 3) determine how we can use today's and tomorrow's technological tools to provide accurate and timely information for resource managers in the decisionmaking process.

To better understand the tools we are using and are planning to use, it is important first to provide a framework of reference. A simplified version of the decisionmaking process will be used as a framework of reference as shown in Figure 1.

The process of collecting and organizing data is not new. However, the tools we use to collect and organize data are rapidly changing. In the past simple

visual observation, manual recording, and organizing were considered adequate. Manual artwork and subjective manipulation of statistical data were the basis of generating and arraying alternatives to aid decisionmaking.

In the world today, ample evidence demonstrates the inadequacies of past methods of collecting and organizing data. Roads have been built across unstable slides; timber has been harvested over wide areas destroying watersheds which trigger erosion; overgrazing by cattle, sheep, and other animals destroy vegetation and add to erosion of productive soils. Vast areas of our land have been made barren as a result of strip mining.

If we are to survive on this earth, we must learn to effectively manage the use of earth's resources. Today, a growing awareness of problems we, ourselves, have caused has precipitated a sense of urgency to adopt effective tools to aid resource managers in making effective management decisions.

Widespread public recognition of our past mistakes and resulting problems has triggered a demand for solutions. We no longer can afford to treat symptoms; nor can we lightly jump from identification of problems to immediate solutions. A systematic process of collecting and organizing data must still be followed. Accelerating this process without sacrificing the value of essential data is vital. Objective, critical, and thorough analysis of past practices of collecting and organizing data is required before we can identify new ways and means of accelerating this process. Next, we must identify the best tools presently available and tools that must be developed to accelerate the process. Finally, we need to combine tools and processes into one integrated information system that can be used effectively in the decisionmaking process.

COLLECTING DATA

Collecting data is not a problem. There is no limit as to the amount and kind of data that can be collected. In fact, volumes of pertinent data already exist. However, these data exist in obscure places, making retrieval an almost impossible task. These data, though vital, are for all purposes lost to us. Also, available data are often incomplete and sometimes contradictory, so retrieving the right data is either impossible or too costly. When found, it will probably be out of date.

Requirements

To objectively select a course of action to improve methods of collecting data, we must examine what data we should collect. A preliminary study by the Forest Service focusing on types of data collected was an eye-opener! Everyone contacted was an expert. It seemed that no one expert agreed with another.

In-depth questioning finally identified basic types of data required by resource specialists. First, five basic generic types of data were identified: 1) topography, 2) soils, 3) geology, 4) vegetation, and 5) climate. Further questioning identified more specific types of data needed by resource specialists. These are represented in Table I.

In each of the categories of basic generic data, there are important relationships. Where the source of data occurs, what type of data exists at that

particular location, when the type of data occurs, and how much of the data exists at the given location is vital for accurate interpretation.

Duplication

During the analysis, it became obvious that each resource specialist combined several specific data to produce criteria essential to interpretation of a particular phenomena. It became equally obvious that other resource specialists combined many of the same specific data for their criteria. Unfortunately, in many cases these same specialists reproduced the same data independently, resulting in an expensive and time-consuming duplication of effort. An example occurs in slope data where several resource specialists may independently specify a percentage range of slope criteria such as: 1) 0-25, 25-45, 45-65, 65 and over, 2) 0-35, 35 and over, or 3) 0-45, 45 and over. Consequently, each resource specialist would be required to construct separate slope maps.

Multiply this example by the many other possibilities of duplication and we see we can reduce time and costs in data collection by standardizing requirements. Recognition of specific data needed under a basic generic data base provides a framework that results in maximum utilization of a minimum amount of specific data.

Techniques

Data collecting techniques in the Forest Service are shown in Table II. These techniques are identified with basic generic data categories to provide a framework for future evaluation and update.

Tools

Today, we have excellent tools to collect spatial data that can be recorded on magnetic tapes. Controlled aerial photography provides the initial stereo pairs of photographs that can be photogrammetrically scanned in a systematic manner, recording spatial data (x, y, z positions) in known increments. These data are automatically recorded and stored on magnetic tape. At the Forest Service computer center in Fort Collins, Colorado, a Topographic Analysis System (TOPAS) of software programs convert spatial data to map products depicting slope, aspect, elevation, contours, seen areas, perspectives, and many others. This system is shown in Figure 2.

The same aerial photographs also serve as the basic tool for collecting and recording resource data (x, y positions) pertaining to soils, geology, and vegetation. Data recorded on the photos are classified by the resource specialist then transferred manually, sometimes with the aid of stereoplotters, to base maps.

Accelerating Data Collection

In the past, most data collection has been accomplished independently by each resource specialist. Little consideration was given to any standard, scale, accuracy, or systematic process for later combining the results of each individual's effort. Today, it is vital to collect data in each of the soil, geology, and vegetation categories in a standard, coordinated, systematic

manner to avoid duplication of effort. Aerial photography, although a valuable remote sensing tool, still requires time-consuming manual methods to transfer data into a standard format. The ideal objective is to record soils, vegetation, and geologic data in a digital format directly onto magnetic tapes.

Technology developed as a result of LANDSAT research proves that this is possible. However, precise requirements of Forest Service data collection preclude direct application of LANDSAT technology, but equipment used in the LANDSAT experiment can be duplicated in low-flying aircraft. Thus, promising results of the LANDSAT experiment have taken on a new significance.

Cooperative Research

We are optimistic that use of multispectral scanners at low altitudes is the key for accelerating collection of data. To prove this, the Forest Service entered into a cooperative effort in 1973 with the University of Utah, State of Utah, Soil Conservation Service, Intermountain Range and Experiment Station, and the McDonnell Douglas Astronautics Company to explore potential applications of multispectral sensors.

In July 1973, a 700 square mile area, including urban Salt Lake City, Utah, and adjacent Wasatch Front mountains, was flown at an altitude of 8,000 feet above terrain. Equipment in the aircraft included cameras for non-metric color photography (5 inch), near infrared photography (70mm panoramic) and a multispectral scanner for recording analog data in the visible spectral ranges of 0.5 to 0.6 micron and 0.6 to 0.7 micron; the near infrared spectral ranges of 0.7 to 0.8 micron and 0.8 micron to 1.1 microns; and the thermal spectral ranges of 10.4 to 12.6 microns.

Existing ground truth data were collected for the area, such as timber type maps, soil type maps, and climatic data. Also, some ground truth was collected during the flight. From the scanner data and ground truth data, classification maps were generated through interactive computer programs by McDonnell Douglas Astronautics Company. The most promising results were the timber type maps, soil type maps, and pervious-impervious surface classification maps as shown in Figures 3, 4, 5, and 6.[1] Costs were not recorded during this study since the objective of the study was exploratory to determine applications.

The Forest Service has recently prepared a proposal for continuing remote sensing studies in cooperation with McDonnell Douglas Astronautics Company. The purpose of this next phase is to concentrate on data collection relating to vegetation and soils. The objective is to determine the best altitudes and combinations of spectral bands to acquire this data. The study will be designed by remote sensing specialists and users throughout the Forest Service. Results will be published and will include costs, time, and reliability of results. If successful, we plan to put this tool into operation.

Aerial photography is not new. It is an accepted technique for collecting data in the Forest Service. However, users are rapidly discovering broader applications of aerial photography. Even multispectral scanners are not new, but when the term "remote sensing" became widely publicized, awareness of the associated tools followed. We are convinced that we can profitably apply these tools for data collection.

The first thing users must learn is what can be sensed by remote sensing. In the recent past, most of our efforts have been in the visible portion of the electromagnetic spectrum as shown in Figure 7.[2] More recently, we have edged into the near infrared segment of the electromagnetic spectrum. If we expand our use of the electromagnetic spectrum and relate specific data with specific segments or combination of segments of the spectrum, we will have increased our data collection capabilities many times.

Acceptance of New Applications

We are convinced that we do have tools for accelerating the collection of data, and that we can identify the right data to collect. However, we do not have widespread acceptance by users in the application of these tools.

There is widespread acceptance of aerial photography. Why? The user can see the product. He can interpret data from the product. He can make measurements from the product. He can organize the data, analyse, infer, project, predict, study alternatives, and make decisions. Data can be transferred to base maps for graphic display. More recently, from the photos or maps, data can be electronically digitized and stored on magnetic tapes.

Here, then, lies the key to non-acceptance. Remotely sensed data from multispectral scanners is collected on magnetic tapes. If data on a magnetic tape cannot be immediately retrieved, identified, and displayed graphically, then it has little or no value to the user. We are back to the days when data was stored in obscure places and for all purposes lost to us. The data on magnetic tapes must be made visible, either in the form of an image as on a photograph or as a map.

Relative Costs

A concentrated effort to determine exact costs, or at least a range of costs, for past, present, and proposed methods of collecting data failed to yield information of sufficient reliability to record. More important was the inference that the initial cost was not the overriding factor. Rather, the time taken to collect data appears to be more important. The right data, collected in a minimum time frame and stored in a manner that allows immediate retrieval and identification, appears to be the most desirable. Obviously, economy of money is an important constraint, and the skills of people carry a high price tag. Consequently, the most economical method of collecting data appears to be one that frees skilled people from time-consuming, laborious tasks that can best be done by new tools such as remote sensing.

Tools for accelerating the collection of data are available. If we are to gain acceptance of these tools, we must continue to explore the next logical step in the decisionmaking process.

ORGANIZING DATA

We have determined that we can store collected data either directly onto magnetic tapes from multispectral scanners or through photogrammetric scanning of stereo pairs of aerial photographs. This is the initial step in organizing data. How about valuable, accessible data that already exists on photographs and maps? It would be folly not to use this data. However, it does not exist in digital format, nor is it stored on magnetic tapes.

Digitizing Existing Data

Over the years, resource specialists have been organizing data on maps and cross-referencing to statistical data. Identification codes have been devised to describe the data in legends on maps. This information can be digitized and recorded on magnetic tapes with existing tools.

Several Regions of the Forest Service are digitizing existing data. Surface Environmental and Mining (SEAM), based in Billings, Montana, in cooperation with the Forest Service, is encouraging acceptance and use of a total information system which includes digitizing existing information as an integrated subsystem.

Accelerating the Digitizing Process

As a result of SEAM's efforts, Forest Service, Region One, Missoula, Montana, is actively engaged in field testing methods to accelerate the digitizing process. A diagram of Region One's digitizing subsystem and equipment is shown in Figure 8.

Forest Service Region Four, Ogden, Utah, has an operational subsystem using some of the same equipment. By August 1, 1975, Region Four will have acquired additional equipment to update their present system. Based on the success of Region One's efforts with the microdensitometer, Region Four will probably have the same digitizing capability as Region One within a year.

The efforts of SEAM and the Forest Service are concentrated on accelerating the conversion of existing data to digital format. The catalyst in this effort has been our experience with manual digitizing. Existing maps containing data come in all sizes, scales, and types of paper. Limiting factors that affect the initial digitizing activity are the size of the digitizer table, 42 inches by 60 inches, and the computer program limitations, 30 inches by 60 inches.

The time it takes to initially digitize a map also depends on the density of line segments representing data that exist on the map. Thus, digitizing can range from 4 hours to 40 hours per map. Successful implementation of the microdensitometer input station can reduce this to several minutes. Density of information would not be a variable, limiting factor. However, in order to use the microdensitometer, it is necessary to reformat the source map to insure each type of data is represented by contrasting, uniform colors or shades of gray.

Software programs are being designed for the subsystem shown in Figure 8 to reduce the amount of time it takes to initially digitize and edit data for

storage on a magnetic tape in an organized format. The use of interactive, on-line systems when fully operational will accelerate the digitizing and storing of existing data onto magnetic tapes.

To date, we have made and are continuing to make objective, critical, and thorough analyses of past practices of collecting data. As a result, we have begun testing, evaluating, and adopting new applications of remote sensing tools. This has led us to the testing, evaluation, and adoption of digitizing techniques using existing equipment. From these efforts, we conclude that the fastest way to collect and organize data is from source data directly to magnetic tapes in an organized, digital format. Thus, our objective should be to eliminate all unnecessary manual operations between the source of the data and its organized storage on magnetic tapes.

Putting It All Together

In order to more clearly define our last stated objective, a graphic representation of an integrated digitizing system for collecting and organizing data is shown in Figure 9.

Several items of interest can be deduced from Figure 9: 1) remote sensing, using multispectral scanners, aerial photography, and microdensitometers is by far the most valuable tool in collecting data, 2) not all subsystems are operational, 3) there are still too many manual processes implied in some of the subsystems, 4) no single subsystem can provide all data required, 5) a combination of subsystems seems to be the best, 6) field work, ground truth, verification, and interpretation cannot be automated (this suggests interactive subsystems), and 7) all collected data must eventually be recorded and organized on magnetic tapes.

Clearly, a dedicated effort must be made to evaluate each subsystem in the light of an optimum system. An evaluation for the total system for collecting and organizing data should be based on a combined evaluation of subsystems including: 1) initial costs, 2) resources committed, 3) accuracy of input data, 4) time, 5) type of data, 6) density of data, and 7) other.

To date, the Forest Service has tried all subsystems depicted. Some show promise; others are operational. Subsystems that are operational are: 1) topographical, or spatial, data collection and 2) manual digitizing of data from existing maps. One subsystem that needs only the purchase of equipment and some training to make it operational is direct stereoplotting from stereo pairs to magnetic tapes. Use of the microdensitometer is being field tested by Region One, Forest Service, Missoula, Montana, but is not yet operational. Software problems and preparation of source material are the major hurdles to overcome.

A fully operational system for collecting and organizing data on magnetic tapes requires that each subsystem be compatible with all other subsystems; otherwise, we cannot take the next step in the decisionmaking process.

GENERATING GRAPHIC DISPLAYS AND STATISTICAL REPORTS

For each subsystem there are computer programs that can retrieve the data stored on magnetic tapes and generate graphic displays and statistical

reports. In addition, we need computer programs that will combine data from subsystems in any format desired.

Operational Subsystems

We now have computer programs that can provide graphic displays and statistical reports for the two operational subsystems described earlier, 1) topographical or spatial data and 2) manual digitizing of data from existing maps. The topographical or spatial data subsystem (TOPAS) was described earlier and is shown in Figure 2. This subsystem is operational and is being used on a limited basis.

Demand for manual digitizing of data from existing maps is increasing. Implementation of this subsystem was accelerated because of pressure from Forest Service commitments. Several users, under strict deadlines to meet objectives, began experimenting with the application of computer programs for processing digital data from magnetic tapes and generating graphical displays and statistical reports. An operational computer program called COMLUP, an acronym for computer mapping for land use planning, was effectively implemented by these users.

During the past year, four users have successfully used the COMLUP subsystem. Table III displays the users, their requirements, products generated using COMLUP computer programs, and problems they experienced. All four users were satisfied that COMLUP products saved enough time and money to justify the initial expense of digitizing their data, and the Forest Service learned valuable lessons from this experience. Those involved in the operation of the subsystem also have a better understanding of the user's requirements.

Developmental Subsystems

As the LANDSAT experiment has demonstrated, there are computer programs that can provide graphic displays and statistical reports using data directly from multispectral scanners. However, at lower altitudes distortion due to topography and aircraft motion becomes a problem.

Forest Service experiments with McDonnell Douglas Astronautics Company revealed that software programs were needed to take out distortions automatically. Otherwise, graphic displays were distorted and statistical reports inaccurate. For the study on the Wasatch Front it was necessary to take photographs of the distorted image on a TV monitor then use manual devices to transfer the information to accurate base maps. From this point on manual digitizing methods were required to re-record data onto magnetic tapes. Software programs are now being developed to correct this problem.

INTERPRETATION OF DATA

Today resource specialists are a part of interdisciplinary teams. Team approach to land use planning is helping to integrate data into a common framework of reference. As a result, the teams have adopted a landtype map as the first phase in interpretation.

Landtype Maps

Landtype maps represent the combination of generic data that coexist in a specific location. The landtype map synthesizes basic data depicted in Table I. Use of this map is the first step in predicting how a basic unit of land will respond to use and management. An objective of digitizing basic generic data is to gain flexibility in combining variables to generate maps. The landtype map can be generated from these variables.

Landtype maps have been prepared by some Forest Service users by manually and subjectively combining basic generic data. It is possible to digitize existing landtype maps into several other maps such as erosion hazard areas, avalanche areas, and others. However, if any changes occur in basic generic data, it will be necessary to start over and prepare a new landtype map, if the original was prepared manually and subjectively. Digitizing basic generic data will allow users to make changes, combine variables in different sets, and update landtype maps without starting over.

MODELING AND SIMULATION

The capabilities of operational subsystems are limited at present. We are able to generate useful products from TOPAS and COMLUP subsystems. However, we need an interactive operational system that will allow the user to simulate impacts on resources, predict response, select alternatives, and make management decisions.

MANAGEMENT DECISIONS

We have shown in Figure 9 the various subsystems for collecting and organizing data onto magnetic tapes. The need to integrate the subsystems into a total system of collecting and organizing data is apparent. We are convinced that the process can be accelerated best by applying remote sensing tools. The time has come to implement processes that will provide us with capability to model and simulate alternatives.

Although COMLUP provides us with useful products, the processes are not interactive. The Forest Service has been expanding and will eventually replace COMLUP with computer programs that are designed to provide interactive capability. Systems enhancements proposed to accomplish this are shown in Figure 10.

With the adoption of this system, COMLUP will yield to GELO, an acronym for Geographical Location System, and GIM, an acronym for Generalized Information Management System. Once operational, the combination of systems shown in Figure 9 and 10 will be a powerful tool in the decisionmaking process.

CONCLUSIONS

Making the right decisions for managing earth's resources depends on the correct interpretion of data, and the accuracy of predictions pertaining to the response of use and management of earth's resources. It is vital that the right data is available at the right time in the decisionmaking process. Consequently, accelerating all processes from the collection of data to management decisions is an important step. A valuable tool for accelerating these processes is remote sensing.

Identifying the right data to collect to meet the needs of all resource specialists is one important step to take. The next important step is to organize and store the data for instant retrieval and identification. Finally, an interactive data analysis system must be implemented to provide a means for rapidly displaying and arraying alternatives prior to final management decisions.

It is clear that new technological tools have been developed with little understanding as to how they relate and interact in the decisionmaking process. If we are to be of any help to the users, it is mandatory that we begin to put all the pieces together into one information system that allows us to collect and organize data as rapidly and accurately as possible using remote sensors, multispectral scanners, microdensitometers, digitizers, and magnetic tapes. In this system, we need computer software programs to retrieve stored data from magnetic tapes, allow interaction between user and stored data to generate and array alternatives, select alternatives, and model and simulate conditions for making predictions. Finally, this system needs to provide for future followup when new facts are identified and changes need to be made.

ACKNOWLEDGMENTS

The author finds it almost impossible to acknowledge and thank by name all those who have had a part in the development of this paper. Many people have willingly given their time to acquaint the author with background information and concepts.

A special thanks to the users who have tested the subsystems described in this paper. Their support, patience, and candid evaluation has been the catalyst that has brought us as far as we are today.

Finally, a warm appreciation for the operators, editors, and computer specialists who have spent many frustrating hours in keeping the systems running.

REFERENCES

1. Linker, D.W. and Nelson, E.E., Multispectral Data Analysis for Resource Managers in Utah, presented at Second Canadian Symposium on Remote Sensing, Guelph, Ontario, Canada, April 29-May 1, 1974.

2. Remote Sensing of Agriculture, Earth Resources, and Man's Environment, Laboratory for Applications of Remote Sensing, Purdue University, West Lafayette, Indiana.

TABLE I - TYPES OF RESOURCE DATA

BASIC GENERIC DATA	TOPOGRAPHY	SOILS	GEOLOGY	VEGETATION	CLIMATE
SPECIFIC DATA	SLOPE ASPECT ELEVATION	TYPE DEPTH	ROCK STRATA SOIL PARENT MATERIAL DIP AND STRIKE OF SEDIMENTARY AND METAMORPHIC ROCK MINERALS	OVERSTORY UNDERSTORY GROUND COVER	RAINFALL SNOWFALL MAX. AIR TEMP MIN. AIR TEMP MEAN AIR TEMP FROST FREE DAYS

TABLE II - DATA COLLECTING TECHNIQUES

	PAST	PRESENT	PROPOSED
Topography (x, y, and z spatial data)	Field methods using plane table and simple measuring devices.	Photogrammetry, using vertical aerial photos in stereo pairs and stereoplotters.	Small scale photography. Digitizing stereo models, storing on magnetic tapes, computer software programs converting data on magnetic tapes to topographic products.
Soils (x, y)	Field sampling, recording, manual transfer of data to existing low standard maps or roughly sketched maps.	Interpretation of aerial photographs, combined with on-ground verification and sampling. Visual or instrument transfer of data from photos to existing maps.	Single band or multiband black and white or color photography. Sample ground truth, interpretation, and instrument transfer of data to digital format. Store on magnetic tapes, use computer software programs for output products. Multi-spectral sensors, directly to magnetic tapes or cathode ray tubes, and computer software program for output products.
Geology	Field work visual interpretation, transfer to existing maps, manual compilation.	Aerial photography, USGS 7½' quads, instrument transfer, cartographic techniques and reproduction methods.	Small scale photography, LANDSAT imagery, Skylab photography.
Vegetation	Field work, visual observation, manual transfer to existing maps.	Aerial photography including color infrared film, ground verification manual and instrument transfer to base maps.	Multi-band photography, multi-spectral sensors. Record directly to magnetic tapes, convert to digital format, use computer software programs aided by sample ground truth methods to provide output products.
Climate	Measuring devices, maps, reports.	(Not familiar enough with present techniques)	(Same)

TABLE III - SUMMARY OF COMLUP SUBSYSTEM EVALUATION

USER	MAPS DIGITIZED	INPUT SCALES	OUTPUT* SCALES	PRODUCTS FROM COMLUP	PROBLEMS
Caribou N. F.	LANDTYPES LANDTYPE ASS'N FOURTH ORDER STREAM WATERSHEDS FIFTH " SIXTH " SEVENTH " MGT AREAS	1:62,500	1:253,540 1:126,720 1:63,360 1:24,000	ALL COMBINATIONS OF TWO MAP LAYERS, ACREAGES FOR EACH MAP UNIT. COMPUTER MAPS OF 10 CLASSIFICATIONS AND AREA IN EACH CATEGORY OF CLASSIFICATION	TURN AROUND TIME TOO LONG SECURITY OF TAPES. IF ERASED, LOSS IS GREAT LIMITED RESOURCES PREVENT RAPID RESPONSE TO USER
SEAM	OWNERSHIP SUBSURFACE (MINERAL) OWNERSHIP TOWNSHIP - RANGE COUNTY BOUNDARIES	1:126,720	1:126,720	MAGNETIC TAPE	SAME
Ogden Valley Coop	OWNERSHIP SLOPE HYDROLOGY EROSION HAZARD VEGETATION CULTURAL	1:24,000	1:24,000 1:63,360	SUITABILITY MAPS AND STATISTICAL REPORTS	SAME ALSO, USER WOULD LIKE TO HAVE COMPUTER COMPOSITE MORE LAYERS AND EVALUATE WEIGHTED CRITERIA FOR SUITABILITY
S & P F (River Basins)	BASE MAP OWNERSHIP SLOPE VEGETATION SOILS ELEVATION PHYSIOGRAPHIC ETC. SPECIAL AREAS	1:253,540	1:253,540	STATISTICAL REPORTS RESOURCE RESPONSE UNIT MAPS	SAME USER WOULD ALSO LIKE TO HAVE COMPUTER COMPOSITE MORE LAYERS

*Quickly done by computer

1. Define Objectives

2. Identify Problems

3. Collect and Organize Data

4. Generate and Array Alternatives

5. Select Alternatives

6. Provide Follow-up

Figure 1. Decisionmaking process

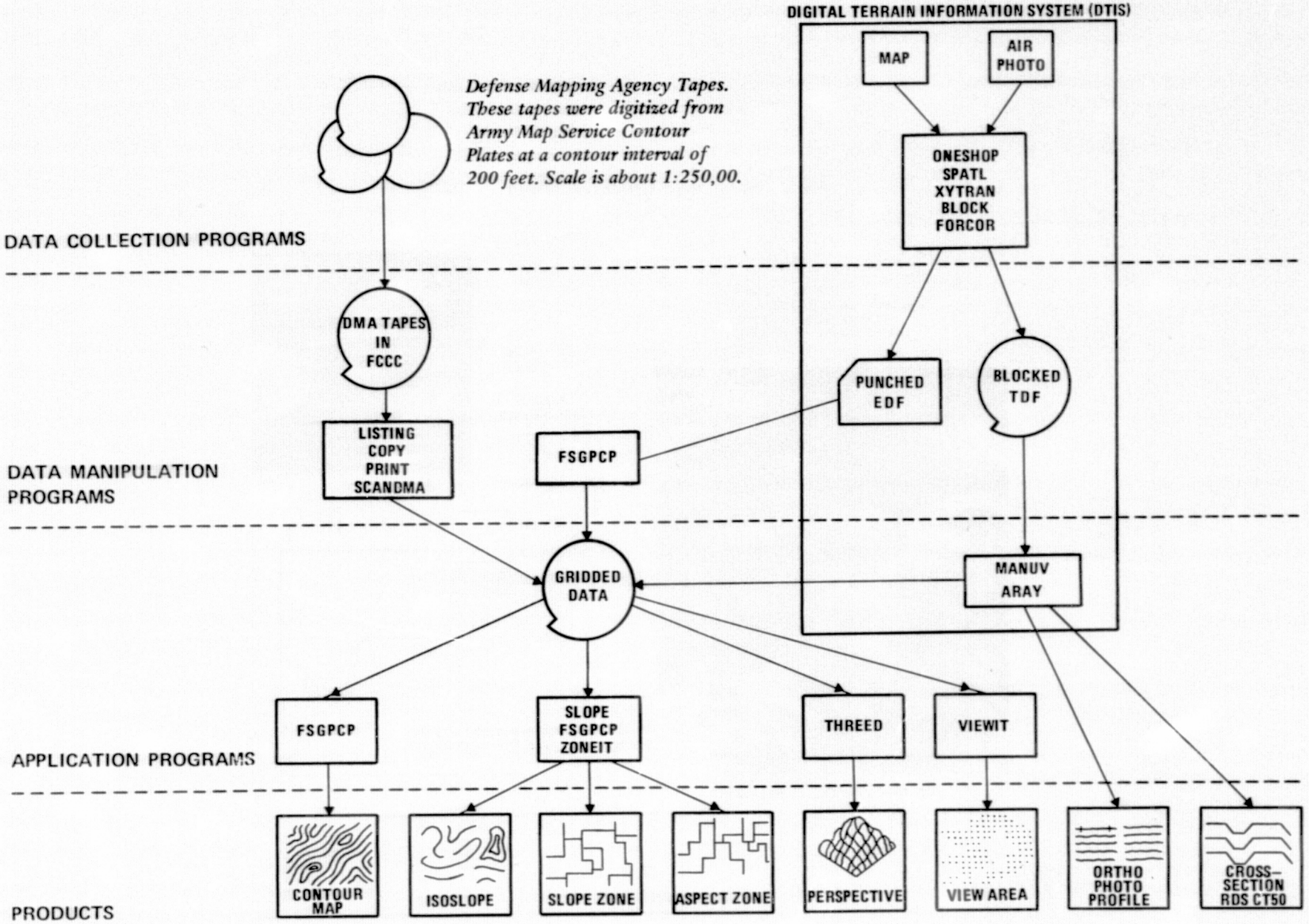


Figure 2. Topographic analysis system (TOPAS).

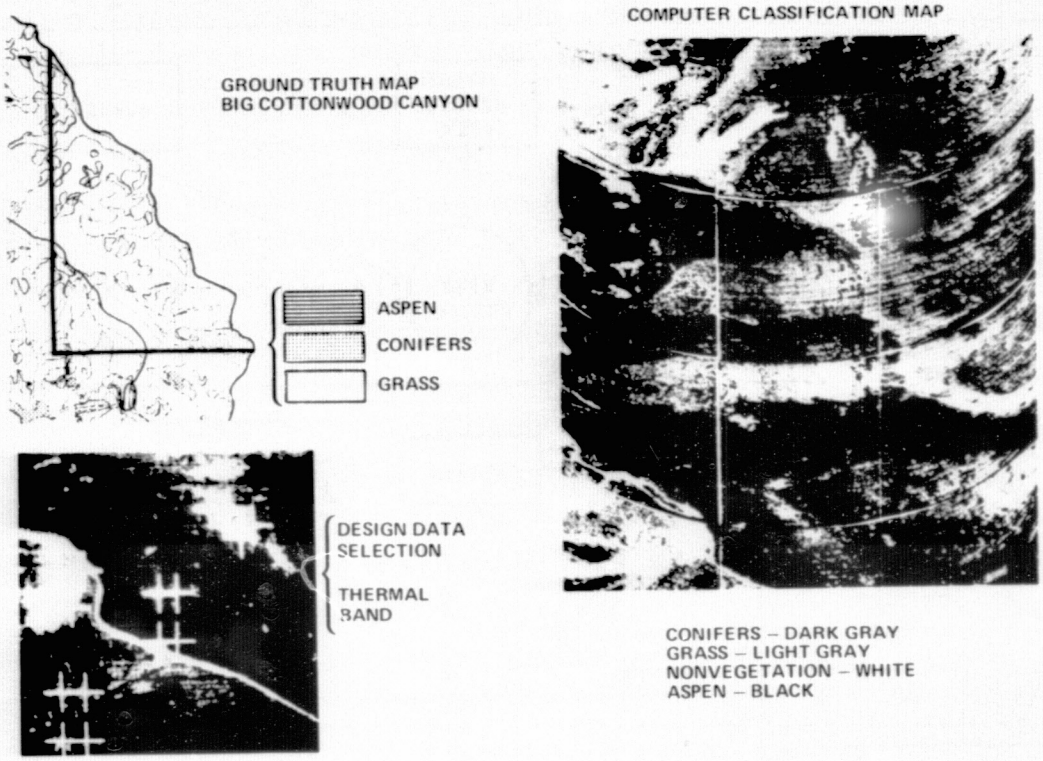


Figure 3. Computer Classification of Plant Types

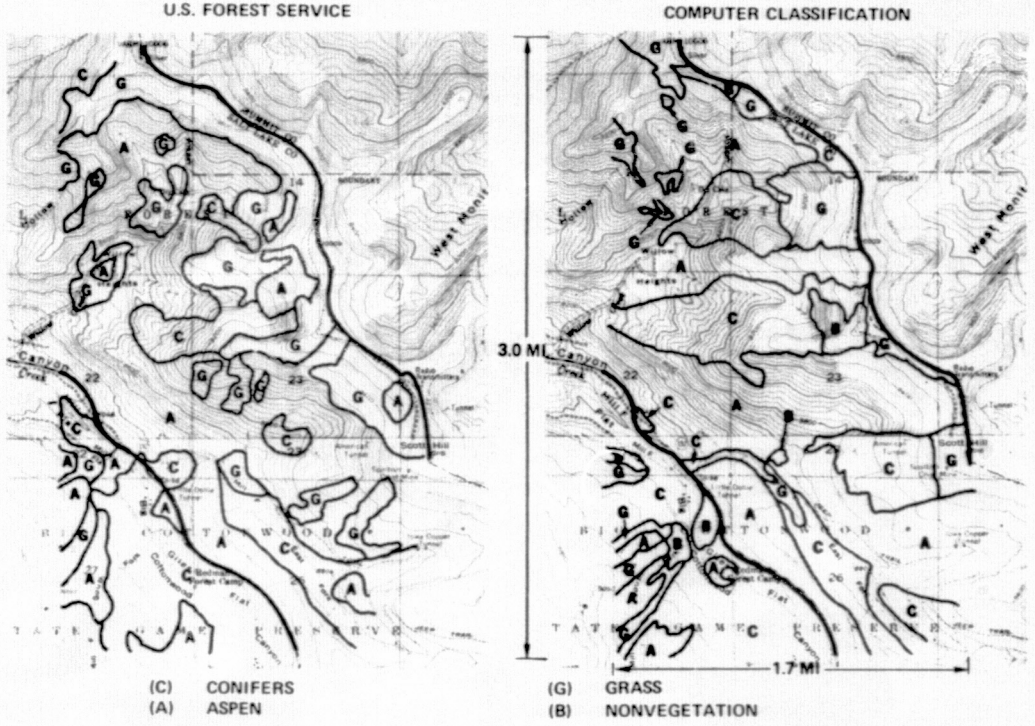


Figure 4. Map Overlays for Plant Types

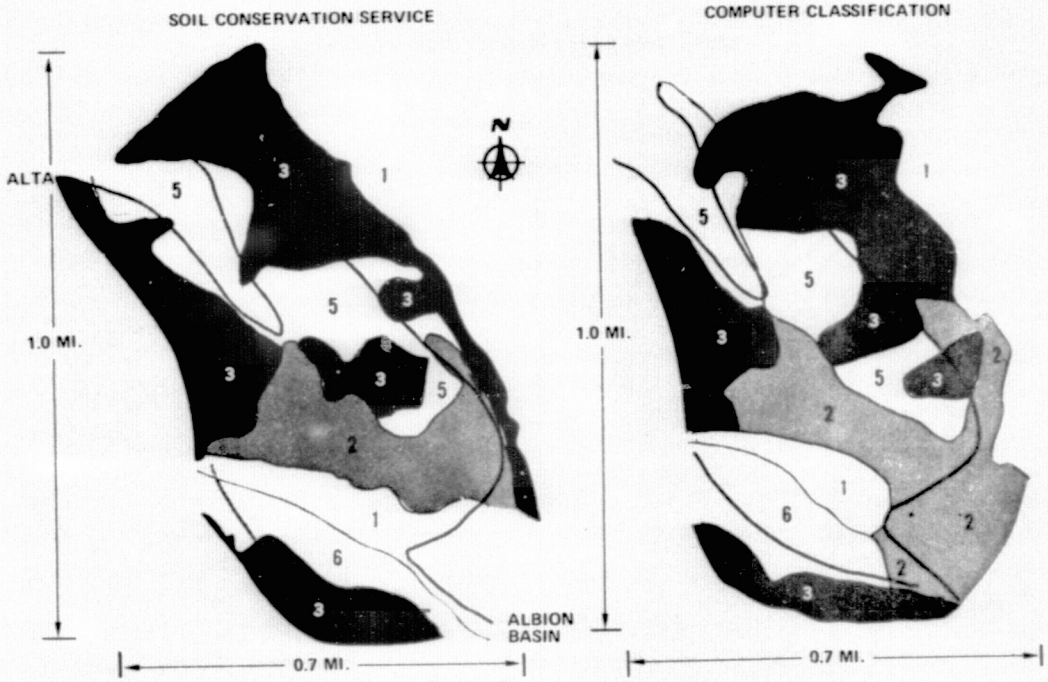


Figure 5. Soil Survey Map

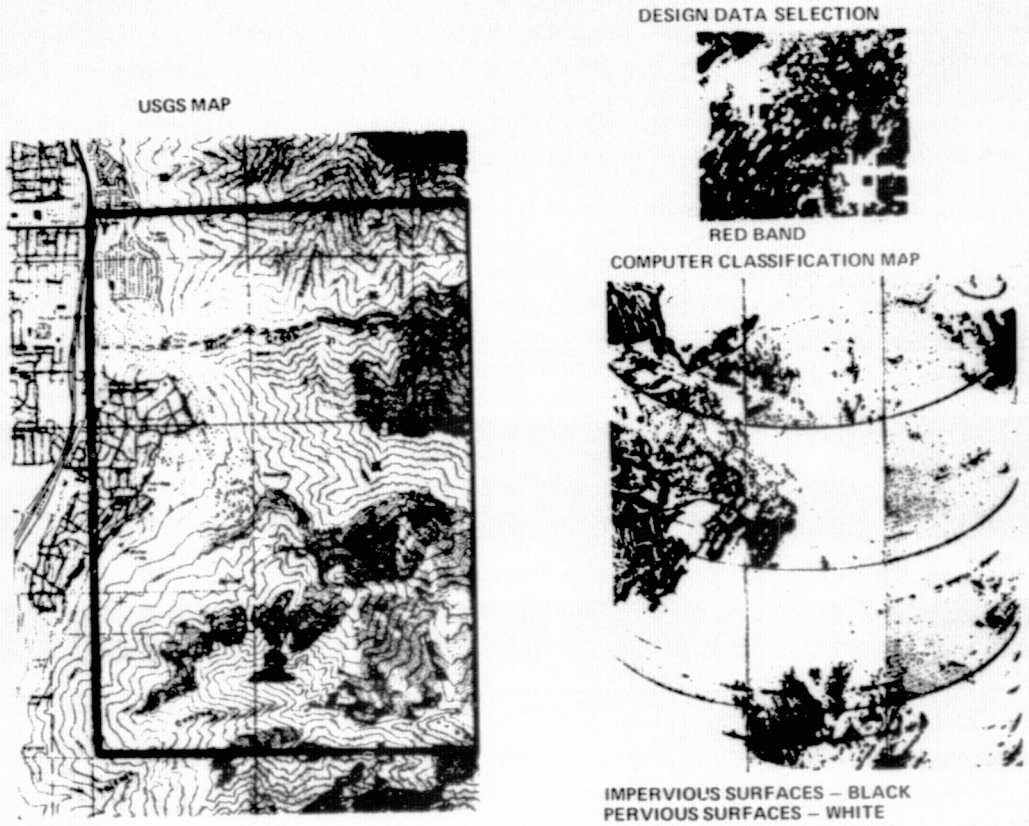


Figure 6. Computer Classification of Impervious Surfaces

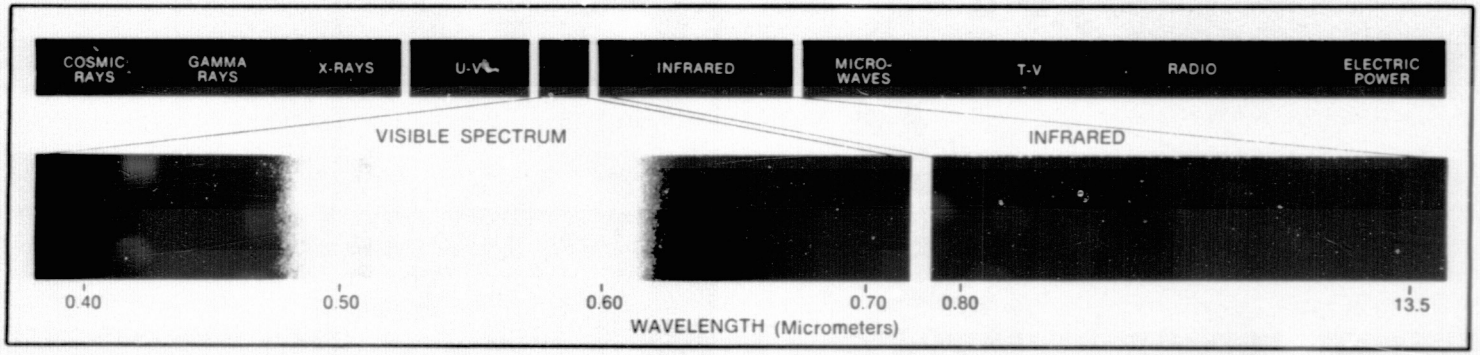
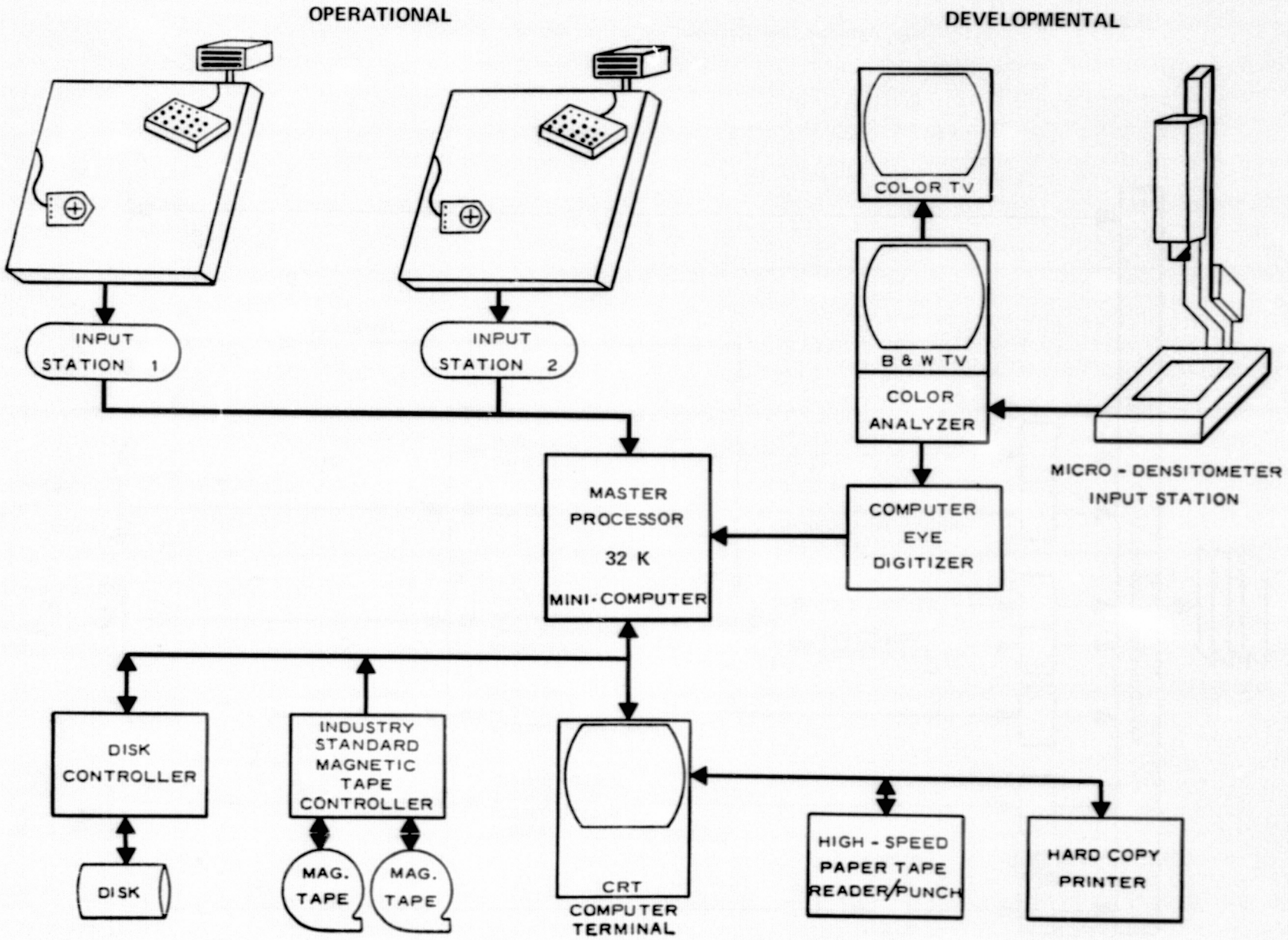


Figure 7. Electromagnetic spectrum



12117

Figure 8. Digitizing subsystems. Forest Service, Missoula, Montana.

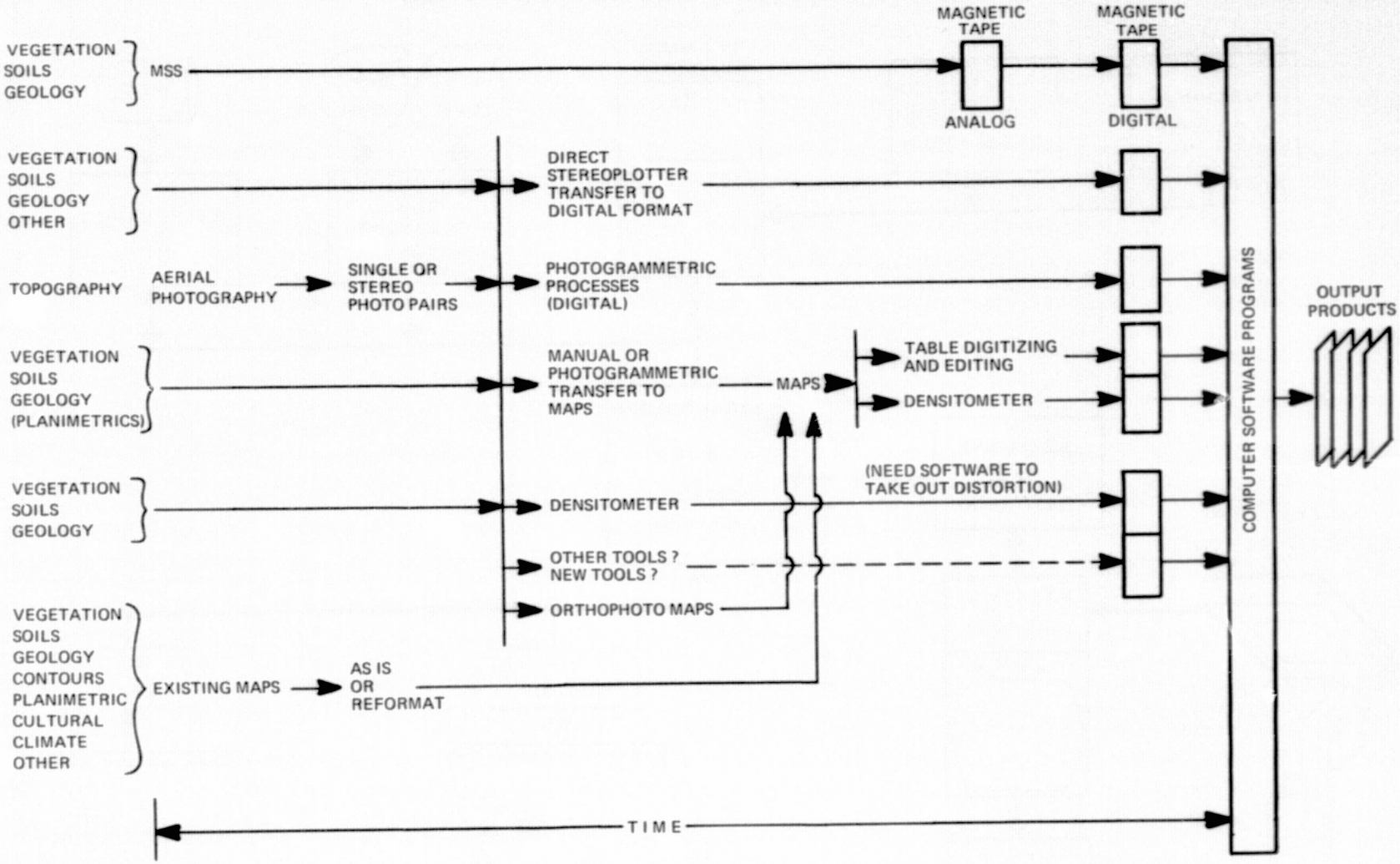


Figure 9. Integrated digitizing system for collecting and organizing data.

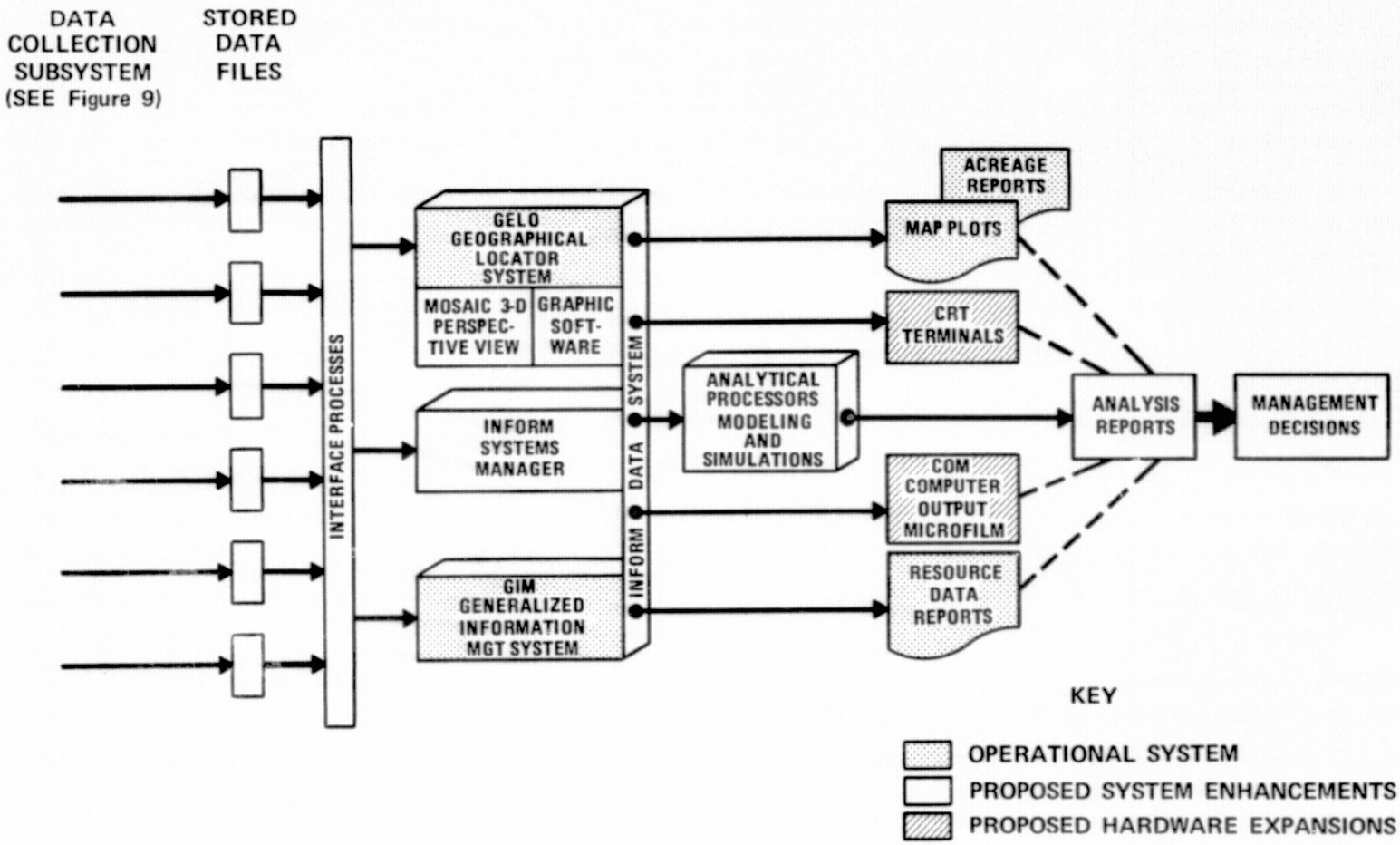


Figure 10. Proposed interactive data analysis system.

SPACE TECHNOLOGY
PUTTING IT IN THE EDUCATIONAL PERSPECTIVE

By Donna B. Hankins, President, Pilot Rock, Inc.

N76-17531

Pilot Rock, Inc., is a California based corporation founded in 1972 for the purpose of creating and producing educational materials. The officers and staff are geologists and earth scientists with photography and teaching orientation. One of the founding precepts of the company was to provide educators with practical, innovative, and manageable audio visual teaching aids in a wide spectrum of educational fields, but primarily geography, geology and social science.

Toward this end, a pilot slide set was prepared, demonstrating primary areas along the entire length of the San Andreas Fault Zone in California and Mexico. This set utilized several National Aeronautics & Space Administration (NASA) infrared research aircraft photos, to more clearly delineate fault traces. Based on an enthusiastic response to initial market sampling of the set, a corporate decision was made to mount a massive program of repackaging NASA generated infrared aircraft imagery into topical teaching sets.

The reasoning behind this decision included the following considerations: the general availability of infrared aircraft imagery generated by Earth Resources Technology Satellites (ERTS), now LANDSAT, and pre-LANDSAT support flights; the haze reduction factors and resolution capability of infrared images; and the fact that the synoptic overview seen in these photos was extremely adaptable to the needs of educators who are generally somewhat familiar with aircraft views. Pilot Rock staff and advisors believed that by becoming knowledgeable in this area first, a solid foundation could be formed to support the creation of teaching aids from other types of imagery.

There are numerous steps in preparing any teaching tool utilizing the photographs and images generated by NASA. First is acquiring the basic library of 35mm slides. This process is an ongoing one, as we reach out to demonstrate a wider range of platforms and sensor types, and involves both intensive microfilm scans and live scanning of hundreds of rolls of film. By previewing thousands of film frames, it is possible to choose the select images that will best demonstrate the following features throughout the United States and globally:

1. A variety of geological features and various geomorphic landforms;
2. Rivers, lakes, nd reservoirs;
3. Agricultural patterns, crops - historic agricultural patterns;
4. Urban centers - street patterns, urban place morphology;
5. Transportation modes - highways, railroads, and airports;

PRECEDING PAGE BLANK NOT FILMED

6. Mining and manufacturing;

7. Seasonal and yearly evidence of change; and

8. A variety of climatic indicators and hazards such as floods, fires, tornadoes and even earthquakes

After the images are selected, they are then converted to 35mm slides. The master frames are carefully located and catalogued, utilizing both the retrieval numbers and frame identification numbers used by NASA and an independent system designed by Pilot Rock, Inc., technical staff. This gives a near instantaneous look at exactly what is available in our library on either a regional basis, by flight and frame number, or site and mission number. Slide library listings are available on request.

As new products go into a design stage, as many as 500 slides may be reviewed representing the range of material desirable in a given teaching package. The very best slides available to describe a given topic are then incorporated into a final set - average size being between 25 to 30 slides. Consulting specialists with known expertise in the theme or topic of the slide package prepare detailed annotations and interpretations of the views seen. Frequently, simple diagrams are utilized to clarify details, and locator maps are used to point out sites of each picture. A reading and reference list completes the package.

The initial effort to acquaint the educational community with such teaching packages has been at University and Junior College levels. In such classes as urban and cultural geography, social science, geomorphology, and various geology classes, these depictions of the earth's surface and its occupancy by humans serve as precise markers for a given point in time. The desirability of the images and photographs lie in having a point against which change can be measured. For example, historic agriculture patterns and urban street patterns are clearly visible, along with the superimposition of modern patterns. As favorable responses to teaching materials in post secondary areas continue to come in, the task ahead is rapidly consolidating and taking a positive shape.

The educational application of remote sensing is in a state of infancy. It is apparent through nearly two years of working with imagery and photography generated by space programs that a far wider scale of use is mandatory. Intelligent management of all Earth and its resources is critical to the survival of the whole system. We believe that a whole range of educational materials should be introduced into elementary and secondary schools as well as colleges and universities at the earliest possible time. The young students of today will be the resource managers, engineers, and planners in a short number of years. Arming these students with basic information and understanding of remote sensing will provide them with the powerful analytic tool for thoughtful stewardship of earth's resources.

First steps to this end should lie in the field of perspectives. Filmstrips for elementary and slide sets for secondary schools can demonstrate an entire range of the perspectives gained in high altitude views. In stages, even the very young student can travel from a ground view of a familiar object such as a house or a distinctive area on a mountain, to a low altitude aircraft view of the same spot. They can then travel to a high altitude photo and finally to a LANDSAT or Skylab overview with the area of interest highlighted by arrows or a circle. Appropriate questions in cassette tape form or printed exercises accompanying the

visuals can lead to a simple definition of what changes take place in the various levels of the pictures. Pattern recognition and texture recognition games can be devised to give the young student a basis for later understanding of spectral signatures important in remote sensing exercises.

Exercises in scale as well as games to define scale as related to perspective, pattern, and texture recognition for elementary students can lead to actual work on scale models of landforms seen in high altitude photos for high school students. The differences in color and color infrared are easy to demonstrate visually, but need specially written guides for understanding at elementary stages. Junior high and high school students can be directed into experiments using black and white, color and color infrared film to photograph several assigned areas or subjects that will graphically demonstrate differences and uses of such film.

Another obvious educational area for use of imagery and photos from aircraft or satellites is in geography, social science, and map studies. Certainly by use of a clearly defined series of multi-level photographs, positive geographic sense can be established in the youngest student. The process of creating understanding of the relationship between maps and high altitude images is particularly simple. Maps become a symbolic representation of a real earth, as they were intended originally, and not the multi-colored puzzles of days gone by.

Pilot Rock, Inc., officers and staff respectfully submit that immediate measures at Federal levels should be undertaken to familiarize elementary and secondary students with the methods, photo/imagery, and applications of remote sensing. This effort may be a major solution for a troubled earth. We also take pleasure in announcing that many of the suggested curriculum aids are in fact being designed by our group. We believe that these uses of imagery, photos and data generated by NASA and the Space Programs reinforce and perpetuate the original intentions of the Space Programs and we are proud to enjoy a pioneer rank in this pioneer field.

GROUND ZERO AND UP - NEBRASKA'S RESOURCES AND LAND USE

By Donald M. Edwards, College of Engineering and Technology, University of Nebraska, Lincoln, Nebraska; and Roger Macklem, Nebraska State Department of Education, Lincoln, Nebraska

N76-17532

ABSTRACT

A one-semester high school course has been developed about the use of remote sensing techniques for land use and earth resources planning and management. The slide-tape-workbook program has been field tested with high school students to show a substantial increase in gain of knowledge and an attitude change in application of remote sensing techniques.

INTRODUCTION

The successful utilization of the technological developments which result from the space programs such as those of NASA must be through the knowledge gained by trained people. With the availability of space craft to the general public a new technology has become available. The proper training of youth, especially at the high school level will better assure the successful application of results obtainable from the space programs.

The purpose of this project was to develop a high school science course with follow-up 4-H and Explorer Post projects to help young people to determine the use of remote sensing techniques in land use and earth resource planning and management. Specific objectives were to determine: 1) what and how satellites and aircraft are used in remote sensing application, 2) what can be interpreted from remote sensing photos, 3) how remote sensing photos can be used in land use and earth resource planning and management and 4) how anyone can take and produce remote sensing photos.

Most important from the developed course was to give science teachers and students through the school curriculum a new alternative of science relevancy.

IMPLEMENTATION

A 125 page laboratory workbook was developed and field tested by high school science teachers (see ACKNOWLEDGMENTS). In the classroom, each student has an individual workbook. A teachers' manual accompanies the students' workbooks. The workbook exercises demand individual and group participation. Five chapters constitute the makeup of the workbook: Chapter 1. Seeing is Believing - Optics and Orbits; Chapter 2. Where It's All At - Nebraska Geography; Chapter 3. Instamatic Learning - Photography in the Classroom; Chapter 4. What Has Less Calories Than Soda Pop? - Water in Nebraska; and Chapter 5. Who is 'Outstanding' In Their Field? - Scientific Land Management.

A 126 color 35 mm. slide program with audio tape and script has been developed to supplement the workbook (Ground Zero and Up - Nebraska's Resources and Land Use).

PRECEDING PAGE BLANK NOT FILMED

The slides present explanations and examples of the use of remote sensing techniques for land use and earth resource planning and management. The entire program is restricted geographically to Nebraska. Another program is being developed to geographically encompass the United States.

The course has been field tested in four high schools. Pilot use of the course in a rural Nebraska high school indicated very positive results (Jones, 1975). Fifteen precent of the students who participated in the course passed the pretests, whereas, 85 percent passed the post-tests. Objective and subjective evaluations of the course at the end of the semester showed that students enjoyed the course. They found the course rewarding while at the same time they generated parental interest in many topics of the course.

Evaluations in other high schools, mainly urban schools have shown similar results.

Script for Slide Program
GROUND ZERO AND UP - NEBRASKA'S RESOURCES AND LAND USE

Splash down! - and now man has turned his attention from the Apollo programs to Skylab and from Skylab to the Space Shuttle. Tomorrow the planets and beyond! But before man takes that trip to the planets and beyond, let's explore what earth resource satellites have provided for mankind. On July 23, 1972, the National Aeronautics and Space Administration launched the first LANDSAT Satellite, then referred to as the Earth Resources Technology Satellite, or ERTS, into space aboard a two-stage Delta rocket. The satellite contains solar ray panels that collect the sun's energy to provide the power for the satellite, and a multi-spectral scanner which detects various reflections from the earth and transmits them back to receiving stations on earth. LANDSAT circles the earth at an altitude of 565 miles. The circular orbit is from the north pole to the south pole on the sunlit side of the earth, completing 14 revolutions each day. This makes possible complete global coverage every 18 days. As the satellite orbits around the world, it transmits its information to United States receiving stations at Goldstone, California; Fairbanks, Alaska; and the Goddard Spaceflight Center outside Washington, D.C. Remote sensing is the measurement or observation of things from a distance. LANDSAT "senses" images from the earth. The devices for obtaining these images and transmitting them back to earth from the satellite are simple in concept, but require a great engineering effort. As the satellite travels from north to south, it scans an area approximately 185 kilometers in width. Each image represents an area approximately 185 X 185 kilometers. Images are reflected light. This light energy travels from the earth to a scan mirror which oscillates and reflects signals through an optical system which breaks up the light energy and is sensed by various detectors. (Figure 1). These detectors convert the various wavelengths into ratio signals transmitting them back to receiving stations on earth where the imagery is processed into photographs. This electrooptical imaging system is the eye of LANDSAT.

Only a small segment of the entire electro-magnetic energy spectrum is commonly used in earth resource and land use determinations. Aboard LANDSAT are sensors to detect various wavelengths. These wave lengths, or as they are more commonly referred to, wave bands, are the visible green band, the visible red band, and two near infrared bands which are just outside the visible band. Satellite passes over Nebraska are in a north-northeast to south-southwest direction, taking approximately seven passes to cover the entire state. (Figure 2). The satellite passes over the

continental United States at about 9:30 a.m. The reason for this time of day is that in the morning hours in North America, the cloud build-up is at a minimum. Also, the sun angle is optimum at this time of the day for accentuation of various ground features.

The following series of pictures will show what earth features the various wave bands best detect. A low elevation air flight shows an area including lakes to the south of Valentine, Nebraska, which is located in the north central part of the State. Very few ground features can be seen as this photo was taken from satellite imagery in the visible green band. This is due to the interference caused by the atmospheric haze, and demonstrates the value of this band for studying such things as air pollution. The same scene taken in the visible red band. Visible red is of importance in that the photosynthetic process in growing vegetation absorbs the visible red portion of the spectrum. The dark areas are wet meadows which are the more vigorously growing vegetation. Again, the same scene but taken in the furthest near infrared band. Water bodies absorb infrared, subsequently, the dark areas are natural reservoirs or lakes. By projecting light through appropriate filters with these three bands, a composite false color image can be made. This is much like generating a colored picture in color television. When superimposing the visible green band, the visible red band, and the near infrared band, and using appropriate filters, certain features can be accentuated. The red areas represent wet meadows, locations of growing vegetation; dark areas represent free bodies of water.

What is the geography of Nebraska? The geographic features of Nebraska are the valleys, the plains, the sandhills, the rolling hills, lakes, rivers, wooded areas, and the manmade features. Starting on the eastern side of the State, the lighter area in the center of this false color composite picture is Omaha. The more red the areas, the more vigorous the vegetative growth. The Platte River flows from the upper left-hand corner to the Missouri River on the right. The downtown area, which is mainly buildings and hard surface streets, is shown by white and light blue areas. Moving outward from the downtown area, the older and more established part of town is darker because of more vegetation and trees. The peripheral area of the city is again lighter in color because new housing developments have fewer trees, and less grass and other vegetation than the older developments. During the winter, other features are brought out as shown by this visible red picture. With the sun lower to the horizon and snow cover on the area, more of the grographic features are visible. Dark areas, shown by the Fontenelle Forest area which is in the loop in the river immediately south of downtown Omaha, represent trees that are above the snow cover. Traveling closer to the earth with Skylab, Epley Airfield, Carter Lake and the Missouri River become very distinct. Skylab is about 276 miles above the earth (Figure 3).

From Skylab, eastern Nebraska is viewed, with Omaha on the right to the Platte River on the left. The river flowing into the Platte River from the northeast is the Elkhorn River. The complex geometry of this part of Nebraska is typical of the more heavily agricultural midwest United States. This complex geometry will be in contrast to the mixed agriculture-rangeland of western Nebraska. Aerial photos can be taken by many types of aircraft. Cameras of the RB-57 aircraft flying at 60,000 feet, using color infrared film, will produce pictures such as this early June photo of the Elkhorn River Valley. Color infrared is sensitive to infrared radiation. The meandering river is contrasted by the white of the sandbars adjacent to it. The untilled portion of the river flood plain shows red, indicating vegetative growth, which are areas reflecting infrared radiation, whereas the fields along both sides show bare soil and dead plant residue. The mining of sand and gravel leaves its mark on the surface of the earth. Gravel pit lakes south of

Grand Island are gravel pit lakes. To the west of Grand Island is Kearney. Along the lower edge of this RB-57 picture is the multichannel Platte River. West of Kearney is Cozad. The dark blue areas along the interstate highway are small bodies of water. Of special interest is the contrast of planning and layout of the town and the farms. Along the way are several man-made reservoirs. What reservoir is this? (Figure 4). This RB-57 photograph shows Johnson Reservoir, located to the south of Lexington. In addition to the lake, note the change in land use pattern contrasted with previous patterns in eastern Nebraska. The darker reds of this early June photo are alfalfa fields. The gray branched patterns are rough untilled areas of deeply eroded terrain suited only to growing grass. Further west along the same side of the Platte River is Jeffrey Reservior, as photographed from an RB-57 in June. Color and patterns are similar as for the Johnson Reservior photo. Westward, at the confluence of the North Platte and South Platte Rivers is North Platte. Differing water depths at the time this photo was taken accounts for the different appearance of the two rivers. West of North Platte is Lake McConaughy, the largest reservoir within the State. Field patterns to the south of the reservoir indicate agricultural cultivation, while north of the reservoir lack of field pattern indicates rangeland. Comparison of the previous August picture with this January picture of Lake McConaughy shows the dune patterns of the sandhills in the rangeland area. The dark patches of the cultivated area are vegetation from the previous growing season which have not been covered by the snow. On the east slope of the Rocky Mountains in Wyoming, a north-south fault is visible. The fault is accentuated by a snow cover. Faults are of importance in the identification of problems in the construction of transportation systems, utility lines, and buildings. Also, of importance is the potential discovery of minerals and fuels along faults. Northwest of Lake McConaughy and east of Alliance are a series of sandhill lakes and meadows among the grass-covered dunes. Different shades of blue for the lakes in this color composite are due to differences in water quality in the lakes. Eastward, to north central Nebraska, this composite photo depicts another series of sandhill lakes, meadows, and streams among the dunes. Immediately to the south is Halsey National Forest, which is a unique forest, having been planted by man in the middle of the sandy soils of the sandhills. It is the largest man-made forest in the world. The forest is readily visible from LANDSAT. It lies near the confluence of the Middle Loup River, upper stream, and the Dismal River, lower stream. The numerous white spots are blow-outs or exposed sand.

Often the excitement of photography is taking the picture yourself. Previous photos and imagery have been taken by high flying aircraft and satellites. Armed with a camera and normal color or color infrared film you can shoot your own pictures and develop them yourself. The three trees taken with normal color film look entirely different when taken with color infrared film. Differences in color intensity of the infrared of the individual trees indicate a difference in species or health of the trees. The dark areas under the trees represent areas with lower evapotranspiration rates and are not shadows. When using color infrared film, the proper lens and filters must be used. To take aerial pictures, it's necessary to get up into the air. A high-winged aircraft with a sliding window would be most desirable. However, perfectly adequate pictures can be taken through a side window of the airplane at a relatively low altitude. This normal color picture of the University of Nebraska Agronomy farm near Mead was taken from about 1000 feet. A photo of the same area taken in color infrared shows features not visible in normal color. Subtle variations within a field provide significant information. Another comparison demonstrating color infrared capabilities invovles Holmes Lake in southwest Lincoln. A normal color shot from low altitude shows the Marina in the upper center of the picture and in the right center edge of the picture is a green "haze" in the small bay. In color infrared this "haze" shows red, indicating some type of plant growth activity. (Figure 5). The shade of blue of the water indicates water

quality. From the shoreline of Holmes Lake, the plant growth becomes more evident. The green material at the water's edge is algae. At the lower left is the paw print of a dog, the white area to the right, a crumpled up cigarette package. Color infrared shows active plant growth in the area indicated as having algae present. A few feet further down the shore is the same phenomena, first in normal color, then color infrared. From a low flying aircraft, trees appear as different shades of red when using color infrared film. The different shades of red indicate either tree specie difference or disease among the trees. There are many other uses that can be made from color and color infrared film. Normal color and color infrared film can be used to identify vegetation and to determine variation in water quality. Most reservoirs have rooted aquatic plants growing near the shore. Some plants just barely reach the water surface. Reeds often grow in dense stands along the shoreline shown by this normal color photo. Color infrared shows vigorous growth activity of these aquatic plants. This type of aquatic vegetation is also visible in color infrared photos from RB-57 aircraft. The dark areas adjacent to the shoreline of the large lake, particularly noticeable in the lower portion of the lake, are areas of rooted aquatic vegetation.

In the sandhills of Nebraska the vegetation is very dependent upon water to remain healthy. Wet meadows are areas where the vegetation has water available at all times. These areas are seen as areas of dark green in normal color. Areas of less moisture appear brown-gray. Color infrared shows this vegetative dependency on water even more strikingly. On the ground the area of deeper red is vegetation which has water always available. From the air, the wet meadow, with the haystacks which appear as white spots, can be seen to spread in both directions from the lake. Trees which surround the lake appear a much deeper red, showing a species difference response in infrared.

Color infrared photos can be used to study water quality, especially sediment loads in lakes. Sediment load of flowing water is evident from this RB-57 color infrared photo of Johnson Lake. The lighter blue, representing sediment laden water, is visible at the inlet to the lake on the left center shoreline. Mixing and dilution of the sediment load occurs in the greater portion of the reservoir, but outflow causes some of the sedimented water to be pulled from the lake. To determine variations in water quality requires water sampling and physical, chemical or biological laboratory tests.

Runoff erosion also contributes sediment to lakes as evidenced by this RB-57 photo of the south shoreline of Lake McConaughy. Sediment load in the water is shown by the light blue areas within the lake. Entire reservoirs viewed from LANDSAT can show differing sediment loads, as seen in these two Missouri River impoundments. On the right is Lewis and Clark Reservoir which is much lighter in tone than Chase Lake. Enlarging and viewing Lewis and Clark Lake on a color composite allows us to see more clearly the sediment load of the incoming river flow and the build-up of sand bars at the upper end of the lake.

Regardless of where people live, land use is of great importance to everyone. Many different types of land use exist in Nebraska, from the agriculturally complex eastern side of Nebraska to the diversely agriculture-rangeland western part of the State. Topographic features result from such activities as tillage practices, harvest of corn and the building of towns and cities. Many field patterns of the intensely cultivated Platte Valley in Eastern Nebraska can be seen from this RB-57 color infrared photo. County roads regularly outline square miles of land on this flat terrain. Vigorously growing crops shows up as bright red. The lighter colored upper portion of the picture is the rougher, more eroded uplands which are much less suited topographically to agricultural tillage.

Looking more closely at a mile by mile and one-half area of agricultural land, terracing, strip cropping and contour farming are indications of conservation farming practices. With proper management, land and earth resources will be available for future generations to use. How is it possible to determine the various types of crops from pictures such as these? A crop calendar tells what stage of growth various crops are at during a specific time of the year. Compare corn and oats for planting and harvesting dates. By knowing when the photo was taken and analyzing sequential pictures, the stage of growth the crop was in and when it was harvested can be determined. Comparison of the photographic data with the crop calendar allows identification of the crop.

From this early June RB-57 photo, agricultural land in eastern Nebraska is observed during land preparation. The darker red areas are forage crops or small grains which began growing early in the spring. White or blue-white fields are those where no vegetation is present. Notice the triangular airport runways.

Contrast this same area in August when most crops are growing well, as indicated by the various shades of red. Blue areas are fields of harvested small grains. Red areas are fields of corn, beans, sorghum, and alfalfa.

Westward in the area of Oshkosh, this RB-57 photo shows another agricultural pattern. The patterns are wheat-fallow strips, wheat showing as red and fallow or bare soil strips showing as white. Sparse rainfall requires that the farmer grow wheat on the land only every other year. To protect the soil from wind erosion the farmer orients the strips perpendicular to prevailing winds and alternates narrow strips of wheat with the bare soil.

Contrast this early June Skylab picture of an area northwest of Columbus in normal color with this picture in color infrared. Color infrared is very helpful for identifying crops in a complex area such as this.

In Holt County is a large area of center pivot irrigation, a very visible landmark to many of our astronauts. On the ground the center pivot irrigation system appears as a long arm with sprinklers on it which rotates in a circle about the irrigation well. The arm is usually one-fourth of a mile long and irrigates about 135 acres of a 160-acre quarter section of land. From LANDSAT the center pivots in the visible red band in July look like many little black dots, each dot being one center pivot irrigation system. From Skylab in color infrared in early June they look much different. Most of the center pivot irrigated areas do not have crops growing; therefore, showing as white dots. Those which appear partially or wholly red probably have alfalfa growing. Looking more closely, the blue portions of some of the circles show areas of moist soil, resulting from tillage or watering patterns.

Irrigation and dryland farming are commonly practiced in the same area. This RB-57 color infrared photo, taken in June, shows areas of growing crops in red and areas to be planted in white. One white fluffy cloud plus part of its dark shadow appear on the upper edge. Contrast the same area taken again in August. (Figure 6). Center pivot irrigation is particularly noticeable because of its darker red color. In the center along the right edge, notice the center pivot system. A wedge of the pie is not covered by the crop. The darker bar in the wedge is a shelterbelt of trees which prevents the farmer from irrigating that portion of the circle. He must reverse his system each time he comes to the shelterbelt to continue irrigating.

Near Bassett, is a number of center pivot irrigation systems, some with good

crop cover, some with poor crop cover. Irregular shades of color in the irrigated areas are places where a crop did not grow. Regular strips across the systems are areas where the crop has already been harvested. At a lower altitude the same type of patterns can be seen in normal color.

Lack of crop cover in portions of the center pivot irrigation system leads to severe erosion problems as evidenced by this low altitude photo of a single system. Further mismanagement leads to such severe erosion that occasionally irrigation systems have to be abondoned. Such is the case with these center pivot irrigated systems viewed from an RB-57.

The sandhills of Nebraska are by the very nature of their soils, very fragile. Under good management they provide excellent grazing for cattle. Supplemental grazing or hay production is provided by well managed center pivot irrigation systems, seen here from low altitude. Loss of vegetative cover on this grazing land leads to wind erosion. Prolonged effects of wind lead to deep and large blow-outs. Wind moves the sand, creating blow-outs and deposits the loose sand downwind from the eroded area. A constant hazard in the sandhills which can result in vegetation loss and increased erosion potential is the grass fire. LANDSAT, in the infrared waveband, recorded in 1972 the pattern resulting in one million dollars of fire damage. Known as the Mullen fire, it burned from just south of Mullen, on the left, eastward for thirty miles, being controlled at the west boundary of Halsey National Forest. A few hours later, embers were fanned by a wind which had shifted to the north and burned another area south of the original burn, stopping near the Dismal River. The white spots are blow-outs. The space program has opened up many avenues for the application of remote sensing methods; such as earth resources identification, urban and rural development, management of water resources, weather forecasting, crop production, plant disease control, and many, many more. Nebraska has been viewed from the ground, from low-flying aircraft at several hundred feet, from the RB-57 at 60,000 feet, to Skylab at 276 miles, and finally LANDSAT at 565 miles. Where do we go from here? What more can be done in making sure that Nebraska and the world will be a better place in which to live?

ACKNOWLEDGMENTS

The authors wish to acknowledge the Nebraska science teachers who wrote the workbook and field tested the entire program; Michael Jones, Winside High School, Winside; Howard Schumann, Northwest High School, Grand Island; James Shank, Omaha Westside High School, Omaha; and Donald Sutton, Seward High School, Seward, Nebraska.

They further wish to acknowledge James Buterbaugh, Melinda Murdock and Orville Friesen of the University Extension Division Instructional Media Center, University of Nebraska, for producing the slides and audio tapes; and to Bob Reck, Paul Seevers and Rex Peterson of the Remote Sensing Center, Conservation and Survey Division, University of Nebraska for providing many of the photos.

This project has been made possible through a Title V Rural Development grant with assistance from NASA, the Nebraska State Department of Education and the College of Engineering and Technology, University of Nebraska, Lincoln.

REFERENCES

Jones, M. E., 1975. Upgrading Attitudes and Increasing Performances in Science Using E.R.T.S. Proceedings, The Nebraska Academy of Sciences. Lincoln, Nebraska.

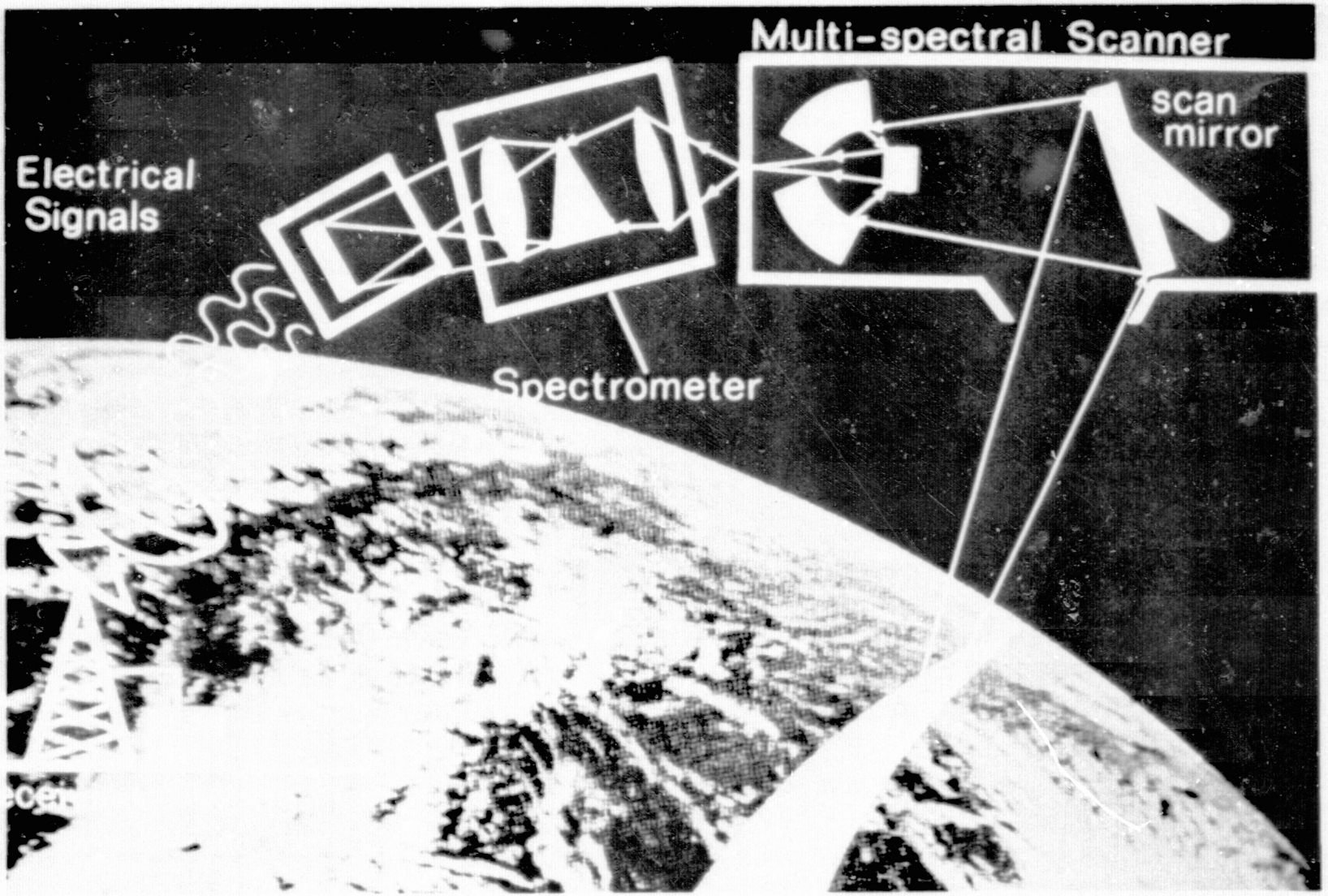


Figure 1.- Schematic view from LANDSAT.

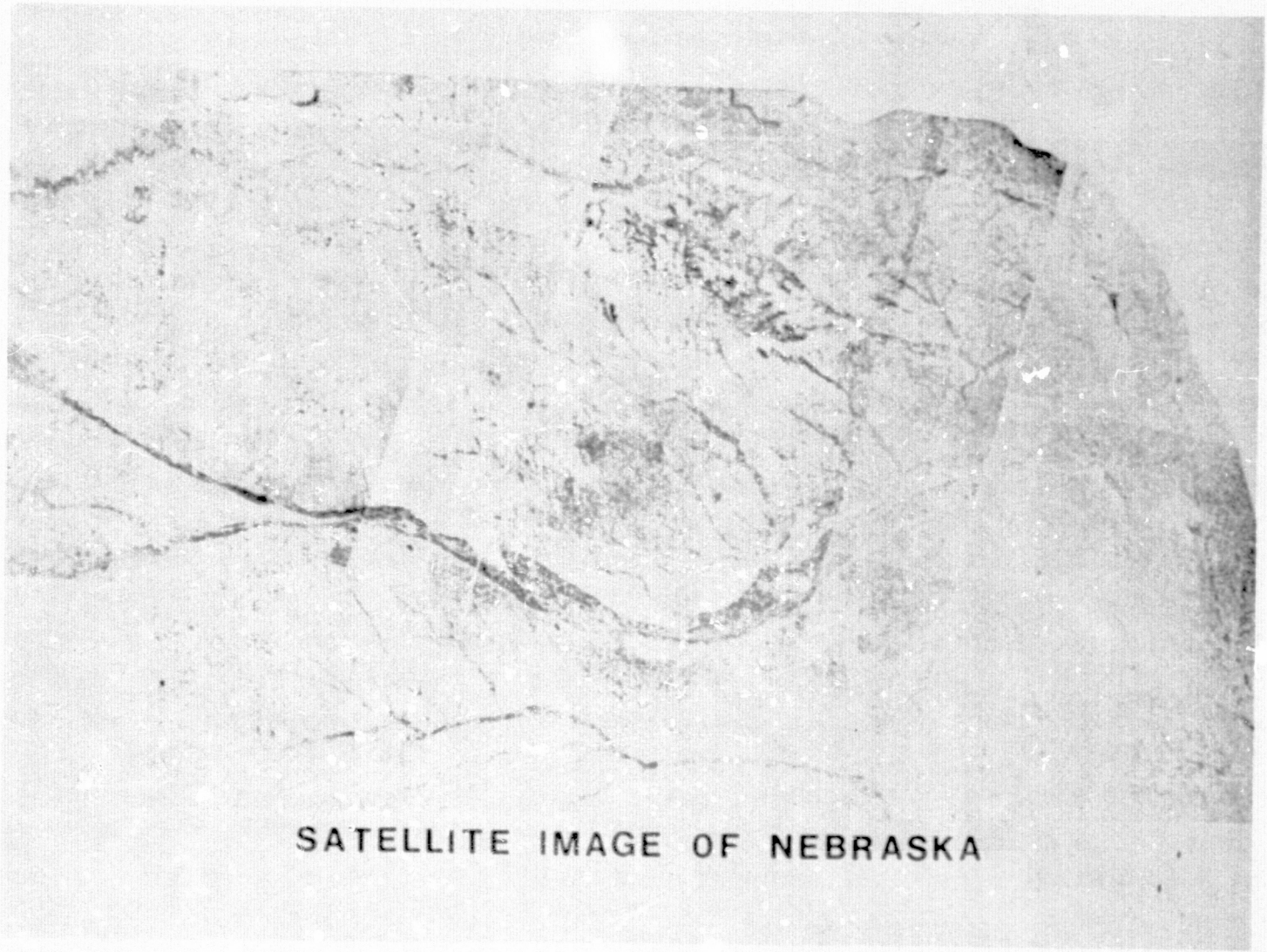


Figure 2.- Satellite imagery of Nebraska.

1233

REPRODUCIBILITY OF THE
ORIGINAL PAGE IS POOR



Figure 3.- Skylab photo of Omaha showing Epley Airport.

REPRODUCIBILITY OF THE
ORIGINAL PAGE IS POOR

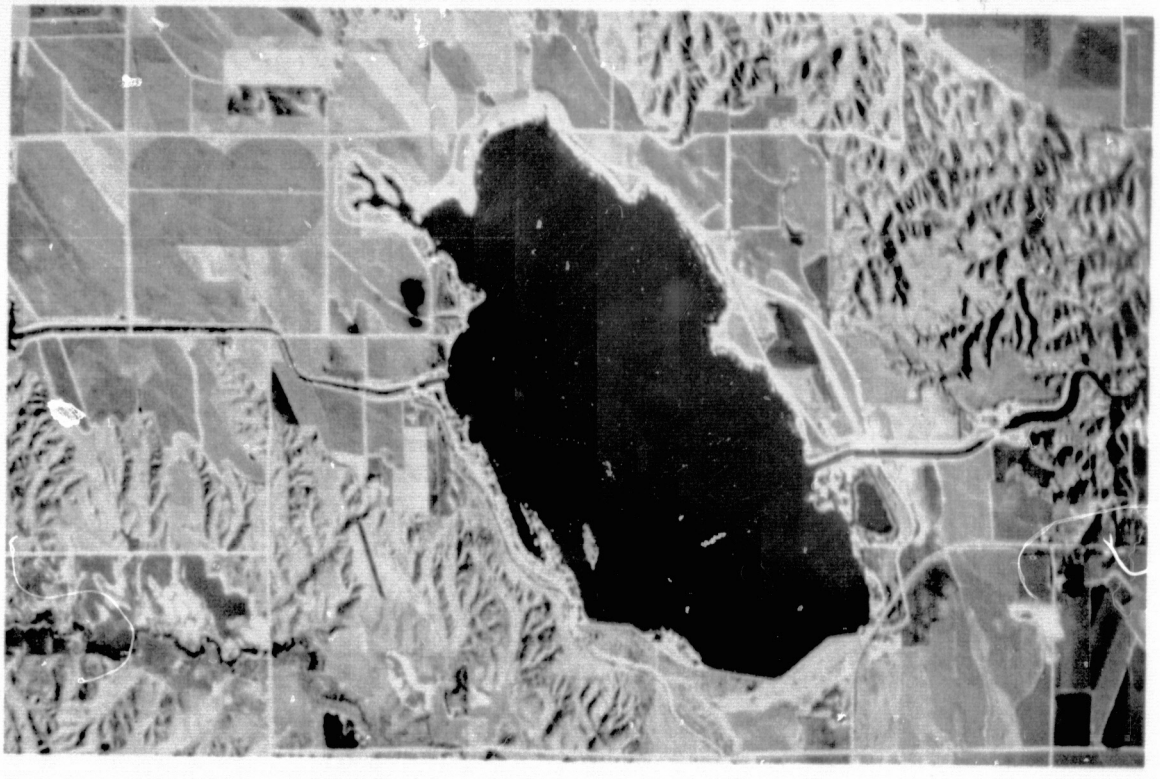


Figure 4.- Aircraft infrared imagery of water quality - Johnson Reservoir, Nebraska.



Figure 5.- Low flying aircraft infrared image of Holmes Lake, Lincoln, Nebraska.

REPRODUCIBILITY OF THE
ORIGINAL PAGE IS POOR

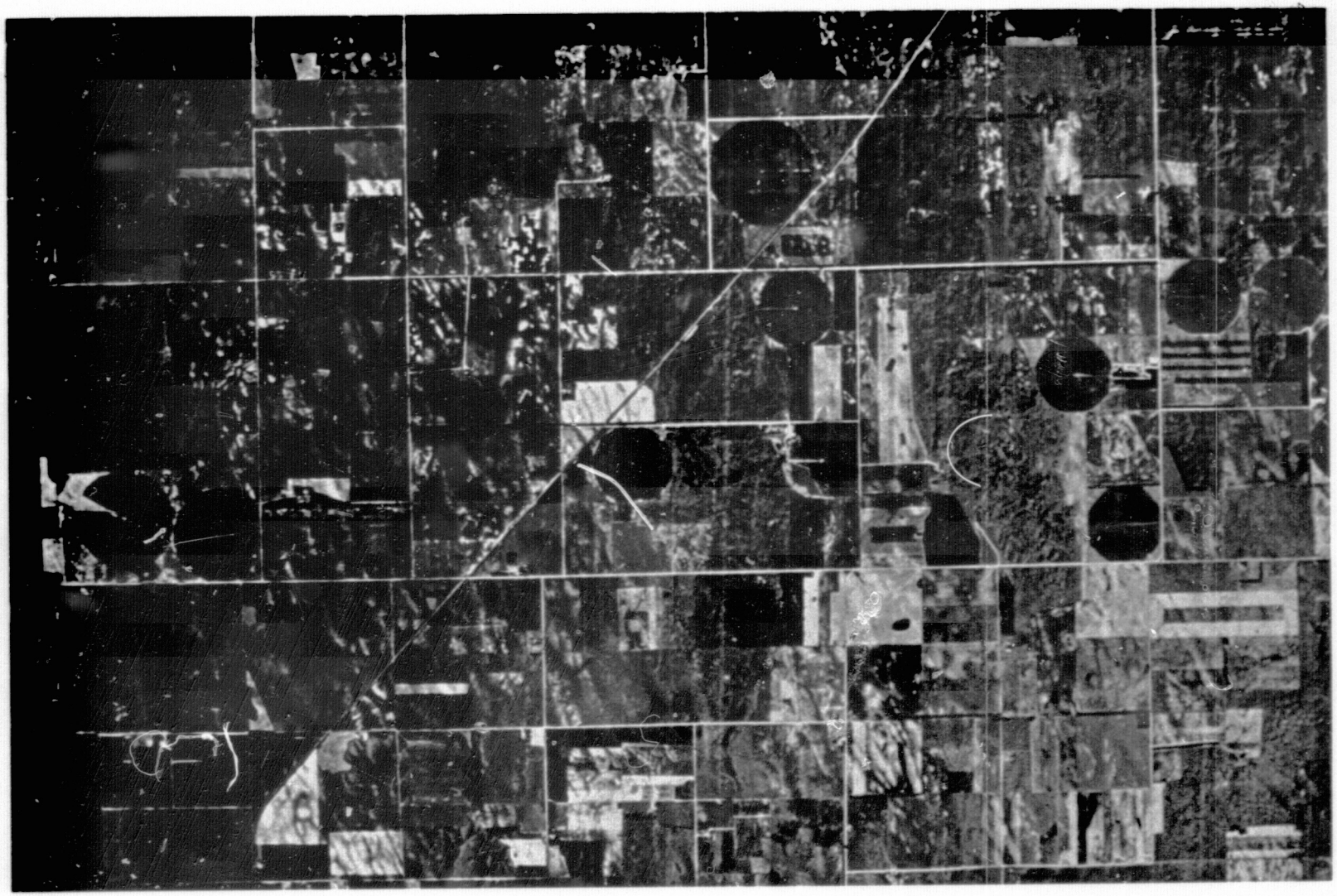


Figure 6.- Aircraft infrared image of agricultural farmland in central Nebraska showing center pivot irrigation.

AN UNSUPERVISED CLASSIFICATION OF MULTISPECTRAL SCANNER DATA USING CORRESPONDENCE ANALYSIS (CLAMS)

N76-17533

by J-M. Monget, Ecole des Mines de Paris (France), and P. Roux, Ecole des Mines de Paris (France)

ABSTRACT

An unsupervised classification method (CLAMS) has been designed as a three step procedure: dimension reduction, classification of channels and clustering of measured reflectance spectra.

The basic concept is that similar channels are most likely to characterize typical shapes of reflectance spectrum. Some results are shown which are in good agreement with the known ground truth.

INTRODUCTION

The problem of unsupervised classification of multispectral scanner data resolves to the design of a clustering algorithm which is able to separate a given set of reflectance spectra into a small number of mutually exclusive "natural" classes without any "a priori" information relevant to them.

The number of classes is usually not available and the criterion used in order to build those clusters must take into account the intensities measured in the n channels simultaneously. This fact leads to the use of a multidimensional approach.

The theoretical background of our work is mainly due to Pr J-P. Benzecri(1) who has introduced correspondence analysis in multidimensional statistics. We have adapted his research to the practical constraints of remote sensing data handling.The clustering method CLAMS, J-M. Monget(2), is mainly organized in three steps :

- the use of correspondence analysis in order to get a close look at the multidimensional structure of the raw data and perform a dimension reduction through the use of a feature space
- the determination on the reduced data of a classification which enables to find which channels are most likely to characterize typical shapes of reflectance spectrum
- the partition of the set of spectra through the use of an adaptative clustering algorithm which is initialized using the results of the preceding step.

A - CORRESPONDENCE ANALYSIS

In the first step we are looking for the structure of the data set regarding the similarity which could exist between the behavior of the channels for the entire test area. In order to do so we represent each channel as a point of a vector space E_I with I dimensions. Each of those J points is weighted by p_j which is the global energy received by the channel j.(Fig 1)

A particular similarity distance between two channels is computed, it is called the χ^2 distance and has the following algebraic formula :

$$d^2_{jj'} = \Sigma\{1/p_i(p^i_j - p^i_{j'})^2 \mid i=1,I\}$$

where :

$$p^i_j = p_{ij}/p_i$$

This measure of similarity is particularly well suited to remote sensing applications because it is equal to zero when the two channels j and j' give two proportional images. Unfortunately the definition of a similarity distance is not enough in order to directly solve our problem of seeking for groups of similar channels because the dimensionality of the initial vector space E_I is much too high. Typically I is equal to several millions of pixels for a LANDSAT image.

Correspondence analysis gives us a mean of choosing a feature space F_n of reduced dimensionality (n = 5 for example) such that the distance between the projections of two channels j and j' in this subspace is a good approximation of the "true" distance $d^2_{jj'}$ existing between j and j' in E_I. The base vectors of F_n are the eigenvectors of the cluster N_J built with the J channels in E_I and their associated weights p_j. The corresponding eigenvalues λ_α are in fact ordered by decreasing order :

$$\lambda_1 > \lambda_2 \cdots > \lambda_n$$

It is in this feature space F_n that we proceed with the other steps of our method.

B - CLASSIFICATION OF CHANNELS

In order to initialize the clustering algorithm applied to the reflectance spectra in F_n, we are previously seeking for a good estimate of the number of "natural" groups and of the associated cluster centers.

Our basic idea is in fact that groups of similar channels are most likely to characterize typical shapes of reflectance spectrum. Thus before clustering, we try to get an idea of the similarity between channels through the building of a dendrogram tree using the distances existing in F_n between all the couples of points (j,j').

In such a representation (Fig2) the heights of the branches are proportional to the diameter in F_n of the classes associated to the corres-

ponding nodes. The decision regarding the number of groups of channels and their nature is usually taken by "cutting" the dendrogram at a given diameter d. In the case illustrated where a ten channel multispectral scanner is used (B. Lacaze (3)), this leads us to six groups listed as follows :

- group 1 : channel A
- group 2 : channel B
- group 3 : channel C
- group 4 : channel D - E - F
- group 5 : channel G - I - J
- group 6 : channel H

C - ADAPTATIVE CLUSTERING OF SPECTRA

The center of gravity of each those groups is used as a potential center for a cluster of reflectance spectra. The adaptative clustering algorithm is based on a minimum distance criterion (E. Diday (4)). It is initiated as previously stated and iterated several times for the complete set of measured spectra in order to get stable clusters. At the end of the process each spectrum is associated to a specific cluster, each of these clusters being characterized by an average reflectance spectrum and associated cluster variance.

D - APPLICATION - UNSUPERVISED CLASSIFICATION OF LANDSAT-1 DATA

We present a classification generated on some sample data collected during the LANDSAT-1 experiment for the FRALIT-A project (P.I. : Dr Verger)

The results are illustrated in Fig 3 for a test area located in the Loire river estuary on the west coast of France. This environment is to be compared with areas which can be found on the East coast of United States where industrial and urban areas often mix with wetlands and forests.

Six typical spectrum shapes have been selected which average signatures are listed in Table I.

AKNOWLEDGMENTS

This research has been supported by the Centre National d'Etudes Spatiales Grant n° 73/1136 and by the Centre National de la Recherche Scientifique under the global sponsorship of the RCP- 353 for the FRALIT-B project.

REFERENCES

1 - J-P. Benzecri et al (1973)
L'analyse des données - Tome 1 : La taxinomie
Tome 2 : L'analyse des correspondances
Dunod Editeur - Paris

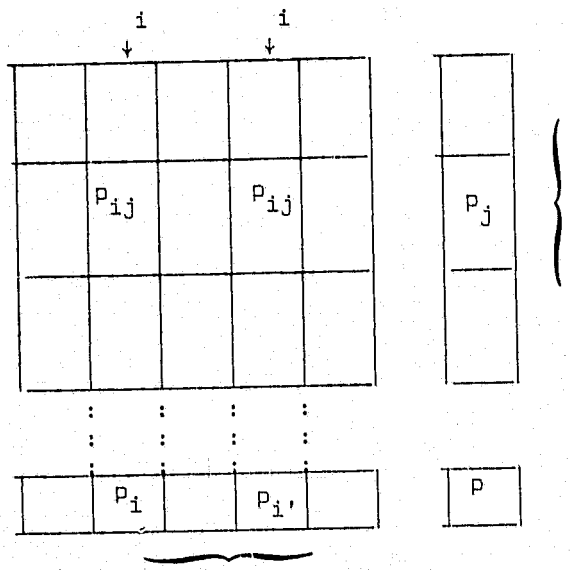
2 - J-M. Monget (1974)
Méthode de regroupement automatique des spectres de réflectance appliquée au problème de la détection à distance des ressources terrestres
Centre de Morphologie Mathématique-Ecole des Mines -Paris
(unpublished report)

3 - B. Lacaze - J-M. Monget - J. Dulac (1974)
Correspondence analysis of multiscanner data for vegetation classification
Proceedings of the 3rd Annual Remote Sensing of the Earth Resources Conference-March 1974 - Tullahoma

4 - E. Diday (1974)
Recent progress in distance and similarity measures in pattern recognition
Proceedings of the Second International Joint Conference on pattern recognition-August 1974-Copenhagen - IEEE 74 CH 0885-4C-

TABLE I - AVERAGE SPECTRAL CHARACTERISTICS OF SIX GROUPS AS DETERMINED BY THE CLAMS SYSTEM FOR THE TEST AREA DISPLAYED ON FIG 3

channel / group	MSS4	MSS5	MSS6	MSS7	
1	32,1	28,0	28,4	14,4	Industrial Suburbs
2	26,8	17,8	9,1	2,8	Water
3	27,4	22,3	34,2	18,6	Residential 1
4	25,8	19,3	38,2	23,6	Residential 2
5	27,1	21,6	31,5	20,2	Agriculture 1
6	24,7	18,4	30,4	19,1	Agriculture 2



Reflectance spectrum S_i = $\{p_{ij} | j=1,J\}$

Image C_j sensed in channel j = $\{p_{ij} | i=1,I\}$

Global reflected energy for spectrum S_i = p_i = $\Sigma\{p_{ij} | j=1,J\}$

Global energy received in channel j = p_j = $\Sigma\{p_{ij} | i=1,I\}$

Total energy received by the spectrometer = p = $\Sigma\{p_{ij} | i=1,I;j=1,J\}$

Figure 1 - Matrix structure of remote sensing data

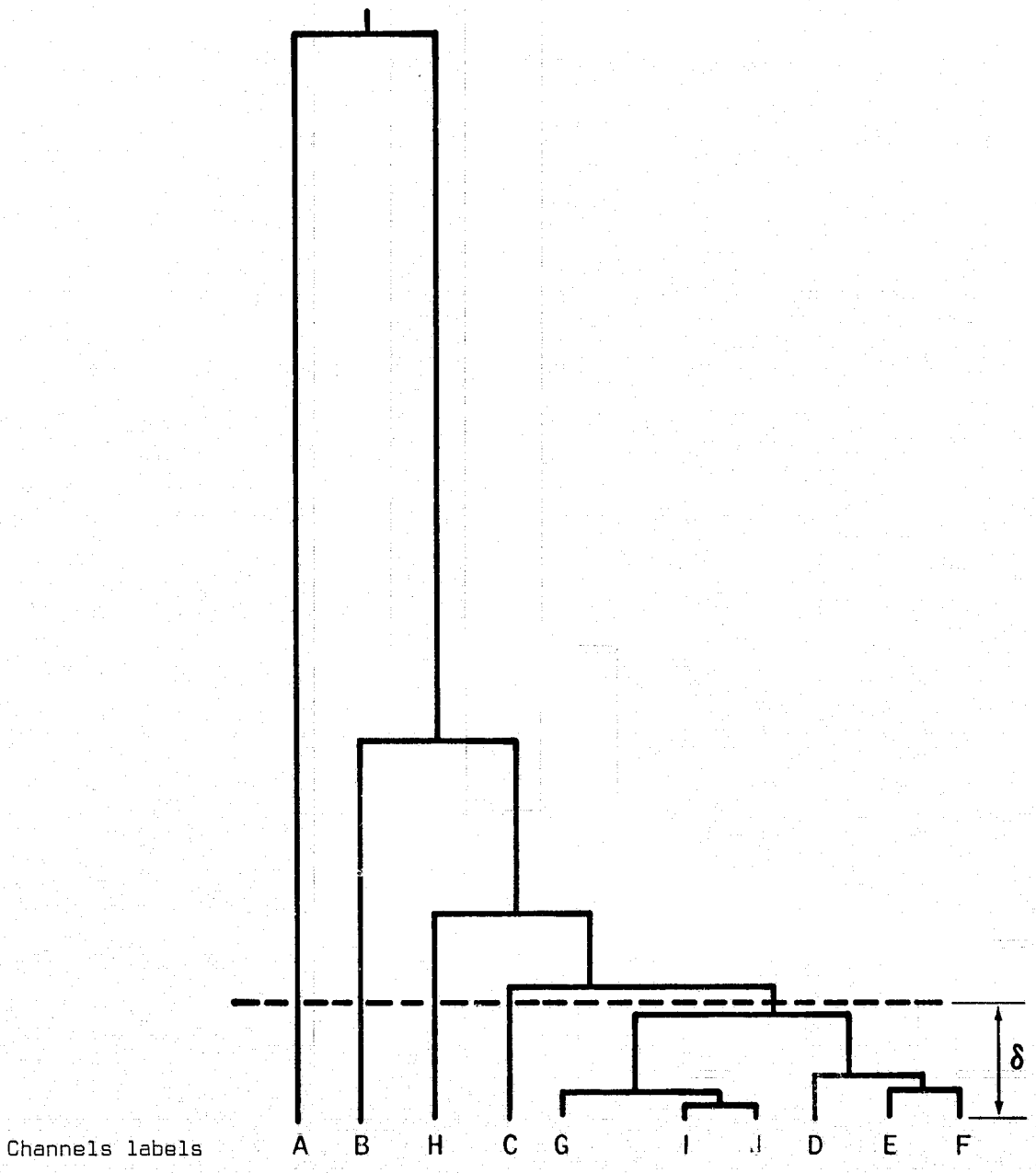
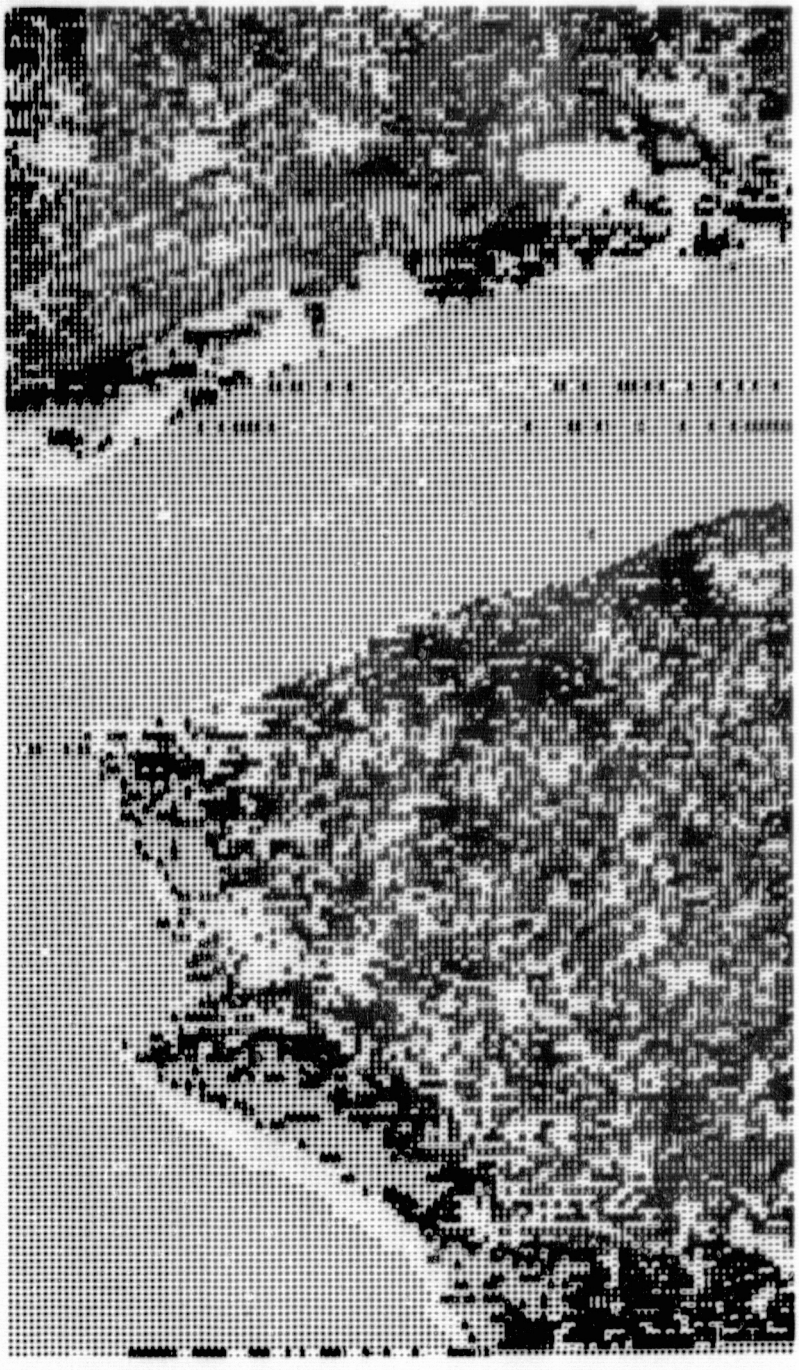


Figure 2 - Similarity structure of the channels in the feature space F_n



Document Ecole des Mines - CNES

Group nomenclature : + - Water
- - Industrial suburb
X or M - Agriculture
. or) - Residential

Figure 3 - Sample unsupervised classification of LANDSAT-1 data

REPRODUCIBILITY OF THE
ORIGINAL PAGE IS POOR

ADVANCES IN AUTOMATIC EXTRACTION OF EARTH RESOURCES INFORMATION FROM MULTISPECTRAL SCANNER DATA†

I-10

By Jon D. Erickson, Environmental Research Institute of Michigan, Ann Arbor, Michigan

N76-17534

ABSTRACT

Recent advances and present status of automatic multispectral scanner data analysis and interpretation are evaluated with problem areas identified and suggested approaches to solutions discussed. The rationale for automatic extraction is given.

The basis of spectral discrimination is briefly examined indicating sources of variability which tend to obscure the spectral attributes of the classes of interest. Spatial and temporal discrimination bases are also discussed.

Automatic processing functions, techniques and methods, and equipment are discussed with emphasis on techniques and equipment required for operational large area surveys with satellite data. Techniques for carrying out major functions of preprocessing for signature extension, feature extraction, discrimination, display, and applications modeling are examined. A Multiplicative and Additive Signature Correction (MASC) technique and a proportion estimation technique are discussed. The development of the Multivariate Interactive Digital Analysis System (MIDAS) multispectral processor system which represents a breakthrough in cost effective high throughput processing for large area surveys from satellites and aircraft is reviewed.

Applications and results are discussed briefly for agricultural crop inventories, environmental monitoring, and resources surveys from ERIM LANDSAT (ERTS) and EREP investigations to indicate the substantial progress achieved to date.

It is concluded that despite the potential indicated in the many successful demonstrations in various application disciplines in the last three years, operational uses of information derived from multispectral sensing of earth resources and land use still awaits employment of cost effective processing systems.

INTRODUCTION

It is a popular view that each of us is an astronaut on a spacecraft called earth traveling around the sun at 80 kilometers per second. Our biological community that lives on the spacecraft has a fragile life support system - the thin film of soil, air, and water in which we dwell. The net number of passengers aboard the spacecraft increases by 1.5 million weekly; their ability to consume its finite supplies in its nearly linear economy has increased tremendously in the last few decades. We see some of the results in the pollution of our environment and the shortages of vital resources. Famine and widespread starvation are seen by some experts as inevitable and imminent as the stork passes the plow.

As astronauts we need to take care of our spacecraft - to check on its status, to monitor its resources, and to see that we are not doing irreparable damage to its vital life support system. From the vantage point of a satellite orbiting the earth, multispectral scanners (first developed some 9-11 years ago by ERIM) are being employed in studies of agricultural crop inventories, environmental monitoring, vegetation assessment, and resource inventories.

I will discuss some of the latest advancements in methodology and hardware for automatic multispectral scanner (MSS) data processing in the context of an Earth Resources Survey Information System, some of the major problems and tasks that remain, and my

†Supported in part by NASA Contracts NAS9-14123, NAS1-13128, and NAS1-11979.

recommendations for their solution. The motivation and rationale for the use of MSS include higher information capacity than film, sensing outside the spectral region of photographic film sensitivity, and electronic recording.

The objective of these information systems is to have fast, reliable, and accurate automatic procedures for extracting information about the amount, location, and condition of objects of user interest and to implement these techniques in a cost effective manner on an operational basis for data from aircraft and satellites -- in short, to have a practical tool for planners and decision makers in many disciplines and institutions.

Processing of multispectral scanner data is now and will remain for some time a "semi-automatic" process requiring a man-machine interaction to achieve the desired results of identifying objects and judging their significance. However, one objective is to reduce the man-machine interaction (which slows the process) to an optimum point through displays and controls which do not unduly impede the process but allow the man to guide the processing to provide information.

The rationale for automatic processing of multispectral scanner data are summarized as follows [1].

1. automatic processing can be done in quasi-real time, that is, before the information content of the data can significantly decay in value.

2. automatic processing of large volumes of data can be accomplished more cost-effectively (not necessarily more cheaply) than manual processing and interpretation but requires non-general purpose computers for operational systems.

3. although the information volume of the desired kind may be small, the data volume is exceedingly high. Automating this data volume reduction to information frees people for creative tasks less well suited for machines.

4. automatic processing gives a potential for a greater consistency of results with objective classification standards. Some would also mention higher accuracy here for automatic over manual processing.

5. derived information from automatic interpretation is in a form for quick and easy correlation and integration with other data bases and/or models in automatic information systems such as automatic mapping and compilation of statistical records or summaries.

6. multispectral scanner data is generated and recorded in electronic form intended for automatic processing in contrast to photography in which film is the recording medium (which has poor radiometric fidelity compared to that needed in automatic processing).

A multistage sampling technique is envisaged for some operational applications whereby an earth resource or land use inventory would be performed using three data-collecting systems: satellites, aircraft, and ground observers, in that sequence. Each of these systems would provide progressively closer looks at progressively smaller areas, and would provide more detailed information about those areas. Then, the more detailed information would be applied to a much larger area for which the limited sample appeared to be representative, as evidenced by the similarity of the small areas to certain surrounding areas as recognized in the space and aircraft data. The first tests of this three stage approach for multispectral scanners have come from LANDSAT (ERTS) experiments.

But to achieve a practical tool, the sensors and automatic processors must replace a sufficient number of ground observers for the costs to be reasonable (a few U.S. dollars per square kilometer is the goal).

Earth Resources Survey Systems are used to gather information to help government, private or foreign users with statutory or other requirements to solve problems or manage resources. These systems consist of remote sensors in aircraft or spacecraft, data formatting and telemetry links, preprocessors, extractive processors, and user applications models. Remote sensors register attributes of the terrain being covered. The sensor data may be relayed to ground facilities through telemetry links. At the facilities, preprocessing and extractive processing are performed, to extract information from data. Finally, user applications

models are used to relate information outputs from the extractive processing, and ancillary data, to the user in terms most meaningful to him.

With the launch of the LANDSAT-1 satellite in 1972, the ability of remote sensors to collect periodic multispectral data was significantly increased over the previous and continuing airborne sensor capability. The potential of coverage of a given site on the earth every 18 days facilitates change detection and opens up possibilities of analysis techniques using the time signature of remote sensible terrain attributes. Finally, the ability of the LANDSAT system to synoptically view 100 n mi^2 "frames" (with 7.2×10^6 picture elements or pixels per frame) facilitates surveys of large areas, and because of this capability, more users of Earth Resources Systems data are actively interested.

At the same time, however, considerable strain is being put on the existing preprocessing and extractive processing hardware and methodology because of the potential of LANDSAT for spectral-spatial-temporal analyses, because of the high data rates involved, because of the need to correlate data with existing airborne sensors for the high spatial resolution view often required, and because of user-imposed timeliness requirements. Additionally, considerable development of the user applications model area is required if the full potential of Earth Resources Information Systems to deliver cost-beneficial results is to be achieved. I characterize this stage of developmental work as the "transition phase" between feasibility and operational use.

At ERIM, we have been exploring for ten years the utility of remote sensing derived information to various natural resources problems, to developing the system methodology and hardware necessary to rapidly provide accurate information to users at low cost, and developing user applications models to enhance the value of earth resources information. Some recent developments towards operational applications in extractive processing methodology and hardware and in user applications model development are reviewed in this paper.

Signature extension techniques and proportion estimation techniques of processing have been investigated to increase the accuracy of large area satellite surveys.

Techniques for spectral-temporal-spatial processing were developed to permit more reliable recognition of classes of vegetation and other terrain categories with distinctive time-varying spectral-spatial signatures.

To perform extractive processing rapidly to meet user timeliness requirements, a high-speed parallel digital, special purpose processor MIDAS (Multivariate Interactive Digital Analysis System) is being developed by ERIM under NASA funding. This low-cost prototype processor implements Bayesian decision or maximum likelihood classification, with versatile data processing, at rates comparable to the data collection rate of LANDSAT making a regional processing center concept realistic. The design philosophy of this processor is discussed.

Last, an example of a user application model developed to predict the yearly production of mallard ducks, an important migratory waterfowl, from remote sensing and ancillary data, is described.

EARTH RESOURCES INFORMATION SYSTEMS

With the launch of the LANDSAT-1 (ERTS-1) satellite in July 1972, the attention of many scientists focused on the application of data from multispectral scanners (MSS) to earth resources problems in the United States and throughout the world. For those of us involved in the design of prototype earth resources information systems to assist in operational resource management, LANDSAT provided a synoptic, periodic broad scale look at the earth's surface attainable only with great difficulty from previously available aircraft sensors.

While data from aircraft sensors will still be sought and used by resource managers because of its relatively high spatial resolution, LANDSAT-like (or better EOS-type) data

from satellites is also definitely here to stay. LANDSAT, because of its wide area coverage, has renewed the interest of resource managers in operational earth resource information systems which can supply them information on a routine basis. For systems designers, this is a challenge for four reasons: 1) the extractive processing techniques have been weak in large area survey capability being instead appropriate to feasibility demonstrations on single scenes which is quite a different thing entirely, meaning signature extension transformation is necessary; 2) the data rate from earth resources sensor systems increased by over an order of magnitude (to 10^{10} data vectors per week) with the launch of LANDSAT-1, creating problems of data acquisition and processing; 3) the demands for timely information from an earth resources system call for throughput requirements two orders of magnitude greater than can be obtained with currently implemented algorithms on general-purpose digital computers; 4) what information is easily extracted from the data by current processors is often not digestible to users. An enzymatic user application model must be included to make the system complete.

To discuss these points in more detail, first refer to Figure 1, which is a familiar block diagram of a typical earth resources survey system. The system begins with a sensor viewing phenomena of the terrain or ocean. The observed phenomena are the reflected or emitted spectral radiance of the scene. Sensor data is collected from remote platforms, so some method of data storage and telemetry are required. The next step in the system is geometric and radiometric preprocessing to permit production of a map-like rendition of the true radiance of the terrain. This step is an absolute necessity in operational large area surveys, but may not be needed in local feasibility demonstrations. Both geographic reference and radiometric feature invariance are a sine qua non to successful systems. The goal is to reduce the effects of distortions of geometry and of radiometric fidelity to negligible levels for further processing and analysis. This step in the procedure may require ancillary information (e.g., knowledge of spacecraft attitude and ground "control points" for performing geometric corrections and knowledge of atmospheric properties for correction of radiometric errors). The accuracy and scanner sensitivity to which these corrections must be performed are dependent on the application being addressed, and may vary widely. The geometric corrections are properly a ground acquisition station function carried out once for all users on the data.

The purpose of signal conditioning, or "preprocessing" is to provide data preparation and handling, to provide geometric and radiometric correction, to provide a convenient input format, to emphasize or enhance aspects of the input signal which are deemed important, to provide in many cases a reduction in the dimensionality of the input data, and most importantly, to provide invariance.

An almost universal approach to recognition is to extract properties or features from the original signal, and to perform the recognition on the feature profile of the input signal. This serves several functions. First, by reducing the input pattern to its essential features, the memory required for storing the signatures is reduced. Secondly, by reducing the input pattern to unique independent features, a considerable amount of invariance to exact form is obtained. Finally, a degree of invariance to noise and background may be achieved.

The next step in the system is extractive processing, designed to extract information pertinent to the user from the data. For example the user may wish to know how many lakes there are in Minnesota (claims of 10,000 not withstanding), and extractive processing could be used to map all water bodies and count them.

Most decision mechanisms are based on multivariate discriminate analysis that partitions measurement space on the basis of the training set signatures which then allows a decision to be made for an appropriate classification for each input pixel.

The function of display is attendant with each and every one of the other functions of a multispectral processing system as one facet of the man-machine interaction. Interactive

controls and commands allow the intervention of the operator to direct that certain things be done which would not otherwise be done automatically.

The user application model is the next step in the system. It is a crucial step because it translates the information extracted from the remote sensing data, adds ancillary information that a user may have at his disposal, and creates a product which can help a user make a decision. For example, suppose the previously mentioned user wanted to estimate the migratory water-fowl produced in Minnesota. Because these birds nest in or near water, the amount of water present is an important but not the only variable. The number of water-fowl present to breed is important, as are the food supply predator information. These ancillary variables are required to calculate the number of migratory waterfowl.

Carrying this example a bit further, the user may want to know the number of water-fowl to be able to set hunting limits in the fall. He will need to consider other ancillary information, such as what neighboring states are doing, before making a decision. This is the user's decision model.

The impression that user and decision models are necessarily formal, mathematical models implemented on computers is not true. Rather these models are more nearly well defined procedures that managers follow to arrive at conclusions or to convert earth resources processed data to a form they can use. The trend is to increasing formalism and mathematics in user models where inputs and outputs are usually quantifiable. Decision models, with their typical socio-economic ancillary inputs, probably will seldom be formalized to the stage where computer implementation is feasible.

With this perspective on an earth resources system, it is perhaps pertinent to point out that with increasing development of high data rate sensors (by NASA) and of user interest in outputs from the system in more timely fashion (to have maximum impact on decisions, information must be timely), the squeeze is on the middle of the system (pre-processing, extractive processing, and user model areas.) In the remainder of the paper we consider some recent advancements in extractive processing and preprocessing and in user model development which we feel begin to close the gap between the sensor's abilities to collect data and the user's desires to digest it, and the ability of extractive processing systems to keep up with the data.

THE BASIS OF EXTRACTIVE PROCESSING

Detection and discrimination of an object by multispectral sensing requires differences in the radiation received from the object and its surroundings. This radiation "contrast" is due to differences in reflectance, emittance, or temperature between the object and its surroundings.

Discrimination means devising a decision rule, based on measurements from a sample from each of two or more given classes, which will enable us to assign new samples to the correct classes when we do not know to which they belong. Classification means to assign samples into groups which shall be as distinct as possible. In discrimination the existence of the classes is given; in classification it is a matter to be determined. Supervised learning or discrimination should achieve greater efficiency because it takes advantage of available human knowledge and intelligence. In some cases, such human assistance is not possible, and an unsupervised learning approach may be required. The user defines which process is employed. Having made the distinction we use the terms interchangeably. The terms identification and recognition will also be employed for convenience.

Basic to this process of discrimination is the concept of a signature. In general, a signature is any collection of observable features of a material or its condition that can be used for precise classification. The features that make up a signature may all be observed simultaneously or in a sequence of observations spread over a considerable time period.

A basic element of spectral information extraction is the realization that spectral signatures cannot be completely deterministic. That is, spectral reflectivity and emissivity measurements of natural objects exhibit some dispersion around a mean value (i.e., spectral signatures are statistical in character). Thus, as we will use the term, a spectral signature is a probability density function (or set of such functions) which characterize the statistical attributes of a finite set of observations of a material and can be used to classify the material or its condition to some degree of fineness.

At the basis of discrimination theory is the necessity to realize that optimum discrimination techniques require not only that the procedures be tailored to recognize the item or material of interest, but also simultaneously, that they be tailored to reject other items or materials that lie in the vicinity of the desired materials but that are not of interest, i.e., the backgrounds in which the items of interest are embedded. Two types of error are possible: failure to classify all of the desired class actually present as that class and misclassification of other classes as that class. Photo interpreters commonly call these errors of omission and commission, respectively.

Examination of measurements of the spectral reflectivity and emissivity of materials as available through the Earth Resources Spectral Information System [2] can aid in the development of effective discrimination procedures (and sensors and missions also) by providing insight into the basic optical properties of the materials of interest and their natural variability. The field measurement program associated with the Large Area Crop Inventory Experiment [LACIE] is intended to support the discrimination technique development in this manner.

Pattern recognition as applied to automatic multispectral processing is discussed in terms of a statistical description of features where each pattern or picture element (pixel) is considered as a vector in n-dimensional space whose components are the simultaneous response in each spectral band from one ground resolution element. The goal of the recognition system is to define partitions in this space such that each region can be identified with a class of patterns, through the techniques of statistical decision theory.

Pattern recognition is accomplished by comparing information derived from unknown input pixels with similar data derived from known sample patterns (called signatures, paradigms, or prototypes) which come from training sets. The specification of these signatures is accomplished utilizing a learning algorithm. The important ansatz is that these signatures are truly "representative" of the class and all of the class dispersion. Based on these comparisons, a decision is made as to the nature of the input patterns.

The key to multispectral recognition is invariance. For example, it is desirable that the classification assigned to an object or pattern of interest be independent of the position of that object in the field of view, the aspect at which it is viewed; the background against which it is seen, partial obscuration of the object, minor changes within a class, and changes in illumination or atmospheric condition. It is not too difficult to provide any one of these invariances. To provide all of the desired invariances with a practical amount of hardware, however, requires that the preprocessing and feature extraction mechanism extract the essence of the classes to be identified.

Without the employment of signature extension procedures to match the conditions from training areas to unknown areas so that signatures, after correcting can apply to the unknown areas, multispectral recognition will remain a scientific curiosity without becoming a practical tool.

ADVANCES IN PROCESSING METHODOLOGY

The automatic processing R&D objective is simply stated as follows: To make large area and small area MSS-based Earth Resources Survey (and land use and pollution monitoring) informations systems practical by:

a. increasing accuracy of information extraction (mensuration, location, and correct classification)
b. decreasing cost (through powerful processing techniques which can use reduced ground observations and fast processing on low cost equipment)
c. developing means to disseminate information in user applications terms (e.g., volume of production not simply area planted to a crop)
d. decreasing time for information extraction to preserve information value from decay
e. demonstrating utility in user applications of simplest technique to meet desired performance and documenting performance achieved with various techniques to allow design of operational systems
f. employing multistage area sampling and bias correction wherever accuracy requirements can be met through this cost-saving approach
g. relaxing costly constraints on data acquisition imposed solely by weak processing techniques.

My assessment of the status of information extraction processing techniques is as follows:

1. A variety of techniques have been demonstrated to be feasible in many applications under limited conditions appropriate to showing feasibility but not generally appropriate to prototype operational conditions over large areas, that is, signature extension techniques are required.

   a. The accuracy achieved in most applications is acceptable, in others it needs to be improved before operational use will be undertaken.

   b. Little or no time constraint for processing has yet been imposed.

   c. Too much ground observation has been used.

   d. Adequate documentation of the procedures to be used with these techniques is becoming available.

2. These limitations are being lessened to the point where operational-prototype information systems are feasible in some applications.

3. The simple step of extracting adequately representative signatures for training is still somewhat elusive.

4. Further processing technique development is necessary.

The global coverage of LANDSAT opens the way for large area surveys to be accomplished at 80 meter resolution. Large areas imply greater variability between training areas and unknown areas thereby requiring signature extension techniques to overcome the significant classification degradation due to this masking effect. Atmospheric scattering and absorption by haze and water vapor modifies the spectral characteristics of reflected sunlight and this can vary with time and place. The 80 meter resolution is coarse by aircraft platform standards and greatly increases the effect of mixtures of objects within a pixel because a significant number of pixels are on boundaries. Proportion estimation techniques which can account for these boundary pixels by estimating the proportions of objects in a pixel are important.

ERIM has investigated both types of techniques with results that indicate some promise and progress.

Type 1 signature extension techniques employ a transformation of signatures to match conditions. Type 2 signature extension techniques remove the effects of variable conditions

through preprocessing as in ratioing adjacent bands. The most useful technique developed to date is a type 1 technique called MASC (for Multiplicative and Additive Signature Correction).

The types of variations which can be corrected for by the MASC Algorithm are listed in Table I. Variations which are the same for all targets, e.g., instrumental gain, and atmospheric state, can be corrected for exactly. Variations which are dependent on target type, e.g., non-Lambertian effects and reflectance changes due to different soil color, etc., can be corrected for in an average way. That is, the MASC corrections are averages over target types. That atmospheric state and sun-target-geometry are potentially important variations in the scanner signal can be seen in Figure 2 and Table II. In Figure 2 is plotted the path radiance as a function of wavelength for several atmospheres (characterized by visibility). Variations in the path radiance of over 30% are possible. Table II shows the effect on both path and total radiance of different scanner view angles. Again the effect can be substantial. Experimental evidence for the importance of these effects was obtained in the CITARS experiment using LANDSAT-1 data from Indiana and Illinois during 1973-1974. Ground-based optical depth measurements were made simultaneously with the LANDSAT overpasses. Classification accuracy was negatively correlated [3] with the difference of optical depth as a measure of haze level between test and training areas. A low-classification accuracy resulted from a large difference of haze level [4].

The MASC Algorithm has been applied to three different CITARS data set-pairs. The recognition results in Figure 3 and Figure 4 have been computed on the basis of percent of wheat pixels recognized as wheat (correct wheat), and the percent of non-wheat pixels that were not recognized as wheat (correct "other"). It is clear from the figures that the MASC transformed signatures were superior to the use of untransformed signatures for wheat recognition.

In Figure 5 the results have been computed on the basis of percent of corn pixels recognized as corn (correct corn), percent of soybean pixels recognized as soybean (correct soy), and percent of non-corn and non-soybean pixels which were not recognized as either corn or soybeans (correct "other"). Again the MASC Algorithm proved far superior to the use of untransformed signatures.

In Figure 6 we plot the average probabilities of misclassification (PoM) based on the results in Figures 3, 4, and 5. From this figure it is even more apparent that the MASC transformation can improve recognition results when non-local signatures are used. It is also of interest to note the relative stability of the average PoM for the MASC transformed signatures as compared to the untransformed signatures. Because of the random variations between data sets one would expect that the use of untransformed signatures would lead to a scatter in the recognition accuracies for different data set-pairs. An algorithm which is able to correct for these variations should yield much less variation in the recognition accuracies. From Figure 6 it is apparent that, for these data sets, this is true for the MASC Algorithm. Bias correction is more reliable with less variation.

MASC has also been used, in a blind test, to determine training fields for a data set using signatures from the previous year. In particular, signatures from Hill Co. Montana (16 July 1973) were used, with the MASC Algorithm to determine Wheat training fields in the Hill Co. segment from 11 July 1974. Figure 7 shows the location of Wheat training fields successfully identified for the 1974 data set. This MASC work was reported in [5].

Accurate mensuration or area determination using LANDSAT pixels of 80 meter footprints require more than single class decisions on the significant number of pixels containing more than one class in significant proportions. The following is taken directly from [6].

Our work on estimation of proportions was accomplished in several phases. In the first phase [7,8], a mathematical model was constructed which related the multispectral signatures of a mixture to the signatures of component materials. This model permitted the maximum likelihood estimate of the proportion vector to be formulated in terms of the observed data

point. The computational aspects of the problem required this simplification: that all of the covariance matrices of the signatures of the component materials be taken as equal to their average. Theoretical and empirical results supported the validity of this assumption. With this simplification, proportion estimation becomes a quadratic programming problem. Several existing computational methods of quadratic programming were adapted and tested on simulated scanner data. Results indicated that this method for proportion estimation was feasible.

The second phase of the program [9] included investigating the problem of detecting alien objects--i.e., objects in the scene not represented in the signature set. A procedure was devised for rejecting those pixels which probably contained significant amounts of alien materials. In addition, aircraft scanner data were smoothed over LANDSAT-sized resolution elements to simulate spaceborne scanner data. When proportion estimation techniques were tested on this data, estimates of crop acreage based on the estimated proportions were found to be better than estimates obtained with conventional recognition techniques.

The third phase of the program was devoted largely to reducing computation time required for the procedures. This was accomplished by improving the basic algorithm. It takes about 20 msec on an IBM 7094 computer to process LANDSAT signal assuming there are five signatures. In order to reduce processing time still further, averaging procedures were considered. Averaging improved the speed of estimation by a factor approximately equal to the number of points included in the average; but accuracy of estimation, contrary to theoretical expectations, was unsatisfactory. During this phase, satellite data with associated ground truth information became available. Testing of the procedures on this data, as well as results of other investigators [10,11,12] suggested extensions of the basic proportion estimation procedure.

Investigation of two extensions constitutes the fourth phase of our program currently. One extension is based on the assumption that the number of object classes that can occur simultaneously in a single pixel is very limited. Although our experimental computer program (called LIMMIX) permits taking this limit as large as 4, experience shows that two is an effective value. The other extension (called "nine-point mixtures") incorporates this limiting concept; but, in addition, utilizes spatial information. For a particular pixel, this spatial information is extracted from the signals of adjoining pixels.

These two procedures, LIMMIX and nine-point mixtures, have an important advantage over the original proportion estimation procedure, MIXMAP. A necessary requirement for MIXMAP processing is that the size of the signature set be no larger than the number of spectral channels plus one. However for LIMMIX and nine-point mixtures, the size of the signature set may be, in principle, unlimited even when the number of spectral channels is as low as two.

Preliminary tests of these new procedures were made on LANDSAT data sets. One scene contained a number of lakes and ponds and the objective of the tests was to measure the surface water acreage. The other scenes were agricultural with selected target crops. Results were encouraging.

Analysis of the results obtained by nine-point mixtures reveals that: (1) Nine-point mixtures has performed significantly better than conventional recognition as a crop proportion estimator for each data set examined. (2) Nine-point mixtures has shown itself capable of extremely accurate crop proportion estimation on one agricultural data set. (3) On the other agricultural data set, while nine-point mixtures performed better than conventional recognition, it is clear that better methods of setting the parameters should be investigated. (4) Nine-point mixtures has shown itself capable of extremely accurate proportion estimation of water, even with very small (.3 acre) lakes. (5) Nine-point mixtures appear to be consistent in this respect: it retains much of its accuracy even over small areas, as indicated by both the corn and soybean test, and the water test. (6) Nine-point mixtures is comparable to conventional recognition in processing time for a reasonable number of signatures.

The long operation of the LANDSAT-1 multispectral scanner and now LANDSAT-2 has allowed users to observe areas of interest repeatedly. Because the LANDSAT MSS has four rather broad spectral bands, extractive processing using only spectral information frequently yields imperfect separation of classes of materials of interest. Partially to overcome the degraded performance of LANDSAT spectral channels relative to those available from typical aircraft scanners, users have exploited the spatial information inherent in the LANDSAT along with the spectral data. Further, using the repetitive coverage capability of LANDSAT, some users have used the temporal variation of spectral data as inputs to the pattern recognition processors.

ERIM has explored both applications of information from LANDSAT, with promising results. In one of the approaches we have tried to spatial-spectral processing, the key step is the formation of spatial "features" or quantified attributes of the scene. Spatial features were formed from LANDSAT data over Michigan as shown in Table III [13]. These spatial features were formed by measuring variations in LANDSAT band MSS-7 signal level in a 9 x 9 array of pixels with the pixel of interest at the center. Then both spectral and spatial signatures were extracted for terrain categories in the Ann Arbor-Brighton area.

An optimum feature selection was made based on an algorithm which selects the feature which, along with the features already selected, minimizes the average pairwise probability of misclassification between pairs of signatures. The results of the optimum feature ordering are presented in Table IV. Note that 2 of the first 4 features are spatial features.

Table V summarizes the performance of the pattern recognition classifier using the twenty-two features of Table III. From the number of spatial features used in the classification, their position in the list of optimum features, and the performance of the classifier using the spatial features, one may obtain some intuition of the utility of spatial features, when used with spectral features in pattern recognition. Automatic boundary detection would be useful here.

While it would be premature to suggest that this type of spatial-spectral processing we have performed using LANDSAT data will be ultimately useful in all discipline areas particularly due to its coarsening of the spatial resolution, we still conclude that the combined use of spatial and spectral information in pattern recognition algorithms has definite promise and should be explored further. The work described above was performed for the U.S. Army-MERDC, under subcontract to ERIM from Batelle Memorial Labs.

Another approach we are developing for including spatial information without as elaborate spatial feature extraction and more importantly without the loss of resolution involves the use of multielement techniques employing a 3 x 3 pixel array in which information from 9 pixels is used in classifying the "central" pixel only. These techniques are applicable whenever a pixel is likely to represent the same material as its neighbors, as with agricultural data. The purpose of these rules is to gain recognition accuracy at only a slight extra cost in processing. Six classification rules have been derived, implemented, and tested in a preliminary way [14]. BAYES9 is based on the assumption that a pixel probably represents the same material as its neighbor, the degree of dependence specified by a parameter which can vary from 0 to 1. Preliminary testing indicates BAYES9 with an improved threshold test combines improved accuracy in class area interiors with sensitivity to detail on class boundaries. Improvement over single pixel classification is consistently achieved and therefore should be explored further. Work on automatic boundary detection and sample classifiers is also promising greater accuracy as well as efficiency.

Because of the periodic coverage of LANDSAT, the temporal variation of spectral signatures can be utilized to help discriminate objects. This capability is enhanced with LANDSAT data over the previously available aircraft data because the periodic coverage is obtained from a sun-synchronous orbit, although separate radiometric correction of each pass may be needed. Further, the data are obtained from a relatively stable platform and at small scan

angles from the nadir (typically $\pm 5.5°$). Both facts greatly ease the data registration problem-that of merging data collected at two different times so that pixels are precisely overlaid to form data vectors of twice as many components.

To illustrate the advantage of multitemporal spectral processing, consider the following example of mapping of natural vegetation in northern Michigan. (The work being discussed here was performed for NASA under grant NGR23-005-552).

Table IV shows the signatures of a mixture of hardwoods, conifers, and grass and shrub swamp on two different dates -- June and March. Shown are the mean values of the signatures, with the standard deviations in parenthesis. Notice that in June, the two classes signatures overlap appreciably in each LANDSAT channel -- the mean difference between classes is less than the standard deviation in each channel. A pattern recognition device hopelessly confuses these two classes in June.

But in March, the two classes are more separable, as shown in the second half of Table VI. This separation of some classes at one time of year and not at others can be exploited to improve maps of natural vegetation areas. Now the challenge is to understand how vegetation signatures change with time, so that we may specify exactly when data are to be collected. The effects of misregistration of temporal MSS data on classification accuracy is also being studied [15].

A second advantage of the periodic coverage is the ability to monitor the development of agricultural crops. While cloud coverage over agricultural areas significantly influences the amount of periodic coverage available, the coverage can still be used. The potential exists for crop yield prediction, by comparing the crop development, as sensed from LANDSAT, with a crop calendar of normal development.

ADVANCES IN PROCESSING EQUIPMENT

My assessment of current multispectral processing equipment systems to meet the needs of keeping pace with multispectral data acquisition which occurs typically at rates of hundreds of kilopixels/sec or megapixels/sec is given below:

1. Sensor capability generally exceeds processing capability by large factors.
2. General purpose digital and analog implementations of present techniques will not keep pace with the needs of most operational-prototype earth resources information systems.
3. Multiple general purpose digital computer approach is probably too costly (except in very special cases)
4. Implementation of special purpose parallel processing with improved techniques appears promising from both throughput and cost aspects but requires experience in the use of systems like MIDAS.

Despite work on faster techniques, presently available conventionally organized digital computers are too slow (with current algorithms) by orders of magnitude so that even many computers per sensor are still inadequate. The Multivariate Interactive Digital Analysis System (MIDAS) system is an attempt to solve the problem of real time multispectral data processing in an operational system. We have been aware of this problem since the initial design and operation of the first multispectral scanner and processing equipment at ERIM over 10 years ago. A real-time processor (SPARC - SPectral Analysis and Recognition Computer) was completed in 1967, allowing parallel decision operations using a multivariate maximum likelihood algorithm thus making possible for the first time, rapid processing of

12-band data [16]. It was evident that a considerable amount of assistance and time was needed by the user in setting up such a machine and controlling its operation. This led to the evaluation of a hybrid system employing a general-purpose digital computer for control by the user of the system [17], and finally to an all digital system.

Processing of remotely sensed data is an interactive process in which the man and machine must, in fact, be considered as the real processing system. This is not apparent in general purpose computer processing systems using software classifiers since the machine is so slow by comparison to parallel digital approaches that an operator is easily able to keep pace with the task (hours or days is the normal time interval). In this MIDAS system, where the parallel-pipeline digital processor is substantially faster (a LANDSAT frame of 7.2×10^6 pixels could be classified into 16 classes in 40 seconds), the time required by an operator is longer than that used in processing. Increases in processor speed will then provide little improvement in throughput. It becomes evident that well designed, interactive display and control subsystems will, in reality, offer the greatest gains in throughput.

The objective of providing greater speed also includes much lower cost. This is true not only for the operational situation but also for research and development. It has been estimated that processing costs in an operational system can be reduced by about a factor of twenty or more from some typical processing costs based on present day feasibility studies on general purpose computers. Costs may be determined by the time required for training. For LANDSAT costs as low as $500/frame may be possible.

MIDAS represents a breakthrough in the field of multispectral scanner image analysis by providing a low-cost capability for user-oriented, interactive, near-real-time, digital analysis to produce thematic mapping with instantaneous or multi-temporal data. MIDAS is 6 to 10 times cheaper than ILLIAC IV and reliable in operation. MIDAS accepts data from aircraft or spacecraft MSS in the form of high-density digital instrumentation tape, 7- or 9-track multidensity computer-compatible tape, or analog tape, and makes use of proven multispectral processing techniques (including signature extension feature extraction) within an innovative hardware approach resulting in a cost-effective, user-controlled system for multispectral analysis and recognition. Its hardware and software are intended to require a minimum amount of instructional training for successful operation. MIDAS is intended to provide multispectral analysis for applications in disciplines such as agriculture, regional and urban planning, forestry, energy and mineral resource location in geology, pollution detection, hydrology and water resources management, and others. Features may be extracted on the basis that their radiation properties are spectral, spatial, temporal, and (possibly) polarization-dependent, thus giving a very general and powerful capability. MIDAS provides a comprehensive data management and processing log system to greatly aid the user in data retrieval and efficient processing control.

The first MIDAS was built as part of the NASA Advanced Applications Flight Experiment program by ERIM to demonstrate the unique advantages of a modular, special-purpose multispectral processor which offers a wide selection of high-performance subsystems, peripherals, and features. In this machine the parallel digital implementation capabilities of a low-cost processor are combined with a mini-computer to achieve near-real-time operation of a complete processing system that includes multiple, user-selectable, preprocessing functions and color displays.

The overall system hardware is shown in Figure 8. The MIDAS system [18] consists of several principal subsystems: the general purpose computer (DEC-PDP-11/45), used for analysis and control but not preprocessing or classification, the input subsystem, the feature extractor/preprocessor, the control subsystem, the digital classifier, and the output displays. Figure 9 shows the user interactive displays.

The input subsystem accepts data stored on: 1) High Density Digital Tape (HDDT), 2) Computer Compatible Tape (CCT), and 3) Analog Tape. The HDDT input is the desired input medium because of its high data rate and digital format. Data stored on HDDT's at 20,000 bits per inch and played back at 120 inches per second gives a data rate of 2.4 megabits per second per channel. For ten channel data this is a bit rate of 24 megabits per second. Another advantage of HDDT is the efficient storage of data and a NASA standard format for Earth Resources Surveys has been recommended. The data contained on an HDDT may be as much as on fifty CCT's.

The second input medium is 7- or 9-track multidensity CCT. The availability of data from many sensors on a common format is desirable, however, the time to produce such tapes from the original data has been quite long and may make the data out of date. The data rate from CCT is at least an order of magnitude below the system capacity. A 58 megabyte disk is provided on the PDP-11/45 for data storage and storage of classification results.

The third medium of data input is from analog tape through the use of multiple A/D converters. This is an efficient data storage medium capable of maximum data rate for the MIDAS system.

The preprocessor performs signature extension preprocessing calculations as needed. These are: 1) calculation of 2-dimensional radiometric correction functions, both additive and multiplicative; 2) selecting and calculating channel ratio transforms, and 3) calculating a 16 spectral band to 8 or 4 linear combination dimension reduction transform.

The calculation of signature extension correction functions is a step normally required [19] to remove path radiance or other atmospheric and angle dependent variations from LANDSAT or aircraft data.

Ratio transforms [20] may be used in preprocessing to provide data which is relatively insensitive to illumination and transmission variations, where transference of signatures from one frame to another is desired, or where spectral features can be enhanced. There is no clear-cut means of examining a data set to decide, in an a priori manner, which of several possible transforms is needed for a particular scene. The method used would normally be one in which each of several transforms are performed on the training sets and the resulting data is tested for the optimal probability of correct classification using the training set and test set data to choose the transform to be employed.

The purpose of the linear transform [21] is to provide a new set of data in which the spectral data is combined in such a manner that the dimension-reduced, transformed data has essentially the same discriminability for the classes of interest to the user as the untransformed data. This has the desirable effect that the classifier can perform a classification operation in which the accuracy of classification using the smaller number of dimensions is equivalent to that obtained with a larger number of untransformed dimensions.

The digital classifier performs a Bayesian decision with a priori probabilities or a maximum-likelihood decision, assuming a multimodal Gaussian multivariate distribution. This assumption has been well justified at this time by over 100 experiments using multispectral data at ERIM [17] and, as time goes on, by more and more experience at NASA and other centers. Although simpler algorithms can perform well for some data sets [4], a significant percentage of applications demand this powerful decision rule. No penalty in speed and only a small additional cost occurs for using this algorithm.

The actual computations are performed by sets of time-shared arithmetic units arranged in parallel pipelines. Each stage supplies its results to a subsequent stage for further processing. Precision varies between 8 and 16 bits as the data progresses through the pipeline and acquires greater significance.

It will accept up to 16 input signals and can classify the results into one of 17 classes (including the null class) at its output. The decision rate is 200 x 10^3/second

allowing classification of an entire LANDSAT frame in less than one minute, although the system is not limited to a frame at a time nor 4 band MSS data.

A three color video display using a high resolution shadow-mask CRT and a MOS storage for display refresh offers an interactive capability (RAMTEK GX-100B) configured to hold a 5 bit color vector with 512 x 512 elements on the display.

The display offers image display, alphanumerics, vector generation, 2 movable cursors, digital zoom and move or moving window display and table look-up of predetermined colors. This color display and associated black and white interactive CRT for menu selection, histograms and scatter plots, and alphanumeric information display provides the major interface for a fast man-machine interface. A scene or portions of a scene can be displayed immediately upon user request for interactive training set analysis with arbitrary shaped bounding of training and test areas. By having the ability to change colors quickly on the CRT through use of the table look-up, enhanced pictures can be viewed which help locate training sets of arbitrary shape. These enhanced pictures may also be put in hard copy form.

An extremely important device for the MIDAS system is a fast color printer. The most attractive method is the ink-jet printer since it produces a usable output immediately with no delay for color processing. This is capable of producing a picture of about 1.1 x 10^6 elements in 2 minutes or less on a 875 x 1285 point format on 8 1/2 x 11-inch paper or transparency.

Having this fast turnaround for intermediate or final recognition results will permit the user to be much more efficient. This is especially true when enhanced false color maps of training areas can be made quickly. Present LANDSAT data sets can take up to 40 man hours of analysis to locate training sets because of low contrast on single channel black and white hardcopy, and because of the poor quality of available hardcopy.

In developing a complex system of digital hardware such as MIDAS, it is necessary to provide diagnostics which provide a quantitative report on the performance of the hardware for fast, low cost maintenance. Diagnostic programs have been developed which make use of a diagnostic bus designed into the system: 1) an automatic in-place fault isolation diagnostic, 2) classifier sub-assembly diagnostics, 3) off-line individual card diagnostics, and 4) a classification accuracy analysis package.

USER APPLICATION MODEL DEVELOPMENT

One critical portion of the Earth Resources Survey System is the User Application Model, which relates the output of the extractive processors and ancillary data to generate information which a user can employ directly. User models may be very simple -- if the user wants a map of vegetation types, the output of the extractive processing may directly serve him directly, and the user application model is absent. But if a Department of Agriculture official wants to know what is the projected wheat production in Kansas, the user model may combine the total productive acreage of wheat (obtained from a remote sensing system), with some farmer's estimates of the yield of particular fields, and some estimates from the weather service of future weather trends, to calculate the total production of wheat in Kansas.

As an example of a user application model, consider Figure 10. This model predicts the population of migratory waterfowl, given the water supply conditions, the food supply conditions, and ancillary variables such as number of nesting pairs, predation, and mortality. Also shown in Figure 10 on the right are elements of the decision model used by the USDI Fisheries and Wildlife Service. The model shown is, at present, conceptual and represents the work of FWS personnel. ERIM and FWS are working jointly (under NASA funding from LANDSAT and Skylab programs) to develop remote sensing multistage sampling inputs to this model [22]. [See also the paper in this Symposium by E. Work and N. Roller.]

Figure 10 shows at the left, inputs to the user model. Asterisks indicate those types of information obtained from low altitude aircraft-borne observers (supplemented by ground observations), and data potentially derivable from remote sensing techniques. The goal of the user model is to estimate the fall population of mature and immature birds. Old birds are estimated by low altitude aerial survey and ground counts of nesting pairs on a sampled basis. Estimates of summer mortality are also made from ground observations and past experience. The number of breeding pairs, coupled with the May and June pond numbers are used to estimate the number of new ducks. This information is augmented by the number of broods obtained on a sampled basis from ground survey.

Hunting regulations are defined based on the population size, the estimate of harvesting of ducks in Canada, and the carrying capacity of the habitat. Remote sensing has an impact in assessing capacity of habitat, especially in the assessment of quantities and distribution of natural vegetation.

As an example of the annual production equation, Figure 11 shows a linear equation in several variables which FWS personnel have derived to predict new production of mallard ducks. The coefficients of the model are derived on the basis of historical experience. If similar models can be constructed for other species, then the general user-decision model of Figure 11 can become more operational.

CONCLUSIONS

Despite making substantial progress in achieving improved processing techniques, improved throughput parallel processing systems, and showing the practical use of multispectral sensing in various earth resources applications under limited conditions, there is still much to be accomplished before multispectral scanner surveys provide successful, operational user information systems for earth resources inventories environmental surveys. Potential benefits of such information will remain largely "potential" until this "transition phase" work is done.

Pattern recognition with careful feature extraction to obtain uniqueness and invariance of features is an important technique in achieving accuracy in surveys. Contributing to an understanding of how to achieve uniqueness and invariance have been major developments in modeling radiative transfer through the atmosphere, vegetation canopies, rock and mineral surfaces, and other object-of-interest/background combinations. Although no general solution to signature extension has been found, MASC represents a very promising approach. Active MSS sensors which may yield more unique and invariant data than always available from passive MSS sensors are being developed.

Other accuracy developments of significance are the proceduralization of signature extension techniques in agricultural crop inventory applications and documentation of performance, adaptive decision-directed classifier techniques, and geometric correction and rectification schemes. A better understanding of training is still needed. Multi-stage area sampling and bias correction techniques can improve accuracy in some resource-limited situations.

For satellite data the development of proportions estimation techniques which can accurately handle pixels on boundaries which contain more than one class has major importance for accuracy of area determination.

Second only to accuracy is efficiency. The need is very great for modern processors to be fast to keep pace with the sensors and low cost without loss of accuracy. Of course, they also need to be convenient and easy to use as well. The earliest breakthroughs to operational applications may come from developments such as MIDAS, a special purpose MSS processor, augmented by registration capability. Significant developments in linear combinations, fast channel selection, linear decision rules, and table look-up schemes have helped the general purpose computer approach to be efficient. Geological techniques have been developed which are now being used operationally for resource exploration by commercial ventures. These include sequential classifiers and techniques employing laboratory spectra in decision rules.

A substantial research software system embodying accurate and efficient procedures and techniques for information extraction exists at ERIM. It is a single system of flexible, user tested algorithms as well as research techniques still under development (whose use is optional). A computer-based data management system for fast data location and retrieval also is employed routinely.

As for the future, we believe that substantial improvements in the technology will yet be made and we look forward eagerly to participating in the further developments for the benefit of the users of these information systems. The potential of multitemporal coverage may lead to accuracy improvements particularly for agricultural surveys and possibly efficiency improvements as well if the ground observation requirements are reduced more than the data management and registration requirement imposes. With the availability of satellite coverage providing the needed repetitive data in quantity, the development of multitemporal techniques, already begun, can proceed. Spectral-spatial approaches also show potential for improvements over spectral features.

Greater spectral coverage in more bands than LANDSAT at some finer spectral resolution (narrower bands) and radiometric sensitivity (higher signal-to-noise) for automatic processing of future MSS satellite data may also yield benefits. S-192 was a step in this direction but greater sensitivity and finer spatial resolution may also be needed by the users interested in terrain as opposed to oceanography applications.

ACKNOWLEDGEMENTS

I wish to acknowledge my co-workers at the Environmental Research Institute of Michigan whose work I have drawn so heavily upon for this paper. The work discussed here was performed by various ERIM staff, especially Robert Crane, Robert Henderson, Harold Horwitz, Richard Kauth, Frank Kriegler, William Malila, Richard Nalepka, Wyman Richardson, Norman Roller, Fred Thomson, and Ed Work. Various contracts supported the work, including NAS5-21783, NGR23-005-552, NAS1-11979, NAS1-13128, NAS9-14123, and Battelle subcontract to contract DAAK02-73-C-0438. This paper is largely based on [1, 23, 24].

REFERENCES

1. Erickson, J.D., "Automatic Extraction of Information from Multispectral Scanner Data", delivered to the 12th International Congress 1972 of the International Society for Photogrammetry Civic Centre, Ottawa, Canada, 1972, and published in the Archives.

2. V. Leeman, D. Earing, R.K. Vincent, & S. Ladd, "The NASA Earth Resources Spectral Information System: A Data Compilation", May 1971;
V. Leeman, R. Vincent, & S. Ladd, "The NASA Earth Resources Spectral Information System: A Data Compilation First Supplement", 1972; Second Supplement, 1973.

3. J.F. Potter, "Atmospheric Effects in CITARS Data", Lockheed Electronics Co., Houston, (unpublished, 1975).

4. W.A. Malila, D.P. Rice, & R.C. Cicone, "Final Report on the CITARS Effort by the Environmental Research Institute of Michigan", Report NASA CR ERIM 109600-12-F, 4/75.

5. R.G. Henderson, G.S. Thomas, & R.F. Nalepka, "Methods of Extending Signatures and Training Without Ground Information", ERIM Report 109600-16-F, May 1975.

6. H.M. Horwitz, J.T. Lewis, & A.P. Pentland, "Estimating Proportions of Objects from Multispectral Scanner Data", ERIM Report 109600-13-F, May 1975.

7. H.M. Horwitz, R.F. Nalepka, P.D. Hyde, & J.P. Morgenstern, "Estimating the Proportions of Objects Within a Single Resolution Element", Symp on Remote Sensing of Environment, Report No. 10259-1-X, 5/71, WRL, IST, U. of M. Ann Arbor, Michigan.

8. R.F. Nalepka, H.M. Horwitz, and P.D. Hyde, 1972, "Estimating Proportions of Objects From Multispectral Data", Report No. 31650-73-T, WRL, IST, U. of M., Ann Arbor, Mich.

9. R.F. Nalepka, and P.D. Hyde, 1973, "Estimating Crop Acreage From Space-Simulated Multispectral Scanner Data", Report No. 31650-148-T, Environmental Res. Inst. of Mich.

10. W.A. Malila and R.F. Nalepka, 1973, "Atmospheric Effects in ERTS-1 Data and Advanced Information Extraction Techniques", Symposium on Significant Results Obtained from the Earth Resources Technology Satellite-1, Vol. 1, Goddard Space Flight Center, Greenbelt, Maryland.

11. F.J. Thomson, 1973, "Crop Species Recognition and Mensuration in the Sacramento Valley", Symposium on Significant Results Obtained From the Earth Resources Technology Satellite-1, Vol. 1, Goddard Space Flight Center, Greenbelt, Maryland.

12. W. Richardson, 1974, "A Study of Some Nine-Element Decision Rules", Report No. 190100-32-T, Environmental Research Institute of Michigan, Ann Arbor, Michigan.

13. R.J. Kauth, R.B. Crane, and W. Richardson, "Feasibile Demonstration of Processing ERTS Data for Global Terrain Cluttering Mapping", ERIM Report 106600-1-L, 1974.

14. W.R. Richardson and J.G. Gleason, "Multispectral Processing Based on Groups of Resolution Elements", ERIM Report 109600-18-F, March 1975.

15. W.A. Malila, R.H. Hieber, and R.C. Cicone, "Studies of Recognition with Multitemporal Remote Sensor Data", ERIM Report 109600-19-F, March 1975.

16. F.J. Kriegler and M.M. Spencer, "A Statistical-Spectral-Analysis and Target-Recognition Computer, Final Report", U of M Report 8640-17-F, 1968.

17. R.E. Marshall and F.J. Kriegler, "Study of a Hybrid Multispectral Processor", ERIM Report 31650-154-T, 1973.

18. F.J. Kriegler, S. Lampert, M. Gordon, R. Marshall, R. Kistler, and D. Christenson, "MIDAS, Prototype Multivariate Interactive Digital Analysis System - Phase I", ERIM Report 195800-25-F. 1974.

19. R.F. Nalepka and J.P. Morgenstern, "Signature Extension: An Approach to Operational Multispectral Surveys", ERIM Report 31650-152-T, 1973
R. Vincent, G. Thomas, and R.F. Nalepka, "Signature Extension Studies", ERIM Report No. 190100-26-T, 1974.

20. R.F. Nalepka, "Investigation of Multispectral Discrimination Techniques", U of M. Report 2264-12-F, 1970.

21. R.B. Crane, T. Crimmins, and J.F. Reyer, "Feature Extraction of Multispectral Data", Conf. Proc. of Machine Processing of Remotely Sensed Data, Purdue Univ., 1973.

22. E.A. Work, Jr., R. Gilmer, and A.T. Klett, "Utility of ERTS for Monitoring the Breeding Habitat of Migratory Waterfowl", presented at ERTS Significant Results Symposium, Washington, D.C. 1973.

23. J.D. Erickson and F.J. Thomson, "Recent Advancements in Information Extraction Methodology and Hardware for Earth Resources Survey Systems", ICC Conference, Minneapolis, Minn. 1974.

24. J.D. Erickson, "Advances in Automatic Extraction of Information From Multispectral Scanner Data", Proceedings of the Commission VII Symposium 1974 of the International Society of Photogrammetry, Banff, Canada 10/74.

TABLE I.

TYPES OF DATA VARIATION POTENTIALLY CORRECTABLE BY MASC

A. Instrumental - System Gain

B. Environmental

Changes in Atmospheric State
Changes in Sun-Target-Scanner Geometry
(For non-Lambertian targets the correction is an average over target types)

C. Scene

Changes in Reflectance
(Correction is averaged over target types)

TABLE II.

SCAN ANGLE EFFECTS ATTRIBUTABLE TO THE ATMOSPHERE
(Calculated from ERIM Radiative Transfer Model)

Azimuth Relative to Sun, ϕ	Scan Angle Relative to Nadir θ	Spectral Radiances* ($mW/cm^2 \cdot sr \cdot \mu m$) λ = 0.55 μm Path	λ = 0.55 μm Total	λ = 0.75 μm Path	λ = 0.75 μm Total
38°	(-) 6°	2.51	4.70	0.98	2.78
	0°	2.71	4.90	1.06	2.86
218°	6°	2.98	5.17	1.17	2.96

Percent Change From Nadir (θ=0°) Value

ϕ	θ	λ = 0.55 μm Path	λ = 0.55 μm Total	λ = 0.75 μm Path	λ = 0.75 μm Total
38°	(-) 6°	-7.3	-4.2	-7.2	-2.8
	0°	0	0	0	0
218°	6°	10.2	5.5	10.1	3.7

Percent Change From One Side of Nadir to Other

Scan Angle Change	λ = 0.55 μm Path	λ = 0.55 μm Total	λ = 0.75 μm Path	λ = 0.75 μm Total
-6° to +6°	18.9	10.1	18.7	6.6

*Target Reflectance = Background Albedo = 8%
Solar Zenith Angle = 39°
Optical Thickness of Atmosphere = 0.3812 for 0.55 μm
and 0.2854 for 0.75 μm

TABLE III. SPATIAL FEATURES DERIVED

1-4	mean signal level in each LANDSAT channel over 9 x 9 array (μ_4-μ_7)
5-8	standard deviation over 9 x 9 array in each LANDSAT channel (σ_4-σ_7)
9-14	normalized indicator of inter-channel covariance between LANDSAT channels over 9 x 9 array (R_{45}-R_{67})
15-22	average power in 4 spatial frequency bands (from 1/2 pixel to 1/5 pixel) for bands MSS-5 and MSS-7 (Q_{25}-Q_{55} & Q_{27}-Q_{57})

TABLE IV. ORDERING OF SPATIAL-SPECTRAL FEATURES FOR TERRAIN CLASSIFICATION USING JUNE MICHIGAN LANDSAT DATA

No. of Features	Feature No*	Prob. of Misclassification
1	1	77
2	11	41
3	20	24
4	4	18
5	8	14
6	2	13
7	22	12
8	10	11
9	5	10
10	6	8
11	3	8
12	9	8

*See Table III for Identity of Features

TABLE V. PERFORMANCE OF CLASSIFIER USING SPECTRAL/SPATIAL FEATURES

		TRUE CATEGORY				
		WATER	SOIL	URBAN	FOREST	AG
ASSIGNED CATEGORY	WATER	19	1	0	0	0
	SOIL	0	0	0	2	4
	URBAN	0	0	21	0	0
	FOREST	0	1	1	18	9
	AG	0	1	1	3	35
	UNCLASS	2	2	1	1	1
	AVERAGE PER CLASS	50%	17%	87%	75%	71%

OVERALL AVERAGE CORRECT CLASSIFICATION 76%

TABLE VI. SIGNATURES OF TWO VEGETATION CLASSES ON TWO DAYS

JUNE	MSS-5	MSS-5	MSS-6	MSS-7
Hdw/Conif/Grass	27.32	17.82	49.62	27.53
	(0.91)	(1.45)	(5.52)	(3.88)
Shrub/Swamp	27.69	17.25	47.06	25.75
	(1.20)	(1.53)	(5.69)	(3.94)
MARCH				
Hdw/Conif/Grass	29.96	28.07	29.93	15.82
	(3.75)	(3.11)	(2.96)	(1.28)
Shrub/Swamp	23.69	20.25	22.19	11.38
	(1.74)	(4.04)	(3.60)	(2.60)

Mean Signature Values are Shown, With Standard Deviations in Parenthesis.

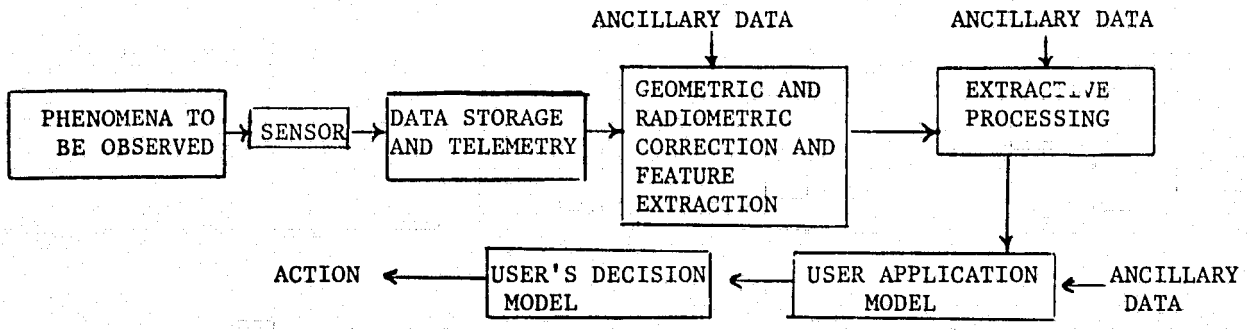


FIGURE 1: TYPICAL EARTH RESOURCES SYSTEM

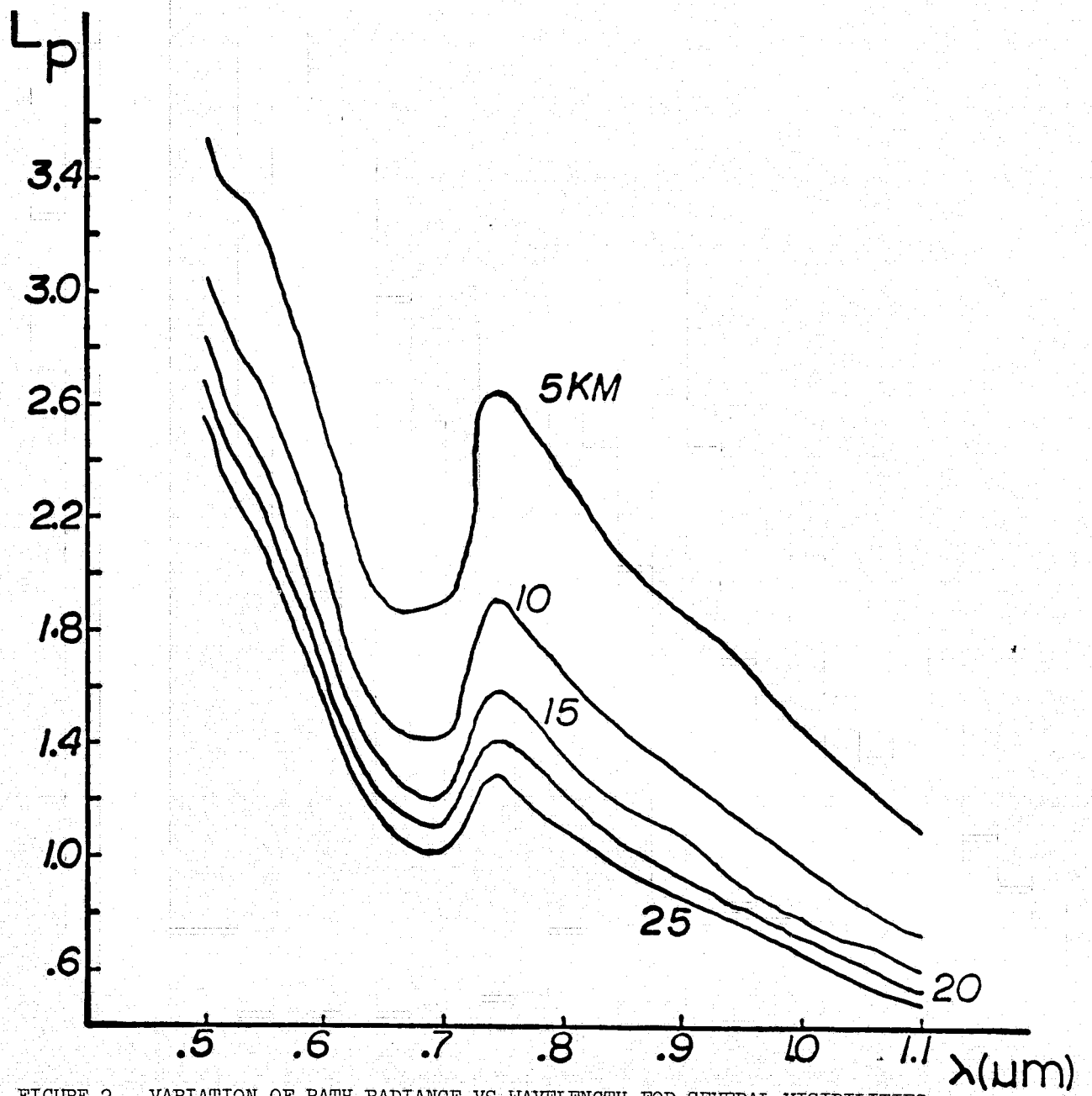


FIGURE 2. VARIATION OF PATH RADIANCE VS. WAVELENGTH FOR SEVERAL VISIBILITIES. (CALCULATED FROM ERIM RADIATIVE TRANSFER MODEL)

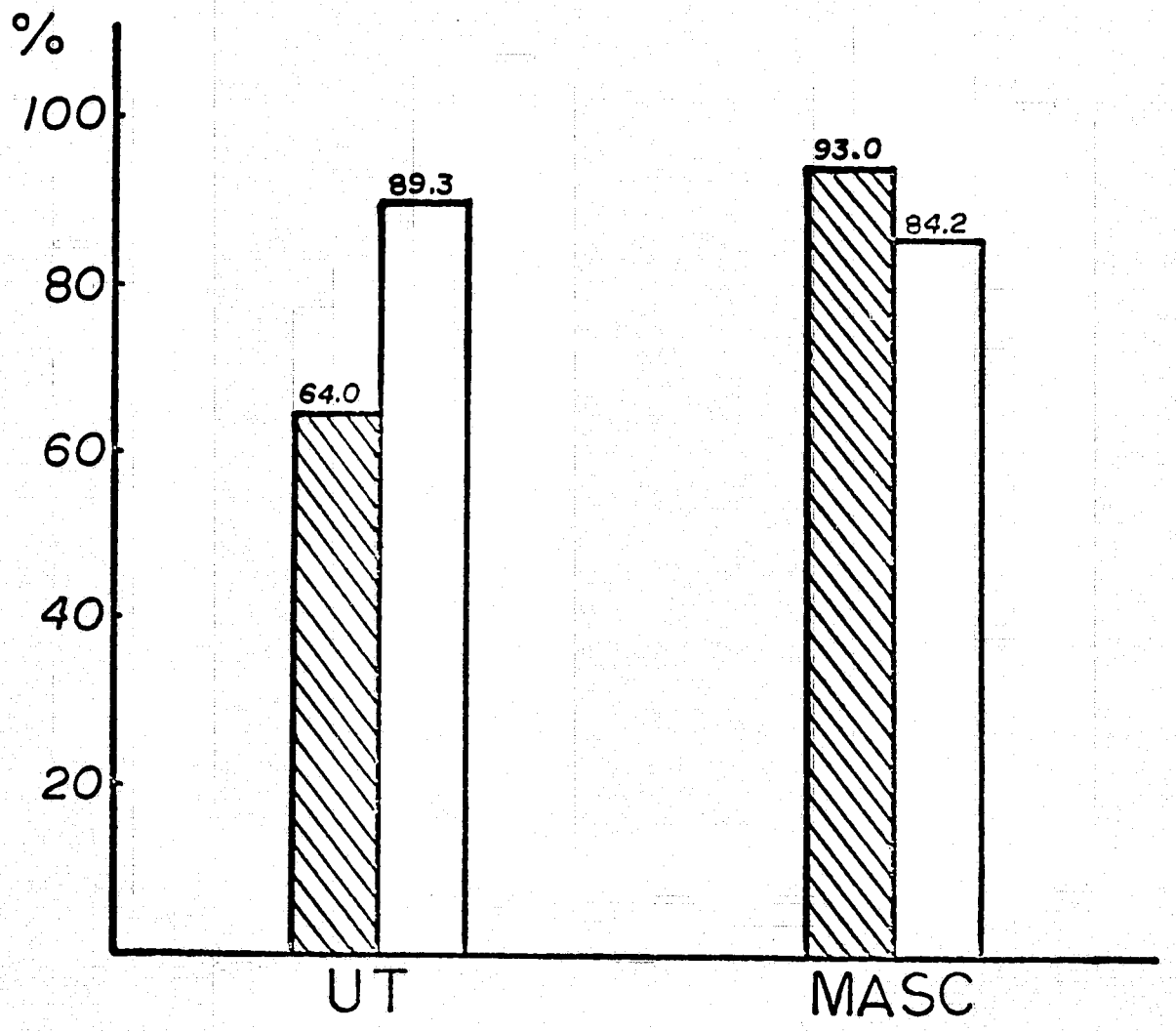


FIG. 3 RECOGNITION OF FAYETTE, ILL., JUNE 10 USING SIGNATURES FROM FAYETTE, ILL., JUNE 11 (UT--untransformed signatures, MASC--MASC transformed signatures. Striped bar is correct wheat recognition; open bar is correct "other" recognition.)

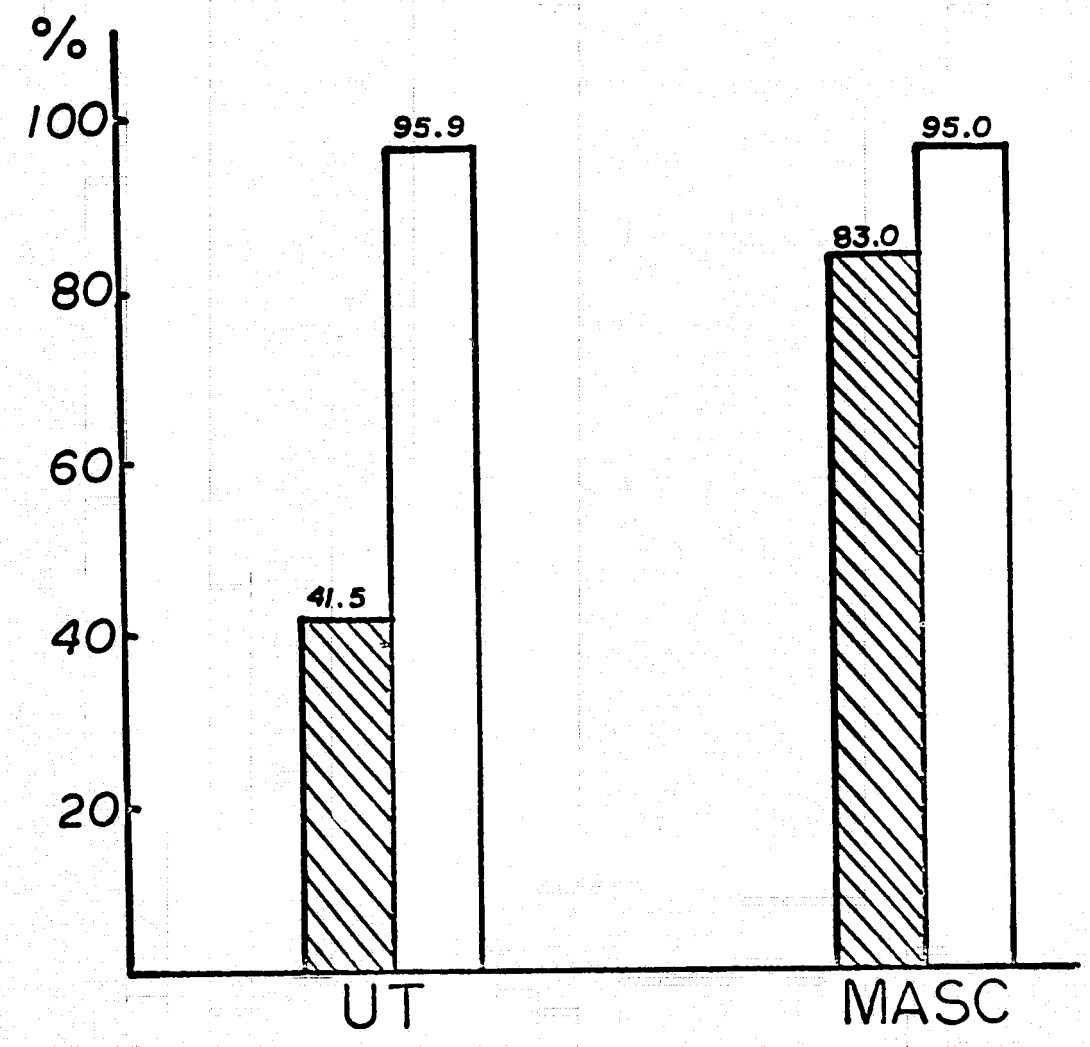


FIG. 4 RECOGNITION OF SHELBY, IND., JUNE 8 USING SIGNATURES FROM FAYETTE, ILL., JUNE 11 (UT--untransformed signatures, MASC--MASC transformed signatures. Striped bar is correct wheat recognition; open bar is correct "other" recognition.)

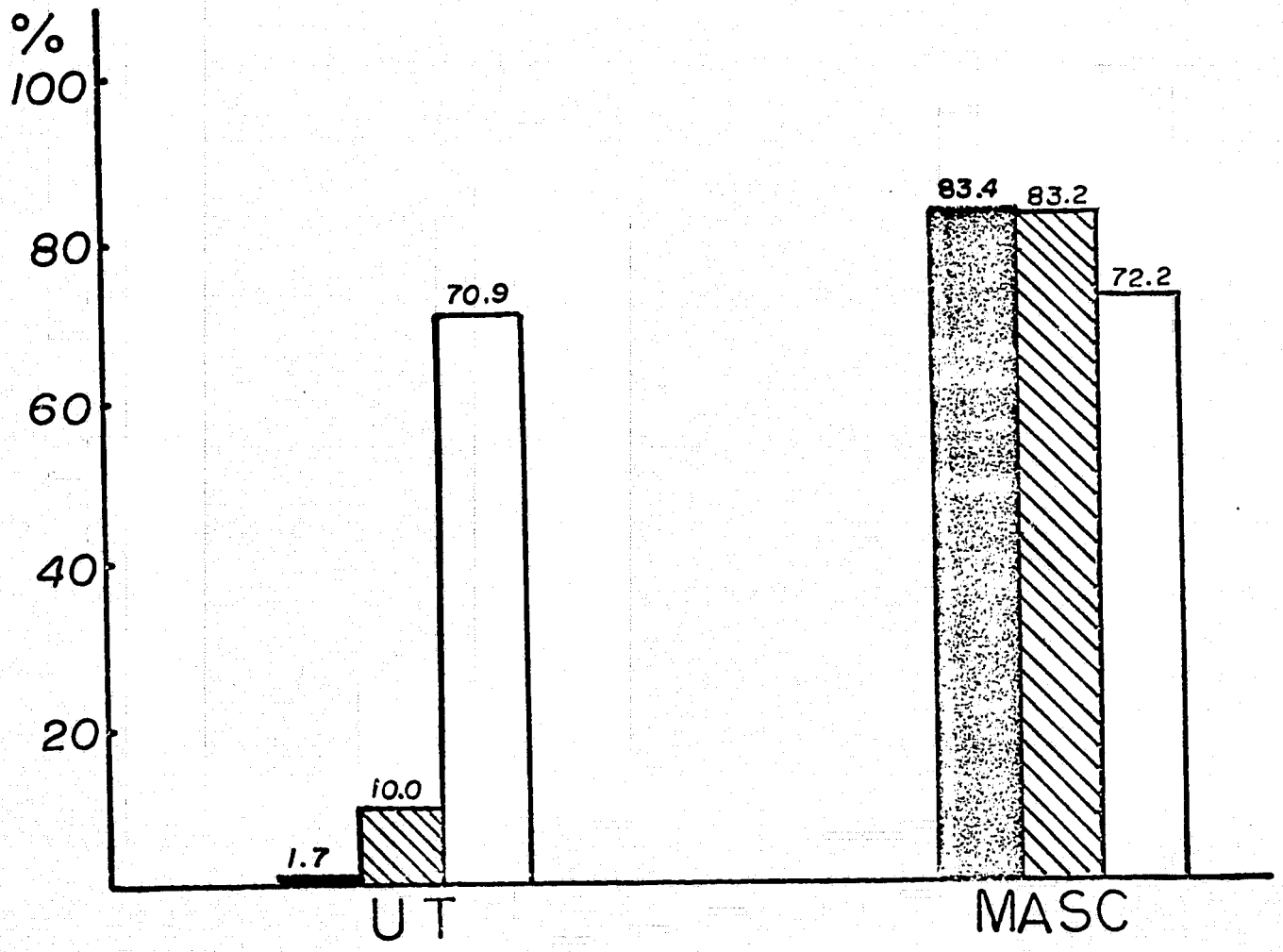


FIG. 5 RECOGNITION OF FAYETTE, ILL., AUGUST 21 USING SIGNATURES FROM WHITE, IND., AUGUST 21 (UT--untransformed signatures, MASC--MASC transformed signatures. Solid Bar is correct corn recognition; striped bar is correct soybean recognition; open bar is correct "other" recognition.)

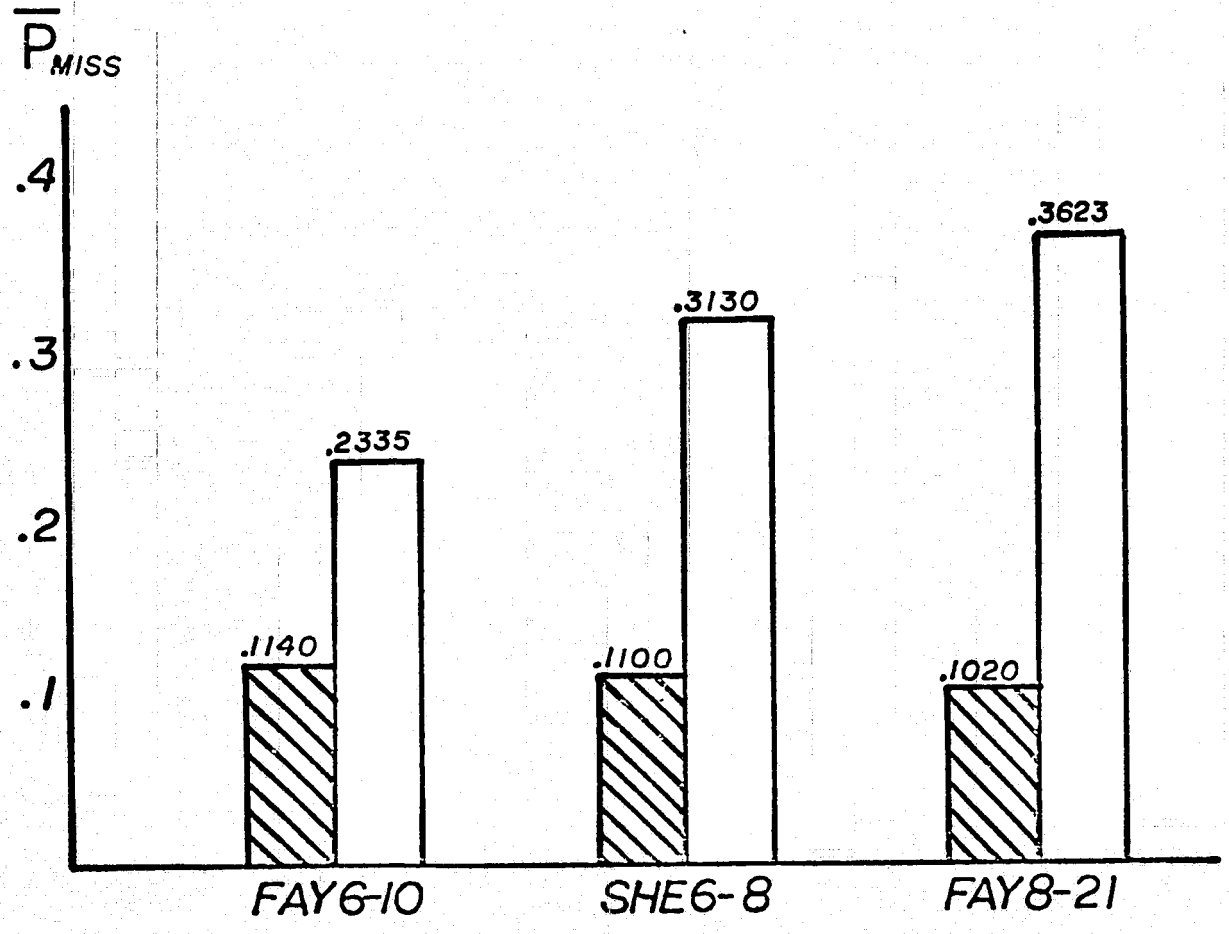
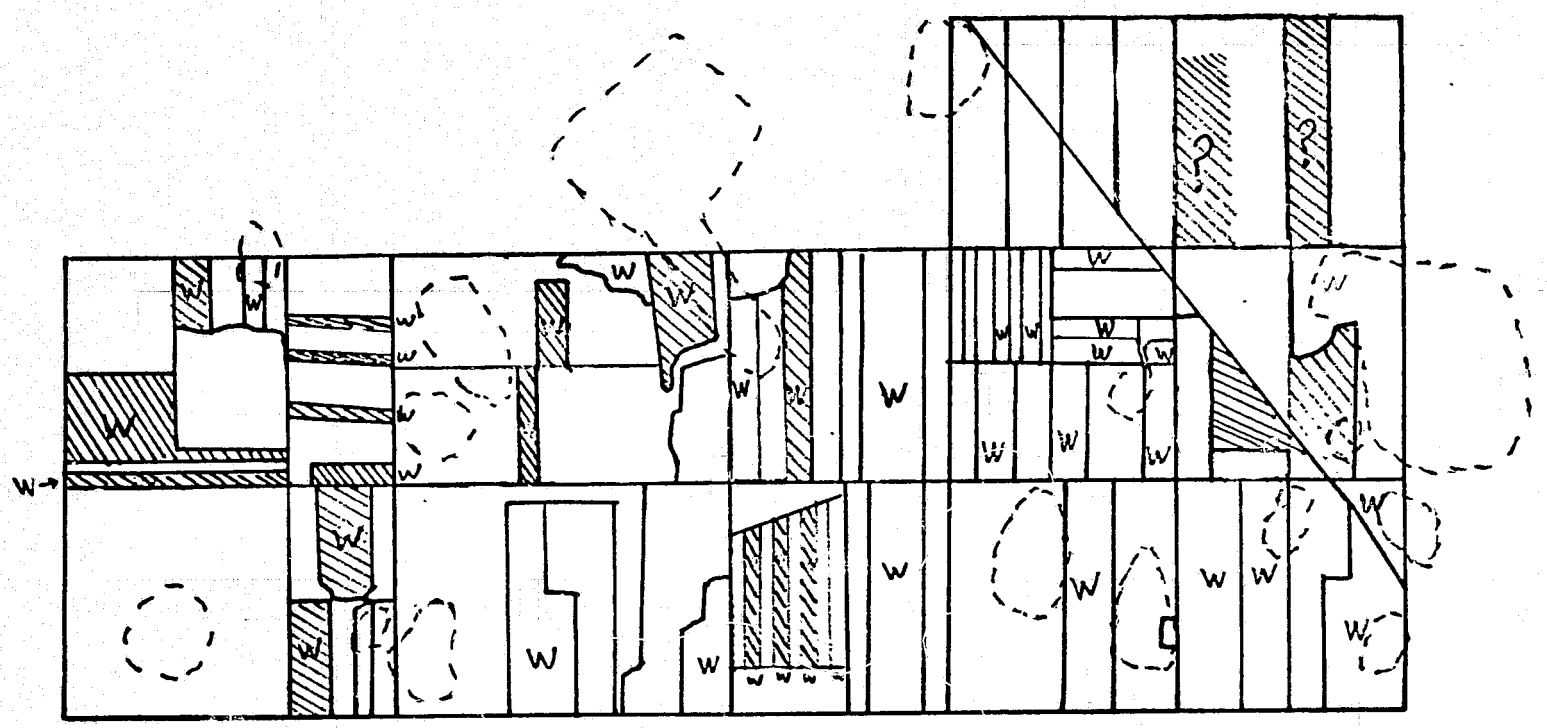


FIG. 6 AVERAGE PROBABILITY OF MISCLASSIFICATION

(Striped bar is for MASC transformed signatures; Open bar is for untransformed signatures)



HILL Co(N) July 11, 1974

Cross Hatched - Fields Identified For Training Using MASC Transformed Signatures From Hill Co(N) July 16, 1973

W - Wheat Fields Identified By Ground Information (No Ground Information Available For Block of Fields in Upper Right)

Dashed Outlines - Clouds or Cloud Shadows

FIGURE 7

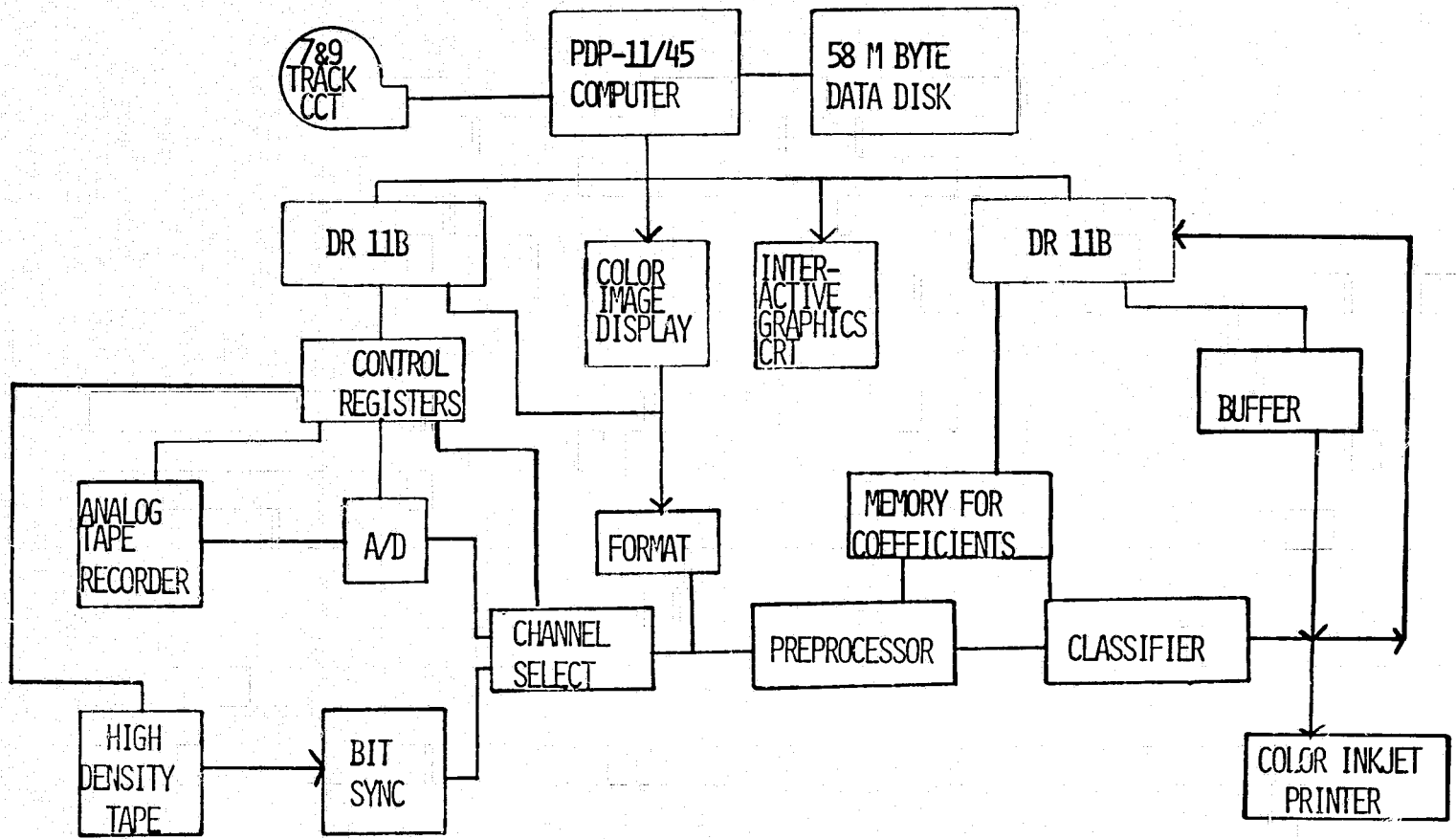


FIGURE 8. OVERALL MIDAS BLOCK DIAGRAM

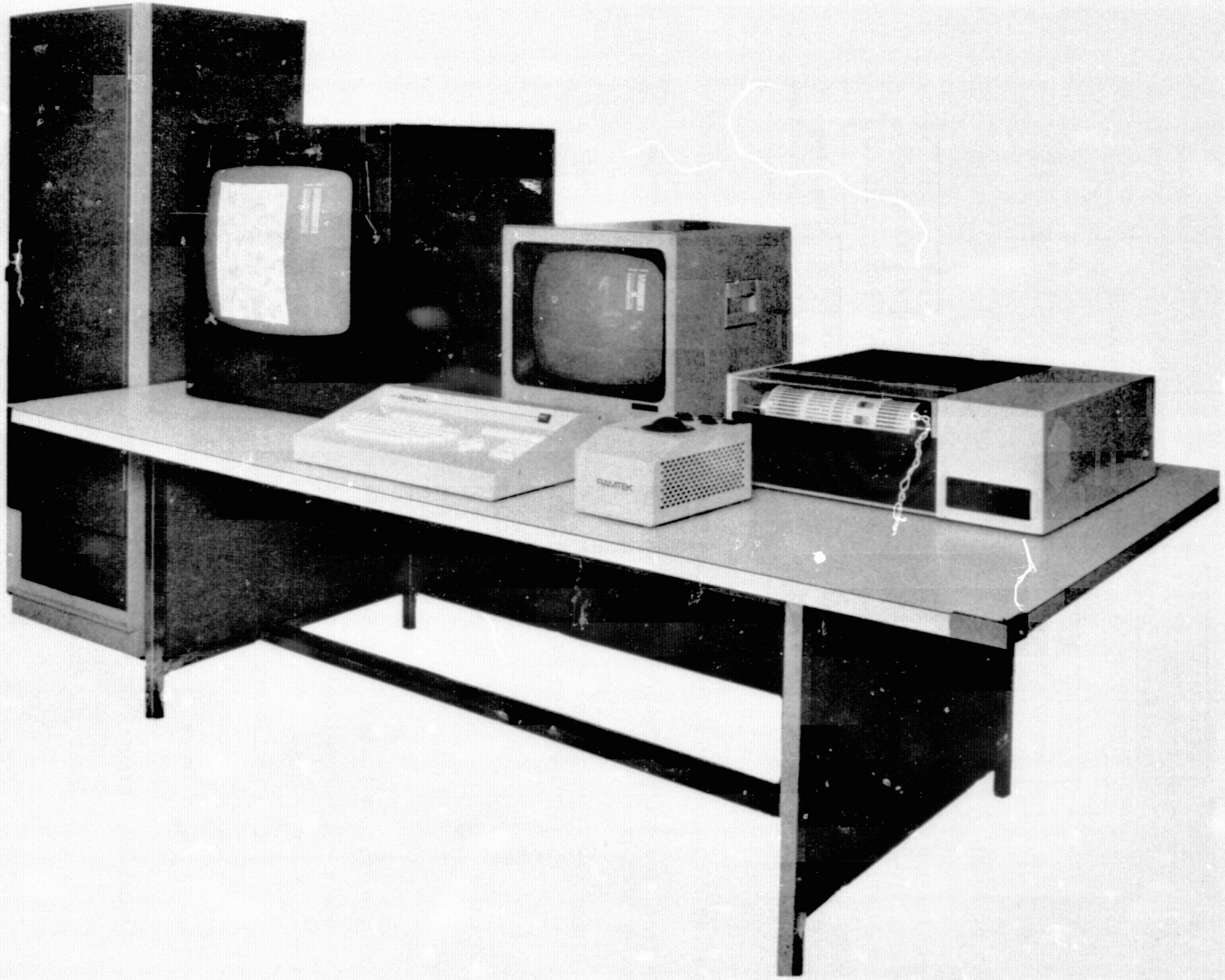
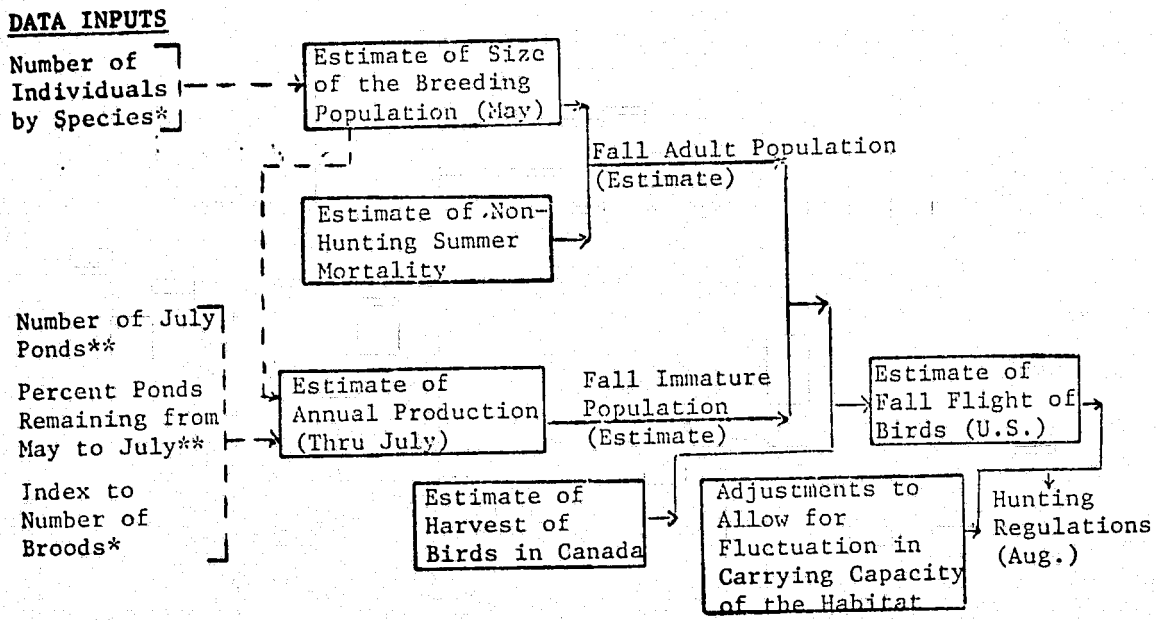


FIGURE 9. MIDAS: A MODERN PROCESSOR FOR EARTH RESOURCES SURVEYS WITH SATELLITE AND AIRCRAFT MULTISPECTRAL SCANNERS, 1975.



*Obtained from aerial observations and adjusted based on selected ground counts

**Obtained from aerial observations--data potentially derived using remote sensing techniques

FIGURE 10. DETERMINING HUNTING REGULATIONS BASED UPON THE ESTIMATED MAGNITUDE OF THE FALL FLIGHT OF MIGRATORY WATERFOWL

$$\hat{Y} = 79.26 + 1.468\ X_1 - 0.624X_2 - 0.028X_3 + 0.016X_4$$

where $\hat{Y}$ = Predicted number of mallard young (millions)

X_1 = July ponds (millions)

X_2 = continental mallard breeding population (millions)

X_3 = percent of ponds remaining from May to July

X_4 = index to number of broods (thousands) unadjusted

FIGURE 11. EXAMPLE OF A MODEL FOR PREDICTING ANNUAL PRODUCTION OF YOUNG MALLARDS. (After Geis, A.D., R. K. Martinson, and D. R. Anderson (1969))

IMAGE 100: THE INTERACTIVE MULTISPECTRAL IMAGE PROCESSING SYSTEM

By Earle S. Schaller, General Electric Company, Space Systems Department, Beltsville, Maryland, and Robert W. Towles, General Electric Company, Ground Systems Department, Daytona Beach, Florida

N76-17535

ABSTRACT

The need for rapid, cost-effective extraction of useful information from vast quantities of multispectral imagery now available from aircraft or spacecraft has resulted in the design, implementation and application of a state-of-the-art processing system known as IMAGE 100. Operating on the general principle that all objects or materials possess unique spectral characteristics or signatures, the System uses this signature uniqueness to identify similar features in an image by simultaneously analyzing signatures in multiple frequency bands. Pseudo-colors, or themes, are then assigned to features having identical spectral characteristics. These themes are displayed on a color CRT, and may be recorded on tape, film, or other media.

The IMAGE 100 concept is based on the premise that man is a necessary link in the image information extraction loop; in many cases he is the "ultimate decision-maker". To this end, the System was designed to incorporate key features such as interactive operation, user-oriented displays and controls, and rapid-response machine processing. Owing to these features, the user can readily control and/or modify the analysis process based on his knowledge of the input imagery. Effective use can thus be made of conventional photographic interpretation skills and state-of-the-art machine analysis techniques in the extraction of useful information from multispectral imagery. This approach results in highly accurate multitheme classification of imagery in seconds or minutes rather than the hours often involved in processing using other means.

Unlike those multispectral data processing systems which assume Gaussian statistics, IMAGE 100 measures signature distributions utilizing histogram routines. Signature shapes are correspondingly approximated (to establish decision criteria) via n-dimensional parallelepiped "building blocks". Special-purpose digital hardware, operating under control of a minicomputer, is used for implementation of the preprocessing and processing algorithms. In addition, other classification techniques such as clustering, Gaussian, or maximum likelihood analysis are available to the user.

In continuous operation at seven locations in the United States, Canada, and Brazil, the System is being applied in such areas as agriculture, forestry, land-use management, water resources, and geology. Through an extensive program of advanced development, IMAGE 100 capabilities are continually being expanded in response to diverse user needs.

INTRODUCTION

The period beginning in the 1960's and continuing into the 1970's has seen a veritable explosion in the availability of remotely sensed image data. Through various aircraft programs, Skylab, and the LANDSAT satellites, thousands of images have been acquired and many of these have been put to use in solving Earth resources management problems for mankind.

Until recently, however, far more imagery had been collected than could practicably be utilized owing to the time and expense involved in analysis or interpretation. Paradoxically, the technology of acquisition - that is, sensors and space platforms - had moved ahead at a much faster pace than had the requisite image information extraction technology.

Even while the LANDSAT spacecraft was only a paper concept in the late 1960's, its data collection capacity was evident. Evident, too, was the fact that Man's capability to acquire data from both aircraft and spacecraft far exceeded his ability to rapidly and cost-effectively extract information vital to Earth resource management. Even more important than the volume of data produced was the fact that the data was multispectral in nature and required sophisticated processing well beyond the state-of-the-art. Recognizing this fact, the General Electric Company began an intensive program of research and development in multispectral image processing in 1967 and developed and tested breadboard processors over the next several years. In July 1973, General Electric introduced the IMAGE 100 Multispectral Analysis System - the most advanced system of its kind in the world today.

IMAGE 100 SYSTEM OVERVIEW

The principal function of the IMAGE 100 System is to extract information from multispectral data for a variety of applications and disciplines. From its inception, the design has been predicated on the concept of the man-machine system. Man is the ultimate interpreter; human intelligence is an indispensable ingredient in the interpretation process. At the same time, the amount and complexity of the data involved plus the myriad of processes necessary to extracting useful information dictate a high degree of automation for efficiency and man-machine interaction for effectiveness. This man-machine concept enables both the man and the machine to become integral elements in the system, and sets the stage for establishment of a synergistic relationship.

The implementation of this concept in IMAGE 100 combines high speed processing, processing flexibility, and, most important, man-machine interaction. The design places in the user's hands a powerful array of analysis and interpretation tools to interact with and operate on the data, and presents him with real-time displays of his processing results in both qualitative and quantitative form.

In its standard configuration the IMAGE 100 System consists of the following elements (Figure 1):

1. Image Analyzer Console
2. Minicomputer with tape drives and other standard peripherals
3. Graphics Display Terminal (including keyboard)
4. Image Memory Unit
5. Input Scanner Unit
6. System Software

The Image Analyzer Console can well be described as the heart of the System; it is here that the color image display, controls, and special-purpose high speed processing logic necessary to real-time analysis and effective interaction are housed.

The minicomputer, including peripherals such as tape drives, disc, and printer/plotter, serves as both the System process controller and a computational device. The computer is of course essential in the input/output process, and serves to initiate and control many of the information extraction processes specified by the user. The computer also accepts, digests, computes, and presents to the user that quantitative data developed in the extraction process.

A third element is the graphics entry/display terminal. Here, the user interacts directly with the computer to initiate certain processing functions (some processing functions are initiated directly at the Image Analyzer Console). This terminal is also used to display the quantitative processing results in both numerical and graphic form.

The Image Memory Unit is the system's real-time image storage device, and the refresh memory for the color video display. It is configured such that four 512 by 512 picture element (pixel) black and white images can be stored at one time. A fifth storage area is normally used to hold up to eight binary thematic images of IMAGE 100 processing results. The image data is stored in digital form, with each pixel's intensity represented by 8 bits of gray level information. It is important to note that each image plane of the memory unit and, consequently, the color display is digitally addressable. This allows the user great flexibility in composing a wide variety of split-screen and other display configurations to suit his needs.

The Input Scanner Unit is a television scanning system designed to permit the input of multi-spectral data, map overlays, and other data in photographic form into the System. The output of the camera is routed to a high speed analog-to-digital converter, and then input to the Image Memory Unit at standard television frame rates.

The IMAGE 100 Software, together with the programmable features of the special-purpose hardware in the Image Analyzer Console, gives the System its power, flexibility, and interactive capability. The software consists of an IMAGE 100 executive and a completely modular array of applications programs which can be "pipelined" together under control of the user. The structure of the software, and the high degree of independence of individual programs, allows enhanced or completely new capabilities to be added with minimal impact on the existing hardware or software.

IMAGE 100 OPERATIONS

Seated at the Image Analyzer Console, the user controls the operation of the System and interacts directly with his data (Figure 2). Immediately before him, at eye level, is the color CRT display—the System's primary display device. Below this is the display control panel which provides full user control over the image display selection and color, as well as all the thematic data displays. On the left side of the console are controls which initiate specific preprocessing functions, and the theme synthesizer panel which controls the storage and logical processing of thematic data. Below these is a series of special function buttons, each of which initiates a specific processing operation via the computer. These buttons are reserved for those routines used most frequently in image processing operations. The last of these, labelled "AUX", produces a display of all auxiliary processing functions available to the user. The list is displayed in numerical order on the graphics display terminal. All the user need do is type the number corresponding to the process he wishes to initiate and processing begins. Software processes requiring user input utilize a simple question/answer (i.e., "conversational") format via the graphics display terminal.

Input Processing

IMAGE 100 is designed to accept multispectral data in both photographic and digital form. Photographic data, in the form of color or black and white transparencies, are input via the Input Scanner Unit as described above. Multispectral data in digital form is input directly via 9-track, high-speed tape drives under control of the minicomputer and loaded into the Image Memory Unit.

A number of specialized hardware and software capabilities have been developed to speed and facilitate the input of both photographic and digital multispectral data. Flicker and difference mode operations have been incorporated to aid in the registration of digitized black and white photographs during the input process, along with provision for shading corrections and video averaging. The input of digital data from tape is accomplished through software which allows the user to select specified image areas, define the image scale, rotate the image to establish the correct viewing geometry, and create a latitude/longitude reference overlay. These options are quickly defined and the digital image data input to the Image Memory Unit in three-to-four minutes.

Image Analysis

Once the data is stored in the System the user is ready to begin his analysis. A number of "preprocessing" functions are available to the user which serve, at least initially, as photo-interpretation aids. Using the controls provided, he can display and view each of the black and white images stored in the Image Memory Unit and arbitrarily assign any image to either the red, green, or blue guns of the color television display. This allows him to create a variety of false color combinations which enhance various image features. Individual bias, gain, and true or complement controls for each gun provide even further manipulation of the image display.

Other hardwired preprocessing functions are also available to the user on the Image Analyzer Console. He may elect to "ratio" the image; that is, take the arithmetic ratio of the pixel values in one black and white image to the corresponding pixel values in another image. This form of image manipulation is a powerful technique in earth resource applications, and one which is often employed in digital processing. When implemented on a general-purpose computer, however, ratioing is a time-consuming process which usually results in the user having to analyze sizeable printouts and mentally visualize the result. In IMAGE 100, standard ratios, difference over sum, and a normalization function are each implemented in hardware operating at video rates. The user can initiate any one of these functions at the press of a console button, and the resulting pre-processed image appears instantly on the color display. It is important to recognize, also, that the subsequent spectral analysis functions of the System can be performed on either the raw or preprocessed data.

The user interacts directly with the image display by means of the joystick on the display control panel. The joystick, in turn, controls the size, shape, and position of an electronic cursor on the display screen.

Before discussing IMAGE 100 information extraction techniques in detail, a brief description of the multispectral analysis concept is in order. In the earth resources context, multispectral analysis is made practical due to the fact that both man-made and natural features radiate and reflect energy differently in different parts of the electromagnetic spectrum. Simultaneous measurement of the energy in several spectral regions can provide a unique key, or "signature", which may be used to identify specific features. LANDSAT data is a prime example of multispectral sensing; each pixel of each LANDSAT black and white image is the measurement of the reflected energy from an 80 meter square area (approximately) on the earth's surface in a particular segment of the electromagnetic spectrum. The energy level is defined in terms of the gray level value of the pixel. Since LANDSAT collects four images simultaneously, there are four pixel values for each 80 meter square area in the image. These four values comprise the "signature" for that area on the ground.

We also know that similar objects or features in a given image have similar signatures. Hence, if we can locate a field of corn in the image and measure its signature, we can use this to identify corn elsewhere in the image and, overlooking this gross oversimplification of the process, we are on the way to a corn crop inventory.

The process just described, that of measuring the spectral properties of a feature and comparing these over the entire image area, is known as "training" and "classification", respectively. These are the fundamental steps of multispectral analysis, and numerous techniques and approaches have been developed to accomplish them. The ultimate goal of all of these is to process the multispectral data in order to accurately identify and categorize features in the image into one or more classes, or themes, as defined by the user. In the example above, corn would be a user-specified theme, and the final product of the multispectral analysis process would be a thematic "map" depicting all the corn in the image.

To initiate the multispectral analysis process in IMAGE 100, the user places the cursor over a feature of interest in the image. This defines the "training" area. The System then measures the spectral values of the feature in each of the stored images, and uses the upper and lower boundary values to define a four-dimensional parallelepiped in spectral space. Then the entire image is scanned, pixel-by-pixel, and compared to the parallelepiped limits. All pixels whose values are found to lie within these limits are classified and displayed as a color overlay on the television display.

This is the first level of training and classification in IMAGE 100, and the entire process takes less than five seconds. The speed of processing and display, here, is of great importance. Training is a user-dominated function, and one which he may choose to repeat frequently, each time comparing the classification results against ground truth and/or his own knowledge of the area. Depending upon the outcome, he may elect to use a larger or smaller training area, or he may select a completely different training area. In any case, re-training, classification, and display of new results is accomplished in what is, effectively, real-time.

Throughout this process, IMAGE 100 provides the user with a display of his quantitative as well as qualitative results using the graphics display terminal. Each time training and classification are performed, the statistical results of the processing are displayed in numerical and graphical form as shown in Figure 3. This display provides a normalized histogram of the number of pixels occurring at each gray level value within the training set boundaries for each of the four images. The display also defines the actual gray level boundaries numerically as well as the number of pixels in the training and alarmed areas.

The user can interact directly with the training set limit data, itself, by typing the number of the image (1 - 4) whose spectral limits he wants to modify. Let's assume he types a "1". The previous display is immediately replaced with a display of that histogram, enlarged now to full screen. The graphics terminal provides an electronic, vertical line cursor, which the user can position along the histogram's horizontal axis, to redefine the upper or lower training set boundary for that image. Each time he does this, the System re-trains, classifies, and displays the result exactly as described earlier. In this case, however, the user is modifying the data directly in the spectral domain, as opposed to the spatial domain.

The four-dimensional parallelepiped resulting from this first phase of processing is actually a gross approximation to the actual training area signature, but one which is quite adequate for many applications without further refinement. If further refinement is necessary, a number of specialized processes can be employed including the limit modification technique just described, as well as a variety of statistical processing algorithms. These include the capabilities for detailed examination of the parallelepiped hyperspace in order to develop an n-dimensional histogram of the training area's signature distribution. Also included are the capability for cluster analysis and maximum likelihood classification.

Once the user is satisfied with the classification result, he stores it on one of the eight binary theme storage areas in the Image Memory Unit. This data forms a thematic map which

can be displayed as an overlay on the image. Each theme has associated with it a particular display color. Any one, any combination, or all eight themes can be displayed at any time. In addition, the System allows the user to perform addition, subtraction, logical "and", "or" and "exclusive or-ing" of thematic data. At any point in the process the user can also request an immediate display of the number of alarmed pixels in each theme storage area. These represent the number of hectares, acres, square kilometers, etc., of each theme he has classified.

A number of other capabilities are provided to manipulate and enhance the image data to aid in the interpretation process. Each of these is an independent processing module. In the interest of space, only a few can be described here.

To facilitate the proper placement of the cursor in training on small features, a "window" technique may be employed. In this mode, the user can select a small display area with the cursor and enlarge it in real-time to any scale he wishes. The display area in which the enlargement is placed is fixed in size, and the system automatically sizes the cursor for the user's selected enlargement scale. An example of a window is shown in Figure 4. The user can now train on the data in the window area and see his results across the entire display. When the user is finished with the window, the System restores the display to its original form.

Another approach to small scale training involves the "single pixel training" feature. In this mode, the user adjusts the cursor to the shape of a cross (+), and places it over the feature of interest. The pixel area in and around the center of the cross on the graphics terminal is then displayed. This display defines the relative location and the gray level values for each pixel. By typing a number corresponding to the relative location of a specific pixel, the user can classify the scene based on that pixel's specific spectral values. This allows the user to train and classify to the most basic resolution element of his data.

Another feature commonly used is called "level-slicing". This technique is used to enhance and analyze individual black and white images. In this process, the user specifies the areas of interest with the cursor, and defines the number of "slices" he wishes to take. The system responds by measuring the minimum and maximum gray level value of the pixels in the area, and divides this by the number of slices. All pixels with gray levels falling within each slice are formed into a binary thematic map and displayed in unique theme colors. Hence, the black and white image is converted to a color map, with subtle gray level differences now emphasized by sharply contrasting colors.

Contrast stretching is another technique used to emphasize subtle gray level variations. The same procedure of area selection and min/max gray level measurement is employed. In this case, however, no color map is generated. Instead, the System creates a new black and white image by expanding the minimum and maximum gray tones in the defined area over nearly the full black-to-white dynamic range of the display. This is an extremely powerful interpretation aid which serves to emphasize low contrast detail found in the original image.

In some instances, the basic rectangular and cross shapes of the cursor are unsuited where irregular shapes, such as geographical and political boundaries, are needed to outline the training area. For this reason, the System allows the user to construct a polygon cursor. Using the System cursor as a cross, the user places the cursor intersection over points along the boundary he wishes to create. The System interprets each of these as the vertex of a polygon. As each vertex is defined, the System connects it with the preceding vertex using a straight line approximation. Up to one hundred vertices may be defined, permitting definition of all forms of training areas including circles. In addition, an unlimited number of polygon cursors may be combined to define virtually any shape in any size. The training area formed is filled in automatically and stored in a theme storage area. This can then be used for the normal training process, or it can be logically "and-ed" with other classification results. If, for example, the user had classified all

coniferous forests in the scene, he could not "and" this with a political boundary theme and create the map of coniferous forest located only in a particular town or county.

When samples of a particular material or class of interest in an image are too small or scattered for machine-training purposes, it is frequently desirable to separate the spectral data into "clusters" where each cluster represents a unique class. Consequently, a semi-supervised cluster analysis software program has been developed to accomplish this function. Using the results of a previous n-dimensional training step, this program attempts to categorize these results into a user-specified number of clusters using a migrating means technique.

Output Processing

The user has several methods for generating output products from his analysis. Hardcopy thematic maps in binary, alphanumeric, and halftone form can be created on the computer's line printer, which features a graphics capability. The System will also record the results on magnetic tape for off-line plotting on any number of commercial plotting devices. High quality color products can be made directly by photographing the color television display, or preferably, by generating a magnetic tape suitable for input to a precision, high resolution, color film recording device.

A recent innovation in the presentation of results involves the use of a cassette video recorder attached to the IMAGE 100 color display. In this way, the user can make a dynamic visual record of each phase of his analysis with voice track annotation. The video cassettes, then, form an audio-visual "laboratory notebook" for subsequent analysis, review, and presentation.

APPLICATIONS EXAMPLES

One IMAGE 100 System is located at General Electric's Image Processing and Analysis Center just outside Washington, D.C. This Center provides processing and analysis services to private industry, universities, and government at all levels. The Center's IMAGE 100 System has been exposed to a wide variety of user applications; highlights of some of these applications may be helpful in understanding how IMAGE 100 is utilized.

Synoptic coverage is one of the principal attributes of LANDSAT data. Each LANDSAT image covers an area 185 km on a side. This fact, coupled with the classification capability inherent in the multispectral data, permits the user to map land-use or inventory crops over large areas both accurately and efficiently. Figure 5 is a multitheme land-use map of Tokyo and environs produced on IMAGE 100. Eight different land-use categories are displayed, each in a unique color (on the original). The area surveyed is some four hundred square miles in size, and the entire classification was accomplished in less than four hours.

In a recent study for a major U.S. agricultural firm, IMAGE 100 was used in an effort to inventory one particular crop in the state of California. Over 4.8 million acres were included in the study area, and the inventory produced a count of some 650,000 acres of the crop in question. This result was within five percent of published figures. Equally important, the study showed that the inventory could be performed operationally at a cost of less than one-tenth cent per acre inventoried, orders of magnitude less than through conventional means.

As an illustration of IMAGE 100's applicability to crop inventories, Figure 6 shows the results of analyzing a 5300 hectare (13,000 acre) area in Williams County, North Dakota. In this example, wheat fields, fallow fields, and pastures were classified to an accuracy of better than ninety-five percent. Owing to the orientation of the fields in the image, the previously mentioned polygon cursor program was utilized in the analysis.

In one of many forestry applications, IMAGE 100 was used for pre-visual detection of stress caused by disease. Scenes (a) and (b) of Figure 7, false color and true color representations of the input image, respectively, show Dutch Elm trees in the Tidal Basin area of Washington, D. C. In less than one hour, all stressed trees in the scene were correctly identified as evidenced by the theme in Figure 7 (c).

IMAGE 100 has also been applied in numerous environmental studies relative to watersheds, navigable rivers, wildlife habitats, and other ecologically and environmentally sensitive areas. One study completed recently focused on the identification of suitable habitats for the North American grizzly bear, an endangered species. Site selection studies for electrical power generation facilities, and the monitoring of strip mining areas used in the production of coal are two significant energy-related applications for which the System is being used.

One of the most common applications is that of water quality mapping. Figure 8 (a) shows the area in and around Manila (the city is located at the mouth of the river at the upper center). Five classes of water quality were mapped based on spectral reflectance as indicated in Figure 8 (b). A land-use analysis of this area, shown in Figure 8 (c), was also performed.

In addition to LANDSAT, IMAGE 100 has been used to process data from a wide variety of other sources. Aerial photography is a common input medium, as is multiband airborne scanner data. For example, data from an airborne side-looking aperture radar has been processed; in this case the radar's separate vertically and horizontally polarized data comprised two "multispectral" channels used in geologic analysis.

Meteorologic data analysis is another and continually growing application of IMAGE 100. Spaceborne meteorological sensors generally provide multiband (visual and infrared) imagery for which IMAGE 100 is ideally suited. As an illustration, four scenes of a hurricane, each taken one hour apart, were displayed on one channel of the IMAGE 100 display. The temperatures of the clouds comprising the storm were identified by their gray level, and mapped continually throughout the storm's development. In this case, the System's storage capacity allowed twenty hours of data to be processed at one time.

Ranging somewhat far afield, it is interesting to note that the System has also been applied in medical data processing—namely the analysis of color and fluoroscopic photography of skin cancer and disease of the retina.

ADVANCED DEVELOPMENT AND FUTURE GROWTH

The IMAGE 100 System is supported by an extensive and continued advanced development program within the General Electric Company. Much of this effort draws its focus from the widespread application of the System by various users in different disciplines, and benefits from their experience and particular applications needs. In the period since the first System was delivered, the number of applications software packages in use has more than doubled. This new software represents improvements in both the efficiency and effectiveness of the processing operations. In one case, for example, new software has reduced the time required to input a four band image from four minutes to a few seconds. New capabilities are added continually in response to user requirements, and the modular concept and structure of the software has enabled many of these to be added literally overnight.

To date, the minicomputer has been dedicated exclusively to the IMAGE 100 operations. That is, during all image processing operations the computer has been an integral, on-line System element. This results primarily from the fact that the computer operates under the vendor's single or dedicated task disc operating system. During interactive image processing, the IMAGE 100 System usually completes the processing task and displays the results in far less time than the user requires to determine his next step. As a result, the computer spends much of its time waiting.

Just as Nature abhors a vacuum, computer people abhor an idle computer. For this reason, then, the entire applications software system is now being converted to full-scale multitask operation. IMAGE 100 activities will take place in a high-priority, user-controlled partition, with significant processing time and resources for a very effective batch "background" operation. The latter will be used to perform the myriad of tape copying, output processing, and other housekeeping tasks associated with a large image processing operation as well as optimizing utilization of the computer for software development and other general-purpose needs. Additional image processing tasks such as bulk classification of entire frames of imagery, image processing and formatting, image output to color recording devices can also be accommodated in the "background" mode, thus further improving the cost-to-benefit ratio. At the same time, this has virtually no impact on the interactive ability of the user to analyze and process image data in the "foreground".

Conceptually, the multitask approach does far more than improve the efficiency of computer utilization. As a concept, it is a major step toward a next generation system of multiple interactive terminals, all controlled by a single processor unit. Such an approach is practical today and, depending on the size of the computer, as many as eight or more users may be allowed to work simultaneously on different applications—with different images—in a single facility or remotely via a communications link to a central processor.

A current development effort of particular significance adds the capability for inputting and processing multispectral scanner data directly from high density recorders. This development, much of which is on-contract, covers the recorder interface electronics and software for tape input control, formatting, display, and processing of eleven-channel data. Software/hardware for accommodating higher-dimension data (i.e., up to 64 channels) from both computer-compatible tape (universal format) and high density tape is also under development.

CONCLUSION

IMAGE 100 is enjoying widespread acceptance within the earth resources community in that seven Systems are in operation in the United States, Canada, and Brazil. Additional Systems are committed for delivery in the United States, the Far East, and the Middle East in the near future. It is significant that with the ever-increasing number and diversity of System users and corresponding applications has come attendant expansion of IMAGE 100's capabilities, as well as advancement in the science (or art?) of image information extraction.

The IMAGE 100 Users Group recently organized will surely promote even more dramatic advancements through the free exchange of new ideas, techniques, procedures, and/or software programs developed by each member organization.

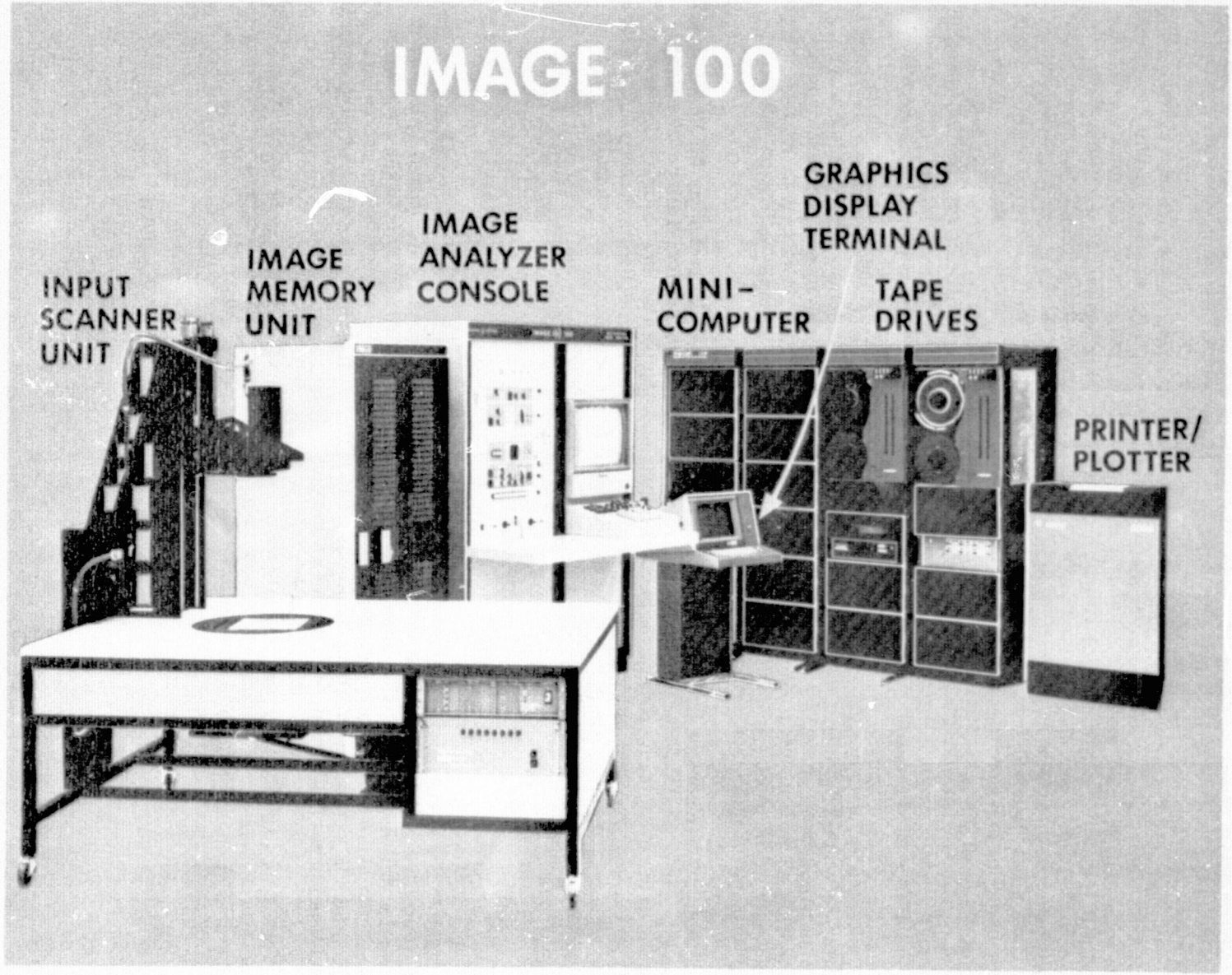


Figure 1. - IMAGE 100 System equipment configuration

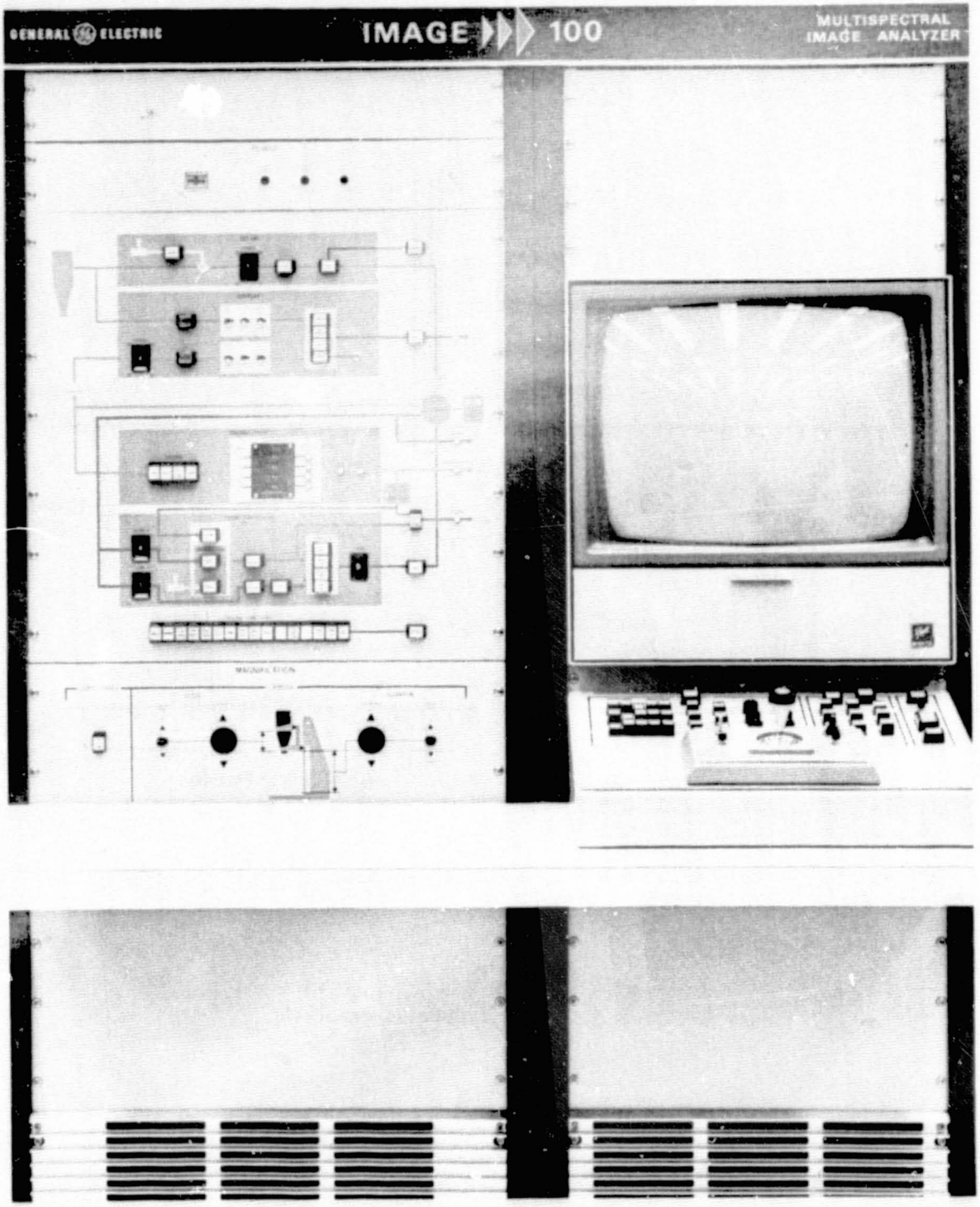
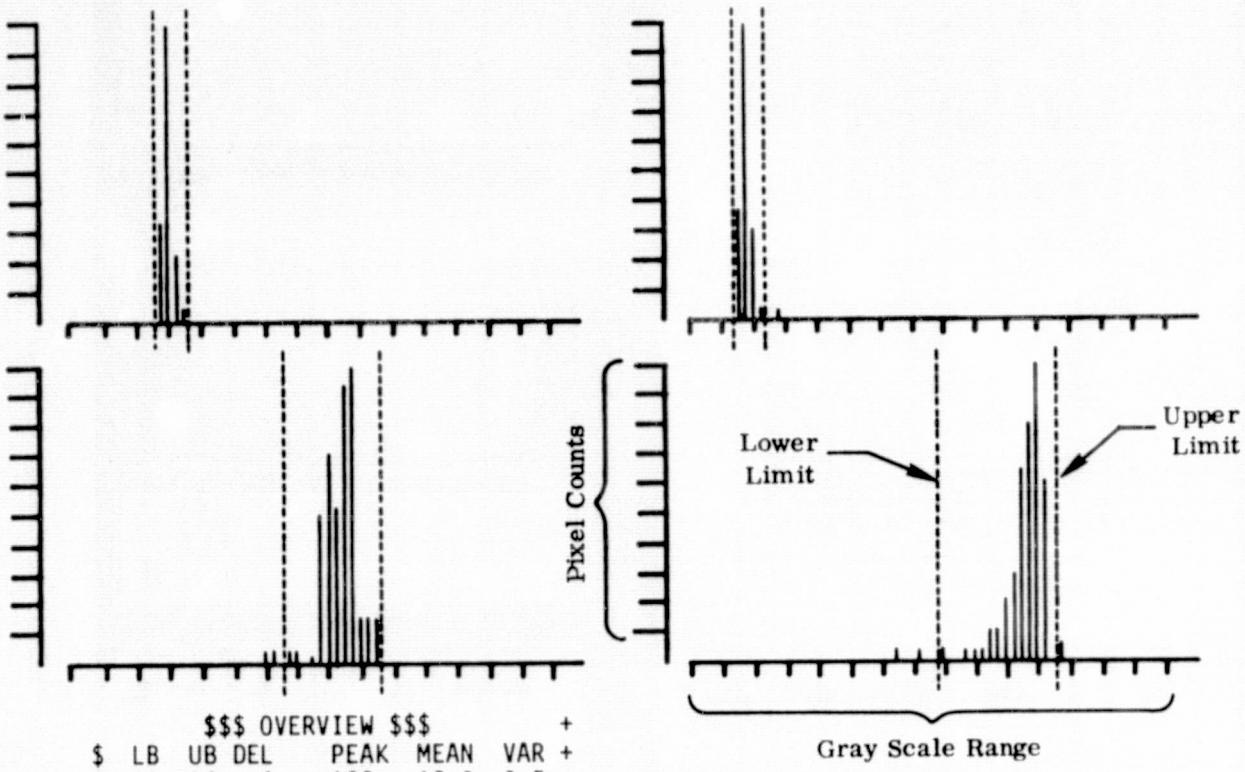


Figure 2. - IMAGE 100 Image Analyzer Console




```
          $$$ OVERVIEW $$$                +
$  LB   UB DEL    PEAK  MEAN  VAR +
1  11   14   4    122.  12.0  0.5 +
2   6    9   4    112.   7.0  0.5 +
3  27   38  12     45.  33.6  4.0 +
4  32   46  15     46.  42.6  5.8 +
TRAINING AREA=   196. PIXELS      +
ALARMED AREA= 41730 PIXELS(16.1%)+
TYPE  CHANNEL $  OR E(X)IT
```

Figure 3.- 1-D Histogram Display (4 Channels)

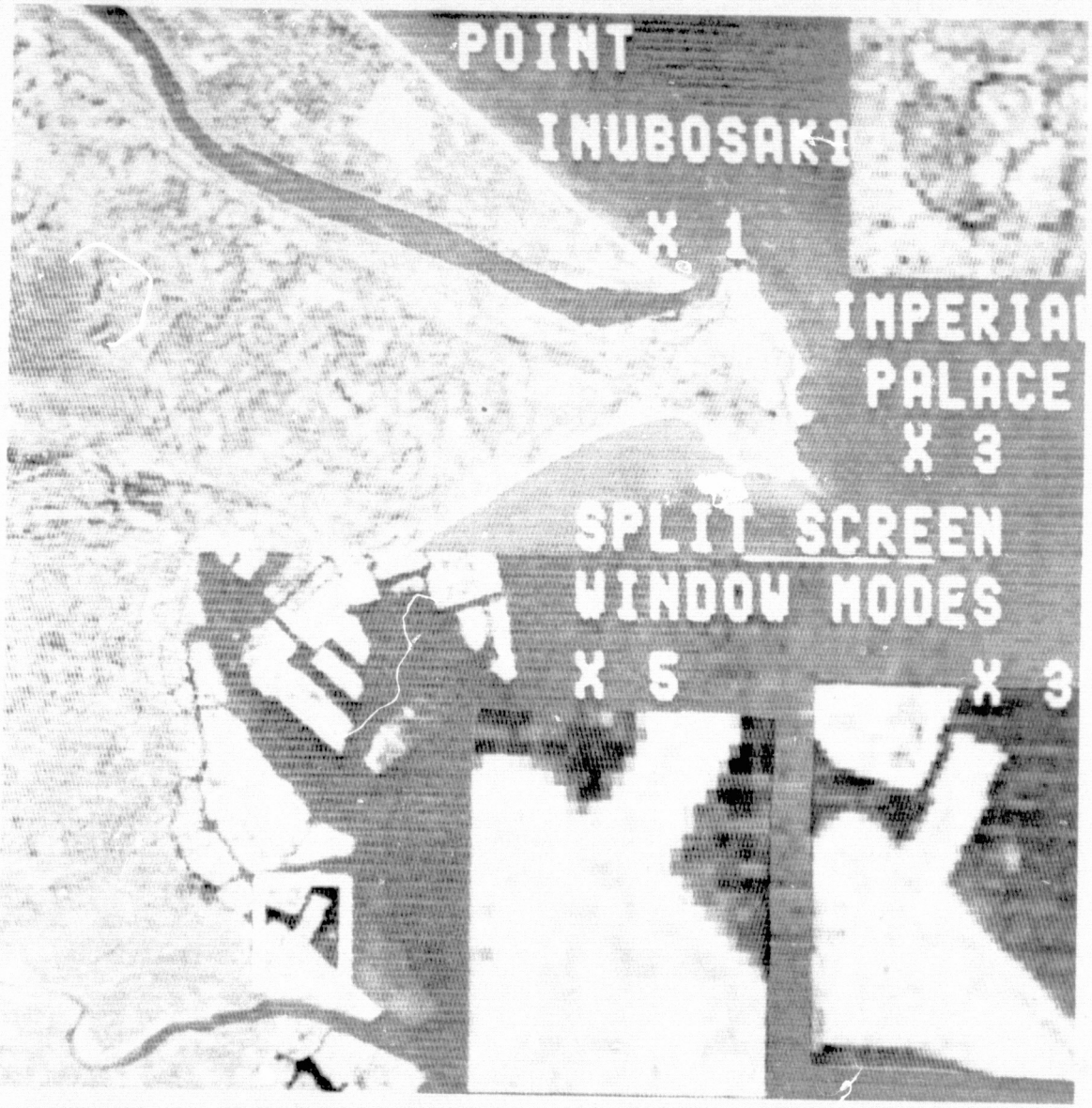


Figure 4. - Example of IMAGE 100 window display and split-screen modes.



Figure 5. - Thematic Map of Tokyo showing eight land-use categories

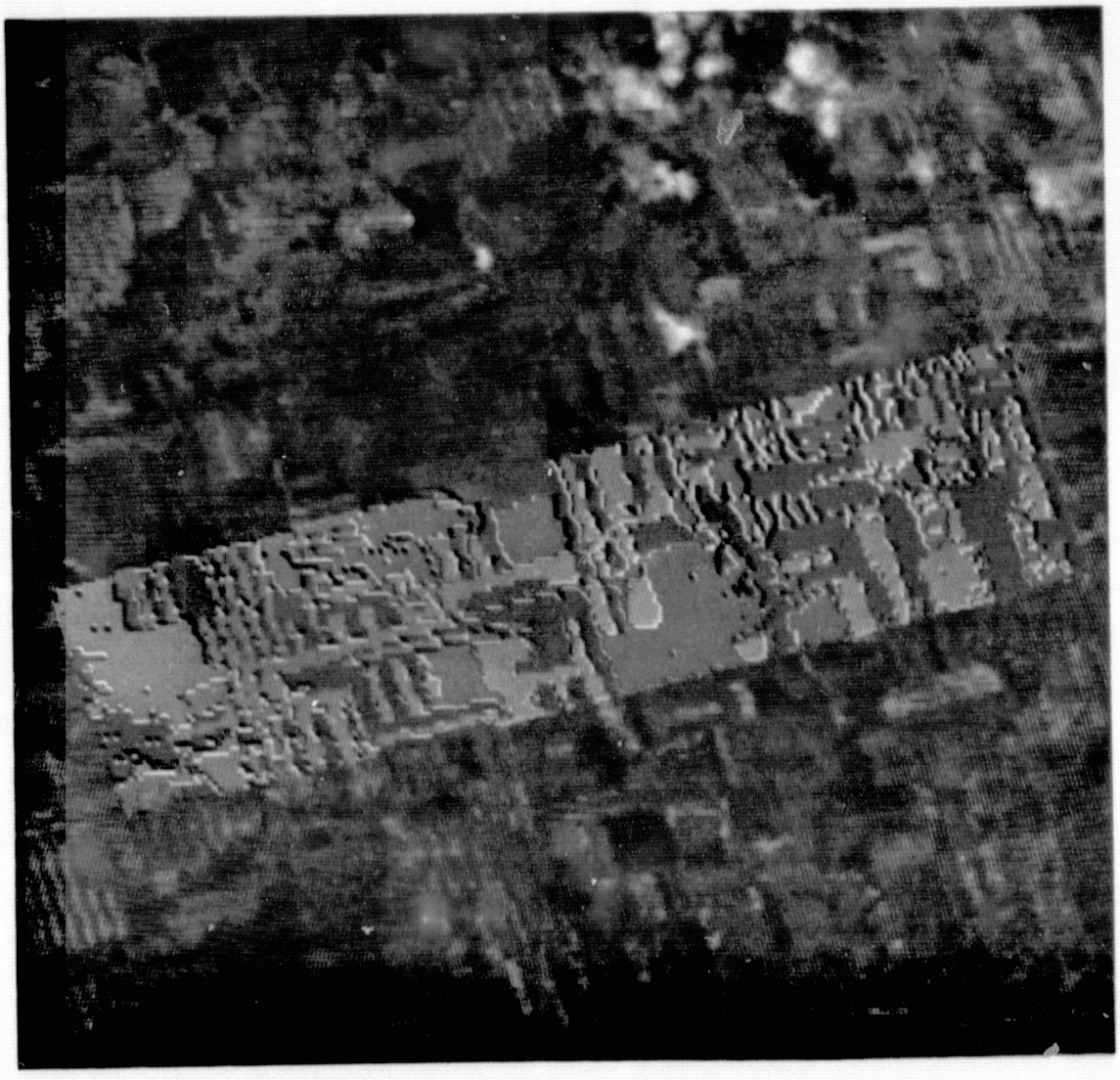
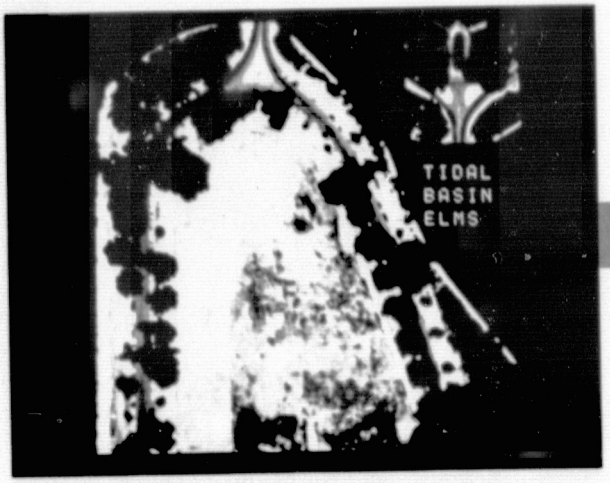
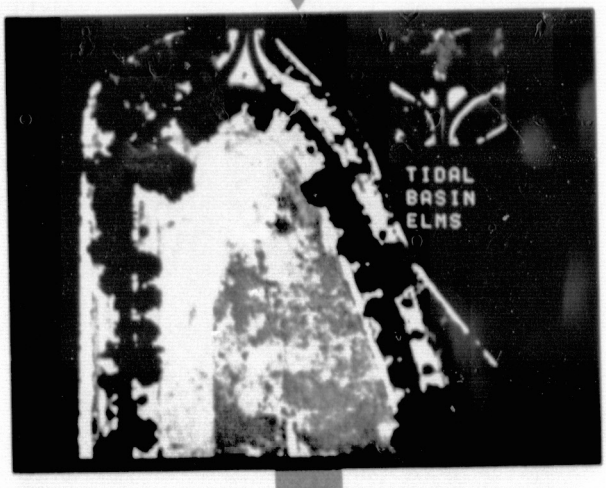


Figure 6. - North Dakota agricultural area, with wheat fields (orange theme), fallow fields (yellow theme), and pastures (blue theme) identified.

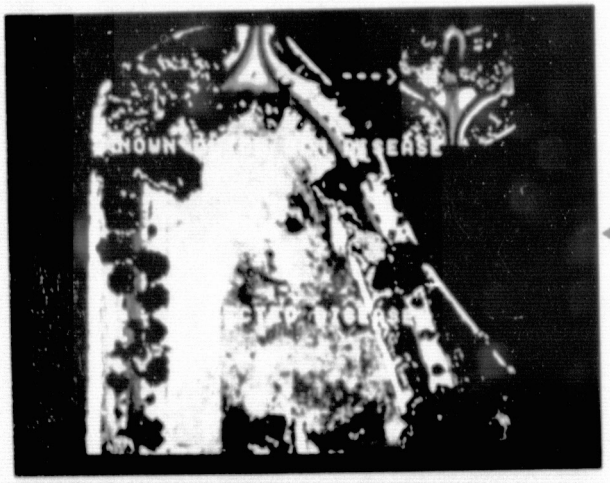
REPRODUCIBILITY OF THE
ORIGINAL PAGE IS POOR



(a) False color infrared input scene (aircraft multispectral camera data)

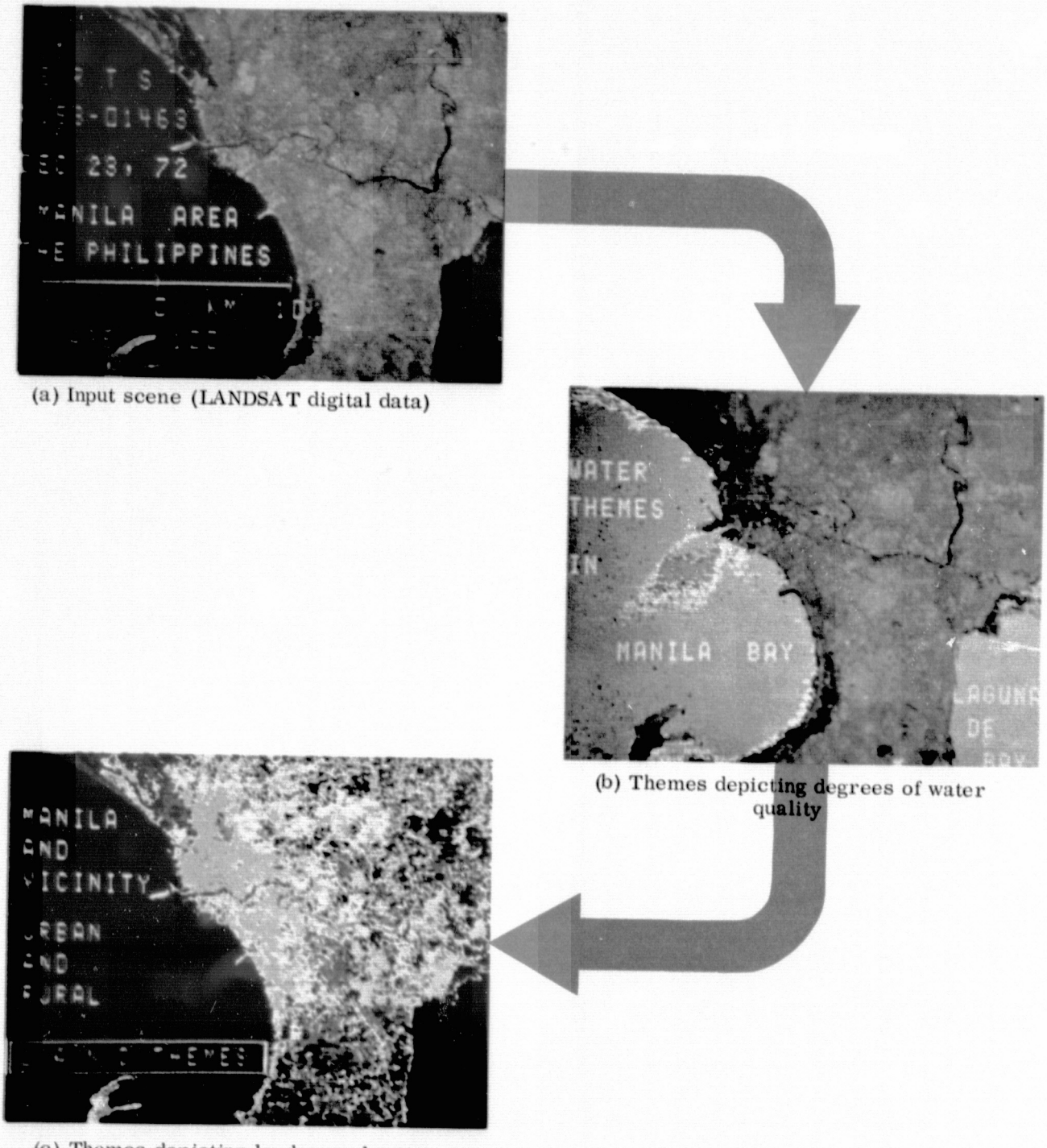


(b) True color input scene



(c) Theme identifying diseased trees

Figure 7. - Pre-visual detection of tree disease example.



(a) Input scene (LANDSAT digital data)

(b) Themes depicting degrees of water quality

(c) Themes depicting land-use classes

Figure 8. - Water quality and land-use classifications in Manila, Philippines area.

GEOLOGIC ANALYSES OF LANDSAT-1 MULTISPECTRAL IMAGERY OF A POSSIBLE POWER PLANT SITE EMPLOYING DIGITAL AND ANALOG IMAGE PROCESSING

I-12

By Jon R. Lovegreen, Woodward-Clyde Consultants, Eastern Region, Clifton, New Jersey, William J. Prosser, Woodward-Clyde Consultants, Central Region, St. Louis, Missouri, and Richard A. Millet, Woodward-Clyde Consultants, Eastern Region, Clifton, New Jersey

N76-17536

ABSTRACT

A site in the Great Valley subsection of the Valley and Ridge physiographic province in eastern Pennsylvania was studied to evaluate the use of digital and analog image processing for geologic investigations. Ground truth at the site was obtained by a field mapping program, a subsurface exploration investigation and a review of available published and unpublished literature. Remote sensing data were analyzed using standard manual techniques. LANDSAT-1 imagery was then analyzed using digital image processing employing the General Electric (GE) Multispectral Image 100 system and using analog color processing employing the Woodward-Clyde Consultants' VP-8 Image Analyzer. This study deals primarily with: (1) linears identified employing image processing and correlation of these linears with known structural features and with linears identified employing manual interpretation; and (2) the identification of rock outcrops in areas of extensive vegetative cover employing image processing. The results of this study indicate that image processing can be a cost-effective tool for evaluating geologic and linear features for regional studies encompassing large areas such as for power plant siting. Digital image processing can be an effective tool for identifying rock outcrops in areas of heavy vegetative cover. Analog image processing can be an effective tool for defining regional linears and regional differences in lithology. Neither technique can completely replace the use of standard manual interpretation techniques but can be used as an additional cost-effective tool to better understand the geologic and structural characteristics of a site region.

INTRODUCTION

The site is located near the Schuylkill River in the Great Valley subsection of the Valley and Ridge physiographic province; refer to Figure 1. The Great Valley is a northeast-southwest-trending lowland, approximately 20 miles wide near the site, which is primarily in agricultural use and typified by low hills and intervening valleys. North of the site is Blue Mountain marking the southern boundary of the forested Appalachian Mountain subsection of the Valley and Ridge physiographic province. The Reading Prong (also predominantly forested), marking the northern boundary of the Piedmont physiographic province, lies south of the site as does the Triassic Basin (Fenneman, 1938).

Geologic conditions near the site are complex and not fully understood. The Great Valley is underlain by highly folded and thrust-faulted lower Paleozoic sedimentary sequences of sandstone, shale, slate, limestone and dolomite; refer to Figure 1. The structural setting of the Great Valley is characterized by a northeast-southwest alignment of fold axes, linears, fault traces and fracture patterns resulting from Paleozoic orogenies; refer to Figure 2. Blue Mountain and the Appalachian Mountains are underlain by folded Paleozoic sedimentary sequences of sandstone, shale, conglomerate and coal. The Reading Prong is an upland underlain by a highly deformed Precambrian crystalline complex composed primarily of granite gneiss. The Triassic Basin is a lowland underlain by sandstone and shale which have been intruded by diabase dikes. A more detailed description of the geologic and structural setting of the site region can be obtained from Fisher, et. al. (1970).

PRECEDING PAGE BLANK NOT FILMED

Purpose

The overall purpose of this ongoing study is to evaluate the use of image processing as a cost-effective tool to supplement standard manual interpretation techniques of remote sensing data. Of particular interest are the use of image processing to: (1) identify linears; (2) correlate the linears identified in (1) with identified structural features; (3) correlate linears identified in (1) with linears identified by other techniques (manual interpretation of remote sensing data, field studies, etc.); (4) identify rock outcrops of similar gross characteristics in a heavily vegetated region; and (5) distinguish between outcrops of different gross characteristics in a heavily vegetated region.

This report discusses only the results obtained to date from digital and analog image processing of LANDSAT imagery. LANDSAT imagery was selected for the initial phase of this study because it is readily available in both digital and analog formats from the EROS Data Center in Sioux Falls, South Dakota; it is relatively inexpensive; and it provides a synoptic view of the study area. Future phases of the study are scheduled to evaluate additional forms of remote sensing data including satellite photography, SLAR imagery, infrared photography and imagery, and aerial photography.

Procedure

The extensive program to gather ground truth included a field investigation program (including borings, backhoe and dozer trenches, geophysical surveys, and geologic mapping) and a review of published and unpublished literature relevant to the site. This program to gather ground truth was coordinated with the acquisition and manual interpretation of remote sensing data including standard black and white aerial photography at scales of 1:12,000 and 1:20,000; false-color near-infrared (IR) photography at a scale of 1:9600; thermal IR imagery at a scale of 1:30,000; Skylab false-color near-IR photography at a scale of approximately 1:432,000 (I.D. 3-869-076); and LANDSAT-1 multispectral scanner (MSS) imagery at a scale of 1:1,000,000 (I.D. E-1080-15185 and E-1170-15191 dated 11 October 1972, and 9 January 1973, respectively).

The ground truth and remote sensing data were used to generate regional and local geologic maps and geologic sections necessary to understand geologic conditions at the site and site region. These data also were used to identify regional and local linears and structural features necessary to understand structural and seismic conditions at the site and site region.

Subsequent to this standard approach of evaluation and definition of geologic and structural conditions at a power plant site, a study area (refer to Figures 1 and 2) was selected for evaluation by using image processing of remote sensing data. To date, image processing of LANDSAT-1 imagery has been conducted. Digital image processing (DIP) was conducted on the General Electric (GE) Image 100 Analysis System in Beltsville, Maryland and analog image processing (AIP) was conducted on Woodward-Clyde Consultants' VP-8 Image Analyzer in Kansas City, Missouri.

The use of DIP (employing color enhancement) on the GE Image 100 Analysis System involved the loading of four computer compatible tapes (CCTs) into a PDP 11/35 computer. Each CCT contained the digital data for one MSS band of LANDSAT-1 image E-1080-15185. The LANDSAT image generated from these data was then displayed on a cathode ray tube (CRT) at scales of 1:630,000, 1:105,000; 1:52,000, and 1:26,000.

Typically, a 1:1 resolution scene (one CRT picture element (pixel) assigned to one LANDSAT pixel) at a scale of 1:105,000 containing all four LANDSAT MSS bands was examined on the CRT; refer to Figure 3. From this working scene a 2:1 resolution working scene (two CRT pixels in the x and y directions assigned to one LANDSAT pixel) or a 4:1 resolution working scene (four CRT pixels in the x and y directions assigned to one LANDSAT pixel) at scales of 1:52,000 and 1:26,000, respectively, were examined in order to select training sites (areas for which ground truth was available). The GE Image 100 then extracted

the four dimensional spectral properties of the selected training sites in a process known as training and assigned a color to the training site. The 1:1 resolution scene (encompassing the study area) was then scanned and all pixels of similar spectral properties were assigned (alarmed) the same color as the training site in a process known as classification. The training process was repeated until the entire study area had been classified or until training had been conducted in all areas of interest. The result of the classification process is a color enhanced image known as a thematic map. The thematic maps were recorded by: color photographs of the thematic map displayed on the CRT; the generation of histograms defining the spectral characteristics of the training site; and halftone (black and white) printouts of all alarmed pixels in a thematic map. These data were then analyzed and interpreted to define geologic and linear features within the study area.

The use of AIP (employing color enhancement) on Woodward-Clyde Consultants' VP-8 Image Analyzer involved the use of MSS bands 5 and 7 of LANDSAT-1 image E-1080-15185 (7 by 7 in.) positive transparencies. The transparencies were placed on a light table where tney were scanned by a vidicon camera. The resultant image was displayed on both a CRT (Figure 4) and a pseudo 3-D monitor. Color enhancement of the image was accomplished by enhancing (assigning a color to) selected sections of the gray scale (the gray scale observed on the CRT actually represents film densities on the positive transparency) either by dividing the gray scale into equal sections or into sections of unequal width which could be correlated with ground truth data. The VP-8 Analyzer has the capability of dividing the gray scale into 8 sections. In addition the pseudo 3-D monitor was used to display the image in three dimensions; the length and width of the image are two dimensions and the gray levels are the third. The results of AIP were recorded by: color photography of the thematic map displayed on the CRT and/or of the 3-D image displayed on the pseudo 3-D monitor.

RESULTS

Digital Image Processing

Linears. - DIP was found to enhance linears parallel to and associated with the northeast-southwest trending structural setting of the study area and the Great Valley in particular. Significantly, however, DIP also enhanced linears trending northwest-southeast, approximately normal to the structural trend. These northeast-southwest trending linears were observed in the Great Valley and in some instances extended to Blue Mountain or the Reading Prong; refer to Figures 5 and 6. At Schuylkill Gap these northwest-southeast trending linears are parallel to the Schuylkill River suggesting possible structural control of the gap and river drainage.

The northwest-southeast trending linears are believed by the authors to be related to a secondary fracture system in the Great Valley which has a similar orientation. This orientation is consistent with the tectonic setting and causative stresses of the region (Fisher, 1970). The enhancement of these linears is important because manual examination of the LANDSAT-1 image tended to discriminate linears parallel to the regional structural trend with a resultant lack of discrimination of linears normal to this trend.

Comparison of linears resulting from DIP with mapped structural features on the Pennsylvania state geology map (Gray and others, 1960) has not been studied in sufficient detail to evaluate this capability. Preliminary results, however, show that the Blue Mountain Structural Front (refer to Figures 5 and 6) and a thrust-fault contact between the Reading Prong and Great Valley can be defined using thematic maps obtained from vegetative and land-use classifications. The enhancement of these structures, however, is a function of topography and land use. Thus, the enhancement does not define the structures; but it does suggest anomalous relationships which are known (in this case) to be structural features.

Comparison of linears resulting from DIP with linears drawn inhouse (refer to Figure 7) and by others (Gold, et. al., 1973) resulting from standard manual interpretation techniques indicate that DIP can be used to supplement results obtained from these techniques. To

date linears obtained from DIP have not duplicated the linears obtained by manual interpretation. Less than 20% of the linears interpreted from DIP were observed by manual interpretation and vice versa. However, the same sense of structural setting is obtained from DIP as from manual interpretation (i.e., a dominant northeast-southwest trending linear system and a less dominant northwest-southeast trending system). Consequently, DIP appears to be an additional tool available to the photo interpreter which can be used to identify linears. It is a tool which has the added benefit of not being subject to human limitations such as fatigue, temperament, or variations in methods of identification. Therefore, results obtained from DIP can be duplicated.

Geology. - Preliminary efforts to extrapolate geologic conditions from a small data base of ground truth to a large region in an area of heavy vegetation such as is found in the Great Valley has been partially successful to date. Rock outcrops of similar gross characteristics including interbedded sandstone and shale or quartzite have been defined with a maximum accuracy of 30%. The highest correlation was obtained when the largest available outcrops, such as abandoned quarries approximately 230 m^2 in area, were used as training sites; refer to Figure 8.

The use of DIP to distinguish between outcrops of different gross characteristics will require substantial additional work to be effective. To date efforts to distinguish outcrops of sandstone and shale from quartzite, or from carbonate strata, have not been successful. It was found that when using DIP in an area with outcrops of one rock type, the outcrops could be identified with 30% accuracy as discussed previously. However, when classification was conducted over a large region where several rock types were present, enhancement did not distinguish between rock types. The reasons for the difficulty encountered in classifying specific rock outcrops are believed to be related to: the use of a fall LANDSAT image rather than a winter image (the latter would tend to minimize vegetative interference); the spatial limitations of LANDSAT imagery coupled with the small outcrop areas; and the use of a composite LANDSAT image composed of all four MSS bands rather than one MSS band (or combination of MSS bands) which would be more responsive to the wavelengths of geologic features (such as MSS band 5 or 7).

A major problem encountered while evaluating the 4:1 scale scenes (1:26,000) was the inability to distinguish between pixels which contained rock outcrop and adjacent pixels which were vegetated, a road, or a plowed field, etc. In order to reduce this problem, ratioing was conducted. As discussed by Vincent (1973), ratioing involves the dividing of the spectral signatures of all pixels in one LANDSAT MSS band by the corresponding pixels in another band. This can serve to reduce atmospheric and solar illumination effects. During this study the ratio of MSS bands 5/4 provided the best enhancement of rock outcrops.

Analog Image Processing

Linears. - AIP was found to enhance linears parallel to and associated with the northeast-southwest trending structural setting of the study area and the Great Valley in particular; refer to Figures 9 and 10. AIP also enhanced linears trending normal to this setting which, as discussed previously, is significant because this "normal" trend was less readily observed during manual interpretation. In addition to enhancement of the imagery, the pseudo 3-D display was used to define linears; refer to Figure 11.

Of particular interest were a series of linears observed in the Great Valley. Among these linears are a northwest-southeast trending linear from Reading, Pennsylvania to Blue Mountain (Figure 9); an arcuate shaped linear trending eastward from Blue Mountain and then southwest toward Lake Ontelaunee (Figures 9 and 10); a north-south trending linear aligned with the Lehigh River from Lehigh Gap in Blue Mountain to the Reading Prong south of Allentown, Pennsylvania (Figure 9); a northeast-southwest trending linear which intersects the Susquehanna River near Harrisburg, Pennsylvania (Figure 9); and several northeast-southwest trending linears crossing the Schuylkill River north of Reading, Pennsylvania (Figure 9). The origin and significance of these linears are not known at the present time and are currently being studied.

Comparison of linears resulting from AIP with mapped structural features on the Pennsylvania state geology map (Gray, et. al., 1960) requires additional study. The preliminary results are similar to those obtained from DIP. Structural features related to or expressed as topographic and vegetative anomalies such as Blue Mountain Structural Front and the thrust-fault contact between the Great Valley and the Reading Prong, are readily observed due to distinctly different spectral characteristics and resultant enhancement colors; refer to Figure 11.

Comparison of linears resulting from AIP with linears drawn inhouse (Figure 7) and by others (Gold, et. al., 1973), using standard manual interpretation techniques, indicates that AIP can be used to supplement these techniques. To date, linears interpreted from AIP have not duplicated linears obtained by manual interpretation. Less than 30% of the linears interpreted from AIP were observed by manual interpretation and vice versa. However, the same sense of structural setting is obtained from AIP as from manual interpretation (i.e., a dominant northeast-southwest trending linear system and a less dominant northwest-southeast trending system). As is the case for DIP, AIP is an additional tool available to the photo interpreter which can be used to identify linears.

Geology. - The extrapolation of geologic conditions from a small data base of ground truth to a large region which is heavily vegetated using AIP has been a qualified success. Enhancement of regional geologic conditions has produced thematic maps which differentiate the folded sandstone and shale sequences of the Appalachian Mountains from the sandstone, shale and carbonate sequences of the Great Valley and differentiates the sedimentary strata of the Great Valley from the crystalline complex of the Reading Prong and the volcanics and sedimentary strata of the Triassic Basin; refer to Figures 10 and 12. The differentiation between these three gross geologic regions is due primarily to vegetation and elevation differences. As Figure 12 shows, relatively high elevations with forests such as the ridges of the Appalachian Mountains, the Reading Prong, and the ridges underlain by volcanics in the Triassic Basin have similar spectral reflectance values and similar color enhancement. These enhancements differ from the lowland areas of the intervening valleys in the Appalachian Mountains, the Great Valley, and the lowlands underlain by sedimentary strata in the Triassic Basin. It has also been possible to differentiate interbedded sandstone and shale from carbonate strata in selected areas in the Great Valley; refer to Figure 12. In other areas, however, such as the Reading Prong and in the Appalachian Mountains, it has not been possible to differentiate between lithologic units within a lowland or highland region.

COMPARISON OF DIP AND AIP

Differences in the method of enhancement of LANDSAT imagery by DIP and AIP and differences in the format of the imagery used for the two processes led to noticeably different results. DIP incorporates digital data into the enhancement process, it therefore inherently has better frequency resolution than spatial resolution. Consequently, during this study DIP tended to lend itself to the very precise identification of subtle differences between adjacent objects. This preciseness can be used to locate anomalies (vegetation and land use in this case) which may then be interpreted for linears, as shown in Figures 5 and 6. This preciseness is also particularly valuable when there is a need to identify rock outcrops in a heavily vegetated region using a small data base of ground truth. The value of the precise frequency resolution is tempered however, by the problem of spatial resolution which caused difficulty in locating and identifying small outcrops. Ratioing, particularly MSS bands 5/4 reduces this problem. It should also be noted that lower altitude (non-LANDSAT) imagery could alleviate this problem.

AIP incorporates analog data derived from LANDSAT digital tapes into the enhancement process, it therefore has lower frequency resolution than does DIP and has the same spatial resolution problems. The lack of frequency resolution and spatial resolution tended to be beneficial in this study with regard to identifying regional linear and geologic features

as shown in Figures 9-12. Regional linears were more readily appparent from AIP than DIP as were different lithologic units.

Thus, DIP tended to make precise definition of the spectral signature of a small area and locate units of similar spectral signature which resulted in the enhancement of many small discrete areas. AIP on the other hand, tended to make coarse definition of regional features which resulted in the enhancement of a few large, less discrete areas.

CONCLUSIONS

1. Image processing can be a cost-effective tool which can be used to supplement standard manual interpretation techniques of remote sensing data.

2. DIP can be an effective tool for identifying rock outcrops in areas of heavy vegetative cover. However additional studies of DIP of LANDSAT imagery and lower altitude imagery and photography are required to obtain satisfactory results for geologic mapping in areas of heavy vegetation.

3. Ratioing of LANDSAT MSS bands 5/4 by DIP assists in the identification of rock outcrops in areas of heavy vegetative cover.

4. DIP has not been effective to date in distiguishing between outcrops of different lithologies in areas of heavy vegetative cover.

5. AIP can be an effective tool for defining regional linears and regional differences in lithology.

6. DIP lends itself to precise differentiation between units with different spectral signatures. AIP lends itself to coarse definition of large areas.

7. Neither DIP nor AIP can completely replace the use of standard manual interpretation of remote sensing data. They can be used, however, as an additional cost-effective tool to better understand the geologic and structural characteristics of a site region.

ACKNOWLEDGMENTS

We wish to acknowledge the assistance provided by the Professional Development Committee of Woodward-Clyde Consultants, William S. Gardner, Chairman, in the inception and support of this study. We also wish to express appreciation to Richard J. Woodward, Howard M. McMaster and F. M. Babcock for their assistance and motivation. Earl Schaller, Bob Breault, Bill Dallam and Ned Buckman provided guidance and great patience in assisting our work with the GE Image 100. Ray Hinkle of Woodward-Clyde Consultants, Eastern Region, made available data developed from his current study of land use and vegetation classification in the Great Valley using DIP and AIP.

REFERENCES

FENNEMAN, N.M., 1938, Physiography of eastern United States: New York, McGraw-Hill, 691p.

FISHER, G.W., PETTIJOHN, F.J., REED, J.C. Jr., and WEAVER, K.N., [ed.], 1970, Studies of Appalachian geology: Central and southern: New York, Interscience Pub., 460p.

GODDARD, E.M. [chairman], 1965, Geologic map of North America: U.S. Geol. Survey Map, 1 sheet.

GOLD, D.P., PARIZEK, R.R., and ALEXANDER, S.S., 1973, Analysis and application of ERTS-1 data for regional geological mapping in McMurtry, G.J., and Petersen, G.W. [ed.], Interdisciplinary applications and interpretations of ERTS data within the Susque-

hanna River Basin, Resource inventory, land use, and pollution: NASA Annual Rept., 1 June 1972 to 30 May 1973, Contract No. NAS 5-23133 (UN159), p. 120-134.

GRAY, Carlyle, 1960, Geologic map of Pennsylvania: Pa. Topo. and Geol. Survey Map, 2 sheets.

REED, J.E. Jr., 1970, Tectonic map of central and southern Appalachians in Fisher, et. al., [ed.], Studies of Appalachian geology: Central and southern: New York, Interscience Pub., 1 sheet.

SOUTHWICK, D.L., 1967, Engineering geology of northeast corridor - Washington D. C. - Boston, Massachusetts - Bedrock geology: U.S. Geol. Survey Misc. Geol. Map I-514-A.

VINCENT, R.K., 1973, Spectral ratio imaging methods for geological remote sensing from aircraft and satellites: American Soc. Photogrammetry Proc., Sioux Falls, S.D., p. 377-397.

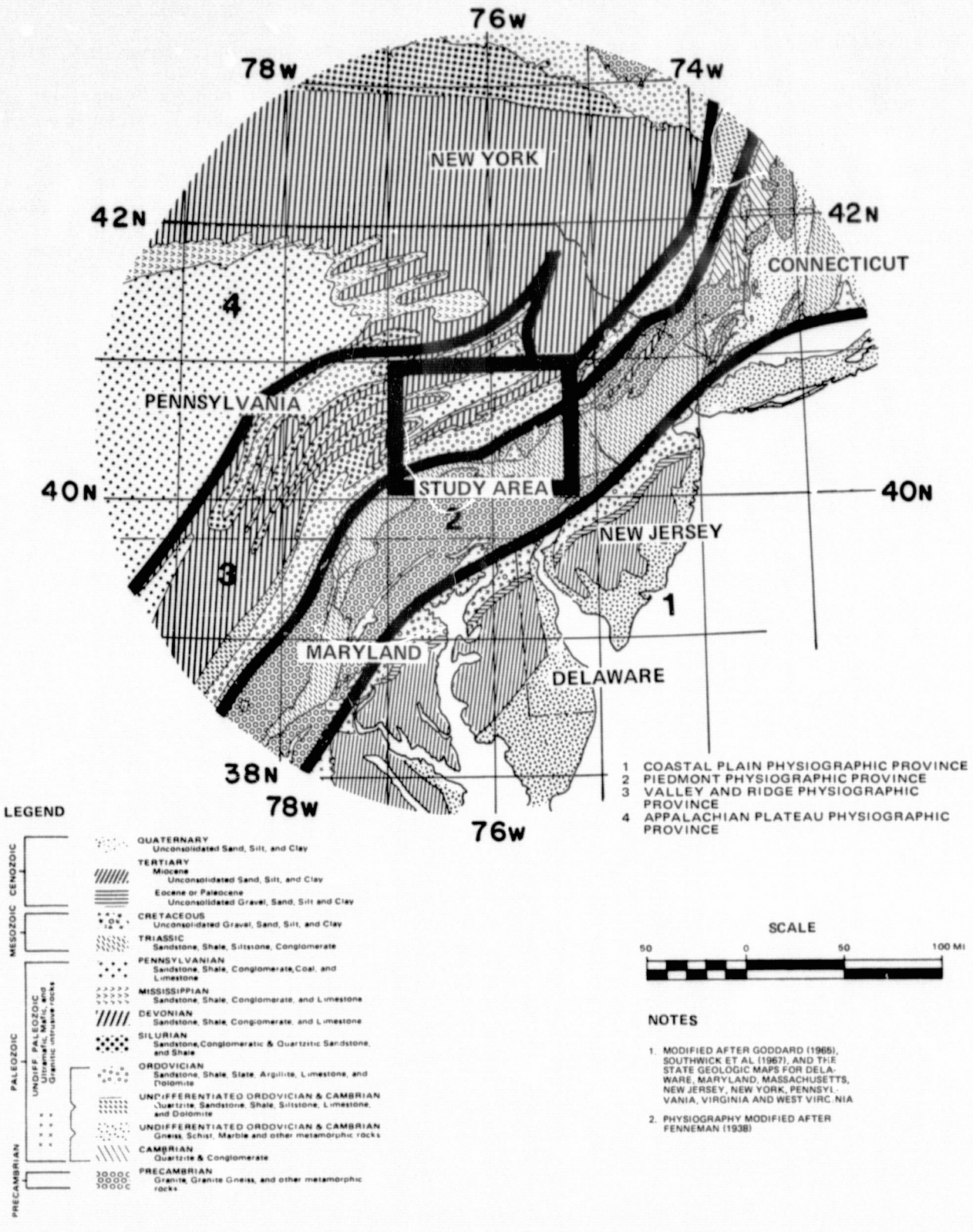
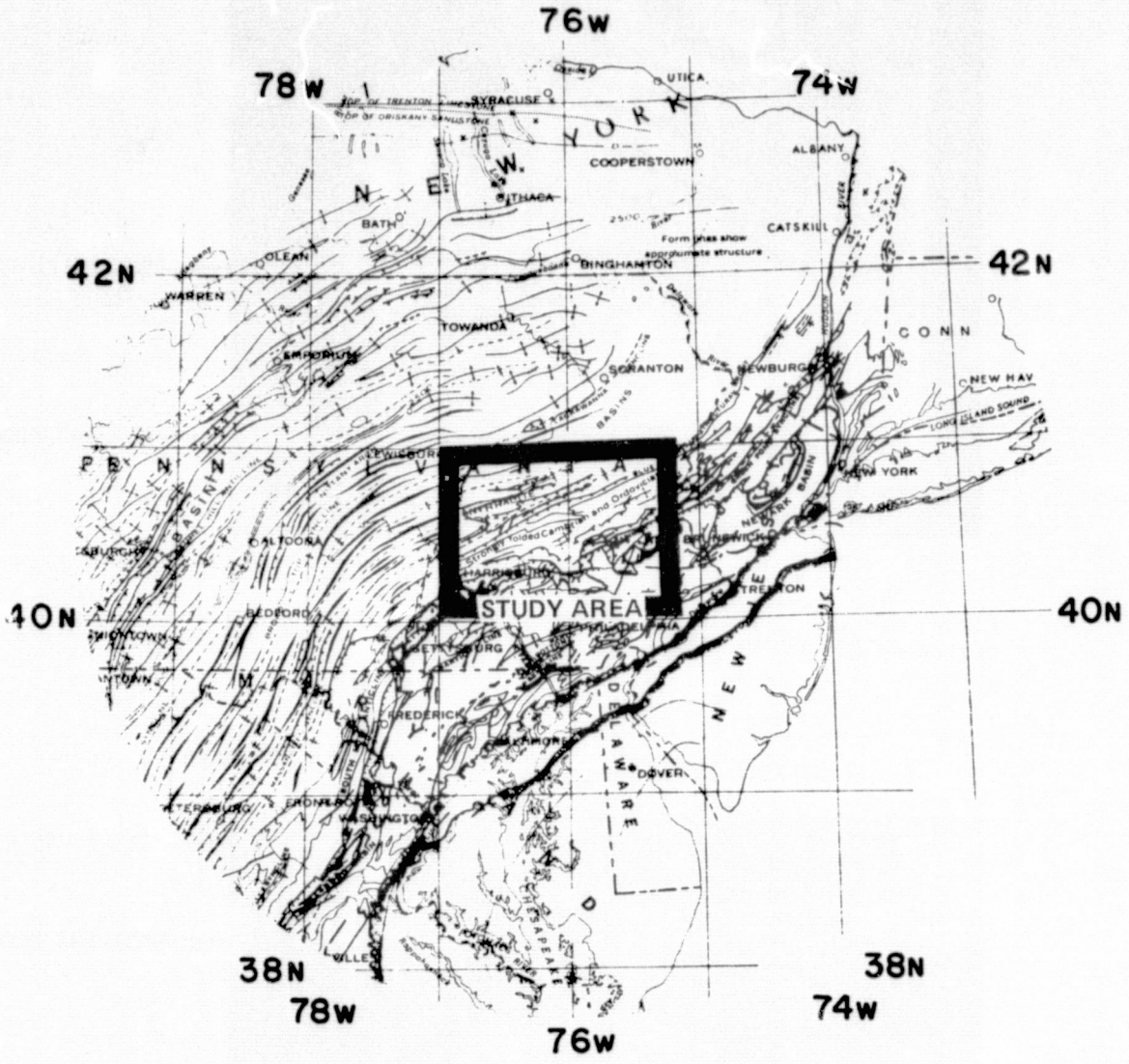


Figure 1.- Geologic setting of study area.



LEGEND

STRUCTURAL FEATURES

- THRUST FAULT — Saw teeth on upper plate, K, klippe
- NORMAL FAULT — Teeth on downthrown side
- TIGHTLY COMPRESSED ANTICLINE
- ANTICLINAL AXIS — Arrow shows direction of plunge
- ANTICLINAL AXIS — Axis of overturned anticline
- SYNCLINAL AXIS — Arrow shows direction of plunge
- STIKE SLIP FAULT — Arrow shows direction of movement
- UNCLASSIFIED FAULT
- STRIKE AND DIRECTION OF DIP OF BEDS

SCALE

50 0 50 100 MI

NOTE

1. MODIFIED AFTER: REED (1970)

Figure 2.- Structural setting of study area.

REPRODUCIBILITY OF THE ORIGINAL PAGE IS POOR

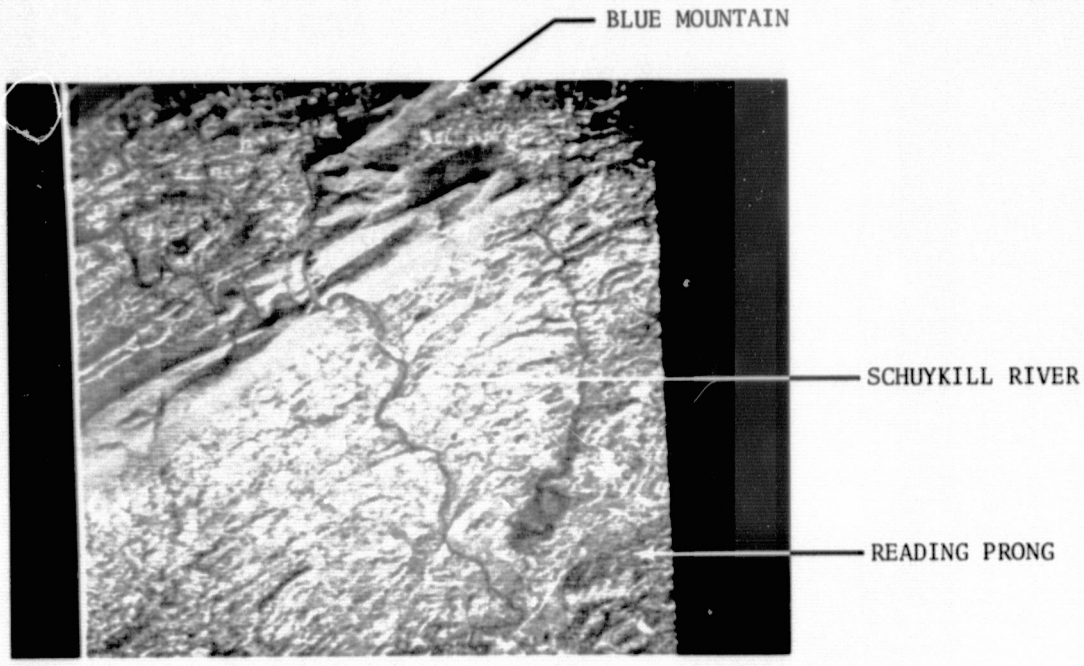


Figure 3.- 1:1 resolution working scene of study area displayed on CRT of GE Image 100 Analysis System.

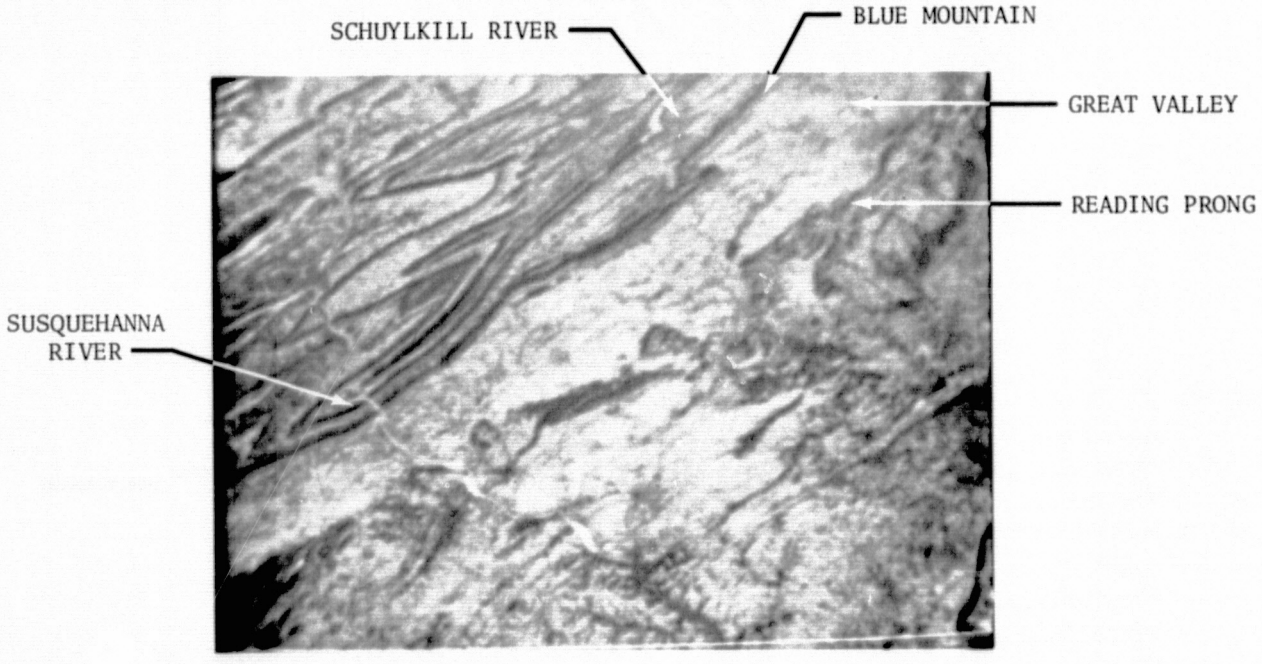


Figure 4.- Study area displayed on CRT of Woodward-Clyde Consultants' VP-8 Image Analyzer.



Figure 5.- Total forest thematic map developed by digital image processing of a 2:1 resolution working scene. Note linears.

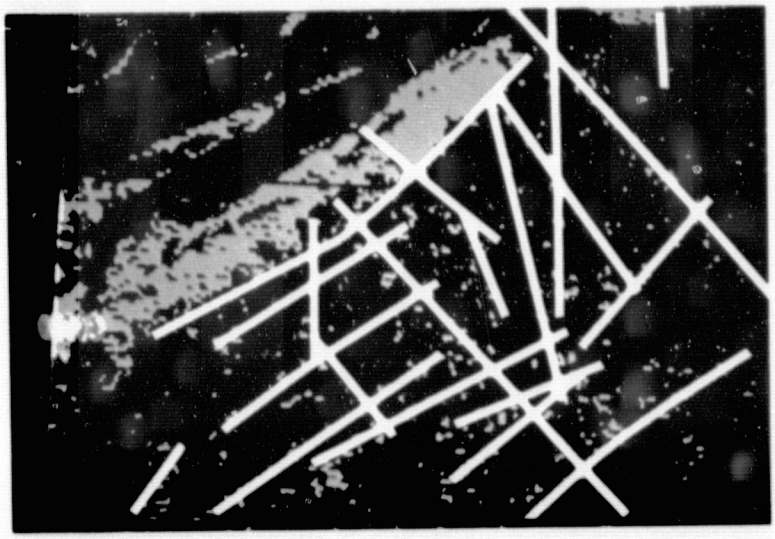


Figure 6.- Thematic map of vegetation developed by digital image processing of a 2:1 resolution working scene. Note linears.

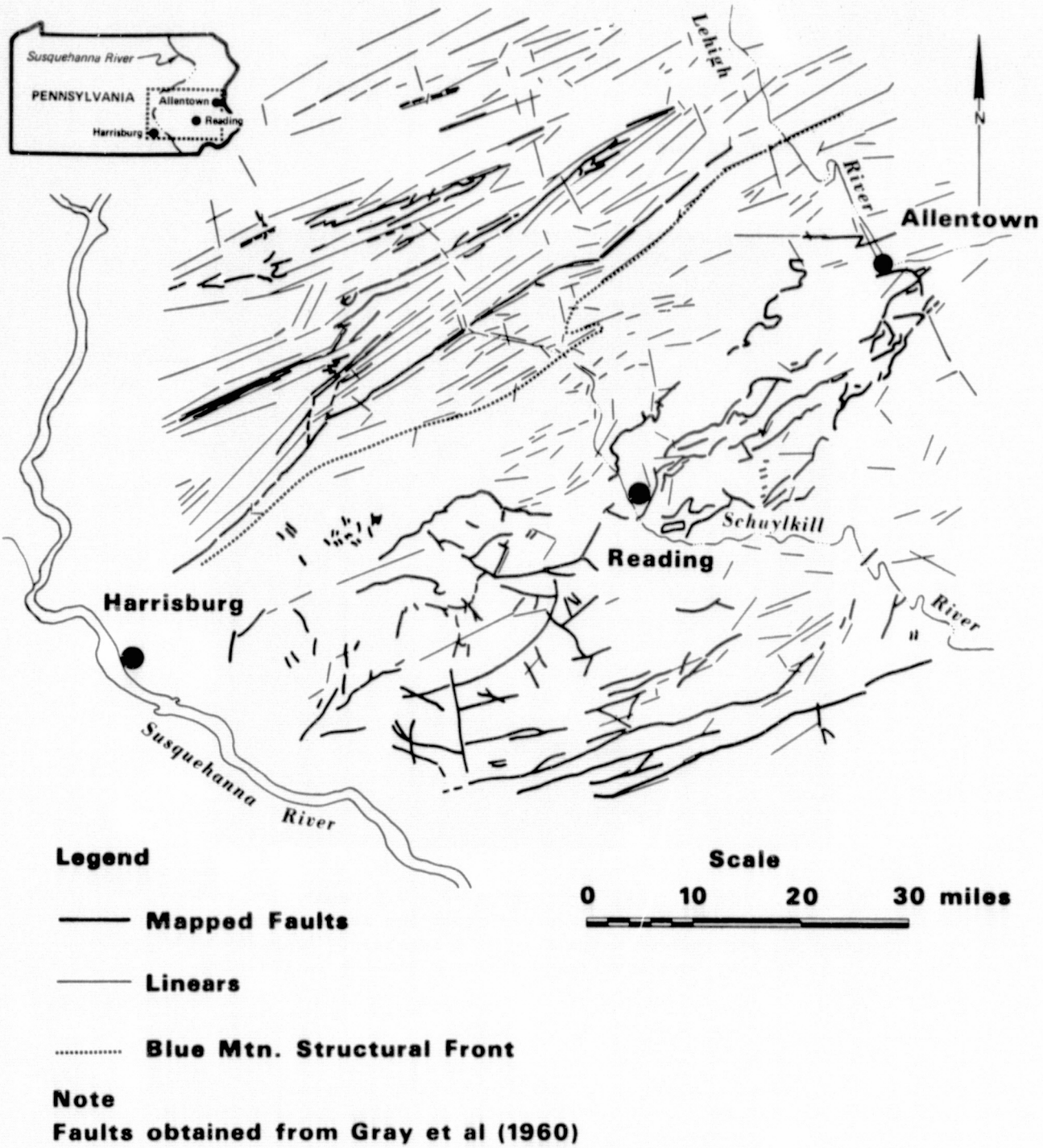


Figure 7.- Linears defined by manual interpretation of LANDSAT-1 image

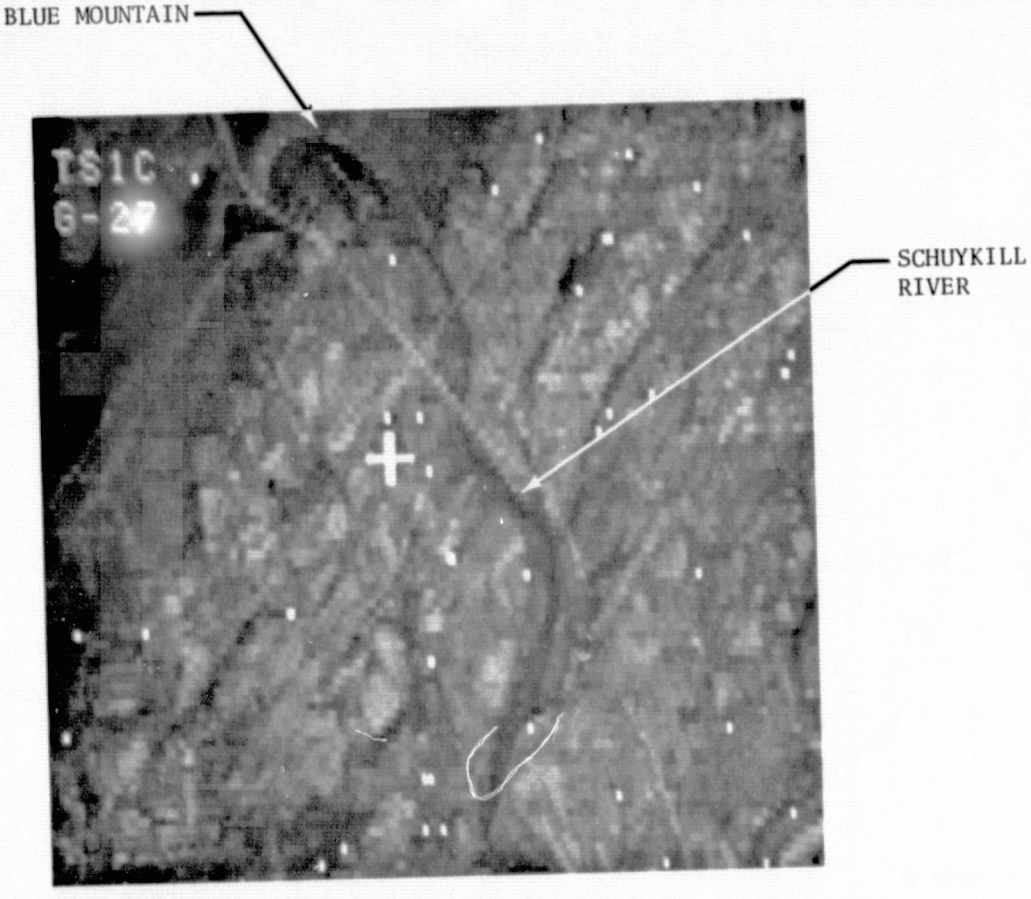


Figure 8.- Digital image processing of a 4:1 resolution working scene with an interbedded sandstone and shale training site. Cursor indicates training site location. Alarmed pixels (white) have spectral signatures similar to training site.

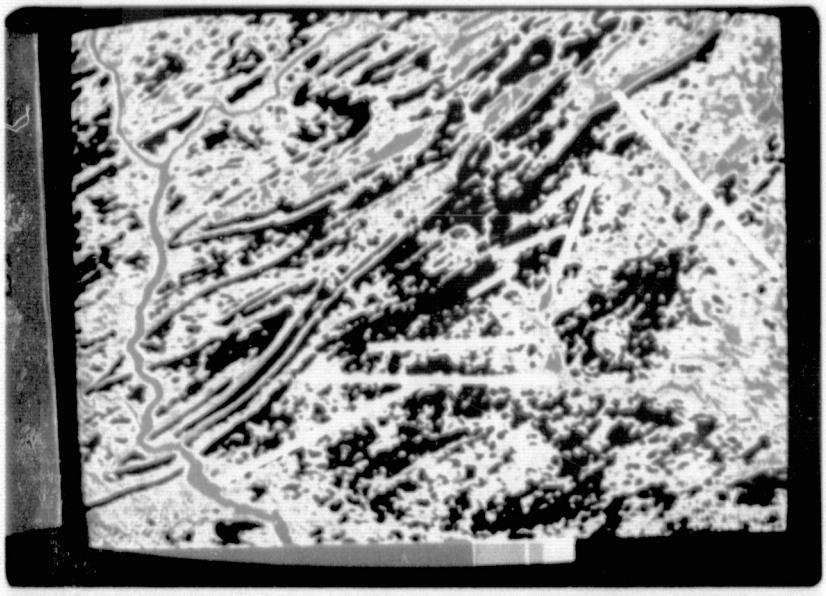


Figure 9.- Analog image processing of LANDSAT imagery. Note linears.

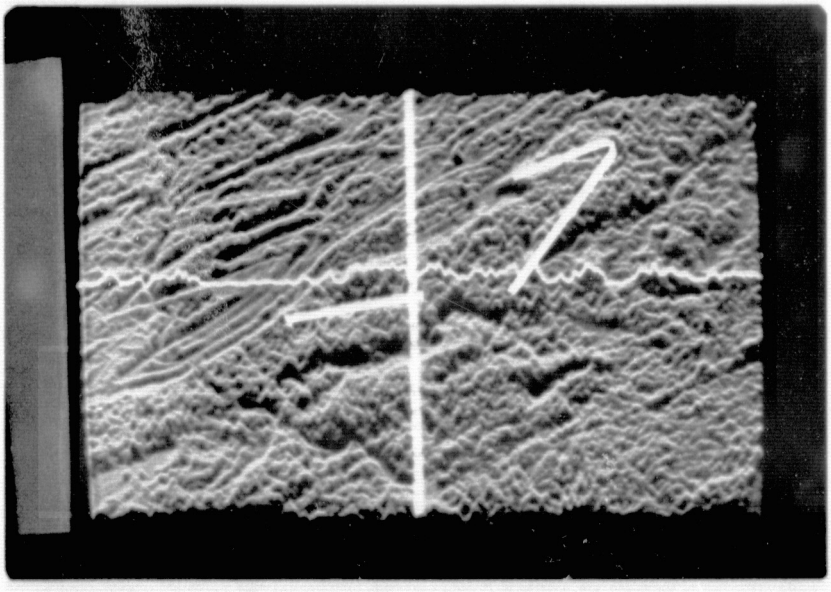


Figure 10.- Pseudo 3-D display of LANDSAT imagery. Vertical dimension represents gray level values. Dark areas are displayed as depressions; light areas as peaks. Note linears.

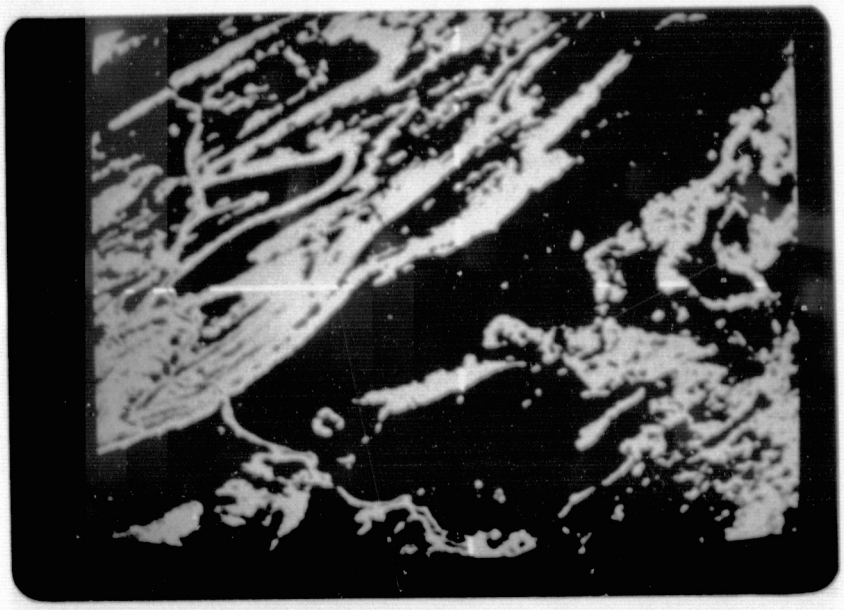


Figure 11.- Analog image processing of LANDSAT imagery. Note definition of Blue Mountain from the Great Valley and the Great Valley from the Reading Prong.

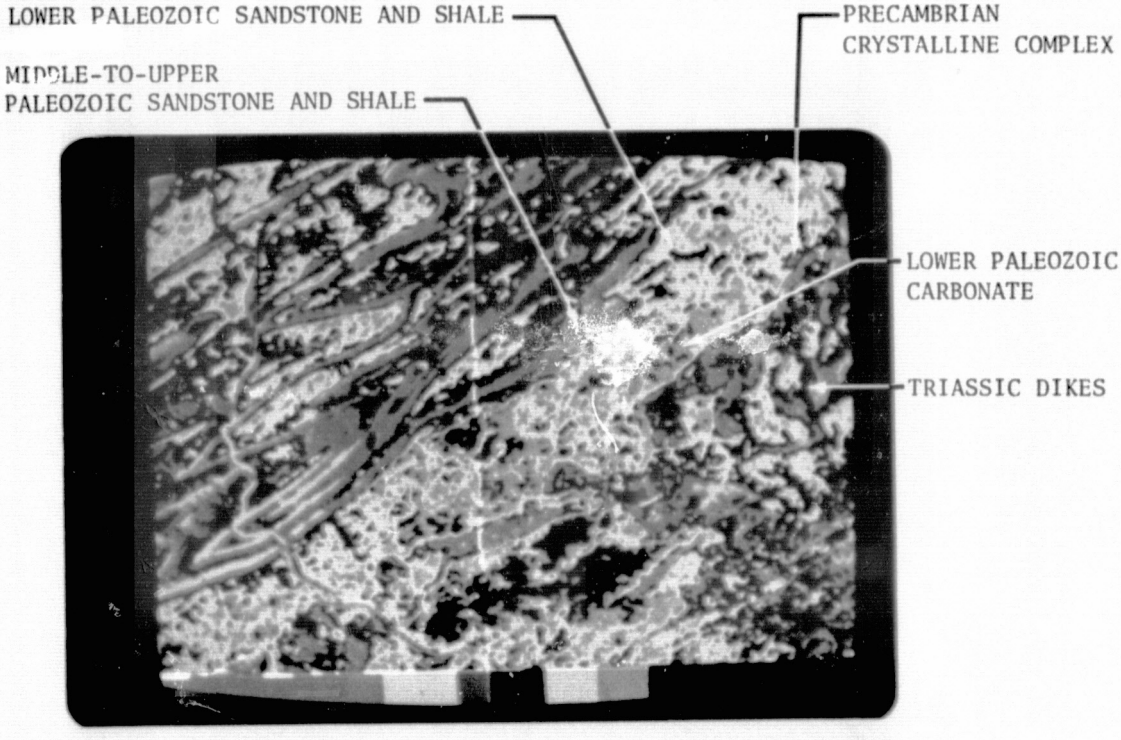


Figure 12.- Analog image processing of LANDSAT imagery. Note definition of geology as a function of elevation and vegetation.

THE SCREWWORM ERADICATION DATA SYSTEM (SEDS)

By Dr. Matthew J. Quinn, NASA, Johnson Space Center, Houston, Texas

N76-17537

ABSTRACT

This paper contains a description of the Screwworm Eradication Data System (SEDS) in general system terms and outlines some of the thinking that went into arriving at the final configuration. One of the objectives of the SEDS was to build a versatile, yet economical, interactive system on the existing Digital PDP 11/45 computers used in the Skylab Production Processing System. Previous experience on various interactive system had given us some background in the best methods of handling image data, registering and correcting the data, and extracting useful information from the images.

INTRODUCTION

The screwworm has been eliminated in many parts of the United States by air-dropping sterile screwworms in areas where screwworms breed. The reproduction of the screwworm can be more or less predicted based on weather conditions -- cold weather slows the breeding, warm weather fosters it, and some moisture appears to enhance breeding conditions which, in turn, improves the chances of screwworm population growth.

The United States has excellent weather coverage from reporting stations all over the country. Temperature, cloud cover, moisture, and other quantities are collected by the US Weather Service. Other countries are often not as well equipped to report in remote areas mainly because the communications are normally not available.

Therefore, to obtain temperature and moisture conditions from remote areas, the NOAA ITOS (Improved TIROS Operational Satellite) was selected to give data from the Very High Resolution Radiometer (VHRR). The VHRR is a two-channel scanning instrument sensitive to energy in the visible spectrum from 0.6 to 0.7 micrometers and the infrared spectrum from 10.5 to 12.5 micrometers.

The ITOS Satellite passes over the United States and Mexico at 9 a.m. local time and again at 9 p.m. Because the orbit has been planned to be sun-synchronous, the daytime picture received on the ground has about the same lighting each day for both the visible and IR scenes. Obviously, the night pass only yields an IR scene. This data can be used to analyze the weather conditions and, in turn, can aid in predicting where potential screwworm breeding areas are located; assuming that the fly is present along with other important survival factors which include the presence of warm-blooded animals.

The Screwworm Eradication Program is a continuing program of the Animal and Plant Health Inspection Service of the US Department of Agriculture (USDA). Since 1962, a USDA laboratory in Mission, Texas has been raising and sterilizing screwworm flies. Each week the laboratory raises up to two hundred million flies and loads them on aircraft to be dropped in selected areas. Because the native female screwworm flies mate only once, by overwhelming the native screwworm population with an overabundance of sterile male screwworms, the USDA has been successfully wiping out the native screwworm population since the eggs laid by the native females mated to sterile males fail to hatch.

Since the sterile screwworm is air-dropped over the remote areas, the information needed by the USDA is where the native screwworms are most likely to breed. Based on studies of the screwworm mating habits, the data obtained from the ITOS Satellite can be used to predict optimum air-drop areas. Locating most likely areas of screwworm breeding and subsequent reproduction is an important tactical parameter in the campaign against this costly pest. The objective of the SEDS is to give the best prediction of screwworm activity to the area epidemiologists and the pilots who will drop the sterile flies.

METHODS OR TECHNIQUES

The ITOS Satellite data is received on S-Band at 1697.5 Mhertz and collected at both Wallops Island, Virginia and San Francisco, California on instrumentation tapes at a speed of 60 inches per second. The data is in a 900 Kilohertz video format which must be first digitized to be used in the PDP 11/45. Since the instantaneous field of view is 0.6 milliradians, the video data is digitized to give pixels at the subpoint of one-half nautical mile. The capability for non-linear sampling intervals was built into the hardware to keep the resolution of all the pixels approximately one-half nautical mile.

The data is input into the PDP 11/45 along with the IRIG B time code to insure that no data is lost and after a data verification check, the imagery can be screened for cloud cover. Then the imagery is registered to a Lambert Conformal Conic Projection (centered on 24 degrees N and 102 degrees W) grid map by selecting up to one hundred gcp's (ground control points). The pin-pointing of the gcp's is relatively easy because an interactive television system was designed as part of the system and using this a controller can "zero" into any area appearing on the screen by enclosing that area by a cursor. The cursor is easily operated by a "joystick" on the control panel accompanying the display. As the operator finds the area containing a geographical feature of known location, he merely switches to a magnification mode. Each pixel is blown up into nine pixels thereby easing the job of identifying the particular pixel associated with the gcp. The gcp is them identified by a preassigned number whose

location has been stored in the computer. This procedure allows the image to be registered to within two pixels or approximately one nautical mile near the satellite subpoint. The one sigma error falls outside of one mile on the edges of the imagery. This two dimensional least square fit corrects the instrument distortion, the earth curvature distortion, and random errors. The data value corrections include radiometric, atmospheric, and emissivity corrections. These corrections are made by comparing the given value with known calculated values and measured ground truth values.

The interactive display was built using shift register memory. In the past we used disc memories to furnish the necessary storage and found that the timing problems gave us system problems.

We also used RAM (random access memory) for display storage. This approach gave us excellent technical results, but was expensive. The shift register approach seemed to give us the advantage of the RAM memories while giving the economies of the disc approach. So far, we have been pleased with the compromise and are enthusiastic about shift register technology for display storage. Some properties of the interactive display are listed in Table I.

The PDP 11/45 processes the data into six different outputs. These outputs of the system are:

1. color enhanced images
2. character density maps
3. level sliced isothermal maps
4. screwworm population dynamics maps
5. rainfall maps
6. data base tapes

Most of the outputs are processed onto microfilm on the III Film Recorder (FR 80). The design goal is to provide output to the user within 48 hours after receiving the data in the mail. This allows only an eight-hour shift to process the data.

SUMMARY

We have learned a lot about such diverse things as unmanned satellites and screwworms. We have been impressed at how good the image is when all aspects of the system are fully understood and used to its full potential. Finally, we were pleased to see how well our display turned out using shift register technology.

REPRODUCIBILITY OF THE ORIGINAL PAGE IS POOR

DISPLAY CHARACTERISTICS

- STANDARD 525-LINE, 30 FRAME PER SECOND TELEVISION
- SPATIAL RESOLUTION 576 PIXELS BY 432 LINES
  ASPECT RATIO OF 4:3
- MONOCHROME OR COLOR OPERATING MODES
  4 INTENSITY LEVELS FOR EACH COLOR
  6 BIT PIXELS -- 2 BITS RED, 2 BLUE, 2 GREEN
- SCROLL TOP TO BOTTOM; BOTTOM TO TOP
- DISPLAY LEFT TO RIGHT; RIGHT TO LEFT
- DATA COMPRESSION SELECT
- 9 TO 1 HARDWARE IMAGE MAGNIFICATION
- X Y CURSOR POSITIONING
- OPERATOR ENTRY CAPABILITY
- INDIVIDUAL COLOR ENABLE

TABLE I

LANDSAT ACTIVITIES IN THE REPUBLIC OF ZAIRE

By Dr. Sendwe K. Ilunga, ERTS-ZAIRE, Earth Satellite Corporation.

N76-17538

The goal of my presentation is to provide the LANDSAT data user community an overview of the LANDSAT data utilization program of the Republic of Zaire, under the auspices of the Office of the President.

Our organization is entitled ERTS-ZAIRE. ERTS is not used in the common English context but rather in a French context: Etudes des Ressources Terrestres par Satellite, or in English, "Study of Terrestrial Resources by Satellite," which is an appropriate description of our objectives.

ERTS-ZAIRE operates under the highest authority of our country; that privileged position has contributed greatly to our progress. Our team has shown that LANDSAT-1 data could contribute significantly to the inventory and analysis of our natural resources, thereby contributing to the improvement of management and planning by our national decisionmakers. ERTS-ZAIRE progress has been rapid, and we are proud as Africans to show that space technology has a value to nations like ZAIRE.

ERTS-ZAIRE activities started soon after the successful LANDSAT-1 launch in July 1972. A team of five Zairian research associates already trained in the broad aspects of the major application fields was sent to the U.S.A. for special training in image interpretation techniques. Our gratitude goes to Professor Colwell and to his coworkers for channeling us through six weeks of training sessions and field activities. Our national proposal to participate in LANDSAT-1 activity was favorably examined by NASA, but could not be included because of scheduling problems. However, a large number of LANDSAT-1 acquisitions were programed over Central Africa, and we have now purchased a LANDSAT-1 data base.

In January 1974, ERTS-ZAIRE, under approval of the Office of the President, hosted a National ERTS Applications Symposium in Kinshasa. More than fifty national and regional resources managers attended. The recommendation of the symposium was that ERTS-ZAIRE should intensify its activity to satisfy the needs of the whole Zairian user community, and to extend the benefits of LANDSAT data utilization to other African countries.

ERTS-ZAIRE has begun a systematic effort to develop and evaluate LANDSAT false color composites, adapted to the African tropical and subtropical ecosystems. Scale 1:200,000 enlargements of the false color composites have been prepared to facilitate applications involving comparison with national resource reconnaissance maps which are also at a 1:200,000 scale.

Our current program is emphasizing topics of economic significance to the national development program of Zaire:

A) Agricultural land use capability analysis, including evaluation of the effects of large-scale burnings,

B) Mineral resources evaluation, and

C) Production of mapping materials for poorly covered regions.

Some technical observations made by the ERTS-ZAIRE team during its two years of experience with LANDSAT data include:

1. For the wet tropics, band 5 plus band 7 false color composites seem to provide a useful interpretation base.

2. False color renditions of vegetation and especially the tropical rain forest by means of the bands 5/7 images filtered to present vegetation in green-blue tones seem to offer an advantage over standard false color products generated by NASA and by the EROS Data Center.

3. Initial experimentation with red-green combinations of band 6 and band 7, to enhance local differences in forest vegetation reflectivities, has shown unexplained large-scale patterns which vary with the seasons. ERTS-ZAIRE is interested in discussing this observation with countries in which similar ecosystem types occur, such as Brazil, Ecuador, Bolivia, the Philippines, Indonesia, Thailand, Puerto Rico, etc.

4. Transparent overlays made from existing maps, or from map printing plates carrying the topography and cultural features, were superimposed on our LANDSAT false color enlargements at scale 1:200,000. This format is gaining acceptance.

5. Temporal composites of LANDSAT imagery are essential to understanding the rapid changes occurring all over Africa related either to seasonal vegetation growth or to human actions like agricultural or pastoral burnings.

The results obtained by the ERTS-ZAIRE team were reported to the director of the Office of the President, Citoyen Bisengimana Rwema, and were instrumental in his decision to consider the installation of a LANDSAT receiving station in Kinshasa. A preliminary report analyzing the pros and cons of such a high-technology undertaking was submitted in July 1974, and contacts were established with NASA. By December 1974, the Office of the President made known its decision to proceed with the receiving station project, at Zaire's expense, and signed a memorandum of understanding with NASA in January 1975.

Two stipulations of the Memorandum of Understanding between NASA and ERTS-ZAIRE have a wide significance:

- The Kinshasa Receiving Station has the capability to acquire LANDSAT data not only over our own national territory, the largest of Africa, but also to provide imagery for 37 other African countries, from Liberia to Tchad to Kenya to Botswana to Namibia.

- ERTS-ZAIRE has agreed to provide free access to all LANDSAT data that its Station may acquire. Our future policy expressly stated during the recent African Regional Conferences in Remote Sensing held in Bamako and Accra will be to acquire data free of charge for the African countries willing to experiment on their own with LANDSAT data over their territories; eventually, ERTS-ZAIRE will require a reasonable participation in the costs whenever a country expresses its wish to utilize LANDSAT data on a pre-operational or profit-producing base.

Our wish is to have components of the Kinshasa Receiving Station in operation by November 24, 1975, our National Celebration Day and 10th anniversary of our renewal; but, in all likelihood, early 1976 should be a realistic goal for our station starting regular production. Experience gained by Zairian technical and management personnel at the INTELSAT Station of N'SELE during the past two years of operation by an all-Zairian team justifies our hope that the LANDSAT/METSAT station of Kinshasa will operate with an all Zairian team as well, after the usual one-year guarantee period during which contractor personnel will work together as a team with their Zairian counterparts.

So, in agreement with the terms of our understanding with NASA, ERTS-ZAIRE intends to provide LANDSAT data to users of the 37 African countries covered in part or in total by the acquisition circle of the Kinshasa Receiving Station. That policy statement was received by the many African delegations participating in the two African Regional Conferences on Remote Sensing held two months ago, in Bamako and in Accra, respectively. ERTS-ZAIRE is well aware of the extra burden resulting from its commitment to cover the needs on LANDSAT data for so many sister countries. We have started right now to size our efforts in equipment acquisition and in training of personnel in accordance with that African-wide demand. International organizations like UNDP and the Economic Commission for Africa have indicated their willingness to combine their resources with ERTS-ZAIRE's own facilities, to develop a properly sized and adequately staffed training complex in Kinshasa. The willingness of ERTS-ZAIRE personnel to engage in bilingual Anglo-French services is one of the reasons why Kinshasa looks forward to its selection as the home of an "African Training Center for Remote Sensing," similar to the ones already in existence in Latin America and in the Indian subcontinent for the Far East.

REMOTE SENSING AS AN INNOVATION: HOW CAN WE IMPROVE ON ITS RATE OF ADOPTION?

By Buzz Sellman, Earth Resources Branch, NASA/Goddard Space Flight Center

N76-17539

ACKNOWLEDGEMENT

The author's perspective on technological innovation dissemination is primarily the result of work performed at the Environmental Research Institute of Michigan (ERIM) and sponsored by the National Science Foundation. The author wishes to acknowledge gratefully his debt to NSF and Dr. Larry Tombaugh, project monitor, and to the ERIM staff.[1]

INTRODUCTION

The efforts by NASA to transfer operationally effective technologies to the public and private sectors has been very successful in some areas, for example, in NASA's contribution to improvements in diagnostic, preventive, and emergency medical situations.[2] However, other efforts have been less successful, such as the earth resources investigation programs designed to apply contemporary remote sensing technologies to "user" needs.

The reasons for the different levels and rates of success are certainly complex, but some of the more important elements and assumptions governing the technology dissemination process can be evaluated in order to improve the rate of adoption of remote sensing. This discussion places particular emphasis upon the potential adopter's environment and arena of work, and his or her expectations and measures of success.

THE INNOVATION DISSEMINATION PROCESS

Remote sensing scientists and technologists, acting as change agents, have collaborated with land planning and management officials in an attempt to use contemporary remote sensing systems for survey, monitoring, and resource evaluation

---

[1]National Science Foundation, Grant Number-GI 34809X1. Two of the final reports from this study are particularly relevant to this paper. Buzz Sellman and Katherine Warner, "The Prospects for Improving Highway Planning Through Remote Sensing Information Systems: A Case Study for Michigan," Report 193500-6-F2, ERIM, Ann Arbor, Michigan, July, 1975. R. Keith Raney, "The Application of Remote Sensing Technology To Local Environmental Planning and Public Policy Formulation," Final Report 193500-6-F, ERIM, Ann Arbor, Michigan, June, 1975.

[2]Toward a Better Tomorrow With Aeronautical and Space Technology, prepared for Committee on Aeronautical and Space Sciences, United States Senate (Washington: U.S. Government Printing Office, 1973).

PRECEDING PAGE BLANK NOT FILMED

programs. Potential adopters of remote sensing systems are also found in the private sector, for example in the forest product and mining industries.

The overall objective of change agents has been to develop evidence compelling enough to persuade the potential user community to adopt remote sensing systems as a new data source and information format for planning and management. If prospective clients (potential adopters) for the technology are considering remote sensing systems for the first time, it is useful to consider these systems as innovations.

Figure 1 depicts an "ideal" innovation dissemination sequence and the relationship between the change agent and the potential adopter. The potential adopter may be aware of the innovation but has not yet reached an informed attitude, either favorable or unfavorable. The role of the change agent is to work with the potential adopter through a discovery, testing and evaluation period to determine whether or not it is in the interest of the potential adopter to become a user.

This is at least a joint educational process. Traditionally, change agents have concentrated on educating potential adopters on the state-of-the-art of remote sensing systems, and sorely neglected to study, evaluate, and become comfortable with the potential adopter's environment, and especially his state-of-the-practice. This omission on the part of change agents is at the heart of the failure of many remote sensing "transfer" efforts to result in permanent, sustaining users of remote sensing systems.

Of the many criteria that pace the rate of innovation adoption, previous research has concluded that the following are crucial to the potential adopters decision to become a permanent user of the innovation.[3]

Relative advantage is the potential adopter's perception of the benefits to be derived from the innovation. These are generally evaluated in economic terms, but the prospective client may perceive an opportunity, through adoption of the innovation, to enhance his personal or professional status as well.[4]

Compatibility of the innovation with current practices determines the scope of adjustment, both institutional and programmatic, to adopt efficiently the innovation.

Innovations that are perceived to be very complex will generally require more time for adoption. While potential adopters will be far more comfortable with simple, straight-forward solutions to their demands, the prospect for such solutions should not be offered unless and until the change agent is satisfied that he can deliver them.

It is generally mandatory that a potential adopter participate in a trial of the innovation. The trial should be a fair and sufficient test of the innovation

---

[3]This section synthesizes some of the research work of Everett M. Rogers with F. Floyd Shoemaker, Communication of Innovations: A Cross Cultural Approach, 2nd edition (New York: The Free Press) 1971, chap. 4.

[4]An interesting and enlightening review of the differences between technical payoffs and power payoffs is found in, Anthony Downs, "A Realistic Look at the Final Payoffs from Urban Data Systems," Public Administration Review, September, 1967, pp. 204-210.

in as near an operational setting as possible.

Finally, the potential adopter must be able to observe the innovation, especially the results or output, before he can decide whether or not he will become a user.

Prospective clients of remote sensing systems may require that additional criteria be tested and satisfied as well, but an assessment of the innovation with respect to the five criteria discussed above must take place prior to adoption by prospective clients.

The participation of the change agent diminishes as the potential adopter becomes more involved in testing and evaluation, and if adoption occurs, the change agent can gradually withdraw from the "transfer" process. A successful innovation dissemination process transforms the potential adopter into a permanent and sustaining user. Having achieved technical independence from the change agent, he is now in a position to act as a change agent with others of similar interests and professional responsibilities.

FINDING A MIDDLE GROUND FOR CHANGE AGENTS AND POTENTIAL ADOPTERS

Of the many assumptions governing the posture of technologists attempting to transfer remote sensing system capabilities to the "user" community, the following two are generally acclaimed as very favorable and compelling reasons for adoption.

The first is that there are large area inventory requirements facing land resource planners, and that newer demands are exceeding the capacities of convential inventory techniques to keep pace with ever expanding data demands. A corollary to this first assumption is that decision-making is also increasing in pace and importance and there is a need to rapidly and efficiently translate the "needed" large data volumes into information formats that public and private officials can bring to bear on land resource management issues.

The second assumption is that the availability of better information, especially of the type that has never been previously available, will result in better planning and management decisions.[5]

While these assumptions appear reasonable in theory, they deserve closer scrutiny in practice. This is especially true if they are to continue to constitute the basis for high expectations on the favorable impact of remote sensing on land planning and management issues.

Computerized urban data systems have not transformed or revolutionized metropolitan planning and decisionmaking per se, despite the enormous data volumes they can handle and the programmable information outputs that they provide for analysis of urban issues. In short, measurable progress in the quality of planning and decisionmaking is not an immediate and determined product of more data and better information. As such, advancement toward this end cannot be achieved soley because the state of the art in data collection and information extraction has been improved through remote sensing systems, or any others.

---

[5]Anthony Downs, p. 204.

There is a need for a change in style on the part of change agents and a reordering of the emphasis that remote sensing ought to play for land resource planning and management goals.

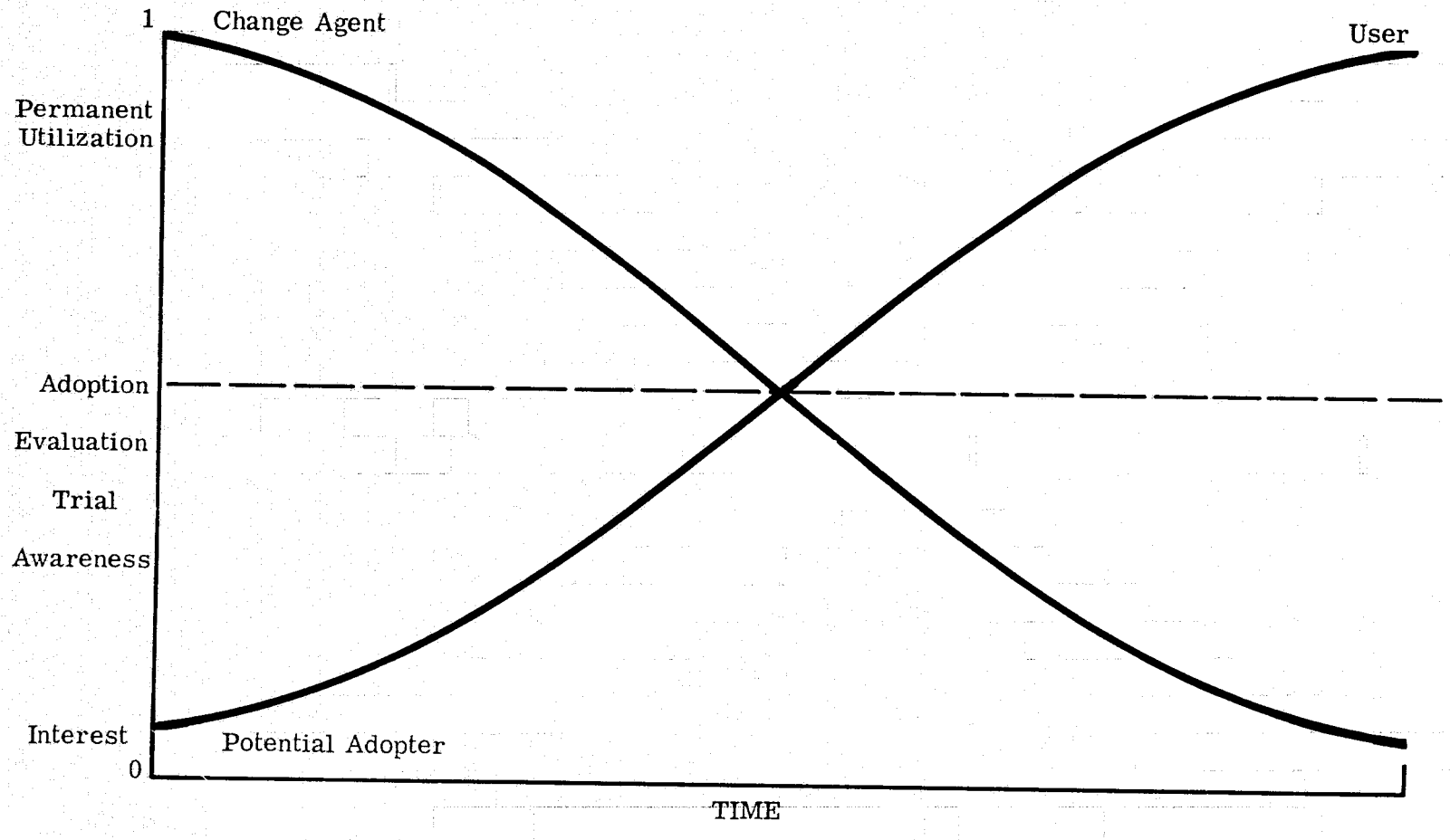
Change agents will need more time to work with potential adopters, and any time gained should be used by them to become far more educated about the potential adopters' state of the practice. This new role and emphasis must be recognized as a legitimate and necessary function of change agents if they are to successfully transfer remote sensing systems into the "user" community.

A new emphasis is needed because technologists overestimate the utility of remote sensing systems to "solve" problems and underestimate the complexity of the potential adopters current data and informational problems; that is, the techniques and practices presently employed to effect planning and management goals and the capacity to change those practices.

If this means lowering the alleged significance (impact value) of remote sensing during negotiations with potential adopters, so much the better. If it means agreeing on a more modest set of goals for the technology, so much the better.

A potential adopter will probably be far more receptive to a collaborative effort as a result of such a change in emphasis. He will still require performance based on the criteria of relative advantage, compatibility, complexity, trial ability, and observability. Yet the legitimate role and value of remote sensing systems is more likely to be discovered in the process.

It should be remembered that remote sensing is in clear competition with other solutions to land planning and management information demands. One of the most formidable competitors, especially in the eyes of potential adopters of remote sensing, is the decision to do nothing new. If advances in the state of the art (new and improved) continue to be the emphasized message of remote sensing change agents, potential adopters probably won't believe it, and more importantly, probably won't buy it.



"IDEAL" INNOVATION/DISSEMINATION SEQUENCE

FIGURE 1

M-DAS - SYSTEM FOR MULTISPECTRAL DATA ANALYSIS

By Robert H. Johnson, Bendix Aerospace Systems Division
Ann Arbor, Michigan

N76-17540

ABSTRACT

M-DAS is a ground data processing system designed for analysis of multispectral data. M-DAS operates on multispectral data from LANDSAT, S-192, M^2S and other sources in CCT form. Interactive training by operator-investigators using a variable cursor on a color display is used to derive optimum processing coefficients and data on cluster separability. An advanced multivariate normal-maximum likelihood processing algorithm is used to produce output in various formats: color-coded film images, geometrically corrected map overlays, moving displays of scene sections, coverage tabulations and categorized CCTs.

The analysis procedure for M-DAS involves three phases: (1) screening and training, (2) analysis of training data to compute performance predictions and processing coefficients, and (3) processing of multichannel input data into categorized results. Typical M-DAS applications involve iteration between each of these phases. A series of photographs of the M-DAS display are used to illustrate M-DAS operation.

INTRODUCTION

M-DAS is the Multispectral Data Analysis System developed and produced by The Bendix Corporation. M-DAS, shown in Figure 1, interactively processes multispectral scanner data from LANDSAT and from M^2S the Bendix airborne multispectral scanner. M-DAS also has capabilities to measure ground control points, compute and resample multispectral data to a precision coordinate system; to digitize film data; and to record output data on film.

From left to right in Figure 1 the components of M-DAS are:

(1) The Decwriter, used for some operator commands and hard copy printout of analysis data.

(2) The Color Moving Window Display, this presents a color coded display of a 320 by 240 pixel field of data. The operator may move this display through the 25 by 100 n mi field contained on LANDSAT CCT to view areas for training set designation, and color coded categorized results.

PRECEDING PAGE BLANK NOT FILMED

(3) The Operator Interaction Panel, provides controls to move the display field, change scale, display mode, position and shape cursor and to enter and modify training set data.

(4) The PDP-11/35 CPU, which performs M-DAS control and some processing functions. A disk memory is included which retains problem data for many investigators who share M-DAS.

(5) The MCP - Multivariate Categorical Processor - which provides high speed operation in categorizing multispectral data.

(6) The MDIP - Multichannel Digital Input Processor. This unit interfaces the optional High Density Tape Recorder to input 14 track M^2S tapes.

(7) Dual Magnetic Tape Units, these units accept the LANDSAT or M^2S CCT's (Computer Compatible Tapes), and also produce output CCT's of categorized or geometrically resampled data.

The M-DAS System design incorporates considerable experience in multispectral data processing. Bendix has operated a service center for multispectral data processing since 1968, and the M-DAS techniques have been proved on this center. A prototype M-DAS System has been delivered to Argentina, and a second system is being installed in Japan. Bendix currently operates two more systems as service facilities.

To illustrate the operation, a set of photographs was taken of the M-DAS color moving window display during the analysis of a LANDSAT scene covering the east shoreline of Saginaw Bay in Lake Huron.

The sequence of photographs shows three M-DAS modes of operation: Training, Analysis, and Categorization. The M-DAS operator selects training sets of multispectral data from small areas in the scene for which he has ground truth or which appear to be homogeneous in the image of the scene. The analysis mode evaluates the statistics of this training data to determine the optimum coefficients for categorization and to predict the performance of the categorization. The categorization uses the coefficients from analysis and for each multispectral pixel makes a decision to assign that pixel to the most likely category.

M-DAS Training

M-DAS training involves interaction between the investigator-operator and the multispectral data. The operator first controls the area viewed by the color moving window display to move it to view an area containing training sets.

Figure 2 shows the initial display during this mode on the sample analysis of LANDSAT data. The display shows the full 46 Km width in a false color mode with LANDSAT bands 7, 5 and 4 assigned respectively to red, green and blue.

Figure 3 shows the area in Saginaw Bay selected for extraction of initial training sets, expanded to fill the M-DAS display. The width of the displayed image is now 20 Km.

In Figure 4, the gamma function has been changed to display each channel in a composite which better shows water body differences. Figure 5 shows the color sliced mode where one band, in this case LANDSAT band 4, is assigned a programmed set of color-intensity-saturation combinations to each radiance level. In this case the shades of grey and cold colors represent low intensities, and bright and warm colors represent high intensities.

Figure 6 shows the M-DAS quadrilateral cursor positioned to designate the first training set, near offshore water. Figure 7 shows the next, deeper water training set. A sample of a small inland training set is shown in Figure 8.

Up to 99 training sets assigned to up to 49 groups may be designated in the analysis of a set of multispectral data from LANDSAT or M^2S. As each training set is defined by the quadrilateral cursor, it is assigned to a group and a color for later categorized displays.

M-DAS Analysis

With these and several additional training sets, the first operation of M-DAS in the analysis mode was run. The following photographs show the display of data on the moving window display of the data from analysis of these sets.

The analysis mode will be typically run iteratively several times during the processing of one LANDSAT scene. Before each of these runs, new training sets will be added, and the categorization of previous training sets will be viewed and these sets will be modified to improve their homogeneity.

Figure 9, shows the first part of the analysis display. This summarizes the training set-group associations and the number of samples (pixels) in each set.

Figures 10 and 11 show the statistical data presented for each group (category). This data shows the means and variances of the training data associated with the group in each measurement channel (LANDSAT band). Following this the Eigenvalues for this category are shown. The Eigenvalue shows the overall statistical separability of this group from all other groups. A value of 100 means that on the average there are 10 standard deviations ($\sqrt{100}$) between this group and the others in the most productive direction in 4 space for the decision on the group shown.

Further data for each group is displayed: the coefficients to transform the input (LANDSAT measurement) variables into the decision space of the eigenvalues. On the right the contribution of each input variable to the decision variables for this group are shown.

The last data displayed for each group is a table that shows the separation of each other group, in units of standard deviations of the subject group and in decision axis system. With some familiarization the M-DAS operator-investigator can quickly tell if his training sets represent separable clusters and if inspection, retraining or consolidation of groups is required.

The above data is repeated for each group and the operator can stop the display to closely study any part of the data. A printout of this data may also be obtained.

A prediction of categorization performance in the form of a truth table as shown in Figure 12 is also available at this point. This table shows the probability of correct identification of each training set based on its multivariate normal statistics, and the probability of each type of false categorization.

M-DAS Categorization Processing

Using the coefficients derived from the analysis above, the display of scene data is resumed, but this time in the categorization mode. In this mode each pixel is displayed in the color assigned to the group that pixel is categorized to. The display, cursor and other functions may be performed while categorizing as with the false color and color sliced modes. The next series of slides show this categorized display after analysis of the first seven training sets.

Figure 13 shows the 20 Km wide section of the scene at Sand Point and the cursor is recalled to show the training set for close offshore water where it was originally placed. The training set is reasonably homogeneous as shown by the uniform category within the boundaries of the cursor.

Recall of training set 2, as shown in Figure 14 shows that this is not a satisfactory or homogeneous training set. At this time it is deleted and repositioned as shown in Figure 15, and re-entered.

Other training sets are also checked and modified as shown on Figure 16 for the small area of distinct vegetation in training set 3. In this display several areas in the land are shown as black which means that these areas are not sufficiently alike any of the seven groups designated so far to be categorized. The threshold, in terms of the number of standard deviations from the mean of each group, that controls the extent of the black areas is selected by the M-DAS operator.

As shown in Figure 16, a new training set and group is assigned in one of the contiguous black areas, beginning to build the number of distinctive categories recognized in these scenes. After the addition of this new set and the refinement of the others as shown above, the analysis mode is run again. The new results are then viewed as shown in Figure 17, where the orange color shows the new added category.

This process of refinement, addition of new categories, and reanalysis can be continued until the desired separations are made or until all separable categories in the data are obtained. Typically more than 20 categories can be extracted from a LANDSAT scene. Where training is initially conducted from ground truth samples, the process later will converge to refinement and addition of new categories where ground truth is not available, and the same categories will be obtained for each area in the scene as the process is converged.

The categorized or false color display may also be expanded as shown in Figure 18 by placing the cursor over the desired area for expansion and expanded by a factor of two as in Figure 19, or of four as in Figure 20

M-DAS output products include the categorized display, as shown at a 25 mi scale in Figure 21. Color film recordings may also be made and may be geometrically corrected and scaled to overlay with precision on map bases. Other outputs include area tables for each category within operator specified boundaries as shown in Figure 22, and categorized scene data on a CCT, to enter in a digital data base.

PERFORMANCE

M-DAS uses multivariate normal, maximum likelihood categorization. The computations for each pixel are made in a transformed multivariate space which rejects the components with negative correlation with the decision required. Because of this, M-DAS offers both very high sensitivity in processing LANDSAT data and can process all eleven channels simultaneously of M^2S data. Typically 20 to 30 categories can be derived from a LANDSAT scene.

Using the iterative training-analysis-categorization approach as described previously, different operators can analyze the same scene with M-DAS and obtain the same results. This repeatability results from the accuracy of the M-DAS categorizer and the insensitivity of the iterative process to the initial training sets selected or to errors in initial training.

M-DAS also has high throughput in performing the complete job of analysis of LANDSAT or M^2S data. It is a balanced system in providing efficient means to converge and identify the groups or clusters inherent in the scene data, high categorization accuracy to extend the range of training data applicability, and a high speed hardware for processing categories. Typically a full LANDSAT scene can be analyzed in one working day, 8 hours; 6-1/2 of this 8 hours are used for interactive training and analysis and the remainder for producing categorized, geometrically corrected film.

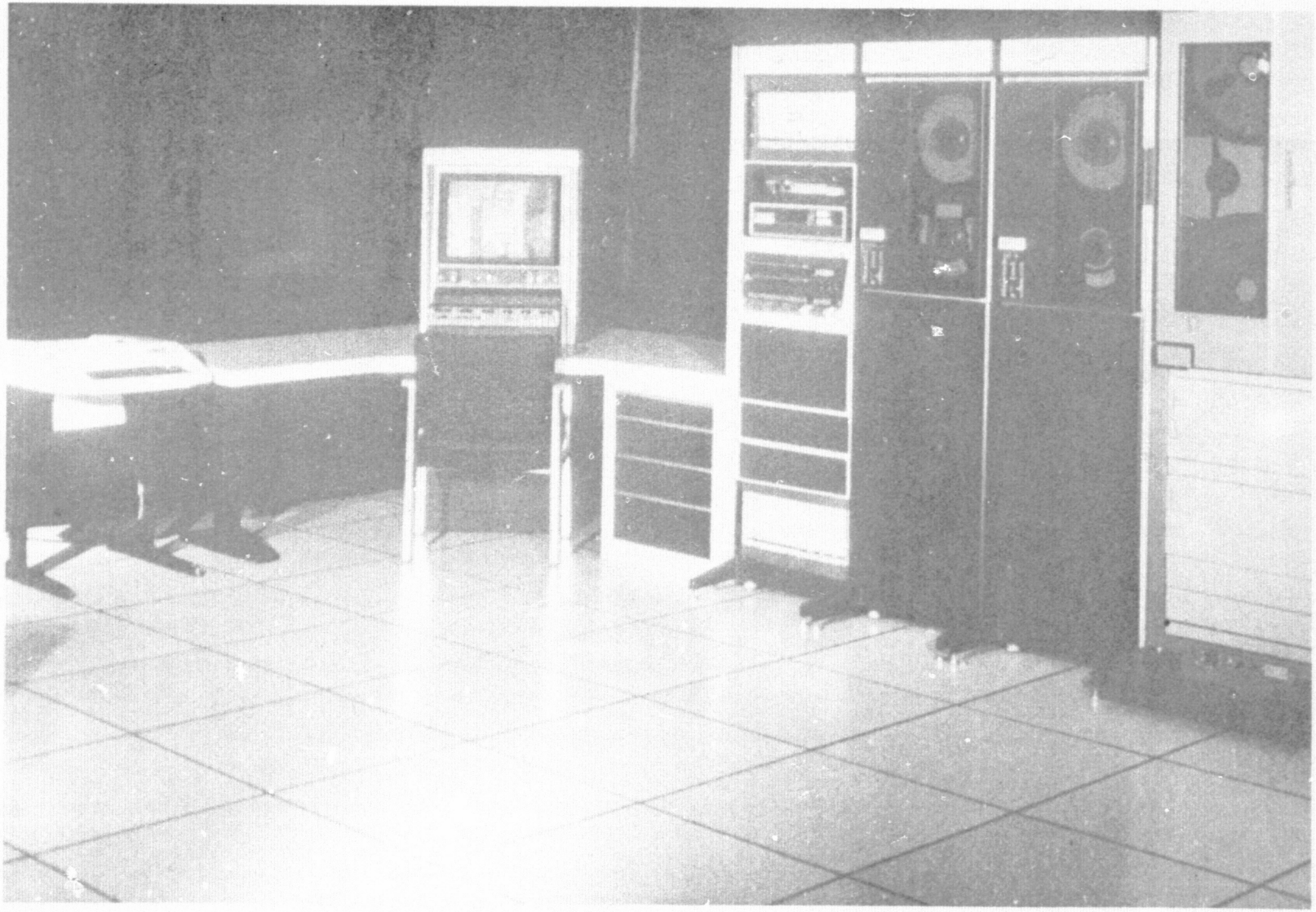


Figure 1.- M-DAS mini data analysis station showing, from left to right, a decwriter, a color moving window display, an operator interaction panel, a PDP-11/35 computer, a multivariate categorical processor, a multichannel digital input processor, and dual magnetic tape units.

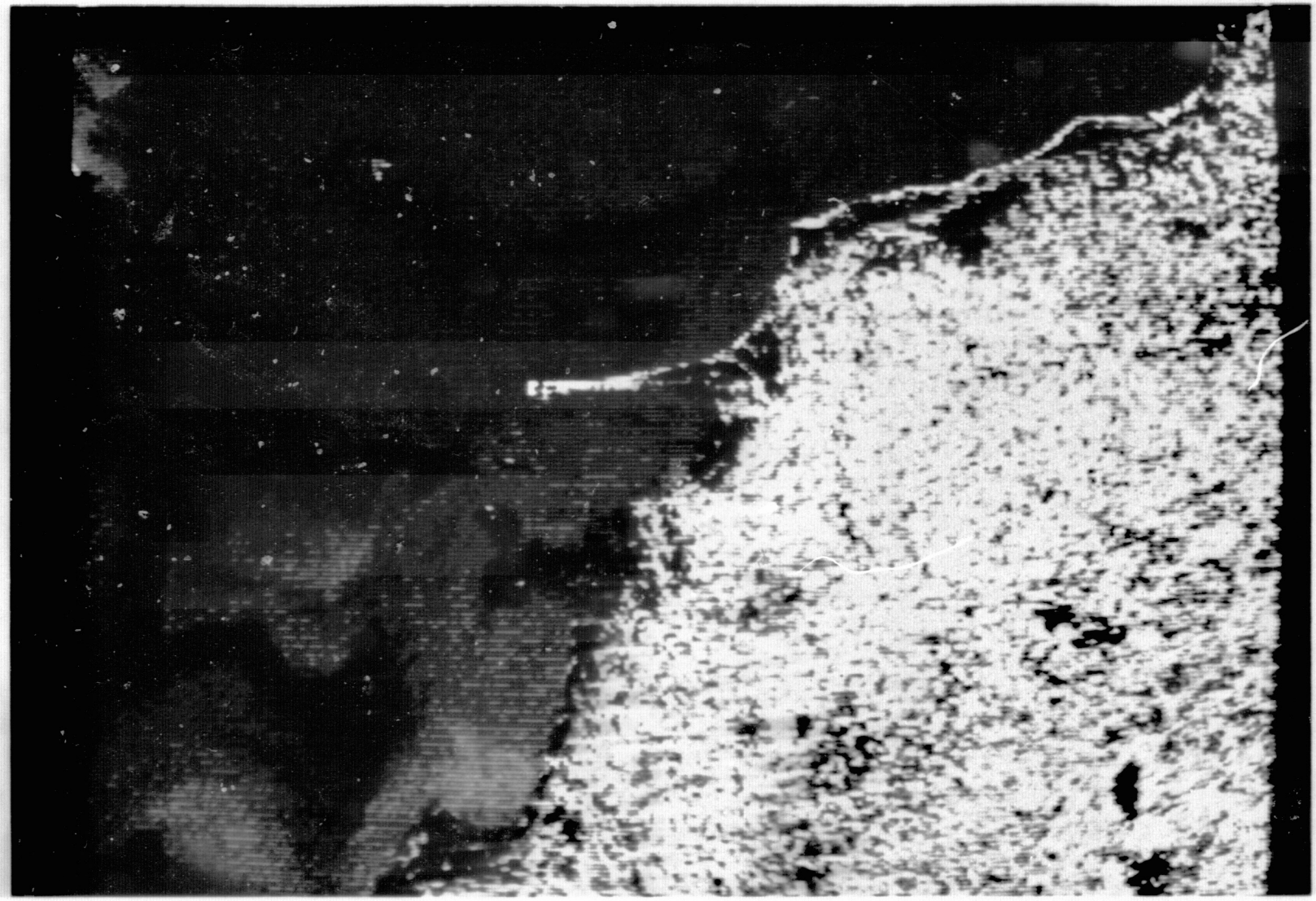


Figure 2.- M-DAS using bands 4, 5, and 7 that shows initial display of LANDSAT data of Sand Point in Saginaw Bay, Michigan.

REPRODUCIBILITY OF THE ORIGINAL PAGE IS POOR

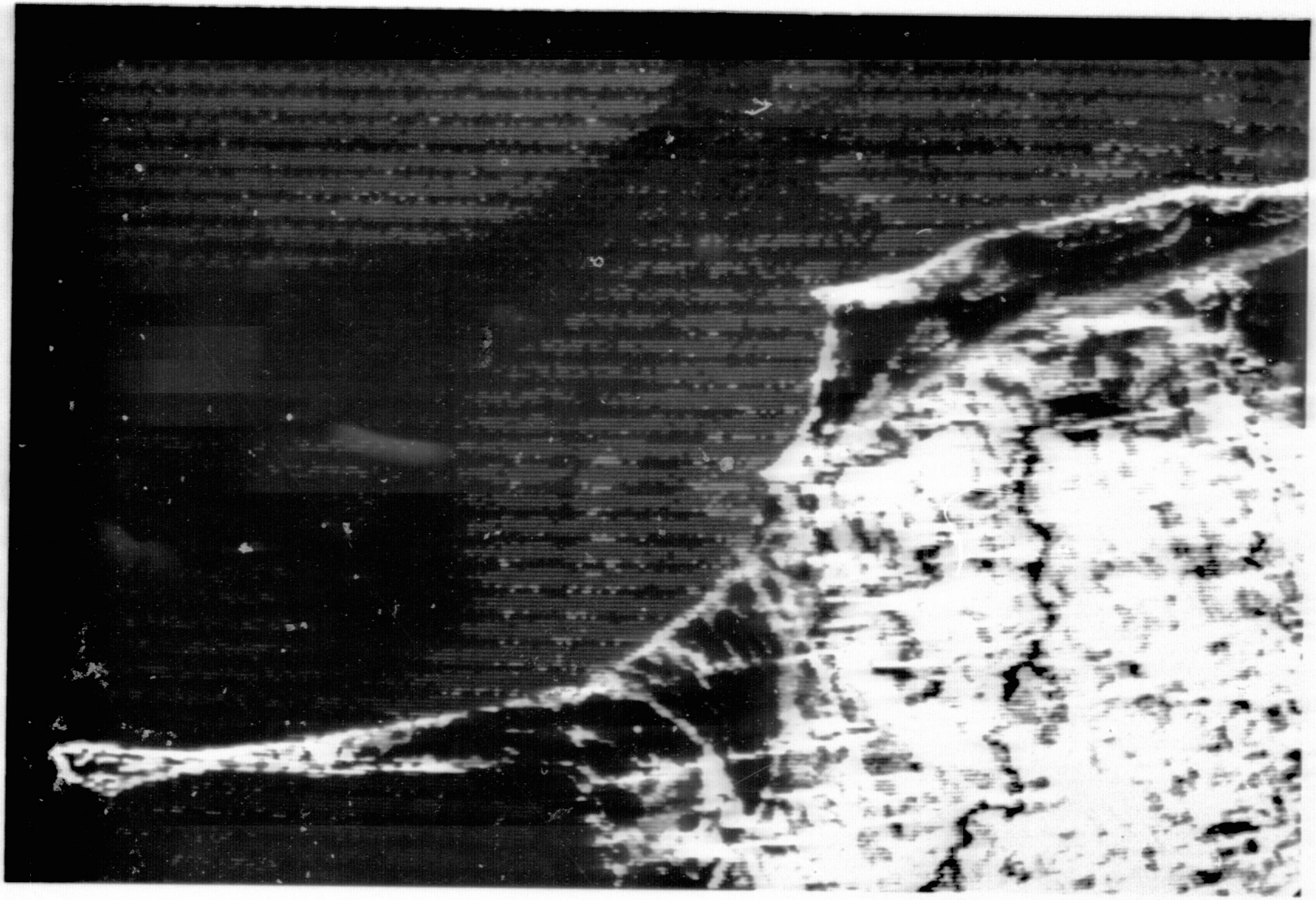


Figure 3.- M-DAS using bands 4, 5, and 7 that shows an expanded image of figure 2.

REPRODUCIBILITY OF THE
ORIGINAL PAGE IS POOR

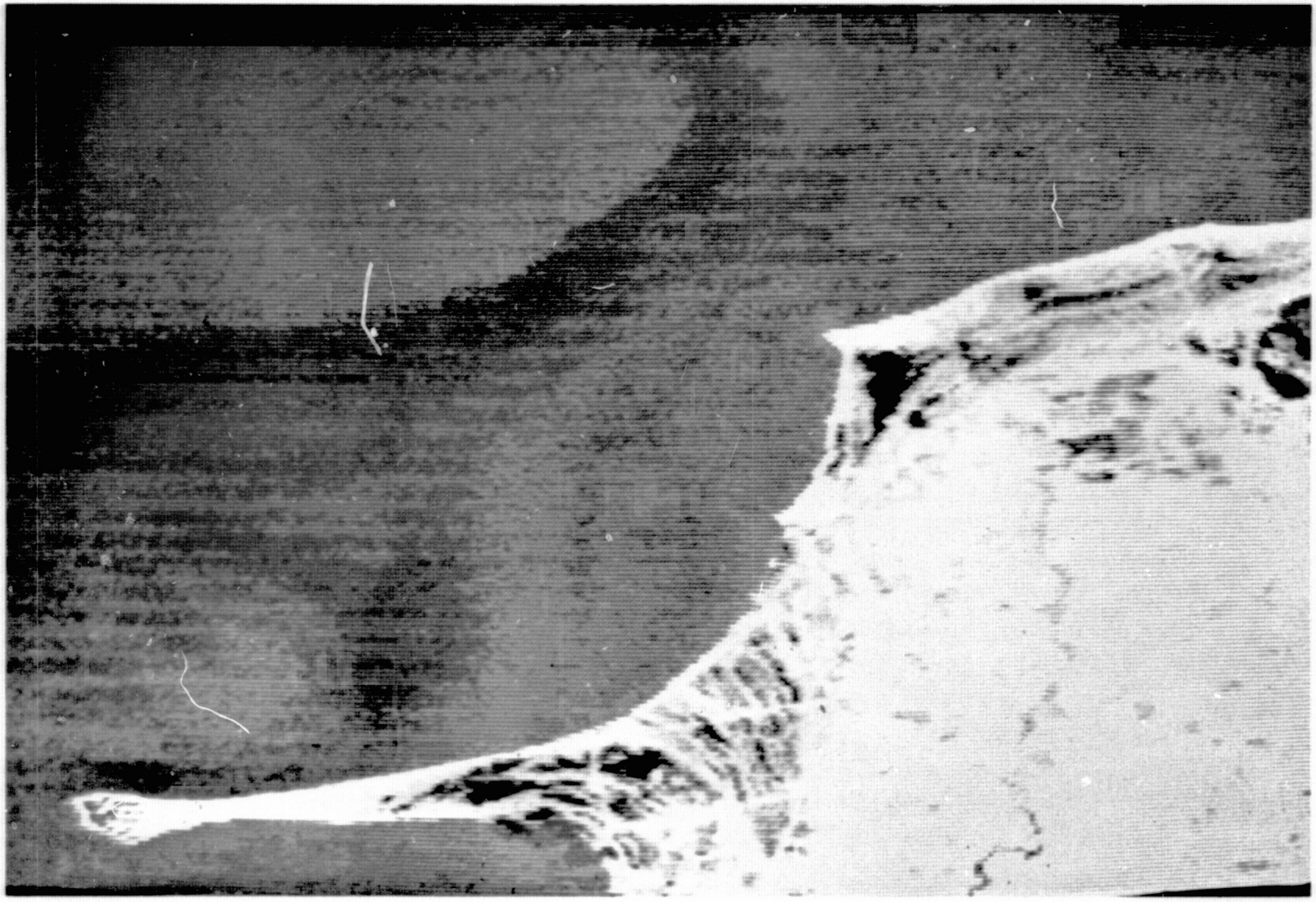


Figure 4.- M-DAS using bands 4, 5, and 7 that shows color sliced image with gamma function changed of Saginaw Bay, Michigan.

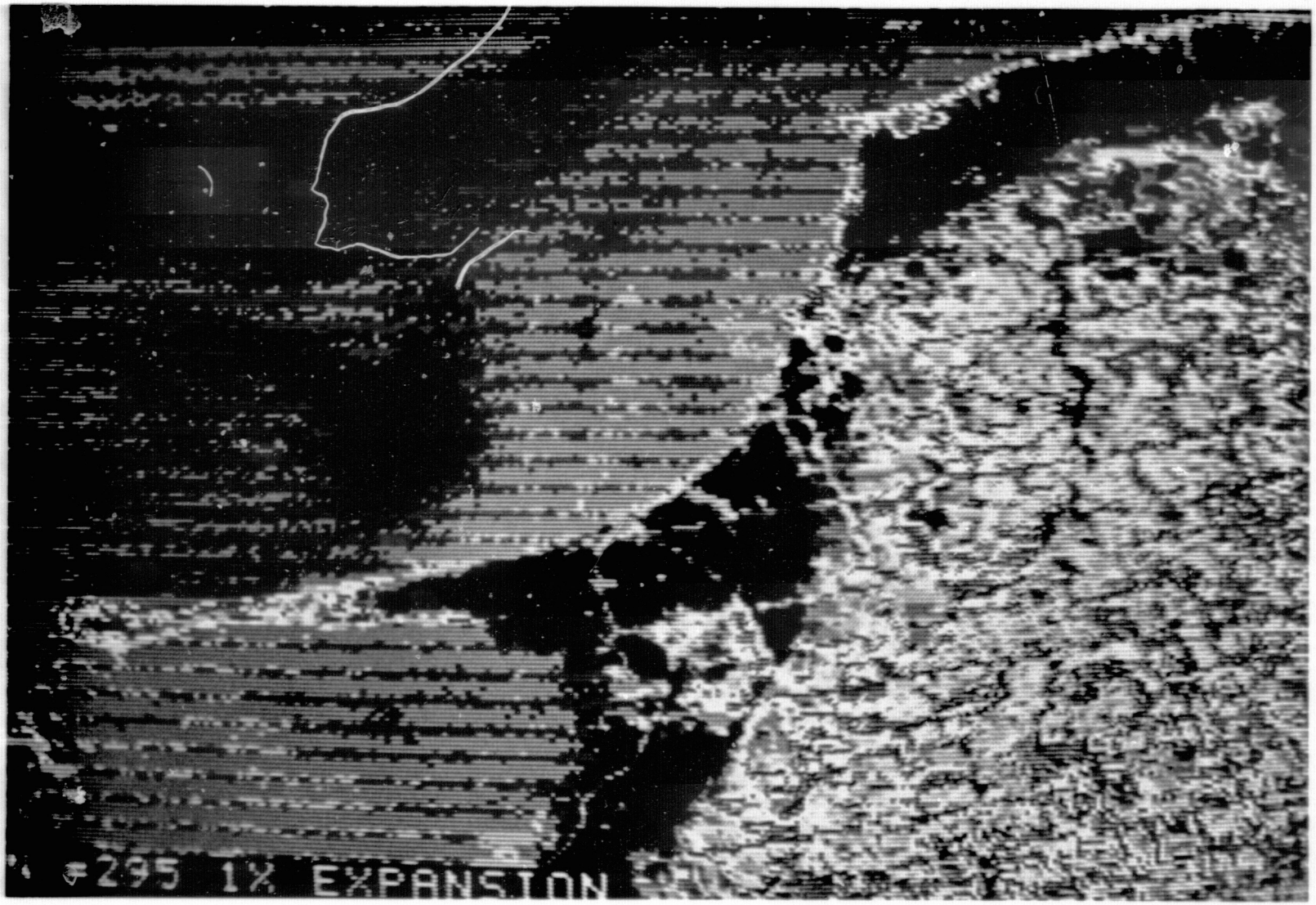


Figure 5.- M-DAS using bands 4, 5, and 7 that shows color sliced imagery with a band 4 assigned set of color-intensity saturation combinations.

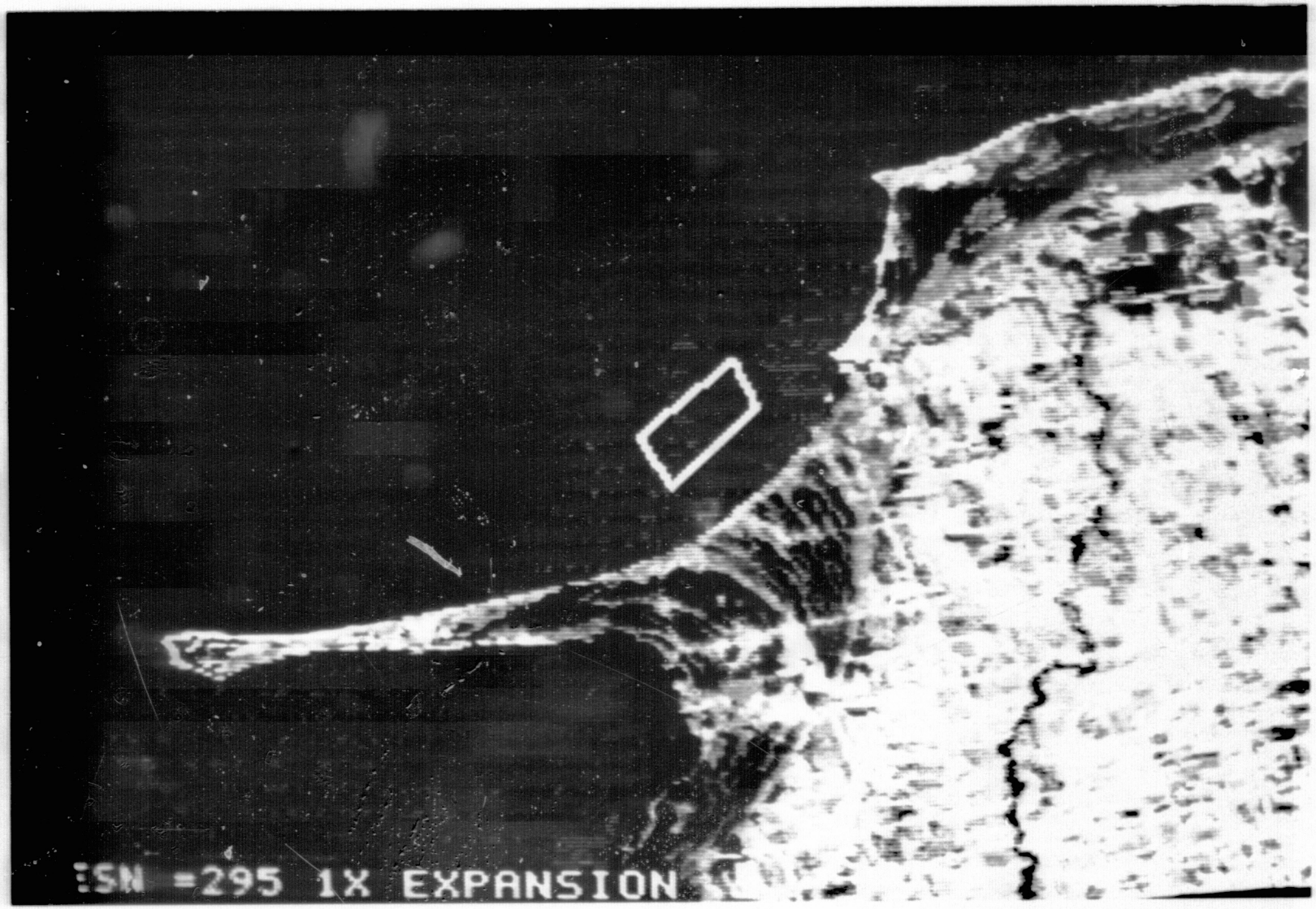


Figure 6.- M-DAS image using bands 4, 5, and 7 that shows offshore training set of Saginaw Bay, Michigan.

REPRODUCIBILITY OF THE ORIGINAL PAGE IS POOR

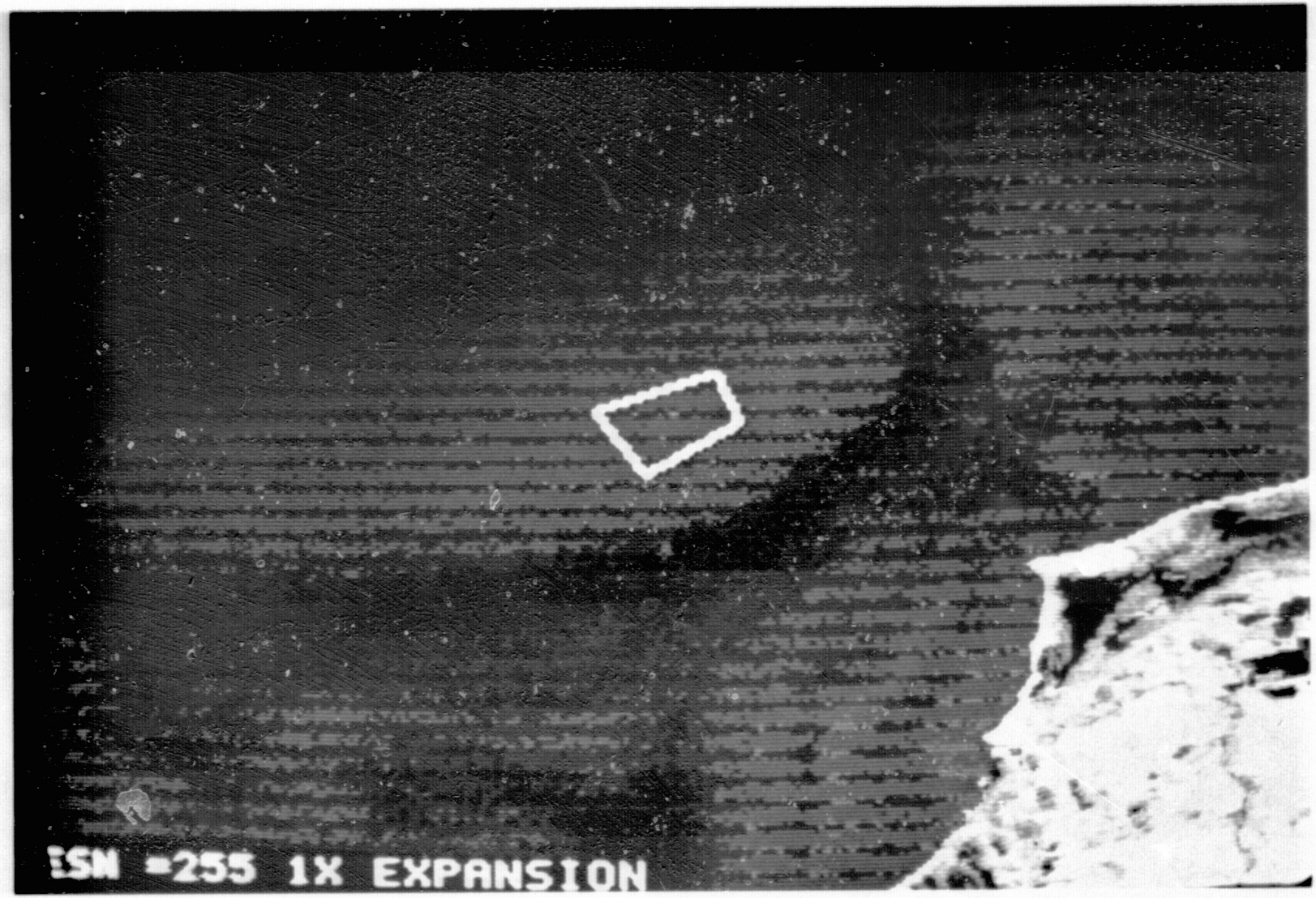


Figure 7.- M-DAS using bands 4, 5, and 7 that shows deeper water training set of Saginaw Bay, Michigan.

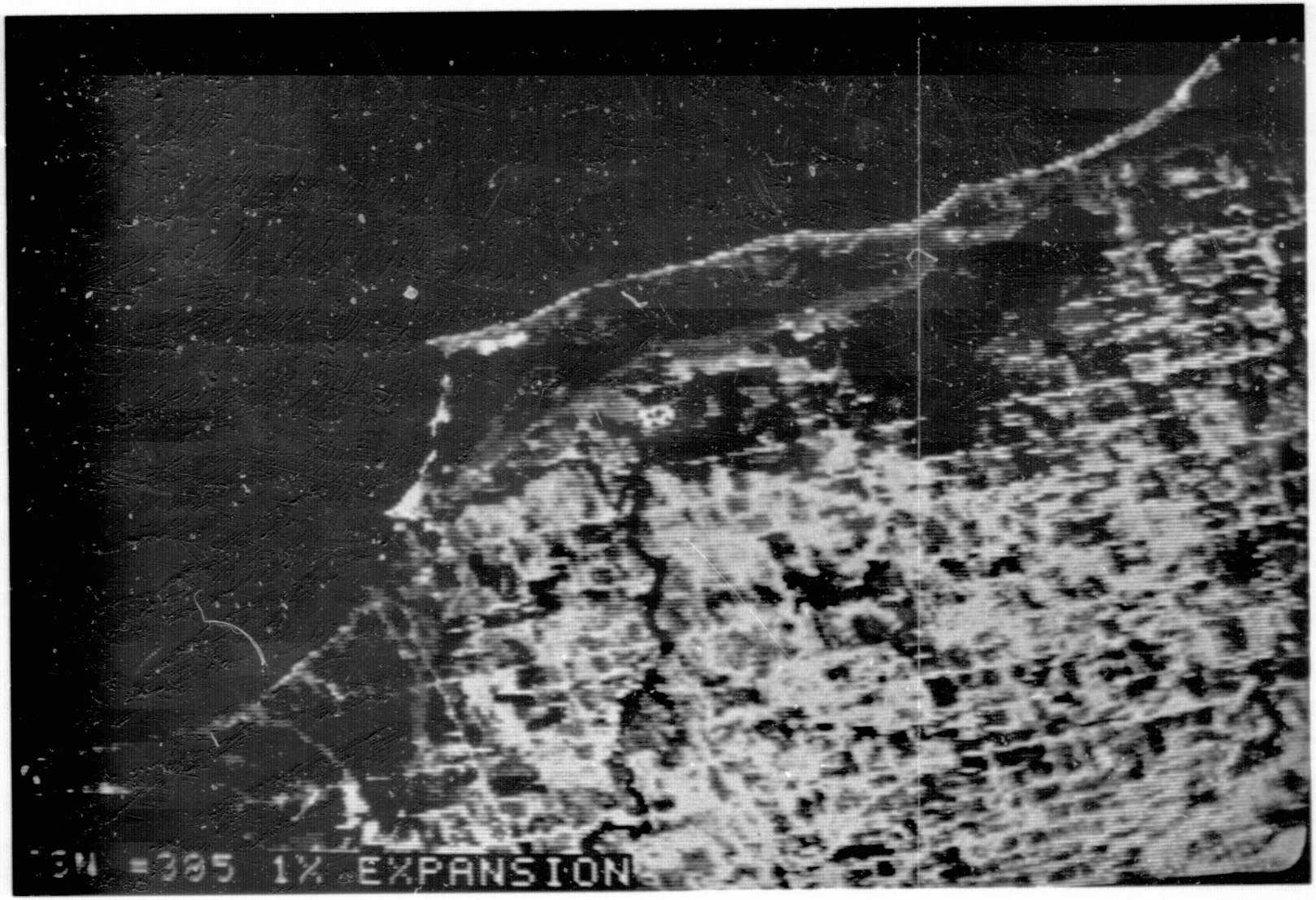


Figure 8.- M-DAS image using bands 4, 5, and 7 that shows inland training set of Saginaw Bay, Michigan.

REPRODUCIBILITY OF THE
ORIGINAL PAGE IS POOR

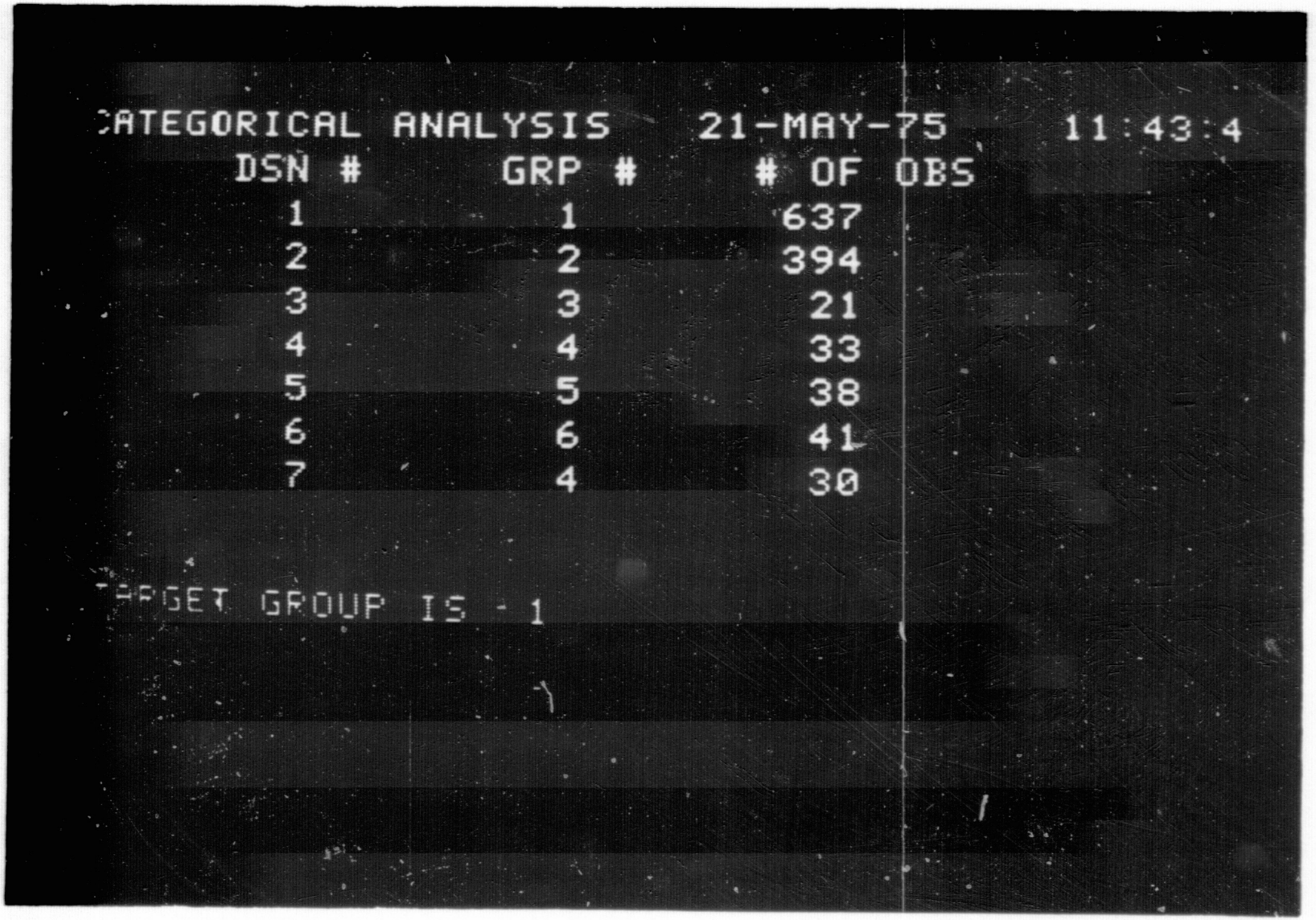
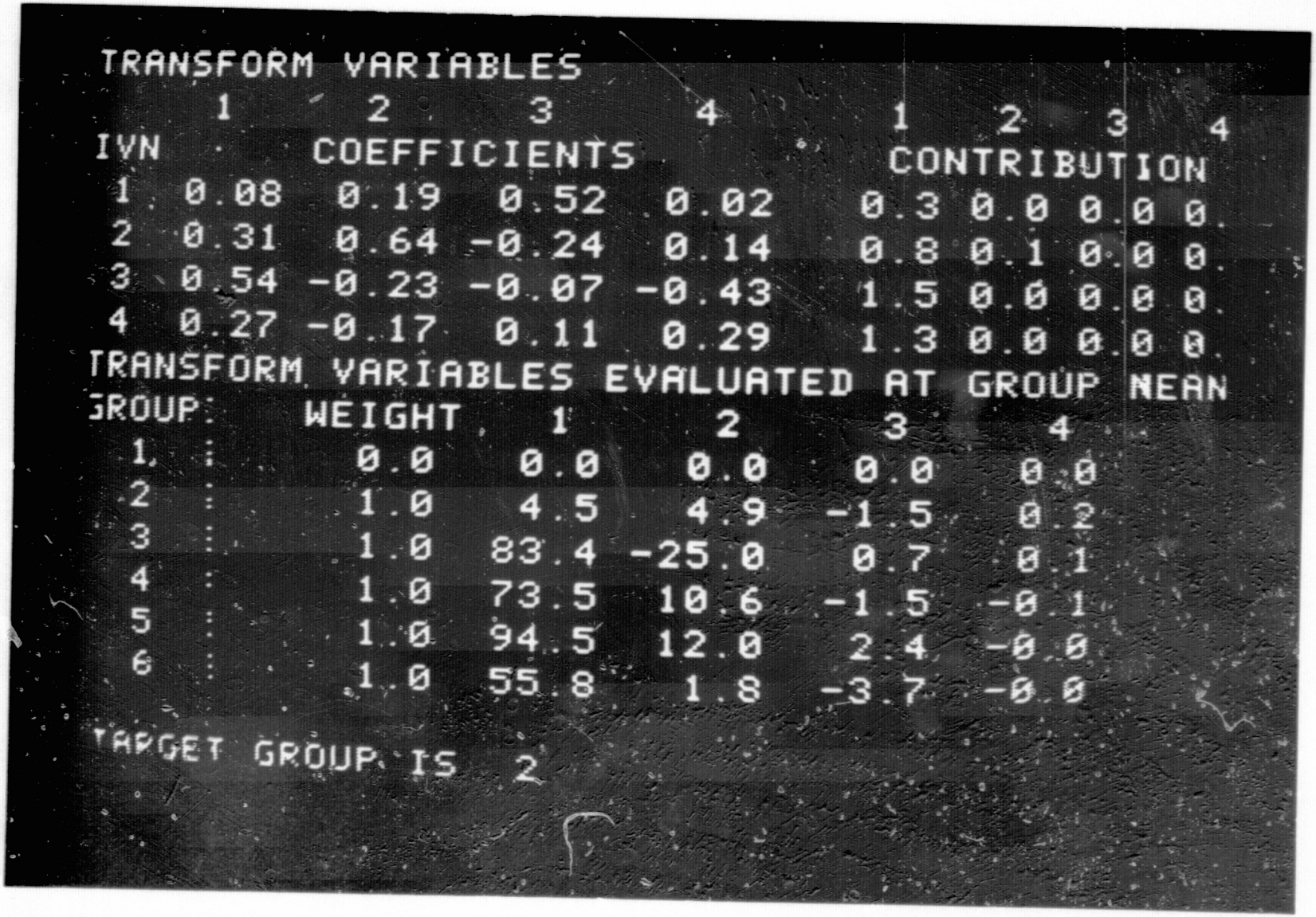


Figure 9.- M-DAS analysis display showing training group association for the training sets.



TRANSFORM VARIABLES

IVN	COEFFICIENTS 1	2	3	4	CONTRIBUTION 1	2	3	4
1	0.08	0.19	0.52	0.02	0.3	0.0	0.0	0.
2	0.31	0.64	-0.24	0.14	0.8	0.1	0.0	0.
3	0.54	-0.23	-0.07	-0.43	1.5	0.0	0.0	0.
4	0.27	-0.17	0.11	0.29	1.3	0.0	0.0	0.

TRANSFORM VARIABLES EVALUATED AT GROUP MEAN

GROUP	WEIGHT	1	2	3	4
1	0.0	0.0	0.0	0.0	0.0
2	1.0	4.5	4.9	-1.5	0.2
3	1.0	83.4	-25.0	0.7	0.1
4	1.0	73.5	10.6	-1.5	-0.1
5	1.0	94.5	12.0	2.4	-0.0
6	1.0	55.8	1.8	-3.7	-0.0

TARGET GROUP IS 2

Figure 10.- M-DAS analysis display showing means and variances for the training set.

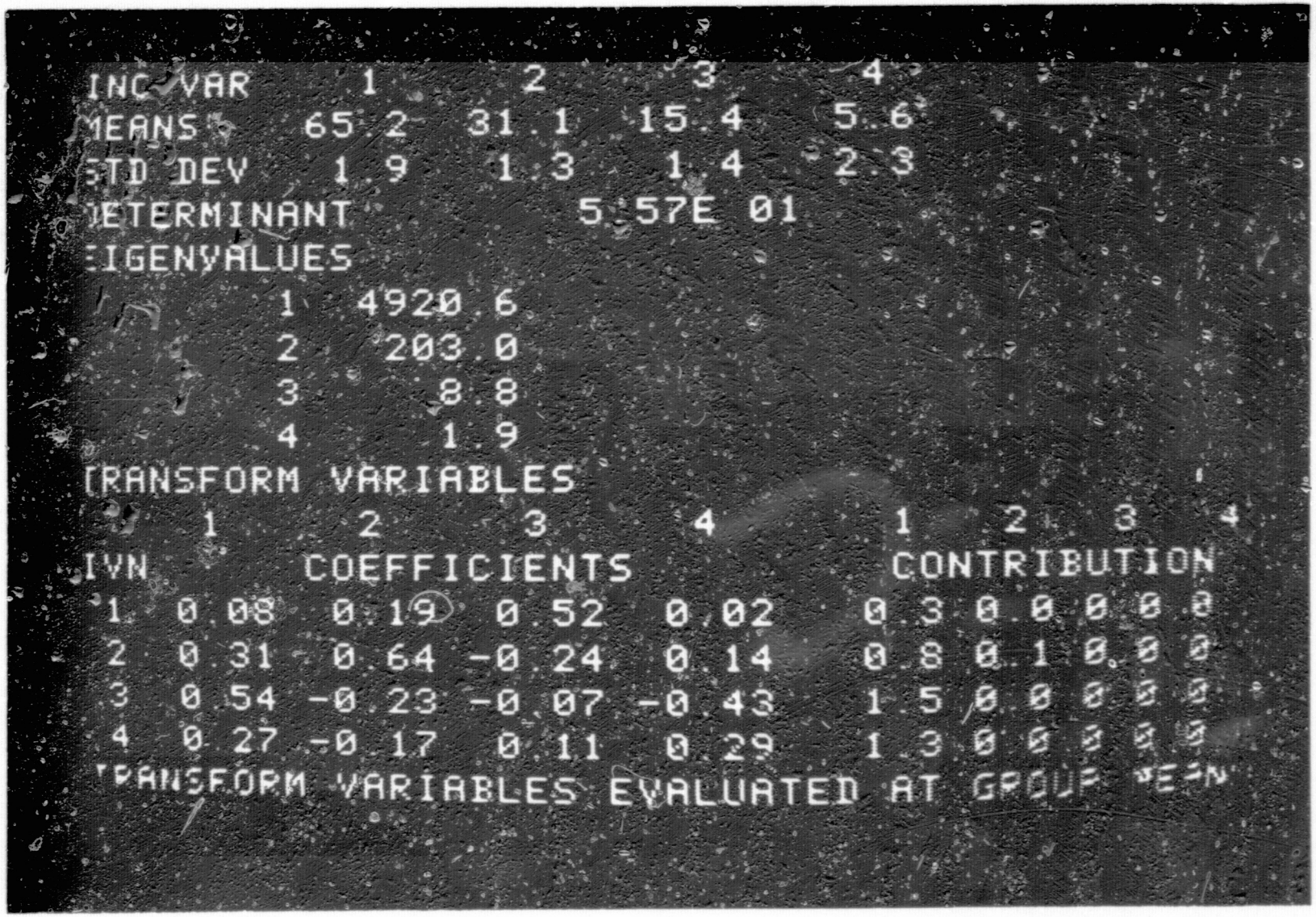
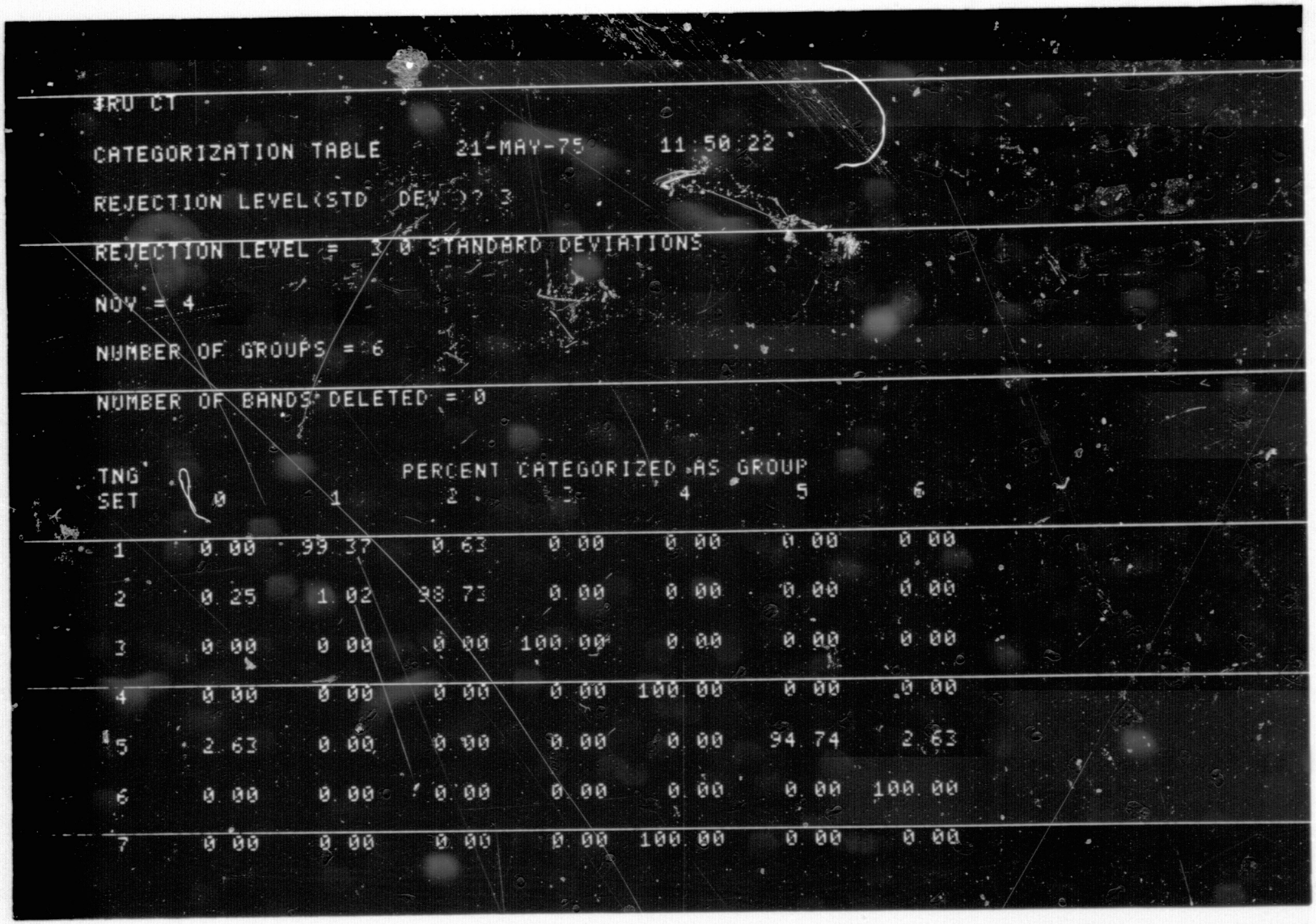


Figure 11.- M-DAS analysis display showing eigenvalues for the training set.



```
$RU CT

CATEGORIZATION TABLE     21-MAY-75     11:50:22

REJECTION LEVEL(STD DEV)? 3

REJECTION LEVEL =  3.0 STANDARD DEVIATIONS

NOV = 4

NUMBER OF GROUPS = 6

NUMBER OF BANDS DELETED = 0

TNG                    PERCENT CATEGORIZED AS GROUP
SET      0        1        2        3        4        5        6
  1    0.00    99.37     0.63     0.00     0.00     0.00     0.00
  2    0.25     1.02    98.73     0.00     0.00     0.00     0.00
  3    0.00     0.00     0.00   100.00     0.00     0.00     0.00
  4    0.00     0.00     0.00     0.00   100.00     0.00     0.00
  5    2.63     0.00     0.00     0.00     0.00    94.74     2.63
  6    0.00     0.00     0.00     0.00     0.00     0.00   100.00
  7    0.00     0.00     0.00     0.00   100.00     0.00     0.00
```

Figure 12.- M-DAS analysis display showing prediction of performance in the form of a truth table.

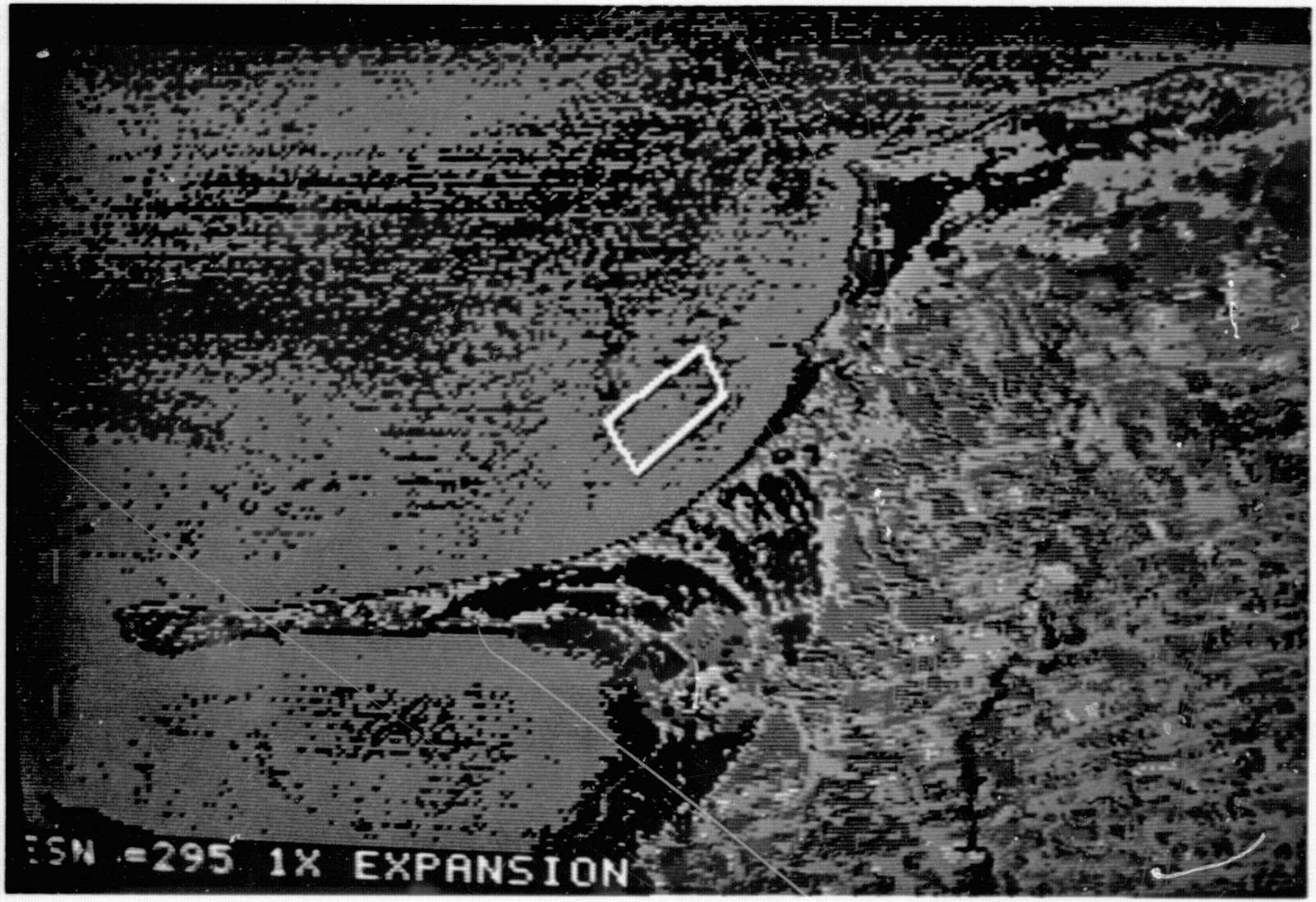


Figure 13.- M-DAS categorized image showing original training set.

1341

REPRODUCIBILITY OF THE
ORIGINAL PAGE IS POOR

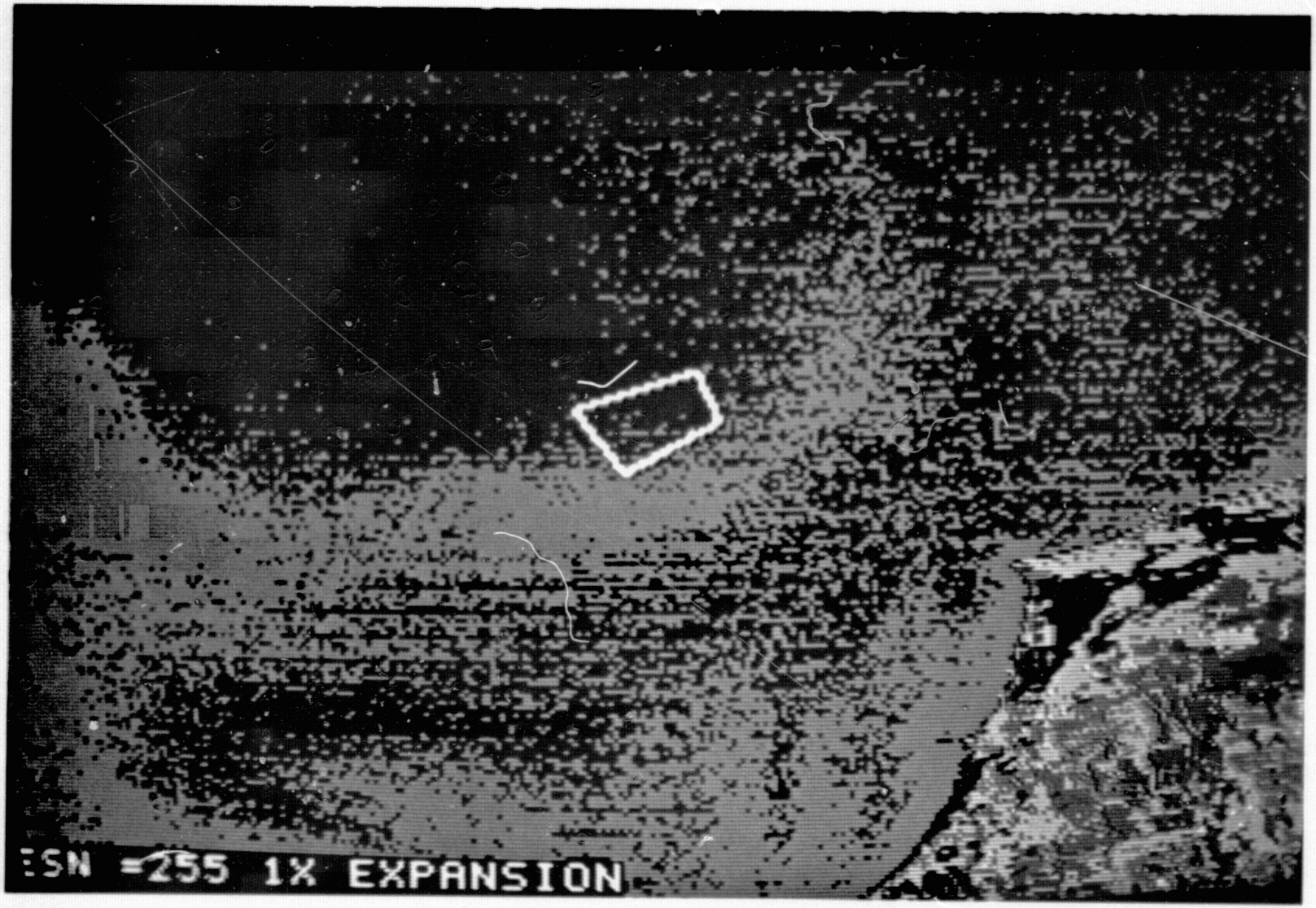


Figure 14.- M-DAS categorized image showing deeper water training set.

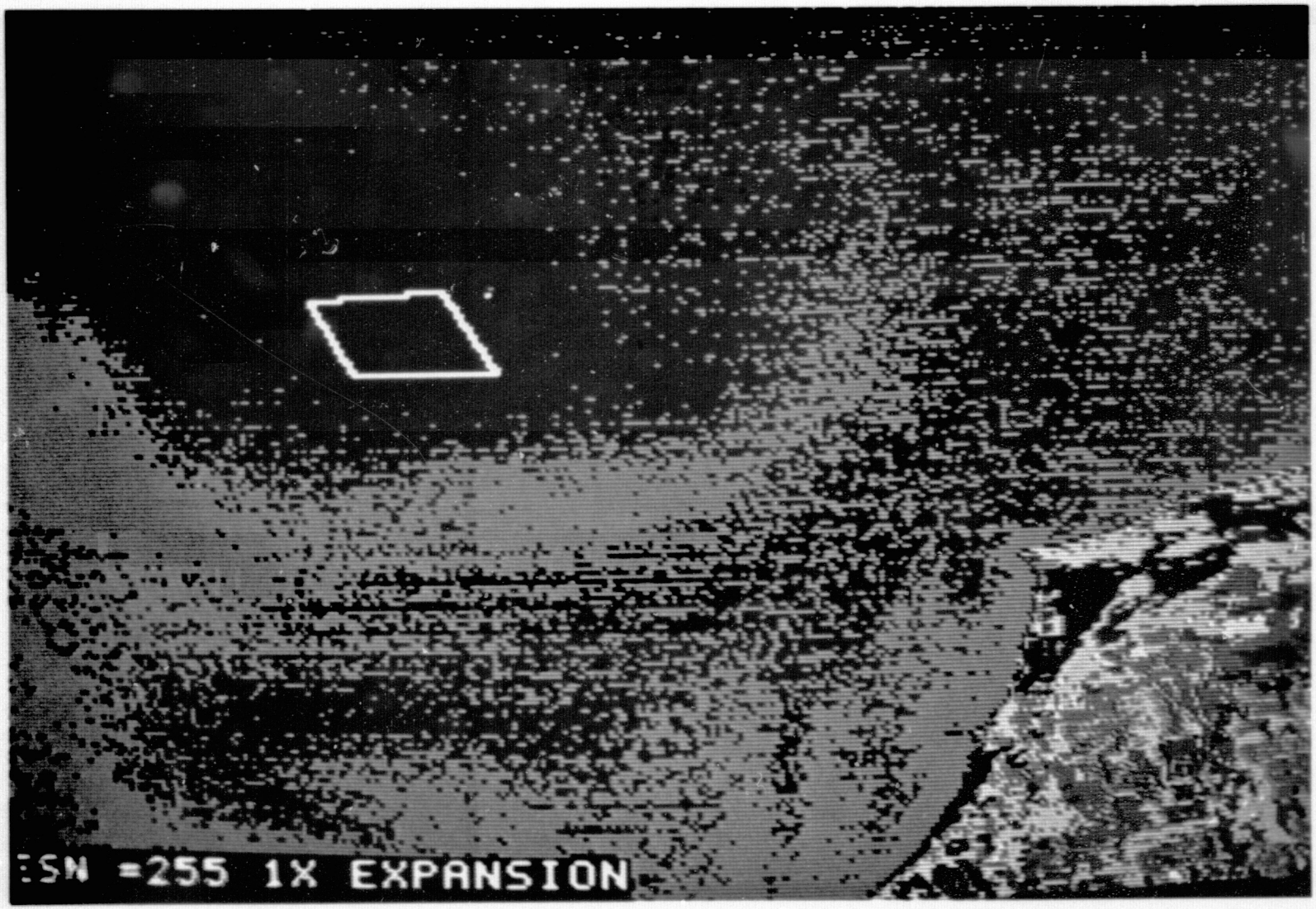


Figure 15.- M-DAS categorized image showing homogeneous repositioned training set.



Figure 16.- M-DAS categorized image showing new training set.



Figure 17.- M-DAS categorized image with orange color showing new category.

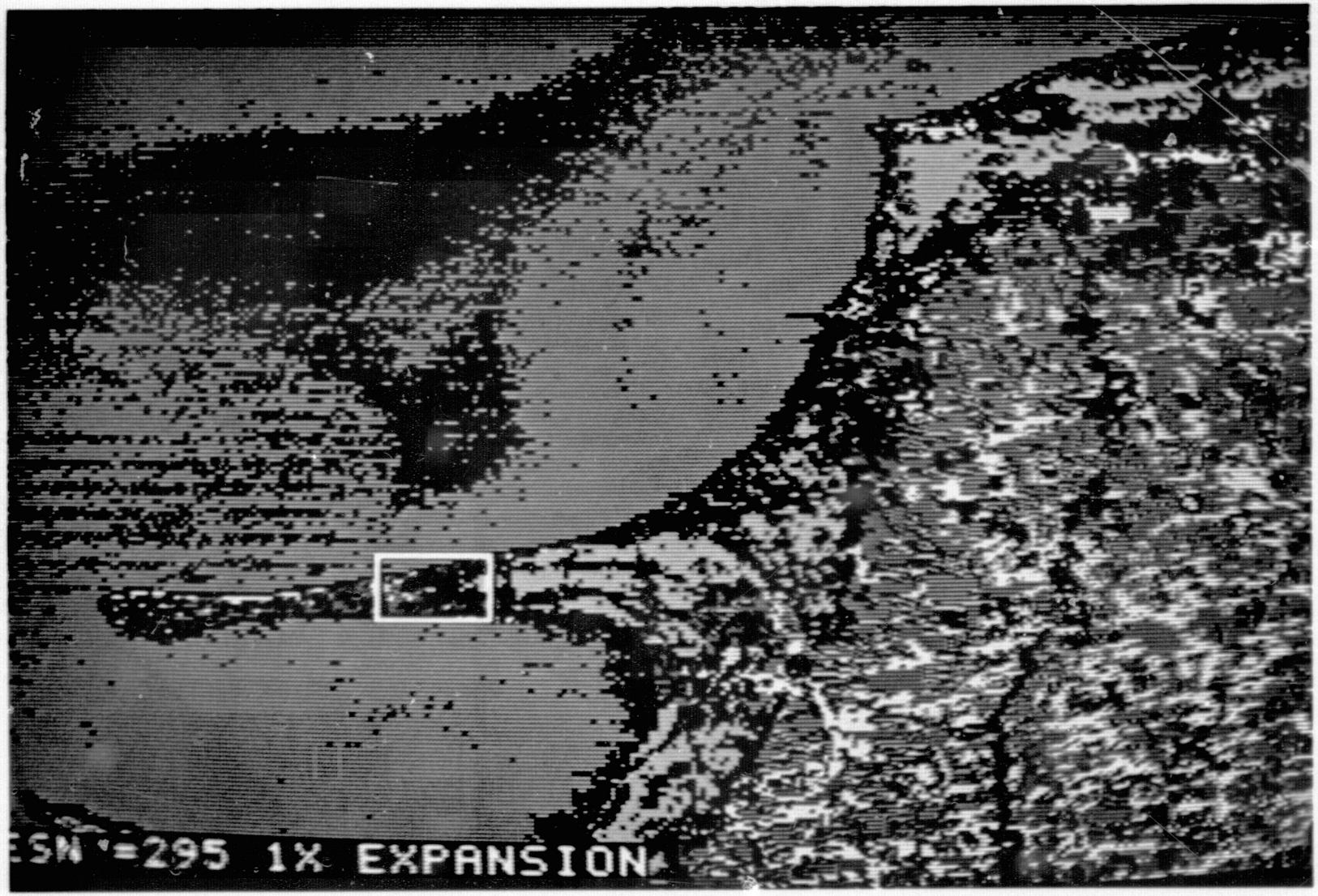


Figure 18.- M-DAS categorized image expanded by a factor of 1.

REPRODUCIBILITY OF THE
ORIGINAL PAGE IS POOR

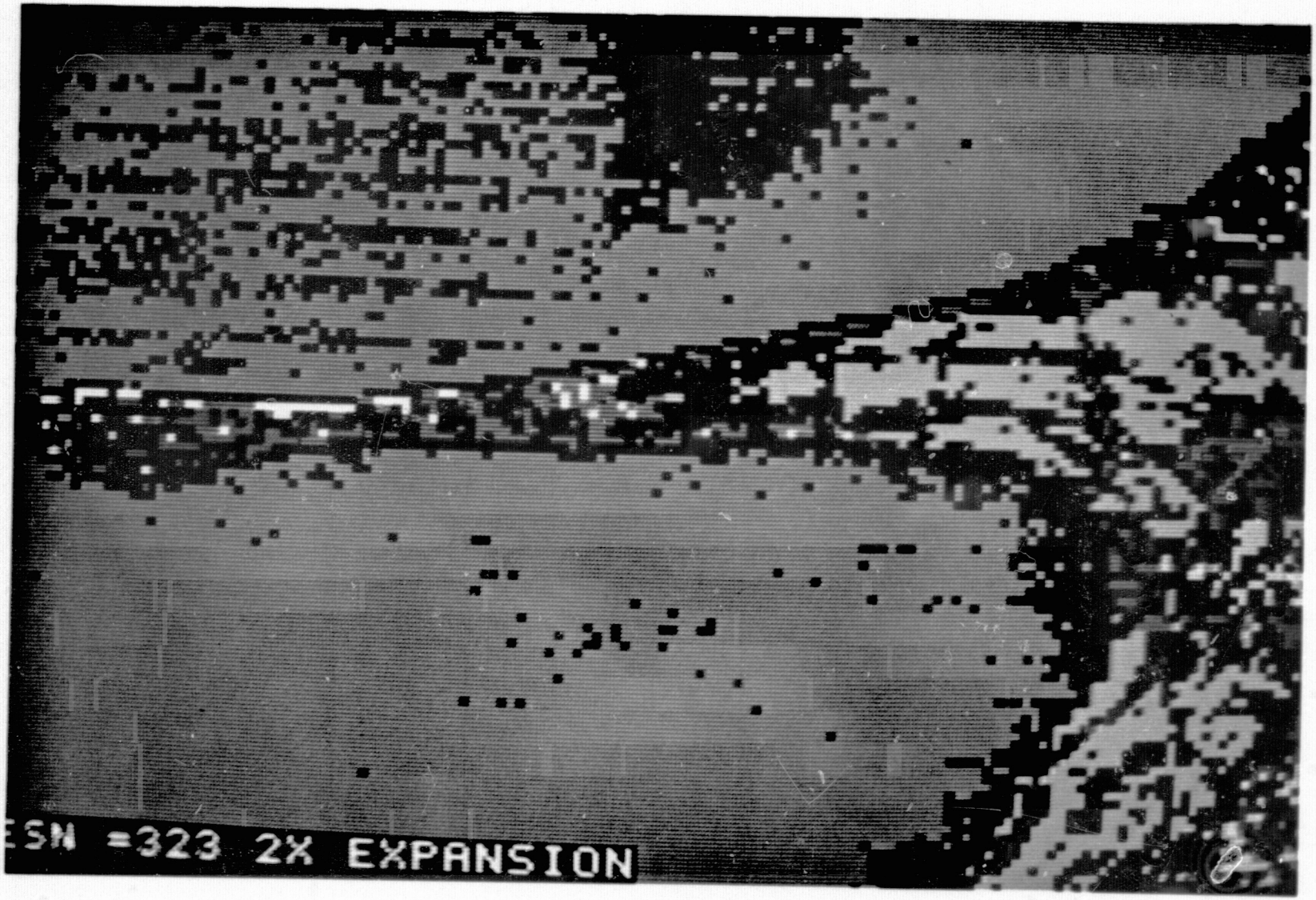


Figure 19.- M-DAS categorized image expanded by a factor of 2.

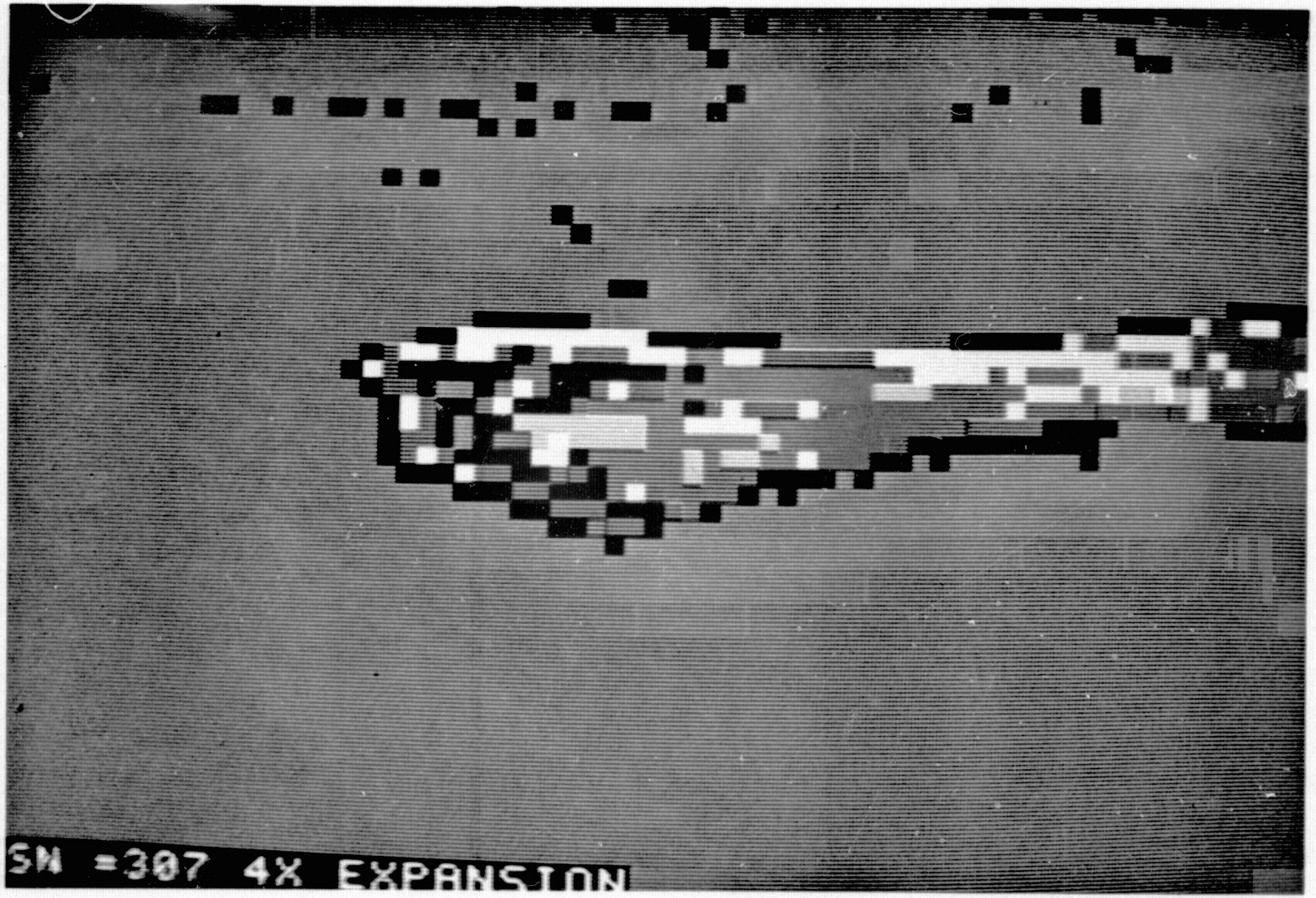


Figure 20.- M-DAS categorized image expanded by a factor of 4.

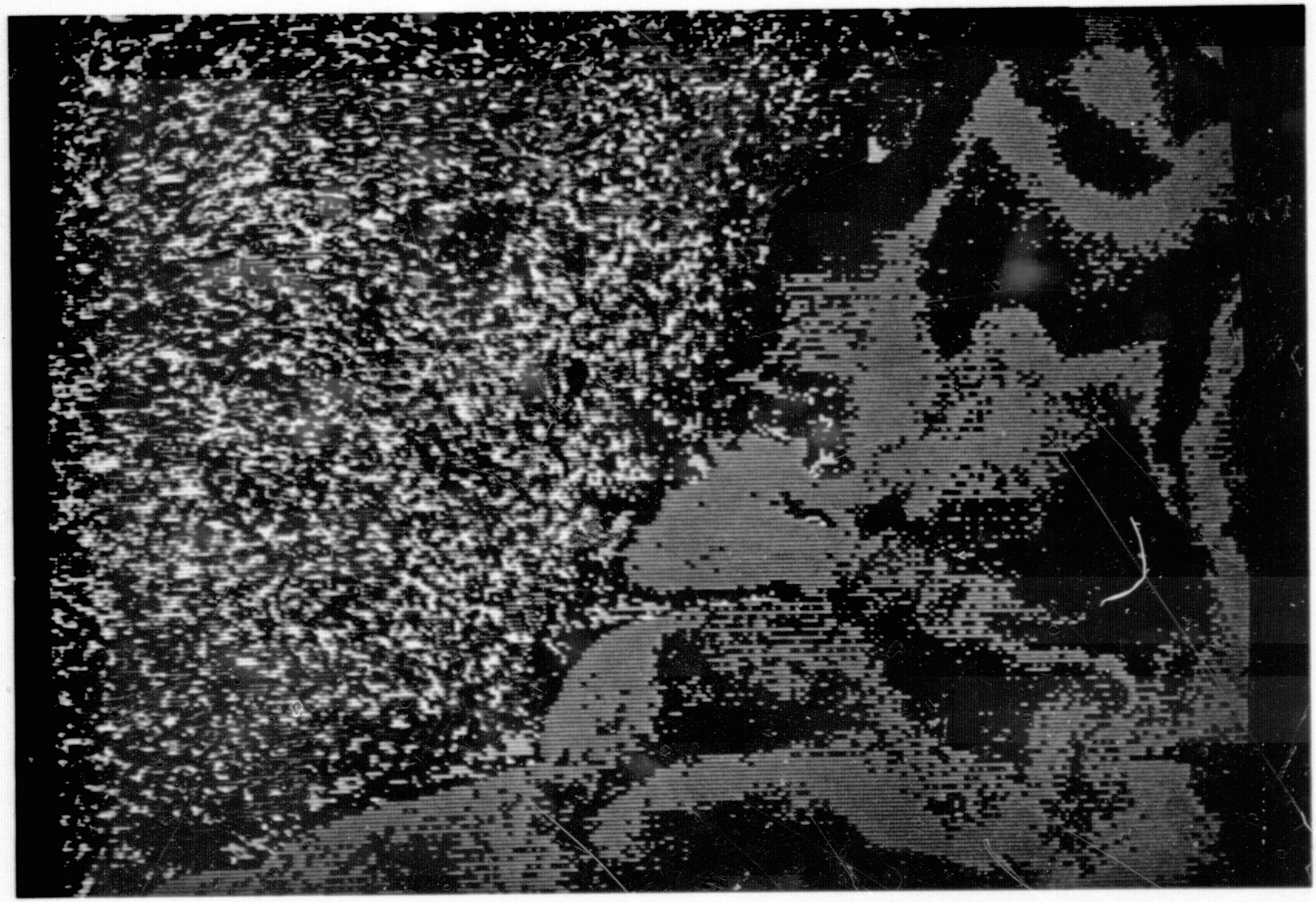
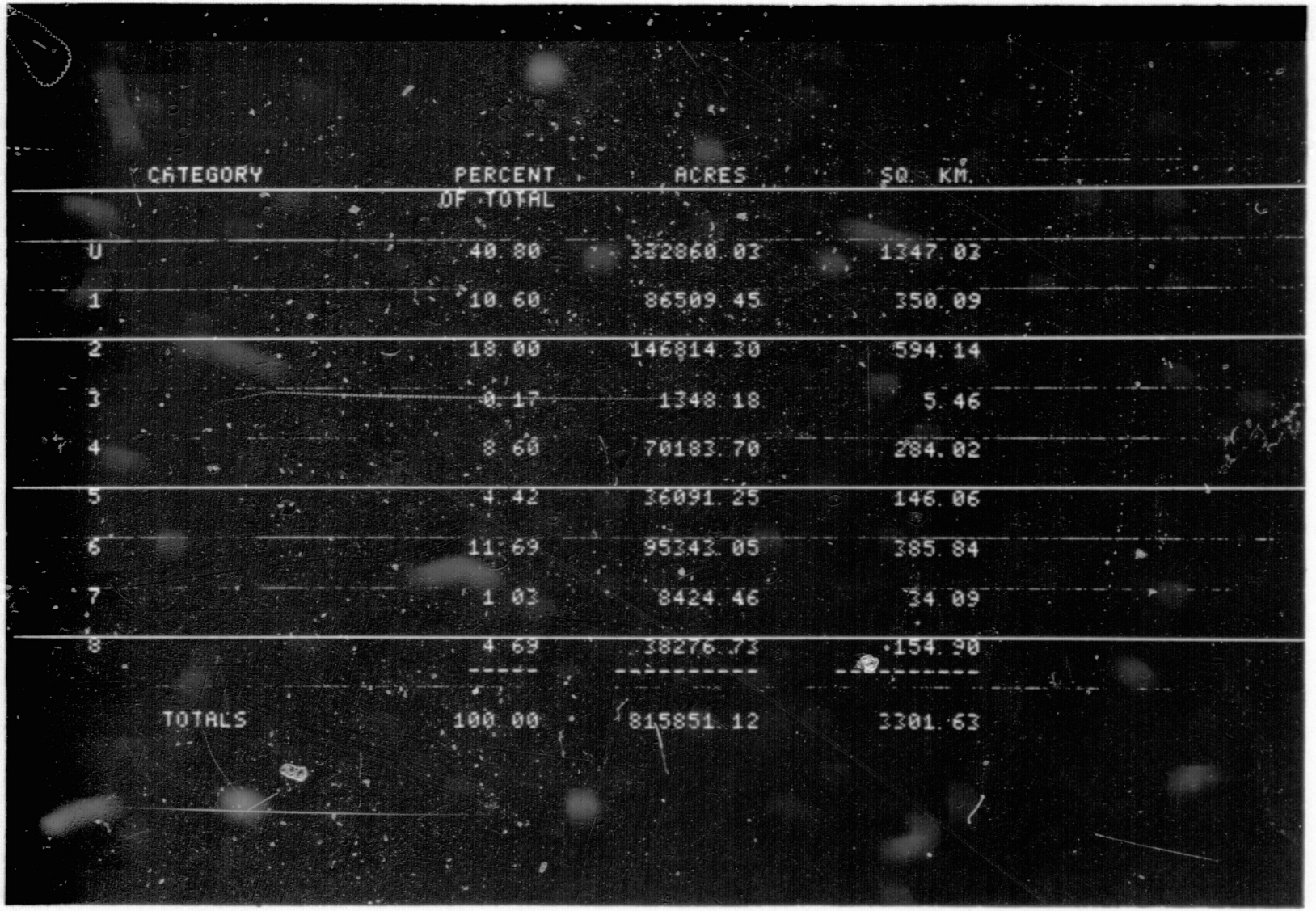


Figure 21.- M-DAS categorized image at a 25-mile scale.



CATEGORY	PERCENT OF TOTAL	ACRES	SQ. KM.
U	40.80	332860.03	1347.02
1	10.60	86509.45	350.09
2	18.00	146814.30	594.14
3	0.17	1348.18	5.46
4	8.60	70183.70	284.02
5	4.42	36091.25	146.06
6	11.69	95343.05	385.84
7	1.03	8424.46	34.09
8	4.69	38276.73	154.90
TOTALS	100.00	815851.12	3301.63

Figure 22.- M-DAS display showing area tables for each category.

ERIPS - EARTH RESOURCE INTERACTIVE PROCESSING SYSTEM

By Dr. Matthew J. Quinn, NASA, Johnson Space Center, Houston, Texas

N76-17541

ABSTRACT

This paper contains a description of the ERIPS (Earth Resources Interactive Processing System) which is the interactive analysis and production system for earth resources applications at Johnson Space Center. The system is located in the Mission Control Center (MCC) and consists of equipment which was originally used for Apollo. The computer is one of five IBM System/360 Model 75J computers in the Real Time Computer Complex in the MCC.

INTRODUCTION

The ERIPS is an interactive computer system used in the analysis of remotely sensed data. It consists of a set of software programs which are executed on an IBM System/360 Model 75J computer under the direction of a trained analyst. The software was a derivative of the Purdue LARSYS program and has evolved significantly in the past three years to now include an extensive pattern recognition system and a number of manipulative, preprocessing routines which prepare the imagery for the pattern recognition application.

The original purpose of the system was to analyze remotely sensed data, to develop and perfect techniques to process the data, and to determine the feasibility of applying the data to significant Earth Resources problems.[1] The system has since developed into a production system. Therefore error recovery and multijobbing capabilities have been added to the system.

EQUIPMENT

The ERIPS hardware consists of an interactive display and an IBM System/360 Model 75J computer. The computer is one of five IBM System 360/75's that were purchased in 1965 to support the Apollo Program. One computer performed the entire computational load for an Apollo mission using one megabyte of main memory and four megabytes of LCS (Large Capacity Storage). Additionally, the core memory is supplemented with eight packs of 2314 disc storage providing direct access storage for more than 200 megabytes of data. The companion disc packs are removable and interchangeable between 2314's. Each pack contains 11 discs with 20 recording surfaces giving over 25 megabytes of data storage.

The access times of these three memories are the following: The main memory access time is 750 nanoseconds. On each main storage reference cycle, the effective cycle time is halved because the storage has four-way interleaving of consecutive double words to and from storage. The CPU requires two computer cycles to complete a storage reference before it can start another reference. Therefore, the four-way interleaving is effectively reduced to two-way. The advantage in using four-way is that a channel request for storage has a better chance of being honored. If the CPU is addressing storage in a four-way

interleaved system, the channel has a three out of four chance of accessing storage meaning only one out of four segments will be busy. On a two-way system, the probability would be reduced to only one out of two chances of accessing storage.

The LCS access time is eight microseconds; however, since the two units within the LCS are two-way interleaved which permits an overlap in the read/write storage cycles, the sequential access rate is effectively four microseconds for each eight byte access.

The access time of the 2314 disc is from 25 milliseconds to 135 milliseconds with an average time of 75 milliseconds.

Only recently the 2314 disc systems have been supplemented with 42 ITEL 7330 disc systems. Each system can store 100 Megabytes of data with an access time from seven milliseconds to 50 milliseconds with an average time of 27 milliseconds.

The remainder of the computer equipment is as follows:
- IBM System/360 J
- Eight nine track, 800 bpi
  IBM2403 Model 3 tape drives
- IBM 1403 and 1443 printers
- Unit record equipment

The console equipment was originally used in Apollo program and was selected because it closely met the requirements for an interactive display capability. There are two consoles which can independently support two users. Each console contains (1) a black and white conversational television monitor with alphanumerics/vector capability used to communicate with the program, (2) a black and white image monitor capable of displaying 16 shades of gray with an alphanumerics/vector overlay capability, (3) a 97 key keyboard with alphabetic and function keys, and (4) a Grafacon tablet and pen used to position the cursor on the monitors. The two consoles share (1) a color monitor capable of displaying images in eight colors with the same overlay capability as the black and white monitors, (2) a hard copy device which can print the contents of the conversational monitor on paper, and (3) a photographic hardcopy device which can photographically reproduce the contents of the image monitor on photo paper. This hardcopy has the capability of reproducing 64 levels of gray.

The image monitors have a resolution of 612 by 439 picture elements. The original Grafacon tablet and pen used to position the cursor on the screen has been updated into a more convenient "joystick" control by means of an action control switch.

APPLICATIONS

The system contains the following software packages:
(1) Image manipulation and display - which allows the data to be handled according to many user-specified parameters.
(2) Image load - which allows the image to be loaded from magnetic tape onto disks.
(3) Image merge - which allows adjacent images to be merged into a single image.

(4) Image differencing - which allows the absolute differencing of corresponding channels of two images.
(5) Image registration - which consists of four alternative techniques to be used to register images.
(6) Pattern recognition module - which allows pattern recognition to be performed on the data.
(7) Statistics package - which gives various mean and covariance calculations on the data.
(8) Iterative and adaptive clustering routines - which gives unsupervised data groupings on the data.
(9) Maximum likelihood classification - which gives two forms of the maximum likelihood classifier.

The various routines can be called up by an analyst using a "menu" system for selecting the appropriate routine. The menu control makes the system somewhat easier to use since the computer will check each entry for errors. If the entry is a proper request, it will be passed on to the application program. On the other hand, if the request is improper, an error message will be printed on the screen.

SUMMARY

The paper presented the ERIPS interactive computer system in use at the Johnson Space Center to analyze remotely sensed data. The system was originally developed as a research tool to perfect techniques for analyzing the remotely sensed data, but has developed into a production system.

REFERENCE

1 Earth Resources Interactive Processing System by Mike Felix unpublished internal note, 1975.

LOW-COST DATA ANALYSIS SYSTEMS FOR PROCESSING MULTISPECTRAL SCANNER DATA

By Sidney L. Whitley, NASA-JSC Earth Resources Laboratory
@ NSTL, Bay St. Louis, Mississippi

N76-17542

ABSTRACT

The NASA Earth Resources Laboratory (ERL) has developed a sophisticated, research-oriented Data Analysis System (DAS) which is used for evaluating complex remote sensor systems and for development of techniques for application of remotely sensed data. Realizing that most potential users of remotely sensed data cannot afford such an expensive system, the ERL has developed some modular hardware components which may be added to one's existing facilities to establish a low-cost data analysis system for processing multispectral scanner data. The ERL has also developed software modules that are compatible with small general purpose digital computers to process and analyze remote sensor data, and to convert it to information needed by users. The software modules are written in FORTRAN IV language for ease of transfer to other computer systems.

ERL defined the basic hardware and software system requirements for some low-cost data analysis systems consisting of an image display system, a small general purpose digital computer, and an output recording device. The software modules consist of: a LANDSAT MSS data reformatting program; a series of spectral pattern recognition programs required to generate surface classification maps and tabular information; programs to convert computer generated maps from image space to a geographically referenced base; programs to extract data and irregularly shaped areas and to produce thematic maps of the designated areas; and programs to tabulate acreages of selected classification categories. Some off-the-shelf, inexpensive digital image display systems are described.

The minimum size computer is specified including word size, number of memory cells, cycle time, recommended hardware features, and peripherals. Most potential users have computers in their facilities which meet or exceed the minimum computer requirements of the low-cost data analysis system.

Several currently available output recording devices are discussed. These include standard computer line printers, electrostatic printer plotters, and color film recorders.

Although the modules may be assembled in a number of configurations, four configurations are presented. Hardware costs are given for these configurations and their capabilities are discussed.

INTRODUCTION

The NASA Earth Resources Laboratory (ERL) has developed a sophisticated, research oriented Data Analysis System (ERL-DAS), shown in figure 1, which is used for evaluating complex remote sensor systems and for developing techniques for application of remotely sensed data to solve or monitor resource management problems. The system has the capability for

PRECEDING PAGE BLANK NOT FILMED

reading and processing data from several multispectral scanner systems (MSS) flown on aircraft and spacecraft, as well as data from ground based data collection systems on boats and trucks. Most potential users of digitally recorded remote sensor data cannot afford and do not need such an extensive data analysis capability. Because of this, the ERL has accepted a challenge to define, assemble and evaluate several configurations of low-cost data analysis systems for processing multispectral scanner data. Throughout this paper the term system is defined to be a set of hardware, a set of software and a procedure for their use. Whitley (ref. 1) describes the procedure used by ERL for processing MSS data with the ERL-DAS. A very similar procedure for use of low-cost data analysis systems is being prepared.

ERL's low-cost data system designs employ a modular approach to take advantage of equipment available in a user's facility, and to give the user a choice of components based upon his survey requirements. The hardware for a low-cost data analysis system can be logically divided into three modules: (1) an image display device; (2) a computer with appropriate peripherals; and (3) an output recording device. The software for the low-cost data analysis system has also been modularized as follows: (1) reformat programs to convert the data from their original formats to formats that are easier to use; (2) a spectral pattern recognition module for classification of surface materials; (3) a geographical reference module for converting data from sensor reference systems to a geographical reference system such as the UTM projection; (4) a data base module for storage, update, and retrieval of up to 30 bytes of information from disparate sources describing resource survey units (e.g., 40 acre plots); and (5) applications modules which extract information from the data stored in the data base module.

IMAGE DISPLAY SYSTEMS

Printer/Plotters

A number of display systems are now available for displaying digitally encoded imagery data. The simplest display system is a line printer where symbols are chosen to approximate grey shades. This type of display device requires the support of a computer program called PICTOUT which can be adapted for use with anyone's existing line printer. Recently, electrostatic printer/plotters have been introduced with the capability of printing a picture element as a character or as a shade of grey. Figure 2 shows an example of grey scale imagery printed by an electrostatic printer. A number of electrostatic printer/plotters are available from computer equipment manufacturers, and may be obtained for a cost of approximately $12,000.

CRT Displays

A Portable Image Display Systems (PIDS), shown in figure 3, was designed and built to ERL specifications by Comtal Corporation in 1974. The PIDS was designed to enable MSS data users to identify the location of known training samples and test fields on tape, and to review the results of surface classification as a color coded display. The PIDS reads MSS imagery data from 9-track computer compatible tapes and displays the data as shades of grey or false colors on the screen of a color TV monitor. The input data may contain up to 2000 elements/swath and the flight line length may be unbounded.

The user has complete flexibility in selecting as many as 64 levels of color or grey to represent any picture element. The scale of PIDS-displayed LANDSAT imagery is about 1:43,000. Any selected 256 x 240 elements may be displayed on the screen. The user can advance, reverse, or shift laterally within an image.

To enable data users to select training samples and test fields, the PIDS has a cursor symbol, "+", which can be positioned anywhere within the screen by rolling a "track-ball" control in the direction of desired cursor movement. The coordinates (scan line number and picture element number) of the cursor position are displayed in light-emitting diodes on the front panel of the PIDS. Polygon shaped training samples or test fields may be defined with the cursor, stored, and transmitted, along with sample identification, on command to a punched paper tape output device (or to a keypunch, card punch, or the bus of a digital computer) for further processing by spectral pattern recognition. The PIDS operates on 110-115 V AC electrical power, and is mounted on wheels for ease of movement from office to office. Only a few minutes of training are required for learning to operate the PIDS.

The PIDS has been shipped to this symposium and is on display. This PIDS, the prototype model, cost approximately $40,000, but production versions may be purchased for approximately $32,000.

An Image Processing System (IPS), figure 4, such as the Comtal Model 8100, may be integrated with a small general purpose digital computer so that the user may interact with the data processing and analysis steps to a large degree. The purpose of the IPS is to display color coded MSS imagery for training or test field location, and to give the user greater flexibility in analyzing the imagery data; 512 scan lines by 512 picture elements are displayed on the screen to 256 levels of color or grey. The system was designed for easy enhancement of the data being displayed.

Data is read from tape into the computer to which the IPS is coupled and is reformatted for display on the IPS display. The user may define a polygon shaped training sample, then have the computer develop statistics for that training sample before a decision is made to accept or reject the sample. A variety of interactive analysis steps are possible, but their discussion is beyond the scope of this paper.

Use of the IPS is dependent upon availability of the computer with which it is integrated. It is recommended that the IPS be used in a time-sharing environment where other tasks can be performed concurrently by the computer, as an investigator uses very little of the computer's capacity during time-consuming tasks such as training sample and test field definition. The IPS must be installed in a fixed location, but it may be physically separated from the computer and operated as a terminal.

The hardware cost of the IPS is approximately $40,000. When used in a time-sharing mode it is necessary to add an operator's console costing approximately $2,500 to $3,000.

COMPUTERS

Almost any small (or large) general purpose digital computer may be used in a low-cost data analysis system. The software which has been developed by ERL for low-cost data systems may be transferred to run on almost any computer with a FORTRAN IV compiler if experienced programmers convert certain instructions that may not be compatible with his computer. Some of the smaller computers may be made to operate more efficiently by adding a few capabilities to their systems software package that make imagery data manipulation easier.

Table I shows the characteristics of a minimum and desired computer configurations. The minimum computer capability required for a low-cost data system is shown in the second column of Table I. If a computer of the minimum capability is used, the data processing time will be longer. It may be necessary to process the imagery data through the computer two or more times to classify the data. Addition of computer memory is recommended where high throughput rates are required. The third column of Table I shows an adequate computer configuration for most potential users of remote sensing, even for state-sized survey areas.

TABLE I - COMPUTER REQUIREMENTS FOR LOW-COST DATA ANALYSIS SYSTEM

CATEGORY	MINIMUM	DESIRED
Central Processor Unit with Operators Console	Yes	Yes
Memory	16K, 16 bit words	64K, 16 bit words (Dual Port)
Tape Drives (CCT)	Two 7 or 9 track	Two 9 track, 3.05 MPS, (120 IPS), 315 Bytes/cm (800BPI)
Disc (Rotating Memory Device)	12M, 16 bit words	46M, 16 bit words
Line Printer	Yes	Yes
Electrostatic Printer	---	Yes
Card Reader	Yes	Yes
Floating Point Hardware	---	Yes
Micro Programmable Writable Control Storage	---	Yes
Operating System	---	Yes
FORTRAN Compiler	Yes	Yes
APPROXIMATE COST	$75-80K	$150K

Computer cycle time is not critical in the selection of a candidate computer for a low-cost data system. A cycle time of 1 microsecond is acceptable; but if high volume throughput is required, cycle times of 660 or 330 nanoseconds are recommended. The speed of geographical reference conversion is dependent on the computer's data manipulation (multiplication, division) efficiency. Hardware or firmware floating point processors are recommended if geographical reference conversion is required.

Although computer tape drives of any speed may be used in a low-cost data system, it is recommended that tape speed be as high as possible (up to 3.05 meters (120 inches)/second) as most modern computers can process data very rapidly. The tape drives should be able to read 800 and 1600 bytes/inch packing densities.

Disc drives (Rotating Memory Devices) are required in the low-cost data system to store a LANDSAT size image during geographical reference conversion (UTM). A disc is also very useful for storage and quick retrieval of all software modules used in the low-cost data analysis system.

Small computers which are adequate for use in a low-cost data system along with all the necessary peripherals may be purchased for $75,000 to $150,000 depending on throughput rates required. The operating costs for these small computers (without equipment amortization or housing) are in the range of $30 to $75 per clock hour.

OUTPUT RECORDING DEVICES

The output recording device for a low-cost data system may be either a computer line printer, an electrostatic printer/plotter, or a black and white or color film recorder. The selection of an output device for a low-cost data system should be based upon the required: output speed, control of scale, quantity of output, dynamic range, number of copies of output to be produced, etc. Several output recording devices are discussed below.

Line Printer

A conventional line printer may be used as an output recording device for a low-cost data analysis system. The surface classification map is recorded on line printer paper, and characters represent the surface material mapped on each print position. This type of output recording device is inexpensive to implement, and is appropriate for small scale survey applications. Its application is best where scale is not critical and where extensive duplication of products is not necessary. The output can be manually color coded if desired.

Electrostatic Printer/Plotter

The electrostatic printer/plotter produces all the characters available on a standard line printer in various letter sizes, and also produces up to 16 distinct grey levels for a given print position. The output format of the electrostatic printer/plotter may be up to 22 inches wide. Coordinate lines, scan line counts, and picture element numbers may be written over the imagery data for annotation purposes. A sample of imagery is shown in figure 2.

The advantages of the electrostatic printer/plotter are its low cost and ease of implementation. The application of the electrostatic printer/plotter is best where limited control of scale is required, and where limited duplication of products is anticipated. Electrostatic printer/plotters are available and are competitively priced from several sources at approximately $12,000.

Film Recorders

When large volumes of data are to be processed, where good geometric precision is needed, and where multiple copies of the output product are required, it is necessary to incorporate a black and white or color film recorder in the low-cost data analysis system as an output recording device. If only grey-shade map products are required, a simple black and white strip or frame film recorder may be used. If a greater dynamic range exists in the data, and it is important to display the greater range, it is necessary to incorporate a color film recorder in the system.

Color Film Recorders

At least two currently available color film recorders are compatible with low-cost data analysis systems. One such system is manufactured by DICOMED and records its output on 12.7 cm (5 inch) color film in frames. The resolution and linearity are good. The system operates in a stand-alone mode and contains a small digital computer for control purposes. The system costs approximately $140,000. A Stand-Alone Color Film Recorder (SACFR) is currently under development for ERL by HRB-Singer. The SACFR is an upgraded version of the ERL-DAS film recorder. The SACFR output is recorded on 24.1 cm (9.5 inch) wide color film as a positive or negative image or on 24.1 cm (9.5 inch) wide color paper. A sample of the film recorder output is shown in figure 5. The system records high resolution, linear images in a continuous strip. The SACFR has a built-in capability for expansion (magnification) and, when used with the appropriate computer software routines, can produce precise map scales. Scales of any size may be produced without loss of resolution or geometric degradation. Magnification is accomplished electronically rather than optically. The cost for production versions is estimated to be $115,000. The prototype SACFR is scheduled for delivery in February 1976.

SOFTWARE

The software modules for the low-cost data analysis system were developed on either a UNIVAC 1108 computer or a Varian Data Machines V-73 small general purpose digital computer. All software was written in FORTRAN IV language for ease of transfer to other computer systems. The software modules which were developed on the UNIVAC 1108 computer have been converted by ERL personnel to run on the V-73 computer (using 32K memory locations or less). The V-73 systems software package has been extended a modest degree by ERL systems programmers to specifically facilitate remote sensor data processing. These extensions to the V-73 systems package already exist in most larger computer systems.

The software developed for the low-cost Data Analysis System consists of the following modules: (1) PATREC Module; (2) GEOREF Module; (3) DATA BASE Module; and (4) APPLICATIONS Module.

PATREC Module

The purpose of the PATREC Module is to convert LANDSAT MSS bulk tape recorded data, and other supporting data into surface classification maps. A block diagram of the PATREC Module is shown in figure 6. The PATREC Module consists of several computer programs: ERTREF, DAPIDS, ISOFLD, STATS, ELLIPSE, and ASSIGN.

Program ERTREF accepts the original LANDSAT bulk tape format and converts it to a format called DASTAP. The DASTAP format is more convenient to read and manipulate than the original LANDSAT format.

Program DAPIDS accepts the DASTAP format and converts it to a DISTAP format which is the format expected by the PIDS. Basically the DISTAP format consists of some general header information (including scan line count) and each picture element of the imagery is expressed as 6-bit word (64 levels). This format is flexible in that each scan line of imagery data may contain up to 2000 picture elements.

Program ISOFLD accepts as input the LANDSAT imagery data in the DASTAP format, and cards containing the coordinates of polygon shaped (n-sided) training samples and sample identification as defined by the user on the PIDS. The purpose of program ISOFLD is to extract data for training samples from LANDSAT data tapes, and to produce a new tape in the DASTAP format which contains only training sample data.

Program STATS accepts training sample data from Program ISOFLD in the DASTAP format only. This program is a simplified version of one which was developed by the Laboratory for Remote Sensing (LARS) at Purdue University. Program STATS produces tabulations of histograms, means, standard deviations, covariance matrices, and spectral plots for each training sample. Program STATS also calculates the relative separability of materials desired to be classified based upon a divergence criteria. Program STATS produces signatures for each material in the form of means and a covariance matrix, and they are written in the SIGTAP format.

Program ELLIPSE accepts signatures as determined by program STATS in the SIGTAP format. Program ELLIPSE converts each of the signatures defined by STATS into an elliptically shaped decision boundary and stores it in a table. The boundaries of the four dimensional tables are output onto tape in the TABTAP format for use in program ASSIGN. Programs ELLIPSE and ASSIGN are also known as program ELLTAB. These two programs were described by Jones, 1974 (ref. 2), and their theory was described by Eppler, 1974 (ref. 3).

Program ASSIGN accepts and stores decision tables for each classification category in computer memory. Program ASSIGN also accepts as input the bulk LANDSAT imagery in the DASTAP format and classifies all data by a table look-up implementation of maximum likelihood spectral pattern recognition and produces a surface classification map in the DISTAP format. Program ASSIGN runs very rapidly and can classify an entire LANDSAT scene to 24 classification categories in approximately an hour, depending upon the computer system used.

GEOREF Module

The GEOREF Module converts a LANDSAT scene from sensor coordinates (scan lines, picture elements, latitude and longitude of the scene center) to a geographically referenced system, the UTM projection. Ground control points are identified on the PIDS and are input by cards into the GEOREF program along with the LANDSAT imagery in the DISTAP format. The geographically referenced image is output on tape in the DISTAP format to a precision of approximately 300 meters RMS error at 1:250,000 scale. The design goal for GEOREF is the National Map Accuracy Standard for 1:250,000 scale. GEOREF will continue to be refined to approximately a 100 meter RMS error at this scale. The corrected imagery is referenced to Northings and Eastings of the UTM.

To implement program GEOREF on a small scale digital computer, it is recommended that the system contain a disc with at least 12,000,000 words of 16 bits/word storage. The GEOREF program may be implemented on a computer using tape as a storage medium when small area surveys are required.

DATA BASE Module[1]

The DATA BASE program is a highly specialized information storage and retrieval system. The objective of this program is to store up to 30 bytes (8-binary bits/byte) of geographically referenced information about plots of real estate (e.g., 40 acres each) for an entire state. The most predominate material for an entire plot may be stored in one byte, the soil type in another, etc.

The program accepts geographically referenced surface classification maps generated by program GEOREF in the DISTAP format. Other types of information such as soil type, rainfall, terrain slope, census data, etc., are entered into the program by punched cards or tape. The program maps the input information into the appropriate set of bytes describing each plot of real estate. Provisions are made for correcting errors in the stored data down to the byte level.

If the DATA BASE Module is established for a state the size of Mississippi, and if the plots of real estate are selected to be 40 acre plots, then 30 bytes of information for each plot may be stored on two 9-track, 315 bytes/cm (800 bytes/inch) computer compatible tapes.

Information may be retrieved from the DATA BASE Module by entering an ordered set of UTM coordinates on punched cards which describe an "n-sided" polygon. The program will retrieve the 30 bytes of data from each plot contained within or on the boundary of the polygon shaped region. The retrieved information will be used as input data by a family of applications programs to extract management information.

Applications Module[1]

The applications module consists of a set of programs which processes management information from the DATA BASE. One applications program might predict the yield of soybeans in an agricultural region which is characterized by two soil types A and B (stored in the DATA BASE). It is known that soil type A can produce X bushels/acre, with a given average rainfall and fertilizer application, while soil type B produces Y bushels/acre under the same conditions. The program would calculate a soybean production estimate for the polygon-shaped region based on information contained within the DATA BASE.

[1]Software under development

LOW-COST DATA ANALYSIS SYSTEM CONFIGURATIONS

Several low-cost data analysis system configurations have been defined which represent various levels of complexity and capability. These configurations are made up of hardware and software modules described earlier.

Configuration 1

Configuration 1 which is shown in figure 7 is composed of an electrostatic printer/plotter as an image display device and output recording device, and a small general purpose digital computer. This configuration represents a very inexpensive system and may be implemented on most potential users' existing facilities without purchase of additional equipment. If such a hardware system were purchased new, the total cost would be approximately $90-$150K, depending on the computer peripherals and memory. The Configuration 1 system is characterized by slow training sample selection, efficient data processing, and limited output capability, but this system is adequate for small area, special purpose surveys. The primary expenditure for implementation of Configuration 1 by most potential users is the cost of manpower for software conversion of existing documented programs.

Configuration 2

Configuration 2, shown in figure 8, is composed of a PIDS, a small general purpose digital computer and an electrostatic printer/plotter. This hardware configuration is quite inexpensive and may in some cases be implemented by purchasing only a PIDS and implementing ERL's software on existing equipment. If the system were to be purchased outright, the component costs would be $32K for the PIDS, $80K to $140K for the computer, and $12K for the electrostatic printer/plotter, or a total system cost of $124K to $184K. If a computer with an electrostatic plotter exists in the user's facility, it is only necessary to spend $32K. Configuration 2 is characterized by efficient data screening and training sample selection procedures, efficient data processing, and a highly useable grey scale map output capability. The PIDS may be used as an output for color coded classification maps of limited survey areas. The PIDS screen may be photographed. The most likely expenditures for implementation of Configuration 2 are for the purchase of the PIDS, and the cost of manpower to convert ERL's software to run on the user's computer facilities.

Configuration 3

Configuration 3, which is shown in figure 9, is composed of a stand-alone PIDS, a small general purpose digital computer, and a stand-alone color strip film recorder. This hardware configuration is fairly inexpensive for its capabilities. The system may be implemented by purchasing a PIDS and a color strip film recorder, and by using existing computer facilities. In this case the user would be required to spend only $147K. The components of the system may be purchased for a cost of $32K for the PIDS, $90K to $150K for the computer, and $115K for the color strip film recorder, or a total hardware cost of $237K to $297K. Configuration 3 is capable of efficient data screening, training and test field definition; efficient data processing, and high volume, high precision, color-coded output products of the type shown in figures 10 and 11. To implement Configuration 3, most users must purchase the PIDS and film recorder, but may convert ERL's software to run on their existing computer.

Configuration 4

Low-cost Data Analysis System Configuration 4, shown in figure 12, is composed of an Image Processing System (IPS), and operator's console, a small general purpose digital computer and a color strip film recorder. In this configuration the IPS is integrated with the computer. The computer is equipped with an operating executive which allows multiple tasks to be performed on a time-sharing basis. The IPS is an off-the-shelf system and interface units have been designed for a number of widely available small general purpose digital computers. The IPS costs $40,000, the operator's console costs approximately $3,000, the computer costs $150,000, and the film recorder costs approximately $115,000. The hardware cost for implementing Configuration 4 is $158,000 if the user's computer is adequate, and only $308,000 if a new computer must be purchased. Configuration 4 permits a user to read a set of data from a LANDSAT tape, have the imagery displayed on the IPS screen, adjust colors to enhance the data, select training samples, develop statistics for the sample, analyze the sample for adequacy as a training sample, and then accept or reject the sample in real time. Every step required to process a set of data on the Configuration 4 system may be made interactive so that a high priority investigation may be completed quickly and accurately. To implement Configuration 4 most users must purchase an IPS and a film recorder, but may convert ERL's software to run on their existing computer. Figures 10 and 11 are also examples of products that could be expected from Configuration 4.

All hardware components described in this paper are off the shelf and readily available. If desired, specifications can be provided by the ERL. Seven of the nine computer programs described are operational on either a UNIVAC 1108 computer or VDM V-73 small general purpose computer. Two of the nine programs are under development: DATA BASE and APPLICATION. All programs are, or will be, available to the public through the Computer Software Management and Information Center, COSMIC, University of Georgia, Athens, Georgia 30602.

REFERENCES

1. Whitley, Sidney L. : A Procedure for Automated Land Use Mapping Using Remotely Sensed Multispectral Scanner Data. NASA TR R-434, 1975

2. Jones, Clay: Implementation of an Advanced Table Look-Up Classifier for Large Area Land Use Classification. Proceedings of the Ninth International Symposium on Remote Sensing of Environment, Vol II, Environmental Research Institute of Michigan (Ann Arbor, Michigan), April 1974

3. Eppler, W. G.: An Improved Version of the Table Look-Up Algorithm for Pattern Recognition. Proceedings of the Ninth International Symposium on Remote Sensing of Environment, Vol II, Environmental Research Institute of Michigan (Ann Arbor, Michigan), April 1974

1365

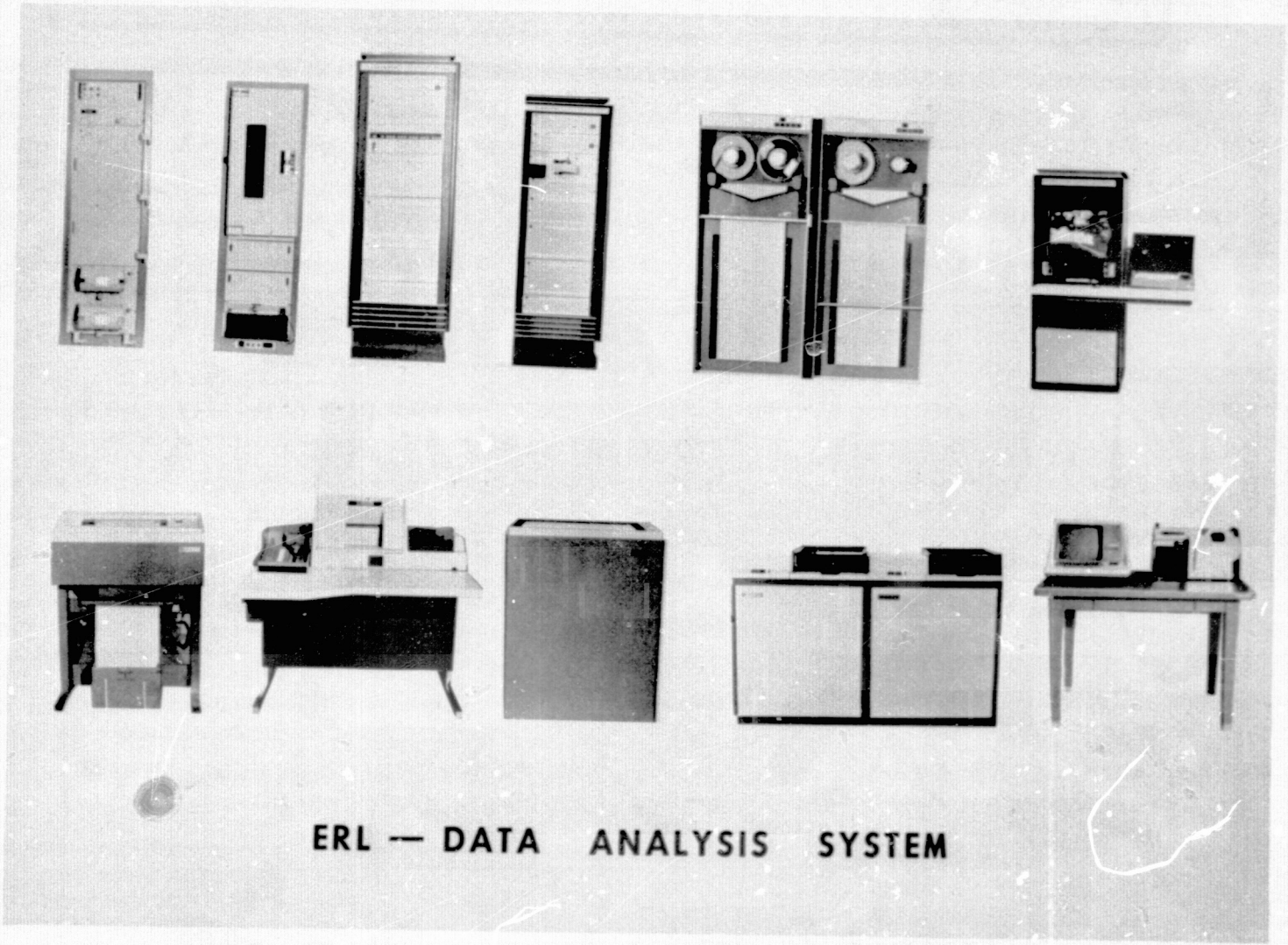


Figure 1.- Earth Resources Laboratory - Data Analysis System.



Figure 2.- Grey scale map.

1366

REPRODUCIBILITY OF THE
ORIGINAL PAGE IS POOR



Figure 3.- Portable image display system.

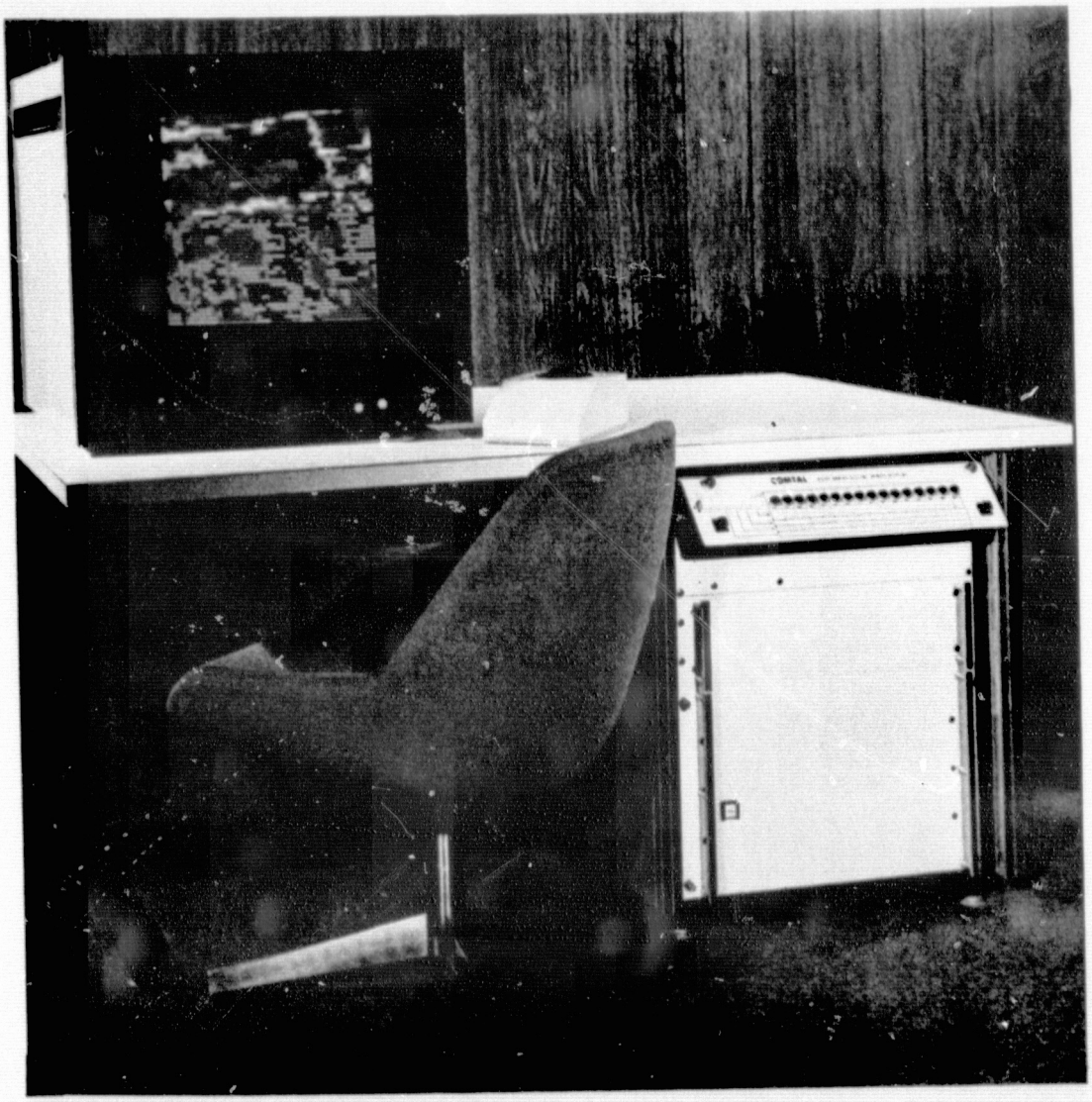


Figure 4.- Image processing system.



Figure 5.- Simulated color infrared image which has been geographically referenced at 1:250,000 scale.

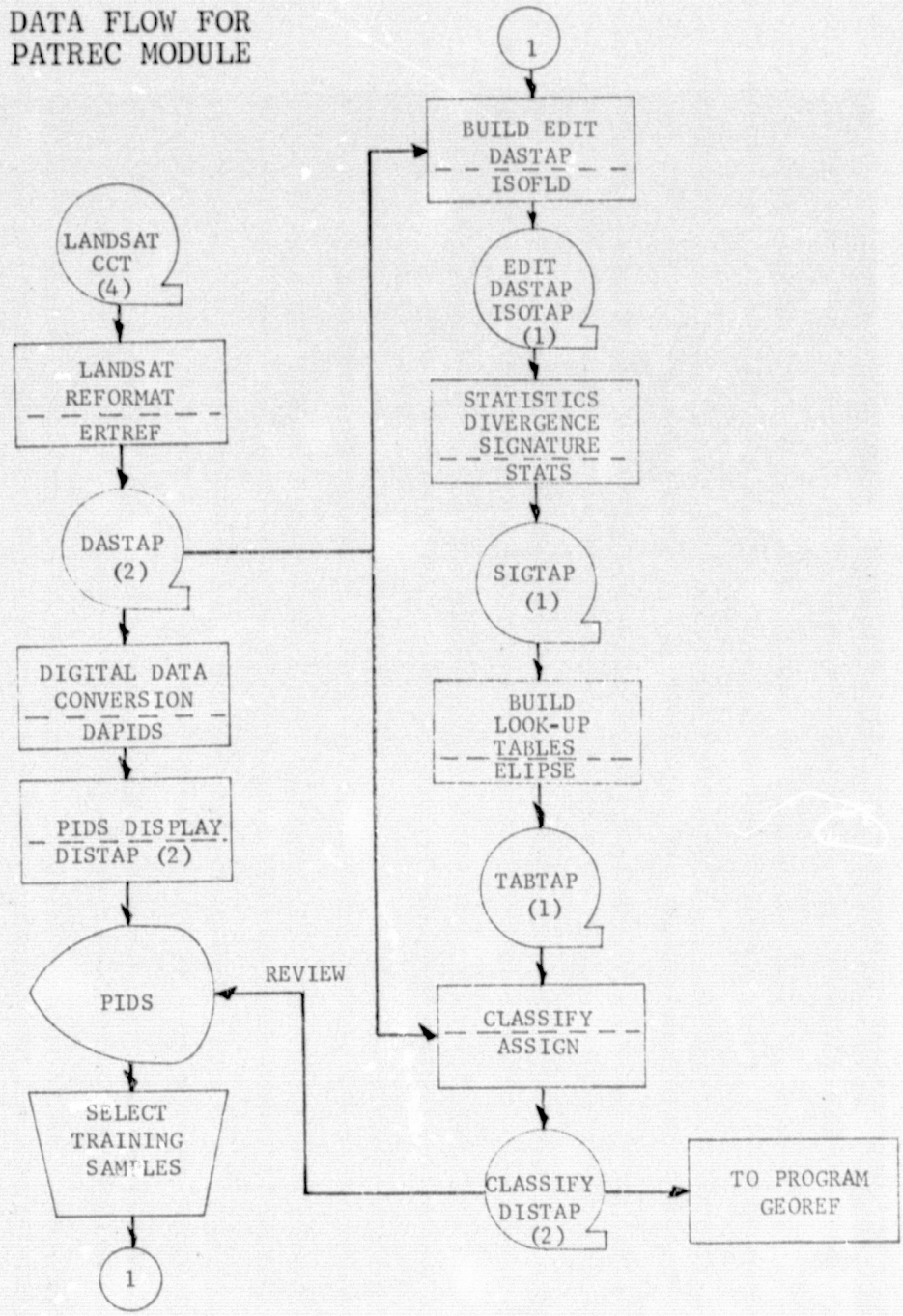


Figure 6.- Block diagram of software PATREC Module.

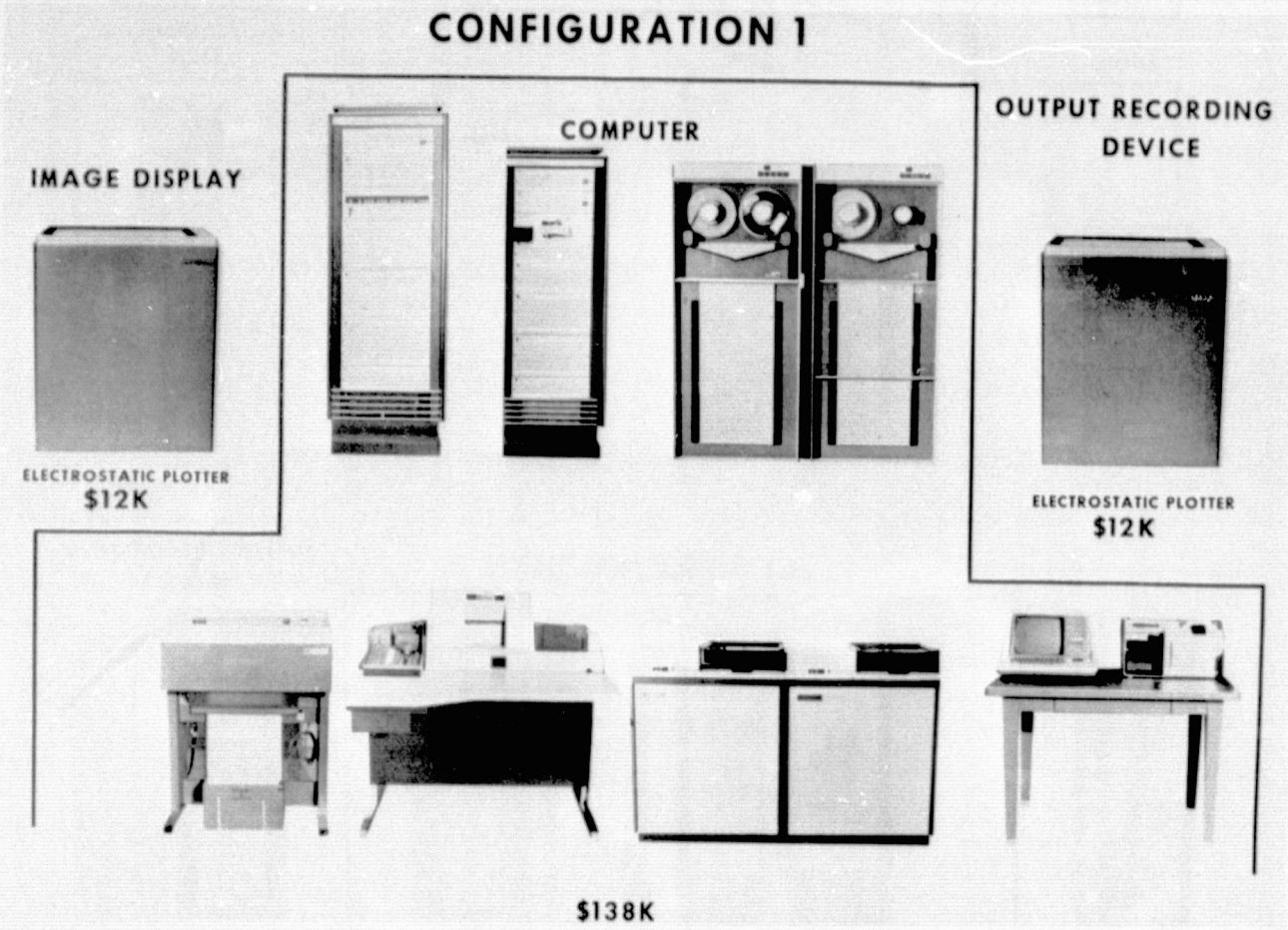


Figure 7.- Low-cost data analysis system, configuration 1.

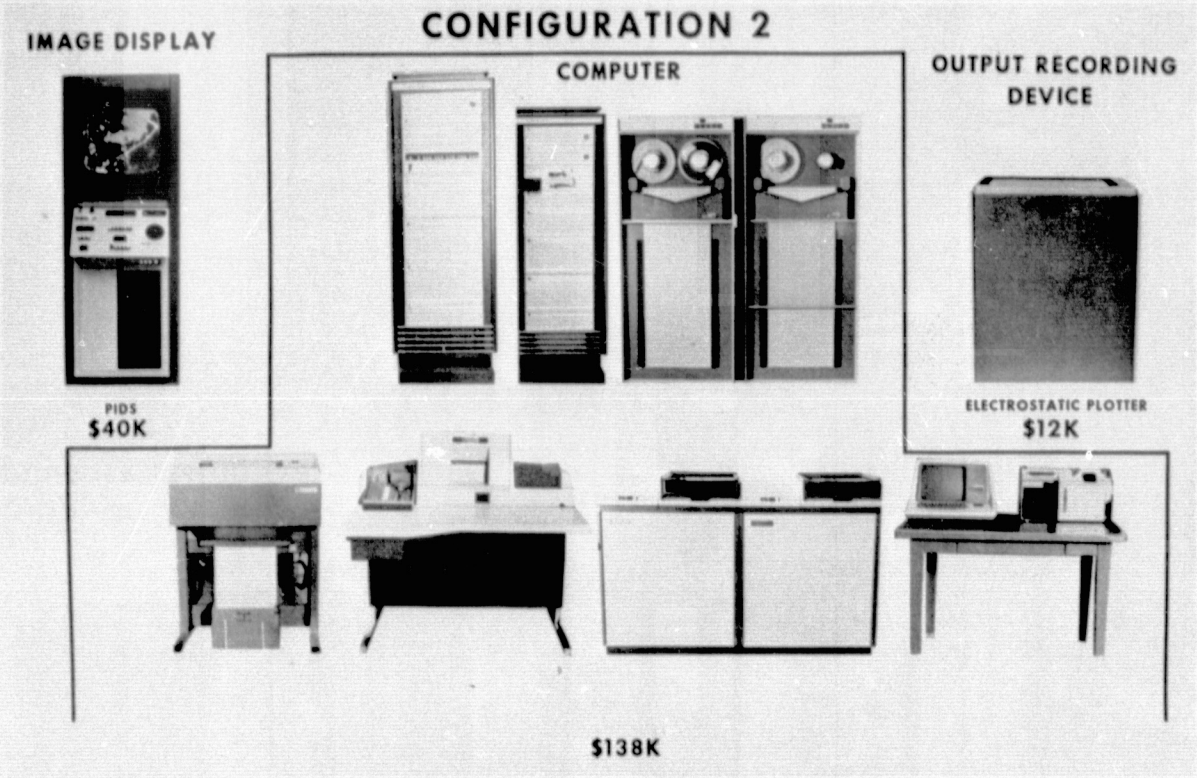


Figure 8.- Low-cost data analysis system, configuration 2.

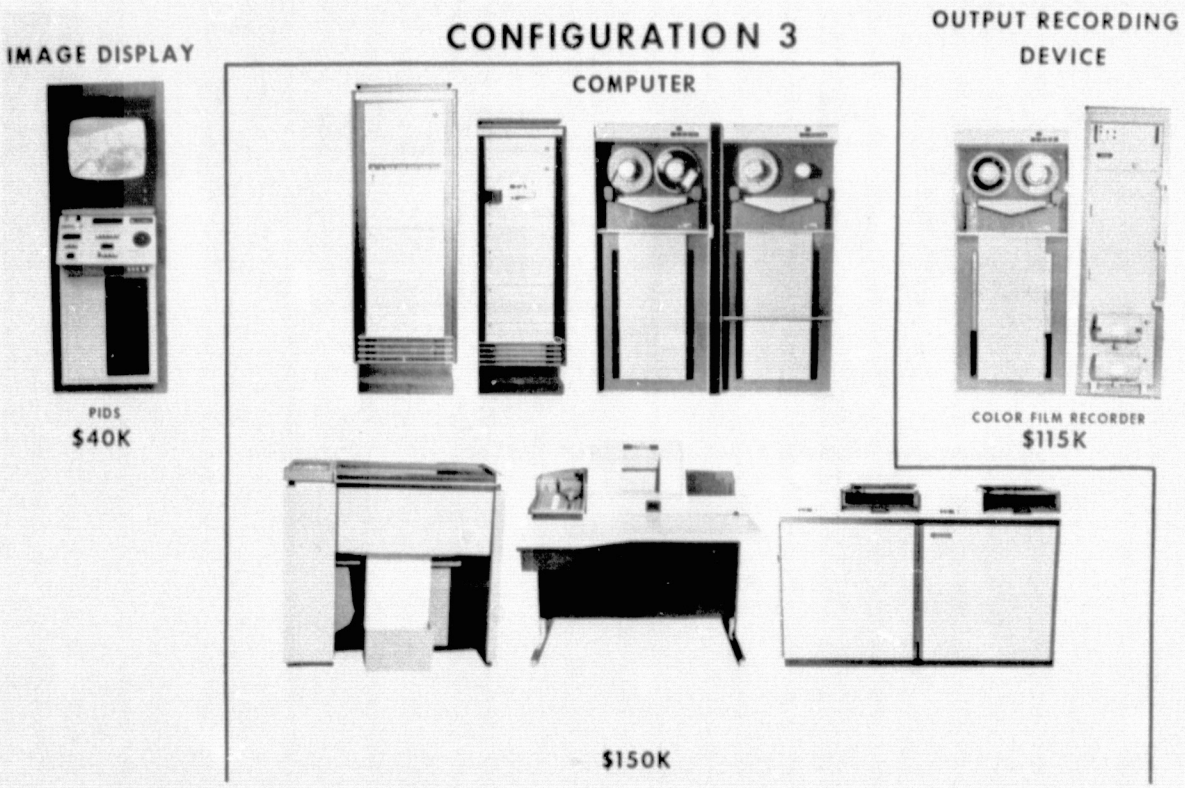


Figure 9.- Low-cost data analysis system, configuration 3.

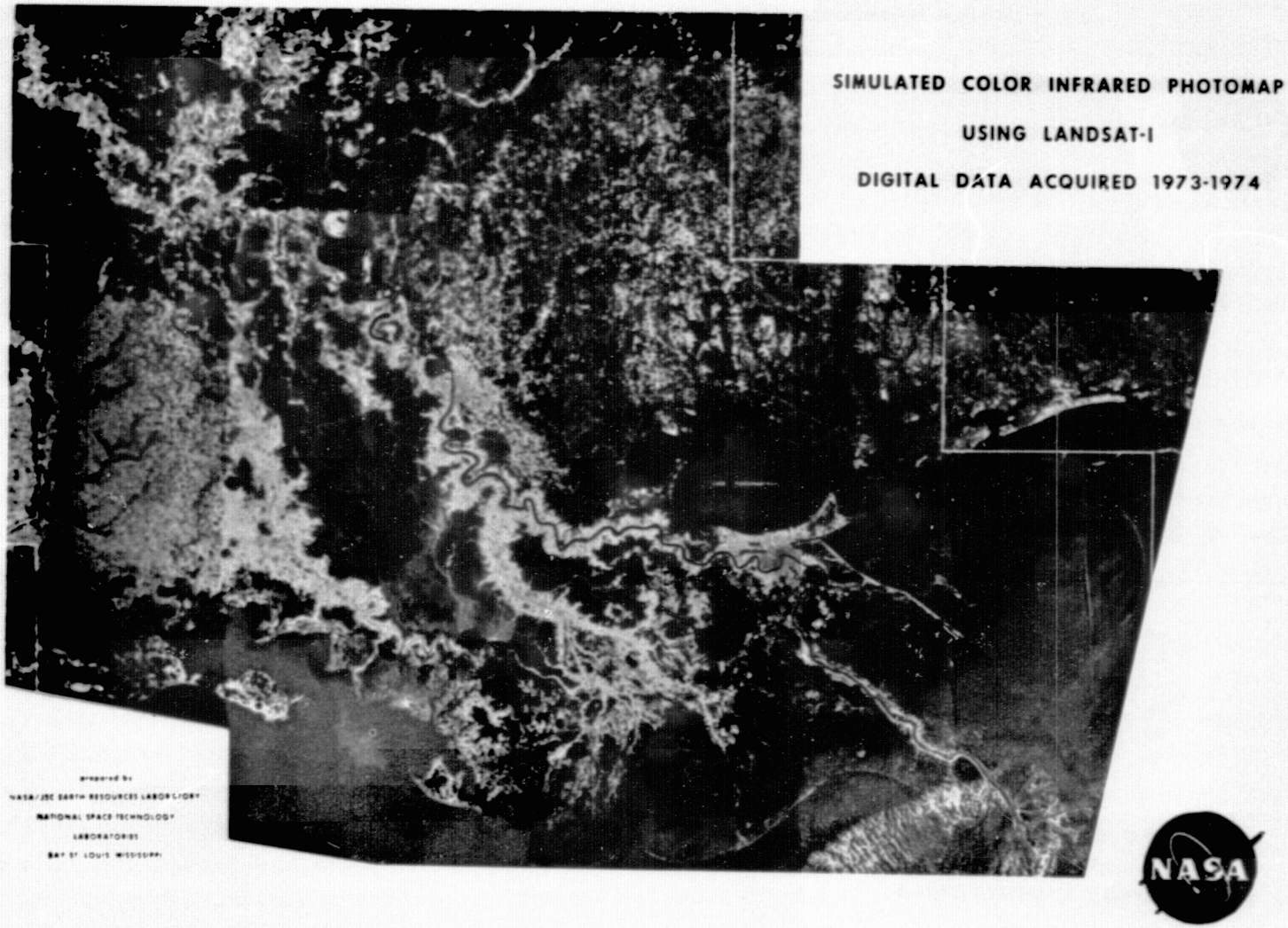


Figure 10.- Mosaic of South Louisiana prepared from seven LANDSAT-1 scenes.

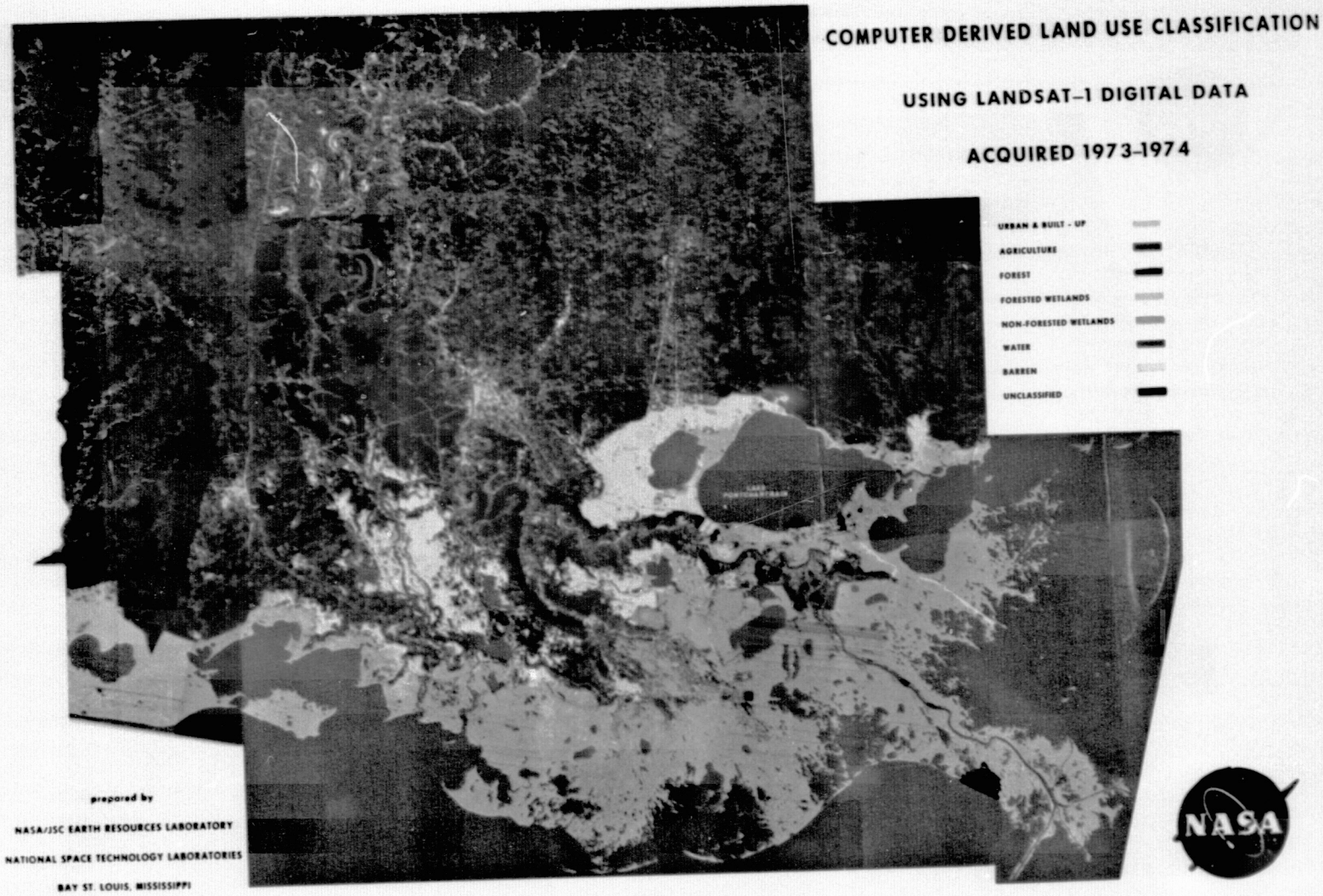


Figure 11.- Surface classification map of South Louisiana prepared from LANDSAT-1 MSS data.

REPRODUCIBILITY OF THE
ORIGINAL PAGE IS POOR

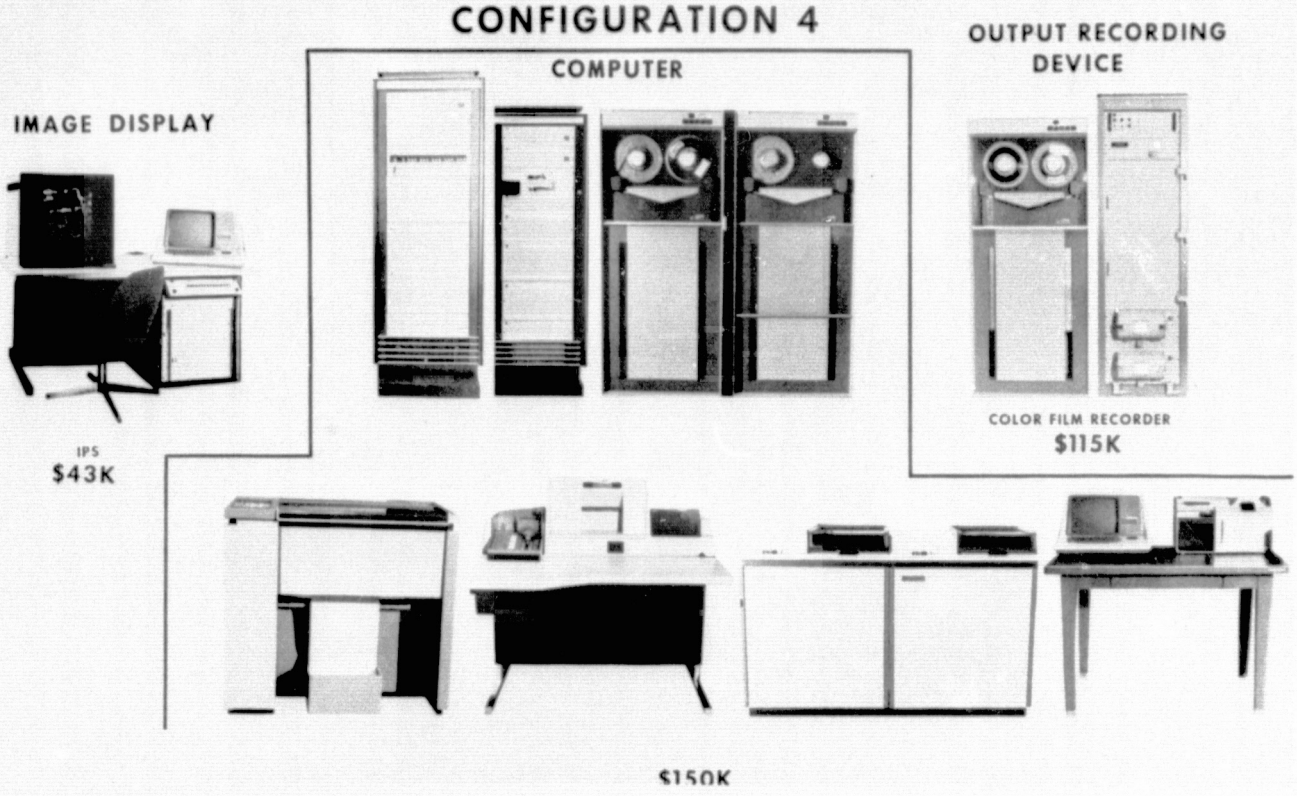


Figure 12.- Low-cost data analysis system, configuration 4.

THE INTEGRATION OF MANUAL AND AUTOMATIC IMAGE ANALYSIS TECHNIQUES WITH SUPPORTING GROUND DATA IN A MULTISTAGE SAMPLING FRAMEWORK FOR TIMBER RESOURCE INVENTORIES: THREE EXAMPLES

By Michael Gialdini, Stephen Titus, James Nichols,
and Randall Thomas, The Remote Sensing Research Program,
University of California, Berkeley, California

N76-17543

ABSTRACT

An approach to information acquisition is discussed in the context of meeting user-specified needs in a cost-effective, timely manner through the use of remote sensing data, ground data, and multistage sampling techniques. The roles of both LANDSAT imagery (2 examples) and Skylab photography (1 example) are discussed as first stages of three separate multistage timber inventory systems and results are given for each system. Emphasis is placed on accuracy and meeting user needs.

INTRODUCTION

The Forest and Rangeland Renewable Resources Planning Act passed in 1974 specifies new guidelines to the Secretary of Agriculture for assessment, planning and reporting on the renewable resources situation in the U.S. to the President. For example, the U.S. Forest Service under the Secretary of Agriculture will be responsible for 1) developing and maintaining resource management plans for the National Forest System (N.F.S.) and 2) developing and maintaining an inventory of all N.F.S. lands and renewable resources. The inventory is required to be updated every ten (10) years, and an annual evaluation report must be submitted to outline the progress in implementing the management plans. Since sound forest management practices are dependent upon the availability of accurate, timely, and economical forest inventory data, which includes timber inventory volume surveys, localized inventory updates may be required more frequently than every 10 years to insure that the objectives of the management plans are being met. Consequently, all federal agencies charged with managing the renewable resources of the U.S. must maintain current inventory information concerning those resources within their jurisdiction.

Outside the U.S. and on some marginal forest lands within the U.S., there is a need for low-cost "volume only" timber surveys. As indicated above, on National Forest Land within the U.S. there is a necessity for periodic detailed timber resource inventories in order to implement sound management practices. This paper will discuss a general information system approach to resource inventory utilizing remote sensing data and supporting ground information and will cite three examples (2 based on LANDSAT imagery and 1 based on Skylab photography) of applications of this approach.

PRECEDING PAGE BLANK NOT FILMED

GENERAL APPROACH

There are seven major steps to be followed in the design and implementation of a remote sensing based information system. To be meaningful, the main criterion for any such system is to be responsive to user requirements and specifications. This necessitates consideration of the capabilities and limitations of the given user agency in the context of the eventual operational use of the system. These steps, in order, are as follows:

1. Definition of Output Products
2. Evaluation of Inputs
3. Development of Estimators
4. Allocation of Effort
5. Data Collection
6. Data Analysis
7. Generation of Output Products

In order to be efficient in subsequent steps of the information system, it is vital to first define the required output products. Designing the inventory with specific goals set before any measurements are made will insure useful, accurate and cost-effective results. Often, inventory results are generated from unrelated data gathered at various times and from a number of sources, leading to unreliable information. User agencies are the obvious sources of output product definitions. Whether the inventory system is to be implemented by a contractor or to be done "in-house," the importance of the user's involvement in definition of reasonable and necessary output products cannot be emphasized too strongly.

After the output products have been defined, the data inputs can be evaluated in terms of the optimum combination that will allow the estimations and measurements necessary for accurate results. A list of potential inputs includes manual ground data collection, large-scale sampling photography, medium-scale photo products, high-flight photo products, satellite photo products, aircraft MSS data, satellite MSS data, and automatic ground data collection. Selection of inputs to be used in the information system will be based on the outputs desired and on relationships between those outputs and features that can be estimated or measured from the various inputs. Basic selection criteria include the use of the optimum combination of inputs without attempting to derive all necessary information from one source, the use of only those inputs that are cost-effective, and maintaining the specified inventory accuracy by using those inputs with the higher correlations to the parameters of interest.

Given the outputs desired and inputs to be used, the sampling-estimation system (e.g. multistage sample) can be designed to meet the user-specified accuracy requirements. In conjunction with the estimator development, a cost-effective allocation of effort should be determined based on the accuracy requirements, the total effort required at the various sample stages, the cost of the effort, and the budget available. In this way, an optimal sampling-estimation system can be developed that will specify the various parameters to be measured or estimated at

a number of stages. In addition, precision statements can be associated with the final estimates and specified output products prior to data collection and analysis.

Data collection, data analysis, and generation of output products will all be accomplished according to plans and specifications determined from the steps above. The system outlined will insure that the output products meet the user needs and provide useful, reliable inventory information in a timely and cost-effective manner.

To better demonstrate the application of this systems approach, the following sections of this paper will cite case study examples.

1973 TIMBER VOLUME INVENTORY

Objective

In order to test the usefulness of LANDSAT-1 imagery for wildland resource inventories, a timber inventory was performed in which the LANDSAT-1 imagery acted as the first stage of a multistage sampling design. The objective of the inventory was to estimate the standing volume of merchantable timber within the Quincy Ranger District 87,000 hectares, (215,000 acres) of the Plumas National Forest in California. Secondary objectives of the inventory were: (1) to test the operational efficiency of the sampling procedures of the multistage sample design; (2) to test the effectiveness of a computer classification of LANDSAT-1 data; (3) to determine the value of LANDSAT-1 data and aircraft data in reducing the sampling error; and (4) to compare the costs of this timber inventory with those for an equivalent inventory using conventional procedures.

Methods

A three-stage sampling design was tested in which "timber volume" was the variable estimated. At each stage timber volume estimates were made from sampling units whose probabilities of selection in the sample were proportional to the corresponding predicted volumes, as interpreted from the next smaller scale imagery. Timber volume estimates were made from three stages: (1) the first stage involved automatic classification of the timberland on the LANDSAT-1 data tapes into four timber volume classes. Within the classified area, samples were selected (called primary sampling units, PSU) from which a more refined estimate of timber volume could be made in the second stage; (2) the second stage involved the acquisition of low altitude photography of selected primary sampling units to select photo plots on which to make a second timber estimate by comparison with photo-volume tables; (3) the third stage involved selecting individual trees within selected sample photo plots by photo measurement of all merchantable trees. Selected trees were then precisely measured (for volume) on the ground and these volume measurements in turn were expanded through the various stages of the sample design to estimate total timber volume over the national forest land within the Quincy Ranger District.

Results

The total volume of timber on the Quincy Ranger District of the Plumas National Forest was estimated to be 11.5 million cubic meters (approximately 2.44 billion board feet) based on eight selected photo plots located within four primary

sampling units. The sampling error associated with this estimate was 8.2 percent, which falls well below the acceptable S.E. of 20 percent for the District. This indicates that the true volume of merchantable trees on the Quincy District will fall into the interval 9.97-13.1 million cubic meters with .80 probability.

There were only thirty-one trees total measured by an optical dendrometer on the ground at the eight plots (thirty-two trees should have been measured but one plot out of the eight contained only three merchantable trees which could be measured). The field work required one week's time by a two-man crew, and the total area of the ground plots measured was 1.3 hectares (3.2 acres), representing a sampling fraction of about 1/67,000.

Critique

The sampling system used to estimate only total volume was very successful with only a minimum sample size. However, in terms of needs in developed countries for detailed timber management planning, volume estimates alone are not enough. Growth data, particularly, is as important as volume of growing stock for planning purposes. Additionally, estimates are needed for mapped subdivisions of the forest based on major vegetation type and stand condition classes.

1974 TOTAL TIMBER RESOURCE INVENTORY

Objective

Results of the volume inventory successfully demonstrated the utility of a LANDSAT-based multistage sampling system for a single Ranger District. The objectives of the 1974 timber inventory were to expand the area covered to include the entire Plumas NF 470,245 hectares (1,162,000 acres), and to incorporate other features into the multistage sampling system to estimate additional parameters necessary for detailed timber management planning. Parameters to be estimated included volume, growth, number of trees, surface area and areas, subdivided into various species and size classes. Additionally, estimates were desired for the entire forest, ranger districts, and by major vegetation types and stand condition classes.

Methods

The sampling-estimation system design for this inventory was based on a number of assumptions and results relating to the particular problem at hand and results of the volume inventory for the Quincy Range District in 1973. Multistage sampling proved useful in the Quincy inventory, for combining three information sources: LANDSAT MSS data, large-scale photo data, and ground measurements. The specifications for sampling unit sizes were based on results of work with the Quincy District: Primary sampling units were rectangular blocks of 45 x 5 pixels (approx. 2.57 kilometers x 400 meters), and large-scale and ground plot sizes were nominally .16 hectares (0.4 acre) circular plots. Stratification is an essential part of many inventories and was introduced this year both in order to reduce variance and because strata estimates were desired as well as total forest estimates. Sample size and allocation were based on precision control for volume only. Although a number of other parameters were also of interest, the population information was

inadequate except for volume, and the sample allocation problem for multiparameter sampling still has not been adequately resolved.

The 1973 Quincy inventory used sample selection probabilities proportional to estimated size (PPES) since volume was the only parameter of interest. The 1974 inventory, however, was concerned with estimating a number of parameters in addition to volume. It has been demonstrated (Wensel, 1974) that greatly inflated variances can be obtained for some parameters if (1) PPES or probability proportional to size (PPS) type sampling is used; and (2) the variables are not all positively and highly correlated with each other. Since growth and volume may be negatively correlated, it was decided that an equal selection probability system would reduce the possibility of inflated variances. For this reason, the primary use of LANDSAT MSS data in the first stage was shifted from defining selection probabilities to determining stratification and acreages within strata based on computer classification.

Figure 1 provides a generalized overview of the 5 stage sampling system. Stratification, into four major vegetation types: mixed conifer, eastside pine, high-elevation true fir, and oak-woodland, was used to reduce variability and to provide estimates for subdivisions of the population. The Stage I sample of 40 primary sampling units (PSU) was allocated proportionally to an area in each stratum; PSU's were selected with probability proportional to the number of acres of timber in each PSU in the stratum of interest. Within each selected PSU, a Stage II systematic sample of ten photo plots was located utilizing centerpoints of large scale low-altitude stereo triplets flown along the center of the longitudinal axis of the PSU. For Stage III, a double sampling link with the ground was provided by selecting a random sample of photo plots for further detailed measurements on the ground. To avoid the use of arbitrary volume tables which potentially can induce a bias into volume estimations, a Stage IV subsample of trees on the ground plots was selected using the "3-P" sample selection technique, probability proportional to prediction. Trees selected were measured with an optical dendrometer to obtain precise measures of volume, surface area and height. A supplementary Stage V sample was used to demonstrate the potential for measuring growth by incorporating remeasurement of permanent plots with the existing four stage system.

Results[1]

Table I summarizes results for the entire forest. While it is interesting to compare these estimates and FS estimates, this is difficult for a number of reasons. Three of the five estimates are not available in previous FS summaries, viz. number of trees, basal area growth, and surface area. Board foot volume is difficult to compare since our estimates are based on a regression model for board foot volume actually recovered, and may or may not be comparable to the FS rule or table. Second, our estimates are for trees 5.0" DBH and larger, and FS estimates are for 11.0" DBH and larger. Third, FS estimates are only for commercial forest land, whereas ours are for all federal forest land. Fourth, the most recent FS estimates date from 1969, and possible changes in stocking levels further complicate the issue. Fifth, FS estimates are for net utilized volume and ours are for gross volume. In the longer term these problems can all be resolved by specifying more completely the measurement techniques that are required. In the mean time, however, our estimate of 16.8 MBF/acre is larger than a FS estimate of 12.1 MBF/

[1]To be meaningful to the user community, the measurement values will be given in traditional units.

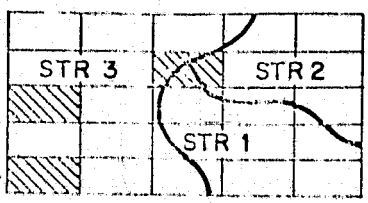
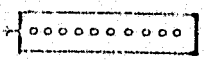
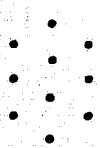
STAGE		DESCRIPTION
0		Stratification of the population (heavy lines).
I		A sample of 45 x 5 pixel PSU's.
II		A sample of .16 hectares (0.4 acre) Photo Plots (SSU) in each selected PSU.
III		A subsample of .16 hectares (0.4 acre) Ground Plots (TSU) selected from the set of photo plots.
IV		A subsample of trees located within the set of Ground Plots.
V		A sample of USFS permanent plots for growth data remeasurement.

Figure 1. Plumas 1974 Multistage Timber Inventory Overview

TABLE I: PLUMAS NATIONAL FOREST 1974 SUMMARY OF ESTIMATES

Parameters of Interest (Conifers, 5.0" DBH and Larger)	Estimate-Mean/Acre	Standard Error	Relative Standard Error(%)
Number of Trees	63.86	7.79	12.19
Square Foot Basal Area	80.69	5.21	6.46
Square Foot Basal Area Growth (5 year)	5.41	0.35	6.42
Cubic Foot Volume	2387.47	186.79	7.82
Scribner Board Foot Volume	16777.05	3173.71	8.19
Square Foot Surface Area	7370.01	465.37	6.31

acre obtained by averaging the total board foot volume on commercial forest land over the total forest acreage. This difference seems entirely plausible in view of the factors listed above, especially the net versus gross volume problem. A similar comparison with cubic foot volume shows a FS estimate of 2402 CF/acre compared with our estimate of 2387 CF/acre. Measurement definitions still confound the comparison since ours is gross volume for the entire tree and theirs is net volume to a 4.0" top diameter inside bark. Both estimates are for all trees 5.1" DBH and larger. Even considering problems of specification, the estimates obtained in the 1974 inventory compare very favorably with previous FS results. These specification discrepancies do not represent defects in the sampling-estimation system, but rather are measurement details which would be resolved before applying the system in a truly operational context.

The relative standard error (RSE), the standard error of the estimate divided by the estimate, for the five parameters of major interest are shown in Table I. With the exception of number of trees, all are in the range 6.31 to 8.19 percent. While the RSE for cubic foot volume, 7.82 percent, does not meet the specified desired level of five percent, the overall results are satisfactory. Using procedures outlined by Cochran (1963, p. 139), it was estimated that the stratification scheme reduced the sampling variance to about 0.9 percent of that which would have been obtained using simple random sampling. More detailed stratification into both major type and stand condition classes should achieve much greater gains in precision, and should allow achievement of desired precision levels without increasing sample size.

For timber management planning, estimates by vegetation type-condition classes are of major interest. Table II summarizes the results for each type-condition class and the five parameters of major interest. Since sample size was not controlled, the RSE for these estimates were larger than those achieved in the stratified sample, ranging from about 14 to 80 percent. The magnitude of the RSE is roughly proportional to the area of each type-condition class; for example, true fir, mixed conifer, and eastside pine considered as a group showed RSE of 27-80, 14-34, and 19-39 percent respectively. This is a reflection of the proportionately larger sample size in types with larger acreages. It is easily seen that the estimates reflect the differing stand conditions in each major vegetation type. For example, board foot volume increases as stand size, but drops off substantially in poorly stocked stands. It should be noted that the areas classified as poorly stocked include land which would be further subdivided into noncommercial forest land or perhaps otherwise reserved from intensive management so that the proportion of land in this category would not be as high as is indicated by this summary. These summaries represent the biological current state of the ecosystem without introducing the many management and environmental protection constraints on activities.

Critique

The success of the 1974 LANDSAT-based total timber inventory is demonstrated by the achievement of RSE less than 8.0 percent for most parameters of major interest at a total cost of approximately $34,000. In addition, opportunities were identified for improving various components of the inventory system that can provide a corresponding improvement in precision of estimates and provide important guidelines for directing future research effort. For example, LANDSAT data computer classification results are still being analyzed, but it appears that information content is sufficient to enable a more detailed stratification to be

TABLE II PLUMAS NATIONAL FOREST 1974, SUMMARY OF ESTIMATES BY TYPE-CONDITION CLASS

Type Condition Class	Number of Trees per Acre	Square Foot Basal Area Per Acre	Square Foot Basal Area Growth 15 year Per Acre	Cubic Foot Volume Per Acre	Scribner Board Foot Volume Per Acre	Square Foot Surface Area Per Acre	Area (Acres)
(TF)[a] Regeneration	93.87	114.52	8.80	2865.20	19781.87	10818.72	11239.78
" Immature	96.24	84.86	5.01	2633.77	18507.13	7625.56	51612.20
" Mature	116.96	158.25	12.70	4232.66	28734.02	14720.02	6146.67
" Overmature	-	-	-	-	-	-	-
" Poorly Stocked	27.70	36.58	2.51	1081.03	7677.22	3338.17	44015.97
(MC)[b] Regeneration	79.88	83.49	5.78	2153.80	14493.25	7740.17	63486.48
" Immature	76.30	107.88	7.07	3172.94	22231.04	9857.41	213461.15
" Mature	100.72	131.33	7.89	4345.98	31275.91	11749.99	177863.43
" Overmature	68.39	127.84	8.84	3908.45	27659.81	11656.98	21996.67
" Poorly Stocked	22.18	40.29	2.40	1434.79	10500.94	3529.29	186068.69
(EP)[c] Regeneration	76.10	54.02	6.75	1038.54	6535.98	5148.36	38110.10
" Immature	84.52	89.73	7.09	2106.89	13846.98	8522.41	117052.45
" Mature	72.08	96.49	5.70	2600.55	18099.39	9086.22	51720.85
" Overmature	-	-	-	-	-	-	-
" Poorly Stocked	19.27	23.14	1.81	625.31	4331.15	2153.31	133736.53

[a] TF = True Fir

[b] MC = Mixed Conifer

[c] EP = Eastside Pine

made to vegetation type and condition. The second component requiring further attention is the specification of regression models that relate photo variables to ground variables.

1974 MANUAL PHOTO-INTERPRETATION TIMBER VOLUME INVENTORY

Objective

In order to determine the information content of Skylab S190 infrared Ektachrome (CIR) imagery for wildland resource inventories, a timber inventory based entirely on manual photo interpretation techniques was performed. In this study the S190 imagery was utilized as the first stage in a multistage sampling design. The objectives included: 1) determining the abilities of human photo interpreters to distinguish timber volume classes on S190 data; 2) determining the efficiencies of simple random sampling as applied to a multistage sampling design and 3) the demonstration of a method of obtaining timber volume information of a reasonably large area (49,700 hectares located within the Plumas National Forest) that is timely, cost-effective and does not require the use of a computer.

Methods

Gross timber volume was the variable estimated in the sampling design based on random sampling at each of three stages. Sampling units were selected at each stage at random because it was not known how well human interpreters could differentiate between timber and non-timber classes on S190 imagery in the first stage, and by utilizing random sampling techniques, the ability to separate these classes could be established quantitatively. In the first stage timber volume was estimated from the percentage of area occupied by each of 4 timber volume classes (non-timber, 0-10,000 board feet/acre, 10-20,000 board feet/acre, and greater than 20,000 board feet/acre) within 1,036 hectares (2 mi. x 2 mi.) squares delineated on an enlarged portion of the S190 imagery. For the second stage, randomly selected squares from the first stage were transferred by visual inspection onto 1:60,000 and 1:120,000 color-infrared resource photography and then divided into five rectangular flight lines. Photo interpreter delineations of the timber volume classes were measured within each square and areal percentages of the volume classes were calculated. A number of these rectangular blocks were selected at random for the acquisition of large-scale high-resolution aerial photography coverage (similar to the preceding case examples). Measurements of individual tree crown diameters and estimates of tree heights were made on .16 hectare (0.4 acre) plots located on the large-scale photography to arrive at the third stage photo volume estimate. The individual tree photo volumes were calculated from regression estimators derived from precise measurements of volume made on randomly selected trees with a Barr & Stroud dendrometer during the ground phase of the study. The ground measurements were then expanded through the various stages of the sample design to estimate the total timber volume located on the 49,700 hectares study area.

Results

Before the timber volume calculations were performed, an analysis of variance and correlation analysis was performed on the timber volume class interpretations on

the enlarged Skylab S190 imagery. In order to determine how accurately a human interpreter could differentiate timber volume classes, 18 of the 48 total PSU's were delineated and interpreted for volume classes on Zeiss scale 1:60,000 infrared Ektachrome high altitude imagery. The 18 selected were the only ones for which stereo coverage was already on hand. A skilled interpreter delineated the 3 timber volume classes and the non-timber class on the high altitude imagery and precisely determined the percentage of the total area covered by each class with an area calculation device. These results, assumed to be an accurate account of ground conditions, were correlated with the interpretation results of each of three interpreters on the enlarged portion of the S190 imagery.

The correlations between the ground conditions and the photo-interpreters' timber volume class estimations on the S190 imagery were very low (.01-.3) but achieved.5-.62 for the non-timber. A comparison of a timber vs. non-timber identification on S190 seemed more promising as a first stage sample stratification due to higher correlations with ground conditions as well as correlations between interpreters on S190 of greater than .80. This indicated that random sampling with probability of selection proportional to the percentage of the PSU covered by timber would be more efficient than the simple random sampling used initially. Timber volume class estimations within PSU's could then be made on the 1:60,000 and 1:120,000 resource photography as a second stage sample. Subsequent selection of the rectangular flight lines from the PSU's could be made using variable probability sampling with probability proportional to estimated volume within each rectangle. From this stage on, the sampling-estimation procedures would follow the steps outlined in the 1973 volume-only inventory summarized earlier in this paper.

Final results of this manual interpretation inventory are still pending. Given the additional information derived from the analysis of variance-correlation analysis, the sampling-estimation system has been redefined and the current data is being reanalyzed in anticipation of more precise volume estimation.

SUMMARY

The results of the case study examples cited above indicate the utility and cost-effectiveness of remote sensing aided inventory systems when used with proper sampling designs, appropriate satellite and aircraft imagery, and subsequent ground data collection. The development and implementation of these systems must be based on meeting user requirements, which are best specified through continual interaction between the remote sensing community and the user-agencies. The ultimate goal is the operational implementation of remote sensing aided information systems by the user-agencies alone.

REFERENCES

Cochran, W. G., 1963. Sampling Techniques. Second Edition. John Wiley & Sons, Inc., New York. 413 pp.

Wensel, Lee C., 1974. Selection Probabilities in Multiparameter Sampling. Proceedings of Workshop of the Society of American Foresters Inventory Working Group. Fort Collins, July 1974.

DESIGN CRITERIA FOR A MULTIPLE INPUT LAND USE SYSTEM*

By

Frederic C. Billingsley and Nevin A. Bryant
Jet Propulsion Laboratory
California Institute of Technology
Pasadena, California 91103

N76-17544

ABSTRACT

There exists a need for geographic information systems that are current and comprehensive. Polygon overlay and grid cell information systems access data for selected areas, but their data files are time consuming to generate and frequently costly to process. Updating of land use changes for such systems may become prohibitively expensive. A recent response has been to process LANDSAT and other digital imagery in classification algorithms to derive land use maps. Such maps, however, cannot interface directly with existing geocoded information storage and retreival systems.

In response to the present dilemma, a design is presented that proposes the use of digital image processing techniques to interface existing geocoded data sets and information management systems with thematic maps and remote sensed imagery. The basic premise is that geocoded data sets can be referenced to a raster scan that is equivalent to a grid cell data set, and that images taken of thematic maps or from remote sensing platforms can be converted to a raster scan. A major advantage of the raster format is that x, y coordinates are implicitly recognized by their position in the scan, and z values can be treated as Boolean layers in a three-dimensional data space. Such a system should permit the rapid incorporation of data sets, rapid comparison of data sets, and adaptation to variable scales by resampling the raster scans.

INTRODUCTION

In the fields of land use planning and natural resource analysis there exists a continually growing need for geographic information systems that are current and comprehensive. Two basic approaches have been undertaken to fulfill agencies' needs, and both have encountered limitations which have restricted their widespread application.

In response to the desire to access data for selected areas, polygon and grid cell geocoded information systems have been developed. Such systems rely on the tabular formatting of the input data, a costly and time consuming process. Often the system falls into disuse because the updating of major segments of the data base, particularly land use changes, becomes prohibitively expensive. At other times the system is found by the full range of potential users to have limited applicability because of the data formatting restrictions inherent in the grid cell or polygon overlaying and comparison technique.

In response to the desire to provide up-to-date land use information, investigators have studied the feasibility of using LANDSAT and other digital imagery for land use mapping. The consensus which appears to be evolving is that while remotely sensed imagery can provide timely coverage and cost-effective land use

---

* This research presents the results of one phase of research carried out at the Jet Propulsion Laboratory, California Institute of Technology, under Contract No. NAS 7-100, sponsored by the National Aeronautics and Space Administration.

PRECEDING PAGE BLANK NOT FILMED

maps of sufficient accuracy using automated data processing techniques, the end product is still a map, and cannot interface directly with existing geocoded information storage and retrieval systems. What appears to be needed is the conjunction of existing geocoded data sets and information management systems with thematic maps and remotely sensed imagery via digital image processing of raster scans made of those maps and images.

CONCEPT

The basic premise in designing a raster scan based Multiple Input Land Use System (MILUS) is that a digital image processing language and its associated algorithms can efficiently execute file manipulation of areally referenced data. The geocoded data set in the tabular data base can be referenced to a raster scan in which each pixel is equivalent to a grid cell or polygon node. Current information on land use can be derived from scanned imagery, while additional data sets could be generated through scanning photographs of thematic maps or converting digitized information to a raster format. Figure 1 illustrates the variety of input formats possible.

A major advantage of the raster format is that x, y coordinates are implicitly recognized for each position in a scan, and z values can be treated as Boolean layers in a three-dimensional data space. Figure 2 illustrates how such a formatting procedure would permit the extension of the data base "images" both horizontally (to include more area) and vertically (to include more variables) without requiring a reformatting of the existing data. A further advantage of using a data base of registered "images" is that updating of a particular component, such as land use, would be accomplished by simply replacing a data plane.

Perhaps the greatest economics associated with the raster scan data base format will be associated with the interrogation of particular areas of interest to the user and cross-referencing of data planes. It is envisioned that the user would extract from the major file (on tape or a mass storage device) a data region of interest. Extraction of a region from the primary set of data planes assures that high resolution data, equivalent to grid cells of one acre (or smaller if needed), can be accessed for interactive interrogation. The area of immediate interest, be it defined by an administrative district (e.g.: census tract) or other polygon, would be accessed by generating a raster scan data plane outlining the area as a binary mask. The binary mask approach, which by image multiplication would present the information processor with data only from the area as defined, permits a flexibility in administrative area choice not presently available in tabular geobase file systems. The user would now have the option to aggregate data by undefined regions such as water sheds while being able to also conform to conventional geobase file units, such as census blocks or tracts in the DIME file system [1] .

The overall design concept for the proposed Multiple Impact Land Use System (MILUS) is presented in Figure 3. It should be noted that the raster scan data base is not designed to supplant existing tabular data files and information storage and retrieval systems, but rather make available additional data not originally included and permit the entry of updated information. The two-dimensional data base files are to be connected by a general purpose interface with the user's information processing system and geographically oriented to the tabular data base coordinates via a tabular-to-raster conversion interface.

It is envisioned that the two dimensional data base of registered images would provide most of the land use and environmental information, while existing tabular data bases, particularly the census DIME files in urban areas, would contain the majority of demographic and economic information.

IMPLEMENTATION

The design of a raster scan data base conversion and management system must be concerned with several subsystems. In order to permit the rapid construction of geocoded multiple variable files from remotely sensed data and mapped information, and be used in conjunction with existing tabular data bases and information processing systems, several types of digital image processing routines must be available. As Figure 3 demonstrates, software and associated hardware are needed to: 1.) Incorporate raw two-dimensional and additional tabular data sets to raster formats, 2.) Perform special purpose digital image processing, 3.) Provides an interface between tabular and raster data bases, and 4.) Interface with an information system processor and provide a binary mask two-dimensional data base file processor. Many of the necessary procedures have been developed for VICAR (Video Image Communication and Retrieval), the digital image processing language developed at the Jet Propulsion Laboratory's Image Processing Lab [2]. Cost-effective construction of master data bases of registered "images" will require streamlining of existing procedures and further development of interactive capabilities.

The reduction of two-dimensional data (maps and scanned imagery) to registered fine-mesh grid cell data planes should contribute the greatest potential return to users. Land use and other social and economic information is mapped at widely varying scales, as each administrative constituency is primarily concerned with its own use of the information it gathers. Comprehensive regional plans have usually required the reduction of all information to the same scale, and as a result, much of the time and money spent in formulating regional plans has been devoted to constructing the basic maps from which decisions can be made. Maps can be photographed and then scanned with a precision microdensitometer at a sampling rate commensurate with the desired minimum grid cell size. The same procedure can be applied to aerial photo transparencies, while scanned imagery can have resampling algorithms transform pixel shape and equivalent land area (IFOV) to desired grid cell sizes. While the generation of registered "image" data planes from mapped and scanned imagery should prove cost-effective when compared with existing geocoding procedures, the registering of other collateral information to a geocoded base may still require extensive manual manipulation. It is expected, for instance, that use of coordinate digitizer input would be restricted to specified high-priority items or as a means to interface tabular data sets with the registered data planes (e.g. coordinate digitize census tract/block boundaries to interface with the census DIME file).

The other primary component of MILUS, file access and geocoded data manipulation based upon digital image processing techniques, should provide the user with an information system that is both more flexible and more cost-effective than existing systems. The use of pixels for grid cells permits several economies in addition to that derived from not needing x-y notation for each grid cell. Briefly, they include: 1.) The ability to assign a value ranging from 0 to 225 to a grid cell if pixel values are in byte format. 2.) Ability to capitalize on the mathematical characteristic that 11 prime numbers exist between 0 and 225.

3.)Ability to use binary (one bit) masks to extract areas of interest by simple multiplication. 4.) Ability to store data at a given areal resolution and retrieve it at any desired resolution by using raster resampling algorithms. 5.) Ability to use a histogram of pixel values to derive area percentages within a designated portion of the raster scan. 6.) Ability to use table-stretch algorithms to manipulate pixel values within a raster scan and between two rasters to generate a third, and 7.) Ability to apply a subarea access routine to a rectangular area within the major data set and place it on a disk file for interactive interrogation.

The seven VICAR file and data manipulation procedures just described, can be used to accomplish a wide variety of geographic information system applications. Some examples in addition to those outlined in the preceding section (CONCEPT) would include:

a. Being able to prepare a data base of registered images to suit the needs of a particular region, such as one of the local COG (Council of Governments) area, and then call from mass storage the particular area of interest at the level of grid cell resolution deemed necessary.

b. By using the byte format to provide a large number of values per data plane, the user will be able to incorporate extended map legends in the grid cells. The prime numbers would constitute one level of classes and the full range of 0-225 would be the range of values for each class on a second data plane. Should it prove that the byte per pixel format does not provide enough prime numbers for a master data plane, the option would exist to use half-word, word, or even dual precision word formats.

c. Being able to rapidly generate derived data sets by using table-stretch and binary masking procedures. Application of these methods have already been performed to determine water quality from LANDSAT imagery [3] and should prove more efficient than the polygon overlay algorithms (such as PIOS [4]) presently developed.

d. Being able to obtain a histogram of pixel values within designated subareas of a raster will permit the user to derive a numerical value (such as acreage or percent cover) for variables not included in an existing tabular data base. Thus, the user could add land use or other information by census tract to the DIME file.

CONCLUSIONS

The United States and the world at large has entered an era of limited resources. In the past, a surplus of land and materials in the U.S. permitted freedom of action, and rarely did the democratic decision-making process need to consider the merits of a project on anything other than its immediate economic cost-benefit. Limited resources have narrowed freedom of choice considerably, and in order to assure the citizenry that an orderly democratic process is being adhered to, legislators are requiring comprehensive analyses of alternatives prior to making far-reaching decisions. National and state-wide land use

planning acts are being contemplated to serve these purposes, and their implementation will require a broad ranging technological effort to provide the required information expeditiously. In addition, the potential users of land use information extends beyond planning agencies to tax accessors, public works, transportation, forestry, etc., all of whom should create a demand for data at a variety of resolutions other than that provided by LANDSAT, and very likely with many different modeling applications in mind. The proposed Multiple Input Land Use System (MILUS) based on the raster scan format should prove flexible enough to serve most user needs in a cost-effective manner through the provision of time-sharing terminals tied in to a regional center.

The projected demands to be placed upon geographic information systems will place a strong emphasis upon the capability to store and retrieve large amounts of data and manipulate data sets for portions of the files efficiently. A major drawback facing most geo-coding procedures is that they rely on sequential commands applied to tabular data strings, and as such require a large investment in formatting or processing data that is inherently two dimensional. Raster scan data bases will avoid many of these problems and possess additional advantages. The video communications field has been and is continuing to address both the problems of mass storage and applications of rapid interactive processing that places a minimal reliance upon computer software routines. The specialized requirement of geographic information systems should derive considerable benefit from the image processing field in the future.

REFERENCES

1. Bureau of the Census, U.S. Department of Commerce, "The DIME Geocoding System", Report No. 4 of the Census Use Study, Washington D.C., July, 1970.

2. Billingsley, F. C., "Digital Image Processing for Information Extraction", International Journal of Man-Machine Studies, V, p. 203, 1973.

3. Blackwell, R. J., "The Trophic Classification of Lakes Using ERTS Multispectral Scanner Data", Proceeding American Society of Photogrammetry, 41st Annual Meeting, March 9-14, Washington, D.C., p.772-782.

4. Comprehensive Planning Organization, Polygon Information Overlay System, San Diego, California, September 15, 1971.

Figure 1

MULTIPLE INPUT LAND USE SYSTEM

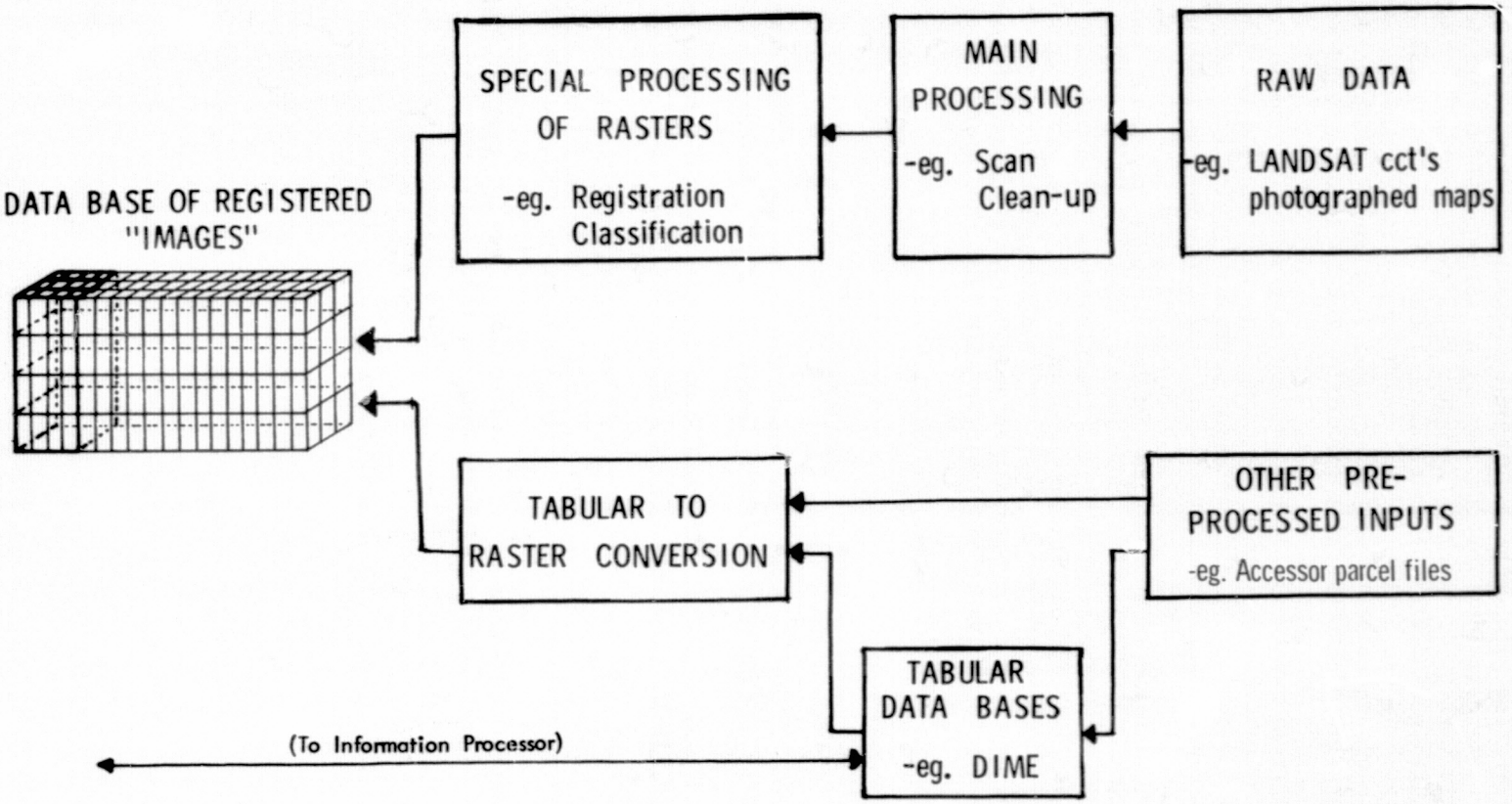


Figure 2

MULTIPLE INPUT LAND USE SYSTEM

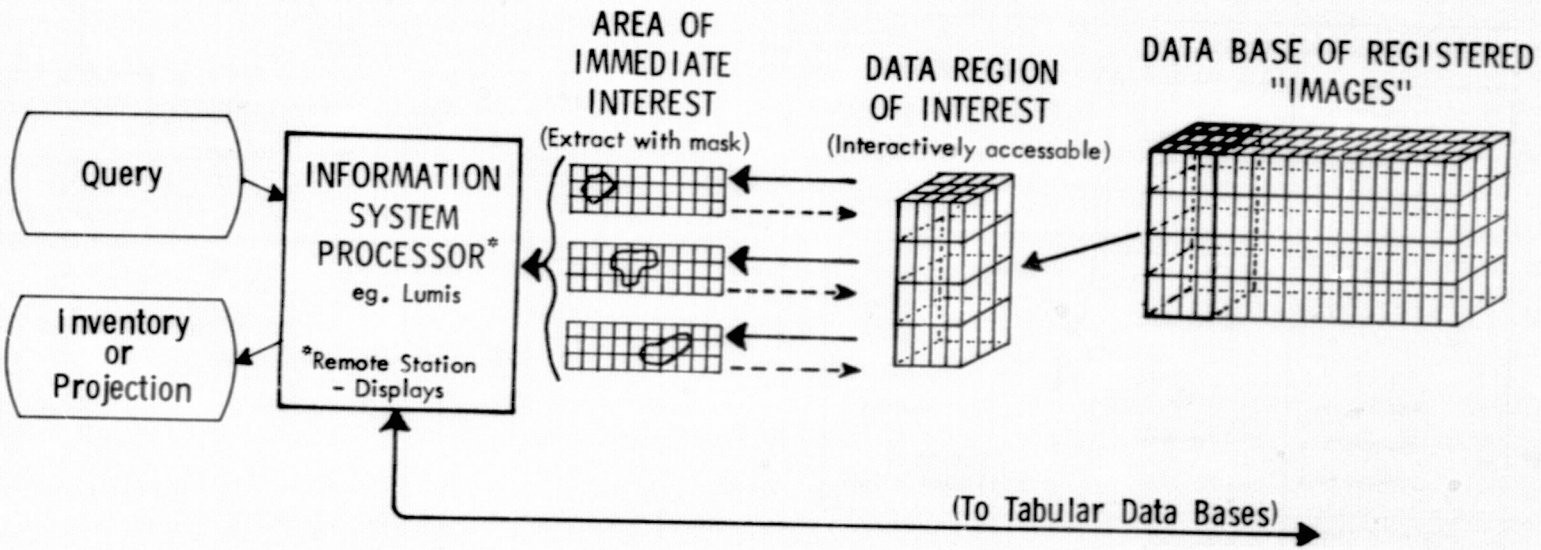
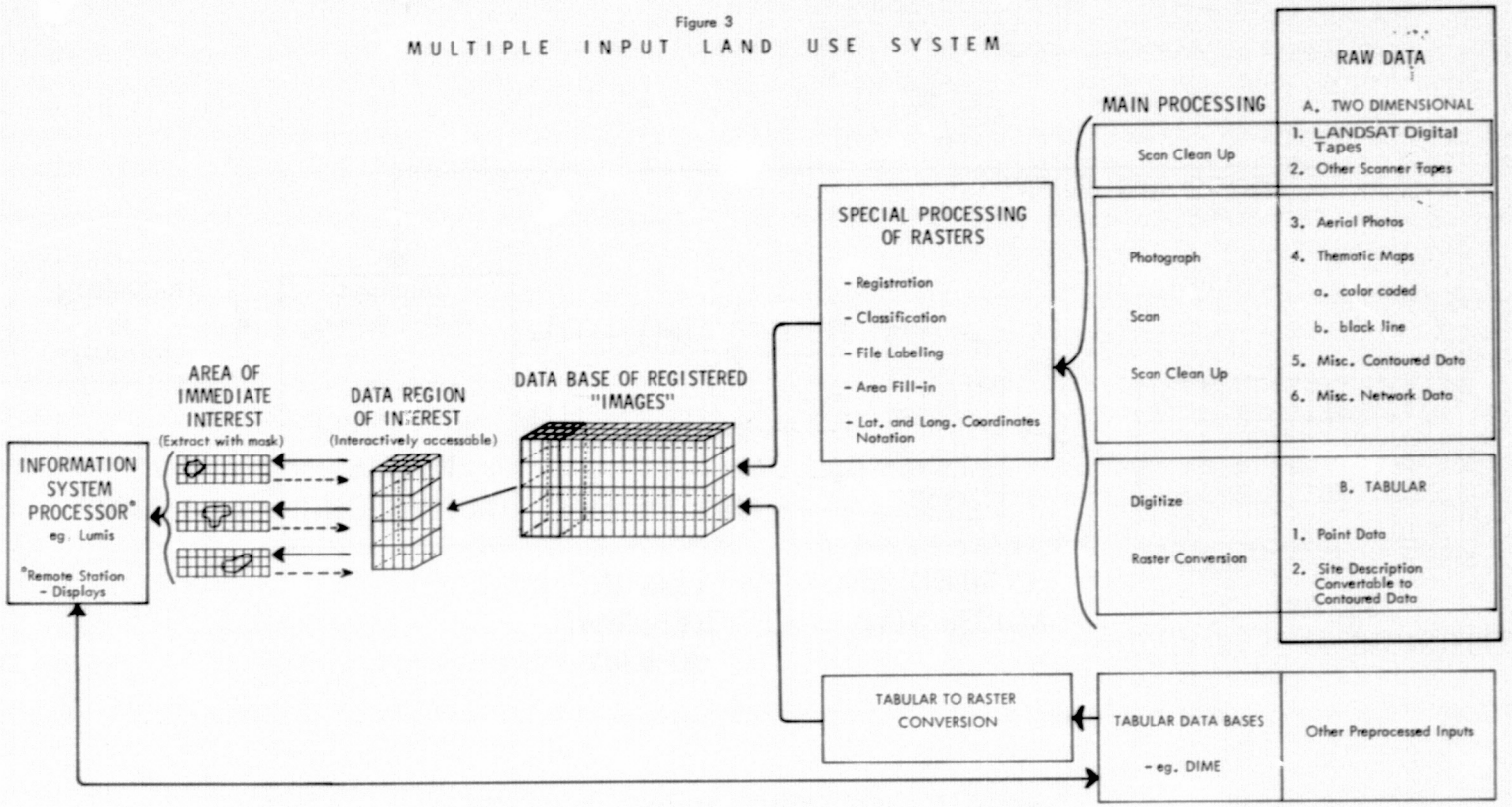


Figure 3

MULTIPLE INPUT LAND USE SYSTEM



- Tabular Data Base Provides Majority of Demographic and Economic Information.
- Two-Dimensional Data Base Provides Majority of Land Use and Environmental Information.
- Two-Dimensional Data Base Provides Various Administrative Boundaries as Binary Overlays.
- Tabular and Two-Dimensional Data are Interfaced and can be Accessed Simultaneously.
- Several User Query Stations May be Used Interactively.

USER SERVICES AVAILABLE FROM USDA'S AERIAL PHOTOGRAPHY FIELD OFFICE

Ronald A. Dickson
Assistant Chief
Western Aerial Photography Laboratory
ASCS - U.S. Department of Agriculture

N76-17545

ABSTRACT

The U. S. Department of Agriculture's Aerial Photography Field Office (APFO), has been in the aerial photography business since the mid-1930's. Consequentially the APFO has compiled a large and unique library of photographic negatives covering virtually all the cultivated area of the nation. This coverage is being continually updated on an average cycle of about seven years, and has generally been flown at a scale of 1:20,000 with an 8 1/4-inch lens. More recently the scale is 1:40,000 using a six-inch lens.

With the launch of LANDSAT-1, APFO was given the additional responsibility of furnishing reproductions of LANDSAT imagery to agencies of the Department of Agriculture. Recently an agreement was reached whereby APFO is furnishing LANDSAT imagery and supporting NASA aircraft imagery to NASA-funded Principal Investigators who are working within the agriculture discipline.

In addition, APFO holds and reproduces Skylab imagery and a variety of aircraft photography (including infrared) from various government agencies.

APFO makes in excess of 650,000 reproductions annually. Two-thirds of this total represents reproductions for users other than ASCS which have been procured through the user services system. This volume represents a majority of the aircraft imagery sold in the nation. The primary reasons for this sales volume are the availability of continually updated photography in the populated areas and the local exposure of this imagery to the general public through the ASCS county office system.

All photography reproduced by APFO is processed through automated systems which are monitored and controlled to meet user requirements. APFO is in the process of acquiring several new pieces of processing and monitoring equipment to update this system.

ASCS is now proceeding with the consolidation of the Eastern Aerial Photography Laboratory in Asheville, North Carolina, with the Western Laboratory in Salt Lake City, Utah. The combined facility will be temporarily housed in the current facility at Salt Lake City. A new facility which will be colocated with the Forest Service's National Geometronics Center is being planned for occupancy in late 1976.

INTRODUCTION

The Agricultural Stabilization and Conservation Service's Aerial Photography program was originated in the mid-1930's under the Agricultural Adjustment Act. The basic responsibility of this program is to furnish photographic enlargements that have been rectified to represent the cropland area at a specific scale to approximately 3,000 ASCS County Offices throughout the continental United States and Hawaii. This photography is then used as a tool in the implementation of various farm programs requiring the determination of acreages. Consequently, the ASCS Aerial Photography Field Office (APFO) has compiled a large and unique library of photographic negatives covering the cultivated eighty percent of the nation. This coverage is being continually updated on an average cycle of seven-year intervals and has generally been flown at a scale of 1:20,000 with an 8 1/4-inch lens. More recently the scale is 1:40,000 using a 6-inch lens.

With the launch of LANDSAT-1, APFO was given the additional responsibility of furnishing reproductions of LANDSAT imagery to agencies of the Department of Agriculture. Recently an agreement was reached whereby APFO is furnishing LANDSAT imagery and supporting NASA aircraft imagery to NASA-funded Principal Investigators who are working within the agricultural discipline.

Products Available

APFO makes in excess of 650,000 reproductions annually. Two-thirds of this total represents reproductions for users other than ASCS which have been procured through the user services system. This volume represents a majority of the aerial photography sold in the nation. The primary reasons for this sales volume are the availability of continually updated photography in the populated areas and the local exposure of this imagery to the general public through the ASCS county office system.

The standard product for ASCS use is an enlargement rectified to the scale of 660' per inch on 24" x 24" paper. Other standard enlargements made from conventional aircraft photography are produced at scales ranging from 2000'/" to 200'/" on 12" x 12", 17" x 17", and 38" x 38" paper. Contact prints and photo indexes are also available.

Reproductions of LANDSAT imagery are available at a variety of scales ranging from 1:3,369,000 (70mm) to 1:250,000 (40" x 40") on black and white or color paper and film.

APFO receives a master file of all LANDSAT imagery from NASA in the form of 70mm negatives and 9 1/2-inch positives. At the present time a Houston Fearless EN46 fixed focus enlarger is being modified and will be equipped with a Tropel Lens System to facilitate the inhouse generation of precision 1:1,000,000 scale, 9 1/2-inch transparencies which are used in the production of color composite negatives and 1:250,000 scale enlargements.

The APFO has accumulated a library of over 1,600 color composite negatives of LANDSAT imagery. Based on workload projections, this library is expected to grow to in excess of 5,000 negatives within the next twelve months. A computer listing of color composite negatives on file is maintained and may be sorted by scene identification number, latitude and longitude, general geographical location, and file number. It is planned that this listing

will be made available to the public in the near future. Most color composites are false color infrared using MSS Bands, 4, 5, and 7. Reproductions from these negatives are available at the standard cost of the color product.

Beginning July 24, 1972, through October 19, 1974, APFO produced LANDSAT indexes of the United States. These are in the form of strip mosaics produced on 20" x 24" paper. There are forty-five indexes, each consisting of approximately 500 scenes. In addition to the LANDSAT indexes, APFO generated indexes for Skylab Missions 2, 3, and 4, depicting coverage of the United States.

Prices for all products produced are established by a Federal pricing committee to cover the actual cost of this service by agencies of the Federal Government.

Ordering Process

Orders for ASCS aircraft photography may be initiated in the locality of the area of interest by contacting the local ASCS Office. Each county office has photo indexes, order forms, and personnel available to assist in ordering photography within that county. In addition to the county offices, a user may contact APFO directly for assistance.

Satellite imagery and NASA aircraft photography must be ordered directly from the Aerial Photography Field Office in Salt Lake City. One may either contact the User Services Section by letter or telephone concerning his needs or do research at the laboratory where a microfilm browse file, catalogs, photographic indexes, and trained personnel are available. Currently LANDSAT data is being retrieved by remote terminal from the Marshall Earth Resources Information Transfer System (MERITS) at Huntsville, Alabama. However, plans are being implemented whereby APFO will establish and maintain its own LANDSAT data retrieval system patterned after the Marshall system.

In addition to ASCS photography and LANDSAT imagery, APFO holds and reproduces Skylab imagery and a variety of aircraft photography, both black and white and infrared, from various government agencies.

Contracting

The Aerial Photography Field Office handles the new aerial photography contracts for ASCS. There are thirty prequalified contractors on the current bidders' list. Normally, ASCS secures approximately 200,000 square miles of new photography each year. Most of this coverage during the last three years has been at a scale of 1:40,000. By October 1976, ASCS will do the new photography contracting for Forest Service and Soil Conservation Service. Where possible, our own agency has entered into cooperative agreements with other Federal, State, and local Governments on a cost-sharing basis.

Quality Assurance

The responsibility of the Quality Assurance Section is to insure that all photographic materials received and released meet established quality and accuracy specifications. A thorough cartographic and photographic inspection is performed on all materials received from contractors of ASCS photography

to insure adherence to photogrammetric and photographic quality requirements. Densitometric measurements are performed using digital, transmission densitometers as an aid in establishing production controls.

All LANDSAT materials received from Goddard Space Flight Center are carefully inspected for resolution, light uniformity, and density specifications to determine compatibility with NASA Data Processing facility requirements under the Memorandum of Understanding established between NASA and ASCS.

Strict quality control procedures are conducted to maintain prescribed controls during printing and processing. All outgoing products are required to meet specifications consistent with user requirements that have been established by NASA. In order to further facilitate adherence to these standards, a computerized program is being installed to evaluate characteristics of all raw photographic materials received and generate data for input to processing controls.

Programs are also being written to produce product shipping reports and funds remaining reports on the Principal Investigator program. GSFC will be furnished these reports on 9-track magnetic tapes as required.

Analytical Aerotriangulation

ASCS has developed a system of extension of control through analytical aerotriangulation designed to provide rectification parameters to correct near vertical aerial photographs to common scales. Because required results are less rigorous than those generally considered acceptable for photogrammetric functions, input in terms of accuracy, time, and expense is greatly reduced. However, results achieved are sufficient for many uses not requiring "mapping standard accuracies."

The system hardware consists of specially designed point transfer stations, 2.5 micron monocomparators with digitizers, and a minicomputer system.

The software consists of a Refinement Program, a Relative Orientation Program, and a Block Adjustment Program capable of handling 500 photographs in 15 strips. The Resection Program determines rectification parameters of each photograph and a ground coordinate value for each point.

The big advantage to the Department of Agriculture lies in the digitization of data. Data is now sorted, printed, and stored automatically. Rectifying projectors are set automatically through paper tape input. Coordinate values are established over a project area at intervals within two miles, thus creating the capability of determining a real coordinate value for any point within a project area.

The automatic data processing system is also used to support a variety of tasks related to record keeping and generation of reports and will be used to maintain the LANDSAT data retrieval system. Hardware is comprised of two Data General Nova 1200 processors with 32 thousand words of internal memory and a 256-thousand word Alpha-Data, fixed-head disc each. Two 12-million word

disc packs and a nine-track magnetic tape drive are accessible to either processor through a multi-communications adaptor. Input/output is also facilitated through high-speed paper tape reader-punches, teletypes, and a Matrix printer. Plans call for the addition of a graphic display terminal.

Photographic Processes

All photography reproduced by APFO is processed through automated systems which are monitored and controlled to meet user requirements.

Automatic dodging, Log-Etronic printers are used extensively in the production of both black and white and color contact prints. One exception to this is in the printing of contact prints from LANDSAT negatives. In this case a Log-E Mark II printer has been modified by removing the cathode ray tube and the photo multiplier tube and equipping it with a point light source which peaks in the ultra violet range at 365 microns to give maximum resolution.

Color composite negatives from LANDSAT imagery are registered using 1:1,000,000 scale positive transparencies and exposing on a Klimsch vacuum printer equipped with a point light source and two filter wheels. One filter wheel has narrow band cut-off filters to control color and the other has neutral density filters to control the exposure of each individual band.

Enlargements from 9" x 9" format film are produced using rectifying projectors. A large volume of this work is handled on automated numerical rectifiers designed and manufactured by H. Dell Foster Company. Rectification parameters are input automatically through punched paper tape generated through the analytical data system. Saltzman rectifying projectors are also used, two of which have been equipped with Pavelle 403 color light sources with subtractive Dicroic filters for making color enlargements. Exposure on all rectifiers is controlled through the use of densitimers.

Enlargements from smaller format negatives are produced on a Durst 138-S enlarger with full-color capabilities using opal lamps and gelatin filters.

Black and white enlargements, photo indexes, and contact prints are processed through Kreonite or Pako processors using a two-tank developer (Startone), one-tank fixer (ammonium thiosulfate), and a two-tank wash. These processors are carefully controlled by using sensometric strips to read speed and gamma. Conversion is currently being made to use one, standard, resin-coated black and white product (EKCo Kodabrome) for all paper prints.

Black and white film products are reproduced on EKCo SO-467 (blue sensitivity) film and processed in 11CM Versamat processors using EKCo 641 chemistry. Direct duplicating film products are processed using the same chemistry and EKCo 2422 film.

Currently all color processing is being accomplished on an 11-tank Autopan-Automat processor which is set up to handle four different systems: (1) Color transparencies from negatives made on EKCo 4109 print film are processed in a modified C-22 developer used with E-4 secondaries; (2) Color composite negatives and (3) color internegatives made from positive transparencies are

made on EKCo 2445 aerocolor negative film using the modified C-22 chemistry and altering the development times; and (4) Color prints from negatives in sizes from 10" x 10" to 40" x 40" are made on RC-37 paper using EKCo plus 3 chemistry. Prints can also be made directly from positive transparencies in the Autopan on EKCo 1993 Ektachrome paper using R-5 chemistry. A second Autopan processor is being installed in which this process or a Cibea-Chrome process will be used. A Pako-Pro 60 processor is also being installed to process color contact prints on RC-37 roll stock using EKCo plus 3 chemistry.

Future Plans

ASCS is now in the process of consolidating the Eastern Aerial Photography Laboratory in Asheville, North Carolina, with the Western Laboratory at Salt Lake City, Utah. The combined facility, known as the ASCS Aerial Photography Field Office, will be temporarily housed in the current building in Salt Lake City. A new facility which will be colocated with the Forest Service's National Geometronics Center in Salt Lake City is being planned for occupancy in late 1976. Eventually all photographic processing for the Forest Service and the Soil Conservation Service, as well as ASCS, will be handled through this office.

Careful consideration is being given to planning and the procurement of equipment to facilitate the production of products that are consistent with the requirements of remote sensing.

THE TEXAS REMOTE SENSING TRAINING PROJECT

By John B. Wells, Office of Information Services,
Office of the Governor, Austin, Texas

N76-17546

ABSTRACT

During the late spring of 1973, the Office of the Governor and the Remote Sensing Task Force were informed of the possibility of participating in the Purdue Terminal Project. The Remote Sensing Task Force requested the Governor's Office of Information Services to respond to the request for participation and to seek funding for the project. The Office of Information Services prepared the Response To Request Plan For Participation In Purdue Terminal Project and submitted it to the LARS Committee. The project was approved by the LARS Committee in late 1974. Funding requirements were met by the Office of Information Services, the U.S. Department of Housing and Urban Development (HUD), and the U.S. Civil Service Commission (CSC).

The Texas Remote Sensing Project was designed to train federal, state and regional agency managers, scientists and engineers. It was recognized that few of the potential students would have backgrounds in remote sensing or computer technology. A one-week seminar was designed and implemented to alleviate this situation. The objectives of the seminar were to build vocabulary, introduce technical subject areas and give students enough training to allow them to relate remote sensing technology to operational agency projects. The seminar was designed to perform the dual function of conveying enough remote sensing information to be of value as a stand-alone and preparing students for detailed pattern recognition training.

The LARSYS III portion of the training project was executed exactly as designed in the LARSYS training materials package. However, the LARSYS package did not contain a LANDSAT training module. Two LANDSAT training modules were developed using Texas LANDSAT data. One module contained central Texas data and the second module contained coastal zone data.

There were five overall objectives of the project. They were:

1. To orient the appropriate personnel in state agencies, COG's and local governments to the advantages and limitations of remote sensing and computer technology.

2. To train the appropriate personnel in the proper utilization of remote sensing and computer technology.

3. To gain experience in the identification of requirements and the application and evaluation of the utilization of remote sensing and computer technology to satisfy information requirements.

4. To promote multi-entity, multi-level cooperation in pilot projects which identify information requirements, apply remote sensing and computer technology, and evaluate the results.

5. To develop the organizational capabilities and mechanisms necessary to most effectively utilize remote sensing and computer technology.

The significant accomplishments of the project were as follows:

1. The Remote Sensing Training Project was funded, staffed and conducted.

2. Over sixty agency managers, scientists and engineers were given training in the current field of remote sensing.

3. Over thirty individuals were trained in the details of computer aided remote sensing data analysis.

4. The LARSYS III computer programs have proven to be of value and are to be moved to Texas A & M University for access by government agencies.

5. Operational program applications of remotely sensed data have been determined by agency students.

6. The Texas Parks and Wildlife Department has approved and funded a project to map state wildlife habitat using LANDSAT-1 data and LARSYS III analysis.

7. The agencies of the state have established organization and communications procedures to accept, evaluate and use remote sensing technology.

Current remote sensing technology and the LARSYS III digital analysis techniques have proven to be of value to state agencies charged with the responsibility of managing and regulating the use of natural resources. The accomplishments stated above are only a beginning in the process of bringing the tools of this technology into widespread use.

The primary difficulties encountered in the execution of the Remote Sensing Training Project were not related to the technology. They were:

1. Funding

2. Organizational communications

The Remote Sensing Training Project has been a valuable experience for the participants. It has assisted in the introduction of remote sensing technology to state government. Operational applications have been determined which will continue after the termination of the training effort.

INTRODUCTION

During the late spring of 1973, the Office of the Governor and the Remote Sensing Task Force was informed of the possibility of participating in the Purdue Terminal Project. The Remote Sensing Task Force requested the Governor's Office of Information Services to respond to the request for participation and to seek funding for the project.

The Office of Information Services prepared the Response to Request Plan For Participation In Purdue Terminal Project and submitted it to the LARS Committee. This document contains the project background, project involvement, participants and goals.

The project was approved by the LARS Committee in late 1974. The funding requirements were met by the Office of Information Services, the U.S. Department of Housing and Urban Development (HUD), and the U.S. Civil Service Commission (CSC). The HUD funds were from the 701 planning appropriations and the CSC funds were under the intergovernmental Personnel Act of 1970. The Office of Information Services funds were appropriated by the Texas Legislature for the operation of the office. Coordination of these three funding sources to fund a single project became a problem and resulted in a late start date. The project was scheduled to begin on January 1, 1974, but delays were encountered. Instructor training began in March 1974 and student training started in April.

PROJECT OVERVIEW

The Texas Remote Sensing Project was designed to train federal, state and regional agency managers, scientists and engineers. It was recognized that few of the potential students would have backgrounds in remote sensing or computer technology. A one week seminar was designed and implemented to alleviate this situation. The seminar was intensive and covered the following subject areas:

1. Project background
2. Geographic base systems
3. The Electromagnetic Spectrum
4. Remote sensing overview
5. Sensors
6. Data handling and processing
7. Photo interpretation
8. Image interpretation
9. Pattern recognition
10. Mathematical tools
11. Introduction to LARSYS III
12. Photo interpretation field trip

The objectives of the seminar were to build vocabulary, introduce technical subject areas and give students enough training to allow them to relate remote sensing technology to operational agency projects. The seminar was designed to perform the dual function of conveying enough remote sensing information to be of

value as a stand-alone and preparing students for detailed pattern recognition training via LARSYS III. This approach was successful and it is felt that the seminar was an essential part of the training project.

The LARSYS III portion of the training project was executed exactly as designed in the LARSYS training materials package. However, the LARSYS package did not contain a LANDSAT training module. Two LANDSAT training modules were developed using Texas LANDSAT data. One module contained central Texas data and the second module contained coastal zone data.

The seminar starting dates were:

1. April 1, 1974
2. May 6, 1974
3. June 10, 1974
4. July 15, 1974
5. August 19, 1974
6. November 4, 1974

The November 4, 1974 seminar was an abbreviated series designed especially for students which are to be working on operational remote sensing projects in the future.

Students have come from federal, state and regional government. The agencies are as follows:

1. NASA
2. U.S. Department of Agriculture (S.C.S.)
3. U.S. Department of the Interior (U.S.G.S.)
4. Water Quality Board
5. Water Rights Commission
6. Water Development Board
7. Parks & Wildlife
8. Historical Commission
9. Department of Agriculture
10. University of Texas
11. Stephen F. Austin University
12. Capitol Area Planning Council

13. Highway Department

14. Office of Information Services

15. General Land Office

16. Texas Forest Service

17. University of Texas at San Antonio

18. U.S. Fish and Wildlife Service

19. Governor's Division of Planning Coordination

20. Texas A & M University

There were five overall objectives of the project. The overall objectives are restated here and a statement of the measure of attainment is included under each.

1. To orient the appropriate personnel in state agencies, COG's and local governments to the advantages and limitations of remote sensing and computer technology.

   Results--Twenty agencies were represented in the training activities. However, no local governments were able to attend, though there were several inquiries from local governments. The participation of federal agencies was surprising and not anticipated. This may indicate that there is a large demand in federal agencies for remote sensing training that has not been recognized.

2. To train the appropriate personnel in the proper utilization of remote sensing and computer technology.

   Results--In the majority of cases, the proper agency personnel did attend the training program.

3. To gain experience in the identification of requirements and the application and evaluation of the utilization of remote sensing and computer technology to satisfy information requirements.

   Results--Considerable experience was gained in the identification of remote sensing requirements for operational programs. The utility of LANDSAT data was determined to be of major value for its ability to give synoptic, current information over wide areas.

4. To promote multi-entity, multi-level cooperation in pilot projects which identify information requirements, apply remote sensing and computer technology and evaluate the results.

   Results--There is no doubt that a basis for multi-entity, multi-level cooperation in pilot and operational projects has been established. Progress has been made in the establishment and funding of projects which will require extensive cooperation.

5. To develop the organizational capabilities and mechanisms necessary to most effectively utilize remote sensing and computer technology.

   Result--The framework to develop organizational capabilities and mechanisms has been established through the Governor's Office, the Remote Sensing Task Force and the Remote Sensing Training Project. This framework must now be exercised to strengthen the established mechanisms.

Specific objectives were developed for the project. These objectives are restated here and the comment associated with each indicates whether or not it is felt that the objective was accomplished or if comment is required. The specific objectives were as follows:

1. Develop and conduct a training program for state personnel in remote sensing technology.

   Accomplished

2. Define the general information requirements of user agencies in planning and managing natural resources.

   Accomplished

3. Define the specific information requirements of user agencies to be satisfied by digital remote sensing techniques.

   Accomplished

4. Provide the means to evaluate and refine the utility and applicability of aircraft and satellite generated digital remote sensing products for state level uses.

   Comment--This objective was designed to open channels of communication between operational users and researchers. The groundwork accomplishing this objective is now being laid with the identification and funding of operational projects.

5. Provide technical design information to and support establishment of the NRIS for the State of Texas.

   Comment--This objective proved to be too broad and was not accomplished within the short time frame of the Remote Sensing Training Project.

6. Investigate the utility of a land use inventory and information system based on digital remote sensing methods.

   Comment--It was proven that digital remote sensing data can provide land use information if the user can adequately define his needs. It was found that more difficulty is encountered in defining "land use inventory" than utilizing digital data to produce an inventory once a definition is achieved.

7. Utilize digital remote sensing techniques to satisfy specific information requirements generated by existing programs of user agencies in a more economical, timely, accurate or comprehensive manner.

   Accomplished--The Texas Parks and Wildlife Department has authorized a project to map the wildlife habitat of Texas using LANDSAT data.

8. Select pilot demonstration areas of the state on the basis of priority identified by the user agencies.

   Accomplished--By far, the major interest has been in the coastal zone. The second major interest has been in the entire state.

9. Develop a resource inventory data base which would serve as a source of information required for the implementation of present and future state and national programs such as the Coastal Zone Management Act, National Land Use Act, National Dam Safety Act and various earth resources and land information programs of the Department of Interior.

   Comment--The framework to develop a resource data base has been accomplished. The task is a monumental one that will require much time and effort to accomplish.

10. Develop and test automated analysis of remote sensing information in pilot demonstration areas.

    Accomplished

11. Promote increased cooperation among the various state and federal entities by involvement in a cooperative, integrated and comprehensive state remote sensing program.

    Accomplished

12. Establish and exercise an official point of interface within the Office of the Governor for state/federal cooperative programs in remote sensing, data collection, data storage and retrieval.

    Accomplished

13. Develop those mechanisms necessary for a cooperative effort between the State of Texas, Purdue University, and NASA in which available technology necessary for the utilization of remote sensing products can be transferred to the State and utilized to aid in solution of state problems.

    Accomplished--The LARSYS III system will be moved to Texas A & M University for use by federal, state and regional government.

All of the specific objectives were accomplished in a major measure with the exception of objective five (5).

SIGNIFICANT ACCOMPLISHMENTS

Most of the original objectives of the Remote Sensing Training Project have been met. The significant accomplishments of the project are as follows:

1. The Remote Sensing Training Project was funded, staffed and conducted.

2. Over sixty agency managers, scientists and engineers were given training in the current field of remote sensing.

3. Over thirty individuals were trained in the details of computer aided remote sensing data analysis.

4. The LARSYS III computer programs have proven to be of value and are to be moved to Texas A & M University for access by government agencies.

5. Operational program applications of remotely sensed data have been determined by agency students. These operational program applications are:

   a. Coastal zone mapping

   b. Wildlife habitat mapping

   c. Land use mapping

   d. Urban expansion mapping

   e. Soil type classification mapping

   f. Area surface water inventory

6. The Texas Parks and Wildlife Department has approved and funded a project to map state wildlife habitats using LANDSAT-1 data and LARSYS III analysis.

7. The agencies of the state have established organization and communications procedures to accept, evaluate and use remote sensing technology.

Current remote sensing technology and the LARSYS III digital analysis techniques have proven to be of value to state agencies charged with the responsibility of managing and regulating the use of natural resources. The accomplishments stated above are only a beginning in the process of bringing the tools of this technology into wide spread use.

CONCLUSIONS

The primary difficulties encountered in the execution of the Remote Sensing Training Project have not been related to the technology. Technical presentation of material, use of the LARSYS III programs and all hardware functions have operated with relative ease. This would tend to prove that the technology can be assembled and transferred.

There have been two primary problems associated with the project, they are:

1. Funding and

2. Organizational communications

Funding arrangements for installation and continuation of the project have been most difficult. This is due to the budgeting process of the State of Texas and the fact that federal agencies are reluctant to provide funds for these activities. NASA has not developed the mechanisms to fund such technology transfer activities to a state.

Organizational communications involving entities with different responsibilities, authorities and objectives are difficult unless common interests can be identified. The Texas natural resources agencies have recognized this and have formed a Task Force on Remote Sensing. The Task Force serves to improve communications and to unify objectives. The Governor's Office has been designated the proper office to coordinate state agency communications and to serve as a single point contact for federal agencies. These organization efforts were occurring during the time that the Remote Sensing Training Project was in progress. Internal state communications should improve measurably in the future.

The federal agencies, NASA, Department of Agriculture, and the Department of the Interior, have not organized to communicate rapidly and effectively. The federal agencies have not recognized the need for an extensive educational effort required to precede the transfer of complex technology to state, regional and local government. The problems of funding and communication can be solved by the development of a plan to accomplish stated goals and objectives.

The Remote Sensing Training Project has been a valuable experience for the participants. It has assisted in the introduction of remote sensing technology to state government. Operational applications have been determined which will continue after the termination of the training effort.

RECOMMENDATIONS

Recommendations are made in three areas:

1. Organization

2. State participation

3. The LARSYS training package

These recommendations are made to meet specific needs and were developed as a result of executing the training project.

Organization

It is recognized that it has been difficult for the state, NASA and Purdue University to work together in the execution of the Remote Sensing Training Project.

Much valuable experience has been gained by these three parties and this experience should be utilized to improve future technology transfer efforts. There appears to be a set of requirements that could be developed to increase the probability of success of technology transfer programs such as the Remote Sensing Training Project.

NASA should develop a statement of the definition of technology transfer. This should be a statement of policy to be used in judging the scope of technology transfer projects and should be as definitive as possible.

Each participating entity should formulate a specific set of objectives for each technology transfer project. These objectives should be stated and should reflect the interest of each entity. The objective statements should be examined to resolve conflicts. The collective objectives then become the objectives for the project.

The criteria to be used for measuring the success of a project should be defined before the project is begun. All participants should agree upon the project measurement criteria and data should be systematically gathered during the entire project period. If the project plan of execution changes, appropriate changes should be made to the project measurement criteria and data collection should be modified.

Current technology is complex and is not easily understood by technically trained individuals from the operational environment of state agencies. It is essential that instructors be technically competent and possess the ability to teach others. Instructors must be interested in the success of the project and must individualize the instruction process with each student. Education of the potential user is an essential part of the technology transfer process and it requires proper consideration and emphasis.

A detailed plan should be formulated by all of the participants involved in executing a project. The plan should detail the responsibilities of each participant and specify the proper communication procedures to be used. Specific individuals should be designated to perform project tasks. Specific individuals should be designated from each participating entity to perform the project management and reporting function.

All project funding requirements should be resolved before a project goes into execution. A technology transfer plan will usually require funding from at least two sources and possibly more. It is important that the funding time phase requirements of each participant be specified and that the project cash flow is consistent with the project requirements.

The project should be monitored continuously to determine if improvements could be made during execution. A project change procedure should be formulated and approved project changes should be implemented.

State Participation

The two basic approaches to transferring technology from the federal government to state governments are:

1. Through individual state agencies

2. Through an executive or agency coordination function

Both of these approaches can be efficient methods of technology transfer and a combination of both can be utilized. The method chosen will depend upon the specific objectives formulated for each individual project.

It is the responsibility of a state to organize to receive, disseminate and perpetuate the new technologies which will improve state government. Each state is structured in a different manner and it cannot be assumed that the Governor or Executive Office has the authority to organize a state in such a manner. Organizational authority may be in the Executive, Legislative or Judicial branches of state government or in any combination of the three. However, state governments should be given the incentive to organize. This can be accomplished by providing internal and external influences.

The purpose of state government organization is to provide a single point contact for federal agencies, academic institutions and private industry. The single point contact should coordinate internal and external communications. Project funding requirements should also be coordinated by the state single point contact. It is desirable for state government to form an association of agency directors. This improves agency communications and provides a mechanism for the development of cooperative projects.

The LARSYS Training Package

The LARSYS training package was found to be a very workable set of instructional tools and results were good. It has been determined that a seminar presentation is required prior to introducing students to the detailed training provided by LARSYS. Any orientation program or seminar should at least contain information to build vocabulary in remote sensing, introduce the mathematics of digital data analysis and familiarize students with current computer technology.

The LARSYS training package can and should be improved. Considerable condensation of material can be accomplished by combining "mini courses," decreasing dependence on written material and utilizing LANDSAT data rather than aircraft data for student problems.

The terminal demonstration and hands-on terminal "mini courses" can be combined into one computer terminal session. The LARSYS Exercise "mini course" can and should be condensed considerably. "The Guide to Multispectral Data Analysis Using LARSYS," should be revised to utilize LANDSAT data. The supervised and unsupervised approaches to data analysis should be taught concurrently.

The entire LARSYS training relies too heavily upon written materials and instructions. The written material tends to be inconsistent and to utilize terminology which may be unfamiliar to the reader. There is no glossary of terms included with the written material. The objectives of the written material could possibly be better achieved through audio-visual presentation.

There is no doubt that the LARSYS training package is a success. It is a first step in the vital process of user education which must be accomplished to achieve technology transfer. The training package should be continually refined and further developed.

ACKNOWLEDGMENTS

This report is a review of the activities of the Remote Sensing Training Project conducted by the Governor's Office of Information Services for the State agencies of the Texas Interagency Council on Natural Resources and the Environment.

The Remote Sensing Training Project has been a result of the collective effort and funding by the State of Texas, the National Aeronautics and Space Administration, the U.S. Department of Housing and Urban Development, the U.S. Civil Service Commission, Purdue University and individuals from the University of Texas. Mr. John B. Wells, Governor's Office of Information Services, was responsible for the direction of the project and served as an instructor. Mr. J.C. Humphrey, Governor's Office of Information Services, served as an instructor. Mr. John Cornwell, Lockheed Electronics, assisted with project planning and execution. Mr. Leo Childs and Mr. Gerald McKain, NASA, Johnson Space Center, served as NASA coordinators. Dr. Robert Holz, Dr. Jan Cannon and Dr. Ed Powers from the University of Texas served ably as lecturers. Dr. Philip Swain, Mr. Terry Phillips, Mr. Carl Walker and Ms. Susan Schwingendorf served as Purdue University coordinators.

INTERACTIVE DIGITAL IMAGE MANIPULATION SYSTEM

By Janice Henze, ESL Incorporated, 495 Java Drive, Sunnyvale, California and
Dr. Robert DeZur, ESL Incorporated, 495 Java Drive, Sunnyvale, California

N76-17547

ABSTRACT

The Interactive Digital Image Manipulation System (IDIMS) developed by ESL Incorporated is a currently available system designed for manipulation, analysis, interpretation and processing of a wide variety of image data. LANDSAT (ERTS) and other data in digital form can be input directly into the system. Photographic prints and transparencies are first converted to digital form with an on-line high-resolution microdensitometer. The system is implemented on a Hewlett-Packard 3000 Computer with 128 K bytes of core memory and a 47.5 megabyte disk. It currently includes a true color display monitor, with processing memories, graphics overlays, and a movable cursor.

Image data formats are flexible so that there is no restriction to a given set of remote sensors. Conversion between data types is available to provide a basis for comparison of the various data. Multispectral data is fully supported, and there is no restriction on the number of dimensions. In this way multispectral data collected at more than one point in time may simply be treated as a data collected with twice (three times, etc.) the number of sensors. There are various libraries of functions available to the user:

1. Processing Functions
   copying, expanding, reducing, rotating images
   arithmetic manipulations of images
   intensity transformations of image values
   statistical information concerning images
   Fourier operations
   Fourier filters
   image generating functions
   manipulations of complex-valued images

2. Display Functions
   utilities such as selecting images, viewing split-screen images, etc.
   functional mappings
   pseudo color mappings
   timing-dependent functions such as flickering between images, zoning through images, etc.
   graphics overlay and mensuration functions

3. System Functions
   tape input, output, and reformatting
   cancel, pause, or continue processing a function
   receiving help or documentation for functions

4. Earth Resources Applications Functions
   classification and clustering algorithms
   training set manipulation
   mensuration
   multistage analysis
   geometric manipulation
   dimensionality reduction
   radiometric correction

statistical information
density slicing
utility functions

The system architecture is such that IDIMS may be used in a number of modes. It may be used as a stand-alone system for processing and evaluation of image data. In this context, multiple users may utilize the system in both interactive and batch modes. In instances where rapid bulk throughput is required, an array processor interfaced with the central processor would enable the system to meet the heavy loads. An alternate scheme is to use IDIMS as a preprocessing and post-processing system for a larger computer facility. In conclusion, IDIMS provides a flexible framework for technique development as well as a facility for processing and evaluation of image data.

INTRODUCTION

The Interactive Digital Image Manipulation System (IDIMS) is intended to be an analysis and technique development tool for a non-programming user. The overall architecture of IDIMS is designed to facilitate expansion and modification with respect to both hardware and software. Wherever possible, flexibility and generality have been incorporated in order to provide a realistic environment for image processing, since neither processing techniques nor the state of the art of remote sensing are likely to remain static. The burden of bookkeeping and efficient image input and output is assumed by the system, so that the user and the program developer are free to concentrate their efforts on the actual problems at hand.

The heart of the IDIM System is a 175 nanosecond cycle time minicomputer,[1] with a multi-programming operating system. See Figure 1 for a photograph of the System. Multiple users may interact by means of terminals, and batch jobs may be submitted to run in the background. The computer is supported by 128K bytes of core memory and a 47.5M byte moving head disk. Digital images are input to the system by means of magnetic tape. Results of processing may be viewed and photographed from a high resolution color display,[2] or they may (where applicable) be printed on the user's terminal or on a line printer. Final results may be transferred back to magnetic tape. IDIMS is capable of interfacing to a precision microdensitometer,[3] which can be used to scan and record images. As can be seen from Figure 2, it forms a truly comprehensive image processing system.

GENERAL SYSTEM FEATURES

The command language of IDIMS is simple, easy to learn, and it contains many sophisticated features for the more advanced user. There are four types of statements which are accepted:

1. System control commands
2. Processing function commands
3. Display control commands
4. Parameter declarations

In addition, the user may declare and name frequently used parameters. Parameters omitted or incorrectly entered will cause a prompt for a correct value. Upon demand, the system will display the results of each processing command. The user may modify the resultant displayed image using the display control statements available.

The images with which a user works are named by him and kept track of in his catalog. An image name may be up to 35 characters in length. An image may be deleted only by the user who named it, or by the IDIM system manager. A processing history of each catalogued image is maintained and available upon request.

All IDIM functions are referred to by names (or abbreviations) which may be up to 8 characters in length. There is no restriction except name uniqueness on the number of functions which may be implemented on the system. The advanced user may find it convenient to combine a frequently used sequence of processing functions into a single function. IDIMS has an advanced macro capability for this purpose. A macro, once defined, is used in a manner identical to any other processing function.

During each session, a complete history of all commands, replies, prompts, and messages is maintained and available. It may be accessed during a session, and unless suppressed, it will be listed at the termination of a session.

The use of disk space by individual users and by the total system is controlled by parameters set by the system manager. Through this facility the manager can efficiently use whatever peripheral storage is available for use by the IDIM system and its users. During a session, a user may work with as many images as will fit on the disk. Upon termination, however, most, if not all, of the images will be automatically stored to tape in order to leave working space for the next user. The image catalog is updated to reflect the fact that the images have been moved from the disk to the tape library.

When being used in session mode, the IDIMS Command Translator is always in one of four states:

1. Interpreting a previous user statement - the user cannot enter any statements when the system is in this state. Normally this state lasts only a short time, perhaps 1/2 to 3 seconds.

2. Executing a system function - the user cannot enter any statements when the system is in this state. Most system functions, however, can be terminated by typing CONTROL-Y[4].

3. Executing a processing function - the user can enter any non-command statement, i.e., display control statement, parameter declaration statement. Also, some system function commands may be entered. This implies that a user need not sit idle during processing of his data.

4. Idle State. When the system is idle, any IDIMS statement may be entered. When the system is in this state, there will be a line-number prompt on the user's terminal.

Batch use of IDIMS is identical to interactive use with the exception that no interaction is available. An error in a command will cancel only the command involved and those subsequent commands which depended on the command in error for their function.

HARDWARE ARCHITECTURE

The hardware is structured around a central data bus, as shown in Figure 3. A minimal system configuration consists of a processor, 128K bytes of core memory, 1 moving head disk, 1 tape drive, 1 user terminal (serving also as an operator's console), and probably either a display or a line printer. A typical configuration consists of a processor, 128K bytes of core memory, 1 moving head disk, 2 or 3 tape drives, 3 or 4 user terminals (one of which would serve as an operator's console), a display, and a line printer. A small high speed swapping disk for holding operating system routines would be a good candidate for most installations also, because of the resulting improvement of the system when heavily loaded.

IDIMS may be tailored to meet specific needs. It is designed around a "two machine concept," in which the minicomputer acts as the command translator and general monitor, and a larger more powerful computer would perform the actual image processing. A variation of this would be to use a special purpose array processor to execute the processing functions. In installations where it is desirable to digitize and record data directly, a microdensitometer (scanner and recorder) may be included in the configuration. The IDIM system software is coded in a system programming language specific to the minicomputer, but all the processing functions are coded in FORTRAN, to facilitate implementation on other machines. The primary objective is to provide flexible low cost analysis of image and remote sensor data, with the capability of expansion to process large quantities of data.

SOFTWARE DESIGN

The software design of IDIMS is modular, and follows a hierarchical pattern. There is an overall monitor, or command translator, which initiates, controls, and receives information from various son processes. The sons include a process which constantly looks for input from user terminals, a process which handles all display functions, and various processes to carry out the image manipulations requested by each user. The programs to carry out all the different image manipulations reside in a library. When a function is requested, the appropriate program is obtained from the library; this program is then assigned the necessary system resources, and the function is allowed to execute. Upon completion, the resources are relinquished. The library structure facilitates addition of new processing functions, and cuts down on the resources which must be expended on all currently inactive functions. A schematic view of the system structure is shown in Figure 4.

In order to provide a framework for both image analysis and convenient development of new analysis methods, there are a number of additional software features. Providing a simple interface between the user and the image data is done by offering a comprehensive file management system which is transparent to the user. Each user is given a catalog, and assigned a number of library tapes. The first time an image is entered into IDIMS, full information such as its size, data type, and spectral organization (if any) must be furnished. The user must also supply a name for the image. All of this information is placed in the catalog, and further references to the image (by name) simply generate appropriate references to the catalog. At the end of a session, images which the user wishes to retain for further work remain on-line or are stored on one or more of the library tapes, and the catalog is updated to reflect this. Images no longer needed are simply deleted. During any subsequent sessions, the images are referred to merely by name, and are automatically brought back onto the disk, if necessary.

In addition to keeping track of the image itself, the file management system also maintains any image-related files generated during the course of processing the image. History files are automatically kept for each image which contain a history of all processing including function names, parameter values supplied to each function, time and dates of processing, and the name of the user who performed the processing. This enables an image to be regenerated, if necessary, and also provides a reference so that a particular sequence of processing may easily be repeated for another similar image.

A very important type of file is a statistics file, which is created and updated by certain statistical functions. For example, the first time a histogram is calculated for an image, the resultant histogram is placed in a statistics file. If a histogram is again requested, the histogram residing in the file is checked to see whether it contains enough information to generate the new one. (i.e., the number of histogram levels in the new request must be less than or equal to the number of gray levels in the old one.) If so, the histogram is compiled using the information in the statistics file, rather than recomputed from the original image data. An example of data stored in another type of statistics file are the results of image clustering. Means for each cluster and covariance

matrices (by bands) for each cluster are entered in the file. These statistics may then be used as input to other functions, such as classification and evaluation routines. A third type of image-related file is used to contain information pertaining to the graphics and mensuration commands which are executed on the display. If a user generates any graphics or annotation on an image, all appropriate defining elements are stored, and the mensuration file is kept permanently upon demand.

There are additional uses for such files. As can probably be imagined, they could hold data relating to how and when the image data was collected, correction factors that might need to be applied (geometric, radiometric), or any other similar type of information. The usefulness of this file management at first seems small, until the full magnitude of keeping track of all the collateral information is considered. Even if the statistics of an image were known, it would be an extremely tedious task of negligible worth to enter them by hand in order to save their recomputation.

The program developer is provided with a number of programming aids in the form of input and output interface routines. These include routines to print error messages, prompt the user for missing or incorrect parameter values, perform well-formatted image input and output, and check for errors in image I/O operations.

The image input and output routines work with line and sample numbers, band numbers, and other information directly pertinent to images. They translate I/O requests into the standard format in terms of record sizes, block factors, and record addresses, and then they initiate the requests by means of operating system routines. This keeps the burden of the I/O off of the program developer and provides uniformity throughout the repertoire of processing functions. The error checking routines are provided to assure that I/O operations have executed successfully. For example, parity errors, unexpected end of files, incompatible image sizes and other errors are recognized. These are partially for the user's benefit, but they are intended primarily to aid the program developer. For the benefit of the user, there is error recognition done by the command translator to ascertain the validity of image and function names.

The parameter prompter is used by all processing functions to request values for necessary parameters, if they have not already been supplied. All the programmer has to do is specify the names and expected formats of the parameters (such as integer, character string, or floating point), and the users will be prompted accordingly and asked to supply the values. For example, if a user is entering an image into his catalog for the first time, and does not supply the size of the image, he would be asked for integer values representing the number of lines and the number of samples in the image.

To conclude the section on software a discussion of the flow of control is in order. See Figure 5 for a schematic representation of this. There is a monitor which constantly looks for input from a user's terminal. When an input is received, it is given to the overall monitor, or command translator, to determine what has been requested. If it is a display request, it is then given to the display controller to process accordingly. If it is a function request, it is given to the user task monitor, which then initiates execution of the appropriate function. In the case that it is an answer to a prompt for parameters, it is returned to the display or function that requested it. Both the display controller and the processing function access the images and image-related files through the I/O routines provided by the system. The display controller also maintains its own specialized files on both the display refresh disk and the system disk. At completion of a function, the necessary files are updated by the monitor/command translator, and the next command is awaited.

The four statement types mentioned above (system commands, processing commands, display control commands, and parameter declarations) are distinguished from one another largely on the basis of special characters. There are three characters used by the various statements:

1. colon :
2. greater than)
3. plus +

A statement containing a greater than character (>) is considered either a system or processing command. System commands are merely a predefined subset of all the commands. A statement containing a colon (:) is considered a parameter declaration statement. A statement containing neither is considered a display control statement. No legal statement may contain both a colon and a greater than character. Statements are continued from line to line by using a plus (+) as the last character before the carriage return in all lines but the last. (In batch use, the plus character must be the last non-blank character in the input card image.)

Processing Commands

The format of processing commands is in general:

Input specification>Function specification>Output specification

System functions are distinguished from other processing functions in that they require no outputs. Both processing and system functions will be more fully described in ensuing sections of this paper. Multiple input images, functions, and output images may be specified in each of their respective fields. Two examples follow:

1. IMAGE1 IMAGE2 IMAGE3>ADD>OUTPUT.IMAGE
2. INPUT.IMAGE>MAP REGISTER>OUTPUT.IMAGE

In the first example, the function ADD requires multiple inputs. In the second example, INPUT.IMAGE will first undergo an intensity transformation, and will then be registered geometrically to produce OUTPUT.IMAGE. Functions with multiple inputs or outputs must appear as the first or last function, respectively, since each function works on the output of the function preceding it.

The input specification is fairly general in that both spatial subsections and spectral band modifiers may be specified along with the image name:

IMAGE.NAME(SL SS NL NS) [SB1 SB2 ... SBn],
where SL = starting line of the subsection,
SS = starting sample of the subsection,
NL = number of lines in the subsection,
NS = number of samples in the subsection,
SB1 = spectral band list1,
SB2 = spectral band list2,
...
and SBn = spectral band listn.

For example, if a user wished to process only the last 10 lines and samples of bands 3 through 5 and band 1 of a 512 by 512 seven band image, the correct specification would be:

IMAGE.NAME (503 503 10 10) [3-5 1]

Lines 503 through 512 and samples 503 through 512 are defined by the spatial subsection field. Bands 3 through 5, and band 1 are defined by the spectral band modifier.

Users may also access one another's images (but not delete them!) by prefacing the name of the image with the user's name, and including the entire name in quotes. That is, 'JAN.MONTEREY.BAY' refers to the image named MONTEREY.BAY which exists in the catalog of user JAN. The user is not required to specify his own identification when referring to his own images.

Display Command

When operating in an interactive mode, any user with access to an on-line display may view the results of his processing. This may be done automatically (if the user is in the automatic display mode), or it may be done by explicit command (if the user is in the manual display mode). To display an image in the manual mode, the user specifies the image name followed by a greater than character: IMAGE.NAME〉. The display mode may be set using a system command. The default mode is set by the IDIMS manager.

Once the image is on the screen, it may be processed in many ways by issuing display control commands. The commands address features of the display such as the overlays, the function processing memories, the pseudo color processing memories, the cursor, and of course, the images. The commands are enumerated in a later section.

Parameter Declarations

Where required, parameters are input to each function in an IDIMS command. The parameters may be input in the command statement as local parameters, they may be specified as a named parameter list and referred to by name in the command statement, or the user may be prompted for them during execution. Parameter lists are defined as follows:

List-name: Param1 = Value-list1 Param2 = Value-list2 ... Paramn = Value-listn

(Plus signs may be used to continue a parameter list declaration to a number of lines in succession, just as they may be used to continue command lines.)The "list-name" is a unique alphanumeric string (starting with a letter) that contains 8 or fewer characters. It identifies the parameter list declaration. "Paramk" is an alphanumeric string which corresponds to a parameter name necessary for some function. "Value-listk" is a value or list of values of a compatible data type with the named parameter, Paramk. When the parameter list is referred to by name as an argument of some function, it is as if the user typed in all of the parameter names and their associated values, just as they appear in the declaration. A parameter list is specified as an argument of a function by enclosing its name in parentheses immediately following the function name:

```
MAPPING: FROM = 0 100 255 TO = 0 200 255
...
INPUT〉MAP (MAPPING) 〉OUTPUT
```

In this example, the lists of "from" and "to" values represent intensity transformations to be performed on an image. When more than one parameter list name is specified, the parameters are treated as one set by the function. If a parameter is specified more than once, the last value specified will be used.

Parameters may be input directly (locally) to each function according to the format:

FUNCTION (Param1 = Value-list1 ... Paramn = Value-listn)

The example in the preceding paragraph would then correspond to:

INPUT⟩ MAP (FROM = 0 100 255 TO = 0 200 255) ⟩OUTPUT

When local parameters are used, their values cannot be referenced by another function. Named and local parameters may be used together, and, as mentioned above, the last occurrence of a parameter will supersede any previous occurrences.

The user will be prompted for parameters during execution of a command whenever he fails to supply the required parameters or a parameter is in error. They will be requested by name. When the user inputs the requested parameters, processing will continue.

PROCESSING FUNCTIONS

In general, there are 12 categories of functions on the IDIM System.

1. System Functions
2. Utility Functions
3. Intensity Transformation Functions
4. Statistical Functions
5. Tape Output Functions
6. Display Functions
7. Earth Resources Related Functions
8. Fourier Functions.
9. Fourier Filter Functions
10. Complex Functions
11. Mensuration Functions
12. Macro Functions

The full repertoire of each type of function is listed in Table I, with a more detailed breakdown of the earth resources related functions in Table II.

The system functions are primarily related to the processing during a session. That is, processing may be cancelled, halted temporarily or resumed under system command. The setting of various modes (such as automatic vs. manual display) may be accomplished. Help may be obtained interactively in the form of documentation on a function (or functions). The various system-kept files may be accessed, such as image histories, session histories, and image catalogs, and images may be explicitly stored to tape or deleted.

Utility functions are available to enter images into the catalog, generate specific image types (wedges, constants, grids, etc.), mosaic images together, print them in various forms on the line printer, and perform numerous tasks. Arithmetic functions work with images on an element by element basis, adding, averaging, scaling, multiplying, or ratioing images. These can all be performed either on independent images or on the spectral bands of a single image (or images).

Image enhancement functions range from intensity transformations, which may be applied selectively to various bands of an image or used to perform histogram equalization, to Fourier manipulations and filters designed to help remove noise, blur, or other undesirable features from images. Some of these are in the form of macro functions.

Histograms are available with a number of options (i.e., showing cumulative distributions or absolute distributions) and tape output compatible with other computer facilities is provided.

A wide range of display functions is available as an aid in viewing and interpreting the results of processing image data. Both true color and black and white images may be displayed. In the case of LANDSAT and other multispectral data, any 3 bands may be displayed as red, green and blue on the display including the traditional "false color" representation with infrared data being assigned one of the visible colors. Images may be selected for viewing in either a normal or split screen state. Images too large to fit on the screen are automatically reduced, and the user is informed of the reduction factor.

Functional intensity transformations are available on the display in the form of "look-up tables" in the refresh cycle of the display so that it is possible to see the effects of a mapping before actually issuing the command to map the digital version of the image. Transformations may be fine-tuned in this manner. In addition to functional processing in the refresh cycle, there is also the capability of performing pseudo coloring of a monochrome image to distinguish more easily between the various image intensities. This is especially useful when viewing the results of an image classification. Users are given permanent libraries of functional and pseudo color maps. It is possible to flicker among various images or mappings (functional or pseudo color) in order to compare results.

A graphics overlay on the screen is used to display various kinds of information, including histograms, profile cuts, tic marks, annotations, and coordinate values of points picked under control of the trackball. There are various mensuration commands which allow the user to define points, lines, and conic sections by means of the trackball, to name them, and to delete them selectively. It is possible to obtain information, such as slopes, intercepts, and coefficients about any of these, and to obtain area information about an outlined polygonal region.

One very helpful feature is the ability to subsection and expand images on the screen. Subsections are chosen from the original image by means of the trackball, and redisplayed. They are expanded as they are displayed, if desired. Any information which was written on the overlay with respect to the original image may be reconstructed to correspond with the subsectioned, enlarged image, and vice versa. This is helpful in maintaining the correlation between features in the original and the enlarged version.

The main goal of the functions discussed in this section is to provide a helpful framework for the user to analyze his data. The types of functions available for analysis of multispectral data is described in the next section.

EARTH RESOURCES PROCESSING FUNCTIONS

Clustering Algorithm

For unsupervised classification IDIMS features an iterative algorithm called ISOCLS (Iterative Self-Organizing Clustering). This procedure will, ideally, separate all of the data into distinct groups or clusters, the center of each cluster being represented by its mean. The process is initialized by assigning each data point to the nearest estimated cluster center (absolute distance is calculated to each cluster mean). After assigning all of the data to clusters, new means are calculated and tests are made to see if clusters should be split or combined. A cluster is split if the standard deviation of the cluster exceeds a specific threshold value. Two clusters are combined if the distance between the cluster centers is smaller than the specified threshold. A cluster is deleted if it has fewer than some specified number of points. The data is reassigned after each split or combine and the process continues until the desired number of iterations have been obtained.

Several parameters are set by the user that controls the operation of ISOCLS. For example, the number of classes, the number of iterations, the initial mean values, maximum standard deviations and minimum separation distances are input by the user at run time. The values set for each of the parameters determine the accuracy and cost of each run. Statistics generated by ISOCLS can be used to run IDIM's maximum likelihood classifier.

Classification Algorithms

IDIMS currently offers the user a choice of classification algorithms; these include a maximum likelihood classification algorithm, a table look-up procedure, and a minimum distance classifier.

Maximum likelihood classification. - The supervised classification algorithm, CLASFY, implemented on IDIMS is essentially that utilized in the LARSYS AA package at Purdue. It assumes that the class-conditional distributions of the data to be recognized are multivariate normal (or the union of several multivariate normal distributions) and that class probability occurrences are all equal; the discriminant functions turn out to be the logarithm of the product of these two distributions. Classification is done on a pixel-by-pixel basis.

Table look-up classifier. - The ESL table look-up classifier, CELTA (Classification by ELliptical TAbles), is an improved version of Dr. W. G. Eppler's table look-up classification algorithm. In this procedure, the maximum likelihood classifier is run systematically so that intensity values in each of the selected channels are converted to addresses in a look-up table which contains the computer class that would be generated by the maximum likelihood classifier.

The table look-up approach is based on prestoring in fast, random-access core memory all possible measurement vectors for each of the prescribed classification categories and substitutes simple comparison operations in place of the lengthy calculations required by more conventional approaches. Each set of spectral values is considered once in the process reducing the comparison time considerably. After the table has been created, the raw data of the study area is run through the computer and the spectral values for a given point are used to look up a computer class in the table. This classification scheme is very efficient when a small number of classes and channels are being used and spectral data that falls outside of some threshold value is unimportant to the investigator.

Features of CELTA include a sufficient test for disjointness, an expeditious method of calculating probability densities in the table building phase, and an option that allows a slight relaxation of the maximum likelihood decision rule. Basically CELTA is restricted to no greater than 4 band images; preprocessing in the form of data compression, feature selection, or dimensionality reduction is required for multispectral images having 5 or more bands.

Minimum distance classifier. - IDIMS also has available the minimum distance classifier MINDST for classification of multispectral images. Statistics used are generated by several of the available routines. Basically, using the spectral mean values for each class (or cluster) the "spectral distances" from a given pixel element are calculated, and that pixel is assigned to the class having the minimum distance. Classification is done on a pixel-by-pixel basis.

Geometric Manipulation

The geometric correction algorithm REGISTER currently used on IDIMS applies linear, second, or third order transformations of the data to effect scale changes, rotations, and skew corrections due to the earth's rotation. These transformations approximately correct a LANDSAT scene to a N-S oriented image having a sampling scale of about 79 meters per data point in both the N-S and E-W directions. If line printer maps are desired, the geometry is adjusted for line

printer aspect ratio. When needed, the corrected image is scale-adjusted to match that of any desired map scale. The basic routine REGISTER translates, rotates, stretches and/or shrinks an image so that the resultant image will reflect true ground distance.

Statistical Routines

To generate the necessary statistics to run the maximum likelihood classifier, either ISOCLAS or the routine STAT is utilized. The latter determines means, variances and covariance statistics for each training field selected, or for combinations of them. The analyst has the option of printing the means, standard deviations, covariance and correlation matrices, histograms, and coincided spectral plots for these training fields or the classes they represent. In addition, STAT allows the investigator to determine optimum features and class separability.

The IDIMS function PEVAL evaluates the classification performance of a previously classified image. Specifically:

1. New output images are created with analyst-specified training and test fields outlined.

2. Thresholding is applied to the previously classified image and thresholded pixels are replaced with the analyst-specified threshold values in the new output image.

3. The larger number of classes in the original image are combined to produce fewer groupings in the new image.

4. Percentages of the total number of pixels in the training and test fields assigned to each new class are printed out.

IDIMS also provides standard correlation and regression routines which are used mainly with multistage analysis procedures.

Radiometric Correction Functions

As an approach to sensor miscalibration (banding) IDIMS currently utilizes a histogram normalization routine. For LANDSAT type imagery the input image is read by bands and independent histograms are generated for each line taken by the six LANDSAT sensors. The resulting 24 histograms are analyzed and the means and standard deviations calculated. The means are normalized to the maximum and minimum value and the middle four values averaged. Multiplicative factors are utilized to alter these statistical parameters to generate a new output image.

Missing or erroneous image data are identified and corrected during a data review procedure. "Bad" lines, for example, are replaced by an "averaging" process taken across several of the surrounding lines of imagery. Various intensity mappings from the repertoire of those available on IDIMS are also used for certain aspects of radiometric correction. These routines are delineated in Table I.

Currently being implemented on IDIMS is a statistical routine for sun angle correction of the reflective data on multispectral imagery.

Utility Functions

Intensity mappings. - The intensity mapping process is used to perform position invariant intensity transformations using a piecewise linear function. This capability allows the user to emphasize intensity detail in a controlled fashion that might otherwise be difficult to see. Gamma correction techniques may also be applied.

Density slicing. - Density slicing allows the user to group density ranges into different density levels or colors. This is used frequently when analyzing thermal IR data as a means of differentiating heat ranges. In the visible region it is often used to separate the range of each density slice. The user may select the number of density slices and the range of each density slice. He has a choice of color contouring or dynamic contouring done either automatically or under trackball control.

Spectral ratioing. - The ratio of one spectral band to another band or linear combination of bands is often used to emphasize detail not readily apparent in the original scene. This process can enhance detail which has little visible difference by emphasizing the relative response between different spectral bands. Ratioing eliminates common brightness trends between bands and emphasizes the difference between them. The resulting pictures are generally of lower contrast than the input images and these can be contrast stretched to further emphasize differences. Different spectrally ratioed pictures are used to produce color composites.

The IDIMS routine SPECRATO performs ratios of the form:

$$\frac{uB_i}{\Sigma w_j B_j}$$

where the u and w_j are weights specified by the user and the B_k are the spectral values for the kth band in the multispectral image.

Since IDIMS has the arithmetic functions ADD, MULTIPLY, etc. which can be used in conjunction with SPECRATO, the algorithm is effectively

$$\frac{\Sigma u_i B_i}{\Sigma w_j B_j}$$

where the u_i and w_j are weights supplied by the user.

Random sampling. - The IDIMS function RANDSAMP permits the user to specify the percentage of an input image to sample and the size of individual rectangular sampling units. Rectangles of this size are then randomly located throughout the image (no overlap) until the percentage requirement is met.

Tape reformatting. - The IDIMS function UNPKCCT is used to unpack or convert a LANDSAT formatted tape (CCT) into a line-by-line image required for processing on the ESL system.

Line printer maps. - The IDIMS function LPMAP produces a line-printer map of an image. The maps are laid down in strips of 125 columns. The column numbers are indicated along the top of each strip and the line numbers along the left hand margin.

Multistage Analysis

ESL's approach to resource inventory type problems with remote sensing data is to apply multistage statistical and prediction analysis. This procedure provides a cost-effective, optimum allocation of efforts for maximum information procurement.

Frequently the number of classes needed for a complete classification can be reduced by eliminating areas that can be classified easily from tone and texture. Large areas can be divided

into several smaller areas each containing a few classes and each representing one general land use or stratum; each stratum can then be classified using only the classes that might occur in that stratum. Strata boundaries are delineated from photos, image displays, etc., entered into the system, and put into common registry with the multifeature images.

Generally speaking, satellite imagery is used to roughly classify the attribute(s) under study within some political or geographical boundary or other strata. These subregions are subdivided into sample plots, and optimum choices are made for utilizing high altitude photography over some of them to further improve the estimates being made. Certain of these "visited" sample plots are selected for low altitude photography to further improve the estimates, and finally a subset of the low altitude coverage plots are visited "on the ground" to provide final verification of these quantities. Statistical inferences and correlations are continually made for those plots not photographed or visited and precise error estimates and confidence limits presented.

In order to accomplish these tasks, IDIMS includes the ability to:

1. Precisely register and transform coordinates from one image form to another. These forms include geographical maps, satellite imagery, high altitude and low altitude aircraft photographs, and the like.

2. Approximate political or geographical boundaries and strata by irregular polygons and to mask or exclude regions of no interest from the analysis.

3. Describe primary sample units and generate the statistics and prediction techniques for selecting those units for further study; this is repeated for the several layers of information available. The IDIMS function SAMPLET describes the primary sampling unit and generates the statistics required for determining units selected for further study.

4. Generate statistical routines - correlation and regression analysis - to infer subclass estimates based on the sampling procedure and to predict the accuracy of results and error bounds.

Training Set Manipulation

The IDIMS routine TSSELECT serves as an interactive training set selection module from which statistics are generated to run the maximum likelihood classifier. The capabilities permit the interactive selection, annotation, and editing of intensive study areas, training areas, and training fields; these regions may be either rectangular or irregular polygons in shape. Many unique features of IDIMS are incorporated in the module to facilitate the efficient selection of training areas and the generation of the required statistics.

Dimensionality Reduction

IDIMS currently uses a version of the Karhunen-Loeve linear transformation to concentrate information into one or several uncorrelated principal components images and to achieve improvement of signal-to-noise ratio. Normally this technique is utilized with multispectral imagery having more than 5 or 6 bands.

CONCLUSION

IDIMS provides an excellent tool for analysis of multispectral data. It combines a wide and powerful range of processing functions with the ability to interactively monitor results. A user is not locked into a rigid menu, but rather is able to decide various processing strategies based on the exact nature of his problem. Development of new processing techniques is also facilitated by the

structure of IDIMS; new or better algorithms and functions leading to more comprehensive methods of analysis are easily implemented on the system.

For people with unusual data handling requirements, IDIMS can be tailored to meet those requirements. Both from a software and a hardware point of view, it is designed to be flexible, economical, and capable of serving as a powerful aid in the analysis of all types of image data.

FOOTNOTES

1. Hewlett Packard 3000 Minicomputer with Multiprogramming Executive Operating System

2. COMTAL 8000 Series Color Display

3. Perkin Elmer PDS 1010A Microdensitometer

4. CONTROL-Y is typed on most terminals by typing the character "Y" while holding the control (CNTL) key.

TABLE I. REPERTOIRE OF FUNCTIONS

PROCESSING FUNCTIONS

SYSTEM

CANCEL
CONTINUE
DELETE
END
HELP
HISTORY
LISTCAT
PAUSE
SESSION
SET
STORE

FOURIER

CFFT
CFFT1
CIFT
CIFT1
FFT
IFT

FOURIER FILTER

DEFOCUS
EXPFILT
GAUSS
IPOLFILT
POLFILT
SINC

MENSURATION

POE

UTILITY

CONSTANT
COPY
ENTER
EXPAND
FLIP
GNOISE
GRID
INSERT
MINGLE
MIRROR
MOSAIC
NOISE
PICPRINT
PLOT
POLYNOM
RADIUS
REDUCE
REGISTER
ROT 180
SENTER
TRANSPOS
UNTIE
WEDGE
WINDOW

COMPLEX

RE
IM
MAG
PHASE
REALIM
CONJ
MAGPHASE
CORRECT
COMPOLAR
SPECPOW
SPECPOWL

ARITHMETIC

ADD
AVERAGE
BYTE
DIVIDE
MULTIPLY
NORMAL
SCALE
SPECRATO

INTENSITY TRANSFORMATION

HANDFLT
MAP
PEXP
PLOG
POWER
REDIST
SIGNALS

STATISTICAL

HISTOG

TAPE OUTPUT

TRANSFER
EBRTAPE

MACRO

AUTOCOR
CEPSTRUM
CROSSCOR
HOMOMORPHIC
MAGPOWER

UTILITY

CENTER
COLOR
FREE
GRAB
INIT
INTENSITY
RELEASE
SAVE
SELECT
SPLIT

PSEUDO COLOR

ACM
CONTOUR (CC)
DPT
DYCC
GPT
PIECEWISE LINEAR (PLPL)
PSEUDO
RECALLP
SAVEP

GRAPHICS

DISPLAY CURSOR (DC)
GRAPHICS
HISTOG
HISTOGV
PROFILE
TIC

TIME DEPENDENT

FLICKER
FLICKERM
FLICKERP
TZONE

INTENSITY TRANSFORMATION

BITS
CPLM
DFM
EXP
GAMMA
LOG
MAP
MZONE
RECALLM
REDIST
SAVEM
SIGMAS
TLM
TUBEC

MENSURATION

ANNOTATE	(AN)
BEGIN	(BM)
DELETE	(DE)
DEFINE POINT	(DP)
END	(EM)
EXTEND LINE	(EX)
FIT CONIC	(FC)
FIT LINE	(FL)
MENSURATION INFORMATION	(MI)
MODE	(MO)
RECONSTRUCT	(RO)
OVERLAY	
SUBSECTION	(SB)
SHADOW	(SM)
MEASUREMENT	

EARTH RESOURCES FUNCTIONS

CLASSIFICATION
DENSITY SLICING
DIMENSIONALITY REDUCTION
GEOMETRIC CORRECTION
MENSURATION
MULTISTAGE ANALYSIS
RADIOMETRIC CORRECTION
STATISTICAL
TRAINING SET SELECTION

MISCELLANEOUS

(SEE TABLE II)

TABLE II. EARTH RESOURCES RELATED FUNCTIONS

CLASSIFICATION

CELTA (TABLE LOOK-UP)
CLASFY (MAXIMUM LIKELIHOOD)
CLASTRAT (CLASSIFICATION OF IMAGE STRATA)
ISOCLS (CLUSTERING)
MINDST (MINIMUM DISTANCE)

DENSITY SLICING

CC (CONTOURING)
DYCC (DYNAMIC CONTOURING)
TZONE (TIMED ZONING)
MZONE (MANUAL ZONING)

DIMENSIONALITY REDUCTION

KARLO (KARHUNEN-LOEVE)
LARSEP (LARSYS SEPARABILITY)

GEOMETRIC CORRECTION

REGISTER (NORTH/SOUTH, SKEW, ASPECT RATIO)

MENSURATION

MI AREA (AREA INFORMATION)

RADIOMETRIC CORRECTION

HISTNORM (SENSOR CALIBRATION)
RADIOMET (SUN ANGLE CORRECTION)

STATISTICAL

HISTOG (INTENSITY DISTRIBUTION)
ISOCLAS (CLUSTERING, STATISTICS)
CLASTRAT (CLASSIFICATION OF IMAGE STRATA)
STAT (CLASS STATISTICS)

TRAINING SET SELECTION

RANDSAMP (RANDOM TRAINING SET SAMPLING)
TSSELECT (INTENSIVE STUDY AREA SELECTION, TEST SET SELECTION, ARBITRARY POLYGONAL TRAINING SET SELECTION)

MULTISTAGE ANALYSIS

SAMPLET (PRIMARY SAMPLE UNIT SELECTION AND STATISTICAL ANALYSIS)
CLASTRAT (CLASSIFICATION OF IMAGE STRATA)

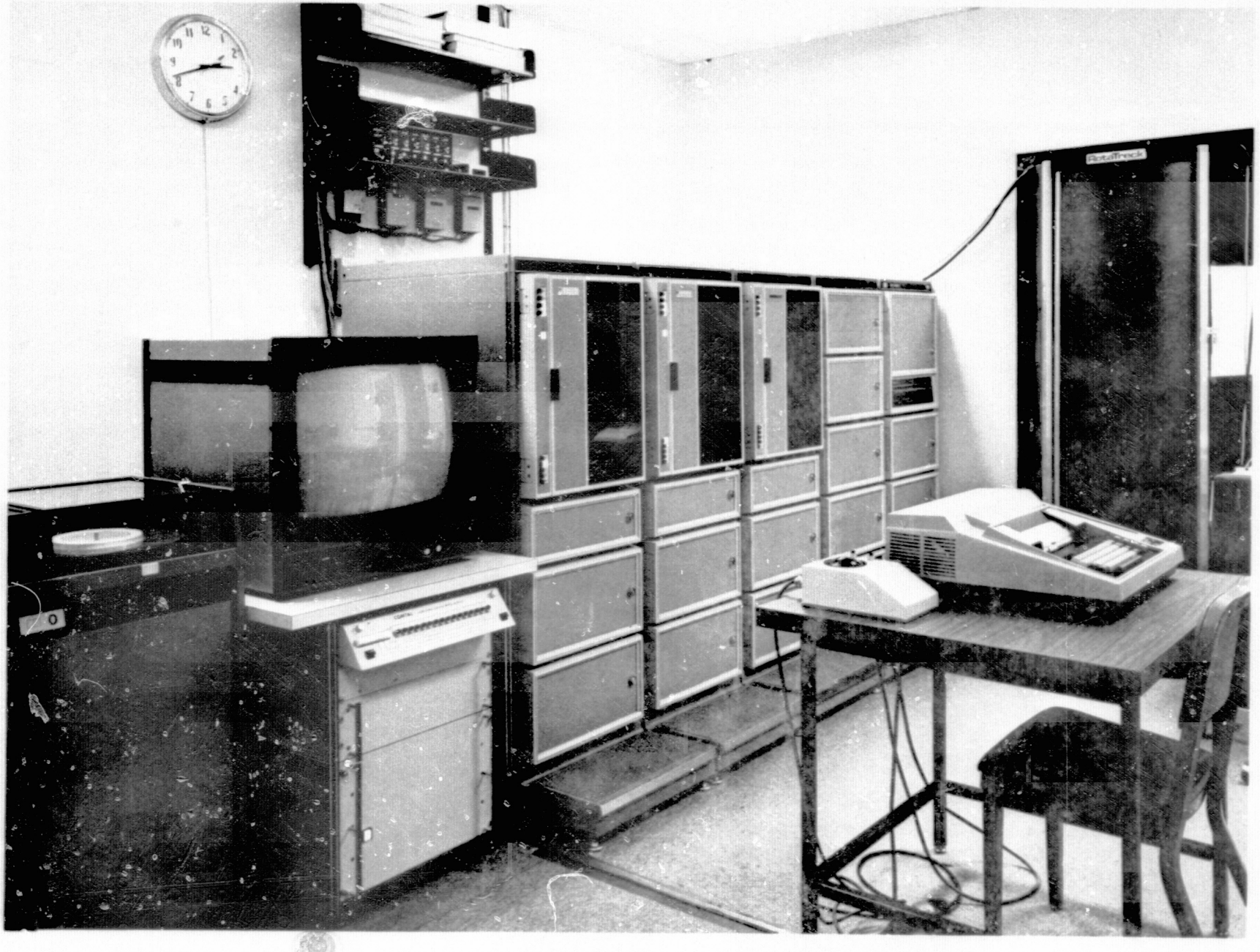


FIGURE 1. PHOTOGRAPH OF THE IDIM SYSTEM

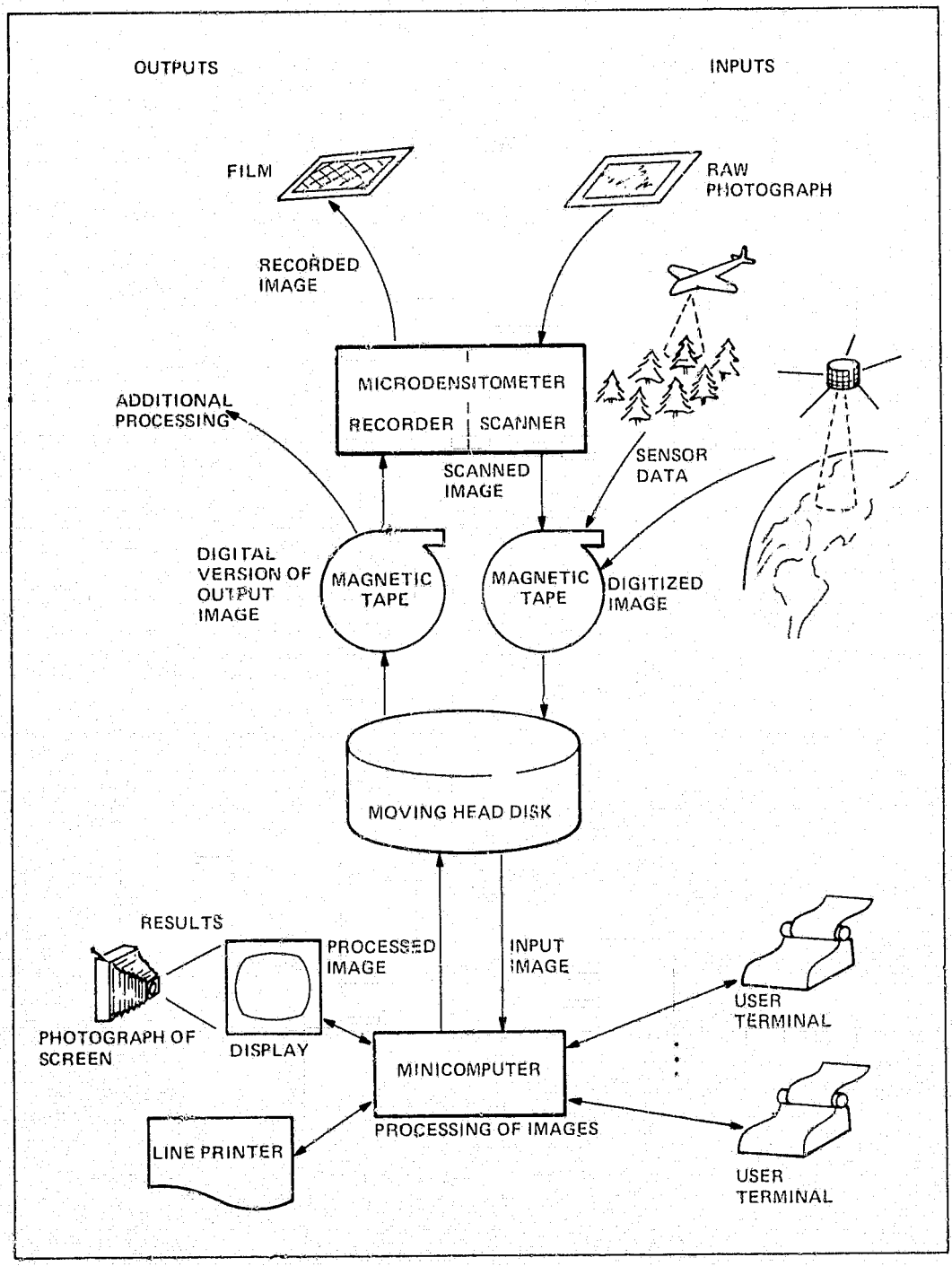


FIGURE 2. IDIMS INPUT/OUTPUT RESOURCES AND CAPABILITIES

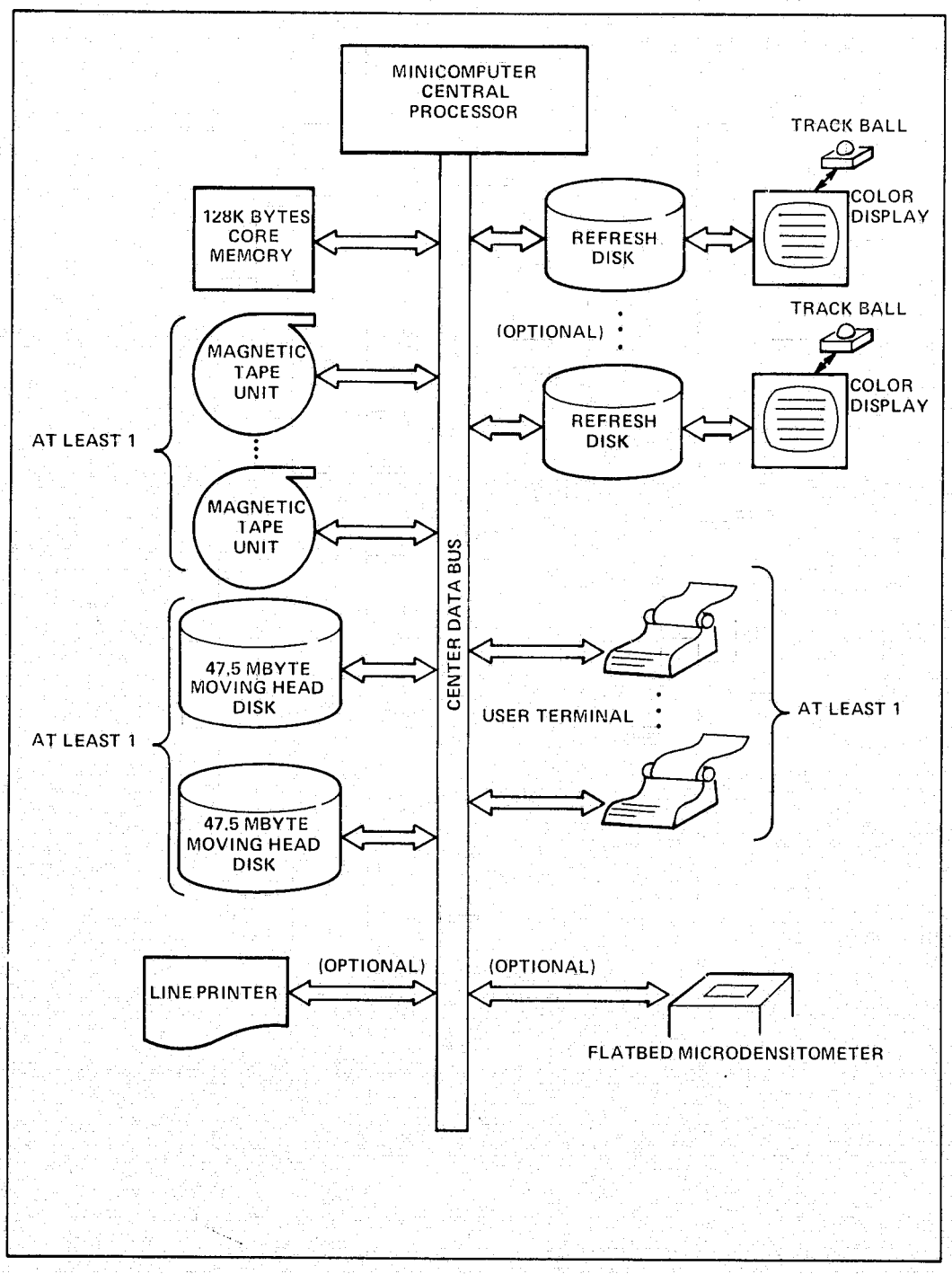


FIGURE 3. IDIMS HARDWARE STRUCTURE

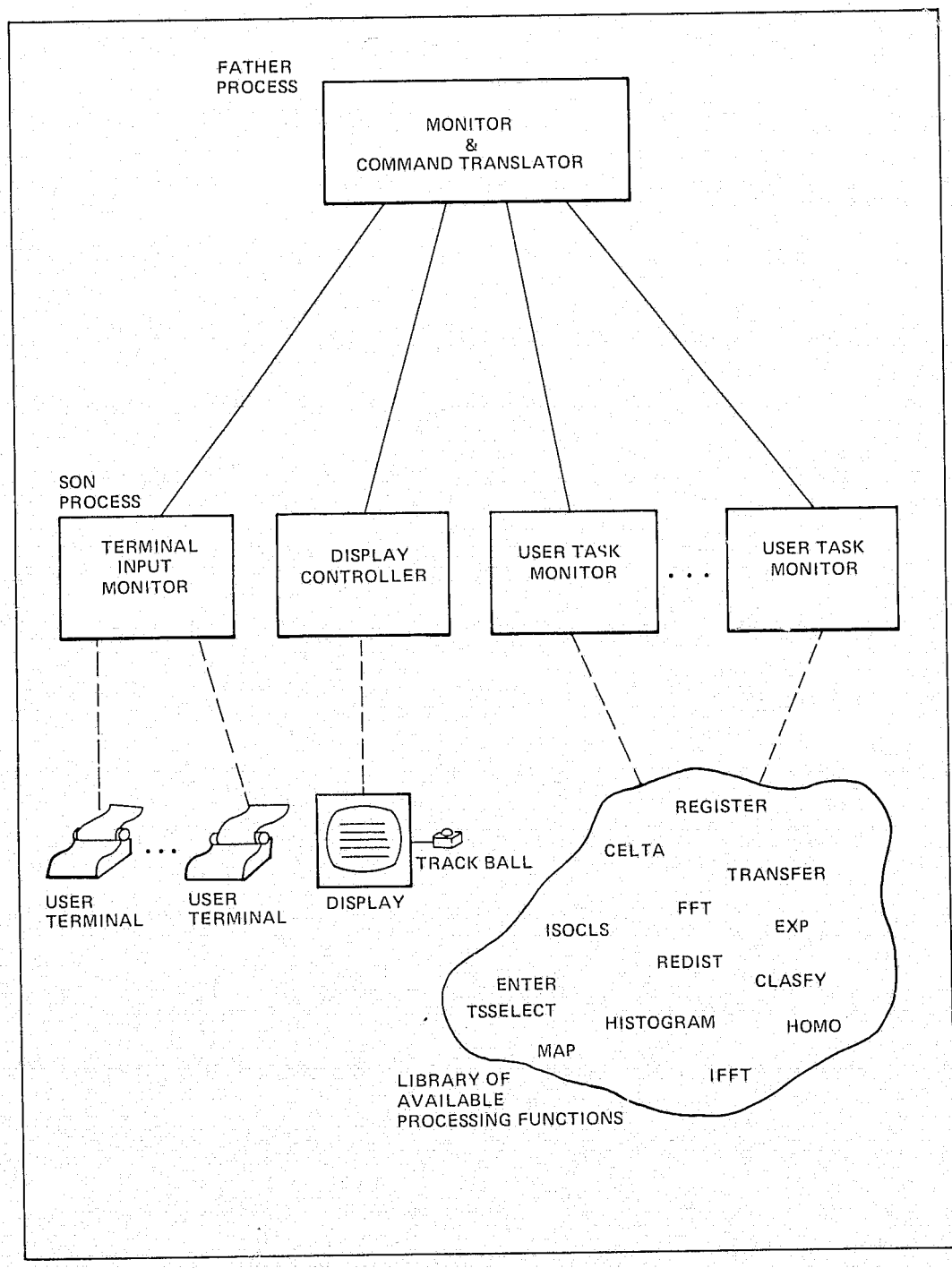


FIGURE 4. IDIMS SOFTWARE HIERARCHY

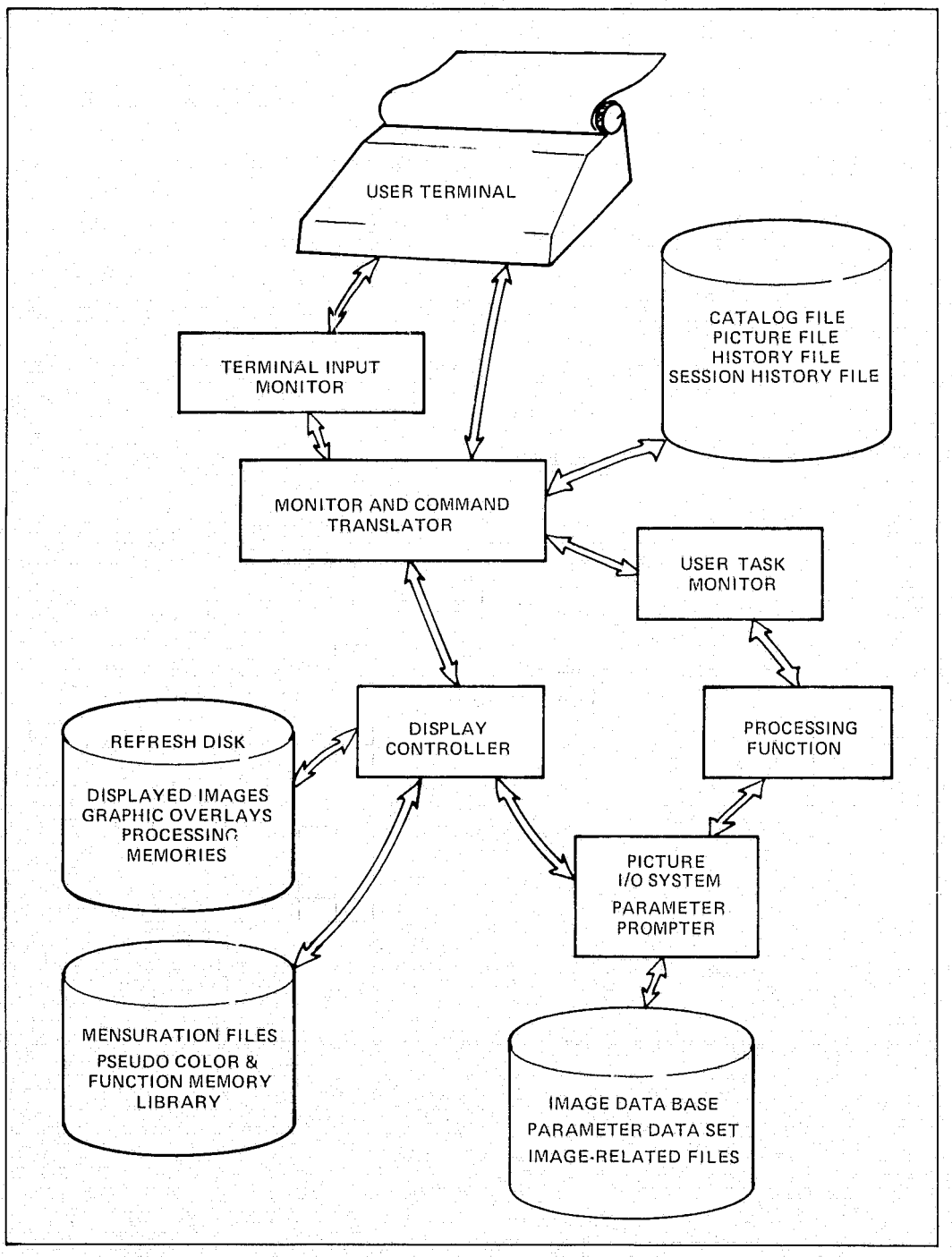


FIGURE 5. IDIMS FLOW OF CONTROL

IMAGE ANIMATION FOR THEME ENHANCEMENT AND CHANGE DETECTION

By Wm. E. Evans, Stanford Research Institute, Menlo Park, California

N76-17548

ABSTRACT

Animated displays have proved useful in enhancing subtle temporally related changes in scenes viewed by satellites capable of providing repetitive coverage. The detectability of fixed features is also improved through the help of the powerful visual integration process. To expedite the process of assembling and displaying well-registered, time-lapse sequences and to provide means for making quantitative measurements of radiances, displacements, and areas, an Electronic Satellite Image Analysis Console (ESIAC) has been constructed. During the LANDSAT-1 program, this equipment was applied to the needs of a number of earth resource investigators with interests principally related to dynamic hydrology. The measurement of the areal extent of snow cover within defined drainage basins is discussed as a representative applications example. The oral presentation was illustrated with short color movie sequences.

INTRODUCTION

Imagery from LANDSAT or the Synchronous Meteorological Satellites, because of its precisely repetitive nature, is ideally suited both for subjective enhancement via time-lapse display and for objective measurements of changes with time.

Detailed temporal analysis often is neglected because the facilities and techniques required to create well-registered multidate sequences are somewhat specialized and not generally available. Preparation of even a simple movie loop is annoyingly time consuming, and then one is still left with the problem of extracting quantitative data. When operating from digital tapes, spatially related trends are even more difficult to follow unless some provision is made also for time-lapse viewing of either the image or some other transformation of the raw data.

Through the use of video editing and animation techniques that are relatively standard in the television industry but perhaps less familiar in instrumentation, it becomes possible to extend significantly the utility of currently available satellite imagery by reducing the turn-around time required to achieve practically useful displays and to achieve useful accuracies at costs that appear commensurate with the amount of professional time saved.

Research meteorologists at SRI became impressed with the power of time-lapse sequences early in the life of ATS-1 (Serebreny et al., 1967, 1970). For their use, the first ESIAC (Electronic Satellite Image Analysis Console) was developed specifically to facilitate both viewing and quantitative measurements in the time domain.

During the LANDSAT-1 program, there was opportunity to improve the hardware and to extend the operating techniques to better fit the needs of earth resource investigators. To obtain a representative sample of real-life problems, an arrangement was made to provide image processing assistance to a number of LANDSAT-1 Principal Investigators employed by the U.S. Geological Survey, Water Resources Division. These projects included:

PRECEDING PAGE BLANK NOT FILMED

- Mapping of seasonal changes in ephemeral desert vegetation coverage in the Southwestern United States.
- Tracking of the dispersion of estuarine discharges into Lake Ontario and Long Island Sound.
- Temporal analysis of riparian vegetation in the Southeastern United States.
- Measurement of areal extent of snowcover in the Pacific Northwest.
- Inventory of playa lakes in Texas.
- Measurement of glacier motion in Alaska.

While the disciplines ranged from Botany to Glaciology, the common bond of interest was a need to monitor temporal changes in water distribution on the earth. In this presentation, we will emphasize the functions that were found to be most useful during these hydrological studies.

During our work we have become convinced that just as still photos are virtually indispensable when working with individual images whether the actual analysis be done manually or by machine, so there is a basic need for some form of animated imagery as the workhorse tool for guidance in temporal studies. Nothing else seems to communicate the message to humans quite so quickly or clearly as time-lapse sequences, flicker comparisons, and the like. And even while striving hard to achieve machine processing, humans seem destined to remain in the loop for the foreseeable future--if only to formulate the problems and check the results.

To illustrate this point, a short movie sequence depicting imagery from one of the synchronous meteorological satellites LANDSAT was shown. It was accompanied by the following remarks. "The area shown is the Southeastern United States, the pictures were taken about 18 minutes apart, and the movie was photographed from the ESIAC screen. First, the sequence is shown in slow motion and some organized cloud motion is evident. Next, when the presentation is speeded up, note how much more information is conveyed. It does not take a professional meteorologist to see that the wind motions are clearly different at different elevations or to infer that there are probably mountains present to cause the uplifting and condensation over the Ozarks. Note also how well the eye can map the shape of the Florida peninsula even though we are viewing it through a considerable amount of cloud cover.

As many of you know, while remarkable progress has been made in machine tracking of well-defined cloud cells, meteorologists routinely use film-loop sequences similar to these to easily follow complex multilayer situations, which thus far have eluded even the most sophisticated machine pattern recognition procedures."

Time-lapse sequences of LANDSAT imagery normally are superficially more more confusing than cloud sequences--principally because the surface features that change lack the large-area organization of the clouds. Again, the remarkable capability of the human eye-brain combination enables an observer to read through the clutter and integrate out basic patterns or to quickly detect small areas of anomalistic behavior. This gives hope that we may be able to teach machines to do the same thing; or at a minimum, we may be able to provide machine processing to enable a human operator to make classifications more efficiently.

HARDWARE

The present ESIAC provides 600 TV frames of analog video disc storage, organized into two 300-frame files, each independently addressable by a separate moving head. The memories can be loaded either from film or hard copy input stations or from digital tape via a fast digital-to-analog converter. The operator is provided with several display screens and with simple video mixing controls that permit him to add positive or negative amounts of images from the disc memories or from a wide variety of other input sources (e.g., map viewing camera, calibration grids and gray scales, cursor, and system-generated overlays). The readout heads can then be stepped sequentially through any number of disc tracks at any desired rate to create a custom-designed animated display.

Displacements are measured with the aid of an electronic cursor, digitally positioned under the control of a track ball.

Areas are measured by electronically counting the total number of picture elements per frame that meet specified classification criteria. (This procedure will be described more fully later.) The preferred input medium for most operations is 70-mm positive film transparencies. Tape input, while providing the ultimate in precision, usually has been too expensive and time consuming to be justified for "first cut" analyses of long time sequences. Filmed images are much easier to scale and to register, particularly when image rotation is required.

An overall view of the equipment is given in the photograph and line drawing of Figure 1.

OPERATING PROCEDURE

After the first image is sized and stored on the disc memory, other images of a desired sequential series are placed in front of the camera, brought into register with the previously stored image, then stored. For film input, registration is achieved with the aid of a set of film micropositioners while viewing either a composite image or a sequentially flickered image pair. If a color composite display or multispectral signal processing is desired, each of the multiband images is entered separately. These are combined as required during playback.

For tape input, a trial entry is made, then the stored trial image is shifted electrically to achieve register with previous entries, as judged by superposition or flicker comparisons. The digital image is then reentered with the required offsets, and the correction data are recorded for future use.

The image sequence is then critically studied at various rates, preferably by the specialist who knows what to concentrate on and what to ignore.

Brightness, contrast, polarity, and color balance of the displays are altered as necessary to achieve optimum presentation of the theme of interest. Critical frame pairs can then be flickered alternately, or viewed in positive-negative superposition. Often displacement changes become more evident when viewed against a fixed grid or background map outline.

Extremely subtle fixed features can be detected and positively separated from film or system artifacts when they integrate in the eye/brain, in spite of the presence of an enormous amount of transient "noise" in the form of vegetation change, clouds, cloud shadows, and sun angle effects.

QUANTITATIVE MEASUREMENTS

Creation of a sequential display normally is only a necessary first step for an actual project task--needed to help the operator identify some feature or theme of interest. Usually the desired end product is some quantitative measure of the specified theme. To provide area measurements, ESIAC is fitted with a set of level decision circuits (LDCs) capable of operating on the video signals. These LDCs are essentially fast one-bit analog-to-digital converters having threshold decision levels adjustable by the operator. Level decisions can be made independently and simultaneously in two or more spectral bands or on additive combinations of two signals. The binary outputs can be combined logically to create a binary video signal that can then be displayed as a two-dimensional binary thematic mask or template that can be viewed either alone or superimposed on the original scene. The white or TRUE picture elements in the mask are totaled in a digital counter and continuously displayed to provide a measure of area.

To aid in the quantitative interpretation of multispectral data and to provide guidance in the setup and adjustment of controls on the Level Decision Circuits, an auxiliary display is provided to present the video information in two-dimensional color space at the same time that it is being viewed as a conventional image on the main display (Image Space Display). The Color Space Display is a dynamic version of the plot shown in Figure 2.

In a typical application, vertical (y-axis) displacements are caused to be proportional to infrared radiances at the same time that horizontal (x-axis) displacements are made proportional to radiances in a visible band. For imagery such as LANDSAT, where reference gray scales are available on the film, a unique data entry procedure permits samples of these scales to be replicated and used to define both axes and the 45° diagonal. The two-dimensional color coordinates of any pixel or small group of pixels (as specified by the cursor intersection in the main image display) can be read directly from this graphic presentation in units linearly correctable to absolute radiance values for the scene.

A summary impression of the spectral statistics for an entire image can be obtained very quickly by observing the brightness distribution over the diagram. Scenes containing significant areas of snow or clouds, for example, produce color maps showing most of the energy distributed along the "neutral" diagonal. A heavily vegetated scene, on the other hand, will generate a scatter diagram with most of its energy above and to the left of the diagonal. Water bodies normally map into the lower right region. Regions of the color space display can be selectively intensified by a z-axis signal derived from one of two sources: (1) a cursor intersection specifying a particular small region of the Image Space Display or (2) by the binary thematic map signal. Case (1) is used to measure the two-band color coordinates of identifiable scene features, while case (2) is useful in monitoring the spectral effect of adjustments to the Level Decision Circuits.

The Color Space Display can be time-lapsed, along with the Image Space Display. A liberal education in the realities of multispectral processing can be gained through a few hours' study of time sequences of actual image data. A seemingly endless variety of "special situations" appear to conspire to provide annoying exceptions to classification algorithms that work "most of the time." Much can be learned, moreover, by watching for any time- or space-organized patterns traced by these exceptions during an animated sequence.

AN APPLICATION EXAMPLE: SNOW AREA MEASUREMENT

To illustrate the use of this equipment, let us turn our attention to an earth resource monitoring application of considerable economic importance: the measurement of the areal extent of snow cover. More specifically, let us consider the problems that arise in monitoring the snowpack within well-defined drainage basins in mountainous terrain.

Figure 3 is an orientation map showing the location of the LANDSAT orbital tracks and nominal frame centers for the Northwestern United States. The coverage afforded by one particular 100 × 100 nautical mile frame in the North Cascades region of Washington state is indicated. The next figure (Figure 4) shows the LANDSAT image for that location for 2 September 1972. Alongside the image is an outline map defining a number of individual drainage basins that we have been studying. The barber-pole frame defines the coverage of the last or working stage of zoom (Figure 5), which singles out a particular 272 km^2 drainage basin--that of Thunder Creek between Lake Ross and Lake Chelan. Snowmelt from this basin drains into Thunder Creek and helps drive hydroelectric power plants located at Diablo and Ross dams--just outside the upper left corner of the enlarged view. The basin boundary overlay is derived from a template stored in the video memory and defines the precise region within which the snow area measurements must be confined by a procedure to be described later.

Our objective is to measure the acretion and ablation for this snowpack with particular emphasis on the critical spring melt period. As a first step, the operator views monochrome and/or color time sequences of scenes similar to the one shown in the upper left panel of Figure 5 and studies the general behavior of the snowpack in space and time. For quantitative measurements on individual dates, he stops the animation and attempts to create a binary thematic map that represents the best visual match to the observed snowpack for that date.

Since the snow appears to be visually well defined in the MSS-5 image, our first attempts were to operate on video signals from band 5 images and to count all those pixels within the basin where the radiance exceeded some threshold level. As in all such thresholding schemes, the all-important question is, "Where does one set the threshold level?"

The binary thematic masks obtained by "slicing" the single date image at five different threshold levels are shown in the last five panels of Figure 5, along with measures of their areas. We found the area-above-threshold to be a very sensitive function of the threshold setting (see Figure 6 for typical curves made for Mt. Rainier). The functional slope is so steep that it appears completely impractical to use preassigned threshold levels. Our initial hope was that by electronically overlaying masks such as those of Figure 5 over the full-tone scale image--sometimes

even displayed in color--and giving an operator the opportunity to study the match dynamically while adjusting the threshold level, we would be able to arrive at a setting that would be representative of the snow-covered area within the basin. Results with this method, while encouraging at first, showed discouragingly high variances between operators and even for repetitive trails by the same operator. For certain times of the year--particularly in early winter when the cover was light and the sun angle was low--variances of ±30 percent of the snow-covered area were common and variances well in excess of 100 percent were not rare. Through careful study of multidate time-lapse sequences and topo map overlays we verified what has been suspected from the beginning--that a major source of difficulty is the effect of sun angle. Snow on south-facing slopes is illuminated nearly perpendicularly and exhibits high radiance to the satellite, while the radiance of snow on the north-facing slopes may be much lower due to illumination at near-grazing angle or it may be completely shadowed.

An operator who is well acquainted with the terrain can learn to watch for this effect and concentrate on the south-facing slopes. The measured value should then always be less than the true value. Perhaps in time a set of "shadow factors" for the major basins of interest could be developed and applied to improve the accuracy of the readings.

Problems with sun angle and shadows can be greatly alleviated by employing more than one spectral band and making the classification decision on the basis of radiance ratios; i.e., on color rather than on brightness alone.

Figure 7 is a two-band color space plot of selected portions of a mountain snow scene. By properly manipulating the Level Decision Circuits, the binary thematic mask can be made to correspond only to those scene constituents having bispectral radiance responses within the diagonal shaded region. This procedure largely eliminates problems with variable illumination and shadowing, but uncovers another problem--partial tree cover. Classifications of snow-covered area made by human photo-interpreters from aircraft imagery frequently extends to significantly lower altitudes than those made from LANDSAT imagery. This is because the humans count the snow under the trees and infer the presence of tree-hidden snow by watching small clearings and streambeds. One might expect that all possible combinations of conifer trees like those at A and snow like that at B mixed together within individual pixels would plot along the line AB. Indeed, with the LDCs adjusted to respond only to a small spectral region centered around the approximate midpoint of line AB, the resulting mask does a respectable job of mapping the tree line. A complication arises when one considers the large size of the triangular region of the color diagram required to include all possible snow-tree mixtures when all possible illumination levels are allowed for each of the constituents. We have not yet found a satisfactory completely objective solution for the snow-tree mixture problem, but image analyses using both the image space and color space displays in the manner just described help the operator to interpret each scene and permit him to more intelligently direct his subjective "bias" when making threshold settings.

EDITING THE BINARY MASK

The operator is provided with capability to make localized revisions to the binary mask when it becomes obvious that the best available objective extraction procedure is not doing an adequate job. He can, for example, lower the thresholding

level in the vicinity of a tree-covered mountain top to record snow that is largely screened by trees, without at the same time causing "blooming" that would create a poor match to the picture for other portions of the mask. As a last resort, he can make additions or erasures to the mask by drawing these in with a light pen, perhaps to delete isolated clouds or cloud shadows. This capability, while exercised as sparingly as possible because it introduces additional time and subjectivity, has been found crucial to the successful completion of many analysis tasks. During the oral presentation a movie sequence was used to illustrate the procedure for generating and editing a binary thematic mask.

BOUNDING THE DATA

Confining the snow measurements within precisely specified drainage basins is a relatively straightforward procedure that makes good use of the registered storage and time-sequenced display features. A hand-drawn, silhouette-type basin outline is prepared, including several stream forks and other landmarks known to be visible on the satellite imagery for a cloud-free summer scene. This drawing is then viewed by the camera, scaled, registered to the summer scene, and converted to a binary mask by one of the LDCs. Since scene data for all other dates in the sequence also will have been registered to the summer scene, the basin-derived mask can be logically ANDed with the scene-derived mask before being measured and photographed. (Unless a scene is completely cloud covered, we find that subtle ground-feature information will nearly always provide enough date-to-date correlation to permit keeping registration errors below one TV element or one LANDSAT pixel, depending upon which is limiting. This is true even when the scene is largely snow-covered or largely featureless, such as the Arizona Desert.)

CONCLUSIONS

Animated sequences of coregistered images provide a powerful form of enhancement for numerous themes, both moving and fixed, that are of interest in repetitive imagery from satellite-borne sensors. Through electronically produced animated displays and associated interactive controls, the remarkable pattern recognition capability of the human eye-brain combination can be effectively teamed with the quantitative precision of machine storage and processing.

Even for applications where multidate displays are not required, equipment of the type described has proved extremely useful in the critical quantitative analysis of individual scenes, particularly where the imagery is available only in photographic form.

ACKNOWLEDGMENTS

Much of the work reported here was performed under Contract NAS5-21841 issued by Goddard Space Flight Center, Greenbelt, Maryland, and was in support of projects in dynamic hydrology headed by Dr. Mark F. Meier USGS (WRD), Tacoma, Washington. The ESIAC was an in-house development of the SRI Atmospheric Sciences Laboratory.

BIBLIOGRAPHY

Evans, W. E., "Time-Lapse Analysis of ERTS Imagery Using Special Electronic Viewing/Measuring Equipment," Proceedings of Second Annual Remote Sensing of Earth

Resources Conference, University of Tennessee Space Institute, Tullahoma, Tennessee 37388, March 26-28, 1974.

Evans, W. E., and S. M. Serebreny, "A Data Products System for ERTS Imagery, Time Lapse Viewing and Measuring," Proceedings of Third Earth Resources Technology Satellite Symposium, pp. 1725-1741, December 10-14, 1973.

Serebreny, S. M., W. E. Evans, R. G. Hadfield, and E. J. Wiegman, "Detection of Cloud Displacement Using Video Techniques," Final Report No. 6672, for the Meteorological Satellite Laboratory, Environmental Science Services Administration, Washington, D.C., Contract Number E-167-67-(N), by Stanford Research Institute, Menlo Park, California (September 1967).

Serebreny, S. M., W. E. Evans, R. G. Hadfield, and E. J. Wiegman, "Electronic System for Utilization of Satellite Cloud Pictures," Amer. Met. Soc., 51, 9, pp. 848-855 (1970).

Serebreny, S.M., W. E. Evans, E. J. Wiegman, "Study of Time-Lapse Processing for Dynamic Hydrologic Conditions", Final Report No. 2165, for Goddard Space Flight Center, Greenbelt, Maryland, by Stanford Research Institute, Menlo Park, California (November 1974).



FIGURE 1a PHOTOGRAPH OF ESIAC

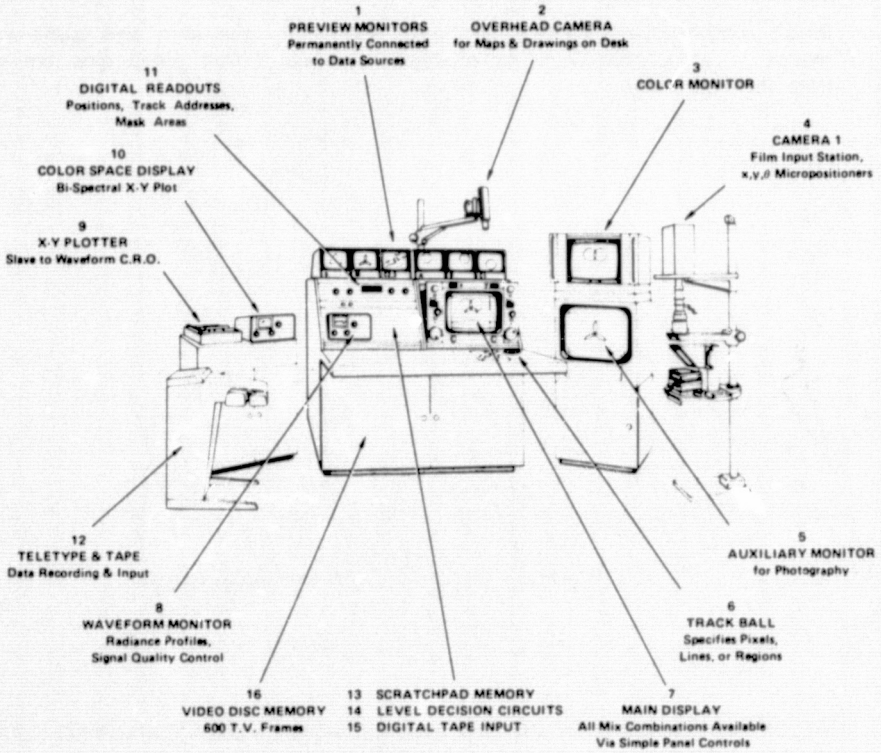


FIGURE 1b ESIAC EQUIPMENT CONFIGURATION

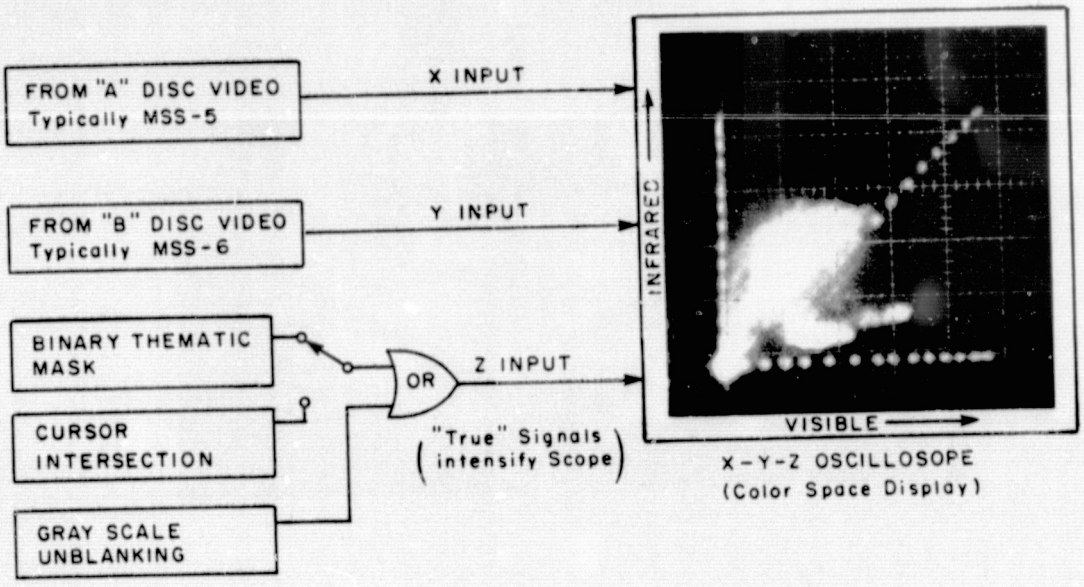


FIGURE 2 ESIAC COLOR SPACE DISPLAY

Energy concentrations resulting from dense vegetation, clear water and turbid water regions in an LANDSAT scene of South Carolina. Dots along axes are gray steps from the film record.

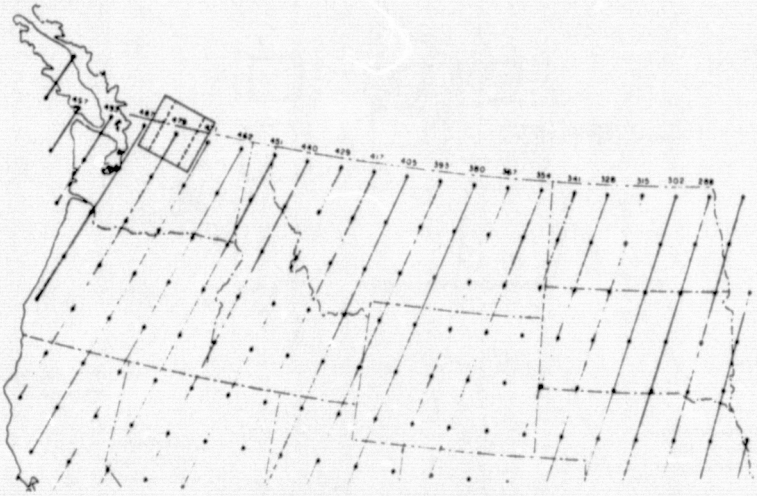


FIGURE 3 MAP OF NORTHWESTERN UNITED STATES WITH OVERLAY SHOWING LANDSAT ORBITAL TRACKS AND NOMINAL CENTERS OF DATA FRAMES

Location and coverage of the frame containing the Thunder Creek drainage basin is shown shaded.

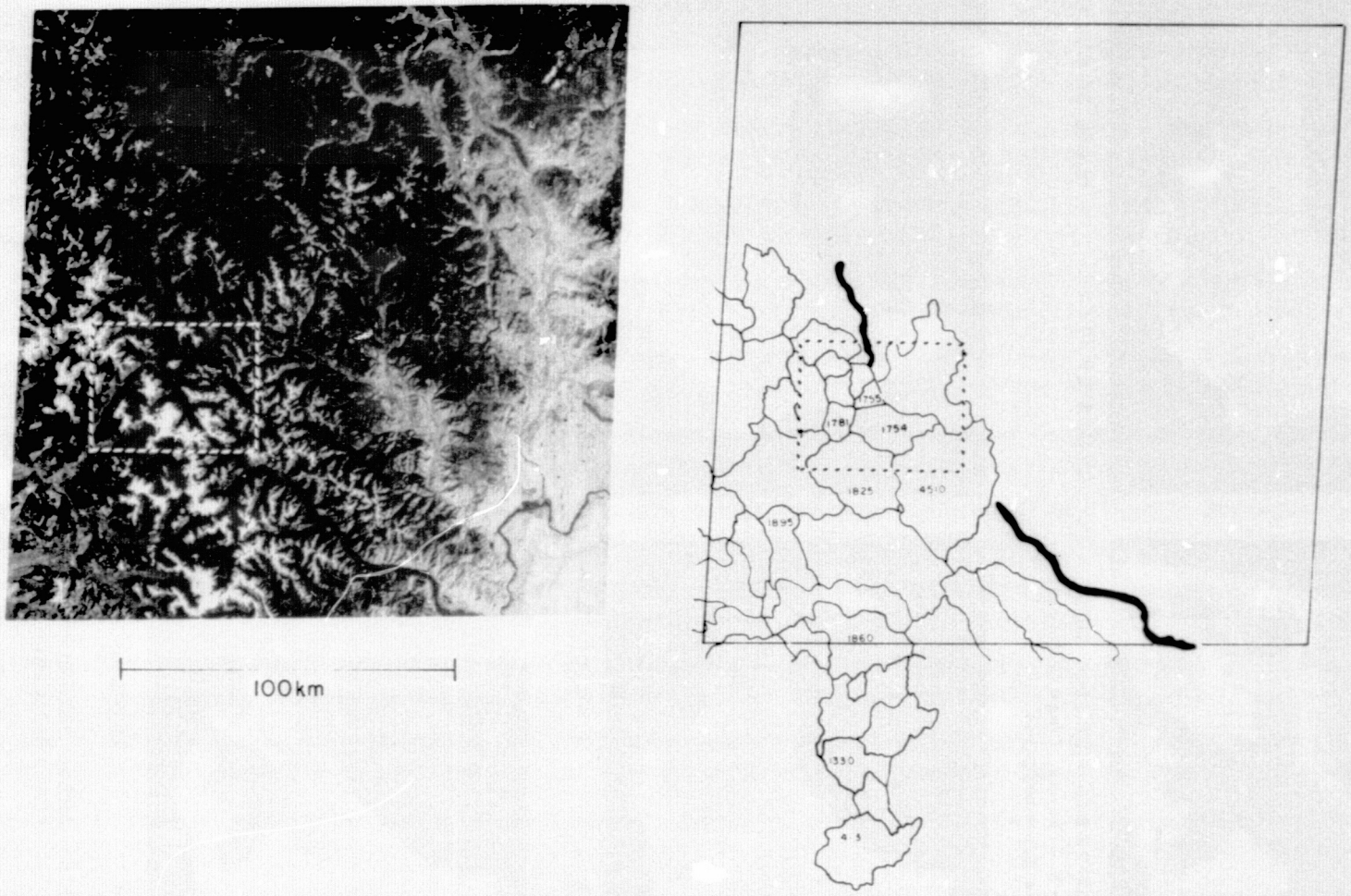
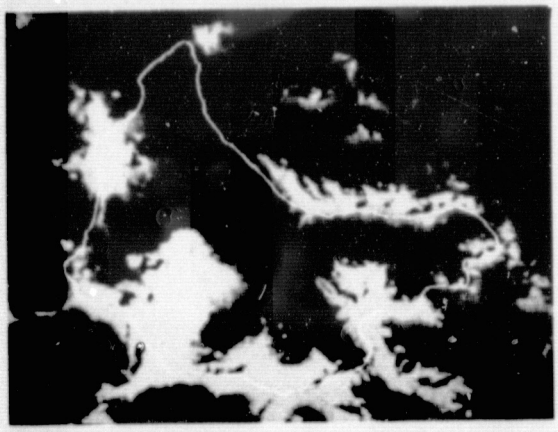
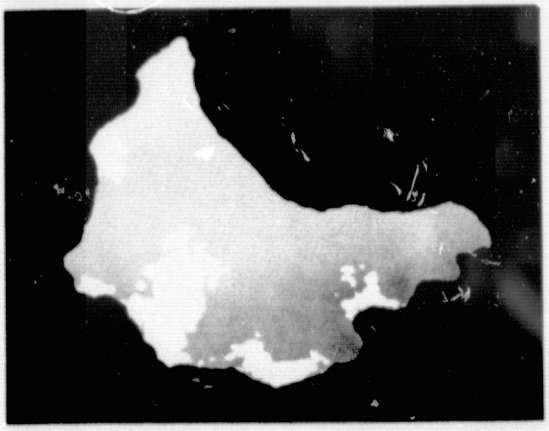


FIGURE 4 LANDSAT IMAGE NO. 1041-18253 FOR 2 SEPTEMBER 1972

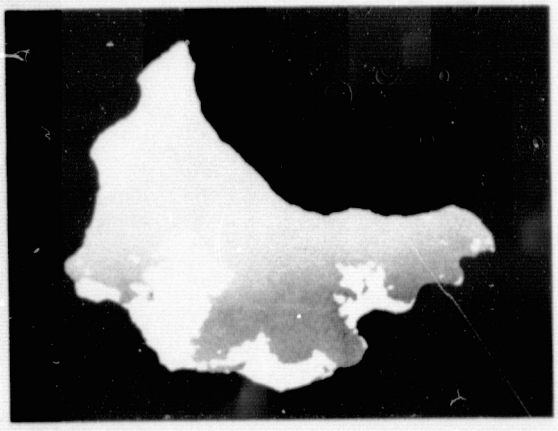
North Cascade Mountain region of Washington and Canada. (Location shown shaded in Figure 2.) Map shows several drainage basin outlines and a rectangular area to be enlarged (in Figure 4). Slide used in oral presentation was in color.



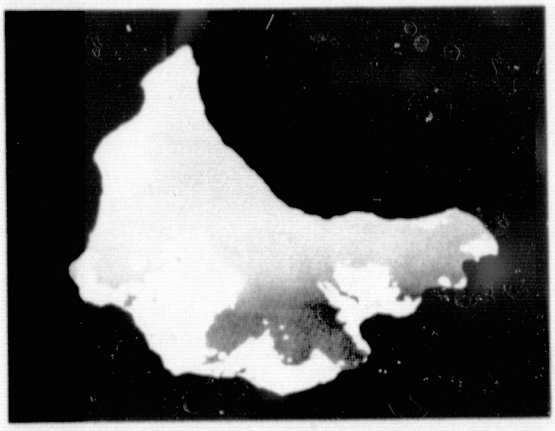
MSS-5 IMAGE 26.8Km HIGH SECTION OF E1041-1823-5. (Thunder Creek Drainage Basin Outline Superimposed)



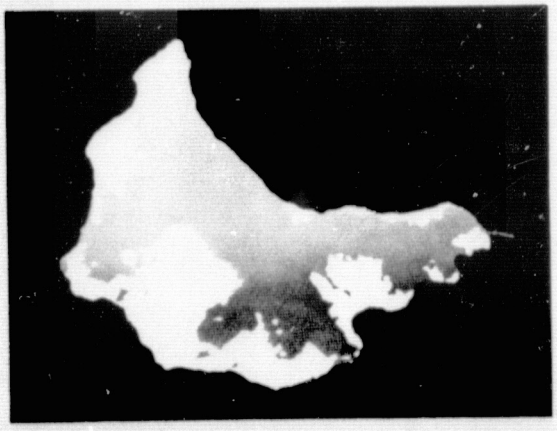
GRAY STEP 10 15.6% OF BASIN



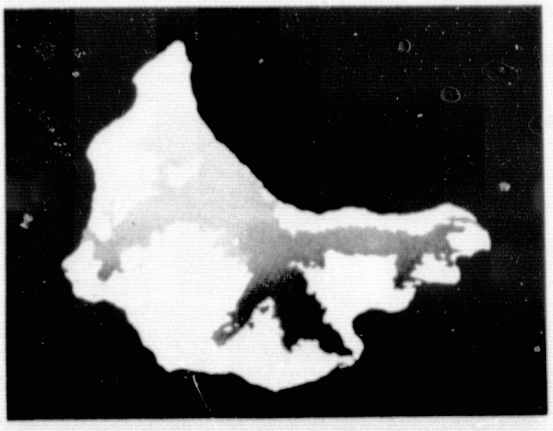
GRAY STEP 8 21.4% OF BASIN



GRAY STEP 6 31.0% OF BASIN



GRAY STEP 4 35.0% OF BASIN



GRAY STEP 2 52.5% OF BASIN

FIGURE 5 AREAL DISTRIBUTION OF BRIGHTNESS ABOVE THRESHOLD FOR 2 SEPTEMBER 1972 (BAND 5, 0.6-0.7 μ)

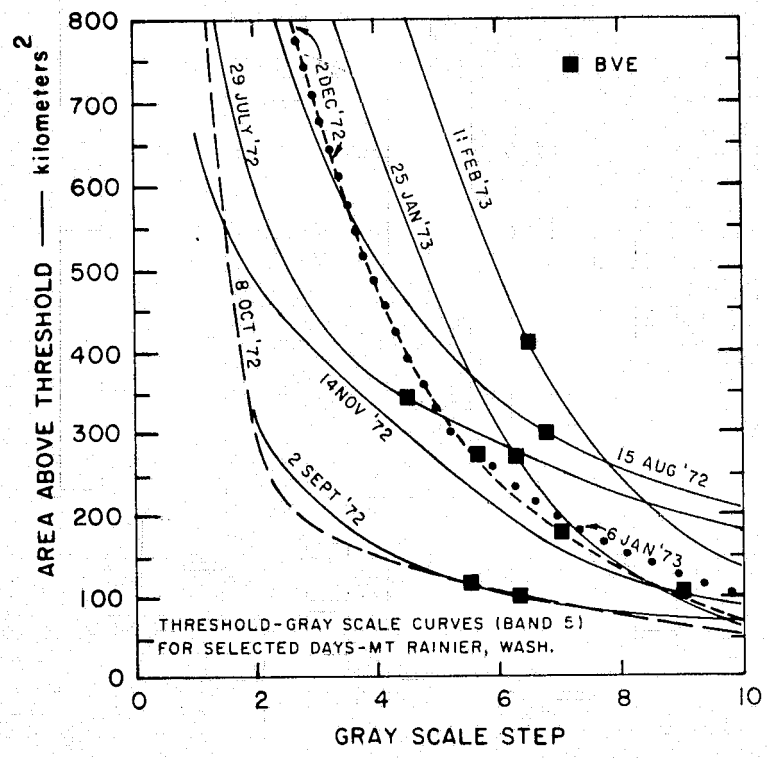
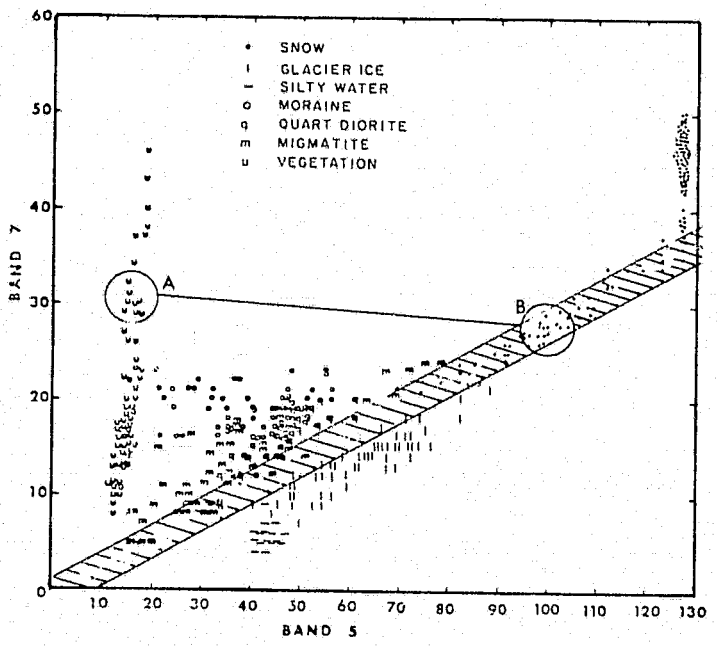


FIGURE 6 AREA VERSUS THRESHOLD LEVEL FOR NINE DATES

Region counted was 45 km diameter circle centered on Mt. Ranier. Plotted points are Best Visual Estimate (BVE) averages for two operators.



SOUTH CASCADE GLACIER 11 AUG. 73

FIGURE 7 TWO BAND RADIANCE DIAGRAM SHOWING RESPONSES FROM SNOW AND FROM RELATIVELY "PURE" PATCHES OF SELECTED COMPETING THEMES

Ratio slicing can be used to extract snow within the shaded band. Data from digital tape of LANDSAT scene 1384-18311 (11 August 1973).

THE TOTAL EARTH RESOURCES SYSTEM OF THE 1980's: A VIEW OF THE FUTURE

By Dr. Charles E. Cheeseman and David W. Keller
General Electric Space Division, Valley Forge, Pennsylvania

N76-17549

ABSTRACT

The Earth Resources Program is in a rapidly maturing phase of its development. Operational systems must soon evolve but the momentum of R&D must also be maintained. This paper considers the scope, configuration and applications of the 1980's total Earth Resources System; it addresses the questions "Where is the Earth Resources Program going?" and, "How does it get there?" A description of future remote sensing systems is provided as are some near-term goals to achieve them.

INTRODUCTION

The Earth Resources Program had its beginnings in the mid 1960's as small groups of scientists and engineers seriously began to explore how remote sensing from space could be used and how the systems to accomplish it might look. Their early efforts were based upon space photographs from the Gemini and, later, the Apollo Programs; their results implied the utility of remote sensing for future Earth Resources applications.

In 1970, the pace of the program turned sharply upward as the Earth Resources Technology Satellite (now called LANDSAT) effort began in earnest. With the launch of LANDSAT 1 in 1972 came the first repetitive multispectral data with which resource management applications and techniques could be investigated on a broad front. After two and one-half years of successful operation, LANDSAT 1 was joined in January, 1975 by its companion, LANDSAT 2, and the focus of the program began to transition from exploration to demonstration of utility.

In the early 1970's, NASA created the Earth Resources Program Office at the Johnson Space Center to provide coordination, integration, planning and review of all Earth Resources Program activities. As the program rapidly matured, one of the early realizations by the ERPO and General Electric was that a major overall planning and systems engineering study was required to give structure of future efforts and to investigate the total scope of the systems likely to be required for operational and R&D use in the 1980's.

In mid-1973, GE's Space Division, assisted by the Environmental Research Institute of Michigan, began to study the form of the future system for the ERPO with the following objectives:

- To define system performance requirements for the total operational and research Earth Resources System in the 1980's.
- To identify critical research and technology development needs.
- To define the role of Space Shuttle in the total system.

In short, this study asks, "Where are we going, how should we get there, and what role should Shuttle fulfill?"

The study was organized to address the total Earth Resources system (Figure 1) in the broadest sense: distinguishing characteristics of the resources form the input and information from user models forms the output.

The effort began with an innovative treatment of resource management requirements which traced information needs back to budgets, laws, and charters. These requirements were then used to structure a 1980's Scenario and to define thirty broad resource management missions (or applications) which could be confidently expected to be carried out by the future system. A classical systems approach was then followed to assess the current state-of-the-art, structure system requirements,

and define the necessary platforms, sensors, and ground system architecture. The study of two of the thirty resource management missions in additional detail was conducted to illuminate problems of transition from R&D to operational systems. The Space Shuttle's role in the system received special attention and a mission able to be served by an early Shuttle flight was defined.

CURRENT STATE OF THE ART

An assessment of the current state of the art was an integral part of the structuring of the future Earth Resources system, for today's technology forms the jumping off point from which the path to the 1980's must be made. The current state of the art was examined, and the results organized with the study's fundamental purpose in mind: defining the nature of the total system of the 1980's.

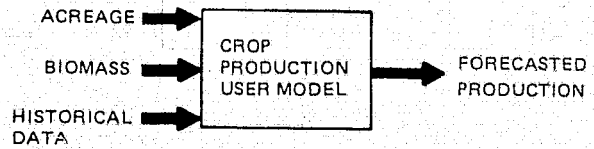
Each of the technological components of the remote sensing system was addressed in the context of the different functions of the system. And, just as importantly, the relative state of the art among these technologies was established to identify imbalances which must be corrected for smooth progress in the future.

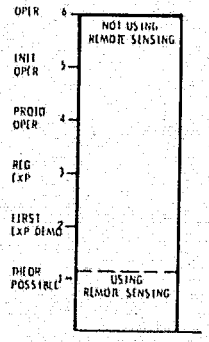
Earth Resources program activities to date have produced a capability in sensors and other flight hardware which is extremely advanced in relation to the extractive and distributive portions of the system (Figures 2 and 3). This has been proper, for the efforts to date have been exploratory in nature and data acquisition has been necessary to evaluate potential. But we are now entering an era of program maturation in which the uniform development of all system elements will be necessary to transition to operational systems. Substantial technology lags exist and must be corrected.

USER MODELS: A SYSTEM ASSESSMENT

Particular focus was placed in the User Model System element, as it is the least understood and poorest defined segment of the future system. User models are any explicit process or procedure used to transform information extracted from remotely-sensed data into a form directly useful as a resource management decision input. User models form the interface between the system and the resource managers whom it serves. A significant fraction of applications do not permit the direct use of extracted information (such as acreage) but require an additional transformation, in conjunction with ancillary data, to produce the final system output (such as a forecasted production level). User Models are thus an information interface.

Little substantive user model work is underway in the remote sensing community. The resource management specialists, on the other hand, are conducting a truly amazing amount of research into mathematical models of a wide variety of resource management processes. Alas, this research for the most part does not acknowledge the existence, much less exploit the technology of remote sensing.





- USER MODELS ARE THE BRIDGE FROM SYSTEM TO USER
- NO BROAD-BASED EFFORTS EXIST
- DEVELOPMENT AS A SYSTEM ELEMENT SHOULD BE STARTED

The development of appropriate user models should be given the same type (not to say level) of attention now afforded to sensors or any other system element, for user models are required if applications systems are to become a mature reality. But methodologies for developing user models are nonexistent. Questions arise such as "does the forcing function lie with the resource manager of NASA?" and "how should the steps of model development be synchronized with sensor or preprocessing system development?" NASA, in the near term, should select those modelling efforts which are key to significant beneficial missions and develop them in partnership with the operational users.

THE EARTH RESOURCES PROGRAM SCOPE AND INTERFACES

In historical context, the 1970 Earth Resources Program regarded its users as a relatively well-identified group of scientific investigators lodged in government, industry, and academic institution who were, for the most part with NASA funding, working to develop the bridge between remote sensing technology and the resources to be managed.

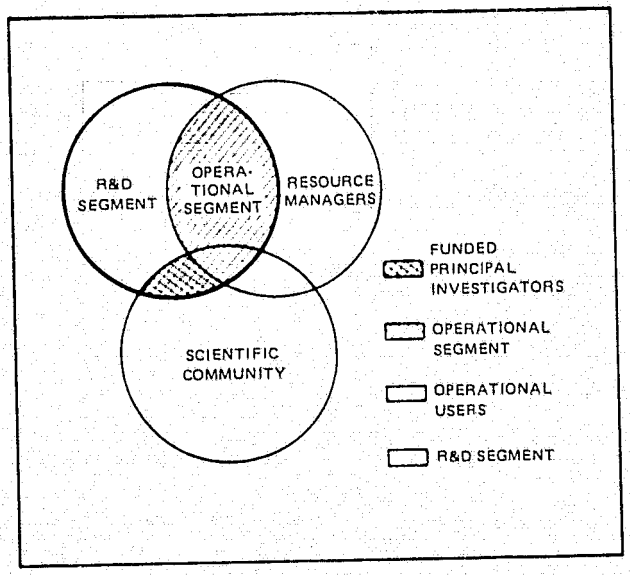
The Earth Resources Program of the 1980's will be larger in scope and, more importantly, different in substance from the program of 1970.

The 1980 Earth Resources Program, will be comprised of an R&D Segment and an Operational Segment, each interfacing with two major communities of operational users: the resource managers and the scientists.

The scope of the R&D Segment will encompass, as today, the activities necessary to develop and turn over for operational use a wide variety of sensors, flight vehicles, data processing and extraction equipment, and applications techniques. Since the program will encompass the Operational Segment, R&D on operations technology will be necessary to a degree not formerly present.

As the operationally-served market becomes more visible, the investigators are being recognized as a necessary R&D element of the program rather than an externally-served market.

The scope of the Operational Segment will encompass those activities necessary to acquire, process, and distribute the informational products of the system. The system will be serving resource managers in both the public and private sectors of our economy, in their functions of surveying, assessing and managing the exploitation of the nations' resources. In parallel, the need of the scientific community - mainly in the Earth and Life Sciences - to expand basic bodies of scientific knowledge will be satisfied.

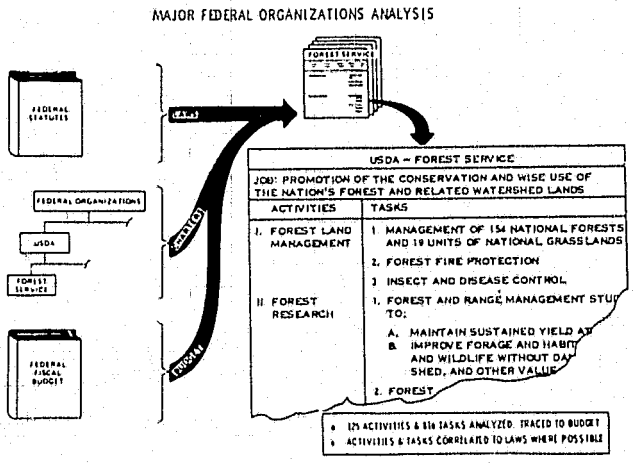


FEDERAL USER REQUIREMENTS

Five major federal organizations were analyzed to provide a set of resource management-related programs which were traceable, comprehensive, legally backed and could be analyzed in great detail for their informational requirements.

The federal organizations selected for analysis were those that are primarily involved in resource management functions:

- Department of Interior
- Department of Agriculture
- Department of Commerce's National Oceanic and Atmospheric Administration
- Environmental Protection Agency
- U.S. Army Corps of Engineers



The analysis produced results in steps of successive depth. At the top level, the missions and functions of each organization which are related to the management of resources were defined. An internally consistent set of resource management-related organization charts for the five agencies is the result. At the second level, a traceable set of activities and tasks necessary to accomplish these management functions were produced and correlated to the information classes established in the discipline analysis. And at the most detailed level, quantitative values were assigned to the information needs associated with each task. A composite is depicted in Figure 4 for all federal organizations.

The primary value of this portion of the user requirements analysis lies in its comprehensiveness and depth in defining legally based, traceable work elements related to the interdisciplinary management of a resource.

THE STATUTORY BASIS

Public demand for the products of an Earth Resources System will arise, at least in part, from an identifiable corpus of public law at the local, state, and especially national levels. The results of a survey of existing and pending legislation were used as one of the traceable elements of the information requirements analysis. Each statute was linked where possible to the specific user charter and tasks which it enables. A brief summary of the conclusions from this statutory survey follows.

Most of the statutory language on resource management is very general, and just as frequently the government agency is not directed but is merely authorized to conduct studies and surveys. Several important resource management functions, such as the activities of the Bureau of Land Management and the Geological Survey, are based upon the extremely broad language contained in the enabling legislation of those agencies. Much of the language pertaining to data collection on natural resources empowers the agency to conduct research or investigations without specifying a funding level or objectives (Soil Conservation Act, Wildlife Protection Act, Fish Resources Act). Some legislation is relatively more precise in the language used in calling for surveys, both in terms of the type of information to be collected and its frequency of collection, and some even set funding ceilings for these activities. Examples of this type of legislation are two agricultural laws, the Cotton Act and the Bankhead-Jones Farm Tenant Act, which call for regular crop acreage estimates and land inventory and monitoring.

Generally, statutory information requirements are most specific when they are tied to reports to be issued to Congress or to enforcement procedures. This latter case is at once both an obstacle and an opportunity for remote sensing data applications. The admissability of such data in court is still an unresolved issue, although there have been some encouraging signs in recent court decisions. If ERS data become generally admissible in such cases as water pollution, land use, and pesticides, the likelihood of seeing mandated ERS provisions in future legislation, particularly environmental legislation, will undoubtedly increase. Activities are underway to prepare new legislation on quite a number of environmental control and planning subjects which will generate demand for remotely-sensed information.

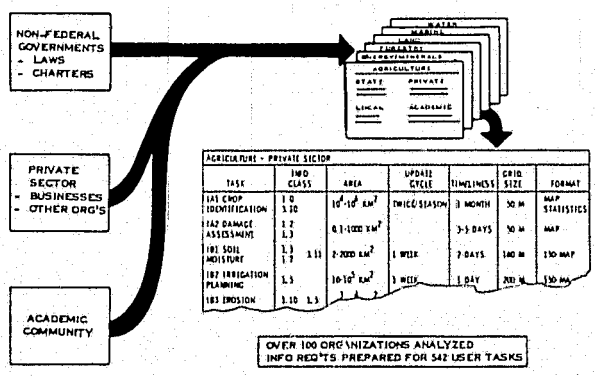
The Coastal Zone Management Act is a prototype of these bills; Land Use Planning Legislation, as yet not successfully introduced, is a near-term potential statute. Longer range, additional legislation to manage and protect the outer continental shelf out to several hundred miles can be expected.

A significant factor in future government ERS demand, indeed in private demand as well, will be the demonstration of practical feasibility of such applications as crop estimates, environmental protection, and others of a repetitive nature. If such feasibility can be convincingly demonstrated, it is quite likely that future legislation will begin to explicitly recognize ERS capabilities.

NON-FEDERAL REQUIREMENTS

A major analysis of the information requirements of non-Federal organizations was carried out to determine the potential of this little-analyzed sector. The most critical problem faced was the selection of representative organizations. As in the Federal case, the task began with the study of the jobs of each organization and relating them to information input points. Over one-hundred organizations were eventually analyzed, many with direct interviews. The results were compiled in the same format as used for the Federal organizations. Figure 5 illustrates the results of the analysis.

In the study of non-federal organizations several trends emerged. High-speed, near real-time data delivery is almost universally sought. Although the specific time period varies from several minutes for such events as forest fires and tornadoes to a day or two for insect infestation to perhaps a week or a few weeks for potential energy source surveys, the operationally-oriented users repeatedly stressed the need for rapid data delivery. This was particularly true in the private sector where the factors of "time is money" and "beat the competition" are major influences.



Many user representatives indicated that their data requirements were supplied by another organization - usually an agency of the Federal Government. Although they anticipated placing no direct requirements on the TERSSE, they strongly urged utilization of the TERSSE output by the supplying agency. In the agriculture field, for example, the vast majority of data collection and distribution is performed by the various elements of the Department of Agriculture. Users of this data indicated a need for improvements in accuracy, timeliness and global coverage.

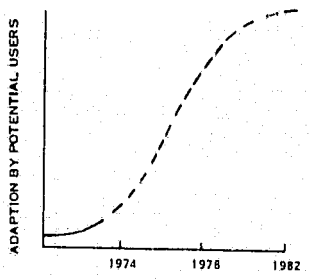
The results of this study of non-federal organizations show that the needs of this community overlap and complement those of the major Federal organizations, and that there is a significantly larger number of potential users for TERSSE data in this category than in the Federal category. Thus, the major system challenge is achieving the design flexibility and system performance necessary to serve this community.

THE PRIVATE SECTOR

Specific attention was devoted to the private sector. This user sector is at once both potentially dominating of a future system and also currently the least understood. Its involvement in the ERS Program is difficult to measure because its research is largely privately funded and thus not required to be reported. But exciting results were the product of the TERSSE study team interviews and assessment of this sector.

The private sector's primary motivations spring from its need to achieve an acceptable rate of return on invested capital. As a result, the early years of remote sensing from space saw little private interest and virtually no privately-financed participation. But that is now changing.

We are currently at an ER program turning point with regard to private sector involvement. A small percentage of private users are now aware of and working with LANDSAT and Skylab data. These aware users are the leaders; they are motivated and enthusiastic. They have demonstrated their capability to evaluate ERS data utility and have, in many cases, instituted application of ERS products without NASA funding. (Indeed, they are spending significant sums for data products and analysis services.) The uncertainties of program continuity was the most-often-cited non-technical reason for hesitancy and the resulting inference is that additional program flights will strongly increase private sector commitment and demand.



The utilization of ERS data by the private sector is following a typical S-shaped acceptance curve, with the current position lying at the initial upturn. TERSSE team interviews indicate that several system improvements (over LANDSAT 1 and 2) are required: increased timeliness, more processed information and less data, and more rapid coverage by better sensors. System improvements in repeat cycle, timeliness, and multispectral resolution, would contribute to private sector acceptance.

Much of the private sector traditionally receives (and expects to continue to receive) information from government agencies. And such will be the case with a significant fraction of TERSSE users. But private concerns who are aware of and using ERS data are, in many cases, making significant outlays for data products. Extrapolation of these outlays to include a high acceptance by the private sector indicates that major system operating revenues could be derived from the private sector if ERS acceptance is obtained through program continuity and system improvement.

THE 1980's MISSIONS

Missions: Statements of Purpose

Resources management missions are the objective of the total Earth resources system. A fundamental question addressed in the study was, "what missions can we expect the future systems to be capable of ?" We assessed in combination the potential of remote sensing, user information needs, and the current state-of-the-art. The result, when combined with the 1980's scenario, led to a set of top-level resource management missions (Figure 6) which are needed and which can be expected to be performed by 1980's systems.

Their form is that of broad descriptions of activities which lead to the production of information useful in the management of a resource. They have been organized according to the resource to be managed. They each embody many Earth and Life Sciences disciplines and they each serve many types and classes of operational user organizations.

The Linking of Specific User Jobs

The management of a particular resource is carried out by a collection of resource managers, each with a different individual purpose and charter, and each playing a different role in the economic or political forces brought to bear on it. In most situations, these organizations or individuals work in concert with each other while fulfilling their extractive, productive, distributive, or replenishing resource function. And in most cases it is necessary to understand these interrelationships in order to define a system to serve them usefully.

Specificity has been added to the mission statements by the assignment of detailed user tasks to each. These tasks are, in the Federal and State government cases, traceable to laws, charters, and budgets. In all cases, the assigned tasks are traceable to the analysis of user information and product requirements.

The resulting mission descriptions are thus broad statements of purpose to which have been linked specific statutorily-based or traditional user tasks in the Federal and non-Federal government, private, and academic sectors.

SYSTEM REQUIREMENTS

The central question of the study was, "What is the form of the total Earth Resources System of the 1980's?" This system will be made up of multiple platforms and sensors serving many users through a multi-path ground system. The approach to defining the system's form began with the definition of specific mission requirements for each of the thirty identified missions and their associated user tasks. Conceptual configurations were then synthesized and evaluated against performance requirements in three major areas:

- Platforms
- Sensors
- Ground Systems

A total system architecture was the final result. It illustrates the complementary roles of the several data acquisition platforms and their associated sensors; it defines the information flow through the system to each of the users in terms of the processing types, timeliness required, and output product. And, since it is neither fiscally nor technically possible to simultaneously implement all thirty missions (or applications), the overall system architecture has been configured to permit incremented implementation of specific missions as they become economically beneficial and technically feasible.

Specifying the functional requirement for each of the thirty missions and their associated user tasks was the first step in the system definition process. Major system functions were structured into an end-to-end flow which reflects the acquisition of the data and its successive transformation into operationally useful resource management information products. It is critical in such a flow to acknowledge not only the functions performed at each step in the flow (such as rotation to a geographically based grid) but also to identify ancillary data necessary to the flow and the point where it enters.

A set of system requirements for each of the missions was then derived. Aggregations of the requirement data are illustrated in Figure 7.

An important conclusion from this data concerning the so-called "one-time user" resulted; while a significant number of user tasks fell into the one-time category (approximately 20 percent) the majority of them belong to a class of tasks that are recurring in nature. The result is a continuous queue of one-time tasks which should be continually serviced.

THE PLATFORMS

No single type of observation platform can satisfy the range of requirements of the 1980's system. Differences in resolution capabilities, response time, repeat cycle, solar illumination, and the related cost-effectiveness of varying types of performance will lead to the use of multiple types of platforms. A set of seven was derived to satisfy the mission requirements (Figure 8). This set comprises the necessary building blocks to satisfy any combination of the thirty TERSSE missions (Figure 9).

Included are the:

- Earth synchronous satellite: capable of rapid response, and flexible acquisition of data for applications with critical timeliness requirements.
- Three types of Sun synchronous satellite: The systematic surveyors, capable of repetitive surveys requiring global coverage with relatively constant lighting.
- Shuttle Sortie: A platform capable of tailored orbit's lighting, and coverage cycles useful for infrequent coverage.
- Non-Sun-synchronous satellite: A polar satellite whose nodal crossing time is tuned to provide varying lighting angles or to coincide with other Earth rhythms such as tides.
- Aircraft: The most flexible platform, capable of extremely high resolution; and useful for regional applications.

The final platform assignments to the thirty missions result in several conclusions. Most important is the fact that applications with the breadth of the TERSSE missions need the advantages of several platforms operating in concert. Some systems will also require multiple platforms of a single type to be properly accomplished. A second conclusion reached is that the non-Sun-synchronous platform is by far the most useful single platform type. But it will be so only if there are many versions of the type with orbits and repeat cycles tailored to individual applications. And a final conclusion results from consideration of implementation phasing and program evolution: although the TERSSE platform assignments may be the ultimate means to implement entire missions, this does not indicate that other platforms should be ignored in the transition period to full maturity.

DATA DISSEMINATION

The ground system is the interface between the collection system (remote sensing platforms and sensors) and the user community. Existing systems are adequate for the present needs because these needs are experimental, or R/D, in nature. The present need is for a thorough, broadly-oriented analysis of relatively limited quantities of data. This is in contrast to the needs of the TERSSE timeframe, where the users will be operational, requiring the routine and timely handling of large quantities of data (each for more narrowly-oriented use). The range of issues addressed in considering the ground system are shown below.

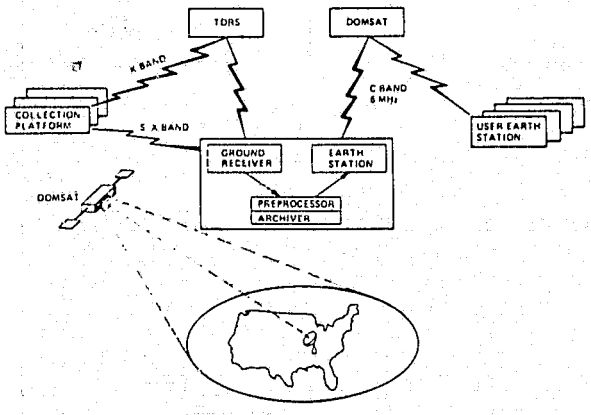
In order to select a ground system concept which would be responsive to future R&D and operational needs, nine alternative ground system configurations were postulated and evaluated using thirteen specific criteria. The nine concepts considered ranged from a fully-centralized to a highly decentralized and physically-distributed multiple center concept. The concept selected as best serving all 30 TERSSE resource management missions, shown in Figure 10, is a hierarchial architecture with distributed extractive processing and centralized preprocessing.

The architectural structure of the TERSSE ground system is mission-tailored and parallels the users' organizational structures. Some users are organizationally centralized (e.g., for World Crop Survey). However, most users exist as a decentralized and geographically-distributed network, even

in those with heavy Federal involvement. This characteristic leads to the recommended TERSSE ground system concept of lead Federal facilities with distributed systems branches and outlets located in the facilities of the distributed operational users. The majority of applications will evolve to require standard output products, routinely issued in user-oriented formats. On the other hand, some applications are by their very nature ad hoc; their output products will not be standard and will require greater flexibility in the user interface. The users' terminal equipment will range from simple read-only devices to full-capability interactive extractive processing equipment.

The Use of DOMSATS

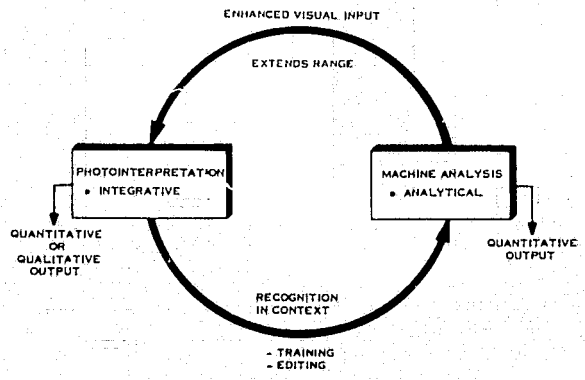
The combination of plummeting channel costs and the advent of low-cost Earth stations make the feasibility of multi-point extractive processing an attractive possibility. Total coverage of the United States is possible with a single DOMSAT channel; this will allow the placement of subscribers and their extractive processors at convenient geographic locations.



The TERSSE ground system architecture utilizes this DOMSAT capability to redistribute remotely sensed data to the several Information Analysis Centers after it has been preprocessed and archived at a single national center.

Machine Analysis and Photointerpretation

Photointerpretation uses the integrative and pattern recognition powers of the human. Automated machine analysis uses the rapid quantitative and analytical capability of digital computers. These two techniques for extractive processing can and should be combined into an integrated approach which synergistically utilizes the natural features of each.



This situation is well suited for a time shared interactive man/machine system which can iterate rapidly between the two modes. But, for fuller use of the man/machine capabilities, better display capabilities are required in future systems.

THE TOTAL SYSTEM

The broad scope and wide diversity of potential uses and missions of remote sensing in the 1980's cannot be effectively served by a single system. Rather, the Earth Resources Program of the Shuttle time frame will be composed of several relatively independent systems each with more restricted disciplinary objectives and scope than LANDSAT or Skylab. The future systems will be more like current NOAA and DOD programs which, because of their precise scope, are able to be justified, designed, and implemented with a high degree of benefit and satisfaction on the part of the served community. The future ER systems will also differ from today's R&D systems by their necessary implementation as a total, end-to-end process.

Considering each of the missions singularly, there is a remote sensing portion and a ground portion which, together, represent the "system" for each mission. For the example shown in Figure 11 (Survey and Inventory of Ground Water for Urban and Agricultural Consumption) the four platforms and their remote sensors feed the ground system. This example shows the specific data and information flow including the processing and in situ data required.

The Lead Mission Concept of System Evolution

TERSSE is the sum of 30 separate systems each with different requirements and serving different users who have various degrees of readiness for the operational use of remote sensing. The implementation of TERSSE must recognize and take advantage of these differences instead of attempting a one time implementation of a singular "super system" that will serve all. The approach which takes these differences into account is the "Lead Mission Concept."

Simply stated, the Lead Mission Concept stipulates that a specific earth resources management mission will be selected and the "system" for implementing it will be developed. As this specific mission's requirements are satisfied, the requirements for other (generally similar or related) resource management missions will be satisfied with little or no change to the specific system of the "lead" mission. It is through this process of selecting lead missions and implementing their systems that the entire TERSSE will eventually evolve.

This concept focuses the system design and operation on critical system development steps and the implementation of cost effective solutions for promising missions. At the same time, the concept provides data to a maximum number of other emerging applications and missions. Thus, the Lead Mission Concept of system evolution will serve as the bridge between the exploratory investigation and the operational application of remote sensing to a resource management mission.

The selection of a particular resource management mission as a lead mission involves the consideration of four factors: benefits, users, technical, and ER Program. The benefits factor indicates that a lead mission should have a major identified benefits potential. The benefits can include both economic and social components and can be either national or global in scope. The user factor indicates that the user organization must be clearly identified and must be willing to actively support the mission. The general public awareness of the user and his mission is also an influencing element of this factor.

The technical factor indicates that the necessary system developments are both identified and feasible. A clear plan for implementing the system should be available which builds upon the existing technology in a logical manner. The ER Program factor is an indication of the synergism that will accrue to the entire program from the particular lead mission under consideration. The capability for spinning off data useful to a maximum number of other applications that will produce widely applicable ERS advances should be considered.

TWO CANDIDATE LEAD MISSIONS

One of the major conclusions reached early in the study was that the Earth Resources Program must position itself in the near future to solve the very difficult problems associated with bringing to operational use those missions identified as cost/beneficial and technically feasible. A part of this process is the development of an understanding of the form and function of a system designed to perform an operational mission. With this in mind, two of the thirty TERSSE missions were selected for more detailed study.

In question were the detailed resource manager (user) functions, their current methods of performing their function, the information flows and information requirements embodied in their function and the characteristics of the observation system which would, in the future, assist in the management of the resource involved.

The two missions selected for study were (1) World Crop Survey and (2) Land Resources Management. These missions represent opposite ends of the TERSSE spectrum in several regards. The World Crop Survey Mission is fundamentally a polar satellite job, while the more fragmented Land Resource Management tasks are best suited to Shuttle Sortie flights and aircraft, augmented by the contextual overview of the polar spacecraft.

The World Crop Survey mission is primarily involved with aggregating a large number of information segments (i.e., field contents) into a few global answers distributed via a very few users. The Land Resources Management mission, on the other hand, has value primarily in its devotion to identification, classification, and location of many single cells of homogeneous use of interest and preserving the essential granularity of such information. It serves a multiplicity of resource managers requiring widely-varying product formats and contents.

As a consequence of this polarity, the two case studies provide more than just a detailed examination of the nature of two primary TERSSE missions. They also jointly serve as a strong reinforcement to the conclusions that different missions require different systems and that each mission must be analyzed in its entirety early in the development process to permit proper system development decisions.

World Crop Survey

Significant attention has been given recently to the economic and social benefit which would accrue from an increase in the accuracy and timeliness of crop forecasts. But substantial questions need to be answered concerning the performance of the system which is to produce such increases.

Our study of the World Crop Survey mission leads to the conclusion that the existing format and distribution methods for USDA crop reports are entirely satisfactory to the users of such data. What is needed is an improvement from 80-85% accuracy to 95% or better in foreign crop data, particularly production forecasts. Also, an increase in the timeliness of such data on the order of six months is needed, with a monthly update cycle.

To effect this improvement will require advances in several areas over the current LANDSATs 1 and 2. The system must insure that two looks per monthly reporting period are obtained in active growth periods (which are occurring for some crop in some location almost constantly). This requirement, when combined with cloud-cover limitations, leads to a seven or eight-day orbital repeat cycle for the polar spacecraft.

A major improvement in data processing productivity and efficiency is needed. A timeliness of 48 hours from overflight to acreage estimate is necessary if the data gathered in two "looks" per reporting period is to be used 90% of the time.

With regard to spatial resolution, the major effect of increased resolution is to include smaller fields in the data sample, as aggregated acreage accuracies are entirely adequate on a global basis with relatively poor resolution. Analysis of Skylab S190B data suggests that fields as small as 8 hectares (20 acres) must be recognizable. Thus, while the 80-meter IFOV of LANDSATs 1 and 2 is adequate for demonstration, an improvement to 40-50 meter IFOV is recommended to include smaller fields in the data sample for an operational system.

Land Resources Management

Land resources management is not really a single mission (nor even a few missions). It is rather a complex set of missions, in which informational requirements, and hence output products, depend on several factors: the specific management decision to be made, the use being considered for the land, and the geographic extent over which the decision is to be made. A large number of

agencies and organizations are involved in land management planning and decisions. Many of these problems or decisions are one-time or very infrequently made and they are best addressed on an 'ad-hoc' basis. A single optimized system solution is not feasible. Rather, each operational problem should be addressed in an individual way, with small groups of related problems (for example, the same decision in several different cities) being treated in parallel.

Although different land resource management problems have different information requirements, generalizations can be made concerning the remote sensing platforms and sensors to be used. All of the land missions have relatively long periods of time between required data updates. Annual data updates would be extraordinary to this user community; they currently work with updates every ten years, and even that is not always feasible.

Because of the detail needed, land resource management agencies will continue to require remotely sensed data of very high resolution, say IFOV's of one to twenty meters.

Major output products for all these missions are maps and map overlays. This is the data presentation medium with which the majority of users are accustomed to working. However, most users, as well, will in the future require a fully-digital data base in which all basic information is included to permit simple compilation, rapid accessibility, and flexible updating of the vast array of statistical data required.

The foregoing set of general requirements lead to the conclusion that the ad hoc land resource missions are best served by the Shuttle Sortie and high-altitude aircraft carrying both film cameras and multispectral scanners. A contextual overview should be provided by polar satellites.

CONCLUSIONS: A 1980's SCENARIO

NASA's 1980's Earth Resources Program

NASA-sponsored research will have passed through the intensive search of the 1970's for initial useful applications and study of multi-spectral analysis techniques. It will be entering a new phase where much higher level mathematics, coupled with new computational technology, sensor sophistication, and the increased use of external data will be under investigation to provide much greater detail about the dynamics of resources. Use of remote sensing inputs to models will be common.

Significant new sensor and applications advances will have been made through the flight of LANDSAT-3, Nimbus VII, and subsequent conventionally launched polar spacecraft flights. Microwave sensing, both active and passive, will be mature system elements. A second generation of land, water, and atmospheric pollution sensors will be flight-ready.

The first relatively simple shuttle sorties will have flown, demonstrating the utility of this flight mode for sensor development. The role of the scientist/astronaut in such flights will have been relatively primitive but the experience gained will have established the basis for extension of crew involvement into higher order tasks such as onboard data analysis.

Preparation for the use of the sortie flight mode in a quick reaction surveillance mode will be underway and a standard "piggy-back" package for use on nearly all flights will have been developed and be in use.

The development of a synchronous satellite capability for moderately high resolution (approx. 50-100m) will be underway to demonstrate the utility of this system element and to establish the operations technology necessary for its conversion to operational use.

The use of prototype projects to perform final development of a system segment will be in widespread use. New operational improvements will be added in complete sections, including platform, sensors, ground processing techniques and equipment, user models, and operations procedures. Substantial involvement by the receiving agency will be present.

The Operational Segment

A Federal Government agency will have operated an initial LANDSAT-based operational system for several years, gaining the experience necessary to assimilate new technology and to effect a major expansion of this system. The areas of expansion will include both increases in the number of Federal bureau "subscribers" and also more formal and extensive services to the private sector, state, regional, and local government bureaus.

The expanded operational system will include several polar-orbiting spacecraft with different orbital repeat cycles and ascending node times which will be tailored to the system users' requirements.

A substantial fleet of long-range, high-performance aircraft will be owned and/or operated by a Federal Agency in much the same fashion as the agency operates the polar and geosynchronous satellite system segments. The aircraft will be optimally based throughout the U.S. and other territories of interest using existing airport facilities where feasible. These aircraft will be used not only for operational data collection where they are economically superior to satellites but also as elements in prototype projects. NASA and other agencies will continue to operate specialized aircraft for sensor and applications development and for use in ptototype projects not requiring large fleet sizes.

A hierarchy of ground facilities will have been set up for operational data handling. Major Federal facilities will be owned and operated by several Federal users. Such Federal users will also be chartered to perform preprocessing, extractive processing and distribution to designated state, regional, and local government users. Other users will establish this capability independently in cases where special requirements dictate.

A tracking and data relay satellite system will be operating in cooperation with multiple polar-orbiting spacecraft to relay high-rate data to U.S. ground station . An increased capacity version of the spacecraft will have been designed for launch by the shuttle and tug.

Near-Term Steps

To realize the progress, significant action is called for on a broad front. We must recognize that different operational missions will require different systems for their implementation . We must learn to single out these lead missions and develop total applications packages which demonstrate the technology and economic benefits of the systems they precede.

In the area of technology development, signature extension over larger geographical areas is critical to the large-area survey missions in order that the time and cost of training classifiers can be cut. Visible and infrared scanners need steady progress toward improved spectral and spatial resolution. And a new community of users must be served by collection of simultaneous film and electronic at 10-20 meter resolutions in the 1980's. Microwave sensing over the ocean is relatively advanced; but the need is great for a high-resolution radar specifically designed for use over land. In the area of data processing, we must develop a user-tailored approach to gridding and superimposing data from different types of sensors taken at different times from different orbits or flight lines. Manual analysis and machine analysis must be further combined in their synergistic forms. And the technology coming into being in the form of domestic communications satellites and large data bases must be exploited.

User models must receive more attention, for they are the bridge between the remote sensing system and the resource manager. And our ability to operate complex, multi-platform systems must be increased in parallel with the development of such systems.

The 1980's systems will enter the decade with the momentum of three and possibly four LANDSAT's behind them. They will have new, improved sensors and ground techniques on which to rely. And those systems will have the Space Shuttle for both low-cost satellite placement and as an orbiting laboratory from which to conduct R&D. The next few years will cast the die from which the 1980's total Earth Resources System will be struck. Major challenges exist but, with vigorous effort, the 1980's systems will produce tangible economic benefits and serve man globally.

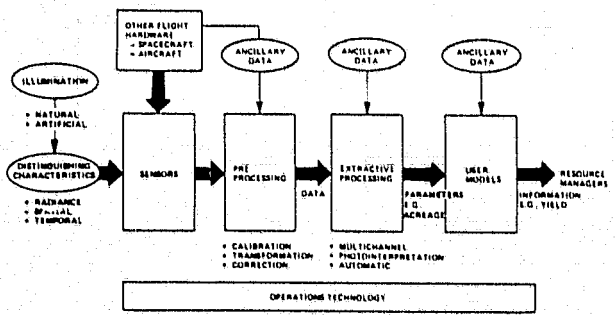


Figure 1. Total Earth Resources System

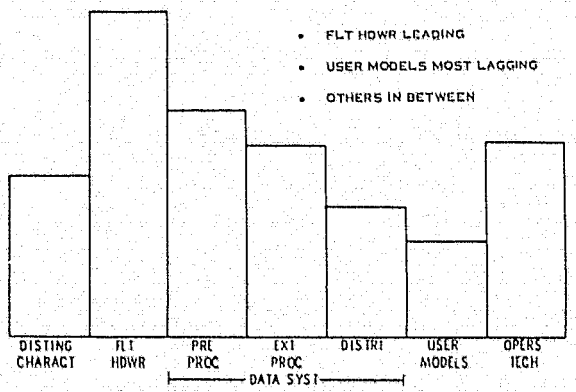
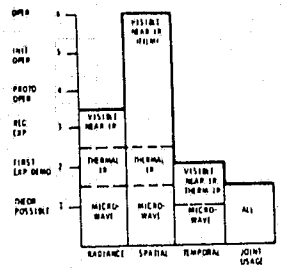


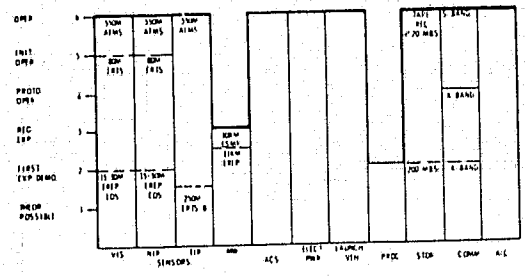
Figure 2. Top Level System State-of-the-Art

DISTINGUISHING CHARACTERISTICS



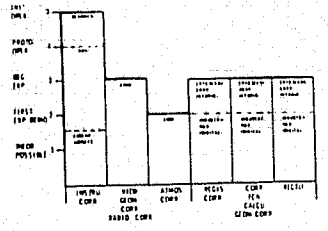
- WITH EXCEPTION OF RADIANCE/SPATIAL IN VISIBLE AND NEAR IR, TECHNOLOGY NOT WELL DEVELOPED
- JOINT USAGE HOLDS GREAT PROMISE BUT FEW STUDIES IN THIS AREA
- DEVELOPMENT AND MEASUREMENT EFFORTS WILL CONTINUE TO BE HAMPERED BY THE ATMOSPHERE

FLIGHT HARDWARE



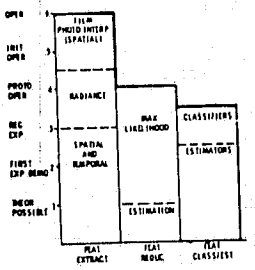
- SENSORS–NO MAJOR BREAKTHROUGH STEADY PROGRESSION OF TECHNOLOGY, MICROWAVE LAGGING OTHER PORTION OF SPECTRUM
- ACS, ELECT PWR, A/C AND LAUNCH VEHICLES NOT LIMITING
- ON-BOARD PROCESSING IN ITS INFANCY
- X-BAND COMM DEVELOPMENT PROGRESSING TOWARD 10^3 MBPS

DATA PRE-PROCESSING



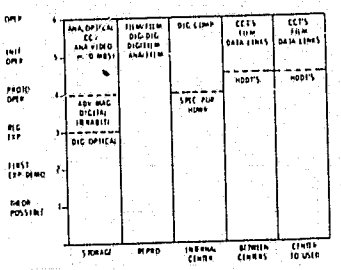
- RADIOMETRIC CORRECTION IMPLEMENTATION IN PRODUCTION ENVIRONMENT NOW FEASIBLE
- SUB-PIXEL GEOMETRIC ACCURACIES ACHIEVABLE USING NEW INTERPOLATION TECHNIQUES
- CORRECTION OF ALL DATA TO SAME REFERENCE GRID IS REQUIRED
- SPEED/ACCURACY IS LIMITATION. REQUIRES SPECIAL PURPOSE HARDWARE

EXTRACTIVE DATA PROCESSING



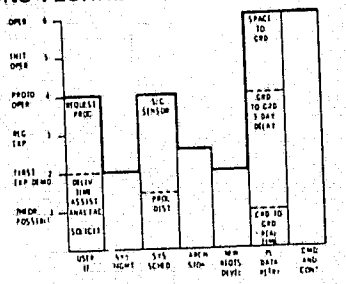
- BASIC QUESTIONS: WHAT CHARACTERISTICS ARE TO BE PROCESSED; WHAT PARAMETERS NEEDED FOR RESOURCE MANAGEMENT ARE DESIRED AS OUTPUTS?
- DIGITAL PROCESSING USING COMBINATIONS OF GP AND SP HARDWARE IS SOLUTION TO CURRENT SPEED/ACCURACY PROBLEMS

DATA STORAGE/REPRODUCTION/DISTRIBUTION



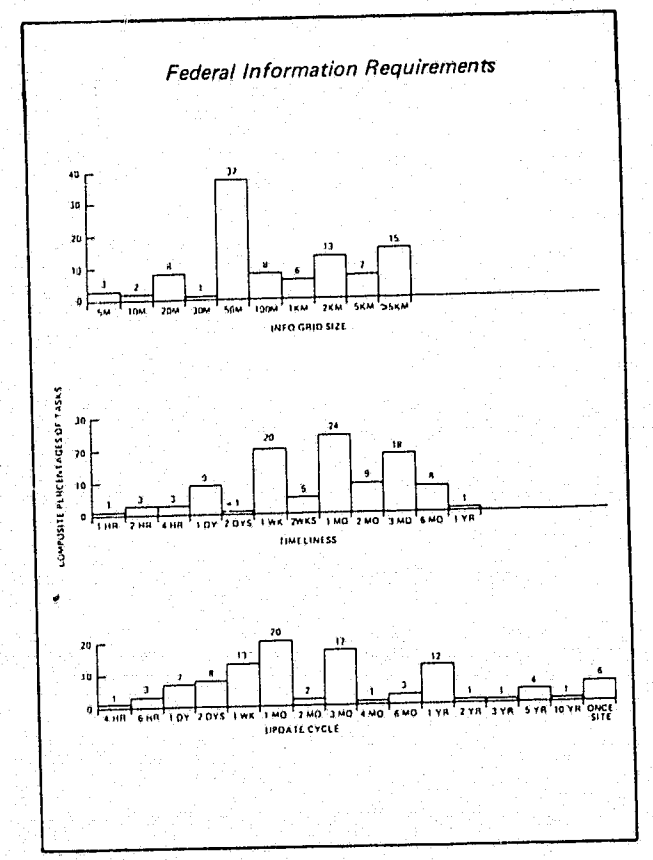
- DATA STORAGE NEED IS A NEW STANDARD HIGH DENSITY, READY ACCESS, COMPUTER COMPATIBLE STORAGE MEDIUM
- MAJOR REPRODUCTION QUESTION: WHAT ARRAY OF PRODUCTS ARE NEEDED? CURRENT SOA IS NOT TECHNOLOGY LIMITING
- TIMELY BULK DATA TRANSFER BETWEEN CENTERS NEEDS DEVELOPMENT

OPERATIONS TECHNOLOGY



- HARDWARE/SOFTWARE IS NOT TECHNOLOGY LIMITING
- MAJOR ADVANCE IS NEEDED IN CONCEPTS, PHILOSOPHY AND APPROACH TO THE OPERATION AND MANAGEMENT OF LARGE MULTI-ELEMENT EARTH RESOURCES SYSTEMS

Figure 3. System Element State-of-the-Art



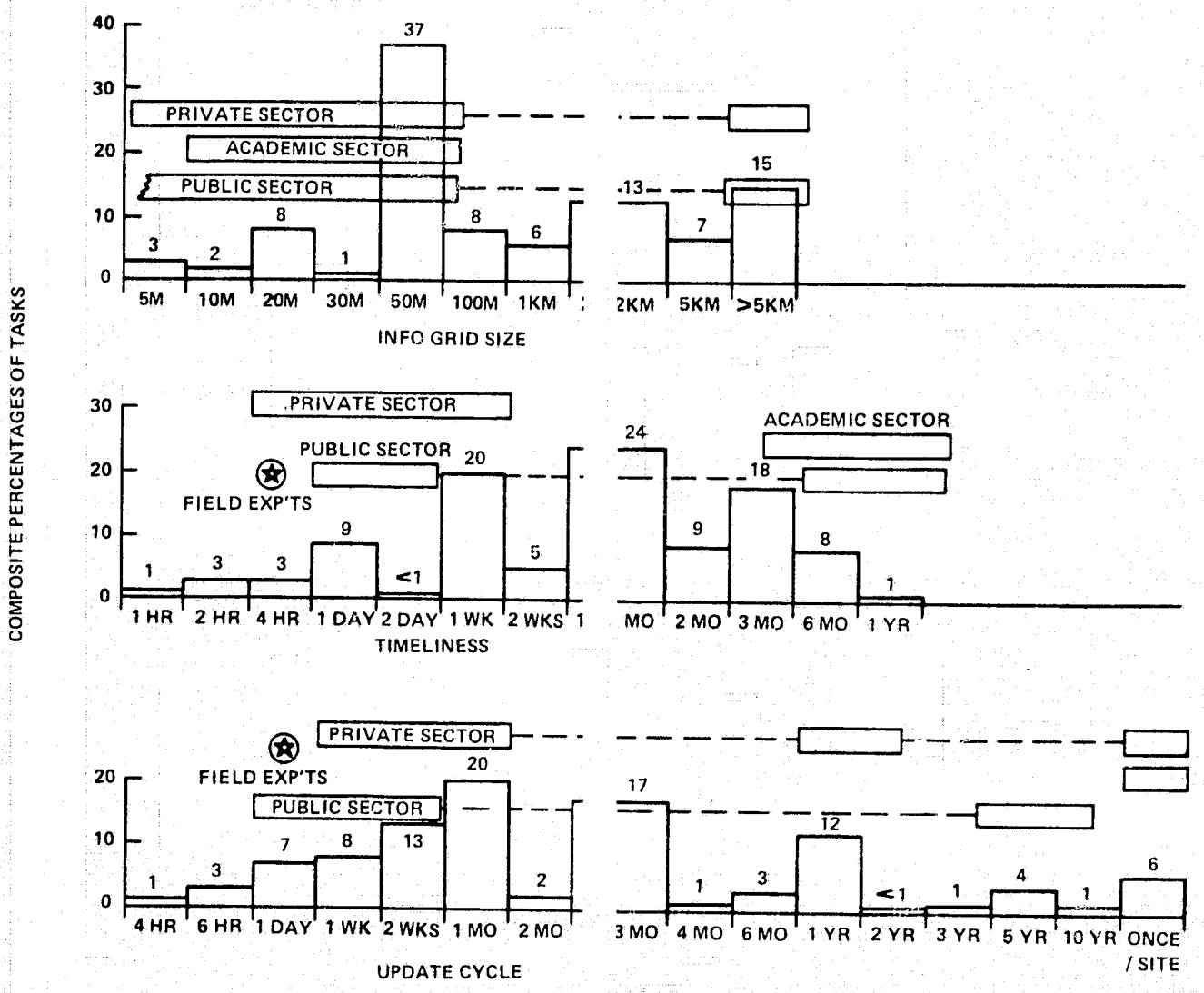
– SOME CONCLUSIONS –

- MANAGEMENT OF NEARLY EVERY RESOURCE IS SOMEONE'S STATUTORY RESPONSIBILITY, BUT THE QUALITY AND LEVEL OF MANAGEMENT VARIES WIDELY.
- THE "BUREAUCRATIC RHYTHM" OF THE CALENDAR DOMINATES THE CYCLIC NEED FOR INFORMATION, E.G., 7, 14, 30, 90 DAYS
- THE FEDERAL ORGANIZATIONS ARE THE "AGGREGATORS" OF RESOURCE INFORMATION AND SERVE A WIDE RANGE OF SECOND-TIER USERS.
- A SIGNIFICANT NUMBER OF EMERGING STATUTORY REQUIREMENTS RELATED TO ENVIRONMENT AND PLANNING WILL CREATE NEW DEMAND FOR REMOTELY-SENSED INFORMATION IN THE NEXT FIVE YEARS.

Figure 4. Federal Information Requirements

COMPOSITE FEDERAL AND NON-FEDERAL REQUIREMENTS

The unweighted non-Federal requirements are superimposed below on the previously described Federal requirements to illustrate the areas of commonality and difference. The non-Federal requirements are not given a vertical dimension, as the demand relative to the Federal sector was not estimated.



- MAJOR NEED EXISTS FOR RAPID DATA BY OPERATING MANAGERS
- SUBSTANTIAL REQUIREMENT FOR LARGE-SCALE DATA; MANY SUCH USERS, FAMILIAR WITH THEIR AREA OF CONCERN, DO NOT NEED GEOMETRIC PRECISION
- PRIVATE SECTOR PROPRIETY IS A CRITICAL REQUIREMENT
- MANY PRIVATE USERS EXPECT DATA FROM STATE AND FEDERAL GOVERNMENTS.

Figure 5. Composite Federal and Non-Federal Requirements

WHAT WE CAN EXPECT OF THE 1980's SYSTEMS

AGRICULTURE

- Survey U.S. cropland to prepare statistical summaries and production forecasts for major crops.
- Monitor U.S. pasture and cropland to detect and assess insect, disease, and stress damage.
- Survey U.S. cropland to evaluate current farming practices and classify areas on the basis of productivity.
- Survey and monitor U.S. cropland to calculate short-and-long-run demand for irrigation water.
- Survey major crops on a global basis to inventory acreage and forecast world production.
- Survey pasture and range areas to prepare statistical summaries of forage acreages, calculate supportive capacity for livestock, and assess current grazing practices.

ENERGY/MINERALS

- Survey geological features to detect sites indicative of the location of mineral deposits.
- Survey surficial thermal patterns to detect potential geothermal sources.
- Survey waters of outer continental shelf areas to detect oil film possibly indicative of submarine oil deposits.
- Monitor surface mining and oil drilling operations to detect resultant environmental pollution.
- Monitor oil and gas pipelines to detect breaks or other environmental dynamics.
- Monitor deepwater ports to detect and assess oil pollution.
- Monitor powerplant operations to detect and assess thermal pollution in adjacent waters.

FOREST

- Survey and monitor forestland to prepare forecasts of timber production, classify areas according to productive status, and assess the efficiency and ecological soundness of timber production and harvesting operations.
- Monitor forests and grassland/brushland areas to detect and assess insect, disease, and stress damage.
- Survey and monitor forests and grassland/brushland areas to assess fire potential, detect the outbreak of fire, assess the dynamics of fire, and assess damage.

LAND

- Survey and map current land use patterns within the U.S. in support of State land use planning and the management of Federal lands.
- Survey and map the vegetation, landforms, topography, geology, and soil of the U.S. land area.
- Continuously survey lake and coastal shoreline morphology and the navigational channels within the coastal zone in support of shipping and recreation.
- Survey, identify, and map the location of geological hazards over the U.S. land area.
- Survey the U.S. flood plain areas and identify and assess potential flood hazard areas.

MARINE

- Survey and map the physical and chemical properties of the global oceans for optimum ship track routing, drilling operations, and other open ocean operations.
- Monitor and assess those dynamic processes of the ocean potentially harnessable as sources of energy.
- Survey and map the distribution and quantity of commercial and sport fish species in U.S. coastal and off-shore waters, their food supplies, and other environmental factors necessary to predict future catches.
- Monitor the health of the global oceans by surveying the source, distribution and movement of the main pollutants in the marine environment, and marine organisms.
- Survey and monitor hazards to navigation on the high seas, such as sea ice, icebergs, and severe wave conditions.

WATER

- Survey and inventory the volume and distribution of surface and ground water to assess available supplies for urban, agricultural, and hydroelectric consumption.
- Survey and map Great Lakes ice cover and type to determine the passibility of navigational channels, optimum routing of lake shipping, and port accessibility.
- Survey and monitor quality surface water throughout the U.S. and surrounding coastal zones with particular attention to lake eutrophication and sources of water pollution.
- Survey and monitor surface water, snow cover, glaciers, and ground water levels and movement to identify potential flood conditions and to trace the movement of floodwaters.
- Survey and monitor the surface water volume and indicator species of vegetation in wetlands and estuaries to evaluate the ecological productivity of wetland areas.

Figure 6. What We Can Expect of the 1980's Systems

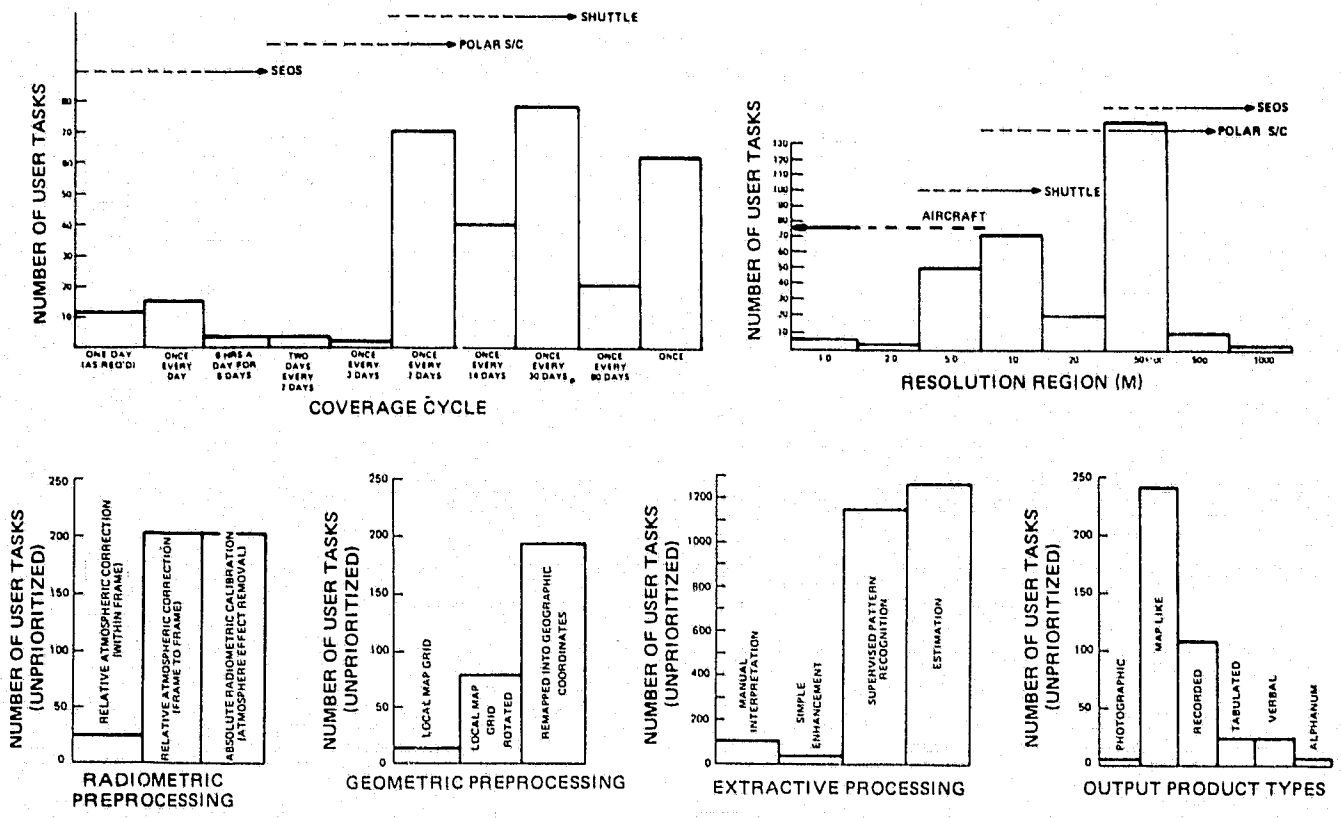


Figure 7. Typical Requirements Aggregations

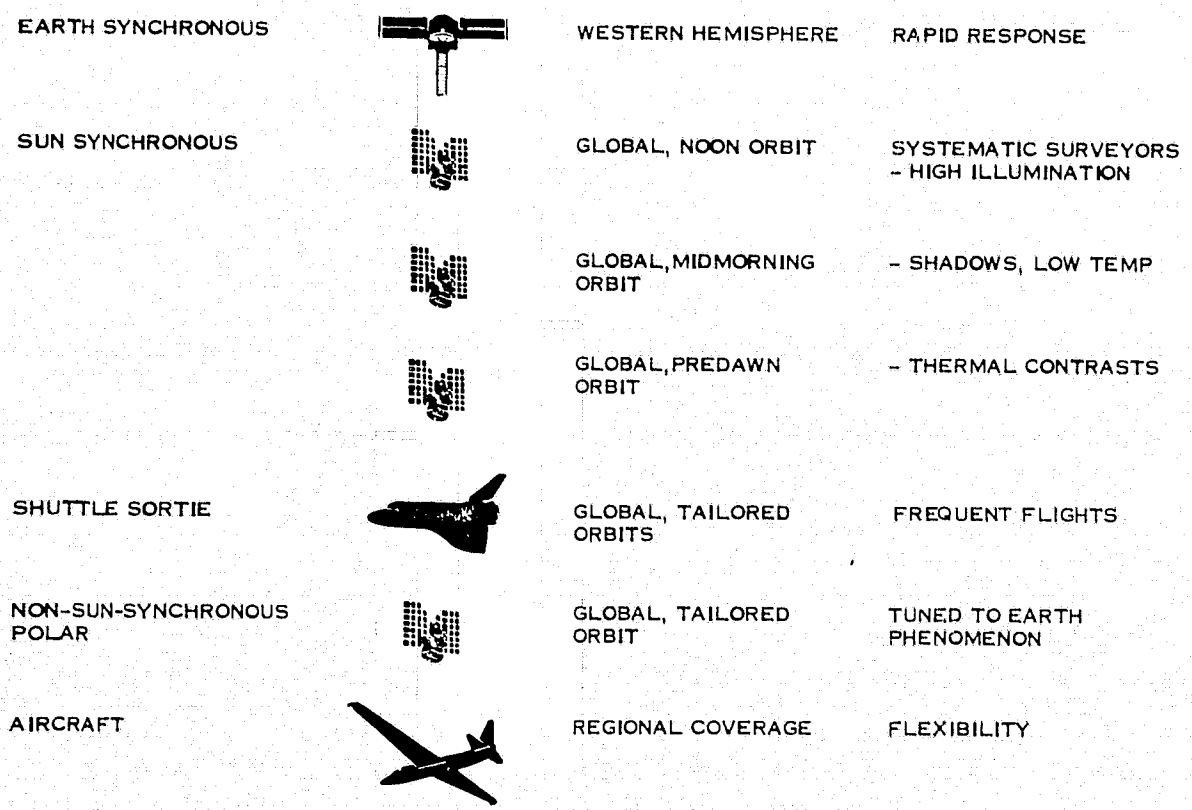
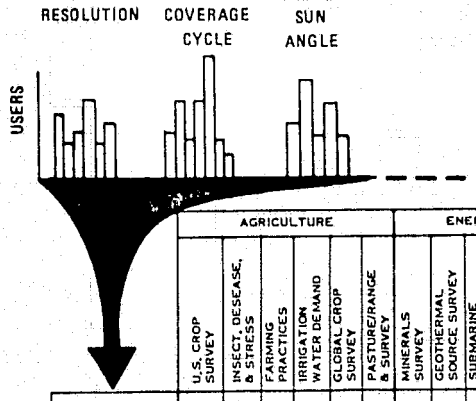


Figure 8. Seven Basic Platform Types



- SEVEN BASIC PLATFORMS REQUIRED
- MOST MISSIONS REQUIRE MULTIPLE PLATFORMS
- ASSIGNMENT CHOICES DEPENDENT ON SYSTEM EVOLUTION RATE, FORM

	AGRICULTURE						ENERGY MINERALS							FORESTRY			LAND USE				MARINE				WATER					
	U.S. CROP SURVEY	INSECT, DESEASE, & STRESS	FARMING PRACTICES	IRRIGATION WATER DEMAND	GLOBAL CROP SURVEY	PASTURE/RANGE & SURVEY	MINERALS SURVEY	GEOTHERMAL SOURCE SURVEY	SUBMARINE OIL SURVEY	EXTRACTION POLLUTION MONITOR	PIPELINE MONITOR	OIL POLLUTION MONITOR	THERMAL POLLUTION MONITOR	TIMBER INVENTORY	INSECT, DISEASE STRESS	FIRE MONITOR & ASSESSMENT	U.S. LAND USE INVENTORY	LAND FORM & COVER MAPPING	COASTLINE SURVEY	GEOLOGICAL HAZARD MAPPING	OCEAN DYNAMICS MONITOR	FISH ENVIRONMENT & LOCATION	MARINE POLLUTION MONITOR	NAVIGATION HAZARD MONITOR	URBAN/AG SUPPLY INVENTORY	HYDROELECTRIC SUPPLY INVENTORY	GREAT LAKES ICE	WATER QUALITY MONITOR	FLOOD MONITOR	COASTAL WETLANDS MONITOR
EARTH SYNC	B					B	B	A	A	B								B				A	A		A		A	B	B	B
PREDAWN SUN SYNC							A								A															
MORNING SUN SYNC		A		A						A	A											A			A					
NOON SUN SYNC	A	A	A	A	A	A	A			A	A		A	B	A	B	B	A		A		A	B		A	A		A	A	A
SHUTTLE SORTIE	B		B		B		B			B			B	A		B	A	A	B		-			B						B
NON SYNC S/C																					A			A						
AIRCRAFT		B		B			B			A		A			B	A	A		A	A	B			B	B		B			

A – PROVIDES ALL OR MAJOR PART OF DATA NEEDS
B – PARTIAL SATISFACTION OF DATA NEEDS

Figure 9. Platform Assignments

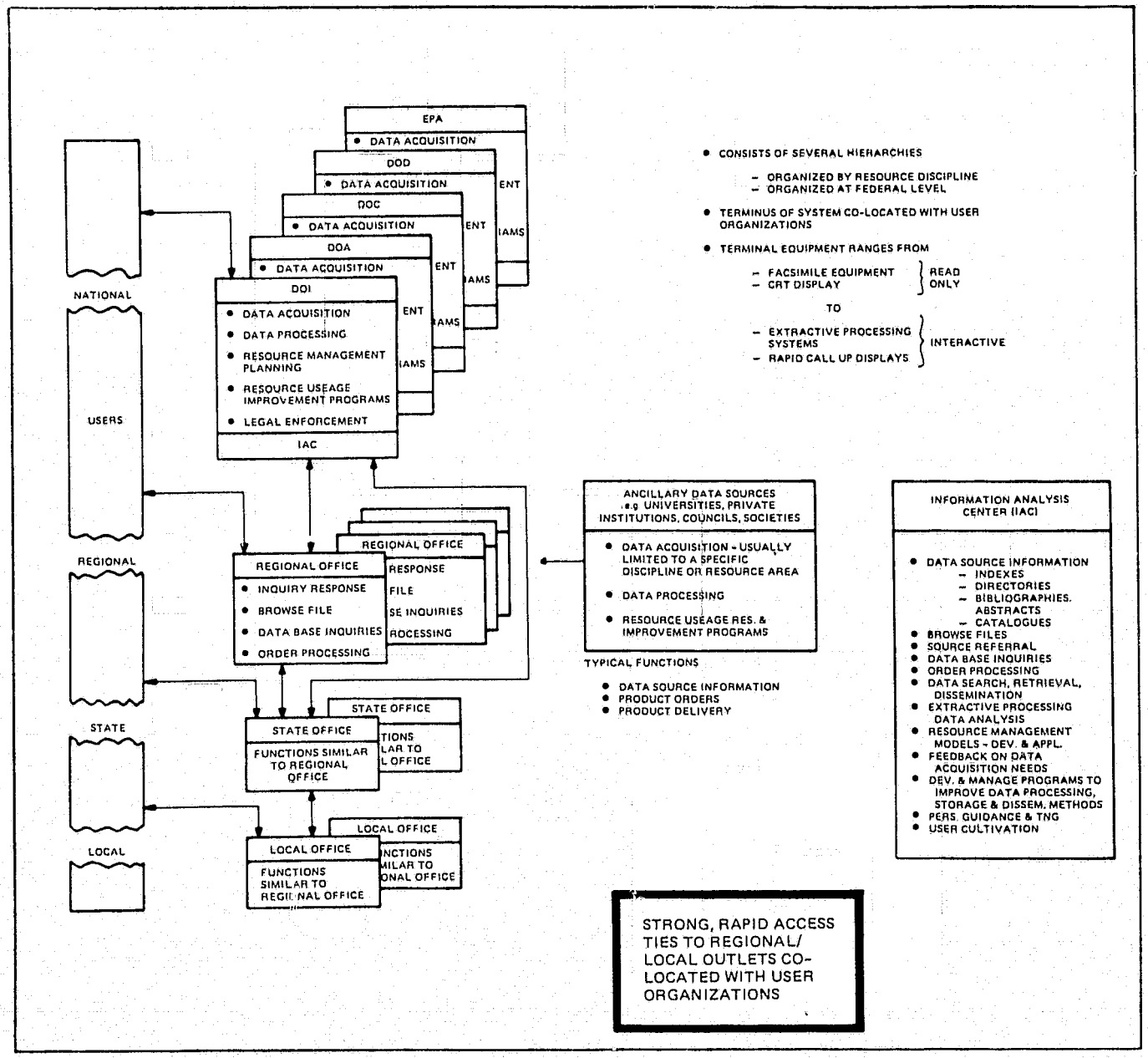


Figure 10. Selected Ground System Architecture - User Oriented Hierarchy

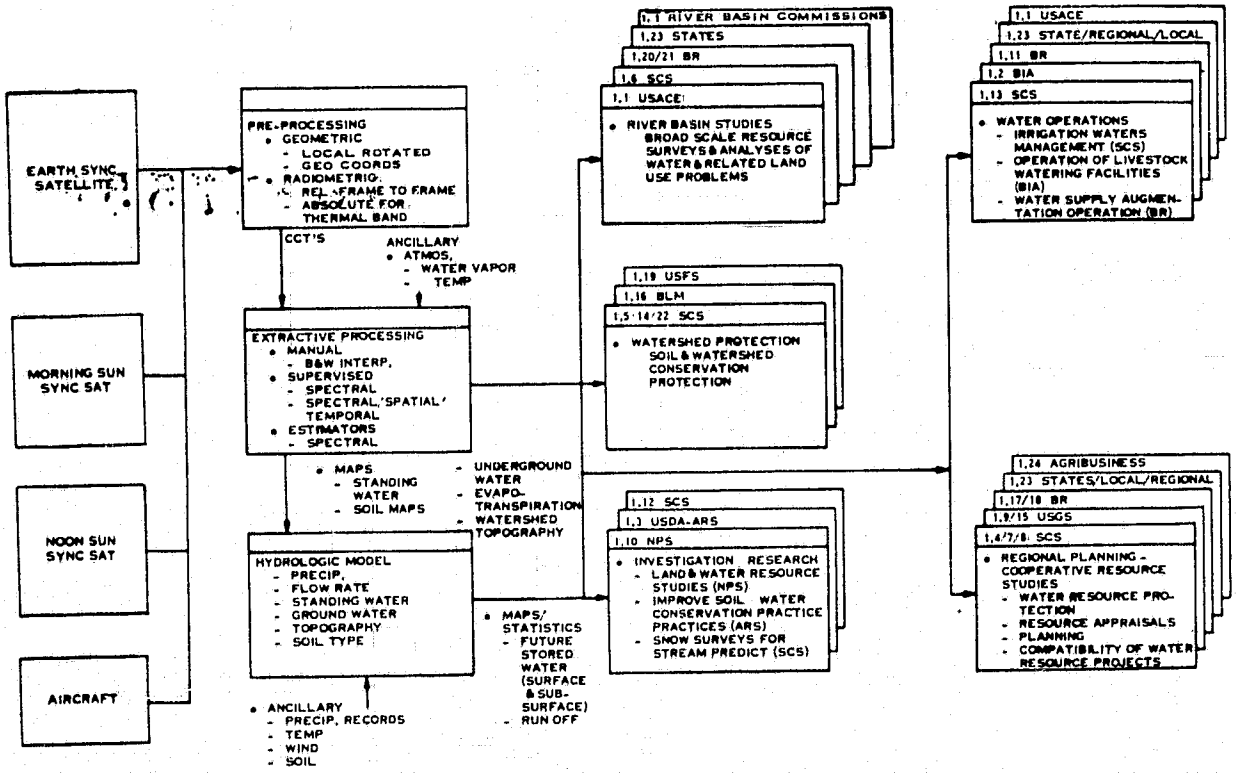


Figure 11. A Single-Mission System for Surface Water Inventory

EARTH RESOURCES SURVEY AND THE SPACE SHUTTLE

I-26

W. Kent Stow and Roman W. Andryczyk
General Electric Space Division, Valley Forge, Pennsylvania

N76-17550

ABSTRACT

There are four specific and distinct roles for Earth Resource applications which the Space Shuttle can serve while operating in its sortie mode. These four roles correspond to the evolutionary stages leading to the operational employment of remotely sensed data by a resource manager in the solution of his management problem. The four basic roles of the Shuttle sortie in such an evolution are: (1) Technique Development Platform, (2) Sensor Development Platform, (3) Applications Development Platform, and (4) Operational Mission Platform. Current planning indicates that most Shuttle flights will have missions other than Earth Resources as their primary objective. Generally these missions do not consume all of the Shuttle capability and there is often room for another mission to share the same flight. The maximum exploitation for Earth Resources of the available frequent sortie flight opportunities requires that the Earth Resources missions be configured to fit the Shuttle with minimum interference to the prime missions. This further implies the utilization of a highly autonomous yet flexible packaging (implementation) concept referred to as the Standard Package concept.

INTRODUCTION

Within the next five years, the introduction of the Space Shuttle will cause significant changes in the overall space program and in the Earth Resources Program in particular(1). This paper addresses the impact that the Shuttle is expected to have on the Earth Resources Program and outlines several concepts for exploiting the Shuttle characteristics. The two principal topics of this paper are (1) the utilization of the Space Shuttle in its sortie mode for Earth Resources and (2) the application of an Earth Observations Standard Package to Earth Resources missions.

Beginning in 1979 the Space Shuttle will provide several unique capabilities previously unavailable to the Earth Resources Program, ERP. Included, of course, are the impressive physical parameters of available payload weight and volume as well as the Orbiter provided support services (power, thermal, data management, etc.). Equally (if not more) important however, are the unique capabilities and practices afforded by the Shuttle such as:

- Frequent flight opportunities.
- Capability for on-orbit servicing of spacecraft.
- Capability of data (film, tape, etc.) return to earth.
- Retrieval and reuse of spacecraft and experiments.
- Presence of man on-board the Orbiter.
- Controlled variability of orbital characteristics.

The four roles of the Space Shuttle in its sortie mode are:

- Technique Development
- Sensor Development
- Applications Development
- Operational Mission Platform

By Technique Development is meant those early investigations which provide the underlying scientific framework upon which the application of remote-sensing to a resource management problem is built. Signature research is typical of these investigations. Sensor Development, the second stage (and second shuttle sortie role) is focused on the engineering of the sensor and on the gathering of data which will permit design of the sensor for its ultimate operational application. Applications Development, the third stage and role, involves the use of nearly-developed or prototype system elements (including sensors) to investigate and demonstrate the workings of the entire applications program. And, finally, Operational Missions are those activities which have successfully completed the development process and are routinely carried out in satisfaction of operational user's needs. While few applications will require development from scratch in all four stages, and many will require no flight-data for one or more steps, the unique features of the Shuttle sortie mode will lead, in many cases, to significant advances in the technological and economical efficiency with which all four stages may be carried out.

The Standard Package concept consists of sensor and support subsystems configured in a modular flexible packaging implementation which will fly on Shuttle flights on a non-interfering, space available basis to acquire remotely sensed data on targets of opportunity and for specialized missions. In order to maximize the flight opportunities and minimize any impact to the prime missions the concept must maintain standard interfaces (electrical, mechanical, crew utilization) with respect to the Shuttle Orbiter and Spacelab. These requirements have been met by establishing a "building block" approach to the implementation whereby a "system" can be quickly configured from an inventory of modular components to meet a wide variety of mission requirements.

SHUTTLE SORTIE MODE FOR EARTH RESOURCES

The development of a particular Earth Resources application (mission) is a staged process which carries an embryonic technology through several successive steps to its final operational implementation. All system elements must enter the development process at an early stage and the steps in the development of each require the acquisition of data. The Shuttle when used in the Sortie mode has four distinct roles which span the total development cycle of the Earth Resources Program. These four roles correspond to the evolutionary stages leading to the operational employment of remotely sensed data by a resource manager in the solution of his management problem. The four basic roles of the Shuttle sortie in such an evolution are: (1) Technique Development Platform, (2) Sensor Development Platform, (3) Applications Development Platform, and (4) Operational Mission Platform.

Shuttle as a Technique Development Platform

A sortie mission which contributes to establishing the basic scientific relationship between remote sensing and the resource management function involved in an application is called a technique development mission. Spaceflight for technique development is generally preceded by ground measurements and aircraft flights; the motivation for spaceflight exists if remote sensing conditions in orbit are to be significantly different from those on the ground or from aircraft. Shuttle flights necessary to carry out this type of mission typically call for varied viewing conditions, such as sun angle, and may or may not require special sensor developments.

Technique development from shuttle promises to be one of the more efficient uses of the frequent flight opportunities and the recoverability of experiment hardware offered by the Shuttle sortie. Technique developments are, by their very nature, disposed to be cut-and-try efforts; this is precisely why aircraft have proven to be of such value to technique developments in the past (and why they will also continue to be so in the future). The frequent flight and intact recovery of hardware will permit the use of hardware not designed for the rigors of long (say, years) spaceflight but for obtaining the specific sets of measurements required to scientifically interrelate the resource phenomenon and the

remote sensing technique under study. Repair, refurbishment and, more importantly, modification of the experiment hardware will lead to a technique development phase which is both time and cost-efficient. As has been learned in aircraft programs, however, the intact recovery and frequent flight opportunities of Shuttle must not become a justification for flying hardware of poor quality. There exist advocates of Shuttle-era cost-savings through low-quality hardware who have not experienced the heartbreak of cheap flights.

As an example of using the Shuttle as a technique development platform consider the acquisition of multi-aspect visible and near-infrared canopy signatures. Suits [2] and others have modeled (Figure 1) various portions of the basic problem: how does the (multispectral) reflectance of a given vegetative canopy vary with viewing and illumination angles and can this variation be used to more effectively discriminate vegetation types and condition ?

Figure 2 illustrates a concept for the spectrometer hardware required, in this instance illustrating the use of a developmental model of the SEOS telescope as the primary optical device and a two-axis steerable gimbal to point it. A payload such as this could be accommodated by a single pallet section (with allowance for launch stowage overhand). The payload is compatible with either other Earth Resources hardware or non Earth Resources missions with similar orbit requirements.

Technique development, as a program element separate from sensor development or applications system development, is a viable use of the Shuttle sortie platform. It promises to be a valuable bridge between the ground-and-aircraft-based technique developments and subsequent steps in the total development process.

Shuttle for Sensor Development Missions

A sortie mission which contributes to the advancement of sensor performance or the development of a new sensor, is, as far as the particular sensor and measurement is concerned, a Sensor Development Mission. The use of the Shuttle for sensor development is not limited to a particular Earth Resources discipline and has the advantages of greater flexibility and adaptibility due to its more frequent flight opportunities and wider capabilities. For example, the increased power and payload weight capabilities suggest the development of advanced scanners which can be assembled into complete systems in small "building block" modules allowing for spatial resolution which is tailored to the specific application, addition or deletion of spectral bands as required by the particular mission and improvements in spectral sensitivity. In the domain of microwave sensors the opportunity exists for advancing the state of the art in spatial resolution through the use of larger apertures or higher frequencies, increasing measurement resolution by using higher output power (to achieve better S/N ratios) or developing specialized instruments such as a radar capable of measuring ocean wave spectra. Figure 3 illustrates the use of the Shuttle for developing the SIMS, Shuttle Imaging Microwave System, sensor.

However, sensor development does not imply the wasteful extension of effort in areas which have previously proven fruitless simply because flight opportunities exist. Sensor Development missions must therefore be chosen carefully based upon previous developments in the discipline during the pre-Shuttle era and on the needs of the missions which are to be served by the sensor. In the pre-shuttle era it was often the emergence of a single flight opportunity which gave impetus to the primacy of one sensor above another. This resulted in wasted costs and efforts for those sensors not qualifying coupled with a disproportionate jump in costs associated with those chosen.

The concept of sortie flights for sensor development allows for many configurations of equipment in the payload bay. A Shuttle flight could have as but one of its objectives the development of one (or several) new sensor types contained in a single pallet. Since the sensors being developed are

contained on a single pallet the problem of complex interfaces is reduced due to ability to specify the configuration at an early date. The integration of the sensor now involves only the pallet to be used plus a minimal Spacelab interface and can take place completely prior to integration in the Shuttle at the launch facility. The value of a constant interface with the experiment carrier has been proven many times on the Nimbus satellite program which has flown over fifty experiments on different missions but using the same, standardized spacecraft and interfaces.

The availability of the Spacelab environment presents several attractive features when considering sensor development. Standard rack-mounted laboratory and commercial hardware can be used within the Spacelab to provide power, signal and data conditioning for a developmental sensor contained on a pallet in the payload bay. The improvements inherent in this feature over developing a sensor entirely for a space environment include the use of the same checkout and test equipment both on the ground and in orbit. This feature also provides the ultimate in flexibility and adaptability for a sensor in that the sensor may be reconfigured somewhat in flight or when returned at the end of the flight.

Another advantage to be gained in sensor development during the Shuttle era centers around the fact that frequent and ongoing flight opportunities allow for greater flexibility in the development of a data system for interpretation of sensor measurement. While parallel development of the sensor and its data handling system are mandatory (whether considering a satellite or Shuttle application) the Shuttle, with its possibilities of flying the same basic sensor in several progressive configurations allows for optimal development of both the sensor performance and the data system needed. In the case of the Rad/Scat the ground data handling system design followed the development of the instrument by at least a year and the nature of the sensor and the Skylab carrier vehicle allowed for no improvements once the hardware design was completed. Shuttle-era flexibility in sensor configuration implies the capability to optimize the data system for the sensor being developed.

Shuttle for Applications Development Missions

This type of sortie mission, an ASVT, would provide a demonstration of an Earth Resources management mission specifically designed to fulfill a requirement for data from an operational user. (ASVT stands for Application System Verification Test.) It consists of the assembly and integration of a complement of sensors necessary to fulfill the data requirements of the user for the particular earth resources management mission to be undertaken, the integration of these sensors into a total system, the flight and data collection using the sensors selected and the processing of the data gathered to demonstrate that the system has met its requirements. It is logically the last sequence before a remote sensing system goes operational and relies heavily on the results of sensor development missions. The unique characteristic of an application development mission is that is represents an entire "turn key" package which can be made operational by the user once the mission has verified the concept. It is complete with documentation, hardware and all necessary software to support operational use. As an example of an ASVT consider the pallet segment shown in Figure 4 which depicts a potential set of sensors for conducting a specific ASVT in the urban land use resource area.

The TERSSE study [1] has identified 30 broad Earth Resources management missions of which 19 could be served in an applications development mode by Shuttle. These include (but are not limited to) crop surveys, thermal pollution monitoring, timber inventories, land use inventories, geological hazard mappings, ocean dynamics monitoring and water quality monitoring. Many of these missions require a sensor complement which includes scanners (visible, IR and thermal), photographic coverage (multispectral and black and white), and imaging microwave sensors (radiometer/scatterometer and/or radar). Table I lists the missions which have been identified by their resource discipline category.

The potential also exists for applications demonstration via Shuttle wherein only the critical elements of the operational mission are executed and some synopticity and repeat coverage can be sacrificed. The restriction of the demonstration to a smaller critical geographical area, or to an important portion of the year permits the use of a Shuttle sortie flight (or flights) for the demonstration. Since launch costs for sortie flights will be shared among the payloads carried, cost advantages are nearly certain to exist over automated spacecraft launched for specific applications development. This is not to say that automated spacecraft will not be used for applications development but only that Shuttle can be examined for support of applications development where cost savings warrant the reduction of synopticity or repeat coverage. Partial solutions quickly are the province of the Shuttle sortie - this capability should not be overlooked for application development.

Shuttle for Operational Missions

Operational missions are distinguishable from other Shuttle sortie activities by virtue of the fact that they serve a user agency administrated function. In this case the Shuttle is the vehicle by which the payload (the actual operational sensor complement) achieves orbit; the data is returned to the user for processing, reduction, analysis and dissemination. User agencies which have been identified include federal government related groups, non federal government related (regional, state, county or local), institutional and private or commercial. Operational missions consist of sensors of various technology disciplines which have been developed and proven on previous flights (Shuttle, aircraft or pre-Shuttle era spacecraft), integrated into an operational system designed to fly in any of several Shuttle sortie configurations (i.e., with Spacelab, pallet mounted, etc.) and previously flown as an applications development mission. Figure 5 shows one concept of the SEOPS standard package used as the Shuttle accommodation for an operational mission of inventorying the U.S. timber volume.

Although flying an operational mission, the Shuttle sortie flight may not be the primary platform in use for the earth resources management task in question. It is possible to view the role of the Shuttle sortie operational flight as that of a complementary or secondary platform in a system which includes sensors in geosynchronous or polar orbit. The problem of global water inventory and management provides an interesting example. Geo-synchronous sensors would be used to provide constant low resolution data of large areas while polar spacecraft sensors provide better resolution over designated regions periodically. However, even with coverage such as this, Shuttle sortie flights could be operationally valuable to fill in cases of sudden changes in water inventory such as flooding. In this fashion, although flying an operational mission, the Shuttle sortie flight in question is not the primary platform in the earth resources management system.

Several questions remain unanswered at this point on the use of Shuttle for operational missions. Launch cost reimbursement by the user is implicit in the concept, and a schedule of costs will be necessary before any operational user can decide whether the service provided is worth the cost. Data availability policy must be established: does the user have sole rights, will current NASA policy prevail into the operational era, or will there be some middle ground sought ? And if an operational payload is flown aboard Shuttle in combination with other payloads what guarantees of data collection and priority can NASA provide the user ? Operational users expect value for cost, propriety, and consistency of data, whether they be sister Federal Agencies or private corporations. Substantial attention must be given these issues before operational resource management missions are flown on Shuttle.

FREQUENT FLIGHT OPPORTUNITIES: A PROGRAM REVOLUTION

In examining characteristics of the Shuttle for exploitive value, no single feature of the Shuttle concept will have so much impact and potential as the opportunity for frequent flights. Today's

Earth Resources Program may be characterized as follows:

1. Spacecraft projects dominate the development of system elements such as signatures, sensors, and data systems.
2. Because of the infrequent availability of flights, all phases of an applications development are necessarily attacked simultaneously: signature research, sensor development, and applications development are combined in a single program.
3. As a result, major budget commitments precede proof of concept and increases in confidence level.

The Earth Resources Experiment Package (EREP) which flew aboard Skylab is the sine qua non of the single-flight-program. Skylab was a once-in-a-decade opportunity which could not be ignored. And EREP has produced valuable contributions to the Earth Resources Program. But the constraints of a single flight opportunity are inescapable. Figure 6 illustrates the situation. Costs rise rapidly as the flight project is approved and hardware is built, but increases in confidence from the three simultaneous steps do not occur until after the beginning of data analysis (the small bump in the cost survey represents data processing costs which are usually not accounted for until late in the project). And the more mature steps (e.g. application development) are not able to capitalize upon the results of the earlier ones.

The Earth Resources R&D Program of the 1980's as a result of frequent-flight-opportunities, should be characterized as follows:

1. System development needs will dominate the conduct of the Program; flights will be scheduled when and as they are useful to the development of a particular system element.
2. Developments will be attacked sequentially and iteratively; signature research, sensor development, and applications development will be kept separate when it is warranted.
3. Low cost will be achieved through reuse and modification of hardware facilities as the development process proceeds.

Figure 6 also illustrates the phased program concept made possible in the Shuttle era by frequent flight opportunities. Technique development flights deliver proven signatures to the sensor development project which, in turn, uses multiple flights to develop sensor hardware for transfer to the total applications system development effort. Costs are more gradually increasing and the confidence associated with the process is more nearly in line with its cost.

A major Earth Resources Program management restructuring will be necessary to achieve these benefits. Application Development Managers will need to be created, assigned, and given the authority to control all aspects of the development of their system, such as signatures, sensors, or data processing, and to schedule Shuttle flights as they become useful at each step. A concomitant amount of Shuttle Program responsivity and flexibility will be required by the Application Development Manager. Such restructuring will not be simple, and the details are not at all visible at this point; however, this aspect of management in the Shuttle Era must be recognized and given early attention.

STANDARD PACKAGE CONCEPT

The innovative technique of providing accommodations to payloads and flying them on most Shuttle flights (more than 30 per year), or providing flight opportunities to payloads on a non-scheduled space available basis, as well as quick reaction capability from space, is a sound and feasible one. The Standard Package concept provides this capability.

Since most Shuttle flights will be dedicated to other than earth observation missions, the opportunity for frequent flights can be exploited only by configuring Earth Resources missions (or any other missions) to fit on the Shuttle with minimum interfaces to the prime payload. This requirement implies the need for an autonomous yet highly flexibile packaging concept. Further, a high degree of standardization must be inherent if costs are to be minimized.

Standard Package is a unique concept in obtaining valuable information for managing the earth's resources and environment. It will provide a new set of capabilities which match many earth observations missions and which complement other platforms such as LANDSAT and aircraft. It is a system consisting of proven standardized modular elements designed for mission flexibility and ease of Shuttle integration. It consists of earth observation sensors and support subsystem which are to fly on Shuttle on a space available, non-interfering basis to acquire data on targets of opportunity and specialized missions, with quick accessibility of the information to the user community. As such, it is not only standard in that it can fly on most flights and has a standard interface with Shuttle; but it is also selectable in that it consists of an "erector set" of modular components which can be rapidly assembled to meet a variety of mission opportunities.

Three basic implementation concepts for the Standard Package are shown in Figure 7. These three: "Bridge," "Cradle," and "Mini-Cradle" each contain basic sensor and support subsystem packages. These range from the single instrument capability of the "Mini-Cradle" to the full capability afforded by the larger concept versions. Because the Standard Package is designed to be a modular stand-alone system, it can be interfaced and integrated with other primary payloads into the Space Shuttle. There is a unique and meaningful role to be performed by this concept in the Shuttle Era of the '80's.

CONCLUSION

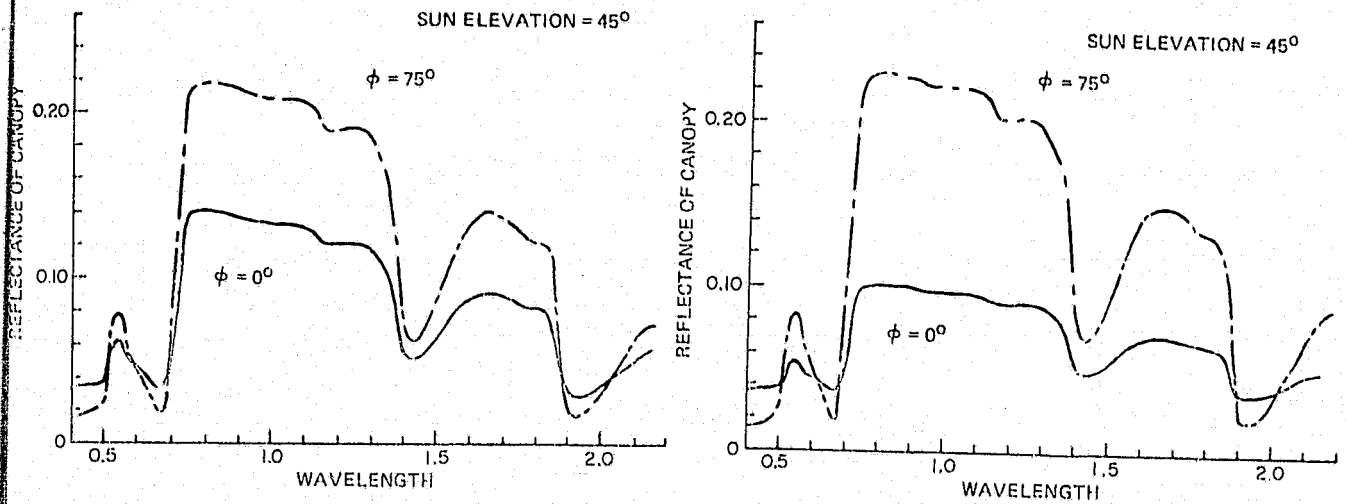
The Space Shuttle in its sortie mode is a primary development platform for the Earth Resources Program and its roles span the range from Technique Development to ASVT Support. As an operational platform, the Shuttle's unique features of tailorable sensors, tailorable orbits and lighting, and hard-copy return qualify it for primary platform status in several cases and as a support platform in many others. Specific objectives now exist for all four roles of the Shuttle sortie and, when considered collectively, can result in an integrated program which will rapidly advance the application of NASA's Earth resources technology in the early years of Shuttle flights.

The Space Shuttle opens a whole new era in providing mankind with the opportunity to fly and recover payloads from the space environment at regular intervals with low cost. Shuttle, however, must do more than articulate the objectives of low cost, flexibility and easy accessibility. It must turn these concepts into realities in a future which demands benefits, yet provides limited budgets.

REFERENCES

1. "Definition of the Total Earth Resources System for the Shuttle Era, TERSSE;" contract final report NAS 9-13401, General Electric Space Division, December 1974.

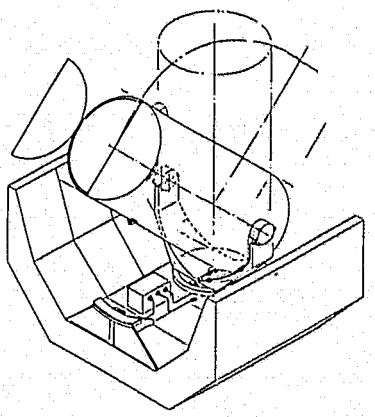
2. G. H. Suits, "Calculations of the Directional Reflectance of a Vegetative Canopy," Journal of Remote Sensing of Environment, Vol. II, pp 117-125, 1972.



(a) Unstressed Corn Canopy

(b) Stressed Corn Canopy

Figure 1. - Effect of Viewing Angle (ϕ) on Reflectance

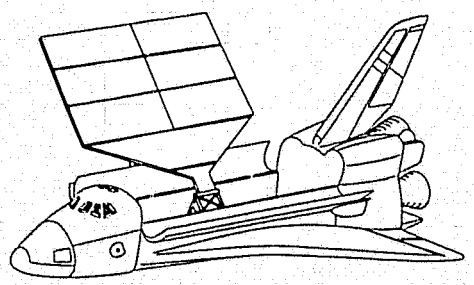


OBLIQUE SIGNATURE RESEARCH EXAMPLE

- FOCUS IS ON DETERMINING DISTINGUISHING CHARACTERISTICS OF RESOURCE
- SENSING EQUIPMENT TAILORED TO RESEARCH NEEDS
- FEW CONTROLLED SITES / SEVERAL OVERFLIGHTS REQUIRED FOR TECHNIQUE DEVELOPMENT

- VEGETATIVE CANOPY SIGNATURES CONTAIN INFO UNOBTAINABLE BY NADIR-LOOKING SENSORS
  - CROP IDENTIFICATION
  - STRESS DETECTION
- VALUE / UTILITY OF OBLIQUE AND MULTI-ANGLE DATA NOT KNOWN
  - SOLAR ILLUMINATION VARIABILITY
  - OPTIMUM ANGLES

Figure 2. - Shuttle Role: Technique Development



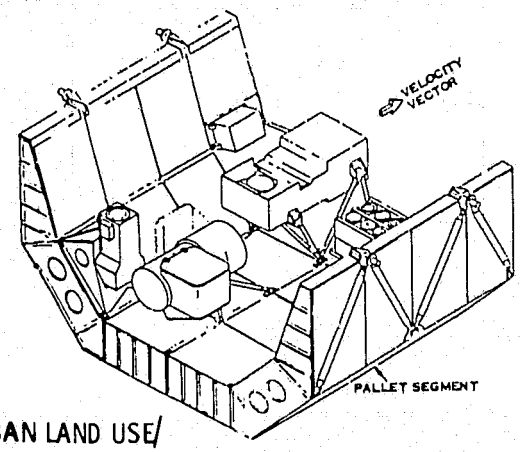
SHUTTLE IMAGING MICROWAVE SYSTEM

- INITIAL INVESTMENT HIGH; COST PER FLIGHT REDUCED BY MULTIPLE FLIGHTS INTERSPERSED BETWEEN SENSOR MODS/UPDATES
- BASIC SENSOR STRUCTURE ABLE TO BE TRANSITIONED TO ASVT USE AT COMPLETION OF SENSOR DEVELOPMENT FLIGHTS

Figure 3. - Shuttle Role: Sensor Development

TABLE I. - SHUTTLE SORTIE APPLICATIONS DEVELOPMENT MISSIONS (ASVT'S)

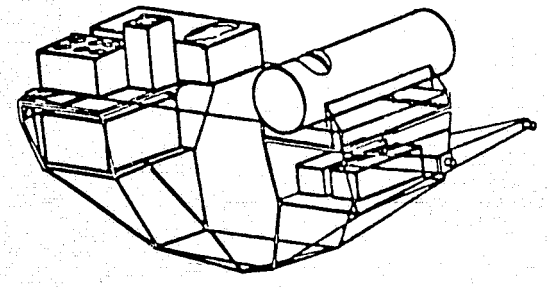
AG1	US CROP SURVEY	LAND 1	US LAND USE INVENTORY
AG3	FARMING PRACTICES	LAND 2	LAND FORM & COVER MAPPING
AG5	GLOBAL CROP SURVEY	LAND 4	GEOLOGICAL HAZARDS MAPPING
E/M1	MINERAL SURVEY	MAR 1	OCEAN DYNAMICS MONITORING
E/M3	SUBMARINE OIL SURVEY	WAT 1	URBAN AG SUPPLY INVENTORY
E/M4	EXTRACTION POLLUTION MONITOR	WAT 2	HYDROELECTRIC SUPPLY INVENTORY
E/M7	THERMAL POLLUTION MONITOR	WAT 3	GREAT LAKES ICE
FOR 1	TIMBER INVENTORY	WAT 4	WATER QUALITY MONITOR
FOR 2	INSECT DISEASE STRESS	WAT 6	COASTAL WETLANDS MONITOR
FOR 3	FIRE MONITOR & ASSESSMENT		



URBAN LAND USE/
CENSUS PAYLOAD

- SENSORS MAY REQUIRE LITTLE OR NO DEVELOPMENT PRIOR TO FLIGHT
- MAJOR FOCUS IS ON PROVIDING DATA TO REMAINDER OF SYSTEM FOR END-TO-END DEMONSTRATION
- MULTIPLE BUT INFREQUENT FLIGHTS REQUIRED

Figure 4. - Shuttle Role: ASVT Development



SEOPS-TIMBER
INVENTORY CONFIGURATION

- SENSORS AND SUPPORT EQUIPMENT ARE AN OPERATIONAL FACILITY
- DATA COLLECTION IS A ROUTINE OPERATION FOR AN OPERATIONAL RESOURCE MANAGER ON A REIMBURSABLE LAUNCH SERVICES BASIS

Figure 5. - Shuttle Role: Operational Mission

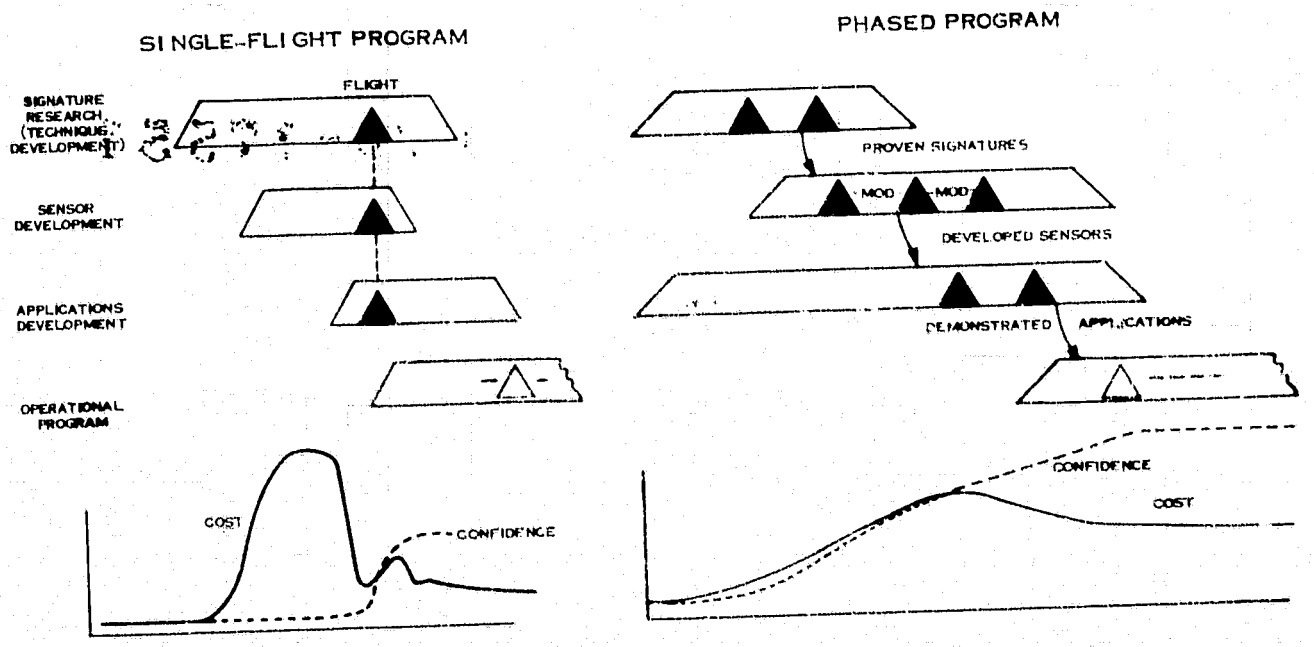


Figure 6. - Single-Flight Program Versus Phased Program

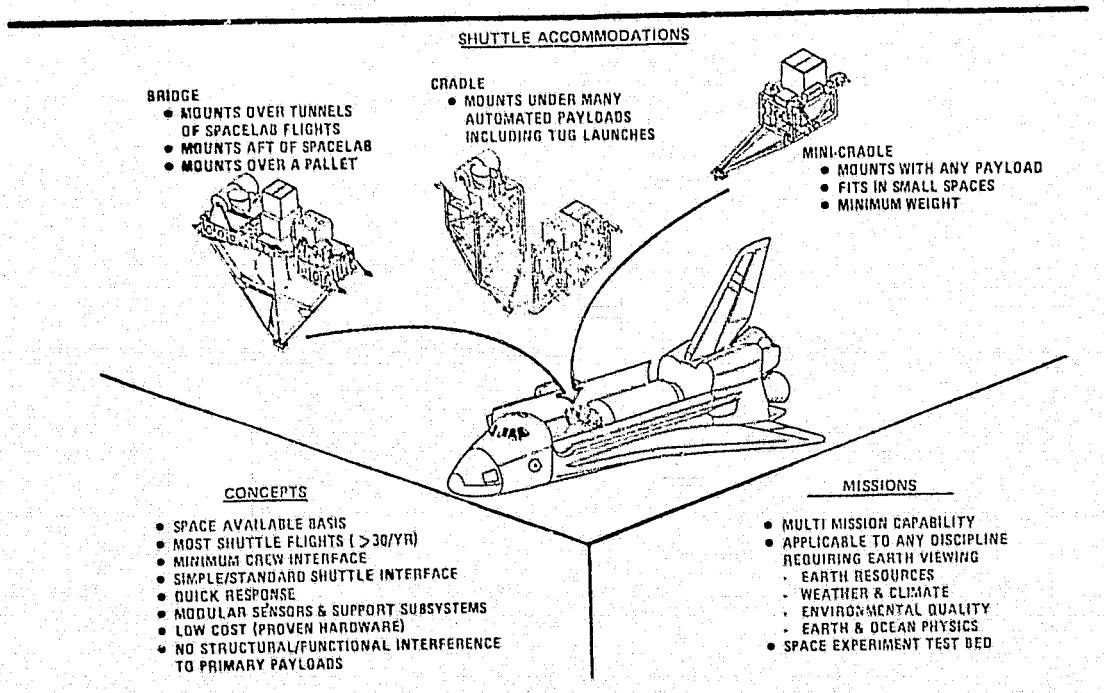


Figure 7. - Standard Package

REPRODUCIBILITY OF THE
ORIGINAL PAGE IS POOR

SENSOR EQUIPMENT OF THE GERMAN EARTH SCIENTIFIC AIRPLANE PROGRAM

By Peter Seige, DFVLR Institut fur Satellitenelektronik,
Oberpfaffenhofen, West Germany

N76-17551

ABSTRACT

The German airplane program for earth scientific research will support the work of a vast staff of earth scientists mainly from universities and federal agencies. Due to their fields of interest, which are in oceanography, hydrology, geology, ecology, and forestry, five test areas were selected which are spread all over Germany. The sensor package, which was designed in accordance with the requirements of this group of scientists, will be installed in a DO 28 D2 type airplane. The sensor equipment consists of a series of 70-mm cameras having different film/filter combinations, a photogrammetric camera, an infrared radiometer, an 11-channel multispectral line scanner, a LANDSAT-compatible radiometer, and a complex avionic system. Along with the airplane, a truck will be equipped with a set of radiometers and other sensor devices for exiensive ground-truth measurements. This also includes a cherry picker. The first phase of the flight program will start in the fall of 1975 and will last for 1 year in order to cover all seasons.

INTRODUCTION

The German airplane program for earth scientific research, which is funded by the Federal Republic of Germany, will support the work of a vast staff of earth scientists, approximately 40 for the time being. In order to concentrate the program, five test areas were selected, representing the main areas of interest of the various working teams presently participating in the airplane program (fig. 1). These test areas are spread all over Germany, reaching from the Northern and Baltic Sea as far south as the Bavarian Mountain regions.

Test area 1 covers the Ja[illegible] bay near the city of Wilhelmshaven, which is an area of shallow waters. There the main interest is to study the interaction between sea and coast. Objects of interest are the sediment transport, pollution problems, icing, and sea currents.

Also of oceanographic interest is test area 2, which is divided into an area of the North Sea in the surroundings of the island of Helgoland and a strip of the Baltic Sea near the city of Kiel. In these areas, white caps will be studied as well as surface temperatures and chlorophyll distribution.

Test area 3 covers an area near Frankfurt and serves as an object to study phenomena of the biosphere of a densely populated area. Cold air streams, land use, and water pollution are the objects of main efforts.

A part of the Black Forest near Freiburg was selected as test area 4 in which mainly vegetation and land use problems will be studied.

Test area 5 is located in the southern part of Germany near the Bavarian Mountains. The main purpose of the studies in this area is to learn more about the

ecology of a terrain bordering a high mountain chain. Geohydrological long-term observations will be performed as well as the classification of natural surfaces.

The shape and size of the various test areas vary between rectangles measuring about 20 to 40 km and single flight strips of lengths up to 70 km.

This short description of the various test areas and the groups of scientists participating in the program already shows that a wide variety of sometimes rather opposing requirements has to be taken into account. The sensor package has thus been designed with maximum flexibility in order to meet all demands. One common condition, however, is that the test areas should be covered at least once per season, which means that the minimum survey phase will be 1 year.

Airplane Sensor Equipment

As the required flight altitudes range from 1000 to 15 000 ft., it was decided to take an unpressurized two-engine aircraft of the type Dornier DO 28 D2 (figs. 2 and 3). Its weight, without sensor loading and additional instrumentation, is about 2600 kg. The minimum speed guaranteeing still acceptable flight conditions will be about 80 kn, which is essential with regard to camera surveys at low altitudes and unfavorable lighting conditions. The maximum flight time of the airplane amounts to approximately 8 hr, which will be reduced in this case to about 3-1/2 hr due to the weighty sensor package. This time, however, is sufficient as all test areas lie within easy reach.

In order to meet the requirements of the various earth scientific disciplines, it was decided to include in the sensor package (fig. 4) a multispectral line scanner, an infrared radiometer, a set of 70-mm cameras, a photogrammetric camera, a zenith-oriented camera, and a four-channel LANDSAT-compatible radiometer.

The most important sensor unit onboard, however, will be a multispectral line scanner (table I). It was decided to use an 11-channel multispectral line scanner provided with 10 channels in the visible and near-infrared part of the spectrum and one in the thermal infrared band between 8 and 14 μ. The spatial resolution is specified to 2.5 mrad, with a total field of view amounting to 100 degrees. The scan speed is variable between 10 and 100 scans per second. For reference (table I), the system has two internal black bodies, which bracket the predicted terrain temperatures, and a calibration lamp. In addition, the skylight can be used as a reference, but this is only of importance under certain weather conditions. A liquid-nitrogen-cooled HgCdTe detector is used for the thermal infrared band, resulting in a temperature resolution of about 0.25°C. Each of the 11-channel detectors is connected to a preamplifier, an automatic gain control, and a data-processing part. The data are digitized and converted to a manchester biphase level code. The stream of 8-bit words is buffered and formatted to a data frame (fig. 5), which is recorded on a 14-track tape, one track per channel.

The data frame consists of two synchronization words, some housekeeping data, the calibration values, 13 words of additional housekeeping and/or external data, and 803 words of video information. The tape speed is controlled by the scan speed so that a maximum bit density packing of 10 kbit/in. will be guaranteed at any speed. This helps to save a lot of tape material that would be wasted otherwise, especially at lower scan speeds.

In order to calibrate the system in the visible part of the spectrum, an integrating sphere is used provided with a tungsten lamp which is again calibrated to a standard. For the thermal infrared channel, a black body is used which can be cooled down to -20°C. The calibration values thus obtained will provide the input data for a subsequent quantitative interpretation of the video data, as far as the sensor characteristics are concerned.

The DFVLR received the scanner in January of this year (fig. 6). Since then, an extensive laboratory test program was performed as well as a number of test flights (fig. 7), some of them already in the earlier described test areas. The scanner delivered very good results, as shown in Figure 8. The example shows the DFVLR facilities in Oberpfaffenhofen from a flight altitude of 1000 feet in channels 2 and 9. Differences in the spectral behavior of the scene are especially obvious in the lower part of the picture where different field types are displayed.

During the first year's measuring phase, it is intended to use the scanner for nearly all flights, in the daytime as well as at night. It was calculated that this phase of the program will provide the earth scientists with a data collection of about 2.8 million scan lines.

In addition to the multispectral scanner, the airplane is equipped with a precision radiation thermometer (fig. 4), which gives a very exact reference for the measurements obtained at the thermal band of the scanner. When selecting such a radiometer for flight applications, you have to be sure that the response time is short enough to guarantee a sufficient spatial resolution. In this case, an infrared radiometer with a response time of 5 msec was chosen. The accuracy was specified to 0.05°C above 0°C. The total field of view measures 2° in this configuration. The spectral band has been limited to 9.5 to 11.5 μ. Before and after each flight, the radiometer will be compared to a small portable black body to check the proper function of the sensor.

Another radiometric device belonging to the airplane equipment will be a four-channel LANDSAT-compatible radiometer. It is capable of detecting, simultaneously, the radiation in the four LANDSAT channels; that is, the radiation between 0.5 and 0.6, 0.6 and 0.7, 0.7 and 0.8, as well as 0.8 and 1.1 μ. The instrument will be set up in such a way that it is directed towards the zenith in order to detect the total incident radiation of the entire hemisphere, that is, the field of view will amount to 2 π steradian. During an overflight, data will be collected on the ground in the same mode so that a comparison between the two measurements may allow an interpretation of the atmospheric conditions between the ground scene and the aircraft. Special consideration will be given to the aerosol content of the atmosphere.

In addition to the radiometric measuring devices, a set of cameras onboard the aircraft will provide the opportunity to carry out an extensive photographic mission at the same time. The setup consists of six Hasselblad cameras. Five of them are the standard type provided with a 70-mm rollfilm. Depending on the size of the test area, it will use either 500- or 70-exposure magazines. The sixth camera is a photogrammetric-type 70-mm camera, which means that an additional precision reseau is imaged onto the film permitting a photogrammetric interpretation of the film material gathered. For this type of camera, magazines with 200 exposures as a maximum are available.

As an alternative, 100- or 50-mm lenses are available, corresponding to a field of view of 43° and 75°, respectively. The 100-mm objectives are preferable from the operational point of view because they are already available with an automatic

aperture control. One camera will be equipped with a lens having a short focal length of 30 mm for flights near the coastline. The result will be a horizontal field of view of 110°, enabling the experimenter to correlate the oceanographic phenomena to some known landmarks. A seventh Hasselblad camera onboard the aircraft will be directed to the sky to image the cloud distribution during the operation. This will help the interpreter to distinguish ground phenomena, such as cloud shadows, from objects of special interest. This camera is equipped with a special lens combination. The field of view thus obtained covers nearly all the hemisphere above the airplane. All seven camera units are controlled by a central logic to guarantee an exact synchronization of the exposure times. Furthermore, the photographic equipment contains a Zeiss photogrammetric camera. Its field of view covers 93°, and the focal length is 153 mm. The magazine accepts up to 120 m of film material having a width of 24 cm. Due to their high imaging quality, the pictures made by this camera are mainly used for photogrammetric purposes. Depending on the test area, the camera will be loaded with black and white, color, or color infrared film. Here again, the exact time information is imaged onto the filmstrip. The total film material delivered by all the cameras has been estimated to be approximately 150 000 exposures during the first phase of the program.

For standard flights, the Hasselblad cameras 1 through 4 are supplied with the LANDSAT-compatible filters to get some correlation with the LANDSAT pictures. Camera 5 and the 70-mm reseau camera will be supplied with various filters, depending on their special functions and requirements. The film material (fig. 9) used in cameras 1 through 4 will be black and white, respectively, panchromatic IR film. The two remaining cameras will use color reversal, color infrared, water penetration or high-resolution black-and-white film in accordance with the earth scientists' requirements for the different test areas.

A special unit has been added to the camera bodies (fig. 10) permitting the registration of a time code onto the film format. These units are fed by an onboard time code generator delivering a 48-bit time information. The bit stream is converted into a digital number pattern by means of light-emitting diodes. An optical system images the time information onto the lower end of the film format as a 12-digit information. Eleven digits are occupied by the time, from day down to 1/100 seconds, while the twelfth digit shows the camera identification so that a later correlation is possible. These 12 digits occupy a space of 8 by 2 mm on the filmstrip so that only a minor part of the ground scenery is lost.

Nearly all the sensors mentioned above have been mounted adjustable within the aircraft so that at least part of the aircraft movements will be compensated (fig. 11). The multispectral scanner has been equipped with an internal roll compensation having a limitation of ±10° so that the system is self-sufficient with respect to this movement. Furthermore, the scanner, the photogrammetric camera, and the 70-mm camera package have been mounted each on a drift frame, which are synchronized to one another. This guarantees that, at any time, all the sensors will be parallel with respect to each other and that, in addition to this, the images or the scan lines are oriented perpendicular to the flight direction. The drift frames will be controlled either by the navigation sensor of the photogrammetric camera or by the avionic system of the aircraft, the details of which will be described later. In other words, there is the possibility to choose between a manual and an automatic drift compensation depending on the kind of mission to be flown. The zenith camera and the LANDSAT-compatible radiometer can also be manually adjusted to the angle of attack of the airplane.

In conjunction with the extensive sensor package, the DO 28 D2 is equipped with an avionic system consisting of a Doppler Radar, a DME, a vertical gyro, a barometric altimeter, a radar altimeter and a gyro, to name only a few of the sensors used. Part of their output data, as for example the altitude measurements, the drift angle, and the speed, are displayed directly to the operator so that he can calculate the essential values, as for example the v/h ratio, which is important for selecting the proper scan speed, or the exposure interval for the different cameras.

The avionic system was designed so that the requirements of the operator, the pilot, and the experimenters can be satisfied at the same time.

The avionic package, the scanner system, and the remainder of the earth scientific sensor equipment are connected by a complex electronic interface system (fig. 12), which generates out of the wide variety of information a data frame compatible to the 11 data frames of the multispectral scanner; that is, having the same word structure, the same length, the same synchronization words, and so on. This data frame is recorded on one of the three remaining free tracks of the 14-track tape connected to the scanner system (fig. 13).

In order to guarantee a synchroneity between the 11 scanner channels and the additional generated data frame, the interface system is controlled by the scanner master clock and the necessary timing signals. This synchroneity is essential for the ground data processing. The data frame registers information from the avionic equipment such as the drift angle, the roll and pitch, the radar and the barometric altitude, magnetic heading, VOR frequencies, DME information, and the geographical coordinates. The earth scientific sensor package delivers information such as data from the four channels of the LANDSAT-compatible radiometer and the infrared radiometer, both including the selected gain factors. The camera set delivers information such as when there was an exposure of one or all cameras, if there were false exposures, and so on. There are, in addition, many more housekeeping and control data building up the data frame, which will not be explained in detail. However, the most important datum registered within this frame is the time information generated by an onboard time code generator. This system serves as a central unit onboard the airplane. All the above mentioned data are registered once per scan line so that it is possible, for example, to correlate a single line with the center line of a photographic picture by means of the time information which is registered on the film format and in the data frame once per scan line with a resolution of a 1/100th of a second. The basic idea of the setup described here is to have all the necessary data available in a concentrated form for further evaluation. On the ground, the most important values of the data frame are printed as a routine in the form of a list. This printout will be attached to the scanner pictures in order to give a quick control of the flight status during the operation time of the scanner.

Ground Data Collecting System

Although it is called an airplane program in addition to the flight program, there will be extensive ground data collecting activities in order to provide the necessary ground-truth values. The missions will take place at the same time and at the same locations as the flight programs, and the data will be gathered by means of a set of sensors matching those onboard the aircraft. For this purpose, a truck (fig. 14) and a cherry picker (fig. 15) have been equipped with the necessary sensors. The platform of the cherry picker can be lifted up to 10 meters above the ground, which will be sufficient in most cases. The instrumentation for

gathering the ground-truth data can be divided into five categories: radiometric sensors, photographic equipment, instrumentation for measuring the soil humidity and soil temperature, meteorological sensors, and geometrical devices.

The different radiometers will pick up the incident and reflected energy in the spectral band between 0.3 and 14 μ. Similar to the scanner in the aircraft, a spectral radiometer will be the core of the ground data collecting sensor package. It will cover a spectral band between 0.4 and 2.6 μ having a spectral resolution of about 2 percent of the peak wavelength. The field of view will be 20°. The main purpose of this instrument is to measure the spectral reflectance of natural objects for correlation with the scanner data recorded during the flights. The sensor package also encloses a LANDSAT-compatible radiometer, which is directed to the sky to pick up the incident radiation from the entire hemisphere; that is, the field of view will be 2 π steradian. The same instrument arrangement will be on the aircraft. Comparison of data gathered on the ground and by aircraft will allow some interpretation of the atmospheric conditions between ground and aircraft. Special attention will be given to the aerosol content. Corresponding to the flight sensor package, an infrared precision radiation thermometer will be included in the ground data collecting system, with the purpose of picking up the radiation in the band between 8 and 14 μ. The accuracy of this instrument amounts to approximately 0.25°C. Last but not least, the system contains two pyranometers for measuring the incident radiation in different spectral bands limited by a set of different filters.

The photographic equipment consists of two 70-mm cameras, one for imaging the ground and environmental scene by means of different film/filter combinations and a second one, provided with a fish-eye, for imaging the cloud coverage of the entire hemisphere during the data collecting phase.

The soil temperature will be taken at selected points by means of a number of soil thermometers. This will help in particular to determine daily variations of the temperature. In addition to this, the soil humidity will be measured by conventional methods.

The ground-truth data collection includes the measurements of meteorological basic parameters, as for example humidity, temperature, barometric pressure, windspeed, wind direction, dust concentration, and haze conditions. Most of the parameters and radiometric values mentioned will either be stored on magnetic tape or on paper strip charts by means of multichannel recorders.

To complete the ground data collection system, a number of geometrical ground references will be used, including color panels and geometrical marks. The above described ground data collection activities are in special cases supplemented by additional activities of the experimenters.

CONCLUSION

Previous to the main program, which will start at the beginning of 1976, a number of test runs will take place in selected areas to determine the most favorable points for gathering ground-truth values and to get acquainted with the sensor package onboard the aircraft. Evaluation of the data so far gathered has not yet been terminated, but we can already say this: The correlation of the flight data and the ground-truth values has proved to be of vital importance to get good results from a quantitative interpretation of the remote sensing data.

TABLE I

ELEVEN-CHANNEL SCANNER CHARACTERISTICS

Characteristics	Value or Type	
Spectral Bands	λc (microns)	$\Delta\lambda$ (microns)
Channel 1	0.410	0.06
Channel 2	0.465	0.05
Channel 3	0.515	0.05
Channel 4	0.560	0.04
Channel 5	0.600	0.04
Channel 6	0.640	0.04
Channel 7	0.680	0.04
Channel 8	0.720	0.04
Channel 9	0.815	0.09
Channel 10	1.015	0.09
Channel 11	11.00 (nominal)	Selectable
Scan Mirror	Rotating optical flat 4 inches diameter Rotation rate: 10 to 100 rps	
Collecting Optics	Dall-Kirkham telescope. 65 CM^2 Collecting area (combined with scan mirror)	
Field of View (FOV)	100 degrees ± 10 degrees for aircraft roll compensation	
Instantaneous Field of View (IFOV)	2.5 milliradians	
V/H	Variable 0.025 to 0.25 radians per second (10 to 100 scans per second)	
Digital Electronics		
Bit Packing Density	10 000 bits/in. (dependent on tape recorder speed control)	
Calibration Sources		
Visible Sources (3)	a) Skylight reference b) Tungsten-halogen lamp c) Black level	
Low Temperature Thermal (BB1)	Field filling (temperature controlled)	
High Temperature Thermal (BB2)	Field filling (temperature controlled)	
Data Recording Devices (customer selected)		
Tape Recorder	Digital data from signal processor	
M^2S Operator Displays		
Thermal Reference Temperature	Digital (optional)	
Indicating Lamps	System status indicators	
Scan Line Count	Digital numerics	

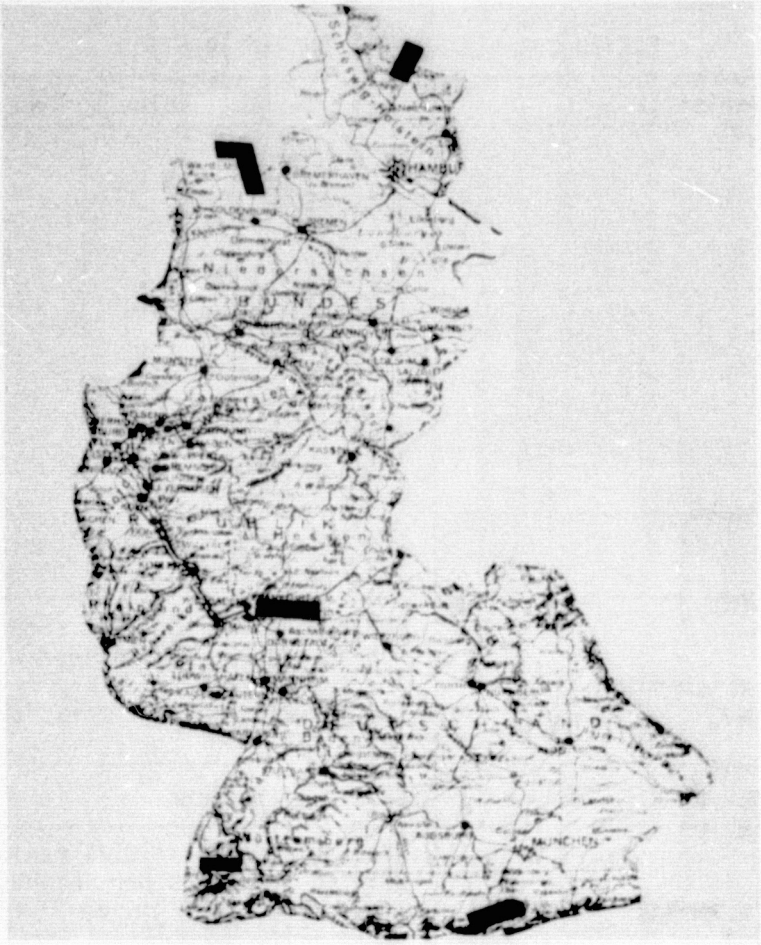


Figure 1.- Location of five test areas in Germany.

- AIRCRAFT : DORNIER DO 28 D2
- NUMBER OF ENGINES : TWO
- POWER OF ENGINES : 2 x 360 PS (100%)
- MAXIMUM SPEED : 177 K IAS
- VS_1 WITH ZERO FLAPS : 57 K IAS
- MAXIMUM GROSS WEIGHT : 3720 kg
- MAXIMUM FLIGHT TIME FOR GROSS WEIGHT : 8 h
- MAXIMUM FLIGHT TIME WITH SENSOR LOADING : 3 1/2 h
- MAXIMUM FLIGHT ALTITUDE : 25000 ft

Figure 2.- Specifications of earth scientific sensor carrier.

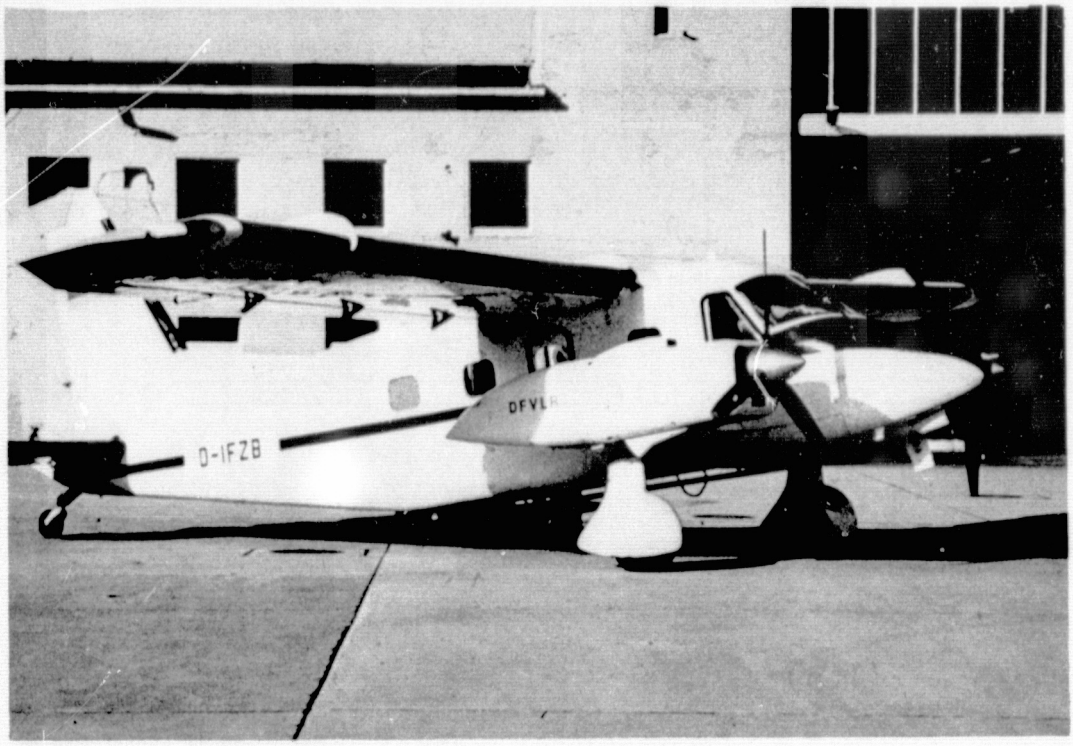


Figure 3.- Dornier DO 28 D2 aircraft.

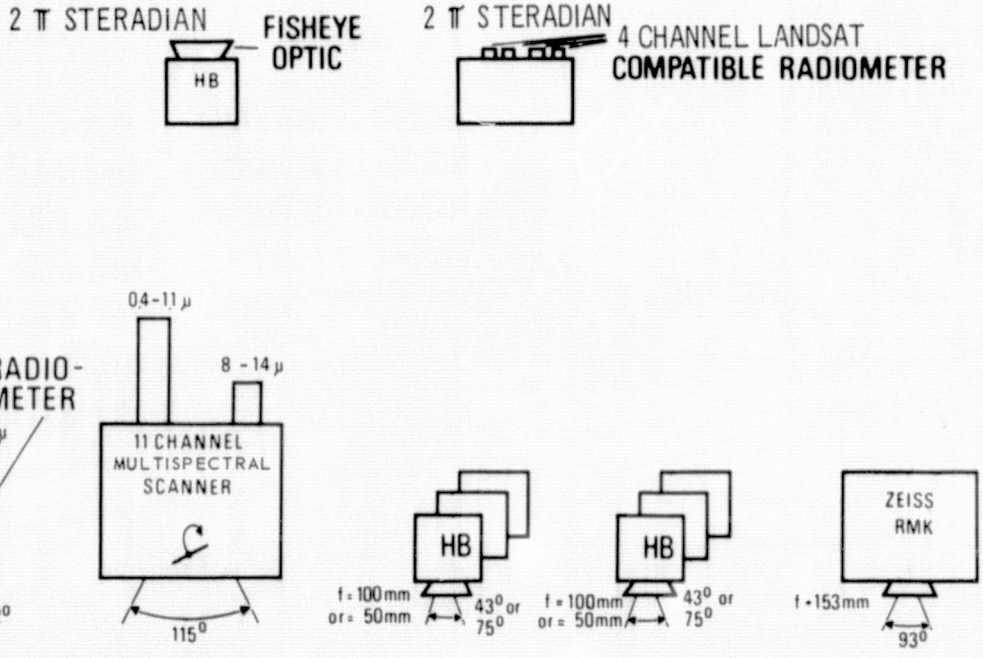


Figure 4.- Earth scientific sensor package.

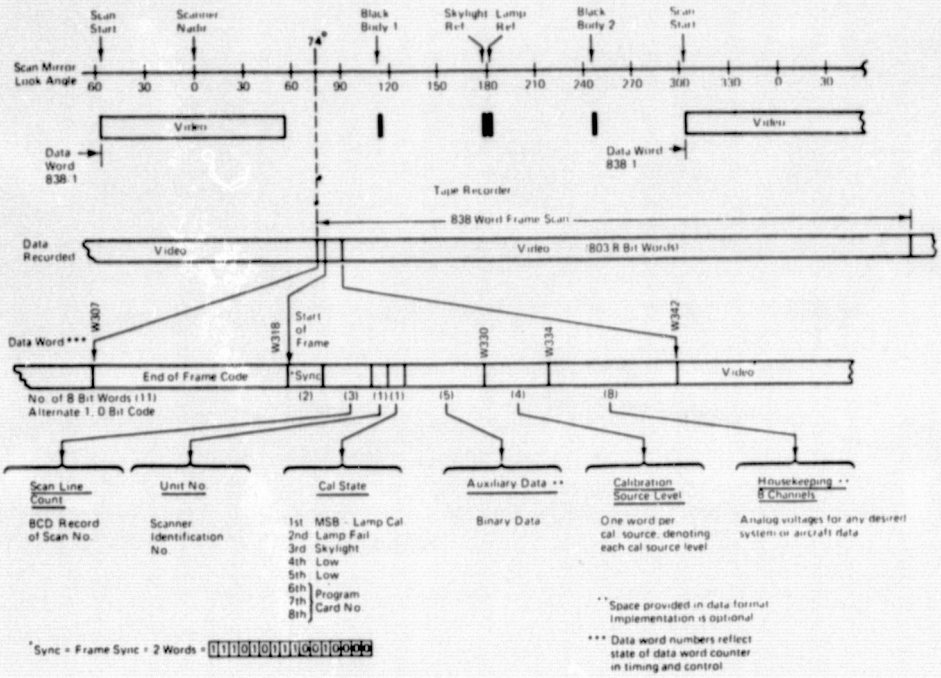


Figure 5.- Eleven-channel scanner data frame.

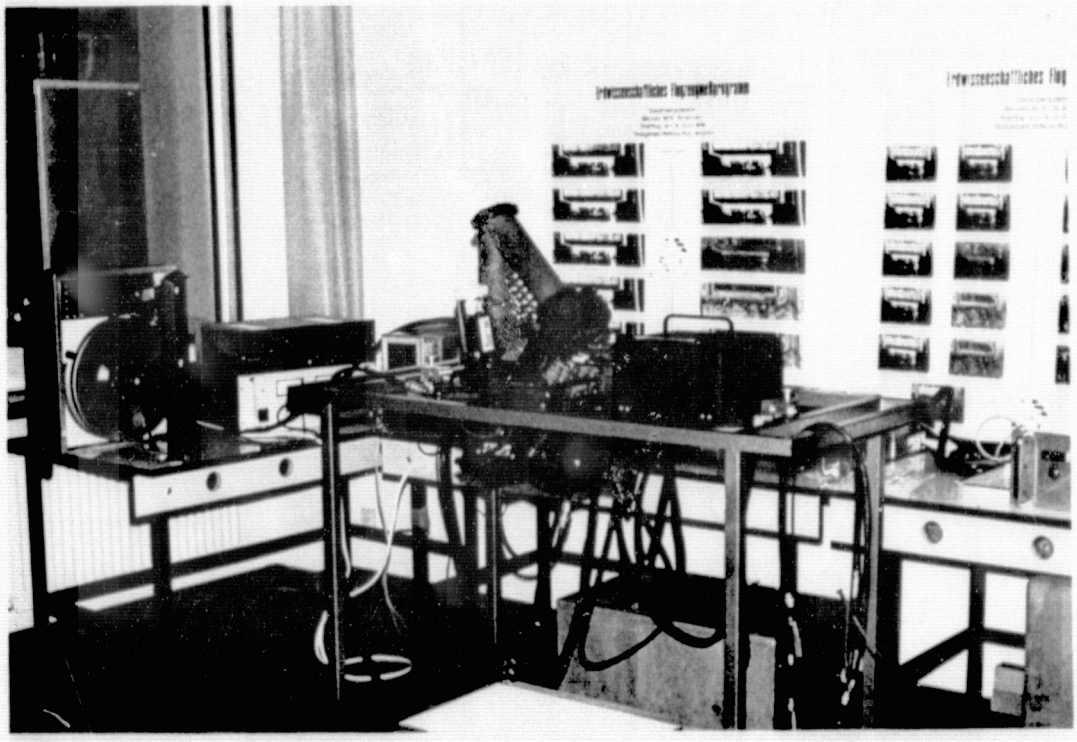


Figure 6.- Eleven-channel scanner laboratory setup.

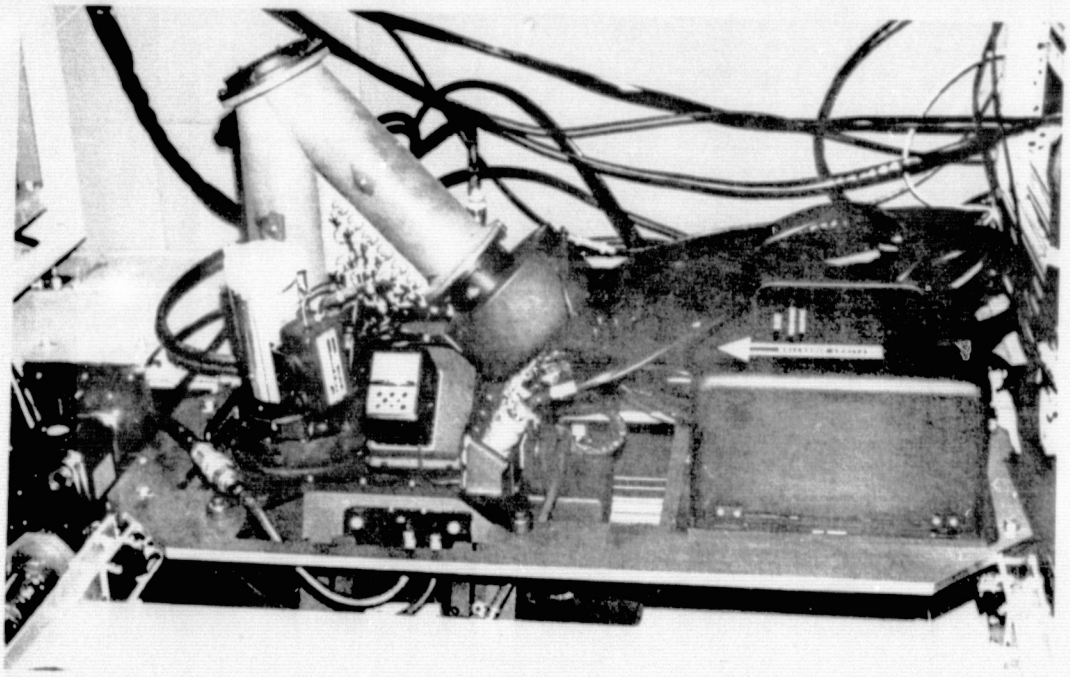


Figure 7.- Eleven-channel scanner aircraft installation.

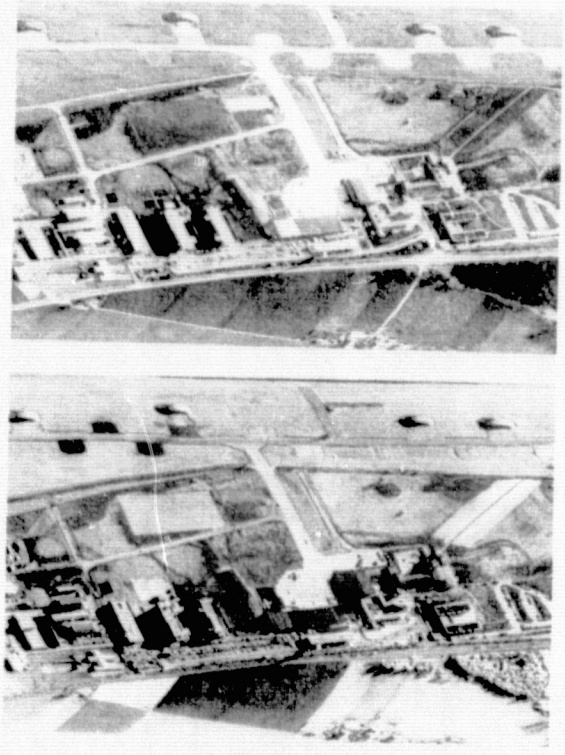


Figure 8.- DFVLR facilities imaged in channels 2 and 9 by the scanner.

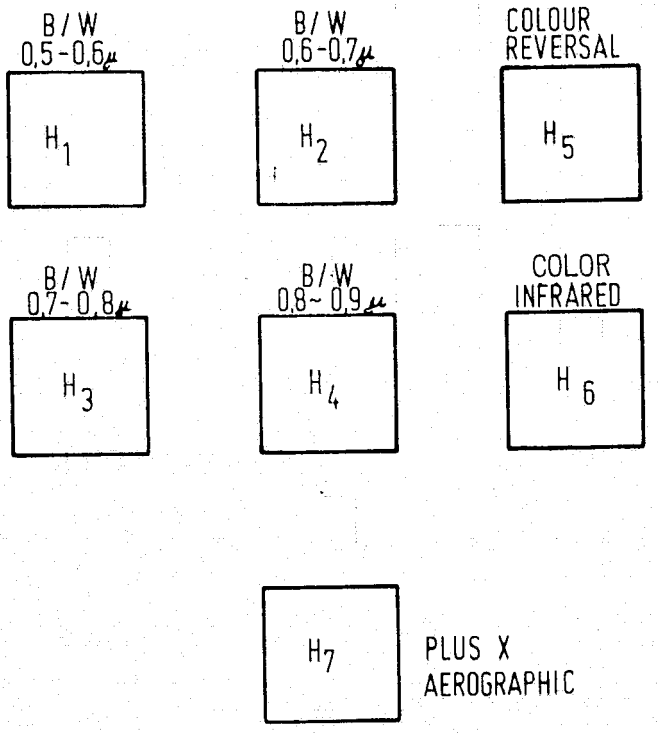
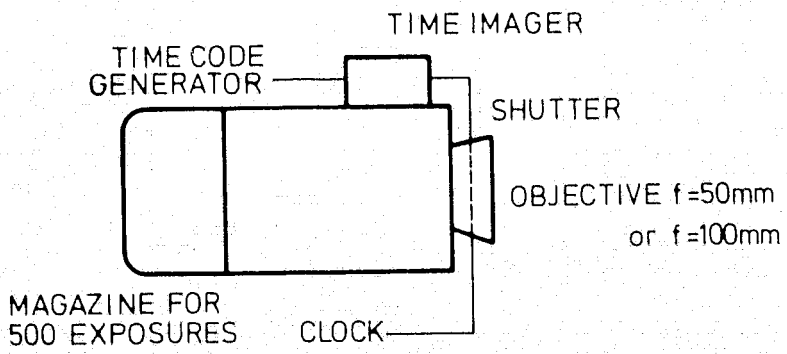


Figure 9.- Camera/film combinations.



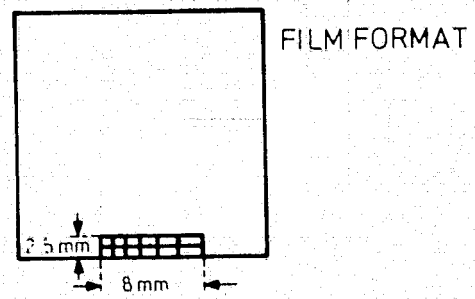


Figure 10.- 70-mm camera modifications for time registration.

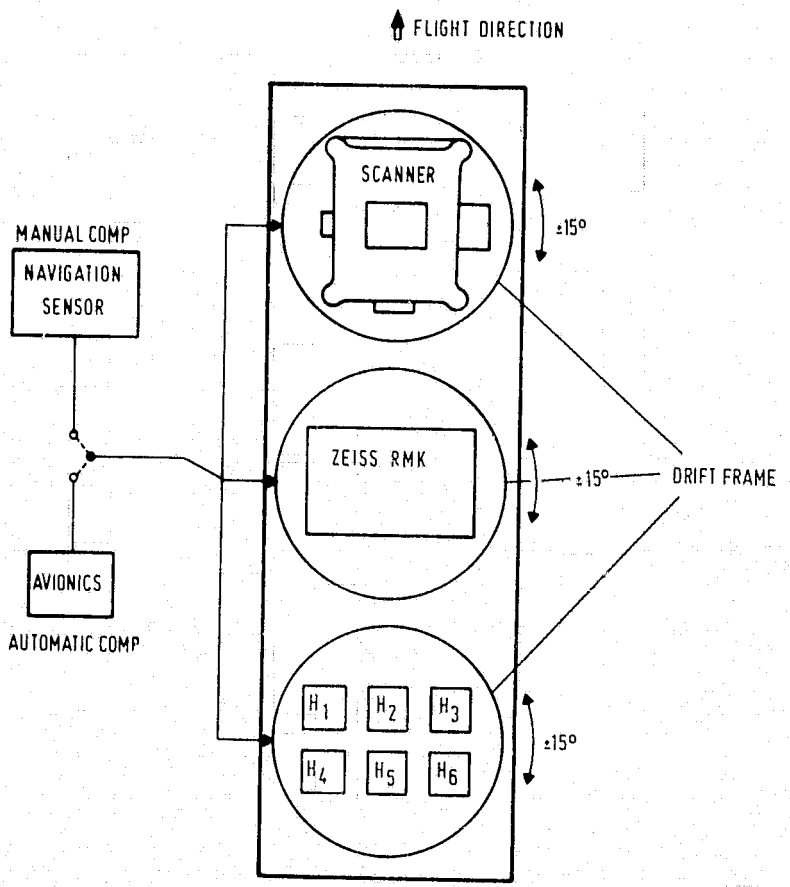


Figure 11.- Drift compensation mounting.

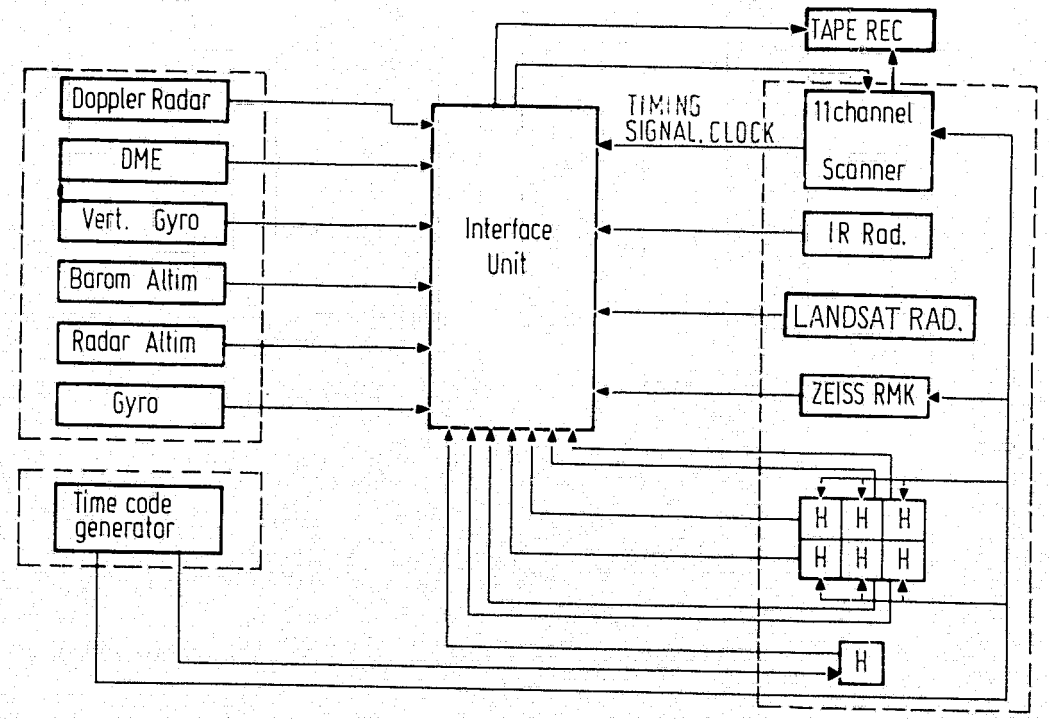


Figure 12.- Onboard data processing.

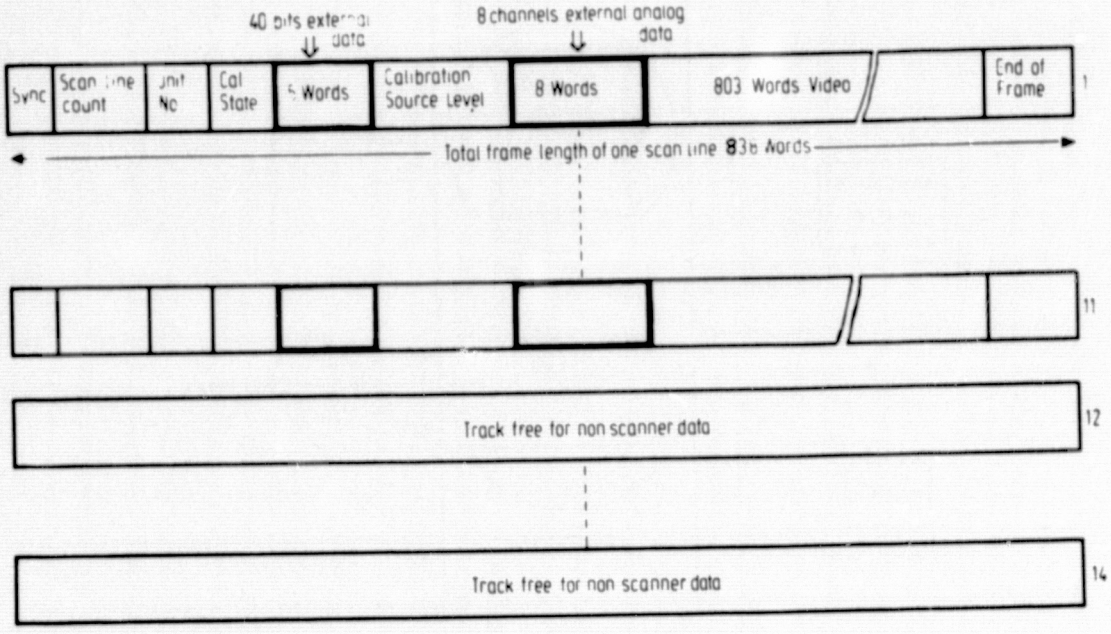


Figure 13.- Data organization on 14-track tape.



Figure 14.- Truck for collecting ground-truth data.

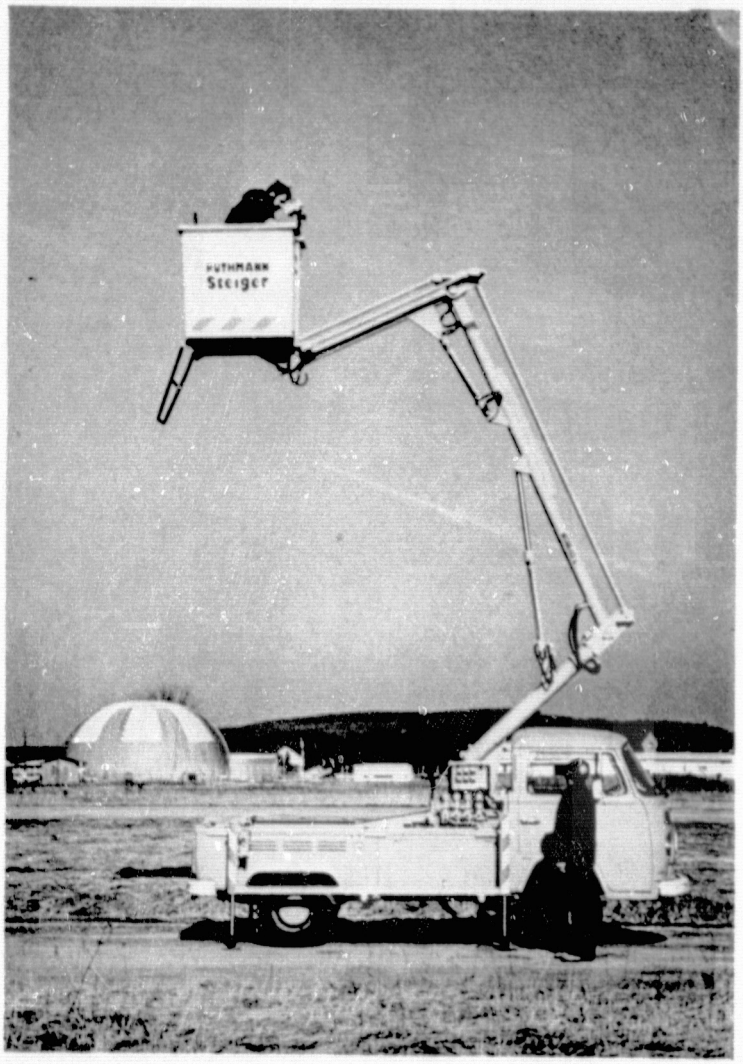


Figure 15.- Cherry picker.